

# Deep Soil Test Borings to Determine Shear Wave Velocities Across South Carolina

---

*Sponsoring Agencies:*  
South Carolina Department of Transportation



Federal Highway Administration



*Principal Investigators:*  
Dr. Inthuorn Sasanakul  
Civil and Environmental Engineering  
University of South Carolina  
Dr. Sarah Gassman  
Civil and Environmental Engineering  
University of South Carolina

October 2019

**Technical Report Documentation Page**

1. Report No. FHWA-SC-19-04	2. Government Accession No.	3. Recipient's Catalog No.
4. Title and Subtitle Deep Soil Test Borings to Determine Shear Wave Velocities Across South Carolina		5. Report Date October 2019
		6. Performing Organization Code
7. Author(s) Inthuorn Sasanakul, Sarah Gassman		8. Performing Organization Report No.
9. Performing Organization Name and Address University of South Carolina Civil and Environmental Engineering 300 Main St., Columbia, SC 29208		10. Work Unit No. (TRAIS)
		11. Contract or Grant No. SPR No. 731
12. Sponsoring Agency Name and Address South Carolina Department of Transportation PO Box 191 Columbia, SC 29202-0191		13. Type of Report and Period Covered Final Report
		14. Sponsoring Agency Code
15. Supplementary Notes Pitak Ruttithivaphanich and Siwadol Dejphumee		
<p>16. Abstract</p> <p>Having an accurate shear wave velocity profile and a better understanding of dynamic behavior of the deep soil deposits in the South Carolina Coastal Plain are critical for seismic hazard analyses of critical transportation infrastructure. This research presents a study that obtained comprehensive field and laboratory measurements of shear wave velocity and dynamic soil behaviors for two sites in the South Carolina Coastal Plain where data was limited. Site A is located near Conway in Horry County and Site B is located in Andrews in Williamsburg County. Geotechnical borings were drilled at these two locations to depths of 505 and 615 ft to perform extensive geotechnical and geological site characterization. Shear wave velocity profiles were developed using several geophysical testing methods including P-S suspension logging, full waveform sonic logging, a combined multi-channel analysis of surface waves and spectral analysis of surface waves, and a combined multi-channel analysis of surface waves and microtremor array measurement methods. The developed profiles were compared, and similarities and differences were discussed in this report.</p> <p>Shear modulus and damping behaviors over a wide range of strains for soil and rock samples collected from both sites were evaluated using resonant column and torsional shear methods. It was found that the behaviors of materials obtained from Tertiary and Cretaceous deposits deviated from the empirical predictions based on plasticity index and geologic age. Based on the results, the predictive curves for shear modulus and damping curves are not recommended for older soil deposits, particularly for those samples with cementation.</p>		

17. Key Word Shear Wave Velocity, Shear Modulus, Damping Site Response Analysis, Geophysical Test, Resonant Column Test, Torsional Shear Test		18. Distribution Statement No restrictions.	
19. Security Classif. (of this report) Unclassified.	20. Security Classif. (of this page) Unclassified.	21. No. of Pages 621	22. Price

## Disclaimer

---

The contents of this report reflect the views of the author who is responsible for the facts and the accuracy of the data presented. The contents do not necessarily reflect the official views of the South Carolina Department of Transportation or Federal Highway Administration. This report does not constitute a standard, specification, or regulation.

The State of South Carolina and the United States Government do not endorse products or manufacturers. Trade or manufacturer's names appear herein solely because they are considered essential to the object of this report.

## Acknowledgments

---

This project was funded by the South Carolina Department of Transportation and the Federal Highway Administration under grant SPR 731. Their support is greatly appreciated.

The authors would like to acknowledge personnel from the South Carolina Department of Transportation for their assistance throughout the project. The SCDOT research development personnel included: Terry Swygert and Meredith Heaps. The implementation committee of this project included: Nicholas Harman, Jeremy Harmon, Bill Jones, Trapp Harris, Renee Gardner, and Blake Gerken (FHWA), and Ani Garignan and Emad Ghebi formerly with SCDOT.

The authors would like to express special thanks to the following individuals who provided support to this project.

William (Billy) Camp	S&ME
Kyle Murrell	S&ME
Levi Ekstrom	S&ME
Christopher Stryffeler	formerly with S&ME
Brady Cox	UT Austin
Antony Martin	GEOVision
John Diehl	GEOVision
Scott Howard	SCDNR
Joe Gellici	SCDNR
William Doar	SCDNR
Michael Waddell	USC
Camille Ransom	SCDHEC
Joy McLaurin	Farmers Grain & Milling

Finally, the authors would like to thank the staff and students at the University of South Carolina for their administrative and technical support of this project. The following graduate students; Pitak Ruttithivaphanich, Siwadol Dejphumee, William Ovalle Villamil, and Kazi Islam assisted with field measurements, laboratory testing, and data compilation and analysis. The following undergraduate students; Veronica Bense, Nicolet Chavancak, Ryan Devine, Javonte Isaac, E'Lexus Nelson, and Bryce Reeve, assisted with laboratory testing.

## Executive Summary

---

This report presents the findings from a study undertaken to obtain deep soil profiles at two sites in the South Carolina Coastal Plain. Site A is located near Conway in Horry County and Site B is located in Andrews in Williamsburg County. Geotechnical borings were drilled to depths of 505 and 615 ft for Sites A and B, respectively. Shear wave velocity profiles were generated using P-S suspension logging, full waveform sonic logging, combined multi-channel analysis and spectral analysis of surface waves (MASW-SASW), and combined multi-channel analysis of surface waves and microtremor array measurement (MASW-MAM) methods. Soil and rock samples were collected for further characterization in the laboratory. Resonant column and torsional shear testing methods were utilized to evaluate dynamic soil behaviors for a wide range of strains.

The shear wave velocity profiles using P-S suspension logging were obtained to a depth of 470 ft for Site A and a depth of 600 ft for Site B. Profiles to a depth of 220 ft were obtained from the MASW-SASW method for both sites. For the combined MASW-MAM method, profiles were obtained to a depth 4921 ft for Site A and a depth of 2625 ft for Site B. Overall, the average shear wave velocities obtained from the surface methods within the top 200 ft were lower than that of the P-S suspension logging data. This resulted in a different NEHRP site class when using the average shear wave values in the top 100 ft for Site A, but not site B. The P-S suspension logging provided detailed characteristics of the soil profile and the results agreed with the visual observation of samples. However, the P-S suspension logging method did not provide the depth of the B-C boundary, as the boundary was below the bottom of each borehole.

The results from both surface methods were in agreement within the top 220 ft where the MASW-SASW results could be compared. The MASW-MAM method is a unique method utilizing passive ambient wave sources and specialized sensors that allows deep profiling and identified an estimated depth to the B-C boundary of 580 ft for Site A and 1343 ft for Site B. Results from both surface methods show that spatial variation of both sites are high, especially for Site A. The shear wave profiles from the surface wave methods represent the average profiles over a large volume of soil; whereas, the profiles from the borehole methods represent localized profiles within the tested borehole. Results from the different methods provide understanding of the range of uncertainty in the shear wave velocity profiles that should be accounted for when performing site response analysis.

Visual observation of samples collected from both sites showed that materials were highly variable with frequent transitions between soil-like to rock-like material. Highly cemented sand or clay with thicknesses varying from a few inches to several feet depth were observed at several depths throughout the soil profiles. The location of these rock-like materials corresponded with the high shear wave velocities observed from the P-S logging profile.

Many soil and rock samples were tested to evaluate dynamic soil behaviors, specifically to determine the variation of shear modulus and damping for a wide range of strains. Overall, it was found that the material behaviors deviate from the predicted behaviors obtained based on soil index properties and geologic age provided in the literature. Relatively high damping values were observed particularly at low strains and the values were significantly affected by loading frequency applied using different testing methods. The effect of soil plasticity in relation to geologic age was evaluated for the shear modulus and damping relations, and no clear trend was observed for Tertiary and Cretaceous soil deposits. As a result, the shear modulus and damping behaviors were not accurately predicted for these soils. It is hypothesized that cementation is likely to be a significant factor affecting the dynamic soil behavior; however, detailed evaluation of cementation in relation to shear modulus and damping was beyond the scope of this study.

Data from this study can be used directly to perform site-specific site response analysis for the sites studied herein with the recommendation to perform sensitivity analyses to account for uncertainty in the shear wave velocity profiles, depth of competent rock, dynamic soil behavior, and impacts of interbedded rock and cemented layers. Predictive equations found in the literature for shear modulus and damping curves are not recommended for Tertiary and Cretaceous deposits because this study showed that soil plasticity and geologic age alone are not dominant factors for older soil deposits, particularly for those samples with cementation.

# Table of Contents

---

Disclaimer .....	iv
Acknowledgments.....	v
Executive Summary .....	vi
Table of Contents.....	viii
List of Figures .....	x
List of Tables .....	xii
1. Introduction.....	1
1.1. Research Objectives.....	1
1.2. Research Tasks.....	2
1.3. Organization of The Report .....	2
2. Background.....	3
3. Methodology .....	6
3.1. Sites Studied and Project Team .....	6
3.2. Field Investigation .....	7
3.2.1. Borehole Geotechnical Investigation.....	7
3.2.2. P-S Suspension Logging Method.....	8
3.2.3. Full Waveform Sonic Logging Method.....	9
3.2.4. Combined Multi-Chanel Analysis and Spectral Analysis of Surface Waves (MASW-SASW) Method.....	9
3.2.5. Combined Multi-Channel Analysis of Surface Waves (MASW) and Microtremor Array Measurement (MAM) Method.....	10
3.3. Laboratory Testing of Soils and Rocks.....	14
3.3.1. Geological Logging .....	15
3.3.2. Soil Classification and Index Property Measurements .....	15
3.3.3. Small Strain Dynamic Properties Measurements.....	15
4. Results and Analysis .....	17
4.1. General Observation of Geotechnical Borehole Drilling.....	17
4.2. Geotechnical and Geological Description of Soil Profiles .....	17
4.3. Field Measurements of Shear Wave Velocity Profiles .....	21
4.3.1. Summary of Surface Wave Data Analyses .....	21
4.3.2. Comparison of $V_s$ Profiles for Site A.....	25

4.3.3. Comparison of $V_s$ Profiles for Site B.....	29
4.4. Laboratory Measurements of Dynamic Behaviors .....	34
4.4.1. Dynamic Behaviors of Materials from Site A .....	34
4.4.2. Dynamic Behaviors of Materials from Site B.....	37
4.4.3. Data Analysis and Interpretation of Dynamic Soil Properties .....	42
5. Conclusion, Recommendations, Implementation, and Future Research Needed .....	60
5.1. Conclusions.....	60
5.2. Recommendations.....	61
5.3. Implementation Plan .....	62
5.4. Future Research Needed .....	63
References.....	64
Appendix.....	68
Appendix A: Geotechnical Boring Logs, P-S Logging, and MASW-SASW Testing Results	
Appendix B: MASW-MAM Testing Results	
Appendix C: FWS Logging Results	
Appendix D: Geological Logging Results	
Appendix E: Index Testing Results	
Appendix F: Resonant Column and Torsional Shear Testing Procedures and Results	
Appendix G: Statistical Analysis of $G/G_{\max}$ and Damping Curves	

## List of Figures

---

<b>Figure 2.1</b> Shear Wave Velocity Profiles for (a) Charleston-Savannah and (b) Myrtle Beach (adapted from Andrus et al. 2014).....	4
<b>Figure 2.2</b> Locations of Soil Specimens from Zhang et al. (2005) and this Study (labeled as Site A and Site B) (adapted from Zhang et al. 2005).....	5
<b>Figure 3.1</b> Study Sites .....	6
<b>Figure 3.2</b> Project Organizational Chart .....	7
<b>Figure 3.3</b> Surface Geophysical Testing Locations at Site A: (a) MASW and SASW Testing Arrays, (b) MASW and MAM Testing Arrays.....	12
<b>Figure 3.4</b> Surface Geophysical Testing Locations at Site B: (a) MASW and SASW Testing Arrays, (b) MASW and MAM Testing Arrays.....	13
<b>Figure 4.1</b> Soil Classification and Geological Information for Site A.....	19
<b>Figure 4.2</b> Soil Classification and Geological Information for Site B .....	20
<b>Figure 4.3</b> Inversion Results for Site A from MASW-SASW Method: (a) Dispersion Curves, and (b) Selected $V_s$ Model.....	22
<b>Figure 4.4</b> Inversion Results for Site B from MASW-SASW Method: (a) Dispersion Curves, and (b) Selected $V_s$ Models .....	23
<b>Figure 4.5</b> Median Inversion Results for Site A from MASW-MAM Method Shown for Each Inversion Parameterization (i.e., layering ratios $X = 1.5, 2.0, 2.5, 2.0a,$ and $2.0b$ ): (a) Dispersion Curves, (b) H/V Curves, (c) $V_s$ Profiles Shown to a Depth of 4900 ft, and (d) $V_s$ Profiles Shown to a Depth of 328 ft.....	24
<b>Figure 4.6</b> Median Inversion Results for Site B from MASW-MAM Method Shown for Each Inversion Parameterization: (a) Dispersion Curves, (b) H/V Curves, (c) $V_s$ Profiles Shown to a Depth of 2625 ft, and (d) $V_s$ profiles Shown to a Depth of 328 ft .....	25
<b>Figure 4.7</b> $V_s$ Profiles for Site A: (a) Shown to a Depth of 800 ft, and (b) Shown to a Depth of 300 ft....	27
<b>Figure 4.8</b> (a) Variation of SPT N Value with Depth, and (b) Comparison between $V_s$ Profiles between the $V_s$ -SPT Correlation and Results from Geophysical Methods for Site A.....	28
<b>Figure 4.9</b> Calcareous Sand/Sandstone Samples from Site A at Depths: (a) 194-200 ft, and (b) 450-456 ft .....	29
<b>Figure 4.10</b> $V_s$ Profiles for Site B: (a) Shown to a Depth of 1800 ft, and (b) Shown to a Depth of 300 ft. ....	31
<b>Figure 4.11</b> Samples from Site B: (a) Limestone from 23-26 ft, (b) Claystone from 300-305 ft, (c) Silty Clay from 394 ft, and (d) Sandstone from 580-584 ft.....	32
<b>Figure 4.12</b> (a) Variation of SPT N Value with Depth, and (b) Comparison between $V_s$ Profiles between the $V_s$ -SPT Correlation and Results from Geophysical Methods for Site B.....	33

<b>Figure 4.13</b> RC Testing Results for Soil Samples from Site A: (a) $G/G_{max}$ Curves, and (b) Damping Curves .....	35
<b>Figure 4.14</b> TS Testing Results for Soil Samples from Site A: (a) $G/G_{max}$ Curves, and (b) Damping Curves .....	36
<b>Figure 4.15</b> RC Testing Results for Rock Samples from Site A: (a) $G/G_{max}$ Curves, and (b) Damping Curves .....	37
<b>Figure 4.16</b> RC Testing Results for Soil Samples from Site B: (a) $G/G_{max}$ Curves, and (b) Damping Curves .....	39
<b>Figure 4.17</b> TS Testing Results for Soil Samples from Site B: (a) $G/G_{max}$ Curves, and (b) Damping Curves .....	40
<b>Figure 4.18</b> RC Testing Results for Rock Samples from Site B: (a) $G/G_{max}$ Curves, and (b) Damping Curves .....	41
<b>Figure 4.19</b> Photos of Rock Samples that Exhibited Relatively High Damping .....	42
<b>Figure 4.20</b> Variation of Shear Wave Velocity with Confinement for Site A .....	43
<b>Figure 4.21</b> Variation of Shear Wave Velocity with Confinement for Site B .....	43
<b>Figure 4.22</b> Variation of Damping with Confinement for Site A .....	44
<b>Figure 4.23</b> Variation of Damping with Confinement for Site B.....	44
<b>Figure 4.24</b> Effect of Testing Frequency on: (a) Normalized $G/G_{0.5Hz}$ , and (b) Normalized $D/D_{0.5Hz}$ .....	47
<b>Figure 4.25</b> Dynamic Properties of Quaternary Age Soils: (a) $G/G_{max}$ Curves, and (b) Damping Curves	49
<b>Figure 4.26</b> Dynamic Properties of Tertiary Age Soils: (a) $G/G_{max}$ Curves, and (b) Damping Curves .....	50
<b>Figure 4.27</b> Dynamic Properties of Cretaceous Age Soils: (a) $G/G_{max}$ Curves, and (b) Damping Curves	51
<b>Figure 4.28</b> (a) $G/G_{max}$ Curves, and (b) Damping Curves Generated from Predictive Model for Quaternary Age Soils: Ten Mile Hill Formation and Penholoway Alloformation .....	56
<b>Figure 4.29</b> (a) $G/G_{max}$ Curves, and (b) Damping Curves Generated from Predictive Model for Tertiary Age Soils: Williams Burg Formation and Lower Bridge Member .....	57
<b>Figure 4.30</b> (a) $G/G_{max}$ Curves, and (b) Damping Curves Generated from Predictive Model for Cretaceous Age Soils: Peedee Formation and Black Creek Group .....	58
<b>Figure 4.31</b> Variation of $D_{min}$ with PI for Soils of Different Geological Ages (after Andrus et al. 2003).	59

## List of Tables

---

<b>Table 3.1</b> A Summary of Laboratory Testing of Soil and Rock Samples .....	14
<b>Table 4.1</b> Summary of Average Shear Wave Velocities and Possible B-C Boundary for Site A.....	29
<b>Table 4.2</b> Summary of Average Shear Wave Velocities and Possible B-C Boundary for Site B .....	33
<b>Table 4.3</b> Material Properties of Tested Samples for Site A.....	34
<b>Table 4.4</b> Material Properties of Tested Samples for Site B .....	38
<b>Table 4.5</b> Comparison of $V_s$ of Soil Samples for Site A .....	45
<b>Table 4.6</b> Comparison of $V_s$ of Soil Samples for Site B .....	46
<b>Table 4.7</b> Model Parameters for Quaternary Deposit (Ten Mile Hill and Penholoway Formation) .....	54
<b>Table 4.8</b> Model Parameters for Tertiary Deposit (Williamsburg Formation and Lower Bridge Member) .....	54
<b>Table 4.9</b> Model Parameters for Cretaceous Deposit (Peedee Formation and Black Creek Group).....	55

# 1. Introduction

---

The South Carolina Coastal Plain consists of a deep soil basin with variable thicknesses of sedimentary deposits across the area. The deep soil basin condition, where the depth to the top of rock is greater than 500 ft, is not properly described by the National Earthquake Hazards Reduction Program (NEHRP) site coefficient, thus site-specific site response analysis (SSRAs) is typically required to determine the design response spectra for structures situated on deep soil basin sites. Shear wave velocity ( $V_s$ ) profiles, the depth of soil sediment to the top of soft rock (i.e., the B-C boundary), and the variation of soil modulus and damping with shear strain are the primary inputs for site response analysis. These parameters have significant impacts on the results of SSRAs.

The overall goal of this research was to reduce uncertainties in SSRAs for the South Carolina Department of Transportation (SCDOT) seismic design. The research goal was achieved through extensive field and advanced laboratory investigations of deep  $V_s$  profiles for two sites in South Carolina. The research presented herein is the first geotechnical and geological investigation where several field methods were used and advanced laboratory testing was performed. The research developed a set of high quality geotechnical and geophysical data as well as geological information that can be used to perform SSRAs and can be used to further interpret other sites in the Coastal Plain.

Two sites located in the South Carolina Coastal Plain were identified by the SCDOT where the deep  $V_s$  profiles and geological information were very limited and/or not available. Site A is located near Conway in Horry County and Site B is located in Andrews in Williamsburg County. The target depth of borehole was approximately 500 and 600 ft deep for Site A and Site B, respectively. Borehole geotechnical and geophysical methods were performed to characterize soil and rock properties and develop the  $V_s$  profiles. These profiles were compared with the  $V_s$  profiles developed from non-invasive surface geophysical methods to evaluate differences in testing methods.

## 1.1. Research Objectives

The research program was designed to accomplish the following objectives:

1. Conduct geotechnical field exploration at two sites and develop comprehensive soil boring logs;
2. Conduct field geophysical testing using different methods at two test sites to develop shear wave velocity profiles and compare the similarities and differences between these profiles;
3. Collect soil and rock samples and conduct a series of geotechnical laboratory tests to determine the physical, mechanical and small strain dynamic properties of the materials in accordance with applicable ASTM and AASHTO standards; and
4. Evaluate parameters that are useful for SSRAs to be conducted for future SCDOT projects at these two sites. These parameters include: average shear wave velocity in the top 100 ft ( $V_{s100ft}$ ), depth to the top of soft or competent rock (i.e., the B-C

boundary), and representative normalized shear modulus ( $G/G_{\max}$ ) and damping ( $D$ ) curves. These parameters are compared with the database currently available to SCDOT engineers and contractors.

## **1.2. Research Tasks**

To meet the objectives, the project was divided into four work tasks spanning a 33-month period. The tasks are listed as follows:

Task 1: Preparation of field and laboratory testing program

Task 2: Field investigation

Task 3: Laboratory testing of soils and rocks

Task 4: Final data compilations and documentation

## **1.3. Organization of The Report**

This report has been organized into five chapters including the introduction to the project presented here. Chapter 2 presents the background of this project. Chapter 3 presents methodology used for Tasks 2 and 3. The results and analysis are presented in Chapter 4, including key findings and comparisons of  $V_s$  profiles generated from different methods and geotechnical and geological boring logs, small strain dynamic properties of soil and rock samples and factors affecting the small strain dynamic properties and comparisons of results with empirical relationships, and a new relationship proposed for Cretaceous age deposits. Chapter 5 presents conclusions, recommendations, and the implementation plan. Appendices A-G include all of the data and detailed information necessary for the report.

## 2. Background

---

The Atlantic Coastal Plain is a geological condition found in the Central and Eastern United States. The coastal plain consists of unconsolidated sediments as thick as 3,000 ft underlain by very hard rock with shear wave velocity,  $V_s$  of over 8500 ft/s. In South Carolina, this very hard rock layer is located close to or at the ground surface in Columbia and its depth increases toward the coast as well as increasing in depth from North to South (Chapman and Talwani 2002). The deep sediments consist of unlithified sediments with weakly lithified units that are formed during Cretaceous, Tertiary (Neogene and Paleogene period), and Quaternary periods (Chapman et al. 2006). Many geologic formations have been identified within the SC Coastal Plain and a wide variety of materials were found within these formations, including sand, clay, gravel, limestone, and marl (SCDNR 2005). This unique geological and geotechnical condition poses significant challenges to seismic hazard analyses for the South Carolina Coastal Plain.

A  $V_s$  profile of soil sediment to the top of “competent” rock (a boundary defined as having a  $V_s$  of 2500 ft/s) and associated dynamic properties (i.e. shear modulus reduction and damping curves) are important parameters for seismic hazard analyses (Kavazanjian et al. 1997). In the Western United States, where most of the current seismic design criteria have been developed, the top of the competent rock is relatively shallow; hence the required  $V_s$  profile is typically no more than 100 ft deep. In the South Carolina Coastal Plain, the depth to the top of competent rock can be much deeper than 100 ft. The sediment from the ground surface to the top of competent rock typically consists of sediment deposits composed of complex layers of materials at different stages of the chemical weathering process. Due to limited data availability for the dynamic properties of the South Carolina Coastal Plain and high cost in site investigation, geotechnical engineers are required to account for high level of uncertainty for the design.

Andrus et al. (2014) compiled  $V_s$  profiles obtained from the literature for several locations in South Carolina. These profiles were measured by different borehole and non-intrusive geophysical methods. Ranges of shear wave velocity were correlated with geological units. An average  $V_s$  of approximately 623 ft/s was recommended for the Quaternary deposit, and 1312-2100 ft/s was recommended for the Tertiary deposit. The top of rock (i.e., B-C boundary) was defined where the  $V_s$  was greater than 2500 ft/s for the Tertiary and older deposits. The  $V_s$  data for the Cretaceous deposit was very limited and typically assumed to be higher than 2500 ft/s. Representative  $V_s$  profiles suggested by Andrus et al. (2014) for the Charleston-Savannah and Myrtle Beach areas are shown in Fig. 2.1. They were developed by averaging several  $V_s$  profiles obtained primarily for depths no deeper than 100 ft. Available  $V_s$  data at depths greater than 100 ft were limited to a few locations. Therefore, additional  $V_s$  data at deeper depths are needed for the South Carolina Coastal Plain in order to reduce uncertainties in estimating  $V_s$  for different soil types and geological formations as well as the estimated depth to the top of competent rock.

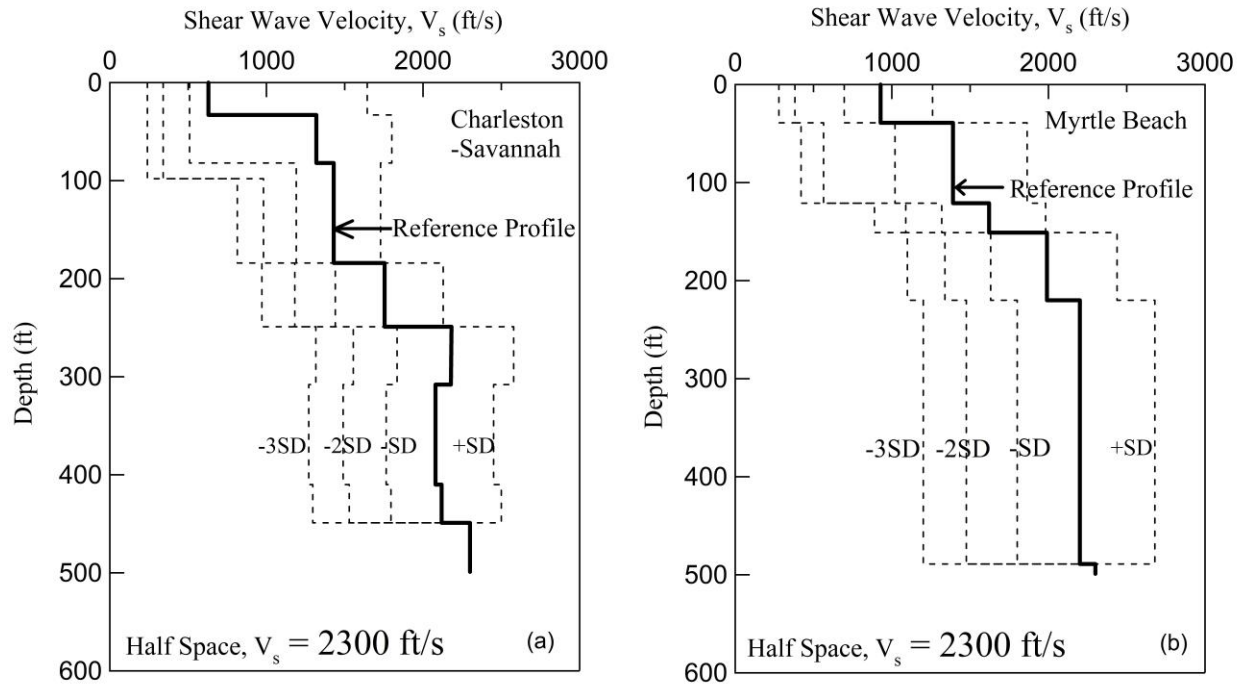


**Figure 2.1** Shear Wave Velocity Profiles for (a) Charleston-Savannah and (b) Myrtle Beach (adapted from Andrus et al. 2014)

Recently, additional deep soil boring investigations have been performed for several projects in the South Carolina Coastal Plain (i.e., GeoVision 2008, GeoVision 2010, S&ME 2015, and F&ME 2017); however, compared to other areas of the world with seismic hazards, practitioners in South Carolina face significant challenges due to lack of data (e.g., recorded ground motions, and deep geotechnical boreholes) and the unique geological conditions (e.g., deep un lithified sediments) that are different than the sites in the Western United States where a large amount of data has been used to develop the USGS simplified procedure. A sensitivity analysis is typically performed to address some of the uncertainties in the site response analysis, but there is no consensus or guidance on how to address these uncertainties or quantify the impact of the assumptions (Camp 2018).

In addition to the  $V_s$  profiles, the variation of shear modulus and damping with shearing strain are important inputs for site response analysis. Andrus and his colleagues (Andrus et al. 2003, Zhang et al. 2005, and Zhang et al. 2008) developed predictive equations for estimating the normalized shear modulus ( $G/G_{max}$ ) and damping ( $D$ ) for South Carolina soils based on geologic age, confining pressure, and soil plasticity. Results were compiled from resonant column and torsional shear tests from 122 soil specimens, 78 of which were from three locations in South Carolina (see Fig. 2.2). The previous study indicated that the geologic age and confining pressure have a larger impact on small strain dynamic properties than soil plasticity. They also reported that Quaternary-age soil dynamic behavior is more linear than Tertiary soil and residual/saprolite soil. This

approach is useful for an estimation of  $G/G_{max}$  and  $D$  variation over a range of strain when laboratory testing is not possible. However, more data are needed for strata deeper than 100 ft, particularly for older deposits (e.g. Tertiary and Cretaceous soil) and other geologic formations for the SC Coastal Plain. Recently, additional  $G/G_{max}$  and  $D$  data for soils in the lower Coastal Plain were obtained by S&ME (2015) and F&ME (2017), thus there is a need to update the Andrus et al. (2003) database and the associated prediction model. Currently, due to a large variation of material properties in the SC Coastal Plain, the site response analyses are performed using both predicted curves proposed by Andrus et al. (2003), or generic curves available in the literature. The generic curves were typically developed from uncemented sand or clay and the confining pressure and plasticity index generally governs dynamic soil properties (e.g. Vucetic and Dobry 1991, Seed et al. 1986, Sun et al. 1988, Ishibashi and Zhang 1993, and Darendeli 2001).

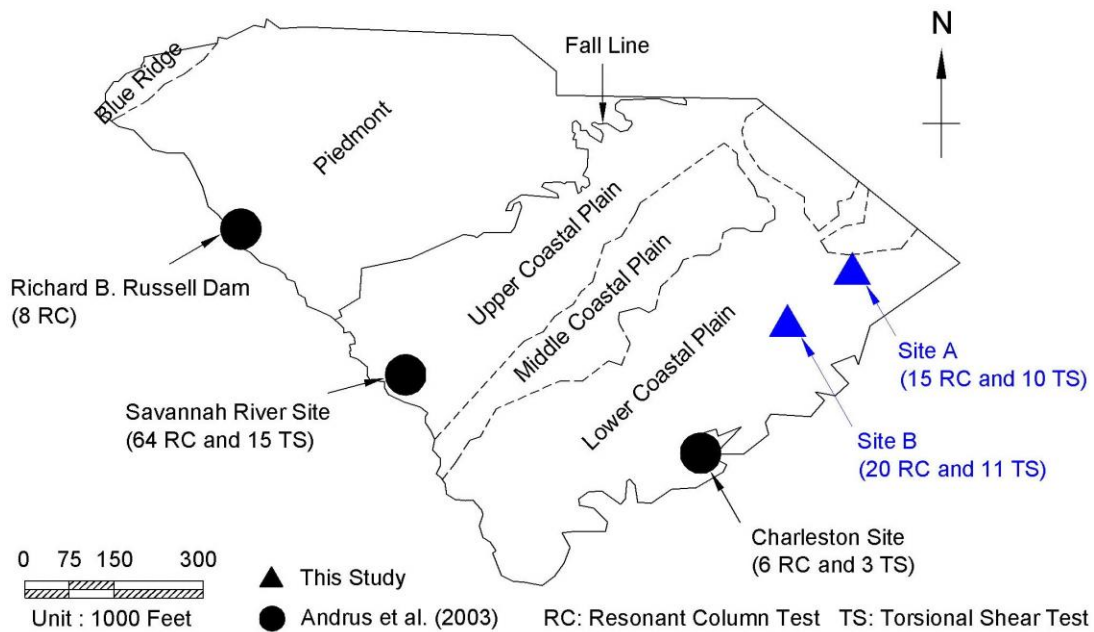


**Figure 2.2** Locations of Soil Specimens from Zhang et al. (2005) and this Study (labeled as Site A and Site B) (adapted from Zhang et al. 2005)

### 3. Methodology

This chapter presents a summary of the methodology used for characterizing deep shear wave velocity profiles and dynamic soil properties. More detailed information can be found in the Appendices.

#### 3.1. Sites Studied and Project Team

Two sites in South Carolina were selected as shown in Fig. 3.1. Site A is located near Conway in Horry County. Site B is located in Andrews in Williamsburg County. The sites are located in the Lower Coastal Plain and were chosen because deep soil borings have not been performed in these areas and the  $V_s$  profiles and dynamic soil properties were unknown. To obtain the  $V_s$  profiles and define the depth to the top of competent or soft rock ( $V_s = 2500$  ft/s), several geophysical testing methods were used: P-S suspension logging, full waveform sonic logging (FWS), a combined multi-channel and spectral analysis of surface waves (MASW-SASW) method, and a combined multi-channel analysis of surface waves and microtremor array measurement (MASW-MAM) method. Soil and rock samples were collected and tested in the laboratory to obtain small strain dynamic properties using resonant column (RC) and torsional shear (TS) methods. The success of this project required effective coordination and execution of the field exploration, geophysical testing activities, and specialized laboratory testing. An organizational chart showing the project team is presented in Fig. 3.2.

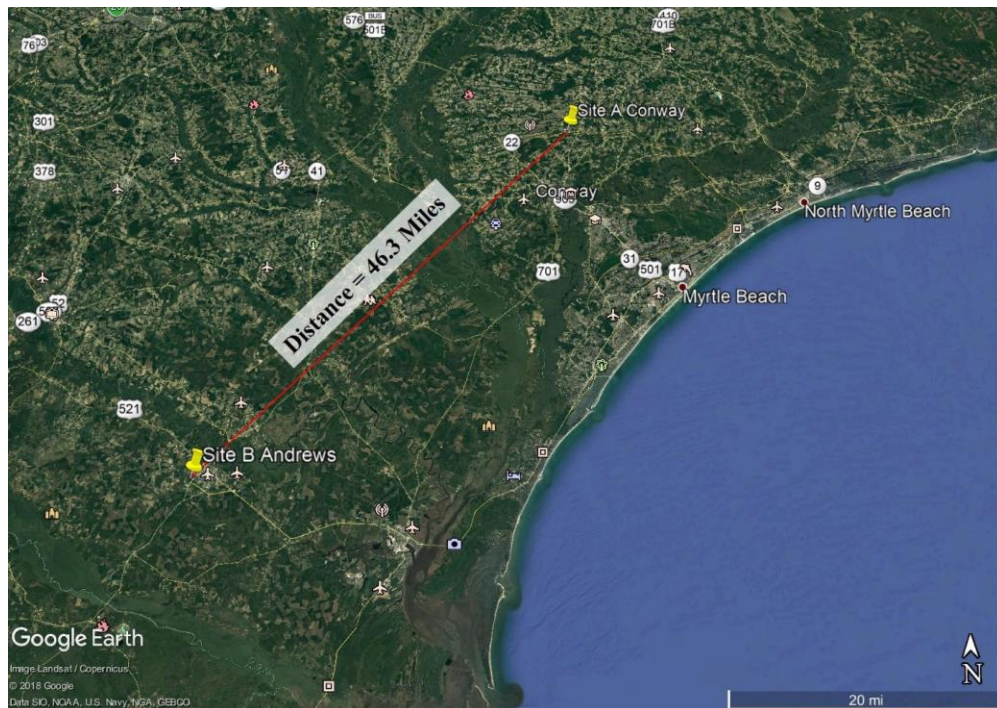
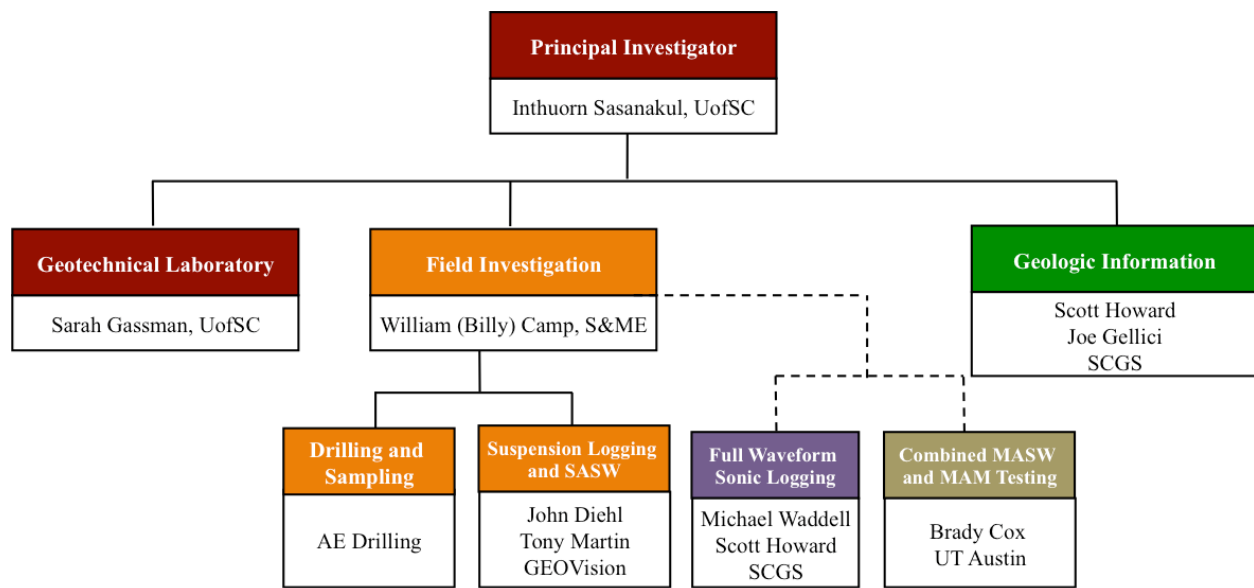


Figure 3.1 Study Sites



**Figure 3.2** Project Organizational Chart

### 3.2. Field Investigation

#### 3.2.1. Borehole Geotechnical Investigation

The geotechnical borings were drilled by AE Drilling under the supervision of S&ME. The methods utilized a combination of mud-rotary drilling, in general accordance with ASTM D5783, and wireline coring procedures, in general accordance with ASTM D2113. Each borehole was approximately 6-inch in diameter to allow for insertion of the geophysical testing equipment. Standard Penetration Test (SPT) split-barrel (split-spoon) sampling and/or thin-walled (Shelby) tube sampling were performed continuously from the ground surface until hard materials (i.e. SPT N-value is over 50 blows per ft) were consistently encountered. SPT split-barrel tube sampling was performed in general accordance with ASTM D1586/D1586M. In SPT sampling, a standard 2-inch diameter split steel tube was driven into undisturbed soil at a select depth using a 140-lb hammer falling a distance of 2.5 ft. The number of blows required to drive the sampler each 6-inch interval was recorded. The N-value represents the number of blows required for 1-foot penetration into the soil after an initial 6 inch “seating” drive depth was recorded. In this study “continuous” 2 ft interval SPT sampling was performed. Field logging was performed in general accordance with ASTM D5434. As the split-barrel samples were collected, visual classification of the soil was performed in general accordance with ASTM D2488 and the samples were then sealed in plastic bags.

Shelby tube sampling was performed in general accordance with ASTM D1587/D1587M. Several Shelby tube samples were collected from both sites. In cases where damage to the Shelby tube sample was considered likely, a pitcher-barrel sampler was used to attempt the sample. A pitcher-

barrel sampler consists of a spring-mounted, 2.5 ft long, thin-walled tube inner barrel with a rotating exterior cutting shoe/barrel. When used in softer materials the spring extends the tip of the thin-walled tube beyond the cutting shoe to collect the sample. In stiffer materials the spring is compressed which results in the cutting shoe leading the thin-walled tube as it is advanced. The recovered tube samples were cleaned at each end, and then sealed with wax in general accordance with ASTM D4220/D4220M.

Once hard material was consistently encountered, the mud-rotary tooling was replaced with H-sized soil/rock coring tools. Coring was accomplished by advancing an outer steel casing with rock carbide or diamond bit, and an inner sample barrel that was locked into the drill string annulus. A triple-tube split inner barrel wireline coring system was used in an effort to enhance core recovery. Once implemented, continuous core runs were conducted at 5 ft intervals. The core samples were collected and visually classified in general accordance with ASTM D2488. The samples were then wrapped in cellophane and placed in polyurethane lined wooden boxes, which were then labeled and prepared for transportation. This procedure was continued until the borehole termination depth was reached. At the termination depth, the borehole was flushed until the geophysical testing was ready to begin logging, at which point the drillers removed tooling and P-S suspension logging commenced.

### **3.2.2. P-S Suspension Logging Method**

The P-S Suspension Logging was performed by GEOVision in general accordance with the procedure outlined in Appendix A. This method is a borehole geophysical method performed by lowering a probe into an open, fluid-filled borehole. The probe measured approximately 25 ft long and included a combined reversible polarity solenoid horizontal shear-wave source and compressional-wave source, which was paired with two biaxial receivers and separated by a flexible isolation cylinder. The receiver pair was centered approximately 12.5 ft above the bottom end of the probe and the receivers were located 1 m apart. The probe was suspended by an armored, multi-conductor cable that was wound about the drum of a winch. The winch was used to meter the cable travel as the probe was lowered into the fluid-filled borehole. The source was triggered after the probe was lowered in 1.5 ft increments.

Pressure waves generated by the source propagated horizontally outward into the fluid surrounding the probe. When the pressure wave impacted the borehole wall, it was converted to compression and shear waves that travel along the length of the borehole wall and convert back to pressure waves near the two biaxial receivers. The system recorded the time it took for the compression and shear waves to reach the two receivers. As the testing was conducted, the operator observed the recorded data and adjusted the gains, filters, delay time, pulse length, and sample rate to improve the quality of the data being recorded.

The recorded data was digitally processed to separate the compression and shear waves using different filtering techniques, such as adjusting the filter frequency and applying Digital Fast Fourier Transform - Inverse Fast Fourier Transform low-pass filtering. The compression and shear

wave velocities were calculated from the distance and time of travel for each waveform from source to receiver 1, and from receiver 1 to receiver 2. These velocities were plotted against the depth of each testing interval.

### **3.2.3. Full Waveform Sonic Logging Method**

The FWS logging was performed by a team from the South Carolina Geological Survey (SCGS), Department of Natural Resources. Similar to the P-S Suspension Logging method, this method was performed by lowering a FWS tool into an open, fluid-filled borehole (Minear 1986). The FWS tool consists of one transmitter and three to four receivers. The transmitter generates source waves and the receivers record four types of waves: compression wave (P-wave), shear wave (s-wave), pseudo Rayleigh wave, and Stoneley wave. In this study, the Mount Sopris 2SAA-1000/FWS probe with two transmitters and three receivers were used to acquire the shear wave data at 0.5 ft intervals with a logging rate of 10 ft/min. During acquisition, the in-coming waveforms from each receiver at every sample interval were recorded for real-time analysis by WellCAD® software. The logging rate and cable tension were constantly monitored to ensure quality control on the incoming signals, alert the operator if there was a problem with the tool, and maintain data quality. Semblance Analysis was used to determine P-wave and shear wave velocity (Kimball et al. 1984). More detailed information about the FWS logging method can be found in Appendix C.

### **3.2.4. Combined Multi-Channel Analysis and Spectral Analysis of Surface Waves (MASW-SASW) Method**

The combined MASW-SASW test was performed by GEOVision. Both MASW and SASW methods were performed utilizing a series of receivers in linear arrays recording data simultaneously during dynamic loading at the surface. The MASW method collects multi-channel seismic data while the SASW method collects surface wave phase data traveling from the source to each receiver. Both methods used a linear array of geophone receivers that were setup to record surface waves traveling from the source to each receiver (e.g. Rix et al. 1991 and Stokoe et al. 1994). Multiple linear arrays incorporating different receiver spacing and locations were used to analyze surface waves of differing wavelengths and frequencies. The Rayleigh and Love waves generated by the sources travel at similar speeds to shear waves and can therefore be used to estimate a representative shear wave velocity for individual layers of soil or rock. Rayleigh waves were measured using a vertical source and an array of vertical receivers, and were representative of vertically polarized shear waves as they traveled through a layered medium. Love waves were measured using a horizontal source and an array of horizontal receivers oriented perpendicular to the orientation of the linear array and were representative of horizontally polarized shear wave as they traveled through a layered medium. Both methods generate dispersion curves and data modeling is performed to obtain the  $V_s$  profile. Depending upon the dispersive nature of the Rayleigh and Love waves traveling along a layered medium, reflecting and refracting off separate layers, each waveform creates small differences in the return time. Electrical impulses were generated as waves passed each receiver location and were stored for each dynamic load session.

Dynamic loads for these techniques typically range from small hammers and sledgehammers to accelerated weight drops and movement of heavy equipment. Resolution of the wave data was heavily dependent on the precision of the array layouts and how well the receivers were coupled to the exposed surface.

In addition to a sledgehammer, a Caterpillar 336F excavator (bucket drop and moving back and forth in place) was used as the energy source to extend the depth of investigation to 200 ft, or greater. Both 1 and 4.5 Hz geophones were used. The MASW data were acquired along three collocated arrays. Two arrays used 48 vertical 4.5 Hz geophones spaced 5 and 10 ft apart, respectively and one array used 9 vertical 1 Hz geophones with variable spacing. The length of the arrays for each site was different and ranged from 230 to 490 ft. Depending on the site, type of energy source, and geophone arrays, the source-receiver offset ranged from 5 to 295 ft. The SASW data were acquired along a single array at each site. For SASW, the 1 Hz vertical geophones were used with several receiver spacings that ranged from 148 to 394 ft the MASW-MAM arrays are shown in Figs. 3.3(a) and 3.4(a) for Site A and Site B, respectively.

The SASW dispersion curves were generated using the software WinSASW V3 and were combined with the MASW dispersion curves generated using the software Seismic Pro Surface V8.0 for both sites. The representative Rayleigh wave dispersion curve was modeled using forward and/or inverse modeling in the software Seisimager to develop several  $V_s$  models corresponding to different receiver spacing. During this process an initial velocity model generated based on soil boring logs and the iterative process of forward or inverse modeling is performed until a  $V_s$  model with low root mean square error (RMS) between the theoretical and experimental dispersion data is developed. More detailed information can be found in Appendix A.

### **3.2.5. Combined Multi-Channel Analysis of Surface Waves (MASW) and Microtremor Array Measurement (MAM) Method**

The combined MASW-MAM method was performed by a team led by Dr. Brady Cox from the University of Texas at Austin. The MASW method was performed using the same procedure as the combined MASW-SASW; however, a sledgehammer was used as the source, different arrays of geophones were used, and the source-receiver offset ranged from 16 to 65 ft from the end of geophone array.

For the MAM method, three-component broadband seismometers were used to record ambient vibrations. The MAM testing at Site A was performed using two roughly-triangular arrays and one circular array as shown in Fig. 3.3(b). Each array utilized ten three-component seismometers, resulting in a maximum array spacing of 164, 984, and 3937 ft for the inner circular array and two outer triangular arrays, respectively. The MAM testing at Site B was performed using three nested circular arrays as shown in Fig. 3.4(b). Ten seismometers were incorporated in the 164 ft and 1492 ft arrays and eight seismometers were in the 1476 ft array.

From the MAM arrays at both sites, all of the data recorded at each seismometer station were computed to generate the representative horizontal to vertical (H/V) spectral ratios curves. The inversion process was performed using a multi-mode approach by matching various combinations of fundamental, first higher, second higher, and other Rayleigh and Love modes to the experimental dispersion data. The inversion was performed using the Software Geopsy by applying the neighborhood algorithm to locate earth models within a pre-defined parameterization that yield the lowest possible misfit values between the theoretical and experimental data. In this study, about 500,000 to 750,000 trial layer earth models for each distinct parameterization was used to obtain a large number of acceptable models controlled by the experimental data and model parameterization. The inverse process resulted in over 100  $V_s$  profiles associated with theoretical dispersion curves from each acceptable inversion parameterization obtained from soil boring logs for both sites. In this study, the median  $V_s$  profiles are obtained and recommended for each site. More detailed information can be found in Appendix B.



**Figure 3.3** Surface Geophysical Testing Locations at Site A: (a) MASW and SASW Testing Arrays, (b) MASW and MAM Testing Arrays

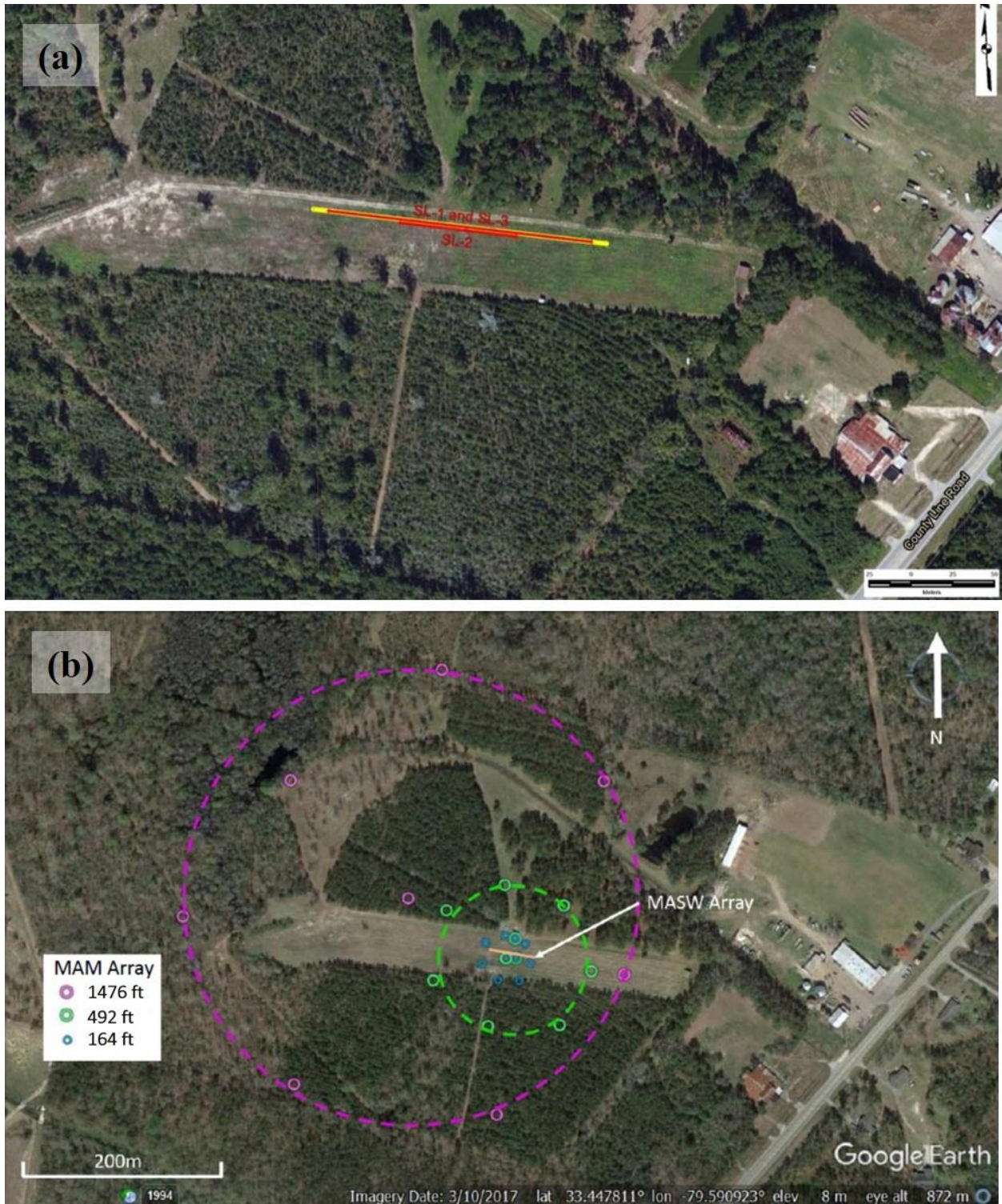


**Figure 3.4** Surface Geophysical Testing Locations at Site B: (a) MASW and SASW Testing Arrays, (b) MASW and MAM Testing Arrays

### 3.3. Laboratory Testing of Soils and Rocks

Following completion of the field investigation, samples were transported in secure containers to the Geotechnical Laboratory at the University of South Carolina. A summary of the laboratory testing is presented in Table 3.1. Testing methods are described as follows.

**Table 3.1** A Summary of Laboratory Testing of Soil and Rock Samples

Analysis	Standard Method	Parameter	Number of Tests
<i>Identification</i>			
Description and Identification of Soils (Visual-Manual Procedure)	ASTM D2488	Angularity, shape, color, moisture condition, consistency, etc	221
Classification of Soils for Engineering Purposes			
AASHTO	AASHTO M 145-87	Soil Type	221
Unified Soil Classification System (USCS)	ASTM D3282 ASTM D2487		
<i>Index Properties</i>			
Moisture Content of Soil and Rock	ASTM D 2216	$w_n$	223
Liquid Limit, Plastic Limit, and Plasticity Index of Soils	ASTM D 4318	LL, PL, PI	191
Grain Size Analysis (Sieve Analysis)	ASTM D 422 ASTM D 6913	$C_u, C_c, D_{10}, D_{50}, \%$ fines	221
Wash Sieving	ASTM D 1140-17		
Specific Gravity (rock samples only)	ASTM C 127-88 AASHTO T 85-91	$G_s$	15
<i>Dynamic Soil and Rock Properties</i>			
Resonant Column Test	ASTM D 4015	G,D	35
Torsional Shear Test	n/a	G,D	21

### **3.3.1. Geological Logging**

Geological logging of the core samples was performed by Mr. Joe Gellici, professional geologist from the South Carolina Geological Survey, Department of Natural Resources. A detailed description of the core samples can be found in Appendix D. The results were correlated with geophysical logs (gamma-ray logs), visual observation of core samples, and formations determined at other core holes in the same area in an attempt to determine the geological formation associated with each of the core samples.

### **3.3.2. Soil Classification and Index Property Measurements**

Each sample was visually classified and measurements of index properties were performed in the Geotechnical Laboratory at the University of South Carolina according to the ASTM standards provided in Table 3.1. The USCS symbols and index properties were used to update the geotechnical boring logs provided by S&ME.

### **3.3.3. Small Strain Dynamic Properties Measurements**

Following completion of the field sample collection, selected core samples were carefully wrapped and sealed to preserve the moisture content and then stored prior to laboratory testing. The samples obtained from the Shelby tube and core samplers were tested for dynamic soil properties using the resonant column (RC) method according to ASTM D4015 and the torsional shear (TS) method. An ASTM standard for the TS test does not exist currently, but this test method is well established (e.g., Kim 1991 and Sasanakul 2005). Both RC and TS methods are the most widely used methods to evaluate modulus reduction ( $G/G_{\max}$ ;  $G_{\max}$  is low-strain shear modulus) and damping over a range of strains for soils. These tests require highly specialized skills and experience. A more detailed description of the sample preparation and RC/TS testing procedure can be found in Appendix F.

A Stokoe-type RC/TS apparatus located in the Geotechnical Laboratory at the University of South Carolina was used in this project. This type of apparatus has been used world-wide for dynamic testing of soils for research and commercial purposes. The equipment can operate both RC and TS testing (e.g., Isenhower 1979, Lodde 1982, Ni 1987, Hwang 1997, and Darendeli 2001). The equipment is the fixed-free type, where the soil specimen is fixed in place at the bottom and the driving force is applied at the top. The general principle employed in the RC test is to excite the soil specimen with a steady-state torsional motion over a range of frequencies to identify the first mode resonant frequency. The shear modulus can then be evaluated utilizing the well-defined boundary conditions and the specimen geometry and mass. Material damping is determined by the half power bandwidth or free vibration decay method. The difference between the TS test and the RC test is mainly in the excitation frequency. In the TS test, a slow cyclic loading in the range of 0.01 to 10 Hz is applied to the specimen. In this project, the TS test was performed at a frequency of 0.5 Hz. Shear modulus and damping were determined based on the characteristic of the hysteresis loop. The drive system and equipment damping for this apparatus were calibrated

according to Sasanakul and Bay (2008, 2010). In the RC test, the first mode resonant frequency is used for the analysis. For this study, the resonant frequency ranged from 10 to 150 Hz for soil samples and 400 to 600 Hz for rock samples.

It is extremely important to handle undisturbed soil samples with care as sample disturbance can have a significant effect on testing results. Each soil sample was carefully cut from the tube. First, each end of the selected portion of the tube was cut using a tube cutter. Next, the side of each tube was cut vertically using a band saw. In most cases, the tube springs opened after cutting, and the soil sample was removed. When the tube did not spring open, the opposite side of the tube was cut to remove soil with minimal disturbance. In addition to the undisturbed soil samples, three additional sand samples taken from the Shelby tube samples were prepared by reconstitution. The sample preparation was conducted by dry pluviation in layers to achieve the field unit weight estimated based on weight and volume relationships of soil in a given section of the Shelby tube sample. Due to a limited number of Shelby tube samples, soil samples from the core sampler were also used for RC and TS testing. Soil specimens were carefully hand-trimmed to a diameter of approximately 1.4 inches and a height of about 3.0 inches using a trimming device and wire saw. Water content and index properties were determined using the trimmings.

Intact rock samples were carefully selected from the core samples. Specific gravity of each rock specimen was measured according to ASTM C127-88 and AASHTO T85-91 prior to testing. The rock sample preparation method is similar to Tuff (i.e., igneous rock sample) preparation done by Jeon (2008). For this study, the typical diameter of the specimens was approximately 2.4 inches and the sample was not re-cored. Each specimen was cut to a specified length in order to achieve the diameter to length ratio of approximately 1:2. The top and bottom of each specimen was trimmed using rotary grinding and sandpaper to create a smooth and flat surface. The specimen was attached to the top and bottom pedestals of the testing device using epoxy glue that was allowed to cure for approximately 24 to 48 hours. Due to the torque limitation of the equipment, only the RC test was performed on the rock specimens.

In this study, each soil specimen was tested with at least three confining pressures of  $0.5\sigma'_{mo}$ ,  $\sigma'_{mo}$ , and  $2\sigma'_{mo}$ , where  $\sigma'_{mo}$  is the mean in-situ confining stress. Due to the maximum safe confining pressure achievable in the laboratory of approximately 150 psi, the maximum confining pressures for deep samples were at  $\sigma'_{mo}$  and the other two confining pressures were at  $0.5\sigma'_{mo}$  and  $0.25\sigma'_{mo}$ . Each rock sample was tested with no confinement and at least two additional confinements of  $0.25\sigma'_{mo}$ ,  $0.5\sigma'_{mo}$ , and/or  $\sigma'_{mo}$ . It was noted that effect of confinement on dynamic properties of rock was minimal as discussed in Sections 4.4.2 and 4.4.3.

## 4. Results and Analysis

---

This project generated a large set of data from a field and laboratory investigation of two sites in the South Carolina Coastal Plain. All of the data and detailed analysis can be found in the appendices. This chapter summarizes key findings and observations from the field and laboratory investigation that are useful for engineering design and future SCDOT studies.

### 4.1. General Observation of Geotechnical Borehole Drilling

For Site A, three boreholes were drilled during a 19-day period, from 1/18/2017 to 2/5/2017. The original plan was to drill to a target depth of 515 ft. The presence of thick sand layers, particularly at depths below 272 ft, caused drilling difficulties during when completing the first borehole. In addition, a significant amount of borehole fluid circulation was lost when advancing below 505 ft and as a result, the borehole became unstable and had to be terminated at 505 ft, 10 feet from the target borehole depth. The P-S logging was only performed between the depths of 300 and 470 ft while the drilling casing/core rod was left in place at the upper 300 ft to maintain the open borehole in the unstable thick sand layers. The FWS logging was not performed at this site due to the instability of the borehole. To allow additional data collection, two additional boreholes were drilled at this site. A second borehole was successfully drilled to the same 505 ft depth as the first borehole utilizing PVC casing to stabilize the hole which allowed additional P-S logging to be performed from the surface to a depth of 300 ft. The P-S logging data of the second borehole was analyzed and combined with the data from the first borehole. The third borehole was drilled to a depth of 300 ft and data from the first borehole was used to select additional Shelby tube sample locations in soil zones.

For Site B, two boreholes were drilled during a 32-day period, from 2/6/2017 to 3/9/2017. The first borehole was drilled to the target depth of 615 ft as planned. The P-S logging and FWS logging were performed at this borehole to a depth of 600 ft. A second borehole was drilled to a depth of 150 ft and data from the first borehole was used to select Shelby tube sample locations in soil zones.

### 4.2. Geotechnical and Geological Description of Soil Profiles

Results from geotechnical and geological logging are summarized in Fig. 4.1 for Site A and Fig. 4.2 for Site B. An overview description of each soil profile is presented below.

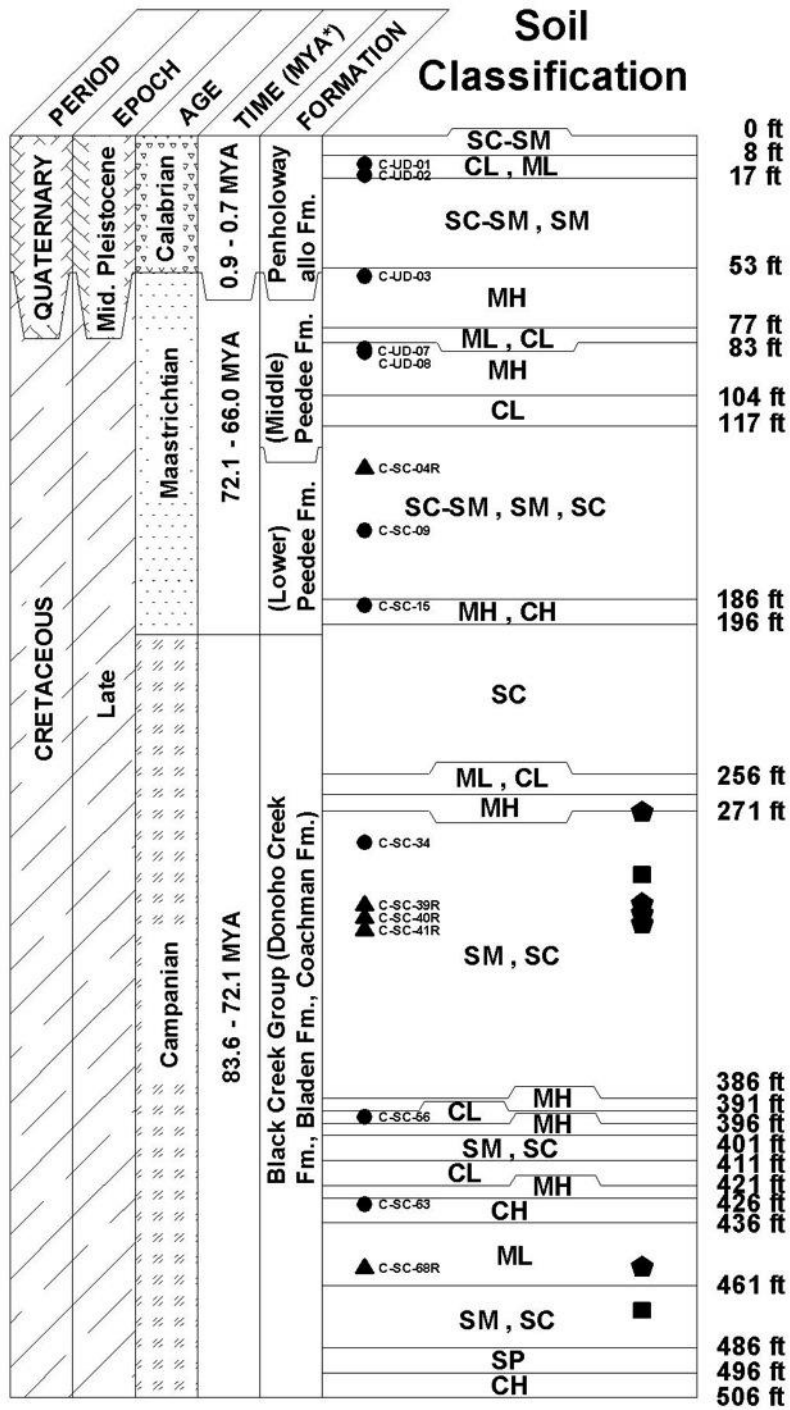
Site A consisted of soil deposits from Quaternary and Cretaceous periods. Younger material from Quaternary deposits, located in the top 53 ft, are Penholoway alloformation. Because this formation has not been used since the early 1980, it is considered informally as an alloformation (Doar 2018). The deposits consisted of silty and clayey sands interbedded with a relatively thin layer of low plasticity clay and silt. Cretaceous deposits consist of Peedee formation located between 53-196 ft and Black Creek group formation and possible Donoho Creek, Bladen, and Coachman formations located below 196 ft. The deposits were composed of a variety of materials, with clayey sand and silt layers appearing to be dominant. These layers were interbedded with layers of low to high plasticity clay and silt with thicknesses ranging from 1 to 2 ft. Relatively thin

rock layers consisting mainly of sandstone or calcareous sand with thicknesses of less than 3 ft were intermittently observed within these layers. Approximately 16-26 ft thick sandstone and limestone layers interbedded with thin clayey sand layers were found at depths between 300-345 ft, and additional sandstone/limestone layers at depths of 450-460 ft. As discussed previously, drilling difficulties were encountered because of sand layers at depths below 272 ft. Below these unstable layers, at depths between 387-461 ft, silty and clayey soils with wide range of plasticity were observed. These layers were underlain by relatively thick silty and clayey sand layers which again caused drilling difficulties. These sands were very fine to medium loose.

Site B consisted of Quaternary, Tertiary and Cretaceous periods. Quaternary deposits located in the top 11 ft are Ten Mile Hill formation. The deposits consist of silty and clayey sand. Below the Quaternary deposits are Tertiary and Cretaceous deposits. The boundary between Tertiary and Cretaceous occurred at a depth of 228 ft below the ground surface. There were two formations including Williamsburg and Rhems formations in the Tertiary section. The shelly limestone layers were found at a depth between 19-48 ft. The soil layers directly below the limestone/sandstone at 43-262 ft were mainly sandy soils with weak to strong cementation. Two additional layers of limestone/sandstone at depths of 115 and 197 ft were observed in the Tertiary deposit interbedded with layers of low and high plastic clayey and silty soils. The level of cementation of these materials was highly variable. At a depth of 230 ft, the Cretaceous deposits from Peedee, Donoho Creek, and Bladen formations consisted of mostly cemented clayey and silty soils interbedded with layers of sand. The thickest sand layer was greater than 30 ft thick and found at a depth of 508 ft. Shell fragments were also observed within these sand layers.

Based on the visual observation and geological classification for both sites, a layer of competent rock was not encountered at the depths investigated.

# Site A: B-CON (Conway)



\* Estimated age in millions of years; MYA = million years ago  
 ● soil sample: UD-undisturbed, SC-core sample  
 ▲ rock sample    ◆ sandstone    ■ limestone

Figure 4.1 Soil Classification and Geological Information for Site A

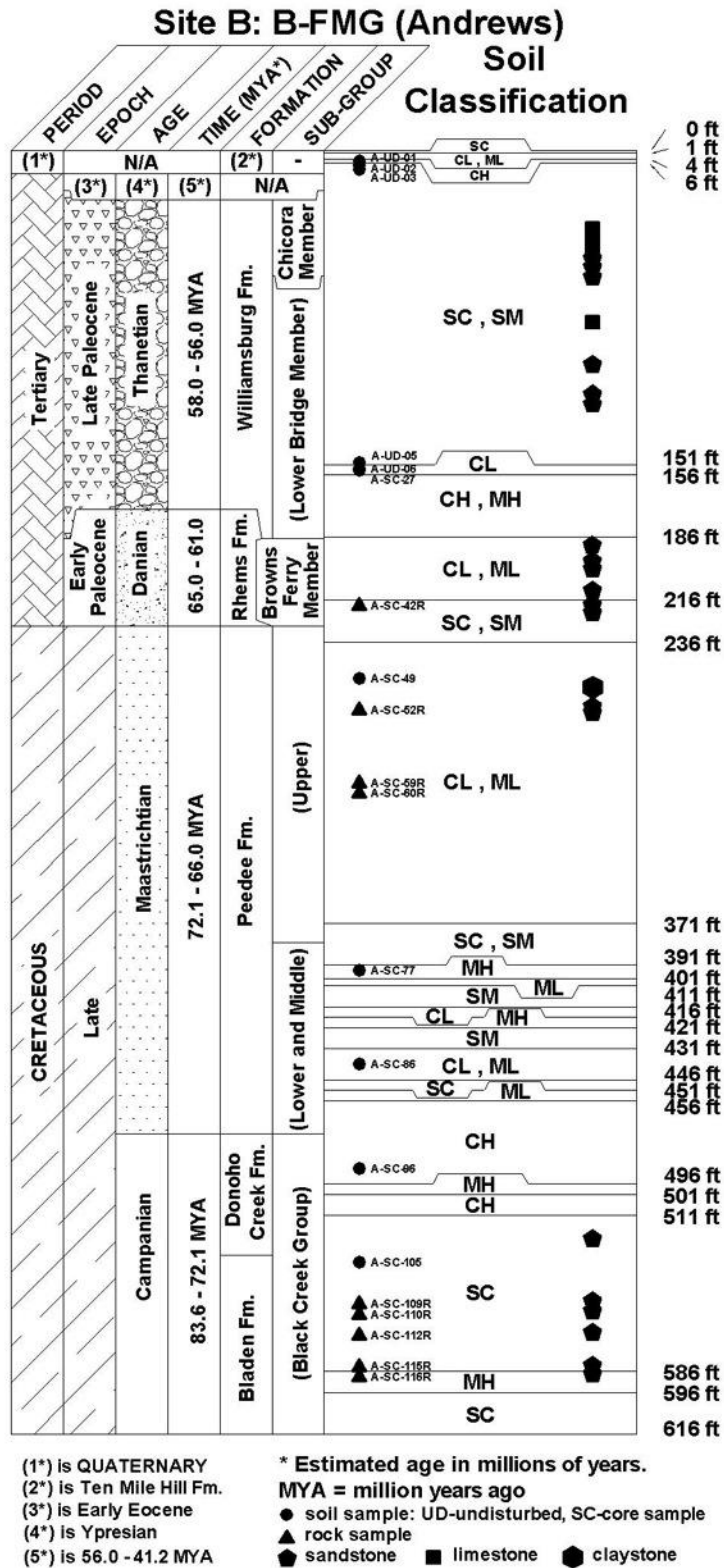


**Figure 4.2** Soil Classification and Geological Information for Site B

### **4.3. Field Measurements of Shear Wave Velocity Profiles**

In this study, the  $V_s$  profiles were obtained from the borehole P-S suspension logging, FWS logging, combined MASW-SASW, and combined MASW-MAM methods. As described previously, the P-S logging was performed from the ground surface to a depth near the bottom of the boreholes. The FWS logging was performed in a similar manner to the P-S logging but could only be completed at Site B. Thus, the borehole methods provided  $V_s$  profiles to a depth of 470 ft for Site A and a depth of 600 ft for Site B. The MASW-SASW tests generated  $V_s$  profiles down to a depth of approximately 220 ft for both sites. The combined MASW-MAM generated profiles down to depths of 4921 ft for Site A and 2625 ft for Site B. This method can generate deeper profiles than other surface wave methods because unlike the typical MASW and SASW which use an active energy source, the MAM method uses passive ambient noise as the wave source and a large array spacing (over 3000 ft) as described previously. This method can produce experimental dispersion curves over a wide frequency range (longer wavelength) resulting in very deep  $V_s$  profile models. More detailed analyses of the MASW-MAM method for this study can be found in section 4.3.1 and Appendix B.

#### **4.3.1. Summary of Surface Wave Data Analyses**

This section includes a summary of surface wave data analyses from the combined MASW-SASW and MASW-MAM methods. Both methods are not commonly performed in SC. In fact, the MASW-MAM method was used for the first time in this study to characterize a deep  $V_s$  profile. It is important to understand that these surface wave methods are not direct measurements of shear wave velocity and the results rely heavily on knowledge and experience of the data analyst. The data analyses presented in this section were conducted by experts in the field and approaches require expert analysis and experience and therefore are not used as part of routine wave velocity profile collection. More detailed information can be found in Appendices A and B.

##### ***4.3.1.1. MASW-SASW Data Analysis and Results***

As mentioned in Section 3.2.4, both MASW and SASW methods generate dispersion curves. These curves were combined as shown in Fig. 4.3(a) and Fig. 4.4(a) for Site A and Site B, respectively. For Site A, there appears to be two phase velocity trends in the data: a higher velocity trend that appears dominant over a wide frequency range (longer wavelength) and a lower velocity trend that occurs over a narrower frequency range (shorter wavelength). For Site B, the Rayleigh wave propagation is very complex with dominant higher mode Rayleigh wave energy at frequencies between 10 and 20 to 25 Hz and no evidence of the fundamental mode Rayleigh wave over this frequency range. This type of dispersion curve signature indicates that there is a shallow high velocity layer at the site.

For Site A, the representative dispersion curve shown in Fig. 4.3(a) was modeled using inverse modeling with the effective modeling solution in the software Seisimager to develop several  $V_s$  models corresponding to different receiver spacing. An example of a selected  $V_s$  model for Site A

is shown in Fig. 4.3(b). The effective mode solution was necessary for inverse modeling the dominant higher mode Rayleigh wave energy at high frequencies associated with a higher velocity (stiff) surface layer and a smooth transition from the fundamental to the first higher mode at low frequencies associated with an abrupt increase in  $V_s$  at depth. The  $V_s$  models developed from effective mode inversion of the Rayleigh wave dispersion curves corresponding to 246 ft (75 m) SASW receiver spacing is recommended by GeoVision (see Appendix A), as it is the most representative of the average  $V_s$  profile for Site A as shown in Fig. 4.3(b).

For Site B, the representative dispersion curve shown in in Fig. 4.4(a) was modeled using the forward modeling with a multi-mode solution (mode with highest relative energy) in the software Seismager, and effective mode modeling solution (3D global solution) in the software WinSASW V3 to develop the  $V_s$  models shown in Fig. 4.4(b). The shallow high velocity layer presented at this site was modeled with variable  $V_s$  and thickness. The best representative  $V_s$  profile was selected based on the best fit data at the higher mode energy between 10 to 15 Hz. Two profiles generated from the multi-mode model and the effective mode model were very close with a difference of 6% for the average  $V_s$  at the top 100 ft as shown in Fig. 4.4(b).

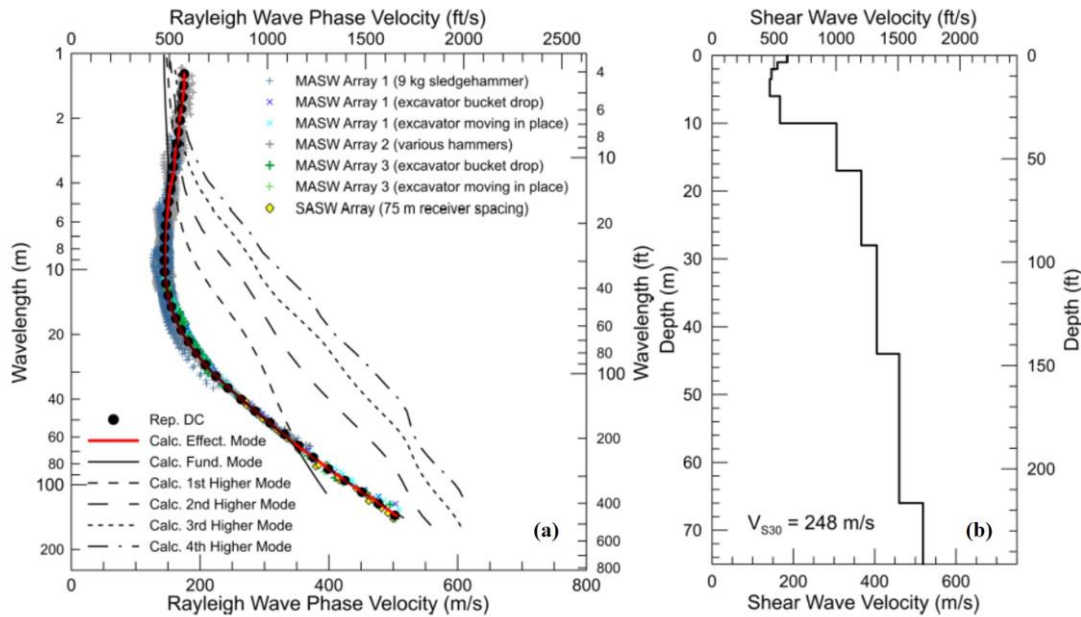


**Figure 4.3** Inversion Results for Site A from MASW-SASW Method: (a) Dispersion Curves, and (b) Selected  $V_s$  Model

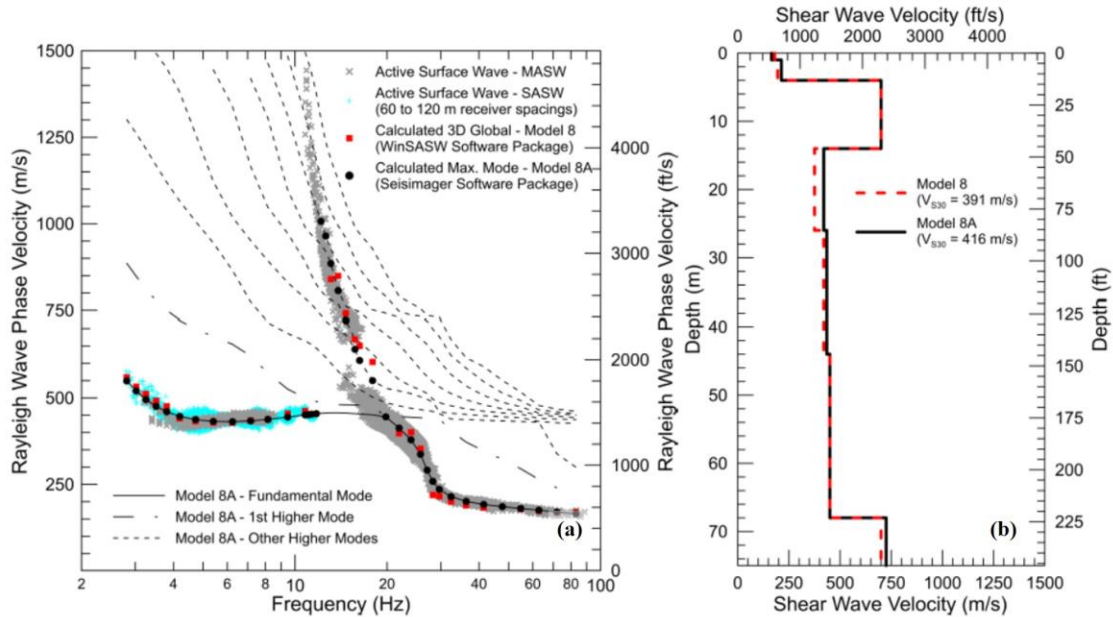


**Figure 4.4** Inversion Results for Site B from MASW-SASW Method: (a) Dispersion Curves, and (b) Selected  $V_s$  Models

#### 4.3.1.2. MASW-MAM Data Analyses and Results

In addition to the dispersion curves shown in Figs. 4.5(a) and 4.6(a), the horizontal to vertical (H/V) spectral ratio curves were generated by the combined MASW-MAM method (see Section 3.2.5) for Site A and Site B as shown in Fig. 4.5(b) and Fig. 4.6(b), respectively. The H/V curves represents the fundamental site frequency and based on Figs 4.5(b) and 4.6(b) a consistency of low-frequency peak is shown suggesting that the fundamental site frequency is relatively uniform across the footprint of the MAM arrays. Typically, the frequency corresponding to a well-defined peak can be used to estimate the fundamental shear wave resonant frequency of the site and/or the lowest-frequency peak of the fundamental mode Rayleigh wave ellipticity (Lermo and Chavez-Garcia 1993, Lachet and Bard 1994, SESAME 2004). However, there were a few other peaks observed and these peaks are believed to be indicative of shallow velocity impedance contrasts. When a more moderate impedance contrast is present, the frequency corresponding to the peak may be more representative of the fundamental site frequency (Bonney 2004). The higher frequency peak is visually variable in its peak location, width, and amplitude across the extent of the arrays. This indicates that the depth and stiffness of a shallow velocity contrast is spatially variable across the sites.

The inversion process was performed as described in Section 3.2.5. The median  $V_s$  profiles obtained from each site are shown in Figs. 4.5(c) and (d) for Site A and Figs. 4.6(c) and (d) for Site B. The median  $V_s$  profile obtained from an inversion parameterization of 2.0a was recommended by the UT Austin (see Appendix B) to be a representative  $V_s$  profile for each site.

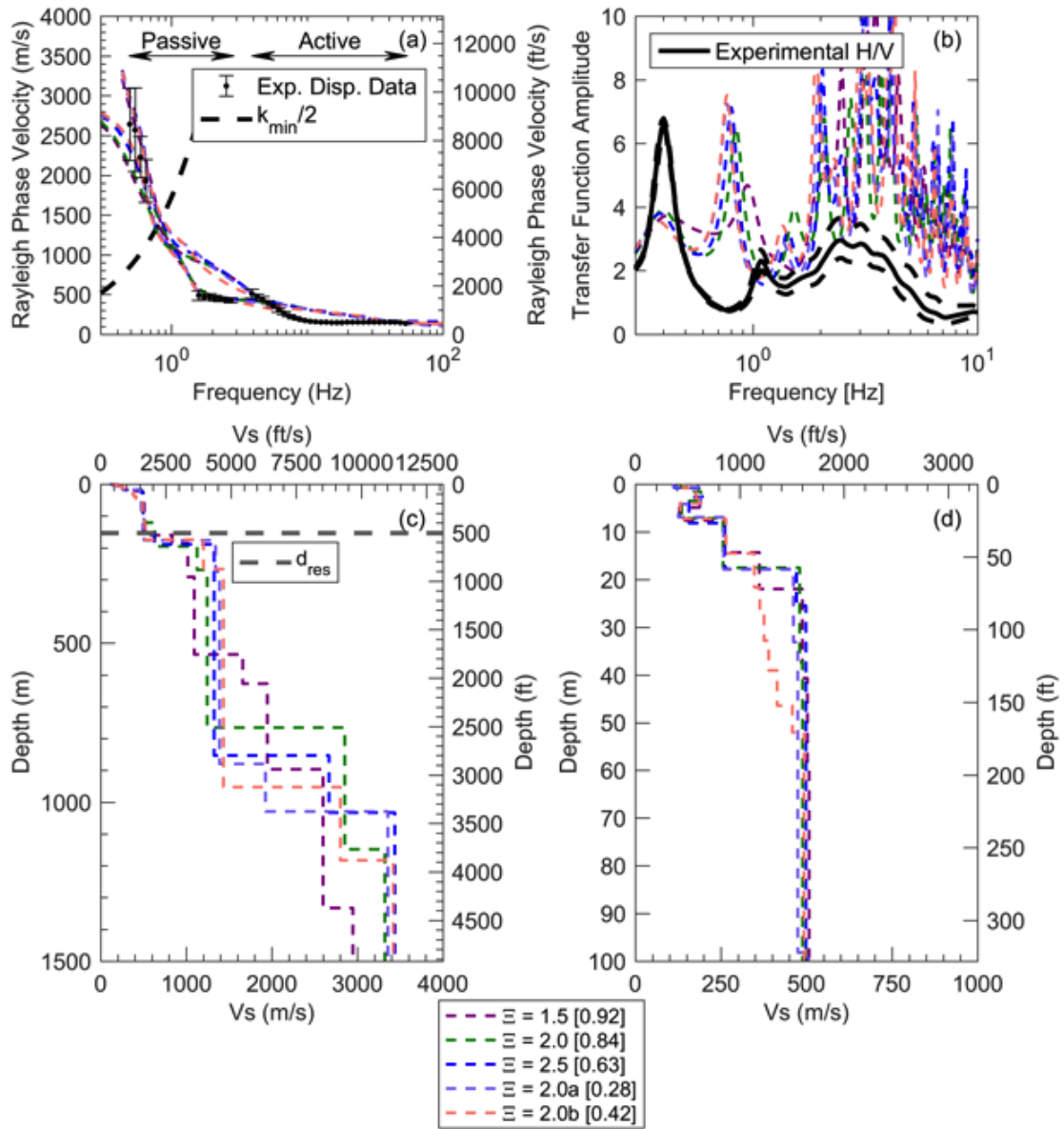


**Figure 4.5** Median Inversion Results for Site A from MASW-MAM Method Shown for Each Inversion Parameterization (i.e., layering ratios  $\chi = 1.5, 2.0, 2.5, 2.0a,$  and  $2.0b$ ): (a) Dispersion Curves, (b) H/V Curves, (c)  $V_s$  Profiles Shown to a Depth of 4900 ft, and (d)  $V_s$  Profiles Shown to a Depth of 328 ft

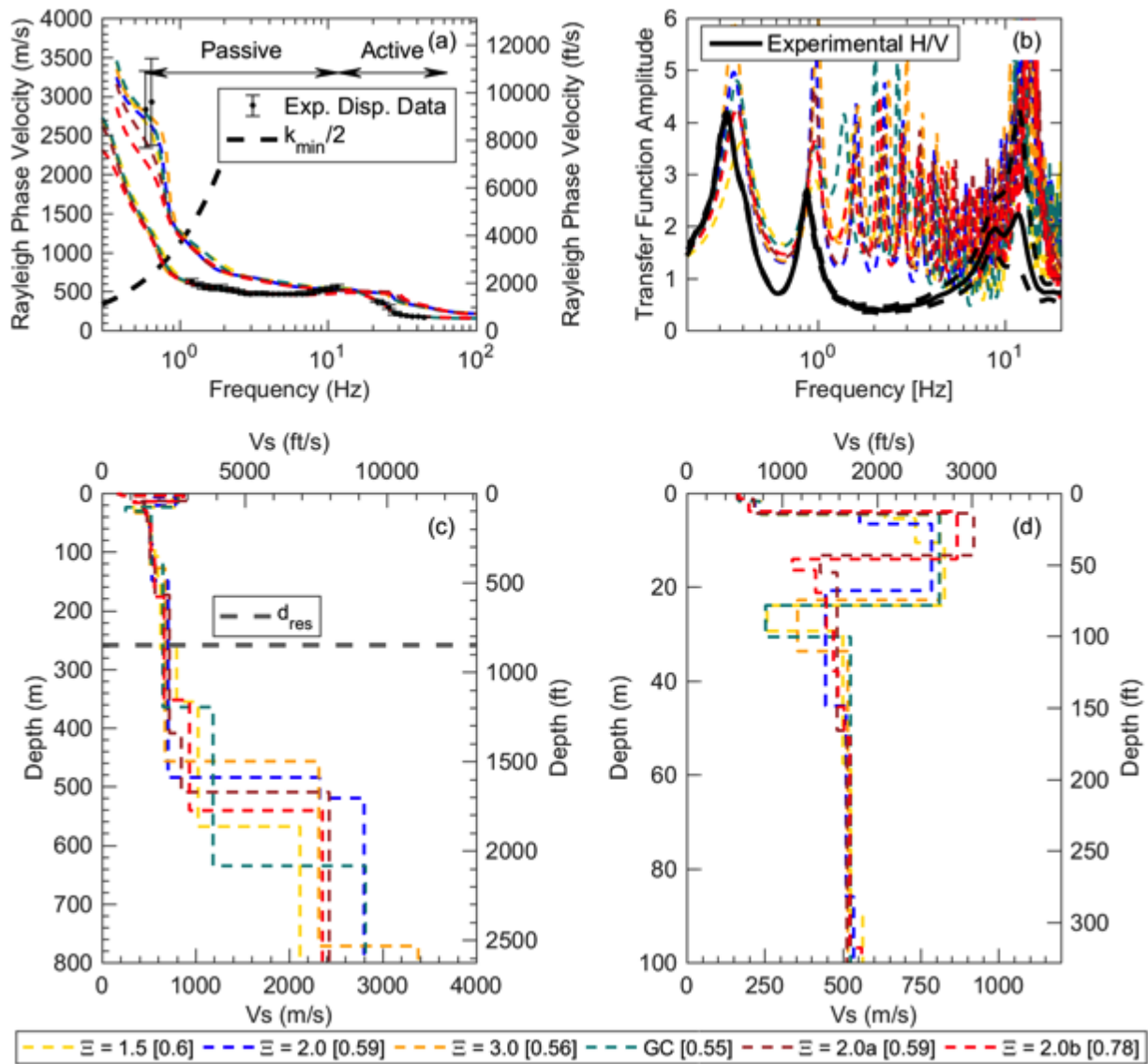


**Figure 4.6** Median Inversion Results for Site B from MASW-MAM Method Shown for Each Inversion Parameterization: (a) Dispersion Curves, (b) H/V Curves, (c)  $V_s$  Profiles Shown to a Depth of 2625 ft, and (d)  $V_s$  profiles Shown to a Depth of 328 ft

### 4.3.2. Comparison of $V_s$ Profiles for Site A

Fig. 4.7 presents the  $V_s$  profiles found from P-S logging, MASW-MAM and MASW-SASW methods for Site A. For comparison purposes, profiles are shown to depths of 800 ft and 300 ft in Fig. 4.7(a) and 4.7(b), respectively. These depths are chosen to provide overall observation of the B-C boundary provided by the MASW-MAM method and allow more detailed comparisons between different geophysical methods at shallower depths. It was noted that several  $V_s$  profiles were generated from both surface geophysical methods during the inversion process of the data analyses as mentioned in Section 4.3.1. The profiles were selected based on the subcontractors'

recommendations based on data quality, boring logs, and geological information at the site. Additional  $V_s$  profiles and more detailed data analysis and interpretation can be found in Appendices A, B, and C. The P-S logging method measured the  $V_s$  profile with a resolution of 1.5 ft, therefore soil layers with thickness greater than 1.5 ft and the variation of  $V_s$  in very stiff and/or cemented soil layers as well as rock layers are captured by the P-S logging method.

For Site A, approximately seven to ten different layers were obtained from the MASW-SASW and the combined MASW-MAM methods based on the surface wave data interpretation. The  $V_s$  generally increased as the depth increases. For both methods, the  $V_s$  ranged from 490-985 ft/s for the Quaternary deposit (Penholoway alloformation) and from 985-1640 ft/s for the Cretaceous deposit (Peedee, Donoho Creek, Bladen, and Coachman formations) below 53 ft. There was no clear separation indicating difference in the  $V_s$  profile for each formation. Some discrepancies between the borehole and surface geophysical methods were observed; however, in general, the  $V_s$  for the younger Quaternary deposits were lower than the older Cretaceous deposits. The lower values of  $V_s$  were likely related to the lower confinement at the shallower depths.

At depths between 374-482 ft, the  $V_s$  ranged from approximately 2,600 to 3,280 ft/s and the core samples from these layers were described visually in the geologic log as alternating layers of loose and hard beds caused by carbonate cementation. These materials are calcareous clayey sand with strong reaction with hydrogen chloride (HCl). There were some trace of shell fragments and muscovite throughout the core. The USCS classifications of these materials are SC and SM.

At depths between 150-295 ft, similar calcareous clayey or silty sand was also found, but the core samples were relatively loose and more friable. The reaction to HCl was weak to moderate indicating less carbonate cementation. This observation is consistent with the lower  $V_s$  values measured for this material, ranging from 1312-1967 ft/s. There were a few thin layers of strong carbonate cemented sand that are consistent with the spikes in the  $V_s$  profile within these depths.

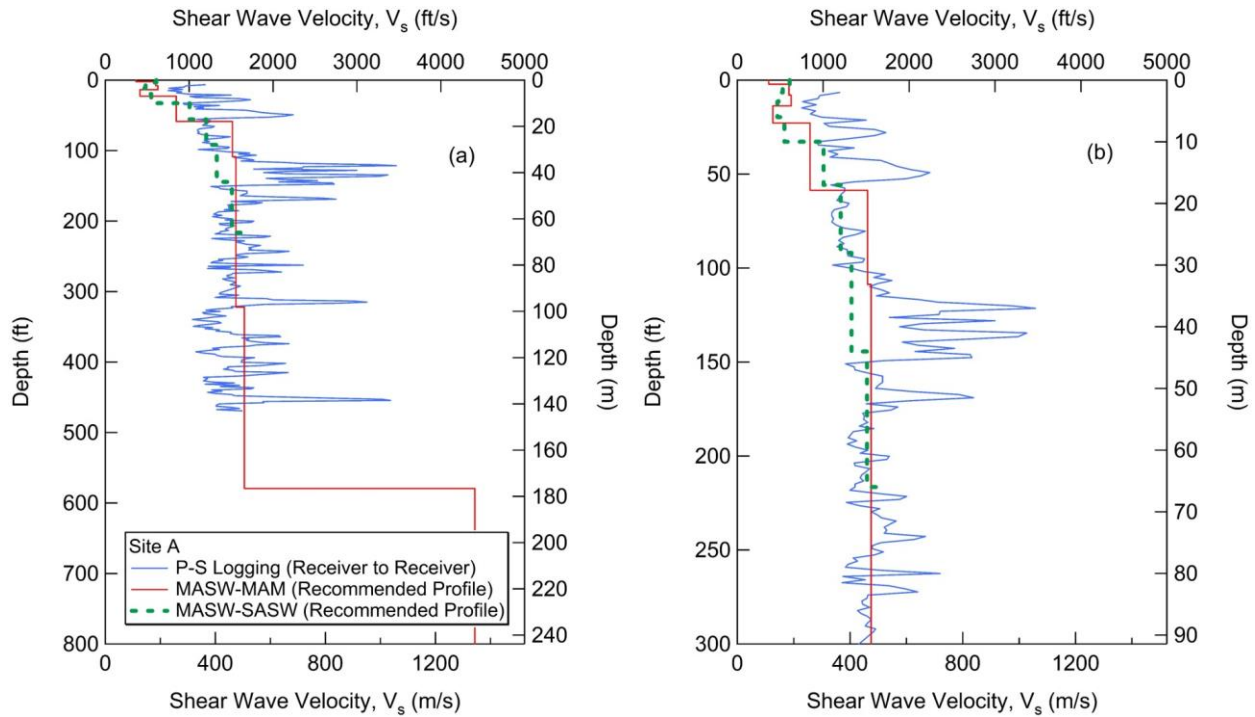


**Figure 4.7**  $V_s$  Profiles for Site A: (a) Shown to a Depth of 800 ft, and (b) Shown to a Depth of 300 ft

At depths between 296-505 ft, two sharp spikes for  $V_s$  of 2953-3280 ft/s at a depth of 315 ft and 456 ft were consistent with sandstone samples described as shelly sandstone. This material appeared to be phosphatic grains tightly cemented with carbonate and had very strong reaction with HCl. Drilling difficulties were encountered at this depth range (300-505 ft) and half of the attempts to collect core samples failed. In addition to the shelly sandstone, the collected samples were mostly classified as loose fine to medium sand with a small percentage of clay, and reaction to HCl was none to weak. These materials were interbedded with a few thin layers of low to high plasticity clay and silt, cemented clay, and sandstone. The  $V_s$  values, with the exception of the sandstone layer, are between 1050-2165 ft/s. The lower  $V_s$  values are consistent with loose, relatively weak cemented sands and the higher values were consistent with cemented clay. Photographs of calcareous sand/sandstone from Site A are shown in Fig. 4.9. Even though the  $V_s$  values for these materials are over 2300 ft/s, they were only found sporadically throughout the borehole depth. As a result, the top of soft rock layer with consistent  $V_s$  of 2300 ft/s or higher was not reached and was located at a deeper depth. The MASW-MAM method suggests that the stiff layer with a very high  $V_s$  of over 4000 ft/s may be located at a depth below 580 ft.

A comparison between SPT N-values and  $V_s$  in the top 120 ft is shown in Fig. 4.8. The SPT-N values with depth are plotted in Fig. 4.8(a) and the  $V_s$  profiles found from the P-S, MASW-MAM and MASW-SASW methods are plotted with depth in Fig. 4.8(b). In addition, the  $V_s$  values found using the  $V_s$ -SPT correlations of Andrus et al. (2009) for sand and Seed and Idriss (1981) for all soils are plotted in Fig. 4.8(b). The results found using the Andrus et al. (2009) and Seed and

Idriss (1981) correlations matched reasonably well with the results from MASW-SASW and MASW-MAM methods at shallow depths (<30 ft) (the Andrus et al. (2009) correlation has a better match). The  $V_s$  profiles from the SPT correlation using Andrus et al. (2009) approach are lower than Seed and Idriss (1981) approach, particularly at deeper depths. The top 50 ft of the  $V_s$  profile from the P-S logging method was much higher than other methods.

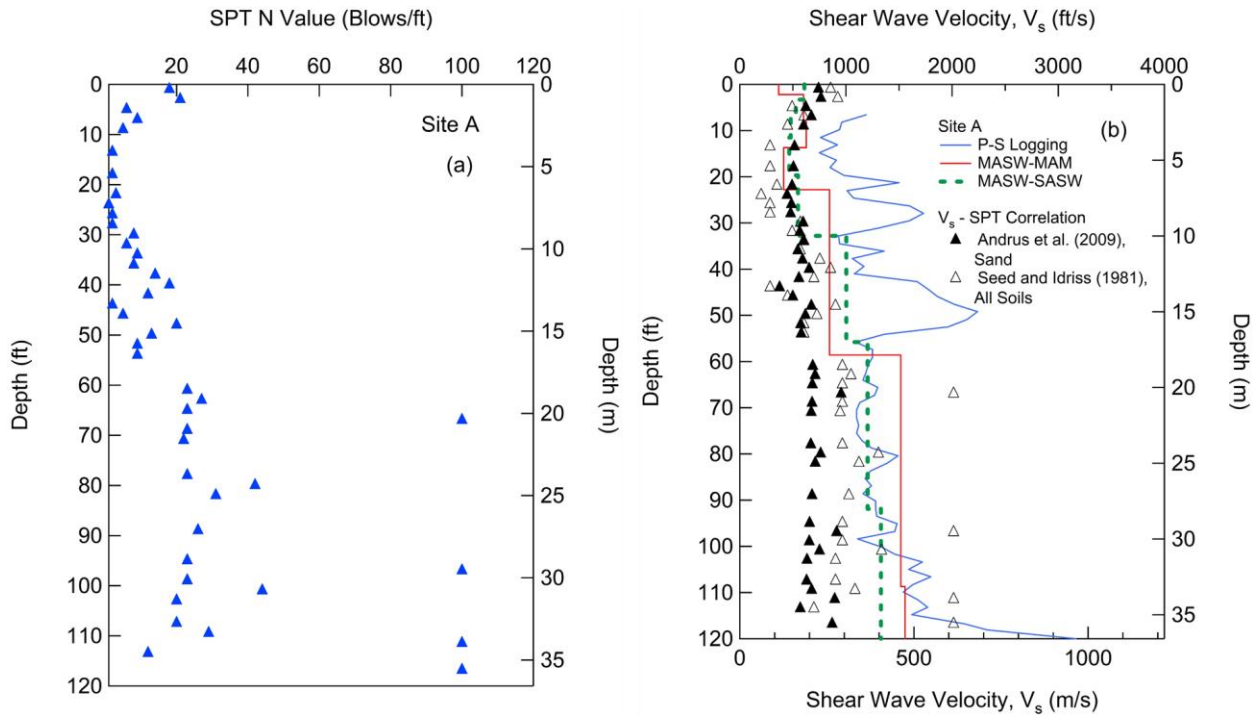


**Figure 4.8** (a) Variation of SPT N Value with Depth, and (b) Comparison between  $V_s$  Profiles between the  $V_s$ -SPT Correlation and Results from Geophysical Methods for Site A

The average  $V_s$  in the top 100 ft and 200 ft of the profile obtained from the three different testing methods are presented in Table 4.1. Results from the P-S logging show higher average values of  $V_s$  than that of the other two methods resulting in a different NEHRP site class. There are a few possible explanations for this discrepancy. The surface methods (MASW-SASW and MASW-MAM methods) characterize the average  $V_s$  based on wave propagation characteristics through a large volume of soil/rock and the profiles typically consist of a limited number of representative layers. Conversely, the P-S logging method can be used to characterize the average  $V_s$  of the localized soil/rock properties within the tested borehole, thus the profiles provide high level of details with higher resolution. It is possible that the depth and stiffness of cemented or soft rock layers is spatially variable across the site causing a large discrepancy between local and global  $V_s$  profiles. The other explanation could be related the problem with borehole drilling at Site A. The P-S logging data at depth below 300 ft was obtained from the uncased borehole. While the P-S logging data at the top 300 ft was obtained from the offset cased hole about approximately 1 month

after the first set of data was collected. The actual reason remains unknown but it is also important to note that the average  $V_s$  for the P-S logging method did not include data from the top 6 ft. In addition, Table 4.1 shows that the B-C boundary was not reached based on the  $V_s$  profiles from the P-S logging and SASW methods. The combined MASW-MAM provides a possible B-C boundary at a depth of 580 ft.

**Table 4.1** Summary of Average Shear Wave Velocities and Possible B-C Boundary for Site A

Method	100 ft		200 ft		B-C Boundary (ft)
	Average $V_s$ (ft/s)	NEHRP Site Class	Average $V_s$ (ft/s)	NEHRP Site Class	
P-S logging	1225	C	1464	C	N/A
MASW-SASW	817	D	1039	D	N/A
MASW-MAM	860	D	1106	D	580

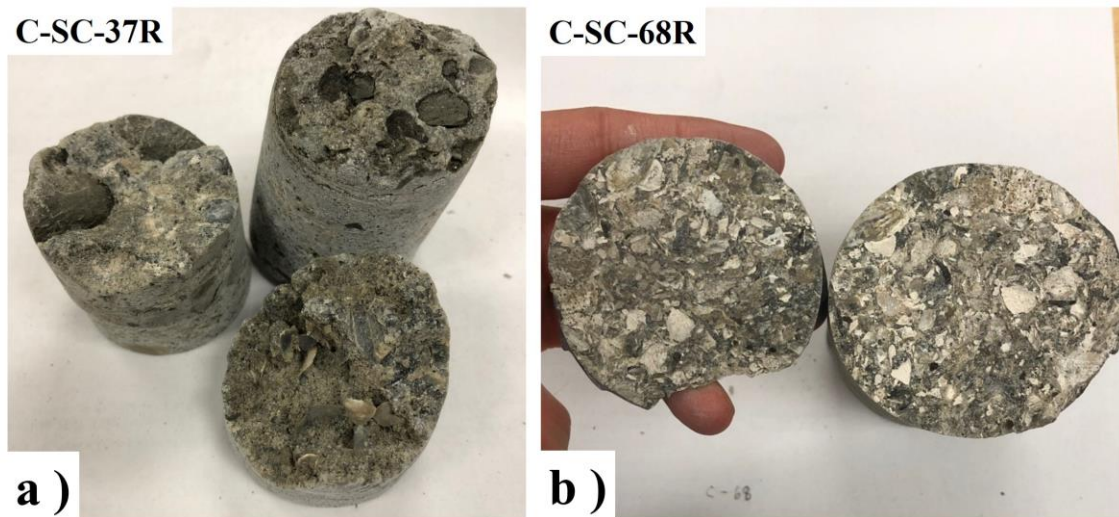


**Figure 4.9** Calcareous Sand/Sandstone Samples from Site A at Depths: (a) 194-200 ft, and (b) 450-456 ft

#### 4.3.3. Comparison of $V_s$ Profiles for Site B

Fig. 4.10 presents the  $V_s$  profiles found from P-S logging, MASW-MAM, MASW-SASW, and FWS methods for Site B. For comparison purposes, profiles are shown to depths of 1800 ft and 300 ft in Fig. 4.10(a) and 4.10(b), respectively. For Site B, the MASW-SASW and the MASW-MAM methods suggested  $V_s$  profiles with six to eight layers of soil. The  $V_s$  slightly increased as the depth increased, with the exception of the layer between 13 to 43 ft. Overall, the  $V_s$  profiles from the MASW-SASW and MASW-MAM methods were similar, but the MASW-MAM provided slightly higher  $V_s$  values. The MASW-MAM method provided the  $V_s$  profile down to a

depth of 1343 ft; whereas, the MASW-SASW provided to a depth of 220 ft.

Similar to the results from Site A, the  $V_s$  profile obtained from the P-S logging method was more sensitive to layering than the two surface methods. The presence of limestone layers at shallow depths (20-43 ft) resulted in a  $V_s$  that is much higher (3280-5250 ft/s). Based on the visual classification, the limestone as shown in Fig. 4.11(a) was described as shelly limestone (biomicrite) with highly variable carbonate cementation. Some zones were well-indurated and cemented with a fine-grained carbonate cementation, other zones were friable where bivalves fragments occurred in a soft micritic (clay-size) matrix. The samples had high moldic porosity with the appearance of a shell hash (coquina), but most of the shells had either been replaced with calcite/micrite, or all of the shells had dissolved leaving a calcite-cemented clay matrix in its place. Even though the  $V_s$  values of the limestone layer were relatively high, the recovered core samples were not entirely intact and could not be used for resonant column and torsional shear testing.

Below the limestone layer (20-43 ft), layers of sand and calcite-cemented sandstone were observed at depths between 43-263 ft. These layers appeared to alternate based on the difficulty in recovering core samples and the spikes observed in the  $V_s$  profile as shown in Fig. 4.10 The sand was classified as SC. The  $V_s$  values for sand were approximately 984-1640 ft/s, while the  $V_s$  values for calcite-cemented sandstone were approximately 2297-3280 ft/s.

At a depth between 263-269 ft, calcareous sandstone layers were observed. These layers were underlain by low plasticity clay or sandy clay for depths between 263 to 364 ft. These thick clay layers were described as weakly to moderately cemented with carbonation or calcareous, sandy clay (mostly clay) with trace of shell fragments. This cemented clay had moderate to strong reaction with HCl. The clay layers were interbedded with claystone as shown in Fig. 4.11(b) and sandstone laminae. The  $V_s$  values for these layers ranged between 1772-2756 ft/s.

At a depth between 367-525 ft, the deposits were highly variable. A sharp spike was observed at the depth of 367 ft in the P-S logging data, with a  $V_s$  value of 4298 ft/s. The material observed at this depth was described as calcareous, clayey sand with strong reaction with HCl. Below this layer, at a depth of 387 ft, the  $V_s$  value was significantly lower and had a value of 984 ft/s.  $V_s$  increased to 2493 ft/s at the depth of 427 ft. The materials observed within these layers were described as laminated calcareous, silty clay as shown in Fig. 4.11(c). The core samples consist of dense clay interlaminated with very thin silty lenses. The material was friable (can break with hand) but firm. Below this layer, at a depth of 443 ft, a layer of calcareous sandy clay with strong cementation was found and had a  $V_s$  of approximately 2953 ft/s. Below this layer, the cementation appears to be weaker which was consistent with the lower  $V_s$  of 1476 ft/s from 466-508 ft. Another spike in  $V_s$  of over 3280 ft/s was observed at the depth of 525 ft and was attributed to the existence of a sandstone layer.

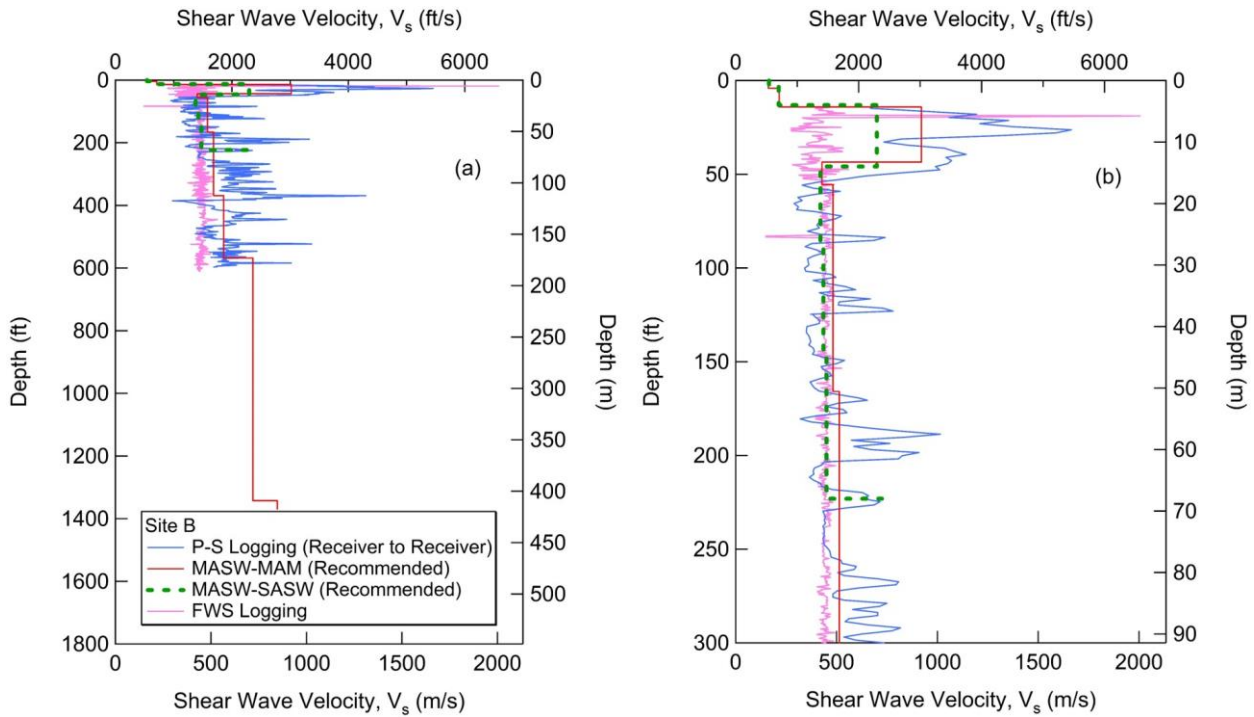


**Figure 4.10**  $V_s$  Profiles for Site B: (a) Shown to a Depth of 1800 ft, and (b) Shown to a Depth of 300 ft.

At a depth between 526-615 ft, more calcareous sandy clay or clayey sand layers were found with the  $V_s$  ranging between 1640-2297 ft/s. These layers were underlain by approximately 13-16 ft of thick layers of sandstone as shown in Fig. 4.11(d), which were consistent with a  $V_s$  of 3028 ft/s. Near the bottom of the borehole, interlaminated/interbedded sand and clay was found. These materials had very little to no reaction with HCl, except where shell fragments occur, and the  $V_s$  was approximately 1640-1968 ft/s. Although the average  $V_s$  is 2034 ft/s between the depth 509-594 ft, based on the core logs and the  $V_s$  profile from the P-S suspension logging data, a consistent layer of rock with  $V_s$  over 2300 ft/s was not reached at the bottom of the borehole (615 ft). In comparison, results from the MASW-MAM method suggested that a layer with  $V_s$  of 2363 ft/s begins at a depth of approximately 568 ft.

The  $V_s$  profile obtained from the FWS logging method is also presented for comparison. Overall, the  $V_s$  values from FWS were lower than the other three methods and there was no variation of  $V_s$  with depth, with the exception of the results at approximately 18-19 ft depth where the limestone layers were observed.

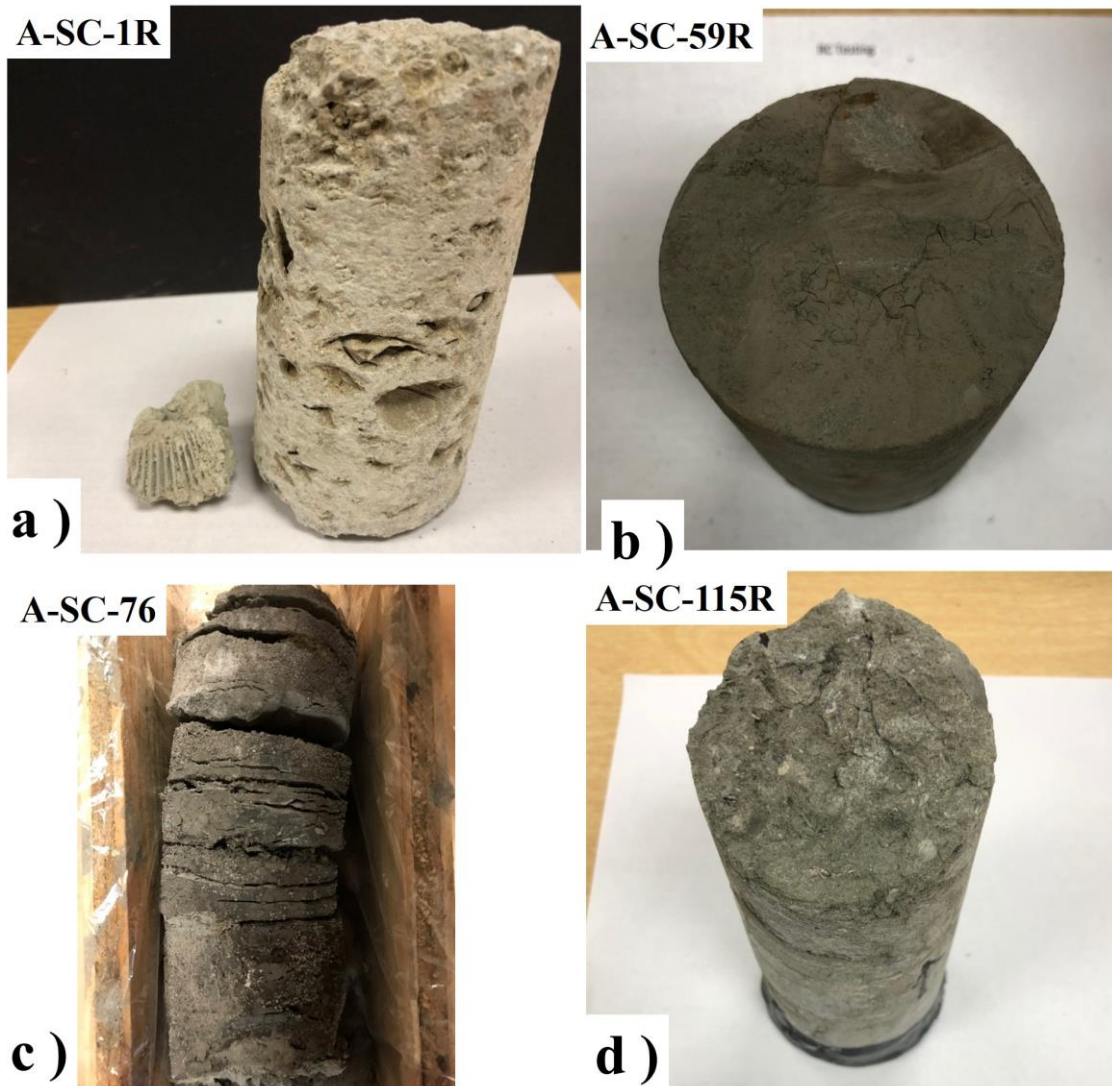


**Figure 4.11** Samples from Site B: (a) Limestone from 23-26 ft, (b) Claystone from 300-305 ft, (c) Silty Clay from 394 ft, and (d) Sandstone from 580-584 ft

A plot of SPT N-values in the top 26 ft is shown in Fig. 4.12(a) and the corresponding  $V_s$  values obtained using the  $V_s$ -SPT correlations of Andrus et al. (2009) and Seed and Idriss (1981) are plotted in Fig. 4.12(b). The results of the P-S, MASW-MAM, MASW-SASW and FWS methods are also shown. Similar to Site A, the correlated results matched reasonably well with the results from MASW-SASW and MASW-MAM methods in the top 12 ft. P-S logging data is not available in the top 11 ft, therefore the results from the  $V_s$ -SPT correlations and surface wave methods are beneficial. Again, the  $V_s$ -SPT N-value correlation approach by Seed and Idriss (1981) shows a better match with results from the geophysical method at depths below 12 ft, however the SPT data is limited at this site because SPT testing was limited to soils above the limestone layer encountered at the depth of approximately 11 ft where the SPT blow count is above 100 blow/ft.

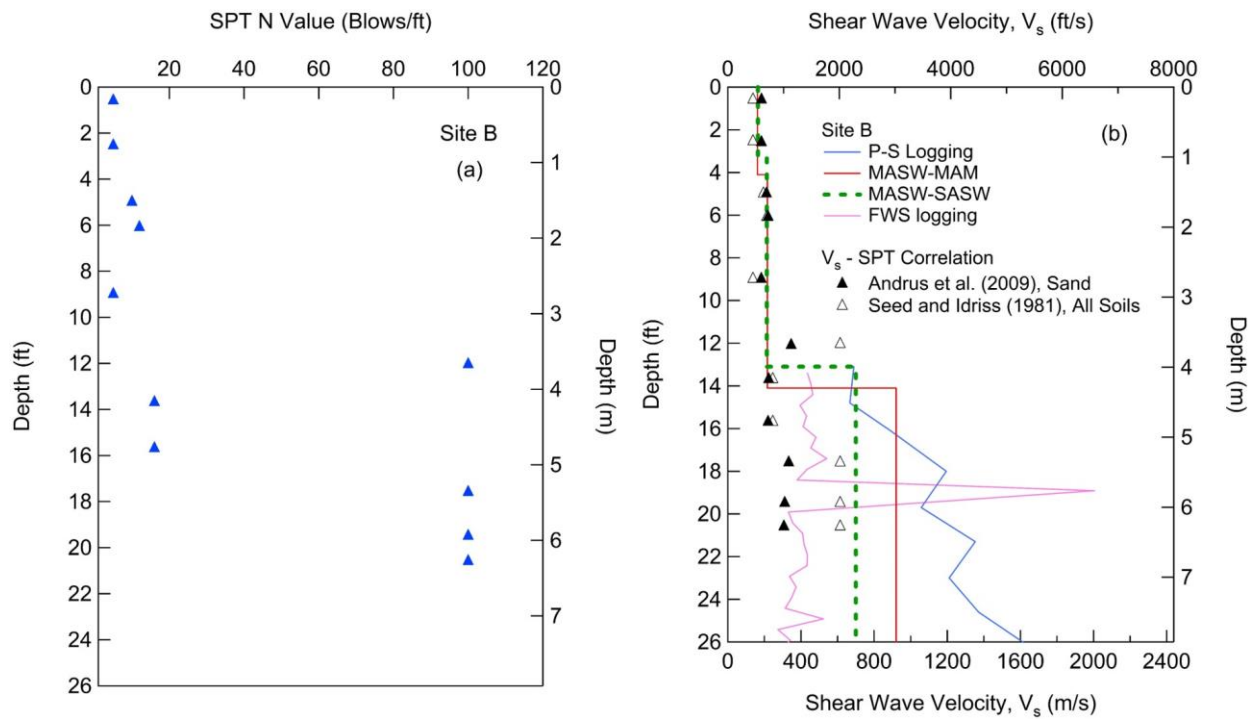


**Figure 4.12** (a) Variation of SPT N Value with Depth, and (b) Comparison between  $V_s$  Profiles between the  $V_s$ -SPT Correlation and Results from Geophysical Methods for Site B

The average  $V_s$  in the top 100 ft and 200 ft of the profile obtained from different testing methods are presented in Table 4.2. Similar to Site A, results from the P-S logging shown higher average values of  $V_s$  than that of the other three methods, but all of the methods yielded the same site class. The combined MASW-MAM provided a possible B-C boundary at a depth of 1343 ft. Analysis of the MASW-MAM test method for Site B can be found in Section 4.3.1.2 and Appendix B. In general, the deeper  $V_s$  profile generated for the combined MASW-MAM method is a result of a dispersion curve that included a wider range of frequencies than other surface wave methods as was shown in Fig. 4.6.

**Table 4.2** Summary of Average Shear Wave Velocities and Possible B-C Boundary for Site B

Method	100 ft		200 ft		B-C Boundary (ft)
	Average $V_s$ (ft/s)	NEHRP Site Class	Average $V_s$ (ft/s)	NEHRP Site Class	
P-S logging	1795	C	1650	C	N/A
FWS logging	1385	C	1429	C	N/A
MASW-SASW	1364	C	1408	C	N/A
MASW-MAM	1465	C	1536	C	1343

#### 4.4. Laboratory Measurements of Dynamic Behaviors

A total of 35 soil and rock samples were tested to evaluate normalized shear modulus and damping curves for a wide range of strains. The effects of confinement, testing frequency, geological age, and plasticity index were examined. All of the soil samples were tested using both the RC and TS methods. The rock samples were tested using the RC method only. More detailed information and testing procedures can be found in Section 3.3 and Appendix F.

##### 4.4.1. Dynamic Behaviors of Materials from Site A

RC and TS tests were performed on five samples from Shelby tubes and ten samples from the core sampler. The material properties and testing confinements are presented in Table 4.3. Soil samples were mostly clayey soils with a high plasticity index. Rock samples were classified as sandstone.

**Table 4.3** Material Properties of Tested Samples for Site A

Sample ID <sup>1</sup>	Depth (ft)	$\sigma'_{mo}$ <sup>2</sup> (psi)	Soil / Rock Type	%Finer	PI	$\omega_i$ <sup>3</sup> (%)	$\omega_f$ <sup>4</sup> (%)	Total Unit Weight (lb/ft <sup>3</sup> )	$\sigma'_m$ <sup>5</sup> (psi)
C-UD-01	11	5	CH	95.1	28	43.4	37.1	113	2, 5, 9
C-UD-02*	16	6	SC-SM	8.0	np <sup>6</sup>	0.0	0.0	95	6, 12, 23
C-UD-03	56	17	CH	91.6	44	35.3	37.1	116	9, 17, 35
C-UD-07	84	25	CH	87.0	43	40.7	35.8	112	13, 25, 51
C-UD-08	87	26	CH	93.8	47	42.6	37.7	113	13, 26, 52
C-SC-09	158	48	SC	30.6	14	20.3	26.4	116	24, 48, 96
C-SC-15	188	57	MH	70.2	19	31.2	28.3	116	29, 57, 114
C-SC-34	283	83	SC	43.6	15	30.1	27.0	109	41, 83, 124
C-SC-56	393	113	CH	95.7	34	36.5	36.1	109	26, 56, 113
C-SC-63	428	121	CH	80.0	39	43.5	40.5	109	61, 121, 147
C-SC-04R	133	45	Sandstone	-	-	-	-	157	0, 22, 45, 90
C-SC-39R	308	93	Sandstone	-	-	-	-	167	0, 46, 92
C-SC-40R	313	110	Sandstone	-	-	-	-	166	0, 55, 110
C-SC-41R	318	103	Sandstone	-	-	-	-	165	0, 52, 103
C-SC-68R	454	160	Sandstone	-	-	-	-	165	0, 80, 120

1. UD represents Shelby tube sample, and SC represents core sample; R is for rock sample

2.  $\sigma'_{mo}$  represents in-situ mean confining stress ( $K_0=0.5$  assumed)

3.  $\omega_i$  represents initial water content

4.  $\omega_f$  represents final water content

5.  $\sigma'_m$  represents testing mean confining stress

6. np represents non-plastic

\* reconstituted sample

All of the results from RC and TS testing for soil samples are presented in terms of normalized modulus ( $G/G_{max}$ ) and damping in Figs. 4.13 and 4.14, respectively. Both tests were carried out between strain levels of  $10^{-5}\%$  to 0.5% and when  $G/G_{max}$  values reached approximately 0.5. Similar results from the RC and TS testing were obtained for the  $G/G_{max}$  curves, but some differences were observed for the damping curves. These differences are due to the effects of

testing frequency discussed in the next section. The degradation of  $G/G_{\max}$  curves occurs at strains  $10^{-3}$  to  $10^{-2}\%$ . Damping values start to increase at strains higher than  $10^{-2}\%$ .

All of the results from RC testing for rock samples are presented in Fig. 4.15. The RC tests were performed up to  $G/G_{\max}$  values of 0.9 when degradation was observed at slightly below  $10^{-3}\%$ . A slight effect of confinement was observed and is discussed in the next section.

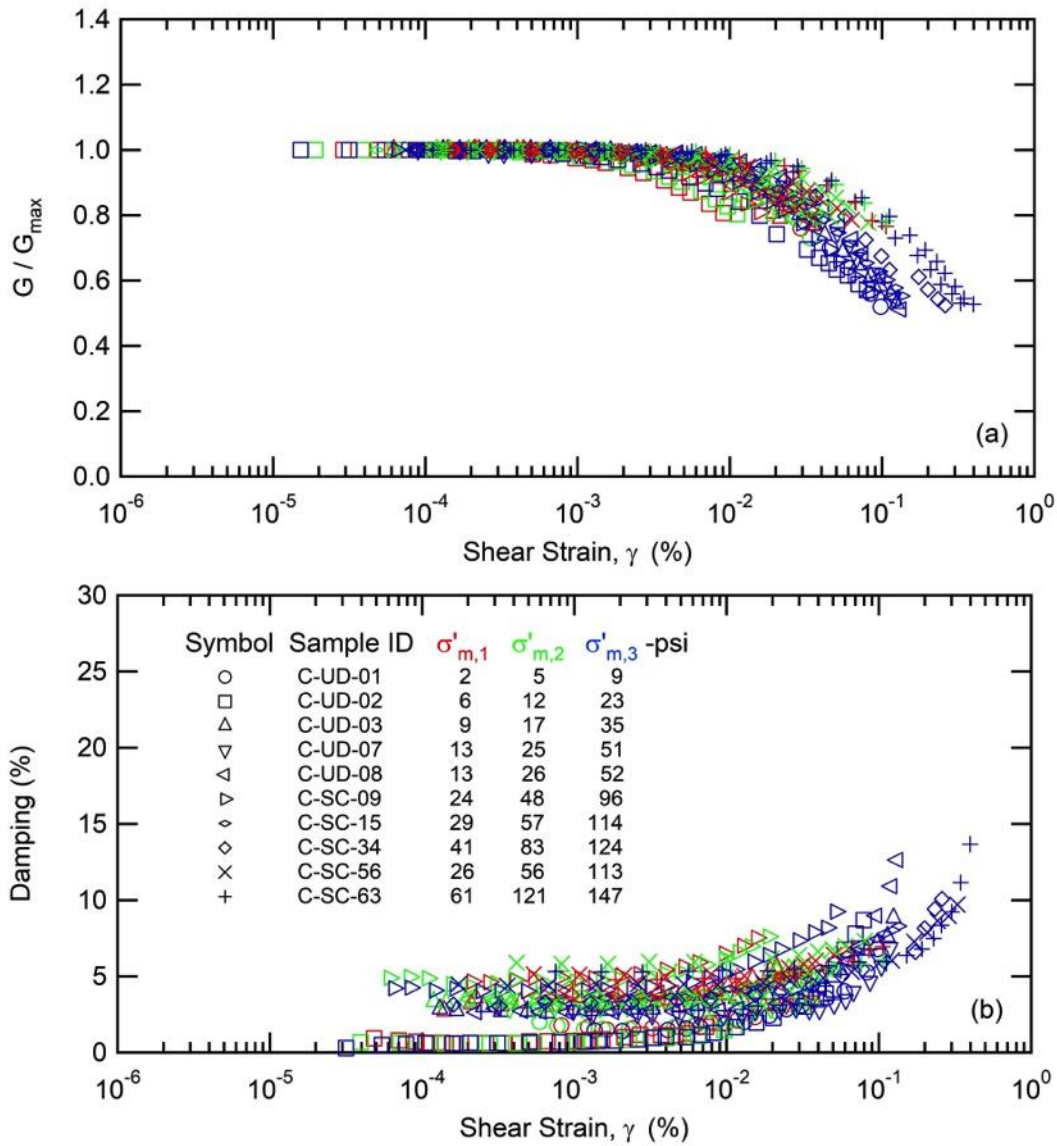


**Figure 4.13** RC Testing Results for Soil Samples from Site A: (a)  $G/G_{\max}$  Curves, and (b) Damping Curves

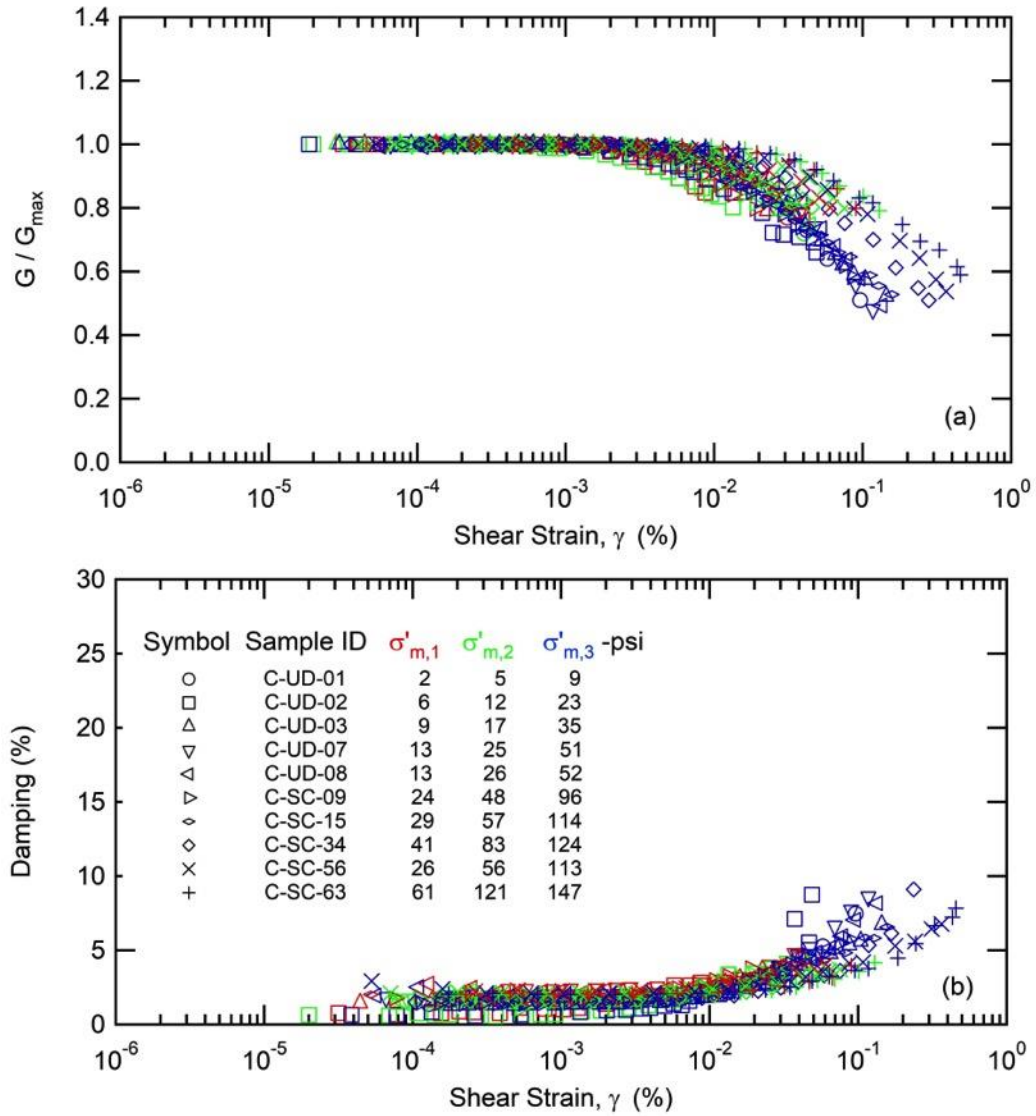


**Figure 4.14** TS Testing Results for Soil Samples from Site A: (a)  $G/G_{\max}$  Curves, and (b) Damping Curves

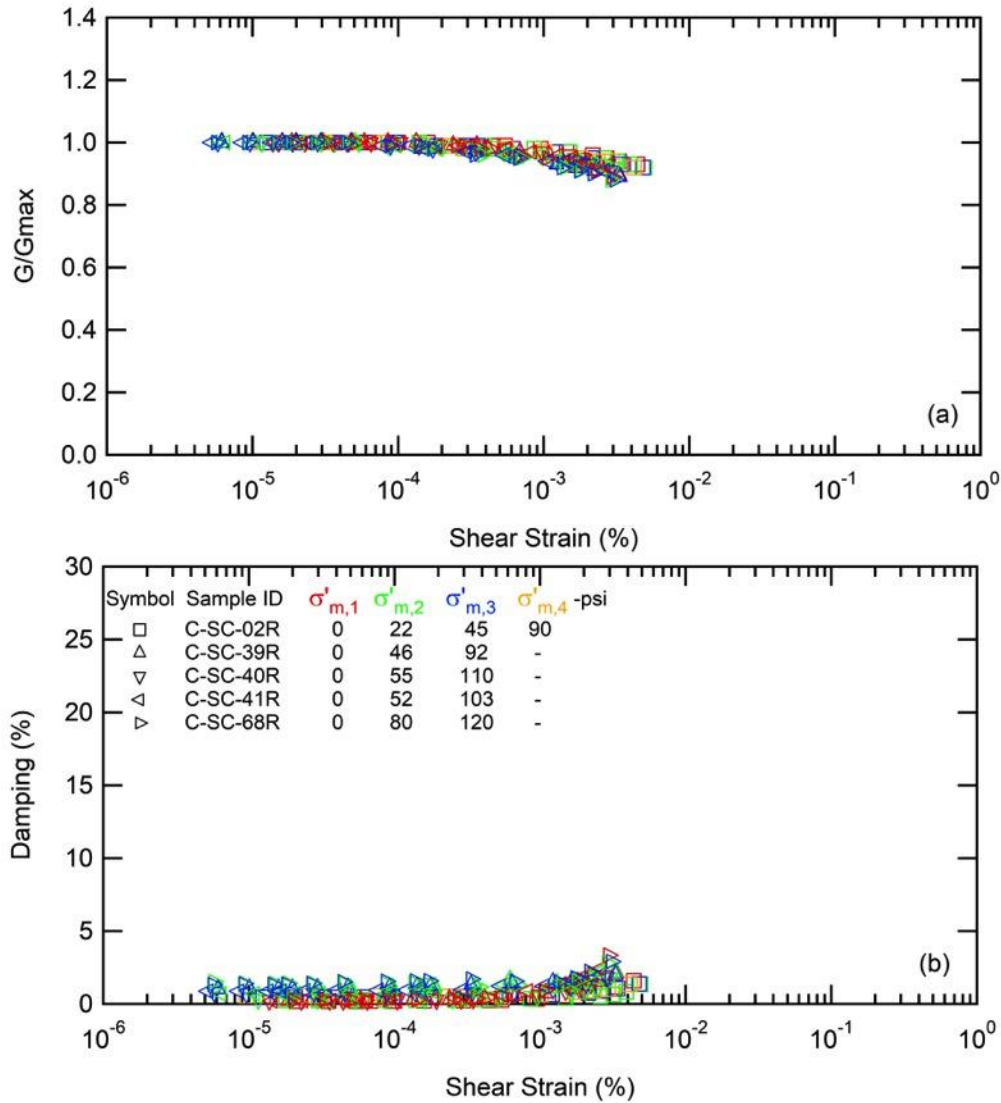


**Figure 4.15** RC Testing Results for Rock Samples from Site A: (a)  $G/G_{max}$  Curves, and (b) Damping Curves

#### 4.4.2. Dynamic Behaviors of Materials from Site B

RC and TS tests were performed on five samples from Shelby tubes and fifteen samples from the core sampler. The material properties and testing confinements are presented in Table 4.4. Soil samples were mostly sand for the depths of 5-10 ft, and clay or silt with high plasticity index at the depths below 150 ft. Sample A-UD-03 and A-UC-05 were tested at dry state prepared by reconstitution as discussed in Section 3.3.3. Rock samples were classified as either sandstone or claystone.

**Table 4.4** Material Properties of Tested Samples for Site B

Sample ID <sup>1</sup>	Depth (ft)	$\sigma'_{mo}$ <sup>2</sup> (psi)	Soil / Rock Type	% Finer	PI	$\omega_i$ <sup>3</sup> (%)	$\omega_f$ <sup>4</sup> (%)	Total Unit Weight (lb/ft <sup>3</sup> )	$\sigma'_m$ <sup>5</sup> (psi)
A-UD-01	5	2	SC	30.5	27	22.6	17.6	127	1, 2, 4
A-UD-02	7	3	SM	23.2	1	14.3	13.9	109	3, 5, 11
A-UD-03*	9	3	SM	14.3	np <sup>6</sup>	0.0	0.0	110	3, 7, 13
A-UD-05*	150	41	SP	0.0	np	0.0	0.0	92	21, 41, 83
A-UD-06	153	43	ML	57.5	11	26.0	23.5	121	22, 43, 86
A-SC-27	153	43	CL	64.2	13	33.3	30.2	120	22, 43, 86
A-SC-49	253	68	CH	68.0	33	30.2	24.8	119	34, 68, 136
A-SC-77	393	110	MH	62.0	24	35.4	33.5	105	55, 110, 138
A-SC-86	438	122	CH	72.6	29	25.7	24.3	121	31, 61, 122
A-SC-96	488	136	CH	74.9	33	31.3	30.9	119	32, 68, 136
A-SC-105	533	148	SC	42.9	20	25.6	22.1	121	37, 74, 111
A-SC-42R	218	68	Sandstone	-	-	-	-	161	0, 34, 68, 135
A-SC-52R	268	89	Sandstone	-	-	-	-	160	0, 45, 89, 133
A-SC-59R	303	100	Claystone	-	-	-	-	152	0, 50, 100
A-SC-60R	308	98	Claystone	-	-	-	-	148	0, 49, 98
A-SC-109R	553	184	Sandstone	-	-	-	-	167	0, 46, 92
A-SC-110R	558	174	Sandstone	-	-	-	-	168	0, 44, 87, 130
A-SC-112R	568	177	Sandstone	-	-	-	-	167	0, 44, 89
A-SC-115R	583	197	Sandstone	-	-	-	-	163	0, 49, 98
A-SC-116R	588	190	Sandstone	-	-	-	-	167	0, 47, 95

1. UD represents Shelby tube sample, and SC represents core sample; R is for rock sample

2.  $\sigma'_{mo}$  represents in-situ mean confining stress ( $K_0=0.5$  assumed)

3.  $\omega_i$  represents initial water content

4.  $\omega_f$  represents final water content

5.  $\sigma'_m$  represents testing mean confining stress

6. np represents non-plastic

\* reconstituted sample

Results from RC and TS testing in terms of normalized modulus and damping for soil samples are presented in Figs. 4.16 and 4.17. Both tests were carried out between strain levels of  $10^{-5}\%$  to  $0.5\%$  and when  $G/G_{max}$  values reached approximately 0.5. The degradation of  $G/G_{max}$  curves for most of the samples occurred at strains  $10^{-3}$  to  $10^{-2}\%$ . Damping values started to increase at strains higher than  $10^{-2}\%$ . Samples A-UD-01, A-UD-02, and A-UD-03 behaved more nonlinearly than other samples. This may be a result of testing these samples at very low confinement. Therefore, results for both  $G/G_{max}$  and damping at high strains at depths of 5-10 ft could vary greatly due to non-linear behavior and should be used along with other data to make design parameter selection.

Results for RC testing for rock samples are presented in Fig. 4.18 Similar to rock testing results from Site A, a very slight effect of confinement was observed. Relatively higher damping was observed for three samples A-SC-59R, A-SC-60R, and A-SC-115R. It was noted that samples A-SC-59R and A-SC-60R were classified as claystone, whereas sample A-SC-115R (i.e., sandstone)

appeared to contain some amount of fines within the sandstone matrix. Photos of these samples are shown in Fig. 4.19.

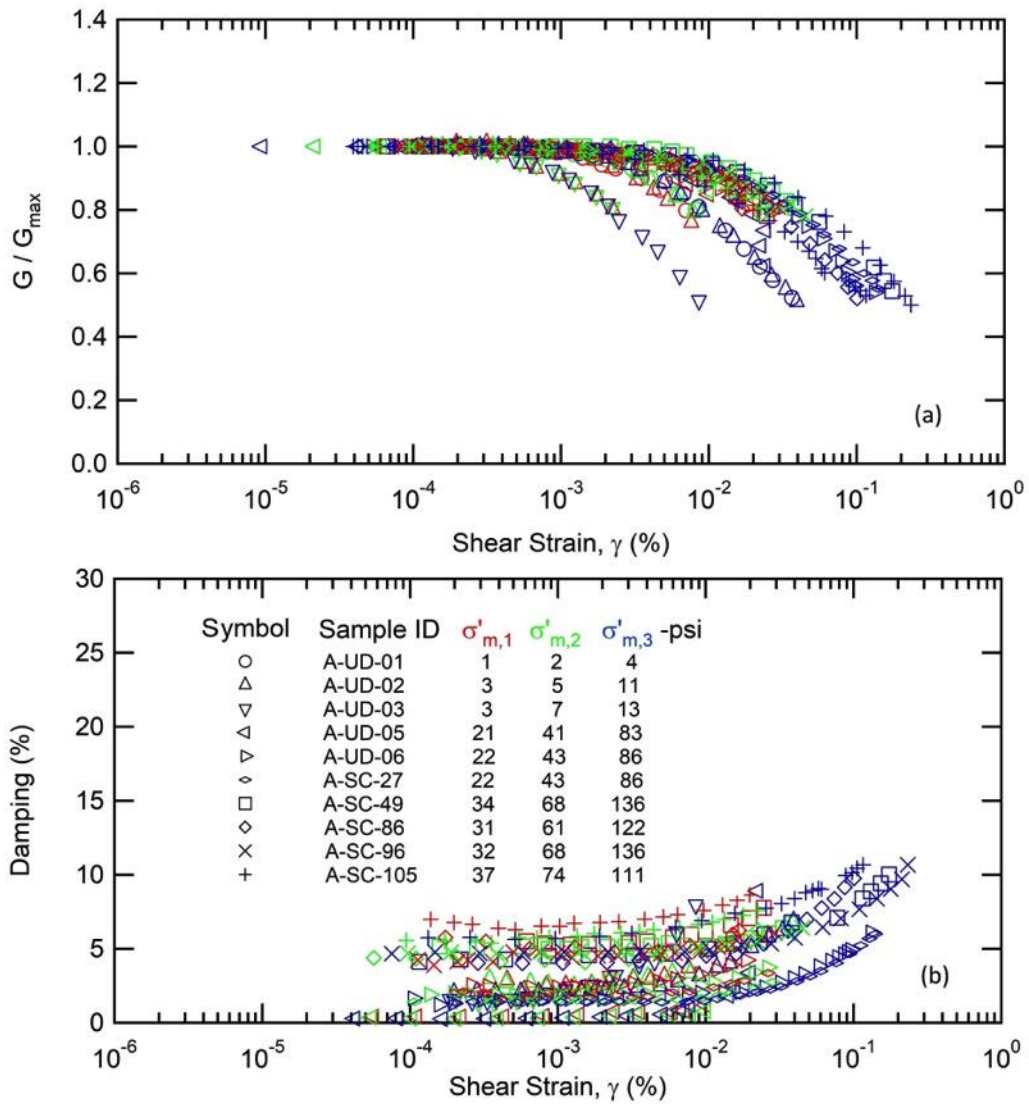


**Figure 4.16** RC Testing Results for Soil Samples from Site B: (a)  $G/G_{\max}$  Curves, and (b) Damping Curves

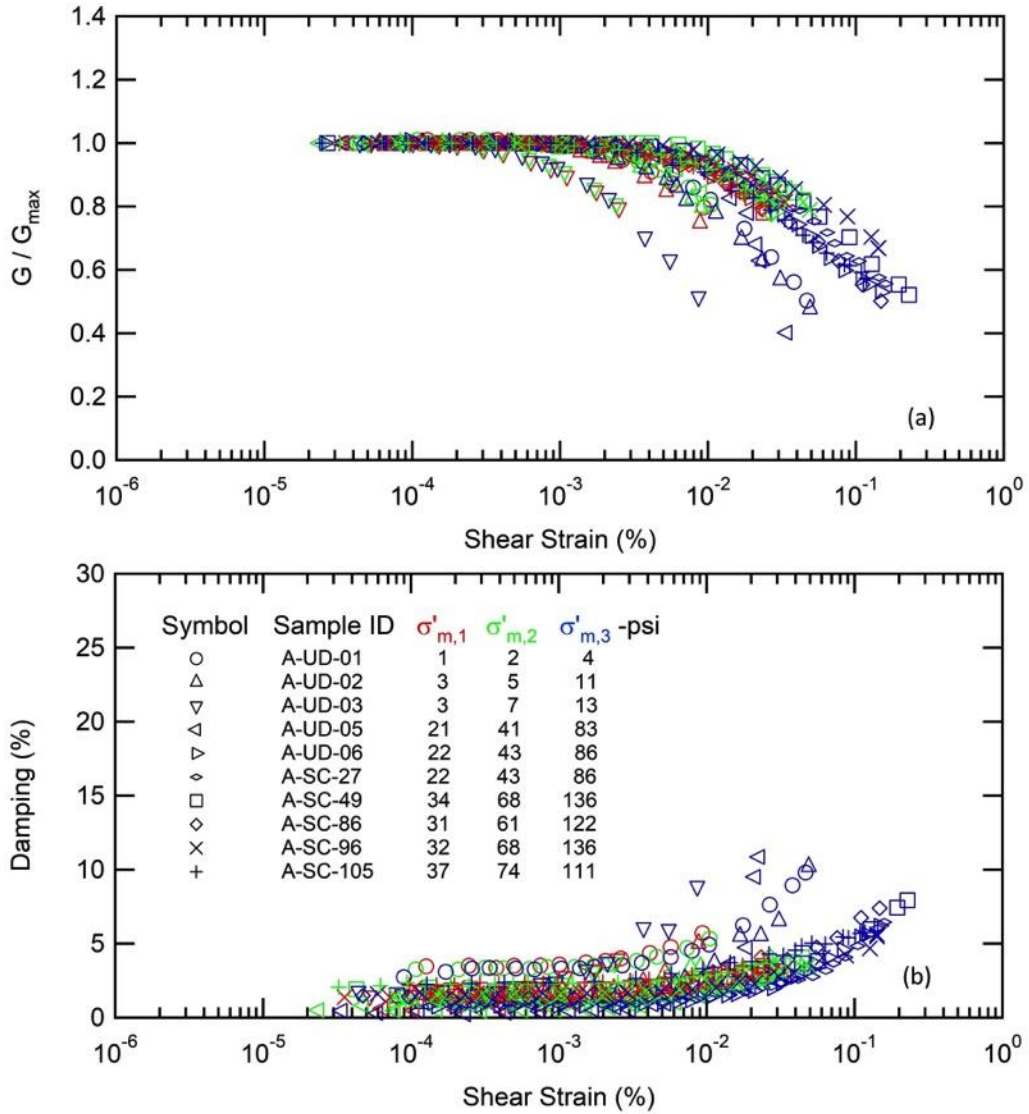


**Figure 4.17** TS Testing Results for Soil Samples from Site B: (a)  $G/G_{max}$  Curves, and (b) Damping Curves

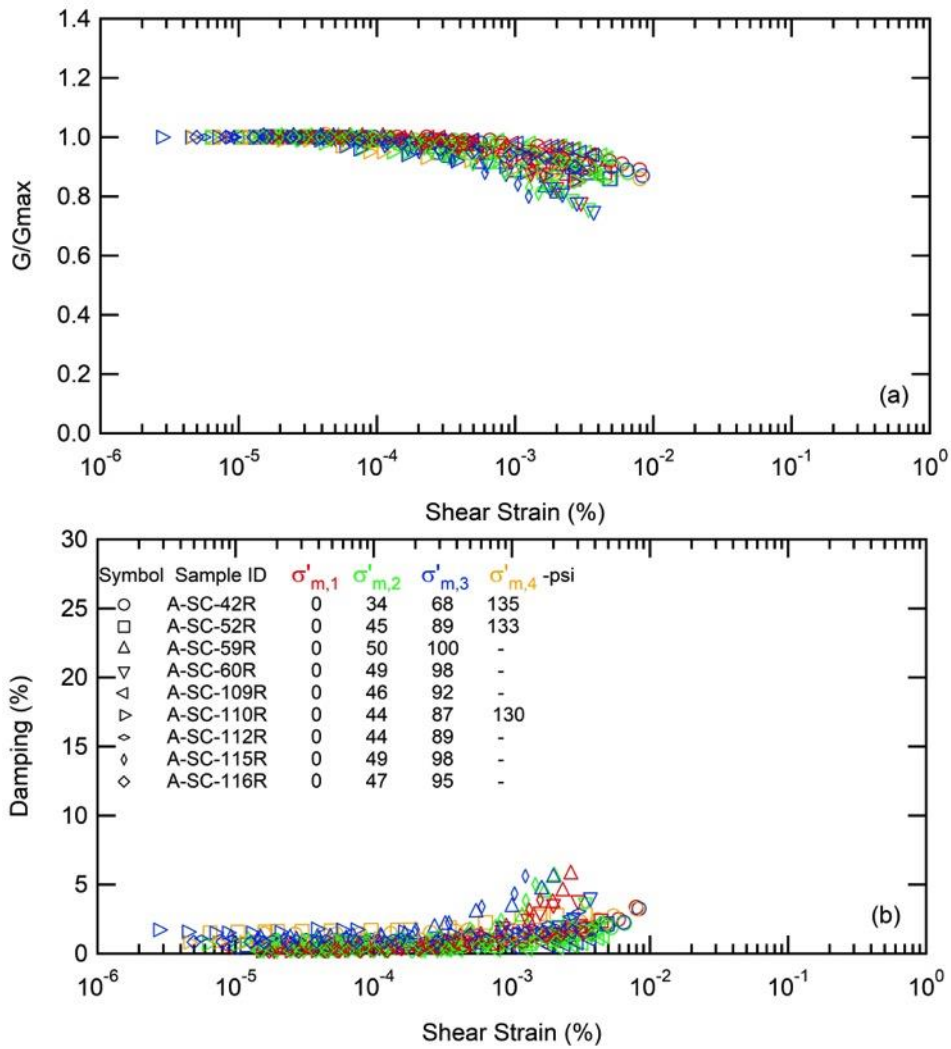


**Figure 4.18** RC Testing Results for Rock Samples from Site B: (a)  $G/G_{max}$  Curves, and (b) Damping Curves

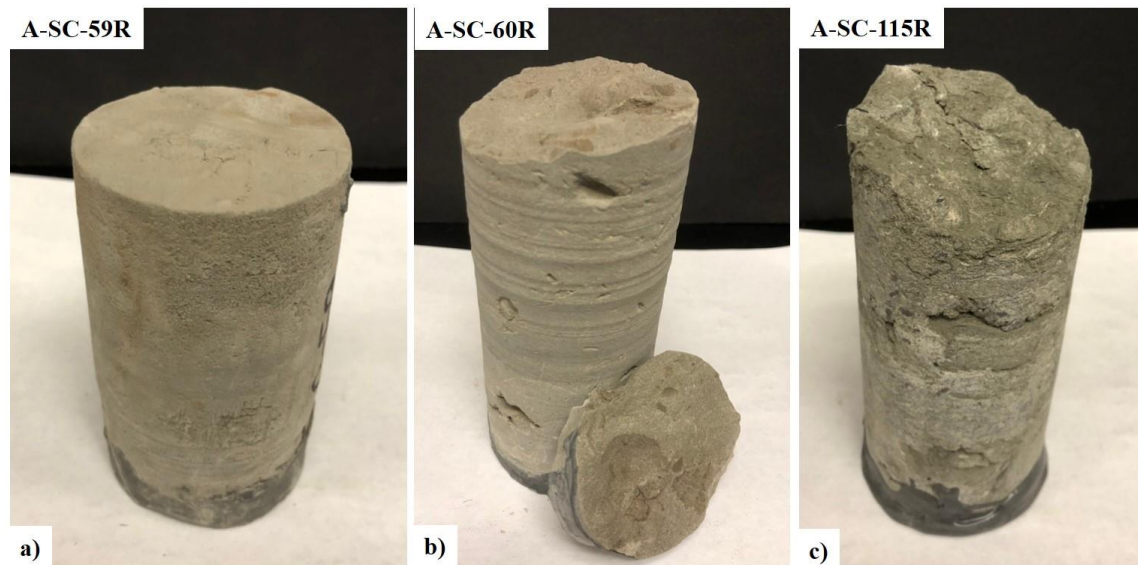


**Figure 4.19** Photos of Rock Samples that Exhibited Relatively High Damping

#### **4.4.3. Data Analysis and Interpretation of Dynamic Soil Properties**

This section presents further analysis of factors affecting the dynamic soil properties from both sites. These factors including confinement, testing frequency, geologic age, and soil plasticity are typical factors that have been studied extensively in the literature. Effects of these factors on the dynamic properties of soils from the South Carolina Coastal Plain deposits are discussed.

##### ***4.4.3.1. Effect of Confinement***

Shear wave velocities of soil and rock samples are presented in Figs. 4.20 and 4.21 for Sites A and B, respectively. At both sites, the  $V_s$  ranged from 540 to 1280 ft/s for the soil samples and from 4100 to 4300 ft/s for the rock samples for the confinement ranging from zero to a maximum of 140 psi. Effects of confinement on  $V_s$  were observed to be minimal for the rock samples as the  $V_s$  increased with confinement by approximately less than 1% from zero to 140 psi confinement. For the soil samples,  $V_s$  increased by 2-5 ft/s per increment of 1 psi confinement. It should be noted that this observation does not account for soil properties, geological age, and other factors.

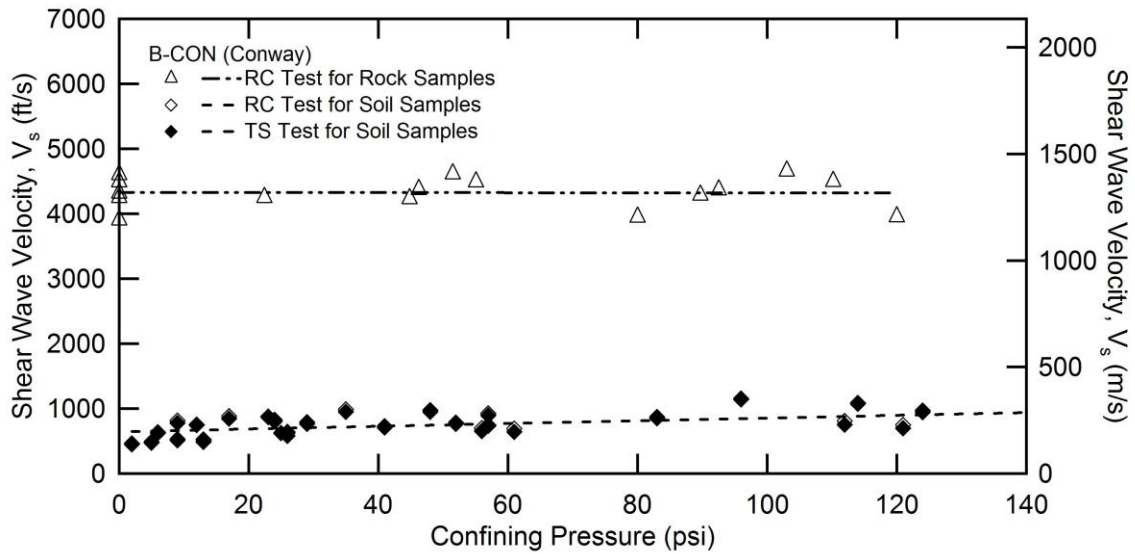


**Figure 4.20** Variation of Shear Wave Velocity with Confinement for Site A

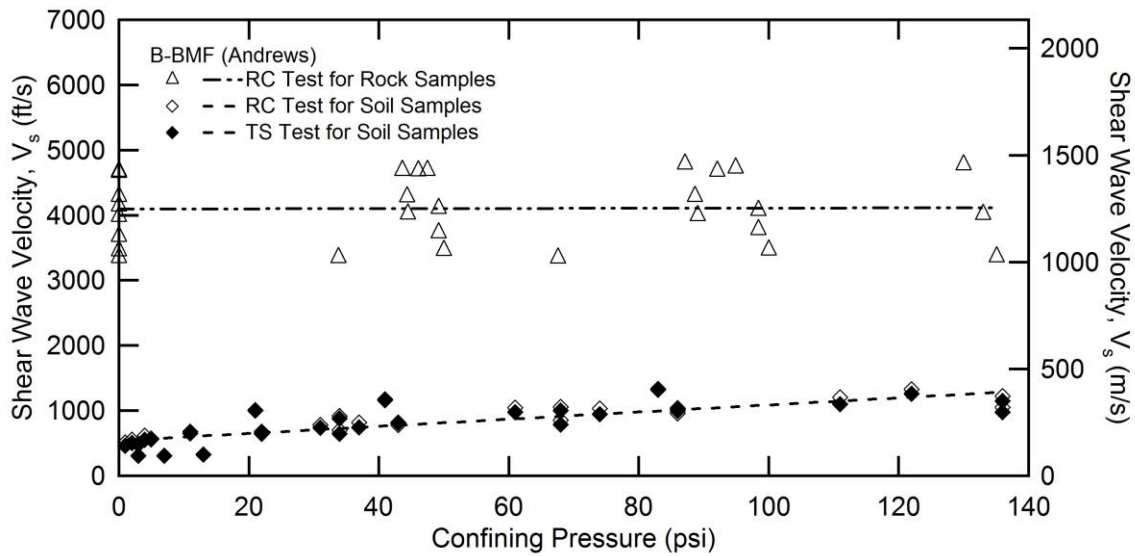


**Figure 4.21** Variation of Shear Wave Velocity with Confinement for Site B

As shown in Figs. 4.22 and 4.23, the low-strain damping ( $D_{min}$ ) ranged from 1.5 to 5% for the soil samples and from 0.2 to 1.2 % for the rock samples at both sites regardless of the testing method used. However, the data was more scattered compared with the  $V_s$  data in Figs 4.20 and 4.21. Furthermore, the data for the soil samples is less scattered in the TS testing results when compared to the RC testing results, and the effects of confinement were observed to be minimal. A large variation of damping for soil was due to the difference in testing frequency between RC and TS tests, which is discussed in Section 4.4.3.2.

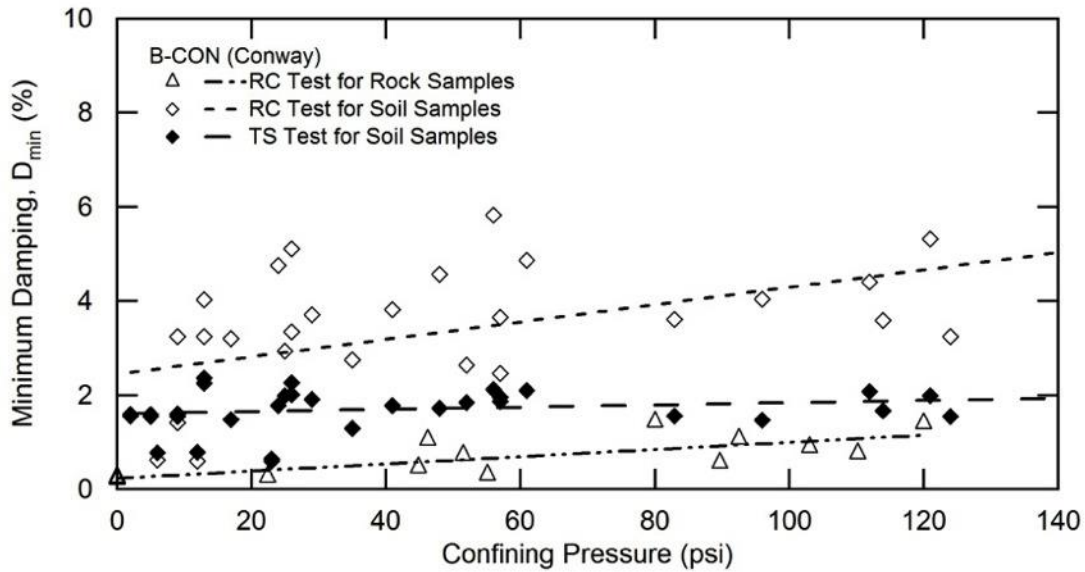


**Figure 4.22** Variation of Damping with Confinement for Site A

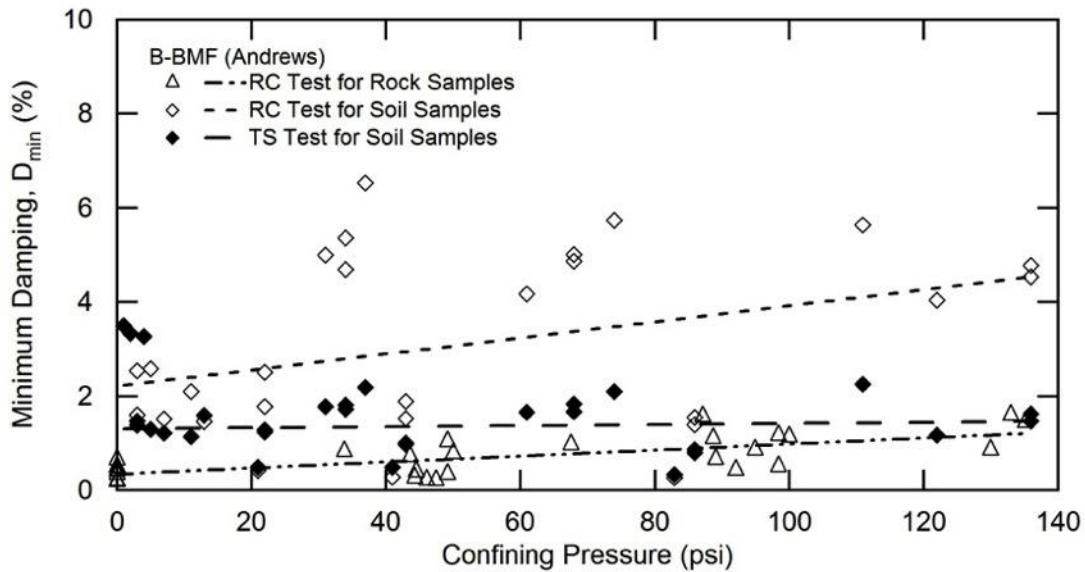


**Figure 4.23** Variation of Damping with Confinement for Site B

The  $V_s$  results obtained from the RC tests at in-situ mean confining stress is presented in Tables 4.5 and 4.6 in comparison with the  $V_s$  data obtained from the three field methods. The results are separated into two groups: soil samples and cemented soil/rock samples. The  $V_s$  of the soil samples from the RC tests are lower than the results from the field tests. In contrast, the  $V_s$  of the cemented soil/rock samples are higher than the results from the field tests. Other contributing factors include the differences in stress conditions between the laboratory and the field, and sample disturbance. It is also important to note that the soil samples represent a wide variety of soil types including silty clay, clayey sand, and high plasticity clay or silt. These samples had relatively weak cementation. The cemented soil/rock samples were very hard and had some imperfections. In some samples, interbedded lenses of clay or silt were present, whereas some samples appeared to be solid hard rock. The higher  $V_s$  observed for the rock samples compared to those found with the field methods is possibly due to the fact that the solid rock sample was selected and tested without taking in to account the existence of rock fractures and interlayering system that exists in the field. Furthermore, laboratory testing provides dynamic soil properties and behaviors at higher strains (see Section 4.4.3.2) than field-testing which is limited to low strain.

**Table 4.5** Comparison of  $V_s$  of Soil Samples for Site A

Sample ID	Depth (ft)	Soil/Rock Type	$\sigma'_{mo}$ (psi)	Shear Wave Velocity (ft/s)			
				Resonant Column Test	MASW-MAM	MASW-SASW	P-S Suspension Logging
C-UD-01	11	CH	5	509	413	479	873
C-UD-02	16	SC-SM	6	635	413	466	873
C-UD-03	56	CH	17	989	846	1004	1719
C-UD-07	84	CH	25	736	1516	1204	1231
C-UD-08	87	CH	26	764	1516	1204	1231
C-SC-04R	133	Sandstone	45	4253	1557	1329	2383
C-SC-09	158	SC	48	1157	1557	1509	1537
C-SC-15	188	MH	57	1088	1557	1509	1444
C-SC-34	283	SC	83	873	1557	-	1480
C-SC-39R	308	Sandstone	93	4374	1557	-	1480
C-SC-40R	313	Sandstone	110	4490	1557	-	1934
C-SC-41R	318	Sandstone	103	4650	1557	-	1934
C-SC-56	393	CH	113	698	1659	-	1596
C-SC-63	428	CH	160	749	1659	-	1411
C-SC-68R	454	Sandstone	1101	3975	1659	-	2013

**Table 4.6** Comparison of  $V_s$  of Soil Samples for Site B

Sample ID	Depth (ft)	Soil/Rock Type	$\sigma'_{mo}$ (psi)	Shear Wave Velocity (ft/s)			
				Resonant Column Test	MASW-MAM	MASW-SASW	P-S Suspension Logging
A-UD-01	5	SC	2	614	708	699	-
A-UD-02	7	SM	3	477	708	699	-
A-UD-03	9	SM	3	304	708	699	-
A-UD-05	150	SP	41	1171	1582	1476	1441
A-UD-06	153	ML	43	1013	1582	1476	1441
A-SC-27	153	CL	43	956	1582	1476	1441
A-SC-42R	218	Sandstone	68	3349	1685	1476	1701
A-SC-49	253	CH	68	850	1685	-	1838
A-SC-52R	268	Sandstone	89	4000	1685	-	1838
A-SC-59R	303	Claystone	100	3465	1685	-	2115
A-SC-60R	308	Claystone	98	4072	1685	-	2115
A-SC-77	393	MH	110	797	1859	-	1849
A-SC-86	438	CH	122	1321	1859	-	1849
A-SC-96	488	CH	136	1218	1859	-	1590
A-SC-105	533	SC	148	1367	1859	-	1930
A-SC-109R	553	Sandstone	184	4682	1859	-	1930
A-SC-110R	558	Sandstone	174	4827	1859	-	1930
A-SC-112R	568	Sandstone	177	4290	1859	-	1930
A-SC-115R	583	Sandstone	197	3875	2361	-	2057
A-SC-116R	588	Sandstone	190	4777	2361	-	2057

#### 4.4.3.2. Effect of Testing Frequency

The frequency effects on low-strain shear modulus and damping of selected soil samples from both sites were examined by conducting a series of TS tests at frequencies ranging from 0.001 and 2 Hz. To compare the effect of frequency, results were normalized with the results measured at a frequency of 0.5 Hz. In addition, the TS results are compared with the results from RC tests performed on the same soil sample at frequencies ranging from 20 to 50 Hz as shown in Fig. 4.24. For the shear modulus, the effect of frequency was found to be small (approximately 10%). In contrast, for the damping, the effect of frequency was found to be as high as 50-200%. It is therefore possible that results from RC tests can provide damping twice as much as the results from TS tests. Earthquake motion is composed of a wide range of frequencies. It is important that damping measurements should be performed using both RC and TS methods. Frequency effects on small strain dynamic properties have been recognized and studied by Stokoe et al. (1999), Rix and Meng (2005), and Ruttithivaphanich and Sasanakul (2019). However, the impact of frequency on site response analysis, especially the effect on damping, is not routinely accounted for in practice, and more research on this topic is needed. Because this study showed a pronounced effect of frequency on plastic fine grained soils (i.e. silty and clayey soils), and until further studies are conducted to develop predictive equations for the frequency effects on damping that can be used in practice, it is recommended to perform both RC and TS tests on soil samples to examine the effects of testing frequency on shear modulus and damping.

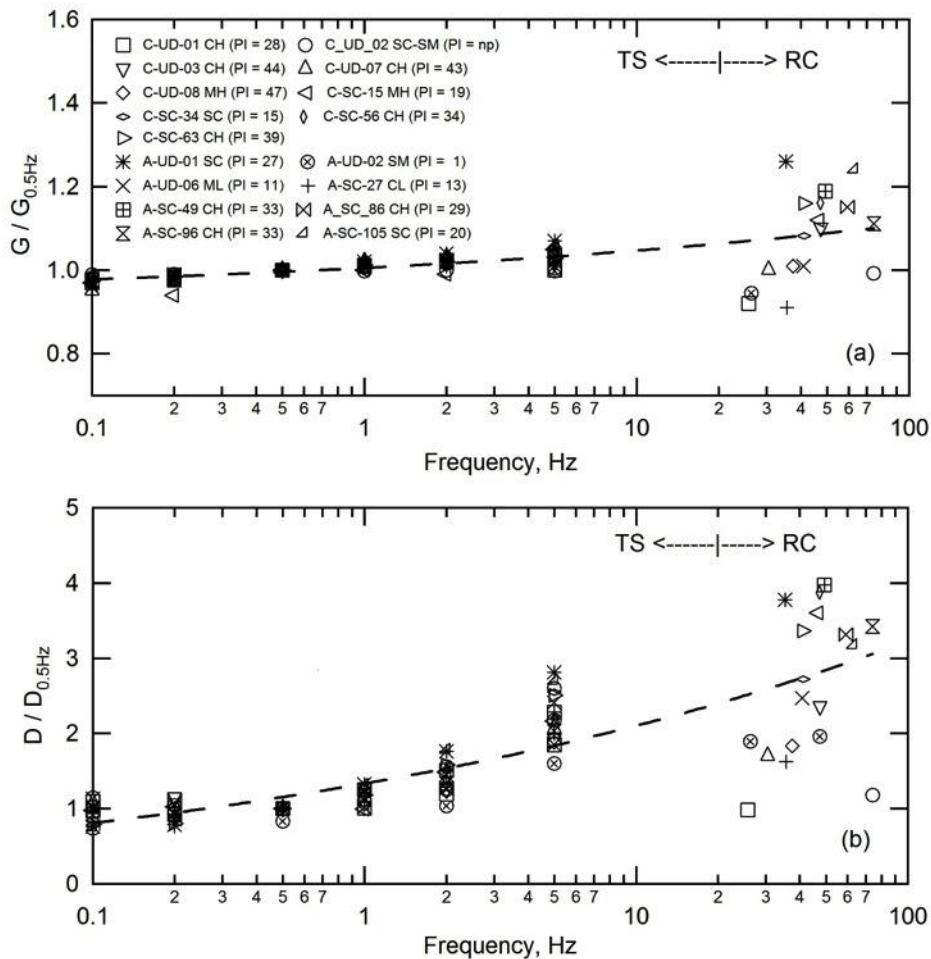


**Figure 4.24** Effect of Testing Frequency on: (a) Normalized  $G/G_{0.5\text{Hz}}$ , and (b) Normalized  $D/D_{0.5\text{Hz}}$

#### 4.4.3.3. Effect of Geological Age and Soil Plasticity

Dynamic behaviors of soil and rock from both sites are separated into three geological age groups: Quaternary (Penholoway allo), Tertiary (Ashley or Cooper Marl), and Cretaceous (Peedee and Black Creek) deposits. Results from RC and TS tests are shown in Figs. 4.25, 4.26, and 4.27 for selected confinements. Results were compared with the empirical relationships proposed by Vucetic and Dobry (1991) for soils of varying plasticity as given by the plasticity index (PI). It is important to note that the Vucetic and Dobry (1991) relationships were obtained from soil tested at confining pressure of 0.25 to 4 atm (4 to 60 psi); therefore, the results should be compared at the confinement within +/- 50% range of the general curves as suggested by Stokoe et al. (1995). In addition, the proposed prediction procedure of  $G/G_{\text{max}}$  and damping curves for specific PI and confinement by Andrus et al. (2003) are plotted for comparison.

For the Quaternary age deposits, five soil samples were available as shown in Fig. 4.25. Comparing results for  $G/G_{max}$  curves with the Vucetic and Dobry (1991) curves with varying ranges of PI, the results aligned with curves for a range of PI that was higher than the PI of the soil samples tested. The rate of increasing in damping at high strains was higher than the Vucetic and Dobry (1991) curves. Comparing results for both  $G/G_{max}$  and damping curves with the Andrus et al. (2003) curves, the results agreed fairly well for the same range of PI and all strain levels. It is important to note that these samples had very little to no cementation.

For the Tertiary age deposits, results from a total of three soil samples and one rock sample are presented in Fig. 4.26. The overall results show the same trend in the slopes and on-set of nonlinearity as Vucetic and Dobry (1991); however, similar to the Quaternary age group, the  $G/G_{max}$  curves generally align with curves for a range of PI that was higher than, but not related to, the PI of these samples. For Sample A-UD-5, the rate of increasing in damping was higher than the Vucetic and Dobry (1991) prediction, but the results agree with the Andrus et al. (2003) curves.

The dynamic behavior of the low plasticity samples (A-SC-27 and A-UD-6) does not match the predicted behavior proposed by Andrus et al. (2003), but is similar to the high plasticity (PI equals 50) predicted behavior of Vucetic and Dobry (1991). It is interesting to observe that the nonlinear behavior of rock sample A-SC-42R was similar to the soil samples. Behaviors of soil and rock deviated from the empirical curves suggesting that the materials within the same age group can be highly variable.

Overall, there was no clear relationship between soil plasticity and both  $G/G_{max}$  and D for the soil samples tested herein. It is important to recognize that the soil preparation process for the measurement of the plastic and liquid limit to determine PI breaks down the structure of cemented soil. Therefore, the effects of PI on dynamic soil behavior may not be relevant to, or less dominant than, the effect of cementation. These findings are based on limited number of samples and therefore more data are needed to quantitatively evaluate the effects (e.g. amount and/or characteristics) of cementation on dynamic soil properties of older soil deposits typically found in the South Carolina Coastal Plain. Consequently, more accurate prediction of dynamic properties can be achieved.

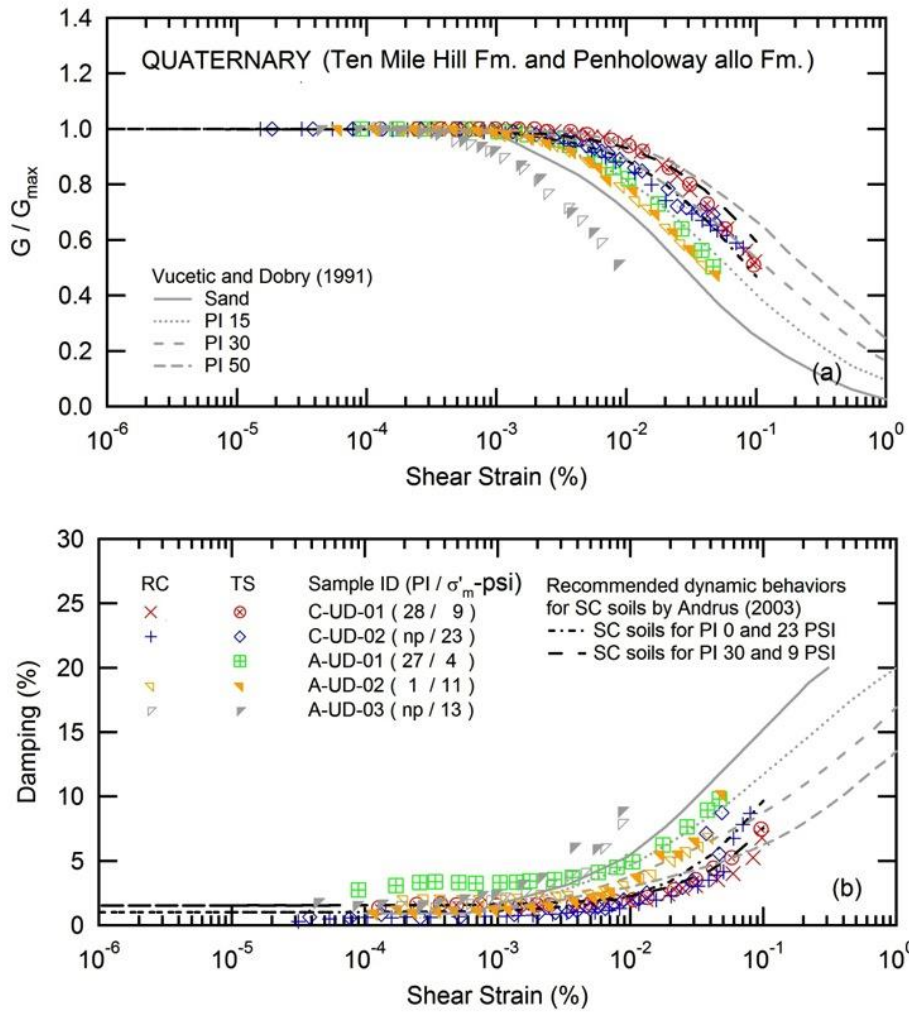


**Figure 4.25** Dynamic Properties of Quaternary Age Soils: (a)  $G/G_{max}$  Curves, and (b) Damping Curves

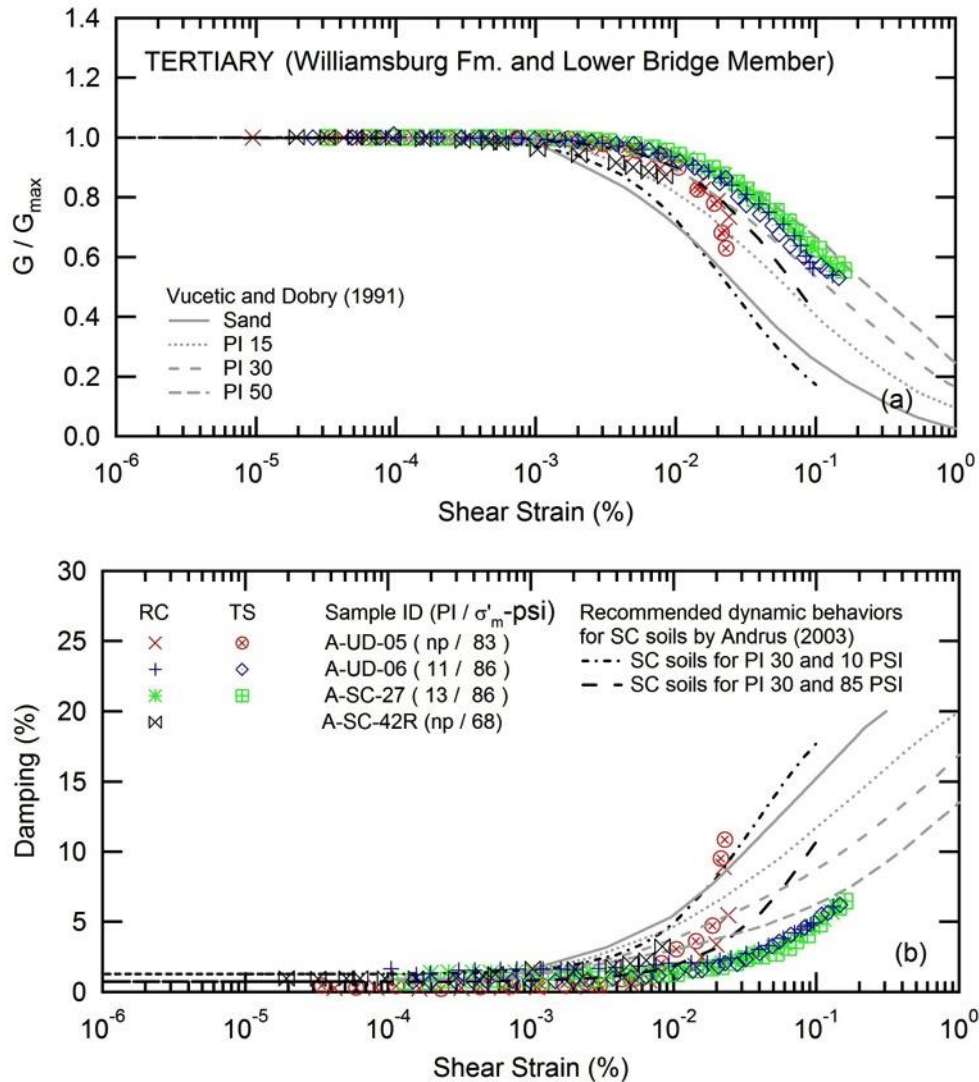


**Figure 4.26** Dynamic Properties of Tertiary Age Soils: (a)  $G/G_{max}$  Curves, and (b) Damping Curves

For the Cretaceous age deposits, the results are compiled from a total of 12 soil samples and 13 rock samples as presented in Fig. 4.27. It is interesting to observe that the  $G/G_{max}$  curves from some of the rock samples started to degrade at lower strains than the soil samples. Overall, the results are plotted within the predicted curves by Vucetic and Dobry (1991) for PI between 30 to 100; hence, the results aligned with curves for a range of PI that was higher than the PI of these samples. Again, there was no clear trend for the effect of plasticity on both  $G/G_{max}$  and  $D$  for the soil samples tested herein. Rock samples appeared to behave more nonlinearly than soil samples. In general, results for  $D_{min}$  were higher than the prediction by Vucetic and Dobry (1991) and similar to the results for Quaternary and Tertiary age groups; the rate of increasing in damping was

higher at higher-strain levels. There was no prediction for Cretaceous age soil according to Andrus et al. (2003), therefore this set of data can be used to improve and expand the SCDOT database for older age soils.

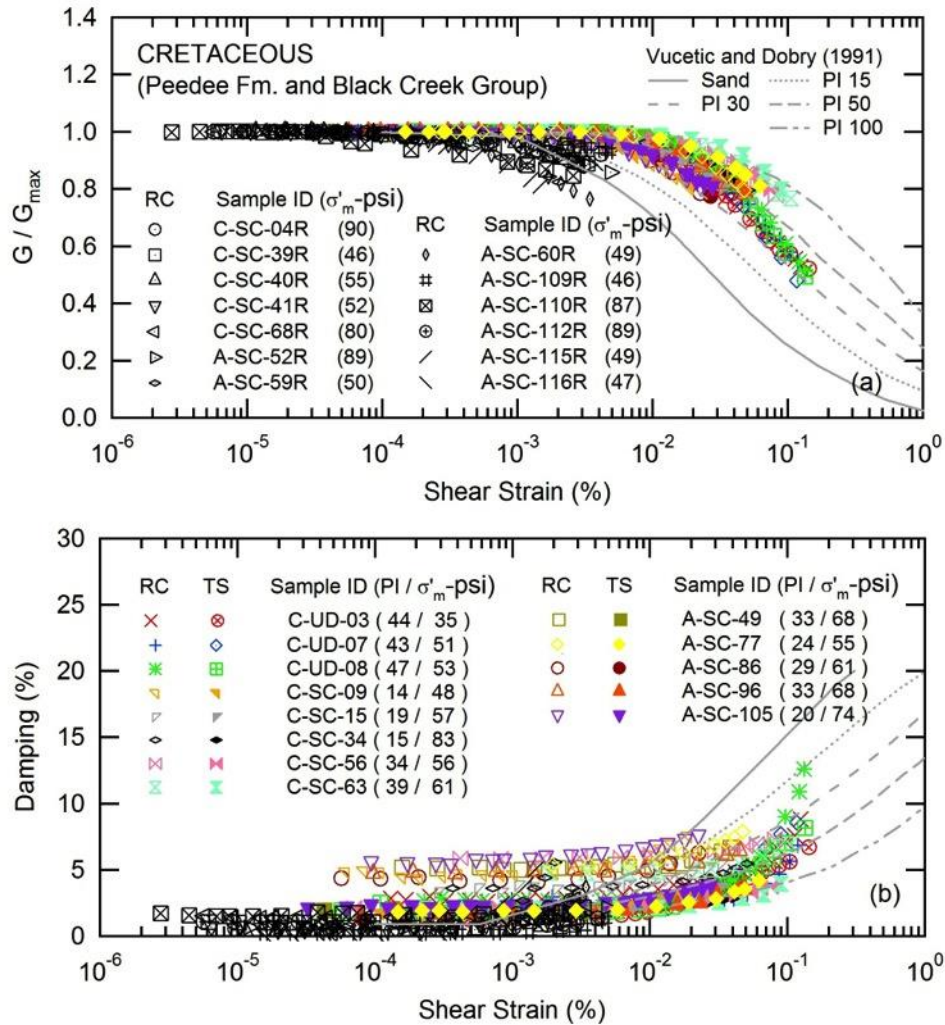


**Figure 4.27** Dynamic Properties of Cretaceous Age Soils: (a)  $G/G_{max}$  Curves, and (b) Damping Curves

#### 4.4.3.4. Statistical Analysis of Predictive $G/G_{max}$ and Damping Curves

As mentioned in the previous section, the predictive  $G/G_{max}$  and damping curves proposed by Andrus et al. (2003) matched only some of the results for the samples of Quaternary and Tertiary age that were tested in this study. Furthermore, Andrus et al. (2003) did not develop predictive curves for the Cretaceous age, of which the majority of the samples tested in this study were from. Since the samples in this study were taken from different locations and geologic formations than those used by Andrus et al. (2003), new predictive curves were developed and assessed for the

new set of data obtained in this study. The same approach of Andrus et al. (2003) was utilized for this effort.

In accordance to the Andrus et al. (2003) procedure, only TS results for soils are used to minimize frequency effects on damping. It is noted that the  $G/G_{\max}$  curves for RC and TS tests for soils are relatively close but the low-strain damping for TS tests are lower. For rock samples, RC test results are used because TS test results are not available. The procedure is described below.

The modified hyperbolic model (Stokoe et al. 1999 and Darendeli 2001) was proposed for the  $G/G_{\max}$  curves as:

$$\frac{G}{G_{\max}} = \frac{1}{1 + \left(\frac{\gamma}{\gamma_r}\right)^\alpha} \quad (4.1)$$

where  $G$  is the shear modulus,  $G_{\max}$  is the low-strain shear modulus,  $\gamma$  is the shear strain,  $\gamma_r$  is the reference strain, and  $\alpha$  is the curvature coefficient. Curve fitting function parameters ( $\gamma_r$  and  $\alpha$ ) were obtained from the  $G/G_{\max}$  curves. The reference strain was corrected for the effect of confinement using the following equation.

$$\gamma_r = \gamma_{r1} (\sigma'_m / P_a)^{k_\gamma} \quad (4.2)$$

where  $\sigma'_m$  is the mean effective confining stress in units of psi,  $P_a$  is a reference pressure of 14.5 psi, and  $k_\gamma$  is an exponent that varies with geologic formation and PI for shear modulus. It is noted that Andrus et al. (2003) uses  $k$  instead of  $k_\gamma$ .

To model the damping curves in relation to  $G/G_{\max}$ , the quadratic polynomial function accounting for the corresponding  $G/G_{\max}$  function proposed by Andrus et al (2003) was adopted and presented as:

$$D - D_{\min} = A \left(G/G_{\max}\right)^2 + B \left(G/G_{\max}\right) + C \quad (4.3)$$

where  $D$  is the damping,  $D_{\min}$  is the low-strain damping, and  $A$ ,  $B$ , and  $C$  are curve fitting parameters. Andrus et al. (2003) proposed  $A = 12.2$ ,  $B = -34.2$  and  $C = 22$  for  $R^2 = 0.785-0.960$  based on data from the Savannah River Site and Charleston (see Figure 2.2).

In this study, soil and rock samples from Sites A and B were from the Quaternary (Ten Mile Hill and Penholoway alloformation), Tertiary (upper soil and Williamsburg Formation and Lower Bridge Member) and Cretaceous (Peedee Formation and Black Creek Group) age groups. Curve fitting was performed resulting in the parameters:  $A = 14.92$ ,  $B = -35.99$ , and  $C = 21.34$  for  $R^2 = 0.789$  for soil, and parameters:  $A = 25.65$ ,  $B = -61.92$ , and  $C = 36.40$  for  $R^2 = 0.611$  for rock.

Furthermore, the  $D_{\min}$  was corrected for the effect of confinement similar to  $\gamma_r$ , by using:

$$D_{\min} = D_{\min 1}(\sigma'_m/P_a)^{-k_D/2} \quad (4.4)$$

where  $k_D$  is an exponent for damping that varies with geologic formation and PI according to Andrus et al. (2003). It is noted that Andrus et al. (2003) assumed  $k = k_\gamma = k_D$ .  $D_{\min 1}$  is the low-strain damping at  $\sigma'_m$  of 14.5 psi presented as:

$$D_{\min 1} = a(\text{PI})+b \quad (4.5)$$

where  $a$  and  $b$  are fitting parameters.

Curve fitting was performed to obtain 5 different model parameters:  $\alpha$ ,  $\gamma_{r1}$ ,  $k_\gamma$ ,  $k_D$ , and  $D_{\min 1}$ . The model parameters and  $R^2$  are presented in Tables 4.7-4.9 as a function of PI for each geologic unit. It is noted that the results from curve fitting using data for all soils in each geologic unit is also presented for a comparison. Statistical analyses of the curve fitting are presented in Appendix G. Overall, the  $R^2$  values for  $k_\gamma$  vary from 0.24 - 0.83 and the  $R^2$  values for  $k_D$  vary from 0.09 – 0.81 for soils. When data from the same age group are combined for all soils, the  $R^2$  values become lower. In addition, the  $R^2$  values for rocks are very low (0.006-0.383). No clear trend was observed for the curve fitting parameters indicating that the dynamic behaviors of these samples are not dependent on PI and/or geologic group. Based on the visual observation and geological logging information of these samples, cementation could be one major factor affecting the dynamic soil properties. As mentioned in Section 4.4.3.3, further quantification of cementation (e.g. by weight) and qualitative evaluation (e.g. types and bonding characteristics) could improve understanding of the sample behavior. However, such studies were outside the scope of this project and thus, findings remain inconclusive.

**Table 4.7** Model Parameters for Quaternary Deposit (Ten Mile Hill and Penholoway Formation)

Geologic Unit	QUATERNARY (Ten Mile Hill Formation and Penholoway alloformation)							
Age	2.6 - 0.01 MYA							
PI	Non-Plastic	1 -10	11 - 20	21 - 30	31-40	41-50	All Soils	Rock
$\gamma_{r1}$ (%)	0.035	-	-	0.130	-	-	0.041	-
$k_{\gamma}$	0.477	-	-	0.575	-	-	0.221	-
$R^{2,*}$	0.211	-	-	0.589	-	-	0.048	-
$D_{min1}$ (%)	0.779	-	-	1.374	-	-	0.845	-
$k_D$	0.740	-	-	0.680	-	-	0.960	-
$R^{2,**}$	0.616	-	-	0.361	-	-	0.542	-
$\alpha$	1.118	-	-	1.237	-	-	1.165	-
No. of Sample	3	-	-	2	-	-	5	-

$R^{2,*}$  is a result of curve fitting in Eq. 4.2,  $R^{2,**}$  is a result of curve fitting in Eq. 4.4.

**Table 4.8** Model Parameters for Tertiary Deposit (Williamsburg Formation and Lower Bridge Member)

Geologic Unit	TERTIARY (Williamsburg Formation and Lower Bridge Member)							
Age	58.0 - 56.0 MYA							
PI	Non-Plastic	1 -10	11 - 20	21 - 30	31-40	41-50	All Soils	Rock*
$\gamma_{r1}$ (%)	0.015	-	0.058	-	-	-	0.035	-
$k_{\gamma}$	0.647	-	0.552	-	-	-	0.619	-
$R^{2,*}$	0.891	-	0.831	-	-	-	0.249	-
$D_{min1}$ (%)	0.572	-	1.418	-	-	-	1.023	-
$k_D$	0.272	-	0.634	-	-	-	0.472	-
$R^{2,**}$	0.810	-	0.928	-	-	-	0.131	-
$\alpha$	1.300	-	1.065	-	-	-	1.143	-
No. of Sample	1	-	2	-	-	-	3	-

$R^{2,*}$  is a result of curve fitting for Eq. 4.2,  $R^{2,**}$  is a result of curve fitting for Eq. 4.4, \*the rock data is not included as there is only one sample in this age group.

**Table 4.9** Model Parameters for Cretaceous Deposit (Peedee Formation and Black Creek Group)

Geologic Unit	CRETACEOUS (Peedee Formation and Black Creek Group)							
Age (MYA)	83.6 - 66.0 MYA							
PI	Non-Plastic	1 -10	11 - 20	21 - 30	31-40	41-50	All Soils	Rock***
$\gamma_{rl}$ (%)	-	-	0.080	0.049	0.062	0.086	0.078	0.038
$k_{\gamma}$	-	-	0.364	0.422	0.794	0.243	0.461	0.163
$R^{2,*}$	-	-	0.578	0.677	0.572	0.540	0.447	0.006
$D_{min1}$ (%)	-	-	2.224	2.087	2.080	1.862	1.978	0.156
$k_D$	-	-	0.220	0.272	0.130	0.086	0.090	-1.833
$R^{2,**}$	-	-	0.312	0.113	0.089	0.014	0.416	0.383
$\alpha$	-	-	1.042	1.252	1.150	1.290	1.183	0.782
No. of Sample	-	-	4	2	4	3	13	13

$R^{2,*}$  is a result of curve fitting for Eq. 4.2,  $R^{2,**}$  is a result of curve fitting for Eq. 4.4, \*\*\*only RC test was performed on rock sample.

Figs. 4.28 to 4.30 show examples of the predicted  $G/G_{max}$  and damping curves for the confining pressure of 14.5 psi. Due to limited data for the Quaternary and Tertiary age groups, it is recommended that lower bound and upper bound curves be used for the site response analysis for these groups. For the Cretaceous group, the effects of PI are not clearly observed, but the  $G/G_{max}$  and D curves for all samples fall within a narrow range and it is suggested that the average curves be used for the site response analysis. For the rock samples, the  $G/G_{max}$  curve degraded at much lower strains than the soil samples. This indicates that the rock may be stiff but brittle. If thick layers of soft rock (or highly cemented soil) are present at a site, it is recommended that RC and TS tests be performed to verify the behavior at medium to high strains. The damping curve for rock samples is observed to be lower than soils. Furthermore, it is important to note that the soil and rock curves were developed for strains up to  $10^{-1}\%$  and  $10^{-2}\%$ , respectively; therefore, extrapolation beyond these strain levels should be performed with caution.

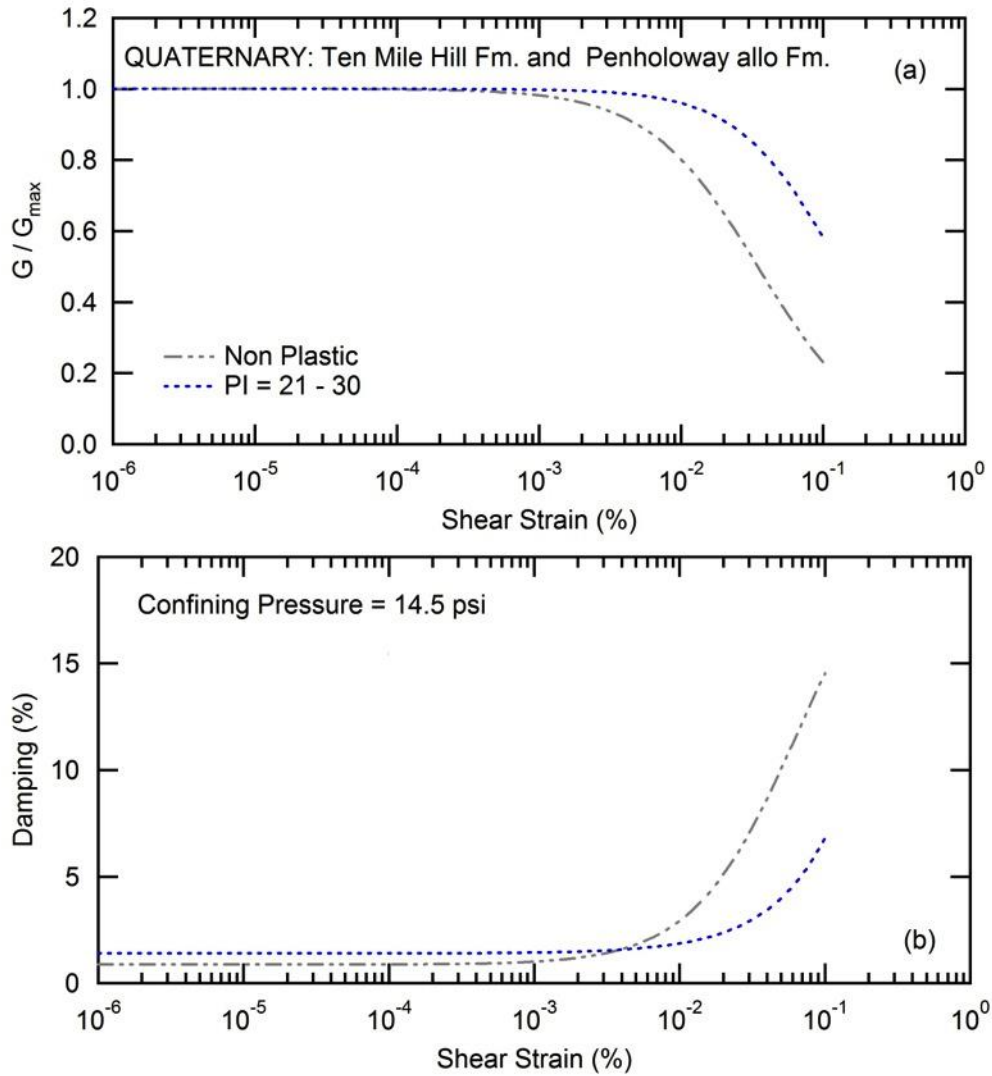


**Figure 4.28** (a)  $G/G_{max}$  Curves, and (b) Damping Curves Generated from Predictive Model for Quaternary Age Soils: Ten Mile Hill Formation and Penholoway Alloformation

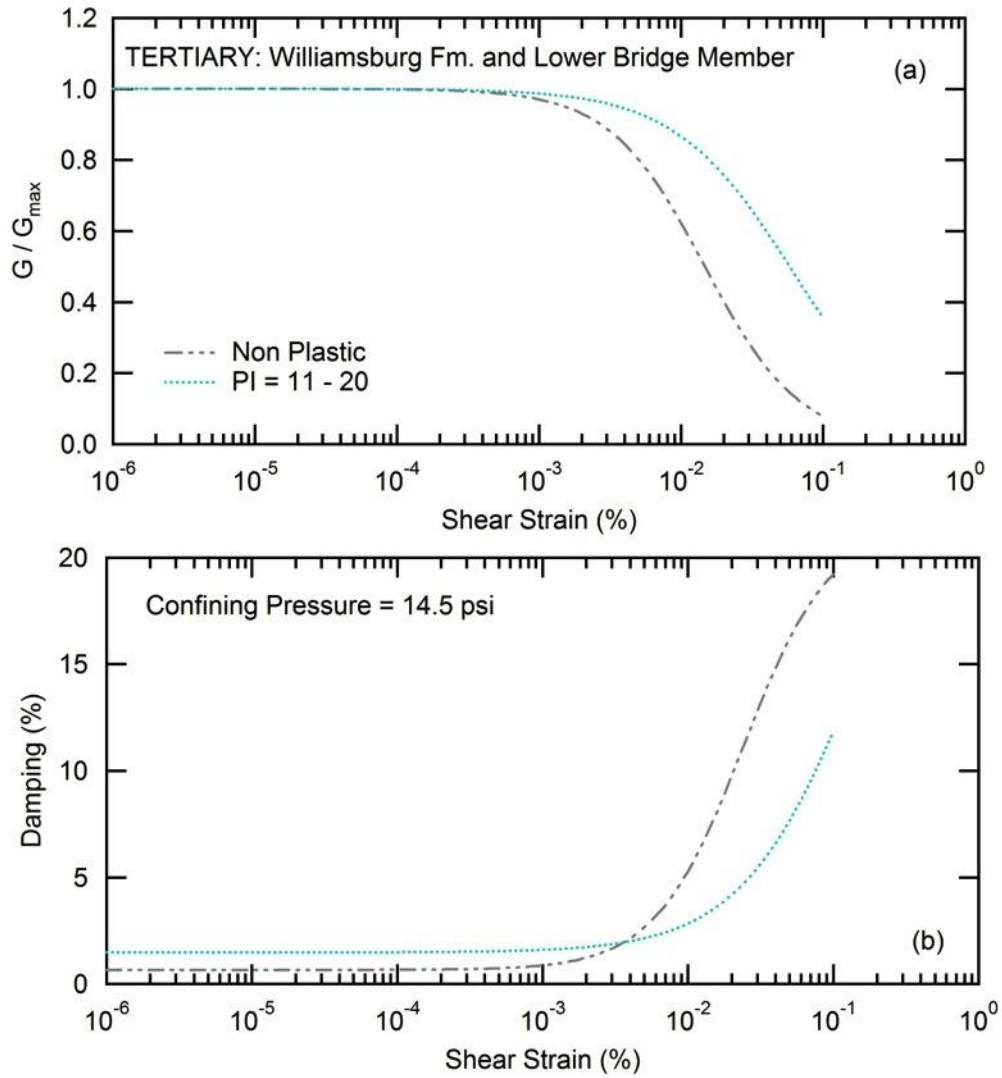


**Figure 4.29** (a)  $G/G_{max}$  Curves, and (b) Damping Curves Generated from Predictive Model for Tertiary Age Soils: Williams Burg Formation and Lower Bridge Member

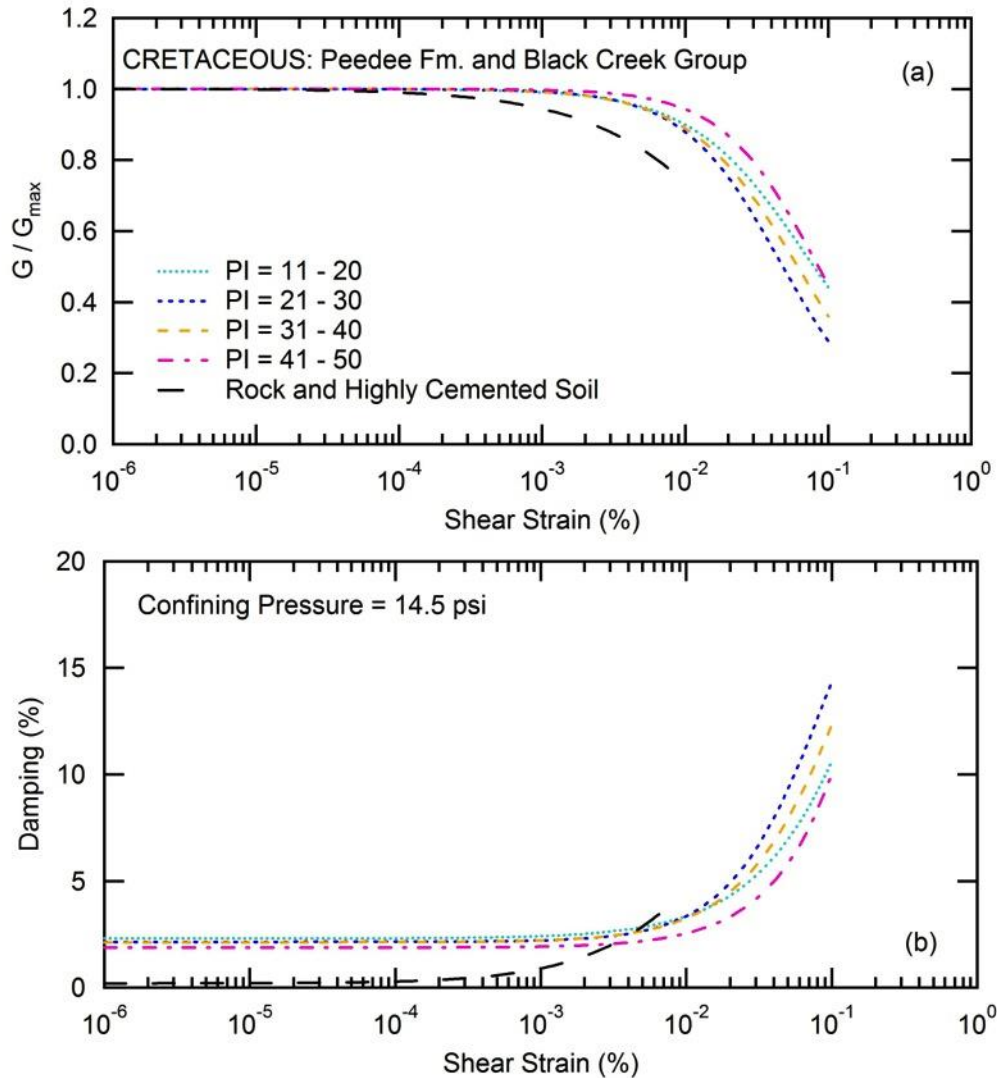


**Figure 4.30** (a)  $G/G_{max}$  Curves, and (b) Damping Curves Generated from Predictive Model for Cretaceous Age Soils: Peedee Formation and Black Creek Group

The effect of soil plasticity on damping at low-strains ( $D_{min}$ ) for the Quaternary, Tertiary and Cretaceous age soils are presented with the relations developed by Andrus et al. (2003) in Fig. 4.31. Results from this study (shown in solid symbols) were limited to PI values up to approximately 50; whereas, Andrus et al. (2003) had data up to 120. Low-strain damping for both geologic ages showed small increases as the PI increased. The rate of increase for the relationship for Tertiary age soils tested in this study was comparable with the trend proposed by Andrus et al. (2003). However, the new set of data generated for Cretaceous age deposits showed less variation with PI, and damping values were higher than Tertiary, Pleistocene, and Holocene age groups. It is important to understand that the majority of the data utilized by Andrus et al. (2003) came from tests performed on soil samples obtained from the Savannah River site. Although these samples

may be from the same or comparable geologic age, the characteristics and behavior of different deposits and formations can be vastly different. For example, sediments of the Peedee Formation may have been deposited in fluvial to delta-plain environments in the western part of the state; whereas, during the same time period, were deposited in shelf environments on the eastern side. The Peedee Formation at Sites A and B consists of a very fine- to coarse-grained, poorly sorted, massive calcareous clayey sands that are rich in shell and nanofossils fragments and with trace amounts of mica, whereas the Peedee Formation at the Savannah River site consists of light-colored fine- to coarse-grained quartz sand and oxidized kaolinite clay (Gellici 2019, Self-trail et al. 2002, Christopher and Prowell 2002, and Fallaw and Price 1995). This information supports the findings in this study that PI and geologic age alone are not dominant factors affecting the dynamic soil properties for older soil deposits, particularly for those samples with cementation. It is highly recommended that the SCDOT continue to collect more data and conduct further detailed geotechnical and geological investigations to characterize soils and rocks particularly for Tertiary and Cretaceous age deposits.

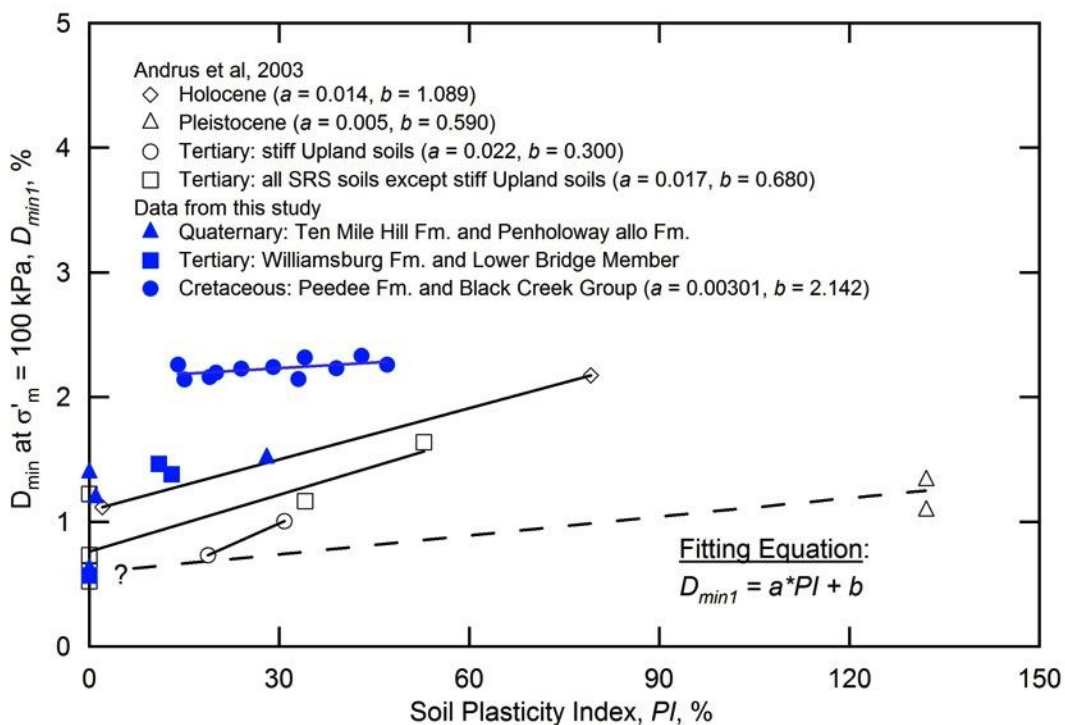


**Figure 4.31** Variation of  $D_{min}$  with PI for Soils of Different Geological Ages (after Andrus et al. 2003)

## 5. Conclusion, Recommendations, Implementation, and Future Research Needed

---

### 5.1. Conclusions

This research presents a study to obtain comprehensive field and laboratory measurements of shear wave velocity and dynamic soil properties for two sites in the South Carolina Coastal Plain: Site A is located near Conway in Horry County and Site B is located in Andrews in Williamsburg County. Geotechnical borings were drilled to depths of 505 and 615 ft for Sites A and B, respectively. Shear wave velocity profiles were generated using P-S suspension logging, FWS logging, combined MASW-SASW, and combined MASW-MAM methods. The profiles using P-S suspension logging were obtained to a depth of 470 ft for Site A and a depth of 600 ft for Site B. Profiles to a depth of 220 ft were obtained from the MASW-SASW method for both sites. For the combined MASW-MAM method, profiles were obtained to a depth 4921 ft for Site A and a depth of 2625 ft for Site B. Overall, the average shear wave velocities obtained from the surface methods at the top 200 ft were lower than that of the P-S suspension logging data. This resulted in a different NEHRP site class when using the average  $V_s$  values in the top 100 ft for Site A, but not site B. The P-S suspension logging provided detailed characteristics of the soil profile within borehole(s) and the results agreed with the visual observation of samples. However, the P-S suspension logging method was not capable of measuring  $V_s$  at very shallow depths (approximately 6-11 ft in this study) and did not provide the depth of the B-C boundary as the boundary was below the bottom of each borehole. Both non-invasive surface methods were performed independently with different teams and these results were in agreement within the top 220 ft where the MASW-SASW results can be compared. The MASW-MAM method is a unique method utilizing passive ambient wave sources and specialized sensors that allows deep profiling and identified an estimated depth to the B-C boundary of 580 ft for Site A and 1343 ft for Site B. Results from both surface methods do show that spatial variation of both sites are high, especially for Site A. While the use of surface wave methods may be more attractive for site investigation as they are relatively lower cost compared to borehole methods, accurate results from the surface wave methods require geological and geotechnical knowledge of the site to effectively perform data processing. Since these methods are not direct measurements, the best representative  $V_s$  profile for each site relied on the experience and skill of the data analysts obtained from utilizing these methods at sites in South Carolina as well as other parts of the country. Furthermore, the  $V_s$  profiles from the surface wave methods represent the average profiles over a large volume of soil. Conversely, the  $V_s$  profiles from the borehole methods represent localized profiles within the tested borehole.

Visual observation of samples collected from both sites showed that materials were highly variable with frequent transitions between soil-like to rock-like material. In the Tertiary and Cretaceous deposits, materials with sand or clay structures with high variation of cementation and shell fragments were found. Highly cemented sand or clay (sandstone or claystone) with thickness

varying from a few inches to several feet was observed at several locations through the entire depth of the soil profiles investigated. The locations of these materials corresponded with the high shear wave velocities observed in the P-S logging profiles.

Resonant column and torsional shear testing allowed observation of shear modulus and damping behavior of material for a wide range of strains. A total of 35 soil and rock samples were tested and several factors affecting the small strain dynamic properties were investigated. Overall, it was found that the dynamic behavior aligned with the generic empirical prediction suggested by Vucetic and Dobry (1991) for a range of PI that was higher than the PI of these samples. Relatively high  $D_{\min}$  values were observed and the rate of increasing in damping with strains was higher than the Vucetic and Dobry (1991) prediction. Damping was significantly affected by testing frequency therefore; results from the more common RC test obtained using high frequencies should be compared with results from TS tests at low frequencies. The effect of soil plasticity on the shear modulus reduction and damping curves for soils with different geological age groups was evaluated and found to have a smaller effect than predictions by previous studies for uncemented soils. The shear modulus of rock and highly cemented soils degraded at lower strains than that of soil. It was found that  $D_{\min}$  slightly increased with soil plasticity for the Cretaceous soil deposits. The effect of soil plasticity on  $D_{\min}$  was much less than the prediction by Andrus et al. (2003). Overall, the results from the laboratory testing program suggest that that plasticity index and geologic age alone are not dominant factors affecting the dynamic soil properties for older soil deposits. It is hypothesized that cementation is a possible dominant factor, however detailed evaluation of cementation in relation with shear modulus and damping is beyond the scope of this study.

## 5.2. Recommendations

Data from this study can be used directly to perform site-specific site response analysis for Site A and Site B with the recommendation to perform sensitivity analyses to account for the uncertainty in the following:

1. ***Variation of  $V_s$  profiles obtained from a specific method.*** This uncertainty is related to variability in data analysis utilized for different method of testing. For example, several possible  $V_s$  models can be obtained from each of the surface geophysical methods. This is because the data analysis depends on knowledge of the geological and geotechnical information at a site and data interpretation performed by data analysts. Sensitivity analysis should be conducted to account for the range of possible profiles.
2. ***Variation of  $V_s$  profiles obtained from different methods.*** High spatial variation was observed, especially at Site A. A lower average  $V_s$  was observed for the top 200 ft obtained by the surface geophysical methods compared to that of the P-S suspension logging method. Sensitivity analysis should be conducted to account for the  $V_s$  profiles from different methods of testing.

3. ***Depth to the B-C boundary.*** The P-S logging method did not provide  $V_s$  profiles beyond the bottom of the borehole at Site A and Site B, and the depth to the B-C boundary was not identified at either site. The depth and characteristics of  $V_s$  profiles from the bottom of the borehole to the projected B-C boundary should be studied as part of the sensitivity analysis.
4. ***Variation of dynamic behaviors (shear modulus and damping curves) of deep sediment.*** The data generated in this report can be readily used for the sites investigated herein. However, the data are limited to depths where the samples were obtained. Use of the shear modulus and damping curves for other depths and other sites requires careful interpretation of soil boring logs. Soil types and index properties should be carefully evaluated to use predictive curves.
5. ***Interbedded rock and cemented layers.*** The presence of rock layers such as limestone at Site B and/or relative thin layers of highly cemented soils should be evaluated to assess their impact on the site response analysis.

For future deep borehole investigations, it is recommended that samples of rock and cemented soils be routinely collected from sites and tested to the extent possible. Laboratory testing should be performed to determine the dynamic behaviors using both resonant column and torsional shear testing for a wide range of strains in order to evaluate the effects of test frequency on low-strain damping.

Based on the results herein, the predictive curves for shear modulus and damping curves suggested by Vucetic and Dobry (1991) and Andrus et al. (2003) can be used for Quaternary deposits. However, these equations are not recommended for Tertiary and Cretaceous deposits because this study showed that soil plasticity and geologic age alone are not dominant factors affecting the dynamic soil properties for older soil deposits, particularly for those samples with cementation.

### **5.3. Implementation Plan**

The following data were obtained in this project and are available for immediate implementation:

1. Soil boring logs for Site A in Conway and Site B in Andrews are summarized in Figs. 4.1 and 4.2, respectively. Additional details are available in Appendix A.
2. Shear wave velocity profiles developed from different methods of testing for each site are shown in Figs. 4.6 and 4.9. Details of the methodology and data analysis to develop each profile are available in Appendices A, B, and C for P-S logging method and MASW-SASW methods, MASW-MAM method and FWS method, respectively. Comparisons of these profiles along with the detailed discussions are included in this report in Section 4.3.
3. Detailed geological information and visual observation of soils and rocks are available in this report and Appendix D.
4. Soil index properties data and soil classifications are available in Appendix E

5. Shear modulus and damping curves and model parameters for the development of these curves are provided in this report in Section 4.4 and data is included in Appendix F. This information can be used for site response analyses.

#### **5.4. Future Research Needed**

Based on the findings of this study, the following research needs were identified:

1. This study makes clear that empirical relationships based on soil plasticity and geologic age do not provide an accurate prediction of the shear modulus and damping curves. Impacts of cemented layers on site response analyses are not clear and should be examined. Importantly, detailed evaluation of cementation and other factors in relation with shear modulus and damping should be investigated in order to develop more accurate predictive models for SCDOT engineers and contractors.
2. Given the high variability in parameters observed within and between the sites studied herein, additional deep  $V_s$  profiles, with extensive sampling and laboratory testing to obtain shear modulus and damping curves, need to be obtained for more locations in the South Carolina Coastal Plain.
3. The surface wave methods show promising results, but require further studies to examine the testing procedures, data analyses protocols, and impacts on the results of site response analyses.

## References

---

- Andrus, R. D., Hayati, H., & Mohanan, N. P. (2009). Correcting Liquefaction Resistance for Aged Sands Using Measured to Estimated Velocity Ratio. *Journal of Geotechnical and Geoenvironmental Engineering*, 135(6), 735-744.
- Andrus, R. D., Ravichandran, N., Aboye, S. A., Bhuiyan, A. H., & Martin, J. R. (2014). Seismic Site Coefficients and Acceleration Design Response Spectra Based on Conditions in South Carolina (No. FHWA-SC-14-02). South Carolina. Dept. of Transportation.
- Andrus, R. D., Zhang, J., Ellis, B. S., & Juang, C. H. (2003). Guide for Estimating the Dynamic Properties of South Carolina Soils for Ground Response Analysis (No. FHWA-SC-03-07,).
- Bonnefoy-Claudet, S. (2004). Nature du bruit de fond sismique: implications pour les études des effets de site (Doctoral dissertation, Université Joseph Fourier (Grenoble)).
- Camp, W.M. (2018) Personal Communication. 17 April.
- Chapman, M. C., & Talwani, P. (2006). Seismic Hazard Mapping for Bridge and Highway Design in South Carolina (No. FHWA-SC-06-09).
- Chapman, M. C., Martin, J. R., Olgun, C. G., & Beale, J. N. (2006). Site-Response Models for Charleston, South Carolina, and Vicinity Developed from Shallow Geotechnical Investigations. *Bulletin of the Seismological Society of America*, 96(2), 467-489.
- Christopher, R. A., & Prowell, D. C. (2002). A Palynological Biozonation for the Maastrichtian Stage (Upper Cretaceous) of South Carolina, USA. *Cretaceous Research*, 23(6), 639-669.
- Darendeli, M. B. (2001). Development of a New Family of Normalized Modulus Reduction and Material Damping Curves. Ph. D. Dissertation, The University of Texas at Austin.
- Doar, R. W. (2018) Personal Communication. 12 March.
- F&ME Consultants (2017). Geotechnical Base Line Report US 21 (Sea Island Parkway) Bridge over Harbor River Beaufort County, South Carolina, SCDOT Project ID: P026862.
- Fallow, W. C., & Price, V. (1995). Stratigraphy of the Savannah River Site and Vicinity. *Southeastern Geology*, 35(1), 21-58.
- Gellici, J. (2019) Personal Communication. 31 May.

GEOvision (2008). P-S Suspension Logging Borehole G-B-1, I-73 Project Little Pee Dee River near Mullins, South Carolina, Report 8451-01.

GEOvision (2010a). Suspension PS velocities Boring GEI-4 and GEI-5 Back Gate Bridge, Murrells Inlet, SC, Report 9459-01.

Hwang, S. K. (1997). Investigation of the Dynamic Properties of Natural Soils. Ph. D. Dissertation, The University of Texas at Austin.

Isenhower, W. M. (1979). Torsional Simple Shear/Resonant Column Properties of San Francisco Bay Mud. Ph. D. Dissertation, The University of Texas at Austin.

Ishibashi, I., & Zhang, X. (1993). Unified Dynamic Shear Moduli and Damping Ratios of Sand and Clay. *Soils and Foundations*, 33(1), 182-191.

Jeon, S. Y. (2008). Dynamic and Cyclic Properties in Shear of Tuff Specimens from Yucca Mountain, Nevada, Ph. D. Dissertation, The University of Texas at Austin.

Kavazanjian Jr, E., Matasović, N., Hadj-Hamou, T., & Sabatini, P. J. (1997). Design Guidance: Geotechnical Earthquake Engineering for Highways, Volume I, Design Principles. Geotechnical Engineering Circular No. 3, Report FHWA-SA-97, 76.

Kim, D. S. (1991). Deformational Characteristics of Soils at Small to Intermediate Strains from Cyclic Test. Ph. D. Dissertation, The University of Texas at Austin.

Kimball, C. V., & Marzetta, T. L. (1984). Semblance Processing of Borehole Acoustic Array Data. *Geophysics*, 49(3), 274-281.

Lachetl, C., & Bard, P. Y. (1994). Numerical and Theoretical Investigations on the Possibilities and Limitations of Nakamura's Technique. *Journal of Physics of the Earth*, 42(5), 377-397.

Lermo, J., & Chávez-García, F. J. (1993). Site Effect Evaluation Using Spectral Ratios with Only One Station. *Bulletin of the Seismological Society of America*, 83(5), 1574-1594.

Lodde, P. F. (1982). Shear Moduli and Material Damping of San Francisco Bay Mud. MS Thesis.

Minear, J. W. (1986). Full Wave Sonic Logging—a Brief Perspective: Transactions of the Society of Professional Well Log Analysts 27th Annual Logging Symposium. Paper AAA.

Ni, S. H. (1987). Dynamic Properties of Sand under True Triaxial Stress States from Resonant Column/Torsional Shear Tests. Ph. D. Dissertation, The University of Texas at Austin.

- Nystrom, P. G., & Maybin, A. H. (2005). Generalized Geologic Map of South Carolina 2005. South Carolina State Documents Depository.
- Rix, G. J., & Leipski, E. A. (1991). Accuracy and Resolution of Surface Wave Inversion in Geotechnical Special Publication no 29. Recent Advances in Instrumentation, Data Acquisition and Testing in Soil Dynamics, 17-32.
- Rix, G. J., & Meng, J. (2005). A Nonresonance Method for Measuring Dynamic Soil Properties. *Geotech. Test. J.*, 281, 1–8.
- Ruttithivaphanich P. & Sasanakul I. (2019). Frequency Effects on Low-Strain Shear Modulus and Damping for Natural Clays and Silts. *Geo-Congress 2019, Philadelphia, Pennsylvania.*
- S&ME (2015). Geotechnical Base Line Report Port Access Road North Charleston, South Carolina, S&ME Project No. 1131-08-554.
- Sasanakul, I. (2005). Development of an Electromagnetic and Mechanical Model for a Resonant Column and Torsional Shear Testing for Soils. Ph. D. Dissertation, Utah State University.
- Sasanakul, I., & Bay, J. (2008), Stress Integration Approach in Resonant Column and Torsional Shear Testing for Soils, *ASCE Journal of Geotechnical and Geoenvironmental Engineering*, Vol. 134, No. 12, December, pp. 1757-1762.
- Sasanakul, I., & Bay, J. A. (2010). Calibration of Equipment Damping in a Resonant Column and Torsional Shear Testing Device. *Geotechnical Testing Journal*, 33(5), 363-374.
- Seed, H. B., & Idriss, I. M. (1981). Evaluation of Liquefaction Potential Sand Deposits Based on Observation of Performance in Previous Earthquakes. In *ASCE National Convention (MO)*, pp. 481-544.
- Seed, H. B., Wong, R. T., Idriss, I. M., & Tokimatsu, K. (1986). Moduli and Damping Factors for Dynamic Analyses of Cohesionless Soils. *Journal of Geotechnical Engineering*, 112(11), 1016-1032.
- Self-Trail, J. M., Christopher, R. A., & Prowell, D. C. (2002). Evidence for Large-Scale Reworking of Campanian Sediments into the Upper Maastrichtian Peedee Formation at Burches Ferry, South Carolina. *Southeastern Geology*, 41(3), 145-158.
- SESAME European project, (2004). Guidelines for the Implementation of the H/V Spectral Ratio Technique on Ambient Vibrations: Measurements, Processing and Interpretation. Deliverable D23.12.

- Stokoe II KH, Wright GW, James AB, & Jose MR (1994) Characterization of Geotechnical Sites by SASW Method. In Woods, RD, Ed., Geophysical Characterization of Sites: Oxford Publ.
- Stokoe, K. H., Darendeli, M. B., Andrus, R. D., & Brown, L. T. (1999). Dynamic Soil Properties: Laboratory, Field and Correlation Studies. In Proceedings of the 2nd International Conference on Earthquake Geotechnical Engineering, pp. 811-846.
- Stokoe, K. H., Hwang, S. K., Lee, J. K., & Andrus, R. D. (1995). Effects of Various Parameters on the Stiffness and Damping of Soils at Small to Medium Strains. Proceedings of the International Symposium, 12-14.
- Sun, J. I., Galesorkhi, R., & Seed, H. B. (1988). Dynamic Moduli and Damping Ratios for Cohesive Soils. Berkeley: Earthquake Engineering Research Center, University of California.
- Vucetic, M., & Dobry, R. (1991). Effect of Soil Plasticity on Cyclic Response. *Journal of Geotechnical Engineering*, 117(1), 89-107.
- Zhang, J., Andrus, R. D., Juang, C. H. (2005). Normalized Shear Modulus and Material Damping Ratio Relationships. *Journal of Geotechnical and Geoenvironmental Engineering*, 131(4), 453-464.
- Zhang, J., Andrus, R. D., Juang, C. H. (2008). Model Uncertainty in Normalized Shear Modulus and Damping Relationships. *Journal of Geotechnical and Geoenvironmental Engineering*, 134(1), 24-36.

# Appendix

---

## **Appendix A: Geotechnical Boring Logs, P-S Logging, and MASW-SASW Testing Results**

---

**Geotechnical Data Summary Report  
Deep Seismic Boreholes for the SCDOT  
Aynor and Andrews, South Carolina  
S&ME Project No. 1426-17-018**



Prepared for:  
**University of South Carolina**  
**Department of Civil and Environmental Engineering**  
**300 Main Street, C227**  
**Columbia, South Carolina 29208**

Prepared by:  
**S&ME, Inc.**  
**620 Wando Park Boulevard**  
**Mt. Pleasant, South Carolina 29464**

**June 29, 2017**



June 29, 2017

Department of Civil and Environmental Engineering  
University of South Carolina  
300 Main Street, C227  
Columbia, South Carolina 29208

Attention: Prof. Inthuorn Sasanakul, PhD, P.E.

Reference: **Geotechnical Data Summary Report  
Deep Seismic Boreholes for the SCDOT**  
Aynor and Andrews, South Carolina  
S&ME Project No. 1413-16-153

Dear Prof. Sasanakul:

S&ME, Inc. (S&ME) is pleased to submit this Geotechnical Data Summary Report for the referenced project. Our services were performed in general accordance with our Proposal No. 14-1600392 REV2, dated June 20, 2016 and FDP Cost Reimbursement Research Subaward Agreement dated November 28, 2017. This data report presents a brief confirmation of our understanding of the project and a discussion of the field exploration program that was implemented.

We appreciate the opportunity to work with the University of South Carolina Department of Civil and Environmental Engineering by providing the geotechnical engineering and geophysical services for this project. Please contact us should any questions arise regarding the information in this data summary report or when further services are needed.

Sincerely,

**S&ME, Inc.**

Christopher Stryffeler P.E.  
Project Engineer  
[cstryffeler@smeinc.com](mailto:cstryffeler@smeinc.com)



William M. Camp, III, P.E., D.GE  
Technical Principal/Vice President  
[bcamp@smeinc.com](mailto:bcamp@smeinc.com)





## Table of Contents

<b>1.0</b>	<b>Project Information .....</b>	<b>2</b>
<b>2.0</b>	<b>Field Exploration Program.....</b>	<b>2</b>
2.1	Geotechnical and Borehole Geophysical Testing.....	2
2.1.1	<i>SPT Hammer Verification and Energy Measurements.....</i>	<i>4</i>
2.1.2	<i>Point A Detailed Narrative .....</i>	<i>5</i>
2.1.2.1	Boring B-CON .....	5
2.1.2.2	Boring B-CONa.....	6
2.1.2.3	Boring B-CONb.....	6
2.1.3	<i>Point B Detailed Narrative.....</i>	<i>7</i>
2.1.3.1	Boring B-FMG .....	7
2.1.3.2	Boring B-FMGa .....	7
2.2	Surface Wave Testing.....	7
<b>3.0</b>	<b>Site Conditions .....</b>	<b>8</b>
3.1	Surface Features.....	8
3.1.1	<i>Surface Features at Point A .....</i>	<i>8</i>
3.1.2	<i>Surface Features at Point B.....</i>	<i>8</i>
3.2	Area Geology.....	8
<b>4.0</b>	<b>Limitations of Report.....</b>	<b>9</b>

## Important Information about Your Geotechnical Engineering Report

### List of Tables

Table 2-1: Boring Summary .....	3
Table 2-2: SPT Hammer Verification and Energy Measurements.....	5

### Appendix

Appendix I: Figures.....	i
Appendix II: Geotechnical Testing Data.....	ii
Appendix III: Borehole Geophysical Testing Data.....	iii
Appendix IV: Surface Wave Testing Data.....	iv

## 1.0 Project Information

The University of South Carolina (USC) received a Request for Proposal (RFP) titled “Deep Soil Test Borings to Determine Shear Wave Velocities across South Carolina” in the spring of 2016 from the South Carolina Department of Transportation (SCDOT). The RFP included field services and laboratory services and USC asked S&ME to help coordinate the field services. The requested scope of field services included two deep soil test borings with Standard Penetration Testing (SPT) and split-barrel sampling, thin-walled tube sampling, and soil coring; and geophysical testing consisting of P-S suspension logging, gamma logging, spontaneous potential logging, and surface wave testing.

The RFP designated the general area for two deep soil test boring locations, designated as Point A and Point B. Point A was to be a 515-ft deep test boring performed near Conway, South Carolina and Point B was to be a 615-ft deep test boring performed near Andrews, South Carolina. Two specific test sites that could accommodate the drilling equipment and the surface wave testing were ultimately identified by USC and S&ME. The Point A or 515-ft deep site was located on SCDOT right-of-way at the end of Morgan Lane, north of Veterans Hwy/Conway Bypass/SC-22 in Aynor, South Carolina. The Point B or 615-ft deep site was located on private property adjacent to a cultivated field approximately a quarter of a mile west of County Line Road behind Farmers Grain & Milling, Inc. at 3167 County Line Road in Andrews, South Carolina.

Site Vicinity Plans (Figures 1, 2, and 4) and Boring Location Plans (Figures 3 and 5) showing the site locations and the approximate boring locations have been included in Appendix I.

## 2.0 Field Exploration Program

The field exploration program, which lasted from January 18 to March 10, 2017, included the performance of two sets of geotechnical borings with accompanying geophysical testing at the Point A and Point B sites. The set of borings at Point A consisted of the initial deep boring B-CON, and offset borings B-CONa, and B-CONb. The set of borings at Point B consisted of the deep boring B-FMG and an offset boring, B-FMGa.

An S&ME Geotechnical Professional provided supervision during all fieldwork. All borings were drilled by AE Drilling, Inc., the drilling subcontractor. Borings B-CON, B-CONa, B-FMG, and B-FMGa were drilled and sampled using an all-terrain vehicle (ATV) mounted CME 550X. Boring B-CONb was drilled using a truck mounted Schramm 450. All downhole and surface geophysical testing was performed by GEOVision, the geophysical subcontractor.

The following sections include a general overview of the field exploration followed by a more detailed narrative of the drilling and sampling activities. Additional information on the geophysical testing is included in the relevant GEOVision reports, which are included as appendices.

### 2.1 Geotechnical and Borehole Geophysical Testing

The geotechnical and borehole geophysical testing performed during this field exploration program included SPT and split-barrel sampling, thin-walled tube sampling, soil coring, P-S suspension logging, and induction/natural gamma logging. Table 2-1 summarizes the types of testing, dates, and depths associated with each boring:

**Table 2-1: Boring Summary**

Location	Boring Number	Type of Testing	Date(s)	Drill Rig	Depths (feet)	Date Grouted
Point A	B-CON	Split-Barrel Sampling	01/18 to 01/21/2017	CME 550X	0 to 118	02/05/2017
		Soil Coring	01/23 to 01/27/2017		119.2 to 502	
		Thin-Walled Tube Sampling	01/18 to 01/21/2017		10 to 109.5	
		P-S Suspension	01/28/2017		301.84 to 469.16	
		Induction/Natural Gamma			490 to 289	
	B-CONa	Thin-Walled Tube Sampling	02/03 to 02/05/2017		0 to 108.5	02/10/2017
	B-CONb	N/A <sup>A</sup>	02/07 to 02/10/2017	Schramm 450	0 to 315	03/10/2017
		P-S Suspension	02/27/2017		6.56 to 293.64	
Induction/Natural Gamma		309.90 to 4.75				
Point B	B-FMG	Split-Barrel Sampling	02/06/2017	CME 550X	0 to 20.7	02/27/2017
		Soil Coring	02/11 to 02/25		20.7 to 615	
		P-S Suspension	02/26/2017		13.12 to 597.11	
		Induction/Natural Gamma			609.75 to 4.55	
	B-FMGa	Thin-Walled Tube Sampling	03/07 to 03/09/2017		0 to 154	03/09/2017

<sup>A</sup> B-CONb was drilled to a depth of 315 feet to facilitate geophysical logging. No geotechnical logging was completed on this borehole.

The geotechnical borings were drilled using a combination of mud-rotary drilling (in general accordance with ASTM D5783) and wireline coring procedures (in general accordance with ASTM D2113). The mud-rotary tooling consisted of NWJ rods with a 4 7/8-in stepped drag bit. Drilling fluid consisting of water and bentonite and/or EZ-Mud drilling polymer was used for both mud-rotary drilling and wireline coring procedures. An approximate 6-inch diameter borehole was drilled to allow for insertion of the geophysical testing equipment. Split-barrel sampling and/or thin-walled tube sampling was performed continuously from the ground surface until hard materials were consistently encountered. Boring B-CONb was drilled using air-rotary drilling procedures (in general accordance with ASTM D5782) with a 10-inch diameter bit.

Split-barrel sampling was performed in general accordance with ASTM D 1586. In split-barrel sampling, a standard 2-in O.D split steel tube is driven into undisturbed soil at a select depth using a 140-lb hammer falling a distance of 30-in. As requested, "continuous" 2-foot interval sampling was performed. The number of blows required to advance the sampler each of the four 6-in intervals is recorded on the field logs. The number of blows recorded for the second and third intervals are then combined and recorded as the Standard Penetration Resistance (N-value). Field logging was performed in general accordance with ASTM D5434. The N-values<sup>1</sup> provide an indication of the relative density of coarse-grained soils and the consistency of fine-grained soils. As the split-barrel samples were collected, a Geotechnical Professional visually and manually classified the soil in general accordance with ASTM D2488 and the SCDOT Geotechnical Design Manual Version 1.1 (GDM). The samples were then sealed and labeled in

<sup>1</sup> The N-values and soil consistency on the boring logs have not been normalized for the specific hammer energy, and thus represent field values.

individual jars and packed for transport to USC. The N-values, field classification of the soils, and other related subsurface information for borings B-CON and B-FMG are presented in the Boring Logs included in Appendix II.

In addition to split-barrel sampling, thin-walled tube sampling was performed in general accordance with ASTM D1587/D1587M. We obtained ten thin-walled samples from boring B-CON, eleven samples from boring B-CONa, and six samples from B-FMGa in strata selected by USC and S&ME. Thin-walled tube sample depths are discussed in further detail in Section 2.1.1.2 and 2.1.1.3. Both Shelby-tube samplers and pitcher-barrel samplers were used during this project. In Shelby-tube sampling, a 2-ft long, thin-walled steel tube with a sharp leading edge is pushed into undisturbed soil at a select depth in the borehole to obtain relatively undisturbed samples of cohesive soils. In cases where damage to the Shelby-tube sample was considered likely, a pitcher-barrel sampler was used to attempt the sample. A pitcher-barrel sampler consists of a spring-mounted, 2.5-ft long, thin-walled tube inner barrel with a rotating exterior cutting shoe/barrel. In softer materials, the spring extends the tip of the thin-walled tube beyond the cutting shoe while in stiffer materials, the spring is compressed resulting in the cutting shoe leading the thin-walled tube. The recovered tube samples were cleaned at each end, sealed with wax, capped, taped, and transported to USC in general accordance with ASTM D4220/D4220M.

Once hard material was consistently encountered, the mud-rotary tooling was replaced with soil coring tools. An H-sized core barrel was used. Coring was accomplished by advancing an outer steel casing with a rock carbide or diamond bit and an inner sample barrel that is locked into the drill string annulus. A triple-tube, split inner barrel wireline coring system was used in an effort to enhance core recovery. Once implemented, continuous core runs were conducted at 5-foot intervals. As the core samples were collected, a Geotechnical Professional visually and manually classified the soil in general accordance with ASTM D2488 and the GDM. The samples were then wrapped in cellophane and placed in polyurethane lined wooden boxes, which were then labeled and prepared for transport to USC. This procedure was continued until the borehole termination depth was reached. At the termination depth, the borehole was flushed until GEOVision was ready to begin logging at which point AE Drilling removed tooling and GEOVision commenced logging.

GEOVision performed the geophysical testing at Point A and Point B on January 28, February 26, and February 27, 2017. The purpose of this testing was to collect in-situ horizontal shear and compressional wave velocity measurements (P-S suspension logging), as well as long and short conductivity and natural gamma data (induction/natural gamma logging). The methods, procedures, results, and certifications for the borehole geophysical testing phase of this project are detailed in GEOVision Report 17016-01 rev 0 dated April 10, 2017. This report has been included in Appendix III.

Upon completion of the geotechnical and geophysical testing, the boreholes were grouted with a Portland cement/bentonite slurry. After completion of the field work, the split-barrel, thin-walled tube, and core samples were transported to USC in Columbia, South Carolina.

### *2.1.1 SPT Hammer Verification and Energy Measurements*

Prior to the start of this project, the SPT hammer efficiency on the drill rig was measured by S&ME in general accordance with ASTM D4633 with a PAX Pile Driving Analyzer™ (PDA). The PDA was used to record and interpret data from two piezoelectric accelerometers which were bolted to a 2-foot long NWJ drill rod internally instrumented with two strain transducers. The accelerometers and strain gages, which

are mounted on opposing axes near the middle of the instrumented rod, monitor acceleration and strain for each hammer blow.

The analyzer converts the data to velocities and forces, computing the maximum transferred hammer energies, driving forces, and stresses. All results are recorded and displayed in real time for each blow. The total drill rod length was 20 to 95 feet while obtaining energy measurements. The N-values during testing ranged from about 19 to 44 blows per foot (bpf).

The SPT hammer energy testing is summarized in the table below. It should be noted that the EFV method was used to determine the energy transferred to the drill rod, and this value was used to compute the transfer efficiency<sup>2</sup>.

**Table 2-2: SPT Hammer Verification and Energy Measurements**

Drilling Company	Drill Rig	Date	Hammer Type (Serial No.)	Hammer Weight <sup>A</sup>	Hammer Drop Height <sup>A</sup>	Rod Size	Average Efficiency
AE Drilling Services	CME 550X ATV	05/20/2016 - 05/23/2016	CME Automatic (SN 613)	139.6 lb	30.0 in	NWJ	91.5%

<sup>A</sup> In accordance with ASTM D1586, the hammer weight shall be 140 ± 2 lbs, and the drop height shall be 30 ± 1 in.

### 2.1.2 Point A Detailed Narrative

S&ME and AE Drilling mobilized to Point A on January 18, 2017. At this site, AE Drilling drilled and sampled three boreholes: borings B-CON, B-CONa, and B-CONb. The site remained active until March 10, 2017 when an upper standpipe was removed from boring B-CONb and the casing was grouted in-place with a Portland cement/bentonite slurry.

#### 2.1.2.1 Boring B-CON

Boring B-CON was drilled using a CME 550X all-terrain vehicle mounted drill rig from January 18 to January 27, 2017. From January 18 to 21, 2017, split-barrel sampling and thin-walled tube sampling were conducted "continuously" from the ground surface to a depth of 118 feet. Mud-rotary procedures were used to advance the borehole after each split-barrel or thin-walled sample. AE Drilling cleared 2 feet from the top of each split-barrel sample, and 3 feet from the top of each thin-walled sample. Thin-walled tube samples were attempted at ten depths: 10 feet, 15 feet, 56 feet, 59 feet, 74 feet, 77 feet, 86 feet, 89 feet, 94 feet, and 107 feet BGL. Both Shelby-tube sampling and pitcher-barrel sampling were used, depending on the lithology. However, only three samples (depths 10 feet, 15 feet, and 86 feet BGL) experienced any recovery without damage, one sample (depth 94 feet BGL) experienced no recovery, and the remaining six samples sustained damaged during sample collection.

On January 23, 2017, drilling operations transitioned to coring procedures. A triple-barrel wireline HQ (94mm) coring system was implemented. Once the tooling was installed, the tip depth was verified to be

<sup>2</sup> Transfer efficiency is defined as the maximum measured energy in the drill rod divided by the assumed maximum rated energy. The assumed maximum rated energy is based on a 140 pound (0.14 kip) hammer falling from a 30 in (2.5 foot) drop height.

119.2 feet BGL. From January 23 to January 27, 2017, the borehole was advanced to a depth of 502 feet BGL. At this depth, the system suffered a 100% loss of fluid circulation. Ben-Seal was added to the drilling fluid in an attempt to regain circulation, but was unsuccessful. After discussing options, costs, and schedules with USC, we opted to terminate the drilling, even though it was 13 ft shorter than planned.

Once the termination decision was made, AE Drilling began removing tooling from the borehole. In an attempt to reduce the chance of a cave-in, AE Drilling only removed 200 feet of core rod, leaving the upper 300 feet cased-off by the core rods. GEOVision inserted their logging equipment through the core rods and conducted the borehole geophysical testing: first, induction/natural gamma logging was performed from 490 to 289 feet BGL and then P-S suspension logging was performed from 301.84 to 469.16 feet BGL. The maximum logging depths were as deep as the tooling would descend, presumably due to sidewall instability. The upper depth was dictated by the presence of the remaining core rod.

Once the first series of geophysical testing was completed, AE Drilling attempted to remove the remaining 310 feet of core rod from the borehole. At a tip depth of approximately 210 feet BGL, the tooling became lodged in the borehole and a portion of the core rod disconnected from the upper section leaving approximately 100 feet of tooling in the borehole between approximate depths of 110 feet and 210 feet BGL. After several attempts to retrieve the core rod, the rods were abandoned and all geotechnical activities were stopped on boring B-CON. The borehole was secured until February 5, 2017 when it was grouted with a Portland cement/bentonite slurry.

#### 2.1.2.2 Boring B-CONa

Boring B-CONa was drilled using a CME 550X all-terrain vehicle mounted drill rig from February 3 to 5, 2017. The purpose of this borehole was to gather eleven supplemental thin-walled tube samples from the site. This was requested by USC because several thin-walled tube samples collected from boring B-CON were damaged. Three 2.0-foot long Shelby-tube samples were collected at depths of 21 feet, 39 feet, and 45 feet BGL. Eight 2.5-foot long pitcher-barrel samples were collected at depths of 47 feet, 50 feet, 53 feet, 70 feet, 76 feet, 92 feet, 102 feet, and 106 feet BGL. All thin-walled samples with the exception of the Shelby-tube sample at 45 feet BGL had recovery. The thin-walled samples at 92 feet and 106 feet BGL sustained damage to the sharp leading edge, but were still prepared for delivery to USC. After completion of all eleven thin-walled tube samples, the borehole was secured until February 10, 2017 when it was grouted with a cement/bentonite slurry mix.

#### 2.1.2.3 Boring B-CONb

Boring B-CONb was drilled using a Schramm 450 from February 7 to 10, 2017. The purpose of this borehole was to collect geophysical data from the surface to a depth of approximately 300 feet (i.e., the portion of B-CON that couldn't be logged). AE Drilling used air-rotary procedures to advance the borehole using a 10-in diameter drill bit to a depth of 315 feet BGL. The hole was then cased with 320 feet of 6-in diameter PVC casing, which was grouted in-place. The borehole was secured until GEOVision reported to the site on February 27, 2017 to conduct the geophysical testing. The geophysical testing was conducted in two phases: P-S suspension logging was performed from 6.56 to 293.64 feet BGL, and induction/natural gamma logging was performed from 309.90 to 4.75 feet BGL. After completion of the geophysical logging, the borehole was secured until March 10, 2017 when it was grouted with a Portland cement/bentonite slurry.

### 2.1.3 *Point B Detailed Narrative*

S&ME and AE Drilling mobilized to Point B on February 6, 2017. At this site, AE Drilling drilled and tested two boreholes (borings B-FMG and B-FMGa). Geotechnical and geophysical data were collected from boring B-FMG from February 3 to 26, 2017. Geotechnical samples were collected from boring B-FMGa from March 7 to 9, 2017. The site remained active until March 9, 2017 when boring B-FMGa was grouted with a Portland cement/bentonite slurry.

#### 2.1.3.1 Boring B-FMG

Boring B-FMG was drilled using a CME 550X all-terrain vehicle mounted drill rig from February 6 to 25, 2017. On February 6, 2017, split-barrel sampling was conducted from the ground surface to a depth of 20.7 feet. During this period, mud-rotary procedures were used to advance the borehole after each split-barrel sample. On February 11, 2017, drilling operations transitioned to coring procedures. Once the tooling was installed, the tip depth was verified to be 20.7 feet BGL. From February 11 to 25, 2017, the borehole was advanced to the termination depth of 615 feet BGL.

Having reached the termination depth near the end of the day on February 25, 2017, the borehole was secured overnight. On February 26, 2017, the borehole was flushed until GEOVision was ready to begin logging at which point AE Drilling removed all tooling and GEOVision inserted their instrumentation into the open borehole. The geophysical data was collected in two phases: P-S suspension logging was performed from 13.12 to 597.11 feet BGL, and induction/natural gamma logging was performed from 609.75 to 4.55 feet BGL. After completion of the geophysical logging, the borehole was secured until the following day, February 27, 2017 when it was grouted with a Portland cement/bentonite slurry.

#### 2.1.3.2 Boring B-FMGa

Boring B-FMGa was drilled using a CME 550X all-terrain vehicle mounted drill rig from March 7 to 9, 2017. The purpose of this borehole was to collect six thin-walled tube samples based on the geotechnical data collected in boring B-FMG. The boring was advanced using mud-rotary procedures. Three 2.0-foot long Shelby-tube samples were collected at depths of 4 feet, 6 feet, and 8 feet BGL. Three 2.5-foot long pitcher-barrel samples were collected at depths of 145 feet, 148 feet, and 151 feet BGL. After completion of all six thin-walled tube samples, the borehole was secured until March 9, 2017 when it was grouted with a cement/bentonite slurry mix.

## 2.2 **Surface Wave Testing**

In-situ seismic measurements using active surface wave techniques were obtained by GEOVision at both Point A and Point B sites from March 6 to 8, 2017. The purpose of this testing was to provide shear wave velocity profiles to a depth of approximately 60 meters. The active surface wave techniques used during the investigation consisted of multi-channel analysis of surface waves (MASW) and spectral analysis of surface waves (SASW) methods. GEOVision also obtained passive measurements using a linear array for comparison purposes. The methods, procedures, results, and certifications for the surface wave testing phase of this project are detailed in GEOVision Report 17016-02 rev a dated May 22, 2017. This report has been included in Appendix IV.

### 3.0 Site Conditions

#### 3.1 Surface Features

##### 3.1.1 *Surface Features at Point A*

Upon arriving at Point A, it appeared that the staked location of the boring would not be stable enough and would not allow for adequate staging room. As such, the boring was relocated to the end of Morgan Lane in the roadway. The ground surface was generally covered with crushed stone or exposed bare earth. No topographic information was provided at the time this report was completed. However, a topographic relief of approximately 1 foot was present between the three boring locations. A drainage feature was present between Morgan Lane and Veterans Hwy/Conway Bypass/SC-22, just south of the boring locations and a detention pond was present north and northwest of the boring locations.

Our exploration was made during a period of generally mild, dry weather with few instances of light wet weather. The exposed ground surface was observed to be generally stable beneath the drill rigs.

##### 3.1.2 *Surface Features at Point B*

Upon arriving at Point B, a roll-off dumpster was in place near the staked location of the boring for use as a drilling fluid and soil retention area. The site was along the edge of a perimeter farm path for a cultivated field. A copse of planted pine trees is present northwest of the boring locations. An additional wooded area was present north and northeast of the boring locations. The ground surface was generally covered with grass. No topographic information was provided at the time this report was completed. However, the area where the borings were located appeared to have a maximum topographic relief of approximately 2 feet and sloped gently down to a shallow swale along the perimeter road south of the boring locations.

Our exploration was made during a period of generally mild, dry weather with few instances of light wet weather. The exposed ground surface was observed to be generally stable beneath the drill rig.

#### 3.2 Area Geology<sup>3</sup>

The sites lie within the Coastal Terraces Region of the Lower Coastal Plain of South Carolina. The topography of this region is dominated by a series of archaic beach terraces, exposed by uplifting of the local area over the last one million years. The lower coastal plain terraces are relatively young Quaternary features, exhibit only minor surface erosion, and can be traced large distances on the basis of surface elevation. Each terrace forms a thin veneer over older, consolidated marine shelf or terrestrial Coastal Plain residual soils that are Cretaceous to Tertiary in age.

---

<sup>3</sup> The information presented in the section 3.2 of this report was gathered from relevant USGS reports available through The National Geologic Map Database (2017, June 28) retrieved from [https://ngmdb.usgs.gov/ngmdb/ngmdb\\_home.html](https://ngmdb.usgs.gov/ngmdb/ngmdb_home.html) and the Mineral Resources On-Line Spatial Data (2017, February 28) retrieved from <https://mrdata.usgs.gov/geology/state/map.html>.

The terrace formation encountered at the surface near Point A was the Waccamaw Formation. This formation is a deeply weathered terrace of the early to middle Pleistocene age. It is typically 0 to 12 feet in thickness in South Carolina and consists of soft limestones and loose gray to buff fine quartz sands in which occasional small quartz pebbles are present. In places, the formation contains a small number of black water-worn phosphatic pebbles that were evidently derived from the Cretaceous.

The terrace formation encountered at the surface near Point B was the Socastee Formation. This formation is a low coastal formation from the Pleistocene age. It is typically 0 to 16 feet thick and consists of variegated quartzose sands, argillaceous sands, and clays.

Materials comprising the terraces typically consist of a strand or beach ridge deposit of clean sands at the seaward margin. Between the strand and the toe of the next inland terrace are mainly finely interlayered clays and sands termed backbarrier deposits. In most areas, the terrace deposits are sufficiently old for a fully developed residual soil profile to have formed from the parent material, but old swamp deposits, stumps, and buried trees have in some areas been covered by the terraces and are usually not evident at the surface.

Over wide areas in both Horry and Williamsburg Counties, seams of poorly consolidated silts or clays occur near the base of the terrace sediments. These sediments were weathered or eroded from the underlying Pee Dee Formation and redeposited a short distance away in a low-energy environment. Under these conditions, the in-place soils often exhibit little strength and can be highly compressible.

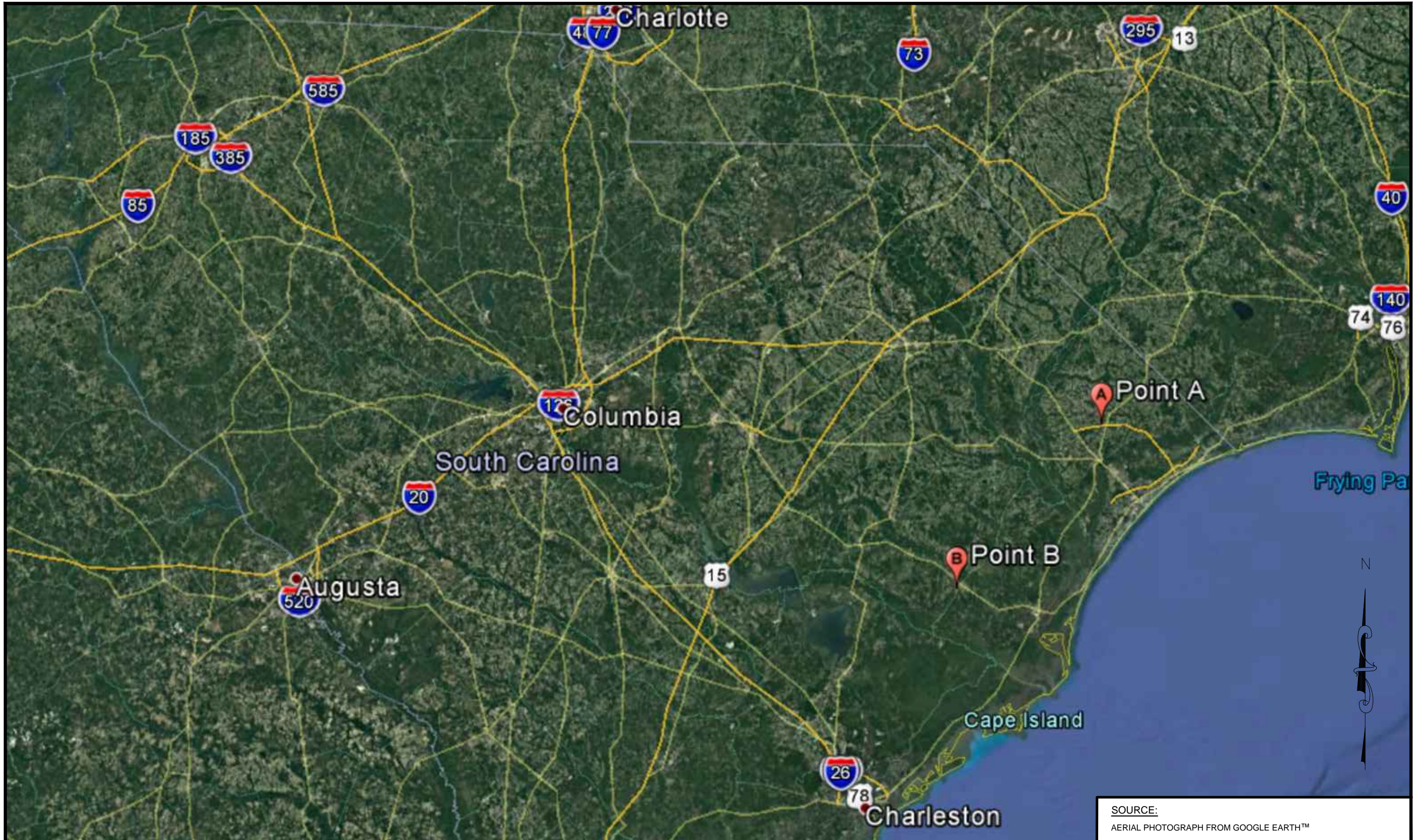
The Pee Dee Formation consists of a thick, massive bedded, dark gray to green, calcareous clay-sand or sand-clay. Ledges of thin limestone or cemented soils are often encountered about every 6 to 8 feet in soil test borings and may range from 6 inches to 4 feet thick. In this part of the county, it is also common for the upper surface of the Pee Dee Formation to be encountered with a highly-cemented marine layer of 12 to 24 inches in thickness, which is where our soundings refused at depths of about 41 to 56 feet. The Pee Dee Formation is estimated to be late Cretaceous age, about 65 million years old. This layer generally forms the bearing layer for deep foundations supporting heavy structures in the area, and is rarely penetrated fully by geotechnical borings.

## **4.0 Limitations of Report**

This geotechnical exploration data report has been prepared in accordance with SCDOT GDM Chapter 21 and with generally accepted geotechnical engineering practice for specific application to this project. The information in this report is based on the applicable standards of our practice in this geographic area at the time this report was prepared. No other warranty, expressed or implied, is made. Environmental assessments of soils, water, wetland, and endangered species were not included in our geotechnical scope of services for this project.

We appreciate the opportunity to be of service to both USC and the SCDOT on this project. If you have any questions concerning this data summary report, please do not hesitate to contact S&ME.

## **Appendix I: Figures**



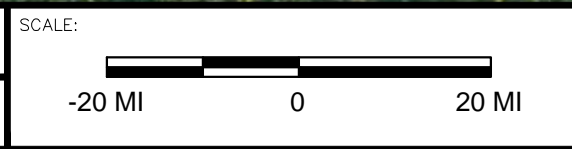
SOURCE:  
AERIAL PHOTOGRAPH FROM GOOGLE EARTH™

DRAWN BY:  
CBS

PROJECT NO.:  
1426-16-153

CHECKED BY:  
BMC, III

DATE:  
06-29-2017



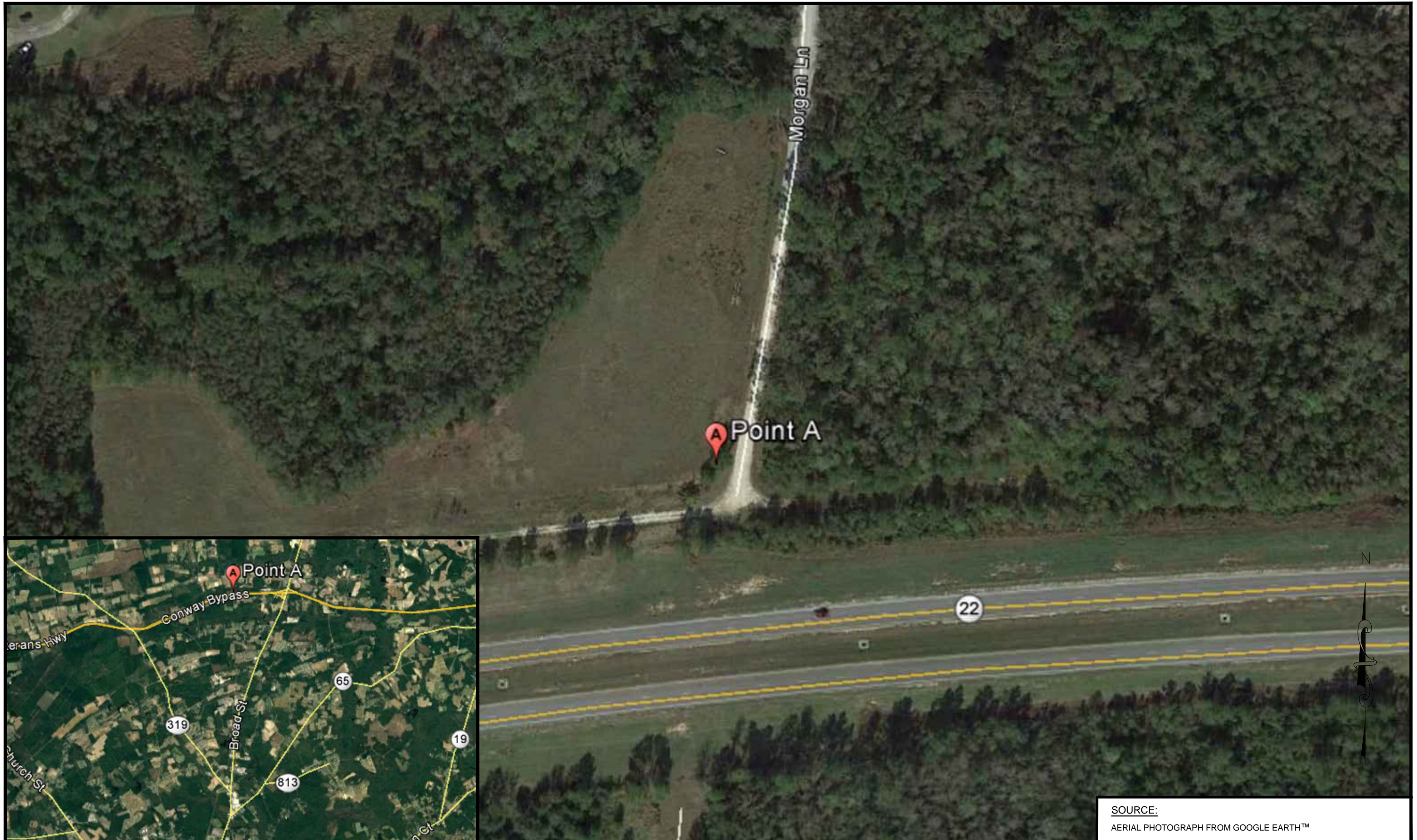
S&ME, Inc.  
620 WANDO PARK BLVD  
Mt PLEASANT, SC 29464

843.884.0005 Phone  
843.881.4890 Fax

[www.smeinc.com](http://www.smeinc.com)

**SITE VICINITY PLAN**  
DEEP SEISMIC BOREHOLES  
AYNOR AND ANDREWS, SOUTH CAROLINA

FIGURE NO.  
**1**



DRAWN BY:  
**CBS**

PROJECT NO.:  
**1426-16-153**

CHECKED BY:  
**BMC, III**

DATE:  
**06-29-2017**

SCALE:  
  
 -100      0      100



S&ME, Inc.  
620 WANDO PARK BLVD  
Mt PLEASANT, SC 29464

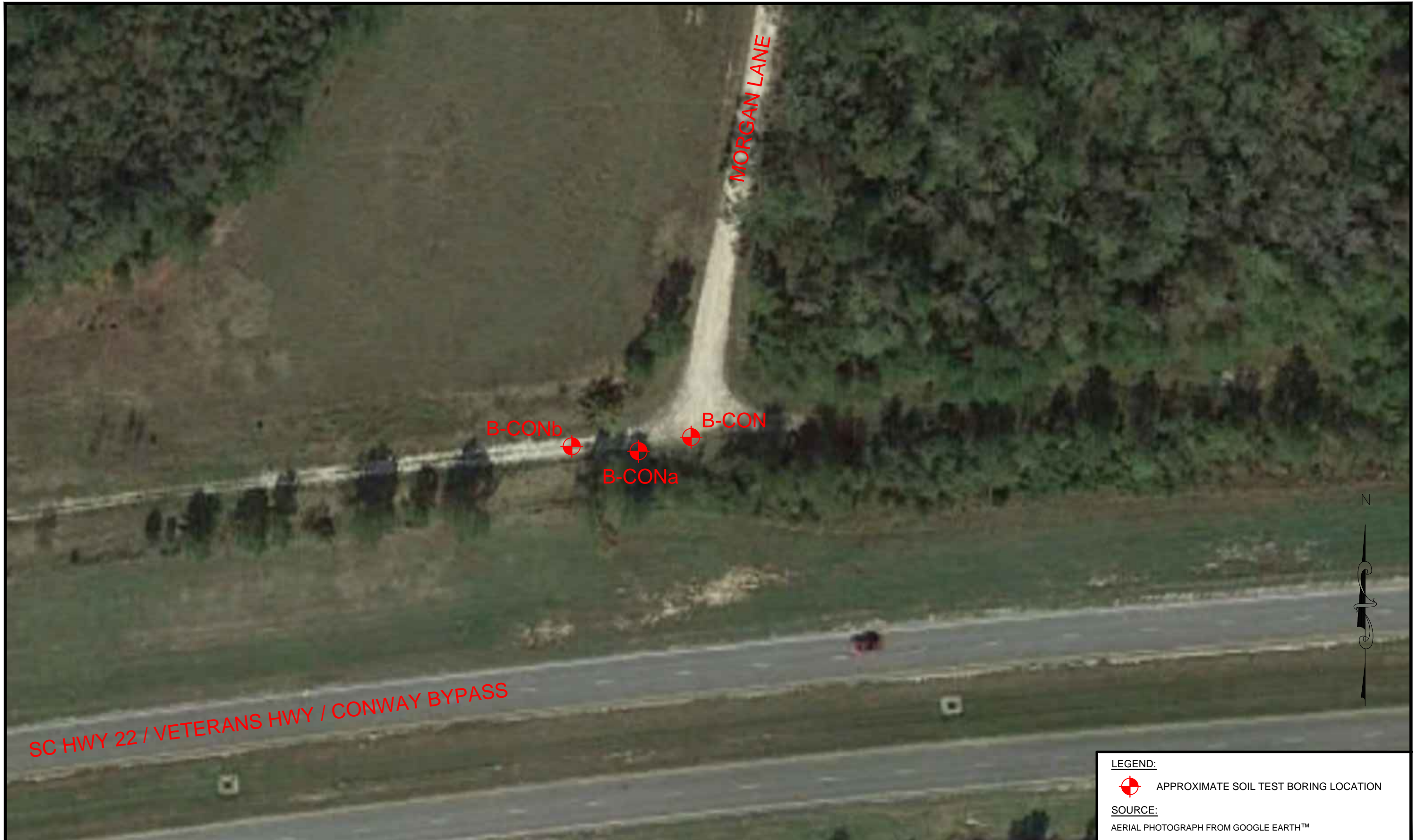
843.884.0005 Phone  
843.881.4890 Fax

[www.smeinc.com](http://www.smeinc.com)

SOURCE:  
AERIAL PHOTOGRAPH FROM GOOGLE EARTH™

**SITE VICINITY PLAN**  
**POINT A**  
 AYNOR, SOUTH CAROLINA

FIGURE NO.  
**2**



**LEGEND:**  
 APPROXIMATE SOIL TEST BORING LOCATION

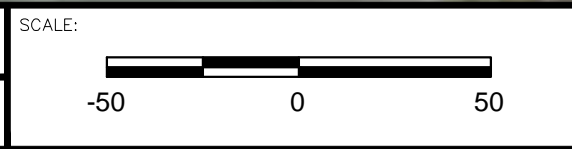
**SOURCE:**  
 AERIAL PHOTOGRAPH FROM GOOGLE EARTH™

DRAWN BY:  
**CBS**

PROJECT NO.:  
**1426-16-153**

CHECKED BY:  
**BMC, III**

DATE:  
**06-29-2017**




S&ME, Inc.  
 620 WANDO PARK BLVD  
 Mt PLEASANT, SC 29464

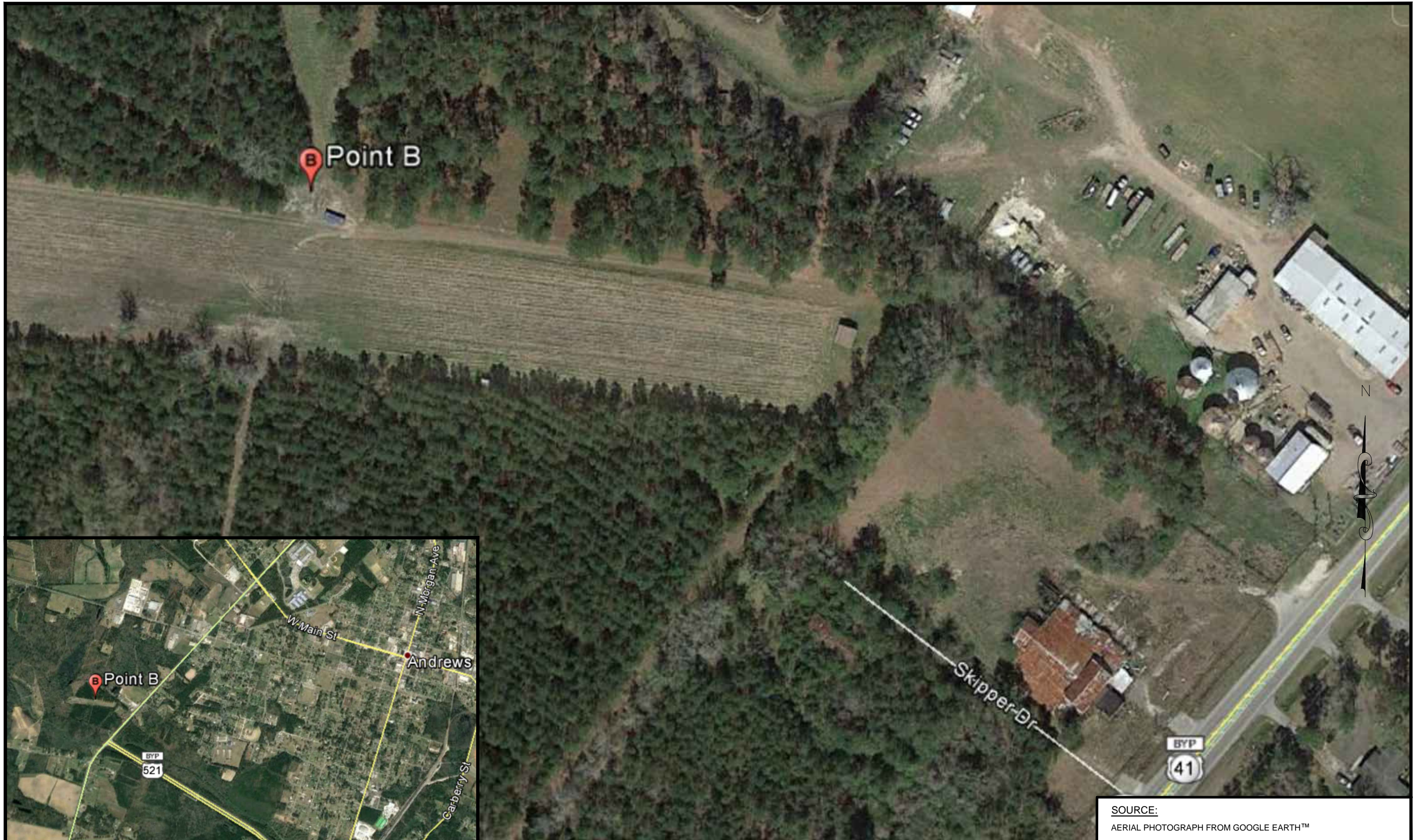
843.884.0005 Phone  
 843.881.4890 Fax

[www.smeinc.com](http://www.smeinc.com)

**BORING LOCATION PLAN**

POINT A  
 AYNOR, SOUTH CAROLINA

FIGURE NO.  
**3**



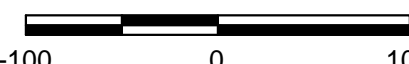
SOURCE:  
AERIAL PHOTOGRAPH FROM GOOGLE EARTH™

DRAWN BY:  
**CBS**

PROJECT NO.:  
**1426-16-153**

CHECKED BY:  
**BMC, III**

DATE:  
**06-29-2017**

SCALE:  
  
 -100      0      100



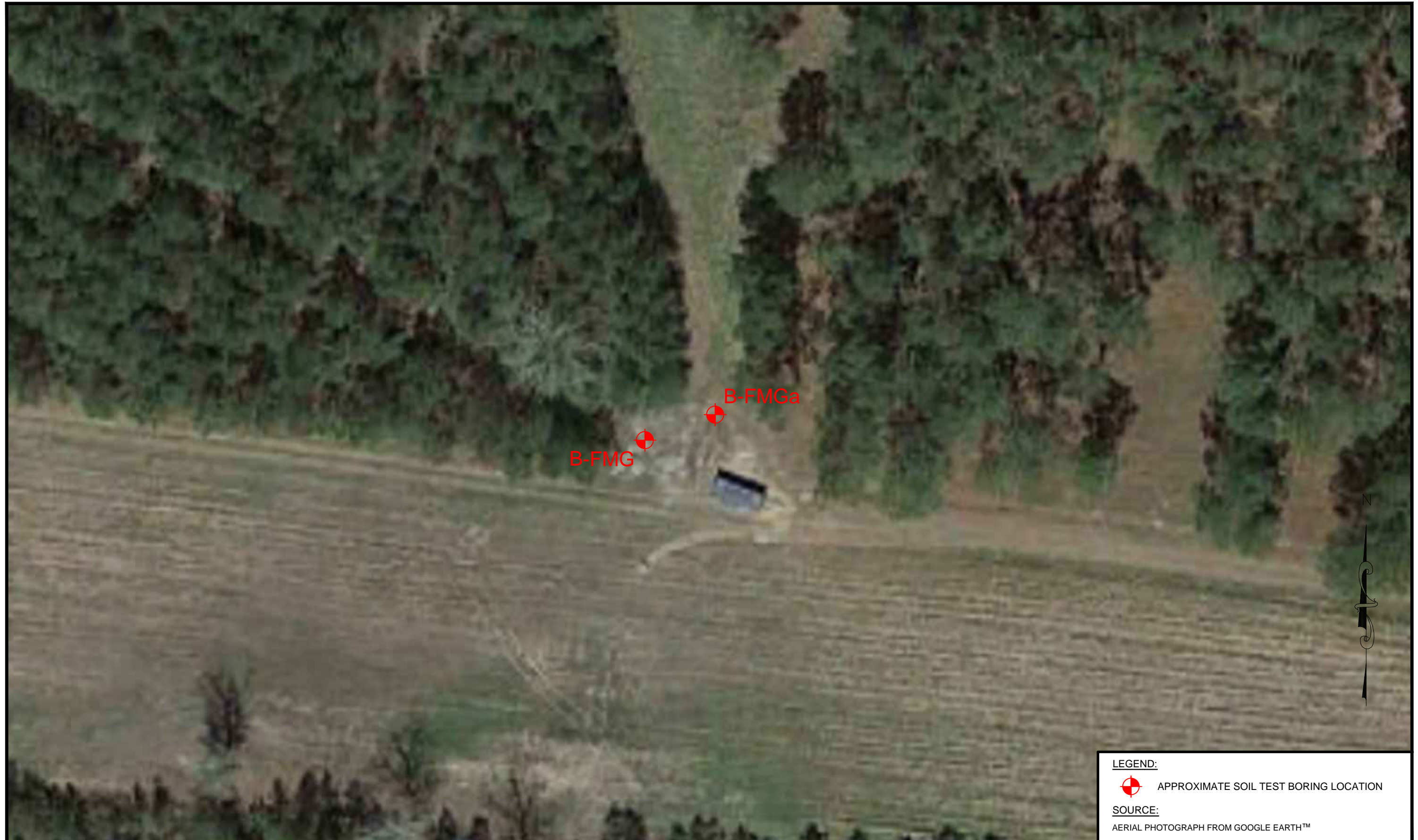
S&ME, Inc.  
620 WANDO PARK BLVD  
Mt PLEASANT, SC 29464

843.884.0005 Phone  
843.881.4890 Fax

[www.smeinc.com](http://www.smeinc.com)

**SITE VICINITY PLAN**  
**POINT B**  
ANDREWS, SOUTH CAROLINA

FIGURE NO.  
**4**



**LEGEND:**  
 APPROXIMATE SOIL TEST BORING LOCATION

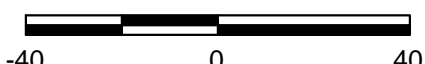
**SOURCE:**  
 AERIAL PHOTOGRAPH FROM GOOGLE EARTH™

DRAWN BY:  
**CBS**

PROJECT NO.:  
**1426-16-153**

CHECKED BY:  
**BMC, III**

DATE:  
**06-29-2017**

SCALE:  




S&ME, Inc.  
 620 WANDO PARK BLVD  
 Mt PLEASANT, SC 29464

843.884.0005 Phone  
 843.881.4890 Fax

[www.smeinc.com](http://www.smeinc.com)

**BORING LOCATION PLAN**

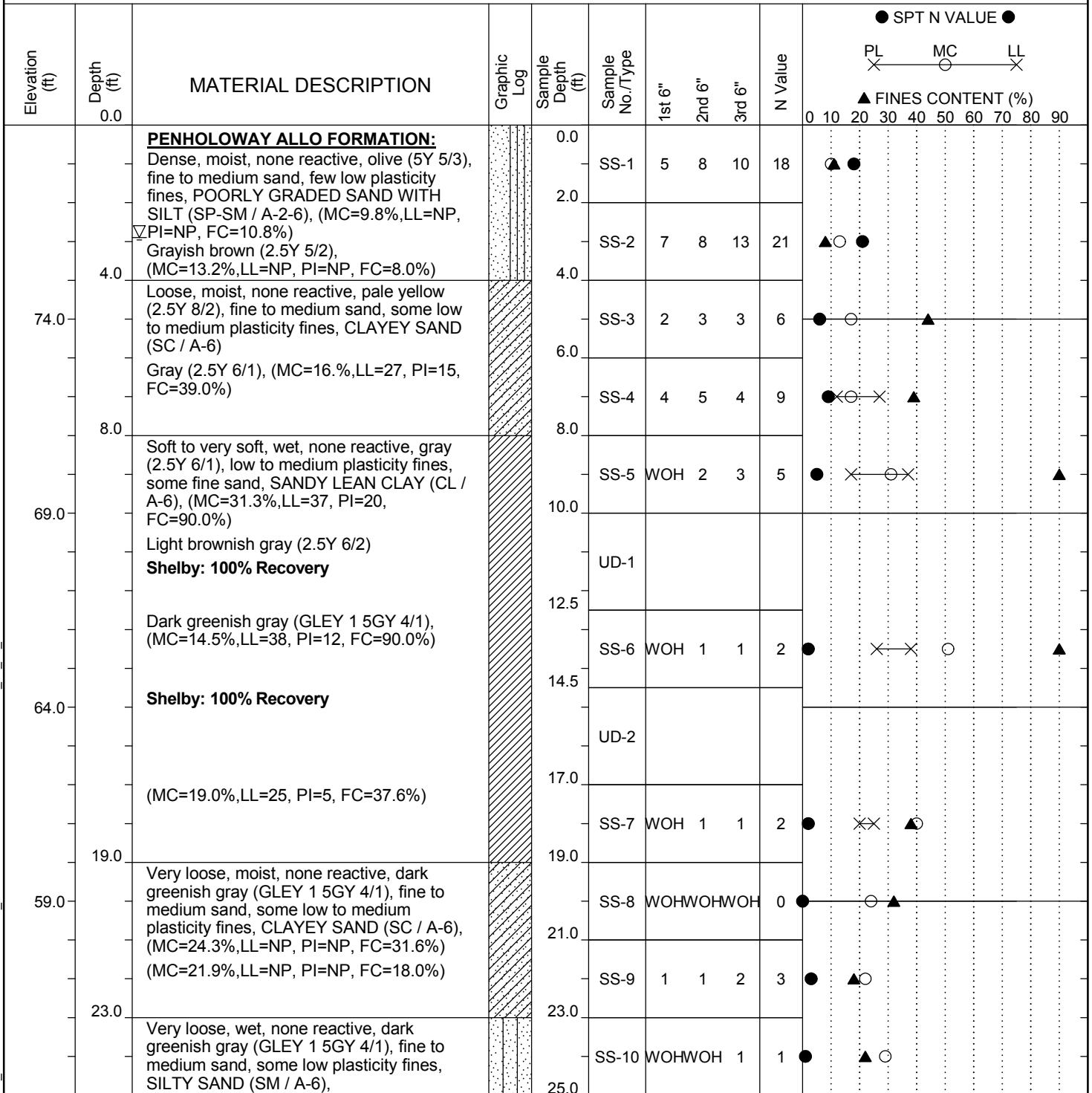
POINT A  
 AYNOR, SOUTH CAROLINA

FIGURE NO.  
**5**

## **Appendix II: Geotechnical Testing Data**

# SCDOT Soil Test Log

<b>Project ID:</b>	1413-16-153	<b>County:</b>	Horry, SC	<b>Boring No.:</b>	B-CON
<b>Site Description:</b>	USC-SCDOT Deep Seismic Holes			<b>Route:</b>	
<b>Eng./Geo.:</b>	JP & CS	<b>Boring Location:</b>	N/A	<b>Offset:</b>	N/A
<b>Elev.:</b>	79.0 ft	<b>Latitude:</b>	33.94557	<b>Longitude:</b>	-79.04754
<b>Total Depth:</b>	502 ft	<b>Soil Depth:</b>	118 ft	<b>Core Depth:</b>	502 ft
<b>Bore Hole Diameter (in):</b>	6	<b>Sampler Configuration</b>		<b>Liner Required:</b>	Y N
<b>Drill Machine:</b>	CME-550	<b>Drill Method:</b>	Mud Rotary	<b>Hammer Type:</b>	Automatic
<b>Core Size:</b>	HQ	<b>Driller:</b>	AE Drilling	<b>Groundwater:</b>	TOB 6 ft
				<b>24HR</b>	2.9 ft



## LEGEND

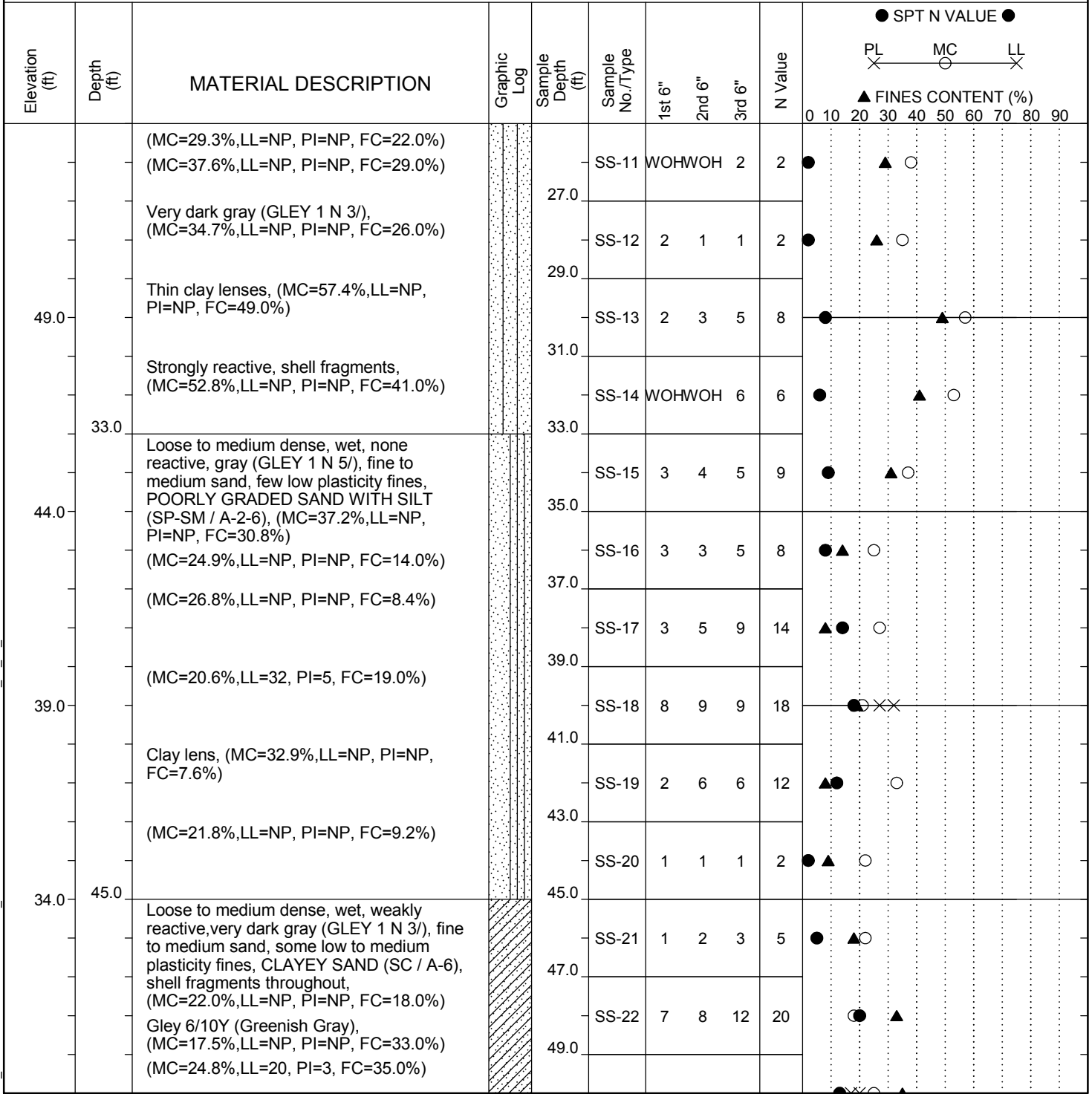
Continued Next Page

SAMPLER TYPE		DRILLING METHOD	
SS - Split Spoon	NQ - Rock Core, 1-7/8"	HSA - Hollow Stem Auger	RW - Rotary Wash
UD - Undisturbed Sample	CU - Cuttings	CFA - Continuous Flight Augers	RC - Rock Core
AWG - Rock Core, 1-1/8"	CT - Continuous Tube	DC - Driving Casing	

SC\_DOT 141316153\_USC-SCDOT DEEP BORINGS\_B-CON.GPJ\_SCDOT DATA TEMPLATE\_01\_30\_2015.GDT 12/20/17

# SCDOT Soil Test Log

<b>Project ID:</b>	1413-16-153	<b>County:</b>	Horry, SC	<b>Boring No.:</b>	B-CON
<b>Site Description:</b>	USC-SCDOT Deep Seismic Holes			<b>Route:</b>	
<b>Eng./Geo.:</b>	JP & CS	<b>Boring Location:</b>	N/A	<b>Offset:</b>	N/A
<b>Elev.:</b>	79.0 ft	<b>Latitude:</b>	33.94557	<b>Longitude:</b>	-79.04754
<b>Total Depth:</b>	502 ft	<b>Soil Depth:</b>	118 ft	<b>Core Depth:</b>	502 ft
<b>Bore Hole Diameter (in):</b>	6	<b>Sampler Configuration</b>		<b>Liner Required:</b>	Y N
<b>Drill Machine:</b>	CME-550	<b>Drill Method:</b>	Mud Rotary	<b>Hammer Type:</b>	Automatic
<b>Core Size:</b>	HQ	<b>Driller:</b>	AE Drilling	<b>Groundwater:</b>	TOB 6 ft
				<b>24HR</b>	2.9 ft



LEGEND

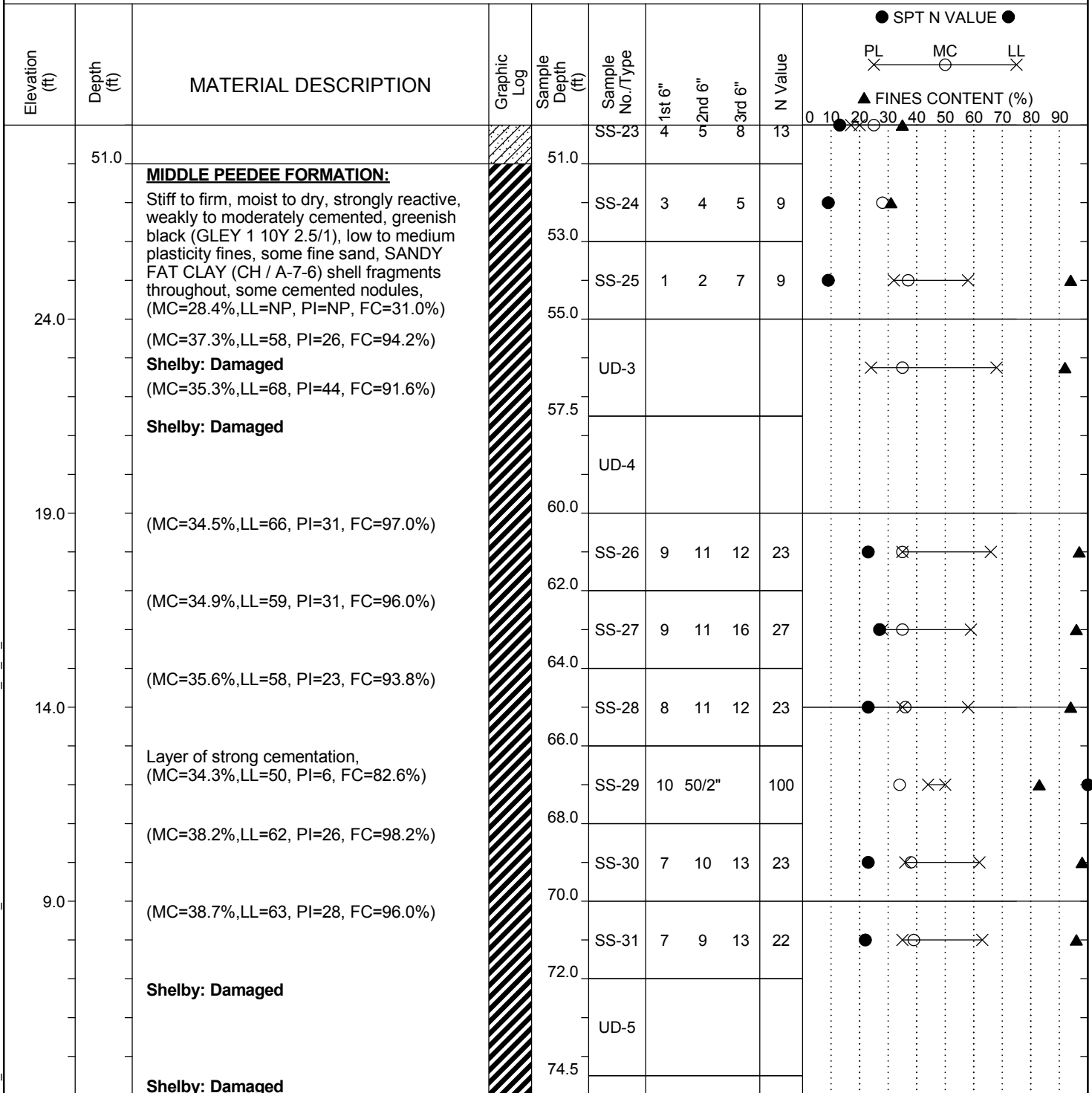
Continued Next Page

SAMPLER TYPE		DRILLING METHOD	
SS - Split Spoon	NQ - Rock Core, 1-7/8"	HSA - Hollow Stem Auger	RW - Rotary Wash
UD - Undisturbed Sample	CU - Cuttings	CFA - Continuous Flight Augers	RC - Rock Core
AWG - Rock Core, 1-1/8"	CT - Continuous Tube	DC - Driving Casing	

SC\_DOT 141316153\_USC-SCDOT DEEP BORINGS\_B-CON.GPJ\_SCDOT DATA TEMPLATE\_01\_30\_2015.GDT 12/20/17

# SCDOT Soil Test Log

<b>Project ID:</b>	1413-16-153	<b>County:</b>	Horry, SC	<b>Boring No.:</b>	B-CON
<b>Site Description:</b>	USC-SCDOT Deep Seismic Holes			<b>Route:</b>	
<b>Eng./Geo.:</b>	JP & CS	<b>Boring Location:</b>	N/A	<b>Offset:</b>	N/A
<b>Elev.:</b>	79.0 ft	<b>Latitude:</b>	33.94557	<b>Longitude:</b>	-79.04754
<b>Total Depth:</b>	502 ft	<b>Soil Depth:</b>	118 ft	<b>Core Depth:</b>	502 ft
<b>Date Started:</b>	1/18/2017		<b>Date Completed:</b>	1/28/2017	
<b>Bore Hole Diameter (in):</b>	6	<b>Sampler Configuration</b>		<b>Liner Required:</b>	Y N
<b>Liner Used:</b>	Y N		<b>Drill Machine:</b>	CME-550	<b>Drill Method:</b>
<b>Drill Method:</b>	Mud Rotary		<b>Hammer Type:</b>	Automatic	
<b>Energy Ratio:</b>	91.5%		<b>Groundwater:</b>	TOB	6 ft
<b>Core Size:</b>	HQ		<b>Driller:</b>	AE Drilling	
<b>24HR:</b>	2.9 ft				



LEGEND

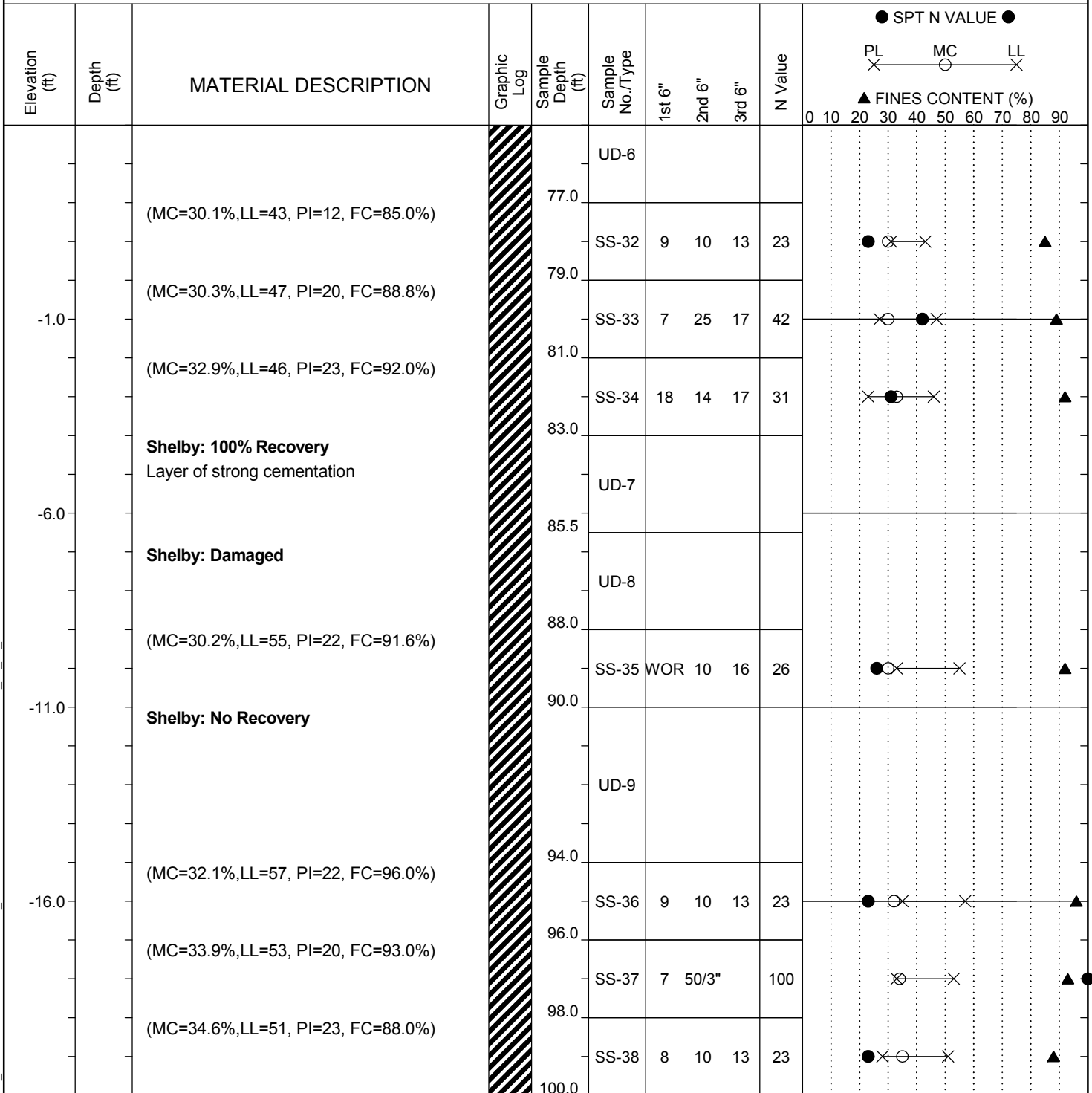
Continued Next Page

SAMPLER TYPE		DRILLING METHOD	
SS - Split Spoon	NQ - Rock Core, 1-7/8"	HSA - Hollow Stem Auger	RW - Rotary Wash
UD - Undisturbed Sample	CU - Cuttings	CFA - Continuous Flight Augers	RC - Rock Core
AWG - Rock Core, 1-1/8"	CT - Continuous Tube	DC - Driving Casing	

SC\_DOT 141316153\_USC-SCDOT DEEP BORINGS\_B-CON.GPJ\_SCDOT DATA TEMPLATE\_01\_30\_2015.GDT 12/20/17

# SCDOT Soil Test Log

<b>Project ID:</b>	1413-16-153	<b>County:</b>	Horry, SC	<b>Boring No.:</b>	B-CON
<b>Site Description:</b>	USC-SCDOT Deep Seismic Holes			<b>Route:</b>	
<b>Eng./Geo.:</b>	JP & CS	<b>Boring Location:</b>	N/A	<b>Offset:</b>	N/A
<b>Alignment:</b>	N/A				
<b>Elev.:</b>	79.0 ft	<b>Latitude:</b>	33.94557	<b>Longitude:</b>	-79.04754
<b>Date Started:</b>	1/18/2017				
<b>Total Depth:</b>	502 ft	<b>Soil Depth:</b>	118 ft	<b>Core Depth:</b>	502 ft
<b>Date Completed:</b>	1/28/2017				
<b>Bore Hole Diameter (in):</b>	6	<b>Sampler Configuration</b>		<b>Liner Required:</b>	Y N
<b>Liner Used:</b>	Y N				
<b>Drill Machine:</b>	CME-550	<b>Drill Method:</b>	Mud Rotary	<b>Hammer Type:</b>	Automatic
<b>Energy Ratio:</b>	91.5%				
<b>Core Size:</b>	HQ	<b>Driller:</b>	AE Drilling	<b>Groundwater:</b>	TOB 6 ft
<b>24HR:</b>	2.9 ft				



LEGEND

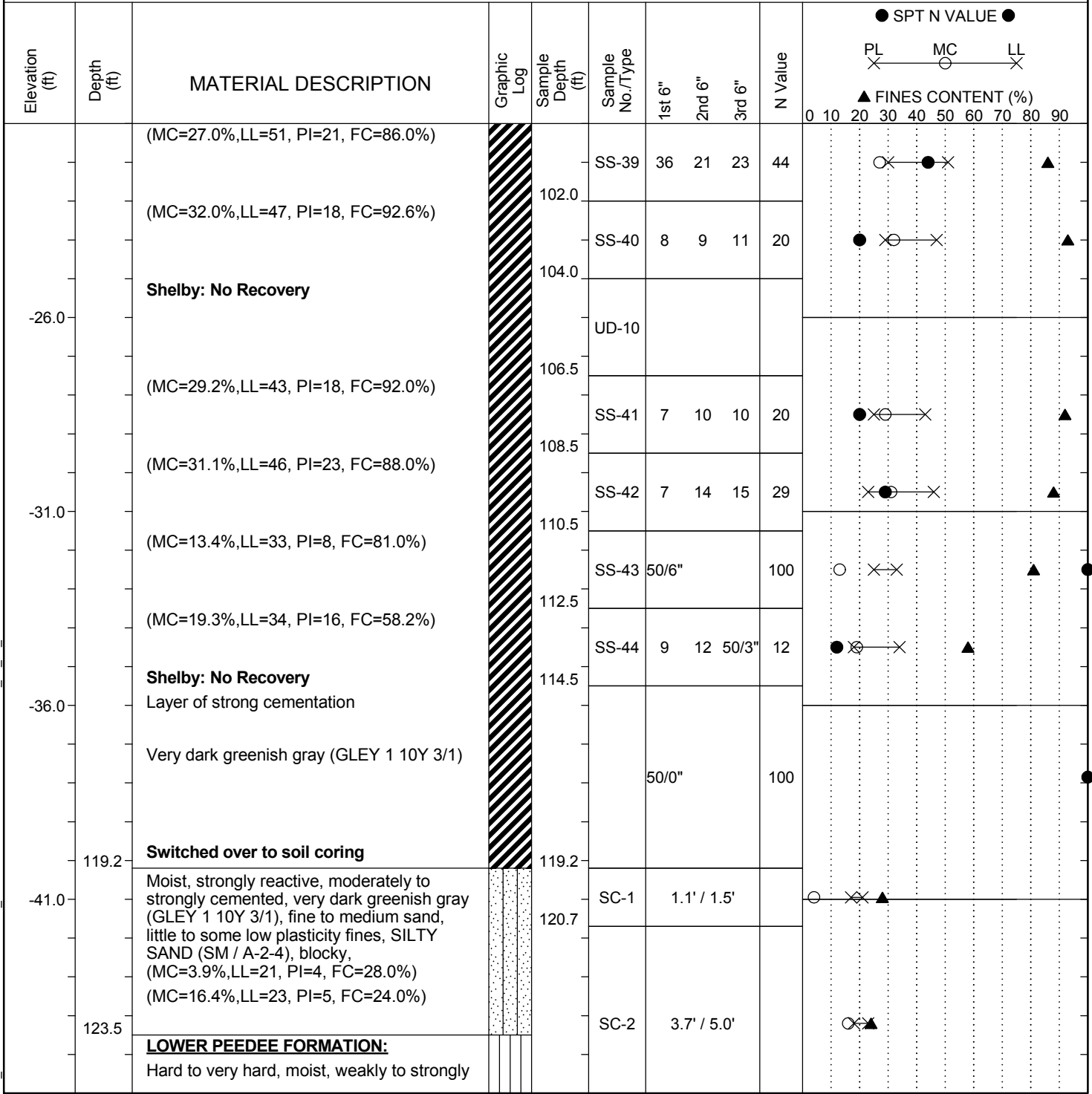
Continued Next Page

SAMPLER TYPE		DRILLING METHOD	
SS - Split Spoon	NQ - Rock Core, 1-7/8"	HSA - Hollow Stem Auger	RW - Rotary Wash
UD - Undisturbed Sample	CU - Cuttings	CFA - Continuous Flight Augers	RC - Rock Core
AWG - Rock Core, 1-1/8"	CT - Continuous Tube	DC - Driving Casing	

SC\_DOT\_141316153\_USC-SCDOT DEEP BORINGS\_B-CON.GPJ\_SCDOT DATA TEMPLATE\_01\_30\_2015.GDT 12/20/17

# SCDOT Soil Test Log

<b>Project ID:</b>	1413-16-153	<b>County:</b>	Horry, SC	<b>Boring No.:</b>	B-CON
<b>Site Description:</b>	USC-SCDOT Deep Seismic Holes			<b>Route:</b>	
<b>Eng./Geo.:</b>	JP & CS	<b>Boring Location:</b>	N/A	<b>Offset:</b>	N/A
<b>Elev.:</b>	79.0 ft	<b>Latitude:</b>	33.94557	<b>Longitude:</b>	-79.04754
<b>Total Depth:</b>	502 ft	<b>Soil Depth:</b>	118 ft	<b>Core Depth:</b>	502 ft
<b>Bore Hole Diameter (in):</b>	6	<b>Sampler Configuration</b>		<b>Liner Required:</b>	Y N
<b>Drill Machine:</b>	CME-550	<b>Drill Method:</b>	Mud Rotary	<b>Hammer Type:</b>	Automatic
<b>Core Size:</b>	HQ	<b>Driller:</b>	AE Drilling	<b>Groundwater:</b>	TOB 6 ft
				<b>Energy Ratio:</b>	91.5%
				<b>24HR</b>	2.9 ft



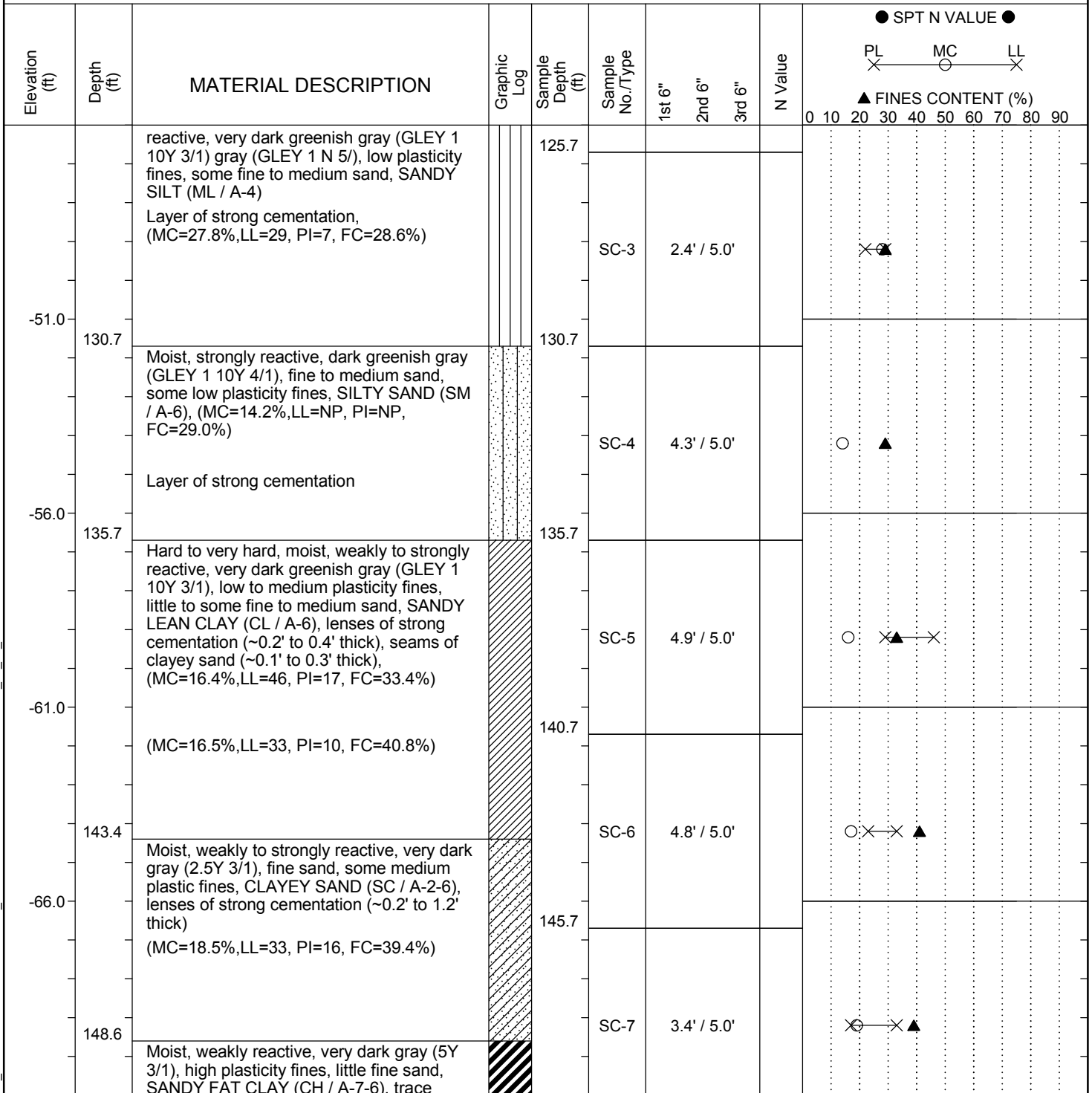
LEGEND Continued Next Page

SAMPLER TYPE		DRILLING METHOD	
SS - Split Spoon	NQ - Rock Core, 1-7/8"	HSA - Hollow Stem Auger	RW - Rotary Wash
UD - Undisturbed Sample	CU - Cuttings	CFA - Continuous Flight Augers	RC - Rock Core
AWG - Rock Core, 1-1/8"	CT - Continuous Tube	DC - Driving Casing	

SC\_DOT\_141316153\_USC-SCDOT DEEP BORINGS\_B-CON.GPJ\_SCDOT DATA TEMPLATE\_01\_30\_2015.GDT 12/20/17

# SCDOT Soil Test Log

<b>Project ID:</b>	1413-16-153	<b>County:</b>	Horry, SC	<b>Boring No.:</b>	B-CON
<b>Site Description:</b>	USC-SCDOT Deep Seismic Holes			<b>Route:</b>	
<b>Eng./Geo.:</b>	JP & CS	<b>Boring Location:</b>	N/A	<b>Offset:</b>	N/A
<b>Elev.:</b>	79.0 ft	<b>Latitude:</b>	33.94557	<b>Longitude:</b>	-79.04754
<b>Total Depth:</b>	502 ft	<b>Soil Depth:</b>	118 ft	<b>Core Depth:</b>	502 ft
<b>Bore Hole Diameter (in):</b>	6	<b>Sampler Configuration</b>		<b>Liner Required:</b>	Y N
<b>Drill Machine:</b>	CME-550	<b>Drill Method:</b>	Mud Rotary	<b>Hammer Type:</b>	Automatic
<b>Core Size:</b>	HQ	<b>Driller:</b>	AE Drilling	<b>Groundwater:</b>	TOB 6 ft
				<b>24HR</b>	2.9 ft



LEGEND

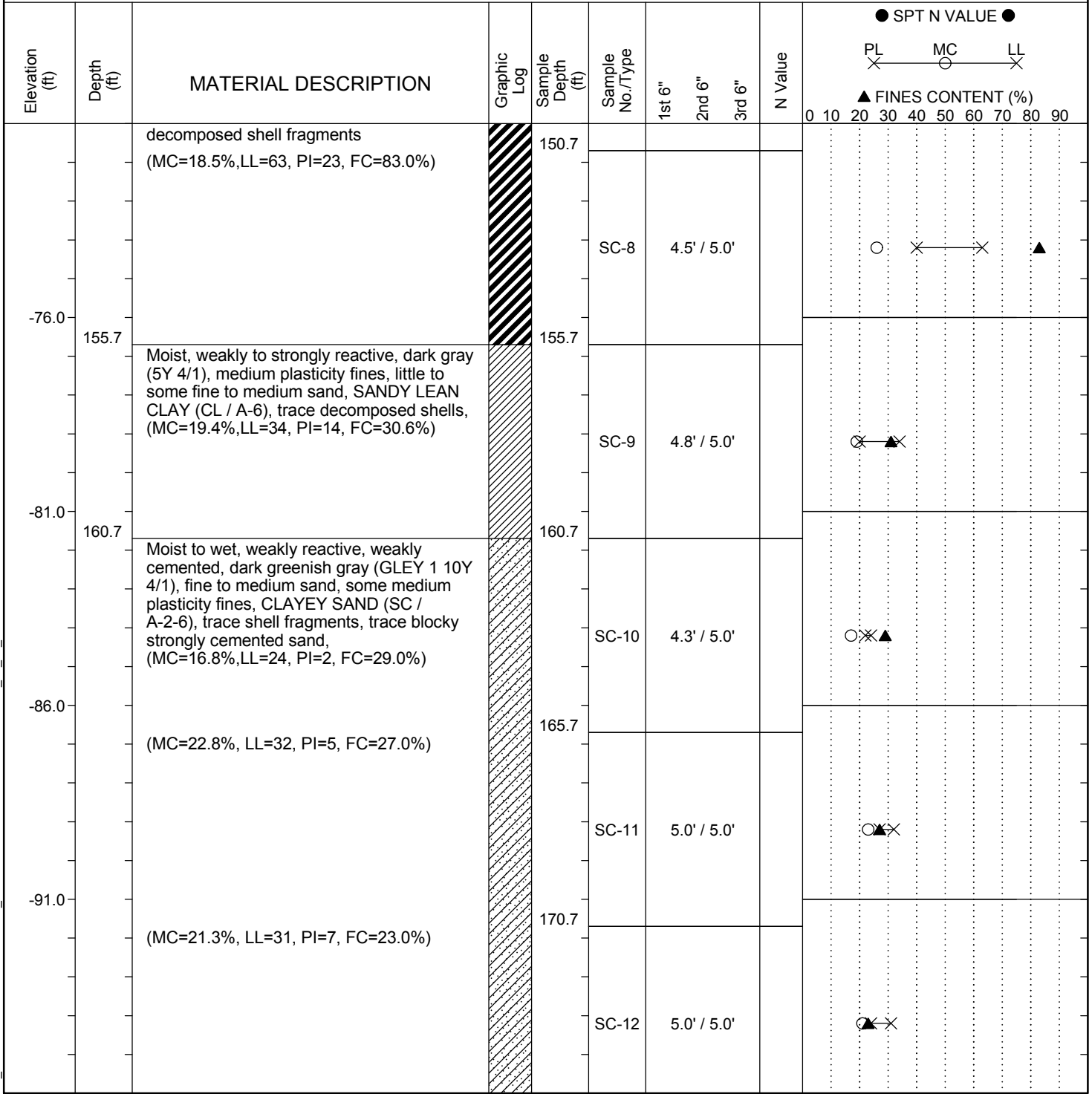
Continued Next Page

SAMPLER TYPE		DRILLING METHOD	
SS - Split Spoon	NQ - Rock Core, 1-7/8"	HSA - Hollow Stem Auger	RW - Rotary Wash
UD - Undisturbed Sample	CU - Cuttings	CFA - Continuous Flight Augers	RC - Rock Core
AWG - Rock Core, 1-1/8"	CT - Continuous Tube	DC - Driving Casing	

SC\_DOT 141316153\_USC-SCDOT DEEP BORINGS\_B-CON.GPJ\_SCDOT DATA TEMPLATE\_01\_30\_2015.GDT 12/20/17

# SCDOT Soil Test Log

<b>Project ID:</b>	1413-16-153	<b>County:</b>	Horry, SC	<b>Boring No.:</b>	B-CON
<b>Site Description:</b>	USC-SCDOT Deep Seismic Holes			<b>Route:</b>	
<b>Eng./Geo.:</b>	JP & CS	<b>Boring Location:</b>	N/A	<b>Offset:</b>	N/A
<b>Alignment:</b>	N/A				
<b>Elev.:</b>	79.0 ft	<b>Latitude:</b>	33.94557	<b>Longitude:</b>	-79.04754
<b>Date Started:</b>	1/18/2017				
<b>Total Depth:</b>	502 ft	<b>Soil Depth:</b>	118 ft	<b>Core Depth:</b>	502 ft
<b>Date Completed:</b>	1/28/2017				
<b>Bore Hole Diameter (in):</b>	6	<b>Sampler Configuration</b>		<b>Liner Required:</b>	Y N
<b>Liner Used:</b>	Y N				
<b>Drill Machine:</b>	CME-550	<b>Drill Method:</b>	Mud Rotary	<b>Hammer Type:</b>	Automatic
<b>Energy Ratio:</b>	91.5%				
<b>Core Size:</b>	HQ	<b>Driller:</b>	AE Drilling	<b>Groundwater:</b>	TOB 6 ft
<b>24HR:</b>	2.9 ft				



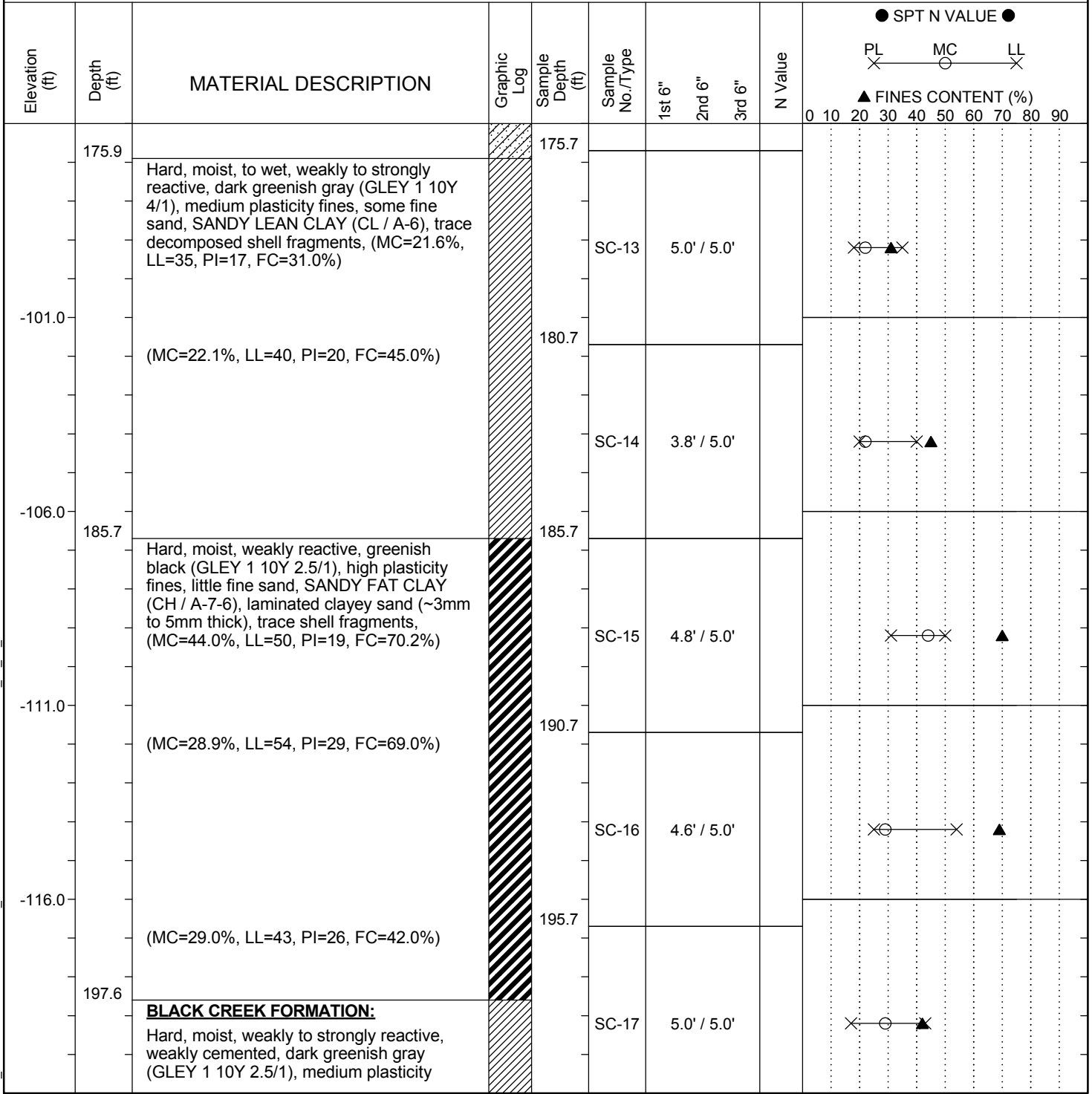
LEGEND Continued Next Page

<b>SAMPLER TYPE</b>		<b>DRILLING METHOD</b>	
SS - Split Spoon	NQ - Rock Core, 1-7/8"	HSA - Hollow Stem Auger	RW - Rotary Wash
UD - Undisturbed Sample	CU - Cuttings	CFA - Continuous Flight Augers	RC - Rock Core
AWG - Rock Core, 1-1/8"	CT - Continuous Tube	DC - Driving Casing	

SC\_DOT\_141316153\_USC-SCDOT DEEP BORINGS\_B-CON.GPJ\_SCDOT DATA TEMPLATE\_01\_30\_2015.GDT 12/20/17

# SCDOT Soil Test Log

<b>Project ID:</b>	1413-16-153	<b>County:</b>	Horry, SC	<b>Boring No.:</b>	B-CON
<b>Site Description:</b>	USC-SCDOT Deep Seismic Holes			<b>Route:</b>	
<b>Eng./Geo.:</b>	JP & CS	<b>Boring Location:</b>	N/A	<b>Offset:</b>	N/A
<b>Elev.:</b>	79.0 ft	<b>Latitude:</b>	33.94557	<b>Longitude:</b>	-79.04754
<b>Total Depth:</b>	502 ft	<b>Soil Depth:</b>	118 ft	<b>Core Depth:</b>	502 ft
<b>Bore Hole Diameter (in):</b>	6	<b>Sampler Configuration</b>		<b>Liner Required:</b>	Y N
<b>Drill Machine:</b>	CME-550	<b>Drill Method:</b>	Mud Rotary	<b>Hammer Type:</b>	Automatic
<b>Core Size:</b>	HQ	<b>Driller:</b>	AE Drilling	<b>Groundwater:</b>	TOB 6 ft
				<b>24HR</b>	2.9 ft



**LEGEND**

*Continued Next Page*

SAMPLER TYPE		DRILLING METHOD	
SS - Split Spoon	NQ - Rock Core, 1-7/8"	HSA - Hollow Stem Auger	RW - Rotary Wash
UD - Undisturbed Sample	CU - Cuttings	CFA - Continuous Flight Augers	RC - Rock Core
AWG - Rock Core, 1-1/8"	CT - Continuous Tube	DC - Driving Casing	

SC\_DOT 141316153\_USC-SCDOT DEEP BORINGS\_B-CON.GPJ\_SCDOT DATA TEMPLATE\_01\_30\_2015.GDT 12/20/17

# SCDOT Soil Test Log

<b>Project ID:</b>	1413-16-153	<b>County:</b>	Horry, SC	<b>Boring No.:</b>	B-CON
<b>Site Description:</b>	USC-SCDOT Deep Seismic Holes			<b>Route:</b>	
<b>Eng./Geo.:</b>	JP & CS	<b>Boring Location:</b>	N/A	<b>Offset:</b>	N/A
<b>Elev.:</b>	79.0 ft	<b>Latitude:</b>	33.94557	<b>Longitude:</b>	-79.04754
<b>Total Depth:</b>	502 ft	<b>Soil Depth:</b>	118 ft	<b>Core Depth:</b>	502 ft
<b>Bore Hole Diameter (in):</b>	6	<b>Sampler Configuration</b>		<b>Liner Required:</b>	Y N
<b>Drill Machine:</b>	CME-550	<b>Drill Method:</b>	Mud Rotary	<b>Hammer Type:</b>	Automatic
<b>Core Size:</b>	HQ	<b>Driller:</b>	AE Drilling	<b>Groundwater:</b>	TOB 6 ft
				<b>24HR</b>	2.9 ft

Elevation (ft)	Depth (ft)	MATERIAL DESCRIPTION	Graphic Log	Sample Depth (ft)	Sample No./Type	1st 6"	2nd 6"	3rd 6"	N Value	SPT N VALUE											
										PL	MC	LL	FINES CONTENT (%)								
	200.7	<p>fines, some fine to medium sand, SANDY LEAN CLAY (CL / A-6), trace shell fragments, trace moderately to strongly cemented sand</p> <p>Hard, moist, weakly reactive, very dark greenish gray (GLEY 1 10Y 3/1), medium to high plasticity fines, little to some fine to medium sand, SANDY FAT CLAY (CH / A-7-6), trace shell fragments, trace mica, stratified clayey sand (~5mm to 0.1' thick), (MC=27.4%, LL=49, PI=28, FC=50.0%) (MC=46.5%, LL=49, PI=26, FC=17.0%)</p>		200.7																	
-126.0				205.7	SC-18	3.4' / 5.0'															
-131.0	210.7	<p>Hard, moist, none to weakly reactive, very dark greenish gray (GLEY 1 10Y 3/1), medium plasticity fines, some fine sand, SANDY LEAN CLAY (CL / A-6), trace shells, trace mica, stratified fat clay, (MC=23.9%, LL=32, PI=11, FC=39.0%)</p> <p>(MC=27.5%, LL=53, PI=23, FC=54.0%)</p>		210.7	SC-19	3.4' / 5.0'															
-136.0				215.7	SC-20	2.8' / 5.0'															
-141.0	218.1	<p>Hard, moist, none to weakly reactive, greenish black (GLEY 1 10Y 2.5/1), high plasticity fines, few fine sand, FAT CLAY WITH SAND (CH / A-7-6), trace shell fragments, laminated clayey sand</p>		218.1	SC-21	5.0' / 5.0'															
	220.7	<p>Moist, none to weakly reactive, very dark greenish gray (GLEY 1 10Y 3/1), fine sand, some low to medium plasticity fines, CLAYEY SAND (SC / A-6), trace shell fragments, few moderately cemented sand, (MC=18.8%, LL=36, PI=22, FC=33.0%)</p>		220.7	SC-22	1.6' / 5.0'															

### LEGEND

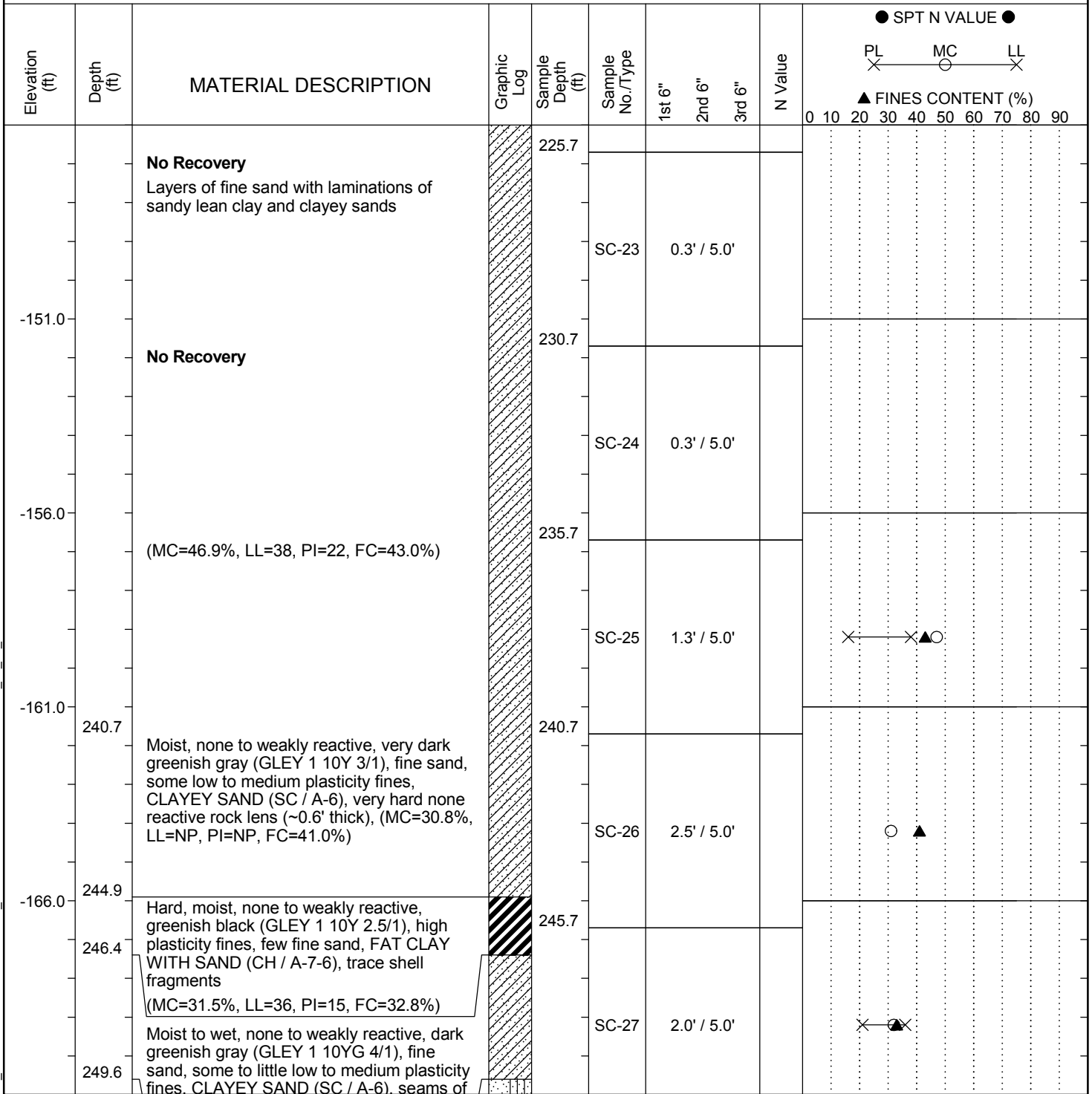
Continued Next Page

SAMPLER TYPE		DRILLING METHOD	
SS - Split Spoon	NQ - Rock Core, 1-7/8"	HSA - Hollow Stem Auger	RW - Rotary Wash
UD - Undisturbed Sample	CU - Cuttings	CFA - Continuous Flight Augers	RC - Rock Core
AWG - Rock Core, 1-1/8"	CT - Continuous Tube	DC - Driving Casing	

SC\_DOT\_141316153\_USC-SCDOT DEEP BORINGS\_B-CON.GPJ\_SCDOT DATA TEMPLATE\_01\_30\_2015.GDT\_12/20/17

# SCDOT Soil Test Log

<b>Project ID:</b>	1413-16-153	<b>County:</b>	Horry, SC	<b>Boring No.:</b>	B-CON
<b>Site Description:</b>	USC-SCDOT Deep Seismic Holes			<b>Route:</b>	
<b>Eng./Geo.:</b>	JP & CS	<b>Boring Location:</b>	N/A	<b>Offset:</b>	N/A
<b>Elev.:</b>	79.0 ft	<b>Latitude:</b>	33.94557	<b>Longitude:</b>	-79.04754
<b>Total Depth:</b>	502 ft	<b>Soil Depth:</b>	118 ft	<b>Core Depth:</b>	502 ft
<b>Bore Hole Diameter (in):</b>	6	<b>Sampler Configuration</b>		<b>Liner Required:</b>	Y N
<b>Drill Machine:</b>	CME-550	<b>Drill Method:</b>	Mud Rotary	<b>Hammer Type:</b>	Automatic
<b>Core Size:</b>	HQ	<b>Driller:</b>	AE Drilling	<b>Groundwater:</b>	TOB 6 ft
				<b>24HR</b>	2.9 ft
				<b>Energy Ratio:</b>	91.5%
				<b>Liner Used:</b>	Y N



**LEGEND**

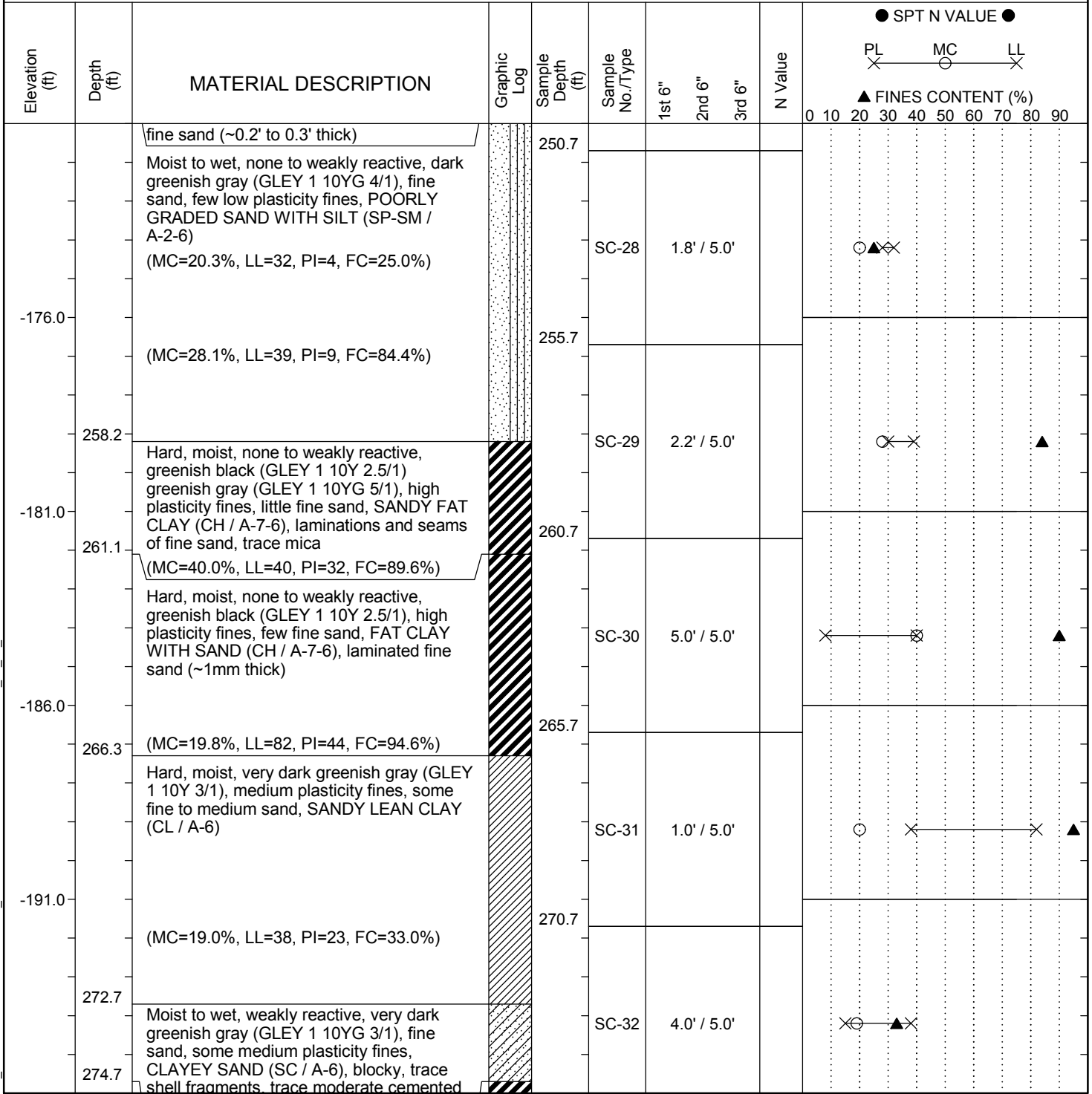
*Continued Next Page*

SAMPLER TYPE		DRILLING METHOD	
SS - Split Spoon	NQ - Rock Core, 1-7/8"	HSA - Hollow Stem Auger	RW - Rotary Wash
UD - Undisturbed Sample	CU - Cuttings	CFA - Continuous Flight Augers	RC - Rock Core
AWG - Rock Core, 1-1/8"	CT - Continuous Tube	DC - Driving Casing	

SC\_DOT\_141316153\_USC-SCDOT DEEP BORINGS\_B-CON.GPJ\_SCDOT DATA TEMPLATE\_01\_30\_2015.GDT 12/20/17

# SCDOT Soil Test Log

<b>Project ID:</b>	1413-16-153	<b>County:</b>	Horry, SC	<b>Boring No.:</b>	B-CON
<b>Site Description:</b>	USC-SCDOT Deep Seismic Holes			<b>Route:</b>	
<b>Eng./Geo.:</b>	JP & CS	<b>Boring Location:</b>	N/A	<b>Offset:</b>	N/A
<b>Elev.:</b>	79.0 ft	<b>Latitude:</b>	33.94557	<b>Longitude:</b>	-79.04754
<b>Total Depth:</b>	502 ft	<b>Soil Depth:</b>	118 ft	<b>Core Depth:</b>	502 ft
<b>Date Started:</b>	1/18/2017		<b>Date Completed:</b>	1/28/2017	
<b>Bore Hole Diameter (in):</b>	6	<b>Sampler Configuration</b>		<b>Liner Required:</b>	Y N
<b>Liner Used:</b>	Y N		<b>Hammer Type:</b>	Automatic	
<b>Drill Machine:</b>	CME-550	<b>Drill Method:</b>	Mud Rotary	<b>Energy Ratio:</b>	91.5%
<b>Core Size:</b>	HQ	<b>Driller:</b>	AE Drilling	<b>Groundwater:</b>	TOB 6 ft
				<b>24HR</b>	2.9 ft



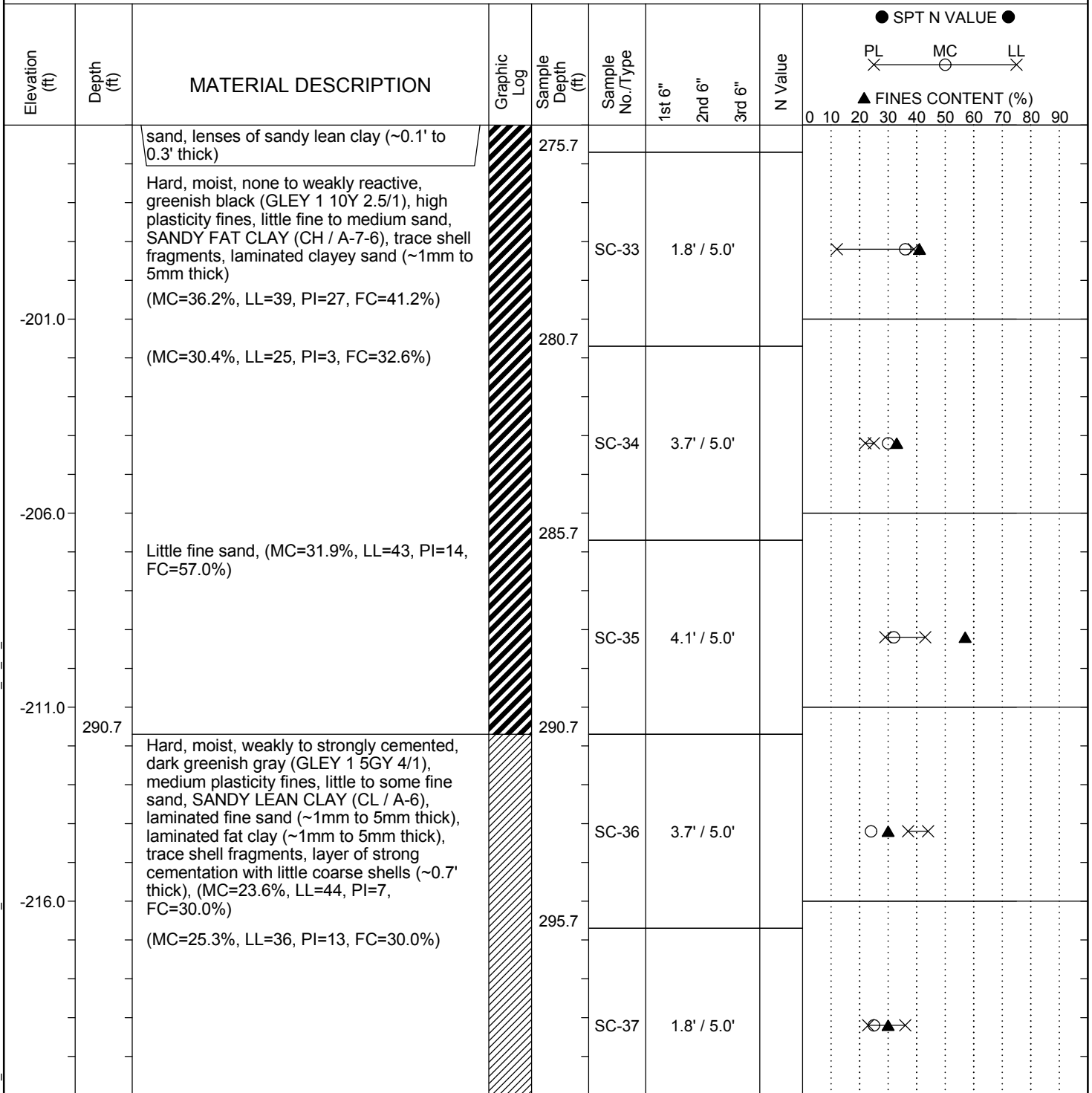
LEGEND Continued Next Page

SAMPLER TYPE		DRILLING METHOD	
SS - Split Spoon	NQ - Rock Core, 1-7/8"	HSA - Hollow Stem Auger	RW - Rotary Wash
UD - Undisturbed Sample	CU - Cuttings	CFA - Continuous Flight Augers	RC - Rock Core
AWG - Rock Core, 1-1/8"	CT - Continuous Tube	DC - Driving Casing	

SC\_DOT\_141316153\_USC-SCDOT DEEP BORINGS\_B-CON.GPJ\_SCDOT DATA TEMPLATE\_01\_30\_2015.GDT 12/20/17

# SCDOT Soil Test Log

<b>Project ID:</b>	1413-16-153	<b>County:</b>	Horry, SC	<b>Boring No.:</b>	B-CON
<b>Site Description:</b>	USC-SCDOT Deep Seismic Holes			<b>Route:</b>	
<b>Eng./Geo.:</b>	JP & CS	<b>Boring Location:</b>	N/A	<b>Offset:</b>	N/A
<b>Elev.:</b>	79.0 ft	<b>Latitude:</b>	33.94557	<b>Longitude:</b>	-79.04754
<b>Total Depth:</b>	502 ft	<b>Soil Depth:</b>	118 ft	<b>Core Depth:</b>	502 ft
<b>Date Started:</b>	1/18/2017		<b>Date Completed:</b>	1/28/2017	
<b>Bore Hole Diameter (in):</b>	6	<b>Sampler Configuration</b>		<b>Liner Required:</b>	Y N
<b>Liner Used:</b>	Y N		<b>Drill Machine:</b>	CME-550	<b>Drill Method:</b>
<b>Drill Method:</b>	Mud Rotary		<b>Hammer Type:</b>	Automatic	
<b>Energy Ratio:</b>	91.5%		<b>Groundwater:</b>	TOB	6 ft
<b>Core Size:</b>	HQ		<b>Driller:</b>	AE Drilling	
<b>24HR:</b>	2.9 ft				



**LEGEND**

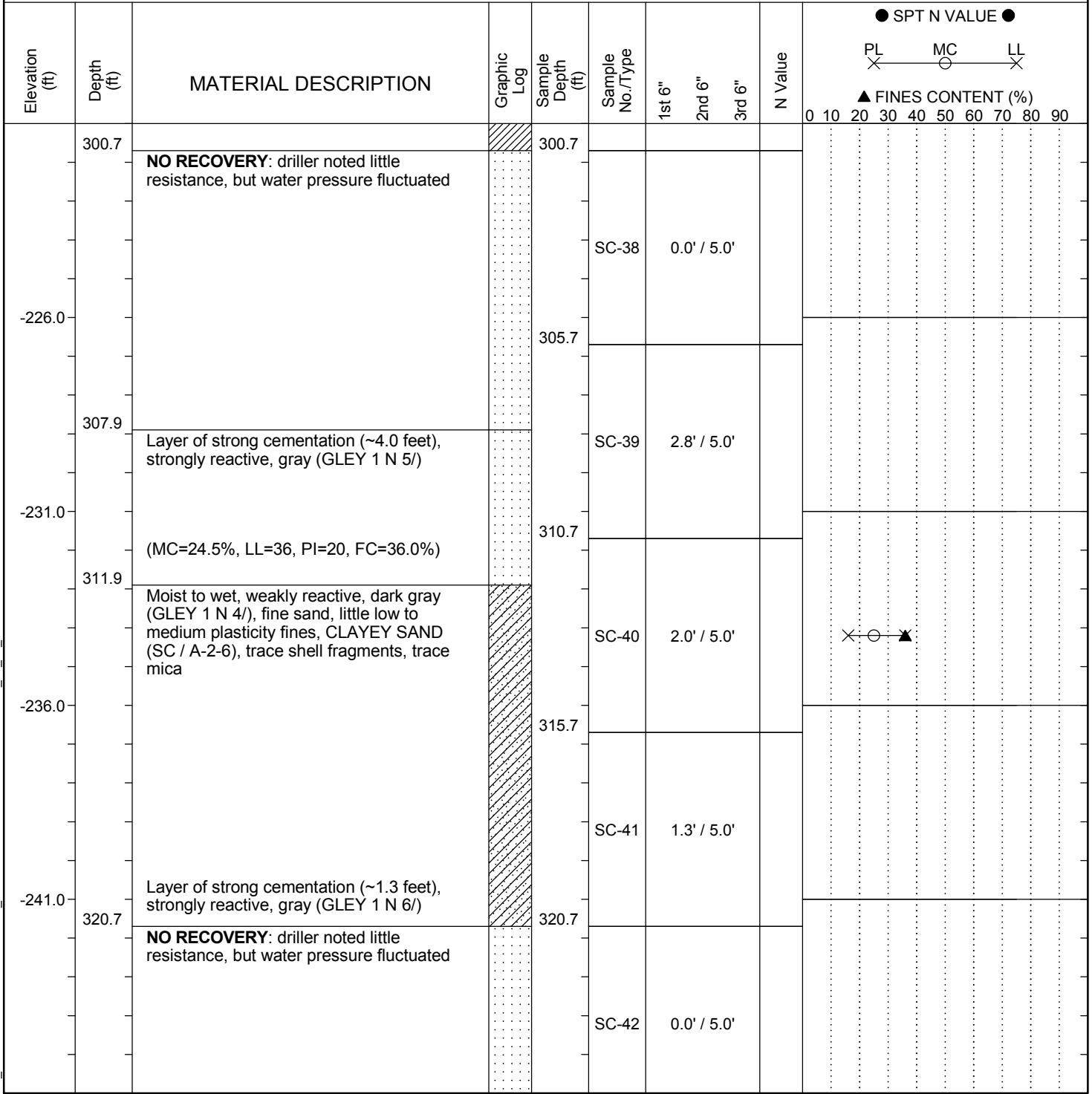
*Continued Next Page*

SAMPLER TYPE		DRILLING METHOD	
SS - Split Spoon	NQ - Rock Core, 1-7/8"	HSA - Hollow Stem Auger	RW - Rotary Wash
UD - Undisturbed Sample	CU - Cuttings	CFA - Continuous Flight Augers	RC - Rock Core
AWG - Rock Core, 1-1/8"	CT - Continuous Tube	DC - Driving Casing	

SC\_DOT 141316153\_USC-SCDOT DEEP BORINGS\_B-CON.GPJ\_SCDOT DATA TEMPLATE\_01\_30\_2015.GDT 12/20/17

# SCDOT Soil Test Log

<b>Project ID:</b>	1413-16-153	<b>County:</b>	Horry, SC	<b>Boring No.:</b>	B-CON
<b>Site Description:</b>	USC-SCDOT Deep Seismic Holes			<b>Route:</b>	
<b>Eng./Geo.:</b>	JP & CS	<b>Boring Location:</b>	N/A	<b>Offset:</b>	N/A
<b>Alignment:</b>	N/A				
<b>Elev.:</b>	79.0 ft	<b>Latitude:</b>	33.94557	<b>Longitude:</b>	-79.04754
<b>Date Started:</b>	1/18/2017				
<b>Total Depth:</b>	502 ft	<b>Soil Depth:</b>	118 ft	<b>Core Depth:</b>	502 ft
<b>Date Completed:</b>	1/28/2017				
<b>Bore Hole Diameter (in):</b>	6	<b>Sampler Configuration</b>		<b>Liner Required:</b>	Y N
<b>Liner Used:</b>	Y N				
<b>Drill Machine:</b>	CME-550	<b>Drill Method:</b>	Mud Rotary	<b>Hammer Type:</b>	Automatic
<b>Energy Ratio:</b>	91.5%				
<b>Core Size:</b>	HQ	<b>Driller:</b>	AE Drilling	<b>Groundwater:</b>	TOB 6 ft
<b>24HR:</b>	2.9 ft				



**LEGEND**

*Continued Next Page*

SAMPLER TYPE		DRILLING METHOD	
SS - Split Spoon	NQ - Rock Core, 1-7/8"	HSA - Hollow Stem Auger	RW - Rotary Wash
UD - Undisturbed Sample	CU - Cuttings	CFA - Continuous Flight Augers	RC - Rock Core
AWG - Rock Core, 1-1/8"	CT - Continuous Tube	DC - Driving Casing	

SC\_DOT\_141316153\_USC-SCDOT DEEP BORINGS\_B-CON.GPJ\_SCDOT DATA TEMPLATE\_01\_30\_2015.GDT 12/20/17

# SCDOT Soil Test Log

<b>Project ID:</b>	1413-16-153	<b>County:</b>	Horry, SC	<b>Boring No.:</b>	B-CON
<b>Site Description:</b>	USC-SCDOT Deep Seismic Holes			<b>Route:</b>	
<b>Eng./Geo.:</b>	JP & CS	<b>Boring Location:</b>	N/A	<b>Offset:</b>	N/A
<b>Alignment:</b>	N/A				
<b>Elev.:</b>	79.0 ft	<b>Latitude:</b>	33.94557	<b>Longitude:</b>	-79.04754
<b>Date Started:</b>	1/18/2017				
<b>Total Depth:</b>	502 ft	<b>Soil Depth:</b>	118 ft	<b>Core Depth:</b>	502 ft
<b>Date Completed:</b>	1/28/2017				
<b>Bore Hole Diameter (in):</b>	6	<b>Sampler Configuration</b>		<b>Liner Required:</b>	Y N
<b>Liner Used:</b>	Y N				
<b>Drill Machine:</b>	CME-550	<b>Drill Method:</b>	Mud Rotary	<b>Hammer Type:</b>	Automatic
<b>Energy Ratio:</b>	91.5%				
<b>Core Size:</b>	HQ	<b>Driller:</b>	AE Drilling	<b>Groundwater:</b>	TOB 6 ft
<b>24HR:</b>	2.9 ft				

Elevation (ft)	Depth (ft)	MATERIAL DESCRIPTION	Graphic Log	Sample Depth (ft)	Sample No./Type	1st 6"	2nd 6"	3rd 6"	N Value	SPT N VALUE											
										PL	MC	LL	FINES CONTENT (%)								
325.7		Very stiff, moist to wet, none reactive, dark greenish gray (GLEY 1 10Y 4/1), medium plasticity fines, some fine to medium sand, SANDY LEAN CLAY (CL / A-6), trace shell fragments, trace subangular fine gravel, trace sub angular coarse sand		325.7	SC-43	0.2' / 5.0'															
-251.0	330.7			NO RECOVERY: driller noted rig chatter and resistance, low flow rate used for drilling fluids	330.7	SC-44	0.0' / 5.0'														
-256.0				335.7	SC-45	0.0' / 5.0'															
-261.0				340.7	SC-46	0.0' / 5.0'															
-266.0		Stiff, moist to wet, none to weakly reactive, dark gray (GLEY 1 N 4/) dark reddish brown (2.5YR 3/4), low to medium plasticity fines, some fine to medium sand, SANDY LEAN CLAY (CL / A-6), few shells, few wood fragments, (MC=40.8%, LL=43, PI=24, FC=45.0%)		345.7	SC-47	1.5' / 5.0'															
	345.7																				

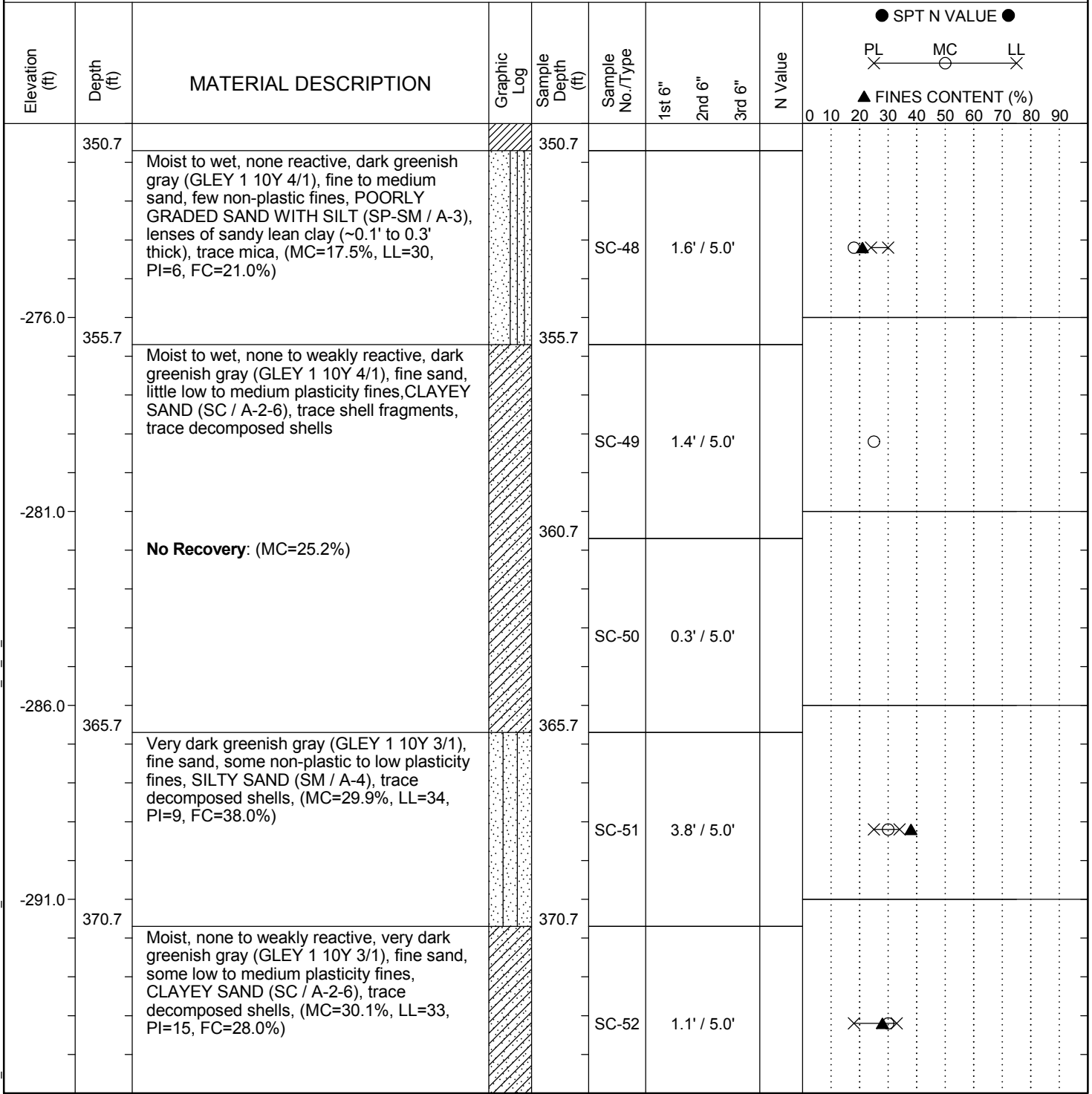
LEGEND Continued Next Page

<b>SAMPLER TYPE</b>		<b>DRILLING METHOD</b>	
SS - Split Spoon	NQ - Rock Core, 1-7/8"	HSA - Hollow Stem Auger	RW - Rotary Wash
UD - Undisturbed Sample	CU - Cuttings	CFA - Continuous Flight Augers	RC - Rock Core
AWG - Rock Core, 1-1/8"	CT - Continuous Tube	DC - Driving Casing	

SC\_DOT\_141316153\_USC-SCDOT DEEP BORINGS\_B-CON.GPJ\_SCDOT DATA TEMPLATE\_01\_30\_2015.GDT 12/20/17

# SCDOT Soil Test Log

<b>Project ID:</b>	1413-16-153	<b>County:</b>	Horry, SC	<b>Boring No.:</b>	B-CON
<b>Site Description:</b>	USC-SCDOT Deep Seismic Holes			<b>Route:</b>	
<b>Eng./Geo.:</b>	JP & CS	<b>Boring Location:</b>	N/A	<b>Offset:</b>	N/A
<b>Elev.:</b>	79.0 ft	<b>Latitude:</b>	33.94557	<b>Longitude:</b>	-79.04754
<b>Total Depth:</b>	502 ft	<b>Soil Depth:</b>	118 ft	<b>Core Depth:</b>	502 ft
<b>Bore Hole Diameter (in):</b>	6	<b>Sampler Configuration</b>		<b>Liner Required:</b>	Y N
<b>Drill Machine:</b>	CME-550	<b>Drill Method:</b>	Mud Rotary	<b>Hammer Type:</b>	Automatic
<b>Core Size:</b>	HQ	<b>Driller:</b>	AE Drilling	<b>Groundwater:</b>	TOB 6 ft
				<b>24HR</b>	2.9 ft
				<b>Energy Ratio:</b>	91.5%
				<b>Date Started:</b>	1/18/2017
				<b>Date Completed:</b>	1/28/2017



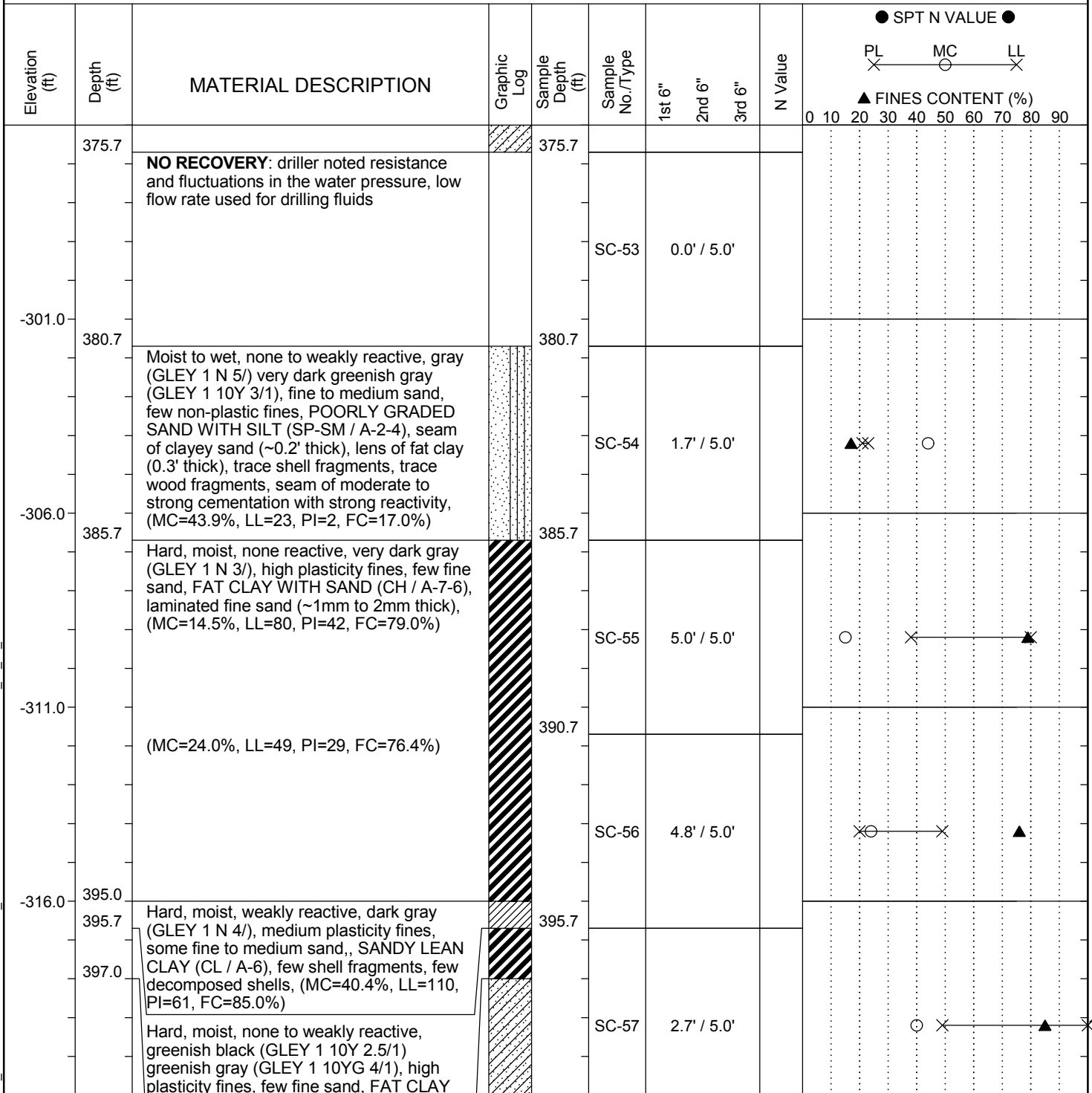
LEGEND Continued Next Page

<b>SAMPLER TYPE</b>		<b>DRILLING METHOD</b>	
SS - Split Spoon	NQ - Rock Core, 1-7/8"	HSA - Hollow Stem Auger	RW - Rotary Wash
UD - Undisturbed Sample	CU - Cuttings	CFA - Continuous Flight Augers	RC - Rock Core
AWG - Rock Core, 1-1/8"	CT - Continuous Tube	DC - Driving Casing	

SC\_DOT\_141316153\_USC-SCDOT DEEP BORINGS\_B-CON.GPJ\_SCDOT DATA TEMPLATE\_01\_30\_2015.GDT 12/20/17

# SCDOT Soil Test Log

<b>Project ID:</b>	1413-16-153	<b>County:</b>	Horry, SC	<b>Boring No.:</b>	B-CON
<b>Site Description:</b>	USC-SCDOT Deep Seismic Holes			<b>Route:</b>	
<b>Eng./Geo.:</b>	JP & CS	<b>Boring Location:</b>	N/A	<b>Offset:</b>	N/A
<b>Elev.:</b>	79.0 ft	<b>Latitude:</b>	33.94557	<b>Longitude:</b>	-79.04754
<b>Total Depth:</b>	502 ft	<b>Soil Depth:</b>	118 ft	<b>Core Depth:</b>	502 ft
<b>Bore Hole Diameter (in):</b>	6	<b>Sampler Configuration</b>		<b>Liner Required:</b>	Y N
<b>Drill Machine:</b>	CME-550	<b>Drill Method:</b>	Mud Rotary	<b>Hammer Type:</b>	Automatic
<b>Core Size:</b>	HQ	<b>Driller:</b>	AE Drilling	<b>Groundwater:</b>	TOB 6 ft
				<b>24HR</b>	2.9 ft



**LEGEND**

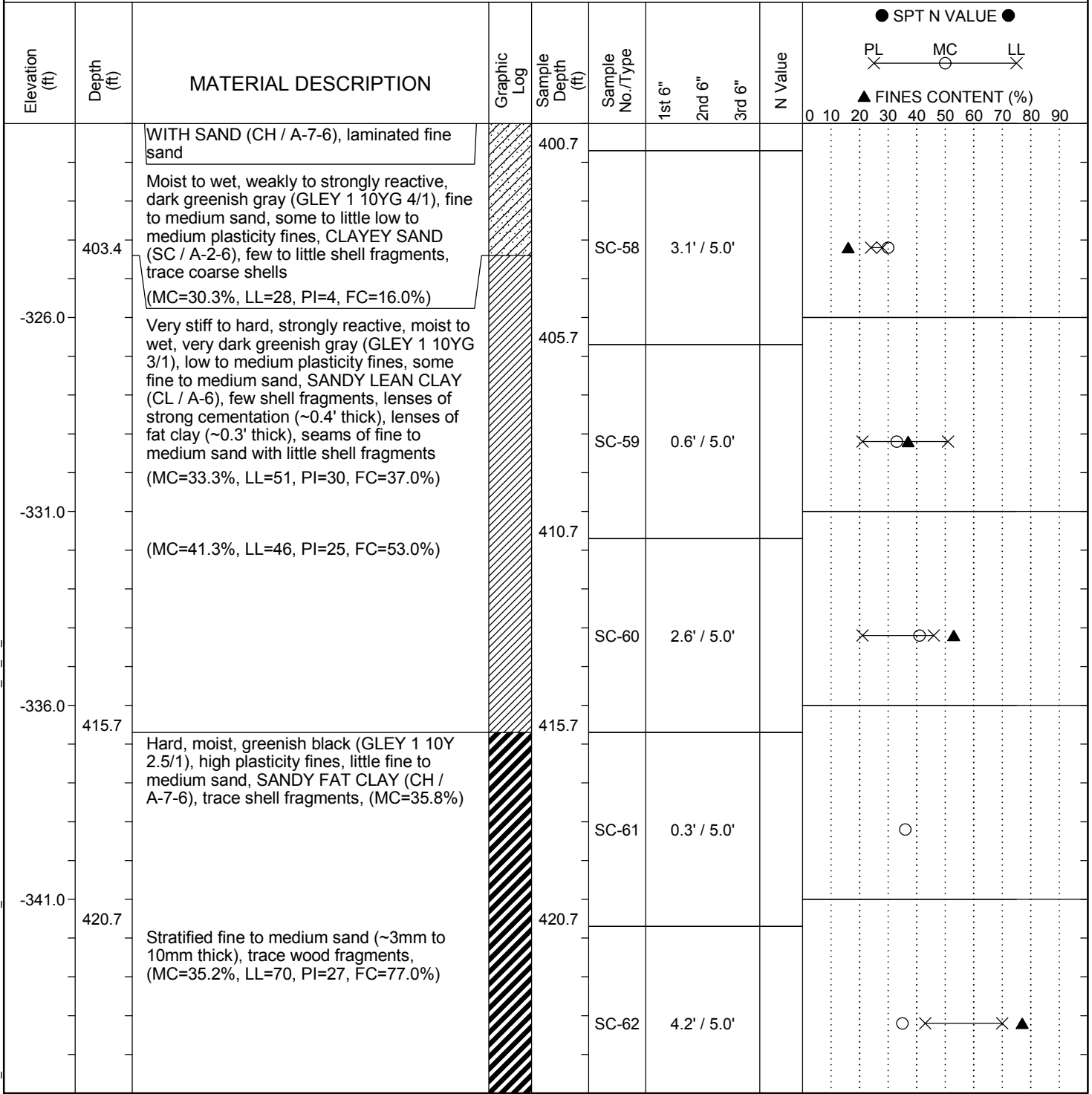
*Continued Next Page*

SAMPLER TYPE		DRILLING METHOD	
SS - Split Spoon	NQ - Rock Core, 1-7/8"	HSA - Hollow Stem Auger	RW - Rotary Wash
UD - Undisturbed Sample	CU - Cuttings	CFA - Continuous Flight Augers	RC - Rock Core
AWG - Rock Core, 1-1/8"	CT - Continuous Tube	DC - Driving Casing	

SC\_DOT 141316153\_USC-SCDOT DEEP BORINGS\_B-CON.GPJ\_SCDOT DATA TEMPLATE\_01\_30\_2015.GDT 12/20/17

# SCDOT Soil Test Log

<b>Project ID:</b>	1413-16-153	<b>County:</b>	Horry, SC	<b>Boring No.:</b>	B-CON
<b>Site Description:</b>	USC-SCDOT Deep Seismic Holes			<b>Route:</b>	
<b>Eng./Geo.:</b>	JP & CS	<b>Boring Location:</b>	N/A	<b>Offset:</b>	N/A
<b>Elev.:</b>	79.0 ft	<b>Latitude:</b>	33.94557	<b>Longitude:</b>	-79.04754
<b>Total Depth:</b>	502 ft	<b>Soil Depth:</b>	118 ft	<b>Core Depth:</b>	502 ft
<b>Bore Hole Diameter (in):</b>	6	<b>Sampler Configuration</b>		<b>Liner Required:</b>	Y N
<b>Drill Machine:</b>	CME-550	<b>Drill Method:</b>	Mud Rotary	<b>Hammer Type:</b>	Automatic
<b>Core Size:</b>	HQ	<b>Driller:</b>	AE Drilling	<b>Groundwater:</b>	TOB 6 ft
				<b>24HR</b>	2.9 ft
				<b>Energy Ratio:</b>	91.5%
				<b>Date Started:</b>	1/18/2017
				<b>Date Completed:</b>	1/28/2017



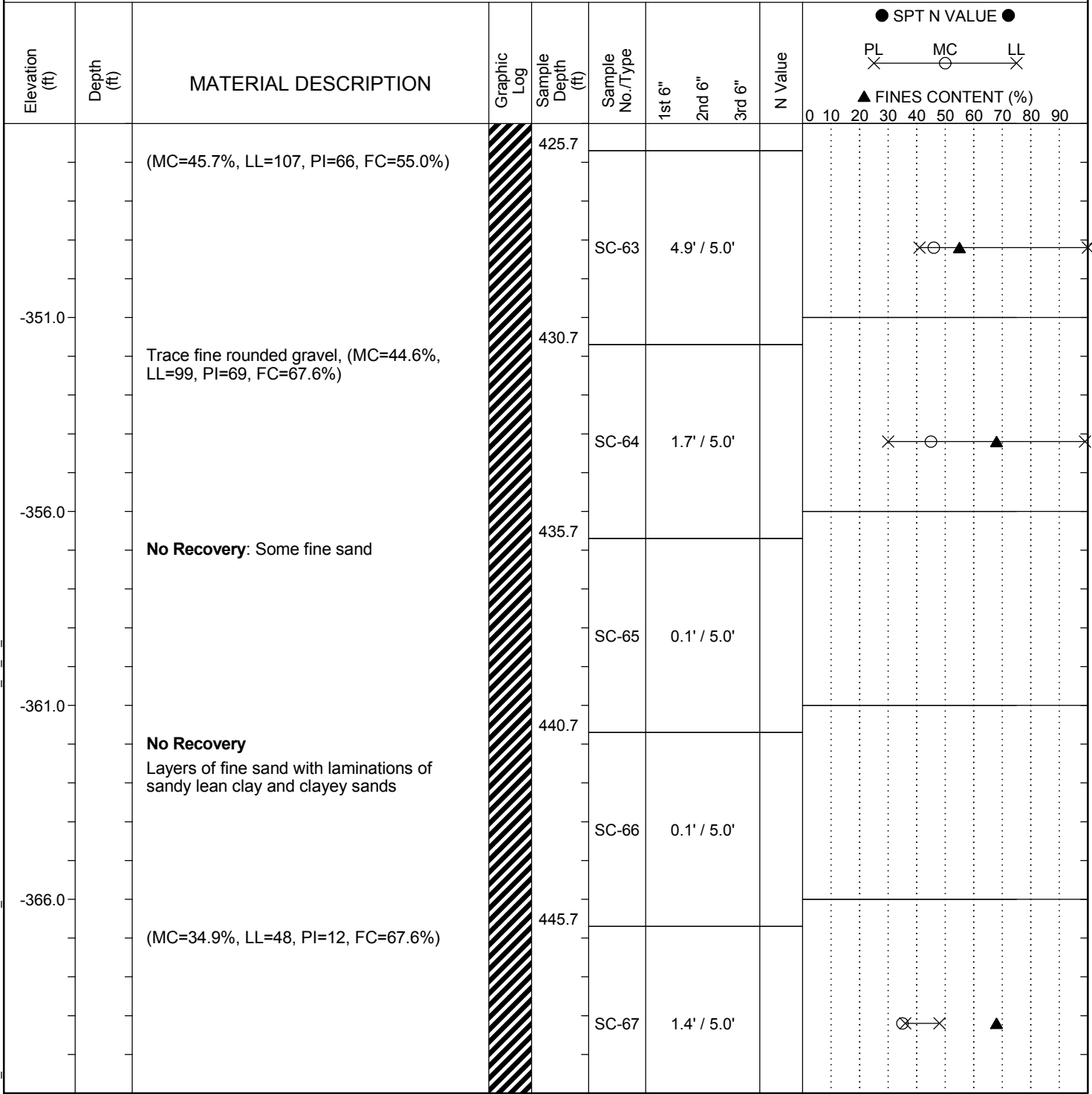
LEGEND Continued Next Page

SAMPLER TYPE		DRILLING METHOD	
SS - Split Spoon	NQ - Rock Core, 1-7/8"	HSA - Hollow Stem Auger	RW - Rotary Wash
UD - Undisturbed Sample	CU - Cuttings	CFA - Continuous Flight Augers	RC - Rock Core
AWG - Rock Core, 1-1/8"	CT - Continuous Tube	DC - Driving Casing	

SC\_DOT\_141316153\_USC-SCDOT DEEP BORINGS\_B-CON.GPJ\_SCDOT DATA TEMPLATE\_01\_30\_2015.GDT 12/20/17

# SCDOT Soil Test Log

<b>Project ID:</b>	1413-16-153	<b>County:</b>	Horry, SC	<b>Boring No.:</b>	B-CON
<b>Site Description:</b>	USC-SCDOT Deep Seismic Holes			<b>Route:</b>	
<b>Eng./Geo.:</b>	JP & CS	<b>Boring Location:</b>	N/A	<b>Offset:</b>	N/A
<b>Elev.:</b>	79.0 ft	<b>Latitude:</b>	33.94557	<b>Longitude:</b>	-79.04754
<b>Total Depth:</b>	502 ft	<b>Soil Depth:</b>	118 ft	<b>Core Depth:</b>	502 ft
<b>Bore Hole Diameter (in):</b>	6	<b>Sampler Configuration</b>		<b>Liner Required:</b>	Y N
<b>Drill Machine:</b>	CME-550	<b>Drill Method:</b>	Mud Rotary	<b>Hammer Type:</b>	Automatic
<b>Core Size:</b>	HQ	<b>Driller:</b>	AE Drilling	<b>Groundwater:</b>	TOB 6 ft
				<b>24HR</b>	2.9 ft
				<b>Energy Ratio:</b>	91.5%
				<b>Liner Used:</b>	Y N



LEGEND

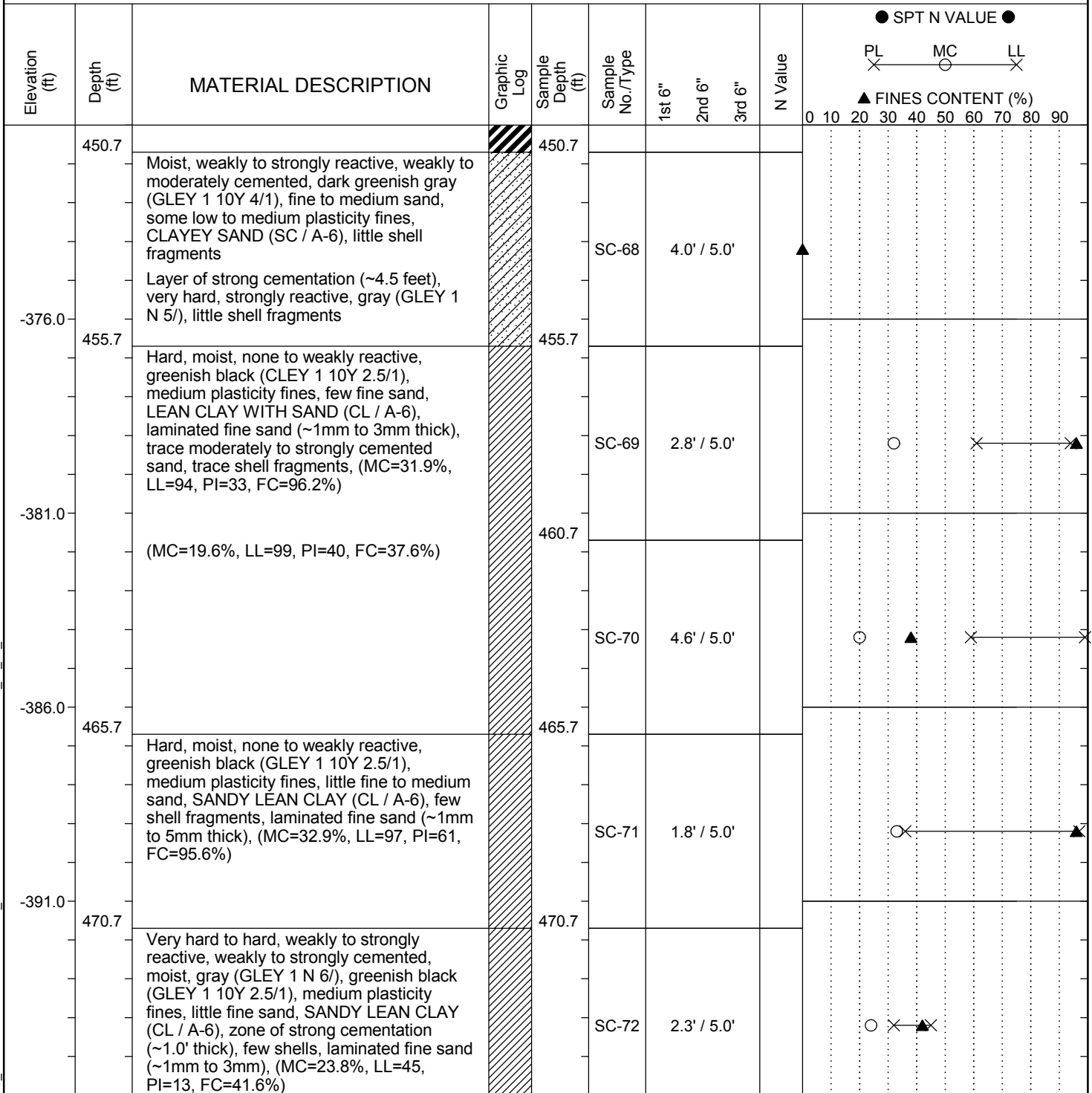
Continued Next Page

SAMPLER TYPE		DRILLING METHOD	
SS - Split Spoon	NQ - Rock Core, 1-7/8"	HSA - Hollow Stem Auger	RW - Rotary Wash
UD - Undisturbed Sample	CU - Cuttings	CFA - Continuous Flight Augers	RC - Rock Core
AWG - Rock Core, 1-1/8"	CT - Continuous Tube	DC - Driving Casing	

SC\_DOT 141316153\_USC-SCDOT DEEP BORINGS\_B-CON.GPJ\_SCDOT DATA TEMPLATE\_01\_30\_2015.GDT 12/20/17

# SCDOT Soil Test Log

<b>Project ID:</b>	1413-16-153	<b>County:</b>	Horry, SC	<b>Boring No.:</b>	B-CON
<b>Site Description:</b>	USC-SCDOT Deep Seismic Holes			<b>Route:</b>	
<b>Eng./Geo.:</b>	JP & CS	<b>Boring Location:</b>	N/A	<b>Offset:</b>	N/A
<b>Elev.:</b>	79.0 ft	<b>Latitude:</b>	33.94557	<b>Longitude:</b>	-79.04754
<b>Total Depth:</b>	502 ft	<b>Soil Depth:</b>	118 ft	<b>Core Depth:</b>	502 ft
<b>Bore Hole Diameter (in):</b>	6	<b>Sampler Configuration</b>		<b>Liner Required:</b>	Y N
<b>Drill Machine:</b>	CME-550	<b>Drill Method:</b>	Mud Rotary	<b>Hammer Type:</b>	Automatic
<b>Core Size:</b>	HQ	<b>Driller:</b>	AE Drilling	<b>Groundwater:</b>	TOB 6 ft
				<b>24HR</b>	2.9 ft



### LEGEND

Continued Next Page

SAMPLER TYPE		DRILLING METHOD	
SS - Split Spoon	NQ - Rock Core, 1-7/8"	HSA - Hollow Stem Auger	RW - Rotary Wash
UD - Undisturbed Sample	CU - Cuttings	CFA - Continuous Flight Augers	RC - Rock Core
AWG - Rock Core, 1-1/8"	CT - Continuous Tube	DC - Driving Casing	

SC\_DOT 141316153\_USC-SCDOT DEEP BORINGS\_B-CON.GPJ\_SCDOT DATA TEMPLATE\_01\_30\_2015.GDT 12/20/17

# SCDOT Soil Test Log

<b>Project ID:</b>	1413-16-153	<b>County:</b>	Horry, SC	<b>Boring No.:</b>	B-CON
<b>Site Description:</b>	USC-SCDOT Deep Seismic Holes			<b>Route:</b>	
<b>Eng./Geo.:</b>	JP & CS	<b>Boring Location:</b>	N/A	<b>Offset:</b>	N/A
<b>Alignment:</b>	N/A				
<b>Elev.:</b>	79.0 ft	<b>Latitude:</b>	33.94557	<b>Longitude:</b>	-79.04754
<b>Date Started:</b>	1/18/2017				
<b>Total Depth:</b>	502 ft	<b>Soil Depth:</b>	118 ft	<b>Core Depth:</b>	502 ft
<b>Date Completed:</b>	1/28/2017				
<b>Bore Hole Diameter (in):</b>	6	<b>Sampler Configuration</b>		<b>Liner Required:</b>	Y N
<b>Liner Used:</b>	Y N				
<b>Drill Machine:</b>	CME-550	<b>Drill Method:</b>	Mud Rotary	<b>Hammer Type:</b>	Automatic
<b>Energy Ratio:</b>	91.5%				
<b>Core Size:</b>	HQ	<b>Driller:</b>	AE Drilling	<b>Groundwater:</b>	TOB 6 ft
<b>24HR:</b>	2.9 ft				

Elevation (ft)	Depth (ft)	MATERIAL DESCRIPTION	Graphic Log	Sample Depth (ft)	Sample No./Type	1st 6"	2nd 6"	3rd 6"	N Value	SPT N VALUE												
										PL	MC	LL	FINES CONTENT (%)									
475.7		Hard, moist, none to weakly reactive, greenish blk (GLEY 1 10Y 2.5/1), medium plasticity fines., few fine sand, LEAN CLAY WITH SAND (CL / A-6), laminated fine sand (~1mm to 2mm), trace shells, (MC=42.7%, LL=100, PI=76, FC=46.0%)		475.7	SC-73	1.5' / 5.0'																
-401.0	480.7	Hard, moist, none reactive, very dark gray (GLEY 1 N 3/), high plasticity fines, few fine sand, FAT CLAY WITH SAND (CH / A-7-6), trace shells, blocky, (MC=35.2%, LL=34, PI=5, FC=38.0%)		480.7	SC-74	0.9' / 5.0'																
-406.0	485.7	<b>NO RECOVERY:</b> driller noted resistance, fluctuating water pressure, low flow rate used for drilling fluid		485.7	SC-75	0.0' / 5.0'																
-411.0	490.7	Wet to moist, greenish gray (GLEY 1 10Y 5/1) very dark gray (GLEY 1 N 3/), fine to medium sand, few low to medium plasticity fines, POORLY GRADED SAND WITH SILT (SP-SM / A-2-4), trace shell fragments, stratified sandy lean clay (~5mm to 0.3' thick), (MC=26.7%, FC=3.0%)		490.7	SC-76	2.5' / 5.0'																
-416.0	495.7	(MC=44.9%, LL=110, PI=48, FC=78.0%)		495.7																		
-419.0	497.7	Moist to wet, greenish black (GLEY 1 10Y 2.5/1), medium plasticity fines, little fine sand, SANDY LEAN CLAY (CL / A-6), trace shell fragments, seams of fine sand		497.7	SC-77	2.9' / 5.0'																

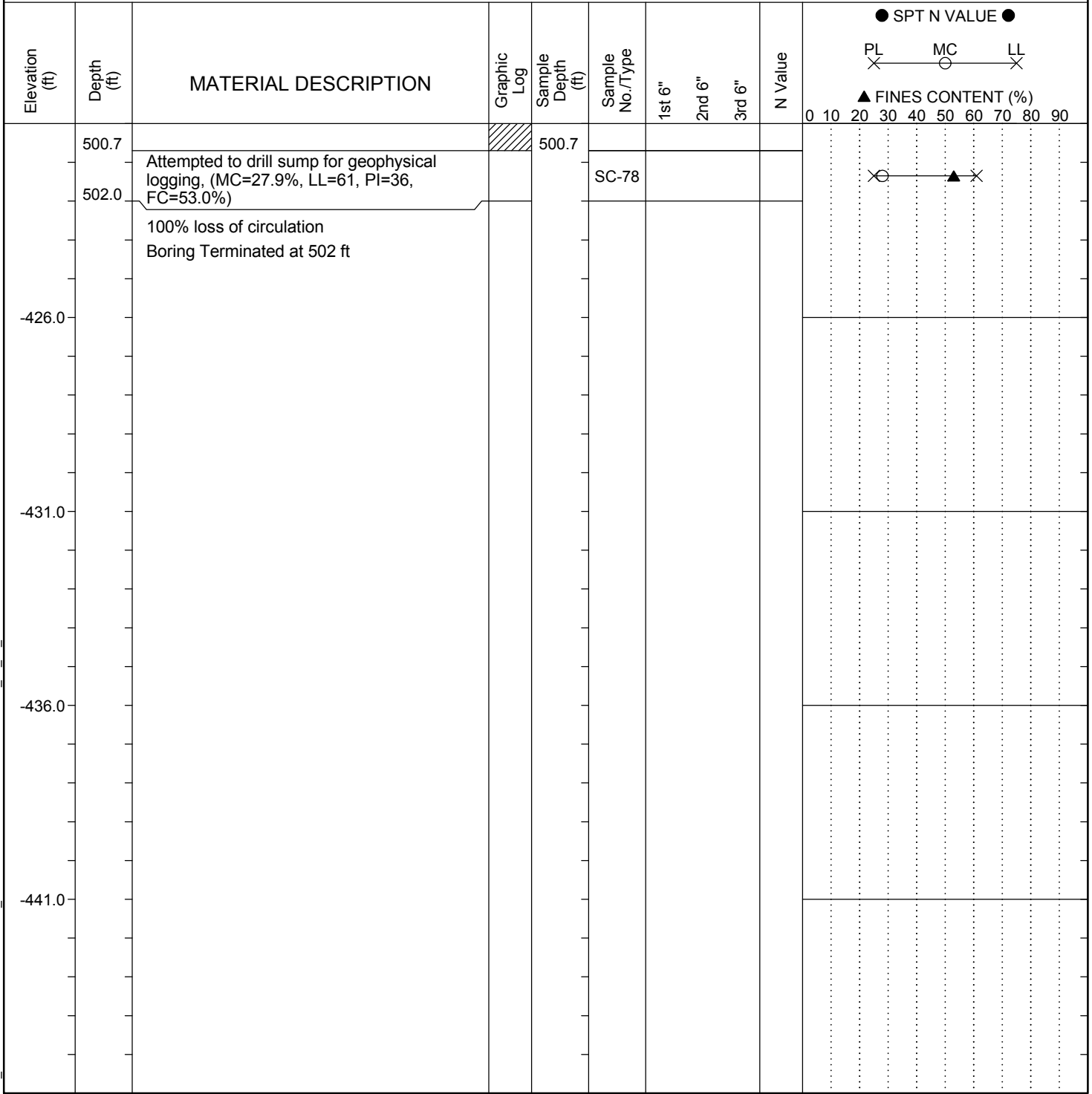
LEGEND Continued Next Page

<b>SAMPLER TYPE</b>		<b>DRILLING METHOD</b>	
SS - Split Spoon	NQ - Rock Core, 1-7/8"	HSA - Hollow Stem Auger	RW - Rotary Wash
UD - Undisturbed Sample	CU - Cuttings	CFA - Continuous Flight Augers	RC - Rock Core
AWG - Rock Core, 1-1/8"	CT - Continuous Tube	DC - Driving Casing	

SC\_DOT 141316153\_USC-SCDOT DEEP BORINGS\_B-CON.GPJ\_SCDOT DATA TEMPLATE\_01\_30\_2015.GDT 12/20/17

# SCDOT Soil Test Log

<b>Project ID:</b>	1413-16-153	<b>County:</b>	Horry, SC	<b>Boring No.:</b>	B-CON
<b>Site Description:</b>	USC-SCDOT Deep Seismic Holes			<b>Route:</b>	
<b>Eng./Geo.:</b>	JP & CS	<b>Boring Location:</b>	N/A	<b>Offset:</b>	N/A
<b>Alignment:</b>	N/A				
<b>Elev.:</b>	79.0 ft	<b>Latitude:</b>	33.94557	<b>Longitude:</b>	-79.04754
<b>Date Started:</b>	1/18/2017				
<b>Total Depth:</b>	502 ft	<b>Soil Depth:</b>	118 ft	<b>Core Depth:</b>	502 ft
<b>Date Completed:</b>	1/28/2017				
<b>Bore Hole Diameter (in):</b>	6	<b>Sampler Configuration</b>		<b>Liner Required:</b>	Y N
<b>Liner Used:</b>	Y N				
<b>Drill Machine:</b>	CME-550	<b>Drill Method:</b>	Mud Rotary	<b>Hammer Type:</b>	Automatic
<b>Energy Ratio:</b>	91.5%				
<b>Core Size:</b>	HQ	<b>Driller:</b>	AE Drilling	<b>Groundwater:</b>	TOB 6 ft
<b>24HR:</b>	2.9 ft				



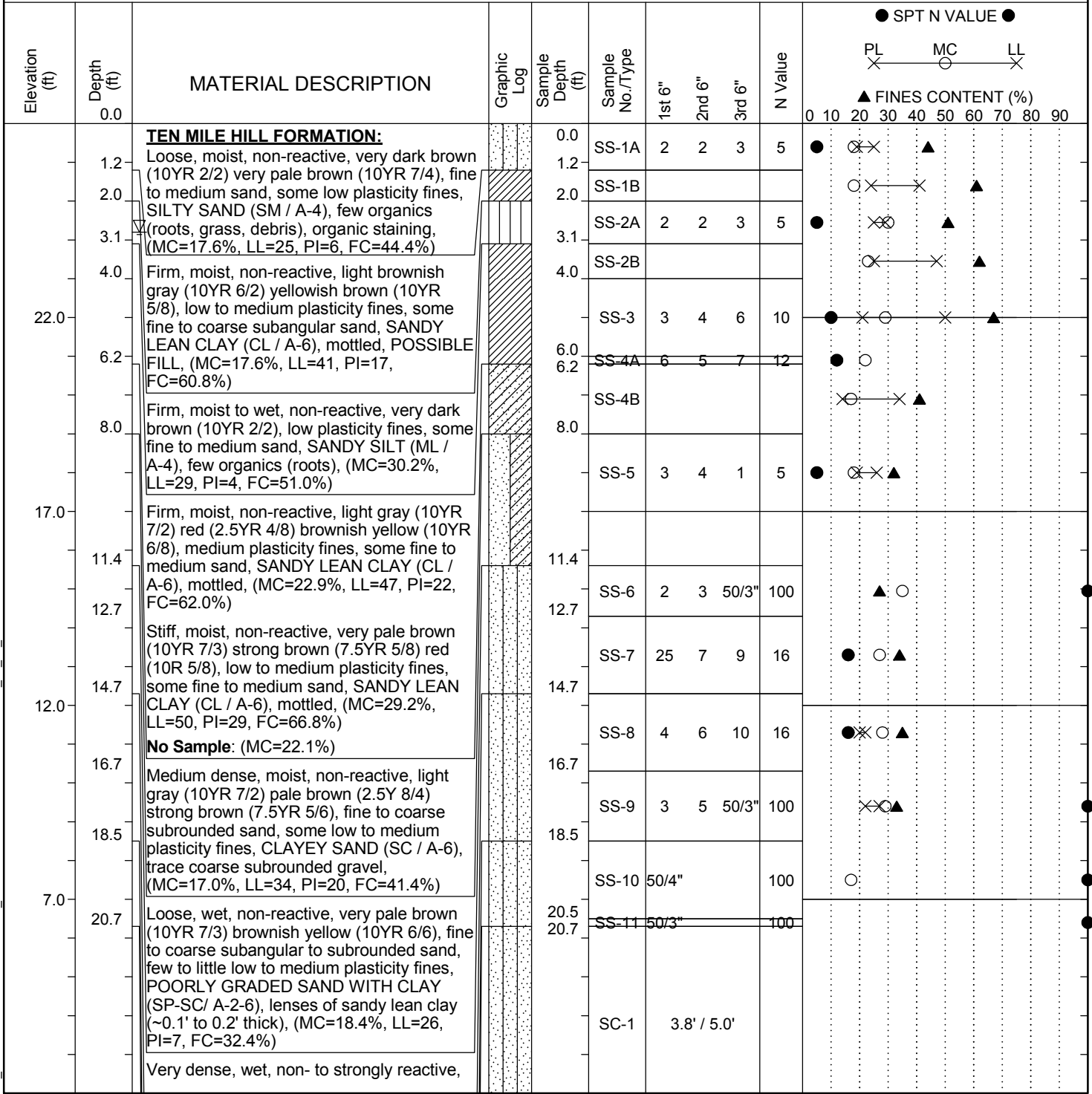
### LEGEND

SAMPLER TYPE		DRILLING METHOD	
SS - Split Spoon	NQ - Rock Core, 1-7/8"	HSA - Hollow Stem Auger	RW - Rotary Wash
UD - Undisturbed Sample	CU - Cuttings	CFA - Continuous Flight Augers	RC - Rock Core
AWG - Rock Core, 1-1/8"	CT - Continuous Tube	DC - Driving Casing	

SC\_DOT 141316153\_USC-SCDOT DEEP BORINGS\_B-CON.GPJ\_SCDOT DATA TEMPLATE\_01\_30\_2015.GDT 12/20/17

# SCDOT Soil Test Log

<b>Project ID:</b>	1413-16-153	<b>County:</b>	Georgetown, SC	<b>Boring No.:</b>	B-FMG
<b>Site Description:</b>	USC-SCDOT Deep Seismic Holes			<b>Route:</b>	
<b>Eng./Geo.:</b>	CS & LE	<b>Boring Location:</b>		<b>Offset:</b>	
<b>Elev.:</b>	27.0 ft	<b>Latitude:</b>	33.447666	<b>Longitude:</b>	-79.59089
<b>Total Depth:</b>	615 ft	<b>Soil Depth:</b>	20.8 ft	<b>Core Depth:</b>	615 ft
<b>Bore Hole Diameter (in):</b>	4	<b>Sampler Configuration</b>		<b>Liner Required:</b>	Y N
<b>Drill Machine:</b>	CME-550	<b>Drill Method:</b>	Mud Rotary	<b>Hammer Type:</b>	Automatic
<b>Core Size:</b>	HQ	<b>Driller:</b>	AE Drilling	<b>Energy Ratio:</b>	91.5%
		<b>Groundwater:</b>	TOB	2.5 ft	24HR 2.8 ft



LEGEND Continued Next Page

<b>SAMPLER TYPE</b>		<b>DRILLING METHOD</b>	
SS - Split Spoon	NQ - Rock Core, 1-7/8"	HSA - Hollow Stem Auger	RW - Rotary Wash
UD - Undisturbed Sample	CU - Cuttings	CFA - Continuous Flight Augers	RC - Rock Core
AWG - Rock Core, 1-1/8"	CT - Continuous Tube	DC - Driving Casing	

SC\_DOT 141316153\_USC-SCDOT DEEP BORINGS\_B-FMG.GPJ SCDOT DATA TEMPLATE\_01\_30\_2015.GDT 12/20/17

# SCDOT Soil Test Log

<b>Project ID:</b>	1413-16-153	<b>County:</b>	Georgetown, SC	<b>Boring No.:</b>	B-FMG
<b>Site Description:</b>	USC-SCDOT Deep Seismic Holes			<b>Route:</b>	
<b>Eng./Geo.:</b>	CS & LE	<b>Boring Location:</b>		<b>Offset:</b>	
<b>Elev.:</b>	27.0 ft	<b>Latitude:</b>	33.447666	<b>Longitude:</b>	-79.59089
<b>Total Depth:</b>	615 ft	<b>Soil Depth:</b>	20.8 ft	<b>Core Depth:</b>	615 ft
<b>Bore Hole Diameter (in):</b>	4	<b>Sampler Configuration</b>		<b>Liner Required:</b>	Y N
<b>Drill Machine:</b>	CME-550	<b>Drill Method:</b>	Mud Rotary	<b>Hammer Type:</b>	Automatic
<b>Core Size:</b>	HQ	<b>Driller:</b>	AE Drilling	<b>Groundwater:</b>	TOB 2.5 ft
				<b>24HR</b>	2.8 ft

Elevation (ft)	Depth (ft)	MATERIAL DESCRIPTION	Graphic Log	Sample Depth (ft)	Sample No./Type	1st 6"	2nd 6"	3rd 6"	N Value	SPT N VALUE											
										PL	MC	LL	FINES CONTENT (%)								
		dark greenish gray (GLE Y 1 10Y 4/1), fine to medium sand, little non-plastic fines, SILTY SAND (SM / A-3), strongly cemented fragments at bottom of sample (top of cemented layer at ~12.3'), (MC=34.8%, LL=NP, PI=NP, FC=27.4%)		25.7																	
		Medium dense, moist to wet, weakly to strongly reactive, dark gray (GLE Y 1 N 4/), fine sand, little non-plastic fines, SILTY SAND (SM / A-3), strongly cemented fragments at top of sample, (MC=27.0%, LL=NP, PI=NP, FC=34.2%)		30.7	SC-2	4.3' / 5.0'															
		Medium dense, wet, weakly to strongly reactive, gray (GLE Y 1 N 5/), fine to medium sand, some non-plastic fines, SILTY SAND (SM / A-4), few strongly cemented nodules, (MC=28.4%, LL=22, PI=2, FC=34.8%)		35.7	SC-3	0.0' / 5.0'															
		Very dense, moist to wet, weakly to strongly reactive, weakly to strongly cemented, very dark greenish gray (GLE Y 1 10Y 3/1), fine to medium sand, some non-plastic fines, SILTY SAND (SM / A-4), few fine to coarse moderately to strongly cemented nodules, (MC=29.0%, LL=27, PI=5, FC=33.2%)		35.7																	
		<b>WILLIAMS BURG FORMATION - CHICORA MEMBER:</b> Very dense, moist to wet, weakly to strongly reactive, strongly cemented, dark greenish gray (GLE Y 1 10Y 4/1), fine to medium sand, little non-plastic fines, SILTY SAND (SM / A-2-4), mostly strongly cemented nodules, trace shell fragments, (MC=16.5%)		40.7	SC-4	2.8' / 5.0'															
		<b>NO RECOVERY</b> Very hard, moist, strongly reactive, strongly cemented, light greenish gray (GLE Y 1 10Y 8/1), fine to coarse subangular sand, little non-plastic to low plasticity fines, SILTY SAND (SM / A-2-4), mostly strongly cemented nodules and layers with honeycombing, little fine to coarse shells		45.7	SC-5	1.2' / 5.0'															
		Less honeycombing <b>NO RECOVERY:</b> (from cuttings) weakly reactive, weakly cemented, light greenish gray (GLE Y 2 10BG 7/1), fine to coarse subangular to subrounded sand, little non-plastic to low plasticity fines, SILTY SAND (SM / A-2-4), Driller noted fluctuating		45.7	SC-6	1.0' / 5.0'															

**LEGEND**

*Continued Next Page*

<b>SAMPLER TYPE</b>		<b>DRILLING METHOD</b>	
SS - Split Spoon	NQ - Rock Core, 1-7/8"	HSA - Hollow Stem Auger	RW - Rotary Wash
UD - Undisturbed Sample	CU - Cuttings	CFA - Continuous Flight Augers	RC - Rock Core
AWG - Rock Core, 1-1/8"	CT - Continuous Tube	DC - Driving Casing	

SC\_DOT\_141316153\_USC-SCDOT DEEP BORINGS\_B-FMG.GPJ\_SCDOT DATA TEMPLATE\_01\_30\_2015.GDT 12/20/17

# SCDOT Soil Test Log

<b>Project ID:</b>	1413-16-153	<b>County:</b>	Georgetown, SC	<b>Boring No.:</b>	B-FMG
<b>Site Description:</b>	USC-SCDOT Deep Seismic Holes			<b>Route:</b>	
<b>Eng./Geo.:</b>	CS & LE	<b>Boring Location:</b>		<b>Offset:</b>	
<b>Elev.:</b>	27.0 ft	<b>Latitude:</b>	33.447666	<b>Longitude:</b>	-79.59089
<b>Total Depth:</b>	615 ft	<b>Soil Depth:</b>	20.8 ft	<b>Core Depth:</b>	615 ft
<b>Bore Hole Diameter (in):</b>	4	<b>Sampler Configuration</b>		<b>Liner Required:</b>	Y N
<b>Drill Machine:</b>	CME-550	<b>Drill Method:</b>	Mud Rotary	<b>Hammer Type:</b>	Automatic
<b>Core Size:</b>	HQ	<b>Driller:</b>	AE Drilling	<b>Groundwater:</b>	TOB 2.5 ft
				<b>24HR</b>	2.8 ft
				<b>Energy Ratio:</b>	91.5%
				<b>Liner Used:</b>	Y N

Elevation (ft)	Depth (ft)	MATERIAL DESCRIPTION	Graphic Log	Sample Depth (ft)	Sample No./Type	1st 6"	2nd 6"	3rd 6"	N Value	SPT N VALUE												
										PL	MC	LL	FINES CONTENT (%)									
50.7		pressure and resistance		50.7																		
		Very hard, moist, strongly reactive, strongly cemented, greenish gray (GLEY 1 10Y 6/1), fine to coarse subangular to subrounded sand, little non-plastic to low plasticity fines, SILTY SAND (SM / A-2-4), honeycombing, some fine to coarse shells			SC-7	0.6' / 5.0'																
-28.0	55.7	Very hard, moist, strongly reactive, strongly cemented, greenish gray (GLEY 1 10Y 6/1), fine to coarse angular to subangular sand, few non-plastic to low plasticity fines, POORLY GRADED SAND WITH SILT (SP-SM / A-2-4), honeycombing, some coarse shells		55.7																		
		Moist to wet, weakly to strongly reactive, weakly to moderately cemented, light greenish gray (GLEY 1 10Y 7/1), fine to medium sand, few non-plastic to low plasticity fines, POORLY GRADED SAND WITH SILT (SP-SM / A-2-4), trace mica, trace shell fragments			SC-8	0.3' / 5.0'																
-33.0		Moist, strongly reactive, strongly cemented, greenish gray (GLEY 1 10Y 6/1), fine to medium sand, little low plasticity fines, SILTY SAND (SM / A-2-4), slight honeycombing, trace shell fragments		60.7																		
		Moist, strongly reactive, strongly cemented, greenish gray (GLEY 1 10Y 6/1), fine to medium sand, little low plasticity fines, SILTY SAND (SM / A-2-4), slight honeycombing, trace shell fragments			SC-9	0.1' / 5.0'																
-38.0	65.7	<b>WILLIAMS BURG FORMATION - LOWER BRIDGE MEMBER:</b> <b>NO RECOVERY:</b> (from cuttings) non-reactive, greenish gray (GLEY 1 10Y 6/1), fine to medium sand, few non-plastic fines, POORLY GRADED SAND WITH SILT (SP-SM / A-2-4), trace shell fragments		65.7																		
		Moist to wet, weakly to strongly reactive, very dark greenish gray (GLEY 1 10Y 3/1), fine sand, few non-plastic fines, POORLY GRADED SAND WITH SILT (SP-SM / A-3) lens of strong cementation (~0.5' thick), (MC=23.6%)		70.7																		
-43.0	70.7			70.7	SC-11	1.0' / 5.0'																

LEGEND Continued Next Page

SAMPLER TYPE		DRILLING METHOD	
SS - Split Spoon	NQ - Rock Core, 1-7/8"	HSA - Hollow Stem Auger	RW - Rotary Wash
UD - Undisturbed Sample	CU - Cuttings	CFA - Continuous Flight Augers	RC - Rock Core
AWG - Rock Core, 1-1/8"	CT - Continuous Tube	DC - Driving Casing	

SC\_DOT\_141316153\_USC-SCDOT DEEP BORINGS\_B-FMG.GPJ\_SCDOT DATA TEMPLATE\_01\_30\_2015.GDT\_12/20/17

# SCDOT Soil Test Log

<b>Project ID:</b>	1413-16-153	<b>County:</b>	Georgetown, SC	<b>Boring No.:</b>	B-FMG
<b>Site Description:</b>	USC-SCDOT Deep Seismic Holes			<b>Route:</b>	
<b>Eng./Geo.:</b>	CS & LE	<b>Boring Location:</b>		<b>Offset:</b>	
<b>Elev.:</b>	27.0 ft	<b>Latitude:</b>	33.447666	<b>Longitude:</b>	-79.59089
<b>Total Depth:</b>	615 ft	<b>Soil Depth:</b>	20.8 ft	<b>Core Depth:</b>	615 ft
<b>Bore Hole Diameter (in):</b>	4	<b>Sampler Configuration</b>		<b>Liner Required:</b>	Y N
<b>Drill Machine:</b>	CME-550	<b>Drill Method:</b>	Mud Rotary	<b>Hammer Type:</b>	Automatic
<b>Core Size:</b>	HQ	<b>Driller:</b>	AE Drilling	<b>Groundwater:</b>	TOB 2.5 ft
				<b>24HR</b>	2.8 ft
				<b>Energy Ratio:</b>	91.5%
				<b>Liner Used:</b>	Y N

Elevation (ft)	Depth (ft)	MATERIAL DESCRIPTION	Graphic Log	Sample Depth (ft)	Sample No./Type	1st 6"	2nd 6"	3rd 6"	N Value	SPT N VALUE											
										PL	MC	LL	FINES CONTENT (%)								
75.7	75.7	<b>NO RECOVERY:</b> (from cuttings) weakly reactive, very dark greenish gray (GLEY 1 10Y 3/1), fine sand, some non-plastic to low plasticity fines, SILTY SAND (SM/ A-4), trace mica		75.7	SC-12	0.0' / 5.0'															
-53.0	80.7	Moist to wet, weakly to strongly reactive, non- to strongly cemented, very dark greenish gray (GLEY 1 10Y 3/1) gray (GLEY 1 N 6'), fine sand, some non-plastic to low plasticity fines, SILTY SAND (SM / A-4), trace mica, lenses of strong cementation (~0.2' to 0.3' thick), (MC=28.0%, LL=NP, PI=NP, FC=40.4%)		80.7	SC-13	2.2' / 5.0'															
-58.0	85.7	Moist to wet, weakly reactive, very dark greenish gray (GLEY 1 10Y 3/1), fine sand, some low plasticity fines, SILTY SAND (SM / A-6), trace mica, trace shell fragments, (MC=32.6%, LL=32, PI=7, FC=35.4%)		85.7	SC-14	0.9' / 5.0'															
-63.0	90.7	<b>NO RECOVERY:</b> (from cuttings) weakly reactive, very dark greenish gray (GLEY 1 10Y 3/1), fine sand, some low plasticity fines, SILTY SAND (SM / A-6), trace mica, trace shell fragments		90.7	SC-15	0.0' / 5.0'															
-68.0	95.7	Moist to wet, weakly reactive, very dark greenish gray (GLEY 1 10Y 3/1), fine sand, little low plasticity fines, SILTY SAND (SM / A-6), trace mica, (MC=34.2%, LL=NP, PI=NP, FC=37.2%)		95.7	SC-16	2.3' / 5.0'															

LEGEND Continued Next Page

SAMPLER TYPE		DRILLING METHOD	
SS - Split Spoon	NQ - Rock Core, 1-7/8"	HSA - Hollow Stem Auger	RW - Rotary Wash
UD - Undisturbed Sample	CU - Cuttings	CFA - Continuous Flight Augers	RC - Rock Core
AWG - Rock Core, 1-1/8"	CT - Continuous Tube	DC - Driving Casing	

SC\_DOT\_141316153\_USC-SCDOT DEEP BORINGS\_B-FMG.GPJ\_SCDOT DATA TEMPLATE\_01\_30\_2015.GDT 12/20/17

# SCDOT Soil Test Log

<b>Project ID:</b>	1413-16-153	<b>County:</b>	Georgetown, SC	<b>Boring No.:</b>	B-FMG
<b>Site Description:</b>	USC-SCDOT Deep Seismic Holes			<b>Route:</b>	
<b>Eng./Geo.:</b>	CS & LE	<b>Boring Location:</b>		<b>Offset:</b>	
<b>Elev.:</b>	27.0 ft	<b>Latitude:</b>	33.447666	<b>Longitude:</b>	-79.59089
<b>Total Depth:</b>	615 ft	<b>Soil Depth:</b>	20.8 ft	<b>Core Depth:</b>	615 ft
<b>Bore Hole Diameter (in):</b>	4	<b>Sampler Configuration</b>		<b>Liner Required:</b>	Y N
<b>Drill Machine:</b>	CME-550	<b>Drill Method:</b>	Mud Rotary	<b>Hammer Type:</b>	Automatic
<b>Core Size:</b>	HQ	<b>Driller:</b>	AE Drilling	<b>Groundwater:</b>	TOB 2.5 ft
				<b>24HR</b>	2.8 ft
				<b>Energy Ratio:</b>	91.5%

Elevation (ft)	Depth (ft)	MATERIAL DESCRIPTION	Graphic Log	Sample Depth (ft)	Sample No./Type	1st 6"	2nd 6"	3rd 6"	N Value	SPT N VALUE											
										PL	MC	LL	FINES CONTENT (%)								
100.7		Moist to wet, weakly to strongly reactive, non- to strongly cemented, very dark greenish gray (GLEY 1 10Y 3/1) gray (GLEY 1 N 6/), fine sand, little medium plasticity fines, CLAYEY SAND (SC / A-2-6), trace mica, trace shell fragments, lenses of strong cementation (~0.4' to 0.5' thick), (MC=36.9%, LL=29, PI=7, FC=44.4%)		100.7	SC-17	2.5' / 5.0'															
-78.0	105.7	Moist to wet, weakly to strongly reactive, non- to strongly cemented, very dark greenish gray (GLEY 1 10Y 3/1) gray (GLEY 1 N 6/), fine sand, some low to medium plasticity fines, CLAYEY SAND (SC / A-6), trace mica, trace shell fragments, lens of strong cementation (~0.1' thick), (MC=28.5%, LL=29, PI=6, FC=33.6%)		105.7	SC-18	3.6' / 5.0'															
-83.0	110.7	Moist, weakly to strongly reactive, non- to strongly cemented, very dark greenish gray (GLEY 1 10Y 3/1) gray (GLEY 1 N 5/), fine sand, some medium plasticity fines, CLAYEY SAND (SC / A-2-6), lens of strong cementation (~0.5' thick), lens of fat clay (~0.3' thick), laminated lean clay (~1mm), (MC=38.6%, LL=30, PI=2, FC=35.8%)		110.7	SC-19	5.0' / 5.0'															
-88.0	115.7	Moist, strongly reactive, strongly cemented, gray (GLEY 1 N 6/), fine sand, little to some medium plasticity fines, CLAYEY SAND (SC / A-2-6), lenses of strong cementation (~0.1' to 0.5' thick), trace fine to coarse shells		115.7	SC-20	0.9' / 5.0'															
-93.0	120.7	Moist, non- to strongly reactive, non- to strongly cemented, gray (GLEY 1 N 6/) very dark greenish gray (GLEY 1 10Y 3/1), fine sand, little non-plastic to low plasticity fines, SILTY SAND (SM / A-2-4), trace mica, lenses of strongly cementation (~0.2' to 0.7' thick), (MC=34.4%, LL=26, PI=2, FC=22.2%)		120.7	SC-21	2.0' / 5.0'															

### LEGEND

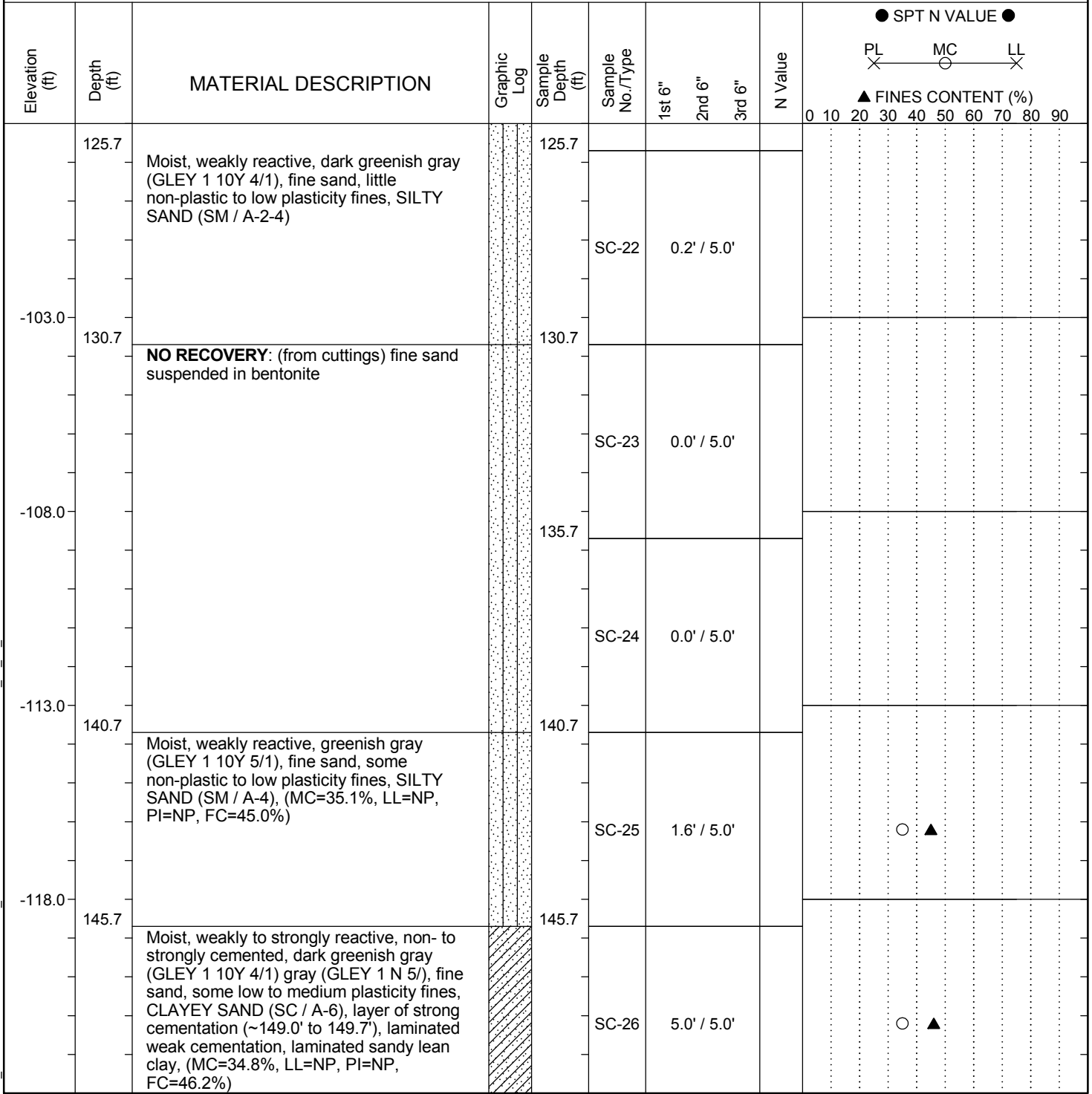
Continued Next Page

SAMPLER TYPE		DRILLING METHOD	
SS - Split Spoon	NQ - Rock Core, 1-7/8"	HSA - Hollow Stem Auger	RW - Rotary Wash
UD - Undisturbed Sample	CU - Cuttings	CFA - Continuous Flight Augers	RC - Rock Core
AWG - Rock Core, 1-1/8"	CT - Continuous Tube	DC - Driving Casing	

SC\_DOT\_141316153\_USC-SCDOT DEEP BORINGS\_B-FMG.GPJ\_SCDOT DATA TEMPLATE\_01\_30\_2015.GDT 12/20/17

# SCDOT Soil Test Log

<b>Project ID:</b>	1413-16-153	<b>County:</b>	Georgetown, SC	<b>Boring No.:</b>	B-FMG
<b>Site Description:</b>	USC-SCDOT Deep Seismic Holes			<b>Route:</b>	
<b>Eng./Geo.:</b>	CS & LE	<b>Boring Location:</b>		<b>Offset:</b>	
<b>Elev.:</b>	27.0 ft	<b>Latitude:</b>	33.447666	<b>Longitude:</b>	-79.59089
<b>Total Depth:</b>	615 ft	<b>Soil Depth:</b>	20.8 ft	<b>Core Depth:</b>	615 ft
<b>Bore Hole Diameter (in):</b>	4	<b>Sampler Configuration</b>		<b>Liner Required:</b>	Y N
<b>Drill Machine:</b>	CME-550	<b>Drill Method:</b>	Mud Rotary	<b>Hammer Type:</b>	Automatic
<b>Core Size:</b>	HQ	<b>Driller:</b>	AE Drilling	<b>Groundwater:</b>	TOB 2.5 ft
				<b>24HR</b>	2.8 ft



**LEGEND**

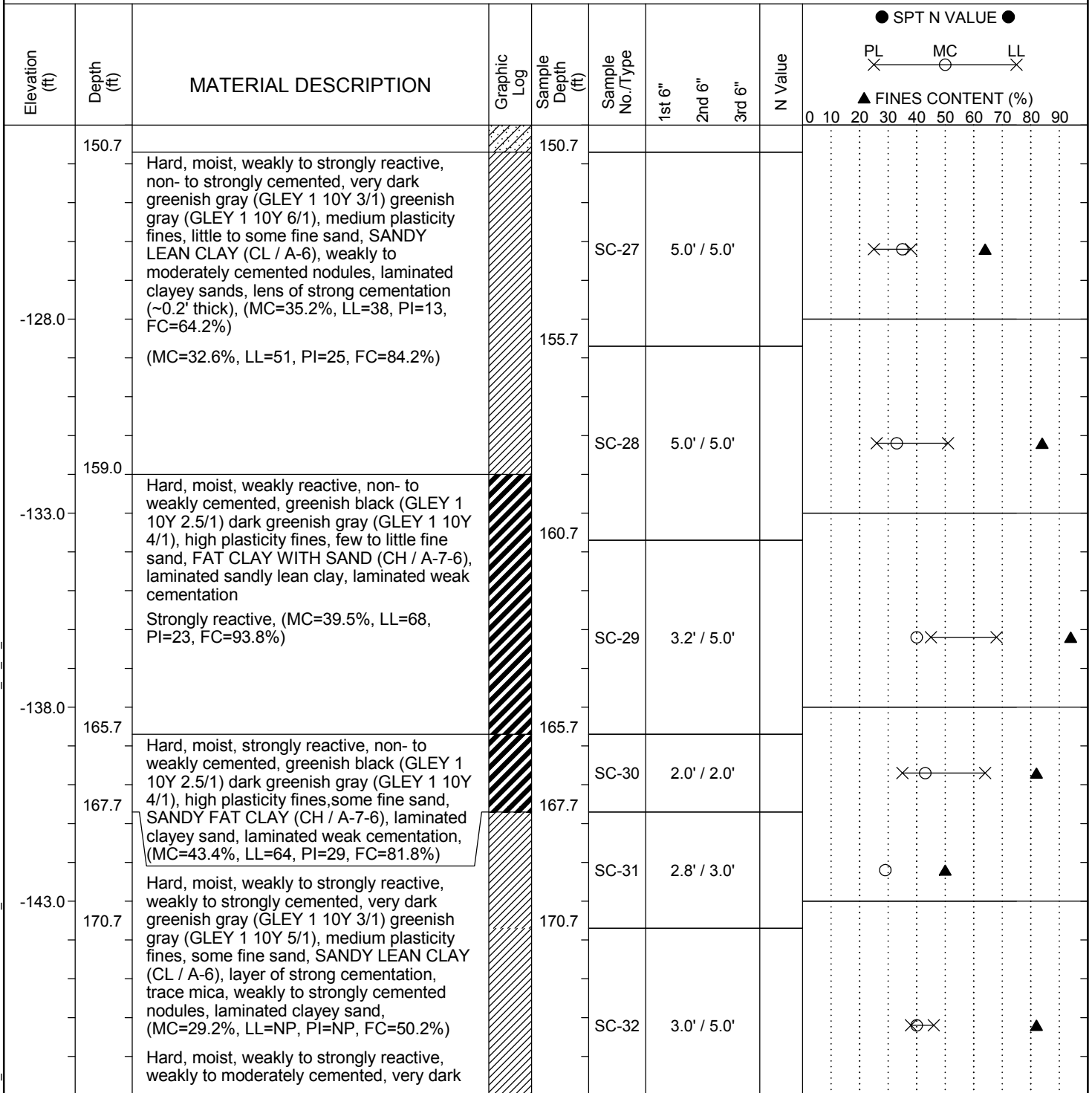
*Continued Next Page*

SAMPLER TYPE		DRILLING METHOD	
SS - Split Spoon	NQ - Rock Core, 1-7/8"	HSA - Hollow Stem Auger	RW - Rotary Wash
UD - Undisturbed Sample	CU - Cuttings	CFA - Continuous Flight Augers	RC - Rock Core
AWG - Rock Core, 1-1/8"	CT - Continuous Tube	DC - Driving Casing	

SC\_DOT\_141316153\_USC-SCDOT DEEP BORINGS\_B-FMG.GPJ\_SCDOT DATA TEMPLATE\_01\_30\_2015.GDT 12/20/17

# SCDOT Soil Test Log

<b>Project ID:</b>	1413-16-153	<b>County:</b>	Georgetown, SC	<b>Boring No.:</b>	B-FMG
<b>Site Description:</b>	USC-SCDOT Deep Seismic Holes			<b>Route:</b>	
<b>Eng./Geo.:</b>	CS & LE	<b>Boring Location:</b>		<b>Offset:</b>	
<b>Elev.:</b>	27.0 ft	<b>Latitude:</b>	33.447666	<b>Longitude:</b>	-79.59089
<b>Total Depth:</b>	615 ft	<b>Soil Depth:</b>	20.8 ft	<b>Core Depth:</b>	615 ft
<b>Bore Hole Diameter (in):</b>	4	<b>Sampler Configuration</b>		<b>Liner Required:</b>	Y N
<b>Drill Machine:</b>	CME-550	<b>Drill Method:</b>	Mud Rotary	<b>Hammer Type:</b>	Automatic
<b>Core Size:</b>	HQ	<b>Driller:</b>	AE Drilling	<b>Energy Ratio:</b>	91.5%
		<b>Groundwater:</b>	TOB	2.5 ft	24HR 2.8 ft



LEGEND

Continued Next Page

SAMPLER TYPE		DRILLING METHOD	
SS - Split Spoon	NQ - Rock Core, 1-7/8"	HSA - Hollow Stem Auger	RW - Rotary Wash
UD - Undisturbed Sample	CU - Cuttings	CFA - Continuous Flight Augers	RC - Rock Core
AWG - Rock Core, 1-1/8"	CT - Continuous Tube	DC - Driving Casing	

SC\_DOT\_141316153\_USC-SCDOT DEEP BORINGS\_B-FMG.GPJ\_SCDOT DATA TEMPLATE\_01\_30\_2015.GDT 12/20/17

# SCDOT Soil Test Log

<b>Project ID:</b>	1413-16-153	<b>County:</b>	Georgetown, SC	<b>Boring No.:</b>	B-FMG
<b>Site Description:</b>	USC-SCDOT Deep Seismic Holes			<b>Route:</b>	
<b>Eng./Geo.:</b>	CS & LE	<b>Boring Location:</b>		<b>Offset:</b>	
<b>Elev.:</b>	27.0 ft	<b>Latitude:</b>	33.447666	<b>Longitude:</b>	-79.59089
<b>Total Depth:</b>	615 ft	<b>Soil Depth:</b>	20.8 ft	<b>Core Depth:</b>	615 ft
<b>Bore Hole Diameter (in):</b>	4	<b>Sampler Configuration</b>		<b>Liner Required:</b>	Y N
<b>Drill Machine:</b>	CME-550	<b>Drill Method:</b>	Mud Rotary	<b>Hammer Type:</b>	Automatic
<b>Core Size:</b>	HQ	<b>Driller:</b>	AE Drilling	<b>Groundwater:</b>	TOB 2.5 ft
				<b>24HR</b>	2.8 ft

Elevation (ft)	Depth (ft)	MATERIAL DESCRIPTION	Graphic Log	Sample Depth (ft)	Sample No./Type	1st 6"	2nd 6"	3rd 6"	N Value	SPT N VALUE											
										PL	MC	LL	FINES CONTENT (%)								
175.7		greenish gray (GLEY 1 10Y 3/1), medium plasticity fines, little to some fine sand, SANDY LEAN CLAY (CL / A-6), laminated clayey sand, laminated weak to moderate cementation, (MC=40.1%, LL=46, PI=8, FC=81.8%)		175.7																	
-153.0		Hard, moist, weakly to strongly reactive, weakly cemented, greenish black (GLEY 1 10Y 2.5/1), high plasticity fines, little fine sand, SANDY FAT CLAY (CH / A-7-6), trace mica, laminated sandy lean clay & clayey sand, (MC=56.2%, LL=54, PI=14, FC=83.4%) (MC=52.9%, LL=54, PI=7, FC=71.2%)		180.7	SC-33	5.0' / 5.0'															
-158.0				185.7	SC-34	4.8' / 5.0'															
-163.0		<b>RHEMS FORMATION - BROWNS FERRY MEMBER:</b> Moist to wet, weakly to strongly reactive, weakly to strongly cemented, very dark greenish gray (GLEY 1 10Y 3/1) gray (GLEY 1 N 5/), fine sand, some medium plasticity fines, CLAYEY SAND (SC / A-6), lenses of strong cementation (~0.2' to 0.3' thick), trace mica, (MC=34.7%, LL=35, PI=9, FC=60.0%)		190.7	SC-35	4.6' / 5.0'															
-168.0		Wet, weakly to strongly reactive, non- to strongly cemented, very dark greenish gray (GLEY 1 10Y 3/1) gray (GLEY 1 N 5/), fine sand, little non-plastic to low plasticity fines, SILTY SAND (SM / A-2-4), lenses of strong cementation (~0.2' to 0.4' thick), trace mica, (MC=34.4%, LL=-, PI=0, FC=12.6%)		195.7	SC-36	1.1' / 5.0'															
		Mostly strong cementation (~0.1' to 0.5' thick) with washed out silty sand at interfaces, trace shell fragments		195.7	SC-37	0.7' / 5.0'															

### LEGEND

Continued Next Page

SAMPLER TYPE		DRILLING METHOD	
SS - Split Spoon	NQ - Rock Core, 1-7/8"	HSA - Hollow Stem Auger	RW - Rotary Wash
UD - Undisturbed Sample	CU - Cuttings	CFA - Continuous Flight Augers	RC - Rock Core
AWG - Rock Core, 1-1/8"	CT - Continuous Tube	DC - Driving Casing	

SC\_DOT\_141316153\_USC-SCDOT DEEP BORINGS\_B-FMG.GPJ\_SCDOT DATA TEMPLATE\_01\_30\_2015.GDT 12/20/17

# SCDOT Soil Test Log

<b>Project ID:</b>	1413-16-153	<b>County:</b>	Georgetown, SC	<b>Boring No.:</b>	B-FMG
<b>Site Description:</b>	USC-SCDOT Deep Seismic Holes			<b>Route:</b>	
<b>Eng./Geo.:</b>	CS & LE	<b>Boring Location:</b>		<b>Offset:</b>	
<b>Elev.:</b>	27.0 ft	<b>Latitude:</b>	33.447666	<b>Longitude:</b>	-79.59089
<b>Total Depth:</b>	615 ft	<b>Soil Depth:</b>	20.8 ft	<b>Core Depth:</b>	615 ft
<b>Bore Hole Diameter (in):</b>	4	<b>Sampler Configuration</b>		<b>Liner Required:</b>	Y N
<b>Drill Machine:</b>	CME-550	<b>Drill Method:</b>	Mud Rotary	<b>Hammer Type:</b>	Automatic
<b>Core Size:</b>	HQ	<b>Driller:</b>	AE Drilling	<b>Groundwater:</b>	TOB 2.5 ft
				<b>24HR</b>	2.8 ft
				<b>Energy Ratio:</b>	91.5%
				<b>Liner Used:</b>	Y N

Elevation (ft)	Depth (ft)	MATERIAL DESCRIPTION	Graphic Log	Sample Depth (ft)	Sample No./Type	1st 6"	2nd 6"	3rd 6"	N Value	SPT N VALUE ●									
										PL	MC	LL							
										▲ FINES CONTENT (%)									
										0	10	20	30	40	50	60	70	80	90
				200.7															
					SC-38	0.1' / 5.0'													
-178.0	205.7	<b>NO RECOVERY:</b> POTENTIAL VOID, loss of water and head pressure		205.7															
					SC-39	0.0' / 5.0'													
-183.0	210.7	Very hard, moist, strongly reactive, strongly cemented, gray (GLEY 1 N 5), medium plasticity fines, some fine sand, SANDY LEAN CLAY (CL / A-6), mostly strong cementation, few shell fragments, clay on inner barrel (not in sample)		210.7															
					SC-40	0.2' / 4.3'													
-188.0	213.9	Hard, moist, weakly to strongly reactive, weakly cemented, very dark greenish gray (GLEY 1 10Y 3/1) greenish gray (GLEY 1 10Y 6/1), medium plasticity fines, little fine sand, SANDY LEAN CLAY (CL / A-6), laminated weakly cemented sands, trace mica (MC=30.8%, LL=43, PI=17, FC=69.8%)		215.0															
					SC-41	1.8' / 0.7'				×	○								
					SC-42	1.9' / 5.0'				×	○								
-193.0	215.7	Very hard to stiff, moist to wet, weakly to strongly reactive, weakly to strongly cemented, greenish black (GLEY 1 10Y 2.5/1) dark greenish gray (GLEY 1 10Y 4/1), medium to high plasticity fines, some fine sand, SANDY LEAN CLAY (CL / A-6), trace mica, lens of strong cementation with few shells (~220.1' to 220.7'), (MC=49.3%, LL=32, PI=6, FC=41.4%)		220.7															
					SC-43	1.8' / 5.0'				×	○								
	222.7	(MC=27.9%, LL=27, PI=5, FC=54.4%) Moist, weakly to strongly reactive, weakly to moderately cemented, dark greenish gray (GLEY 1 10Y 4/1), fine sand, some medium																	

**LEGEND**

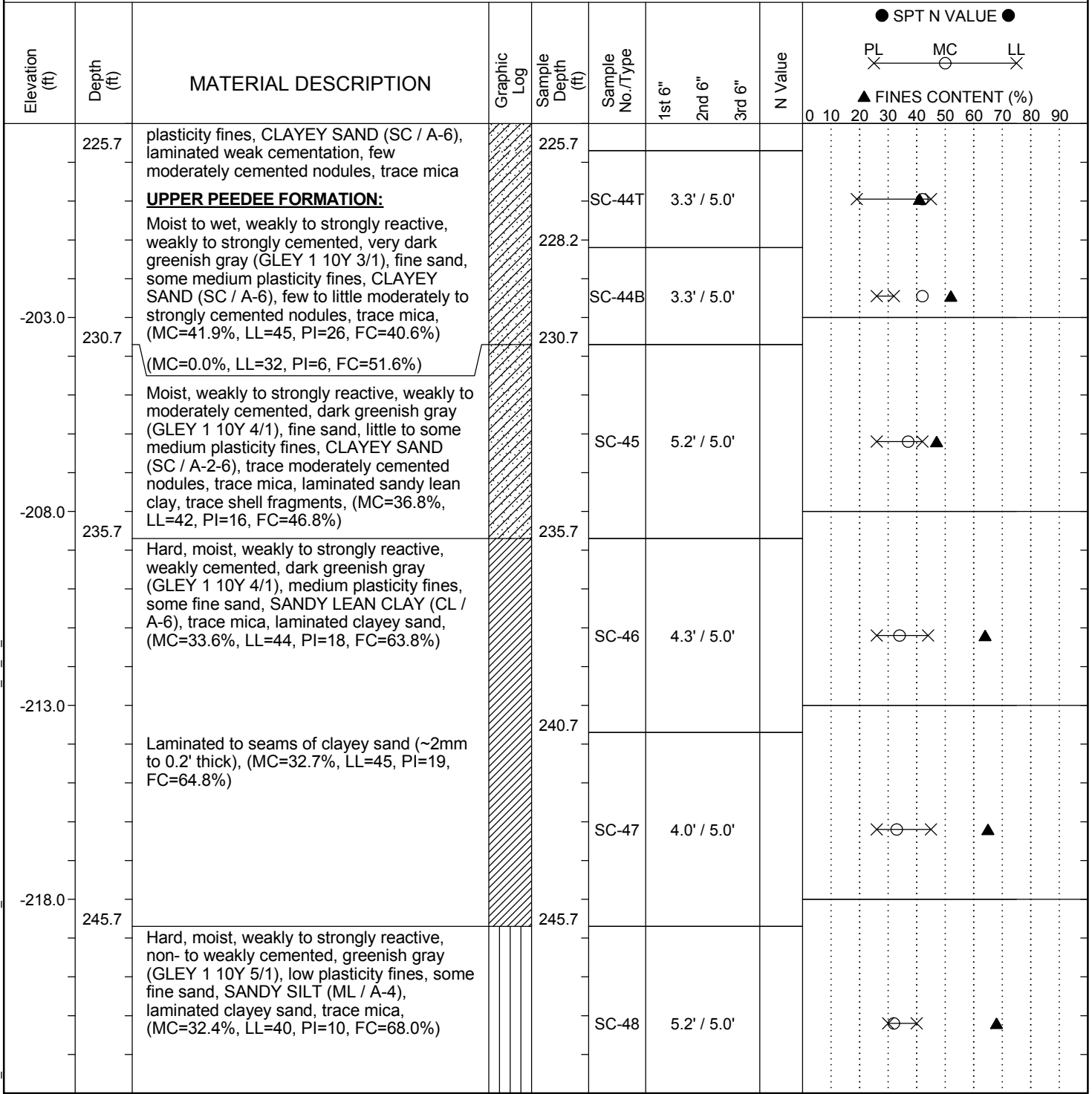
*Continued Next Page*

SAMPLER TYPE		DRILLING METHOD	
SS - Split Spoon	NQ - Rock Core, 1-7/8"	HSA - Hollow Stem Auger	RW - Rotary Wash
UD - Undisturbed Sample	CU - Cuttings	CFA - Continuous Flight Augers	RC - Rock Core
AWG - Rock Core, 1-1/8"	CT - Continuous Tube	DC - Driving Casing	

SC\_DOT\_141316153\_USC-SCDOT DEEP BORINGS\_B-FMG.GPJ\_SCDOT DATA TEMPLATE\_01\_30\_2015.GDT\_12/20/17

# SCDOT Soil Test Log

<b>Project ID:</b>	1413-16-153	<b>County:</b>	Georgetown, SC	<b>Boring No.:</b>	B-FMG
<b>Site Description:</b>	USC-SCDOT Deep Seismic Holes			<b>Route:</b>	
<b>Eng./Geo.:</b>	CS & LE	<b>Boring Location:</b>		<b>Offset:</b>	
<b>Elev.:</b>	27.0 ft	<b>Latitude:</b>	33.447666	<b>Longitude:</b>	-79.59089
<b>Total Depth:</b>	615 ft	<b>Soil Depth:</b>	20.8 ft	<b>Core Depth:</b>	615 ft
<b>Bore Hole Diameter (in):</b>	4	<b>Sampler Configuration</b>		<b>Liner Required:</b>	Y N
<b>Drill Machine:</b>	CME-550	<b>Drill Method:</b>	Mud Rotary	<b>Hammer Type:</b>	Automatic
<b>Core Size:</b>	HQ	<b>Driller:</b>	AE Drilling	<b>Groundwater:</b>	TOB 2.5 ft
				<b>24HR</b>	2.8 ft



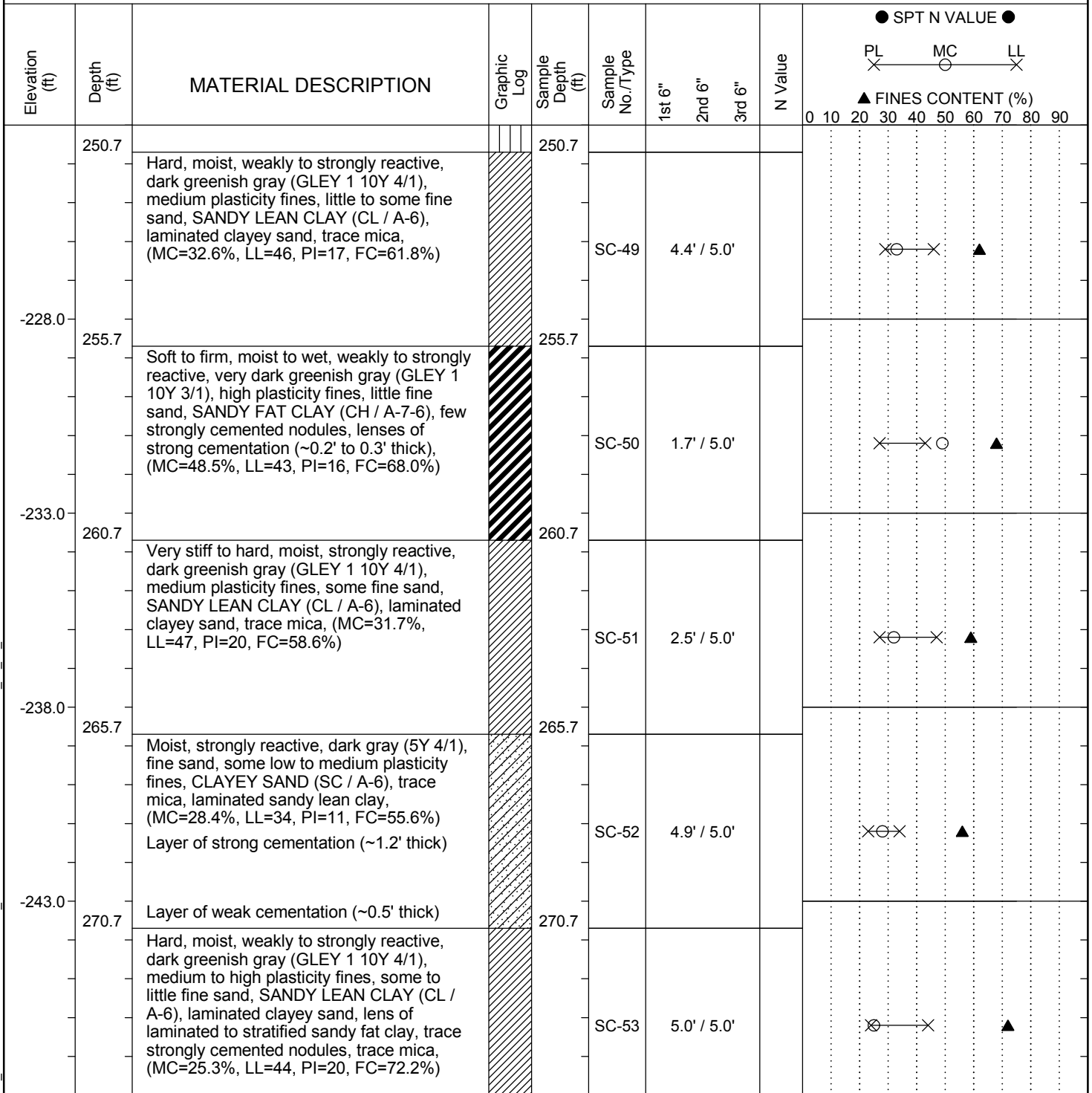
LEGEND Continued Next Page

SAMPLER TYPE		DRILLING METHOD	
SS - Split Spoon	NQ - Rock Core, 1-7/8"	HSA - Hollow Stem Auger	RW - Rotary Wash
UD - Undisturbed Sample	CU - Cuttings	CFA - Continuous Flight Augers	RC - Rock Core
AWG - Rock Core, 1-1/8"	CT - Continuous Tube	DC - Driving Casing	

SC\_DOT\_141316153\_USC-SCDOT DEEP BORINGS\_B-FMG.GPJ\_SCDOT DATA TEMPLATE\_01\_30\_2015.GDT 12/20/17

# SCDOT Soil Test Log

<b>Project ID:</b>	1413-16-153	<b>County:</b>	Georgetown, SC	<b>Boring No.:</b>	B-FMG
<b>Site Description:</b>	USC-SCDOT Deep Seismic Holes			<b>Route:</b>	
<b>Eng./Geo.:</b>	CS & LE	<b>Boring Location:</b>		<b>Offset:</b>	
<b>Elev.:</b>	27.0 ft	<b>Latitude:</b>	33.447666	<b>Longitude:</b>	-79.59089
<b>Total Depth:</b>	615 ft	<b>Soil Depth:</b>	20.8 ft	<b>Core Depth:</b>	615 ft
<b>Bore Hole Diameter (in):</b>	4	<b>Sampler Configuration</b>		<b>Liner Required:</b>	Y N
<b>Drill Machine:</b>	CME-550	<b>Drill Method:</b>	Mud Rotary	<b>Hammer Type:</b>	Automatic
<b>Core Size:</b>	HQ	<b>Driller:</b>	AE Drilling	<b>Energy Ratio:</b>	91.5%
		<b>Groundwater:</b>	TOB	2.5 ft	24HR 2.8 ft



LEGEND

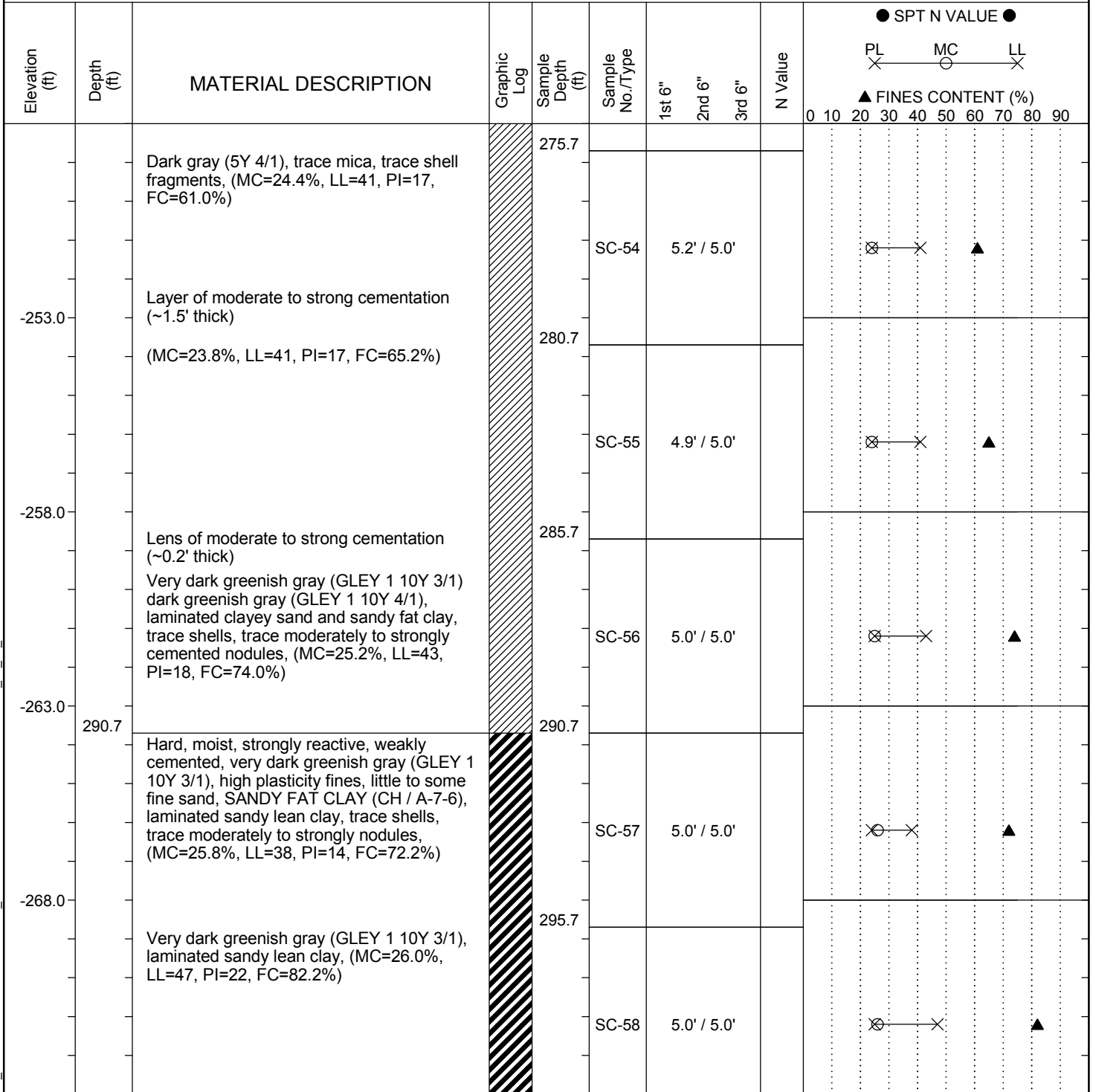
Continued Next Page

<b>SAMPLER TYPE</b> SS - Split Spoon UD - Undisturbed Sample AWG - Rock Core, 1-1/8"		<b>DRILLING METHOD</b> HSA - Hollow Stem Auger CFA - Continuous Flight Augers DC - Driving Casing		NQ - Rock Core, 1-7/8" CU - Cuttings CT - Continuous Tube		RW - Rotary Wash RC - Rock Core	
---	--	--	--	---	--	------------------------------------	--

SC\_DOT 141316153\_USC-SCDOT DEEP BORINGS\_B-FMG.GPJ SCDOT DATA TEMPLATE\_01\_30\_2015.GDT 12/20/17

# SCDOT Soil Test Log

<b>Project ID:</b>	1413-16-153	<b>County:</b>	Georgetown, SC	<b>Boring No.:</b>	B-FMG
<b>Site Description:</b>	USC-SCDOT Deep Seismic Holes			<b>Route:</b>	
<b>Eng./Geo.:</b>	CS & LE	<b>Boring Location:</b>		<b>Offset:</b>	
<b>Elev.:</b>	27.0 ft	<b>Latitude:</b>	33.447666	<b>Longitude:</b>	-79.59089
<b>Total Depth:</b>	615 ft	<b>Soil Depth:</b>	20.8 ft	<b>Core Depth:</b>	615 ft
<b>Bore Hole Diameter (in):</b>	4	<b>Sampler Configuration</b>		<b>Liner Required:</b>	Y N
<b>Drill Machine:</b>	CME-550	<b>Drill Method:</b>	Mud Rotary	<b>Hammer Type:</b>	Automatic
<b>Core Size:</b>	HQ	<b>Driller:</b>	AE Drilling	<b>Groundwater:</b>	TOB 2.5 ft
				<b>24HR</b>	2.8 ft
				<b>Energy Ratio:</b>	91.5%
				<b>Liner Used:</b>	Y N



LEGEND

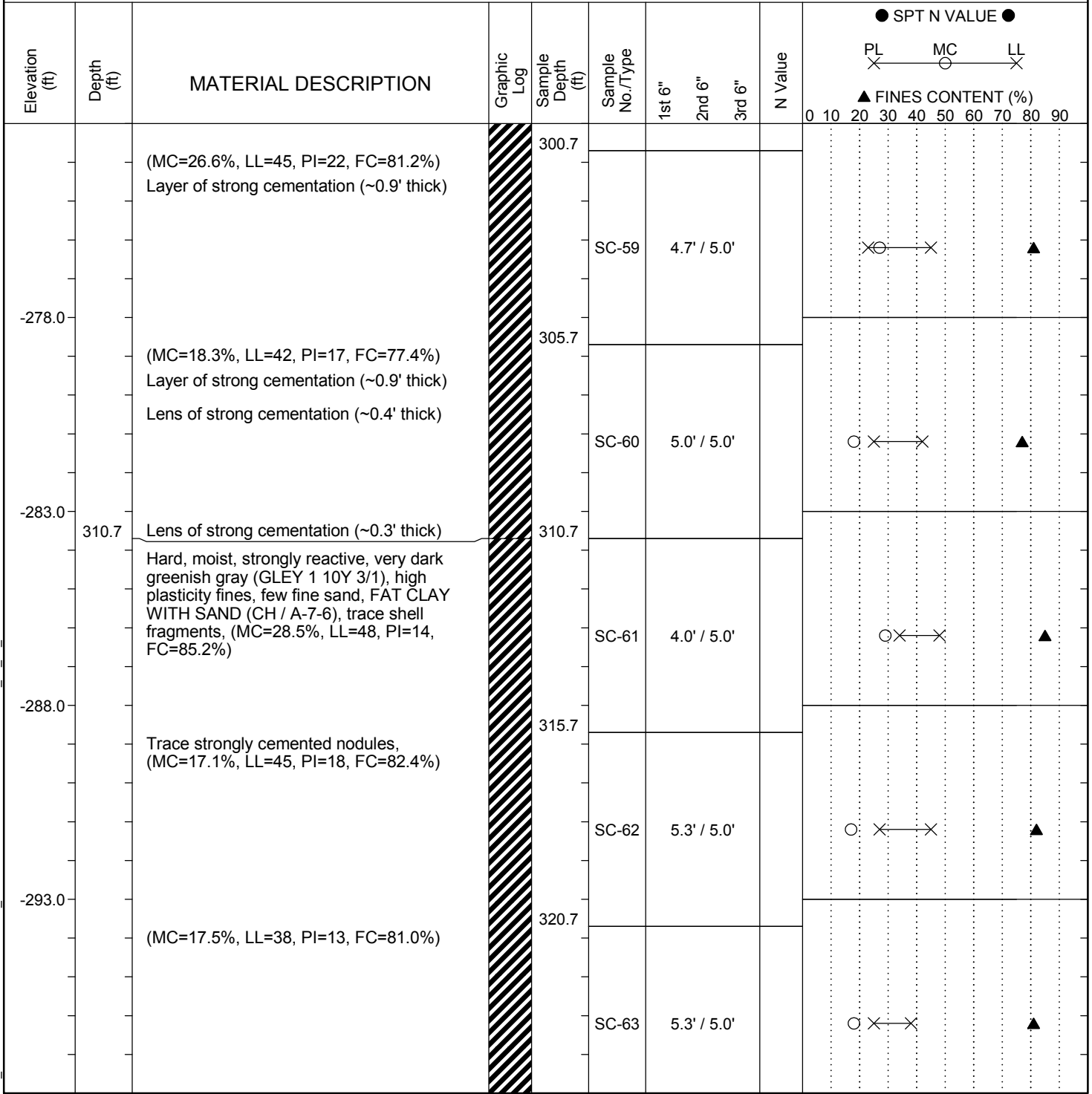
Continued Next Page

SAMPLER TYPE		DRILLING METHOD	
SS - Split Spoon	NQ - Rock Core, 1-7/8"	HSA - Hollow Stem Auger	RW - Rotary Wash
UD - Undisturbed Sample	CU - Cuttings	CFA - Continuous Flight Augers	RC - Rock Core
AWG - Rock Core, 1-1/8"	CT - Continuous Tube	DC - Driving Casing	

SC\_DOT\_141316153\_USC-SCDOT DEEP BORINGS\_B-FMG.GPJ\_SCDOT DATA TEMPLATE\_01\_30\_2015.GDT 12/20/17

# SCDOT Soil Test Log

<b>Project ID:</b>	1413-16-153	<b>County:</b>	Georgetown, SC	<b>Boring No.:</b>	B-FMG
<b>Site Description:</b>	USC-SCDOT Deep Seismic Holes			<b>Route:</b>	
<b>Eng./Geo.:</b>	CS & LE	<b>Boring Location:</b>		<b>Offset:</b>	
<b>Elev.:</b>	27.0 ft	<b>Latitude:</b>	33.447666	<b>Longitude:</b>	-79.59089
<b>Total Depth:</b>	615 ft	<b>Soil Depth:</b>	20.8 ft	<b>Core Depth:</b>	615 ft
<b>Bore Hole Diameter (in):</b>	4	<b>Sampler Configuration</b>		<b>Liner Required:</b>	Y N
<b>Drill Machine:</b>	CME-550	<b>Drill Method:</b>	Mud Rotary	<b>Hammer Type:</b>	Automatic
<b>Core Size:</b>	HQ	<b>Driller:</b>	AE Drilling	<b>Energy Ratio:</b>	91.5%
		<b>Groundwater:</b>	TOB	2.5 ft	24HR 2.8 ft



LEGEND

Continued Next Page

SAMPLER TYPE		DRILLING METHOD	
SS - Split Spoon	NQ - Rock Core, 1-7/8"	HSA - Hollow Stem Auger	RW - Rotary Wash
UD - Undisturbed Sample	CU - Cuttings	CFA - Continuous Flight Augers	RC - Rock Core
AWG - Rock Core, 1-1/8"	CT - Continuous Tube	DC - Driving Casing	

SC\_DOT\_141316153\_USC-SCDOT DEEP BORINGS\_B-FMG.GPJ\_SCDOT DATA TEMPLATE\_01\_30\_2015.GDT\_12/20/17

# SCDOT Soil Test Log

<b>Project ID:</b>	1413-16-153	<b>County:</b>	Georgetown, SC	<b>Boring No.:</b>	B-FMG
<b>Site Description:</b>	USC-SCDOT Deep Seismic Holes			<b>Route:</b>	
<b>Eng./Geo.:</b>	CS & LE	<b>Boring Location:</b>		<b>Offset:</b>	
<b>Elev.:</b>	27.0 ft	<b>Latitude:</b>	33.447666	<b>Longitude:</b>	-79.59089
<b>Total Depth:</b>	615 ft	<b>Soil Depth:</b>	20.8 ft	<b>Core Depth:</b>	615 ft
<b>Date Started:</b>	02/06/2017		<b>Date Completed:</b>	2/18/2017	
<b>Bore Hole Diameter (in):</b>	4	<b>Sampler Configuration</b>		<b>Liner Required:</b>	Y N
<b>Liner Used:</b>	Y N		<b>Hammer Type:</b>	Automatic	
<b>Energy Ratio:</b>	91.5%		<b>Groundwater:</b>	TOB	2.5 ft
<b>Core Size:</b>	HQ	<b>Driller:</b>	AE Drilling	<b>24HR:</b>	2.8 ft

Elevation (ft)	Depth (ft)	MATERIAL DESCRIPTION	Graphic Log	Sample Depth (ft)	Sample No./Type	1st 6"	2nd 6"	3rd 6"	N Value	SPT N VALUE											
										PL	MC	LL	FINES CONTENT (%)								
		(MC=27.2%, LL=46, PI=9, FC=90.0%)		325.7																	
					SC-64	4.6' / 5.0'															
-303.0		(MC=21.2%, LL=45, PI=17, FC=93.0%)		330.7																	
	333.1	Layer of moderate cementation (~0.7' thick)																			
		Hard, moist, strongly reactive, dark greenish gray (GLEY 1 10Y 4/1), medium plasticity fines, few fine sand, LEAN CLAY WITH SAND (CL / A-6), stratified sandy lean clay at top of layer			SC-65	5.0' / 5.0'															
-308.0		Trace blocky clay, (MC=32.1%, LL=49, PI=26, FC=88.6%)		335.7																	
					SC-66	4.5' / 5.0'															
-313.0																					
		Very dark greenish gray (GLEY 1 10Y 3/1), (MC=30.7%, LL=34, PI=13, FC=94.0%)		340.7																	
					SC-67	4.4' / 5.0'															
-318.0																					
	345.7			345.7																	
		Very hard, moist, strongly reactive, moderately to strongly cemented, gray (GLEY 1 N 5/) dark greenish gray (GLEY 1 10Y 4/1), medium plasticity fines, some fine sand, SANDY LEAN CLAY (CL / A-6), mostly moderate to strong cementation, trace shell fragments, (MC=20.5%, LL=37, PI=11, FC=86.2%)			SC-68	5.0' / 5.0'															
-318.0																					
	349.4			349.4																	

### LEGEND

Continued Next Page

SAMPLER TYPE		DRILLING METHOD	
SS - Split Spoon	NQ - Rock Core, 1-7/8"	HSA - Hollow Stem Auger	RW - Rotary Wash
UD - Undisturbed Sample	CU - Cuttings	CFA - Continuous Flight Augers	RC - Rock Core
AWG - Rock Core, 1-1/8"	CT - Continuous Tube	DC - Driving Casing	

SC\_DOT\_141316153\_USC-SCDOT DEEP BORINGS\_B-FMG.GPJ\_SCDOT DATA TEMPLATE\_01\_30\_2015.GDT 12/20/17

# SCDOT Soil Test Log

<b>Project ID:</b>	1413-16-153	<b>County:</b>	Georgetown, SC	<b>Boring No.:</b>	B-FMG
<b>Site Description:</b>	USC-SCDOT Deep Seismic Holes			<b>Route:</b>	
<b>Eng./Geo.:</b>	CS & LE	<b>Boring Location:</b>		<b>Offset:</b>	
<b>Elev.:</b>	27.0 ft	<b>Latitude:</b>	33.447666	<b>Longitude:</b>	-79.59089
<b>Total Depth:</b>	615 ft	<b>Soil Depth:</b>	20.8 ft	<b>Core Depth:</b>	615 ft
<b>Bore Hole Diameter (in):</b>	4	<b>Sampler Configuration</b>		<b>Liner Required:</b>	Y N
<b>Drill Machine:</b>	CME-550	<b>Drill Method:</b>	Mud Rotary	<b>Hammer Type:</b>	Automatic
<b>Core Size:</b>	HQ	<b>Driller:</b>	AE Drilling	<b>Groundwater:</b>	TOB 2.5 ft
				<b>24HR</b>	2.8 ft

Elevation (ft)	Depth (ft)	MATERIAL DESCRIPTION	Graphic Log	Sample Depth (ft)	Sample No./Type	1st 6"	2nd 6"	3rd 6"	N Value	SPT N VALUE											
										PL	MC	LL	FINES CONTENT (%)								
	350.7	Hard, moist, strongly reactive, very dark greenish gray (GLEY 1 10Y 3/1), high plasticity fines, little fine sand, SANDY FAT CLAY (CH / A-7-6), trace shells, trace blocky clay		350.7																	
	-328.0	Hard, moist, strongly reactive, very dark gray (5Y 3/1) grayish brown (10YR 5/2), high plasticity fines, few fine sand, FAT CLAY WITH SAND (CH / A-7-6), trace shell fragments, trace blocky clay, (MC=24.6%, LL=49, PI=14, FC=94.2%) (MC=19.9%, LL=41, PI=11, FC=92.2%)		355.7	SC-69	4.8' / 5.0'															
	-333.0	Hard to very hard, moist, strongly reactive, dark greenish gray (GLEY 1 10Y 4/1), high plasticity fines, little to some fine sand, SANDY FAT CLAY (CH / A-7-6), trace shell fragments, lenses of moderate to strong cementation (~0.2' to 0.5' thick) (MC=26.8%, LL=41, PI=19, FC=82.6%) Hard, laminated sandy lean clay		360.7	SC-70	5.2' / 5.0'															
	-338.0	(MC=12.6%, LL=36, PI=13, FC=63.4%) Grayish brown (10YR 5/2), fine to medium sand, trace strongly cemented nodules		365.7	SC-71	4.6' / 5.0'															
	-343.0	Moist, strongly reactive, weakly to strongly cemented, very dark greenish gray (GLEY 1 10Y 3/1) dark grayish brown (10YR 4/2), fine to medium sand, some medium plasticity fines, CLAYEY SAND (SC / A-6), trace shell fragments Trace moderately to strongly cemented nodules, (MC=19.5%, LL=24, PI=4, FC=34.4%)		370.7	SC-72	5.1' / 5.0'															
					SC-73	5.0' / 5.0'															

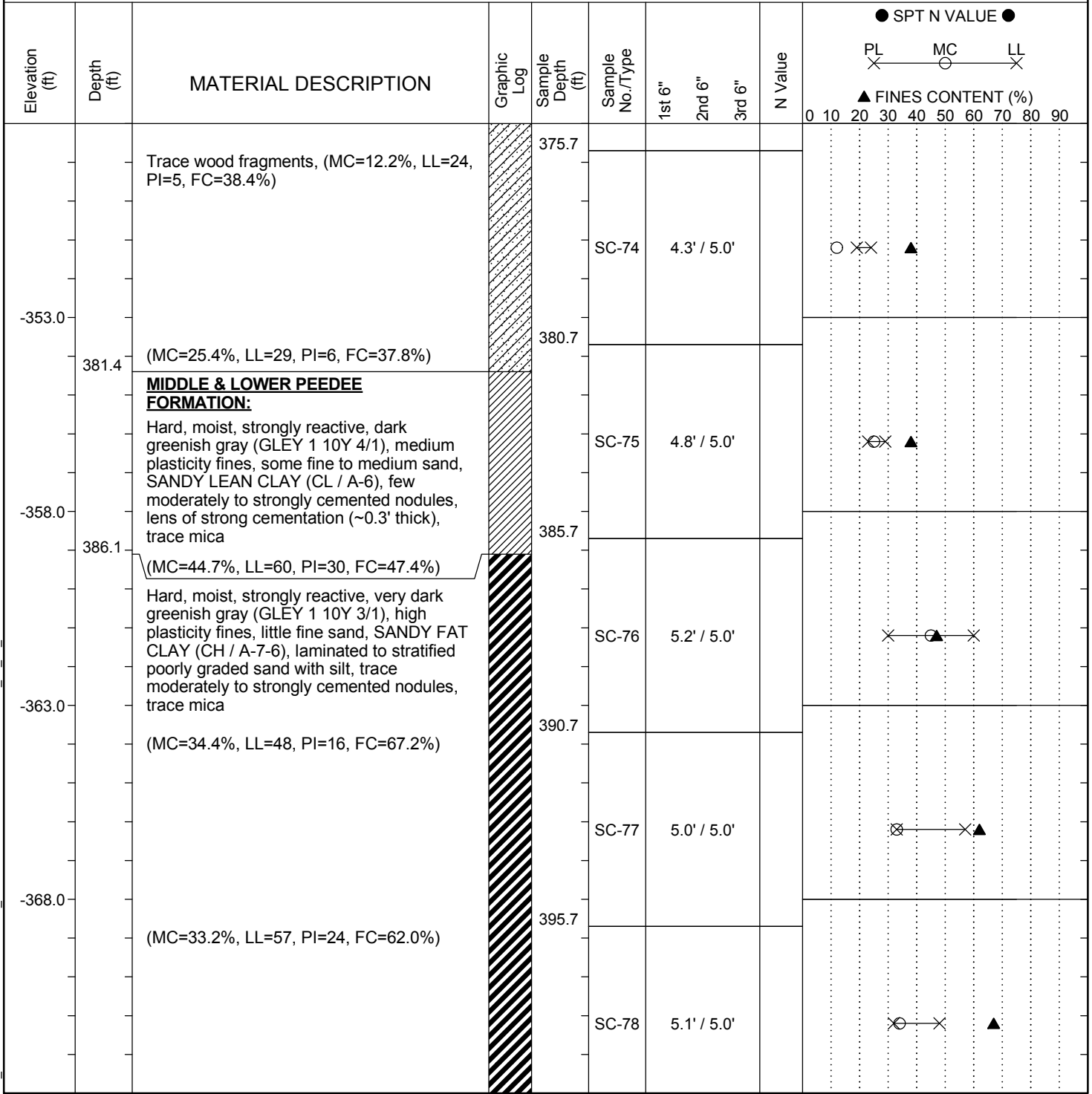
LEGEND Continued Next Page

<b>SAMPLER TYPE</b>		<b>DRILLING METHOD</b>	
SS - Split Spoon	NQ - Rock Core, 1-7/8"	HSA - Hollow Stem Auger	RW - Rotary Wash
UD - Undisturbed Sample	CU - Cuttings	CFA - Continuous Flight Augers	RC - Rock Core
AWG - Rock Core, 1-1/8"	CT - Continuous Tube	DC - Driving Casing	

SC\_DOT\_141316153\_USC-SCDOT DEEP BORINGS\_B-FMG.GPJ\_SCDOT DATA TEMPLATE\_01\_30\_2015.GDT 12/20/17

# SCDOT Soil Test Log

<b>Project ID:</b>	1413-16-153	<b>County:</b>	Georgetown, SC	<b>Boring No.:</b>	B-FMG
<b>Site Description:</b>	USC-SCDOT Deep Seismic Holes			<b>Route:</b>	
<b>Eng./Geo.:</b>	CS & LE	<b>Boring Location:</b>		<b>Offset:</b>	
<b>Elev.:</b>	27.0 ft	<b>Latitude:</b>	33.447666	<b>Longitude:</b>	-79.59089
<b>Total Depth:</b>	615 ft	<b>Soil Depth:</b>	20.8 ft	<b>Core Depth:</b>	615 ft
<b>Date Started:</b>	02/06/2017		<b>Date Completed:</b>	2/18/2017	
<b>Bore Hole Diameter (in):</b>	4	<b>Sampler Configuration</b>		<b>Liner Required:</b>	Y N
<b>Liner Used:</b>	Y N		<b>Drill Machine:</b>	CME-550	<b>Drill Method:</b>
<b>Drill Method:</b>	Mud Rotary		<b>Hammer Type:</b>	Automatic	
<b>Energy Ratio:</b>	91.5%		<b>Groundwater:</b>	TOB	2.5 ft
<b>Core Size:</b>	HQ		<b>Driller:</b>	AE Drilling	
<b>24HR:</b>	2.8 ft				



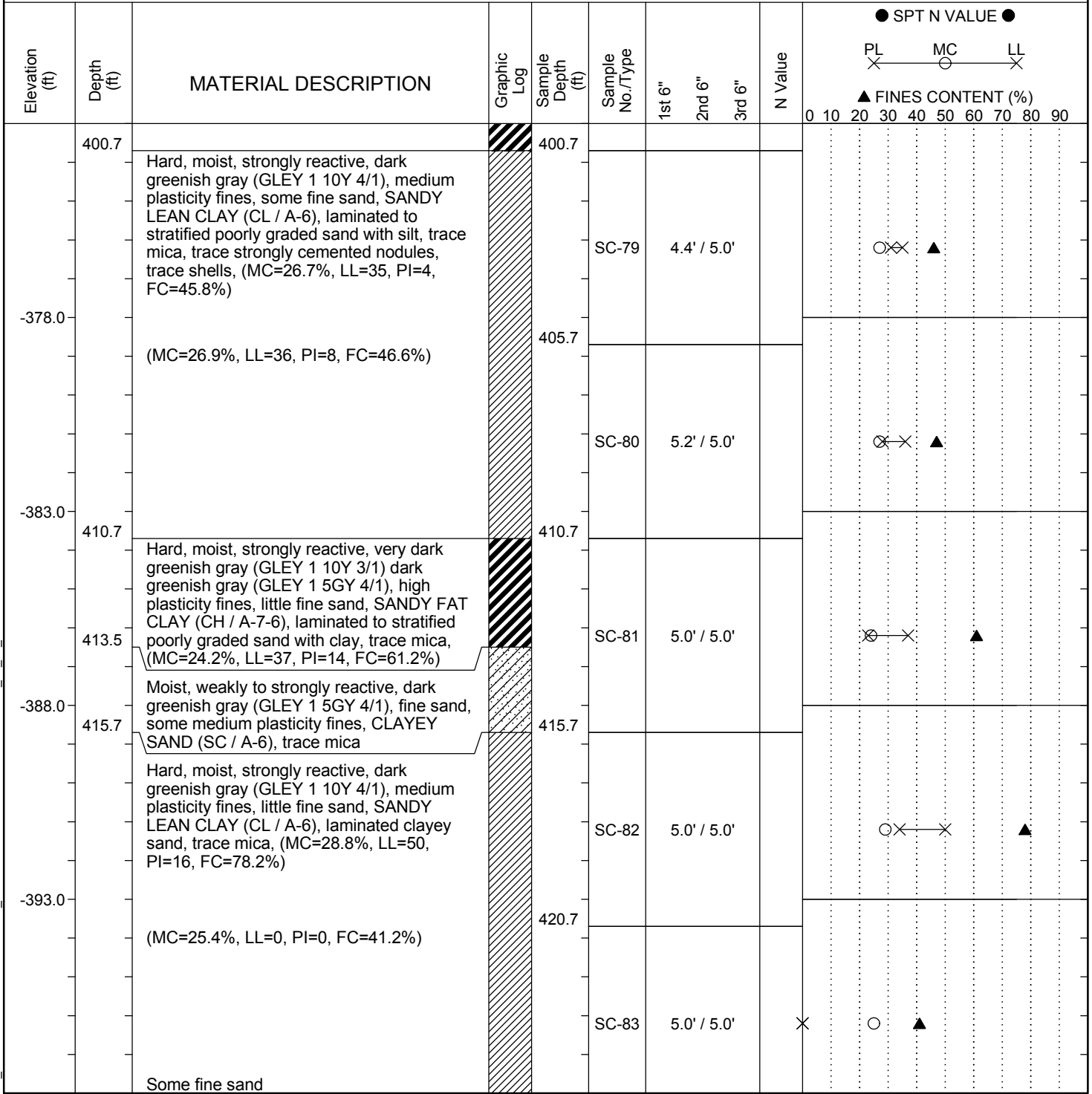
LEGEND Continued Next Page

SAMPLER TYPE		DRILLING METHOD	
SS - Split Spoon	NQ - Rock Core, 1-7/8"	HSA - Hollow Stem Auger	RW - Rotary Wash
UD - Undisturbed Sample	CU - Cuttings	CFA - Continuous Flight Augers	RC - Rock Core
AWG - Rock Core, 1-1/8"	CT - Continuous Tube	DC - Driving Casing	

SC\_DOT\_141316153\_USC-SCDOT DEEP BORINGS\_B-FMG.GPJ\_SCDOT DATA TEMPLATE\_01\_30\_2015.GDT 12/20/17

# SCDOT Soil Test Log

<b>Project ID:</b>	1413-16-153	<b>County:</b>	Georgetown, SC	<b>Boring No.:</b>	B-FMG
<b>Site Description:</b>	USC-SCDOT Deep Seismic Holes			<b>Route:</b>	
<b>Eng./Geo.:</b>	CS & LE	<b>Boring Location:</b>		<b>Offset:</b>	
<b>Elev.:</b>	27.0 ft	<b>Latitude:</b>	33.447666	<b>Longitude:</b>	-79.59089
<b>Total Depth:</b>	615 ft	<b>Soil Depth:</b>	20.8 ft	<b>Core Depth:</b>	615 ft
<b>Bore Hole Diameter (in):</b>	4	<b>Sampler Configuration</b>		<b>Liner Required:</b>	Y N
<b>Drill Machine:</b>	CME-550	<b>Drill Method:</b>	Mud Rotary	<b>Hammer Type:</b>	Automatic
<b>Core Size:</b>	HQ	<b>Driller:</b>	AE Drilling	<b>Energy Ratio:</b>	91.5%
		<b>Groundwater:</b>	TOB	<b>24HR</b>	2.8 ft



**LEGEND**

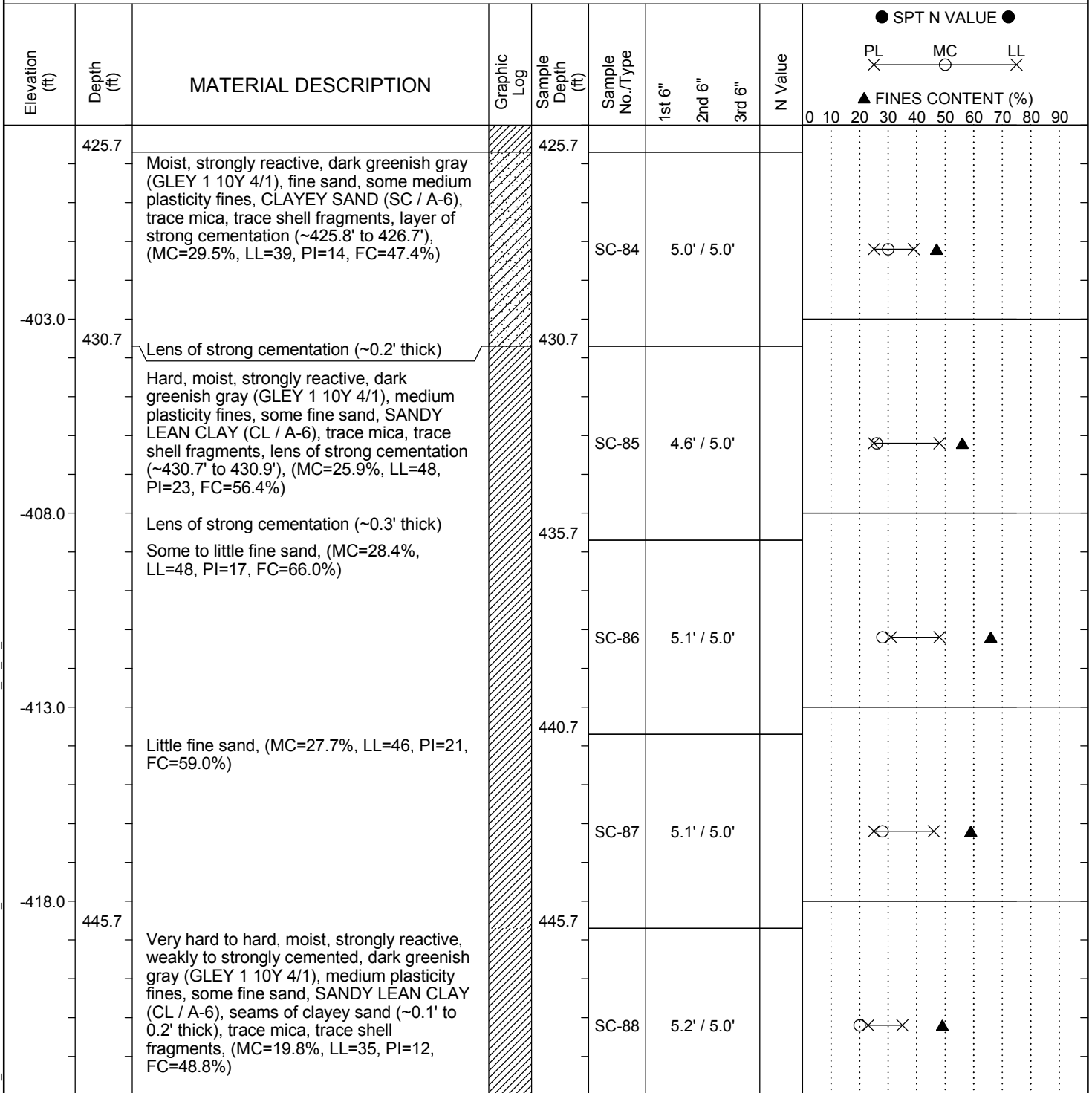
*Continued Next Page*

SAMPLER TYPE		DRILLING METHOD	
SS - Split Spoon	NQ - Rock Core, 1-7/8"	HSA - Hollow Stem Auger	RW - Rotary Wash
UD - Undisturbed Sample	CU - Cuttings	CFA - Continuous Flight Augers	RC - Rock Core
AWG - Rock Core, 1-1/8"	CT - Continuous Tube	DC - Driving Casing	

SC\_DOT\_141316153\_USC-SCDOT DEEP BORINGS\_B-FMG.GPJ\_SCDOT DATA TEMPLATE\_01\_30\_2015.GDT\_12/20/17

# SCDOT Soil Test Log

<b>Project ID:</b>	1413-16-153	<b>County:</b>	Georgetown, SC	<b>Boring No.:</b>	B-FMG
<b>Site Description:</b>	USC-SCDOT Deep Seismic Holes			<b>Route:</b>	
<b>Eng./Geo.:</b>	CS & LE	<b>Boring Location:</b>		<b>Offset:</b>	
<b>Elev.:</b>	27.0 ft	<b>Latitude:</b>	33.447666	<b>Longitude:</b>	-79.59089
<b>Total Depth:</b>	615 ft	<b>Soil Depth:</b>	20.8 ft	<b>Core Depth:</b>	615 ft
<b>Bore Hole Diameter (in):</b>	4	<b>Sampler Configuration</b>		<b>Liner Required:</b>	Y N
<b>Drill Machine:</b>	CME-550	<b>Drill Method:</b>	Mud Rotary	<b>Hammer Type:</b>	Automatic
<b>Core Size:</b>	HQ	<b>Driller:</b>	AE Drilling	<b>Groundwater:</b>	TOB 2.5 ft
				<b>24HR</b>	2.8 ft
				<b>Energy Ratio:</b>	91.5%



**LEGEND**

*Continued Next Page*

SAMPLER TYPE		DRILLING METHOD	
SS - Split Spoon	NQ - Rock Core, 1-7/8"	HSA - Hollow Stem Auger	RW - Rotary Wash
UD - Undisturbed Sample	CU - Cuttings	CFA - Continuous Flight Augers	RC - Rock Core
AWG - Rock Core, 1-1/8"	CT - Continuous Tube	DC - Driving Casing	

SC\_DOT 141316153\_USC-SCDOT DEEP BORINGS\_B-FMG.GPJ SCDOT DATA TEMPLATE\_01\_30\_2015.GDT 12/20/17

# SCDOT Soil Test Log

<b>Project ID:</b>	1413-16-153	<b>County:</b>	Georgetown, SC	<b>Boring No.:</b>	B-FMG
<b>Site Description:</b>	USC-SCDOT Deep Seismic Holes			<b>Route:</b>	
<b>Eng./Geo.:</b>	CS & LE	<b>Boring Location:</b>		<b>Offset:</b>	
<b>Elev.:</b>	27.0 ft	<b>Latitude:</b>	33.447666	<b>Longitude:</b>	-79.59089
<b>Total Depth:</b>	615 ft	<b>Soil Depth:</b>	20.8 ft	<b>Core Depth:</b>	615 ft
<b>Bore Hole Diameter (in):</b>	4	<b>Sampler Configuration</b>		<b>Liner Required:</b>	Y N
<b>Drill Machine:</b>	CME-550	<b>Drill Method:</b>	Mud Rotary	<b>Hammer Type:</b>	Automatic
<b>Core Size:</b>	HQ	<b>Driller:</b>	AE Drilling	<b>Groundwater:</b>	TOB 2.5 ft
				<b>24HR</b>	2.8 ft
				<b>Energy Ratio:</b>	91.5%
				<b>Liner Used:</b>	Y N

Elevation (ft)	Depth (ft)	MATERIAL DESCRIPTION	Graphic Log	Sample Depth (ft)	Sample No./Type	1st 6"	2nd 6"	3rd 6"	N Value	SPT N VALUE ●		FINES CONTENT (%) ▲	
										PL	MC	LL	0
		Little to some fine sand Little fine sand, trace mica to micaceous, (MC=27.9%, LL=45, PI=18, FC=75.2%)		450.7									
-428.0					SC-89	4.8' / 5.0'					⊗	⊗	▲
		Dark olive gray (5Y 3/2), (MC=28.2%, LL=50, PI=27, FC=80.6%)		455.7									
-433.0					SC-90	5.0' / 5.0'					⊗	⊗	▲
		(MC=29.1%, LL=51, PI=27, FC=82.2%)		460.7									
-438.0					SC-91	4.4' / 5.0'					⊗	⊗	▲
		(MC=28.0%, LL=39, PI=16, FC=52.6%)		465.7									
-443.0		Layer of stratified weakly to strongly cemented clayey sand (~0.6' thick) Trace moderately to strongly cemented nodules		470.7							⊗	⊗	▲
	470.7	<b>DONOHO CREEK FORMATION - BLACK CREEK GROUP:</b> Hard, moist, strongly reactive, greenish black (GLEYS 1 10Y 2.5/1), high plasticity fines, little fine sand, SANDY FAT CLAY (CH / A-7-6), trace mica, trace shell fragments, laminated to stratified sandy lean clay, trace wood fragments,		470.7							⊗	⊗	▲
					SC-93	5.1' / 5.0'					⊗	⊗	▲

LEGEND

Continued Next Page

SAMPLER TYPE		DRILLING METHOD	
SS - Split Spoon	NQ - Rock Core, 1-7/8"	HSA - Hollow Stem Auger	RW - Rotary Wash
UD - Undisturbed Sample	CU - Cuttings	CFA - Continuous Flight Augers	RC - Rock Core
AWG - Rock Core, 1-1/8"	CT - Continuous Tube	DC - Driving Casing	

SC\_DOT\_141316153\_USC-SCDOT DEEP BORINGS\_B-FMG.GPJ\_SCDOT DATA TEMPLATE\_01\_30\_2015.GDT 12/20/17

# SCDOT Soil Test Log

<b>Project ID:</b>	1413-16-153	<b>County:</b>	Georgetown, SC	<b>Boring No.:</b>	B-FMG
<b>Site Description:</b>	USC-SCDOT Deep Seismic Holes			<b>Route:</b>	
<b>Eng./Geo.:</b>	CS & LE	<b>Boring Location:</b>		<b>Offset:</b>	
<b>Elev.:</b>	27.0 ft	<b>Latitude:</b>	33.447666	<b>Longitude:</b>	-79.59089
<b>Total Depth:</b>	615 ft	<b>Soil Depth:</b>	20.8 ft	<b>Core Depth:</b>	615 ft
<b>Bore Hole Diameter (in):</b>	4	<b>Sampler Configuration</b>		<b>Liner Required:</b>	Y N
<b>Drill Machine:</b>	CME-550	<b>Drill Method:</b>	Mud Rotary	<b>Hammer Type:</b>	Automatic
<b>Core Size:</b>	HQ	<b>Driller:</b>	AE Drilling	<b>Groundwater:</b>	TOB 2.5 ft
				<b>24HR</b>	2.8 ft

Elevation (ft)	Depth (ft)	MATERIAL DESCRIPTION	Graphic Log	Sample Depth (ft)	Sample No./Type	1st 6"	2nd 6"	3rd 6"	N Value	SPT N VALUE									
										PL	MC	LL							
										▲ FINES CONTENT (%)									
										0	10	20	30	40	50	60	70	80	90
		(MC=29.4%, LL=70, PI=48, FC=66.2%) Few shell fragments, (MC=36.0%, LL=81, PI=55, FC=76.2%)		475.7															
-453.0					SC-94	5.0' / 5.0'					30								
		Greenish black (GLEY 1 10Y 2.5/1) dark greenish gray (GLEY 1 10Y 4/1), some fine sand, laminated to stratified sandy lean clay, trace to few moderately cemented nodules, (MC=29.6%, LL=81, PI=57, FC=67.0%)		480.7															
-458.0					SC-95	4.7' / 5.0'					40								
		Little fine sand, laminated, trace shell fragments, (MC=29.8%, LL=59, PI=35, FC=67.0%)		485.7															
-463.0					SC-96	5.0' / 5.0'					30								
	490.7	Very hard, moist, strongly reactive, non- to weakly cemented, greenish black (GLEY 1 10Y 2.5/1), high plasticity fines, few fine sand, FAT CLAY WITH SAND (CH / A-7-6), laminated, trace shell fragments, (MC=40.3%, LL=80, PI=45, FC=91.8%)		490.7															
-468.0					SC-97	5.1' / 5.0'					40								
	495.7	Very hard, moist, strongly reactive, very dark greenish gray (GLEY 1 10Y 3/1), high plasticity fines, FAT CLAY (CH / A-7-6), trace shells, trace fine sand, (MC=59.1%, LL=80, PI=35, FC=94.8%)		495.7															
					SC-98	5.1' / 5.0'					30								

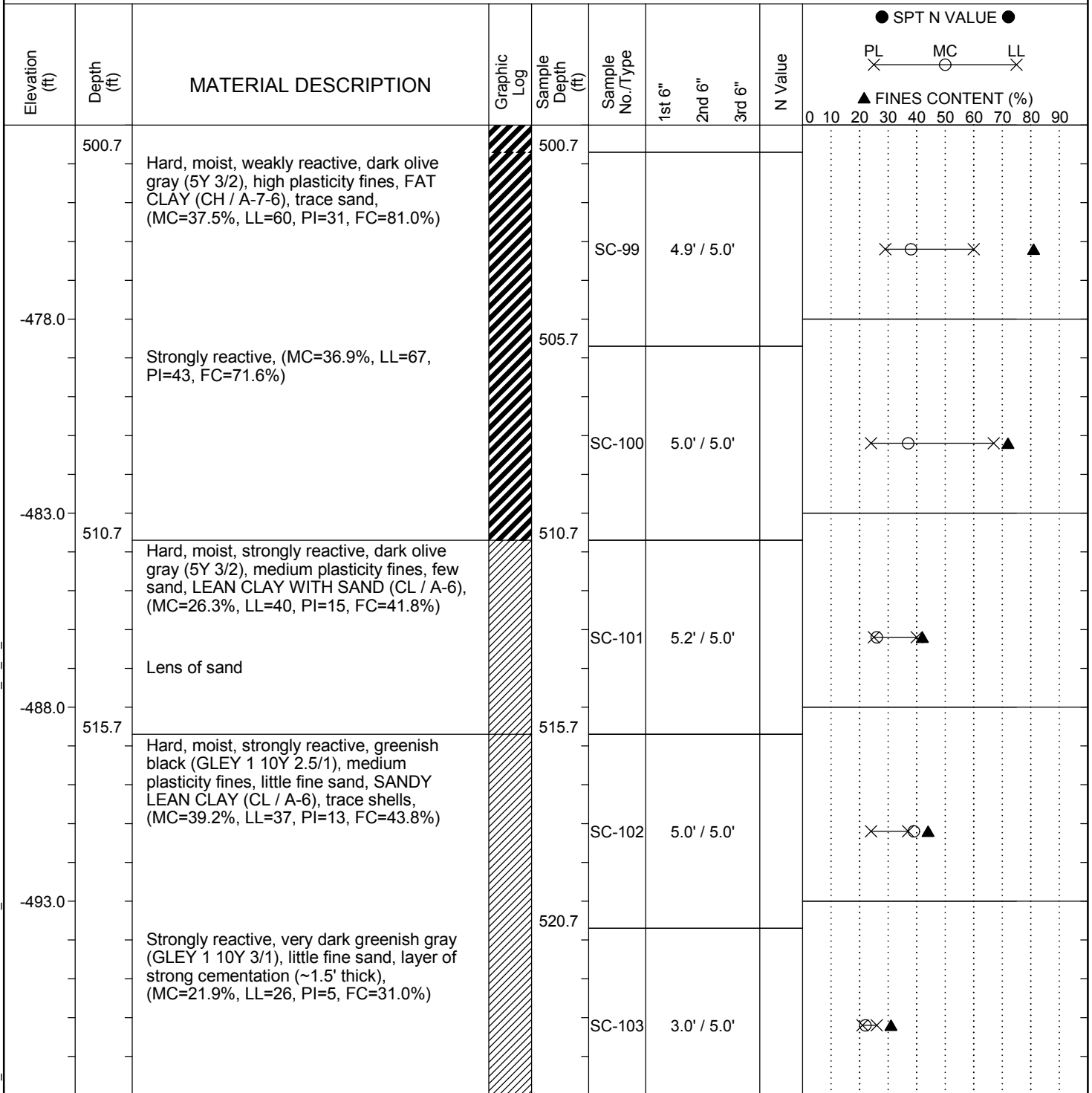
LEGEND Continued Next Page

SAMPLER TYPE		DRILLING METHOD	
SS - Split Spoon	NQ - Rock Core, 1-7/8"	HSA - Hollow Stem Auger	RW - Rotary Wash
UD - Undisturbed Sample	CU - Cuttings	CFA - Continuous Flight Augers	RC - Rock Core
AWG - Rock Core, 1-1/8"	CT - Continuous Tube	DC - Driving Casing	

SC\_DOT\_141316153\_USC-SCDOT DEEP BORINGS\_B-FMG.GPJ\_SCDOT DATA TEMPLATE\_01\_30\_2015.GDT 12/20/17

# SCDOT Soil Test Log

<b>Project ID:</b>	1413-16-153	<b>County:</b>	Georgetown, SC	<b>Boring No.:</b>	B-FMG
<b>Site Description:</b>	USC-SCDOT Deep Seismic Holes			<b>Route:</b>	
<b>Eng./Geo.:</b>	CS & LE	<b>Boring Location:</b>		<b>Offset:</b>	
<b>Elev.:</b>	27.0 ft	<b>Latitude:</b>	33.447666	<b>Longitude:</b>	-79.59089
<b>Total Depth:</b>	615 ft	<b>Soil Depth:</b>	20.8 ft	<b>Core Depth:</b>	615 ft
<b>Bore Hole Diameter (in):</b>	4	<b>Sampler Configuration</b>		<b>Liner Required:</b>	Y N
<b>Drill Machine:</b>	CME-550	<b>Drill Method:</b>	Mud Rotary	<b>Hammer Type:</b>	Automatic
<b>Core Size:</b>	HQ	<b>Driller:</b>	AE Drilling	<b>Groundwater:</b>	TOB 2.5 ft
				<b>24HR</b>	2.8 ft



**LEGEND**

*Continued Next Page*

SAMPLER TYPE		DRILLING METHOD	
SS - Split Spoon	NQ - Rock Core, 1-7/8"	HSA - Hollow Stem Auger	RW - Rotary Wash
UD - Undisturbed Sample	CU - Cuttings	CFA - Continuous Flight Augers	RC - Rock Core
AWG - Rock Core, 1-1/8"	CT - Continuous Tube	DC - Driving Casing	

SC\_DOT\_141316153\_USC-SCDOT DEEP BORINGS\_B-FMG.GPJ\_SCDOT DATA TEMPLATE\_01\_30\_2015.GDT 12/20/17

# SCDOT Soil Test Log

<b>Project ID:</b>	1413-16-153	<b>County:</b>	Georgetown, SC	<b>Boring No.:</b>	B-FMG
<b>Site Description:</b>	USC-SCDOT Deep Seismic Holes			<b>Route:</b>	
<b>Eng./Geo.:</b>	CS & LE	<b>Boring Location:</b>		<b>Offset:</b>	
<b>Elev.:</b>	27.0 ft	<b>Latitude:</b>	33.447666	<b>Longitude:</b>	-79.59089
<b>Total Depth:</b>	615 ft	<b>Soil Depth:</b>	20.8 ft	<b>Core Depth:</b>	615 ft
<b>Bore Hole Diameter (in):</b>	4	<b>Sampler Configuration</b>		<b>Liner Required:</b>	Y N
<b>Drill Machine:</b>	CME-550	<b>Drill Method:</b>	Mud Rotary	<b>Hammer Type:</b>	Automatic
<b>Core Size:</b>	HQ	<b>Driller:</b>	AE Drilling	<b>Groundwater:</b>	TOB 2.5 ft
				<b>24HR</b>	2.8 ft

Elevation (ft)	Depth (ft)	MATERIAL DESCRIPTION	Graphic Log	Sample Depth (ft)	Sample No./Type	1st 6"	2nd 6"	3rd 6"	N Value	SPT N VALUE												
										PL	MC	LL	FINES CONTENT (%)									
		Weakly reactive, some fine sand, (MC=21.1%, LL=31, PI=9, FC=34.2%)		525.7																		
		Strongly reactive, few shells			SC-104	5.0' / 5.0'																
-503.0	530.7	<b>BLADEN FORMATION - BLACK CREEK GROUP:</b> Weakly reactive, greenish black (GLEY 1 10Y 2.5/1), trace shells, (MC=25.7%, LL=39, PI=19, FC=33.4%)			530.7	SC-105	5.0' / 5.0'															
-508.0		Weakly cemented, some fine sand, (MC=28.6%, LL=41, PI=18, FC=31.2%)			535.7	SC-106	5.3' / 5.0'															
-513.0		Very dark greenish gray (GLEY 1 10Y 3/1), (MC=31.0%, LL=43, PI=17, FC=43.0%)			540.7	SC-107	4.5' / 5.0'															
-518.0		Very dark gray (5Y 3/1), (MC=26.7%, LL=40, PI=19, FC=34.0%)		545.7	SC-108	3.0' / 5.0'																

LEGEND Continued Next Page

SAMPLER TYPE		DRILLING METHOD	
SS - Split Spoon	NQ - Rock Core, 1-7/8"	HSA - Hollow Stem Auger	RW - Rotary Wash
UD - Undisturbed Sample	CU - Cuttings	CFA - Continuous Flight Augers	RC - Rock Core
AWG - Rock Core, 1-1/8"	CT - Continuous Tube	DC - Driving Casing	

SC\_DOT\_141316153\_USC-SCDOT DEEP BORINGS\_B-FMG.GPJ\_SCDOT DATA TEMPLATE\_01\_30\_2015.GDT 12/20/17

# SCDOT Soil Test Log

<b>Project ID:</b>	1413-16-153	<b>County:</b>	Georgetown, SC	<b>Boring No.:</b>	B-FMG
<b>Site Description:</b>	USC-SCDOT Deep Seismic Holes			<b>Route:</b>	
<b>Eng./Geo.:</b>	CS & LE	<b>Boring Location:</b>		<b>Offset:</b>	
<b>Elev.:</b>	27.0 ft	<b>Latitude:</b>	33.447666	<b>Longitude:</b>	-79.59089
<b>Total Depth:</b>	615 ft	<b>Soil Depth:</b>	20.8 ft	<b>Core Depth:</b>	615 ft
<b>Bore Hole Diameter (in):</b>	4	<b>Sampler Configuration</b>		<b>Liner Required:</b>	Y N
<b>Drill Machine:</b>	CME-550	<b>Drill Method:</b>	Mud Rotary	<b>Hammer Type:</b>	Automatic
<b>Core Size:</b>	HQ	<b>Driller:</b>	AE Drilling	<b>Energy Ratio:</b>	91.5%
		<b>Groundwater:</b>	TOB	<b>24HR</b>	2.8 ft

Elevation (ft)	Depth (ft)	MATERIAL DESCRIPTION	Graphic Log	Sample Depth (ft)	Sample No./Type	1st 6"	2nd 6"	3rd 6"	N Value	SPT N VALUE													
										PL	MC	LL	FINES CONTENT (%)										
550.7		Moist, strongly reactive, weakly cemented, very dark gray (2.5Y 3/1), fine sand, little low plasticity fines, CLAYEY SAND (SC / A-2-6), layer of strong cementation (~0.8' thick), (MC=31.0%, LL=43, PI=17, FC=43.0%)		550.7	SC-109	1.0' / 5.0'																	
-528.0		Layer of strong cementation (~1.0' thick)		555.7	SC-110	1.0' / 5.0'																	
-533.0		<b>NO RECOVERY</b>		560.7	SC-111	0.0' / 5.0'																	
-538.0		Layer of strong cementation (~1.2' thick)		565.7	SC-112	1.2' / 5.0'																	
-543.0	570.7	Moist, weakly reactive, weakly cemented, very dark greenish gray (GLEYS 1 10Y 3/1), fine sand, little medium plasticity fines, CLAYEY SAND (SC / A-2-6), (MC=25.9%, LL=30, PI=8, FC=25.0%)		570.7	SC-113	3.5' / 5.0'																	

**LEGEND**

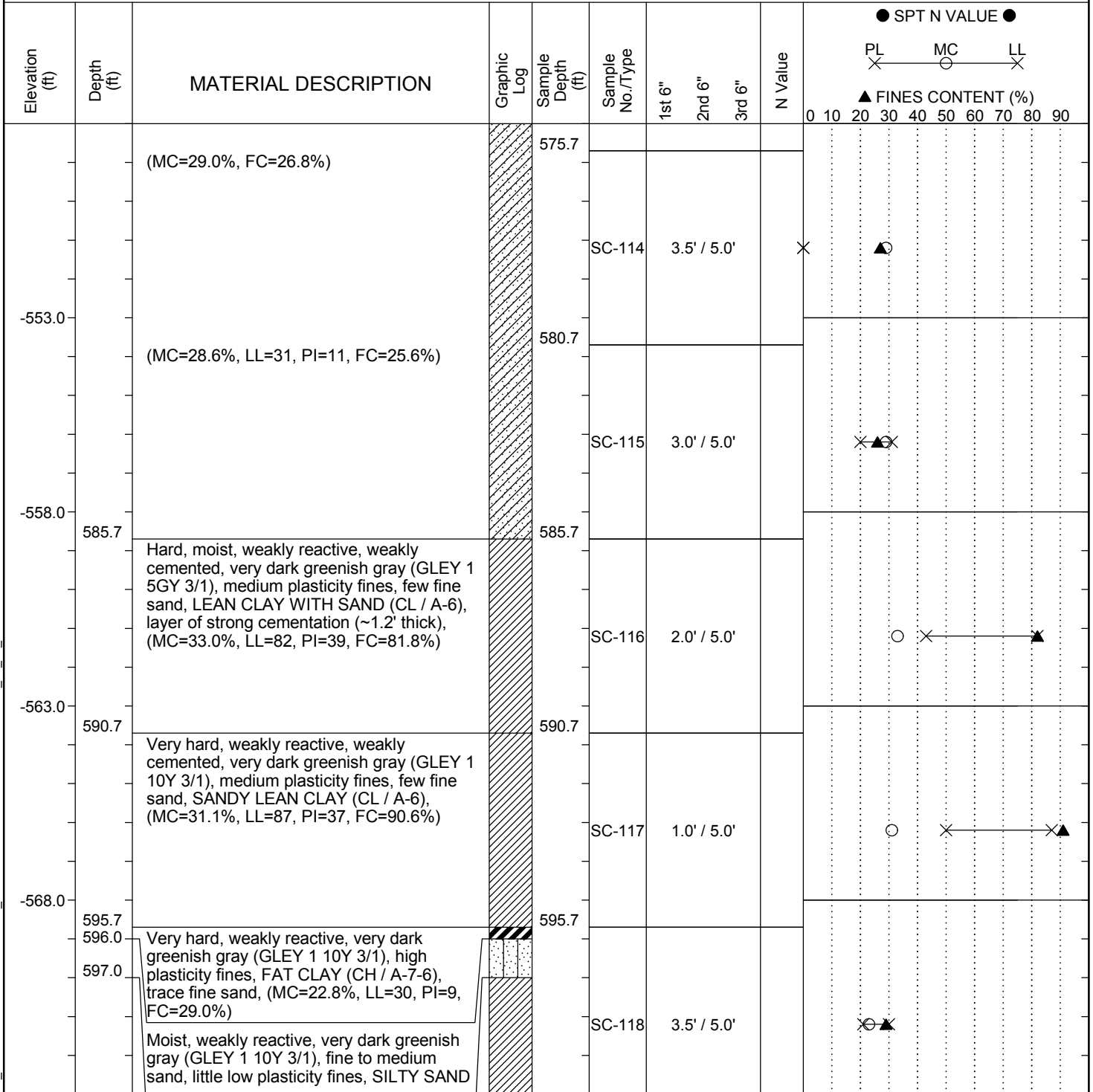
*Continued Next Page*

<b>SAMPLER TYPE</b>		<b>DRILLING METHOD</b>	
SS - Split Spoon	NQ - Rock Core, 1-7/8"	HSA - Hollow Stem Auger	RW - Rotary Wash
UD - Undisturbed Sample	CU - Cuttings	CFA - Continuous Flight Augers	RC - Rock Core
AWG - Rock Core, 1-1/8"	CT - Continuous Tube	DC - Driving Casing	

SC\_DOT 141316153\_USC-SCDOT DEEP BORINGS\_B-FMG.GPJ SCDOT DATA TEMPLATE\_01\_30\_2015.GDT 12/20/17

# SCDOT Soil Test Log

<b>Project ID:</b>	1413-16-153	<b>County:</b>	Georgetown, SC	<b>Boring No.:</b>	B-FMG
<b>Site Description:</b>	USC-SCDOT Deep Seismic Holes			<b>Route:</b>	
<b>Eng./Geo.:</b>	CS & LE	<b>Boring Location:</b>		<b>Offset:</b>	
<b>Elev.:</b>	27.0 ft	<b>Latitude:</b>	33.447666	<b>Longitude:</b>	-79.59089
<b>Total Depth:</b>	615 ft	<b>Soil Depth:</b>	20.8 ft	<b>Core Depth:</b>	615 ft
<b>Bore Hole Diameter (in):</b>	4	<b>Sampler Configuration</b>		<b>Liner Required:</b>	Y N
<b>Drill Machine:</b>	CME-550	<b>Drill Method:</b>	Mud Rotary	<b>Hammer Type:</b>	Automatic
<b>Core Size:</b>	HQ	<b>Driller:</b>	AE Drilling	<b>Groundwater:</b>	TOB 2.5 ft
				<b>24HR</b>	2.8 ft



## LEGEND

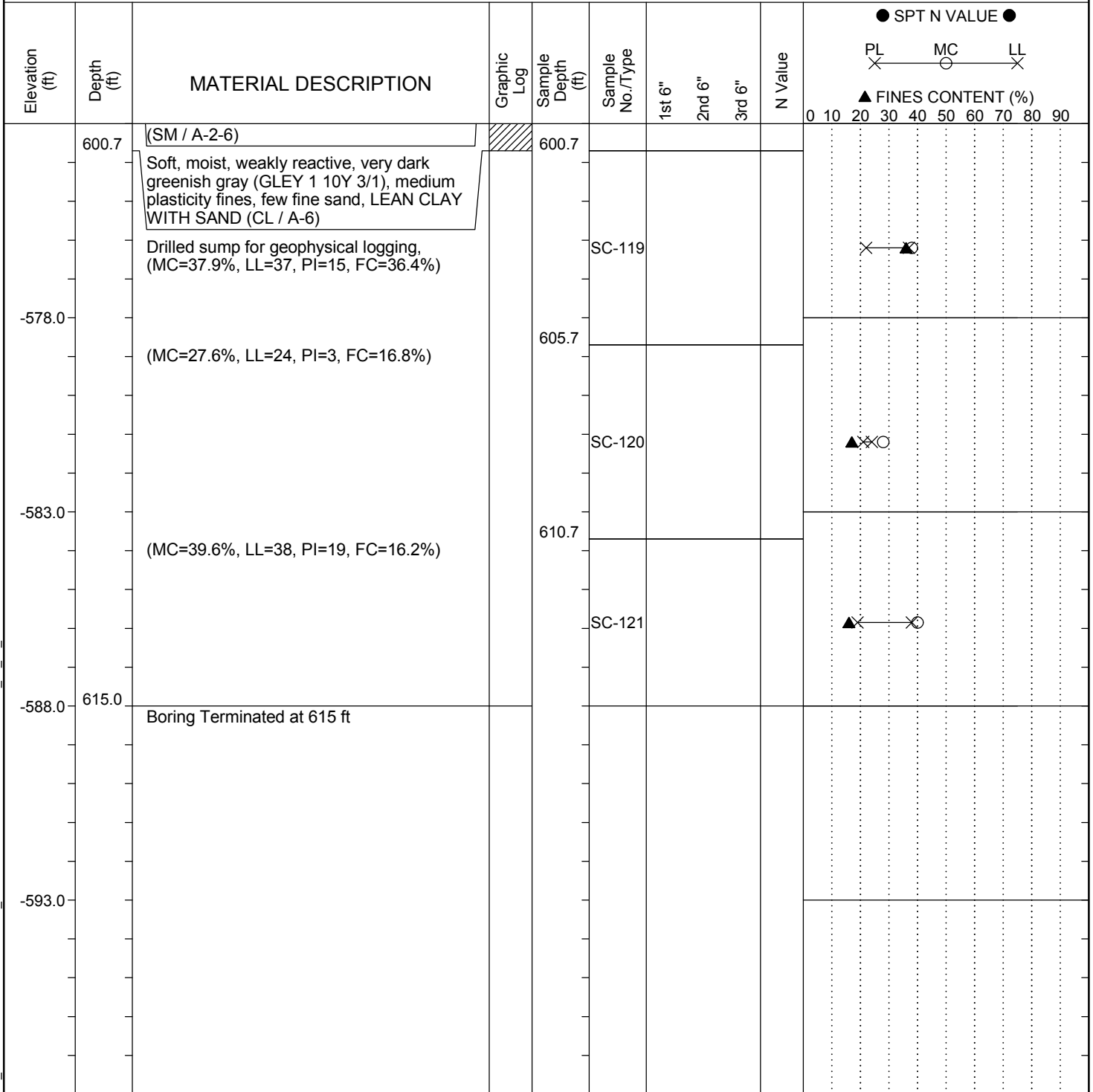
Continued Next Page

SAMPLER TYPE		DRILLING METHOD	
SS - Split Spoon	NQ - Rock Core, 1-7/8"	HSA - Hollow Stem Auger	RW - Rotary Wash
UD - Undisturbed Sample	CU - Cuttings	CFA - Continuous Flight Augers	RC - Rock Core
AWG - Rock Core, 1-1/8"	CT - Continuous Tube	DC - Driving Casing	

SC\_DOT\_141316153\_USC-SCDOT DEEP BORINGS\_B-FMG.GPJ\_SCDOT DATA TEMPLATE\_01\_30\_2015.GDT\_12/20/17

# SCDOT Soil Test Log

<b>Project ID:</b>	1413-16-153	<b>County:</b>	Georgetown, SC	<b>Boring No.:</b>	B-FMG
<b>Site Description:</b>	USC-SCDOT Deep Seismic Holes			<b>Route:</b>	
<b>Eng./Geo.:</b>	CS & LE	<b>Boring Location:</b>		<b>Offset:</b>	
<b>Elev.:</b>	27.0 ft	<b>Latitude:</b>	33.447666	<b>Longitude:</b>	-79.59089
<b>Total Depth:</b>	615 ft	<b>Soil Depth:</b>	20.8 ft	<b>Core Depth:</b>	615 ft
<b>Bore Hole Diameter (in):</b>	4	<b>Sampler Configuration</b>		<b>Liner Required:</b>	Y N
<b>Drill Machine:</b>	CME-550	<b>Drill Method:</b>	Mud Rotary	<b>Hammer Type:</b>	Automatic
<b>Core Size:</b>	HQ	<b>Driller:</b>	AE Drilling	<b>Groundwater:</b>	TOB 2.5 ft
				<b>24HR</b>	2.8 ft
				<b>Energy Ratio:</b>	91.5%
				<b>Liner Used:</b>	Y N



## LEGEND

SAMPLER TYPE		DRILLING METHOD	
SS - Split Spoon	NQ - Rock Core, 1-7/8"	HSA - Hollow Stem Auger	RW - Rotary Wash
UD - Undisturbed Sample	CU - Cuttings	CFA - Continuous Flight Augers	RC - Rock Core
AWG - Rock Core, 1-1/8"	CT - Continuous Tube	DC - Driving Casing	

SC\_DOT 141316153\_USC-SCDOT DEEP BORINGS\_B-FMG.GPJ SCDOT DATA TEMPLATE\_01\_30\_2015.GDT 12/20/17

## **Appendix III: Borehole Geophysical Testing Data**



**SCDOT**  
**BOREHOLE GEOPHYSICS**  
**SOUTH CAROLINA**

**April 10, 2017**  
**Report 17016-01 rev 0**

**SCDOT  
BOREHOLE GEOPHYSICS  
SOUTH CAROLINA**

**Prepared for**

**S&ME, Inc.  
620 Wando Park Boulevard  
Mt. Pleasant, South Carolina 29464  
(843) 884-0005**

**Prepared by**

**GEOVision Geophysical Services  
1124 Olympic Drive  
Corona, California 92881  
(951) 549-1234  
Project 17016**

**April 10, 2017**

**Report 17016-01 rev 0**

# TABLE OF CONTENTS

<b>TABLE OF CONTENTS</b> .....	<b>3</b>
<b>TABLE OF FIGURES</b> .....	<b>4</b>
<b>TABLE OF TABLES</b> .....	<b>4</b>
<b>APPENDICES</b> .....	<b>4</b>
<b>INTRODUCTION</b> .....	<b>5</b>
<b>SCOPE OF WORK</b> .....	<b>5</b>
<b>INSTRUMENTATION</b> .....	<b>7</b>
SUSPENSION VELOCITY INSTRUMENTATION .....	7
INDUCTION / NATURAL GAMMA INSTRUMENTATION .....	10
<b>MEASUREMENT PROCEDURES</b> .....	<b>12</b>
SUSPENSION VELOCITY MEASUREMENT PROCEDURES .....	12
INDUCTION / NATURAL GAMMA MEASUREMENT PROCEDURES .....	13
<b>DATA ANALYSIS</b> .....	<b>15</b>
SUSPENSION VELOCITY ANALYSIS.....	15
INDUCTION / NATURAL GAMMA ANALYSIS .....	17
<b>RESULTS</b> .....	<b>18</b>
SUSPENSION VELOCITY RESULTS .....	18
INDUCTION / NATURAL GAMMA RESULTS .....	18
<b>SUMMARY</b> .....	<b>19</b>
DISCUSSION OF SUSPENSION VELOCITY RESULTS .....	19
DISCUSSION OF INDUCTION / NATURAL GAMMA RESULTS.....	20
QUALITY ASSURANCE .....	22
SUSPENSION VELOCITY DATA RELIABILITY .....	22
<b>CERTIFICATION</b> .....	<b>23</b>

## Table of Figures

Figure 1: Concept illustration of P-S logging system.....	25
Figure 2: Example of filtered (1400 Hz lowpass) suspension record.....	26
Figure 3. Example of unfiltered suspension record.....	27
Figure 4: Borehole B-FMG, Suspension R1-R2 P- and S <sub>H</sub> -wave velocities.....	28
Figure 5. Boring B-FMG, Induction and natural gamma logs.....	39
Figure 6: Boreholes HOR-1328 & Conway Offset, Suspension R1-R2 P- and S <sub>H</sub> -wave velocities.....	40
Figure 7. Boreholes HOR-1328 & Conway Offset, Induction and natural gamma logs.....	49

## Table of Tables

Table 1. Borehole locations and logging dates.....	24
Table 2. Logging dates and depth ranges.....	24
Table 3. Borehole B-FMG, Suspension R1-R2 depths and P- and S <sub>H</sub> -wave velocities.....	29
Table 4. Boreholes HOR-1328 & Conway Offset, Suspension R1-R2 depths and P- and S <sub>H</sub> -wave velocities.....	41

## APPENDICES

<b>APPENDIX A</b>	<b>SUSPENSION VELOCITY MEASUREMENT QUALITY ASSURANCE SUSPENSION SOURCE TO RECEIVER ANALYSIS RESULTS</b>
<b>APPENDIX B</b>	<b>INDUCTION, ELOG, NATURAL GAMMA AND MECHANICAL CALIPER LOGS</b>
<b>APPENDIX C</b>	<b>GEOPHYSICAL LOGGING SYSTEMS - NIST TRACEABLE CALIBRATION RECORDS</b>

## INTRODUCTION

**GEOVision** acquired borehole geophysical data in three (3) boreholes at 2 South Carolina Department of Transportation sites. The work was performed for S&ME, Inc. Analysis and report were reviewed by a **GEOVision** Professional Geophysicist or Engineer.

## SCOPE OF WORK

This report presents results of borehole geophysical measurements acquired in three boreholes between January 28<sup>th</sup> and February 27<sup>th</sup>, 2017 as detailed in Table 1. The purpose of these measurements was to supplement stratigraphic information by acquiring shear wave and compressional wave velocities as a function of depth.

The OYO Suspension PS Logging System (Suspension System) was used to obtain in-situ horizontal shear ( $S_H$ ) and compressional (P) wave velocity measurements in one cased and two uncased boreholes at 1.6 foot intervals. Measurements followed **GEOVision** Procedure for PS Suspension Seismic Velocity Logging, revision 1.5. Acquired data were analyzed and a profile of velocity versus depth was produced for both  $S_H$  and P waves.

A detailed reference for the suspension PS velocity measurement techniques used in this study is:

Guidelines for Determining Design Basis Ground Motions, Report TR-102293,  
Electric Power Research Institute, Palo Alto, California, November 1993, Sections  
7 and 8.

A Robertson Geologging Dual Induction probe (DUIN) was used to collect long and short conductivity and natural gamma data at 0.05 foot intervals.

Measurement procedures followed these ASTM standards:

- ASTM D5753-05 (Re-approved 2010), “Planning and Conducting Boring Geophysical Logging”

- ASTM D6726-01 (Re-approved 2007), “Conducting Boring Geophysical Logging – Electromagnetic Induction”

# INSTRUMENTATION

## Suspension Velocity Instrumentation

Suspension velocity measurements were performed using the suspension PS logging system, manufactured by OYO Corporation, and their subsidiary, Robertson Geologging. This system directly determines the average velocity of a 3.3-foot high segment of the soil column surrounding the borehole of interest by measuring the elapsed time between arrivals of a wave propagating upward through the soil column. The receivers that detect the wave, and the source that generates the wave, are moved as a unit in the borehole producing relatively constant amplitude signals at all depths.

The suspension system probe consists of a combined reversible polarity solenoid horizontal shear-wave source and compressional-wave source, joined to two biaxial receivers by a flexible isolation cylinder, as shown in Figure 1. The separation of the two receivers is 3.3 feet, allowing average wave velocity in the region between the receivers to be determined by inversion of the wave travel time between the two receivers. The total length of the probe as used in these surveys is approximately 25 feet, with the center point of the receiver pair 12.5 feet above the bottom end of the probe.

The probe receives control signals from, and sends the digitized receiver signals to, instrumentation on the surface via an armored multi-conductor cable. The cable is wound onto the drum of a winch and is used to support the probe. Cable travel is measured to provide probe depth data using a sheave of known circumference fitted with a digital rotary encoder.

The entire probe is suspended in the borehole by the cable, therefore, source motion is not coupled directly to the borehole walls; rather, the source motion creates a horizontally propagating impulsive pressure wave in the fluid filling the borehole and surrounding the source. This pressure wave is converted to P and  $S_H$ -waves in the surrounding soil and rock as it impinges upon the wall of the borehole. These waves propagate through the soil and rock surrounding the borehole, in turn

causing a pressure wave to be generated in the fluid surrounding the receivers as the soil waves pass their location. Separation of the P and  $S_H$ -waves at the receivers is performed using the following steps:

1. Orientation of the horizontal receivers is maintained parallel to the axis of the source, maximizing the amplitude of the recorded  $S_H$  -wave signals.
2. At each depth,  $S_H$ -wave signals are recorded with the source actuated in opposite directions, producing  $S_H$ -wave signals of opposite polarity, providing a characteristic  $S_H$ -wave signature distinct from the P-wave signal.
3. The 6.3 foot separation of source and receiver 1 permits the P-wave signal to pass and damp significantly before the slower  $S_H$ -wave signal arrives at the receiver. In faster soils or rock, the isolation cylinder is extended to allow greater separation of the P- and  $S_H$ -wave signals.
4. In saturated soils, the received P-wave signal is typically of much higher frequency than the received  $S_H$ -wave signal, permitting additional separation of the two signals by low pass filtering.
5. Direct arrival of the original pressure pulse in the fluid is not detected at the receivers because the wavelength of the pressure pulse in fluid is significantly greater than the dimension of the fluid annulus surrounding the probe (feet versus inches scale), preventing significant energy transmission through the fluid medium.

In operation, a distinct, repeatable pattern of impulses is generated at each depth as follows:

1. The source is fired in one direction producing dominantly horizontal shear with some vertical compression, and the signals from the horizontal receivers situated parallel to the axis of motion of the source are recorded.
2. The source is fired again in the opposite direction and the horizontal receiver signals are recorded.

3. The source is fired again and the vertical receiver signals are recorded. The repeated source pattern facilitates the picking of the P and  $S_H$ -wave arrivals; reversal of the source changes the polarity of the  $S_H$ -wave pattern but not the P-wave pattern.

The data from each receiver during each source activation is recorded as a different channel on the recording system. The Suspension PS system has six channels (two simultaneous recording channels), each with a 1024 sample record. The recorded data are displayed as six channels with a common time scale. Data are stored on disk for further processing.

Review of the displayed data on the recorder or computer screen allows the operator to set the gains, filters, delay time, pulse length (energy), and sample rate to optimize the quality of the data before recording. Verification of the calibration of the Suspension PS digital recorder is performed at least every twelve months using a NIST traceable frequency source and counter, as presented in Appendix C.

## Induction / Natural Gamma Instrumentation

Formation conductivity and natural gamma data were collected using a DUIN model dual induction probe, manufactured by Robertson Geologging, Ltd. The probe is 7.5 feet long, and 1.5 inches in diameter.

This probe is useful in the following studies:

- Bed boundary identification
- Strata correlation between borings
- Strata geometry and type (shale indication)

The probe receives control signals from, and sends the digitized measurement values to, a Robertson Micrologger II on the surface via an armored 4 conductor cable. The cable is wound onto the drum of a winch and is used to support the probe. Cable travel is measured to provide probe depth data, using a sheave of known circumference fitted with a digital rotary encoder. The probe and depth data are transmitted by USB link from the Micrologger unit to a laptop computer where it is displayed and stored on hard disk.

An Electro-Magnetic (EM) induction probe consists of transmitter and receiver coils. An alternating current is applied to the transmitter coil, causing the coil to radiate a primary EM field. This primary EM field generates eddy currents in subsurface materials, which give rise to a secondary EM field. The secondary EM field is measured as an alternating current in the receiver coils, which is proportional to formation conductivity. The probe coil spacing is optimized to achieve high vertical resolution, minimal borehole influence and large radius of investigation. The Robertson focused dual induction probe has effective coil spacings of 1.6 and 2.6 feet, operates at a frequency of 39 kHz, has 1 millisiemens/meter resolution, and operates over a 5 to 3000 millisiemens/meter conductivity range.

Natural gamma measurements rely upon small quantities of radioactive material contained in soil and rocks to emit gamma radiation as they decay. Trace amounts of uranium and thorium are

present in a few minerals, where potassium-bearing minerals such as feldspar, mica and clays will include traces of a radioactive isotope of potassium. These emit gamma radiation as they decay with an extremely long half-life. This radiation is detected by scintillation - the production of a tiny flash of light when gamma rays strike a crystal of sodium iodide. The light is converted into an electrical pulse by a photomultiplier tube. Pulses above a threshold value of 60 KeV are counted by the probe's microprocessor. The measurement is useful because the radioactive elements are concentrated in certain soil and rock types e.g. clay or shale, and depleted in others e.g. sandstone or coal.

## **MEASUREMENT PROCEDURES**

### **Suspension Velocity Measurement Procedures**

Boreholes were logged filled with fresh water mud. Measurements followed the **GEOVision** Procedure for P-S Suspension Seismic Velocity Logging, revision 1.5. Prior to the logging run, the probe was positioned with the top of the probe even with a stationary reference point. The electronic depth counter was set to the distance between the mid-point of the receiver and the top of the probe, minus the height of the stationary reference point, if any. Measurements were verified with a tape measure, and calculations recorded on a field log.

The probe was lowered to the bottom of the borehole, stopping at 1.6 foot intervals to collect data, as summarized in Table 2. At each measurement depth the measurement sequence of two opposite horizontal records and one vertical record was performed. Gains were adjusted as required. The data from each depth were viewed on the computer display, checked, and saved to disk before moving to the next depth.

Upon completion of the measurements, the probe was returned to the surface and the zero depth indication at the depth reference point was verified prior to removal from the borehole.

## Induction / Natural Gamma Measurement Procedures

Measurement procedures, incorporated into Bechtel Specification 25938-000-3PS-CY05-G0002 Rev. 00, followed these ASTM standards:

- ASTM D5753-05 (Re-approved 2010), “Planning and Conducting Boring Geophysical Logging”
- ASTM D6274-10, “Conducting Boring Geophysical Logging – Gamma”
- ASTM D6726-01 (Re-approved 2007), “Conducting Boring Geophysical Logging – Electromagnetic Induction”

All borings were filled with water during logging. Prior to the logging run, the measurement depths were referenced to ground level. This was done by placing the top of the probe at grade, and the electronic depth counter was set to the probe length. These calculations are recorded on the field logs. Offset distances between probe tip and measurement points are corrected for in the data acquisition software. The probe was lowered to the bottom of the boring where data acquisition was begun, and the probe was returned to the surface at approximately 10 feet/minute, collecting data continuously at 0.05-foot spacing, as summarized in Table 2.

This probe was not calibrated in the field, as it is used to provide qualitative measurements, not quantitative values, and is used only to assist in picking transitions between stratigraphic units, as described in ASTM D5753-05 (Reapproved 2010), “Planning and Conducting Borehole Geophysical Logging”. A functional test was performed prior to the logging run by placing a coil with an effective conductivity value over the probe, and recording the resultant output of the system. The results are recorded on the field logs, as reproduced in the separate Support Document package 16133-03 delivered to S&ME. These functional checks are also presented in LAS 2.0 format in the boring specific sub-directories on the data disks labeled Report 16133-02 that accompany this report.

Natural gamma was not calibrated in the field, as it is a qualitative measurement, not a quantitative value, and is used only to assist in picking transitions between stratigraphic units, as described in ASTM D6274-10, “Conducting Borehole Geophysical Logging – Gamma”.

Upon completion of the measurements, the probe zero depth indication at the depth reference point was verified prior to removal from the boring.

## DATA ANALYSIS

### Suspension Velocity Analysis

Using the proprietary OYO program PSLOG.EXE version 1.0, the recorded digital waveforms were analyzed to locate the most prominent first minima, first maxima, or first break on the vertical axis records, indicating the arrival of P-wave energy. The difference in travel time between receiver 1 and receiver 2 (R1-R2) arrivals was used to calculate the P-wave velocity for that 1.0 meter segment of the soil column. When observable, P-wave arrivals on the horizontal axis records were used to verify the velocities determined from the vertical axis data. The time picks were then transferred into a Microsoft Excel<sup>®</sup> template to complete the velocity calculations based on the arrival time picks made in PSLOG. The Microsoft Excel<sup>®</sup> analysis file accompanies this report.

The P-wave velocity over the 6.3-foot interval from source to receiver 1 (S-R1) was also picked using PSLOG, and calculated and plotted in Microsoft Excel<sup>®</sup>, for quality assurance of the velocity derived from the travel time between receivers. In this analysis, the depth values as recorded were increased by 4.8 feet to correspond to the mid-point of the 6.33-foot S-R1 interval. Travel times were obtained by picking the first break of the P-wave signal at receiver 1 and subtracting the calculated and experimentally verified delay, in milliseconds, from source trigger pulse (beginning of record) to source impact. This delay corresponds to the duration of acceleration of the solenoid before impact.

As with the P-wave records, the recorded digital waveforms were analyzed to locate clear  $S_H$ -wave pulses, as indicated by the presence of opposite polarity pulses on each pair of horizontal records. Ideally, the  $S_H$ -wave signals from the 'normal' and 'reverse' source pulses are very nearly inverted images of each other. Digital Fast Fourier Transform – Inverse Fast Fourier Transform (FFT – IFFT) lowpass filtering was used to remove the higher frequency P-wave signal from the  $S_H$ -wave signal. Different filter cutoffs were used to separate P- and  $S_H$ -waves at different depths, ranging from 600 Hz in the slowest zones to 4000 Hz in the regions of highest velocity. At each depth, the filter frequency was selected to be at least twice the fundamental frequency of the  $S_H$ -wave signal being filtered.

Generally, the first maxima were picked for the 'normal' signals and the first minima for the 'reverse' signals, although other points on the waveform were used if the first pulse was distorted. The absolute arrival time of the 'normal' and 'reverse' signals may vary by +/- 0.2 milliseconds, due to differences in the actuation time of the solenoid source caused by constant mechanical bias in the source, or by borehole inclination. This variation does not affect the R1-R2 velocity determinations, as the differential time is measured between arrivals of waves created by the same source actuation. The final velocity value is the average of the values obtained from the 'normal' and 'reverse' source actuations.

As with the P-wave data,  $S_H$ -wave velocity calculated from the travel time over the 6.33-foot interval from source to receiver 1 was calculated and plotted for verification of the velocity derived from the travel time between receivers. In this analysis, the depth values were increased by 4.8 feet to correspond to the mid-point of the 6.33-foot S-R1 interval. Travel times were obtained by picking the first break of the  $S_H$ -wave signal at the near receiver and subtracting the calculated and experimentally verified delay, in milliseconds, from the beginning of the record at the source trigger pulse to source impact.

Poisson's Ratio,  $\nu$ , was calculated in the Microsoft Excel<sup>®</sup> template using the following formula:

$$\nu = \frac{\left(\frac{v_s}{v_p}\right)^2 - 0.5}{\left(\frac{v_s}{v_p}\right)^2 - 1.0}$$

Figure 2 shows an example of R1 - R2 measurements on a sample filtered suspension record. In Figure 2, the time difference over the 3.3 foot interval of 1.88 milliseconds for the horizontal signals is equivalent to an  $S_H$ -wave velocity of 1745 feet/second. Whenever possible, time

differences were determined from several phase points on the  $S_H$ -waveform records to verify the data obtained from the first arrival of the  $S_H$ -wave pulse. Figure 3 displays the same record before filtering of the  $S_H$ -waveform record with a 1400 Hz FFT - IFFT digital lowpass filter, illustrating the presence of higher frequency P-wave energy at the beginning of the record, and distortion of the lower frequency  $S_H$ -wave by residual P-wave signal.

Data and analyses were reviewed by a **GEOVision** Professional Geophysicist or Engineer as a component of the in-house data validation program.

### **Induction / Natural Gamma Analysis**

No analysis is required with the induction and natural gamma data; however, depths to identifiable boring log features, such as distinct natural gamma transitions, were compared to verify consistent depth readings on all logs. Using WellCAD™ software version 5.1, these data were combined with the Elog and caliper logs, and converted to LAS 2.0 and PDF formats for transmittal to the client. In many of the boreholes at this site, multiple data sets were collected over several different depth intervals, and each separate log is presented.

## RESULTS

### Suspension Velocity Results

Suspension R1-R2 P- and  $S_H$ -wave velocities for borehole B-FMG are presented in Figure 4 and data compiled in Table 3. Nearby boreholes HOR-1328 and Conway Offset were combined for data analysis. Combined velocities for boreholes HOR-1328 and Conway Offset are plotted in Figure 6 and data compiled in Table 4. The associated Microsoft Excel<sup>®</sup> analysis files are included in the data deliverable included with this report. Included in the Microsoft Excel<sup>®</sup> analysis files are Poisson's Ratio calculations, tabulated data and plots.

P- and  $S_H$ -wave velocity data from R1-R2 analysis and quality assurance analysis of S-R1 data are plotted together in Figures A-1 and A-2 in Appendix A to aid in visual comparison. Note that R1-R2 data are an average velocity over a 3.3-foot segment of the soil column; S-R1 data are an average over 6.3 feet, creating a significant smoothing relative to the R1-R2 plots. The S-R1 velocity data displayed in these figures are also compiled in Tables A-1 and A-2.

### Induction / Natural Gamma Results

Induction and natural gamma data for boreholes B-FMG, and HOR-1328 combined with Conway Offset are presented in single page log plots in Figures 5 and 7, respectively, as well as in scaled (1in:20ft) multi-page log plots in Appendix B. Depths on all figures and tables are referenced to ground surface. LAS 2.0 data and Acrobat files of the plots for each boring are included in the data deliverable included with this report.

## SUMMARY

### Discussion of Suspension Velocity Results

Suspension PS velocity data are ideally collected in uncased, fluid filled boreholes drilled with rotary wash methods, as was the case for B-FMG in Andrews, and HDR-1328. The Conway OFFSET hole was cased with 4 inch PVC to 310 feet.

Overall, Suspension PS velocity data quality is judged on 5 criteria, as summarized below.

	Criteria	HDR-1328 + OFFSET	B-FMG
1	Consistent data between receiver to receiver (R1 – R2) and source to receiver (S – R1) data.	Yes	Yes
2	Consistency between data from adjacent depth intervals.	Yes	Yes
3	Consistent relationship between P-wave and S <sub>H</sub> -wave (excluding transition to saturated soils)	Yes. Saturation occurs at 9 ft depth	Yes. Saturation occurs at about 15 ft depth
4	Clarity of P-wave and S <sub>H</sub> -wave onset, as well as damping of later oscillations.	Good	Good
5	Consistency of profile between adjacent borings, if available.	Not applicable.	Not applicable.

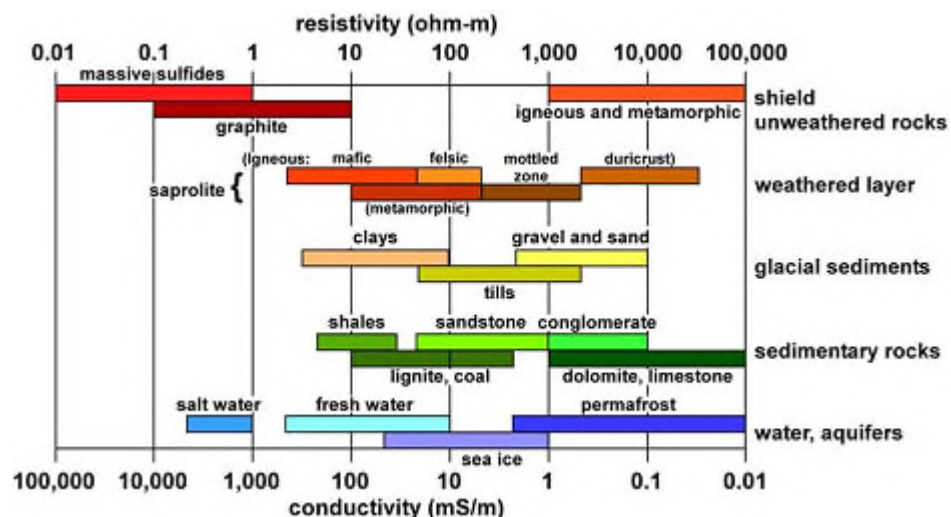
These data indicate good consistency between R1-R2 and S-R1 velocities, and good consistency between adjacent depths in the intervals tested.

## Discussion of Induction / Natural Gamma Results

Both gamma and conductivity are relative logs, not absolute; meaning relative changes in amplitude are more informative than the absolute values. With that in mind, we can provide general guidelines.

Conductivity: generally, conductivity is higher in materials in which electric and electromagnetic fields flow preferentially. For earth materials, typically hard rock, limestone, dry sands and similar exhibit relatively low conductivity (higher resistivity); whereas metallic ores and clays, and silts exhibit relatively high conductivity (low resistivity). For near surface materials, unconsolidated sediment is typically more conductive than consolidated sediment. Water content and salinity also contribute to increased conductivity, e.g., wet soil and sand is more conductive than dry. Here below is a jpg with general ranges, note there is overlap (from <http://emgeo.sdsu.edu/emrockprop.html> Palacky, G. J., 1988, Resistivity characteristics of geologic targets, in Investigations in Geophysics vol. 3: Electromagnetic methods in applied geophysics-theory, vol. 1, edited by M. N. Nabighian, Soc. Expl. Geophys., 53–129.)

Typical near surface soils and hard rock exhibits low conductivity, usually near the low, or left, axis close to (or less than) zero mS/m. In contrast, fat clays could be in the hundreds to low thousands ms/m.



Natural Gamma (NG): Higher in materials that contain uranium, thorium, or potassium (or similar) bearing minerals, or soils / rocks in which these minerals are concentrated. For example, in near surface measurements NG is higher in clays or shales and lower in sandstones and coals. Typical sands or near surface unconsolidated materials are relatively low. Clay seams may spike very high, the higher the value the more concentrated radioactive minerals.

Typical near surface soil often hovers around 100CPS or less, but this can vary by location. Fat clays can cause deflections to the right to several hundred CPS.

Typically, there is an expected correlation between conductivity and natural gamma. For example, a clay seam would be expected to exhibit a NG high and a corresponding conductivity high. A sand would be expected to have a relatively flat NG response and a corresponding low conductivity. However, relative, abrupt changes in amplitude are more indicative of formational or lithologic changes, which may assist with observations in the borehole geologic logs.

The upper and lower sections of the Conway boring overlapped perfectly. However, the OFFSET hole exhibits strong conductivity response from the metallic centralizers installed at 15, 45, 105, 155, 205, and 255 feet below ground surface.

## **Quality Assurance**

These borehole geophysical measurements were performed using industry-standard or better methods for measurements and analysis. All work was performed under **GEOVision** quality assurance procedures, which include:

- Use of NIST-traceable calibrations, where applicable, for field and laboratory instrumentation
- Use of standard field data logs
- Use of independent verification of velocity data by comparison of receiver-to-receiver and source-to-receiver velocities
- Independent review of calculations and results by a registered professional engineer, geologist, or geophysicist.

## **Suspension Velocity Data Reliability**

P- and S<sub>H</sub>-wave velocity measurement using the Suspension Method gives average velocities over a 3.3-foot interval of depth. This high resolution results in the scatter of values shown in the graphs. Individual measurements are very reliable with estimated precision of +/- 5%. Depth indications are very reliable with estimated precision of +/- 0.2 feet. Standardized field procedures and quality assurance checks contribute to the reliability of these data.

## CERTIFICATION

All geophysical data, analysis, interpretations, conclusions, and recommendations in this document have been prepared under the supervision of and reviewed by a **GEOVision** California Professional Geophysicist or Engineer.

Prepared by



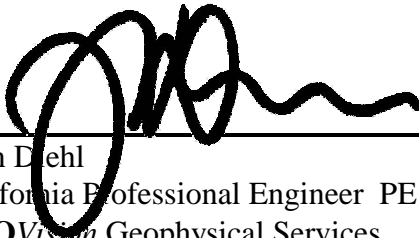
---

Emily Feldman  
Senior Staff Geophysicist  
**GEOVision** Geophysical Services

4/10/2017

Date

Reviewed and approved by



---

John Diehl  
California Professional Engineer PE 30362  
**GEOVision** Geophysical Services



4/10/2017

Date

- \* This geophysical investigation was conducted under the supervision of a California Professional Geophysicist or Engineer using industry standard methods and equipment. A high degree of professionalism was maintained during all aspects of the project from the field investigation and data acquisition, through data processing, interpretation and reporting. All original field data files, field notes and observations, and other pertinent information are maintained in the project files and are available for the client to review for a period of at least one year.

A professional geophysicist's certification of interpreted geophysical conditions comprises a declaration of his/her professional judgment. It does not constitute a warranty or guarantee, expressed or implied, nor does it relieve any other party of its responsibility to abide by contract documents, applicable codes, standards, regulations or ordinances.

Table 1. Borehole locations and logging dates

BOREHOLE DESIGNATION	DATES LOGGED	COORDINATES (US SURVEY FEET) <sup>(1)</sup>		ELEVATION (TOP OF WELL CASING) <sup>(1)</sup> (FEET)
		NORTHING	EASTING	
HOR-1328	1/28/2017			
B-FMG	2/26/2017			
Conway Offset	2/27/2017			

<sup>(1)</sup> Survey data not available

Table 2. Logging dates and depth ranges

BOREHOLE NUMBER	TOOL AND RUN NUMBER	DEPTH RANGE (FEET)	OPEN HOLE (FEET)	SAMPLE INTERVAL (FEET)	DATE LOGGED
HOR-1328	SUSPENSION DOWN01	301.84- 469.16	505	1.6	1/28/2017
HOR-1328	INDUCTION UP01	490 – 289	505	0.05	1/28/2017
B-FMG	SUSPENSION DOWN01	13.12 – 597.11	610	1.6	2/26/2017
B-FMG	INDUCTION UP01	609.75 – 4.55	640	0.05	2/26/2017
Conway Offset	SUSPENSION DOWN01	6.56 – 293.64	310	1.6	2/27/2017
Conway Offset	INDUCTION UP01-02	309.90 – 4.75	310	0.05	2/27/2017

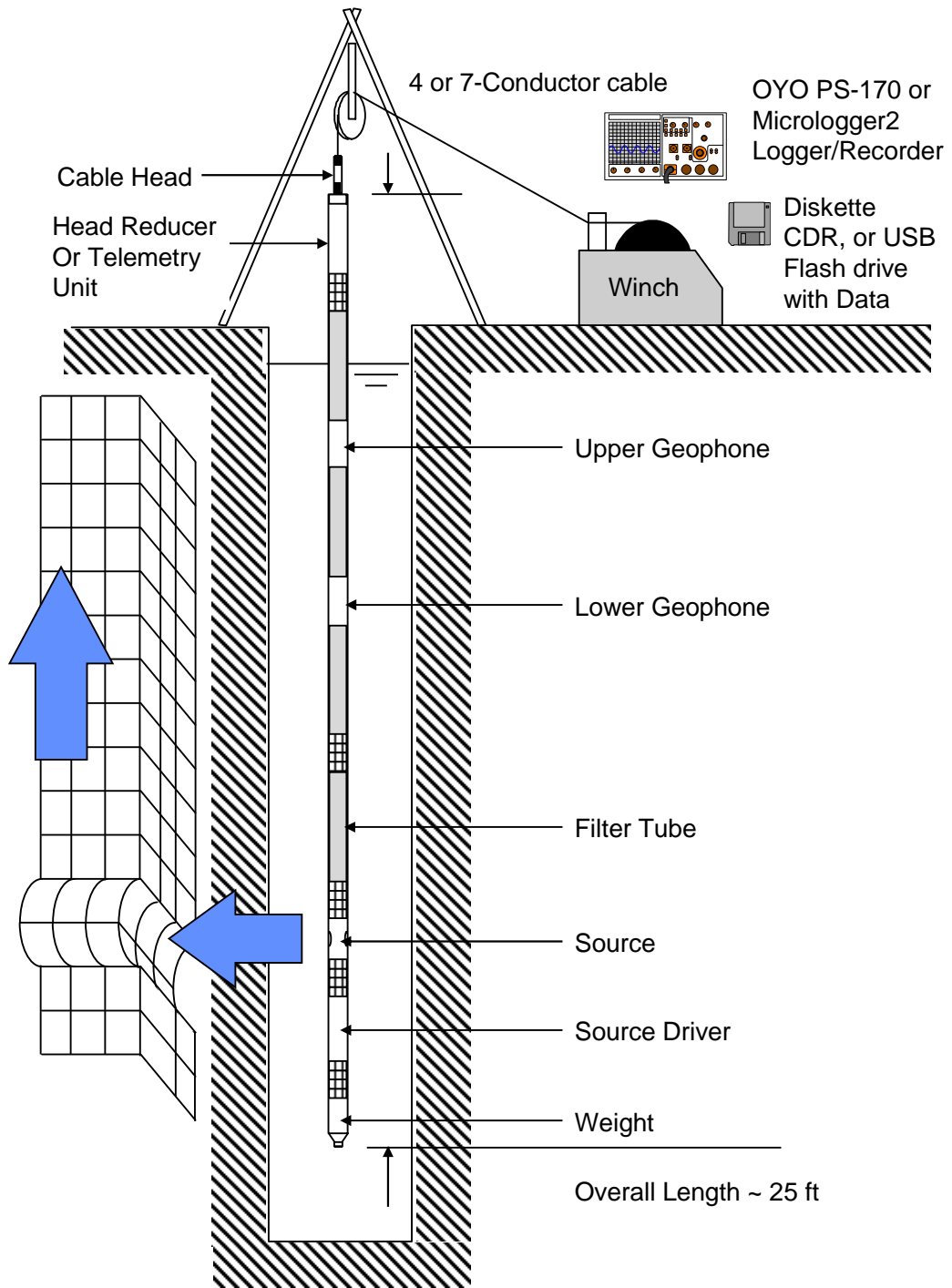


Figure 1: Concept illustration of P-S logging system

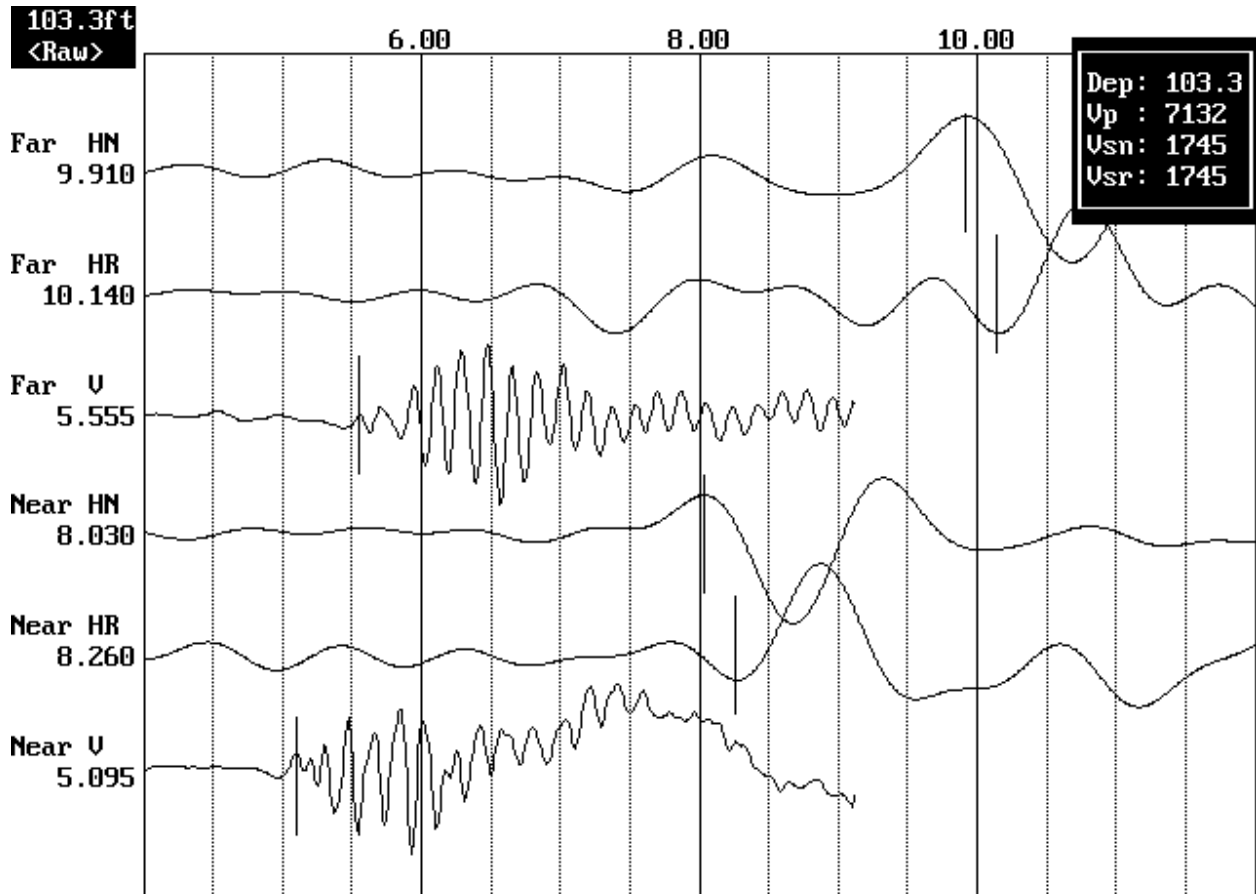


Figure 2: Example of filtered (1400 Hz lowpass) suspension record

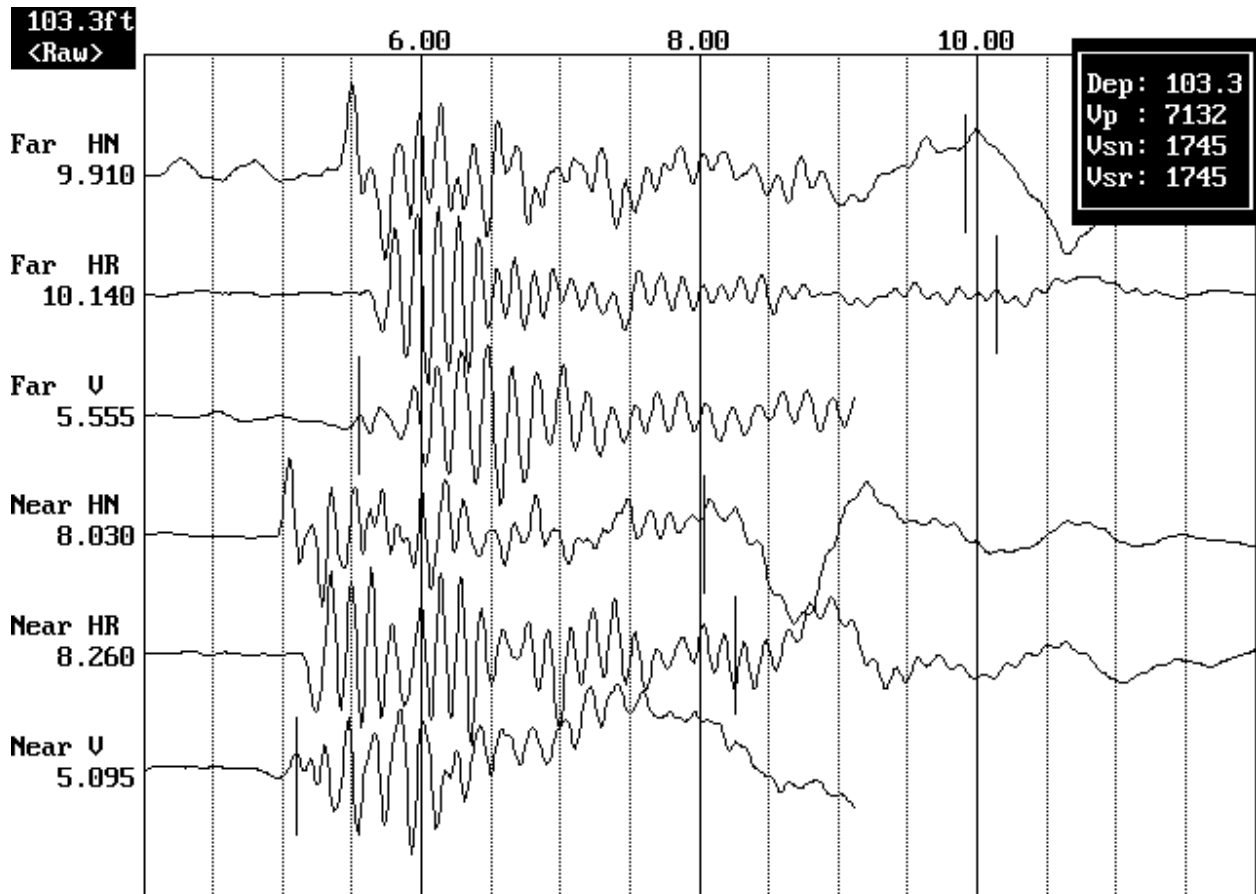


Figure 3. Example of unfiltered suspension record

### SCDOT ANDREWS BORING B-FMG Receiver to Receiver $V_s$ and $V_p$ Analysis

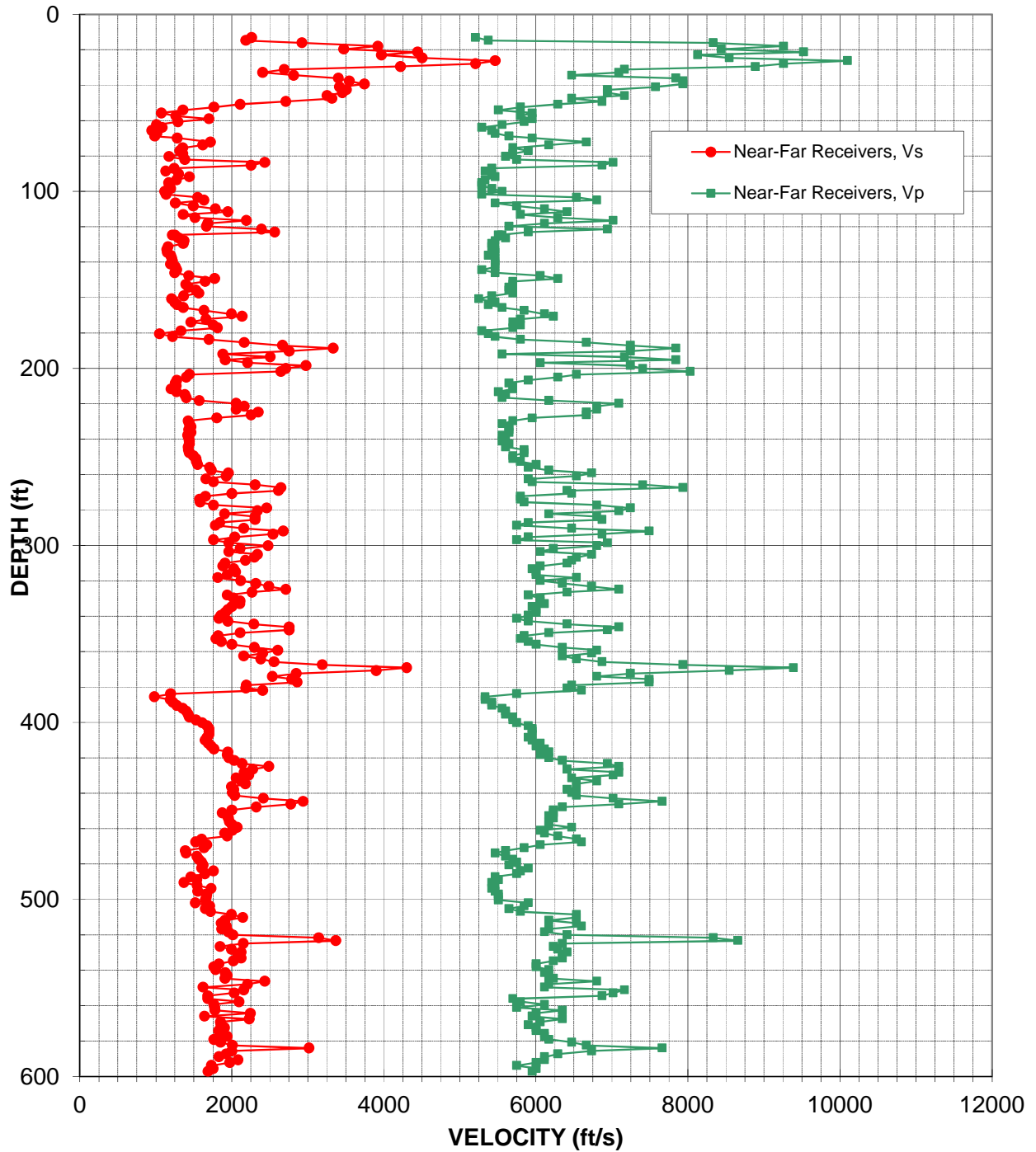


Figure 4: Borehole B-FMG, Suspension R1-R2 P- and  $S_H$ -wave velocities

Table 3. Borehole B-FMG, Suspension R1-R2 depths and P- and S<sub>H</sub>-wave velocities

**Summary of Compressional Wave Velocity, Shear Wave Velocity, and Poisson's Ratio  
Based on Receiver-to-Receiver Travel Time Data - Borehole B-FMG**

American Units				Metric Units			
Depth at Midpoint Between Receivers	Velocity		Poisson's Ratio	Depth at Midpoint Between Receivers	Velocity		Poisson's Ratio
	V <sub>s</sub>	V <sub>p</sub>			V <sub>s</sub>	V <sub>p</sub>	
(ft)	(ft/s)	(ft/s)		(m)	(m/s)	(m/s)	
13.1	2260	5210	0.38	4.0	690	1590	0.38
14.8	2190	5380	0.40	4.5	670	1640	0.40
16.1	2920	8330	0.43	4.9	890	2540	0.43
18.0	3920	9260	0.39	5.5	1200	2820	0.39
19.7	3470	8440	0.40	6.0	1060	2570	0.40
21.3	4440	9520	0.36	6.5	1350	2900	0.36
23.0	3970	8130	0.34	7.0	1210	2480	0.34
24.6	4500	8550	0.31	7.5	1370	2610	0.31
26.3	5460	10100	0.29	8.0	1670	3080	0.29
27.9	5210	9260	0.27	8.5	1590	2820	0.27
29.5	4220	8890	0.35	9.0	1290	2710	0.35
31.2	2690	7170	0.42	9.5	820	2180	0.42
32.8	2410	7090	0.43	10.0	730	2160	0.43
34.5	2810	6470	0.38	10.5	860	1970	0.38
36.1	3400	7840	0.38	11.0	1040	2390	0.38
37.7	3550	7940	0.38	11.5	1080	2420	0.38
39.4	3750	7940	0.36	12.0	1140	2420	0.36
41.0	3420	7580	0.37	12.5	1040	2310	0.37
42.7	3510	6940	0.33	13.0	1070	2120	0.33
44.3	3450	6940	0.34	13.5	1050	2120	0.34
45.9	3250	7170	0.37	14.0	990	2180	0.37
47.6	3320	6470	0.32	14.5	1010	1970	0.32
49.2	2710	6870	0.41	15.0	830	2090	0.41
50.9	2110	6290	0.44	15.5	640	1920	0.44
52.5	1760	5800	0.45	16.0	540	1770	0.45
54.1	1360	5510	0.47	16.5	410	1680	0.47
55.8	1080	5950	0.48	17.0	330	1810	0.48
57.4	1260	5800	0.48	17.5	380	1770	0.48
59.1	1700	5950	0.46	18.0	520	1810	0.46
60.7	1290	5850	0.47	18.5	390	1780	0.47
62.3	1010	5560	0.48	19.0	310	1690	0.48
64.0	1080	5290	0.48	19.5	330	1610	0.48
65.6	950	5420	0.48	20.0	290	1650	0.48
67.3	1020	5460	0.48	20.5	310	1670	0.48
68.9	990	5650	0.48	21.0	300	1720	0.48
69.9	1280	5950	0.48	21.3	390	1810	0.48

**Summary of Compressional Wave Velocity, Shear Wave Velocity, and Poisson's Ratio  
Based on Receiver-to-Receiver Travel Time Data - Borehole B-FMG**

American Units			
Depth at Midpoint Between Receivers	Velocity		Poisson's Ratio
	V <sub>s</sub>	V <sub>p</sub>	
(ft)	(ft/s)	(ft/s)	
72.2	1720	6670	0.46
73.8	1620	6170	0.46
75.5	1360	5700	0.47
77.1	1320	5900	0.47
78.7	1360	5700	0.47
80.4	1170	5600	0.48
82.0	1380	5750	0.47
83.7	2430	7020	0.43
85.3	2250	6870	0.44
86.9	1240	5420	0.47
88.6	1130	5330	0.48
90.2	1300	5420	0.47
91.9	1440	5460	0.46
93.5	1270	5330	0.47
95.1	1170	5290	0.47
96.8	1180	5290	0.47
98.4	1190	5420	0.47
100.1	1120	5560	0.48
101.7	1140	5290	0.48
103.4	1550	6540	0.47
105.0	1630	6800	0.47
106.6	1260	5460	0.47
108.3	1490	5750	0.46
109.9	1780	6120	0.45
111.6	1950	6410	0.45
113.2	1360	5800	0.47
114.8	1520	6290	0.47
116.5	2190	7020	0.45
118.1	1680	6120	0.46
119.8	1670	5650	0.45
121.4	2390	6940	0.43
123.0	2560	5900	0.38
124.7	1220	5510	0.47
124.7	1250	5560	0.47
126.3	1300	5600	0.47
128.0	1370	5460	0.47
129.6	1360	5420	0.47
131.2	1160	5420	0.48
132.9	1150	5460	0.48
134.5	1150	5460	0.48

Metric Units			
Depth at Midpoint Between Receivers	Velocity		Poisson's Ratio
	V <sub>s</sub>	V <sub>p</sub>	
(m)	(m/s)	(m/s)	
22.0	520	2030	0.46
22.5	490	1880	0.46
23.0	410	1740	0.47
23.5	400	1800	0.47
24.0	410	1740	0.47
24.5	360	1710	0.48
25.0	420	1750	0.47
25.5	740	2140	0.43
26.0	690	2090	0.44
26.5	380	1650	0.47
27.0	340	1630	0.48
27.5	400	1650	0.47
28.0	440	1670	0.46
28.5	390	1630	0.47
29.0	360	1610	0.47
29.5	360	1610	0.47
30.0	360	1650	0.47
30.5	340	1690	0.48
31.0	350	1610	0.48
31.5	470	1990	0.47
32.0	500	2070	0.47
32.5	380	1670	0.47
33.0	460	1750	0.46
33.5	540	1860	0.45
34.0	590	1950	0.45
34.5	410	1770	0.47
35.0	460	1920	0.47
35.5	670	2140	0.45
36.0	510	1860	0.46
36.5	510	1720	0.45
37.0	730	2120	0.43
37.5	780	1800	0.38
38.0	370	1680	0.47
38.0	380	1690	0.47
38.5	400	1710	0.47
39.0	420	1670	0.47
39.5	410	1650	0.47
40.0	350	1650	0.48
40.5	350	1670	0.48
41.0	350	1670	0.48

**Summary of Compressional Wave Velocity, Shear Wave Velocity, and Poisson's Ratio  
Based on Receiver-to-Receiver Travel Time Data - Borehole B-FMG**

American Units			
Depth at Midpoint Between Receivers	Velocity		Poisson's Ratio
	V <sub>s</sub>	V <sub>p</sub>	
(ft)	(ft/s)	(ft/s)	
136.2	1190	5380	0.47
137.8	1210	5460	0.47
139.4	1220	5460	0.47
141.1	1190	5460	0.47
142.7	1260	5460	0.47
144.4	1280	5290	0.47
146.0	1250	5460	0.47
147.6	1440	6060	0.47
149.3	1770	6290	0.46
150.9	1650	5700	0.45
152.6	1390	5700	0.47
154.2	1430	5650	0.47
155.8	1530	5650	0.46
157.5	1560	5700	0.46
159.1	1370	5420	0.47
160.8	1210	5250	0.47
162.7	1250	5460	0.47
164.0	1280	5380	0.47
165.7	1360	5560	0.47
167.3	1630	5850	0.46
169.3	2000	6120	0.44
170.6	2140	6230	0.43
172.2	1660	5800	0.46
173.9	1460	5700	0.46
175.5	1750	5800	0.45
177.2	1810	5700	0.44
178.8	1330	5290	0.47
180.5	1050	5380	0.48
182.1	1220	5460	0.47
183.7	1700	5800	0.45
185.4	2160	6670	0.44
187.0	2670	7250	0.42
188.7	3330	7840	0.39
190.3	2750	7250	0.42
191.9	1880	5560	0.44
193.6	2510	7170	0.43
195.2	1920	7840	0.47
196.9	2210	6060	0.42
198.5	2980	7250	0.40
200.1	2710	7410	0.42

Metric Units			
Depth at Midpoint Between Receivers	Velocity		Poisson's Ratio
	V <sub>s</sub>	V <sub>p</sub>	
(m)	(m/s)	(m/s)	
41.5	360	1640	0.47
42.0	370	1670	0.47
42.5	370	1670	0.47
43.0	360	1670	0.47
43.5	380	1670	0.47
44.0	390	1610	0.47
44.5	380	1670	0.47
45.0	440	1850	0.47
45.5	540	1920	0.46
46.0	500	1740	0.45
46.5	430	1740	0.47
47.0	440	1720	0.47
47.5	470	1720	0.46
48.0	480	1740	0.46
48.5	420	1650	0.47
49.0	370	1600	0.47
49.6	380	1670	0.47
50.0	390	1640	0.47
50.5	410	1690	0.47
51.0	500	1780	0.46
51.6	610	1860	0.44
52.0	650	1900	0.43
52.5	510	1770	0.46
53.0	450	1740	0.46
53.5	530	1770	0.45
54.0	550	1740	0.44
54.5	400	1610	0.47
55.0	320	1640	0.48
55.5	370	1670	0.47
56.0	520	1770	0.45
56.5	660	2030	0.44
57.0	810	2210	0.42
57.5	1020	2390	0.39
58.0	840	2210	0.42
58.5	570	1690	0.44
59.0	760	2180	0.43
59.5	580	2390	0.47
60.0	670	1850	0.42
60.5	910	2210	0.40
61.0	830	2260	0.42

**Summary of Compressional Wave Velocity, Shear Wave Velocity, and Poisson's Ratio  
Based on Receiver-to-Receiver Travel Time Data - Borehole B-FMG**

American Units			
Depth at Midpoint Between Receivers	Velocity		Poisson's Ratio
	V <sub>s</sub>	V <sub>p</sub>	
(ft)	(ft/s)	(ft/s)	
201.8	2650	8030	0.44
203.4	1440	6540	0.47
205.1	1400	6290	0.47
206.7	1280	5900	0.48
208.3	1260	5650	0.47
210.0	1270	5700	0.47
211.6	1200	5700	0.48
213.3	1270	5510	0.47
214.9	1380	5600	0.47
216.5	1400	5560	0.47
218.2	1570	6170	0.47
219.8	2060	7090	0.45
221.5	2160	6800	0.44
223.1	2060	6800	0.45
224.7	2350	6670	0.43
226.4	2250	6670	0.44
228.0	1800	5950	0.45
229.7	1420	5700	0.47
231.3	1440	5560	0.46
232.9	1460	5650	0.46
234.6	1440	5650	0.47
236.2	1460	5650	0.46
237.9	1420	5560	0.47
239.5	1440	5600	0.46
241.1	1440	5560	0.46
242.8	1440	5650	0.47
244.4	1420	5600	0.47
246.1	1430	5850	0.47
247.7	1440	5850	0.47
249.3	1490	5700	0.46
251.0	1530	5700	0.46
252.6	1540	5800	0.46
254.3	1550	6010	0.46
255.9	1710	5900	0.45
257.6	1730	6170	0.46
259.2	1960	6730	0.45
260.8	1930	6540	0.45
262.5	1660	5900	0.46
264.1	1760	5950	0.45
265.8	2310	7410	0.45

Metric Units			
Depth at Midpoint Between Receivers	Velocity		Poisson's Ratio
	V <sub>s</sub>	V <sub>p</sub>	
(m)	(m/s)	(m/s)	
61.5	810	2450	0.44
62.0	440	1990	0.47
62.5	430	1920	0.47
63.0	390	1800	0.48
63.5	380	1720	0.47
64.0	390	1740	0.47
64.5	370	1740	0.48
65.0	390	1680	0.47
65.5	420	1710	0.47
66.0	430	1690	0.47
66.5	480	1880	0.47
67.0	630	2160	0.45
67.5	660	2070	0.44
68.0	630	2070	0.45
68.5	720	2030	0.43
69.0	690	2030	0.44
69.5	550	1810	0.45
70.0	430	1740	0.47
70.5	440	1690	0.46
71.0	450	1720	0.46
71.5	440	1720	0.47
72.0	450	1720	0.46
72.5	430	1690	0.47
73.0	440	1710	0.46
73.5	440	1690	0.46
74.0	440	1720	0.47
74.5	430	1710	0.47
75.0	440	1780	0.47
75.5	440	1780	0.47
76.0	460	1740	0.46
76.5	470	1740	0.46
77.0	470	1770	0.46
77.5	470	1830	0.46
78.0	520	1800	0.45
78.5	530	1880	0.46
79.0	600	2050	0.45
79.5	590	1990	0.45
80.0	510	1800	0.46
80.5	540	1810	0.45
81.0	700	2260	0.45

**Summary of Compressional Wave Velocity, Shear Wave Velocity, and Poisson's Ratio  
Based on Receiver-to-Receiver Travel Time Data - Borehole B-FMG**

American Units			
Depth at Midpoint Between Receivers	Velocity		Poisson's Ratio
	V <sub>s</sub>	V <sub>p</sub>	
(ft)	(ft/s)	(ft/s)	
267.4	2650	7940	0.44
269.0	2610	6410	0.40
270.7	2000	6470	0.45
272.3	1650	5800	0.46
274.0	1580	5800	0.46
275.6	1580	5850	0.46
277.2	1760	6800	0.46
278.9	2460	7250	0.43
280.5	2340	7090	0.44
282.2	1900	6170	0.45
283.8	2310	6800	0.44
285.4	2310	6870	0.44
287.1	1840	5900	0.45
288.7	1780	5750	0.45
290.4	2160	6470	0.44
292.0	2680	7490	0.43
293.6	2540	6870	0.42
295.3	2040	5900	0.43
296.9	1760	5750	0.45
298.6	1960	6940	0.46
300.2	2480	6800	0.42
301.8	2110	6230	0.44
303.5	1960	6060	0.44
305.1	2340	6730	0.43
306.8	2300	6540	0.43
308.4	2180	6470	0.44
310.0	1910	6410	0.45
311.7	1880	6060	0.45
313.3	2030	5950	0.43
315.0	2050	6010	0.43
316.6	1940	6010	0.44
318.2	1820	6540	0.46
319.9	2120	6060	0.43
321.5	2310	6350	0.42
323.2	2490	6730	0.42
324.8	2710	7090	0.41
326.4	2270	6410	0.43
328.1	1940	5900	0.44
329.7	2020	6060	0.44
331.4	2110	6060	0.43

Metric Units			
Depth at Midpoint Between Receivers	Velocity		Poisson's Ratio
	V <sub>s</sub>	V <sub>p</sub>	
(m)	(m/s)	(m/s)	
81.5	810	2420	0.44
82.0	800	1950	0.40
82.5	610	1970	0.45
83.0	500	1770	0.46
83.5	480	1770	0.46
84.0	480	1780	0.46
84.5	540	2070	0.46
85.0	750	2210	0.43
85.5	710	2160	0.44
86.0	580	1880	0.45
86.5	700	2070	0.44
87.0	700	2090	0.44
87.5	560	1800	0.45
88.0	540	1750	0.45
88.5	660	1970	0.44
89.0	820	2280	0.43
89.5	780	2090	0.42
90.0	620	1800	0.43
90.5	540	1750	0.45
91.0	600	2120	0.46
91.5	760	2070	0.42
92.0	640	1900	0.44
92.5	600	1850	0.44
93.0	710	2050	0.43
93.5	700	1990	0.43
94.0	660	1970	0.44
94.5	580	1950	0.45
95.0	570	1850	0.45
95.5	620	1810	0.43
96.0	630	1830	0.43
96.5	590	1830	0.44
97.0	550	1990	0.46
97.5	650	1850	0.43
98.0	710	1940	0.42
98.5	760	2050	0.42
99.0	830	2160	0.41
99.5	690	1950	0.43
100.0	590	1800	0.44
100.5	620	1850	0.44
101.0	640	1850	0.43

**Summary of Compressional Wave Velocity, Shear Wave Velocity, and Poisson's Ratio  
Based on Receiver-to-Receiver Travel Time Data - Borehole B-FMG**

American Units			
Depth at Midpoint Between Receivers	Velocity		Poisson's Ratio
	V <sub>s</sub>	V <sub>p</sub>	
(ft)	(ft/s)	(ft/s)	
333.0	2100	6120	0.43
334.7	2000	5950	0.44
336.3	1950	6010	0.44
337.9	1920	6010	0.44
339.6	1860	5900	0.45
341.2	1830	5750	0.44
342.9	1950	5900	0.44
344.5	2290	6410	0.43
346.1	2750	7090	0.41
347.8	2750	6940	0.41
349.4	2110	6170	0.43
351.1	1820	5850	0.45
352.7	1790	5800	0.45
354.3	1860	5900	0.44
356.0	2000	6010	0.44
357.6	2300	6350	0.42
359.3	2600	6800	0.41
360.9	2410	6730	0.43
362.5	2160	6350	0.43
364.2	2380	6540	0.42
365.8	2550	6870	0.42
367.5	3190	7940	0.40
369.1	4300	9390	0.37
370.7	3900	8550	0.37
372.4	2850	7250	0.41
374.0	2530	6800	0.42
375.7	2790	7490	0.42
377.3	2860	7490	0.41
378.9	2190	6470	0.44
380.6	2190	6410	0.43
381.9	2410	6600	0.42
383.9	1200	5750	0.48
385.5	980	5330	0.48
387.1	1190	5330	0.47
388.8	1230	5420	0.47
390.4	1280	5420	0.47
392.1	1360	5560	0.47
393.7	1400	5600	0.47
395.3	1420	5600	0.47
397.0	1440	5700	0.47

Metric Units			
Depth at Midpoint Between Receivers	Velocity		Poisson's Ratio
	V <sub>s</sub>	V <sub>p</sub>	
(m)	(m/s)	(m/s)	
101.5	640	1860	0.43
102.0	610	1810	0.44
102.5	590	1830	0.44
103.0	580	1830	0.44
103.5	570	1800	0.45
104.0	560	1750	0.44
104.5	590	1800	0.44
105.0	700	1950	0.43
105.5	840	2160	0.41
106.0	840	2120	0.41
106.5	640	1880	0.43
107.0	560	1780	0.45
107.5	550	1770	0.45
108.0	570	1800	0.44
108.5	610	1830	0.44
109.0	700	1940	0.42
109.5	790	2070	0.41
110.0	730	2050	0.43
110.5	660	1940	0.43
111.0	730	1990	0.42
111.5	780	2090	0.42
112.0	970	2420	0.40
112.5	1310	2860	0.37
113.0	1190	2610	0.37
113.5	870	2210	0.41
114.0	770	2070	0.42
114.5	850	2280	0.42
115.0	870	2280	0.41
115.5	670	1970	0.44
116.0	670	1950	0.43
116.4	730	2010	0.42
117.0	360	1750	0.48
117.5	300	1630	0.48
118.0	360	1630	0.47
118.5	370	1650	0.47
119.0	390	1650	0.47
119.5	410	1690	0.47
120.0	430	1710	0.47
120.5	430	1710	0.47
121.0	440	1740	0.47

**Summary of Compressional Wave Velocity, Shear Wave Velocity, and Poisson's Ratio  
Based on Receiver-to-Receiver Travel Time Data - Borehole B-FMG**

American Units			
Depth at Midpoint Between Receivers	Velocity		Poisson's Ratio
	V <sub>s</sub>	V <sub>p</sub>	
(ft)	(ft/s)	(ft/s)	
398.6	1530	5700	0.46
400.3	1610	5750	0.46
401.9	1680	5900	0.46
403.5	1700	5950	0.46
405.2	1700	5950	0.46
406.8	1700	5950	0.46
408.5	1680	5900	0.46
410.1	1650	5950	0.46
411.8	1690	6060	0.46
413.4	1730	6010	0.45
415.0	1760	6120	0.45
416.7	1950	6170	0.44
418.3	1940	6060	0.44
420.0	1960	6170	0.44
421.6	2030	6350	0.44
423.2	2140	6940	0.45
424.9	2490	7090	0.43
426.5	2280	6410	0.43
428.2	2160	7090	0.45
429.8	2220	7020	0.44
431.4	2060	6470	0.44
433.1	2120	6800	0.45
434.7	2180	6540	0.44
436.4	2000	6540	0.45
438.0	2030	6410	0.44
439.6	2010	6470	0.45
441.3	2040	6540	0.45
442.9	2420	7020	0.43
444.6	2940	7660	0.41
446.2	2780	7090	0.41
447.8	2320	6350	0.42
449.5	2000	6230	0.44
451.1	1870	6230	0.45
452.8	1940	6170	0.44
454.1	1960	6230	0.45
456.0	1970	6170	0.44
457.7	2000	6170	0.44
459.3	2070	6470	0.44
461.0	2010	6060	0.44
462.6	1900	6120	0.45

Metric Units			
Depth at Midpoint Between Receivers	Velocity		Poisson's Ratio
	V <sub>s</sub>	V <sub>p</sub>	
(m)	(m/s)	(m/s)	
121.5	470	1740	0.46
122.0	490	1750	0.46
122.5	510	1800	0.46
123.0	520	1810	0.46
123.5	520	1810	0.46
124.0	520	1810	0.46
124.5	510	1800	0.46
125.0	500	1810	0.46
125.5	520	1850	0.46
126.0	530	1830	0.45
126.5	540	1860	0.45
127.0	590	1880	0.44
127.5	590	1850	0.44
128.0	600	1880	0.44
128.5	620	1940	0.44
129.0	650	2120	0.45
129.5	760	2160	0.43
130.0	690	1950	0.43
130.5	660	2160	0.45
131.0	680	2140	0.44
131.5	630	1970	0.44
132.0	650	2070	0.45
132.5	660	1990	0.44
133.0	610	1990	0.45
133.5	620	1950	0.44
134.0	610	1970	0.45
134.5	620	1990	0.45
135.0	740	2140	0.43
135.5	900	2340	0.41
136.0	850	2160	0.41
136.5	710	1940	0.42
137.0	610	1900	0.44
137.5	570	1900	0.45
138.0	590	1880	0.44
138.4	600	1900	0.45
139.0	600	1880	0.44
139.5	610	1880	0.44
140.0	630	1970	0.44
140.5	610	1850	0.44
141.0	580	1860	0.45

**Summary of Compressional Wave Velocity, Shear Wave Velocity, and Poisson's Ratio  
Based on Receiver-to-Receiver Travel Time Data - Borehole B-FMG**

American Units			
Depth at Midpoint Between Receivers	Velocity		Poisson's Ratio
	V <sub>s</sub>	V <sub>p</sub>	
(ft)	(ft/s)	(ft/s)	
464.2	1940	6290	0.45
465.9	1600	6540	0.47
467.5	1530	6600	0.47
469.2	1670	6060	0.46
470.8	1630	5850	0.46
472.4	1390	5600	0.47
473.8	1400	5460	0.47
475.7	1540	5600	0.46
477.4	1560	5700	0.46
479.0	1600	5750	0.46
480.6	1620	5650	0.46
482.3	1600	5900	0.46
483.9	1760	5800	0.45
485.6	1650	5750	0.46
487.2	1460	5460	0.46
488.9	1540	5510	0.46
490.5	1370	5420	0.47
492.1	1540	5460	0.46
493.8	1730	5420	0.44
495.4	1550	5460	0.46
497.1	1670	5510	0.45
498.7	1670	5510	0.45
500.3	1650	5510	0.45
502.0	1520	5900	0.46
503.6	1710	5850	0.45
505.3	1650	5650	0.45
506.9	1720	5800	0.45
508.5	2000	6540	0.45
510.2	2140	6540	0.44
511.8	1910	6170	0.45
513.5	1860	6540	0.46
515.1	1930	6600	0.45
516.7	1870	6170	0.45
518.4	1960	6120	0.44
520.0	2010	6410	0.45
521.7	3140	8330	0.42
523.3	3370	8660	0.41
524.9	2150	6350	0.44
526.6	1850	6230	0.45
528.2	2000	6290	0.44

Metric Units			
Depth at Midpoint Between Receivers	Velocity		Poisson's Ratio
	V <sub>s</sub>	V <sub>p</sub>	
(m)	(m/s)	(m/s)	
141.5	590	1920	0.45
142.0	490	1990	0.47
142.5	460	2010	0.47
143.0	510	1850	0.46
143.5	500	1780	0.46
144.0	420	1710	0.47
144.4	430	1670	0.47
145.0	470	1710	0.46
145.5	480	1740	0.46
146.0	490	1750	0.46
146.5	490	1720	0.46
147.0	490	1800	0.46
147.5	540	1770	0.45
148.0	500	1750	0.46
148.5	450	1670	0.46
149.0	470	1680	0.46
149.5	420	1650	0.47
150.0	470	1670	0.46
150.5	530	1650	0.44
151.0	470	1670	0.46
151.5	510	1680	0.45
152.0	510	1680	0.45
152.5	500	1680	0.45
153.0	460	1800	0.46
153.5	520	1780	0.45
154.0	500	1720	0.45
154.5	530	1770	0.45
155.0	610	1990	0.45
155.5	650	1990	0.44
156.0	580	1880	0.45
156.5	570	1990	0.46
157.0	590	2010	0.45
157.5	570	1880	0.45
158.0	600	1860	0.44
158.5	610	1950	0.45
159.0	960	2540	0.42
159.5	1030	2640	0.41
160.0	660	1940	0.44
160.5	560	1900	0.45
161.0	610	1920	0.44

**Summary of Compressional Wave Velocity, Shear Wave Velocity, and Poisson's Ratio  
Based on Receiver-to-Receiver Travel Time Data - Borehole B-FMG**

American Units			
Depth at Midpoint Between Receivers	Velocity		Poisson's Ratio
	V <sub>s</sub>	V <sub>p</sub>	
(ft)	(ft/s)	(ft/s)	
529.9	2120	6410	0.44
531.5	2080	6350	0.44
533.1	2120	6350	0.44
534.8	2020	6230	0.44
536.4	1830	6010	0.45
538.1	1760	6010	0.45
539.7	1790	6170	0.45
541.3	1920	6120	0.45
543.0	1940	6170	0.45
544.6	1910	6230	0.45
546.3	2430	6800	0.43
547.9	2210	6170	0.43
549.5	1620	6120	0.46
551.2	2160	7170	0.45
552.8	2030	7020	0.45
554.5	1680	6870	0.47
556.1	1680	5700	0.45
557.7	2100	5800	0.42
559.4	1760	6120	0.45
561.0	1770	5750	0.45
562.7	1780	6350	0.46
564.3	2240	6010	0.42
565.9	1640	5950	0.46
567.6	2230	6350	0.43
569.2	1850	6060	0.45
570.9	1860	5900	0.45
572.5	1900	6010	0.44
574.2	1830	6010	0.45
575.8	1870	6120	0.45
577.4	1940	6120	0.44
579.1	1760	6170	0.46
580.7	1850	6470	0.46
582.4	2010	6670	0.45
584.0	3020	7660	0.41
585.6	2000	6730	0.45
587.3	1930	6290	0.45
588.9	1830	6120	0.45
590.6	2080	6120	0.43
592.2	1970	6010	0.44
593.8	1730	5750	0.45

Metric Units			
Depth at Midpoint Between Receivers	Velocity		Poisson's Ratio
	V <sub>s</sub>	V <sub>p</sub>	
(m)	(m/s)	(m/s)	
161.5	650	1950	0.44
162.0	640	1940	0.44
162.5	650	1940	0.44
163.0	620	1900	0.44
163.5	560	1830	0.45
164.0	540	1830	0.45
164.5	540	1880	0.45
165.0	580	1860	0.45
165.5	590	1880	0.45
166.0	580	1900	0.45
166.5	740	2070	0.43
167.0	670	1880	0.43
167.5	490	1860	0.46
168.0	660	2180	0.45
168.5	620	2140	0.45
169.0	510	2090	0.47
169.5	510	1740	0.45
170.0	640	1770	0.42
170.5	540	1860	0.45
171.0	540	1750	0.45
171.5	540	1940	0.46
172.0	680	1830	0.42
172.5	500	1810	0.46
173.0	680	1940	0.43
173.5	560	1850	0.45
174.0	570	1800	0.45
174.5	580	1830	0.44
175.0	560	1830	0.45
175.5	570	1860	0.45
176.0	590	1860	0.44
176.5	540	1880	0.46
177.0	560	1970	0.46
177.5	610	2030	0.45
178.0	920	2340	0.41
178.5	610	2050	0.45
179.0	590	1920	0.45
179.5	560	1860	0.45
180.0	640	1860	0.43
180.5	600	1830	0.44
181.0	530	1750	0.45

**Summary of Compressional Wave Velocity, Shear Wave Velocity, and Poisson's Ratio  
Based on Receiver-to-Receiver Travel Time Data - Borehole B-FMG**

<b>American Units</b>			
<b>Depth at Midpoint Between Receivers</b>	<b>Velocity</b>		<b>Poisson's Ratio</b>
	<b>V<sub>s</sub></b>	<b>V<sub>p</sub></b>	
(ft)	(ft/s)	(ft/s)	
595.5	1750	6010	0.45
597.1	1690	5950	0.46

<b>Metric Units</b>			
<b>Depth at Midpoint Between Receivers</b>	<b>Velocity</b>		<b>Poisson's Ratio</b>
	<b>V<sub>s</sub></b>	<b>V<sub>p</sub></b>	
(m)	(m/s)	(m/s)	
181.5	530	1830	0.45
182.0	510	1810	0.46

	LOG TYPE	PROJECT	Andrews / SCDOT
	Dual Induction	WELL	B-FMG
CLIENT S&ME		LOCATION	Andrews
		LOGGER	J. Jordan
		DATE	Feb. 26, 2017

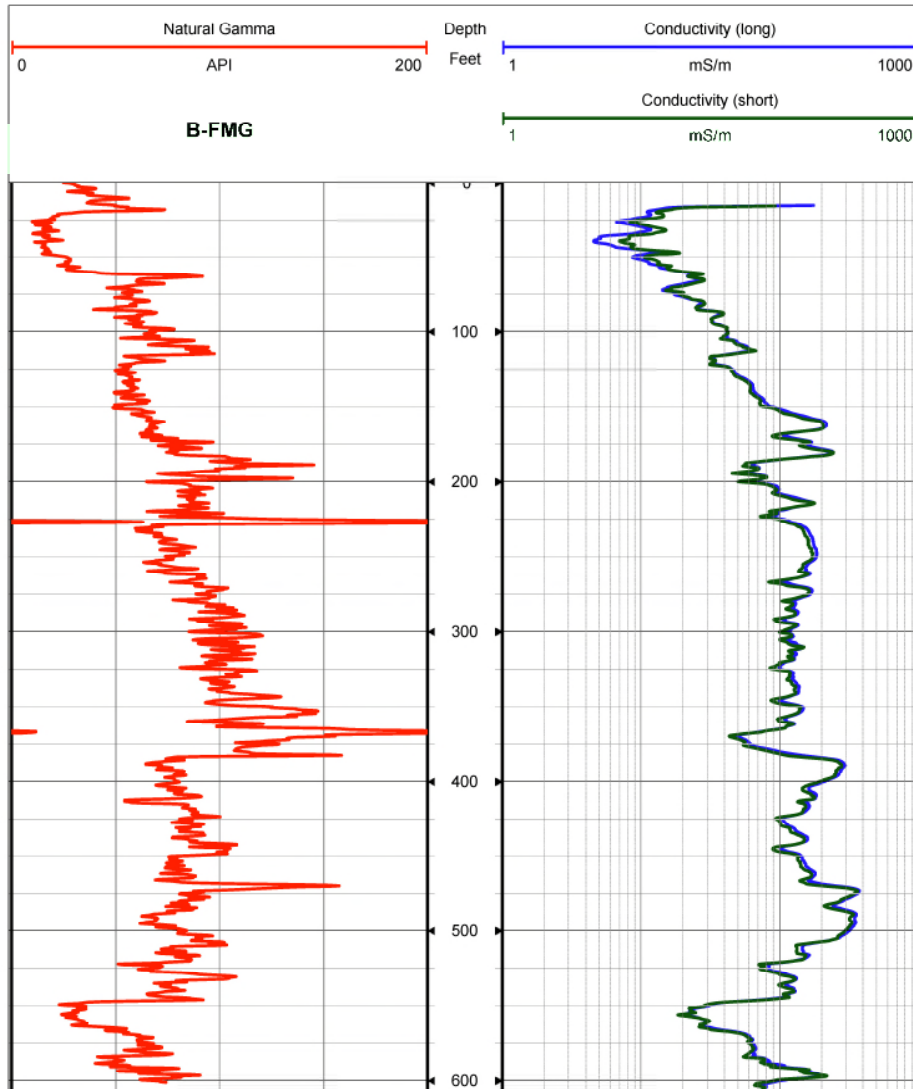


Figure 5. Boring B-FMG, Induction and natural gamma logs

### SCDOT CONWAY BORINGS HOR-1328 & OFFSET Receiver to Receiver $V_s$ and $V_p$ Analysis

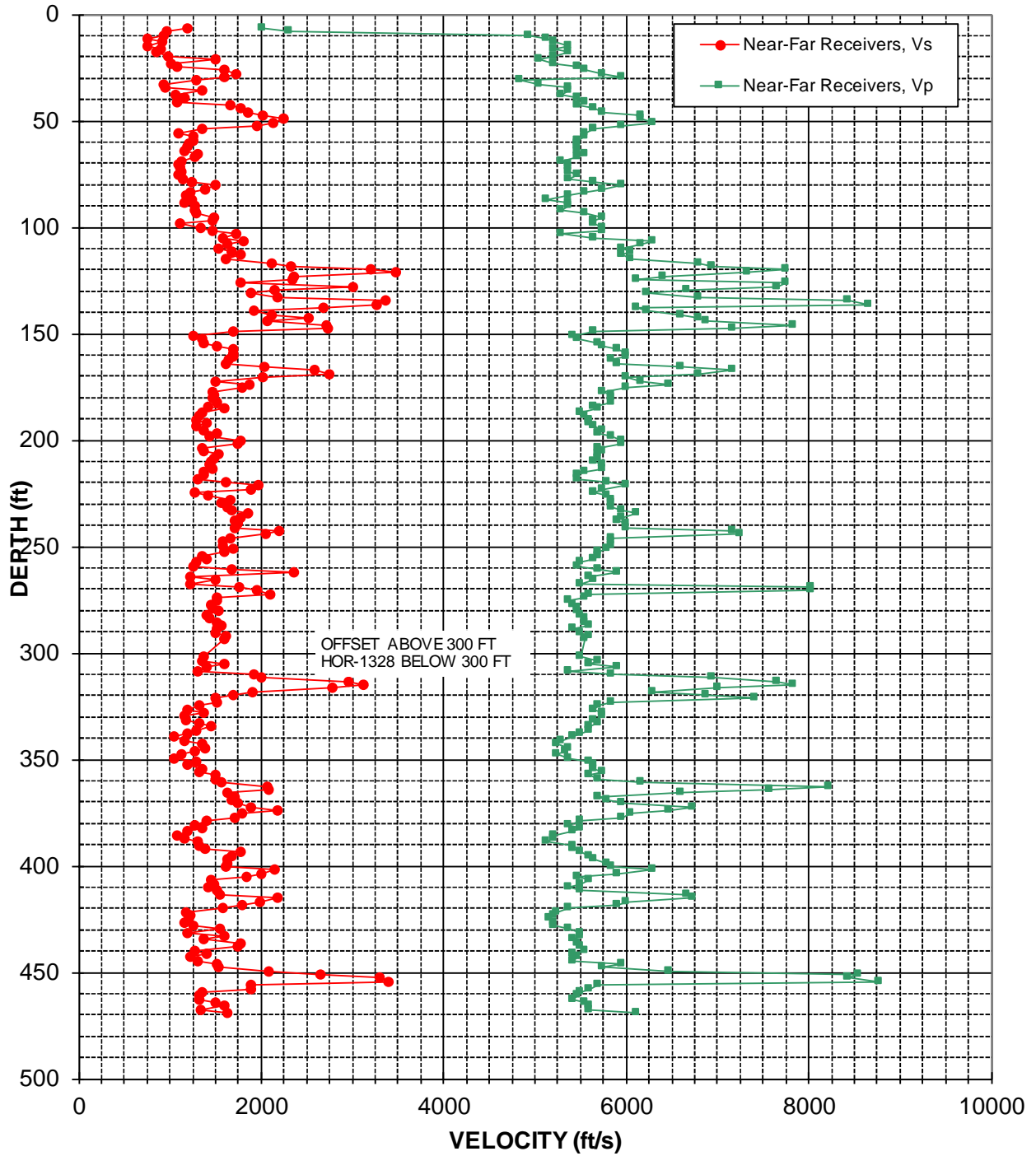


Figure 6: Boreholes HOR-1328 & Conway Offset, Suspension R1-R2 P- and  $S_H$ -wave velocities

Table 4. Boreholes HOR-1328 & Conway Offset, Suspension R1-R2 depths and P- and S<sub>H</sub>-wave velocities

**Summary of Compressional Wave Velocity, Shear Wave Velocity, and Poisson's Ratio  
Based on Receiver-to-Receiver Travel Time Data - Borehole HOR-1328 COMBINED WITH OFFSET**

American Units				Metric Units			
Depth at Midpoint Between Receivers	Velocity		Poisson's Ratio	Depth at Midpoint Between Receivers	Velocity		Poisson's Ratio
	V <sub>s</sub>	V <sub>p</sub>			V <sub>s</sub>	V <sub>p</sub>	
(ft)	(ft/s)	(ft/s)		(m)	(m/s)	(m/s)	
6.6	1190	2020	0.23	2.0	360	620	0.23
8.2	960	2310	0.40	2.5	290	700	0.40
9.8	940	4940	0.48	3.0	290	1510	0.48
11.5	760	5130	0.49	3.5	230	1560	0.49
13.1	920	5210	0.48	4.0	280	1590	0.48
14.8	750	5380	0.49	4.5	230	1640	0.49
16.4	910	5210	0.48	5.0	280	1590	0.48
18.0	850	5380	0.49	5.5	260	1640	0.49
19.7	980	5210	0.48	6.0	300	1590	0.48
21.3	1500	5050	0.45	6.5	460	1540	0.45
23.0	1010	5210	0.48	7.0	310	1590	0.48
24.6	1070	5460	0.48	7.5	330	1670	0.48
26.3	1600	5560	0.45	8.0	490	1690	0.45
27.9	1730	5750	0.45	8.5	530	1750	0.45
29.5	1600	5950	0.46	9.0	490	1810	0.46
31.2	1290	4830	0.46	9.5	390	1470	0.46
32.8	930	5050	0.48	10.0	280	1540	0.48
34.5	940	5380	0.48	10.5	290	1640	0.48
36.1	1360	5380	0.47	11.0	410	1640	0.47
37.7	1060	5290	0.48	11.5	320	1610	0.48
39.4	1170	5460	0.48	12.0	360	1670	0.48
41.0	1080	5560	0.48	12.5	330	1690	0.48
42.7	1670	5460	0.45	13.0	510	1670	0.45
44.3	1770	5650	0.45	13.5	540	1720	0.45
45.9	1860	5750	0.44	14.0	570	1750	0.44
47.6	2020	6170	0.44	14.5	620	1880	0.44
49.2	2240	6170	0.42	15.0	680	1880	0.42
50.9	2140	6290	0.43	15.5	650	1920	0.43
52.5	1960	5950	0.44	16.0	600	1810	0.44
54.1	1360	5650	0.47	16.5	410	1720	0.47
55.8	1090	5560	0.48	17.0	330	1690	0.48
57.4	1250	5560	0.47	17.5	380	1690	0.47
59.1	1250	5460	0.47	18.0	380	1670	0.47
60.7	1210	5460	0.47	18.5	370	1670	0.47
62.3	1190	5460	0.48	19.0	360	1670	0.48

**Summary of Compressional Wave Velocity, Shear Wave Velocity, and Poisson's Ratio  
Based on Receiver-to-Receiver Travel Time Data - Borehole HOR-1328 COMBINED WITH OFFSET**

American Units			
Depth at Midpoint Between Receivers	Velocity		Poisson's Ratio
	V <sub>s</sub>	V <sub>p</sub>	
(ft)	(ft/s)	(ft/s)	
64.0	1160	5460	0.48
65.6	1300	5560	0.47
67.3	1270	5460	0.47
68.9	1130	5290	0.48
70.5	1100	5380	0.48
72.2	1100	5380	0.48
73.8	1120	5380	0.48
75.5	1100	5460	0.48
77.1	1150	5380	0.48
78.7	1240	5650	0.47
80.4	1490	5950	0.47
82.0	1390	5750	0.47
83.7	1230	5560	0.47
85.3	1180	5380	0.47
86.9	1240	5130	0.47
88.6	1160	5380	0.48
90.2	1280	5380	0.47
91.9	1280	5290	0.47
93.5	1290	5560	0.47
95.1	1480	5750	0.46
96.8	1460	5650	0.46
98.4	1110	5650	0.48
100.1	1330	5750	0.47
101.7	1460	5750	0.47
103.4	1720	5290	0.44
105.0	1590	5650	0.46
106.6	1800	6290	0.46
108.3	1630	6170	0.46
109.9	1540	5950	0.46
111.6	1680	6060	0.46
113.2	1770	5950	0.45
114.8	1620	6060	0.46
116.8	2120	6800	0.45
118.1	2330	6940	0.44
120.1	3210	7750	0.40
121.4	3470	7330	0.36
123.0	2360	6410	0.42
124.7	2350	6120	0.41
126.3	1770	7750	0.47
128.0	3000	7660	0.41

Metric Units			
Depth at Midpoint Between Receivers	Velocity		Poisson's Ratio
	V <sub>s</sub>	V <sub>p</sub>	
(m)	(m/s)	(m/s)	
19.5	350	1670	0.48
20.0	400	1690	0.47
20.5	390	1670	0.47
21.0	340	1610	0.48
21.5	340	1640	0.48
22.0	340	1640	0.48
22.5	340	1640	0.48
23.0	340	1670	0.48
23.5	350	1640	0.48
24.0	380	1720	0.47
24.5	460	1810	0.47
25.0	420	1750	0.47
25.5	370	1690	0.47
26.0	360	1640	0.47
26.5	380	1560	0.47
27.0	350	1640	0.48
27.5	390	1640	0.47
28.0	390	1610	0.47
28.5	390	1690	0.47
29.0	450	1750	0.46
29.5	450	1720	0.46
30.0	340	1720	0.48
30.5	410	1750	0.47
31.0	450	1750	0.47
31.5	520	1610	0.44
32.0	480	1720	0.46
32.5	550	1920	0.46
33.0	500	1880	0.46
33.5	470	1810	0.46
34.0	510	1850	0.46
34.5	540	1810	0.45
35.0	490	1850	0.46
35.6	650	2070	0.45
36.0	710	2120	0.44
36.6	980	2360	0.40
37.0	1060	2230	0.36
37.5	720	1950	0.42
38.0	720	1860	0.41
38.5	540	2360	0.47
39.0	920	2340	0.41

**Summary of Compressional Wave Velocity, Shear Wave Velocity, and Poisson's Ratio  
Based on Receiver-to-Receiver Travel Time Data - Borehole HOR-1328 COMBINED WITH OFFSET**

American Units			
Depth at Midpoint Between Receivers	Velocity		Poisson's Ratio
	V <sub>s</sub>	V <sub>p</sub>	
(ft)	(ft/s)	(ft/s)	
129.6	2150	6670	0.44
131.2	1890	6230	0.45
132.9	2180	6800	0.44
134.5	3370	8440	0.41
136.5	3270	8660	0.42
137.8	2690	6120	0.38
139.4	1920	6230	0.45
141.1	2110	6600	0.44
142.7	2530	6800	0.42
144.4	2070	6870	0.45
146.0	2710	7840	0.43
147.6	2730	7170	0.42
149.3	1700	5650	0.45
150.9	1260	5420	0.47
152.6	1360	5460	0.47
154.2	1370	5700	0.47
155.8	1520	5750	0.46
157.5	1690	5900	0.46
159.5	1690	6010	0.46
160.8	1690	6010	0.46
162.4	1640	5850	0.46
164.0	1610	5900	0.46
165.7	2030	6600	0.45
167.3	2580	7170	0.43
169.0	2750	6800	0.40
170.6	2020	6010	0.44
172.2	1500	6170	0.47
173.9	1870	6470	0.45
175.5	1790	6010	0.45
177.2	1460	5750	0.47
178.8	1480	5850	0.47
180.5	1470	5850	0.47
182.1	1520	5850	0.46
184.1	1420	5650	0.47
185.4	1590	5700	0.46
187.0	1350	5510	0.47
188.7	1320	5560	0.47
190.3	1290	5600	0.47
191.9	1390	5600	0.47
193.6	1280	5650	0.47

Metric Units			
Depth at Midpoint Between Receivers	Velocity		Poisson's Ratio
	V <sub>s</sub>	V <sub>p</sub>	
(m)	(m/s)	(m/s)	
39.5	660	2030	0.44
40.0	580	1900	0.45
40.5	660	2070	0.44
41.0	1030	2570	0.41
41.6	1000	2640	0.42
42.0	820	1860	0.38
42.5	580	1900	0.45
43.0	640	2010	0.44
43.5	770	2070	0.42
44.0	630	2090	0.45
44.5	830	2390	0.43
45.0	830	2180	0.42
45.5	520	1720	0.45
46.0	380	1650	0.47
46.5	410	1670	0.47
47.0	420	1740	0.47
47.5	460	1750	0.46
48.0	520	1800	0.46
48.6	520	1830	0.46
49.0	520	1830	0.46
49.5	500	1780	0.46
50.0	490	1800	0.46
50.5	620	2010	0.45
51.0	790	2180	0.43
51.5	840	2070	0.40
52.0	620	1830	0.44
52.5	460	1880	0.47
53.0	570	1970	0.45
53.5	550	1830	0.45
54.0	450	1750	0.47
54.5	450	1780	0.47
55.0	450	1780	0.47
55.5	460	1780	0.46
56.1	430	1720	0.47
56.5	490	1740	0.46
57.0	410	1680	0.47
57.5	400	1690	0.47
58.0	390	1710	0.47
58.5	430	1710	0.47
59.0	390	1720	0.47

**Summary of Compressional Wave Velocity, Shear Wave Velocity, and Poisson's Ratio  
Based on Receiver-to-Receiver Travel Time Data - Borehole HOR-1328 COMBINED WITH OFFSET**

American Units			
Depth at Midpoint Between Receivers	Velocity		Poisson's Ratio
	V <sub>s</sub>	V <sub>p</sub>	
(ft)	(ft/s)	(ft/s)	
195.2	1370	5750	0.47
196.9	1520	5700	0.46
198.5	1430	5850	0.47
200.1	1770	5950	0.45
201.8	1740	5950	0.45
203.7	1360	5700	0.47
205.1	1370	5750	0.47
206.7	1540	5700	0.46
208.7	1490	5700	0.46
210.0	1450	5650	0.46
211.6	1430	5750	0.47
213.3	1470	5750	0.47
214.9	1370	5560	0.47
216.5	1370	5460	0.47
218.2	1310	5460	0.47
219.8	1610	5800	0.46
221.5	1970	6010	0.44
223.1	1890	5750	0.44
224.7	1270	5650	0.47
226.4	1420	5800	0.47
228.0	1660	5850	0.46
229.7	1560	5850	0.46
231.3	1630	5850	0.46
232.9	1680	5950	0.46
234.6	1850	6120	0.45
236.2	1780	5950	0.45
237.9	1710	5900	0.45
239.5	1740	6010	0.45
241.1	1710	6010	0.46
242.8	2190	7170	0.45
244.4	2060	7250	0.46
246.1	1670	5850	0.46
247.7	1570	5850	0.46
249.3	1570	5850	0.46
251.0	1700	5800	0.45
252.6	1600	5700	0.46
254.3	1350	5700	0.47
255.9	1400	5650	0.47
257.6	1290	5510	0.47
259.2	1260	5460	0.47

Metric Units			
Depth at Midpoint Between Receivers	Velocity		Poisson's Ratio
	V <sub>s</sub>	V <sub>p</sub>	
(m)	(m/s)	(m/s)	
59.5	420	1750	0.47
60.0	460	1740	0.46
60.5	440	1780	0.47
61.0	540	1810	0.45
61.5	530	1810	0.45
62.1	410	1740	0.47
62.5	420	1750	0.47
63.0	470	1740	0.46
63.6	450	1740	0.46
64.0	440	1720	0.46
64.5	440	1750	0.47
65.0	450	1750	0.47
65.5	420	1690	0.47
66.0	420	1670	0.47
66.5	400	1670	0.47
67.0	490	1770	0.46
67.5	600	1830	0.44
68.0	580	1750	0.44
68.5	390	1720	0.47
69.0	430	1770	0.47
69.5	510	1780	0.46
70.0	470	1780	0.46
70.5	500	1780	0.46
71.0	510	1810	0.46
71.5	560	1860	0.45
72.0	540	1810	0.45
72.5	520	1800	0.45
73.0	530	1830	0.45
73.5	520	1830	0.46
74.0	670	2180	0.45
74.5	630	2210	0.46
75.0	510	1780	0.46
75.5	480	1780	0.46
76.0	480	1780	0.46
76.5	520	1770	0.45
77.0	490	1740	0.46
77.5	410	1740	0.47
78.0	430	1720	0.47
78.5	390	1680	0.47
79.0	380	1670	0.47

**Summary of Compressional Wave Velocity, Shear Wave Velocity, and Poisson's Ratio  
Based on Receiver-to-Receiver Travel Time Data - Borehole HOR-1328 COMBINED WITH OFFSET**

American Units			
Depth at Midpoint Between Receivers	Velocity		Poisson's Ratio
	V <sub>s</sub>	V <sub>p</sub>	
(ft)	(ft/s)	(ft/s)	
260.8	1680	5700	0.45
262.5	2360	5900	0.40
264.1	1230	5600	0.47
265.8	1490	5650	0.46
267.4	1220	5510	0.47
269.0	1760	8030	0.47
270.7	1960	8030	0.47
272.3	2100	5600	0.42
274.0	1520	5560	0.46
275.6	1510	5380	0.46
277.2	1450	5420	0.46
278.9	1460	5460	0.46
280.5	1540	5460	0.46
282.2	1400	5510	0.47
283.8	1440	5560	0.46
285.4	1520	5560	0.46
287.1	1560	5600	0.46
288.7	1520	5420	0.46
290.4	1490	5510	0.46
292.0	1610	5600	0.45
293.3	1590	5560	0.46
301.8	1370	5510	0.47
303.5	1360	5700	0.47
305.1	1590	5600	0.46
306.8	1400	5900	0.47
308.4	1310	5380	0.47
310.0	1920	5850	0.44
311.7	2000	6940	0.45
313.3	2950	7660	0.41
315.0	3120	7840	0.41
316.6	2780	7020	0.41
318.2	1900	6290	0.45
319.9	1690	6870	0.47
321.5	1500	7410	0.48
323.2	1520	5850	0.46
324.8	1320	5700	0.47
326.4	1200	5650	0.48
328.1	1370	5750	0.47
329.7	1160	5750	0.48
331.4	1180	5650	0.48

Metric Units			
Depth at Midpoint Between Receivers	Velocity		Poisson's Ratio
	V <sub>s</sub>	V <sub>p</sub>	
(m)	(m/s)	(m/s)	
79.5	510	1740	0.45
80.0	720	1800	0.40
80.5	370	1710	0.47
81.0	460	1720	0.46
81.5	370	1680	0.47
82.0	540	2450	0.47
82.5	600	2450	0.47
83.0	640	1710	0.42
83.5	460	1690	0.46
84.0	460	1640	0.46
84.5	440	1650	0.46
85.0	450	1670	0.46
85.5	470	1670	0.46
86.0	430	1680	0.47
86.5	440	1690	0.46
87.0	460	1690	0.46
87.5	480	1710	0.46
88.0	460	1650	0.46
88.5	460	1680	0.46
89.0	490	1710	0.45
89.4	490	1690	0.46
92.0	420	1680	0.47
92.5	410	1740	0.47
93.0	480	1710	0.46
93.5	430	1800	0.47
94.0	400	1640	0.47
94.5	580	1780	0.44
95.0	610	2120	0.45
95.5	900	2340	0.41
96.0	950	2390	0.41
96.5	850	2140	0.41
97.0	580	1920	0.45
97.5	520	2090	0.47
98.0	460	2260	0.48
98.5	460	1780	0.46
99.0	400	1740	0.47
99.5	370	1720	0.48
100.0	420	1750	0.47
100.5	350	1750	0.48
101.0	360	1720	0.48

**Summary of Compressional Wave Velocity, Shear Wave Velocity, and Poisson's Ratio  
Based on Receiver-to-Receiver Travel Time Data - Borehole HOR-1328 COMBINED WITH OFFSET**

American Units			
Depth at Midpoint Between Receivers	Velocity		Poisson's Ratio
	V <sub>s</sub>	V <sub>p</sub>	
(ft)	(ft/s)	(ft/s)	
333.0	1320	5700	0.47
334.7	1440	5600	0.46
336.3	1290	5600	0.47
337.9	1190	5510	0.48
339.6	1040	5420	0.48
341.2	1160	5290	0.47
342.9	1350	5250	0.46
344.5	1380	5380	0.46
346.1	1270	5330	0.47
347.8	1130	5250	0.48
349.4	1050	5380	0.48
351.1	1280	5600	0.47
352.7	1190	5650	0.48
354.3	1360	5650	0.47
356.0	1320	5750	0.47
357.6	1500	5600	0.46
359.3	1490	5700	0.46
360.9	1560	6170	0.47
362.5	2070	8230	0.47
364.2	2090	7580	0.46
365.8	1630	6600	0.47
367.5	1710	5700	0.45
369.1	1680	5800	0.45
370.7	1750	5950	0.45
372.4	1890	6730	0.46
374.0	2190	6470	0.44
375.7	1800	6060	0.45
377.3	1710	5950	0.46
378.9	1410	5510	0.47
380.6	1280	5380	0.47
382.2	1360	5510	0.47
383.9	1200	5420	0.47
385.5	1080	5210	0.48
387.1	1160	5210	0.47
388.8	1310	5130	0.47
390.4	1330	5420	0.47
392.1	1390	5420	0.46
393.7	1780	5510	0.44
395.3	1680	5600	0.45
397.0	1630	5650	0.45

Metric Units			
Depth at Midpoint Between Receivers	Velocity		Poisson's Ratio
	V <sub>s</sub>	V <sub>p</sub>	
(m)	(m/s)	(m/s)	
101.5	400	1740	0.47
102.0	440	1710	0.46
102.5	390	1710	0.47
103.0	360	1680	0.48
103.5	320	1650	0.48
104.0	350	1610	0.47
104.5	410	1600	0.46
105.0	420	1640	0.46
105.5	390	1630	0.47
106.0	340	1600	0.48
106.5	320	1640	0.48
107.0	390	1710	0.47
107.5	360	1720	0.48
108.0	410	1720	0.47
108.5	400	1750	0.47
109.0	460	1710	0.46
109.5	460	1740	0.46
110.0	480	1880	0.47
110.5	630	2510	0.47
111.0	640	2310	0.46
111.5	500	2010	0.47
112.0	520	1740	0.45
112.5	510	1770	0.45
113.0	530	1810	0.45
113.5	580	2050	0.46
114.0	670	1970	0.44
114.5	550	1850	0.45
115.0	520	1810	0.46
115.5	430	1680	0.47
116.0	390	1640	0.47
116.5	410	1680	0.47
117.0	370	1650	0.47
117.5	330	1590	0.48
118.0	350	1590	0.47
118.5	400	1560	0.47
119.0	400	1650	0.47
119.5	420	1650	0.46
120.0	540	1680	0.44
120.5	510	1710	0.45
121.0	500	1720	0.45

**Summary of Compressional Wave Velocity, Shear Wave Velocity, and Poisson's Ratio  
Based on Receiver-to-Receiver Travel Time Data - Borehole HOR-1328 COMBINED WITH OFFSET**

American Units			
Depth at Midpoint Between Receivers	Velocity		Poisson's Ratio
	V <sub>s</sub>	V <sub>p</sub>	
(ft)	(ft/s)	(ft/s)	
398.6	1630	5800	0.46
400.3	1620	5850	0.46
401.9	2150	6290	0.43
403.5	2000	5900	0.43
405.2	1830	5460	0.44
406.8	1460	5600	0.46
408.5	1470	5510	0.46
410.1	1410	5380	0.46
411.8	1520	5510	0.46
413.4	1550	6670	0.47
415.0	2180	6730	0.44
416.7	1980	6010	0.44
418.3	1790	5900	0.45
420.0	1580	5380	0.45
421.6	1170	5250	0.47
423.2	1220	5210	0.47
424.9	1200	5170	0.47
426.5	1170	5210	0.47
428.2	1260	5210	0.47
429.8	1540	5380	0.46
431.4	1190	5510	0.48
433.1	1600	5510	0.45
434.7	1370	5420	0.47
436.4	1770	5460	0.44
438.0	1740	5510	0.44
439.6	1270	5560	0.47
441.3	1390	5420	0.46
442.9	1220	5460	0.47
444.6	1310	5420	0.47
446.2	1510	5950	0.47
447.8	1540	5750	0.46
449.5	2080	6470	0.44
451.1	2650	8550	0.45
452.8	3300	8440	0.41
454.4	3400	8770	0.41
456.0	1880	5700	0.44
457.7	1890	5600	0.44
459.3	1360	5510	0.47
461.0	1330	5460	0.47
462.6	1320	5420	0.47

Metric Units			
Depth at Midpoint Between Receivers	Velocity		Poisson's Ratio
	V <sub>s</sub>	V <sub>p</sub>	
(m)	(m/s)	(m/s)	
121.5	500	1770	0.46
122.0	490	1780	0.46
122.5	660	1920	0.43
123.0	610	1800	0.43
123.5	560	1670	0.44
124.0	440	1710	0.46
124.5	450	1680	0.46
125.0	430	1640	0.46
125.5	460	1680	0.46
126.0	470	2030	0.47
126.5	660	2050	0.44
127.0	600	1830	0.44
127.5	550	1800	0.45
128.0	480	1640	0.45
128.5	360	1600	0.47
129.0	370	1590	0.47
129.5	370	1580	0.47
130.0	360	1590	0.47
130.5	380	1590	0.47
131.0	470	1640	0.46
131.5	360	1680	0.48
132.0	490	1680	0.45
132.5	420	1650	0.47
133.0	540	1670	0.44
133.5	530	1680	0.44
134.0	390	1690	0.47
134.5	430	1650	0.46
135.0	370	1670	0.47
135.5	400	1650	0.47
136.0	460	1810	0.47
136.5	470	1750	0.46
137.0	640	1970	0.44
137.5	810	2610	0.45
138.0	1010	2570	0.41
138.5	1040	2670	0.41
139.0	570	1740	0.44
139.5	580	1710	0.44
140.0	410	1680	0.47
140.5	400	1670	0.47
141.0	400	1650	0.47

**Summary of Compressional Wave Velocity, Shear Wave Velocity, and Poisson's Ratio  
Based on Receiver-to-Receiver Travel Time Data - Borehole HOR-1328 COMBINED WITH OFFSET**

<b>American Units</b>			
<b>Depth at Midpoint Between Receivers</b>	<b>Velocity</b>		<b>Poisson's Ratio</b>
	<b>V<sub>s</sub></b>	<b>V<sub>p</sub></b>	
(ft)	(ft/s)	(ft/s)	
464.2	1490	5560	0.46
465.9	1600	5600	0.46
467.5	1330	5600	0.47
469.2	1630	6120	0.46

<b>Metric Units</b>			
<b>Depth at Midpoint Between Receivers</b>	<b>Velocity</b>		<b>Poisson's Ratio</b>
	<b>V<sub>s</sub></b>	<b>V<sub>p</sub></b>	
(m)	(m/s)	(m/s)	
141.5	460	1690	0.46
142.0	490	1710	0.46
142.5	410	1710	0.47
143.0	500	1860	0.46

	LOG TYPE	PROJECT	Conway / SCDOT Site A
	Dual Induction	WELL	HOR-1328 & Conway Offset
CLIENT S&ME		LOCATION	Conway Site A
		LOGGER	J. Jordan
		DATE	Jan. 28 and Feb. 27, 2017

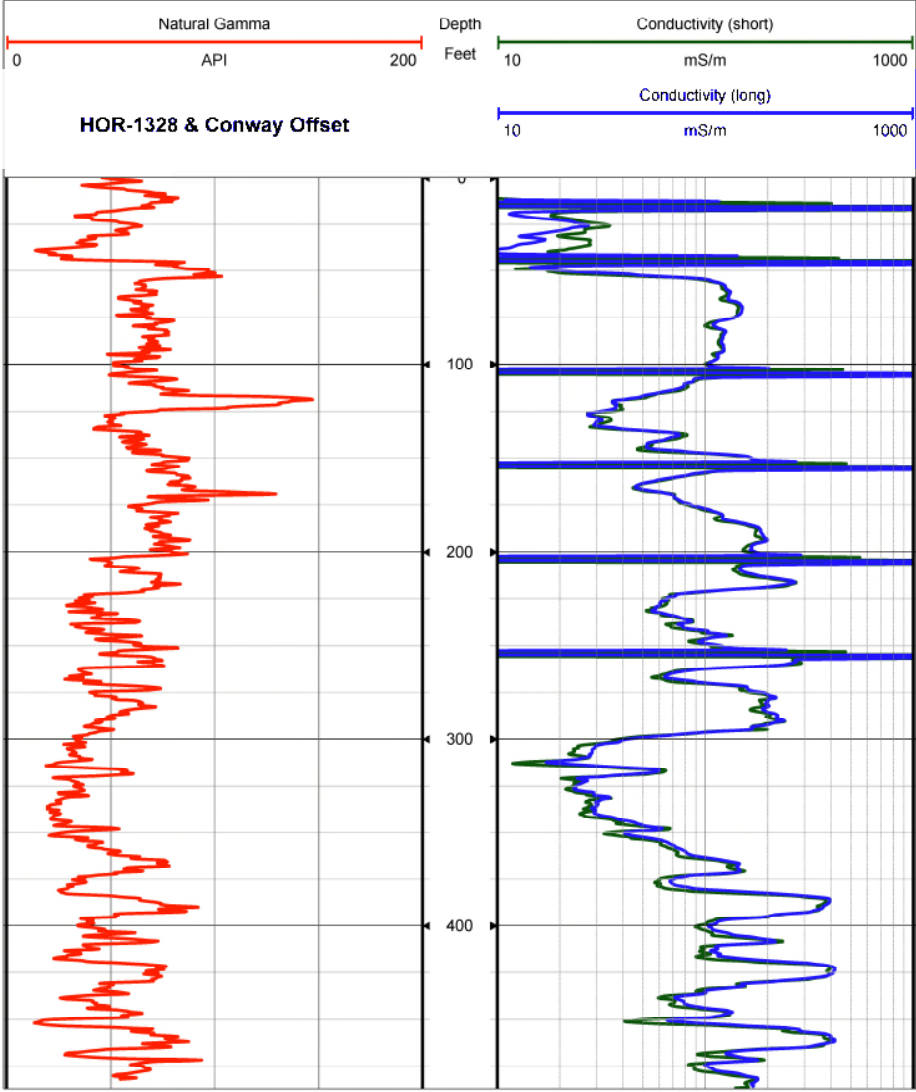


Figure 7. Boreholes HOR-1328 & Conway Offset, Induction and natural gamma logs

## **APPENDIX A**

# **SUSPENSION VELOCITY MEASUREMENT QUALITY ASSURANCE SUSPENSION SOURCE TO RECEIVER ANALYSIS RESULTS**

## SCDOT ANDREWS BORING B-FMG Source to Receiver and Receiver to Receiver Analysis

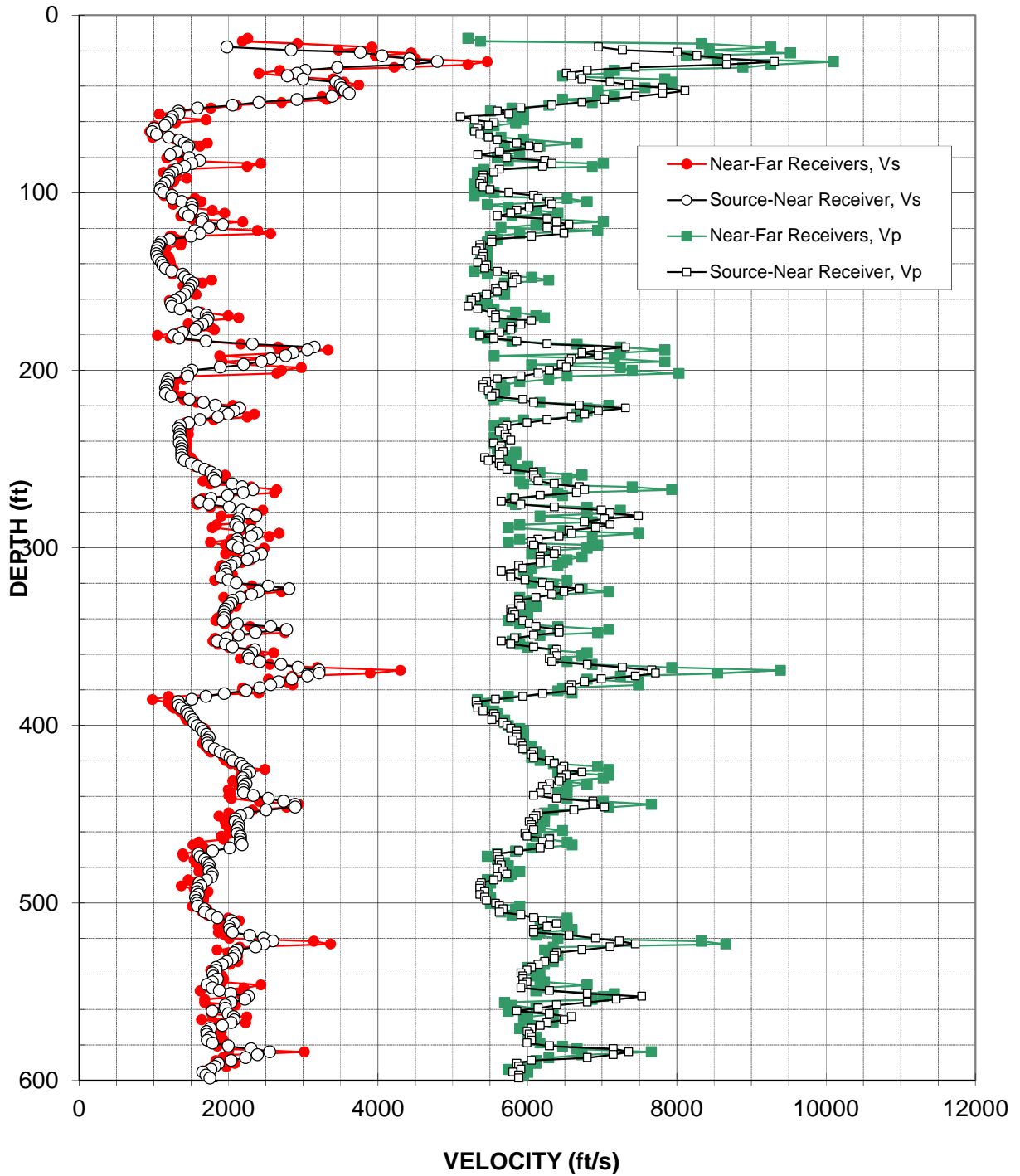


Figure A-1: Borehole B-FMG, Suspension S-R1 P- and  $S_H$ -wave velocities

Table A-1. Borehole B-FMG, S - R1 quality assurance analysis P- and SH-wave data

**Summary of Compressional Wave Velocity, Shear Wave Velocity, and Poisson's Ratio  
Based on Source-to-Receiver Travel Time Data - Borehole B-FMG**

American Units				Metric Units			
Depth at Midpoint Between Source and Near Receiver	Velocity		Poisson's Ratio	Depth at Midpoint Between Source and Near Receiver	Velocity		Poisson's Ratio
	V <sub>s</sub>	V <sub>p</sub>			V <sub>s</sub>	V <sub>p</sub>	
(ft)	(ft/s)	(ft/s)		(m)	(m/s)	(m/s)	
18.0	1980	6960	0.46	5.5	600	2120	0.46
19.6	2840	7280	0.41	6.0	870	2220	0.41
20.9	3770	8010	0.36	6.4	1150	2440	0.36
22.9	4060	8270	0.34	7.0	1240	2520	0.34
24.5	4430	8670	0.32	7.5	1350	2640	0.32
26.2	4800	9310	0.32	8.0	1460	2840	0.32
27.8	4430	8670	0.32	8.5	1350	2640	0.32
29.4	3460	7450	0.36	9.0	1050	2270	0.36
31.1	3030	6810	0.38	9.5	920	2070	0.38
32.7	2920	6530	0.38	10.0	890	1990	0.38
34.4	2790	6590	0.39	10.5	850	2010	0.39
36.0	3000	6730	0.38	11.0	910	2050	0.38
37.6	3440	7110	0.35	11.5	1050	2170	0.35
39.3	3500	7360	0.35	12.0	1070	2240	0.35
40.9	3520	7810	0.37	12.5	1070	2380	0.37
42.6	3560	8120	0.38	13.0	1080	2470	0.38
44.2	3620	7810	0.36	13.5	1100	2380	0.36
45.8	3390	7450	0.37	14.0	1030	2270	0.37
47.5	2920	7030	0.40	14.5	890	2140	0.40
49.1	2410	6730	0.43	15.0	730	2050	0.43
50.8	2060	6330	0.44	15.5	630	1930	0.44
52.4	1590	5920	0.46	16.0	480	1800	0.46
54.0	1330	5600	0.47	16.5	410	1710	0.47
55.7	1340	5750	0.47	17.0	410	1750	0.47
57.3	1250	5100	0.47	17.5	380	1560	0.47
59.0	1230	5300	0.47	18.0	370	1610	0.47
60.6	1190	5550	0.48	18.5	360	1690	0.48
62.2	1150	5480	0.48	19.0	350	1670	0.48
63.9	1000	5340	0.48	19.5	310	1630	0.48
65.5	980	5300	0.48	20.0	300	1610	0.48
67.2	1040	5360	0.48	20.5	320	1640	0.48
68.8	1200	5480	0.47	21.0	370	1670	0.47
70.5	1340	5600	0.47	21.5	410	1710	0.47
72.1	1410	5860	0.47	22.0	430	1790	0.47
73.7	1470	6030	0.47	22.5	450	1840	0.47
74.7	1450	6150	0.47	22.8	440	1870	0.47
77.0	1310	5630	0.47	23.5	400	1720	0.47
78.7	1220	5340	0.47	24.0	370	1630	0.47

**Summary of Compressional Wave Velocity, Shear Wave Velocity, and Poisson's Ratio  
Based on Source-to-Receiver Travel Time Data - Borehole B-FMG**

American Units				Metric Units			
Depth at Midpoint Between Source and Near Receiver	Velocity		Poisson's Ratio	Depth at Midpoint Between Source and Near Receiver	Velocity		Poisson's Ratio
	V <sub>s</sub>	V <sub>p</sub>			V <sub>s</sub>	V <sub>p</sub>	
(ft)	(ft/s)	(ft/s)		(m)	(m/s)	(m/s)	
80.3	1480	5730	0.46	24.5	450	1750	0.46
81.9	1610	6240	0.46	25.0	490	1900	0.46
83.6	1510	6330	0.47	25.5	460	1930	0.47
85.2	1420	6210	0.47	26.0	430	1890	0.47
86.9	1310	5630	0.47	26.5	400	1720	0.47
88.5	1250	5550	0.47	27.0	380	1690	0.47
90.1	1210	5410	0.47	27.5	370	1650	0.47
91.8	1190	5410	0.47	28.0	360	1650	0.47
93.4	1200	5390	0.47	28.5	360	1640	0.47
95.1	1150	5360	0.48	29.0	350	1640	0.48
96.7	1100	5410	0.48	29.5	340	1650	0.48
98.3	1090	5500	0.48	30.0	330	1680	0.48
100.0	1140	5750	0.48	30.5	350	1750	0.48
101.6	1240	6090	0.48	31.0	380	1860	0.48
103.3	1250	6150	0.48	31.5	380	1870	0.48
104.9	1370	6300	0.48	32.0	420	1920	0.48
106.5	1510	6330	0.47	32.5	460	1930	0.47
108.2	1510	6030	0.47	33.0	460	1840	0.47
109.8	1510	5860	0.46	33.5	460	1790	0.46
111.5	1410	5780	0.47	34.0	430	1760	0.47
113.1	1470	5600	0.46	34.5	450	1710	0.46
114.7	1650	6270	0.46	35.0	500	1910	0.46
116.4	1640	6390	0.46	35.5	500	1950	0.46
118.0	1920	6560	0.45	36.0	590	2000	0.45
119.7	1740	6270	0.46	36.5	530	1910	0.46
121.3	1550	6390	0.47	37.0	470	1950	0.47
122.9	1620	6490	0.47	37.5	490	1980	0.47
124.6	1500	6060	0.47	38.0	460	1850	0.47
126.2	1210	5530	0.47	38.5	370	1690	0.47
127.9	1100	5530	0.48	39.0	330	1690	0.48
129.5	1080	5390	0.48	39.5	330	1640	0.48
129.5	1070	5360	0.48	39.5	330	1640	0.48
131.1	1050	5360	0.48	40.0	320	1640	0.48
132.8	1040	5320	0.48	40.5	320	1620	0.48
134.4	1040	5410	0.48	41.0	320	1650	0.48
136.1	1050	5410	0.48	41.5	320	1650	0.48
137.7	1070	5390	0.48	42.0	330	1640	0.48
139.3	1100	5340	0.48	42.5	340	1630	0.48
141.0	1120	5460	0.48	43.0	340	1660	0.48
142.6	1160	5430	0.48	43.5	350	1660	0.48

**Summary of Compressional Wave Velocity, Shear Wave Velocity, and Poisson's Ratio  
Based on Source-to-Receiver Travel Time Data - Borehole B-FMG**

American Units				Metric Units			
Depth at Midpoint Between Source and Near Receiver	Velocity		Poisson's Ratio	Depth at Midpoint Between Source and Near Receiver	Velocity		Poisson's Ratio
	V <sub>s</sub>	V <sub>p</sub>			V <sub>s</sub>	V <sub>p</sub>	
(ft)	(ft/s)	(ft/s)		(m)	(m/s)	(m/s)	
144.3	1240	5600	0.47	44.0	380	1710	0.47
145.9	1390	5810	0.47	44.5	420	1770	0.47
147.6	1420	5830	0.47	45.0	430	1780	0.47
149.2	1470	5860	0.47	45.5	450	1790	0.47
150.8	1530	5810	0.46	46.0	460	1770	0.46
152.5	1500	5680	0.46	46.5	460	1730	0.46
154.1	1470	5580	0.46	47.0	450	1700	0.46
155.8	1450	5600	0.46	47.5	440	1710	0.46
157.4	1420	5460	0.46	48.0	430	1660	0.46
159.0	1350	5320	0.47	48.5	410	1620	0.47
160.7	1290	5250	0.47	49.0	390	1600	0.47
162.3	1230	5250	0.47	49.5	370	1600	0.47
164.0	1240	5210	0.47	50.0	380	1590	0.47
165.6	1360	5340	0.47	50.5	410	1630	0.47
167.6	1590	5530	0.46	51.1	480	1690	0.46
168.9	1700	5580	0.45	51.5	520	1700	0.45
170.5	1730	5580	0.45	52.0	530	1700	0.45
172.2	1720	6060	0.46	52.5	520	1850	0.46
174.1	1650	5920	0.46	53.1	500	1800	0.46
175.4	1590	5780	0.46	53.5	480	1760	0.46
177.1	1560	5780	0.46	54.0	470	1760	0.46
178.7	1390	5630	0.47	54.5	420	1720	0.47
180.4	1270	5360	0.47	55.0	390	1640	0.47
182.0	1340	5550	0.47	55.5	410	1690	0.47
183.6	1700	5860	0.45	56.0	520	1790	0.45
185.3	2320	6270	0.42	56.5	710	1910	0.42
186.9	3150	7320	0.39	57.0	960	2230	0.39
188.6	3060	6960	0.38	57.5	930	2120	0.38
190.2	2860	6730	0.39	58.0	870	2050	0.39
191.8	2760	6960	0.41	58.5	840	2120	0.41
193.5	2560	6590	0.41	59.0	780	2010	0.41
195.1	2440	6560	0.42	59.5	740	2000	0.42
196.8	2210	6460	0.43	60.0	670	1970	0.43
198.4	1890	6530	0.45	60.5	580	1990	0.45
200.0	1510	6300	0.47	61.0	460	1920	0.47
201.7	1450	6150	0.47	61.5	440	1870	0.47
203.3	1460	5920	0.47	62.0	440	1800	0.47
205.0	1200	5600	0.48	62.5	360	1710	0.48
206.6	1180	5460	0.48	63.0	360	1660	0.48
208.2	1190	5410	0.47	63.5	360	1650	0.47

**Summary of Compressional Wave Velocity, Shear Wave Velocity, and Poisson's Ratio  
Based on Source-to-Receiver Travel Time Data - Borehole B-FMG**

American Units				Metric Units			
Depth at Midpoint Between Source and Near Receiver	Velocity		Poisson's Ratio	Depth at Midpoint Between Source and Near Receiver	Velocity		Poisson's Ratio
	V <sub>s</sub>	V <sub>p</sub>			V <sub>s</sub>	V <sub>p</sub>	
(ft)	(ft/s)	(ft/s)		(m)	(m/s)	(m/s)	
209.9	1160	5410	0.48	64.0	350	1650	0.48
211.5	1170	5480	0.48	64.5	360	1670	0.48
213.2	1160	5580	0.48	65.0	350	1700	0.48
214.8	1230	5530	0.47	65.5	380	1690	0.47
216.4	1480	5940	0.47	66.0	450	1810	0.47
218.1	1660	6090	0.46	66.5	510	1860	0.46
219.7	1820	6700	0.46	67.0	560	2040	0.46
221.4	2150	7320	0.45	67.5	650	2230	0.45
223.0	2080	6960	0.45	68.0	630	2120	0.45
224.7	2000	6770	0.45	68.5	610	2060	0.45
226.3	1860	6590	0.46	69.0	570	2010	0.46
227.9	1620	6270	0.46	69.5	490	1910	0.46
229.6	1470	6000	0.47	70.0	450	1830	0.47
231.2	1360	5730	0.47	70.5	410	1750	0.47
232.9	1330	5680	0.47	71.0	400	1730	0.47
234.5	1350	5630	0.47	71.5	410	1720	0.47
236.1	1350	5700	0.47	72.0	410	1740	0.47
237.8	1340	5730	0.47	72.5	410	1750	0.47
239.4	1370	5780	0.47	73.0	420	1760	0.47
241.1	1340	5550	0.47	73.5	410	1690	0.47
242.7	1380	5650	0.47	74.0	420	1720	0.47
244.3	1370	5630	0.47	74.5	420	1720	0.47
246.0	1370	5680	0.47	75.0	420	1730	0.47
247.6	1370	5630	0.47	75.5	420	1720	0.47
249.3	1370	5430	0.47	76.0	420	1660	0.47
250.9	1420	5480	0.46	76.5	430	1670	0.46
252.5	1500	5630	0.46	77.0	460	1720	0.46
254.2	1590	5650	0.46	77.5	480	1720	0.46
255.8	1680	5730	0.45	78.0	510	1750	0.45
257.5	1760	6090	0.45	78.5	540	1860	0.45
259.1	1830	6090	0.45	79.0	560	1860	0.45
260.7	1800	6120	0.45	79.5	550	1860	0.45
262.4	1820	6150	0.45	80.0	560	1870	0.45
264.0	2050	6360	0.44	80.5	620	1940	0.44
265.7	2180	6700	0.44	81.0	670	2040	0.44
267.3	2330	6770	0.43	81.5	710	2060	0.43
268.9	2200	6660	0.44	82.0	670	2030	0.44
270.6	1990	6180	0.44	82.5	610	1880	0.44
272.2	1770	5830	0.45	83.0	540	1780	0.45
273.9	1610	5650	0.46	83.5	490	1720	0.46

**Summary of Compressional Wave Velocity, Shear Wave Velocity, and Poisson's Ratio  
Based on Source-to-Receiver Travel Time Data - Borehole B-FMG**

American Units				Metric Units			
Depth at Midpoint Between Source and Near Receiver	Velocity		Poisson's Ratio	Depth at Midpoint Between Source and Near Receiver	Velocity		Poisson's Ratio
	V <sub>s</sub>	V <sub>p</sub>			V <sub>s</sub>	V <sub>p</sub>	
(ft)	(ft/s)	(ft/s)		(m)	(m/s)	(m/s)	
275.5	1740	5920	0.45	84.0	530	1800	0.45
277.1	2010	6360	0.44	84.5	610	1940	0.44
278.8	2180	6990	0.45	85.0	670	2130	0.45
280.4	2260	7110	0.44	85.5	690	2170	0.44
282.1	2370	7490	0.44	86.0	720	2280	0.44
283.7	2140	7030	0.45	86.5	650	2140	0.45
285.3	2120	6770	0.45	87.0	650	2060	0.45
287.0	2100	7110	0.45	87.5	640	2170	0.45
288.6	2140	6920	0.45	88.0	650	2110	0.45
290.3	2310	6560	0.43	88.5	700	2000	0.43
291.9	2380	6590	0.43	89.0	730	2010	0.43
293.5	2310	6430	0.43	89.5	700	1960	0.43
295.2	2120	6150	0.43	90.0	650	1870	0.43
296.8	2120	6060	0.43	90.5	650	1850	0.43
298.5	2060	6090	0.44	91.0	630	1860	0.44
300.1	2130	6210	0.43	91.5	650	1890	0.43
301.8	2290	6390	0.43	92.0	700	1950	0.43
303.4	2440	6360	0.41	92.5	740	1940	0.41
305.0	2340	6180	0.42	93.0	710	1880	0.42
306.7	2250	6180	0.42	93.5	690	1880	0.42
308.3	2100	6180	0.43	94.0	640	1880	0.43
310.0	2040	5890	0.43	94.5	620	1790	0.43
311.6	1960	5940	0.44	95.0	600	1810	0.44
313.2	1960	5650	0.43	95.5	600	1720	0.43
314.9	1970	5780	0.43	96.0	600	1760	0.43
316.5	1900	5780	0.44	96.5	580	1760	0.44
318.2	2000	5970	0.44	97.0	610	1820	0.44
319.8	2110	6210	0.43	97.5	640	1890	0.43
321.4	2530	6300	0.40	98.0	770	1920	0.40
323.1	2810	6700	0.39	98.5	860	2040	0.39
324.7	2400	6490	0.42	99.0	730	1980	0.42
326.4	2310	6330	0.42	99.5	700	1930	0.42
328.0	2160	6120	0.43	100.0	660	1860	0.43
329.6	2060	5890	0.43	100.5	630	1790	0.43
331.3	2040	5890	0.43	101.0	620	1790	0.43
332.9	2000	5920	0.44	101.5	610	1800	0.44
334.6	1960	5780	0.44	102.0	600	1760	0.44
336.2	1940	5810	0.44	102.5	590	1770	0.44
337.8	1940	5830	0.44	103.0	590	1780	0.44
339.5	1940	5780	0.44	103.5	590	1760	0.44

**Summary of Compressional Wave Velocity, Shear Wave Velocity, and Poisson's Ratio  
Based on Source-to-Receiver Travel Time Data - Borehole B-FMG**

American Units				Metric Units			
Depth at Midpoint Between Source and Near Receiver	Velocity		Poisson's Ratio	Depth at Midpoint Between Source and Near Receiver	Velocity		Poisson's Ratio
	V <sub>s</sub>	V <sub>p</sub>			V <sub>s</sub>	V <sub>p</sub>	
(ft)	(ft/s)	(ft/s)		(m)	(m/s)	(m/s)	
341.1	1930	5940	0.44	104.0	590	1810	0.44
342.8	2120	6030	0.43	104.5	650	1840	0.43
344.4	2560	6120	0.39	105.0	780	1860	0.39
346.0	2780	6430	0.39	105.5	850	1960	0.39
347.7	2360	6430	0.42	106.0	720	1960	0.42
349.3	2140	6090	0.43	106.5	650	1860	0.43
351.0	1980	5830	0.44	107.0	600	1780	0.44
352.6	1850	5650	0.44	107.5	560	1720	0.44
354.2	1960	5780	0.44	108.0	600	1760	0.44
355.9	2060	6090	0.44	108.5	630	1860	0.44
357.5	2350	6390	0.42	109.0	720	1950	0.42
359.2	2310	6360	0.42	109.5	700	1940	0.42
360.8	2260	6390	0.43	110.0	690	1950	0.43
362.4	2280	6300	0.42	110.5	690	1920	0.42
364.1	2420	6330	0.41	111.0	740	1930	0.41
365.7	2710	6810	0.41	111.5	820	2070	0.41
367.4	2930	7280	0.40	112.0	890	2220	0.40
369.0	3210	7670	0.39	112.5	980	2340	0.39
370.6	3210	7720	0.40	113.0	980	2350	0.40
372.3	3060	7450	0.40	113.5	930	2270	0.40
373.9	2850	6990	0.40	114.0	870	2130	0.40
375.6	2670	6770	0.41	114.5	810	2060	0.41
377.2	2560	6590	0.41	115.0	780	2010	0.41
378.9	2420	6560	0.42	115.5	740	2000	0.42
380.5	2240	6590	0.43	116.0	680	2010	0.43
382.1	1940	6210	0.45	116.5	590	1890	0.45
383.8	1700	5940	0.46	117.0	520	1810	0.46
385.4	1510	5580	0.46	117.5	460	1700	0.46
386.7	1330	5320	0.47	117.9	400	1620	0.47
388.7	1330	5340	0.47	118.5	410	1630	0.47
390.3	1370	5340	0.46	119.0	420	1630	0.46
392.0	1440	5410	0.46	119.5	440	1650	0.46
393.6	1460	5550	0.46	120.0	440	1690	0.46
395.3	1490	5580	0.46	120.5	450	1700	0.46
396.9	1530	5530	0.46	121.0	460	1690	0.46
398.5	1540	5680	0.46	121.5	470	1730	0.46
400.2	1580	5730	0.46	122.0	480	1750	0.46
401.8	1640	5780	0.46	122.5	500	1760	0.46
403.5	1660	5860	0.46	123.0	510	1790	0.46
405.1	1710	5860	0.45	123.5	520	1790	0.45

**Summary of Compressional Wave Velocity, Shear Wave Velocity, and Poisson's Ratio  
Based on Source-to-Receiver Travel Time Data - Borehole B-FMG**

American Units				Metric Units			
Depth at Midpoint Between Source and Near Receiver	Velocity		Poisson's Ratio	Depth at Midpoint Between Source and Near Receiver	Velocity		Poisson's Ratio
	V <sub>s</sub>	V <sub>p</sub>			V <sub>s</sub>	V <sub>p</sub>	
(ft)	(ft/s)	(ft/s)		(m)	(m/s)	(m/s)	
406.7	1740	5860	0.45	124.0	530	1790	0.45
408.4	1720	5810	0.45	124.5	520	1770	0.45
410.0	1720	5920	0.45	125.0	520	1800	0.45
411.7	1730	5940	0.45	125.5	530	1810	0.45
413.3	1810	5940	0.45	126.0	550	1810	0.45
414.9	1890	6090	0.45	126.5	580	1860	0.45
416.6	1970	6060	0.44	127.0	600	1850	0.44
418.2	2020	6090	0.44	127.5	620	1860	0.44
419.9	2060	6300	0.44	128.0	630	1920	0.44
421.5	2160	6360	0.43	128.5	660	1940	0.43
423.1	2190	6490	0.44	129.0	670	1980	0.44
424.8	2250	6460	0.43	129.5	690	1970	0.43
426.4	2290	6730	0.43	130.0	700	2050	0.43
428.1	2240	6530	0.43	130.5	680	1990	0.43
429.7	2190	6460	0.44	131.0	670	1970	0.44
431.3	2200	6430	0.43	131.5	670	1960	0.43
433.0	2240	6300	0.43	132.0	680	1920	0.43
434.6	2210	6210	0.43	132.5	670	1890	0.43
436.3	2200	6270	0.43	133.0	670	1910	0.43
437.9	2210	6180	0.43	133.5	670	1880	0.43
439.5	2340	6090	0.41	134.0	710	1860	0.41
441.2	2530	6390	0.41	134.5	770	1950	0.41
442.8	2740	6880	0.41	135.0	840	2100	0.41
444.5	2890	6880	0.39	135.5	880	2100	0.39
446.1	2890	7030	0.40	136.0	880	2140	0.40
447.7	2500	6630	0.42	136.5	760	2020	0.42
449.4	2260	6150	0.42	137.0	690	1870	0.42
451.0	2160	6120	0.43	137.5	660	1860	0.43
452.7	2100	6090	0.43	138.0	640	1860	0.43
454.3	2090	6030	0.43	138.5	640	1840	0.43
456.0	2140	6060	0.43	139.0	650	1850	0.43
457.6	2140	6060	0.43	139.5	650	1850	0.43
458.9	2120	6090	0.43	139.9	650	1860	0.43
460.9	2120	5970	0.43	140.5	650	1820	0.43
462.5	2160	6000	0.43	141.0	660	1830	0.43
464.2	2160	6300	0.43	141.5	660	1920	0.43
465.8	2160	6210	0.43	142.0	660	1890	0.43
467.4	2180	6300	0.43	142.5	670	1920	0.43
469.1	2020	6180	0.44	143.0	610	1880	0.44
470.7	1790	5890	0.45	143.5	550	1790	0.45

**Summary of Compressional Wave Velocity, Shear Wave Velocity, and Poisson's Ratio  
Based on Source-to-Receiver Travel Time Data - Borehole B-FMG**

American Units				Metric Units			
Depth at Midpoint Between Source and Near Receiver	Velocity		Poisson's Ratio	Depth at Midpoint Between Source and Near Receiver	Velocity		Poisson's Ratio
	V <sub>s</sub>	V <sub>p</sub>			V <sub>s</sub>	V <sub>p</sub>	
(ft)	(ft/s)	(ft/s)		(m)	(m/s)	(m/s)	
472.4	1600	5600	0.46	144.0	490	1710	0.46
474.0	1620	5600	0.45	144.5	490	1710	0.45
475.6	1680	5630	0.45	145.0	510	1720	0.45
477.3	1710	5630	0.45	145.5	520	1720	0.45
478.6	1740	5650	0.45	145.9	530	1720	0.45
480.6	1740	5600	0.45	146.5	530	1710	0.45
482.2	1740	5680	0.45	147.0	530	1730	0.45
483.8	1780	5730	0.45	147.5	540	1750	0.45
485.5	1770	5600	0.44	148.0	540	1710	0.44
487.1	1710	5550	0.45	148.5	520	1690	0.45
488.8	1610	5390	0.45	149.0	490	1640	0.45
490.4	1630	5360	0.45	149.5	500	1640	0.45
492.0	1580	5360	0.45	150.0	480	1640	0.45
493.7	1580	5430	0.45	150.5	480	1660	0.45
495.3	1590	5360	0.45	151.0	490	1640	0.45
497.0	1560	5430	0.46	151.5	480	1660	0.46
498.6	1570	5460	0.45	152.0	480	1660	0.45
500.2	1580	5580	0.46	152.5	480	1700	0.46
501.9	1590	5630	0.46	153.0	480	1720	0.46
503.5	1680	5680	0.45	153.5	510	1730	0.45
505.2	1680	5630	0.45	154.0	510	1720	0.45
506.8	1770	5920	0.45	154.5	540	1800	0.45
508.4	1850	6090	0.45	155.0	560	1860	0.45
510.1	2040	6210	0.44	155.5	620	1890	0.44
511.7	2080	6390	0.44	156.0	630	1950	0.44
513.4	2010	6270	0.44	156.5	610	1910	0.44
515.0	2020	6090	0.44	157.0	620	1860	0.44
516.6	2060	6090	0.44	157.5	630	1860	0.44
518.3	2290	6560	0.43	158.0	700	2000	0.43
519.9	2470	6920	0.43	158.5	750	2110	0.43
521.6	2590	7230	0.43	159.0	790	2210	0.43
523.2	2470	7450	0.44	159.5	750	2270	0.44
524.8	2360	7110	0.44	160.0	720	2170	0.44
526.5	2120	6730	0.45	160.5	650	2050	0.45
528.1	2080	6390	0.44	161.0	630	1950	0.44
529.8	2100	6360	0.44	161.5	640	1940	0.44
531.4	2060	6360	0.44	162.0	630	1940	0.44
533.1	1980	6240	0.44	162.5	600	1900	0.44
534.7	1920	6150	0.45	163.0	580	1870	0.45
536.3	1830	6060	0.45	163.5	560	1850	0.45

**Summary of Compressional Wave Velocity, Shear Wave Velocity, and Poisson's Ratio  
Based on Source-to-Receiver Travel Time Data - Borehole B-FMG**

American Units				Metric Units			
Depth at Midpoint Between Source and Near Receiver	Velocity		Poisson's Ratio	Depth at Midpoint Between Source and Near Receiver	Velocity		Poisson's Ratio
	V <sub>s</sub>	V <sub>p</sub>			V <sub>s</sub>	V <sub>p</sub>	
(ft)	(ft/s)	(ft/s)		(m)	(m/s)	(m/s)	
538.0	1830	6000	0.45	164.0	560	1830	0.45
539.6	1790	5920	0.45	164.5	550	1800	0.45
541.3	1800	5940	0.45	165.0	550	1810	0.45
542.9	1850	5940	0.45	165.5	560	1810	0.45
544.5	1780	6000	0.45	166.0	540	1830	0.45
546.2	1710	5940	0.45	166.5	520	1810	0.45
547.8	1780	5920	0.45	167.0	540	1800	0.45
549.5	1880	6300	0.45	167.5	570	1920	0.45
551.1	2030	6810	0.45	168.0	620	2070	0.45
552.7	2270	7540	0.45	168.5	690	2300	0.45
554.4	2220	7190	0.45	169.0	680	2190	0.45
556.0	2040	6810	0.45	169.5	620	2070	0.45
557.7	1960	6390	0.45	170.0	600	1950	0.45
559.3	1960	6150	0.44	170.5	600	1870	0.44
560.9	1780	5860	0.45	171.0	540	1790	0.45
562.6	2000	6300	0.44	171.5	610	1920	0.44
564.2	2070	6590	0.45	172.0	630	2010	0.45
565.9	2080	6490	0.44	172.5	630	1980	0.44
567.5	2040	6270	0.44	173.0	620	1910	0.44
569.1	1920	6180	0.45	173.5	580	1880	0.45
570.8	1760	6060	0.45	174.0	540	1850	0.45
572.4	1710	6000	0.46	174.5	520	1830	0.46
574.1	1710	6030	0.46	175.0	520	1840	0.46
575.7	1760	6060	0.45	175.5	540	1850	0.45
577.3	1720	6060	0.46	176.0	520	1850	0.46
579.0	1790	6000	0.45	176.5	550	1830	0.45
580.6	2000	6300	0.44	177.0	610	1920	0.44
582.3	2300	7150	0.44	177.5	700	2180	0.44
583.9	2550	7360	0.43	178.0	780	2240	0.43
585.5	2390	7150	0.44	178.5	730	2180	0.44
587.2	2230	6810	0.44	179.0	680	2070	0.44
588.8	2040	6060	0.44	179.5	620	1850	0.44
590.5	1870	5860	0.44	180.0	570	1790	0.44
592.1	1820	5890	0.45	180.5	550	1790	0.45
593.7	1770	5920	0.45	181.0	540	1800	0.45
595.4	1660	5810	0.46	181.5	510	1770	0.46
597.0	1700	5890	0.45	182.0	520	1790	0.45
598.7	1750	5890	0.45	182.5	530	1790	0.45
600.3	1800	5890	0.45	183.0	550	1790	0.45
601.9	1870	5970	0.45	183.5	570	1820	0.45

**Summary of Compressional Wave Velocity, Shear Wave Velocity, and Poisson's Ratio  
Based on Source-to-Receiver Travel Time Data - Borehole B-FMG**

<b>American Units</b>			
<b>Depth at Midpoint Between Source and Near Receiver</b>	<b>Velocity</b>		<b>Poisson's Ratio</b>
	<b>V<sub>s</sub></b>	<b>V<sub>p</sub></b>	
(ft)	(ft/s)	(ft/s)	

<b>Metric Units</b>			
<b>Depth at Midpoint Between Source and Near Receiver</b>	<b>Velocity</b>		<b>Poisson's Ratio</b>
	<b>V<sub>s</sub></b>	<b>V<sub>p</sub></b>	
(m)	(m/s)	(m/s)	

## SCDOT CONWAY BORINGS HOR-1328 & OFFSET Source to Receiver and Receiver to Receiver Analysis

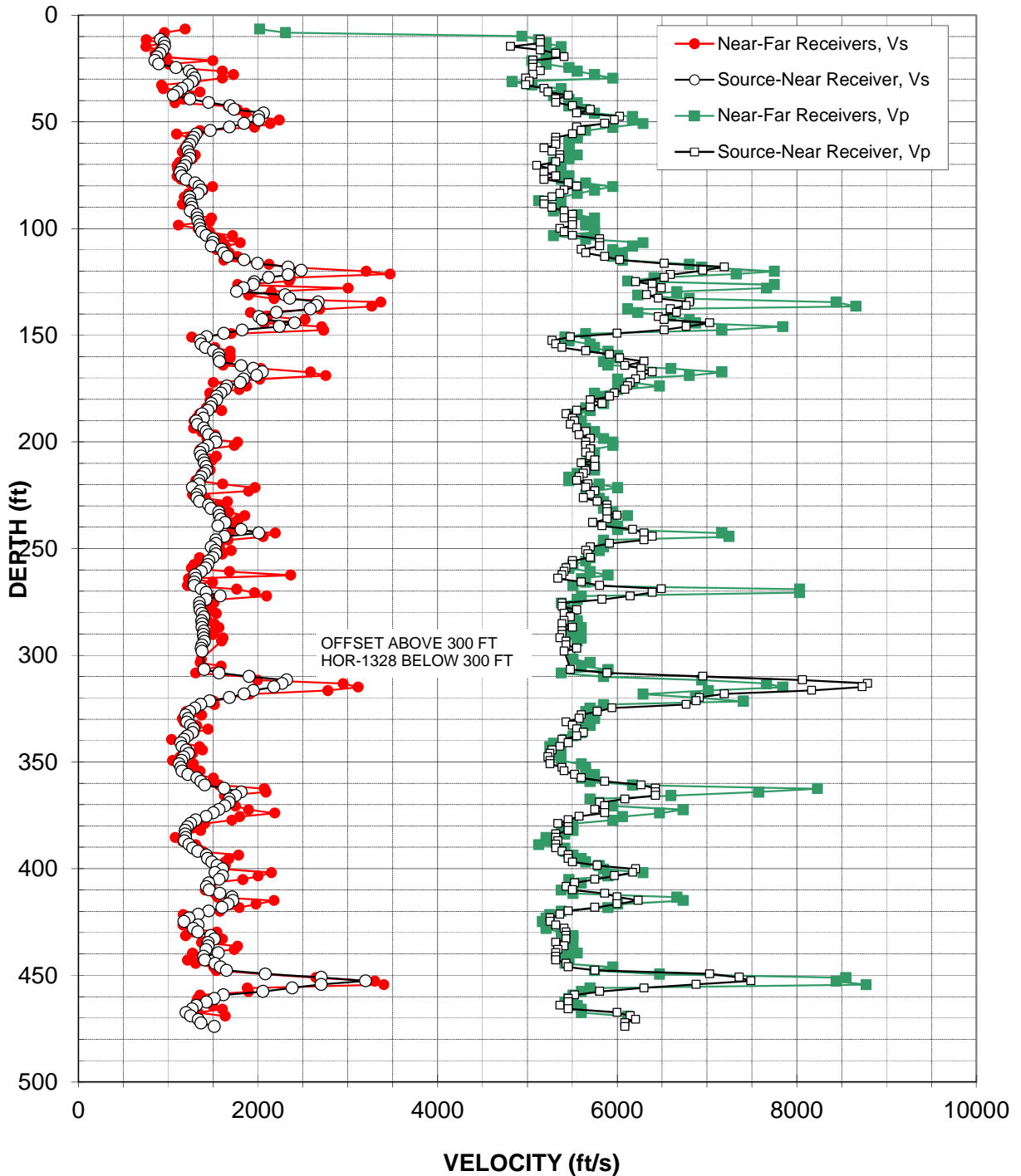


Figure A-2: Boreholes HOR-1328 & Conway Offset, Suspension S-R1 P- and  $S_H$ -wave velocities

Table A-2. Boreholes HOR-1328 & Conway Offset, S - R1 quality assurance analysis P- and S<sub>H</sub>-wave data

**Summary of Compressional Wave Velocity, Shear Wave Velocity, and Poisson's Ratio  
Based on Source-to-Receiver Travel Time Data - Borehole HOR-1328 COMBINED WITH OFFSET**

American Units				Metric Units			
Depth at Midpoint Between Source and Near Receiver	Velocity		Poisson's Ratio	Depth at Midpoint Between Source and Near Receiver	Velocity		Poisson's Ratio
	V <sub>s</sub>	V <sub>p</sub>			V <sub>s</sub>	V <sub>p</sub>	
(ft)	(ft/s)	(ft/s)		(m)	(m/s)	(m/s)	
11.4	910	5150	0.48	3.5	280	1570	0.48
13.0	950	5150	0.48	4.0	290	1570	0.48
14.7	960	4810	0.48	4.5	290	1470	0.48
16.3	940	5150	0.48	5.0	290	1570	0.48
18.0	910	5320	0.48	5.5	280	1620	0.48
19.6	870	5410	0.49	6.0	270	1650	0.49
21.2	850	5060	0.49	6.5	260	1540	0.49
22.9	890	5060	0.48	7.0	270	1540	0.48
24.5	1090	5060	0.48	7.5	330	1540	0.48
26.2	1230	5150	0.47	8.0	380	1570	0.47
27.8	1270	5060	0.47	8.5	390	1540	0.47
29.4	1290	4980	0.46	9.0	390	1520	0.46
31.1	1270	5020	0.47	9.5	390	1530	0.47
32.7	1210	4980	0.47	10.0	370	1520	0.47
34.4	1150	5190	0.47	10.5	350	1580	0.47
36.0	1100	5230	0.48	11.0	340	1590	0.48
37.6	1060	5460	0.48	11.5	320	1660	0.48
39.3	1240	5320	0.47	12.0	380	1620	0.47
40.9	1450	5320	0.46	12.5	440	1620	0.46
42.6	1690	5500	0.45	13.0	510	1680	0.45
44.2	1730	5700	0.45	13.5	530	1740	0.45
45.8	2060	5550	0.42	14.0	630	1690	0.42
47.5	2010	6030	0.44	14.5	610	1840	0.44
49.1	2010	5970	0.44	15.0	610	1820	0.44
50.8	1850	5860	0.44	15.5	560	1790	0.44
52.4	1680	5550	0.45	16.0	510	1690	0.45
54.0	1470	5600	0.46	16.5	450	1710	0.46
55.7	1310	5500	0.47	17.0	400	1680	0.47
57.3	1280	5320	0.47	17.5	390	1620	0.47
59.0	1260	5320	0.47	18.0	390	1620	0.47
60.6	1240	5320	0.47	18.5	380	1620	0.47
62.2	1210	5190	0.47	19.0	370	1580	0.47
63.9	1220	5280	0.47	19.5	370	1610	0.47
65.5	1240	5360	0.47	20.0	380	1640	0.47
67.2	1240	5360	0.47	20.5	380	1640	0.47
68.8	1200	5320	0.47	21.0	370	1620	0.47
70.5	1190	5100	0.47	21.5	360	1560	0.47

**Summary of Compressional Wave Velocity, Shear Wave Velocity, and Poisson's Ratio  
Based on Source-to-Receiver Travel Time Data - Borehole HOR-1328 COMBINED WITH OFFSET**

American Units				Metric Units			
Depth at Midpoint Between Source and Near Receiver	Velocity		Poisson's Ratio	Depth at Midpoint Between Source and Near Receiver	Velocity		Poisson's Ratio
	V <sub>s</sub>	V <sub>p</sub>			V <sub>s</sub>	V <sub>p</sub>	
(ft)	(ft/s)	(ft/s)		(m)	(m/s)	(m/s)	
72.1	1150	5280	0.48	22.0	350	1610	0.48
73.7	1130	5190	0.47	22.5	350	1580	0.47
75.4	1150	5320	0.48	23.0	350	1620	0.48
77.0	1200	5190	0.47	23.5	370	1580	0.47
78.7	1300	5460	0.47	24.0	400	1660	0.47
80.3	1340	5550	0.47	24.5	410	1690	0.47
81.9	1370	5410	0.47	25.0	420	1650	0.47
83.6	1330	5360	0.47	25.5	410	1640	0.47
85.2	1240	5280	0.47	26.0	380	1610	0.47
86.9	1240	5190	0.47	26.5	380	1580	0.47
88.5	1260	5190	0.47	27.0	380	1580	0.47
90.1	1260	5280	0.47	27.5	390	1610	0.47
91.8	1250	5410	0.47	28.0	380	1650	0.47
93.4	1320	5500	0.47	28.5	400	1680	0.47
95.1	1330	5410	0.47	29.0	400	1650	0.47
96.7	1330	5500	0.47	29.5	410	1680	0.47
98.3	1350	5500	0.47	30.0	410	1680	0.47
100.0	1360	5360	0.47	30.5	410	1640	0.47
101.6	1370	5410	0.47	31.0	420	1650	0.47
103.3	1420	5500	0.46	31.5	430	1680	0.46
104.9	1500	5810	0.46	32.0	460	1770	0.46
106.5	1500	5810	0.46	32.5	460	1770	0.46
108.2	1480	5810	0.47	33.0	450	1770	0.47
109.8	1590	5600	0.46	33.5	490	1710	0.46
111.5	1620	5650	0.46	34.0	490	1720	0.46
113.1	1660	5860	0.46	34.5	510	1790	0.46
114.7	1850	6030	0.45	35.0	560	1840	0.45
116.4	2000	6530	0.45	35.5	610	1990	0.45
118.0	2340	7190	0.44	36.0	710	2190	0.44
119.7	2480	6960	0.43	36.5	760	2120	0.43
121.6	2340	6590	0.43	37.1	710	2010	0.43
122.9	2120	6530	0.44	37.5	650	1990	0.44
124.9	1960	6210	0.44	38.1	600	1890	0.44
126.2	1950	6390	0.45	38.5	590	1950	0.45
127.9	1840	6490	0.46	39.0	560	1980	0.46
129.5	1760	6390	0.46	39.5	540	1950	0.46
131.1	2300	6330	0.42	40.0	700	1930	0.42
132.8	2350	6460	0.42	40.5	720	1970	0.42
134.4	2670	6810	0.41	41.0	810	2070	0.41
136.1	2650	6770	0.41	41.5	810	2060	0.41

**Summary of Compressional Wave Velocity, Shear Wave Velocity, and Poisson's Ratio  
Based on Source-to-Receiver Travel Time Data - Borehole HOR-1328 COMBINED WITH OFFSET**

American Units				Metric Units			
Depth at Midpoint Between Source and Near Receiver	Velocity		Poisson's Ratio	Depth at Midpoint Between Source and Near Receiver	Velocity		Poisson's Ratio
	V <sub>s</sub>	V <sub>p</sub>			V <sub>s</sub>	V <sub>p</sub>	
(ft)	(ft/s)	(ft/s)		(m)	(m/s)	(m/s)	
137.7	2580	6590	0.41	42.0	790	2010	0.41
139.3	2210	6660	0.44	42.5	670	2030	0.44
141.3	2010	6460	0.45	43.1	610	1970	0.45
142.6	2050	6530	0.45	43.5	620	1990	0.45
144.3	2410	7030	0.43	44.0	730	2140	0.43
145.9	2240	6770	0.44	44.5	680	2060	0.44
147.6	1820	6530	0.46	45.0	560	1990	0.46
149.2	1620	6000	0.46	45.5	490	1830	0.46
150.8	1430	5480	0.46	46.0	440	1670	0.46
152.5	1360	5280	0.46	46.5	410	1610	0.46
154.1	1370	5320	0.46	47.0	420	1620	0.46
155.8	1420	5390	0.46	47.5	430	1640	0.46
157.4	1500	5650	0.46	48.0	460	1720	0.46
159.0	1560	5920	0.46	48.5	480	1800	0.46
160.7	1560	6030	0.46	49.0	480	1840	0.46
162.3	1570	6300	0.47	49.5	480	1920	0.47
164.3	1810	6090	0.45	50.1	550	1860	0.45
165.6	1950	6270	0.45	50.5	590	1910	0.45
167.2	2050	6390	0.44	51.0	620	1950	0.44
168.9	1980	6270	0.44	51.5	600	1910	0.44
170.5	1840	6210	0.45	52.0	560	1890	0.45
172.2	1800	6150	0.45	52.5	550	1870	0.45
173.8	1650	6120	0.46	53.0	500	1860	0.46
175.4	1640	6090	0.46	53.5	500	1860	0.46
177.1	1590	5970	0.46	54.0	480	1820	0.46
178.7	1540	5920	0.46	54.5	470	1800	0.46
180.4	1540	5700	0.46	55.0	470	1740	0.46
182.0	1480	5830	0.47	55.5	450	1780	0.47
183.6	1480	5700	0.46	56.0	450	1740	0.46
185.3	1440	5550	0.46	56.5	440	1690	0.46
186.9	1380	5430	0.47	57.0	420	1660	0.47
188.9	1390	5500	0.47	57.6	420	1680	0.47
190.2	1310	5530	0.47	58.0	400	1690	0.47
191.8	1330	5480	0.47	58.5	400	1670	0.47
193.5	1400	5550	0.47	59.0	430	1690	0.47
195.1	1420	5650	0.47	59.5	430	1720	0.47
196.8	1450	5580	0.46	60.0	440	1700	0.46
198.4	1530	5700	0.46	60.5	460	1740	0.46
200.0	1530	5650	0.46	61.0	470	1720	0.46
201.7	1440	5650	0.47	61.5	440	1720	0.47

**Summary of Compressional Wave Velocity, Shear Wave Velocity, and Poisson's Ratio  
Based on Source-to-Receiver Travel Time Data - Borehole HOR-1328 COMBINED WITH OFFSET**

American Units				Metric Units			
Depth at Midpoint Between Source and Near Receiver	Velocity		Poisson's Ratio	Depth at Midpoint Between Source and Near Receiver	Velocity		Poisson's Ratio
	V <sub>s</sub>	V <sub>p</sub>			V <sub>s</sub>	V <sub>p</sub>	
(ft)	(ft/s)	(ft/s)		(m)	(m/s)	(m/s)	
203.3	1390	5700	0.47	62.0	420	1740	0.47
205.0	1360	5650	0.47	62.5	410	1720	0.47
206.6	1370	5700	0.47	63.0	420	1740	0.47
208.6	1400	5750	0.47	63.6	430	1750	0.47
209.9	1410	5600	0.47	64.0	430	1710	0.47
211.5	1420	5750	0.47	64.5	430	1750	0.47
213.5	1430	5650	0.47	65.1	440	1720	0.47
214.8	1400	5630	0.47	65.5	430	1720	0.47
216.4	1370	5580	0.47	66.0	420	1700	0.47
218.1	1340	5550	0.47	66.5	410	1690	0.47
219.7	1340	5680	0.47	67.0	410	1730	0.47
221.4	1270	5650	0.47	67.5	390	1720	0.47
223.0	1360	5750	0.47	68.0	410	1750	0.47
224.7	1320	5700	0.47	68.5	400	1740	0.47
226.3	1320	5630	0.47	69.0	400	1720	0.47
227.9	1350	5780	0.47	69.5	410	1760	0.47
229.6	1450	5890	0.47	70.0	440	1790	0.47
231.2	1480	5890	0.47	70.5	450	1790	0.47
232.9	1560	5890	0.46	71.0	480	1790	0.46
234.5	1570	6000	0.46	71.5	480	1830	0.46
236.1	1590	5890	0.46	72.0	480	1790	0.46
237.8	1640	5730	0.46	72.5	500	1750	0.46
239.4	1560	5830	0.46	73.0	470	1780	0.46
241.1	1810	6180	0.45	73.5	550	1880	0.45
242.7	2010	6300	0.44	74.0	610	1920	0.44
244.3	1630	6390	0.47	74.5	500	1950	0.47
246.0	1530	6300	0.47	75.0	470	1920	0.47
247.6	1530	5920	0.46	75.5	470	1800	0.46
249.3	1480	5700	0.46	76.0	450	1740	0.46
250.9	1530	5650	0.46	76.5	460	1720	0.46
252.5	1530	5680	0.46	77.0	470	1730	0.46
254.2	1500	5700	0.46	77.5	460	1740	0.46
255.8	1460	5500	0.46	78.0	440	1680	0.46
257.5	1440	5500	0.46	78.5	440	1680	0.46
259.1	1420	5430	0.46	79.0	430	1660	0.46
260.7	1370	5410	0.47	79.5	420	1650	0.47
262.4	1300	5390	0.47	80.0	400	1640	0.47
264.0	1310	5340	0.47	80.5	400	1630	0.47
265.7	1290	5600	0.47	81.0	390	1710	0.47
267.3	1290	5810	0.47	81.5	390	1770	0.47

**Summary of Compressional Wave Velocity, Shear Wave Velocity, and Poisson's Ratio  
Based on Source-to-Receiver Travel Time Data - Borehole HOR-1328 COMBINED WITH OFFSET**

American Units			
Depth at Midpoint Between Source and Near Receiver	Velocity		Poisson's Ratio
	V <sub>s</sub>	V <sub>p</sub>	
(ft)	(ft/s)	(ft/s)	
268.9	1370	6490	0.48
270.6	1420	6390	0.47
272.2	1580	6150	0.46
273.9	1420	5830	0.47
275.5	1350	5390	0.47
277.1	1350	5390	0.47
278.8	1360	5550	0.47
280.4	1380	5410	0.47
282.1	1400	5480	0.47
283.7	1370	5410	0.47
285.3	1380	5390	0.46
287.0	1380	5500	0.47
288.6	1400	5390	0.46
290.3	1390	5390	0.46
291.9	1400	5360	0.46
293.5	1400	5430	0.46
295.2	1380	5430	0.47
296.8	1370	5550	0.47
298.1	1380	5410	0.47
306.7	1400	5480	0.46
308.3	1570	5890	0.46
310.0	1900	6960	0.46
311.6	2320	8060	0.45
313.2	2270	8790	0.46
314.9	2180	8730	0.47
316.5	1950	8170	0.47
318.2	1850	7190	0.46
319.8	1680	6920	0.47
321.4	1460	6880	0.48
323.1	1360	6770	0.48
324.7	1300	5940	0.47
326.4	1240	5780	0.48
328.0	1190	5600	0.48
329.6	1220	5580	0.47
331.3	1210	5430	0.47
332.9	1250	5500	0.47
334.6	1280	5550	0.47
336.2	1270	5630	0.47
337.8	1210	5550	0.47
339.5	1180	5390	0.47

Metric Units			
Depth at Midpoint Between Source and Near Receiver	Velocity		Poisson's Ratio
	V <sub>s</sub>	V <sub>p</sub>	
(m)	(m/s)	(m/s)	
82.0	420	1980	0.48
82.5	430	1950	0.47
83.0	480	1870	0.46
83.5	430	1780	0.47
84.0	410	1640	0.47
84.5	410	1640	0.47
85.0	410	1690	0.47
85.5	420	1650	0.47
86.0	430	1670	0.47
86.5	420	1650	0.47
87.0	420	1640	0.46
87.5	420	1680	0.47
88.0	430	1640	0.46
88.5	420	1640	0.46
89.0	430	1640	0.46
89.5	430	1660	0.46
90.0	420	1660	0.47
90.5	420	1690	0.47
90.9	420	1650	0.47
93.5	430	1670	0.46
94.0	480	1790	0.46
94.5	580	2120	0.46
95.0	710	2460	0.45
95.5	690	2680	0.46
96.0	660	2660	0.47
96.5	590	2490	0.47
97.0	560	2190	0.46
97.5	510	2110	0.47
98.0	450	2100	0.48
98.5	410	2060	0.48
99.0	400	1810	0.47
99.5	380	1760	0.48
100.0	360	1710	0.48
100.5	370	1700	0.47
101.0	370	1660	0.47
101.5	380	1680	0.47
102.0	390	1690	0.47
102.5	390	1720	0.47
103.0	370	1690	0.47
103.5	360	1640	0.47

**Summary of Compressional Wave Velocity, Shear Wave Velocity, and Poisson's Ratio  
Based on Source-to-Receiver Travel Time Data - Borehole HOR-1328 COMBINED WITH OFFSET**

American Units				Metric Units			
Depth at Midpoint Between Source and Near Receiver	Velocity		Poisson's Ratio	Depth at Midpoint Between Source and Near Receiver	Velocity		Poisson's Ratio
	V <sub>s</sub>	V <sub>p</sub>			V <sub>s</sub>	V <sub>p</sub>	
(ft)	(ft/s)	(ft/s)		(m)	(m/s)	(m/s)	
341.1	1140	5460	0.48	104.0	350	1660	0.48
342.8	1160	5360	0.48	104.5	350	1640	0.48
344.4	1200	5280	0.47	105.0	370	1610	0.47
346.0	1230	5250	0.47	105.5	370	1600	0.47
347.7	1170	5230	0.47	106.0	360	1590	0.47
349.3	1150	5250	0.47	106.5	350	1600	0.47
351.0	1120	5250	0.48	107.0	340	1600	0.48
352.6	1140	5390	0.48	107.5	350	1640	0.48
354.2	1160	5410	0.48	108.0	350	1650	0.48
355.9	1220	5530	0.47	108.5	370	1690	0.47
357.5	1320	5600	0.47	109.0	400	1710	0.47
359.2	1360	5860	0.47	109.5	420	1790	0.47
360.8	1410	6270	0.47	110.0	430	1910	0.47
362.4	1620	6430	0.47	110.5	490	1960	0.47
364.1	1810	6430	0.46	111.0	550	1960	0.46
365.7	1750	6430	0.46	111.5	530	1960	0.46
367.4	1680	6090	0.46	112.0	510	1860	0.46
369.0	1680	5810	0.45	112.5	510	1770	0.45
370.6	1630	5860	0.46	113.0	500	1790	0.46
372.3	1570	5750	0.46	113.5	480	1750	0.46
373.9	1500	5860	0.46	114.0	460	1790	0.46
375.6	1420	5580	0.47	114.5	430	1700	0.47
377.2	1310	5460	0.47	115.0	400	1660	0.47
378.9	1250	5340	0.47	115.5	380	1630	0.47
380.5	1210	5460	0.47	116.0	370	1660	0.47
382.1	1190	5460	0.48	116.5	360	1660	0.48
383.8	1190	5320	0.47	117.0	360	1620	0.47
385.4	1190	5320	0.47	117.5	360	1620	0.47
387.1	1180	5340	0.47	118.0	360	1630	0.47
388.7	1230	5320	0.47	118.5	380	1620	0.47
390.3	1270	5320	0.47	119.0	390	1620	0.47
392.0	1330	5390	0.47	119.5	410	1640	0.47
393.6	1430	5460	0.46	120.0	430	1660	0.46
395.3	1440	5460	0.46	120.5	440	1660	0.46
396.9	1490	5500	0.46	121.0	450	1680	0.46
398.5	1540	5780	0.46	121.5	470	1760	0.46
400.2	1610	6210	0.46	122.0	490	1890	0.46
401.8	1520	6180	0.47	122.5	460	1880	0.47
403.5	1610	5970	0.46	123.0	490	1820	0.46
405.1	1570	5750	0.46	123.5	480	1750	0.46

**Summary of Compressional Wave Velocity, Shear Wave Velocity, and Poisson's Ratio  
Based on Source-to-Receiver Travel Time Data - Borehole HOR-1328 COMBINED WITH OFFSET**

American Units				Metric Units			
Depth at Midpoint Between Source and Near Receiver	Velocity		Poisson's Ratio	Depth at Midpoint Between Source and Near Receiver	Velocity		Poisson's Ratio
	V <sub>s</sub>	V <sub>p</sub>			V <sub>s</sub>	V <sub>p</sub>	
(ft)	(ft/s)	(ft/s)		(m)	(m/s)	(m/s)	
406.7	1450	5530	0.46	124.0	440	1690	0.46
408.4	1430	5430	0.46	124.5	430	1660	0.46
410.0	1460	5500	0.46	125.0	440	1680	0.46
411.7	1570	5860	0.46	125.5	480	1790	0.46
413.3	1710	6000	0.46	126.0	520	1830	0.46
414.9	1720	6240	0.46	126.5	520	1900	0.46
416.6	1670	6000	0.46	127.0	510	1830	0.46
418.2	1600	5750	0.46	127.5	490	1750	0.46
419.9	1450	5460	0.46	128.0	440	1660	0.46
421.5	1340	5360	0.47	128.5	410	1640	0.47
423.1	1230	5250	0.47	129.0	380	1600	0.47
424.8	1180	5250	0.47	129.5	360	1600	0.47
426.4	1330	5320	0.47	130.0	410	1620	0.47
428.1	1280	5410	0.47	130.5	390	1650	0.47
429.7	1330	5430	0.47	131.0	410	1660	0.47
431.3	1470	5430	0.46	131.5	450	1660	0.46
433.0	1510	5430	0.46	132.0	460	1660	0.46
434.6	1450	5320	0.46	132.5	440	1620	0.46
436.3	1450	5410	0.46	133.0	440	1650	0.46
437.9	1420	5340	0.46	133.5	430	1630	0.46
439.5	1560	5320	0.45	134.0	480	1620	0.45
441.2	1390	5320	0.46	134.5	420	1620	0.46
442.8	1410	5320	0.46	135.0	430	1620	0.46
444.5	1520	5430	0.46	135.5	460	1660	0.46
446.1	1580	5460	0.45	136.0	480	1660	0.45
447.7	1650	5750	0.46	136.5	500	1750	0.46
449.4	2080	7030	0.45	137.0	630	2140	0.45
451.0	2710	7360	0.42	137.5	820	2240	0.42
452.7	3200	7490	0.39	138.0	970	2280	0.39
454.3	2710	6880	0.41	138.5	820	2100	0.41
456.0	2380	6300	0.42	139.0	730	1920	0.42
457.6	2060	5810	0.43	139.5	630	1770	0.43
459.2	1610	5530	0.45	140.0	490	1690	0.45
460.9	1510	5460	0.46	140.5	460	1660	0.46
462.5	1430	5460	0.46	141.0	430	1660	0.46
464.2	1310	5360	0.47	141.5	400	1640	0.47
465.8	1270	5460	0.47	142.0	390	1660	0.47
467.4	1200	6000	0.48	142.5	370	1830	0.48
469.1	1250	6150	0.48	143.0	380	1870	0.48
470.7	1340	6210	0.48	143.5	410	1890	0.48

**Summary of Compressional Wave Velocity, Shear Wave Velocity, and Poisson's Ratio  
Based on Source-to-Receiver Travel Time Data - Borehole HOR-1328 COMBINED WITH OFFSET**

<b>American Units</b>			
<b>Depth at Midpoint Between Source and Near Receiver</b>	<b>Velocity</b>		<b>Poisson's Ratio</b>
	<b>V<sub>s</sub></b>	<b>V<sub>p</sub></b>	
(ft)	(ft/s)	(ft/s)	
472.4	1360	6090	0.47
474.0	1510	6090	0.47

<b>Metric Units</b>			
<b>Depth at Midpoint Between Source and Near Receiver</b>	<b>Velocity</b>		<b>Poisson's Ratio</b>
	<b>V<sub>s</sub></b>	<b>V<sub>p</sub></b>	
(m)	(m/s)	(m/s)	
144.0	420	1860	0.47
144.5	460	1860	0.47

## **APPENDIX B**

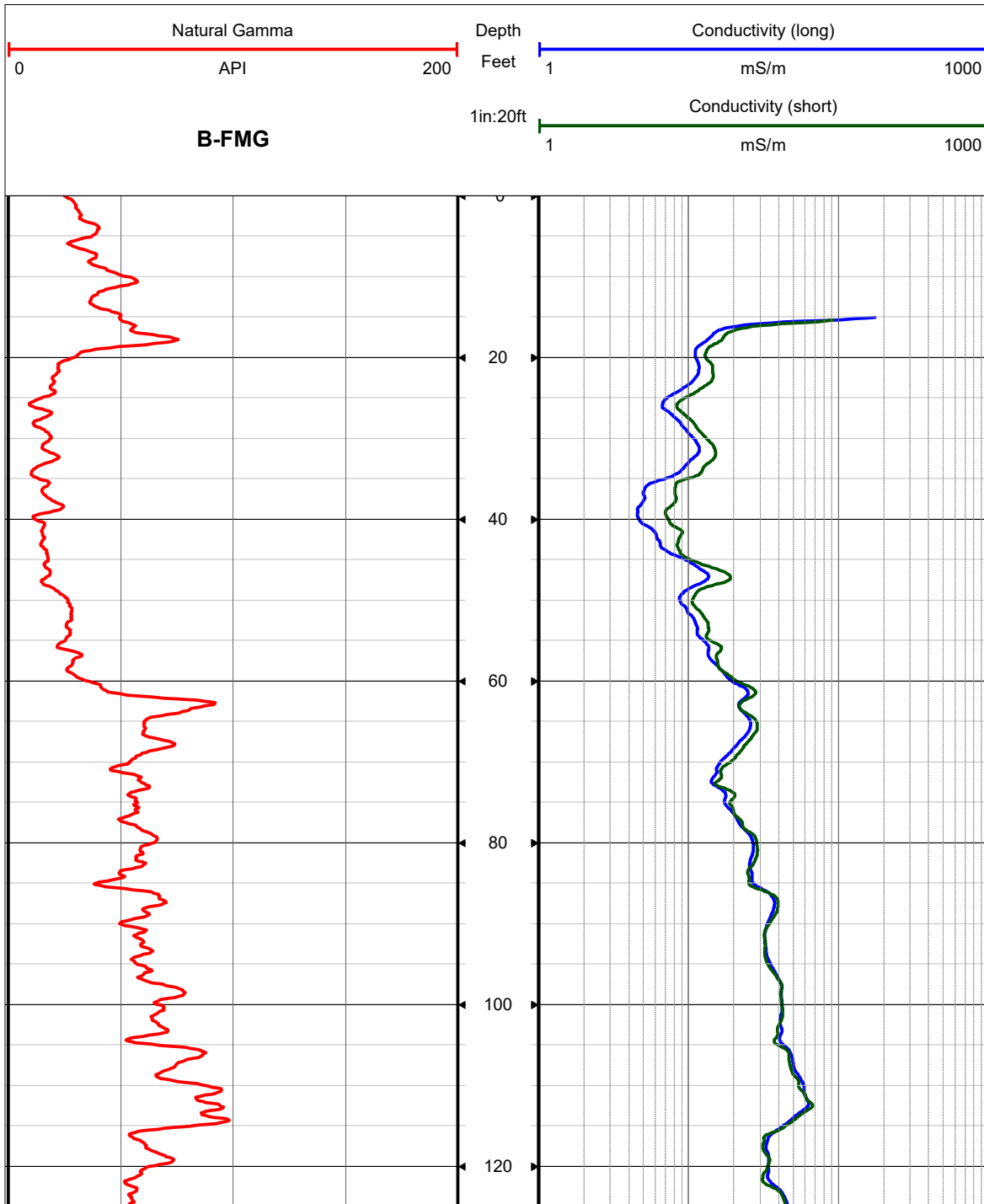
# **INDUCTION, ELOG, NATURAL GAMMA AND CALIPER LOGS**

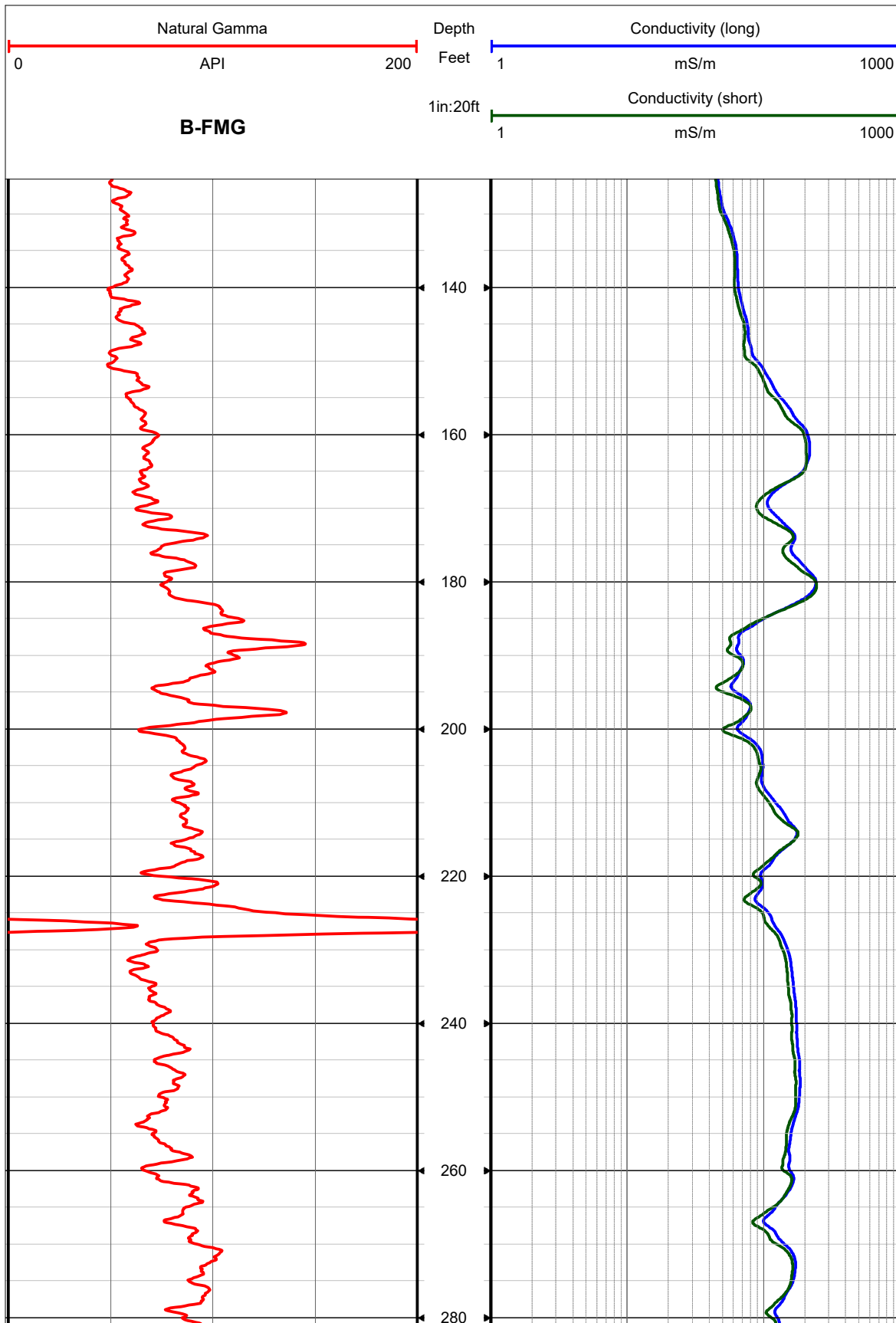


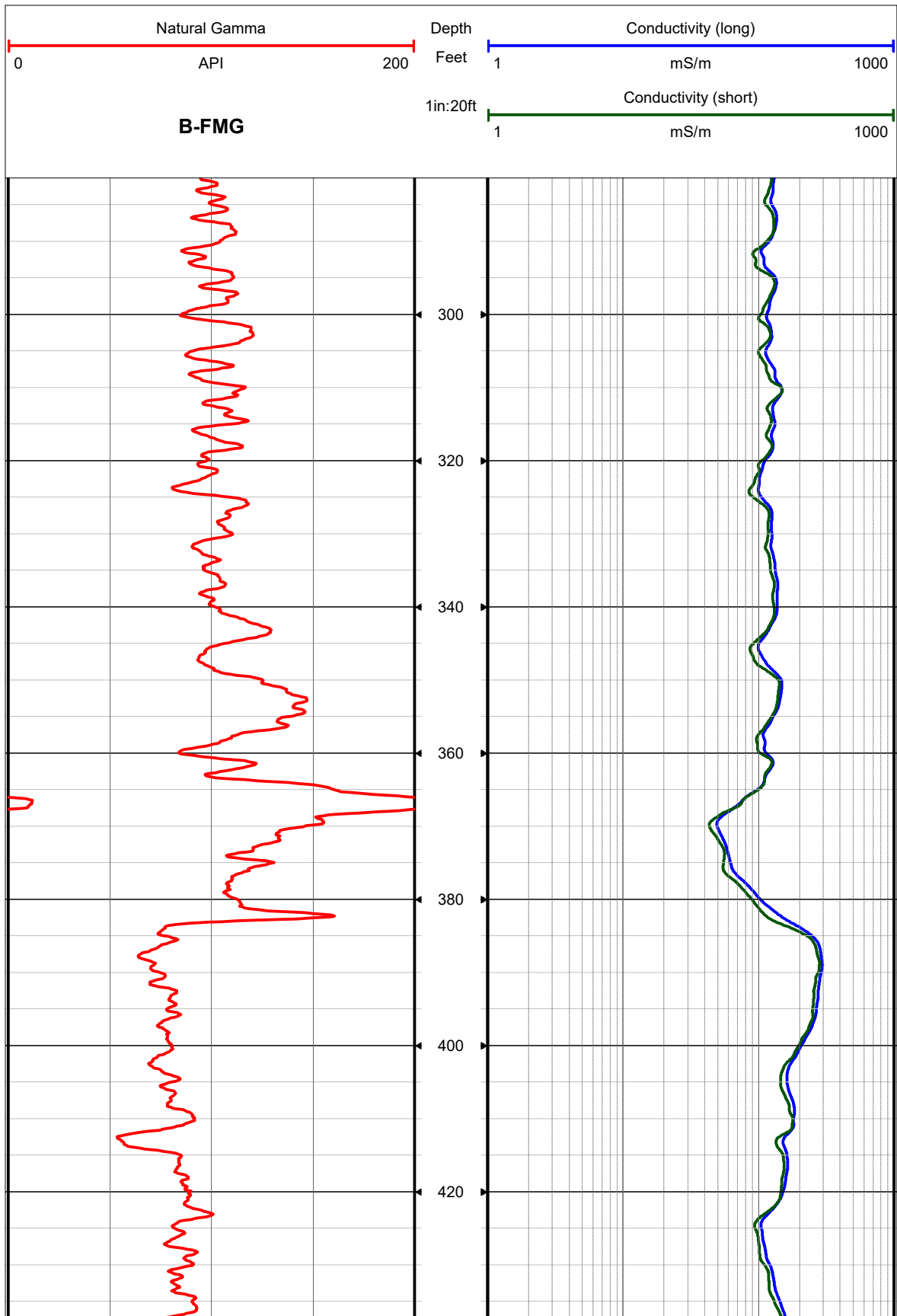
CLIENT S&ME

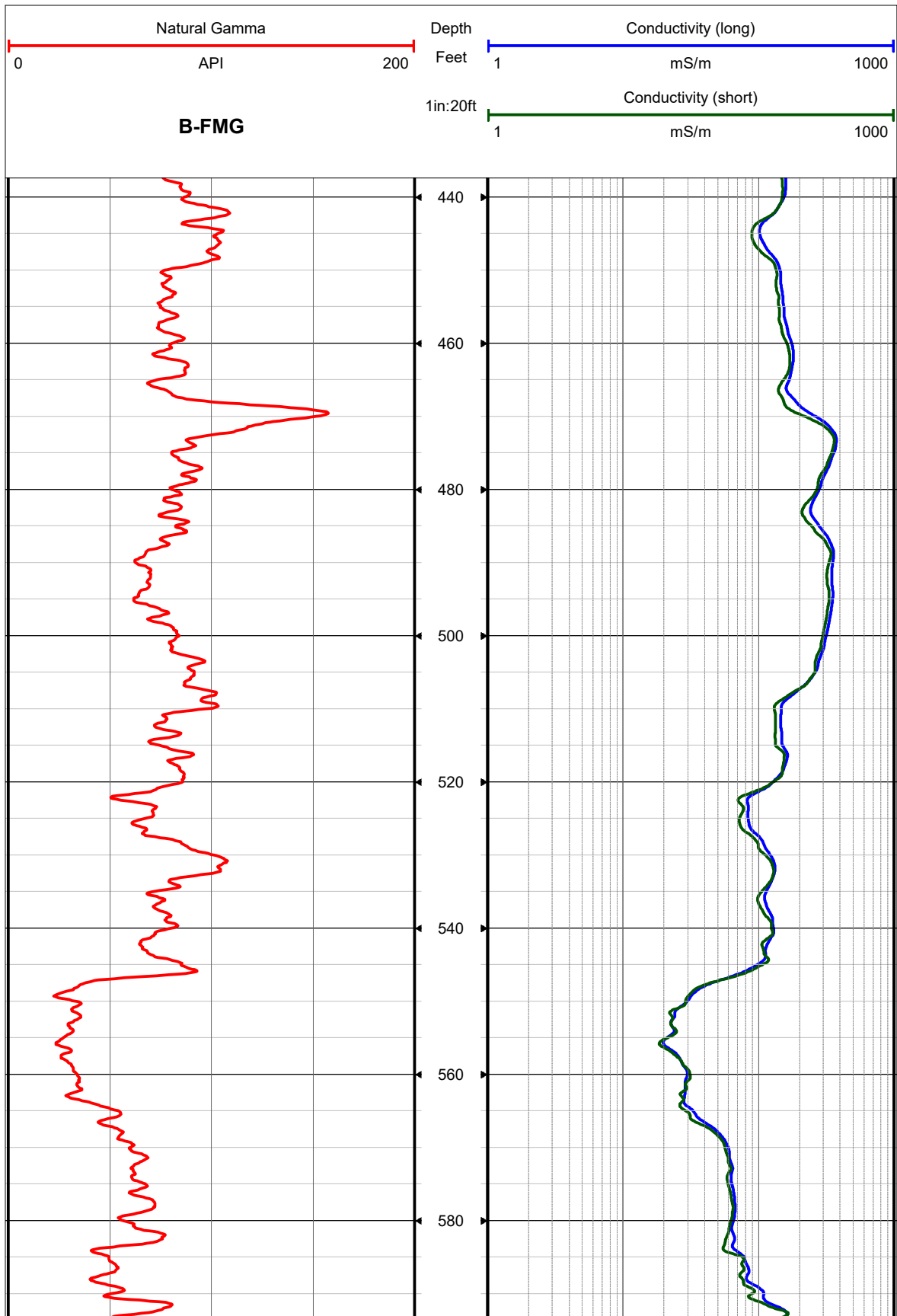
LOG TYPE  
Dual Induction

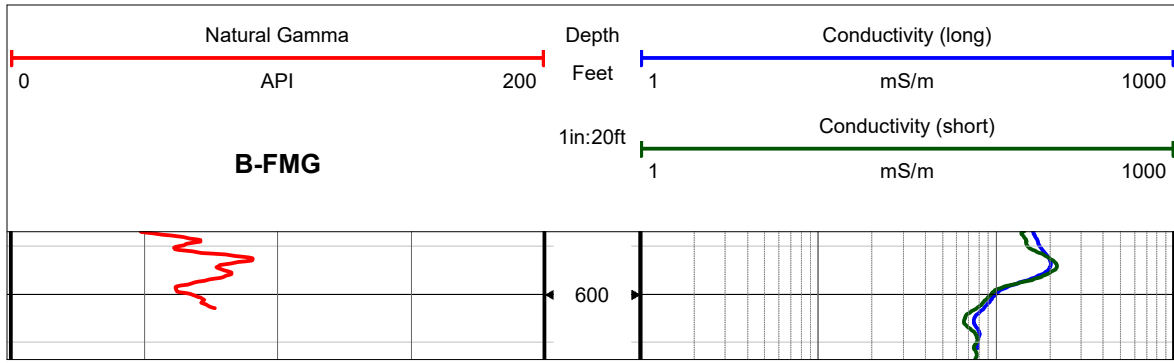
PROJECT Andrews / SCDOT  
WELL B-FMG  
LOCATION Andrews  
LOGGER J. Jordan  
DATE Feb. 26, 2017









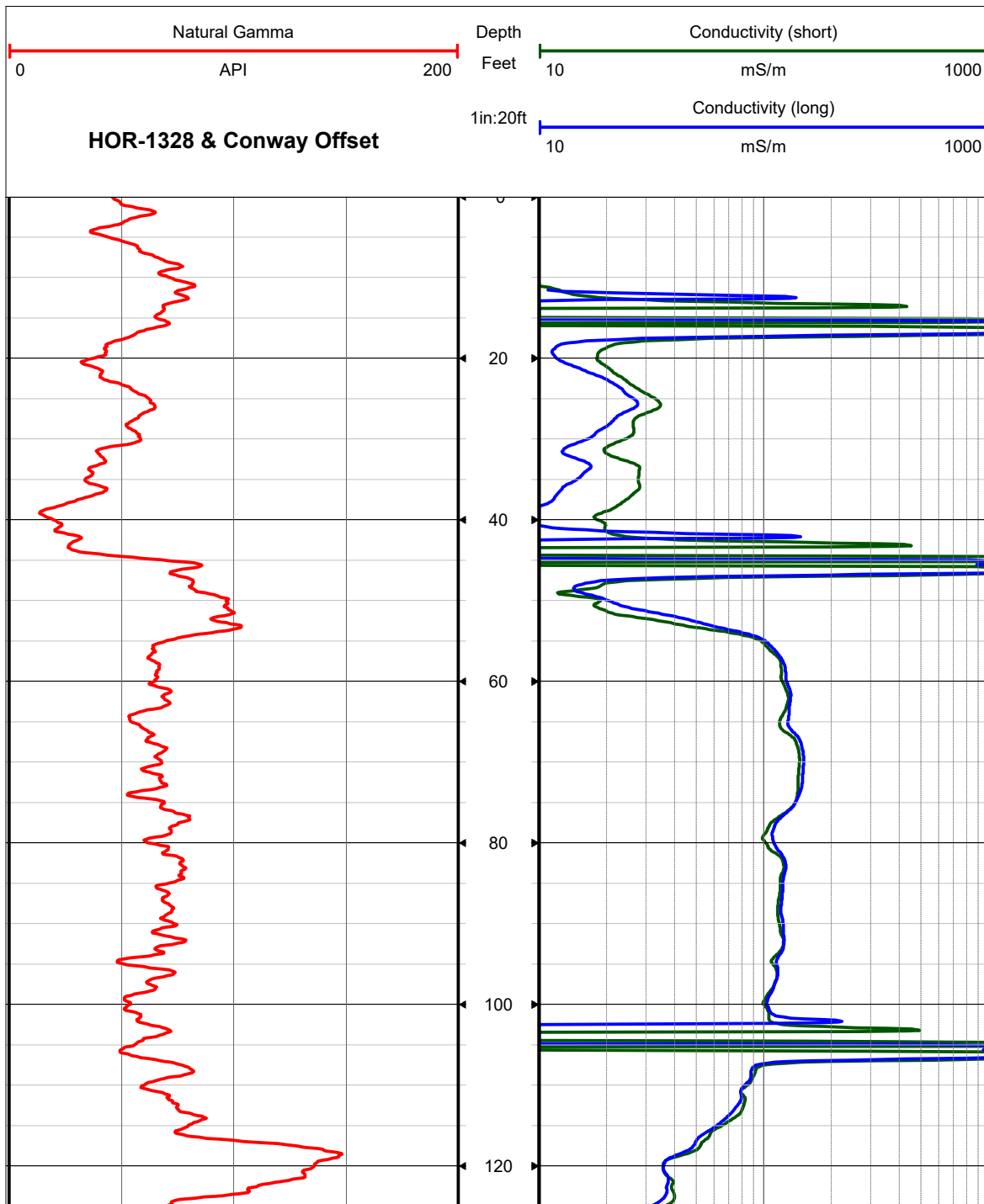


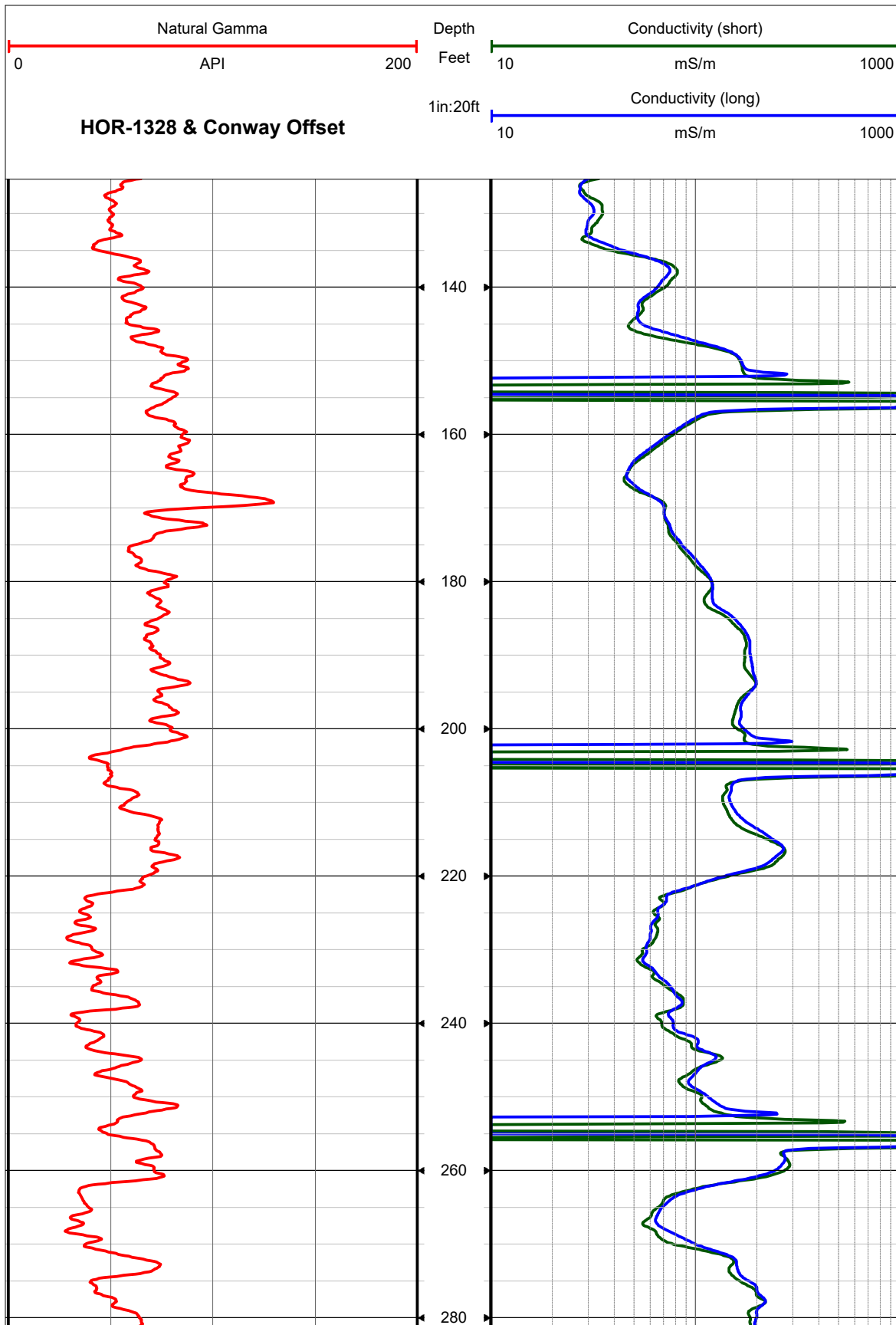


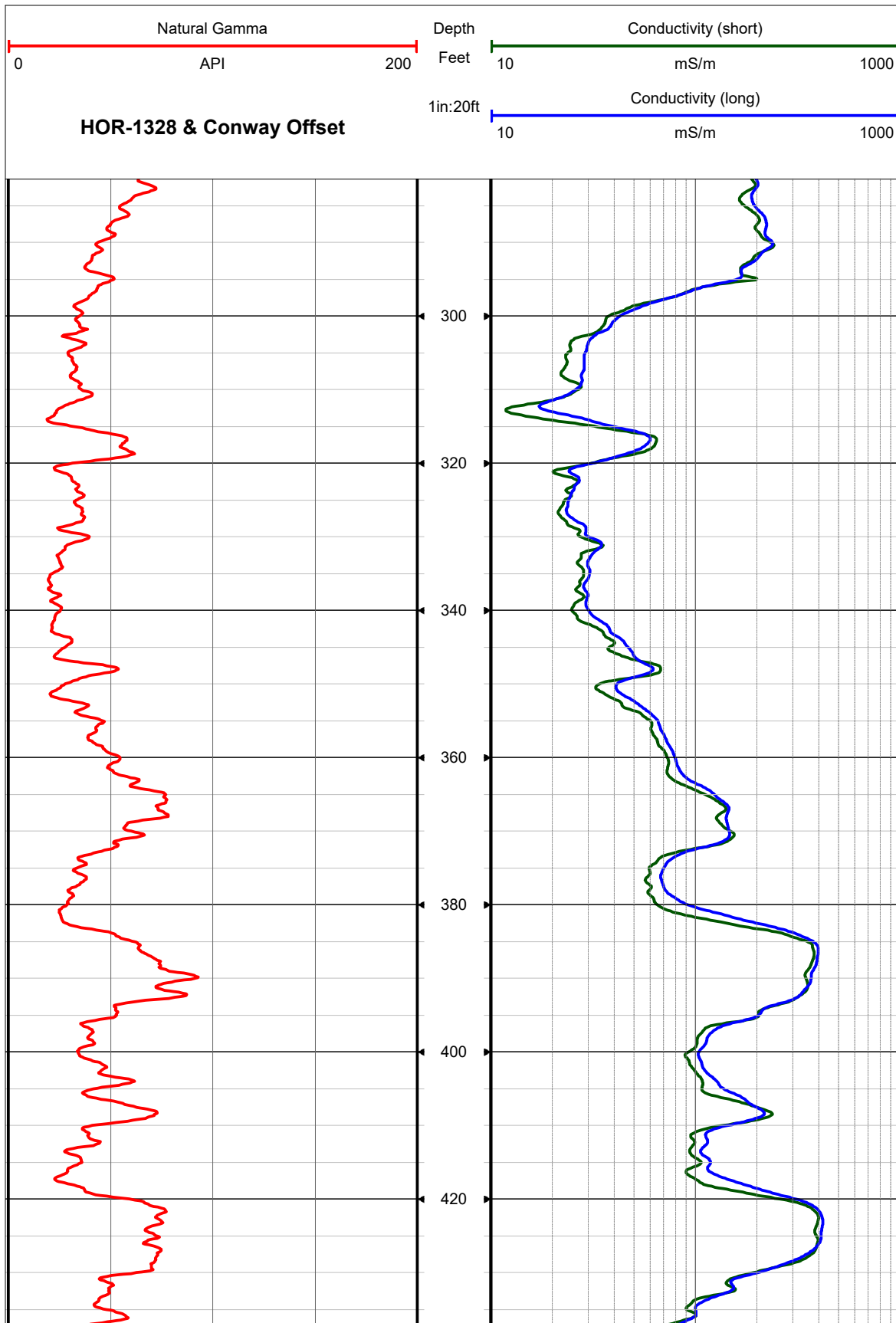
CLIENT S&ME

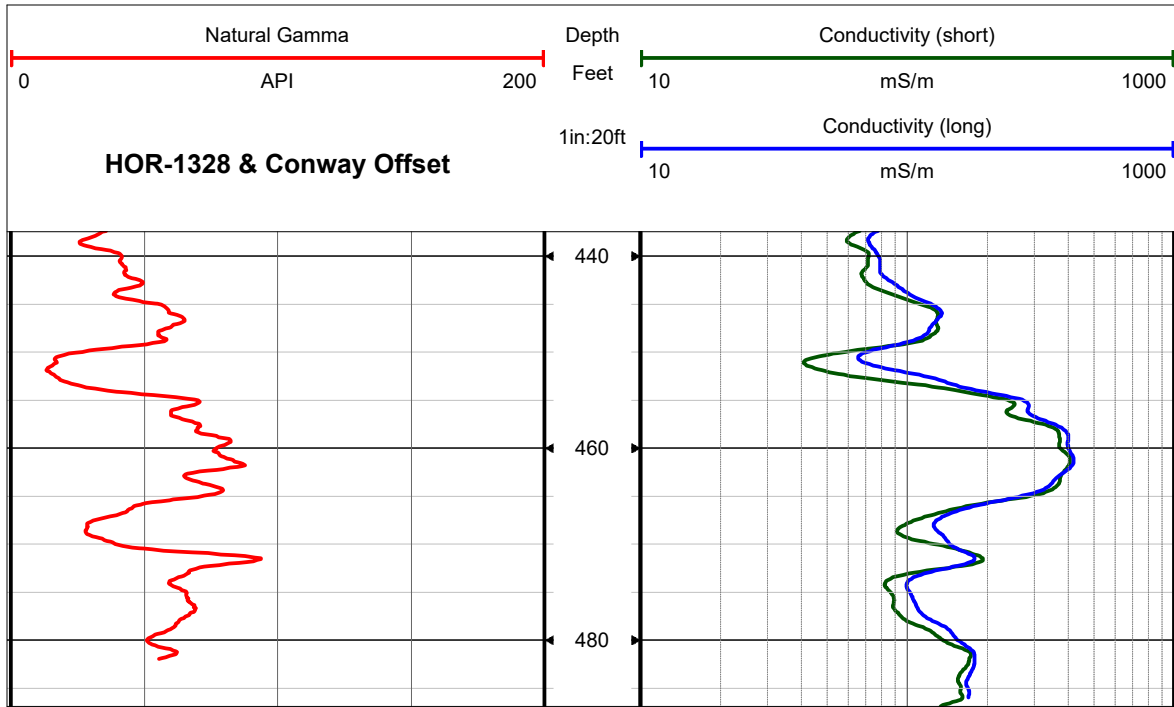
LOG TYPE  
Dual Induction

PROJECT Conway / SCDOT Site A  
 WELL HOR-1328 & Conway Offset  
 LOCATION Conway Site A  
 LOGGER J. Jordan  
 DATE Jan. 28 and Feb. 27, 2017









**APPENDIX C**

**GEOPHYSICAL LOGGING  
SYSTEMS - NIST TRACEABLE  
CALIBRATION RECORDS**



MICRO PRECISION CALIBRATION, INC  
 2165 N. Glassell St.,  
 Orange, CA 92865  
 714-901-5659



# Certificate of Calibration

Calibration CERT #  
 AC-1969

Date: Jan 6, 2017

Cert No. 512200812659896

**Customer:**

GEOVISION  
 1124 OLYMPIC DRIVE  
 CORONA CA 92881

Work Order #: N/A

MPC Control #: AM6767  
 Asset ID: 160023  
 Gage Type: LOGGER  
 Manufacturer: OYO  
 Model Number: 3403  
 Size: N/A  
 Temp/RH: 72.0°F / 54.0%  
 Location: Calibration performed at MPC facility

Serial Number: 160023  
 Department: N/A  
 Performed By: TYLER MCKEEN  
 Received Condition: IN TOLERANCE  
 Returned Condition: IN TOLERANCE  
 Cal. Date: December 16, 2016  
 Cal. Interval: 12 MONTHS  
 Cal. Due Date: December 16, 2017

**Calibration Notes:**

THIS CERTIFICATE SUPERSEDES 512200812635836. REVISED PO SCP-0045 REVISION 1 JAN 04, 2017.

See attached data sheet for calculations. ( 1 Page )

Calibrated IAW customer supplied data form Rev 2.1  
 Frequency measurement uncertainty = 0.0005 Hz  
 Unit calibrated with Laptop Panasonic Model CF-29,s/n: 4FKSA41798  
 Calibrated To 4:1 Accuracy Ratio

This Calibration has been performed in conformance with, and complies to all requirements as set forth in S&ME purchase order SCP-0045 Revision 1, Dated January 04, 2017

**Standards Used to Calibrate Equipment**

I.D.	Description.	Model	Serial	Manufacturer	Cal. Due Date	Traceability #
T1100	UNIVERSAL COUNTER	53131A	3546A09912	HEWLETT PACKARD	Feb 2, 2017	222008122827657
DB8748	GPS TIME AND FREQUENCY RECEIVER	58503A	3625A01225	HEWLETT PACKARD	Jun 17, 2017	222008122553843
LAS0018	ARB / FUNC GENERATOR	33250A	US40001522	AGILENT	Dec 7, 2017	512200812632023

Calibrating Technician:

TYLER MCKEEN

QC Approval:

Jim Williams

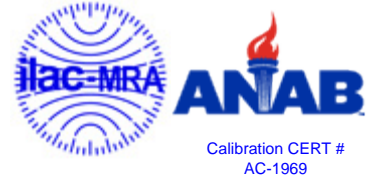
The reported expanded uncertainty of measurement is stated as the standard uncertainty of measurement multiplied by the coverage factor k=2, which for normal distribution corresponds to a coverage probability of approximately 95%. The standard uncertainty of measurement has been determined in accordance with EA's Publication and NIST Technical Note 1297, 1994 Edition. Services rendered comply with ISO 17025:2005, ANSI/NCSL Z540-1, MPC Quality Manual, MPC CSD and with customer purchase order instructions.

Calibration cycles and resulting due dates were submitted/approved by the customer. Any number of factors may cause an instrument to drift out of tolerance before the next scheduled calibration. Recalibration cycles should be based on frequency of use, environmental conditions and customer's established systematic accuracy. The information on this report, pertains only to the instrument identified.

All standards are traceable to SI through the National Institute of Standards and Technology (NIST) and/or recognized national or international standards laboratories. Services rendered include proper manufacturer's service instruction and are warranted for no less than thirty (30) days. This report may not be reproduced in part or in a whole without the prior written approval of the issuing MPC lab.



MICRO PRECISION CALIBRATION, INC  
 2165 N. Glassell St.,  
 Orange, CA 92865  
 714-901-5659



# Certificate of Calibration

Date: Jan 6, 2017

Cert No. 512200812659896

## Procedures Used in this Event

Procedure Name	Description
GEOVISION SEISMIC	Suspension PS Seismic Logger/Recorder Calibration Procedure

Calibrating Technician:

TYLER MCKEEN

QC Approval:

Jim Williams

The reported expanded uncertainty of measurement is stated as the standard uncertainty of measurement multiplied by the coverage factor  $k=2$ , which for normal distribution corresponds to a coverage probability of approximately 95%. The standard uncertainty of measurement has been determined in accordance with EA's Publication and NIST Technical Note 1297, 1994 Edition. Services rendered comply with ISO 17025:2005, ANSI/NCCL Z540-1, MPC Quality Manual, MPC CSD and with customer purchase order instructions.

Calibration cycles and resulting due dates were submitted/approved by the customer. Any number of factors may cause an instrument to drift out of tolerance before the next scheduled calibration. Recalibration cycles should be based on frequency of use, environmental conditions and customer's established systematic accuracy. The information on this report, pertains only to the instrument identified.

All standards are traceable to SI through the National Institute of Standards and Technology (NIST) and/or recognized national or international standards laboratories. Services rendered include proper manufacturer's service instruction and are warranted for no less than thirty (30) days. This report may not be reproduced in part or in a whole without the prior written approval of the issuing MPC lab.

## SUSPENSION PS SEISMIC LOGGER/RECORDER CALIBRATION DATA FORM

### INSTRUMENT DATA

System mfg.:	<u>010</u>	Model no.:	<u>3403</u>
Serial no.:	<u>160023</u>	Calibration date:	<u>12/16/16</u>
By:	<u>Micro Precision</u>	Due date:	<u>12/16/17</u>
Counter mfg.:	<u>Hewlett Packard</u>	Model no.:	<u>53131A</u>
Serial no.:	<u>3546A09912</u>	Calibration date:	<u>2/02/16</u>
By:	<u>Micro Precision</u>	Due date:	<u>2/02/17</u>
Signal generator mfg.:	<u>Agilent</u>	Model no.:	<u>33250A</u>
Serial no.:	<u>U540001522</u>	Calibration date:	<u>12/07/16</u>
By:	<u>Micro Precision</u>	Due date:	<u>12/07/17</u>
Laptop controller mfg.:	<u>Panasonic</u>	Model no.:	<u>CF-29</u>
Serial no.:	<u>4FKSA41798</u>	Calibration date:	<u>N/A</u>

### SYSTEM SETTINGS:

Gain:	<u>2-32</u>
Filter:	<u>10k/off</u>
Range:	<u>5-200 microseconds</u>
Delay:	<u>0</u>
Stack (1 std):	<u>1</u>
System date = correct date and time	<u>Yes, 12/16/16, 11:37 AM</u>

### PROCEDURE:

Set sine wave frequency to target frequency with amplitude of approximately 0.25 volt peak  
 Note actual frequency on data form.  
 Set sample period and record data file to disk. Note file name on data form.  
 Pick duration of 9 cycles using PSLOG.EXE program, note duration on data form, and save as .sps file. Calculate average frequency for each channel pair and note on data form.  
 Average frequency must be within +/- 1% of actual frequency at all data points.

Maximum error ((AVG-ACT)/ACT\*100)%      As found      0.40%      As left      0.40%

Target Frequency (Hz)	Actual Frequency (Hz)	Sample Period (microS)	File Name	Time for 9 cycles Hn (msec)	Average Frequency Hn (Hz)	Time for 9 cycles Hr (msec)	Average Frequency Hn (Hz)	Time for 9 cycles V (msec)	Average Frequency V (Hz)
50.00	<u>50.0</u>	200	<u>001</u>	<u>179.4</u>	<u>50.1</u>	<u>179.6</u>	<u>50.1</u>	<u>180.0</u>	<u>50.0</u>
100.0	<u>100.0</u>	100	<u>002</u>	<u>90.1</u>	<u>100.2</u>	<u>89.9</u>	<u>100.2</u>	<u>90.0</u>	<u>100.0</u>
200.0	<u>200.0</u>	50	<u>003</u>	<u>45.05</u>	<u>199.8</u>	<u>45.05</u>	<u>199.8</u>	<u>45.1</u>	<u>199.6</u>
500.0	<u>500.0</u>	20	<u>004</u>	<u>17.94</u>	<u>501.8</u>	<u>18.00</u>	<u>500.0</u>	<u>17.98</u>	<u>500.8</u>
1000	<u>1000.0</u>	10	<u>005</u>	<u>8.98</u>	<u>1003.0</u>	<u>9.01</u>	<u>999.0</u>	<u>9.01</u>	<u>999.0</u>
2000	<u>2000.0</u>	5	<u>006</u>	<u>4.49</u>	<u>2008.0</u>	<u>4.505</u>	<u>1998.0</u>	<u>4.5</u>	<u>2000.0</u>

Calibrated by:	<u>Tyler McKeen</u>	<u>12/16/16</u>	
	Name	Date	Signature
Witnessed by:	<u>Emily Feldman</u>	<u>12/16/16</u>	
	Name	Date	Signature

## **Appendix IV: Surface Wave Testing Data**



**DRAFT REPORT**

**SURFACE WAVE MEASUREMENTS**

**SCDOT BOREHOLE SITES NEAR ANDREWS  
AND CONWAY, SOUTH CAROLINA**

**GEOVision** Project No. 17016

*Prepared for*

S&ME, Inc.  
620 Wando Park Boulevard  
Mt. Pleasant, South Carolina 29464  
(843) 884-0005

*Prepared by*

**GEOVision** Geophysical Services, Inc.  
1124 Olympic Drive  
Corona, California 92881  
(951) 549-1234

Report 17016-02

May 22, 2017

# TABLE OF CONTENTS

<b>1</b>	<b>INTRODUCTION.....</b>	<b>1</b>
<b>2</b>	<b>OVERVIEW OF SURFACE WAVE METHODS .....</b>	<b>4</b>
<b>3</b>	<b>FIELD PROCEDURES.....</b>	<b>13</b>
<b>4</b>	<b>DATA REDUCTION .....</b>	<b>18</b>
4.1	MASW DATA REDUCTION .....	18
4.2	SASW DATA REDUCTION .....	21
4.3	ARRAY MICROTREMOR DATA REDUCTION .....	23
4.4	COMPARISON OF SURFACE WAVE DISPERSION DATA .....	27
<b>5</b>	<b>SURFACE WAVE MODELING.....</b>	<b>31</b>
<b>6</b>	<b>RESULTS .....</b>	<b>34</b>
6.1	ANDREWS SITE .....	34
6.2	CONWAY SITE.....	43
<b>7</b>	<b>REFERENCES.....</b>	<b>55</b>
<b>8</b>	<b>CERTIFICATION .....</b>	<b>58</b>

## LIST OF TABLES

TABLE 1	ANDREWS SITE – $V_S$ MODEL FROM 3D GLOBAL SOLUTION IN WINSASW SOFTWARE PACKAGE (METRIC UNITS).....	41
TABLE 2	ANDREWS SITE – $V_S$ MODEL FROM 3D GLOBAL SOLUTION IN WINSASW SOFTWARE PACKAGE (IMPERIAL UNITS).....	41
TABLE 3	ANDREWS SITE – $V_S$ MODEL FROM MULTI-MODE SOLUTION (MODE WITH MAXIMUM ENERGY) IN SEISIMAGER SOFTWARE PACKAGE (METRIC UNITS).....	42
TABLE 4	ANDREWS SITE – $V_S$ MODEL FROM MULTI-MODE SOLUTION (MODE WITH MAXIMUM ENERGY) IN SEISIMAGER SOFTWARE PACKAGE (IMPERIAL UNITS) .....	42
TABLE 5	CONWAY SITE – $V_S$ MODEL FOR 45 M SASW RECEIVER SPACING AND COINCIDENT .....	49
TABLE 6	CONWAY SITE – $V_S$ MODEL FOR 45 M SASW RECEIVER SPACING AND COINCIDENT .....	49
TABLE 7	CONWAY SITE – $V_S$ MODEL FOR 60 M SASW RECEIVER SPACING AND COINCIDENT .....	50
TABLE 8	CONWAY SITE – $V_S$ MODEL FOR 60 M SASW RECEIVER SPACING AND COINCIDENT .....	50
TABLE 9	CONWAY SITE – $V_S$ MODEL FOR 75 M SASW RECEIVER SPACING AND COINCIDENT .....	51
TABLE 10	CONWAY SITE – $V_S$ MODEL FOR 75 M SASW RECEIVER SPACING AND COINCIDENT .....	51
TABLE 11	CONWAY SITE – $V_S$ MODEL FOR 90 M SASW RECEIVER SPACING AND COINCIDENT .....	52
TABLE 12	CONWAY SITE – $V_S$ MODEL FOR 90 M SASW RECEIVER SPACING AND COINCIDENT .....	52
TABLE 13	CONWAY SITE – $V_S$ MODEL FOR 114 M SASW RECEIVER SPACING AND COINCIDENT .....	53
TABLE 14	CONWAY SITE – $V_S$ MODEL FOR 114 M SASW RECEIVER SPACING AND COINCIDENT .....	53

## LIST OF FIGURES

FIGURE 1	SITE MAP – ANDREWS SITE .....	2
FIGURE 2	SITE MAP – CONWAY SITE .....	3
FIGURE 3	RELATIONSHIP BETWEEN THE WAVELENGTH OF SURFACE WAVES AND INVESTIGATION DEPTH .....	4
FIGURE 4	TYPICAL SASW SETUP .....	5
FIGURE 5	MASKING AND UNWRAPPING PHASE SPECTRUM TO CALCULATE DISPERSION CURVE .....	6
FIGURE 6	PHASE SHIFT AND F-K TRANSFORMS TO IDENTIFY SURFACE WAVE ENERGY .....	7
FIGURE 7	COMPARISON OF RAYLEIGH AND LOVE WAVE F-V TRANSFORMS FROM A SITE WITH COMPLEX RAYLEIGH WAVE PROPAGATION BUT SIMPLE LOVE WAVE PROPAGATION.....	8
FIGURE 8	TYPICAL ARRAYS USED FOR ARRAY MICROTREMOR MEASUREMENTS .....	9
FIGURE 9	EXAMPLE OF ESAC DATA REDUCTION .....	9
FIGURE 10	REMI™ ANALYSIS OF LINEAR ARRAY MICROTREMOR DATA.....	10
FIGURE 11	EXAMPLE H/V SPECTRAL RATIO DATA .....	11
FIGURE 12	MASW AND SASW FIELD LAYOUT – ANDREWS SITE .....	13
FIGURE 13	MASW AND SASW FIELD LAYOUT – CONWAY SITE.....	13
FIGURE 14	GEOMETRICS GEODE SEISMOGRAPH.....	14
FIGURE 15	LOOKING NORTH AT 4.5 AND 1 HZ GEOPHONES ALONG CONWAY MASW ARRAYS 1 AND 3.....	14
FIGURE 16	1.5 KG HAMMER, AND 4.5, AND 9 KG SLEDGEHAMMER ENERGY SOURCES AT SOUTH END OF CONWAY MASW ARRAY 2.....	15
FIGURE 17	CATERPILLAR 336F EXCAVATOR ENERGY SOURCE – MOVING BACK AND FORTH (LEFT) AND BUCKET DROP (RIGHT).....	15
FIGURE 18	HP 35670A DYNAMIC SIGNAL ANALYZER USED FOR SASW ACQUISITION .....	17
FIGURE 19	COMPARISON OF RAYLEIGH WAVE F-V TRANSFORMS FROM 48 AND 12 CHANNEL RECEIVER GATHERS AT THE ANDREWS SITE, MASW ARRAY 2 .....	19
FIGURE 20	COMPARISON OF RAYLEIGH WAVE F-V TRANSFORMS FROM EXCAVATOR BUCKET DROP AND MOVING BACK AND FORTH ENERGY SOURCES AT THE ANDREWS SITE, MASW ARRAY 2. ....	19
FIGURE 21	COMPARISON OF RAYLEIGH WAVE F-V TRANSFORMS FROM EXCAVATOR BUCKET DROP ENERGY SOURCE FOR THE 48 CHANNEL, 141 M LONG ARRAY 2 AND 9 CHANNEL, 141 M LONG ARRAY 3 AT THE ANDREWS SITE .....	20
FIGURE 22	ANDREWS SITE – RAYLEIGH WAVE DISPERSION DATA FROM MASW ARRAYS 1 TO 3 .....	20
FIGURE 23	CONWAY SITE – RAYLEIGH WAVE DISPERSION DATA FROM MASW ARRAYS 1 TO 3.....	21
FIGURE 24	ANDREWS SITE – RAYLEIGH WAVE DISPERSION DATA FROM SASW ARRAY .....	22
FIGURE 25	CONWAY SITE – RAYLEIGH WAVE DISPERSION DATA FROM SASW ARRAY .....	23

FIGURE 26	ANDREWS SITE – SLOWNESS-FREQUENCY AND PHASE VELOCITY-FREQUENCY IMAGES RESULTING FROM ReMi™ AND ESAC ANALYSIS OF ARRAY MICROTREMOR DATA ACQUIRED ALONG MASW ARRAY 1 .....	24
FIGURE 27	ANDREWS SITE – RAYLEIGH WAVE DISPERSION DATA RESULTING FROM ReMi™ AND ESAC ANALYSIS OF ARRAY MICROTREMOR DATA ACQUIRED ALONG MASW ARRAY 1 .....	25
FIGURE 28	CONWAY SITE – SLOWNESS-FREQUENCY AND PHASE VELOCITY-FREQUENCY IMAGES RESULTING FROM ReMi™ AND ESAC ANALYSIS OF ARRAY MICROTREMOR DATA ACQUIRED ALONG MASW ARRAY 1 .....	26
FIGURE 29	CONWAY SITE – RAYLEIGH WAVE DISPERSION DATA RESULTING FROM ReMi™ AND ESAC ANALYSIS OF ARRAY MICROTREMOR DATA ACQUIRED ALONG MASW ARRAY 1 .....	26
FIGURE 30	ANDREWS SITE – COMPARISON OF DISPERSION CURVES FROM ACTIVE AND PASSIVE SURFACE WAVE DATA .....	27
FIGURE 31	ANDREWS SITE – MASW AND SASW DISPERSION DATA USED FOR DATA MODELING .....	28
FIGURE 32	CONWAY SITE – COMPARISON OF DISPERSION CURVES FROM ACTIVE AND PASSIVE SURFACE WAVE DATA .....	29
FIGURE 33	CONWAY SITE – COMPARISON OF DISPERSION CURVES FROM MASW (FULL OFFSET RANGE RECEIVER GATHERS), SASW (60, 75, AND 90 M RECEIVER SPACING), AND ARRAY MICROTREMOR (HIGHER VELOCITY TREND) DATA .....	29
FIGURE 34	CONWAY SITE – MASW AND SASW DISPERSION DATA USED FOR DATA MODELING .....	30
FIGURE 35	INTERACTIVE ANALYSIS OF SEISMIC REFRACTORS AND REFLECTORS AT ANDREWS SITE .....	33
FIGURE 36	ANDREWS SITE – EFFECTIVE MODE MODELING OF RAYLEIGH WAVE DISPERSION DATA (3D GLOBAL SOLUTION IN WINSASW SOFTWARE PACKAGE) FOR CONSTANT VELOCITY, VARIABLE THICKNESS HIGH VELOCITY LAYER .....	36
FIGURE 37	ANDREWS SITE – MULTI-MODE MODELING OF RAYLEIGH WAVE DISPERSION DATA (MODE WITH MAXIMUM ENERGY IN SEISIMAGER SOFTWARE PACKAGE) FOR CONSTANT VELOCITY, VARIABLE THICKNESS HIGH VELOCITY LAYER .....	37
FIGURE 38	ANDREWS SITE – EFFECTIVE MODE MODELING OF RAYLEIGH WAVE DISPERSION DATA (3D GLOBAL SOLUTION IN WINSASW SOFTWARE PACKAGE) FOR VARIABLE VELOCITY, CONSTANT THICKNESS HIGH VELOCITY LAYER .....	38
FIGURE 39	ANDREWS SITE – MULTI-MODE MODELING OF RAYLEIGH WAVE DISPERSION DATA (MODE WITH MAXIMUM ENERGY IN SEISIMAGER SOFTWARE PACKAGE) FOR VARIABLE VELOCITY, CONSTANT THICKNESS HIGH VELOCITY LAYER .....	39
FIGURE 40	ANDREWS SITE – VELOCITY MODELS SELECTED FOR PURPOSE OF SITE CHARACTERIZATION .....	40
FIGURE 41	CONWAY SITE – MODELING OF RAYLEIGH WAVE DISPERSION DATA FROM 45 M SASW RECEIVER SPACING AND COINCIDENT MASW RECEIVER ARRAYS .....	44
FIGURE 42	CONWAY SITE – MODELING OF RAYLEIGH WAVE DISPERSION DATA FROM 60 M SASW RECEIVER SPACING AND COINCIDENT MASW RECEIVER ARRAYS .....	45
FIGURE 43	CONWAY SITE – MODELING OF RAYLEIGH WAVE DISPERSION DATA FROM 75 M SASW RECEIVER SPACING AND COINCIDENT MASW RECEIVER ARRAYS .....	46
FIGURE 44	CONWAY SITE – MODELING OF RAYLEIGH WAVE DISPERSION DATA FROM 90 M SASW RECEIVER SPACING AND COINCIDENT MASW RECEIVER ARRAYS .....	47
FIGURE 45	CONWAY SITE – MODELING OF RAYLEIGH WAVE DISPERSION DATA FROM 114 M SASW RECEIVER SPACING AND COINCIDENT MASW RECEIVER ARRAYS .....	48
FIGURE 46	CONWAY SITE – SUMMARY OF $V_s$ MODELS .....	54

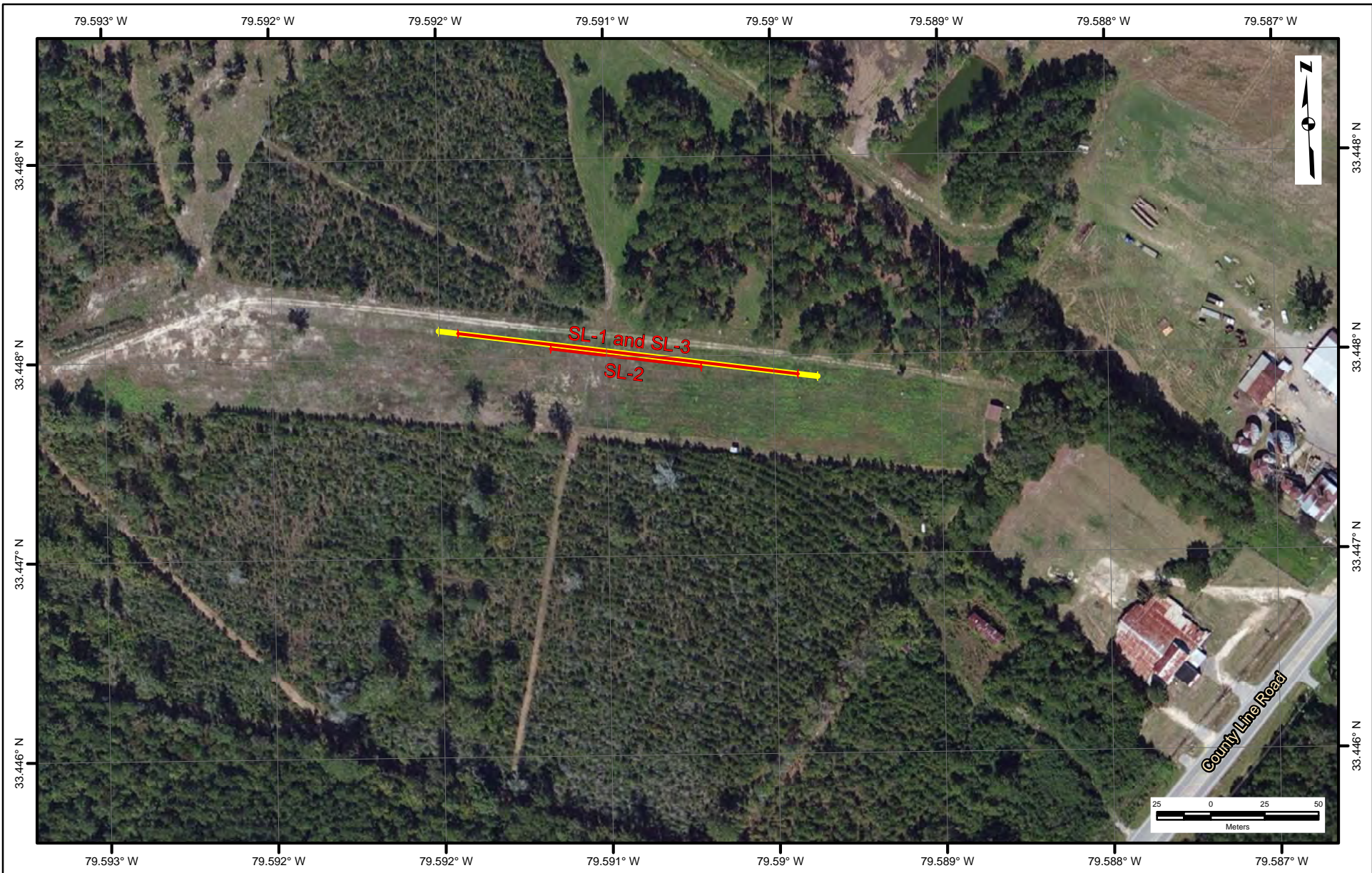
# 1 INTRODUCTION

In-situ seismic measurements using active surface wave techniques were performed at SCDOT borehole sites near Andrews and Conway, South Carolina from March 6<sup>th</sup> to 8<sup>th</sup>, 2017. The Andrews site is located near 3167 County Line Road, Andrews, SC 29510 and the Conway site is located near 8260 Morgan Lane, Anynor, SC 29511.

The purpose of this investigation was to provide shear (S) wave velocity profiles to a minimum depth of 60 meters (m) and as great a depth as the energy source provided would permit. The active surface wave techniques utilized during this investigation consisted of the multi-channel analysis of surface waves (MASW) and spectral analysis of surface waves (SASW) methods. Ambient vibration data were also recorded into the longest MASW array at each site in what is often referred to as the passive MASW or refraction microtremor (ReMi™) method. These data were not used for site characterization and only used to document the performance of linear microtremor arrays, which are routinely used for site characterization in the United States. It is preferable to utilize two-dimensional arrays for ambient vibration (array microtremor measurements) over linear arrays and such data were acquired by the University of Texas, Austin (UTA) as part of a separate investigation.

The location of the surface wave testing arrays at the Andrews and Conway sites are presented in Figures 1 and 2, respectively.

This report contains the results of the surface wave measurements conducted at the Andrews and Conway sites. An overview of the surface wave methods is given in Section 2. Field and data reduction/modeling procedures are discussed in Sections 3 and 4, respectively. Data modeling procedures are discussed in Section 5. Results are presented in Section 6. References and our professional certification are presented in Sections 7 and 8, respectively.



**Legend**

-  MASW Array
-  SASW Receiver Array

**NOTES:**

1. Coordinate System: WGS84 NAD 83
2. Base map source: Esri, DigitalGlobe, GeoEye, Earthstar Geographics, CNES/Airbus DS, USDA, USGS, AEX, Getmapping, Aerogrid, IGN, IGP, swisstopo, and the GIS User Community

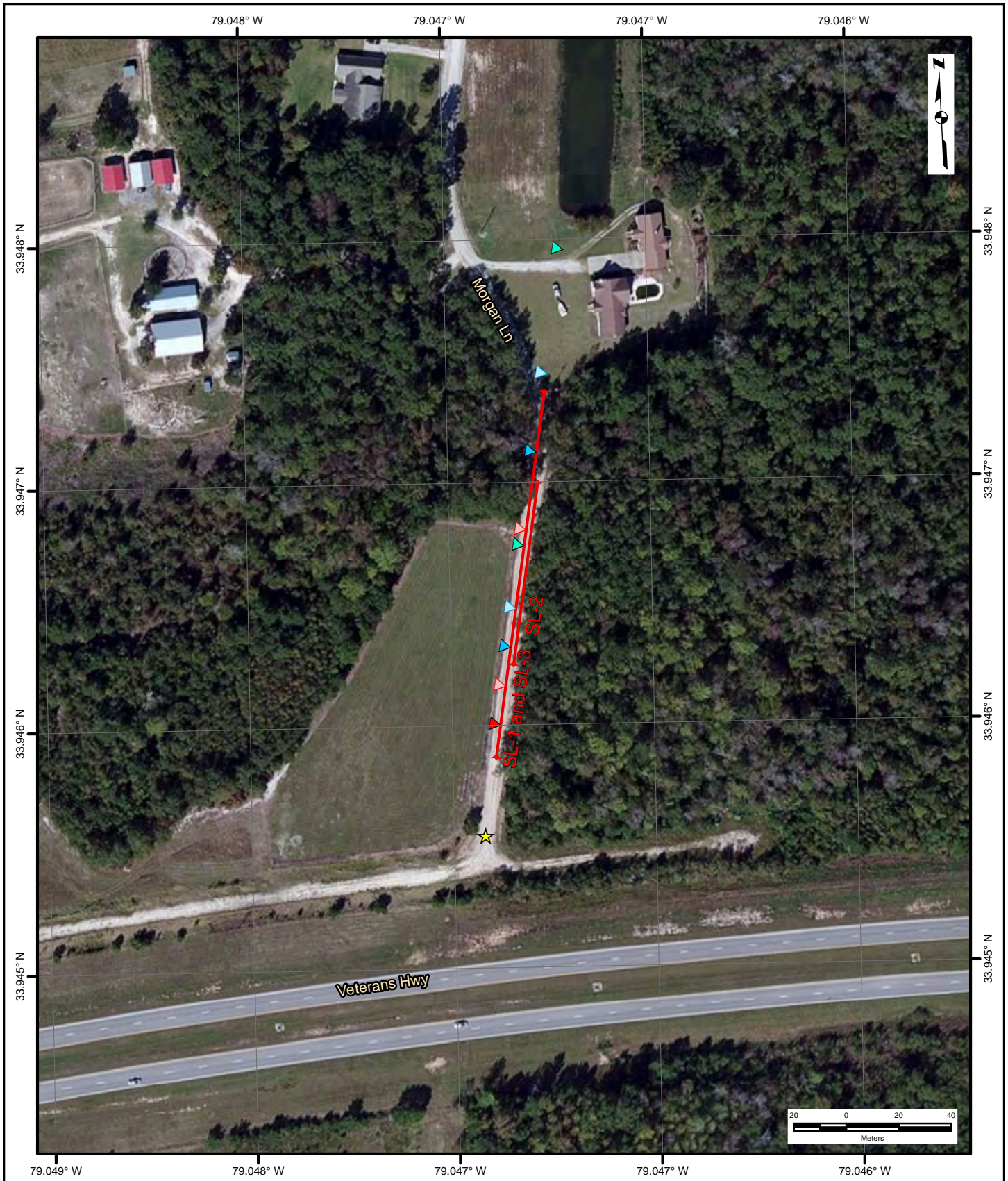


Date:	5/22/2017
GV Project:	17016
Developed by:	L Demine
Drawn by:	T Rodriguez
Approved by:	A Martin
File Name:	17016_1.MXD

**FIGURE 1  
SITE MAP - ANDREWS SITE**

**ANDREWS  
GEORGETOWN COUNTY, SOUTH CAROLINA**

**PREPARED FOR  
S&ME, INC.**



**Legend**

-  MASW Array
-  SASW Receiver Pairs
-  SASW Source Location

**NOTES:**

1. Coordinate System: WGS84 NAD 83
2. Base map source: Esri, DigitalGlobe, GeoEye, Earthstar Geographics, CNES/Airbus DS, USDA, USGS, AEX, Getmapping, Aerogrid, IGN, IGP, swisstopo, and the GIS User Community



Date: 5/22/2017  
 GV Project: 17016  
 Developed by: L Demine  
 Drawn by: T Rodriguez  
 Approved by: A Martin  
 File Name: 17016\_2.MXD

**FIGURE 2  
 SITE MAP - CONWAY SITE**

**CONWAY  
 Horry County, South Carolina**

**PREPARED FOR  
 S&ME, INC.**

## 2 OVERVIEW OF SURFACE WAVE METHODS

Both active and passive (ambient noise) surface wave techniques were utilized during this investigation. Active surface wave techniques include the spectral analysis of surface waves (SASW) and multi-channel array surface wave (MASW) methods. Passive surface wave techniques include the HVSR technique and the array and refraction microtremor methods.

The basis of surface wave methods is the dispersive characteristic of Rayleigh and Love waves when propagating in a layered medium. The Rayleigh wave phase velocity ( $V_R$ ) depends primarily on the material properties ( $V_S$ , mass density, and Poisson's ratio or compression wave velocity) over a depth of approximately one wavelength. The Love wave phase velocity ( $V_L$ ) depends primarily on  $V_S$  and mass density. Rayleigh and Love wave propagation are also affected by damping or seismic quality factor ( $Q$ ). Rayleigh wave techniques are utilized to measure vertically polarized S-waves ( $S_V$ -wave); whereas, Love wave techniques are utilized to measure horizontally polarized S-waves ( $S_H$ -wave).

Surface waves of different wavelengths ( $\lambda$ ) or frequencies ( $f$ ) sample different depths (Figure 2). As a result of variance in the shear stiffness of the distinct layers, waves with different wavelengths propagate at different phase velocities; hence, dispersion. A surface wave dispersion curve is the variation of  $V_R$  or  $V_L$  with  $\lambda$  or  $f$  (Figure 2).

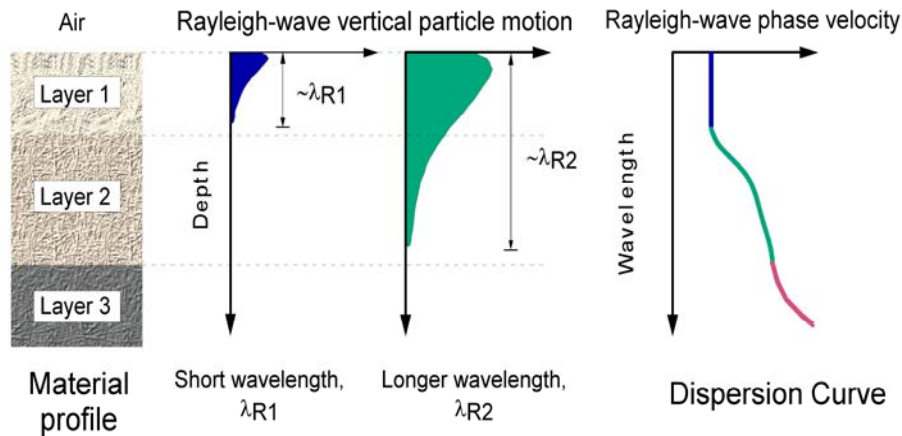


**Figure 3** Relationship between the wavelength of surface waves and investigation depth

The SASW and MASW methods are in-situ seismic methods for determining shear wave velocity ( $V_S$ ) profiles (Stokoe et al., 1994; Stokoe et al., 1989; Park et al., 1999a and 1999b, Foti, 2000). Surface wave techniques are non-invasive and non-destructive, with all testing performed on the ground surface at strain levels in the soil in the elastic range ( $< 0.001\%$ ). SASW testing consists of collecting surface wave phase data in the field, generating the dispersion curve, and then using iterative forward or inverse modeling to calculate the shear wave velocity profile. MASW testing consists of collecting multi-channel seismic data in the field, applying a wavefield transform to obtain the dispersion curve, and data modeling to obtain the  $V_S$  profile.

A detailed description of the SASW field procedure is given in Joh, 1996. A typical SASW setup is shown in Figure 4. A vertical dynamic load is used to generate horizontally-propagating Rayleigh waves and a horizontal force is used to generate Love waves. The ground motions are monitored by two, or more, vertical (Rayleigh wave) or horizontal (Love wave) receivers and recorded by the data acquisition system capable of performing both time and frequency-domain calculations. Theoretical, as well as practical considerations, such as signal attenuation, necessitate the use of several receiver spacings to generate the dispersion curve over the wavelength range required to evaluate the stiffness profile. To identify and/or minimize phase shifts due to differences in receiver coupling and subsurface variability, the source location is reversed. To develop a  $V_S$  model to a 30 meter depth using Rayleigh wave methods, energy sources typically include: small hammers (rock hammer or 3 lb hammer) for short receiver intervals; 10 to 20 lb sledgehammers for intermediate separations, and accelerated weight drops (AWD) or an electromechanical shaker for larger spacings. More energetic sources, such as bulldozers or seismic vibrators (Vibroseis<sup>TM</sup>), can be used to characterize velocity structure to depths of 100 m or more. Energy sources for shallow imaging using Love waves include a hammer and horizontal traction plank, portable hammer impact aluminum source, and inclined or horizontal accelerated weight drop systems. Energy sources for deeper imaging using Love waves include horizontal seismic vibrators. Generally, high frequency (short wavelength) surface waves are recorded across receiver pairs spaced at short intervals, whereas low frequency (long wavelength) surface waves require greater spacing between receivers. Dispersion data averaged across greater distances are often smoother because effects of localized heterogeneities are averaged.

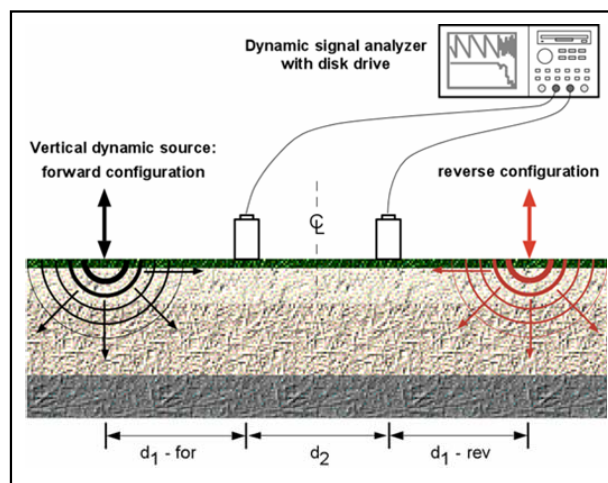


**Figure 4** Typical SASW setup

After the time-domain motions from the two receivers are converted to frequency-domain records using the Fast Fourier Transform, the cross power spectrum and coherence are calculated. The phase of the cross power spectrum represents the phase differences between the two receivers as the wave train propagates past them. It ranges from  $-\pi$  to  $\pi$  in a wrapped form and must be unwrapped through an interactive process called masking. Phase jumps are specified, near-field data (wavelengths longer than two times the distance from the source to first receiver) and low-coherence data are removed. The experimental dispersion curve is calculated from the unwrapped phase angle and the distance between receivers by:

$$V_{R/L} = f * d_2 / (\Delta\phi / 2\pi)$$

where  $V_R$  = Rayleigh wave phase velocity  
 $V_L$  = Love wave phase velocity  
 $f$  = frequency  
 $d_2$  = distance between receivers  
 $\Delta\phi$  = the phase difference in radians

Figure 5 demonstrates phase unwrapping of the cross power spectrum during SASW data reduction.

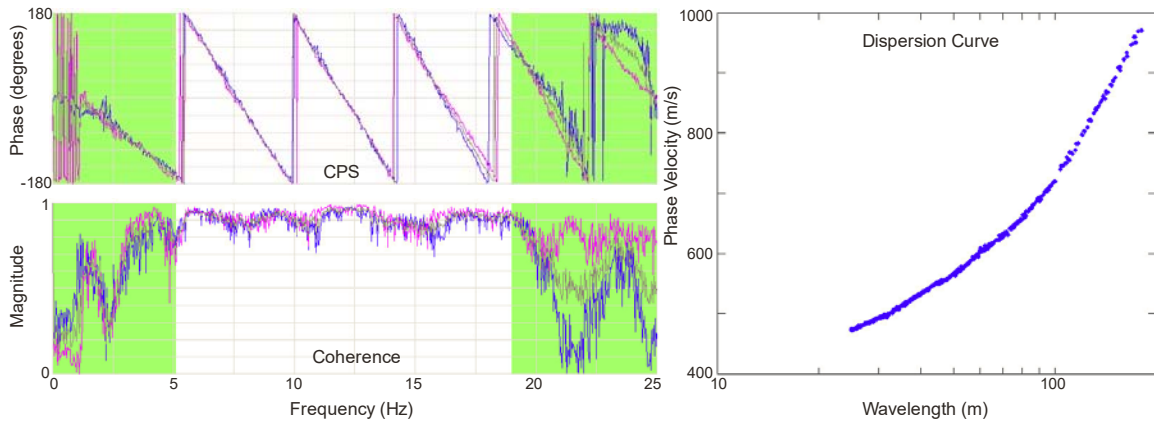


**Figure 5** Masking and unwrapping phase spectrum to calculate dispersion curve

A detailed description of the MASW method is given by Park, 1999a and 1999b. Ground motions are recorded by 24, or more, geophones typically spaced 1 to 3 m apart along a linear array and connected to a seismograph. Energy sources are the same as those outlined above for SASW testing. When applying the MASW technique to develop a one-dimensional (1-D)  $V_S$  model, the surface-wave data, preferably, are acquired using multiple-source offsets at both ends of the array. The most commonly applied MASW technique is the Rayleigh-wave based MASW method, which we refer to as  $MAS_{RW}$  to distinguish from Love-wave based MASW ( $MAS_{LW}$ ).  $MAS_{RW}$  and  $MAS_{LW}$  acquisition can easily be combined with P- and S-wave seismic refraction acquisition, respectively.  $MAS_{RW}$  data are generally recorded using a vertical source and vertical geophone, but may also be recorded using a horizontal geophone with radial (in-line) orientation.  $MAS_{LW}$  data are recorded using transversely orientated horizontal source and transverse horizontal geophone.

A wavefield transform is applied to the time-history data to convert the seismic record from the time-offset domain to the frequency-phase velocity or frequency-wavenumber domain in which the surface-wave dispersion curve can be easily identified. Common wave-field transforms include: the frequency-wavenumber (f-k) transform, slant-stack transform ( $\tau$ -p), frequency domain beamformer, and phase-shift transform. Figure 6 demonstrates application of the phase shift and f-k transforms to identify surface wave energy. Occasionally, SASW analysis procedures are used to extract surface wave dispersion data, from fixed receiver pairs, at smaller wavelengths than can be recovered by wavefield transformation. Construction of a dispersion curve, over the wide frequency/wavelength range necessary to develop a robust  $V_S$  model while

also limiting the maximum wavelength based on an established near-field criteria (e.g. Yoon and Rix, 2009; Li and Rosenblad, 2011), generally requires multiple source offsets.

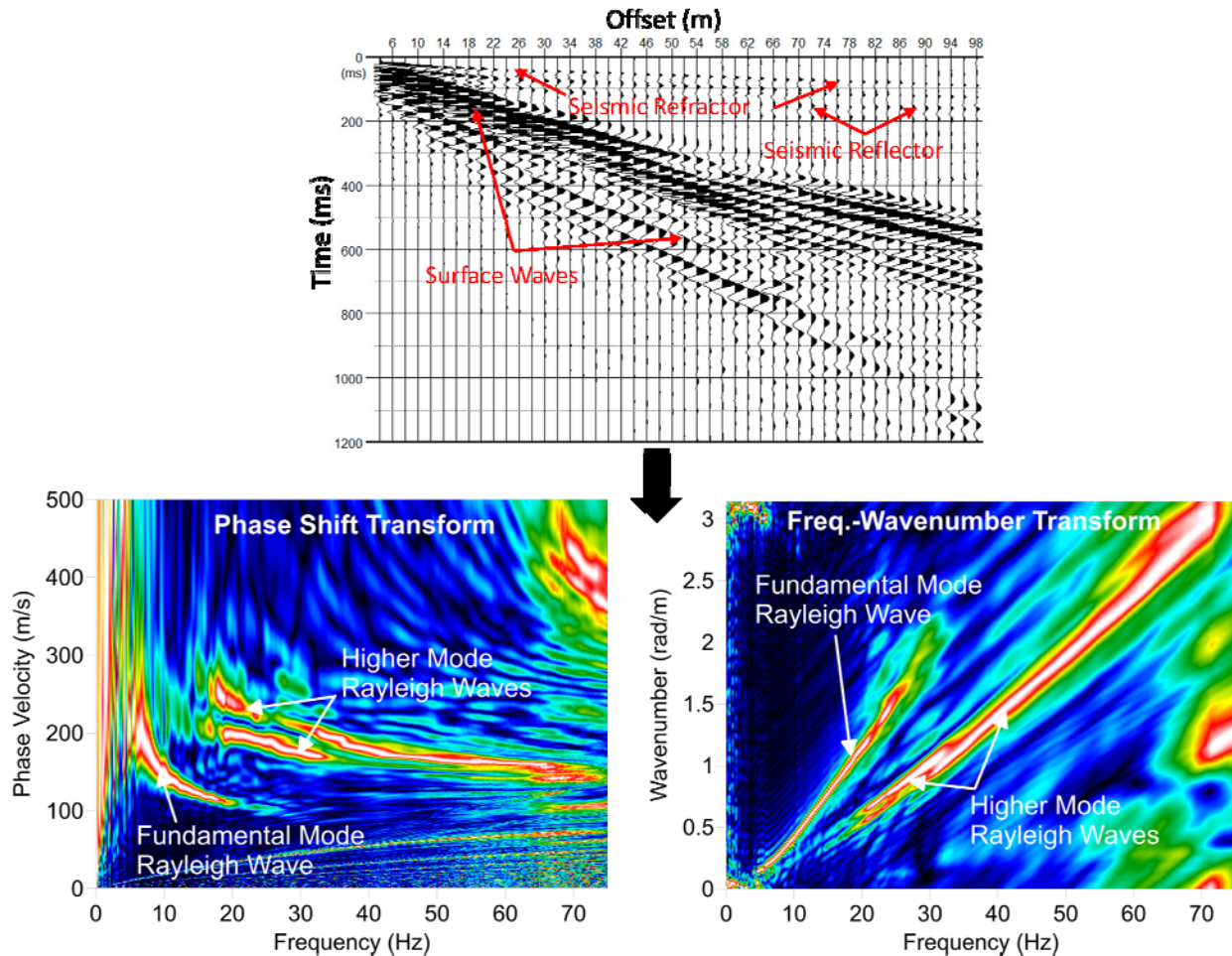


**Figure 6** Phase shift and *f-k* transforms to identify surface wave energy

Although, the vast majority of MASW surveys record Rayleigh waves, it has been shown that Love wave techniques can be more effective in some environments, particularly shallow rock sites and sites with a highly attenuative, low velocity surface layer (Xia, et al., 2012; **GEOVision**, 2012; Yong, et al., 2013; Martin, et al., 2014). Figure 7 provides an example of frequency-velocity (*f-v*) transforms of MAS<sub>R</sub>W and MAS<sub>L</sub>W data from a site where the fundamental mode Love wave was much more easily interpreted. Rayleigh wave techniques, however, are generally more effective at sites where velocity gradually increases with depth because larger energy sources are readily available for generation of Rayleigh waves. Rayleigh wave techniques are generally more applicable to sites with high velocity layers and/or velocity inversions because the presence of such structures is more apparent in the Rayleigh wave dispersion curves than in Love wave dispersion curves. Additionally, Rayleigh wave techniques are preferable at sites with a high velocity surface layer because Love waves do not theoretically exist in such environments. Occasionally, the horizontal radial component of a Rayleigh wave may yield higher quality dispersion data than the vertical component because different modes of propagation may have more energy in one component than the other. Recording both the vertical

and horizontal components of the Rayleigh wave is particularly useful at sites with complex modes of propagation or when attempting to recover multiple Rayleigh wave modes for multi-mode modeling as demonstrated in Dal Moro, et al, 2015. Joint inversion of Rayleigh and Love wave data may yield more accurate  $V_S$  models and also offer a means to investigate anisotropy, where  $S_V$ - and  $S_H$ -wave velocity are not equal, as shown in Dal Moro and Ferigo, 2011.

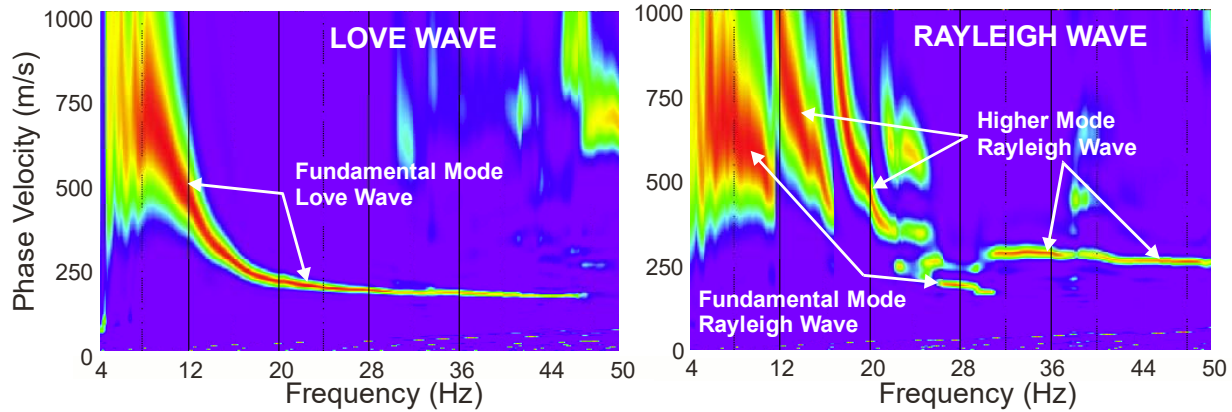


**Figure 7** Comparison of Rayleigh and Love wave  $f$ - $v$  transforms from a site with complex Rayleigh wave propagation but simple Love wave propagation

A detailed discussion of the array microtremor method can be found in Okada, 2003. Unlike the SASW and MASW methods, which use an active energy source (e.g. hammer), the microtremor technique records background noise emanating from ocean wave activity, traffic, industrial activity, construction, etc. The technique uses 4, or more, receivers aligned in a 2-dimensional array. Triangle, circle, semi-circle, and “L” shaped arrays are commonly used, although any 2-dimensional arrangement of receivers can be used (Figure 8). For investigation of the upper 100 m, receivers typically consist of 1 to 4.5 Hz geophones. The nested triangle array, which consists of several embedded equilateral triangles, is often used as it provides accurate dispersion curves with a relatively small number of geophones. With this array, the outer side of the triangle should be equal to or greater than the desired depth of investigation. The “L” array is useful at sites located at the corner of perpendicular intersecting streets. Typically, 10 to 60 minutes of ambient vibration data are recorded, depending on the size of the array. The surface wave dispersion curve is typically estimated from array microtremor data using various  $f$ - $k$  methods such as beam-forming (Lacoss, et al., 1969), and maximum-likelihood (Capon, 1969), and the spatial-autocorrelation (SPAC) method, which was originally based on work by Aki, 1957. The SPAC method has since been extended and modified (Ling and Okada, 1993 and Ohori *et al.*, 2002) to permit the use of noncircular arrays, and is now collectively referred to as extended spatial autocorrelation (ESPAC or ESAC). Further modifications to the SPAC method permit the use of irregular or random arrays (Bettig *et al.*, 2001). Although it is common to apply SPAC methods to obtain a surface wave dispersion curve for modeling, other approaches involve direct modeling of the coherency data, also referred to as SPAC coefficients (Asten, 2006 and Asten, *et al.*, 2015).

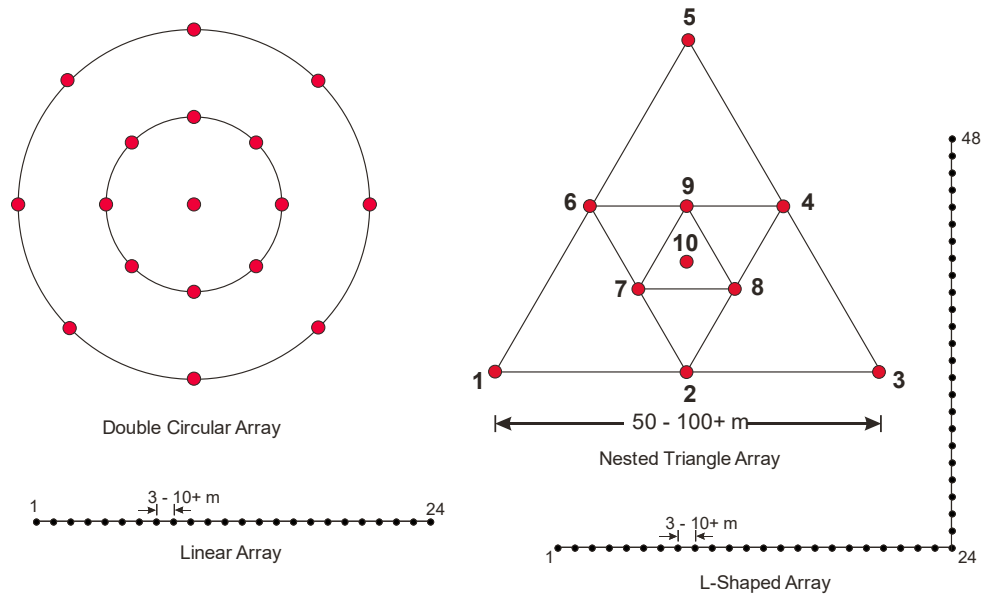


**Figure 8** Typical arrays used for array microtremor measurements

Analysis of array microtremor data using the SPAC method involves computation of the complex coherence for all receiver pair combinations in the array. The real component of the coherence for constant receiver separations and different azimuths are averaged resulting in a plot of coherence as a function of frequency and receiver separation termed the SPAC coefficients. Aki (1957) showed that the SPAC coefficients from a Bessel function of the first kind, zero order. Figure 9 provides an example of ESAC data processing. The velocity-frequency image shows the degree of fit of the Bessel function to the SPAC coefficients. The receiver offset versus coherence plot shows the best fitting Bessel function for the SPAC coefficients at a frequency of 1.7 Hz, which, in this case, is at a velocity of 463 m/s.

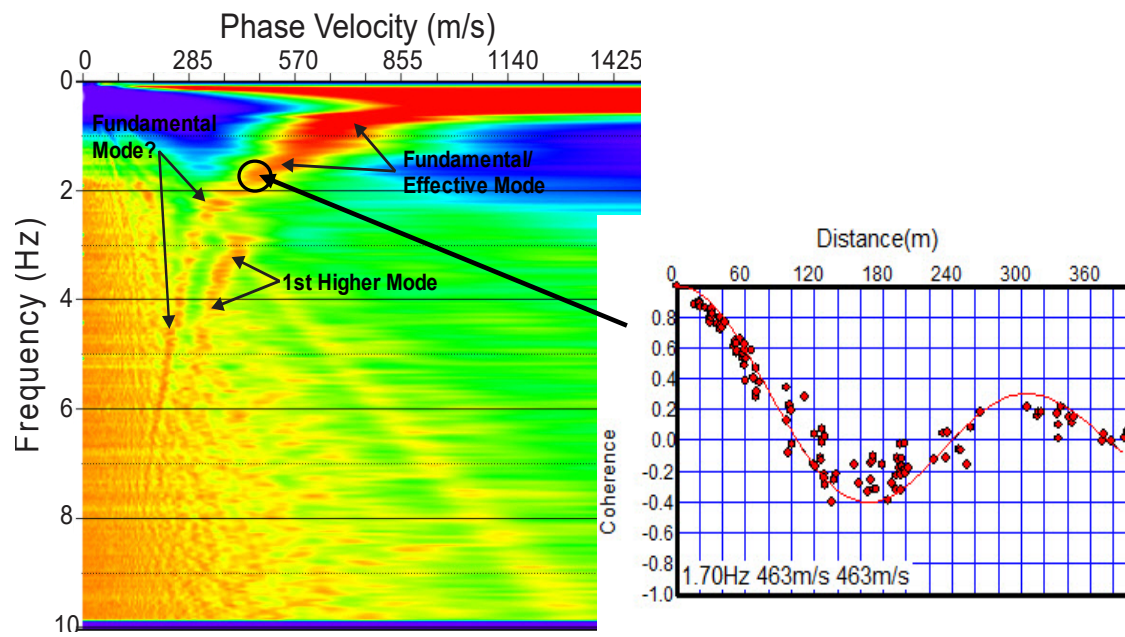


**Figure 9** Example of ESAC data reduction

The refraction microtremor technique (ReMi™), a detailed description of which can be found in Louie (2001), differs from the more established array microtremor technique in that it uses a linear receiver array rather than a two dimensional array. Two dimensional arrays are preferred over linear arrays when applying the array microtremor method and should be utilized whenever possible. Refraction microtremor field procedures typically consist of laying out a linear array of at least 24 4.5 Hz geophones and recording 20, or more, 30 second noise records. These noise records are reduced using the software package SeisOpt® ReMi™ v2.0 by Optim™ Software and Data Services. This package is used to generate and combine the slowness (p) – frequency (f) transform of the noise records. The surface wave dispersion curve is picked at the lower envelope of the surface wave energy identified in the p-f spectrum. It should be noted that other data reduction techniques such as seismic interferometry and ESAC can also be used to extract surface wave dispersion curves from linear array, passive surface wave data. In fact, it is good practice to always interpret linear array microtremor data using two analytical approaches and to combine with active surface wave dispersion data. Figure 10 shows p-f images developed using the ReMi™ technique where resulting dispersion curves are likely reliable and unreliable, respectively.

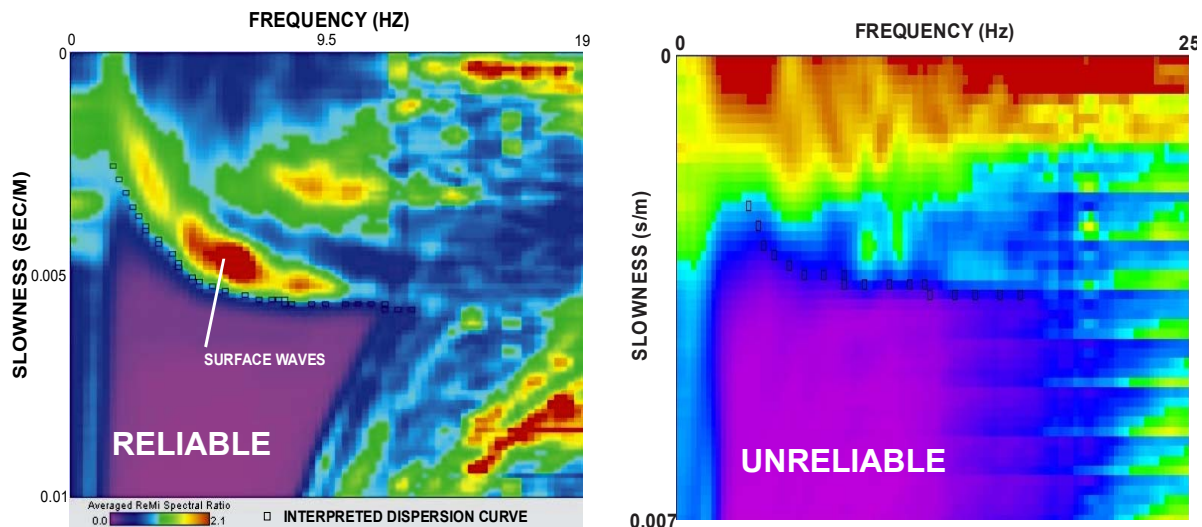


**Figure 10** ReMi™ analysis of linear array microtremor data

The horizontal-to-vertical spectral ratio (HVSr) technique was first introduced by Nogoshi and Igarashi (1971) and popularized by Nakamura (1989). This technique utilizes single-station recordings of ambient vibrations (microtremor or noise) made with a three-component seismometer. In this method, the ratio of the Fourier amplitude spectra of the horizontal and vertical components is calculated to determine the frequency of the maximum HVSr response (HVSr peak frequency), commonly accepted as an approximation of the fundamental frequency ( $f_0$ ) of the sediment column overlying bedrock. The HVSr peak frequency associated with bedrock is a function of the bedrock depth and S-wave velocity of the sediments overlying bedrock. The theoretical HVSr response can be calculated for an S-wave velocity model using modeling schemes based on surface wave ellipticity, vertically propagating body waves, or diffuse wavefields containing body and surface waves. The HVSr frequency peak can also be estimated using the quarter-wavelength approximation:

$$f_0 = \frac{\bar{V}_s}{4z}$$

where  $f_0$  is the site fundamental frequency and  $\bar{V}_s$  is the average shear-wave velocity of the soil column overlying bedrock at depth  $z$ .

Joint inversion of HVSR and surface wave dispersion data may reduce non-uniqueness of the resulting  $V_s$  models in some cases. Figure 11 is an example of HVSR data collected at a site where with bedrock at a depth of about 60 m.

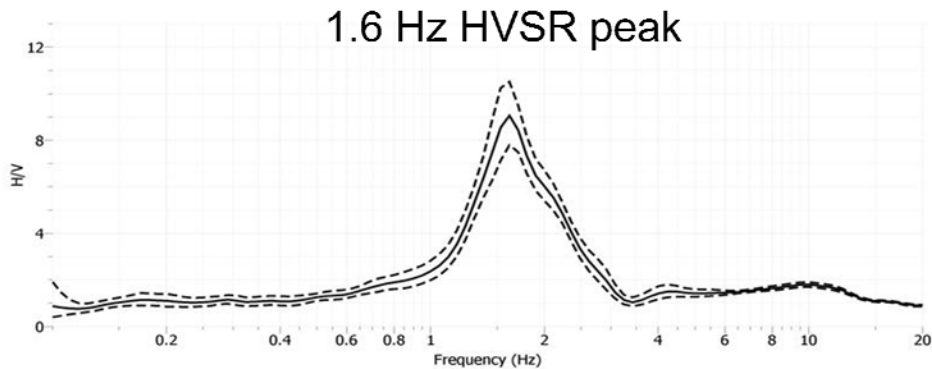


**Figure 11** Example H/V spectral ratio data

The active and passive surface wave techniques complement one another as outlined below:

- SASW/MASW techniques image the shallow velocity structure which cannot be imaged by the microtremor technique and are needed for an accurate  $V_s$  model and  $V_{S30}/V_{S100ft}$  estimate.
- Microtremor techniques often perform well in noisy environments where SASW/MASW depth investigation may be limited.
- In a high noise environment, the microtremor technique will extend the depth of investigation of SASW/MASW soundings.

The dispersion curves generated from the active and passive surface wave soundings are generally combined and modeled using iterative forward and inverse modeling routines. The final model profile is assumed to represent actual site conditions. Several options exist for the Rayleigh wave forward solution: a formulation that takes into account only fundamental-mode Rayleigh wave motion; one that includes all stress waves and incorporates receiver geometry in an SASW test named the 3-D solution (Roesset et al., 1991); one that computes an effective mode for an MASW test but assumes a plane Rayleigh wave and no body wave effects, and a multi-mode solution that models different Rayleigh wave modes. Both fundamental mode and multi-mode forward solutions are available for modeling of Love wave data.

The theoretical model used to interpret the dispersion curve assumes horizontally layered, laterally invariant, homogeneous-isotropic material. Although these conditions are seldom

strictly met at a site, the results of active and/or passive surface wave testing provide a good “global” estimate of the material properties along the array. The results may be more representative of the site than a borehole “point” estimate.

It may not always be possible to develop a coherent, fundamental mode dispersion curve over sufficient frequency range for modeling due to dominant higher modes with the higher modes not clearly identifiable for multi-mode modeling. It may, however, be possible to identify the Rayleigh wave phase velocity of the fundamental mode at 40 m wavelength ( $V_{R40}$ ) in which case  $V_{S30}$  can at least be estimated using the Brown et al., 2000 relationship:

$$V_{S30} = 1.045V_{R40}$$

This relationship was established based on statistical analysis of a large number of surface wave data sets from sites with control by velocities measured in nearby boreholes and has been further evaluated by Martin and Diehl, 2004, and Albarello and Gargani, 2010.

As with all surface geophysical methods, inversion of surface wave dispersion data does not yield a unique  $V_S$  model and there are multiple possible solutions that may equally well fit the experimental data. Based on our experience at other sites, the shear wave velocity models ( $V_S$  and layer thicknesses) determined by surface wave testing are within 20% of the velocities and layer thicknesses that would be determined by other seismic methods (Brown, 1998). The average velocity of the upper 30 m or 100 ft, however, is much more accurate when the fundamental mode solution is valid, often to better than 5%, because it is not sensitive to the layering in the model.  $V_{S30}$  does not appear to suffer from the non-uniqueness inherent in  $V_S$  models derived from surface wave dispersion curves (Martin et al., 2006, Comina et al., 2011). Therefore,  $V_{S30}$  is more accurately estimated from inversion of surface wave dispersion data than the resulting  $V_S$  models.

### 3 FIELD PROCEDURES

MASW data were acquired along three collocated arrays and SASW data were acquired along a single array at each of the Andrews and Conway sites. The geometry of the MASW and SASW arrays at the Andrews and Conway sites are presented in Figures 12 and 13, respectively.

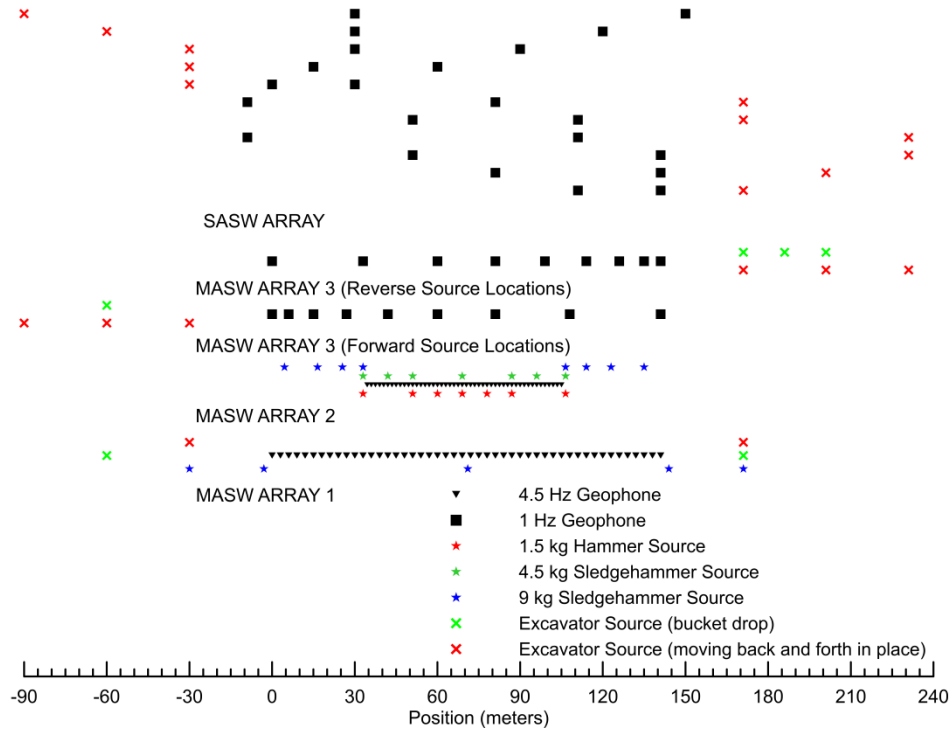


*Figure 12 MASW and SASW field layout – Andrews site*

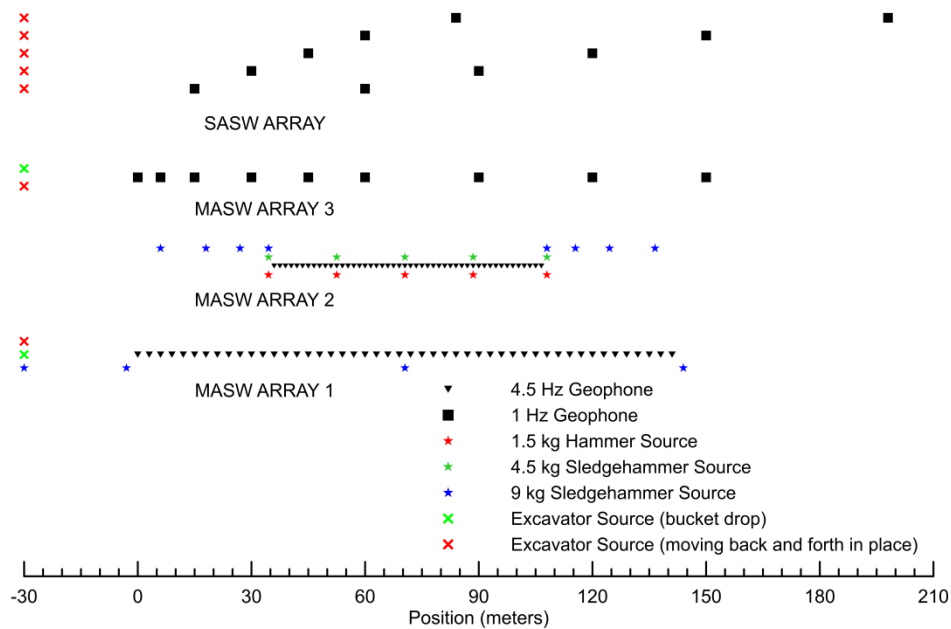


*Figure 13 MASW and SASW field layout – Conway site*

The MASW seismic data acquisition system consisted of two 24-channel Geometrics Geode signal enhancement seismographs combined to form a 48-channel system and a laptop computer running Geometrics Seismodule Controller Software (Figure 14). Other seismic equipment utilized during this investigation consisted of: Geospace 4.5 and 1 Hz vertical geophones (Figure 15), seismic cables, hammer switches, and multiple hammer sources including a 1.5 kg hammer, 12 and 20 lb sledgehammers, and an aluminum plate (Figure 16). A Caterpillar 336F excavator was also used as an energy source (bucket drop and moving back and forth in place) to extend depth of investigation to 60 m, or greater (Figure 17).



**Figure 14** *Geometrics Geode seismograph*



**Figure 15** *Looking north at 4.5 and 1 Hz geophones along Conway MASW Arrays 1 and 3*



**Figure 16** 1.5 kg hammer, and 4.5, and 9 kg sledgehammer energy sources at south end of Conway MASW Array 2



**Figure 17** Caterpillar 336F excavator energy source – moving back and forth (left) and bucket drop (right)

MASW Array 1 at the Andrews and Conway sites consisted of a linear array of 48 vertical 4.5 Hz geophones spaced 3 m apart for a line length of 141 m. The energy sources consisted of a 9

kg sledgehammer utilized at locations offset 3 and 30 m from the end geophones, where possible, and at the center of the array and the excavator (both bucket drops and moving back and forth in place). At the Andrews site, the excavator was located 30 m from the end geophones at each end of the array and 60 m from the end geophone at the western end of the array. At the Conway site, the excavator could only be used at a single location 30 m south of the southernmost geophone. Typically, ten 1 to 2 s seismic records were stacked for each sledgehammer location, ten 1 to 2 s seismic records were saved at each bucket drop location, and ten to thirty 30 s seismic records were saved when the excavator was moving back and forth.

Array microtremor data were acquired at both the Andrews and Conway sites along MASW Array 1; primarily to assess the performance of a linear passive array relative to the MASW technique and to the preferred 2-D array microtremor geometry deployed by UTA. Ambient noise measurements were recorded along each array for at least 15 minutes at a 2 ms sample rate.

MASW Array 2 at the Andrews and Conway sites consisted of a linear array of 48 vertical 4.5 Hz geophones spaced 1.5 m apart for a line length of 70.5 m. This array was collocated with and centered near the center of MASW Array 1. The energy sources consisted of a 9 kg sledgehammer offset 1.5, 9, 18 and 30 m from the end geophones; 1.5 and/or 4.5 kg hammers offset 1.5 m from the near geophones and at 6 to 12 geophones intervals along the array. Typically, ten 1 s seismic records were stacked and saved at source location.

MASW Array 3 at the Andrews and Conway sites consisted of a linear array of 9 vertical 1 Hz geophones with variable spacing as shown in Figures 12 and 13. Array 3 was collocated with Array 1, but extended 9 m beyond the end of Array 1 at the Conway site. The energy sources consisted of an excavator (both bucket drops and moving back and forth in place). At the Conway site, the excavator could only be used at a single location 30 m south of the southernmost geophone. At the Andrews site, the excavator was located 30, 60 and 90 m from the end geophones at each end of the array. Typically, ten 1 to 2 s seismic records were stacked for each sledgehammer location; ten 1 to 2 s seismic records were saved at each bucket drop location; and ten to seventy 30 s seismic records were saved when the excavator was moving back and forth.

All MASW seismic records were stored on a laptop computer with file names and acquisition parameters documented on a field log.

The SASW seismic data acquisition system consisted of an HP 35670A dynamic signal analyzer (Figure 18). Other seismic equipment utilized for acquisition of SASW data consisted of Geospace Model GS-1 1 Hz vertical geophones (Figure 15) and sensor cables. A Caterpillar 336F excavator was used as an energy source for SASW data acquisition (Figure 17).

SASW data were collected at the Conway site using a common source configuration with base receiver spacings of 45, 60, 75, 90, and 114 m as shown on Figure 13. The purpose of the SASW survey was to extend depth of investigation of the MASW survey and, therefore, it was not necessary to use smaller receiver spacings and energy sources. A common source geometry was used at the Conway site instead of the preferred common center point geometry because the source could only be used at a single location to minimize damage to a gravel road. SASW data were collected at the Andrews site using a common source configuration with base receiver

spacings of 30, 45, 60, 90, and 120 m as shown on Figure 14. Reversed source locations were occupied at the Andrews site (Figure 12); however, a common center point geometry was not utilized as MASW data were acquired concurrently and the excavator could not be utilized along the MASW array. The SASW data were collected as the excavator repeatedly drove back at forth over a 2 to 4 m long area at the source location. Ten to twenty-five 32 second records were averaged in the frequency domain to improve signal-to-noise ratio. All field data were saved to disk with acquisition parameters and file names documented on a field log.



*Figure 18 HP 35670A dynamic signal analyzer used for SASW acquisition*

## 4 DATA REDUCTION

### 4.1 MASW Data Reduction

The MASW data were reduced using the software Seismic Pro Surface V8.0 developed by Geogiga using the following steps:

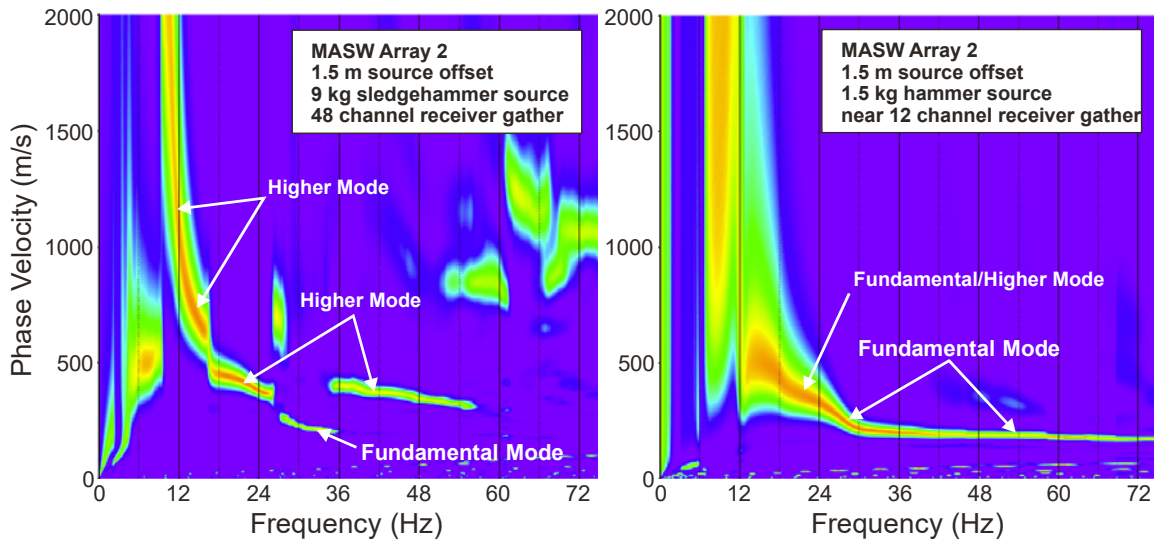
- Input seismic record into software.
- Enter receiver spacing, geometry, offset range used for analysis, etc.
- Apply wavefield transform to seismic record to convert the data from time – offset to frequency – phase velocity space.
- If seismic data were not stacked in the time domain (e.g. excavator source) stack f-v images from each individual seismic record from a fixed source location.
- Identify and pick Rayleigh wave dispersion curve.
- Repeat for all seismic records.
- Apply near-field criteria (maximum wavelength equal 1 to 1.3 times the source to midpoint of receiver array distance).
- Merge multiple dispersion curves extracted from the MASW data collected along each seismic spread (different source types, source locations, different receiver offset ranges, etc.).
- Convert dispersion curves to required format for modeling.
- Calculate a representative dispersion curve for the combined MASW dispersion data using a moving average polynomial curve fitting routine, as necessary.

A unique data acquisition and data reduction procedure used by **GEOVision** for 1-D MASW soundings is the use of multiple source types and source locations during data acquisition and the extraction of multiple (>50) dispersion curves from the different source locations and limited offset range receiver gathers associated with each source location. The use of such a data acquisition and processing strategy ensures that the modeled dispersion curve covers as wide a frequency/wavelength range as possible and is representative of average conditions beneath the array.

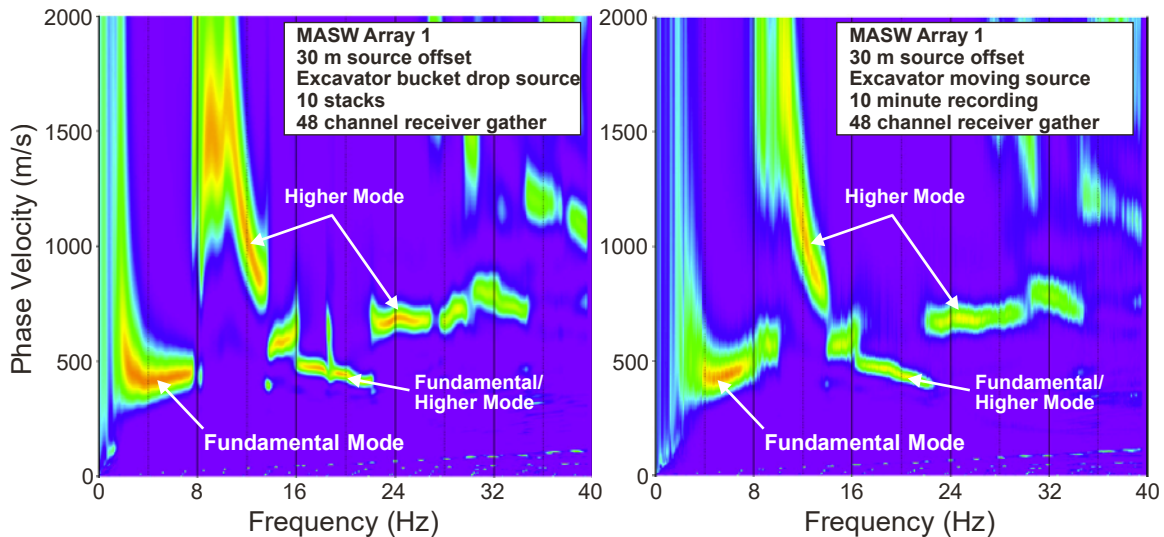
As an example, Figure 19 presents the frequency-phase velocity images of the seismic record offset 1.5 m from the end geophone on MASW Array 2 at the Andrews site. The image on the left is from a seismic record collected using a 9 kg sledgehammer source with all 48 channels used for analysis. The image on the right is from a seismic record collected using a 1.5 kg hammer source with only the near 12 channels used for analysis in order to extract higher frequency (smaller wavelength) dispersion data. The 48 channel receiver gather only recovers the fundamental mode Rayleigh wave at frequencies between about 25 and 35 Hz with the higher mode Rayleigh waves dominant at higher and lower frequencies. The receiver gather comprised of the nearest 12 geophones recovers the fundamental mode Rayleigh wave to a frequency of greater than 75 Hz.

Also unique to this investigation was the use of an excavator energy source (both bucket drops and continuous recording with the excavator moving back and forth in place), which is routinely used for SASW acquisition, to acquire MASW data. MASW data were also collected using only a 9 channel, 1 Hz geophone array to demonstrate the use of smaller numbers of geophones when expensive low frequency geophones are required for data acquisition. Figure 20 compares the f-v

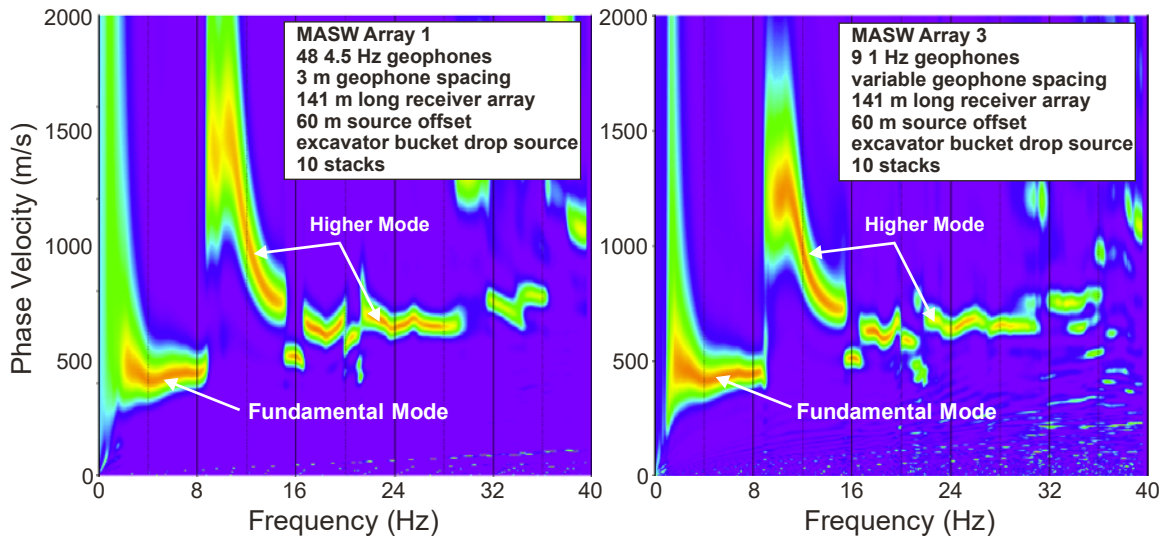
transforms from an excavator bucket drop and excavator moving back and forth for the same source location on MASW Array 1. The Rayleigh wave dispersion data from the two sources are similar; although we expect that the excavator moving back and forth will generate lower frequency energy than the bucket drop. Also note that the fundamental mode Rayleigh wave is clearly defined at frequencies less than 8 Hz using the excavator source (Figure 20 and 21), but not with the hammer source (Figure 19). Figure 21 demonstrates that similar Rayleigh wave dispersion data can be obtained at low frequencies using a 9 channel array with variable geophone spacing and the same length as a 48 channel array with constant geophone spacing.



**Figure 19** Comparison of Rayleigh wave  $f$ - $v$  transforms from 48 and 12 channel receiver gathers at the Andrews site, MASW Array 2

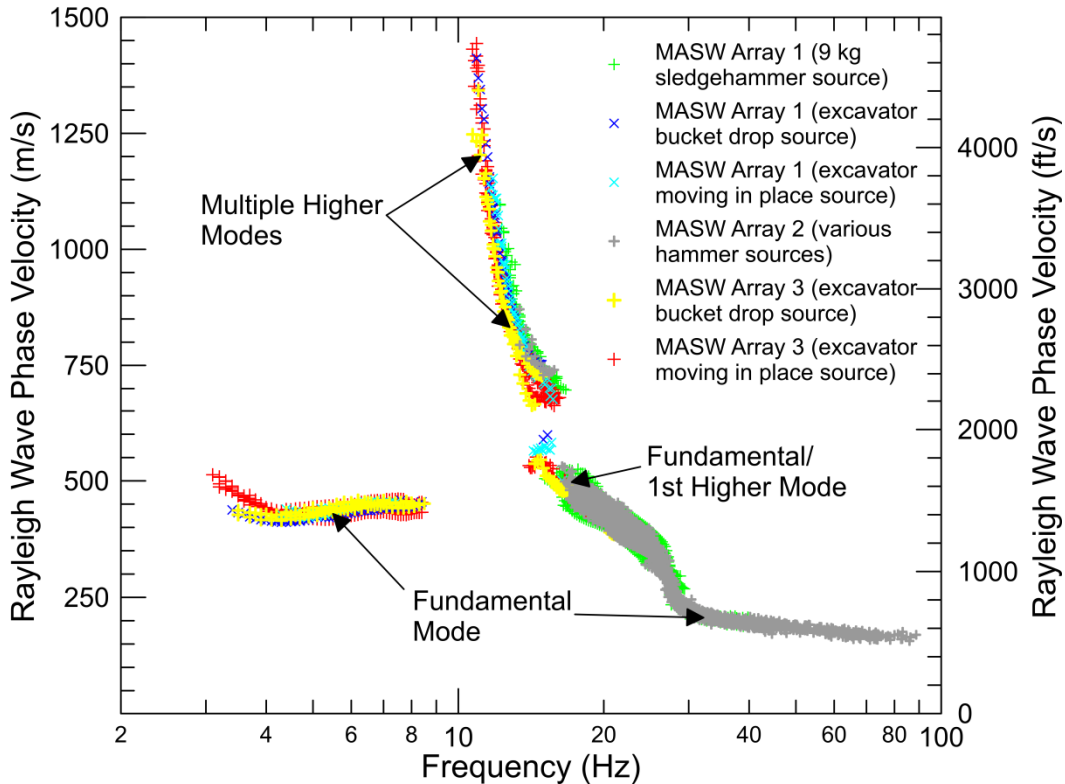


**Figure 20** Comparison of Rayleigh wave  $f$ - $v$  transforms from excavator bucket drop and moving back and forth energy sources at the Andrews site, MASW Array 2.



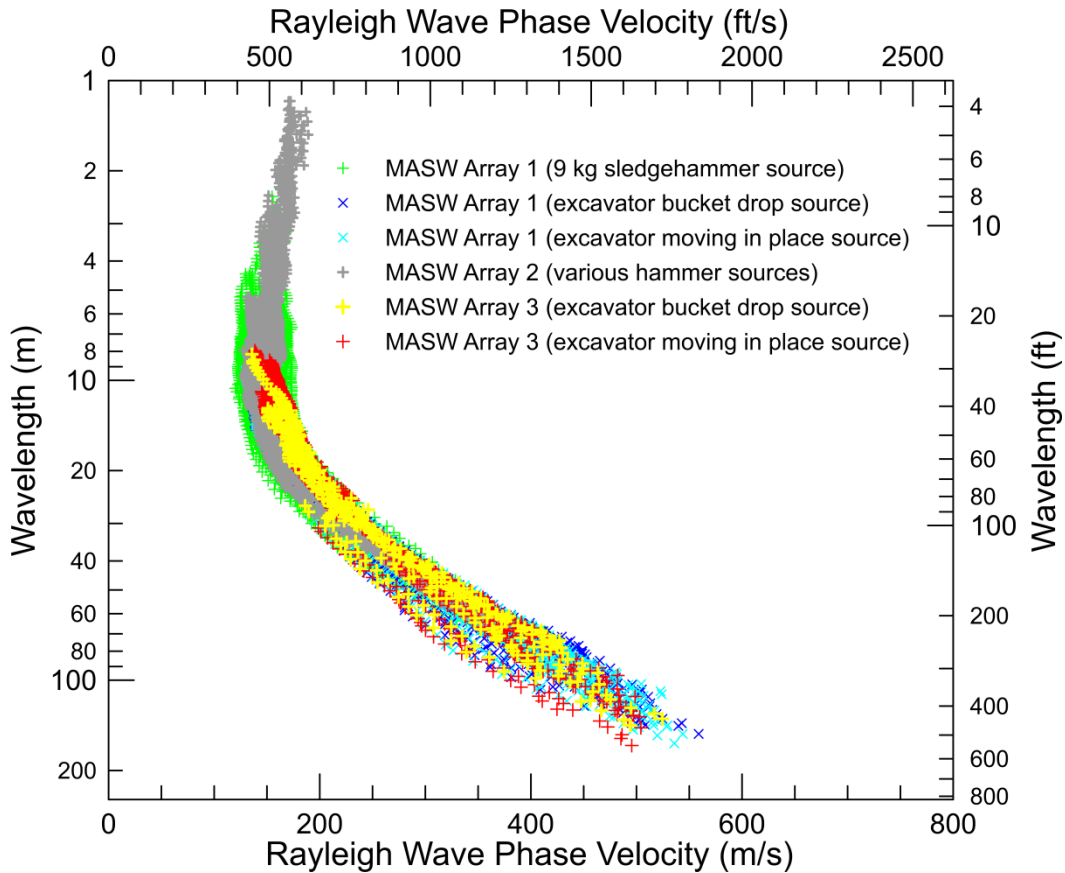
**Figure 21** Comparison of Rayleigh wave  $f$ - $v$  transforms from excavator bucket drop energy source for the 48 channel, 141 m long Array 2 and 9 channel, 141 m long Array 3 at the Andrews site

Figure 22 presents the Rayleigh wave dispersion data from MASW Arrays 1 to 3 at the Andrews site, plotted as log frequency versus Rayleigh wave phase velocity. Rayleigh wave propagation at the Andrews site is very complex with dominant higher mode Rayleigh wave energy at frequencies between about 10 and 20 to 25 Hz and no evidence of the fundamental mode Rayleigh wave over this frequency range. This type of dispersion curve signature indicates that a shallow high velocity layer may be present at the site.



**Figure 22** Andrews site – Rayleigh wave dispersion data from MASW Arrays 1 to 3

Figure 23 presents the Rayleigh wave dispersion data from MASW Arrays 1 to 3 at the Conway site, plotted as Rayleigh wave phase velocity versus log wavelength. There is considerable scatter in the Rayleigh wave dispersion data which is indicative of significant lateral velocity variability beneath the testing arrays. Our data reduction procedure utilizes multiple variable offset range receiver gathers when generating the f-v transforms for each source location to quantify the degree of lateral velocity variability.



*Figure 23 Conway site – Rayleigh wave dispersion data from MASW Arrays 1 to 3*

## 4.2 SASW Data Reduction

The SASW data were reduced using the WinSASW software package and the following steps:

- Input forward and/or reverse-direction phase spectrum and coherence for a receiver spacing.
- Enter receiver spacing, geometry and wavelength restrictions (max. wavelength = 2 times the receiver spacing).
- Mask phase data (either the forward and reverse directions individually or the average).
- Generate dispersion curve.
- Repeat for all receiver spacings and merge all dispersion curves as appropriate.

- Calculate a representative dispersion curve for the combined SASW dispersion data using the moving average polynomial curve fitting routine in the software package WinSASW V3.

Figure 24 presents the Rayleigh wave dispersion data from the SASW array at the Andrews site, plotted as log frequency versus Rayleigh wave phase velocity. The SASW dispersion data have dominant higher mode Rayleigh waves at intermediate frequencies, similar to the MASW dispersion data, which is indicative of a shallow high velocity layer.

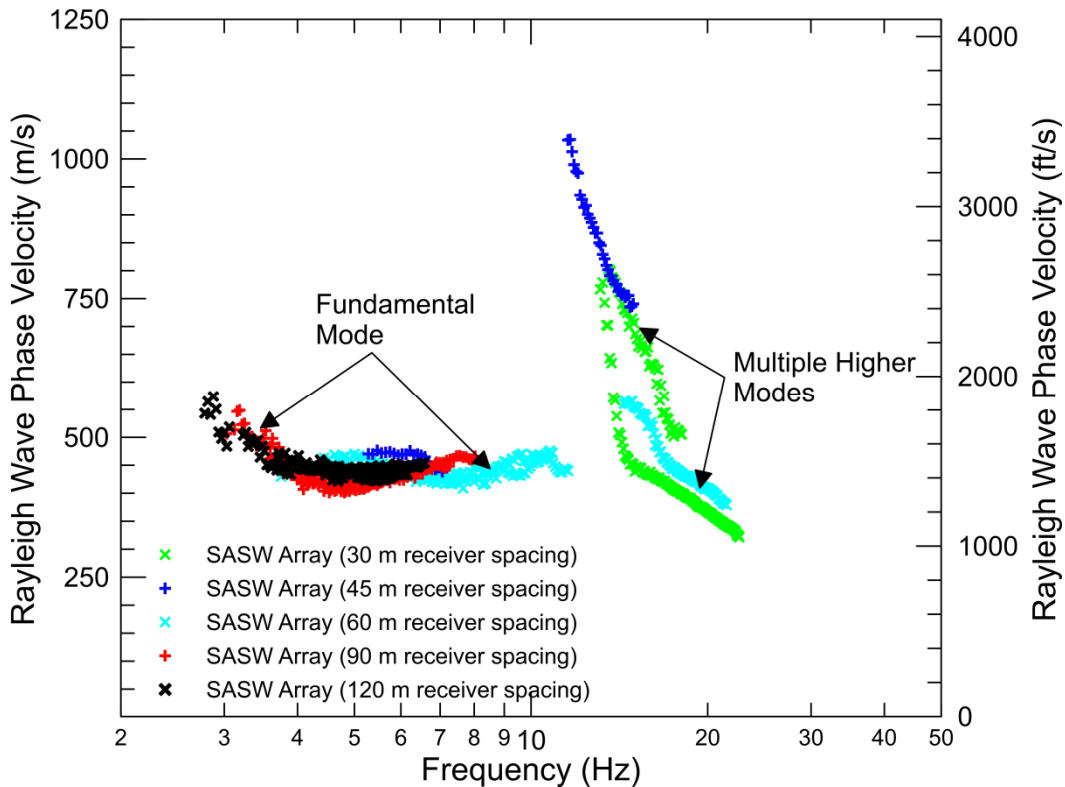


**Figure 24** Andrews site – Rayleigh wave dispersion data from SASW array

Figure 25 presents the Rayleigh wave dispersion data from the SASW array at the Conway site, plotted as Rayleigh wave phase velocity versus log wavelength. These data were acquired using a common source geometry and are, therefore, very sensitive to lateral velocity variability as the different receiver spacings characterize subsurface properties beneath different portions of the array. As with the MASW arrays, there is considerable scatter in the Rayleigh wave dispersion data which is indicative of significant lateral velocity variability beneath the array. The dispersion data from the 45 and 60 m receiver spacings are relatively similar as are the dispersion data from the 90 and 114 m receiver spacings. The dispersion data from the 75 m receiver spacing is between that from the 45/60 and 90/114 m receiver spacings.

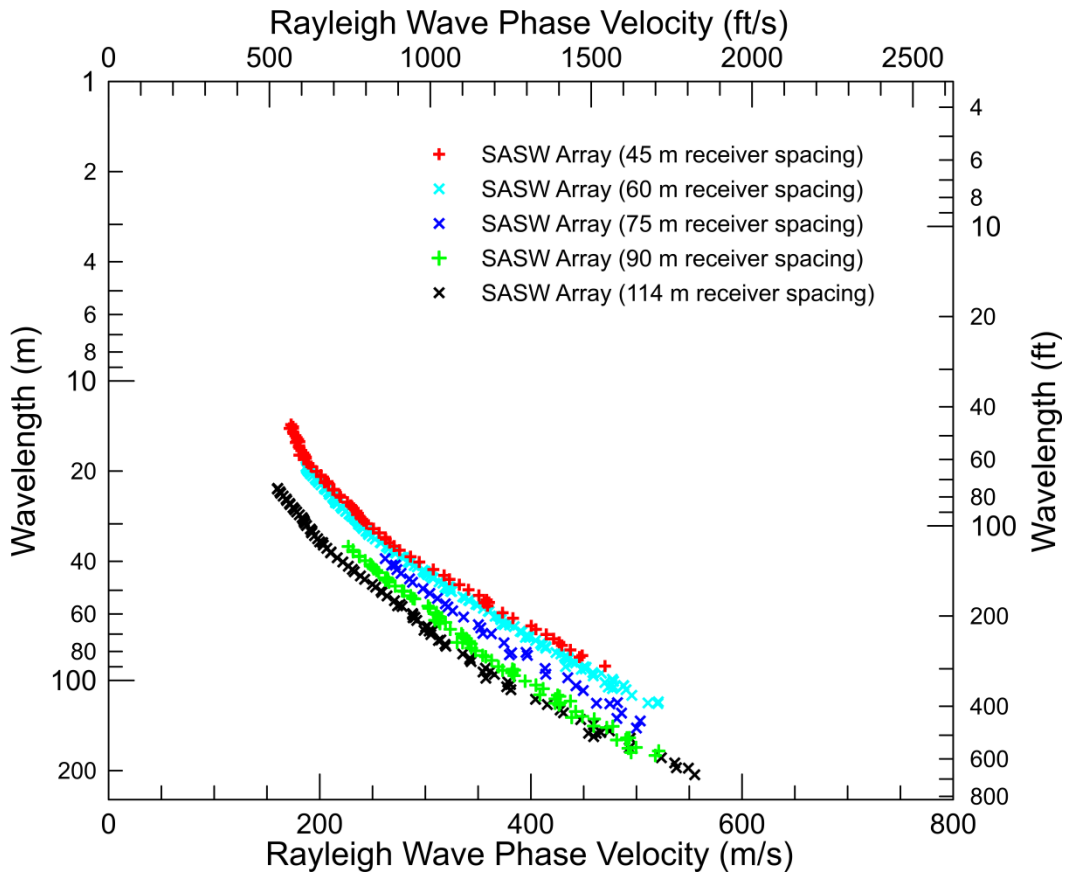


Figure 25 Conway site – Rayleigh wave dispersion data from SASW array

### 4.3 Array Microtremor Data Reduction

Acquisition of array microtremor data was not part of the scope of work for this investigation as UTA acquired surface wave data using the 2D array microtremor method. However, ambient vibration data were collected into the linear 141 m long MASW Array 1 at each site in order to compare to MASW and 2D array microtremor data. Array microtremor data collected along linear arrays were reduced using both the ESAC and ReMi™ methods.

The processing sequence for implementation of the ESAC method in the SeisImager software package is as follows:

- Input all seismic records for a dataset into software.
- Load geometry (x and y positions) for each channel in seismic records.
- Calculate the SPAC coefficients for each seismic record and average.
- For each frequency calculate the RMS error between the SPAC coefficients and a Bessel function of the first kind and order zero over a user defined phase velocity range and velocity step.
- Plot an image of RMS error as a function for frequency (f) and phase velocity (v).
- Identify and pick the dispersion curve as the continuous trend on the f-v image with the lowest RMS error.
- Convert dispersion curves to appropriate format for modeling.

- Combine multiple passive dispersion curves, as appropriate.
- Calculate a representative dispersion curve for the passive dispersion data using a moving average polynomial curve fitting routine, as necessary.

The linear array microtremor data were also reduced using both the Optim™ Software and Data Services SeisOpt® ReMi™ v5.0 data analysis package as follows:

- Conversion of SEG-2 format field files to SEG-Y format.
- Data preprocessing which includes trace-equalization gaining and DC offset removal.
- Inputting receiver geometry.
- Computing the velocity spectrum of each record by p-f transformation in both forward and reverse directions.
- Combining the individual p-f transforms (either all or selected) into one image.
- Picking and saving the dispersion curve.
- Conversion of the dispersion curve to appropriate format for modeling.
- Combination of dispersion curve with other passive dispersion curves as appropriate.
- Calculate a representative dispersion curve for the passive dispersion data using a moving average polynomial curve fitting routine, as necessary.

Interpretation of linear array microtremor data collected at the Andrews site is presented as Figure 26 and resulting Rayleigh wave dispersion curves are presented as Figure 27. The ReMi™ technique requires that the dispersion curve is interpreted along the lower envelope of the surface wave energy, which is subjective. Analysis of linear array microtremor data using the ESAC technique is not subjective; however, the resulting dispersion curve is only accurate if the multi-directional noise criteria are adequately satisfied. As with the MASW and SASW techniques, the linear array microtremor data indicates that Rayleigh wave propagation is quite complex at the site.

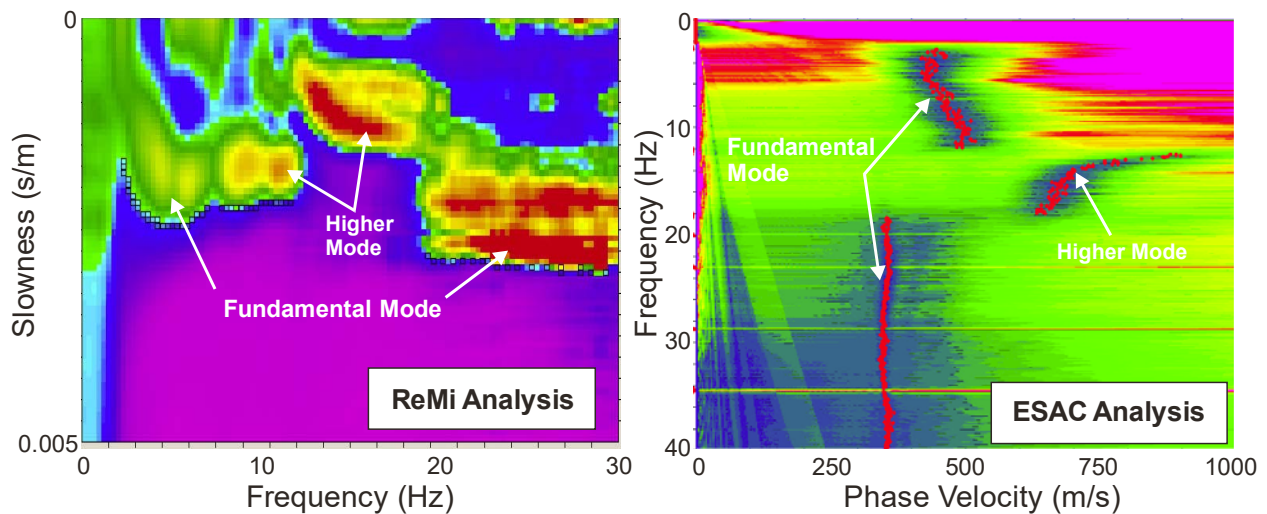


**Figure 26** Andrews site – slowness-frequency and phase velocity-frequency images resulting from ReMi™ and ESAC analysis of array microtremor data acquired along MASW Array 1

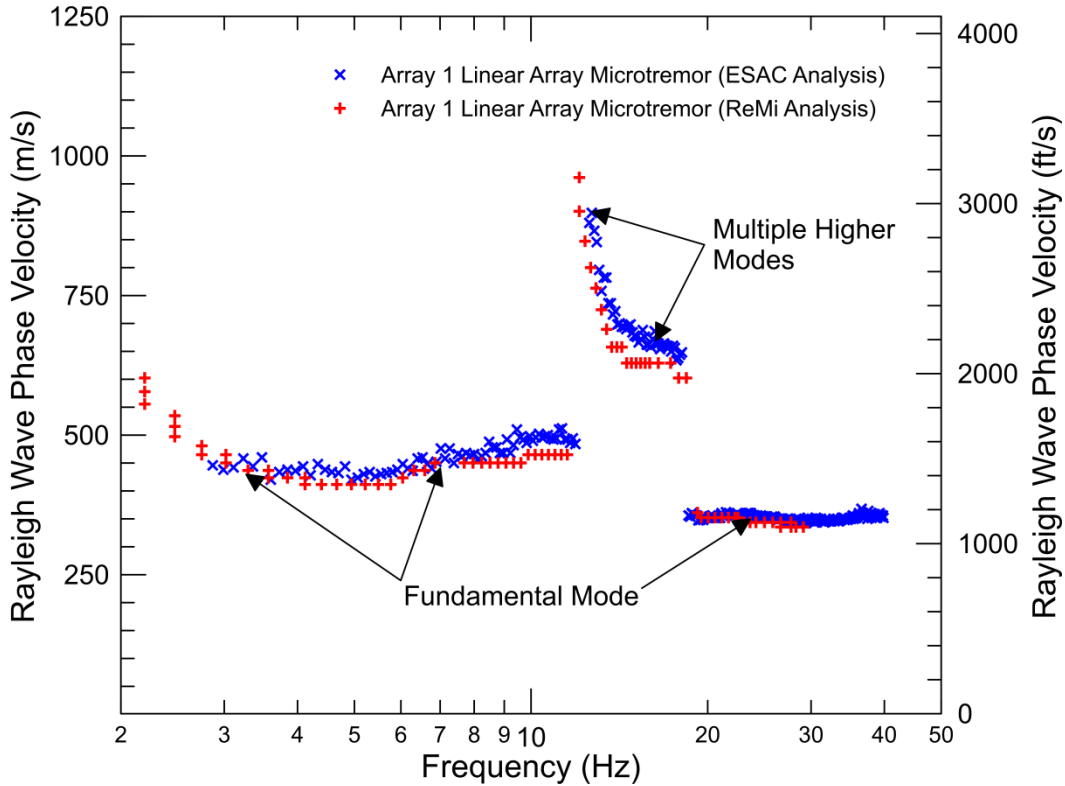


**Figure 27** Andrews site – Rayleigh wave dispersion data resulting from ReMi™ and ESAC analysis of array microtremor data acquired along MASW Array 1

The dispersion curves resulting from ReMi™ and ESAC analysis of the linear array microtremor data collected along Andrews MASW Array 1 (Figure 27) are in acceptable agreement indicating that the dispersion curves may be valid at this site. Only the ReMi™ analysis obtained dispersion data at a frequency below 3 Hz and, therefore, this data should be used with caution.

Interpretation of linear array microtremor data collected at the Conway site is presented as Figure 28 and resulting Rayleigh wave dispersion curves are presented as Figure 29. The linear microtremor array was oriented perpendicular to a highway with moderate traffic, which is generally considered a favorable array set up for recovery of useful surface wave dispersion data. Interpretation of the linear array microtremor data is complicated by the presence of significant lateral velocity variation as identified in the MASW and SASW data. It should be noted that an array oriented parallel to the highway would not have satisfied the multi-directional noise criteria necessary for successful implementation of passive linear arrays. There appear to be two phase velocity trends in the data – a higher velocity trend that appears dominant over a wide frequency range and a lower velocity trend that occurs over a narrower frequency range. The dispersion curves resulting from ReMi™ and ESAC analysis of the linear array microtremor data collected along Conway MASW Array 1 (Figure 29) are in good agreement for the low velocity trend although the ReMi dispersion curve extends to much longer wavelengths (lower frequencies). ReMi™ and ESAC analysis of the high velocity trend result in somewhat different dispersion curves, especially at long wavelengths. Under normal conditions, the dispersion data interpreted from the linear array microtremor data would be considered too complex to be used for site characterization. However, this site has significant lateral velocity variability and the linear array

microtremor data may yield  $V_S$  models comparable to those from active source surface wave testing.

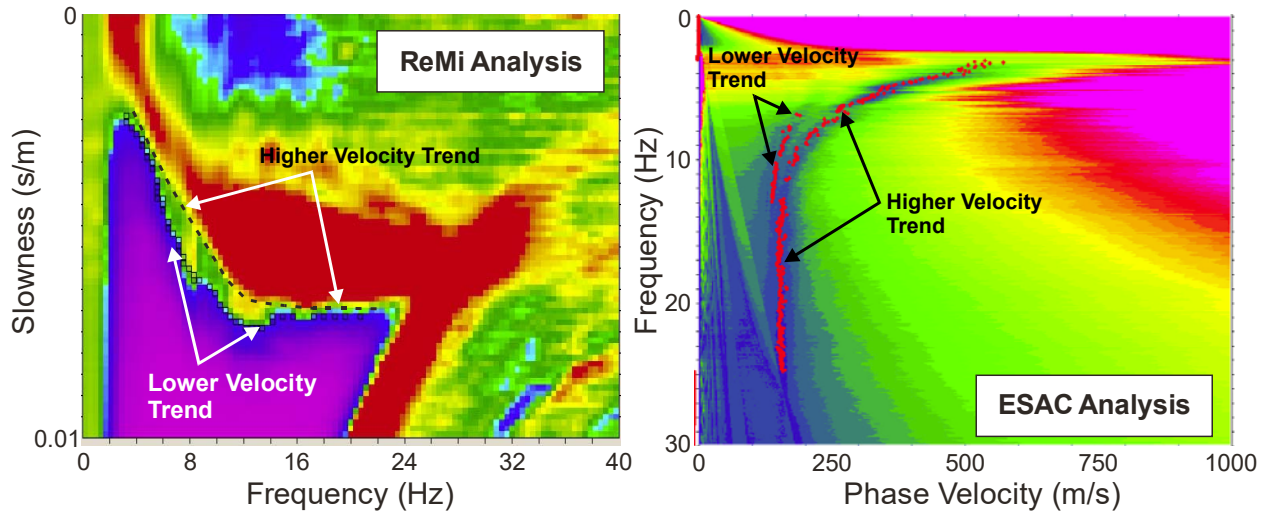


**Figure 28** Conway site – slowness-frequency and phase velocity-frequency images resulting from ReMi™ and ESAC analysis of array microtremor data acquired along MASW Array 1

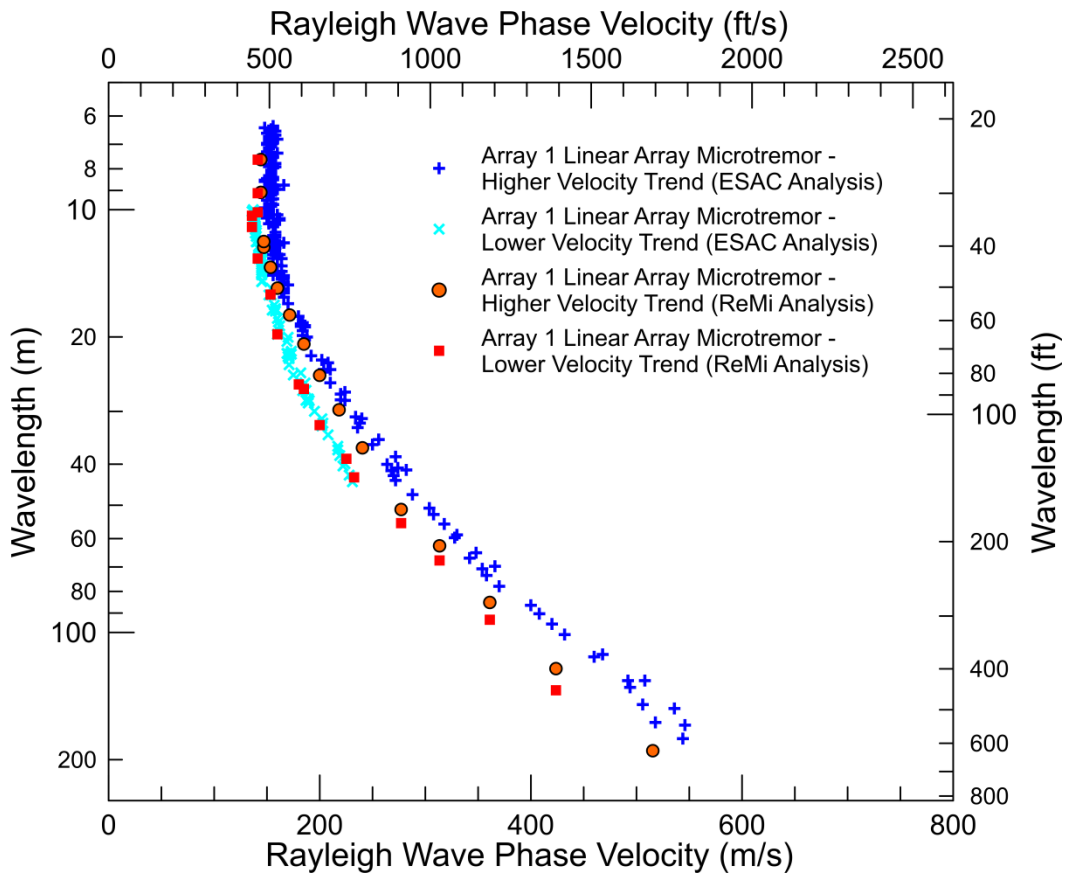


**Figure 29** Conway site – Rayleigh wave dispersion data resulting from ReMi™ and ESAC analysis of array microtremor data acquired along MASW Array 1

#### 4.4 Comparison of Surface Wave Dispersion Data

A comparison of the MASW, SASW, and linear array microtremor data acquired at the Andrews site is presented as Figure 30. There is generally good agreement between the MASW and SASW dispersion data. At frequencies higher than about 20 Hz, the dispersion data from the linear array microtremor data analyzed using the ReMi™ and ESAC techniques are not in good agreement with that from the MASW data. The fundamental and higher mode Rayleigh wave dispersion data linear array microtremor data at frequencies less than 20 Hz is in acceptable agreement with that from active surface wave testing. One exception is that the linear array microtremor data yields lower phase velocities at frequencies less than 3.5 Hz than the active surface wave data. It should be noted that the blade drop energy source also yields lower phase velocities than the moving excavator source at frequencies of less than 4 Hz (Figure 22).

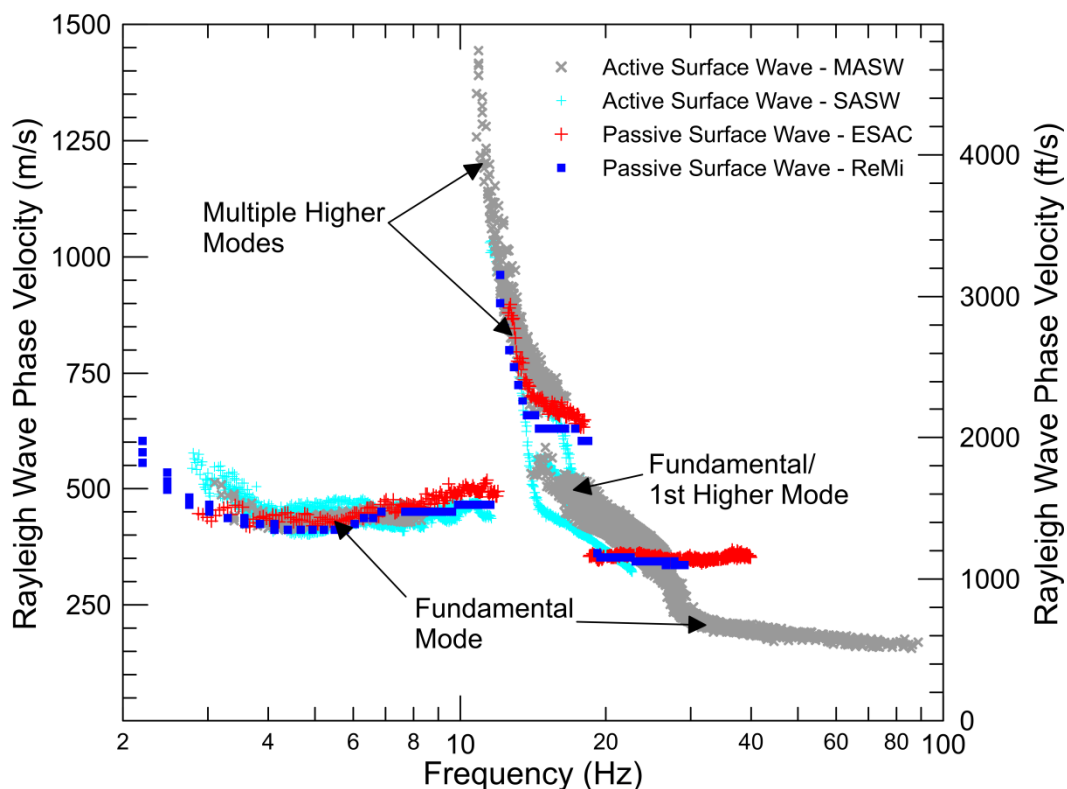


**Figure 30** Andrews site – comparison of dispersion curves from active and passive surface wave data

All MASW dispersion data from MASW Arrays 1, 2, and 3 and SASW data from 60, 90, and 120 m receiver spacings were selected for data modeling. The resulting composite dispersion data is presented in Figure 31. There is some uncertainty in the dispersion data at frequencies less than 4 Hz based on differences in dispersion curves extracted from MASW and SASW with a moving excavator source and those from MASW data collected using a bucket drop source. The linear array microtremor data also has lower phase velocities than the moving excavator source dispersion data at frequencies less than about 4 Hz; although, this data is not expected to be as reliable as that from the active source. Comparison of these dispersion curves to those collected by UTA using the 2D array microtremor method may yield additional information on which data set is more reliable at low frequencies. A larger energy source such as a Caterpillar

D9R or D10R bulldozer or large vibroseis source would have likely yielded more reliable dispersion data at low frequencies.

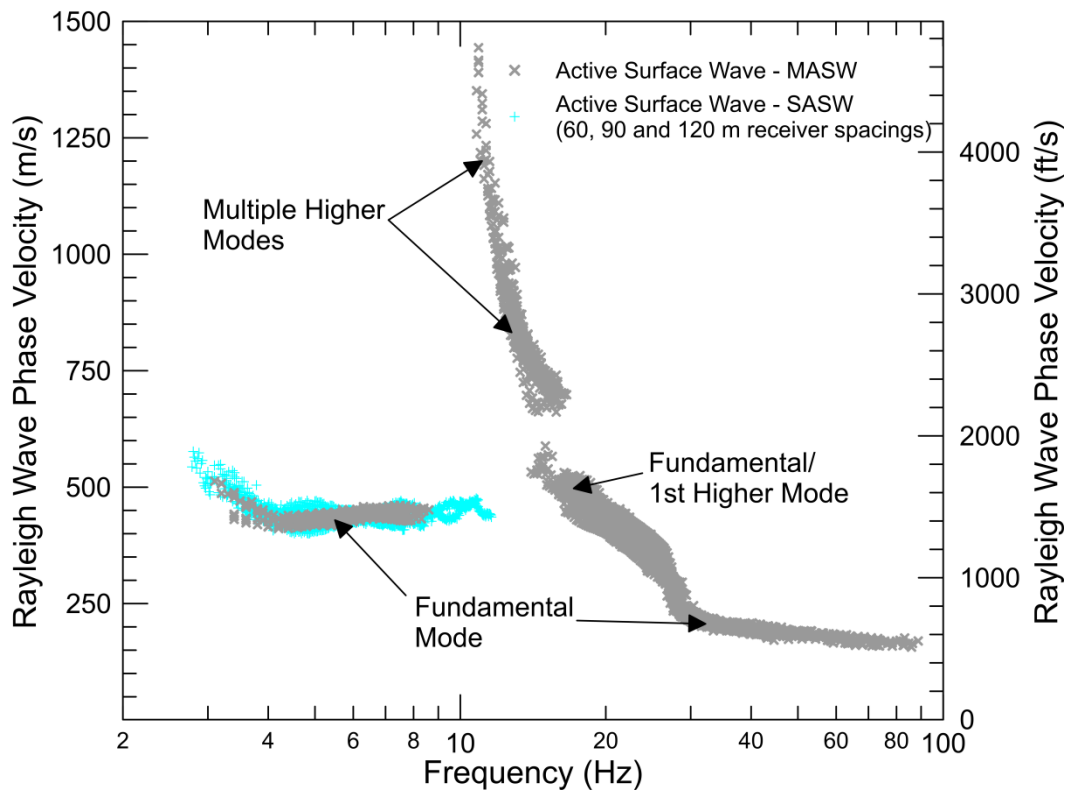


**Figure 31** Andrews site – MASW and SASW dispersion data used for data modeling

A comparison of the MASW, SASW, and linear array microtremor data acquired at the Conway site is presented as Figure 32. There is generally good agreement between the MASW and SASW dispersion data, although there is significant scatter due to lateral velocity variability. The dispersion data from the linear array microtremor data analyzed using the ReMi™ and ESAC techniques is also in acceptable agreement with that from the MASW and SASW data. The higher velocity trend identified from ESAC analysis of the linear array data appears to be in better agreement with the active surface wave data than that identified using the ReMi™ analysis, as shown in Figure 33. This figure compares MASW dispersion data extracted using the full offset range receiver gathers (i.e. all geophones) from Arrays 1, 2, and 3 and the SASW data from the 60, 75, and 90 m receiver spacing to the dominant higher velocity trend dispersion data extracted from MASW Array 1.

Due to the significant lateral velocity variation beneath the testing area, separate  $V_s$  models were developed using the dispersion curves associated with each SASW receiver spacing and MASW dispersion data extracted from receiver gathers over the same position range as the SASW receiver pairs. On MASW Array 3, only 4 geophones spanned each SASW receiver range and the resulting dispersion curves were effectively identical to those from the SASW test. Figure 34 presents the separate dispersion curves used for data modeling.

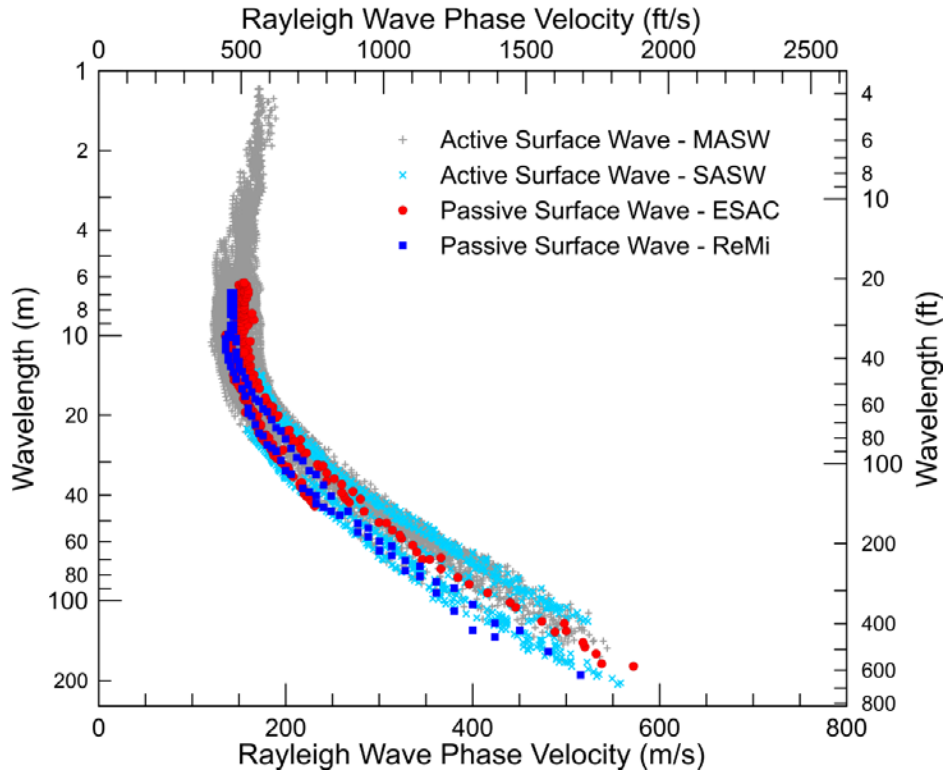


Figure 32 Conway site – comparison of dispersion curves from active and passive surface wave data

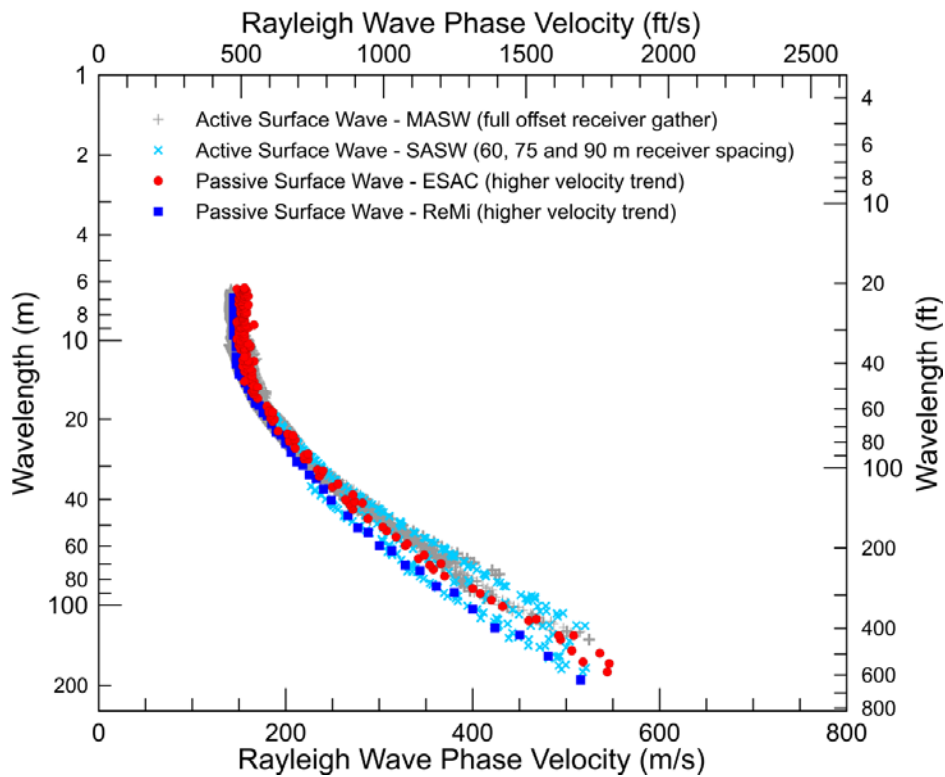
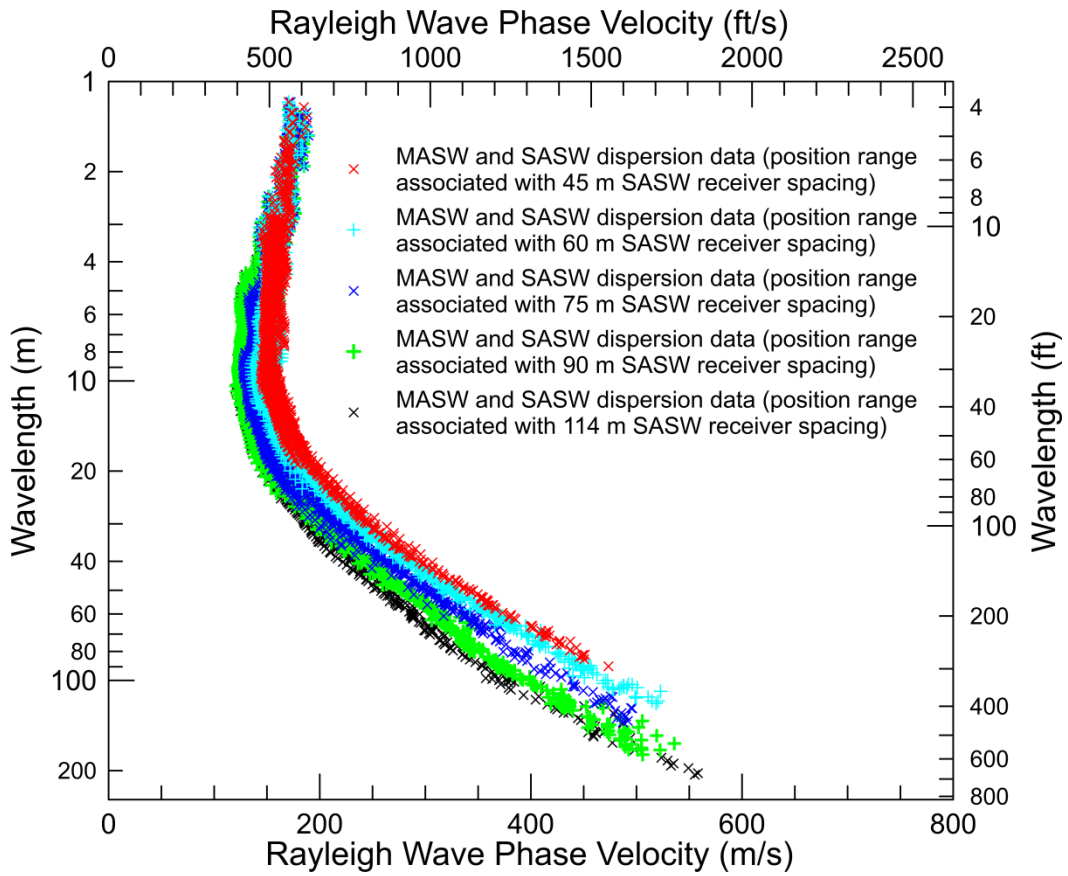


Figure 33 Conway site – comparison of dispersion curves from MASW (full offset range receiver gathers), SASW (60, 75, and 90 m receiver spacing), and array microtremor (higher velocity trend) data



**Figure 34** Conway site – MASW and SASW dispersion data used for data modeling

## 5 Surface Wave Modeling

The representative dispersion curves from the MASW and SASW dispersion data at each sounding location were combined and the moving average polynomial curve fitting routine in WinSASW V3 was used to generate a composite representative dispersion curve for modeling. An equal logarithm wavelength sample rate was used for the representative dispersion curve to reflect the gradual loss in model resolution with depth.

Rayleigh wave dispersion data are generally modeled using either the fundamental, effective mode, or multi-mode solutions in software packages such as WinSASW V3 and Seisimager. The final composite representative dispersion curve for each site was loading into a forward and/or inverse modeling software package to develop a  $V_S$  model. During this process an initial velocity model was generated based on general characteristics of the dispersion curve and the forward or inverse modeling routines were utilized to adjust the layer  $V_S$  until an acceptable agreement with the observed data was obtained. Layer thicknesses were adjusted and the modeling process repeated until a  $V_S$  model was developed with low RMS error between the observed and calculated dispersion curves. Where appropriate, multiple  $V_S$  models were developed to demonstrate model non-uniqueness.

The surface wave dispersion data from the Andrews site is very complex and required forward modeling using a multi-mode routine (Rayleigh wave mode with highest relative energy) in the Seisimager software package and effective mode modeling routine in the WinSASW V3 software package. Conventional multi-mode inversion packages require that the different Rayleigh wave modes be identified on the dispersion curve prior to modeling. This was not possible at the Andrews site because the dominant higher mode energy at intermediate frequencies appears to smoothly transition through multiple modes. Effective mode routines can often be used to simulate such dispersion curves. The 3D global effective mode routine in the WinSASW software package was utilized to simulate the effective mode. The effective mode routine the Seisimager software package did not appear to be useful for modeling the Andrews site dispersion data. It should be noted that the assumptions made in the multi-mode and effective mode analytical routines do not simulate the source and receiver geometry in the MASW survey set up. The 3D array solution in the WinSASW software package can simulate the source-receiver geometry in an SASW experiment; however, the SASW technique was only utilized to derive long wavelength/low frequency dispersion data during this investigation.

The surface wave dispersion data from the Conway site was modeled using the effective mode solution in the Seisimager software package. The effective mode solution was necessary to simulate the dominant higher mode energy at high frequencies associated with a higher velocity surface layer (stiff fill on the gravel road where testing was conducted) and a smooth transition from fundamental to 1<sup>st</sup> higher mode at low frequencies associated with stiff sediments underlying low velocity near surface sediments.

Data inputs into the modeling software include layer thickness, S-wave velocity, P-wave velocity, or Poisson's ratio (Rayleigh wave only), and mass density. P-wave velocity and mass density only have a very small influence (i.e. less than 10% providing realistic parameters used) on the S-wave velocity model generated from a surface wave dispersion curve. However, realistic assumptions for P-wave velocity, which is significantly impacted by the location of the

saturated zone, and mass density will significantly improve the accuracy of the S-wave velocity model.

When modeling surface wave dispersion data, multiple  $V_S$  models exist that equally fit the observed dispersion curve; referred to as non-uniqueness. Non-uniqueness has been found to have very little effect on estimated  $V_{S30}$ , at least at sites with a dominant fundamental mode, or modeled site response.

Constant mass density values of 1.7 to 2.2 g/cm<sup>3</sup> were used in the  $V_S$  profiles for subsurface soils depending on P and S-wave velocity. Within the normal range encountered in geotechnical engineering, variation in mass density has a negligible ( $\pm 2\%$ ) effect on the estimated  $V_S$  from surface wave dispersion data.

During modeling of the Rayleigh wave dispersion data, the compression wave velocity ( $V_P$ ) for unsaturated sediments and weathered rock was estimated using a Poisson's ratio ( $\nu$ ) of 0.3 and the relationship:

$$V_P = V_S [(2(1-\nu))/(1-2\nu)]^{0.5}$$

Poisson's ratio has a larger effect than density on the estimated  $V_S$  from Rayleigh wave dispersion data. Achenbach (1973) provides the approximate relationship between Rayleigh wave velocity ( $V_R$ ),  $V_S$ , and  $\nu$ :

$$V_R = V_S [(0.862 + 1.14 \nu)/(1 + \nu)]$$

Using this relationship, it can be shown that  $V_S$  derived from  $V_R$  only varies by about 10% over possible 0 to 0.5 range for Poisson's ratio where:

$$\begin{aligned} V_S &= 1.16V_R \text{ for } \nu = 0 \\ V_S &= 1.05V_R \text{ for } \nu = 0.5 \end{aligned}$$

Although there can be exceptions, the common range of the Poisson's ratio for unsaturated sediments and rock is about 0.25 to 0.35. Over this range,  $V_S$  derived from modeling of Rayleigh wave dispersion data will vary by about 5%. Therefore, an intermediate Poisson's ratio of 0.3 was selected for modeling to minimize any error associated with the assumed Poisson's ratio.

To reduce errors associated with expected high Poisson's ratio of saturated sediments, seismic refraction first-arrival data were reviewed in the MASW seismic records to determine if there was any evidence of a refractor associated with the top of the saturated zone in the near surface. If a saturated zone refractor was identified, interactive layer-based modeling (horizontal layers) was conducted to estimate the depth to and  $V_P$  ( $>1,500$  m/s) of the saturated sediments, which was then constrained when modeling the dispersion data. Poisson's ratio of saturated, soft sediments can be slightly less than 0.5, and gradually decrease with depth as the sediments become stiffer.

Based on this analysis the top of the saturated zone with  $V_P \sim 1,650$  m/s was constrained at a depth of about 2 m when modeling the Conway data. Interactive analysis of the Andrews data (Figure 35) revealed the presence of a seismic refraction with  $V_P \sim 2,750$  m/s (similar in forward

and reverse direction indicating subhorizontal layer), much higher than expected for shallow saturated zone, at a depth of about 3.5 m. This layer could be as much as 1 meter deeper if there is a thin, hidden layer saturated layer overlying the high velocity layer. Further review of the hyperbolic moveout of seismic reflectors at greater depth revealed that the high velocity layer must have limited, but not resolvable, thickness with  $V_P$  decreasing to that of typical saturated sediments (1,500 to 1,750 m/s) at greater depths.

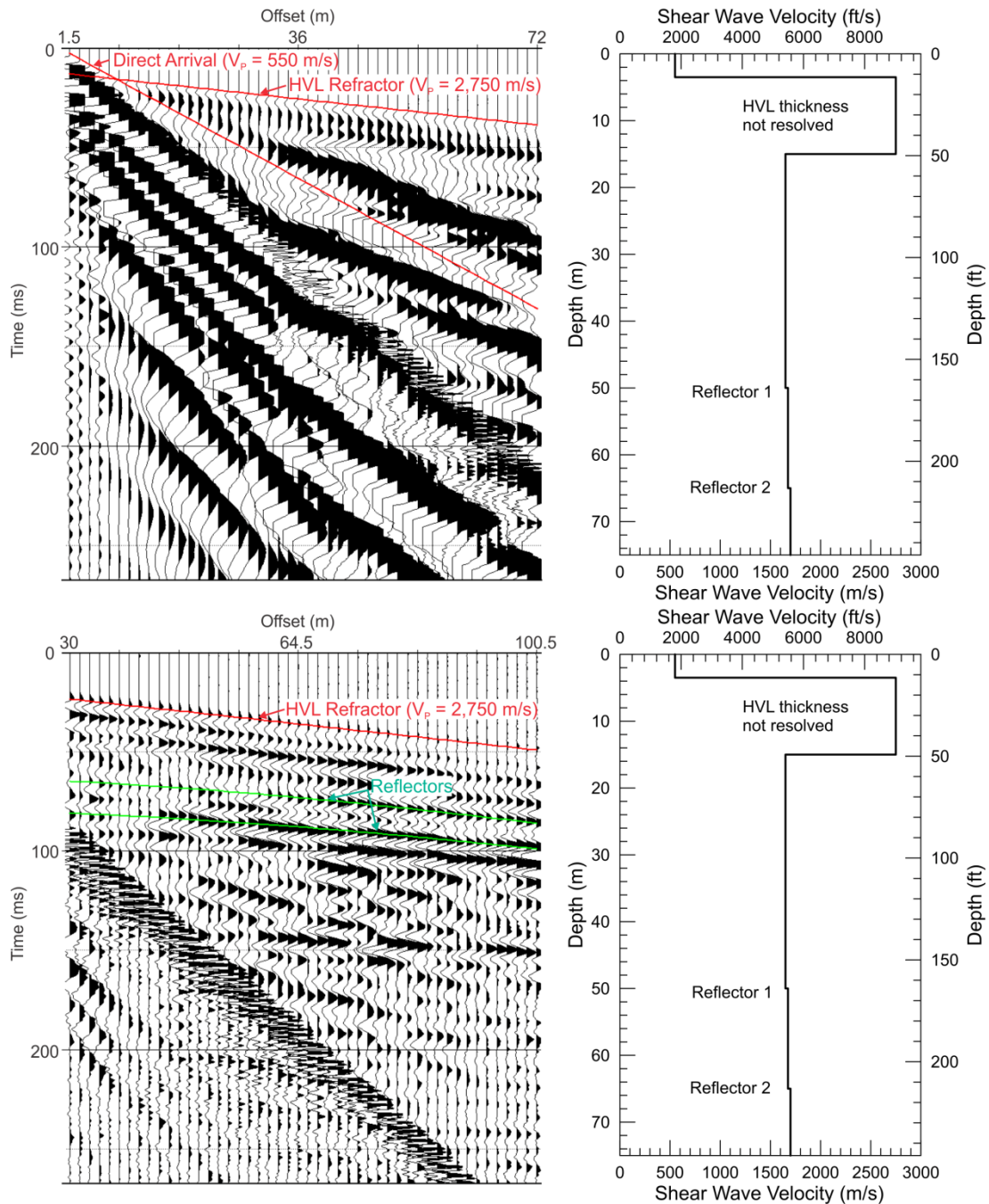


**Figure 35** Interactive analysis of seismic refractors and reflectors at Andrews site

## 6 RESULTS

### 6.1 Andrews Site

The characteristics of the Rayleigh wave dispersion data collected at the Andrews site (Figure 30) indicate that a shallow high velocity layer (HVL) is likely present beneath the site. Additionally, simple interactive review of seismic refractors and reflectors in the Andrews site seismic records, also indicate the presence of a shallow HVL of limited, but irresolvable, thickness. Sediments below the HVL are likely saturated based on the hyperbolic moveout of seismic reflectors at depth and the possibility cannot be discounted that a thin, saturated layer overlies the high velocity layer. The seismic refraction first-arrival data indicates that the HVL has a  $V_P$  of about 2,750 m/s. Depending on whether this layer is saturated or not, expected  $V_S$  might be in the 700 to 1,500 m/s range.

The array microtremor data acquired using a linear array provides similar evidence of the presence of a HVL as the MASW data, but does not recover correct Rayleigh wave dispersion data at frequencies greater than 20 Hz and less than 3.5 Hz.

Sites with a HVL can often be modeled using either multi-mode or effective mode inversion routines. Occasionally, the fundamental mode Rayleigh wave is dominant depending on the depth and velocity of the HVL. Rayleigh wave propagation at the Andrews site is very complicated and it was only possible to attempt modeling of the data using an effective mode solution in an SASW modeling software package (3D global solution in WinSASW V3) and a multi-mode solution (mode with highest relative energy) in the Seisimager software package. Neither of these approaches accurately simulates the source-receiver geometry of an MASW experiment and, therefore, error may be higher than typically observed. The inverse modeling routines in these packages could not be successfully implemented with this data and it was necessary to use a forward modeling approach, which severely limited exploration of the model space. There is significant model non-uniqueness associated with a HVL and it is not possible to independently resolve the thickness and velocity of the HVL, and velocity of the underlying layer.

Figures 36 and 37 present  $V_S$  models for an HVL with variable thickness and assumed constant  $V_S$  of 1,000 m/s, developed using the 3D global solution in WinSASW ( $V_S$  models 1 to 5) and Rayleigh wave mode with maximum energy in Seisimager ( $V_S$  models 1A to 5A), respectively. Layer  $V_S$  below the HVL and resulting  $V_{S30}$  estimates are generally slightly higher in the models developed using Seisimager. As the thickness of the HVL increases, the  $V_S$  of the layer underlying the HVL decreases until at some point velocity becomes unrealistically low. Models are presented for a HVL thickness of 6 to 12 m and arguments can be made that all models are equally valid. It should be noted that the calculated dispersion curve for the  $V_S$  models developed using WinSASW are in better agreement with the higher mode energy between 10 and 15 Hz than those developed using Seisimager; however, the agreement is not as good at frequencies greater than 25 Hz. Calculated higher modes are presented in Figure 37 for  $V_S$  model 3A. As previously discussed, Rayleigh wave propagation is very complex with Rayleigh wave phase velocities in the frequency range of 3 to 10 Hz, 10 to 15 Hz, 15 to 25 Hz, and 25 to 90 Hz representing the fundamental mode, 4<sup>th</sup> to 8<sup>th</sup> higher mode, 1<sup>st</sup> and 2<sup>nd</sup> higher mode, and fundamental mode, respectively.

Figures 38 and 39 present  $V_S$  models for an HVL with variable  $V_S$  and constant assumed thickness of 10 m, developed using the 3D global solution in WinSASW ( $V_S$  models 5 to 7) and Rayleigh wave mode with maximum energy in Seisimager ( $V_S$  models 5A to 7A), respectively. Layer  $V_S$  below the HVL and resulting  $V_{S30}$  estimates are generally slightly higher in the models developed using Seisimager. As the  $V_S$  of the HVL increases, the  $V_S$  of the layer underlying the HVL decreases. Models are presented for  $V_S$  of 750, 1000, and 1250 m/s and arguments can be made that all models are equally valid, although the calculated dispersion curve for the  $V_S$  model with a HVL velocity of 750 m/s is in the best agreement with the higher mode energy between 10 and 15 Hz.

For the purpose of site characterization, we present a  $V_S$  model with a HVL thickness of 10 m and a  $V_S$  of 700 m/s as Figure 40 and Tables 1 to 4. In this figure, Model 8 was developed using the 3D global solution in WinSASW and Model 8A presents the multi-mode model developed in Seisimager. All previously presented models are considered equally valid, but these models appear to best fit the higher mode energy between 10 and 15 Hz.  $V_{S30}$  of Model 8 and Model 8A is 391 and 416 m/s, respectively, a 6% difference.

$V_{S30}$  of the presented  $V_S$  models 1A to 8A (Figures 37, 39, and 40) developed by attempting to fit the Rayleigh wave mode with the highest energy to the observed dispersion data (Seisimager) ranges from 332 to 417 m/s.  $V_{S30}$  of the presented  $V_S$  models 1 to 8 (Figures 36, 38, and 40) developed by attempting to fit the effective mode (WinSASW 3D global solution) to observed dispersion data ranges from 347 to 394 m/s. The lower  $V_{S30}$  estimates are generally associated with models where the high velocity layer has a greater thickness or  $V_S$ . This is a much larger variation than typically observed for  $V_S$  models developed using the fundamental mode Rayleigh wave assumption. The scatter in the observed dispersion data at long wavelengths indicates that there may be about 10% variation in  $V_{S30}$  beneath the testing arrays. The presented  $V_S$  models may reflect some of this lateral velocity variability as the calculated dispersion curves for the various models are not the same. Finally, modeling of the dispersion data was complicated due to the dominant higher mode Rayleigh waves and the resulting error in  $V_{S30}$  is likely much larger than observed at sites with less complex velocity structure.

The Rayleigh wave dispersion data presented above need to be reconciled with dispersion data from the 2D array microtremor array(s) acquired by UTA to confirm the Rayleigh wave phase velocities at frequencies below 3.5 Hz. The Rayleigh wave phase velocity data selected for modeling below 3.5 Hz is biased towards higher velocities resulting from SASW and MASW testing with the energy source consisting of an excavator moving back and forth in place. MASW data collected with an excavator bucket drop source and array microtremor data acquired using a linear array yielded lower Rayleigh wave phase velocities at frequencies below 3.5 Hz. Although, we would expect the moving excavator source to be richer in lower frequency energy than the bucket drop, the low frequency phase velocity data should be validated using another means (e.g. 2D array microtremor, larger energy source such as Caterpillar D9R, or Vibroseis). If Rayleigh wave phase velocities are overestimated at frequencies below 3.5 Hz, then the  $V_S$  of the half space in the velocity models will be overestimated.

The  $V_S$  models presented above need to be reconciled with borehole velocity measurements and  $V_S$  models developed by UTA using the MASW and 2D array microtremor techniques. Additionally, alternate data modeling strategies for treatment of complex dispersion data, such as direct inversion of the v-f transforms, should be investigated.

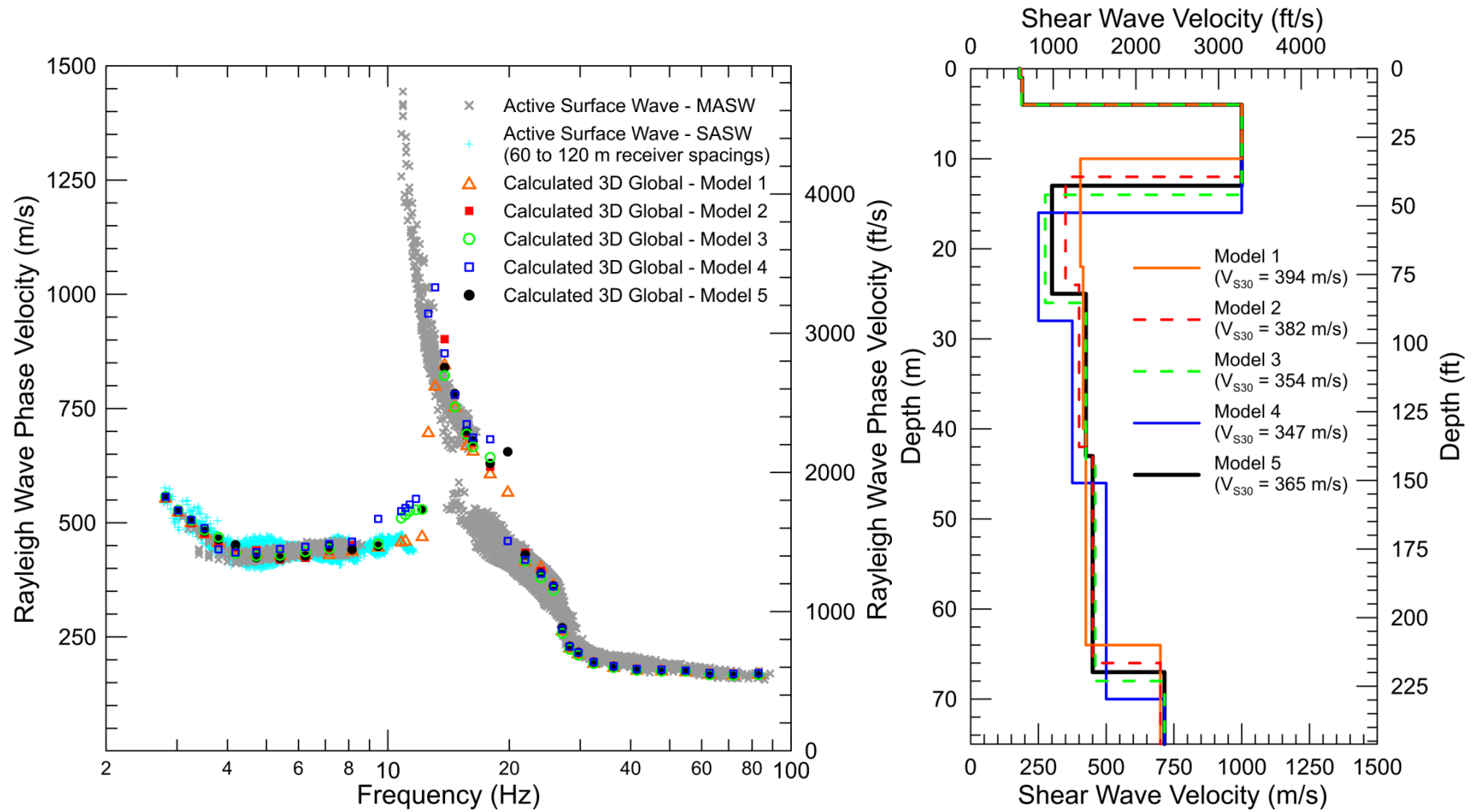


**Figure 36** Andrews site – Effective mode modeling of Rayleigh wave dispersion data (3D global solution in WinSASW software package) for constant velocity, variable thickness high velocity layer

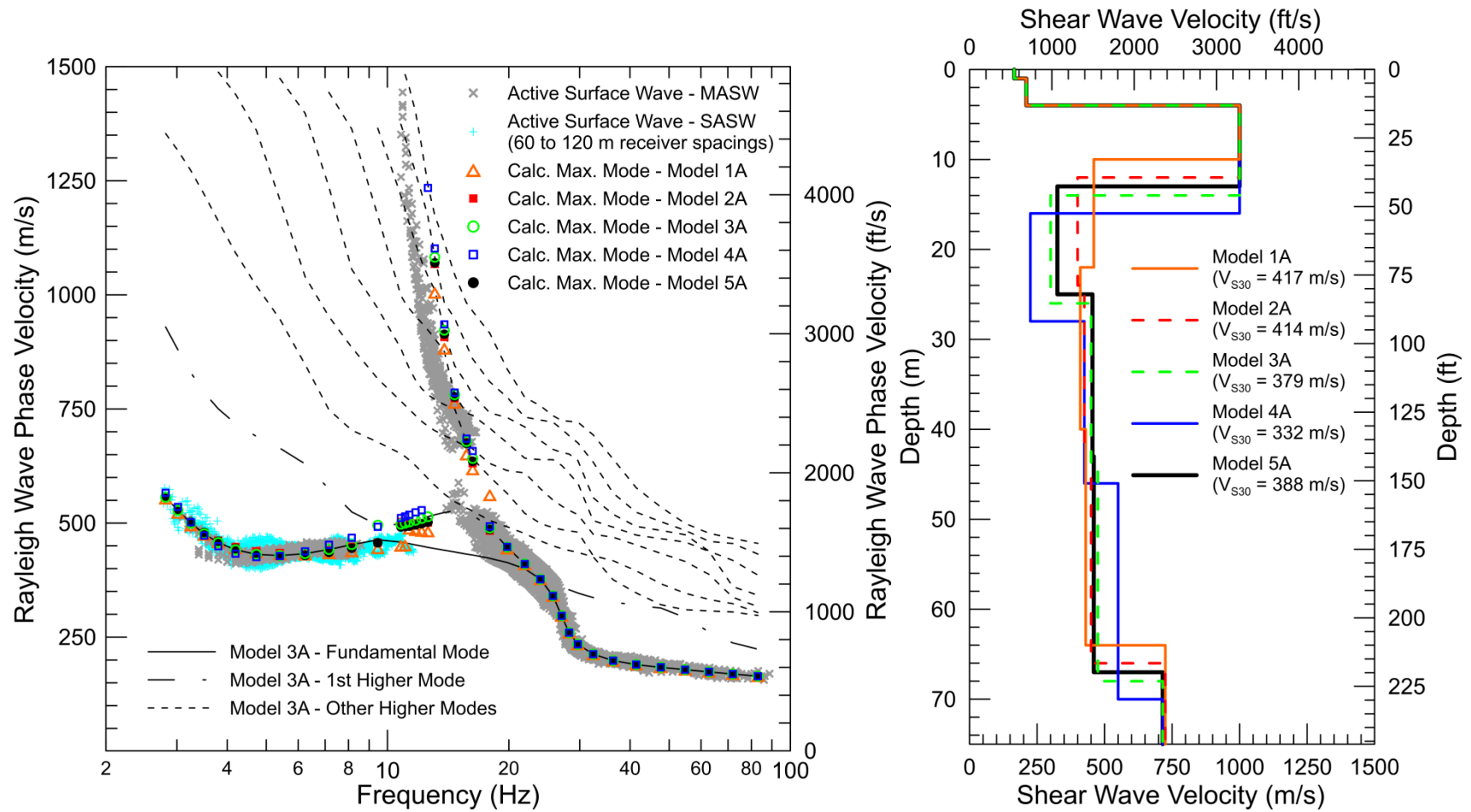


**Figure 37 Andrews site – Multi-mode modeling of Rayleigh wave dispersion data (mode with maximum energy in Seisimager software package) for constant velocity, variable thickness high velocity layer**

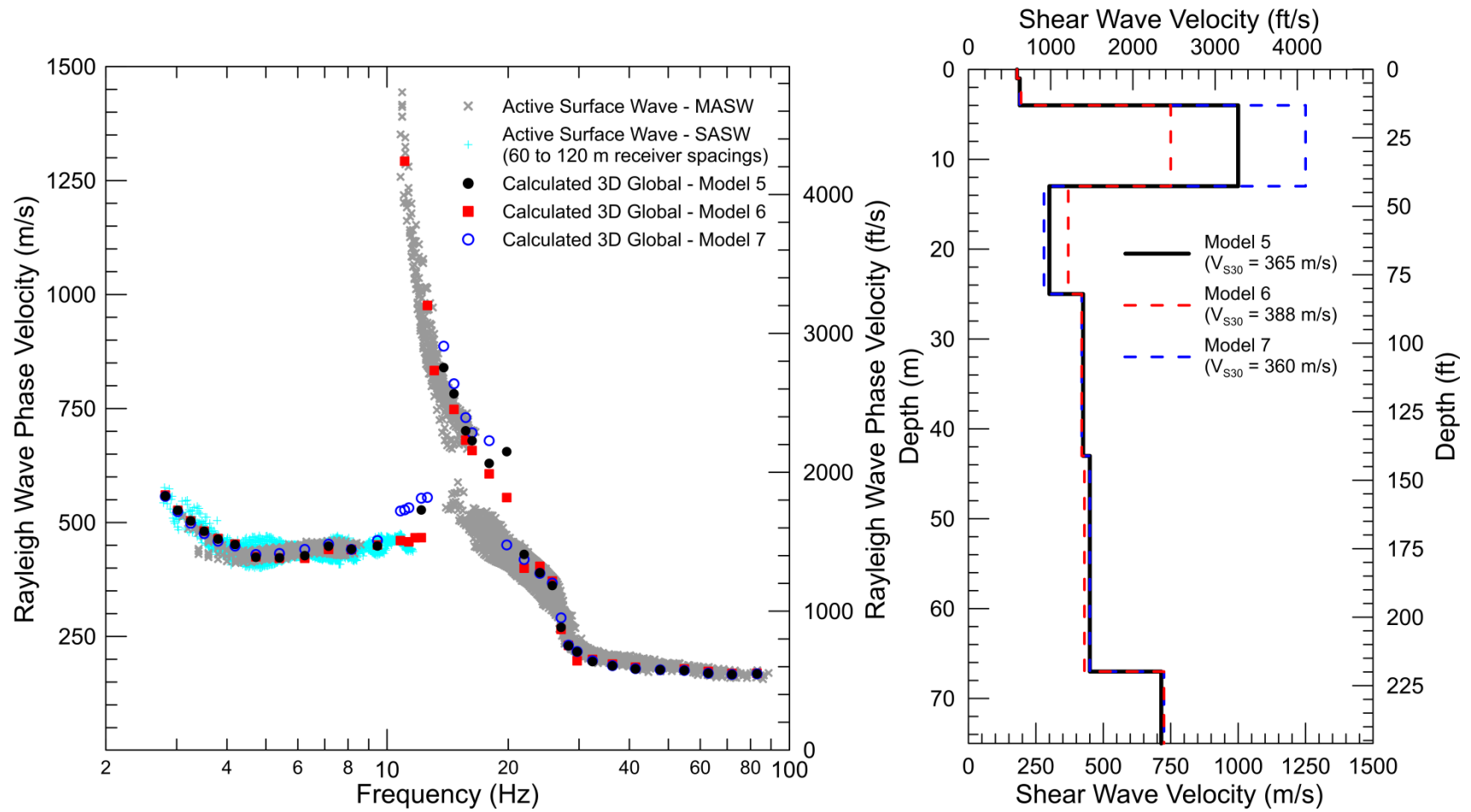


**Figure 38** Andrews site – Effective mode modeling of Rayleigh wave dispersion data (3D global solution in WinSASW software package) for variable velocity, constant thickness high velocity layer

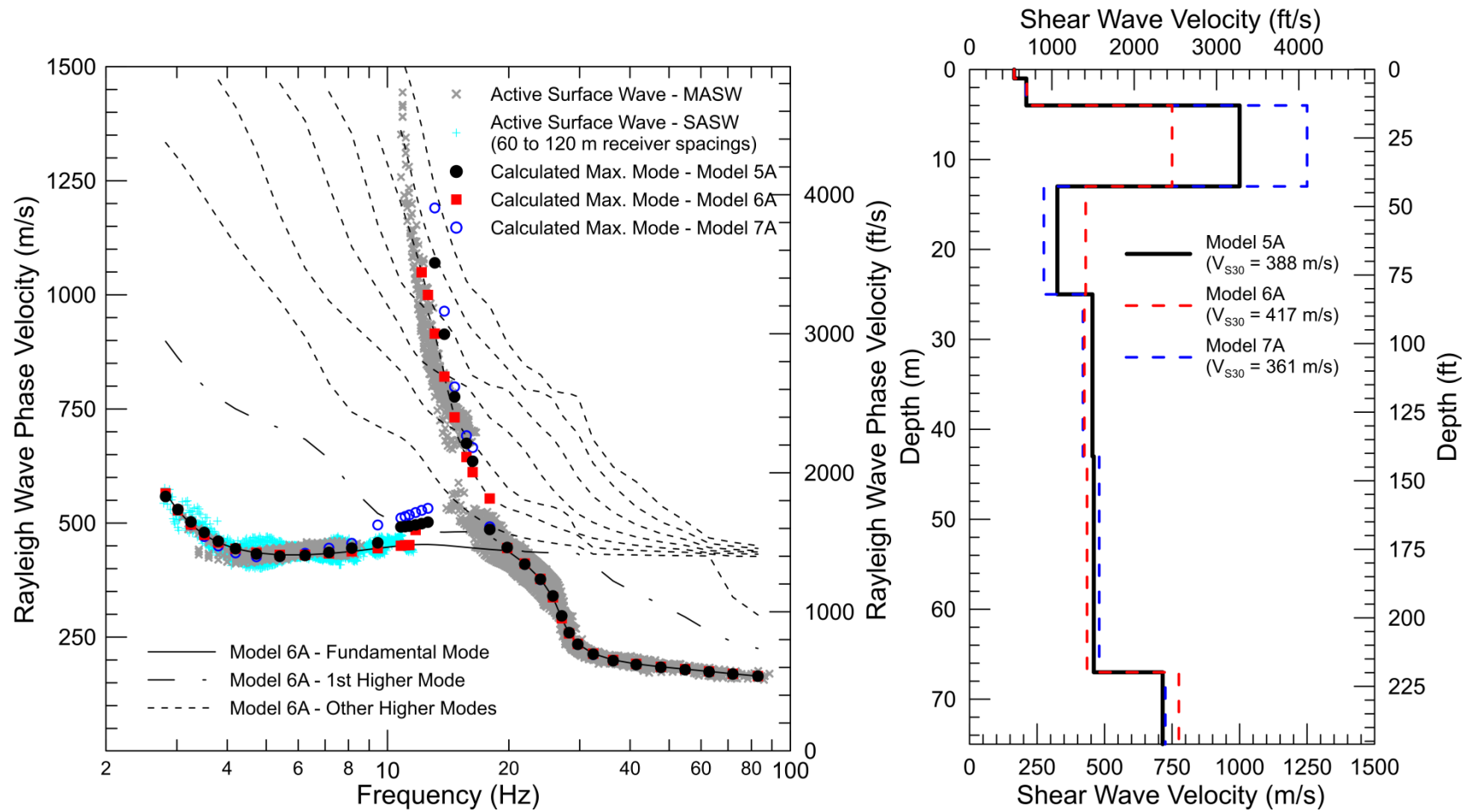


**Figure 39** Andrews site – Multi-mode modeling of Rayleigh wave dispersion data (mode with maximum energy in Seisimager software package) for variable velocity, constant thickness high velocity layer

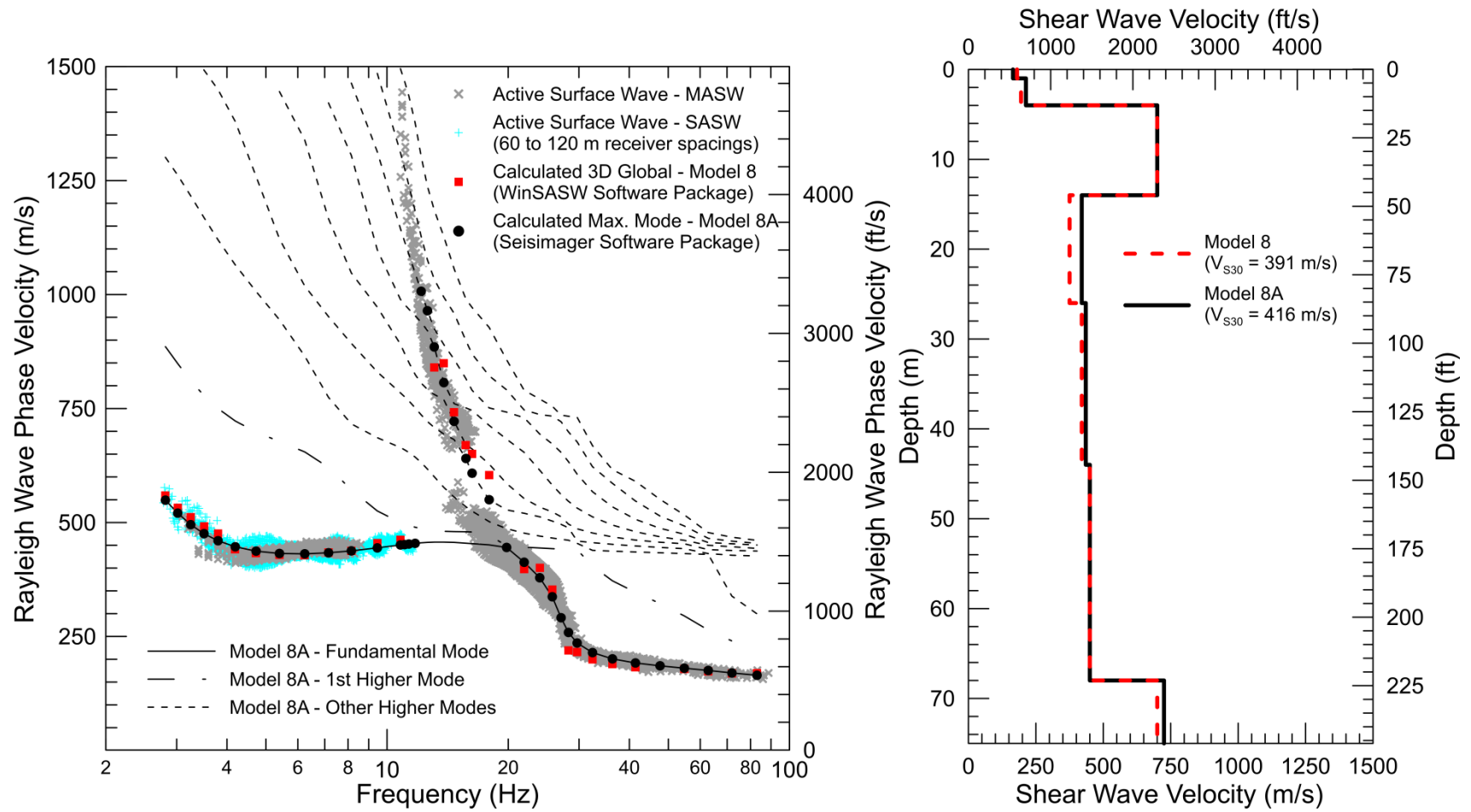


Figure 40 Andrews site – Velocity models selected for purpose of site characterization

**Table 1 Andrews site –  $V_S$  model from 3D global solution in WinSASW software package (metric units)**

Depth to Top of Layer (m)	Layer Thickness (m)	S-Wave Velocity (m/s)	Inferred P-Wave Velocity (m/s)	Assumed Poisson's Ratio	Assumed Density (g/cm <sup>3</sup> )
0	1	180	337	0.300	1.70
1	1	195	365	0.300	1.80
2	2	195	1500	0.491	1.85
4	10	700	2750	0.465	2.10
14	12	375	1600	0.471	1.90
26	18	420	1650	0.465	2.00
44	24	450	1650	0.460	2.00
68	>7	700	1750	0.405	2.10

**Table 2 Andrews site –  $V_S$  model from 3D global solution in WinSASW software package (Imperial units)**

Depth to Top of Layer (ft)	Layer Thickness (ft)	S-Wave Velocity (ft/s)	Inferred P-Wave Velocity (ft/s)	Assumed Poisson's Ratio	Assumed Density (lb/ft <sup>3</sup> )
0.0	3.3	591	1105	0.300	106
3.3	3.3	640	1197	0.300	112
6.6	6.6	640	4921	0.491	115
13.1	32.8	2297	9022	0.465	131
45.9	39.4	1230	5249	0.471	119
85.3	59.1	1378	5413	0.465	125
144.4	78.7	1476	5413	0.460	125
223.1	>23.0	2297	5741	0.405	131

**Table 3 Andrews site –  $V_S$  model from multi-mode solution (mode with maximum energy) in Seisimager software package (metric units)**

Depth to Top of Layer (m)	Layer Thickness (m)	S-Wave Velocity (m/s)	Inferred P-Wave Velocity (m/s)	Assumed Poisson's Ratio	Assumed Density (g/cm <sup>3</sup> )
0	1	165	330	0.333	1.70
1	1	213	420	0.327	1.80
2	2	213	1500	0.490	1.85
4	10	700	2750	0.465	2.10
14	12	420	1650	0.465	2.00
26	18	435	1650	0.463	2.00
44	24	450	1650	0.460	2.00
68	>7	725	1750	0.396	2.10

**Table 4 Andrews site –  $V_S$  model from multi-mode solution (mode with maximum energy) in Seisimager software package (Imperial units)**

Depth to Top of Layer (ft)	Layer Thickness (ft)	S-Wave Velocity (ft/s)	Inferred P-Wave Velocity (ft/s)	Assumed Poisson's Ratio	Assumed Density (lb/ft <sup>3</sup> )
0.0	3.3	541	1083	0.333	106
3.3	3.3	699	1378	0.327	112
6.6	6.6	699	4921	0.490	115
13.1	32.8	2297	9022	0.465	131
45.9	39.4	1378	5413	0.465	125
85.3	59.1	1427	5413	0.463	125
144.4	78.7	1476	5413	0.460	125
223.1	23.0	2379	5741	0.396	131

## 6.2 Conway Site

The characteristics of the Rayleigh wave dispersion data collected at the Conway site (Figures 23 and 25) indicate that there is significant lateral velocity variation beneath the measurement arrays. Therefore, Rayleigh wave dispersion data were reduced from receiver offset ranges coincident with each SASW receiver spacing between 45 and 114 m and  $V_S$  models developed for each of the five combined MASW/SASW data sets as shown in Figure 34. Further review of the Rayleigh wave dispersion data indicates that there is a stiff surface layer associated with the compacted gravel road on which the testing arrays were located. Interactive review of seismic refractors and reflectors in the Conway site seismic records indicate that the saturated zone with a  $V_P \sim 1,650$  m/s, is located at a depth of about 2 m.

If it were not for the complications due to lateral velocity variability, array microtremor data acquired using a linear array perpendicular to the highway would have likely yielded reliable dispersion data to image velocity structure in the upper 75 to 100 m, when combined with MASW dispersion data. Arrays aligned parallel to the highway would not have been effective. A 2D array microtremor array must be used to image velocity structure to greater depths.

Sites with a stiff surface layer can often be modeled using either multi-mode or effective mode inversion routines. At this site, the effective mode modeling routine in the Seisimager software package was used for inverse modeling of the observed Rayleigh wave dispersion curves.

Although this modeling approach does not accurately simulate the source-receiver geometry of an MASW test, it is suitable for modeling dominant higher mode Rayleigh wave energy at the high frequencies associated with a stiff surface layer and a transition from fundamental to first higher mode at low frequencies that can be associated with an abrupt increase in  $V_S$  at depth.

Figures 41 to 45 present  $V_S$  models developed from effective mode inversion of the Rayleigh wave dispersion curves corresponding to the 45, 60, 75, 90, and 114 m SASW receiver spacings, respectively. Depth of investigation ranges from about 45 m, for the 45 m receiver spacing dispersion data, to over 100 m for the 114 m receiver spacing dispersion data. The resulting  $V_S$  models in both metric and Imperial units are presented in Tables 5 to 14. The fundamental mode assumption is not valid for modeling the dispersion data at this site since wavelengths less than 3 to 5 m are dominated by higher mode energy due to the stiff surface layer and wavelengths greater than 70 to 100 m transition from fundamental to 1<sup>st</sup> higher mode.

The five  $V_S$  models are summarized in Figure 46 and illustrate the significant lateral velocity variability at the site, in both in the  $V_S$  and thickness of a low velocity layer below the road fill but also in deeper geologic units, which might imply some shallow dip (e.g. several degrees) in subsurface sediments. The  $V_S$  models associated with the 60 and 75 m SASW receiver spacings are most representative of average velocity structure beneath MASW arrays 1 and 2.  $V_{S30}$  of the five  $V_S$  models, representative of average velocity structure beneath different segments of the arrays, range from 217 to 280 m/s, a 25% variation. Such a large variation in  $V_{S30}$  over a distance of 150 m is not unusual for weathered rock sites but is not common for sediment sites.

The Rayleigh wave dispersion data presented above should be reconciled with dispersion data from the 2D array microtremor array(s) acquired by UTA. The  $V_S$  models should be reconciled with borehole velocity measurements and  $V_S$  models developed by UTA using the MASW and 2D array microtremor techniques.

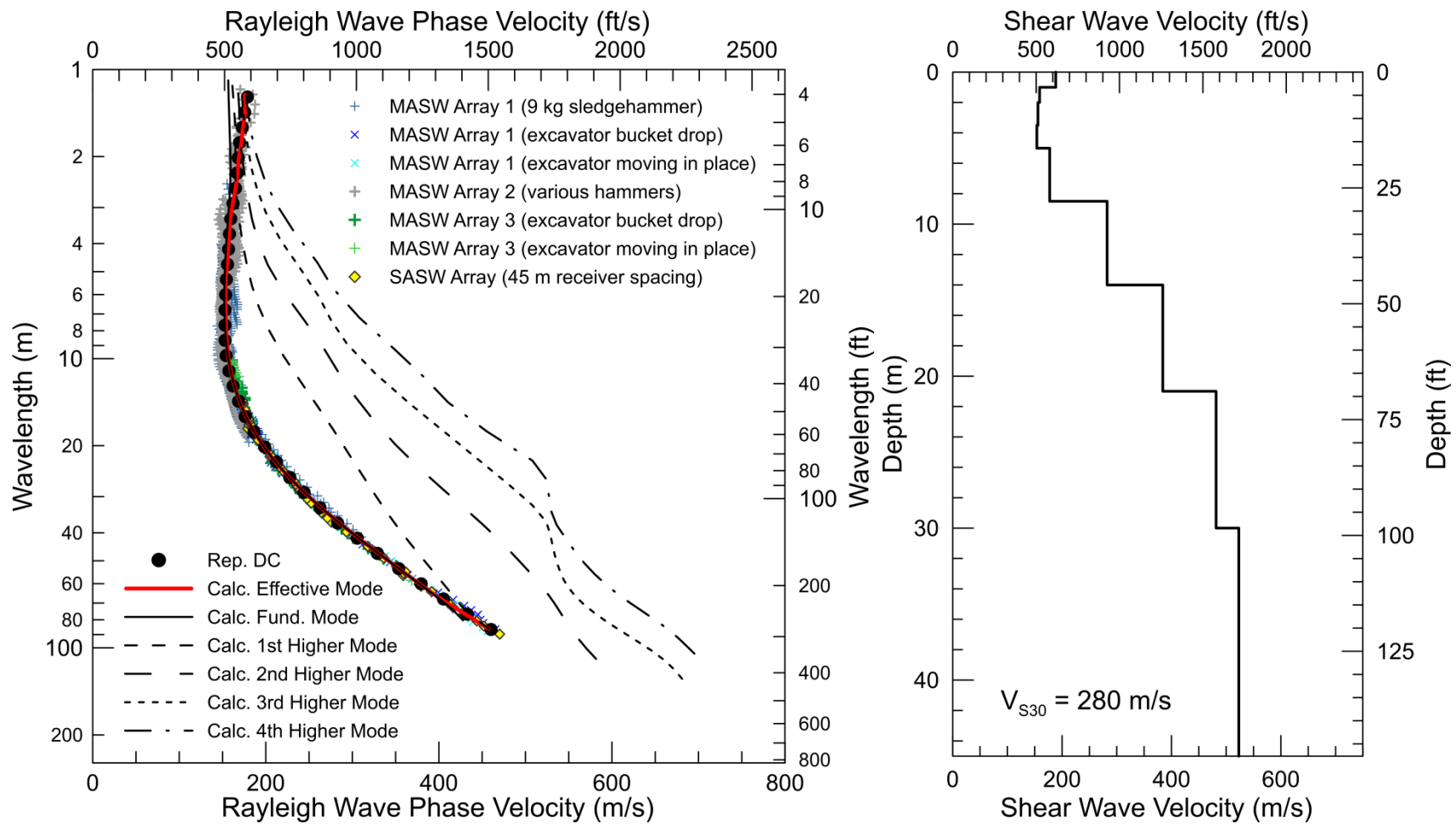


Figure 41 Conway site – Modeling of Rayleigh wave dispersion data from 45 m SASW receiver spacing and coincident MASW receiver arrays

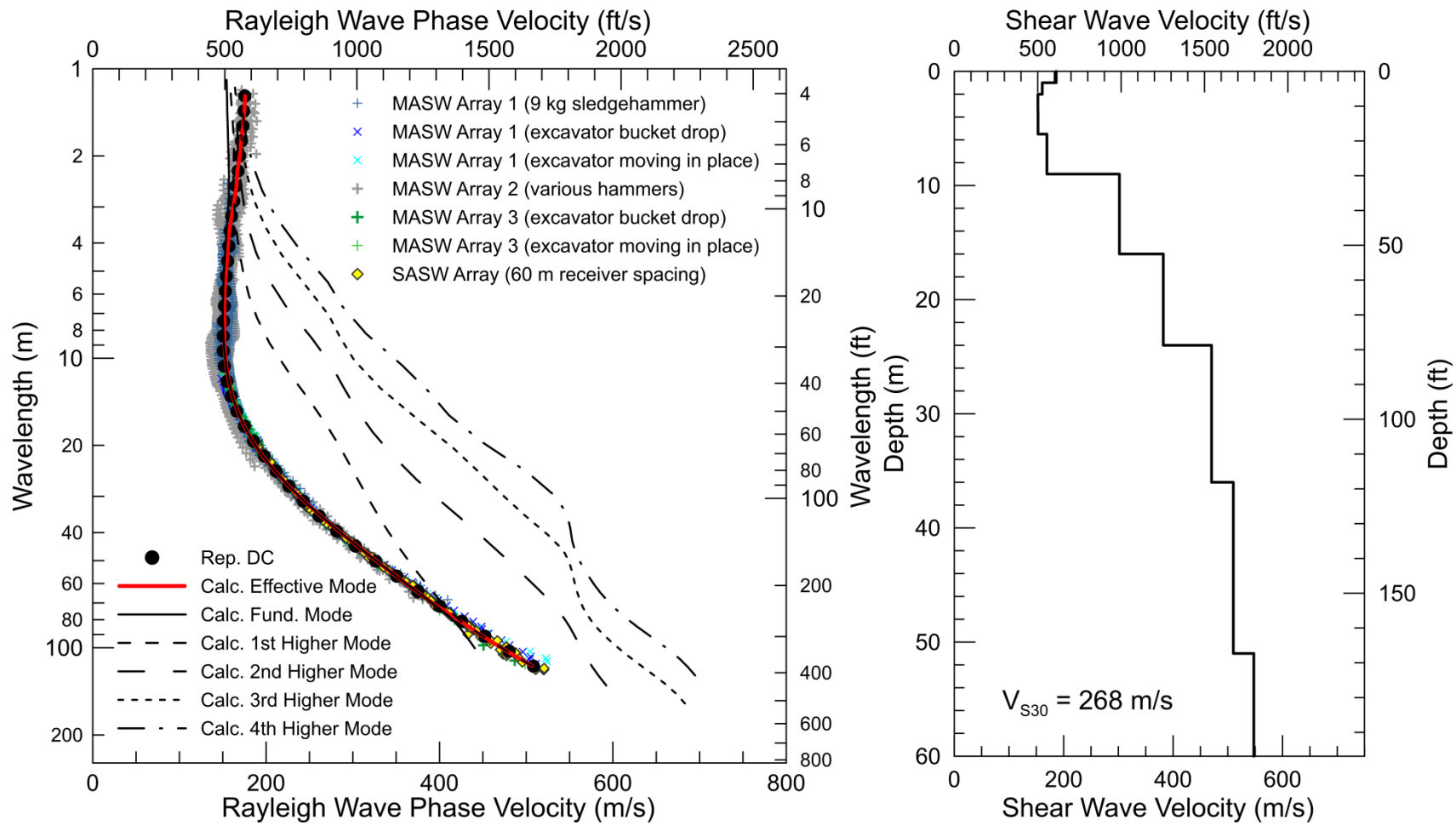


Figure 42 Conway site – Modeling of Rayleigh wave dispersion data from 60 m SASW receiver spacing and coincident MASW receiver arrays

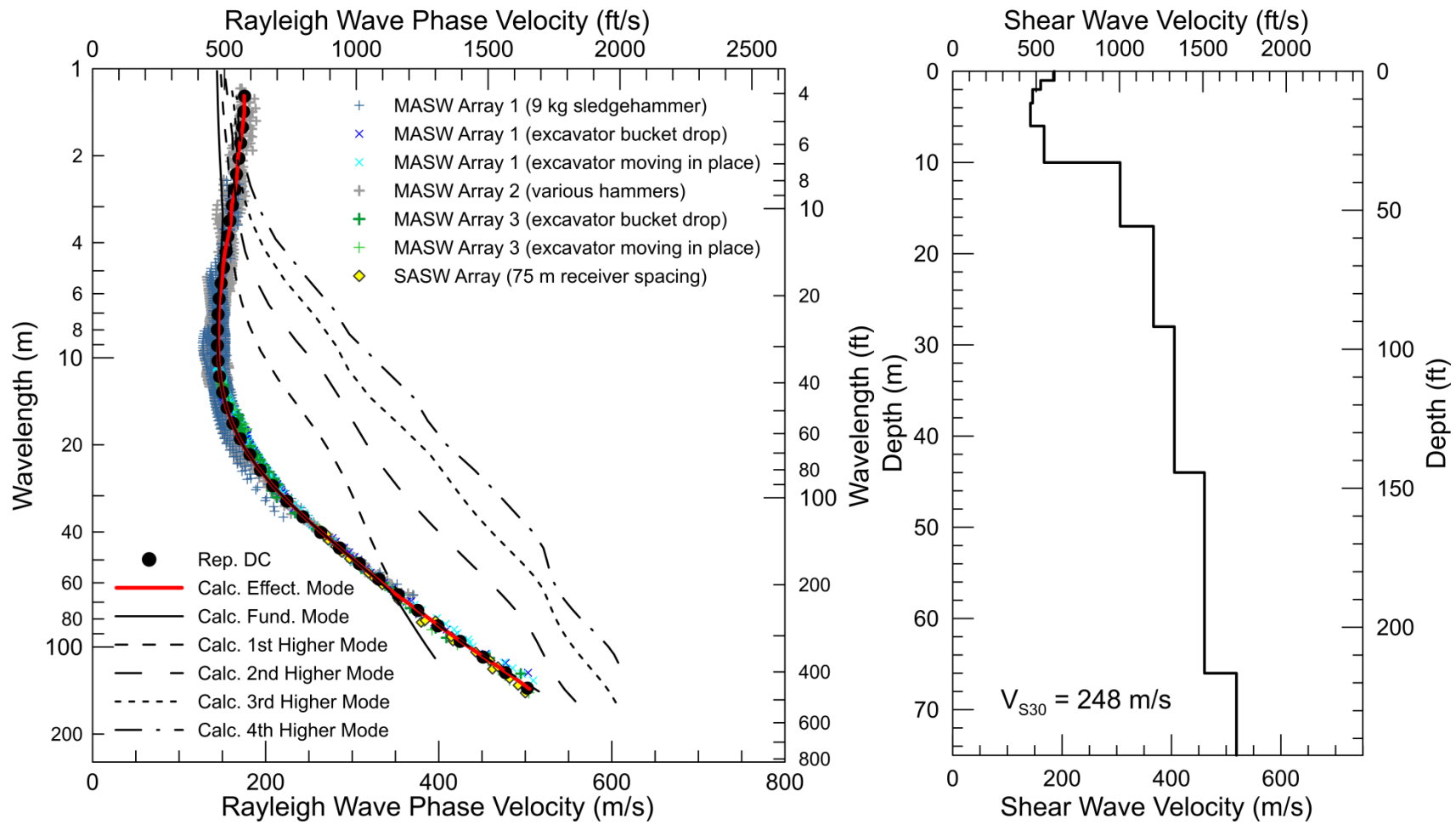


Figure 43 Conway site – Modeling of Rayleigh wave dispersion data from 75 m SASW receiver spacing and coincident MASW receiver arrays

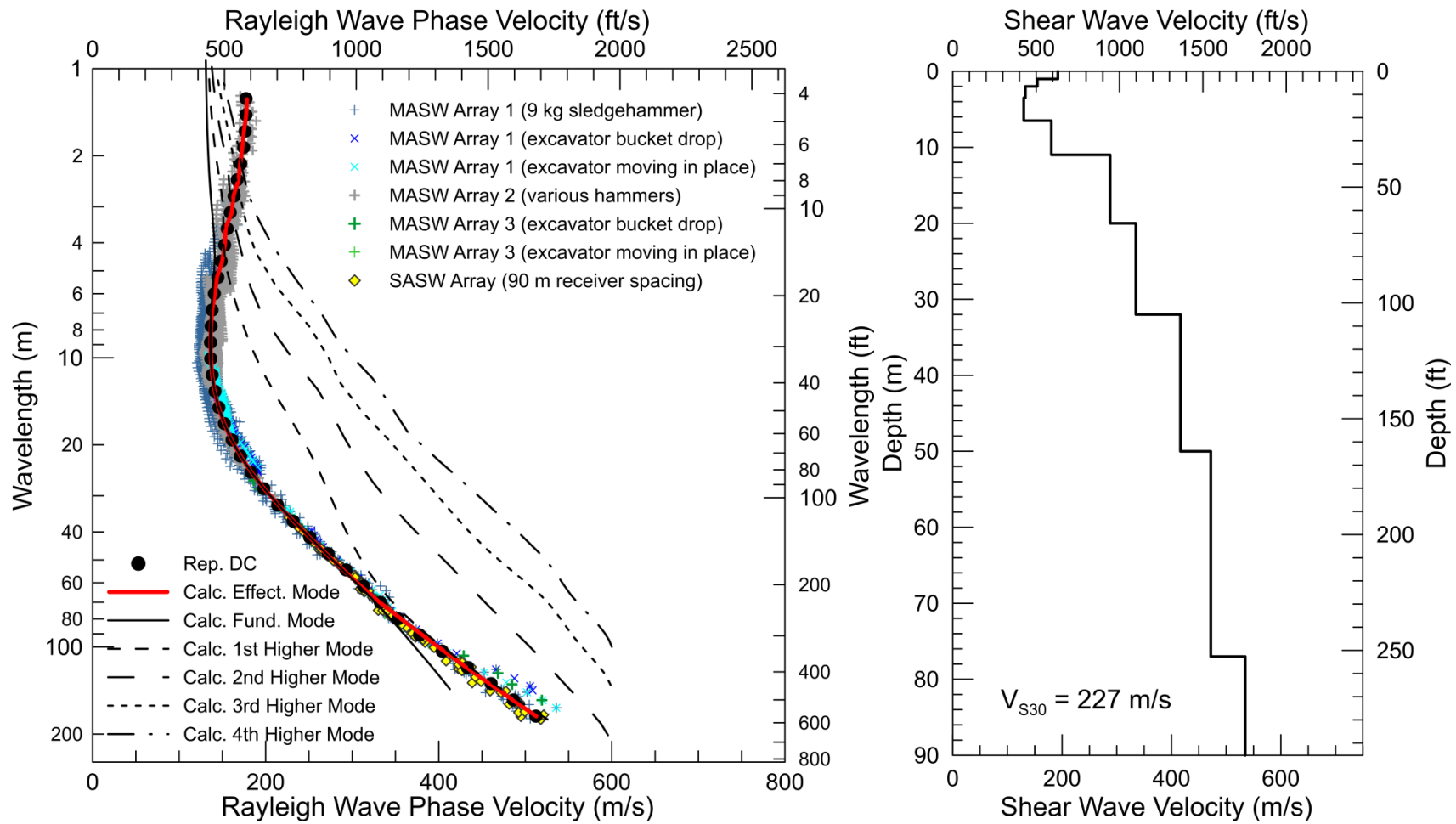
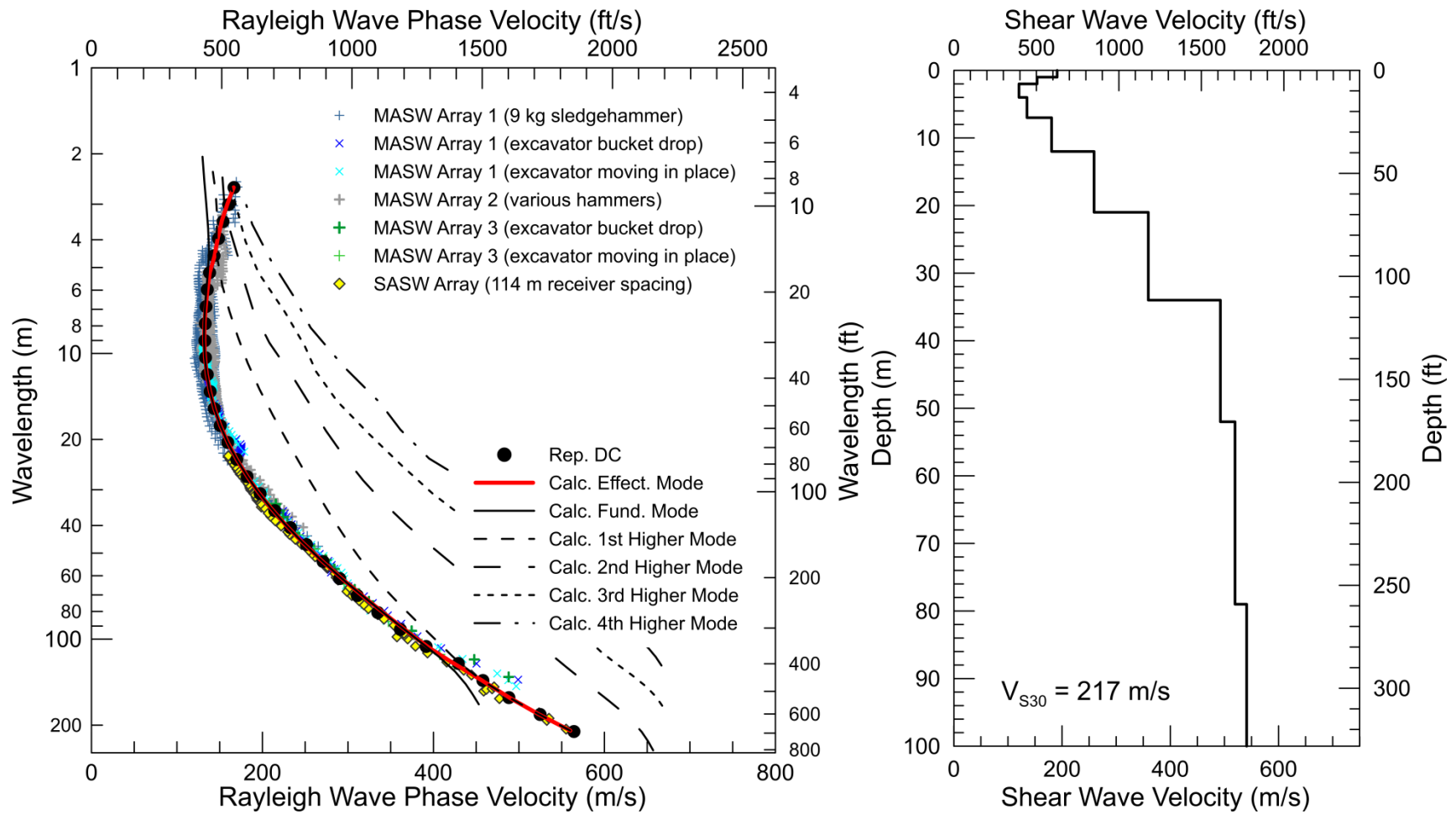


Figure 44 Conway site – Modeling of Rayleigh wave dispersion data from 90 m SASW receiver spacing and coincident MASW receiver arrays



**Figure 45 Conway site – Modeling of Rayleigh wave dispersion data from 114 m SASW receiver spacing and coincident MASW receiver arrays**

**Table 5 Conway site –  $V_S$  model for 45 m SASW receiver spacing and coincident MASW receiver arrays (metric units)**

Depth to Top of Layer (m)	Layer Thickness (m)	S-Wave Velocity (m/s)	Inferred P-Wave Velocity (m/s)	Assumed Poisson's Ratio	Assumed Density (g/cm <sup>3</sup> )
0	1	189	352	0.300	1.80
1	1	159	318	0.333	1.75
2	1.5	156	1500	0.495	1.70
3.5	1.5	154	1550	0.495	1.70
5	3.5	178	1600	0.494	1.80
8.5	5.5	282	1650	0.485	1.90
14	7	384	1650	0.471	1.95
21	9	482	1650	0.453	2.00
30	>15	523	1700	0.448	2.00

**Table 6 Conway site –  $V_S$  model for 45 m SASW receiver spacing and coincident MASW receiver arrays (Imperial units)**

Depth to Top of Layer (ft)	Layer Thickness (ft)	S-Wave Velocity (ft/s)	Inferred P-Wave Velocity (ft/s)	Assumed Poisson's Ratio	Assumed Density (lb/ft <sup>3</sup> )
0.0	3.3	618	1156	0.300	112
3.3	3.3	521	1042	0.333	109
6.6	4.9	511	4921	0.495	106
11.5	4.9	505	5085	0.495	106
16.4	11.5	582	5249	0.494	112
27.9	18.0	927	5413	0.485	119
45.9	23.0	1260	5413	0.471	122
68.9	29.5	1580	5413	0.453	125
98.4	>49.2	1717	5577	0.448	125

**Table 7 Conway site –  $V_S$  model for 60 m SASW receiver spacing and coincident MASW receiver arrays (metric units)**

Depth to Top of Layer (m)	Layer Thickness (m)	S-Wave Velocity (m/s)	Inferred P-Wave Velocity (m/s)	Assumed Poisson's Ratio	Assumed Density (g/cm <sup>3</sup> )
0	1	186	348	0.300	1.80
1	1	161	321	0.333	1.75
2	1.5	153	1500	0.495	1.70
3.5	2	153	1550	0.495	1.70
5.5	3.5	169	1600	0.494	1.80
9	7	302	1650	0.483	1.90
16	8	382	1650	0.472	1.95
24	12	470	1650	0.456	2.00
36	15	510	1700	0.451	2.00
51	>9	548	1700	0.442	2.05

**Table 8 Conway site –  $V_S$  model for 60 m SASW receiver spacing and coincident MASW receiver arrays (Imperial units)**

Depth to Top of Layer (ft)	Layer Thickness (ft)	S-Wave Velocity (ft/s)	Inferred P-Wave Velocity (ft/s)	Assumed Poisson's Ratio	Assumed Density (lb/ft <sup>3</sup> )
0.0	3.3	612	1142	0.300	112
3.3	3.3	528	1054	0.333	109
6.6	4.9	502	4921	0.495	106
11.5	6.6	503	5085	0.495	106
18.0	11.5	556	5249	0.494	112
29.5	23.0	990	5413	0.483	119
52.5	26.2	1254	5413	0.472	122
78.7	39.4	1543	5413	0.456	125
118.1	49.2	1674	5577	0.451	125
167.3	>29.5	1796	5577	0.442	128

**Table 9 Conway site –  $V_S$  model for 75 m SASW receiver spacing and coincident MASW receiver arrays (metric units)**

Depth to Top of Layer (m)	Layer Thickness (m)	S-Wave Velocity (m/s)	Inferred P-Wave Velocity (m/s)	Assumed Poisson's Ratio	Assumed Density (g/cm <sup>3</sup> )
0	1	186	347	0.300	1.80
1	1	161	301	0.300	1.75
2	1.5	146	1500	0.495	1.65
3.5	2.5	142	1550	0.496	1.65
6	4	167	1600	0.494	1.80
10	7	306	1650	0.482	1.90
17	11	367	1650	0.474	1.95
28	16	405	1650	0.468	2.00
44	22	460	1700	0.460	2.00
66	>9	519	1700	0.449	2.05

**Table 10 Conway site –  $V_S$  model for 75 m SASW receiver spacing and coincident MASW receiver arrays (Imperial units)**

Depth to Top of Layer (ft)	Layer Thickness (ft)	S-Wave Velocity (ft/s)	Inferred P-Wave Velocity (ft/s)	Assumed Poisson's Ratio	Assumed Density (lb/ft <sup>3</sup> )
0.0	3.3	609	1139	0.300	112
3.3	3.3	528	987	0.300	109
6.6	4.9	480	4921	0.495	103
11.5	8.2	466	5085	0.496	103
19.7	13.1	548	5249	0.494	112
32.8	23.0	1004	5413	0.482	119
55.8	36.1	1204	5413	0.474	122
91.9	52.5	1330	5413	0.468	125
144.4	72.2	1510	5577	0.460	125
216.5	>29.5	1702	5577	0.449	128

**Table 11 Conway site –  $V_S$  model for 90 m SASW receiver spacing and coincident MASW receiver arrays (metric units)**

Depth to Top of Layer (m)	Layer Thickness (m)	S-Wave Velocity (m/s)	Inferred P-Wave Velocity (m/s)	Assumed Poisson's Ratio	Assumed Density (g/cm <sup>3</sup> )
0	1	192	360	0.300	1.80
1	1	155	310	0.333	1.75
2	1.5	133	1500	0.496	1.65
3.5	3	130	1550	0.496	1.65
6.5	4.5	180	1600	0.494	1.80
11	9	288	1650	0.484	1.90
20	12	335	1650	0.479	1.95
32	18	416	1650	0.466	2.00
50	27	472	1700	0.458	2.00
77	>13	535	1700	0.445	2.05

**Table 12 Conway site –  $V_S$  model for 90 m SASW receiver spacing and coincident MASW receiver arrays (Imperial units)**

Depth to Top of Layer (ft)	Layer Thickness (ft)	S-Wave Velocity (ft/s)	Inferred P-Wave Velocity (ft/s)	Assumed Poisson's Ratio	Assumed Density (lb/ft <sup>3</sup> )
0.0	3.3	631	1181	0.300	112
3.3	3.3	508	1016	0.333	109
6.6	4.9	436	4921	0.496	103
11.5	9.8	426	5085	0.496	103
21.3	14.8	592	5249	0.494	112
36.1	29.5	944	5413	0.484	119
65.6	39.4	1098	5413	0.479	122
105.0	59.1	1366	5413	0.466	125
164.0	88.6	1548	5577	0.458	125
252.6	>42.7	1754	5577	0.445	128

**Table 13 Conway site –  $V_s$  model for 114 m SASW receiver spacing and coincident MASW receiver arrays (metric units)**

Depth to Top of Layer (m)	Layer Thickness (m)	S-Wave Velocity (m/s)	Inferred P-Wave Velocity (m/s)	Assumed Poisson's Ratio	Assumed Density (g/cm <sup>3</sup> )
0	1	191	358	0.300	1.80
1	1	154	308	0.333	1.75
2	2	120	1500	0.497	1.65
4	3	135	1550	0.496	1.70
7	5	181	1600	0.494	1.80
12	9	259	1650	0.487	1.90
21	13	359	1650	0.475	1.95
34	18	493	1650	0.451	2.00
52	27	520	1700	0.448	2.00
79	>21	541	1700	0.444	2.05

**Table 14 Conway site –  $V_s$  model for 114 m SASW receiver spacing and coincident MASW receiver arrays (Imperial units)**

Depth to Top of Layer (ft)	Layer Thickness (ft)	S-Wave Velocity (ft/s)	Inferred P-Wave Velocity (ft/s)	Assumed Poisson's Ratio	Assumed Density (lb/ft <sup>3</sup> )
0.0	3.3	627	1173	0.300	112
3.3	3.3	505	1011	0.333	109
6.6	6.6	395	4921	0.497	103
13.1	9.8	444	5085	0.496	106
23.0	16.4	593	5249	0.494	112
39.4	29.5	850	5413	0.487	119
68.9	42.7	1179	5413	0.475	122
111.5	59.1	1616	5413	0.451	125
170.6	88.6	1705	5577	0.448	125
259.2	>68.9	1775	5577	0.444	128

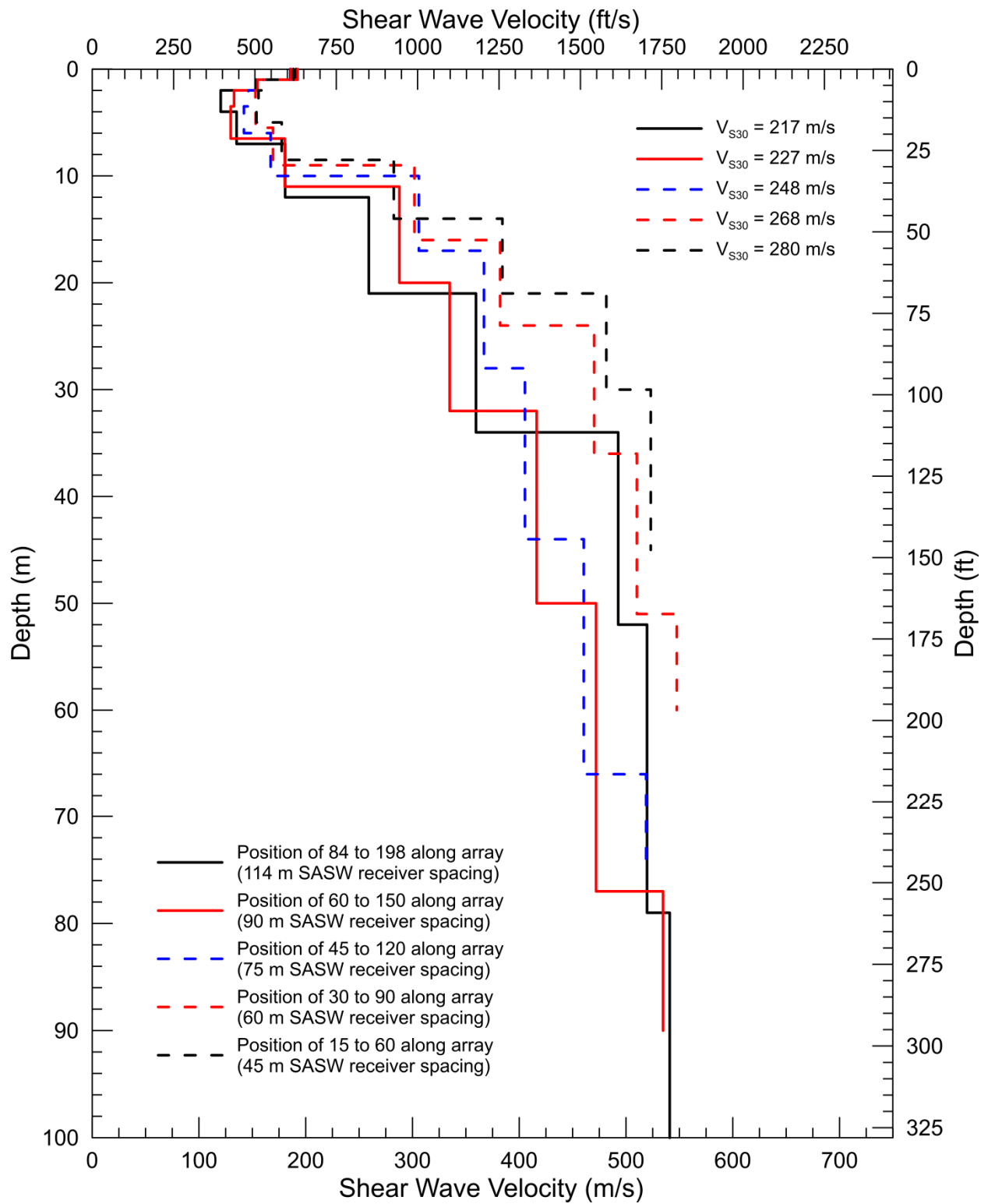


**Figure 46** Conway site – Summary of  $V_S$  models

## 7 REFERENCES

- Achenbach J, 1973, Wave Propagation in Elastic Solids, Elsevier, Amsterdam, Netherlands.
- Aki K, 1957, Space and time spectra of stationary stochastic waves, with special reference to microtremors. *Bull. Earthq. Inst. Univ. Tokyo*, v. 35, pp. 415–457.
- Albarello D and Gargani G, 2010, “Providing NEHRP soil classification from the direct interpretation of effective Rayleigh-wave dispersion curves”, *Bulletin of the Seismological Society of America*, Vol. 100, No. 6, p 3284-3294.
- Asten M, 2006, Site shear velocity profile interpretation from microtremor array data by direct fitting of SPAC curves, in *Proceedings of the Third Int. Symp. Effects of Surface Geol. Seismic Motion*, Vol. 2, LCPC Edition, Grenoble, France, August 30–September 01, Paper No. 99, 1069-1080.
- Asten M, Stephenson W and Hartzell, S, 2015, The use of wavenumber normalization in computing spatially averaged coherencies (krSPAC) of microtremor data from asymmetric arrays, *Proceedings 6<sup>th</sup> International Conference on Earthquake Geotechnical Engineering*, Christchurch, New Zealand, 9 p.
- Bettig B, Bard PY, Scherbaum F, Riepl J, Cotton F, Cornou C and Hatzfeld D, 2001, Analysis of dense array noise measurements using the modified spatial auto-correlation method (SPAC): application to the Grenoble area, *Bollettino di Geofisica Teorica ed Applicata*, Vol 42, p 281–304.
- Brown L, 1998, Comparison of  $V_S$  profiles from SASW and borehole measurements at strong motion sites in Southern California, Master’s thesis, University of Texas, Austin.
- Brown L, Diehl J and Nigbor R, 2000, A simplified method to measure average shear-wave velocity in the top 30 m ( $V_{S,30}$ ), *Proc. 6<sup>th</sup> International Conference on Seismic Zonation*, 1–6.
- BSSC, 2003, *NEHRP recommended provisions for seismic regulations for new buildings and other structure (FEMA 450), Part I: Provisions*, Building Seismic Safety Council, Federal Emergency Management Agency, Washington D.C.
- Capon J, 1969, High-resolution frequency-wavenumber spectrum analysis, *Proc. Institute of Electrical and Electronics Engineers (IEEE)*, Vol. 57, no. 8, p 1408–1418.
- Comina C, Foti S, Boiero D, and Socco LV, 2011, Reliability of  $V_{S,30}$  evaluation from surface-wave tests, *J. Geotech. Geoenviron. Eng.*, p 579–586.
- Dal Moro G, Moura R, Moustafa A, 2015, Multi-component joint analysis of surface waves, *Journal of Applied Geophysics*, Vol. 119, p 128-138.
- Dal Moro G and Ferigo F, 2011, Joint Analysis of Rayleigh- and Love-wave dispersion curves: Issues, criteria and improvements, *Journal of Applied Geophysics*, Vol. 75, p 573-589.
- Ellefsen K, 2003, Seg2\_edit: a program for editing and manipulating SEG-2 files, *U.S. Geol. Surv. Open-File Rept. 03-141*, 11 pp.
- Foti S, 2000, Multistation Methods for Geotechnical Characterization using Surface Waves, Ph.D. Dissertation, Politecnico di Torino, Italy.

- GEOVision, Inc (2012): EPRI (2004, 2006) ground-motion model (GMM) review project: Shear wave velocity measurements at seismic recording stations, <http://www.epri.com/abstracts/Pages/ProductAbstract.aspx?ProductId=000000003002000719>.
- Imai T, Fumoto H, and Yokota K, 1976, P- and S-Wave Velocities in Subsurface Layers of Ground in Japan, Oyo Corporation Technical Note N-14.
- International Committee of Building Officials, 2000 International Building Code, ICC, Hauppauge, NY, Section 1615.1.1
- García-Jerez A, Piña-Flores J, Sánchez-Sesma F, Luzón, F, Perton, M, 2016, A computer code for forward computation and inversion of the H/V spectral ratio under the diffuse field assumption, *Computers & Geosciences*, In Press.
- Joh S, 1996, Advances in interpretation and analysis techniques for spectral-analysis-of-surface-waves (SASW) measurements, Ph.D. Dissertation, University of Texas, Austin.
- Joh S, 2002, WinSASW V2.0, Data Interpretation and Analysis for SASW Measurements, Department of Civil Engineering, Chung-Ang University, Anseong, Korea.
- Lacoss R, Kelly E and Toksöz M, 1969, Estimation of seismic noise structure using arrays, *Geophysics*, v. 34, pp. 21-38.
- Li J and Rosenblad B, 2011, Experimental study of near-field effects in multichannel array-based surface wave velocity measurements, *Near Surface Geophysics*, Vol. 9, 357-366.
- Ling S and Okada H, 1993, An extended use of the spatial correlation technique for the estimation of geological structure using microtremors, *Proc. the 89<sup>th</sup> Conference Society of Exploration Geophysicists Japan (SEGJ)*, pp. 44–48 (in Japanese).
- Louie J, 2001, Faster, Better: Shear-Wave Velocity to 100 Meters Depth from Refraction Microtremor Arrays, *Bulletin of the Seismological Society of America*, vol. 91, no. 2, p. 347-364.
- Martin A and Diehl J, 2004, Practical experience using a simplified procedure to measure average shear-wave velocity to a depth of 30 meters ( $V_{s30}$ ), *Proceedings of the 13<sup>th</sup> World Conference on Earthquake Engineering*, Vancouver, B.C., Canada, August 1-6, 2004, Paper No. 952.
- Martin A, Shawver J and Diehl J, 2006, Combined use of Active and Passive Surface Wave Techniques for Cost Effective UBC/IBC Site Classification, *Proceedings of the 8<sup>th</sup> National Conference on Earthquake Engineering*, San Francisco, California, Paper No. 1013.
- Martin A, Yong A and Salomone L, 2014, Advantages of active Love wave techniques in geophysical characterization of seismographic station sites – case studies in California and the Central and Eastern United States, *Proceedings of the Tenth U.S. National Conference on Earthquake Engineering, Frontiers of Earthquake Engineering*, July 21-25, Anchorage, Alaska.
- Nakamura Y, 1989, A method for dynamic characteristics estimation of subsurface using microtremor on the ground surface, *Quart. Reprt Rail. Tech. Res. Inst.*, Vol. 30, no. 1, p 25–33.
- Nogoshi M and Igarashi T, 1971, On the amplitude characteristics of microtremor (part 2), *J. Seismol. Soc. Japan*, Vol. 24, p 26–40 (in Japanese).

- Ohori M, Nobata A, and Wakamatsu K, 2002, A comparison of ESAC and FK methods of estimating phase velocity using arbitrarily shaped microtremor arrays, *Bull. Seismol. Soc. Am.*, v. 92, no. 6, p. 2323–2332.
- Okada H, 2003, The Microtremor Survey Method, *Society of Exploration Geophysics Geophysical Monograph Series*, Number 12, 135p.
- Park C, Miller R and Xia J, 1999a, Multimodal analysis of high frequency surface waves, *Proceedings of the Symposium on the Application of Geophysics to Engineering and Environmental Problems '99*, 115-121.
- Park C, Miller R and Xia, J, 1999b, Multichannel analysis of surface waves, *Geophysics*, Vol 64, No. 3, 800-808.
- Rix G, 1988, Experimental study of factors affecting the spectral-analysis-of surface-waves method, Ph.D. Dissertation, University of Texas, Austin.
- Roesset J, Chang D and Stokoe K, 1991, Comparison of 2-D and 3-D Models for Analysis of Surface Wave Tests, *Proceedings, 5<sup>th</sup> International Conference on Soil Dynamics and Earthquake Engineering*, Karlsruhe, Germany.
- Stokoe K, Rix G and Nazarian S, 1989, In situ seismic testing with surface waves, *Proceedings, Twelfth International Conference on Soil Mechanics and Foundation Engineering, Vol. 1*, Rio de Janeiro, Brazil, pp. 330-334.
- Stokoe K, Wright S, Bay J and Roesset J, 1994, Characterization of Geotechnical Sites by SASW Method, *ISSMFE Technical Committee 10 for XIII ICSMFE, Geophysical Characteristics of Sites*, A.A. Balkema Publishers/Rotterdam & Brookfield, Netherlands, pp. 146.
- Xia J, Xu Y, Luo Y, Miller R, Cakir R and Zeng C, 2012, Advantages of using Multichannel analysis of Love waves (MALW) to estimate near-surface shear-wave velocity, *Surveys in Geophysics*, 841–860.
- Yong A, Martin A, Stokoe K and Diehl J, 2013, ARRA-funded  $V_{S30}$  measurements using multi-technique method approach at strong-motion stations in California and Central-Eastern United States, Open-File Report 2013-1102, United States Geological Survey, <http://pubs.usgs.gov/of/2013/1102/>.
- Yoon S and Rix G, 2009, Near-field effects on Array-based surface wave methods with active sources, *Journal of Geotechnical and Geoenvironmental Engineering*, Vol. 135, no. 3, 399-406.

## 8 CERTIFICATION

All geophysical data, analysis, interpretations, conclusions, and recommendations in this document have been prepared under the supervision of and reviewed by a **GEOVision** California Professional Geophysicist.

Reviewed and approved by



5/22/2017

---

Antony Martin

Date

California Professional Geophysicist, P. Gp. 989  
**GEOVision** Geophysical Services

- \* This geophysical investigation was conducted under the supervision of a California Professional Geophysicist using industry standard methods and equipment. A high degree of professionalism was maintained during all aspects of the project from the field investigation and data acquisition, through data processing interpretation and reporting. All original field data files, field notes and observations, and other pertinent information are maintained in the project files and are available for the client to review for a period of at least one year.

A professional geophysicist's certification of interpreted geophysical conditions comprises a declaration of his/her professional judgment. It does not constitute a warranty or guarantee, expressed or implied, nor does it relieve any other party of its responsibility to abide by contract documents, applicable codes, standards, regulations or ordinances.

# Appendix B: MASW-MAM Testing Results

---

**Deep Shear Wave Velocity Profiling  
Using MASW and MAM  
Surface Wave Methods:  
SCDOT Deep Borehole Sites near Andrews  
and Conway, South Carolina**

**For:**

**Inthuorn Sasanakul, Ph.D., P.E.**

**Assistant Professor**

**Department of Civil and Environmental Engineering**

**University of South Carolina**

**300 Main Street, C227**

**Columbia, SC 29208**

**Ph: 803-777-7160**

**sasanaku@cec.sc.edu**

**By:**

**Brady R. Cox, Ph.D., P.E.**

**Joseph Vantassel, B.S.**

**The University of Texas at Austin**

**[brcox@utexas.edu](mailto:brcox@utexas.edu)**

**July 31, 2017**

**Geotechnical Engineering Report GR17-18**

**Geotechnical Engineering Center**

**Civil Engineering Department**

**The University of Texas at Austin**

## TABLE OF CONTENTS

1.0	INTRODUCTION .....	3
2.0	DATA ACQUISITION.....	3
2.1.	Multi-channel analysis of surface waves (MASW) .....	3
2.2.	Microtremor Array Measurements (MAM) .....	5
3.0	HORIZONTAL-TO-VERTICAL SPECTRAL RATIOS.....	6
4.0	DISPERSION PROCESSING.....	8
5.0	INVERSION PROCEDURE .....	12
6.0	INVERSION RESULTS.....	15
6.1.	Deep Vs Profiles for Site A.....	15
6.1.1	<b>“Blind” Inversion Results for Site A .....</b>	<b>16</b>
6.1.2	<b>“Informed” Inversion Results for Site A .....</b>	<b>18</b>
6.1.3	<b>Comparison of “Blind” and “Informed” Profiles for Site A .....</b>	<b>20</b>
6.2.	Deep Vs Profiles for Site B .....	26
6.2.1	<b>“Blind” Inversion Results Site B .....</b>	<b>26</b>
6.2.3	<b>Comparison of “Blind” and “Informed” Profiles for Site B.....</b>	<b>30</b>
7.0	SUGGESTIONS FOR SITE RESPONSE.....	36
	REFERENCES .....	37
	Appendix A: Receiver Coordinates .....	40
	Appendix B: Tabulated Dispersion Data, Layering Ratio Inversion Summary Plots and Tabulated Median Vs Profiles for Site A (near Conway, SC).....	43
	Appendix C: Tabulated Dispersion Data, Layering Ratio Inversion Summary Plots and Tabulated Median Vs Profiles for the Site B (near Andrews, SC) .....	53

## 1.0 INTRODUCTION

To characterize the near-surface and deep shear wave velocity ( $V_s$ ) structure for two sites located in eastern South Carolina (one near Conway and one near Andrews), active-source and passive-source surface wave testing were performed by Dr. Brady R. Cox, Mr. Joseph Vantassel, and Mr. Michael Yust from the University of Texas at Austin between 1/13/2017 and 1/14/2017. The multi-channel analysis of surface waves (i.e., MASW) method was employed for active-source testing and two-dimensional (2D) microtremor array measurements (i.e., MAM) were used for passive-source testing. Additionally, in an effort to characterize the lateral variability in depth to bedrock and estimate the fundamental frequency ( $f_0$ ) of each site, horizontal-to-vertical (H/V) spectral ratios were calculated for each broadband seismometer location used in MAM testing. This report details our findings.

## 2.0 DATA ACQUISITION

The first set of combined MASW and MAM measurements was located near Conway, SC (refer to Figure 1) and the second set of measurements was acquired near Andrews, SC (refer to Figure 2). These two test locations will be referred to as “Site A” and “Site B”, respectively. Details regarding the data acquisition at both locations are provided below.

### 2.1. *Multi-channel analysis of surface waves (MASW)*

Figure 1 and Figure 2 show plan views of the active-source MASW test locations at Site A and B, respectively. MASW testing was performed using 4.5-Hz vertical and horizontal geophones (Geospace Technologies GS-11D installed in a PC21 land case) coupled to the ground surface with a 7.6-cm (3-in) spike. Two parallel lines of 24 geophones were placed in a linear array with a spacing of 2 m (6.56 ft) between successive geophones, resulting in an array length of 46 m (151 ft). One of these parallel lines was composed of only vertical geophones, the other, only horizontal geophones. The horizontal geophones were oriented such that they recorded waves polarized perpendicular to the line direction. Vertical geophones were used to record wavefields with strong Rayleigh wave content while the horizontal geophones were used to record wavefields with strong Love wave content. Wavefields with strong Rayleigh wave content were actively-generated by striking vertically on a square aluminum strike-plate with a 7.3 kg (16 lb) sledgehammer at three distinct “shot” locations offset 5, 10, and 20 m (16.4, 32.8, and 65.6 ft) relative to the first geophone

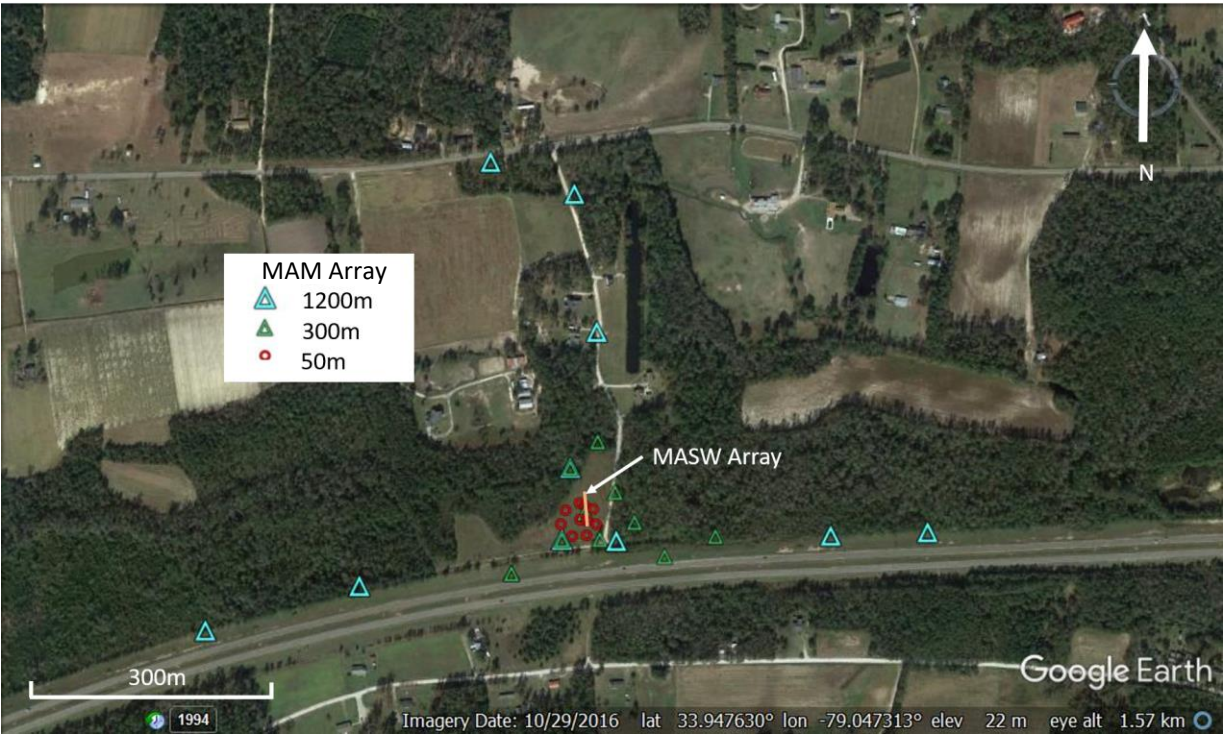


**Figure 1:** Plan view of the multi-channel analysis of surface waves (i.e., MASW) and microtremor array measurement (i.e., MAM) test locations at Site A (near Conway, SC).

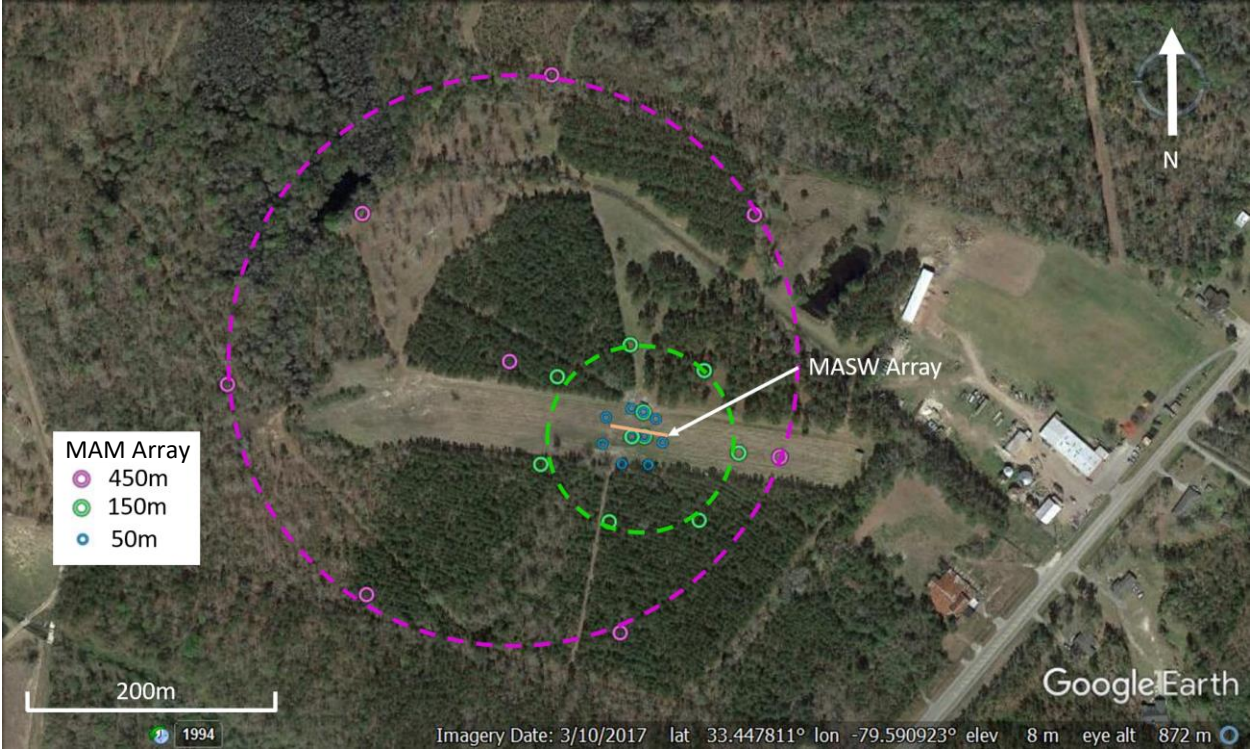


**Figure 2:** Plan view of the multi-channel analysis of surface waves (i.e., MASW) and microtremor array measurement (i.e., MAM) test locations at Site B (near Andrews, SC).

on each side of the array. Five distinct blows were recorded per shot location for subsequent stacking to increase signal-to-noise ratio. Wavefields with strong Love wave content were actively-generated by striking horizontally on both sides of a weighted shear plank with the same sledgehammer at the same distinct “shot” locations aforementioned. Ten distinct blows, five per horizontal strike direction, were recorded per shot location for subsequent stacking. Wavefields were recorded for 2.0 seconds with a 0.5 second pre-trigger delay using a sampling rate ( $\Delta t$ ) of 500  $\mu$ s.

## **2.2. *Microtremor Array Measurements (MAM)***

Three-component broadband seismometers with a flat frequency response between 20 seconds and 100 Hz (Nanometrics Inc. Trillium Compact 20s) were used to record ambient vibrations. Seismometers were oriented to magnetic north and were buried to provide adequate coupling with the ground surface and to mitigate the effects of wind vibrations. Acquisition systems for the Trillium Compact 20s seismometers consist of Nanometrics, Inc. Centaur digitizers (24 bit ADC, 135 dB dynamic range).

MAM testing at Site A was performed using two roughly-triangular arrays and one circular array (refer to Figure 1). Each array setup consisted of ten broadband seismometers. The use of irregular triangular arrays rather than circular arrays was necessary at Site A due to property access issues. The arrays are referred to by their largest sensor separation distance; that is 1200m, 300m, and 50m. Note that the 1200m and 300m arrays shared some common receiver locations, this was done to expedite deployment of each array in the field. For the 50m circular array two additional sensors were placed inside the circles perimeter to improve the array’s theoretical frequency response.

MAM testing at Site B was performed using three nested circular arrays (refer to Figure 2). The arrays are again referred to by their largest sensor separation distance; that is 450m, 150m, and 50m. The 150m and 50m arrays consisted of ten broadband seismometers; the 450m array consisted of eight broadband seismometers. The northwest-most sensor in the 450m array had to be moved from its intended location due to standing water. For the 150m and 50m arrays two additional sensors were added to improve the array’s theoretical response in a similar manner to that done at Site A. Note again that some sensor locations were shared between arrays to expedite field deployment.

Coordinates for all seismometer locations used in MAM arrays at Site A and B are provided in Appendix A. MAM stations were used to record ambient vibrations for periods of 45 minutes to 2 hours, with longer recording times corresponding to the larger arrays. Data were recorded with a sampling frequency of 100 Hz.

### **3.0 HORIZONTAL-TO-VERTICAL SPECTRAL RATIOS**

Horizontal-to-vertical (H/V) spectral ratios were computed for all stations used in MAM testing at Site A and B. If an H/V curve exhibits a well-defined peak, the frequency corresponding to this peak ( $f_{0\_H/V}$ ) can be used to estimate the fundamental shear wave resonant frequency ( $f_{0\_S}$ ) of the site (Lermo and Chavez-Garcia 1993, Lachet and Bard 1994, SESAME 2004) and/or the lowest-frequency peak of the fundamental mode Rayleigh wave ellipticity ( $f_{0\_R}$ ) (Malischewsky and Scherbaum 2004, Poggi and Fah 2010). When a strong impedance contrast is present at a site,  $f_{0\_H/V}$ ,  $f_{0\_S}$ , and  $f_{0\_R}$  are approximately equal to one another. When a more moderate impedance contrast is present,  $f_{0\_H/V}$  may be more representative of  $f_{0\_S}$  (Bonney 2004).

The squared average of the north and east components (i.e., the square root of the average of the squared north and east components) of a given seismometer was used to represent a single horizontal component for H/V calculations. For each individual station/receiver, records were divided into 3 to 6 minute time windows and the H/V spectral ratios from all windows were used to calculate a lognormal median and +/- one standard deviation for that location. The total number of windows for each station ranged from 7 to 19, depending on the total record length. Konno and Ohmachi smoothing with a smoothing constant of 40 was utilized to remove noise spikes in the Fourier spectra for each time window.

The SESAME D23.12 (2004) report provides clarity criteria for inferring  $f_{0\_H/V}$  from H/V curves. The authors of the SESAME (2004) report do not recommend inferring  $f_{0\_H/V}$  from H/V curves that fail to meet these criteria. Figure 3 shows the H/V curves for all MAM stations at Site A passing the SESAME (2004) clarity criteria. Note that of the 30 stations used during MAM testing at Site A, only one did not pass the SESAME (2004) clarity criteria and will not be considered further. The “clear” peak exhibited in the H/V curves has a mean  $f_{0\_H/V}$  of 0.40 Hz and standard deviation ( $\sigma_{f_{0\_H/V}}$ ) of 0.00 Hz. Due to its quality, the low-frequency peak was used to help constrain the depth to basement rock in the surface wave inversion results. The consistency of this low-frequency peak suggests that the fundamental site frequency is relatively uniform across the footprint of the MAM arrays. In addition to this well-defined, “clear”, low-frequency peak, two

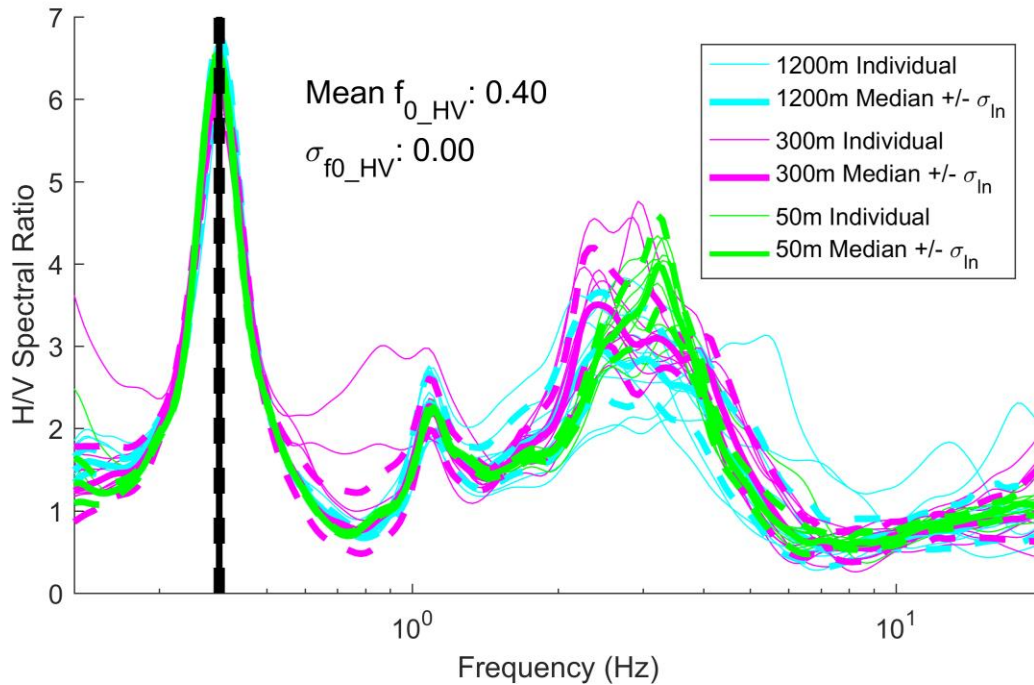


**Figure 3:** Horizontal-to-vertical spectral ratios for all individual MAM stations meeting the SESAME (2004) peak clarity criteria at Site A (near Conway, SC). Also shown are the lognormal median (thick solid lines) and  $\pm$  one standard deviation (thick dashed lines) curves for each array (computed using only the MAM stations meeting the SESAME 2004 criteria). Solid and dashed vertical black lines represent the mean  $f_{0\_HV}$   $\pm$   $\sigma_{f0\_HV}$ , respectively. Note that the H/V curve for each individual station represents a median computed using 7 to 19 time windows ranging from 3 to 6 minutes long.

other peaks are apparent in the H/V curve, at approximately 1 and 3 Hz. These peaks do not pass the SESAME (2004) clarity criteria. These peaks, however, are believed to be indicative of shallow impedance contrasts in the velocity structure, and were used to qualitatively constrain surface wave inversions (as discussed below). The highest frequency peak, centered near 3 Hz, is visually variable in its peak location, width, and amplitude across the extents of the arrays. This indicates that the depth and stiffness of a shallow velocity contrast is spatially variable across the site.

Figure 4 shows the H/V curves from all individual stations used in MAM testing at Site B passing the SESAME (2004) clarity criteria. Of the 28 stations used during MAM testing at Site B, only one did not pass the clarity criteria and will not be considered further. Similarly to Site A, the Site B H/V curves exhibit multiple peaks. All H/V curves exhibit a stable, low-frequency peak with a mean  $f_{0\_HV}$  of 0.33 Hz and a standard deviation ( $\sigma_{f0\_HV}$ ) of 0.00 Hz. This “clear” low

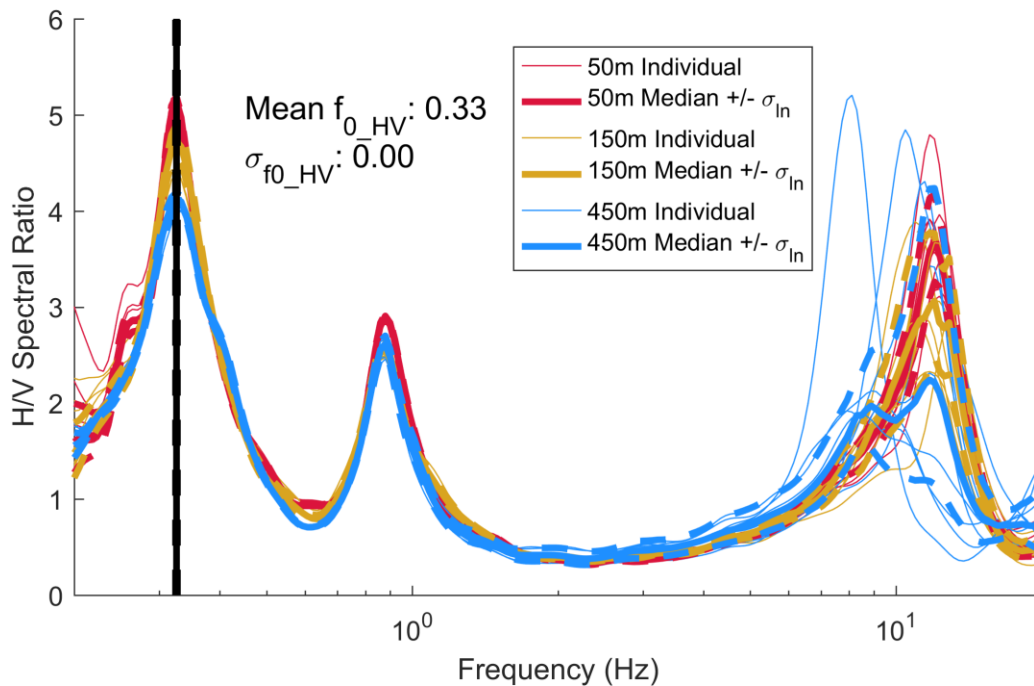


**Figure 4:** Horizontal-to-vertical spectral ratios for all individual MAM stations meeting the SESAME (2004) peak clarity criteria at Site B (near Andrews, SC). Also shown are the lognormal median (thick solid lines) and +/- one standard deviation (thick dashed lines) curves for each array (computed using only the MAM stations meeting the SESAME 2004 criteria). Solid and dashed vertical black lines represent the mean  $f_{0\_HV}$  +/-  $\sigma_{f_{0\_HV}}$ , respectively. Note that the H/V curve for each individual station represents a median computed using 7 to 9 time windows ranging from 3 to 6 minutes long.

frequency peak was used to help constrain the depth to basement rock during surface wave inversion. The consistency of this low-frequency peak suggests that the fundamental site frequency and depth to basement rock are relatively uniform across the footprint of the MAM arrays. The H/V curves exhibit additional peaks at approximately 0.9 and 10 Hz that are indicative of other strong impedance contrasts in the shallow velocity structure. The potential for multiple significant impedance contrasts was used to qualitatively constrain inversion results. As noted for Site A, the highest frequency peak at Site B, centered near 10 Hz, is visually variable in its peak location, width, and amplitude across the extents of the arrays. This indicates that the depth and stiffness of a shallow velocity contrast is spatially variable across the site.

#### 4.0 DISPERSION PROCESSING

MASW Rayleigh and Love wave data were analysed using several different 2D transformation methods (Park et. al 1998, Nolet and Panza 1976, Zywicki 1999) coupled with the

multiple source-offset technique for identifying near-field contamination and quantifying dispersion uncertainty (Cox and Wood 2011). Dispersion data influenced by near-field effects and/or significant offline noise were eliminated. Rayleigh and Love dispersion data from each source-offset location were used to compute mean and +/- one standard deviation Rayleigh and Love MASW dispersion data. The mean and +/- one standard deviation MASW dispersion data for Site A and B are shown in Figure 5 and 6, respectively. The dispersion data are plotted in terms of phase velocity (Rayleigh or Love) as function of both frequency ( $f$ ; left-hand plot) and wavelength ( $\lambda$ ; right-hand plot) in order to best visualize key aspects of the data.

The 2D high resolution frequency-wavenumber (HFK) method (Capon 1969) was used to generate Rayleigh-wave dispersion data for all MAM arrays (both circular and triangular). Additionally, the Modified Spatial Autocorrelation (MSPAC) method (Bettig et al. 2001) was used to compute MAM dispersion data for all circular arrays. These two processing methods often produced similar results. However, HFK tends to work better when ambient noise sources are not azimuthally well-distributed, while MSPAC tends to work better when ambient noise sources are azimuthally well-distributed. Ambient noise sources were found not to be well-distributed during HFK processing, thus, HFK processing was favoured over MSPAC for these datasets. Recordings from each array were divided into 3 to 6 minute windows, which were processed individually. Time windows containing large oscillations, which stem from high-amplitude noise in the near-field (e.g., persons walking near the sensor, cars driving close by, etc.) were eliminated. Dispersion data from all MAM arrays were combined and used to compute mean and +/- one standard deviation dispersion estimates. The mean and +/- one standard deviation MAM dispersion data for Site A and Site B are shown relative to the MASW dispersion data in Figure 5 and Figure 6, respectively.

One must be cautious about using dispersion data at wavenumbers ( $k = 2\pi/\lambda$ ) less than the theoretical array resolution limit associated with the largest array for a given site. At wavenumbers less than the theoretical array resolution limit (i.e.,  $k_{\min}/2$ , Wathelet et al. 2008) the dispersion data may be negatively influenced by limitations of the array aperture (i.e., the array is not large enough to accurately resolve low frequency, high phase velocity dispersion data whose associated wavenumbers are less than the  $k_{\min}/2$  resolution limit). Or in other words, the dispersion data at frequencies below this threshold (wavelengths above this threshold) may be of lower quality and higher uncertainty. However, in an effort to provide informed profiles as deep as possible, the

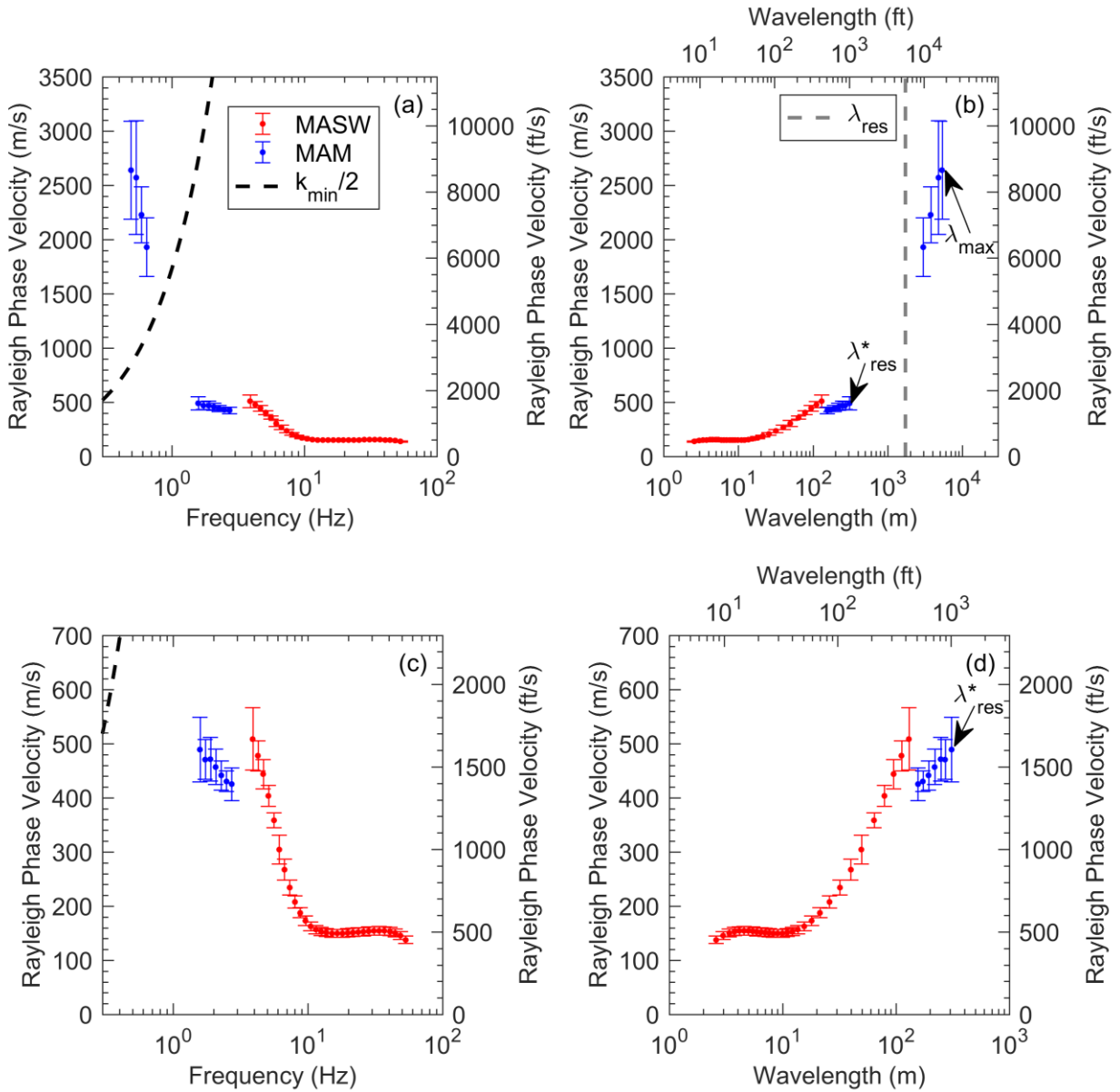


Figure 5: Mean and +/- one standard deviation experimental MASW and MAM dispersion data at Site A in terms of (a & c) frequency and (b & d) wavelength, after resampling. Note that (c) and (d) are zoomed-in views of (a) and (b), respectively.

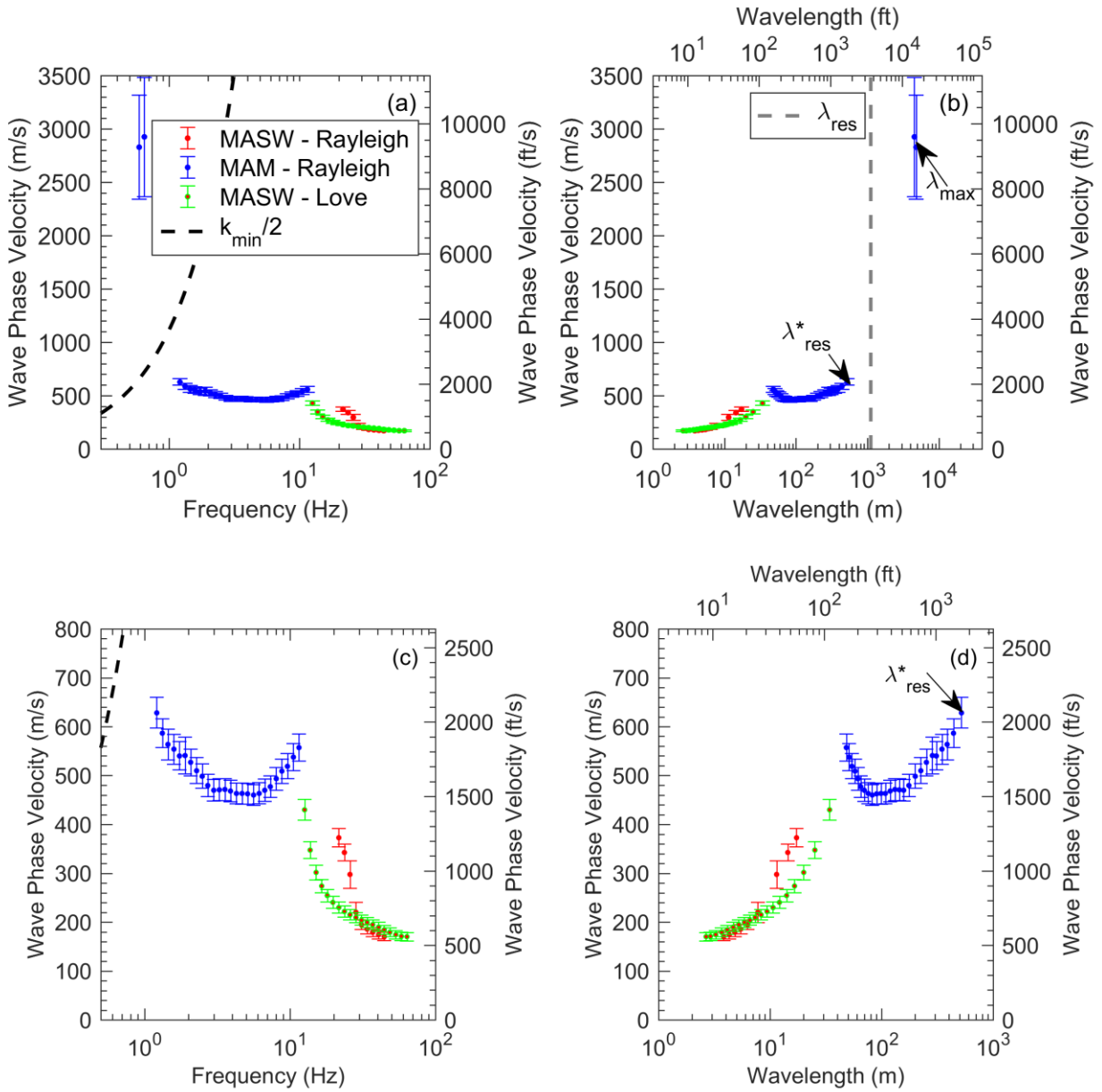


Figure 6: Mean and +/- one standard deviation experimental MASW and MAM dispersion data at Site B in terms of (a & c) frequency and (b & d) wavelength, after resampling. Note that (c) and (d) are zoomed-in views of (a) and (b), respectively.

highly variable low frequency dispersion data points beyond the array resolution limit were used to constrain the inversion process. Without these additional data points it is believed that the inversion would significantly underestimate the velocity structure at depth. Furthermore, the low frequency peaks in the H/V spectral ratios indicated that the deep velocity structure (below the depth easily resolved by the largest arrays used) could be of significance to the site response.

During the inversion process (discussed below), three wavelengths obtained from the experimental dispersion data are used to guide the depth to which the Vs profiles are reported. The first guiding wavelength is referred to as the array resolution wavelength ( $\lambda_{\text{res}}$ ), which is the wavelength corresponding to the longest theoretical wavelength able to be measured reliably from the array geometry. The  $\lambda_{\text{res}}$  value corresponds to the wavelength associated with the  $k_{\text{min}}/2$  array resolution limit. If the useable dispersion data does not reach  $\lambda_{\text{res}}$ , the highest useable dispersion wavelength is defined as  $\lambda^*_{\text{res}}$ . Thus,  $\lambda^*_{\text{res}}$  is the second guiding wavelength. The third guiding wavelength is referred to as the maximum wavelength ( $\lambda_{\text{max}}$ ), which is the wavelength corresponding to the mean values of the lowest frequency and highest phase velocity extracted during dispersion processing. These three guiding wavelengths (i.e.,  $\lambda_{\text{res}}$ ,  $\lambda^*_{\text{res}}$ , and  $\lambda_{\text{max}}$ ) are clearly indicated in Figure 5 and Figure 6, for Site A and B respectively. For Site A,  $\lambda^*_{\text{res}} = 308$  m (1010 ft),  $\lambda_{\text{res}} = 1729$  m (5673 ft), and  $\lambda_{\text{max}} = 5363$  m (17595 ft). For Site B,  $\lambda^*_{\text{res}} = 518$  m (1700 ft),  $\lambda_{\text{res}} = 1113$  m (3652 ft), and  $\lambda^*_{\text{max}} = 4799$  m (15745 ft).

The MASW and MAM dispersion data at each site were combined to increase the bandwidth/wavelength range of the experimental data. Prior to inversion, the combined MASW and MAM experimental dispersion data was resampled in log space using 70 points from 0.2 to 100 Hz.

## **5.0 INVERSION PROCEDURE**

The inverse problem involved in obtaining a realistic layered earth model from surface wave dispersion data is inherently ill-posed, nonlinear and mix-determined, without a unique solution. If detailed borehole data and/or geologic information is available, it can and should be used to help constrain the inversions and limit solution non-uniqueness (Teague et al. 2015). The use of supporting/a-priori information during inversion is the best approach for retrieving Vs profiles that are consistent with the actual subsurface layering. In the absence of a-priori information, the analyst must decide on an appropriate number of layers and ranges for their

corresponding inversion parameters (i.e., trial number of layers and ranges in their respective thicknesses, shear wave velocities, compression wave velocities and mass densities). Selection of these parameters has been shown to significantly impact the results of an inversion.

*Upon request, our initial inversions were performed “blind.”* Meaning, they were not guided by supporting site-specific subsurface information. In order to search for, identify, and encompass the most reasonable layered earth models during our blind inversions, the “layering ratio” approach was utilized. This approach involves conducting multiple inversions for each dispersion dataset utilizing systematically-varied inversion parameters. Each parameterization is defined by a unique layering ratio ( $\Xi$ ), which represents a multiplier that systemically increases the *potential* thickness of each layer in the inversion parameterization based on the *potential* thickness of the layer directly above it (Cox and Teague 2016). The layering ratio approach also allows one to quantify uncertainty in the derived Vs profiles.

**Following the submission of our preliminary “blind” models, we were provided with borehole information that was used to perform subsequent “informed” inversions.** The information provided for Site A was boring log number B-CON started on January 18, 2017. The information provided for Site B was boring log number B-FMG started on February 6, 2017. The boring logs provided information with regard to the soil type and site layering, which were incorporated into the inversion parameterizations. As expressed previously, the incorporation of site specific information assists the inversion process by limiting solution non-uniqueness.

The inversion of surface wave data involves finding layered earth models whose theoretical dispersion curves, which are computed via the “forward” problem, best match the experimentally measured dispersion data. The quality of fit between theoretical and experimental data is typically quantified using a “misfit” value (e.g., Wathelet 2004, Foti et al. 2009). The forward problem used in this study was the transfer matrix approach developed by Thomson (1950) and Haskell (1953) and later modified by Dunkin (1965) and Knopoff (1964). A multi-mode approach was employed, meaning that inversions were performed where the experimental dispersion data could be fit with various combinations of fundamental (R0), first higher (R1), second higher (R2), etc... Rayleigh and Love (L) modes. The inversion was performed using the open-source software Geopsy. This software uses the neighborhood algorithm to locate earth models within a pre-defined parameterization that yield the lowest possible misfit values between the theoretical and

experimental data. Misfit values for this study were computed using Equation 1 (modified from Wathelet 2004).

$$m_{d,e} = w_d m_d + w_e m_e = w_d \sqrt{\sum_{i=1}^{n_f} \frac{(x_{di} - x_{ci})^2}{\sigma_i^2 n_f}} + w_e \sqrt{\frac{(f_{0,R,d} - f_{0,R,c})^2}{\sigma_{f_{0,R,d}}^2}} \quad \text{Eq. (1)}$$

In Equation 1,  $m_{d,e}$  is the combined misfit value based on both misfit relative to dispersion data ( $m_d$ ) and misfit relative to the Rayleigh wave ellipticity peak ( $m_e$ ). The terms  $w_d$  and  $w_e$  are user-defined weighting terms which add up to 1.0. For the dispersion misfit,  $x_{di}$  represents the Rayleigh wave phase velocity of the experimental dispersion data at frequency  $f_i$ ;  $x_{ci}$  is the calculated/theoretical Rayleigh wave phase velocity computed for the trial layered earth model at frequency  $f_i$ ;  $\sigma_i$  is the standard deviation associated with the experimental dispersion data at frequency  $f_i$ ; and  $n_f$  is the number of frequency samples considered for the misfit calculation. Similarly, for the ellipticity peak misfit,  $f_{0,R,d}$  represents the Rayleigh wave ellipticity peak associated with the field data (assumed to coincide with the H/V peak,  $f_{0,H/V}$ ),  $f_{0,R,c}$  represents the calculated/theoretical Rayleigh wave ellipticity peak for the trial layered earth model and  $\sigma_{f_{0,R,d}}$  is the standard deviation associated with the experimental ellipticity peak (i.e., assumed to be equal to the standard deviation in the H/V peak,  $\sigma_{f_{0,H/V}}$ ). While inversions were performed using  $f_{0,H/V}$  from the lowest frequency H/V peak to constrain  $f_{0,R}$ , ultimately only dispersion misfit ( $m_d$ ) is reported in final inversion results below. Note that Geopsy does not allow for computation of the fundamental shear wave resonant frequency ( $f_{0,S}$ ) as a constraint during inversion. However, as noted earlier,  $f_{0,H/V}$  may be a better indicator of  $f_{0,S}$  than  $f_{0,R}$  if a more moderate impedance contrast is present. Thus, we find it valuable to compute the theoretical shear wave transfer function for all ground models and qualitatively compare  $f_{0,H/V}$  to  $f_{0,S}$ .

While there are no universally “good” or “bad” misfit values (Cox and Teague 2016),  $m_d$  values less than 1.0 indicate that, on average (i.e., across the frequency band considered), the theoretical dispersion curve falls within the +/- one standard deviation bounds of the experimental data. Thus,  $m_d$  values in excess of 1.0 suggest a poor fit of the experimental dispersion data and low  $m_d$  values indicated models that fit the mean dispersion data well across the entire bandwidth.

The number of trial models necessary to search the entire parameter space and obtain a large number of acceptable models is controlled by the experimental data and model parameterization (i.e., it is site-specific). We searched 500,000 to 750,000 trial layered earth models for each distinct parameterization (i.e., for each layering ratio), with more trial models used

for parameterizations with more layers (i.e., more degrees of freedom). While it would appear reasonable to extract all Vs profiles with misfit values less than 1.0 for each parameterization, the number of profiles with misfits below 1.0 varies considerably between parameterizations and in some cases is not computationally manageable. **For consistency, the 100 lowest misfit Vs profiles obtained from each inversion parameterization were extracted for further analysis and used to quantify Vs uncertainty. All Vs profiles deemed to be acceptable given the experimental data and associated uncertainty are provided below.**

## 6.0 INVERSION RESULTS

Surface waves at a given wavelength are generally capable of profiling to a maximum depth of 1/3 to 1/2 of their wavelength (Foti et al. 2014, Garofalo et al. 2016a). Thus, Vs profiles obtained from inversion are considered most reliable at depths less than approximately  $\lambda_{\text{res}}/2$ . Or, in other words, the resolution depth ( $d_{\text{res}}$ ) for Vs profiles derived from surface wave inversion is approximately  $\lambda_{\text{res}}/2$ . However, as reliable dispersion data was not available up to the  $\lambda_{\text{res}}/2$  limit at either site,  $d_{\text{res}}$  was set equal to  $\lambda_{\text{res}}^*/2$ . At depths greater than  $d_{\text{res}}$  the Vs profiles are constrained by less reliable dispersion data and should be used with caution. Vs profiles at depths greater than  $d_{\text{res}}$  are reported because, while less certain, they provide guiding information about the deep Vs structure that is more reliable than simply guessing. We clearly delineate the  $d_{\text{res}}$  depth by using a horizontal dashed line in all figures and tables. The Vs profiles for both sites are discussed on a site-by-site basis below.

### 6.1 *Deep Vs Profiles for Site A*

The “blind” and “informed” inversion results for Site A are summarized in Figures 7 and 8, respectively. For the “blind” inversion (Figure 7), three distinct inversion parameterizations yielded Vs profiles with low dispersion misfit values and  $f_{0,S}$  values from theoretical, linear-elastic shear wave transfer functions that agreed well with the experimental  $f_{0,H/V}$  values from the H/V data at Site A. These three inversion parameterizations were created using the layering ratio procedure (Cox and Teague 2016) with layering ratios ( $\Xi$ ) of 1.5, 2.0, and 2.5. These layering ratios resulted in 19, 13, and 10 subsurface layers, respectively. Other layering ratio parameterizations were investigated and found to yield unacceptable fits to the experimental dispersion data and/or experimental H/V data. For the “informed” inversion results (Figure 8), two distinct inversion parameterizations adapted from a layering ratio of 2.0, referred to as 2.0a and

2.0b, yielded acceptable  $V_s$  profiles following the same criteria expressed previously. These parameterizations were developed to follow the layering found in the boring log above the bottom of the boring [153 m (502 ft) at Site A] and the applicable layering from  $\Xi = 2.0$  below the bottom of the boring. These adapted parameterizations included 13 and 18 major subsurface layers, respectively.

### 6.1.1 “Blind” Inversion Results for Site A

Theoretical dispersion curves associated with the best 100  $V_s$  profiles from each acceptable “blind” inversion parameterization are shown in Figure 7a. It is clear from inspection that all theoretical dispersion curves match the experimental dispersion data quite well (i.e., within the uncertainty bounds of the experimental data). The numbers in brackets within the figure legend are the ranges in dispersion misfit ( $m_d$ ) values for each inversion parameterization. The lowest misfit values were achieved using the parameterization derived from a layering ratio of 2.5, with  $m_d$  of 0.61 to 0.65. However, misfit values associated with all other acceptable parameterizations shown in Figure 7a also indicate good fits to the experimental dispersion data. Hence, all of the 300 theoretical dispersion curves shown in Figure 7a are deemed to be possible representations of the experimental data and its corresponding uncertainties.

The  $V_s$  profiles derived from “blind” inversions are shown in panel (c) and (d) of Figure 7.  $V_s$  profiles from a layering ratio of 1.5 exhibit more gradual changes in  $V_s$  below  $d_{res}$  due to using more trial layers. Conversely, layering ratios of 2.0 and 2.5 exhibit more pronounced velocity contrasts, particularly below the resolution limit, because they included fewer trial layers. Figure 7b shows the lognormal median experimental H/V curve with  $\pm$  one standard deviation along with the theoretical, linear-elastic shear wave transfer functions for all 300  $V_s$  profiles derived from blind inversions. Note that the transfer functions were computed using small-strain damping ratios based on the relationships of Darendeli (2001) for soils and set equal to 0.5% for rock.

As discussed earlier, if a sharp velocity contrast is present at a site then experimental H/V curves generally exhibit well-defined peaks, the frequency of which is approximately coincident with the fundamental resonant frequency of the shear wave transfer function. The H/V low frequency peak at Site A passed the peak clarity criteria established by SESAME (2004) for the fundamental site frequency. Thus, it is important that the lowest frequency transfer function peaks occur at the same frequency as the lowest frequency H/V peaks to ensure the velocity models

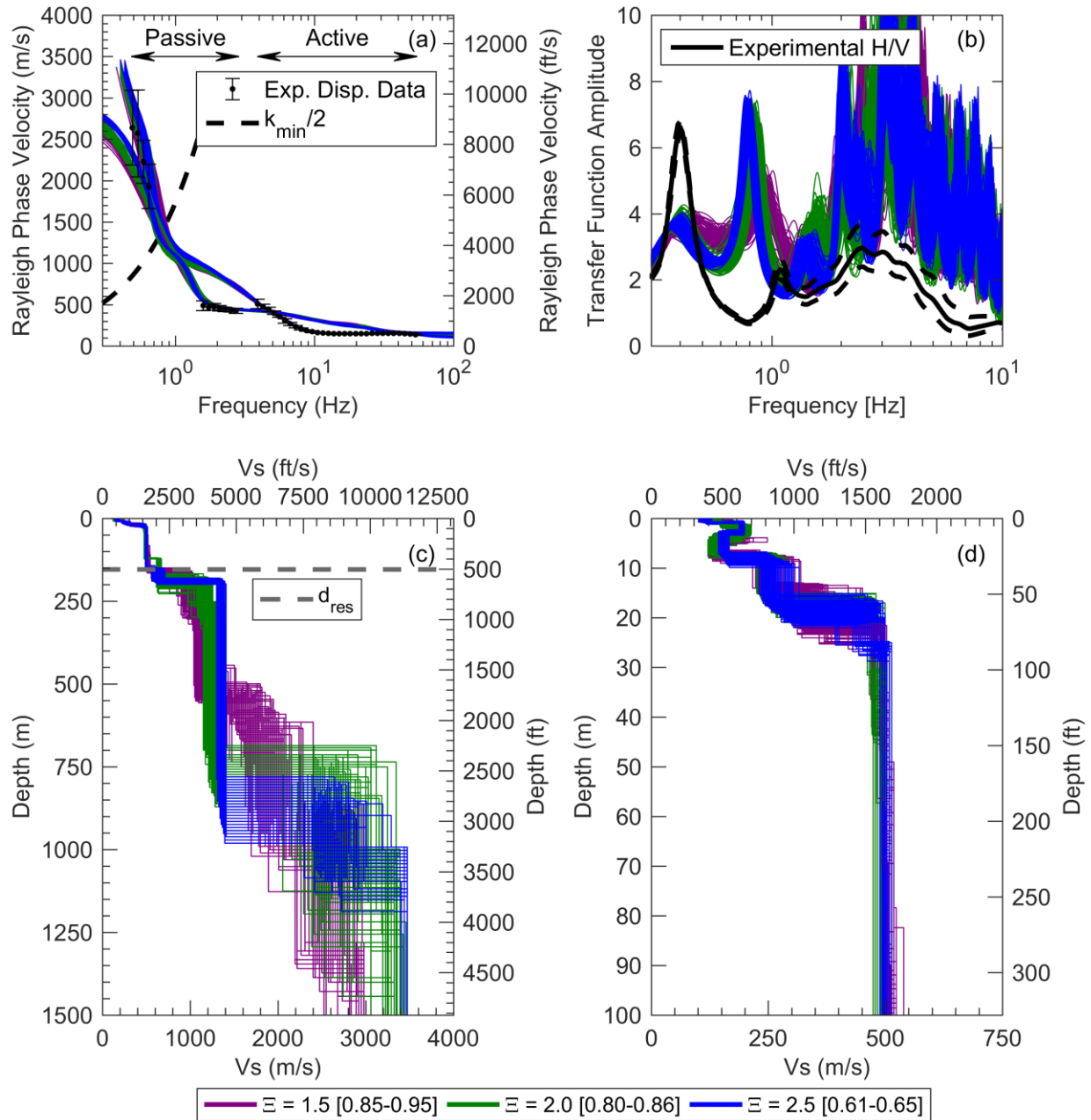


Figure 7: **“Blind” inversion results for Site A** based on a fundamental and 1<sup>st</sup>-higher mode interpretation/inversion of the experimental Rayleigh wave dispersion data. Shown for each inversion parameterization (i.e., layering ratios  $\Xi = 1.5, 2.0,$  and  $2.5$ ) are the 100 lowest misfit: (a) fundamental and 1<sup>st</sup>-higher theoretical Rayleigh wave dispersion curves along with the composite experimental dispersion data; (b) theoretical shear wave transfer functions with the lognormal median and  $\pm$  one standard deviation experimental H/V curve; and (c and d) Vs profiles shown to depths of 1500 m (4921 ft) and 100 m (328 ft), respectively. The array resolution depth limit ( $d_{res} = \lambda_{res}^*/2$ ) is shown at 154 m (505 ft). The dispersion misfit values for each inversion parameterization are indicated in brackets in the legend.

capture the “site signature” (Teague and Cox 2016, Teague et al. 2017). Note that the amplitudes of the experimental H/V curves are not expected to match the amplitudes of the transfer functions, as the H/V amplitude cannot be used directly to infer site response. The dispersion curves, transfer functions, and shear wave velocity profiles for each inversion parameterization used for “blind” inversions at Site A are plotted separately in Appendix B.

### **6.1.2 “Informed” Inversion Results for Site A**

Theoretical dispersion curves associated with the best 100  $V_s$  profiles from each acceptable “informed” inversion parameterization are shown in Figure 8a. It is clear from inspection that all theoretical dispersion curves match the experimental dispersion data quite well (i.e., within the uncertainty bounds of the experimental data). The numbers in brackets within the figure legend are the ranges in dispersion misfit ( $m_d$ ) values for each inversion parameterization. The lowest misfit values were achieved using the 2.0a parameterization, with  $m_d$  of 0.26 to 0.31. However, misfit values associated with the other acceptable parameterization shown in Figure 8a also indicate good fits to the experimental dispersion data. Hence, all of the 200 theoretical dispersion curves shown in Figure 8a are deemed to be possible representations of the experimental data and its corresponding uncertainties.

The final  $V_s$  profiles derived from “informed” inversions are shown in panel (c) and (d) of Figure 8. Differences in the  $V_s$  profiles from inversion 2.0a and 2.0b demonstrate how using additional layers in the parameterization allows for more gradual changes in  $V_s$  during inversion. While the results from 2.0a have lower misfit values, indicating that a more abrupt impedance contrast may be present at approximately 20 m, the possibility for a more gradual transition in stiffness cannot be neglected. Figure 7b shows the lognormal median experimental H/V curve with +/- one standard deviation along with the theoretical, linear-elastic shear wave transfer functions for all 200 informed  $V_s$  profiles. Note that the transfer functions were computed using small-strain damping ratios based on the relationships of Darendeli (2001) for soils and set equal to 0.5% for rock. As discussed for the “blind” inversion results, it is important that the lowest frequency transfer function peaks occur at the same frequency as the lowest frequency H/V peaks to ensure the velocity models capture the “site signature”. The dispersion curves, transfer functions and shear wave velocity profiles for each “informed” inversion performed for Site A are plotted separately in Appendix B.

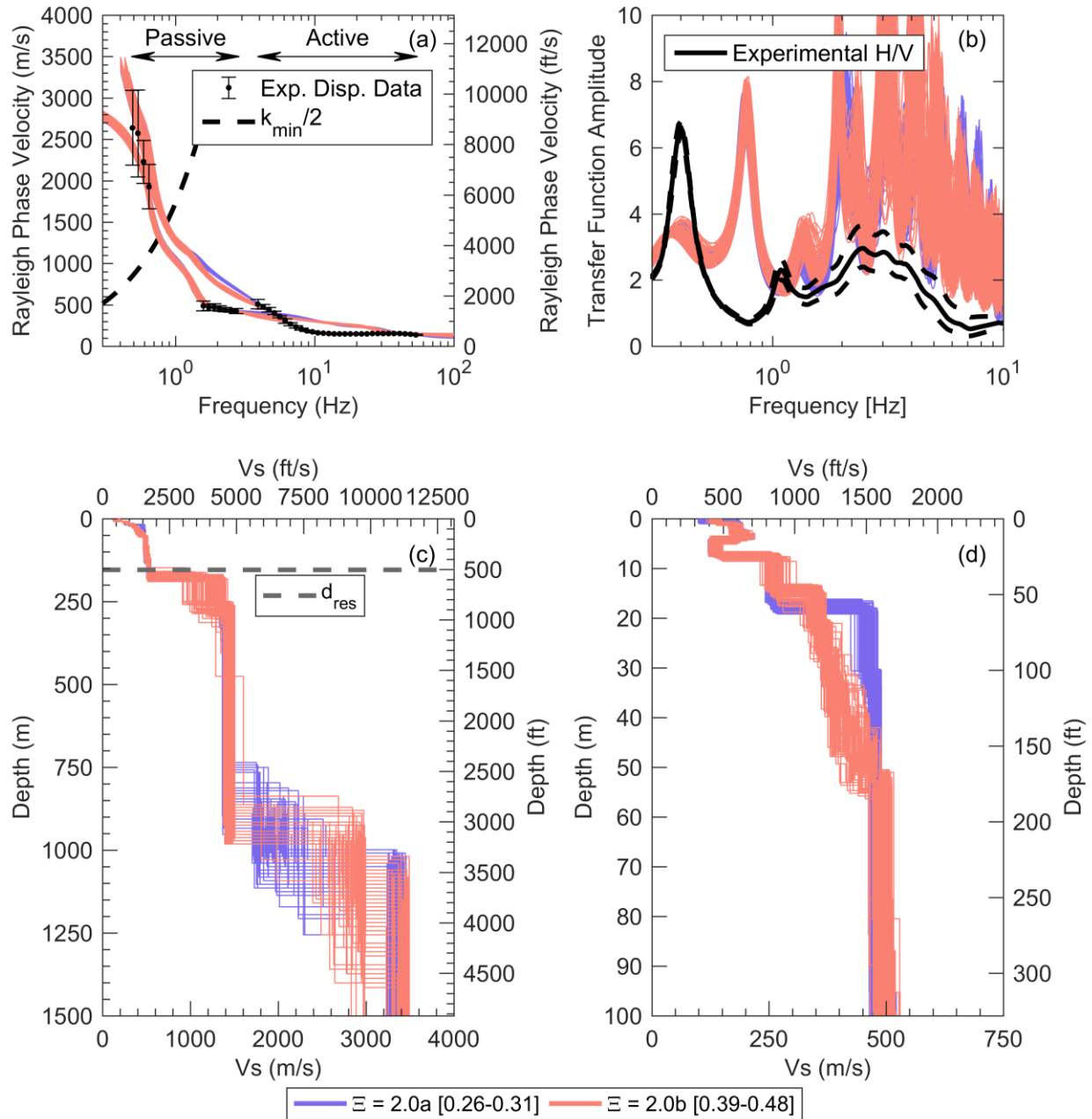


Figure 8: **“Informed” inversion results for Site A** based on a fundamental and 1<sup>st</sup>-higher mode interpretation/inversion of the experimental Rayleigh wave dispersion data. Shown for each inversion parameterization (i.e., adapted layering ratio to include borehole information  $\Xi = 2.0a$  and  $2.0b$ ) are the 100 lowest misfit: (a) theoretical fundamental and 1<sup>st</sup>-higher Rayleigh wave dispersion curves along with the composite experimental dispersion data; (b) theoretical shear wave transfer functions with the lognormal median and +/- one standard deviation experimental H/V curve; and (c and d) Vs profiles shown to depths of 1500 m (4921 ft) and 100 m (328 ft), respectively. The array resolution depth limit ( $d_{res} = \lambda^*_{res}/2$ ) is shown at 154 m (505 ft). The dispersion misfit values for each inversion parameterization are indicated in brackets in the legend.

### 6.1.3 Comparison of “Blind” and “Informed” Profiles for Site A

Figure 9 shows all 500 Vs profiles for Site A site (both “blind” and “informed”) along with the intra- and inter-inversion standard deviation of the natural logarithm of Vs ( $\sigma_{\ln V_s}$ ). The variability within a given layering ratio parameterization (i.e., intra-inversion) is generally lower than the variability between layering ratio parameterizations (i.e., inter-inversion). Within a given layer, the intra-inversion  $\sigma_{\ln V_s}$  is generally less than 0.05, while the inter-inversion  $\sigma_{\ln V_s}$  varies between 0.05 and 0.15. This underscores the need to consider multiple inversion parameterizations when quantifying inversion uncertainty. All  $\sigma_{\ln V_s}$  profiles exhibit localized “spikes” at layer interfaces. These spikes do not represent Vs uncertainty within a given layer, rather, they represent uncertainties in the locations of boundaries between layers. *The lognormal median depth to “engineering” rock (i.e., Site Class B, material with Vs > 760 m/s [2500 ft/s]) at Site A is approximately 178 m (584 ft) with a lognormal standard deviation ( $\sigma_{\ln Z_{rock}}$ ) of 0.063, which is equivalent to a +/- one standard deviation depth range of 167 – 190 m [548 – 623 ft]. The lognormal median depth to “hard” rock (i.e., Site Class A, material with Vs > 1520 m/s [5000 ft/s]) at Site A is approximately 831 m (2726 ft) with a lognormal standard deviation ( $\sigma_{\ln Z_{rock}}$ ) of 0.172, which is equivalent to a +/- one standard deviation depth range of 700 – 988 m [2297 – 3241 ft].* (Note that the Vs profiles were weighted by the inverse of their dispersion misfit values, giving those profiles with lower misfits more weight in the statistical calculations).

The array resolution limit ( $d_{res} = \lambda^*_{res}/2$ ) for Site A is 154 m (505 ft), however while the inversions are not as well constrained below this depth and the results should therefore be used cautiously, the deeper profiles contain important information for site response. Of particular interest is the maximum depth that must be modeled in site response analyses in order to capture the fundamental site frequency inferred from the experimental H/V curves. Figure 10 compares the experimental H/V curve at Site A to the theoretical shear wave transfer functions for ground models truncated at various depths. Figure 10 illustrates that while the velocity models below the array resolution limit may not be as well constrained, their continuation beyond this limit is necessary to be able to capture the measured fundamental site frequency. Figure 10a, 10b, and 10c illustrate the transfer functions when the ground model is cut off at too shallow a depth (i.e., less than 800 m [2625 ft]). These profiles clearly do not yield transfer functions with fundamental frequencies that match the low frequency peak in the experimental H/V. Therefore, they are

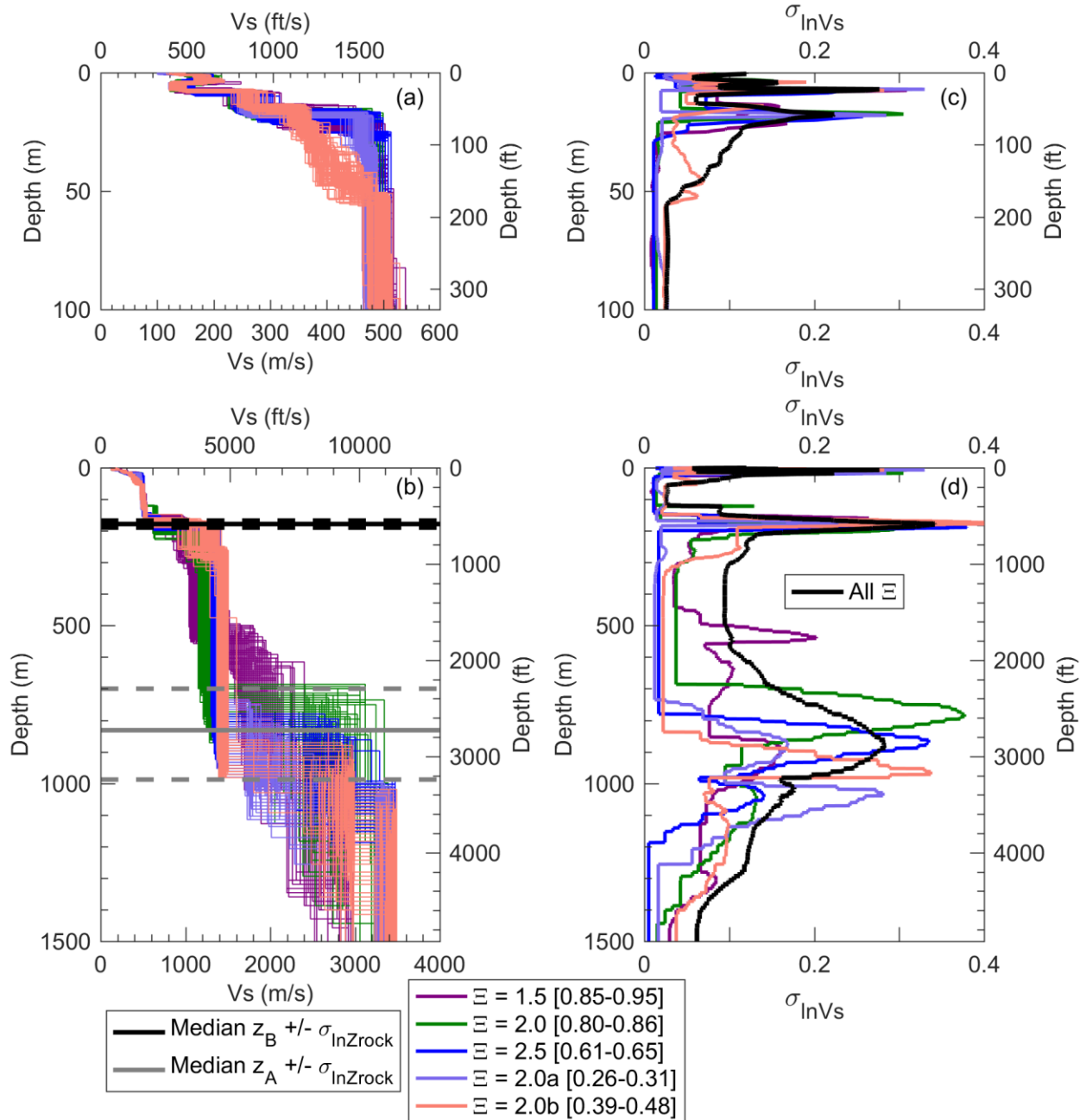


Figure 9: Inversion results for Site A site based on a fundamental and 1<sup>st</sup>-higher mode interpretation/inversion of the experimental Rayleigh wave dispersion data. Shown for each inversion parameterization (i.e., layering ratios  $\Xi = 1.5, 2.0, 2.5, 2.0a,$  and  $2.0b$ ) are the 100 lowest misfit: (a) Vs profiles shown to a depth of 100 m (328 ft); (b) standard deviation of the natural logarithm of Vs ( $\sigma_{\ln Vs}$ ) to a depth of 100 m (328 ft); (c) Vs profiles shown to a depth of 1500m (4921 ft), with the median and  $\pm$  one lognormal standard deviation depths to Site Class B and A (i.e.,  $V_{sB} > 760$  m/s (2500 ft/s) and  $V_{sA} > 1520$  m/s (5000 ft/s)); (d) standard deviation of the natural logarithm of Vs ( $\sigma_{\ln Vs}$ ) to a depth of 1500m (4921 ft).

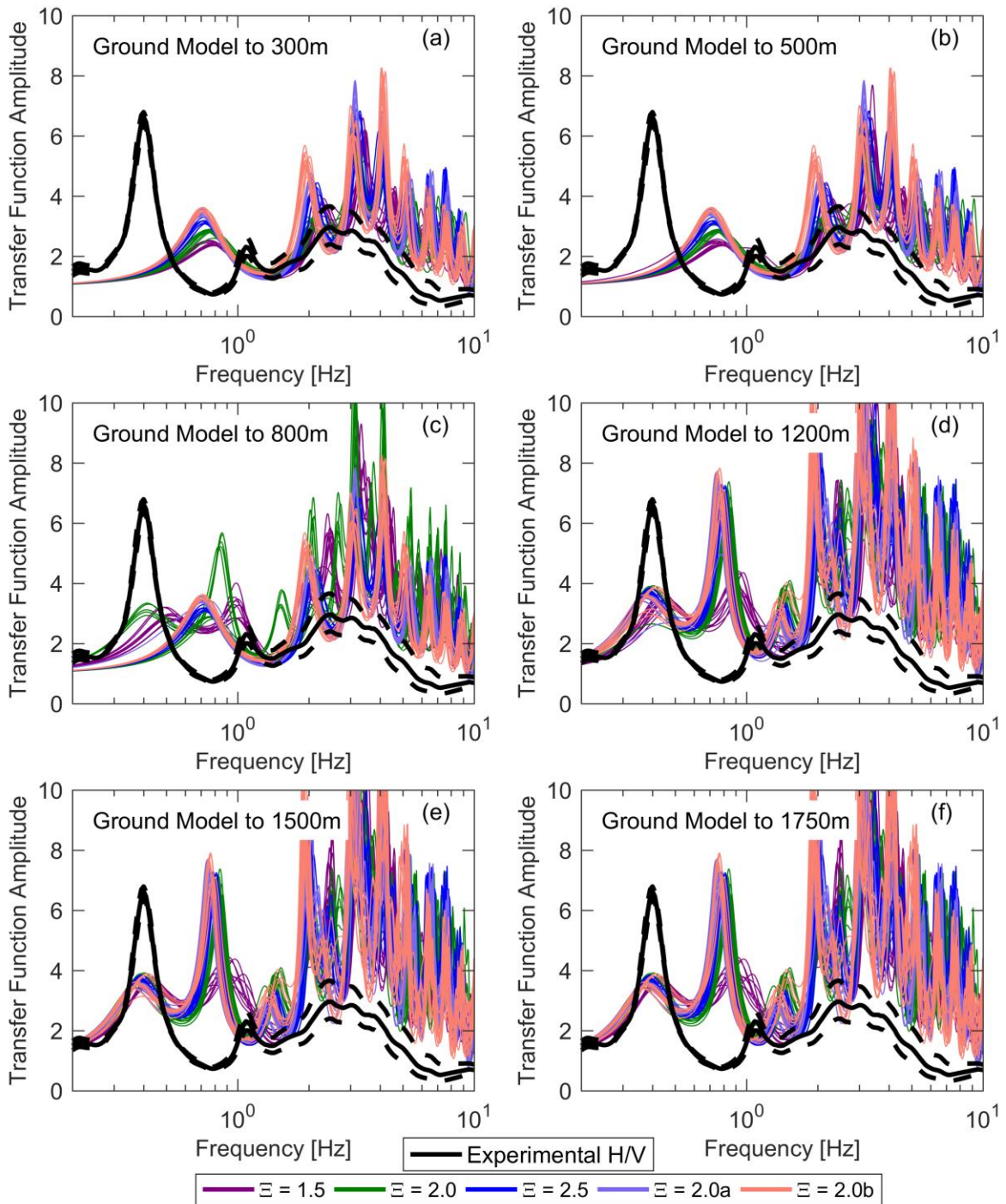


Figure 10: Theoretical shear wave transfer functions for Site A computed from the 10 best ground models for each inversion parameterization (i.e., layering ratios  $\Xi = 1.5, 2.0, 2.5, 2.0a,$  and  $2.0b$ ). Panels (a) – (f) present transfer functions obtained from cutting off the  $V_s$  profiles at different depths. The transfer functions are compared with the lognormal median and  $\pm$  one standard deviation experimental H/V curve.

missing a critical piece of the “site signature”. In contrast, Figure 10d, 10e, and 10f illustrate that extending the Vs profiles to depths greater than about 1200 m (3940 ft) results in transfer functions with a fundamental frequency that matches the low frequency H/V peak, capturing the “site signature”. As noted above, the magnitudes of the H/V and transfer function are not comparable, and only the relative alignment of lowest frequency peaks may be compared. Note that additional peaks in the transfer function, that are not present in the experimental H/V, may indicate influences of higher modes at those frequencies.

Figure 11 shows the distribution of Vs30 values obtained for all 500 Vs profiles derived for Site A. Vs30 values are binned into 5 m/s (16.4 ft/s) intervals with each layering ratio’s contribution indicated by color. ***The median Vs30 value for Site A is 256 m/s (840 ft/s) with a  $\sigma_{\ln Vs30} = 0.0374$ , which is equivalent to a +/- one standard deviation range in Vs30 of 247–266 m/s [810 – 872 ft/s].***

Figure 12 compares the median Vs profiles obtained from each of the five acceptable inversion parameterizations used at Site A. In the near-surface, all median Vs profiles indicate shallow, stiff velocity contrasts at approximately 7 m (23 ft) and 17 m (56 ft). Below the velocity contrast at approximately 17m (56 ft) the velocity remains relatively constant until reaching a significant velocity contrast at depth. This significant velocity contrast occurs at approximately 178 m (584 ft), where material with velocities indicative of engineering rock are encountered. A deeper velocity contrast is presumably present below 700 m (2297 ft), however, the depth and magnitude of this contrast is less certain (refer to Figure 9). ***All of the median Vs profiles for Site A are tabulated in Appendix B.***

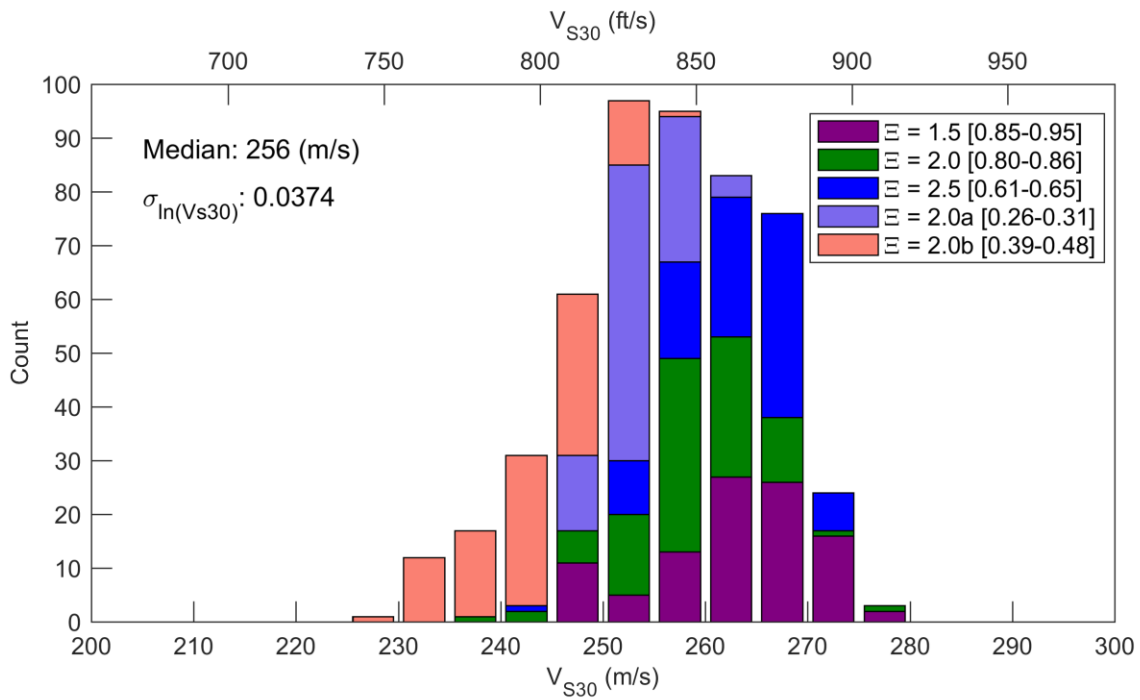


Figure 11: Distribution of Vs30 values obtained from all 500 Vs profiles at Site A, binned in 5 m/s (16.4 ft/s) intervals and organized by layering ratio ( $\Xi$ ) with the dispersion misfit values indicated inside brackets.

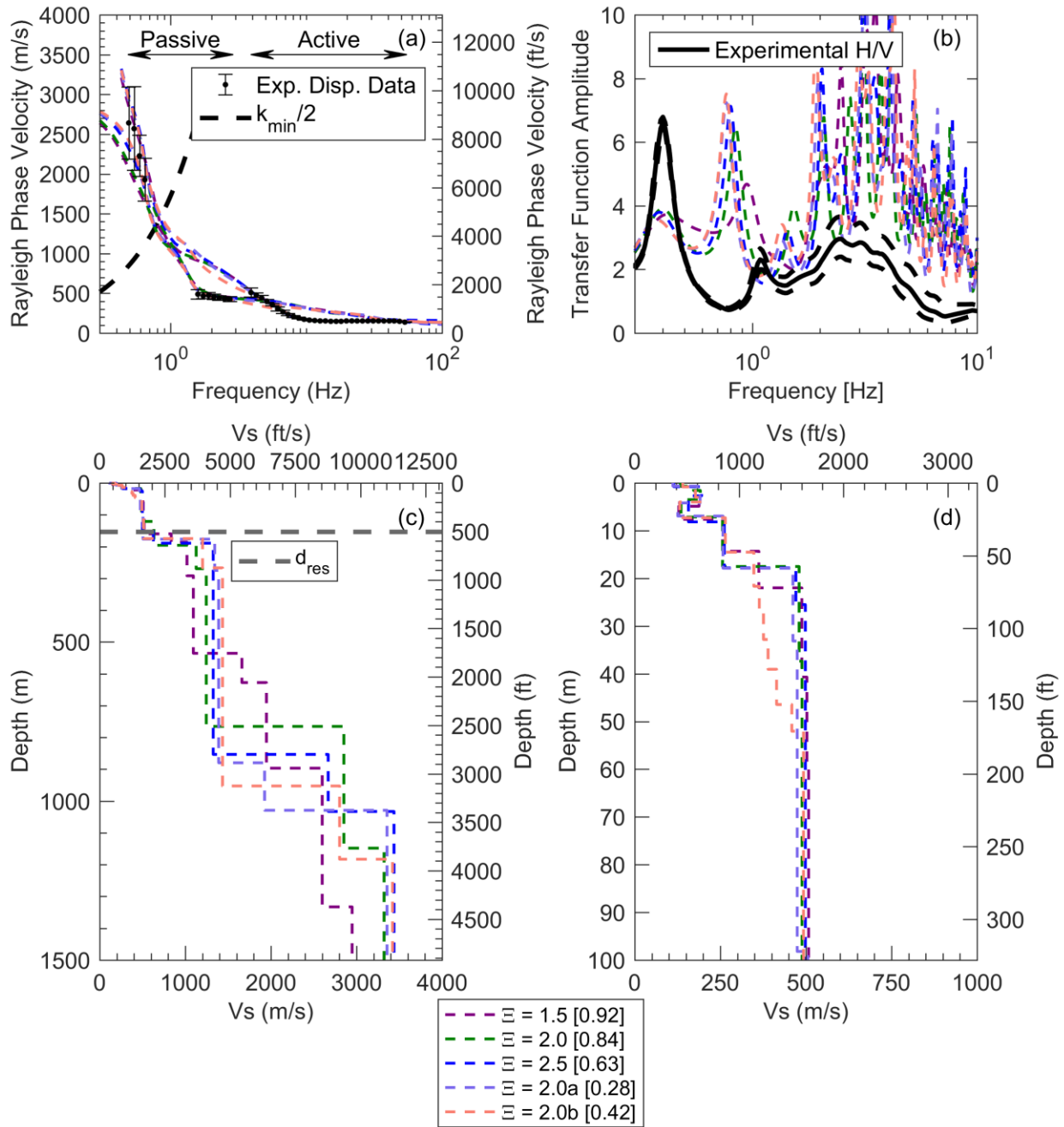


Figure 12: Median inversion results for Site A based on a fundamental and 1<sup>st</sup>-higher mode interpretation/inversion of the experimental Rayleigh wave dispersion data. Shown for each inversion parameterization (i.e., layering ratios  $\Xi = 1.5, 2.0, 2.5, 2.0a,$  and  $2.0b$ ) are the medians of the 100 best: (a) theoretical fundamental and 1<sup>st</sup>-higher Rayleigh wave dispersion curves along with the composite experimental dispersion data; (b) theoretical shear wave transfer function with the lognormal median and +/- one standard deviation experimental H/V curve; and (c and d) Vs profiles shown to depths of 1500m (4921 ft) and 100 m (328 ft), respectively. The array resolution depth limit ( $d_{res} = \lambda_{res}/2$ ) is shown at 154 m (505 ft). The median dispersion misfit values for each inversion parameterization are indicated in brackets in the legend.

## 6.2. *Deep Vs Profiles for Site B*

The “blind” and “informed” inversion results for Site B are summarized in Figures 13 and 14, respectively. For the “blind” inversions (Figure 13), four distinct inversion parameterizations yielded Vs profiles with low dispersion misfit values and  $f_{0,S}$  values from theoretical, linear-elastic shear wave transfer functions that agreed well with the experimental  $f_{0,H/V}$  values from the H/V data at Site B. Three of the four inversion parameterizations were created using the layering ratio procedure with layering ratios ( $\Xi$ ) of 1.5, 2.0, and 3.0. The fourth inversion parameterization was selected based on geological conditions common to the area of the coastal plain of South Carolina and will be referred to as GC. These parameterizations resulted in 17, 11, 8, and 10 subsurface layers, respectively. Other parameterizations were investigated and found to yield unacceptable fits to the experimental dispersion data and/or experimental H/V data. For the informed inversions (Figure 14), two distinct inversion parameterizations adapted from a layering ratio of 2.0, referred to as 2.0a and 2.0b, yielded acceptable Vs profiles following the same criteria expressed previously. These parameterizations were developed to follow the layering found in the boring log above the bottom of the boring [187 m (615 ft) at Site B] and the applicable layering from  $\Xi = 2.0$  below the bottom of the boring. These adapted parameterizations included 12 and 16 major subsurface layers, respectively.

Theoretical dispersion curves associated with the best 100 Vs profiles from each acceptable “blind” inversion parameterization are shown in Figure 13a. It is clear from inspection that all theoretical dispersion curves match the experimental dispersion data quite well (i.e., within the uncertainty bounds of the experimental data). The numbers in brackets within the figure legend are the ranges in dispersion misfit values for each inversion parameterization. The lowest misfit values (0.54 to 0.56) were achieved using the parameterization derived from anticipated geologic conditions (GC) for the “blind” inversions. However, misfit values associated with all other inversion parameterizations also indicate good fits to the experimental dispersion data. Hence, all of the 400 theoretical dispersion curves shown in Figure 13a are deemed to be good representations of the experimental data and its corresponding uncertainties.

### 6.2.1 “Blind” Inversion Results Site B

The “blind” Vs profiles derived from inversion are shown in Figure 13c and 13d. Vs profiles are similar above the resolution depth ( $d_{res}$ ), with the notable exception of depths between

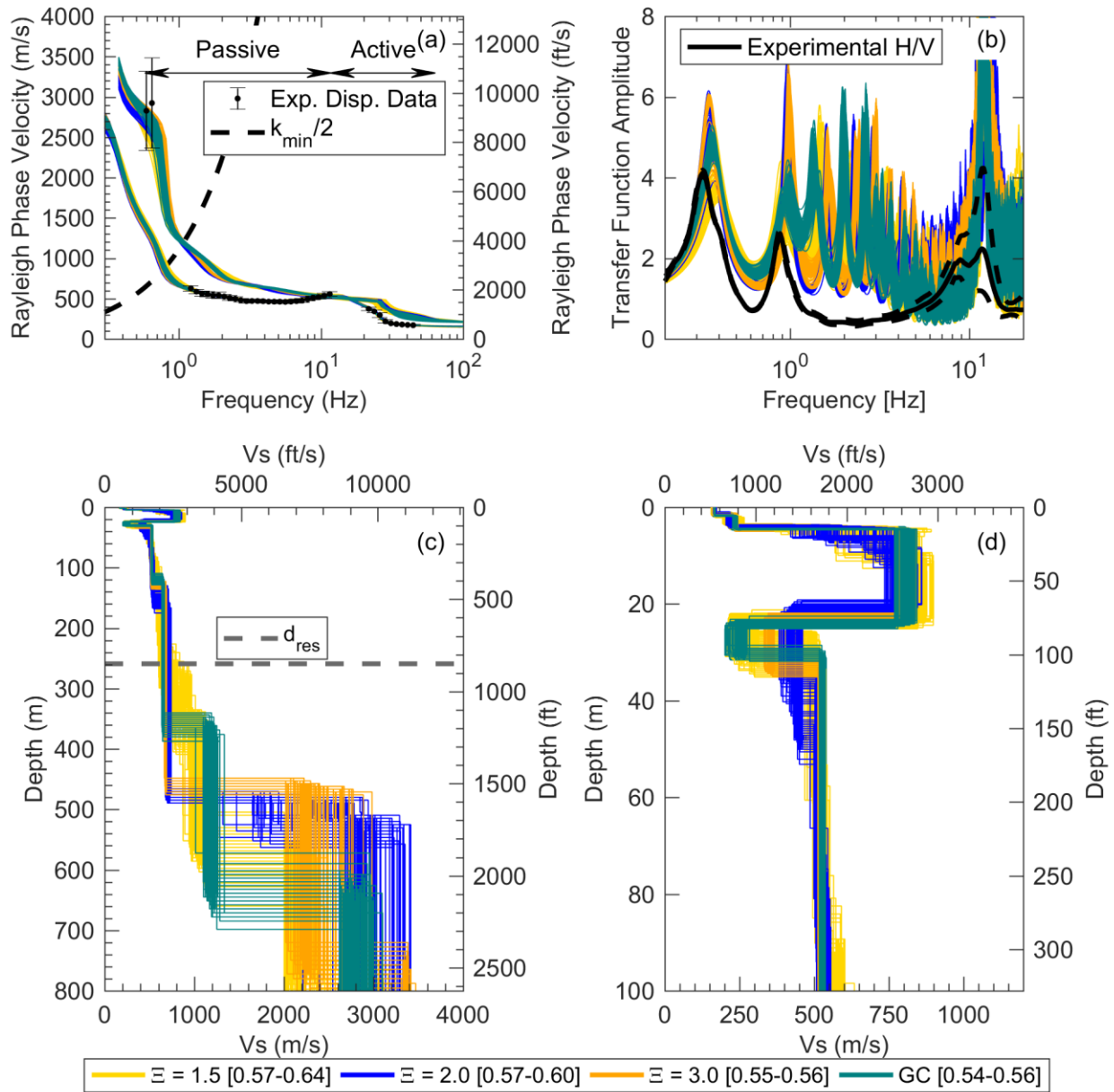


Figure 13: **“Blind” inversion results for Site B** based on a fundamental and 1<sup>st</sup>-higher mode interpretation/inversion of the experimental Rayleigh and Love wave dispersion data. Shown for each inversion parameterization (i.e., layering ratios  $\Xi = 1.5, 2.0$  and  $3.0$  and GC) are the 100 lowest misfit: (a) theoretical fundamental and 1<sup>st</sup>-higher Rayleigh wave dispersion curves along with the composite experimental dispersion data; (b) theoretical shear wave transfer functions with the lognormal median and  $\pm$  one standard deviation experimental H/V curve; and (c and d)  $V_s$  profiles shown to depths of 800 m (2625 ft) and 100 m (328 ft), respectively. The array resolution depth limit ( $d_{res} = \lambda_{res}^*/2$ ) is shown at 259 m (850 ft). The dispersion misfit values for each inversion parameterization are indicated in brackets in the legend.

approximately 20 and 50 m (66 and 164 ft), where the choice of layering parameterization clearly influences the inversion results. Note that the reasons for a poorly constrained solution here include: (1) the gap in the Rayleigh dispersion data between about 10-20 Hz, (2) the presence of a very stiff, shallow layer underlain by a much softer layer near 20 m. It will be noted that the inversion can fit the experimental data with models that either contain a thicker, higher velocity layer in conjunction with a thinner, softer, underlying low velocity layer (i.e., GC), or a thinner, high velocity layer in conjunction with a thicker and stiffer underlying low velocity layer (i.e.,  $\Xi = 2.0$ ). The only way to determine which of these “blind” models is most accurate is to use subsurface layering information from the boring log to constrain the inversion and limit inversion non-uniqueness. As the inversions shown above were performed blind, no site specific subsurface information was available to constrain the inversion. Thus, for the blind inversion results all options must be considered in order to realistically quantify uncertainty.

Figure 13b shows the lognormal median experimental H/V curve with +/- one standard deviation along with the theoretical, linear-elastic shear wave transfer functions for all 400 Vs profiles derived from blind inversions. Note that the transfer functions were computed using small-strain damping ratios based on the relationships of Darendeli (2001) for soils and set equal to 0.5% for rock. The H/V low frequency peak at Site B agrees well with linear-elastic transfer functions calculated from all of the blind inversion results. The dispersion curves, transfer functions and shear wave velocity profiles for each layering ratio inversion parameterization used at Site B are plotted individually in Appendix C.

### **6.2.2 “Informed” Inversion Results Site B**

Theoretical dispersion curves associated with the best 100 Vs profiles from each acceptable “informed” inversion parameterization are shown in Figure 14a. It is clear from inspection that all theoretical dispersion curves match the experimental dispersion data quite well (i.e., within the uncertainty bounds of the experimental data). The numbers in brackets within the figure legend are the ranges in dispersion misfit values for each inversion parameterization. The lowest misfit values were achieved using the 2.0a parameterization, with  $m_d$  of 0.57 to 0.65. However, misfit values associated with the other inversion parameterization also indicate good fits to the experimental dispersion data. Hence, all of the 200 theoretical dispersion curves shown in Figure 14a are deemed to be good representations of the experimental data and its corresponding uncertainties.

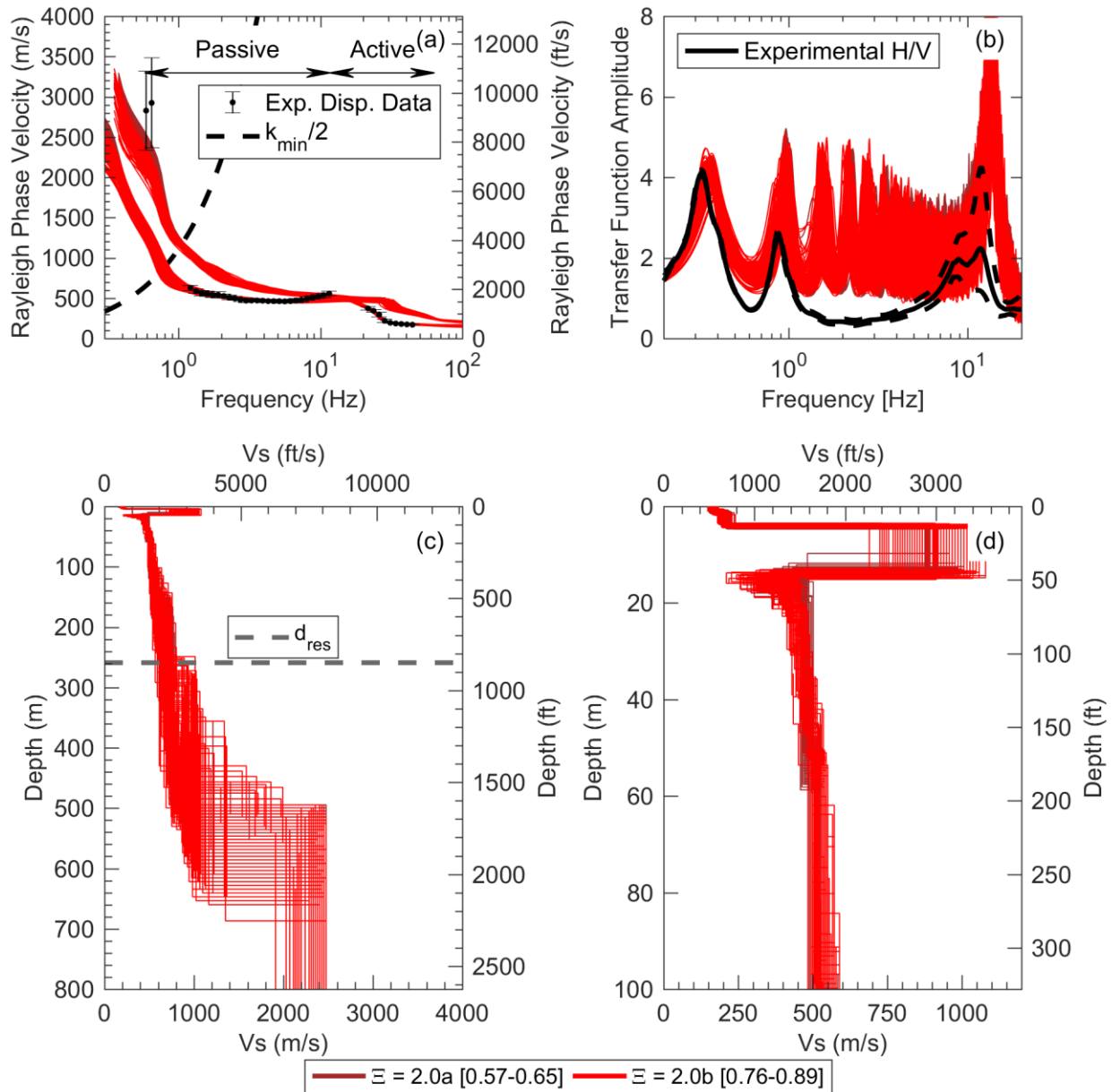


Figure 14: **“Informed” inversion results for Site B** based on a fundamental and 1<sup>st</sup>-higher mode interpretation/inversion of the experimental Rayleigh and Love wave dispersion data. Shown for each inversion parameterization (i.e., adapted layering ratios  $\Xi = 2.0a$  and  $2.0b$ ) are the 100 lowest misfit: (a) theoretical fundamental and 1<sup>st</sup>-higher Rayleigh wave dispersion curves along with the composite experimental dispersion data; (b) theoretical shear wave transfer function with the lognormal median and  $\pm$  one standard deviation experimental H/V curve; and (c and d)  $V_s$  profiles shown to depths of 800 m (2625ft) and 100 m (328ft), respectively. The array resolution depth limit ( $d_{res} = \lambda_{res}^*/2$ ) is shown at 259 m (850 ft). The dispersion misfit values for each inversion parameterization are indicated in brackets in the legend.

The “informed” Vs profiles derived from inversion are shown in Figure 14c and 14d. The “informed” Vs profiles obtained from inversion parameterizations 2.0a and 2.0b are very similar to one another, and in good agreement with those obtained from the “blind” inversions. The notable exception is the region between approximately 20 and 50 m (66 and 164 ft) previously discussed for the “blind” Vs profiles. It will be observed, from comparison with Figure 13d, that the uncertainty of the depth and velocity of the inverse layer has been considerably reduced by the layering information obtained from the borehole log.

Figure 14b shows the lognormal median experimental H/V curve with +/- one standard deviation along with the theoretical, linear-elastic shear wave transfer functions for all 200 “informed” Vs profiles derived from inversion. Once again, the location of the lowest frequency peak in the H/V curves is captured well by the theoretical transfer functions calculated from the inverted Vs profiles. The dispersion curves, transfer functions and shear wave velocity profiles for each inversion parameterization used at Site B are plotted individually in Appendix C.

### 6.2.3 Comparison of “Blind” and “Informed” Profiles for Site B

Figure 15 shows all 600 Vs profiles for Site B (both blind and informed) along with the intra- and inter-inversion standard deviation of the natural logarithm of Vs ( $\sigma_{\ln Vs}$ ). The variability within a given layering ratio parameterization (i.e., intra-inversion) is generally lower than the variability between layering ratio parameterizations (i.e., inter-inversion). Within a given layer, the intra-inversion  $\sigma_{\ln Vs}$  is generally less than 0.05, while the inter-inversion  $\sigma_{\ln Vs}$  is typically less than 0.1, except at layer interfaces. All  $\sigma_{\ln Vs}$  profiles exhibit localized “spikes” at layer interfaces. These spikes do not represent Vs uncertainty within a given layer, rather, they represent uncertainties in the locations of boundaries between layers. This underscores the need to consider multiple inversion parameterizations when quantifying inversion uncertainty. *The lognormal median depth to “engineering” rock (i.e., Site Class B, material with Vs > 760 m/s [2500 ft/s]) at Site B is approximately 390 m (1280 ft) with a lognormal standard deviation ( $\sigma_{\ln Z_{rock}}$ ) of 0.219, which is equivalent to a +/- one standard deviation depth range of 313 – 485 m [1027–1591 ft]. The lognormal median depth to “hard” rock (i.e., Site Class A, material with Vs > 1520 m/s [5000 ft/s]) at Site A is approximately 531 m (1742 ft) with a lognormal standard deviation ( $\sigma_{\ln Z_{rock}}$ ) of 0.122, which is equivalent to a +/- one standard deviation depth range of 470 – 600 m [1542–1969 ft].* Note that the shallow high velocity (Vs>760 m/s) layer starting at approximately 3 m (10 ft) has been excluded from the calculation of the Site Class B boundary.

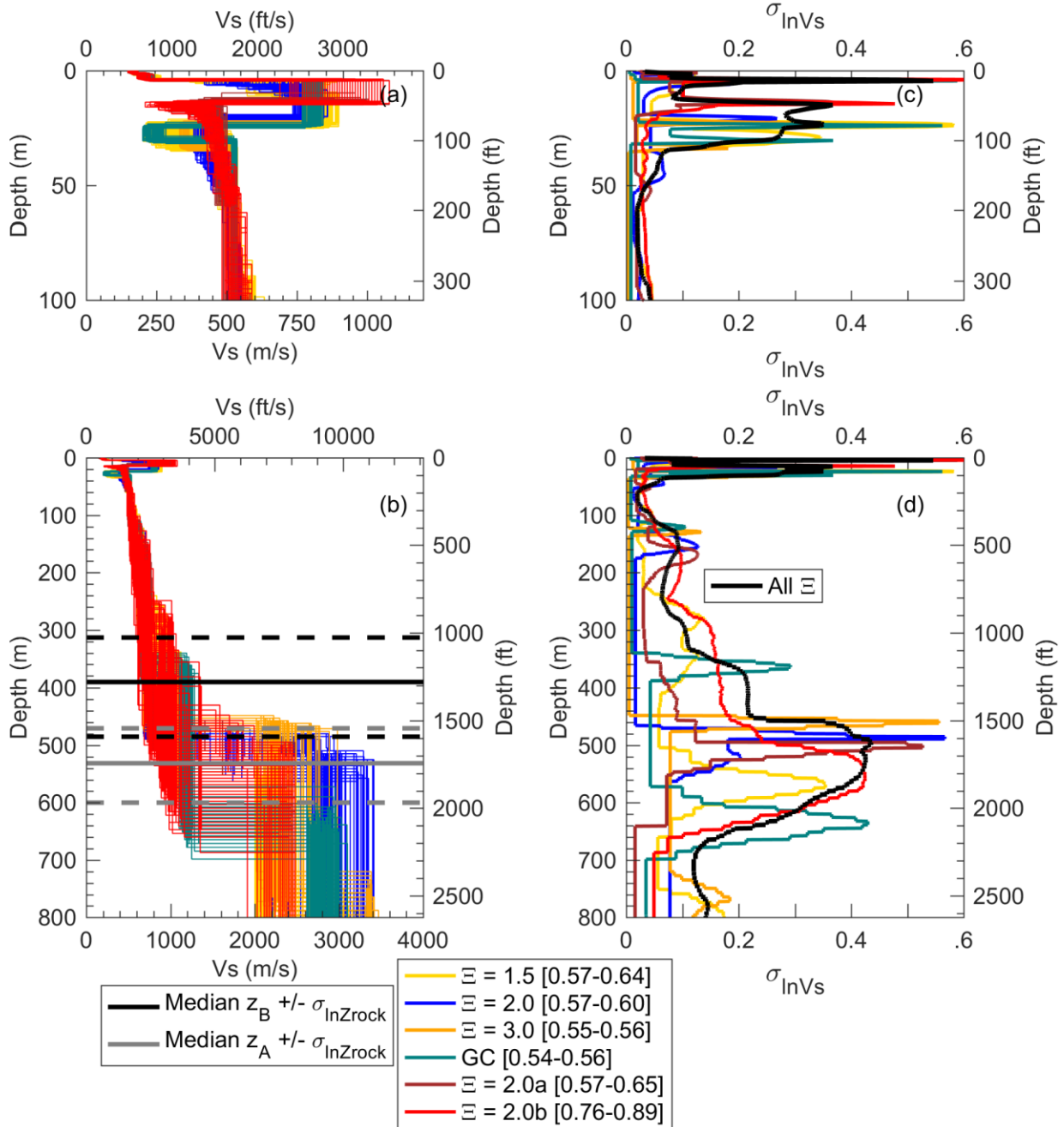


Figure 15: Inversion results for Site B site based on a fundamental and 1<sup>st</sup>-higher mode interpretation/inversion of the experimental Rayleigh and Love wave dispersion data. Shown for each inversion parameterization (i.e., layering ratios  $\Xi = 1.5, 2.0, 3.0, 2.0a,$  and  $2.0b$  and GC) are the 100 lowest misfit: (a)  $V_s$  profiles shown to a depth of 100 m (328 ft); (b) standard deviation of the natural logarithm of  $V_s$  ( $\sigma_{\ln V_s}$ ) to a depth of 100 m (328 ft); (c)  $V_s$  profiles shown to a depth of 800m (2625 ft), with the median and  $\pm$  one lognormal standard deviation depths to site class B and A (i.e.,  $V_{SB} > 760$  m/s (2500 ft/s) and  $V_{SA} > 1520$  m/s (5000 ft/s), note that the shallow high velocity ( $V_s > 760$  m/s) layer starting at approximately 3 m (10 ft) has been excluded from the calculation of the site class boundaries; (d) standard deviation of the natural logarithm of  $V_s$  ( $\sigma_{\ln V_s}$ ) to a depth of 800m (2625 ft).

The array resolution limit ( $d_{\text{res}} = \lambda_{\text{res}}^*/2$ ) for Site B is 259 m (850 ft), however while the inversions are not as well constrained below this depth and the results should therefore be used cautiously, the deeper profiles contain important information for site response. Of particular interest is the maximum depth that must be modeled in site response analyses in order to capture the fundamental site frequency inferred from the experimental H/V curves. Figure 16 compares the experimental H/V curve at Site B to the theoretical shear wave transfer functions for ground models truncated at various depths. Figure 16 illustrates that while the velocity models below the array resolution limit may not be as well constrained, their continuation beyond this limit is necessary to be able to capture the measured fundamental site frequency. Figure 16a, 16b, 16c, and 16d illustrate the transfer functions when the ground model is cut off at too shallow a depth (i.e., less than 600 m [1970 ft]). These depth-truncated profiles clearly do not yield transfer functions with fundamental frequencies that match the low frequency peak in the experimental H/V, and therefore do not match a critical piece of the “site signature”. In contrast, Figure 16e and Figure 16f illustrate that extending the Vs profiles to depths greater than about 800 m (2625 ft) results in transfer functions with a fundamental frequency that matches the low frequency H/V peak, capturing the “site signature”. As noted above, the magnitudes of the H/V and transfer function are not comparable, and only the relative alignment of lowest frequency peaks should be compared. Note that additional peaks in the transfer function, that are not present in the experimental H/V, may indicate influences of higher modes at those frequencies.

Figure 17 shows the distribution of Vs30 values obtained for all 600 Vs profiles derived for Site B. Vs30 values are binned into 10 m/s (32.8 ft/s) intervals with each layering ratio’s contribution indicated by its respective color and indicated in the legend. ***The median Vs30 value is 438 m/s (1437 ft/s) and  $\sigma_{mVs30} = 0.0657$ , which is equivalent to a +/- one standard deviation range in Vs30 of 410–468 m/s [1345 – 1535 ft/s].***

Figure 18 compares the median Vs profiles obtained from each of the six acceptable inversion parameterizations used at Site B. In the near-surface, all median Vs profiles indicate velocity contrasts at approximately 3 m (10 ft) and 20 m (65 ft). As noted above, another significant velocity contrast occurs at approximately 463 m (1519 ft), where material with velocities indicative of engineering rock are encountered. A deeper velocity contrast is likely present between approximately 500-600 m (1640-1970 ft). However, the depth and magnitude of this contrast is not well constrained. ***All of the median Vs profiles for the Site B are tabulated in Appendix C.***

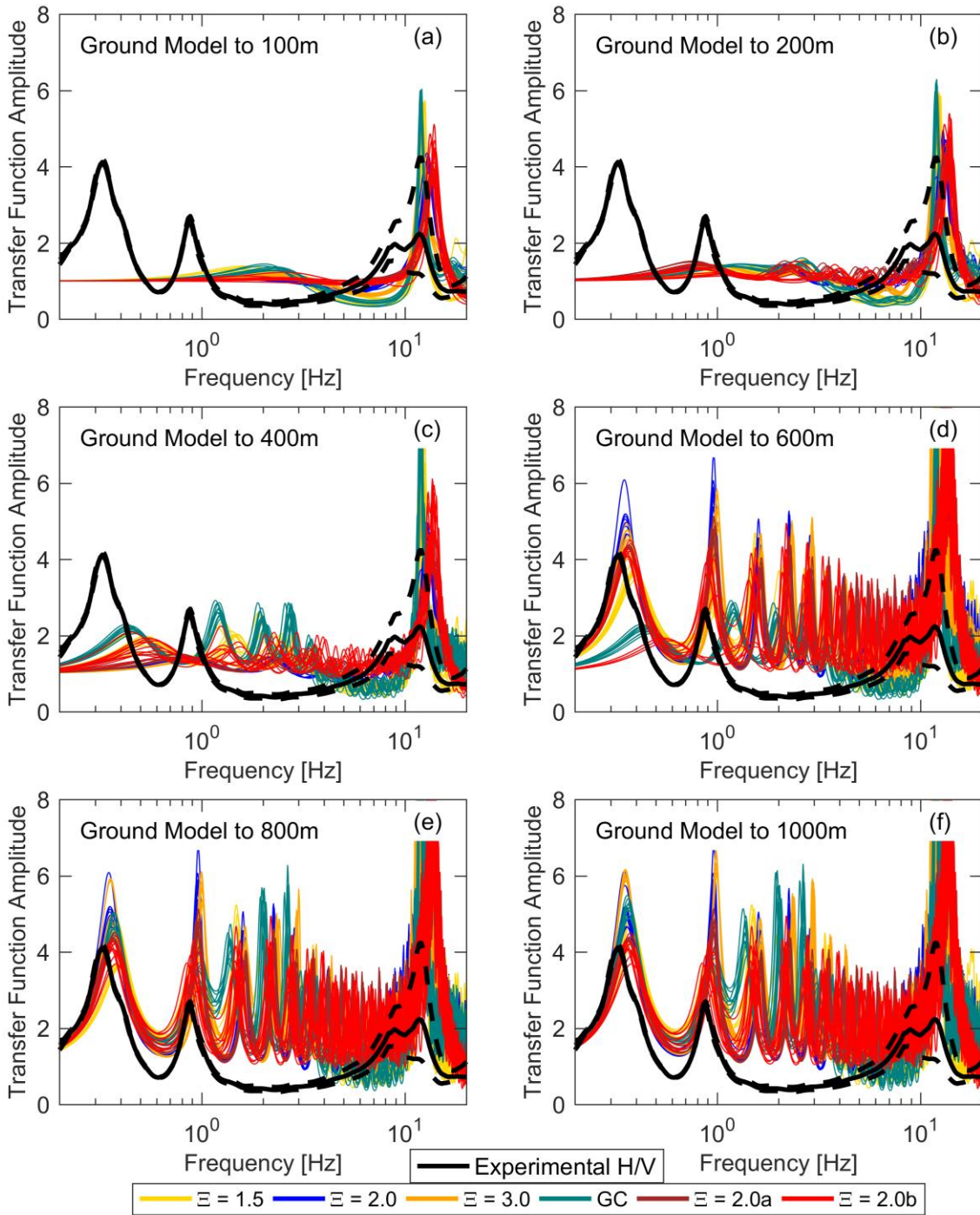


Figure 16: Theoretical shear wave transfer functions for Site B computed from the 10 best ground models for each inversion parameterization (i.e., layering ratios  $\Xi = 1.5, 2.0, 3.0, 2.0a$ , and  $2.0b$  and GC). Panels (a) – (f) present transfer functions obtained from cutting off the Vs profiles at different depths. The transfer functions are compared with the lognormal median and +/- one standard deviation experimental H/V curve.

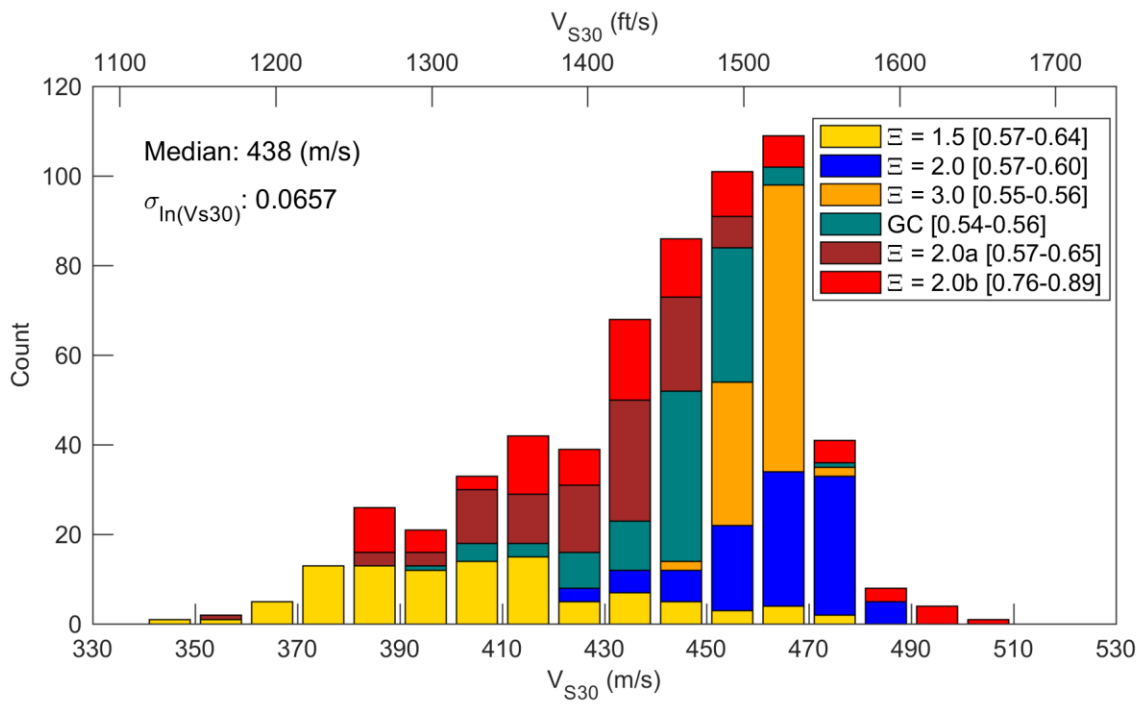


Figure 17: Distribution of Vs30 values obtained from all 600 Vs profiles at Site B binned in 10 m/s (32.8 ft/s) intervals and organized by layering ratio ( $\Xi$ ) parameterization with the dispersion misfit values indicated inside brackets.

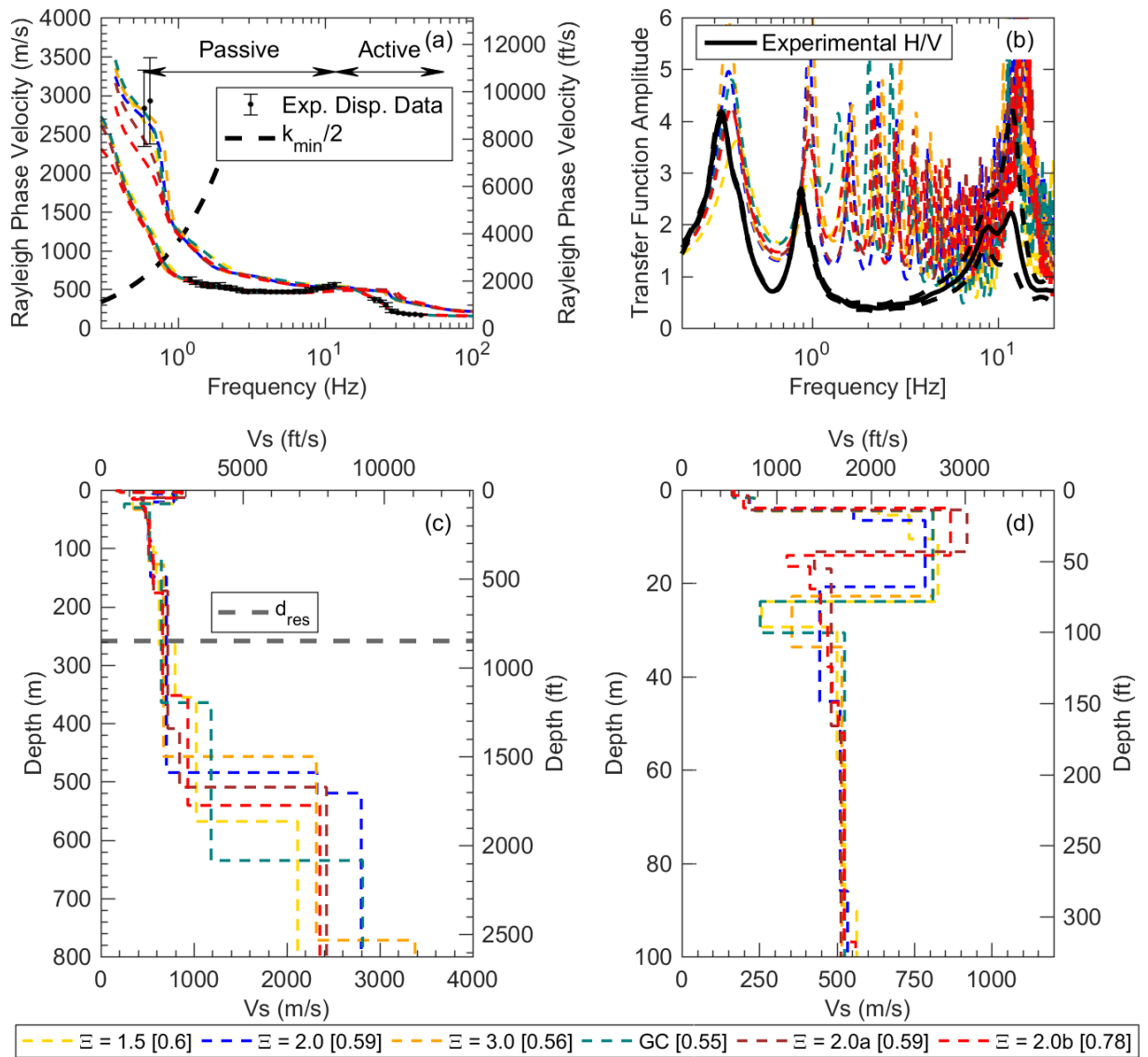


Figure 18: Median inversion results for the Site B based on a fundamental and 1<sup>st</sup>-higher mode interpretation/inversion of the experimental Rayleigh and Love wave dispersion data. Shown for each inversion parameterization are the medians of the 100 best: (a) theoretical fundamental and 1<sup>st</sup>-higher Rayleigh wave dispersion curves along with the composite experimental dispersion data; (b) theoretical shear wave transfer function with the lognormal median and +/- one standard deviation experimental H/V curve; and (c and d) Vs profiles shown to depths of 800 (2625 ft) and 100 m (328 ft), respectively. The array resolution depth limit ( $d_{res} = \lambda^*_{res}/2$ ) is shown at 259 m (850 ft). The median dispersion misfit values for each inversion parameterization are indicated in brackets in the legend.

## 7.0 SUGGESTIONS FOR SITE RESPONSE

It is important to recognize that experimental dispersion curves and/or H/V curves contain valuable information regarding small-strain wave propagation. Since the experimental dispersion data and H/V curves were measured over a large footprint at each site (refer to Figure 1 and Figure 2), we believe that they represent a “site signature” (Teague and Cox 2016, Teague et al. 2017) that contains important information about small-strain wave propagation across the site. All Vs profiles shown in Figures 7-9 and 13-15, while visually variable, well-capture their respective site signatures. Therefore, in order to realistically account for Vs uncertainty in site response, we believe that a number of Vs profiles from each inversion parameterization should be considered for use in subsequent site response analyses for their respective sites.

Based on the sensitivity of the SH transfer functions to the truncation of profiles at depth (refer to Figures 10 and 16), it is recommended that the Vs profiles be extended to the following depths in order to capture the fundamental frequency measured in the H/V experimental data: Site A – at least 1200 m (3940 ft); Site B – at least 800 m (2625 ft). Note that these recommended depths are about 200 m (650 ft) below their respective median plus one sigma depths to Site Class A bedrock ( $Z_A + \sigma_{\ln Z_{\text{rock}}}$ ) for each site. While these depths are well in excess of our ideal depth resolution limits for the size of surface wave arrays deployed at each site, it is clear that truncating the Vs profiles above these depths will not allow for accurate modeling of the fundamental site frequency. This will have consequences not only for matching the fundamental site frequency, but also for accurately predicting higher frequency ground motions affected by higher modes.

**The “informed” inversion results shown in Figure 8 for Site A and Figure 14 for Site B are preferred over the “blind” inversion results shown in Figure 7 for Site A and Figure 13 for Site B. Furthermore, the Vs profiles corresponding to inversion parameterizations 2.0a should be considered as the “best”/most likely profiles obtained from the “informed” inversions. If a single Vs profile for each site is desired for comparison purposes, we recommend using the median Vs profile obtained from the “informed” inversion results and an inversion parameterization of 2.0a.** The median 2.0a Vs profile for Site A is shown in Figure 12 and tabulated in Appendix B, while the median 2.0a Vs profile for Site B is shown in Figure 18 and tabulated in Appendix C. However, we must stress that we recommend using multiple Vs profiles from each acceptable set of inversion parameterizations (refer to Figure 9 for Site A and

Figure 15 for Site B) in order to realistically accounting for Vs uncertainty in site response analyses.

*Tabulated values for all of these Vs profiles, or any number of randomly selected Vs profiles, can be provided in any desired file format (e.g., .txt, .xlsx, .mat) upon request.* Additionally, all of the median Vs profiles tabulated in Appendix B and Appendix C for Site A and Site B, respectively, also well-capture the site signature and are suitable for use in subsequent site response analyses. We welcome the opportunity to provide input regarding the appropriate use of these Vs profiles in your site response studies. **We strongly encourage those conducting site response analyses to avoid the blind application of base-case/bounding-type Vs profiles commonly used to account for epistemic uncertainty and randomized Vs profiles to account for aleatory variability, as these types of Vs profiles will most likely not fit the site signature.** Please refer to Griffiths et al. (2016a), Griffiths et al. (2016b), Teague and Cox (2016), and Teague et al. (2017) for additional information on site response implications associated with using non-unique Vs profiles derived from surface wave inversion in comparison with other commonly used methods of accounting for Vs uncertainty.

## REFERENCES

- Bettig, B., Bard, P.Y., Scherbaum, F., Riepl, J., Cotton, F., Cornou, C., and Hatzfeld, D. (2001). “Analysis of dense array noise measurements using the modified spatial auto correlation method (SPAC): application to the Grenoble area.” *Bollettino de Geofisica Teoria e Applicata*, 42(3-4), 281-304.
- Boaga, J., Cassiani, G., Strobbia, C.L., and Vignoli, G. (2013). “Mode misidentification in Rayleigh waves: Ellipticity as a cause and a cure.” *Geophysics*, Vol. 78(4), p. EN17–EN 28.
- Bonnefoy, S. (2004). Nature du bruit de fond sismique: implication pour les etudes des effects de site, Phd thesis Universite Joseph Fourier (LGIT), Grenoble, France.
- Capon, J. (1969). “High Resolution Frequency-Wavenumber Spectrum Analysis.” *Proceedings of the IEEE*, Vol. 57, Issue 8, pp. 1408–1418.
- Cox, B.R. and Teague, D. (2016). “Layering Ratios: A Systematic Approach to the Inversion of Surface Wave Data in the Absence of A-priori Information.” *Geophysical Journal International*, DOI: 10.1093/gji/ggw282
- Cox, B. and Wood, C., (2011). Surface Wave Benchmarking Exercise: Methodologies, Results and Uncertainties, *GeoRisk 2011: Geotechnical Risk Assessment and Management* (C.H. Juang et al., eds.), ASCE GSP 224, pp. 845-852.
- Dunkin J.W. (1965). “Computation of modal solutions in layered, elastic media at high frequencies.” *Bulletin of the Seismological Society of America*, Vol. 55, pp. 335–358.

- Darendeli, M.B. (2001). "Development of A New Family of Normalized Modulus Reduction and Material Damping Curves." Ph.D. Dissertation, School of Civil, Architectural and Environmental Engineering, The University of Texas at Austin, Austin, TX.
- Electric Power Research Institute (EPRI) "Seismic Evaluation Guidance: Screening, Prioritization and Implementation Details (SPID) for the Resolution of Fukushima Near-Term Task Force Recommendation 2.1: Seismic" Electric Power Research Institute, Palo Alto, CA: 2012, Report 1025287, pp. 206.
- Haskell, N. A. (1953). "The dispersion of surface waves on multilayered media." *Bulletin of Seismological Society of America*, Vol. 43, pp. 17–34.
- Foti, S., Comina, C., Boiero, D., & Socco, L.V. (2009). "Non-uniqueness in surface-wave inversion and consequences on seismic site response analyses." *Soil Dynamics Earthquake Engineering*, Vol. 29, pp. 982–993.
- Foti, S., Lai, C., Rix, G., and Strobbia, C. (2014). *Surface Wave Methods for Near-Surface Characterization*. CRC Press, Boca Raton, Florida.
- Garofalo, F., Foti, S., Hollender, F., Bard, P.Y., Cornou, C., Cox, B.R., Ohrnberger, M., Sicilia, D., Asten, M., Di Giulio, G., Forbriger, T., Guillier, B., Hayashi, K., Martin, A., Matsushima, S., Mercerat, D., Poggini, V., & Yamanaka, H. (2016a). "Interpacific project: comparison of invasive and non-invasive methods for site characterization. Part I: Intra-comparison of surface wave methods." *Soil Dyn. Earthq. Eng.*, **82**, 222–240, doi:10.1016/j.soildyn.2015.12.010.
- Garofalo, F., Foti, S., Hollender, F., Bard, P.Y., Cornou, C., Cox, B.R., Dechamp, A., Ohrnberger, M., Perron, V., Sicilia, D., Teague, D., & Vergnault, C. (2016b). "Interpacific project: comparison of invasive and non-invasive methods for site characterization. Part II: Intra-comparison between surface-wave and borehole methods." *Soil Dyn. Earthq. Eng.*, **82**, 241–254, doi:10.1016/j.soildyn.2015.12.009.
- Griffiths, S.C., Cox, B.R., Rathje, E.M., Teague, D.P. (2016a). "A Surface Wave Dispersion Approach for Evaluating Statistical Models that Account for Shear Wave Velocity Uncertainty," *Journal of Geotechnical and Geoenvironmental Engineering* (accepted November 2015).
- Griffiths, S.C., Cox, B.R., Rathje, E.M., Teague, D.P. (2016b). "Linking Dispersion Misfit and Uncertainty in Vs Profiles to Variability in Site Response," *Journal of Geotechnical and Geoenvironmental Engineering* (accepted November 2015).
- Knopoff L. (1964). "A matrix method for elastic wave problems." *Bulletin of the Seismological Society of America*, Vol. 54, pp. 431–438.
- Lachet, C. and Bard, P.-Y. (1994). "Numerical and theoretical investigations on the possibilities and limitations of Nakamura's technique." *Journal of Physics of the Earth*, Vol. 42, pp. 377–397.
- Lermo, J. and Chavez-Garcia, F.J., (1993). "Site effects evaluation using spectral ratios with only one station." *Bulletin of the Seismological Society of America*, Vol. 83, pp. 1574–1594.
- Malischewsky, P. G. and F. Scherbaum (2004). "Love's formula and H/V-ratio (ellipticity) of Rayleigh waves", *Wave Motion*, Vol. 40, pp. 57–67.
- Nolet, G., and Panza, G.F. (1976). "Array analysis of seismic surface waves: limits and possibilities." *Pure and Applied geophysics*, 114(5), 775-790.
- Park, C. B., R. D. Miller, and J. Xia (1998). "Imaging dispersion curves of surface waves on multichannel record", 68th Annual Meeting of the International Society of Exploration Geophysics, New Orleans, Sept. 13–18, Expanded Abstracts, p. 1377–1380.

- Poggi, V. and Fah, D. (2010). "Estimating Rayleigh wave particle motions from three-component array analysis of ambient vibrations." *Geophysical Journal International*, Vol. 180, pp. 251-267.
- Richart, F.E., Jr., Hall, J.R., Jr. & Woods, R.D., (1970). *Vibrations of Soils and Foundations*. Prentice-Hall, Inc.
- SESAME European project, (2004). Guidelines for the Implementation of the H/V Spectral Ratio Technique on Ambient Vibrations: Measurements, Processing and Interpretation. Deliverable D23.12.
- Teague, D.P., Cox, B.R., Bradley, B.A., Wotherspoon, L.M. (2015). "Development of Realistic Vs Profiles in Christchurch, New Zealand via Active and Ambient Surface Wave Data: Methodologies for Inversion in Complex Interbedded Geology," 6th International Conference on Earthquake Geotechnical Engineering, Christchurch, New Zealand, 1-4 November 2015.
- Teague, D and Cox, B.R. (2016). "Site Response Implications Associated with using Non-Unique Vs Profiles from Surface Wave Inversion in Comparison with Other Commonly Used Methods of Accounting for Vs Uncertainty." *Soil Dynamics and Earthquake Engineering*, <http://dx.doi.org/10.1016/j.soildyn.2016.07.028i>.
- Teague, D.P., Cox, B.R., Rathje, E.M. (2017). "Measured vs. Predicted Site Response at the Garner Valley Downhole Array Considering Shear Wave Velocity Uncertainty from Borehole and Surface Wave Methods," submitted to *Soil Dynamics and Earthquake Engineering*, July 2017.
- Thomson, W. T. (1950). "Transmission of elastic waves through a stratified solid medium." *Journal of Applied Physics*, Vol. 21, pp. 89–93.
- Toro, G. (1995) "Probabilistic models of the site velocity profiles for generic and site-specific ground-motion amplification studies." Technical Report No. 779574, Brookhaven National Laboratory, Upton, N.Y. pp. 147.
- Wathelet, M., Jongmans, D., and Ohrnberger, M. (2004). "Surface-wave inversion using a direct search algorithm and its application to ambient vibration measurements." *Near Surface Geophysics*, Vol. 2(4), pp. 211–221.
- Wathelet, M., Jongmans, D., Ohrnberger, M., and Bonnefoy-Claudet, S. (2008). "Array performances for ambient vibrations on a shallow structure and consequences over Vs inversion." *Journal of Seismology*, Vol. 12, pp. 1–19, DOI 10.1007/s10950-007-9067-x
- Zywicki, D.J. (1999). Advanced signal processing methods applied to engineering analysis of seismic surface waves. Ph.D. Dissertation, School of Civil and Environmental Engineering, Georgia Institute of Technology, Atlanta, GA.

# **Appendix A: Receiver Coordinates**

**Table A1:** Coordinates and elevations for all seismometers used in MAM testing at Site A (near Conway, SC).

Array	Station	Latitude [°]	Longitude [°]	MSL [m]
1200m Triangular Array	11	33.950355	-79.049221	-10.0
	12	33.949925	-79.047898	-12.8
	13	33.945448	-79.042392	-13.4
	14	33.945414	-79.043915	-13.9
	15	33.945371	-79.047283	-16.2
	16	33.946329	-79.047997	-11.2
	17	33.944824	-79.051305	-4.8
	18	33.944265	-79.053715	-7.9
	19	33.945395	-79.048137	-12.8
	20	33.948104	-79.047563	-14.5
300m Triangular Array	11	33.946006	-79.047296	-13.5
	12	33.945619	-79.046999	-11.6
	13	33.945164	-79.046528	-14.2
	14	33.945424	-79.045730	-12.4
	15	33.945394	-79.047544	-12.3
	16	33.946329	-79.047997	-11.2
	17	33.944964	-79.048932	-11.0
	18	33.945740	-79.047776	-11.5
	19	33.945395	-79.048137	-12.8
	20	33.946671	-79.047562	-14.8
50m Circular Array	11	33.945869	-79.047855	-13.5
	12	33.945790	-79.047646	-11.3
	13	33.945590	-79.047601	-11.5
	14	33.945449	-79.047753	-13.8
	15	33.945440	-79.047978	-10.3
	16	33.945597	-79.048153	-11.0
	17	33.945777	-79.048079	-13.2
	18	33.945640	-79.047753	-11.1
	19	33.945834	-79.047780	-12.7
	20	33.945653	-79.047853	-11.2

**Table A2:** Coordinates and elevations for all seismometers used in MAM testing at Site B (near Andrews, SC).

Array	Station	Latitude [°]	Longitude [°]	MSL [m]
450m Circular Array	11	33.449943	-79.591593	-26.0
	12	33.448959	-79.589843	-26.9
	13	33.447229	-79.589605	-26.0
	14	33.445962	-79.590961	-25.9
	15	33.446217	-79.593142	-24.2
	16	33.447711	-79.594353	-25.6
	17	33.448942	-79.593209	-25.1
	20	33.447894	-79.591932	-23.8
150m Circular Array	11	33.448021	-79.590898	-22.0
	12	33.447842	-79.590261	-24.2
	13	33.447255	-79.589958	-26.6
	14	33.446771	-79.590293	-24.1
	15	33.446754	-79.591064	-26.6
	16	33.447160	-79.591657	-24.5
	17	33.447788	-79.591521	-25.7
	18	33.447367	-79.590770	-26.8
	19	33.447540	-79.590779	-24.4
	20	33.447364	-79.590876	-26.5
50m Circular Array	11	33.447565	-79.590883	-20.5
	12	33.447494	-79.590673	-24.2
	13	33.447326	-79.590613	-24.6
	14	33.447164	-79.590734	-24.7
	15	33.447170	-79.590961	-24.6
	16	33.447311	-79.591128	-25.1
	17	33.447501	-79.591100	-24.6
	18	33.447367	-79.590770	-26.8
	19	33.447540	-79.590779	-24.4
	20	33.447364	-79.590876	-26.5

**Appendix B: Tabulated Dispersion Data,  
Layering Ratio Inversion Summary Plots and  
Tabulated Median Vs Profiles for Site A  
(near Conway, SC)**

**Table B1:** Composite Rayleigh wave experimental dispersion data used in surface wave inversion

Frequency	Rayleigh Phase Velocity		Std. Dev.		Wavelength	
	[Hz]	[m/s]	[ft/s]	[m/s]	[ft/s]	[m]
0.492	2639.9	8661.0	452.4	1484.3	5362.9	17594.8
0.539	2570.5	8433.5	523.9	1718.9	4772.3	15657.0
0.589	2227.9	7309.3	259.0	849.7	3779.9	12401.1
0.645	1929.2	6329.5	268.5	880.8	2991.2	9813.8
1.59	488.9	1604.0	59.5	195.1	308.0	1010.5
1.74	470.8	1544.5	36.6	120.1	271.0	889.2
1.90	471.4	1546.7	40.6	133.2	248.0	813.8
2.08	457.2	1500.0	33.0	108.2	219.8	721.2
2.28	441.2	1447.4	27.3	89.6	193.8	636.0
2.49	430.6	1412.7	18.8	61.7	172.9	567.2
2.73	425.4	1395.5	30.2	99.2	156.1	512.1
3.91	508.9	1669.5	57.4	188.2	130.2	427.3
4.28	477.6	1566.9	27.8	91.1	111.7	366.5
4.68	443.7	1455.7	27.2	89.3	94.8	311.2
5.12	403.4	1323.5	19.2	63.1	78.8	258.5
5.60	358.5	1176.3	13.7	44.9	64.0	210.0
6.13	304.5	998.9	26.5	86.9	49.7	163.0
6.71	267.3	876.9	19.3	63.2	39.8	130.7
7.34	234.4	769.2	13.7	44.9	31.9	104.8
8.03	207.6	681.2	11.0	36.1	25.9	84.8
8.79	187.7	615.8	9.1	30.0	21.4	70.1
9.62	173.1	567.9	8.7	28.4	18.0	59.1
10.5	162.8	534.0	8.1	26.7	15.5	50.7
11.5	156.6	513.8	7.8	25.7	13.6	44.6
12.6	153.1	502.3	7.7	25.1	12.2	39.9
13.8	151.2	496.1	7.6	24.8	11.0	36.0
15.1	149.8	491.3	7.5	24.6	9.9	32.6
16.5	149.5	490.3	7.5	24.5	9.1	29.7
18.1	149.8	491.3	7.5	24.6	8.3	27.2
19.8	150.7	494.5	7.5	24.7	7.6	25.0
21.6	151.3	496.5	7.6	24.8	7.0	23.0
23.7	152.1	499.0	7.6	25.0	6.4	21.1
25.9	152.7	501.1	7.6	25.1	5.9	19.3
28.3	153.8	504.7	7.7	25.2	5.4	17.8
31.0	154.4	506.5	7.7	25.3	5.0	16.3
33.9	154.4	506.5	7.7	25.3	4.5	14.9
37.1	154.4	506.5	7.7	25.3	4.2	13.6
40.6	152.9	501.5	7.6	25.1	3.8	12.3
44.5	150.4	493.5	7.5	24.7	3.4	11.1
48.6	145.8	478.2	7.3	23.9	3.0	9.8
53.2	137.9	452.3	6.9	22.6	2.6	8.5

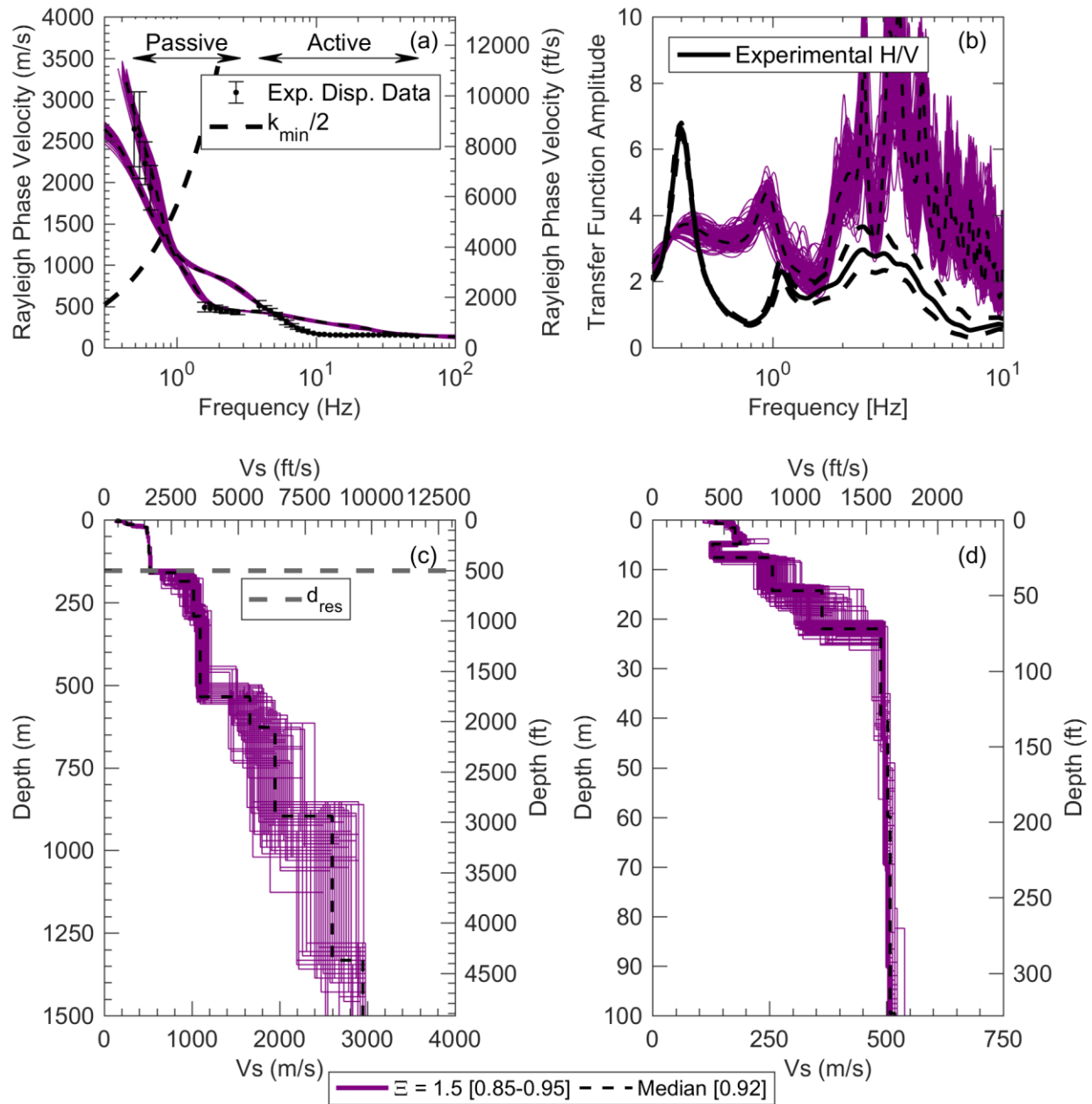


**Figure B1:** “Blind” inversion results for a *layering ratio* ( $\Xi$ ) of 1.5 based on a fundamental and 1<sup>st</sup> higher mode interpretation/inversion of the experimental Rayleigh wave dispersion data acquired at Site A. Shown are the 100 lowest misfit and median: (a) theoretical fundamental and 1st-higher Rayleigh wave dispersion curves along with the experimental dispersion data; (b) theoretical shear wave transfer functions with the lognormal median and +/- one standard deviation experimental H/V curve; and (c and d) Vs profiles shown to depths of 1500 m (4921 ft) and 100 m (328 ft), respectively. The array resolution depth limit ( $d_{res} = \lambda_{res}^*/2$ ) is shown at 154 m (505 ft). The range of dispersion misfit values for the 100 lowest misfit and median profiles are indicated in brackets in the legend.

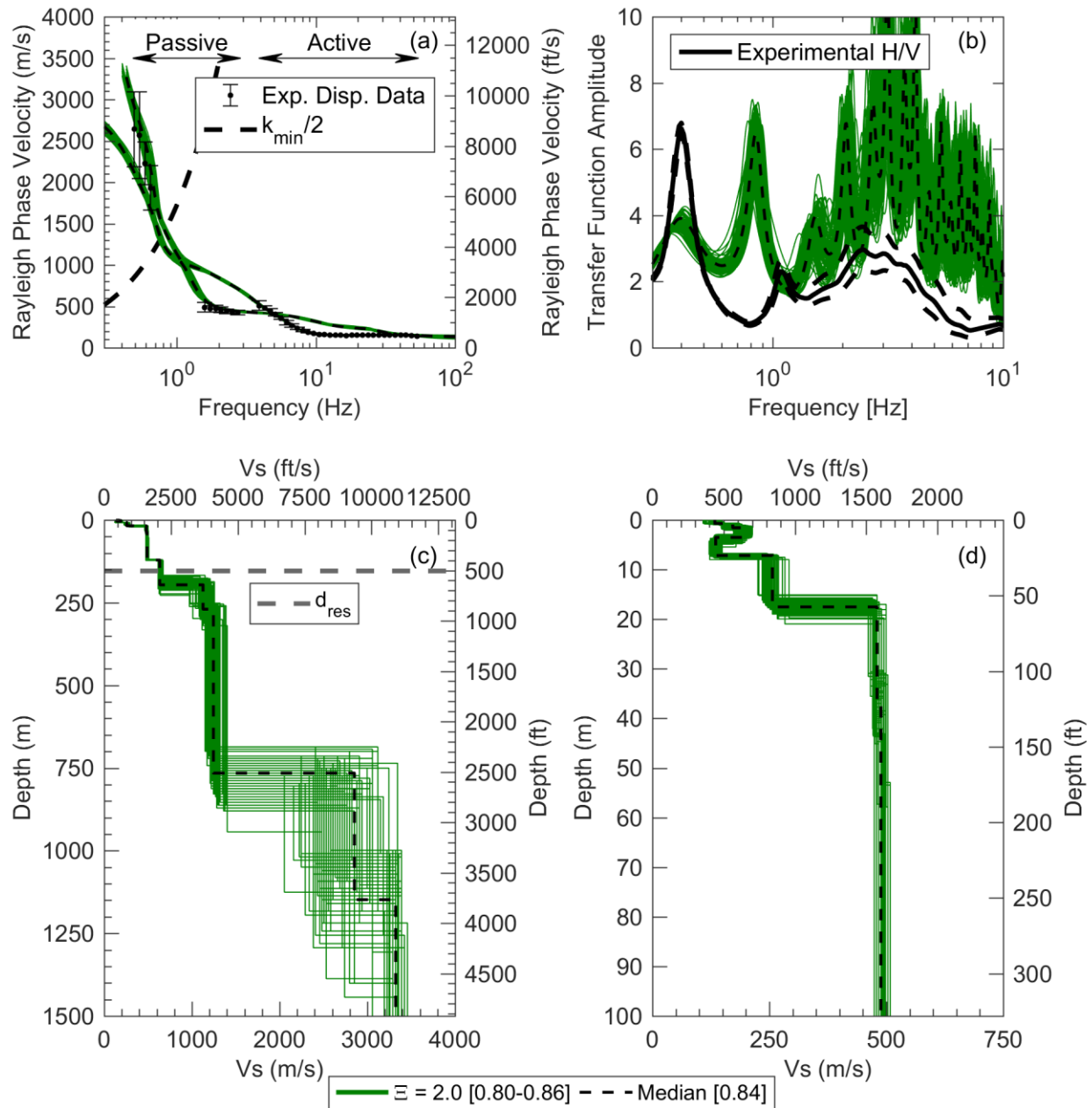


**Figure B2:** “Blind” inversion results for a *layering ratio* ( $\Xi$ ) of 2.0 based on a fundamental and 1<sup>st</sup> higher mode interpretation/inversion of the experimental Rayleigh wave dispersion data acquired at Site A. Shown are the 100 lowest misfit and median: (a) theoretical fundamental and 1st-higher Rayleigh wave dispersion curves along with the experimental dispersion data; (b) theoretical shear wave transfer functions with the lognormal median and +/- one standard deviation experimental H/V curve; and (c and d) Vs profiles shown to depths of 1500 m (4921 ft) and 100 m (328 ft), respectively. The array resolution depth limit ( $d_{res} = \lambda_{res}^*/2$ ) is shown at 154 m (505 ft). The range of dispersion misfit values for the 100 lowest misfit and median profiles are indicated in brackets in the legend.

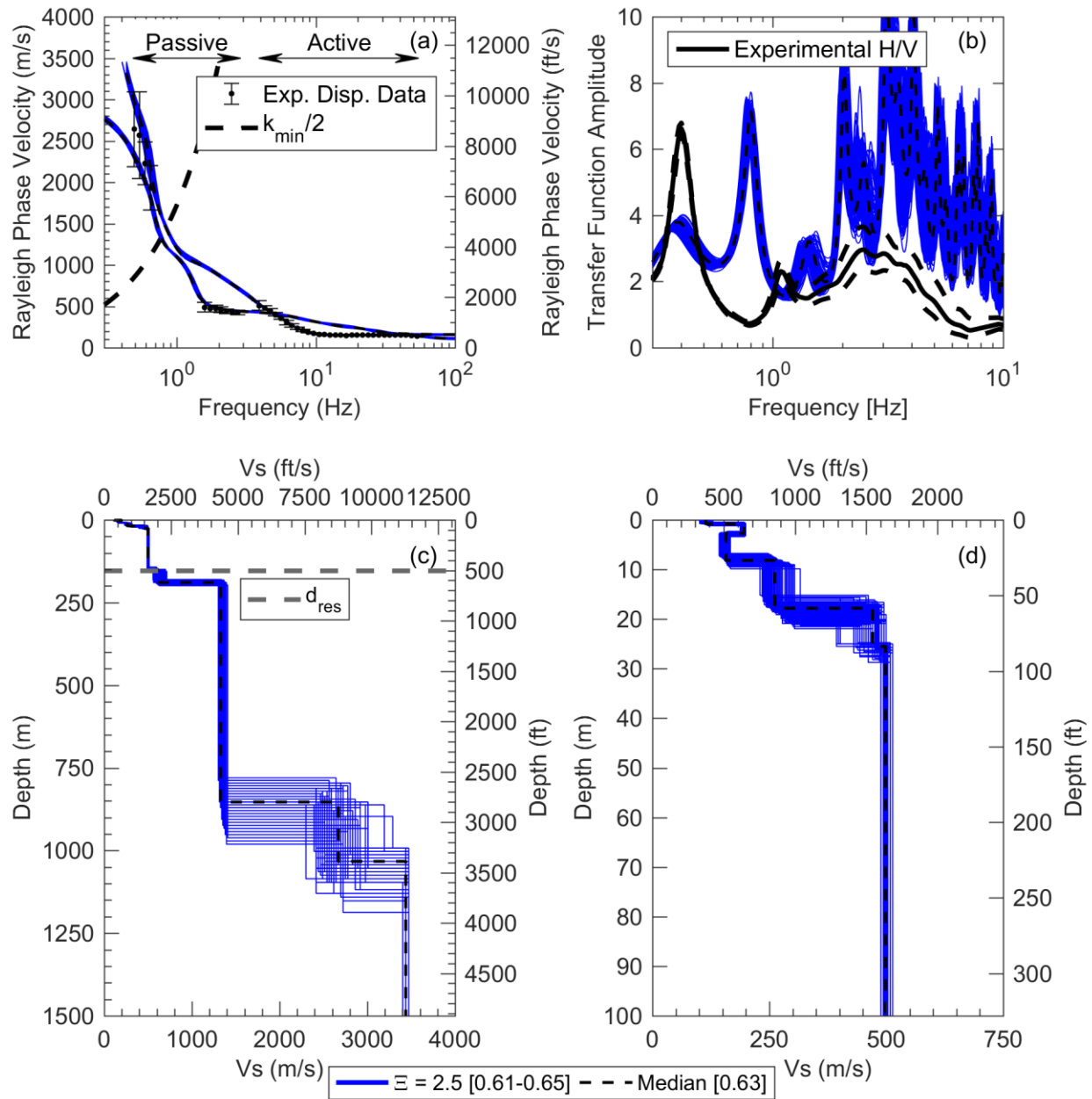


**Figure B3:** “Blind” inversion results for a *layering ratio* ( $\Xi$ ) of 2.5 based on a fundamental and 1<sup>st</sup> higher mode interpretation/inversion of the experimental Rayleigh wave dispersion data acquired at Site A. Shown are the 100 lowest misfit and median: (a) theoretical fundamental and 1st-higher Rayleigh wave dispersion curves along with the experimental dispersion data; (b) theoretical shear wave transfer functions with the lognormal median and +/- one standard deviation experimental H/V curve; and (c and d) Vs profiles shown to depths of 1500 m (4921 ft) and 100 m (328 ft), respectively. The array resolution depth limit ( $d_{res} = \lambda_{res}^*/2$ ) is shown at 154 m (505 ft). The range of dispersion misfit values for the 100 lowest misfit and median profiles are indicated in brackets in the legend.

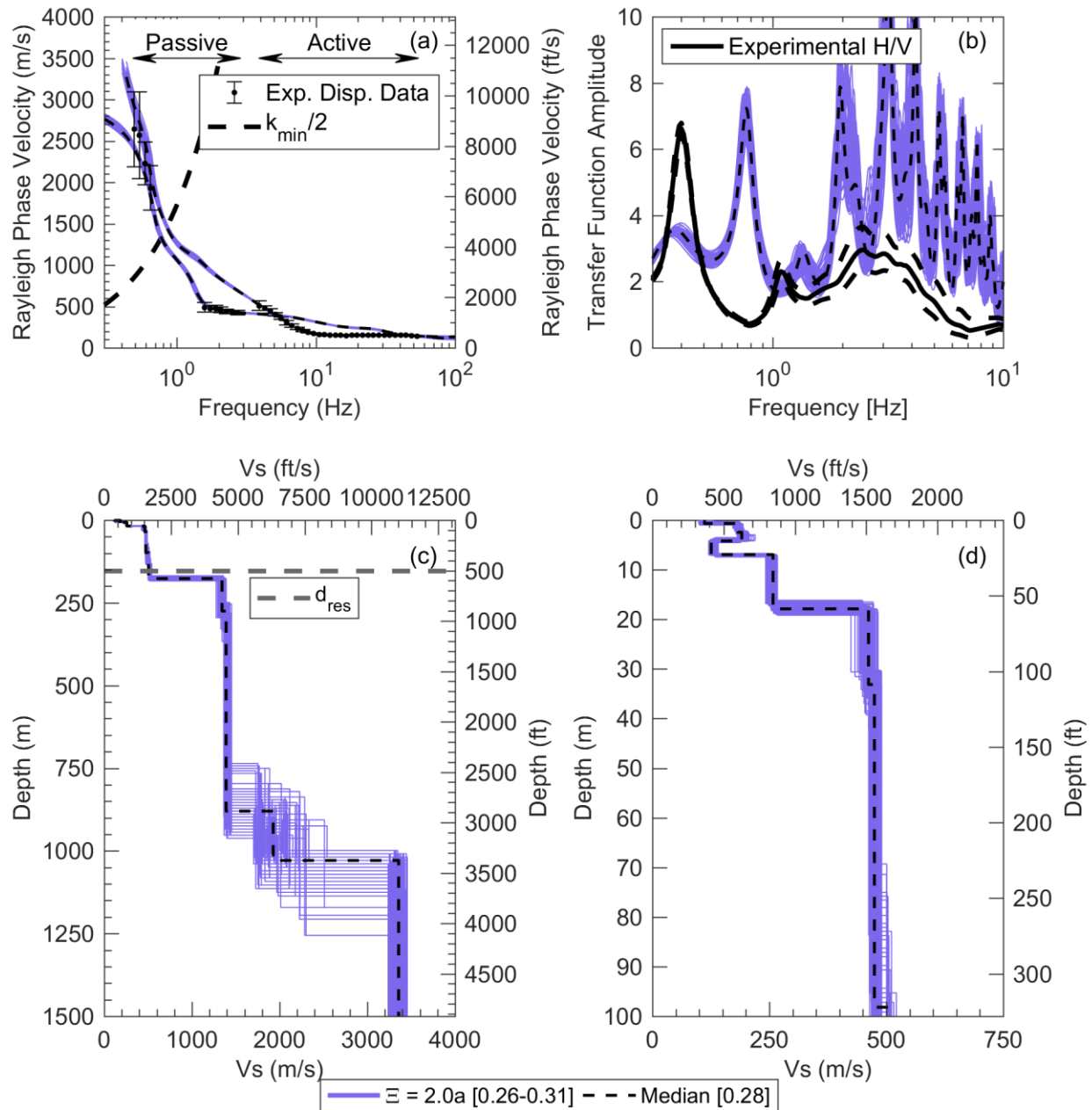


**Figure B4:** “Informed” inversion results for inversion parameterization  $2.0a$ , based on a fundamental and 1<sup>st</sup>-higher mode interpretation/inversion of the experimental Rayleigh wave dispersion data acquired at Site A. Shown are the 100 lowest misfit and median: (a) theoretical fundamental and 1st-higher Rayleigh wave dispersion curves along with the experimental dispersion data; (b) theoretical shear wave transfer functions with the lognormal median and  $\pm$  one standard deviation experimental H/V curve; and (c and d) Vs profiles shown to depths of 1500 m (4921 ft) and 100 m (328 ft), respectively. The array resolution depth limit ( $d_{res} = \lambda_{res}^*/2$ ) is shown at 154 m (505 ft). The range of dispersion misfit values for the 100 lowest misfit and median profiles are indicated in brackets in the legend.

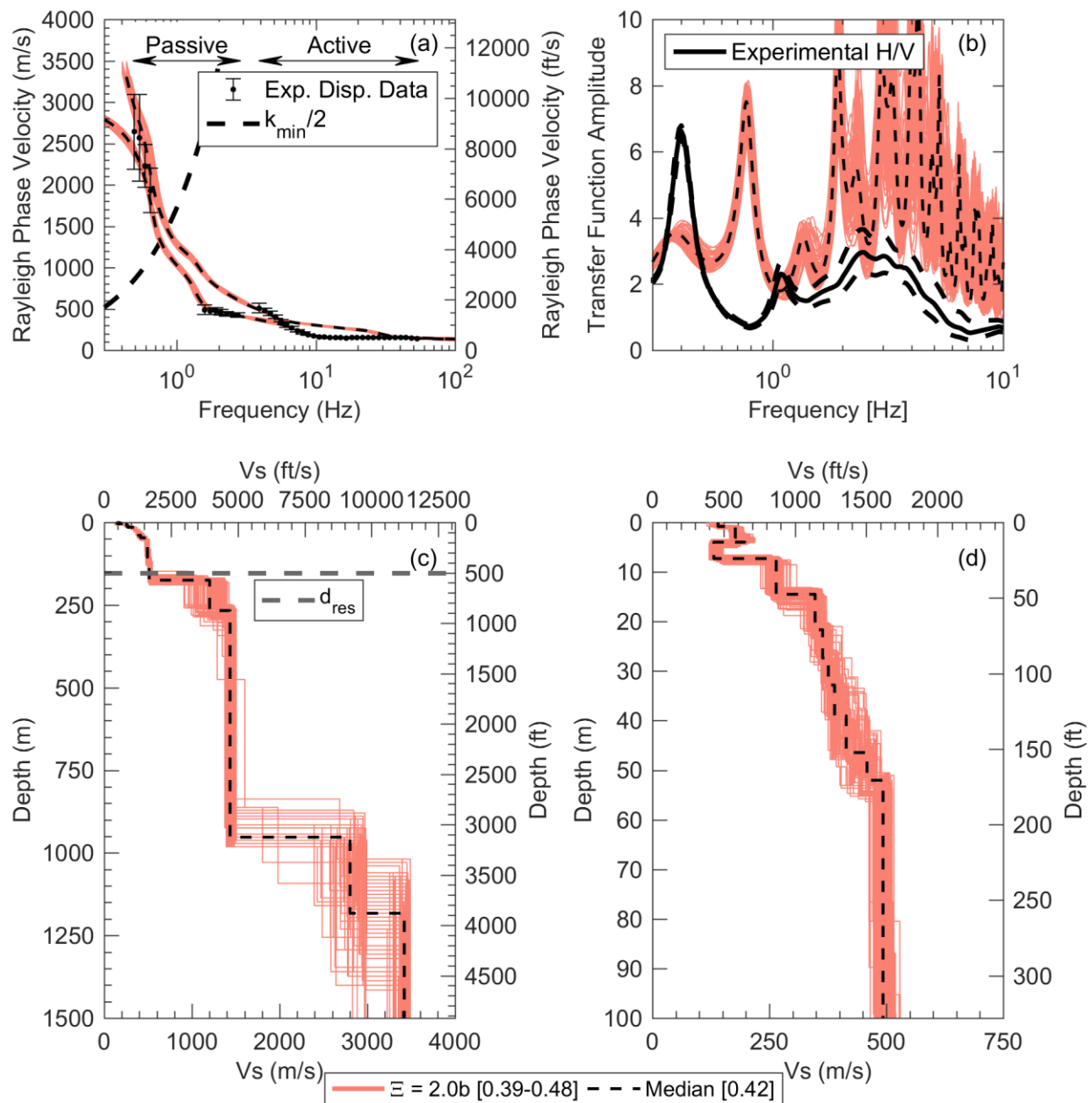


**Figure B5:** “Informed” inversion results for inversion parameterization  $2.0b$ , based on a fundamental and 1<sup>st</sup>-higher mode interpretation/inversion of the experimental Rayleigh wave dispersion data acquired at Site A. Shown are the 100 lowest misfit and median: (a) theoretical fundamental and 1st-higher Rayleigh wave dispersion curves along with the experimental dispersion data; (b) theoretical shear wave transfer functions with the lognormal median and +/- one standard deviation experimental H/V curve; and (c and d) Vs profiles shown to depths of 1500 m (4921 ft) and 100 m (328 ft), respectively. The array resolution depth limit ( $d_{res} = \lambda^*_{res}/2$ ) is shown at 154 m (505 ft). The range of dispersion misfit values for the 100 lowest misfit and median profiles are indicated in brackets in the legend.

**Table B2:** “Blind” median Vs profile and corresponding dispersion misfit value for a layering ratio of 1.5, with the approximate array resolution depth ( $d_{\text{res}} = \lambda^*_{\text{res}}/2$ ) limit indicated with a dashed black line.

Dispersion Misfit: 0.92			
Bottom Depth		Vs	
[m]	[ft]	[m/s]	[ft/s]
0.8	2.5	136.1	446.6
1.6	5.2	168.3	552.2
3.1	10.3	176.9	580.4
4.9	16.0	187.8	616.1
7.6	25.0	128.7	422.1
14.3	47.0	256.5	841.5
22.0	72.1	362.4	1189.1
40.7	133.5	488.1	1601.3
59.8	196.3	502.9	1649.8
99.5	326.6	507.9	1666.3
160.0	524.8	518.1	1699.8
186.3	611.1	835.3	2740.5
291.9	957.5	1019.2	3343.9
535.5	1757.0	1093.7	3588.2
627.6	2058.9	1661.1	5449.7
896.7	2941.8	1947.7	6390.2
1332.7	4372.3	2599.3	8527.8
1500.0	4921.3	2948.2	9672.7

**Table B3:** “Blind” median Vs profile and corresponding dispersion misfit value for a layering ratio of 2.0, with the approximate array resolution depth ( $d_{res} = \lambda^*_{res}/2$ ) limit indicated with a dashed black line.

Dispersion Misfit: 0.84			
Bottom Depth		Vs	
[m]	[ft]	[m/s]	[ft/s]
0.7	2.3	133.5	437.8
1.6	5.1	171.7	563.3
3.5	11.5	191.6	628.5
7.1	23.4	135.2	443.6
17.5	57.5	256.5	841.5
37.3	122.5	480.1	1575.1
121.0	397.0	488.5	1602.7
196.0	643.1	632.7	2075.9
269.6	884.5	1126.8	3697.0
765.4	2511.0	1244.7	4083.7
1148.1	3766.7	2852.1	9357.2
1500.0	4921.3	3322.2	10899.5

**Table B4:** “Blind” median Vs profile and corresponding dispersion misfit value for a layering ratio of 2.5, with the approximate array resolution depth ( $d_{res} = \lambda^*_{res}/2$ ) limit indicated with a dashed black line.

Dispersion Misfit: 0.63			
Bottom Depth		Vs	
[m]	[ft]	[m/s]	[ft/s]
0.8	2.6	113.8	373.4
2.7	8.9	195.4	641.1
8.2	26.8	157.0	515.0
17.8	58.4	261.6	858.4
25.5	83.6	470.6	1544.0
151.0	495.5	498.3	1634.9
189.3	621.1	626.5	2055.4
853.4	2799.7	1325.8	4349.6
1032.8	3388.5	2669.0	8756.6
1500.0	4921.3	3437.4	11277.4

**Table B5:** “Informed” median Vs profile and corresponding dispersion misfit value for inversion parameterization 2.0a, with the approximate array resolution depth ( $d_{\text{res}} = \lambda^*_{\text{res}}/2$ ) limit indicated with a dashed black line.

Dispersion Misfit: 0.28			
Bottom Depth		Vs	
[m]	[ft]	[m/s]	[ft/s]
0.7	2.2	111.4	365.5
2.4	8.0	183.0	600.3
4.2	13.7	191.0	626.6
6.9	22.8	125.8	412.6
17.9	58.6	257.8	845.8
33.1	108.7	462.0	1515.8
98.2	322.1	474.6	1556.9
176.6	579.4	505.5	1658.6
275.0	902.3	1343.1	4406.6
879.8	2886.4	1389.3	4558.2
1029.1	3376.2	1926.2	6319.7
1500.0	4921.3	3356.5	11012.0

**Table B6:** “Informed” median Vs profile and corresponding dispersion misfit value for inversion parameterization 2.0b, with the approximate array resolution depth ( $d_{\text{res}} = \lambda^*_{\text{res}}/2$ ) limit indicated with a dashed black line.

Dispersion Misfit: 0.42			
Bottom Depth		Vs	
[m]	[ft]	[m/s]	[ft/s]
0.8	2.7	140.2	459.9
3.0	9.9	177.2	581.4
4.0	13.1	197.2	647.0
7.3	23.9	131.3	430.8
14.5	47.6	264.6	868.1
21.7	71.1	347.8	1141.2
27.3	89.7	363.8	1193.7
32.8	107.6	376.0	1233.7
39.0	128.1	389.4	1277.6
46.4	152.4	414.3	1359.3
52.0	170.7	458.8	1505.2
110.6	363.0	492.9	1617.2
174.9	573.7	512.1	1680.2
266.9	875.7	1201.5	3941.9
952.7	3125.5	1434.5	4706.4
1182.9	3880.8	2802.1	9193.3
1500.0	4921.3	3420.8	11223.1

**Appendix C: Tabulated Dispersion Data,  
Layering Ratio Inversion Summary Plots and  
Tabulated Median Vs Profiles for Site B  
(near Andrews, SC)**

**Table C1:** Composite Rayleigh wave experimental dispersion data used in surface wave inversion

Frequency	Rayleigh Phase Velocity		Std. Dev.		Wavelength	
	[Hz]	[m/s]	[ft/s]	[m/s]	[ft/s]	[m]
0.589	2828.7	9280.5	489.1	1604.7	4799.2	15745.5
0.645	2924.4	9594.3	558.6	1832.7	4534.2	14875.9
1.21	628.5	2061.9	31.6	103.7	518.7	1701.8
1.33	586.8	1925.1	29.4	96.4	442.6	1452.1
1.45	563.4	1848.3	31.7	104.1	388.3	1274.1
1.59	553.8	1816.8	30.7	100.6	348.8	1144.5
1.74	540.2	1772.3	29.2	95.7	311.0	1020.3
1.90	541.0	1774.9	37.6	123.3	284.6	933.8
2.08	526.7	1728.0	27.2	89.3	253.2	830.8
2.28	510.0	1673.3	26.4	86.5	224.1	735.2
2.49	498.5	1635.6	24.9	81.5	200.2	656.8
2.73	479.6	1573.4	23.0	75.5	176.0	577.4
2.98	469.6	1540.5	22.0	72.3	157.5	516.6
3.26	470.9	1545.1	22.2	72.8	144.3	473.5
3.57	471.1	1545.6	22.5	73.8	131.9	432.9
3.91	468.2	1536.0	21.9	71.9	119.8	393.1
4.28	463.2	1519.7	21.5	70.4	108.3	355.5
4.68	462.9	1518.7	21.4	70.3	98.9	324.6
5.12	462.5	1517.3	21.4	70.2	90.3	296.4
5.60	460.1	1509.4	21.2	69.4	82.1	269.5
6.13	463.6	1521.0	21.5	70.5	75.6	248.1
6.71	469.7	1541.1	23.2	76.0	70.0	229.8
7.34	476.9	1564.7	22.1	72.4	65.0	213.2
8.03	493.2	1618.1	23.1	75.8	61.4	201.5
8.79	508.6	1668.6	24.6	80.6	57.9	189.9
9.62	519.1	1703.0	25.6	84.0	54.0	177.1
10.5	537.6	1763.9	27.5	90.1	51.1	167.6
11.5	557.4	1828.7	27.8	91.2	48.4	158.8
21.6	372.8	1223.2	18.6	61.2	17.2	56.6
23.7	342.5	1123.8	17.1	56.2	14.5	47.5
25.9	297.2	975.2	27.9	91.5	11.5	37.7
28.3	219.7	720.8	20.7	67.9	7.8	25.4
31.0	194.8	639.2	9.7	32.0	6.3	20.6
33.9	185.4	608.2	9.3	30.4	5.5	17.9
37.1	179.6	589.1	9.0	29.5	4.8	15.9
40.6	174.3	571.8	8.7	28.6	4.3	14.1
44.5	170.5	559.5	8.5	28.0	3.8	12.6

**Table C2:** Composite Love wave experimental dispersion data used in surface wave inversion

Frequency	Love Phase Velocity		Std. Dev.		Wavelength	
	[Hz]	[m/s]	[ft/s]	[m/s]	[ft/s]	[m]
11.5	554.6	1819.6	43.9	143.9	48.2	158.0
12.6	429.8	1410.1	21.5	70.5	34.1	111.9
13.8	347.2	1139.2	17.4	57.0	25.2	82.6
15.1	301.2	988.3	15.1	49.4	20.0	65.5
16.5	273.6	897.5	13.7	44.9	16.6	54.4
18.1	254.1	833.7	12.7	41.7	14.1	46.2
19.8	240.3	788.4	12.0	39.4	12.2	39.9
21.6	229.7	753.8	11.5	37.7	10.6	34.8
23.7	221.7	727.3	11.1	36.4	9.4	30.7
25.9	215.0	705.4	10.8	35.3	8.3	27.2
28.3	209.0	685.8	10.5	34.3	7.4	24.2
31.0	204.0	669.2	10.2	33.5	6.6	21.6
33.9	199.3	654.0	10.0	32.7	5.9	19.3
37.1	194.7	638.7	9.7	31.9	5.2	17.2
40.6	190.0	623.4	9.5	31.2	4.7	15.3
44.5	184.1	604.0	9.2	30.2	4.1	13.6
48.6	178.9	586.8	8.9	29.3	3.7	12.1
53.2	174.0	570.7	8.7	28.5	3.3	10.7
58.3	170.7	560.0	8.5	28.0	2.9	9.6
63.7	169.8	557.1	8.5	27.9	2.7	8.7

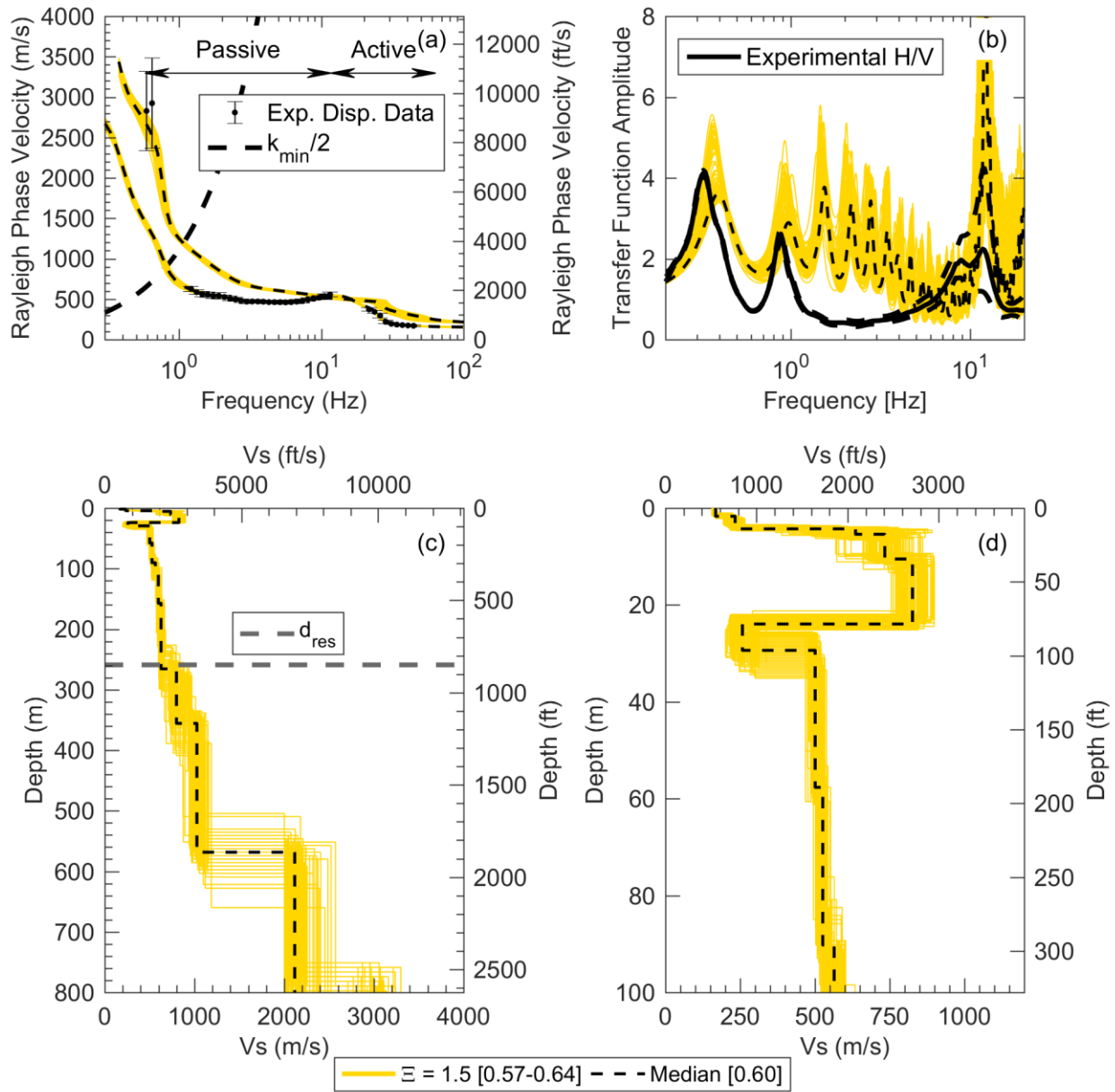


**Figure C1:** “Blind” inversion results for a layering ratio ( $\Xi$ ) of 1.5 based on a fundamental and 1st-higher mode interpretation/inversion of the experimental Rayleigh and Love wave dispersion data acquired at Site B. Shown are the 100 lowest misfit and median: (a) theoretical fundamental and 1st-higher Rayleigh wave dispersion curves along with the experimental dispersion data; (b) theoretical shear wave transfer functions with the lognormal median and +/- one standard deviation experimental H/V curve; and (c and d) Vs profiles shown to depths of 800 m (2624 ft) and 100 m (328 ft), respectively. The array resolution depth limit ( $d_{res} = \lambda^*_{res}/2$ ) is shown at 259 m (850 ft). The range of dispersion misfit values for the 100 lowest misfit and median profiles are indicated in brackets in the legend.

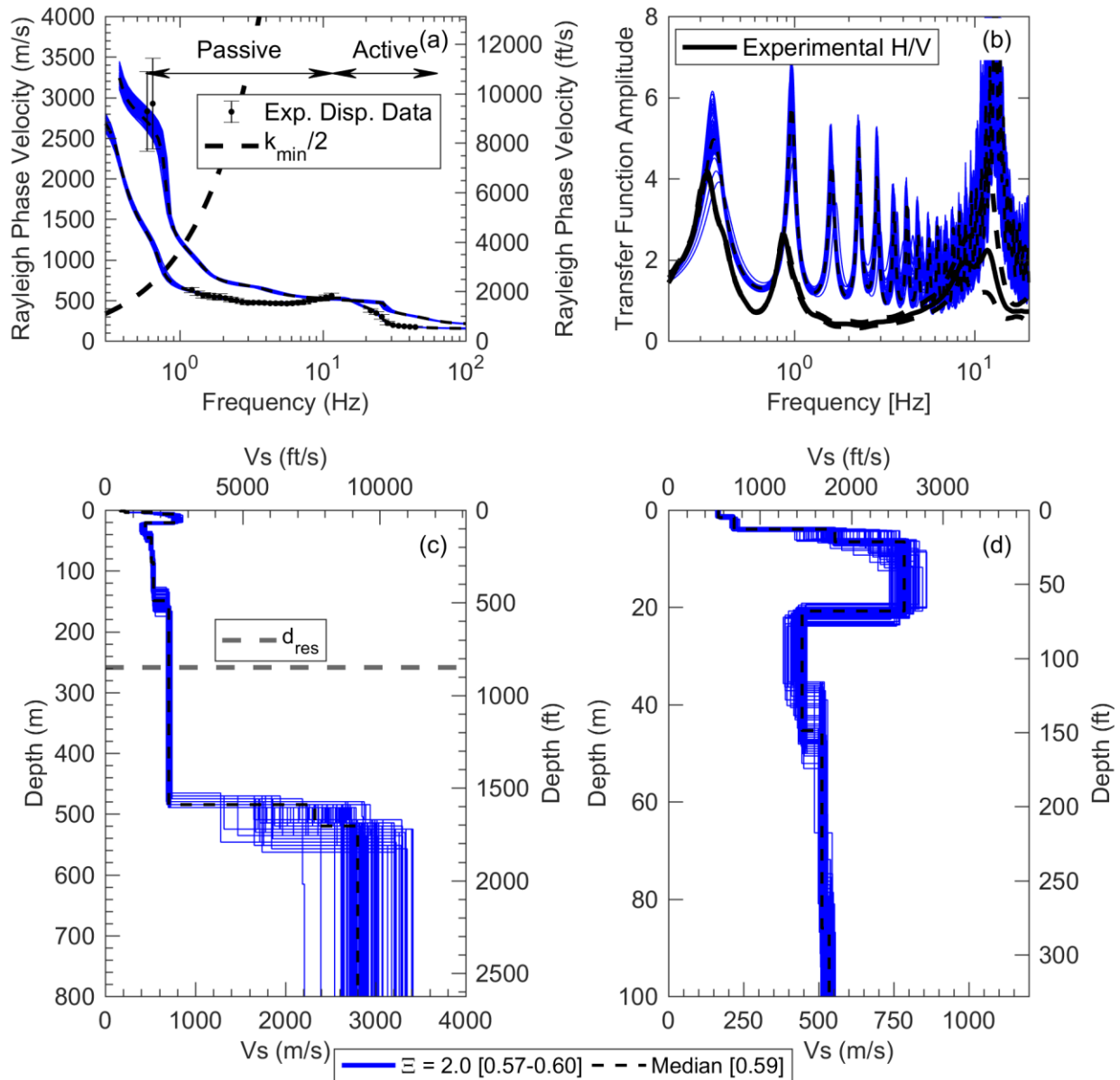


**Figure C2:** “Blind” inversion results for a *layering ratio* ( $\Xi$ ) of 2.0 based on a fundamental and 1st-higher mode interpretation/inversion of the experimental Rayleigh and Love wave dispersion data acquired at Site B. Shown are the 100 lowest misfit and median: (a) theoretical fundamental and 1st-higher Rayleigh wave dispersion curves along with the experimental dispersion data; (b) theoretical shear wave transfer functions with the lognormal median and +/- one standard deviation experimental H/V curve; and (c and d) Vs profiles shown to depths of 800 m (2624 ft) and 100 m (328 ft), respectively. The array resolution depth limit ( $d_{res} = \lambda^*_{res}/2$ ) is shown at 259 m (850 ft). The range of dispersion misfit values for the 100 lowest misfit and median profiles are indicated in brackets in the legend.

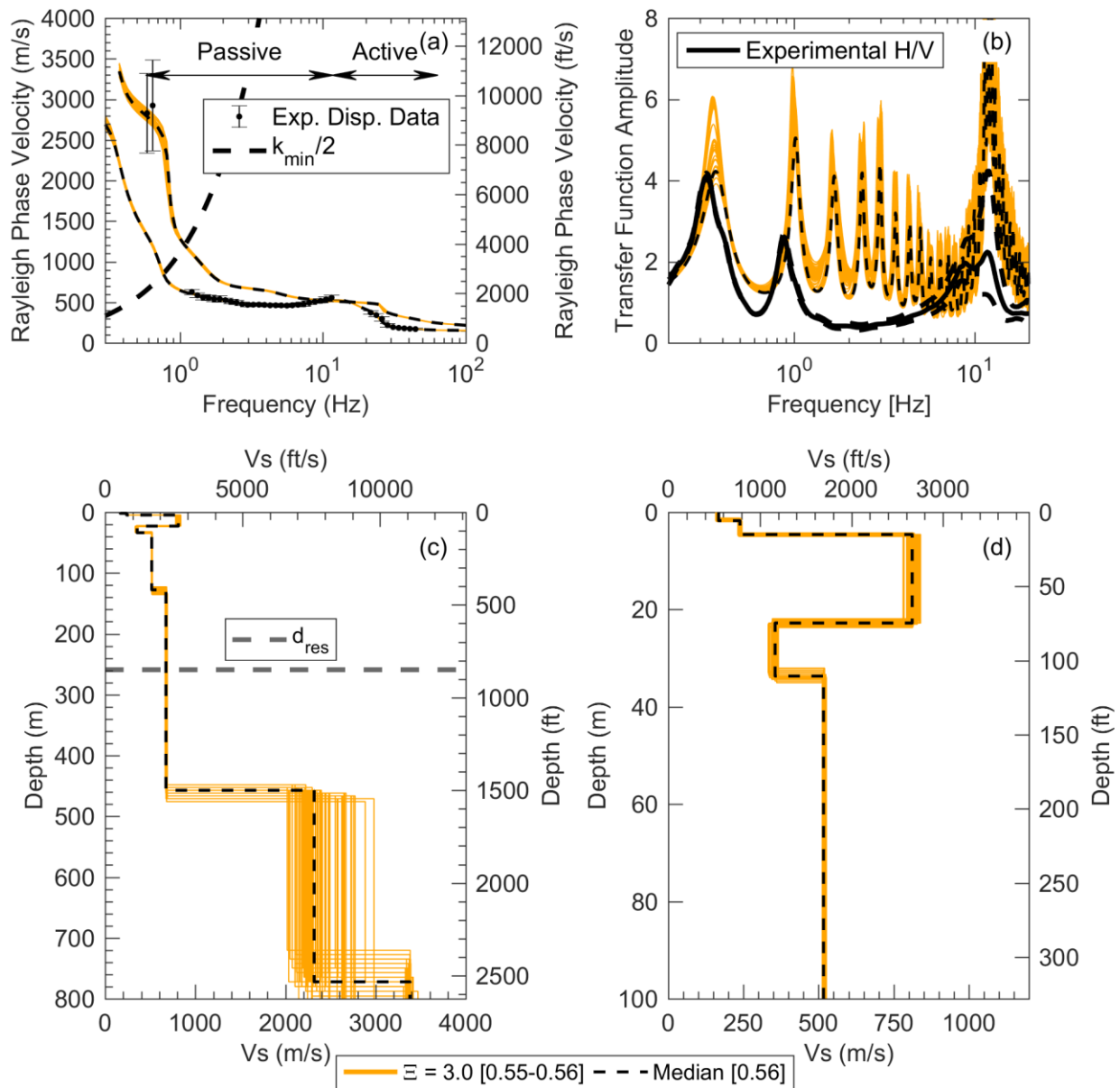


**Figure C3:** “Blind” inversion results for a layering ratio ( $\Xi$ ) of 3.0 based on a fundamental and 1st-higher mode interpretation/inversion of the experimental Rayleigh and Love wave dispersion data acquired at Site B. Shown are the 100 lowest misfit and median: (a) theoretical fundamental and 1st-higher Rayleigh wave dispersion curves along with the experimental dispersion data; (b) theoretical shear wave transfer functions with the lognormal median and +/- one standard deviation experimental H/V curve; and (c and d) Vs profiles shown to depths of 800 m (2624 ft) and 100 m (328 ft), respectively. The array resolution depth limit ( $d_{res} = \lambda^*_{res}/2$ ) is shown at 259 m (850 ft). The range of dispersion misfit values for the 100 lowest misfit and median profiles are indicated in brackets in the legend.

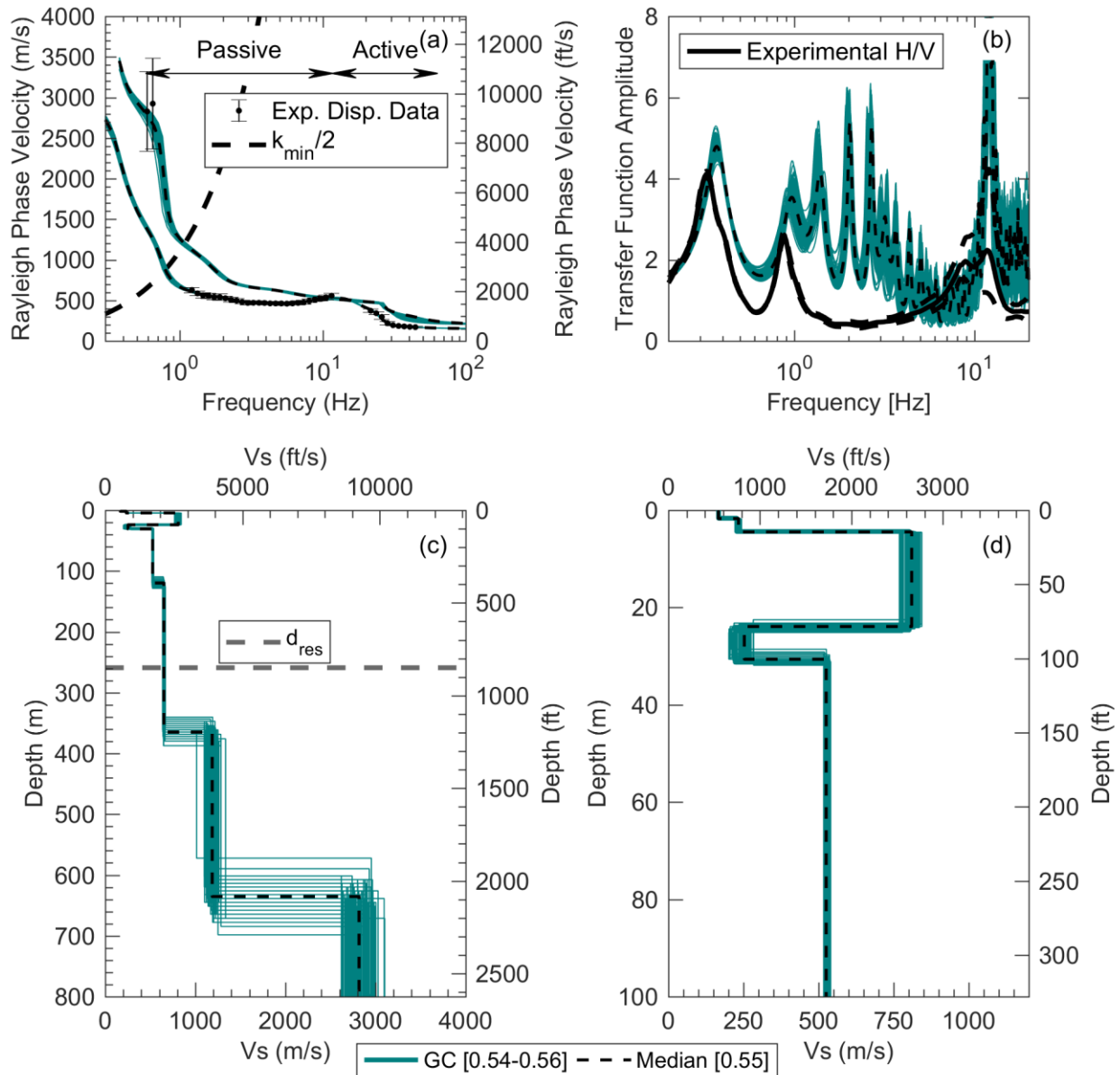


**Figure C4:** “Blind” inversion results for layering based on anticipated geologic conditions (i.e. GC) based on a fundamental and 1st-higher mode interpretation/inversion of the experimental Rayleigh and Love wave dispersion data acquired at Site B. Shown are the 100 lowest misfit and median: (a) theoretical fundamental and 1st-higher Rayleigh wave dispersion curves along with the experimental dispersion data; (b) theoretical shear wave transfer functions with the lognormal median and +/- one standard deviation experimental H/V curve; and (c and d) Vs profiles shown to depths of 800 m (2624 ft) and 100 m (328 ft), respectively. The array resolution depth limit ( $d_{res} = \lambda_{res}^*/2$ ) is shown at 259 m (850 ft). The range of dispersion misfit values for the 100 lowest misfit and median profiles are indicated in brackets in the legend.

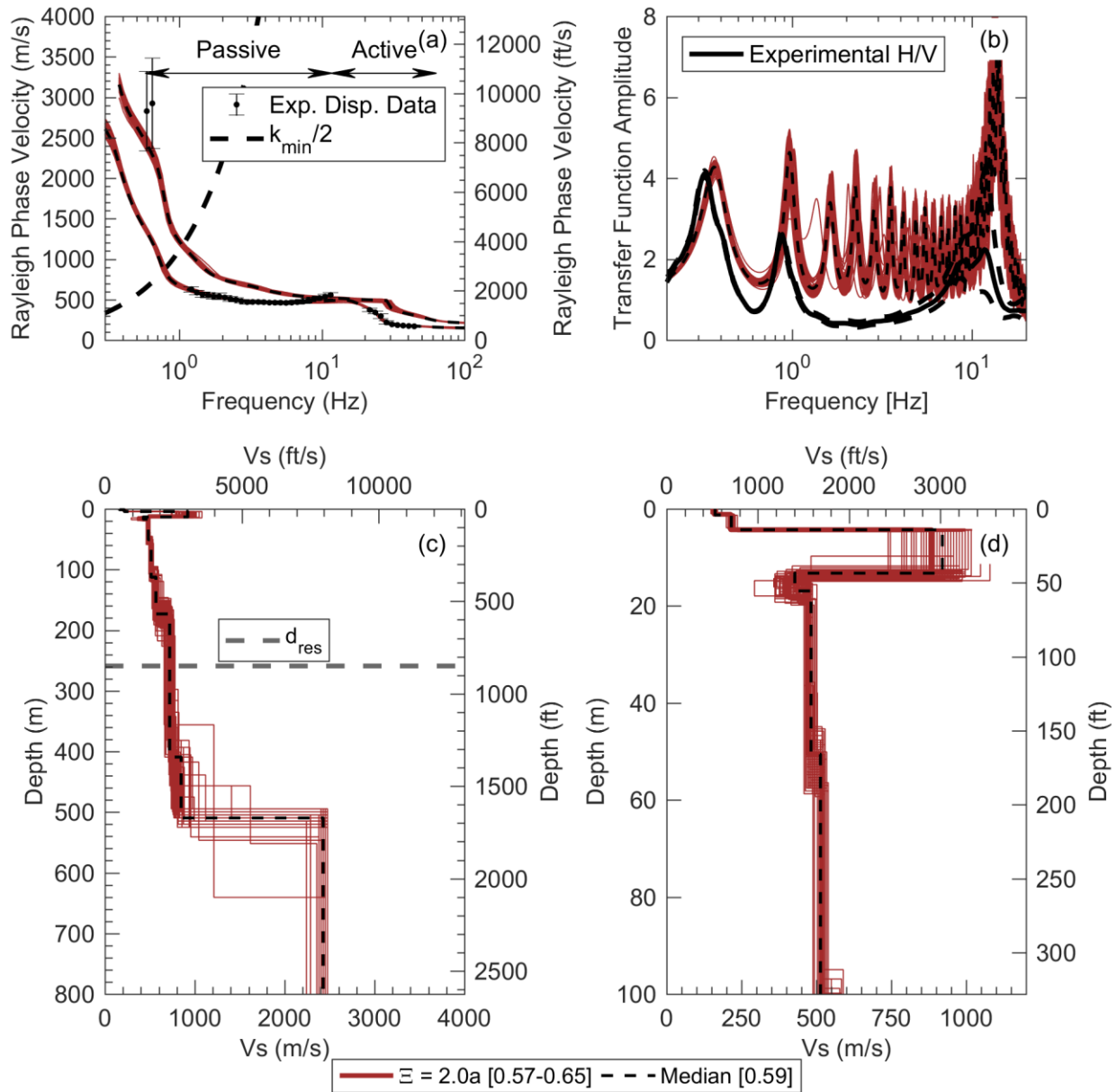


**Figure C5:** “Informed” inversion results for inversion parameterization  $2.0a$ , based on a fundamental and 1st-higher mode interpretation/inversion of the experimental Rayleigh and Love wave dispersion data acquired at Site B. Shown are the 100 lowest misfit and median: (a) theoretical fundamental and 1st-higher Rayleigh wave dispersion curves along with the experimental dispersion data; (b) theoretical shear wave transfer functions with the lognormal median and  $\pm$  one standard deviation experimental H/V curve; and (c and d) Vs profiles shown to depths of 800 m (2624 ft) and 100 m (328 ft), respectively. The array resolution depth limit ( $d_{res} = \lambda_{res}^*/2$ ) is shown at 259 m (850 ft). The range of dispersion misfit values for the 100 lowest misfit and median profiles are indicated in brackets in the legend.

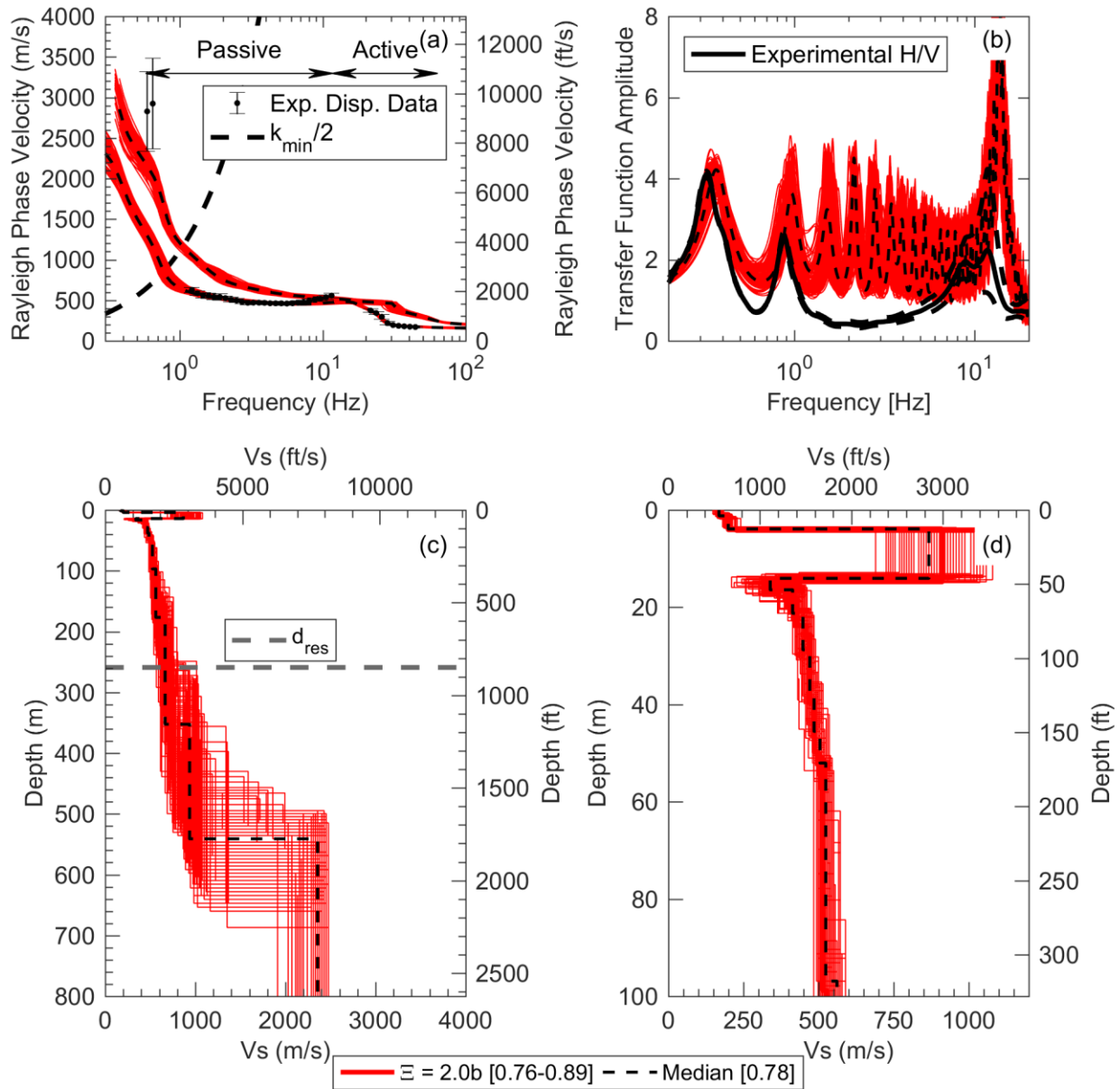


**Figure C6:** “Informed” inversion results for inversion parameterization  $2.0b$ , based on a fundamental and 1st-higher mode interpretation/inversion of the experimental Rayleigh and Love wave dispersion data acquired at Site B. Shown are the 100 lowest misfit and median: (a) theoretical fundamental and 1<sup>st</sup>-higher Rayleigh wave dispersion curves along with the experimental dispersion data; (b) theoretical shear wave transfer functions with the lognormal median and +/- one standard deviation experimental H/V curve; and (c and d) Vs profiles shown to depths of 800 m (2624 ft) and 100 m (328 ft), respectively. The array resolution depth limit ( $d_{res} = \lambda_{res}^*/2$ ) is shown at 259 m (850 ft). The range of dispersion misfit values for the 100 lowest misfit and median profiles are indicated in brackets in the legend.

**Table C3:** “Blind” median Vs profile and corresponding dispersion misfit value for a layering ratio of 1.5, with the approximate array resolution depth ( $d_{res} = \lambda^*_{res}/2$ ) limit indicated with a dashed black line.

Dispersion Misfit: 0.60			
Bottom Depth		Vs	
[m]	[ft]	[m/s]	[ft/s]
1.7	5.5	167.7	550.3
4.3	14.1	233.0	764.5
5.4	17.7	635.9	2086.2
10.5	34.5	733.6	2406.7
23.9	78.5	826.2	2710.7
29.4	96.4	257.4	844.5
57.7	189.2	500.7	1642.7
90.2	295.9	526.1	1726.1
107.7	353.2	564.1	1850.8
157.3	516.0	597.2	1959.3
265.5	871.1	627.1	2057.4
355.6	1166.7	798.7	2620.3
568.4	1864.9	1026.5	3367.8
800.0	2624.7	2117.3	6946.4

**Table C4:** “Blind” median Vs profile and corresponding dispersion misfit value for a layering ratio of 2.0, with the approximate array resolution depth ( $d_{res} = \lambda^*_{res}/2$ ) limit indicated with a dashed black line.

Dispersion Misfit: 0.59			
Bottom Depth		Vs	
[m]	[ft]	[m/s]	[ft/s]
1.5	5.0	166.6	546.4
3.9	12.9	218.8	717.9
6.5	21.4	554.5	1819.2
20.8	68.1	785.2	2576.0
45.3	148.7	444.9	1459.7
86.0	282.1	511.1	1676.8
149.1	489.2	535.0	1755.3
484.6	1589.9	705.0	2313.0
519.8	1705.5	2326.2	7632.0
800.0	2624.7	2801.5	9191.3

**Table C5:** “Blind” median Vs profile and corresponding dispersion misfit value for a layering ratio of 3.0, with the approximate array resolution depth ( $d_{res} = \lambda^*_{res}/2$ ) limit indicated with a dashed black line.

Dispersion Misfit: 0.56			
Bottom Depth		Vs	
[m]	[ft]	[m/s]	[ft/s]
1.7	5.7	167.2	548.6
4.6	15.0	238.4	782.3
22.8	74.7	811.5	2662.4
33.7	110.5	355.3	1165.8
127.6	418.5	516.3	1694.0
457.2	1499.9	674.7	2213.4
772.1	2533.2	2318.1	7605.4
800.0	2624.7	3380.0	11089.3

**Table C6:** “Blind” median Vs profile and corresponding dispersion misfit value for layering based on anticipated geologic conditions CG, with the approximate array resolution depth ( $d_{res} = \lambda^*_{res}/2$ ) limit indicated with a dashed black line.

Dispersion Misfit: 0.55			
Bottom Depth		Vs	
[m]	[ft]	[m/s]	[ft/s]
1.7	5.6	166.4	545.9
4.5	14.6	233.3	765.3
23.9	78.4	809.9	2657.1
30.6	100.5	252.7	829.1
119.7	392.8	525.2	1723.2
364.8	1196.9	650.3	2133.4
635.3	2084.5	1186.7	3893.3
800.0	2624.7	2816.4	9240.3

**Table C7:** “Informed” median Vs profile and corresponding dispersion misfit value for inversion parameterization 2.0a, with the approximate array resolution depth ( $d_{res} = \lambda^*_{res}/2$ ) limit indicated with a dashed black line.

Dispersion Misfit: 0.59			
Bottom Depth		Vs	
[m]	[ft]	[m/s]	[ft/s]
1.3	4.1	161.7	530.6
4.3	14.1	215.8	708.2
13.2	43.5	920.5	3020.1
16.9	55.5	427.9	1403.7
50.6	165.9	482.1	1581.7
112.5	369.0	513.4	1684.5
173.1	568.0	566.6	1859.1
409.2	1342.5	719.5	2360.5
509.6	1671.9	847.2	2779.6
800.0	2624.7	2428.1	7966.3

**Table C8:** “Informed” median Vs profile and corresponding dispersion misfit value for inversion parameterization 2.0b, with the approximate array resolution depth ( $d_{res} = \lambda^*_{res}/2$ ) limit indicated with a dashed black line.

Dispersion Misfit: 0.78			
Bottom Depth		Vs	
[m]	[ft]	[m/s]	[ft/s]
1.2	3.9	168.3	552.2
3.9	12.8	199.3	654.0
14.0	46.1	867.2	2845.1
16.4	53.8	338.9	1111.9
21.2	69.7	413.5	1356.7
28.7	94.3	447.8	1469.1
37.9	124.3	470.6	1544.0
45.5	149.4	484.9	1590.8
52.0	170.7	504.6	1655.4
96.9	317.9	523.7	1718.3
176.6	579.4	561.0	1840.7
352.5	1156.3	664.4	2179.9
540.9	1774.7	935.9	3070.4
800.0	2624.7	2356.7	7732.0

## Appendix C: FWS Logging Results

---

# **Shear wave Velocities Derived From Full Wave Sonic Tool in Borehole WIL-358**

## **Summary Report**

**for**

**Inthuorn Sasanakul, Ph.D., P.E.  
Department of Civil and Environmental Engineering  
University of South Carolina**

**by**

**Michael Waddell<sup>1</sup>, and Scott Howard<sup>2</sup>**

- 1) Retired Associate Research Professor,  
University of South Carolina**
- 2) South Carolina Department of Natural Resources -  
Geological Survey**

**October 13, 2017**

## **Introduction**

One aspect of this project is to look at alternative methods for determining in situ shear wave velocities to the current standard P-wave and S-wave suspension logging technique. We proposed using a Full Waveform Sonic (FWS) tool as an alternative method for determining in situ S-wave velocities. If this FWS method proved to be a reliable method for obtaining s-wave velocities, it could reduce the cost in obtaining s-wave data for earthquake modeling.

The initial scope of work was to log two boreholes, one near Conway, S.C. and the second one near Andrews, S.C. Due drilling problems and poor hole conditions we were not able to log the borehole at Conway, but we were able to log the 610 feet borehole at Andrews (WIL-358, SCDNR Well Identifier).

## **Methodology**

The Full Waveform Sonic (FWS) tool is used extensively in the petroleum industry, groundwater, mining, and geotechnical industries to determine in situ P-wave and S-wave velocities. Sonic logs are widely employed, often in combination with other logs, to provide porosity, permeability, and geo-mechanical properties. This probe is ideal in open-hole applications, such as for fracture identification, determining shear-wave velocities, and cement-bond logging (case hole).

The 2SAA-1000-FWS (Mt. Sopris) probe (Figure 1) uses a high-energy source wave that is generated by a ceramic piezoelectric transducer to excite the adjacent formation. Waves of different frequencies are developed and propagated within the formation, allowing for real-time analysis of the full waveform by WellCAD® software. Under suitable borehole conditions, Compressional (P), Shear (S), Stoneley, and Tube wave arrivals can be detected.

The FWS sonic probe must be used in a fluid-filled hole and consists of one transmitter and three to four receivers (Figure 1). In an open hole the probe generates and receives four types of waves: compression wave (P-wave), shear wave (s-wave), pseudo-

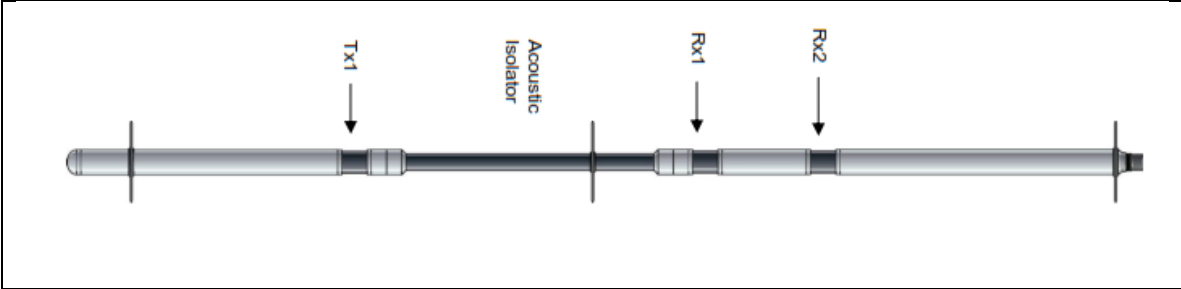


Figure 1. Schematic of the 2SAA-1000-FWS full wave sonic tool. The piezoelectric transmitter is label TX1. In the diagram above there are only two receivers (RX1, RX2). Model used to log WIL 358 borehole has three receivers. An acoustic rubber isolator that separates the transmitted signal from the arriving signals separates the receivers.

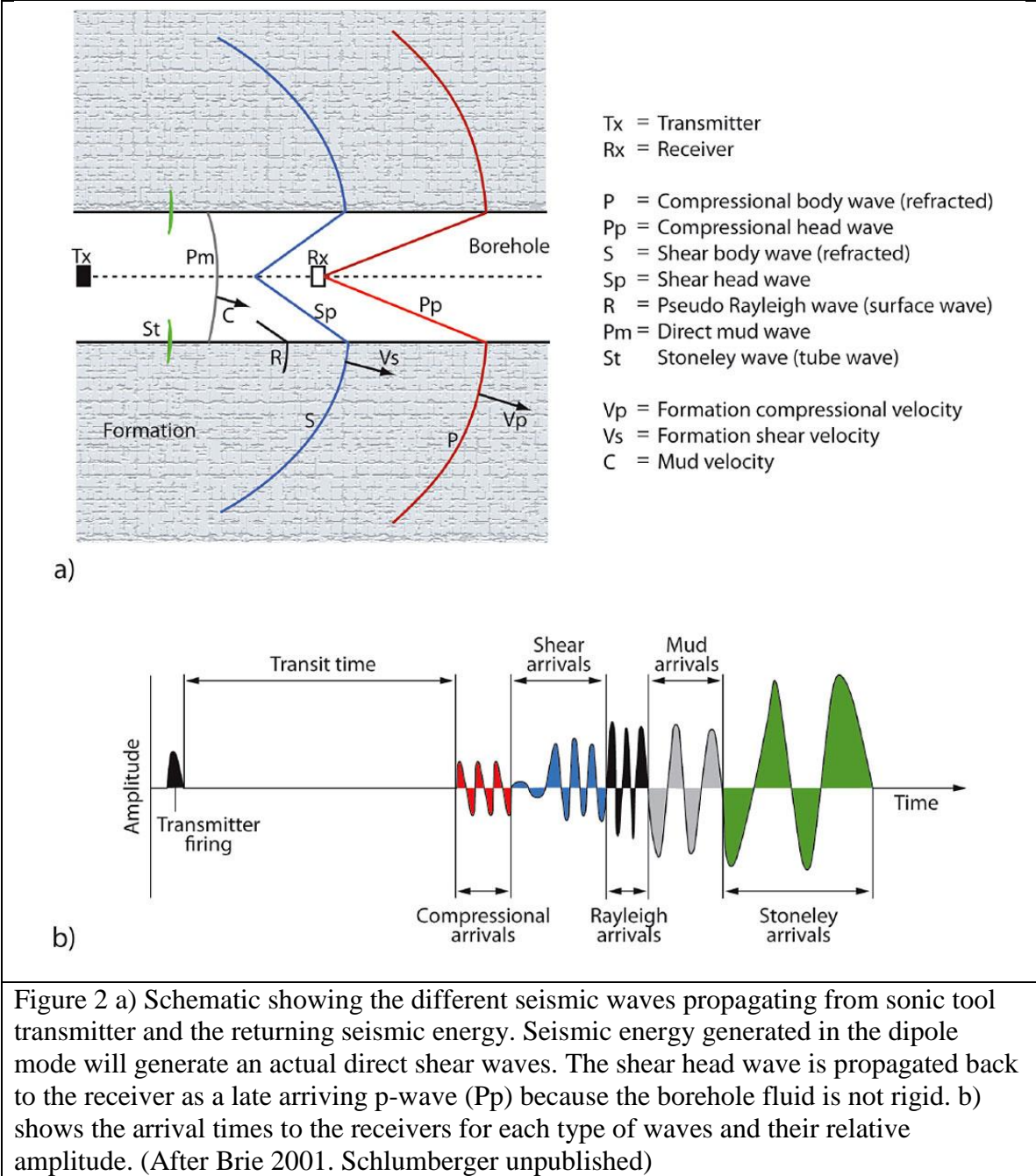
Rayleigh wave, and Stoneley wave (Figure 2). The Stoneley wave is generated at the fluid-solid interface, which in this case would be the borehole mud interacting with the side of the borehole. The pseudo-Rayleigh wave is generally only produced in a fast shear-wave environment. A fast shear-wave environment is when the shear-wave velocity is faster than the mud velocity, and it is generated with a monopole source. There are basically two modes for collecting sonic data in a borehole. The first mode is monopole and the second is dipole. Monopole (axisymmetric) transducers generate omnidirectional acoustic waves around the tool circumference, while dipole (nonaxisymmetric) transducers generate azimuthally oriented acoustic waves (Figure 3).

Two types of borehole shear waves can be produced during data acquisition, direct (refracted) and indirect (induced). Monopole mode generates indirect shear waves, which result when some of the converted compressional energy is transferred from the borehole fluid into the rock formation. Direct shears wave are produced using dipole transmitters that generate shear waves by inducing a flexural wave (asymmetric mode) in the borehole. The flexural mode is similar to shaking a rope causing a sine wave to be produced assuming both ends of the rope at attached to a fix object. The flexural waves travel along the borehole in the plane of the dipole source that generated it. The particle motion of the flexural wave is perpendicular to the direction of propagation similar to an s-wave, and flexural wave slowness is related to s-wave slowness. Flexural waves are dispersive meaning their slowness varies with frequency. However, shear waves cannot propagate through liquids but only through solids that have a shear modulus (rigidity). Therefore in liquids, shear head-wave generated along the borehole is converted into a compressional head wave and propagated back across the borehole fluid to the acoustic receivers as a later-arriving compressional wave (Figure 2a) (Haldorsen et al., 2006).

Sonic probes do not record direct p-wave and s-wave velocities but instead record p- and s-wave slowness (Equation 1; Crain, 2000). Slowness (s) is defined as: the reciprocal of velocity

$$(1) \quad s = 1/\text{Velocity}$$

(Slowness  $\mu\text{s}/\text{ft}$  or  $\mu\text{s}/\text{m}$  )



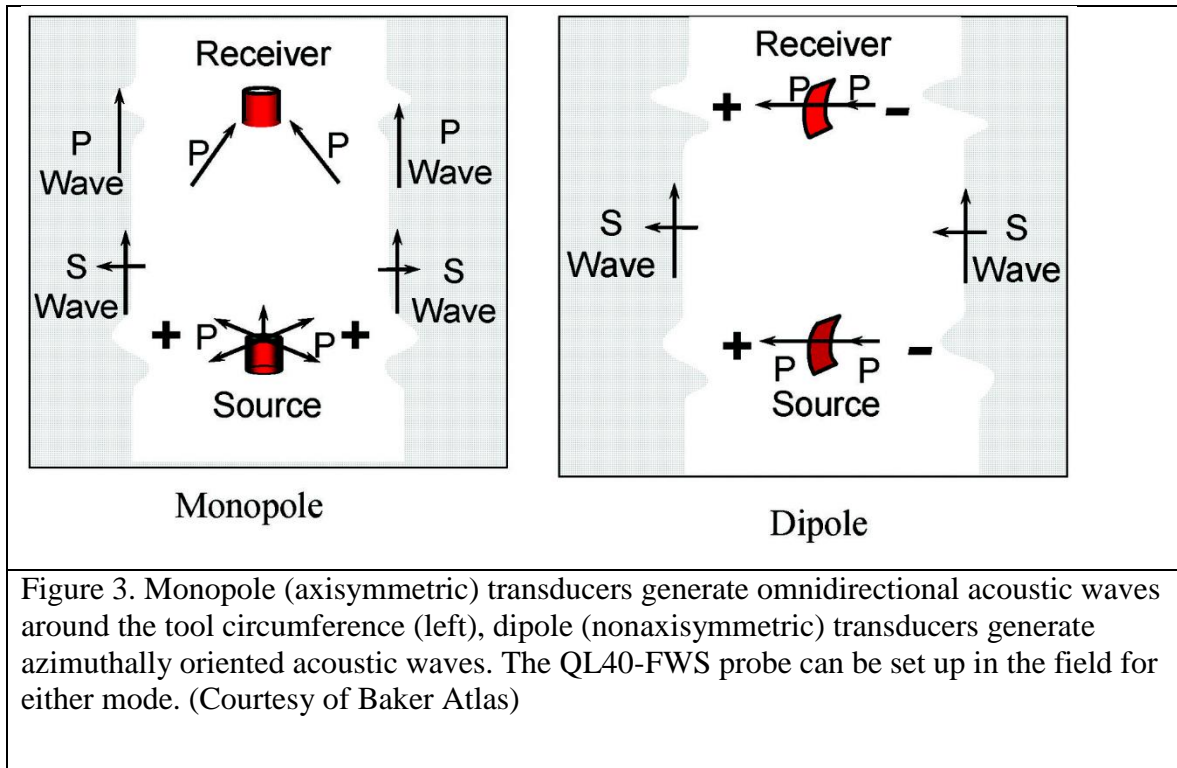


Figure 3. Monopole (axisymmetric) transducers generate omnidirectional acoustic waves around the tool circumference (left), dipole (nonaxisymmetric) transducers generate azimuthally oriented acoustic waves. The QL40-FWS probe can be set up in the field for either mode. (Courtesy of Baker Atlas)

## **Data Acquisition**

The Mount Sopris 2SAA-1000/F-FWS probe used to acquire the shear wave data in WIL-358 consisted of two transmitters and three receivers. The vertical sample interval was every 0.5 feet and the logging rate was 10 feet/minute. During acquisition, the incoming waveforms from each receiver at each sample interval were monitored (Figure 4) for data consistency. The logging rate and cable tension also were constantly monitored to also maintain data quality on the incoming signals and to alert the operator if there was a problem with the tool.

## **Data Analysis**

A typical workflow for determining p- and s-wave slowness from sonic data is semblance analysis. Semblance is a measure of multi-receiver coherence for only the arriving p- and s- waves. At each depth there are three wavelets produced, one wavelet per receiver (Figure 5). The next step is to determine the first break of the p-wave or the s-wave. A theoretical line drawn starting at the transmitter (time zero, T0) thru each of the corresponding first breaks for each receiver (Figure 5). The first breaks are either p-wave or s-wave. The slope of the theoretical line is equal to slowness in either feet/microseconds or meters/microseconds. The Process Semblance algorithm creates a fan of lines with different slopes. Each line has its origin at the transmitter position at time zero. The slope of each line can be expressed as the ratio of time and distance given in ( $\mu\text{s}/\text{m}$ ) or ( $\mu\text{s}/\text{ft}$ ). Along each of these lines a coherence value is calculated using the sonic signal amplitudes found at the intersection of fitted line and data trace. The Semblance is computed in order to get a value for the coherence of the signals.

A typical semblance plot (Figure 6) shows a series of dark solid vertical lines. In the Velocity Analysis Result (middle diagram), the first vertical dark band is the p-wave slowness in microseconds per foot (blue line) and the second vertical dark band is the s-wave slowness in microseconds per foot (red line). The two color lines are the slowness picks for the p-wave and s-wave at each sample point. To the right (Figure 6) are the p-wave and s-wave velocities derived from the following Equation 2:

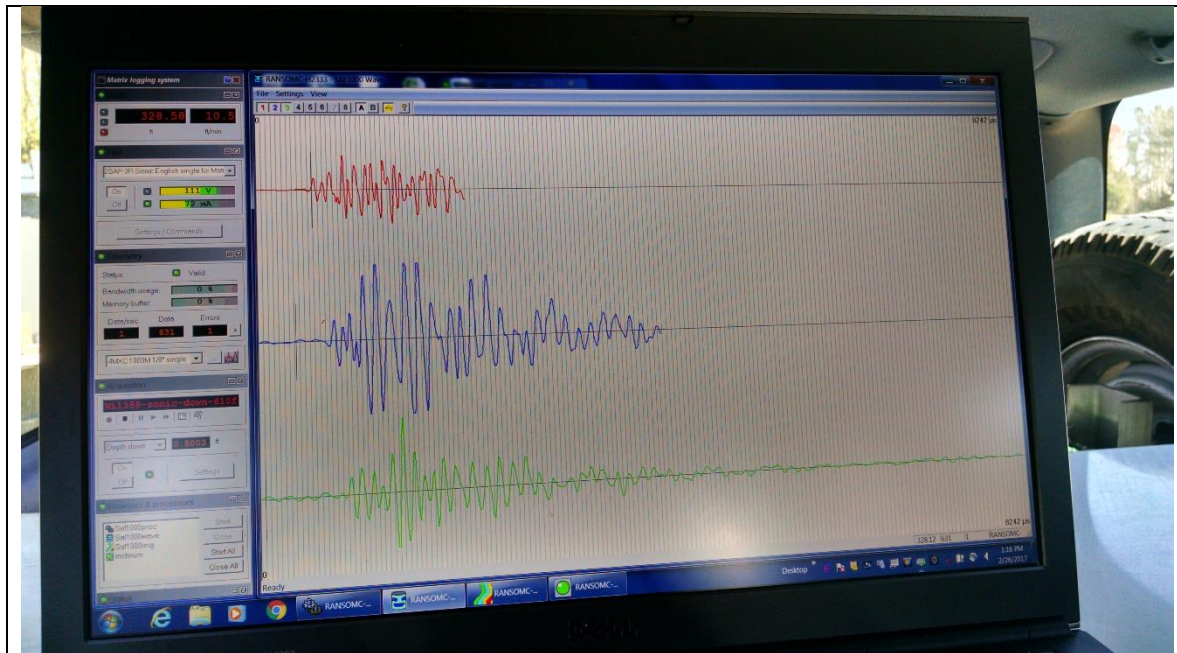


Figure 4. Screen shot of arriving waveforms during data acquisition in borehole WIL-358. The red wave is receiver one, blue receiver two and green receiver three.

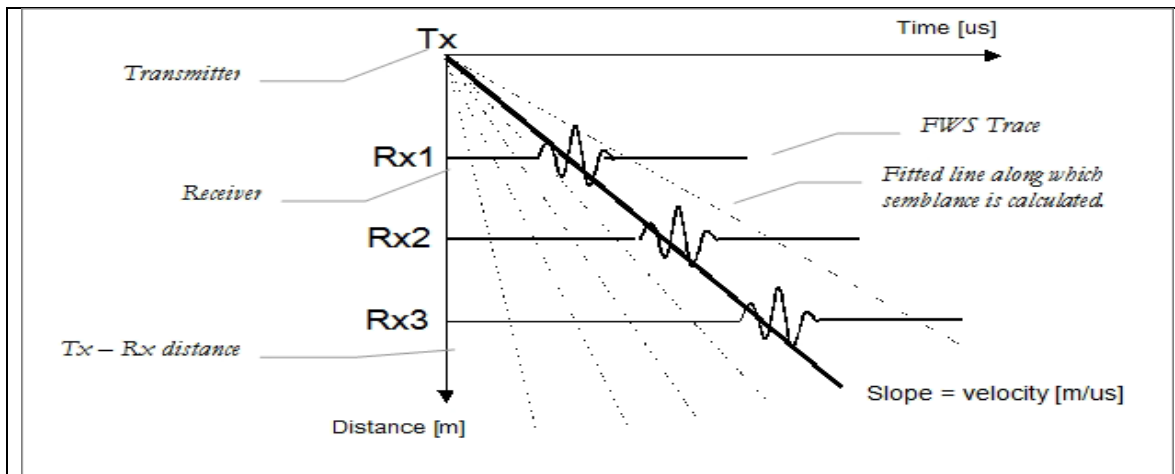


Figure 5. Diagram illustrating the semblance analysis. The transmitter (Tx) is time zero. Rx1 - 3 are the receivers with the arriving wavelets. The solid line is the first break pick of the first arrival. The semblance algorithm generates the dotted lines. A coherence value is generated at the intersection of the fitted line (dotted) and the data trace first break. (2009 Mount Sopris)

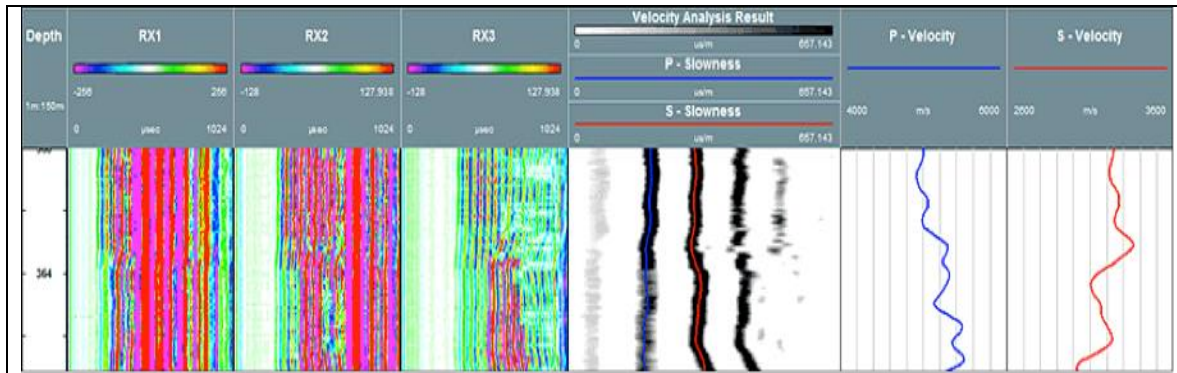


Figure 6. This figure is a typical analysis plot. On the left are the wavelets (color density plots) for each receiver. The middle is the semblance plot under ideal conditions. The darker bands indicate a high correlation of the signal amplitudes at certain slowness values. The first dark vertical band on the left (blue line) is the p-wave slowness (microseconds per foot) and the second dark vertical band (red line) is the s-wave slowness (microseconds per foot). The right two plots blue and red are the p-wave velocity and s-wave velocity converted to feet per seconds.

$$(2) \quad \text{Velocity (ft/sec)} = (1/(\text{slowness } \mu\text{s/ft})) * 10^6$$

Figure 7 is the semblance plot for WIL-358. As can be seen in Figure 7 the semblance plot is very noisy from 75 to 390 feet below land surface (bls). Several attempts were made to filter out the noise but were unsuccessful. A different workflow for velocity analysis was used on this data set (personal communication Jim LoCoco, 2016). This workflow uses the auto first-breaks picker to determine the initial s-wave first breaks for receivers RX1A-2 and RX2A-1. Figure 8 is a screen capture of entire wave from receiver RX2A-1 at 98.18 feet bls. The interpretation begins with locating the first arrival of the p-wave and then the first arrival of the s-wave. The next step is to isolate the p-wave portion of the full waveform and blank out the p-wave data (Figure 8, area covered by the hash lines) leaving the s-wave and late arriving Stoneley wave data.

The first breaks derived from the auto picker are used as guides for manual editing. Figure 9 shows the first breaks for the p-wave and s-wave slowness (yellow and blue columns) after the interpreter has manually edited the first breaks for receivers RX1A-1 and RX2A-1. The primary purpose of manually editing the first breaks is to insure that each pick follows the waveform that is the shear wave first break. Using Equation 3 the p- and s-wave velocities can be calculated.

$$(3) \quad ((1/(\text{RX2-1} - \text{RX1-1})) * 10^6$$

## Results

Using Equation 3, p- and s-wave slowness was converted into p- and s-wave velocities. Figures 9 and 10 are graphs showing the s-wave velocity in seconds/foot. Table 1 shows the s-wave velocities verses depth in tabular form and Figure 10 is a graph of Table 1 data. In Table 1 the data from 0 to 55 feet is questionable because of very low signal-to-noise ratio. The velocities calculated in the upper 18 feet are within the surface casing are not valid. In Figure 10, the s-wave velocities appear to be consistent with coastal plain s-wave velocities obtained from vertical seismic profiles at Savannah River

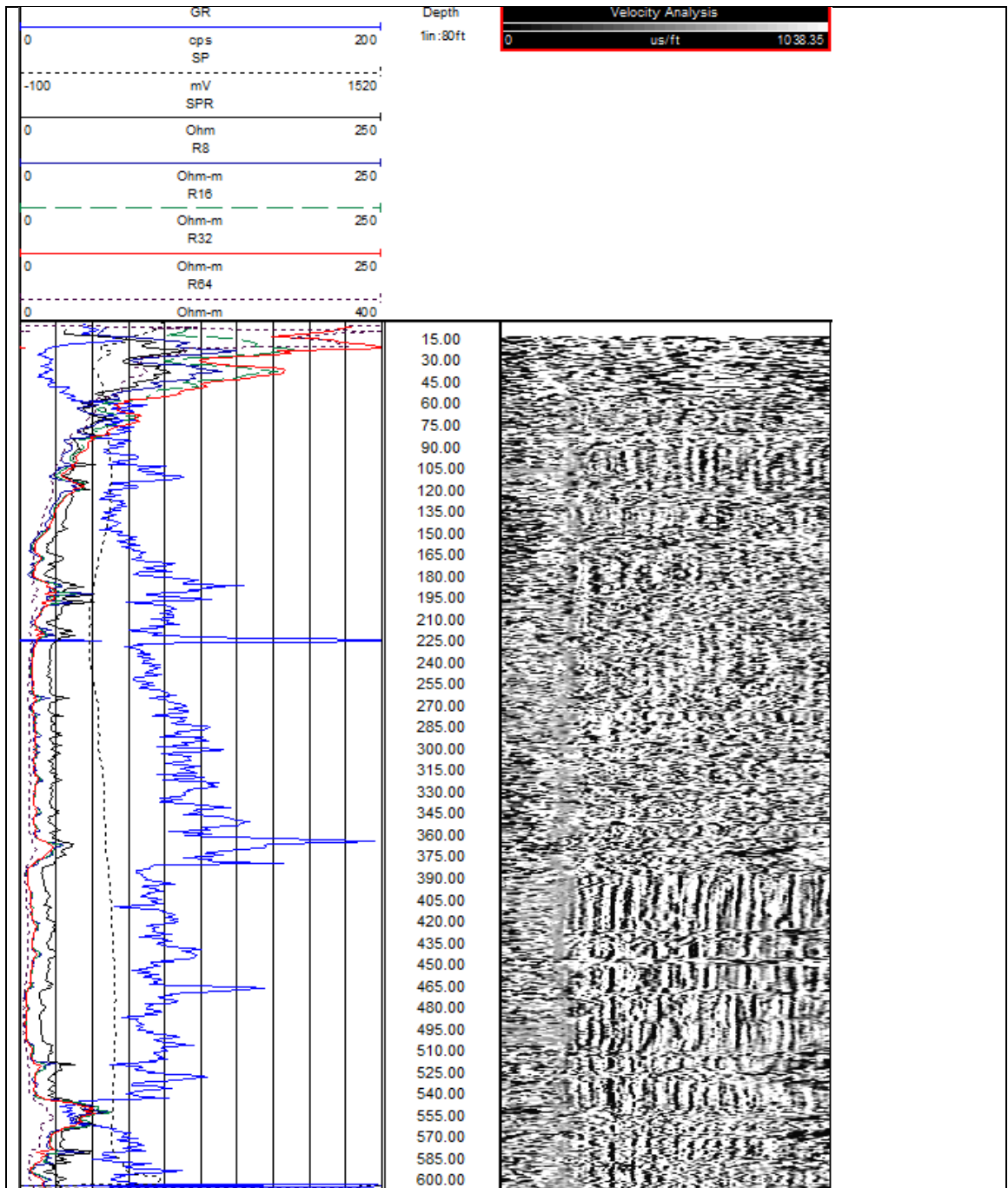


Figure 7. WIL-358 borehole electrical and natural gamma ray logs on the left and semblance plot on the right. On the semblance plot usable data starts at approximately 75 feet below land surface (bls). The data quality from 75 to 390 feet bls is poor.

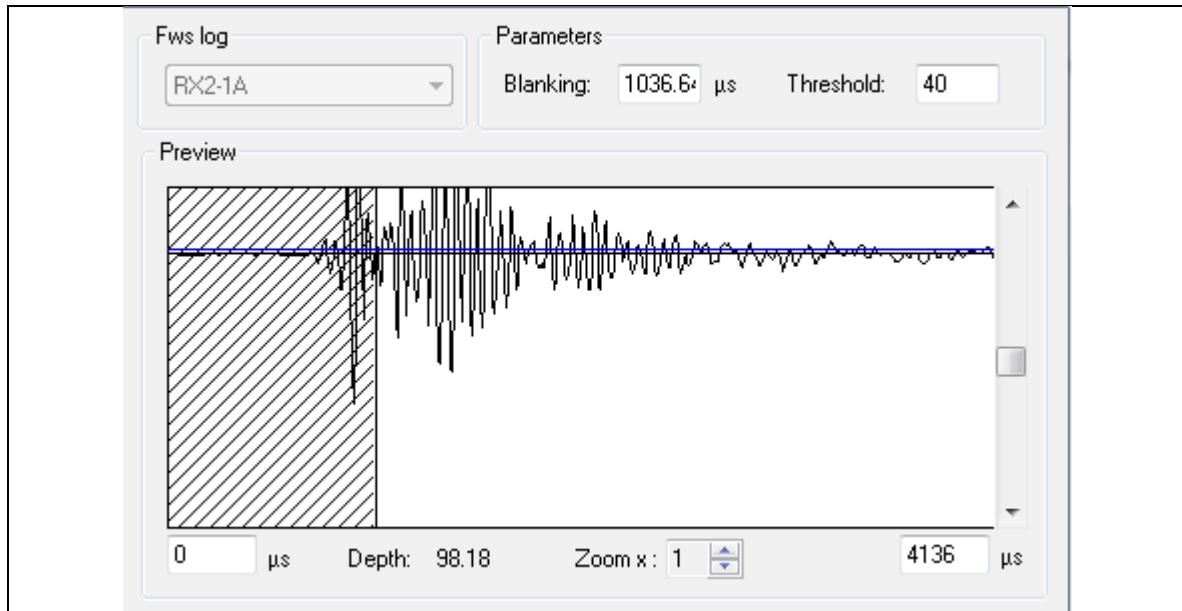


Figure 8. An entire wave from a depth of 98.18 ft. This wave form contains p-, s-, and Stoneley waves. The p-wave data have been blanked out (area within the hash lines). The blanking area stops at the first break for the arriving s-wave.

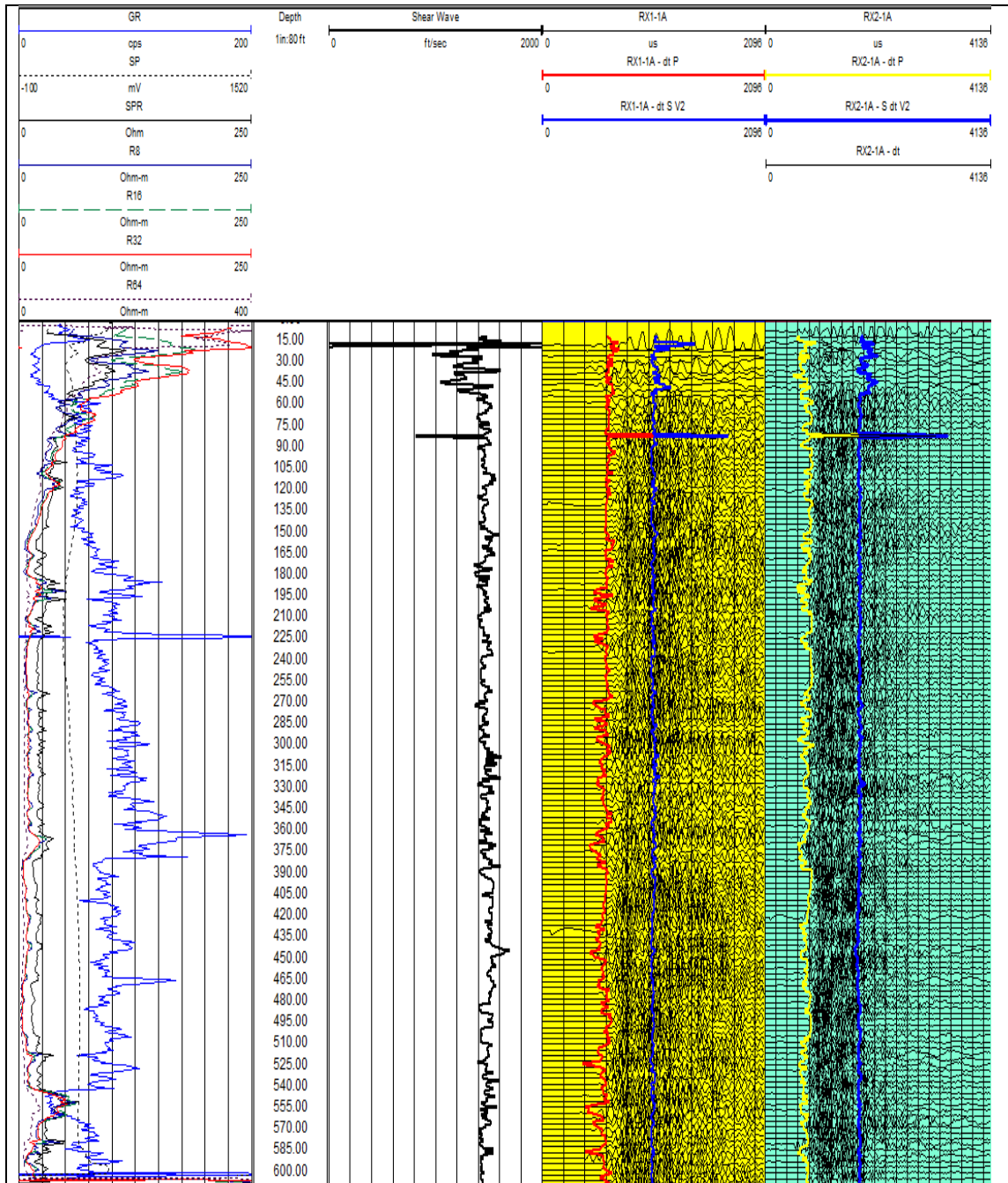


Figure 9. The left panel is electrical logs, natural gamma ray log, spontaneous potential log, which are used for correlating lithology to velocity logs. The next panel is s-wave slowness converted to velocity in ft./sec using equation 3. The yellow panel is the full waveform for receiver RX1A-1. The red line is first breaks for p-wave and the blue is first breaks for s-wave. The green panel is the full waveform for receiver RX-2A-1. The yellow line is the p-wave first breaks and the blue line is the s-wave first breaks.

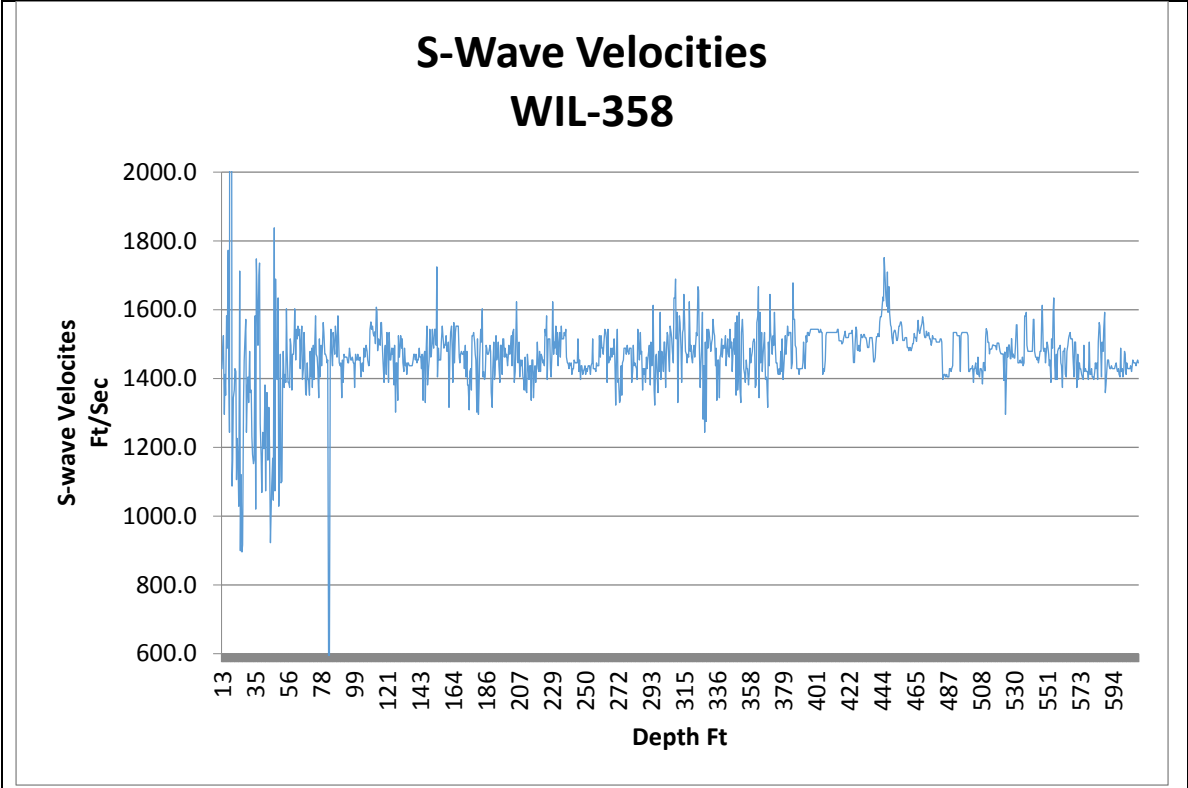


Figure 10. Graphical presentation of s-wave velocities from Table 1.

Site by the Earth Sciences and Resources Institute, University of South Carolina (Waddell and Domoracki, 2002). The perturbations in velocities appear to be related to variations in the geology. The natural gamma log (Figure 9 blue curve left panel) indicates the geology varies with depth. The shear-wave velocities will vary with variation in the degree of compaction of the sediments. This variation in compaction can be observed on the gamma log. Generally, lower gamma counts per second define more consolidated sediments. An exception can be clay, which tends naturally to have higher gamma counts per seconds (kaolinite being an exception).

### **Conclusions**

1. The shear-wave velocities derived from the Full-Wave Sonic tool appear to be consistent with velocities obtained from vertical seismic profiles conducted in the coastal plain.
2. More research needs to be done to understand why the low signal-to-noise ratio was present in the upper 55 feet. Is the low signal-to-noise ratio site specific, or is it characteristic of the shallow clastic sediments in the coastal plain?
3. It appears that the shear wave data quality increases as the clastic sediments become consolidated.
4. To determine if the Full-Wave Sonic data is truly reliable, more wells need to be logged in the upper, middle, and low coastal plain.

### **Recommendations**

1. If the FWS data from well WIL-358 is consistent with the suspension log data this could reduce the cost of obtaining shear-wave velocities.
2. There will have to be an agreement between SCDOT and SCDHEC so that the FWS tool could be used on SCDOT projects.

## **Acknowledgments**

I would thank South Carolina Department of Health and Environmental Control (SCDHEC) for allowing the use of their FWS tool and logging truck. I would also like to thank Camille Ransom at SCDHEC who operated the logging truck and provided insight in the use of the FWS tool.

## **References Cited**

Brie, 2001, Schlumberger Unpublished Report

Crain, 2000, Petrophysical Handbook, [www.spec2000.net](http://www.spec2000.net)

Haldorsen, J.B.U., Johnson, D.L., Sinha, B., Valero, H-P, and Winkler, K., 2006, Borehole Acoustic Waves, Oilfield Review, Spring 2006.

2009, Mount Sopris Instruments 2SAA-1000/F Sonic Probe Manuel, Mount Sopris Instruments, Co., Inc, Golden, CO.

1993, WellCad Software, Advance Logic Technology, Zoning de Solupla BÂT A route de Niederpallen ,L-8506 Redange, Luxembourg.

Waddell, M.G., and Domoracki, W., 2002, Non-Invasive Determination of the Location and Distribution of Free-Phase Dense Nonaqueous Phase Liquids (DNAPL) by Seismic Reflection Techniques, Final Report: Tasks 4, 5, and 6, Earth Sciences and Resources Institute, University of South Carolina, DOE Award Number DE-AR26-98FT40369.

Table 1  
Shear Wave Velocity

Depth (ft)	Velocity (ft/sec)
13.41	1428.6
13.91	1488.1
14.41	1524.4
14.91	1295.3
15.41	1412.4
15.91	1351.4
16.41	1582.3
16.91	1488.1
17.41	1773
17.91	1420.5
18.41	1243.8
18.91	6578.9
19.41	3846.2
19.91	1087
20.42	1162.8
20.92	1344.1
21.42	1366.1
21.92	1428.6
22.42	1420.5
22.92	1106.2
23.42	1225.5
23.92	1146.8
24.42	1028.8
24.92	1712.3
25.42	899.3
25.92	1121.1
26.42	896.1
26.92	915.8
27.42	1336.9
27.92	1453.5
28.42	1506
28.92	1572.3
29.42	1243.8
29.92	1373.6
30.42	1404.5
30.92	1329.8
31.42	1479.3

Table 1  
Shear Wave Velocity

Depth (ft)	Velocity (ft/sec)
31.92	1358.7
32.42	1366.1
32.92	1231.5
33.42	1179.2
33.92	1152.1
34.42	1162.8
34.92	1582.3
35.42	1020.4
35.93	1748.3
36.43	1612.9
36.93	1497
37.43	1700.7
37.93	1736.1
38.43	1269
38.93	1173.7
39.43	1068.4
39.93	1243.8
40.43	1231.5
40.93	1196.2
41.43	1381.2
41.93	1073
42.43	1358.7
42.93	1358.7
43.43	1162.8
43.93	1315.8
44.43	1213.6
44.93	922.5
45.43	1008.1
45.93	1087
46.43	1168.2
46.93	1046
47.43	1838.2
47.93	1073
48.43	1689.2
48.93	1412.4
49.43	1396.6
49.93	1634

Table 1  
Shear Wave Velocity

Depth (ft)	Velocity (ft/sec)
50.43	1028.8
50.94	1116.1
51.44	1470.6
51.94	1096.5
52.44	1101.3
52.94	1381.2
53.44	1479.3
53.94	1373.6
54.44	1412.4
54.94	1388.9
55.44	1602.6
55.94	1479.3
56.44	1388.9
56.94	1388.9
57.44	1373.6
57.94	1515.2
58.44	1497
58.94	1366.1
59.44	1470.6
59.94	1470.6
60.44	1515.2
60.94	1602.6
61.44	1453.5
61.94	1543.2
62.44	1515.2
62.94	1552.8
63.44	1524.4
63.94	1543.2
64.44	1428.6
64.94	1497
65.44	1552.8
65.94	1396.6
66.45	1428.6
66.95	1533.7
67.45	1479.3
67.95	1358.7
68.45	1351.4

Table 1  
Shear Wave Velocity

Depth (ft)	Velocity (ft/sec)
68.95	1445.1
69.45	1396.6
69.95	1396.6
70.45	1351.4
70.95	1479.3
71.45	1404.5
71.95	1488.1
72.45	1373.6
72.95	1497
73.45	1396.6
73.95	1515.2
74.45	1582.3
74.95	1470.6
75.45	1462
75.95	1428.6
76.45	1344.1
76.95	1515.2
77.45	1404.5
77.95	1497
78.45	1436.8
78.95	1506
79.45	1562.5
79.95	1533.7
80.45	1470.6
80.95	1470.6
81.46	1462
81.96	1445.1
82.46	1453.5
82.96	490.2
83.46	490.2
83.96	1470.6
84.46	1543.2
84.96	1479.3
85.46	1436.8
85.96	1533.7
86.46	1497
86.96	1470.6

Table 1  
Shear Wave Velocity

Depth (ft)	Velocity (ft/sec)
87.46	1552.8
87.96	1515.2
88.46	1462
88.96	1582.3
89.46	1515.2
89.96	1445.1
90.46	1436.8
90.96	1445.1
91.46	1344.1
91.96	1453.5
92.46	1388.9
92.96	1470.6
93.46	1462
93.96	1462
94.46	1462
94.96	1462
95.46	1445.1
95.96	1445.1
96.46	1488.1
96.97	1470.6
97.47	1453.5
97.97	1453.5
98.47	1462
98.97	1445.1
99.47	1445.1
99.97	1373.6
100.47	1470.6
100.97	1453.5
101.47	1453.5
101.97	1470.6
102.47	1453.5
102.97	1453.5
103.47	1462
103.97	1404.5
104.47	1436.8
104.97	1445.1
105.47	1420.5

Table 1  
Shear Wave Velocity

Depth (ft)	Velocity (ft/sec)
105.97	1488.1
106.47	1462
106.97	1479.3
107.47	1497
107.97	1479.3
108.47	1453.5
108.97	1436.8
109.47	1438.1
109.97	1542.5
110.47	1564.4
110.97	1543.2
111.47	1552.8
111.98	1533.1
112.48	1523.7
112.98	1535.5
113.48	1501.1
113.98	1607.2
114.48	1594.3
114.98	1481
115.48	1515.2
115.98	1506
116.48	1497
116.98	1562.5
117.48	1562.5
117.98	1488.1
118.48	1445.1
118.98	1388.9
119.48	1479.3
119.98	1497
120.48	1412.4
120.98	1533.7
121.48	1488.1
121.98	1388.9
122.48	1533.7
122.98	1453.5
123.48	1453.5
123.98	1488.1

Table 1  
Shear Wave Velocity

Depth (ft)	Velocity (ft/sec)
124.48	1470.6
124.98	1488.1
125.48	1381.2
125.98	1497
126.48	1302.1
126.98	1445.1
127.49	1445.1
127.99	1336.9
128.49	1524.4
128.99	1462
129.49	1488.1
129.99	1524.4
130.49	1488.1
130.99	1515.2
131.49	1445.1
131.99	1420.5
132.49	1488.1
132.99	1436.8
133.49	1445.1
133.99	1412.4
134.49	1445.1
134.99	1445.1
135.49	1436.8
135.99	1436.8
136.49	1436.8
136.99	1436.8
137.49	1436.8
137.99	1453.5
138.49	1470.6
138.99	1470.6
139.49	1453.5
139.99	1470.6
140.49	1445.1
140.99	1453.5
141.49	1453.5
141.99	1488.1
142.5	1462

Table 1  
Shear Wave Velocity

Depth (ft)	Velocity (ft/sec)
143	1462
143.5	1428.6
144	1470.6
144.5	1336.9
145	1462
145.5	1479.3
146	1329.8
146.5	1462
147	1552.8
147.5	1381.2
148	1428.6
148.5	1453.5
149	1543.2
149.5	1462
150	1470.6
150.5	1543.2
151	1506
151.5	1488.1
152	1543.2
152.5	1543.2
153	1497
153.5	1724.1
154	1404.5
154.5	1488.1
155	1453.5
155.5	1453.5
156	1453.5
156.5	1506
157	1552.8
157.5	1524.4
158.01	1488.1
158.51	1497
159.01	1497
159.51	1524.4
160.01	1479.3
160.51	1479.3
161.01	1506

Table 1  
Shear Wave Velocity

Depth (ft)	Velocity (ft/sec)
161.51	1315.8
162.01	1479.3
162.51	1533.7
163.01	1552.8
163.51	1488.1
164.01	1388.9
164.51	1562.5
165.01	1445.1
165.51	1533.7
166.01	1552.8
166.51	1552.8
167.01	1552.8
167.51	1552.8
168.01	1462
168.51	1445.1
169.01	1470.6
169.51	1479.3
170.01	1470.6
170.51	1470.6
171.01	1479.3
171.51	1428.6
172.01	1497
172.51	1404.5
173.02	1479.3
173.52	1381.2
174.02	1381.2
174.52	1308.9
175.02	1420.5
175.52	1428.6
176.02	1366.1
176.52	1524.4
177.02	1524.4
177.52	1533.7
178.02	1506
178.52	1470.6
179.02	1453.5
179.52	1302.1

Table 1  
Shear Wave Velocity

Depth (ft)	Velocity (ft/sec)
180.02	1515.2
180.52	1295.3
181.02	1373.6
181.52	1462
182.02	1543.2
182.52	1506
183.02	1602.6
183.52	1404.5
184.02	1420.5
184.52	1396.6
185.02	1404.5
185.52	1497
186.02	1488.1
186.52	1470.6
187.02	1470.6
187.52	1479.3
188.02	1497
188.53	1479.3
189.03	1358.7
189.53	1315.8
190.03	1428.6
190.53	1506
191.03	1396.6
191.53	1412.4
192.03	1524.4
192.53	1453.5
193.03	1470.6
193.53	1506
194.03	1436.8
194.53	1388.9
195.03	1497
195.53	1497
196.03	1412.4
196.53	1515.2
197.03	1515.2
197.53	1462
198.03	1488.1

Table 1  
Shear Wave Velocity

Depth (ft)	Velocity (ft/sec)
198.53	1462
199.03	1470.6
199.53	1436.8
200.03	1462
200.53	1497
201.03	1470.6
201.53	1488.1
202.03	1524.4
202.53	1436.8
203.03	1533.7
203.54	1543.2
204.04	1388.9
204.54	1420.5
205.04	1524.4
205.54	1623.4
206.04	1453.5
206.54	1445.1
207.04	1506
207.54	1404.5
208.04	1453.5
208.54	1436.8
209.04	1453.5
209.54	1404.5
210.04	1396.6
210.54	1366.1
211.04	1462
211.54	1366.1
212.04	1358.7
212.54	1470.6
213.04	1445.1
213.54	1396.6
214.04	1436.8
214.54	1436.8
215.04	1336.9
215.54	1453.5
216.04	1453.5
216.54	1344.1

Table 1  
Shear Wave Velocity

Depth (ft)	Velocity (ft/sec)
217.04	1420.5
217.54	1436.8
218.04	1388.9
218.54	1436.8
219.05	1506
219.55	1428.6
220.05	1420.5
220.55	1479.3
221.05	1420.5
221.55	1470.6
222.05	1462
222.55	1445.1
223.05	1453.5
223.55	1436.8
224.05	1543.2
224.55	1524.4
225.05	1582.3
225.55	1396.6
226.05	1515.2
226.55	1515.2
227.05	1515.2
227.55	1428.6
228.05	1404.5
228.55	1479.3
229.05	1623.4
229.55	1470.6
230.05	1506
230.55	1488.1
231.05	1552.8
231.55	1470.6
232.05	1533.7
232.55	1436.8
233.05	1497
233.55	1533.7
234.06	1462
234.56	1552.8
235.06	1515.2

Table 1  
Shear Wave Velocity

Depth (ft)	Velocity (ft/sec)
235.56	1515.2
236.06	1515.2
236.56	1533.7
237.06	1524.4
237.56	1543.2
238.06	1462
238.56	1445.1
239.06	1445.1
239.56	1428.6
240.06	1445.1
240.56	1436.8
241.06	1445.1
241.56	1412.4
242.06	1428.6
242.56	1428.6
243.06	1453.5
243.56	1445.1
244.06	1445.1
244.56	1445.1
245.06	1445.1
245.56	1515.2
246.06	1420.5
246.56	1453.5
247.06	1396.6
247.56	1436.8
248.06	1436.8
248.56	1412.4
249.06	1420.5
249.57	1428.6
250.07	1436.8
250.57	1412.4
251.07	1428.6
251.57	1420.5
252.07	1436.8
252.57	1436.8
253.07	1436.8
253.57	1412.4

Table 1  
Shear Wave Velocity

Depth (ft)	Velocity (ft/sec)
254.07	1436.8
254.57	1445.1
255.07	1515.2
255.57	1428.6
256.07	1428.6
256.57	1428.6
257.07	1420.5
257.57	1445.1
258.07	1436.8
258.57	1436.8
259.07	1436.8
259.57	1524.4
260.07	1462
260.57	1524.4
261.07	1488.1
261.57	1488.1
262.07	1470.6
262.57	1515.2
263.07	1543.2
263.57	1533.7
264.07	1515.2
264.58	1388.9
265.08	1543.2
265.58	1445.1
266.08	1462
266.58	1453.5
267.08	1488.1
267.58	1462
268.08	1488.1
268.58	1470.6
269.08	1515.2
269.58	1470.6
270.08	1322.8
270.58	1445.1
271.08	1543.2
271.58	1388.9
272.08	1396.6

Table 1  
Shear Wave Velocity

Depth (ft)	Velocity (ft/sec)
272.58	1329.8
273.08	1336.9
273.58	1436.8
274.08	1351.4
274.58	1445.1
275.08	1453.5
275.58	1488.1
276.08	1488.1
276.58	1488.1
277.08	1470.6
277.58	1497
278.08	1479.3
278.58	1470.6
279.08	1488.1
279.58	1488.1
280.09	1488.1
280.59	1388.9
281.09	1420.5
281.59	1497
282.09	1436.8
282.59	1445.1
283.09	1436.8
283.59	1428.6
284.09	1396.6
284.59	1543.2
285.09	1497
285.59	1453.5
286.09	1533.7
286.59	1470.6
287.09	1479.3
287.59	1366.1
288.09	1428.6
288.59	1412.4
289.09	1428.6
289.59	1388.9
290.09	1462
290.59	1428.6

Table 1  
Shear Wave Velocity

Depth (ft)	Velocity (ft/sec)
291.09	1462
291.59	1479.3
292.09	1497
292.59	1381.2
293.09	1506
293.59	1436.8
294.09	1470.6
294.59	1612.9
295.1	1366.1
295.6	1322.8
296.1	1462
296.6	1470.6
297.1	1420.5
297.6	1358.7
298.1	1479.3
298.6	1420.5
299.1	1592.4
299.6	1396.6
300.1	1479.3
300.6	1462
301.1	1420.5
301.6	1506
302.1	1506
302.6	1373.6
303.1	1470.6
303.6	1533.7
304.1	1524.4
304.6	1470.6
305.1	1420.5
305.6	1552.8
306.1	1533.7
306.6	1515.2
307.1	1479.3
307.6	1445.1
308.1	1634
308.6	1634
309.1	1689.2

Table 1  
Shear Wave Velocity

Depth (ft)	Velocity (ft/sec)
309.6	1515.2
310.1	1592.4
310.61	1329.8
311.11	1515.2
311.61	1582.3
312.11	1562.5
312.61	1488.1
313.11	1388.9
313.61	1533.7
314.11	1543.2
314.61	1644.7
315.11	1543.2
315.61	1479.3
316.11	1470.6
316.61	1445.1
317.11	1470.6
317.61	1462
318.11	1623.4
318.61	1479.3
319.11	1497
319.61	1462
320.11	1445.1
320.61	1479.3
321.11	1497
321.61	1462
322.11	1488.1
322.61	1533.7
323.11	1524.4
323.61	1666.7
324.11	1655.6
324.61	1506
325.11	1373.6
325.62	1436.8
326.12	1479.3
326.62	1592.4
327.12	1282.1
327.62	1436.8

Table 1  
Shear Wave Velocity

Depth (ft)	Velocity (ft/sec)
328.12	1243.8
328.62	1506
329.12	1275.5
329.62	1543.2
330.12	1488.1
330.62	1543.2
331.12	1533.7
331.62	1506
332.12	1479.3
332.62	1506
333.12	1515.2
333.62	1572.3
334.12	1533.7
334.62	1524.4
335.12	1436.8
335.62	1488.1
336.12	1336.9
336.62	1453.5
337.12	1453.5
337.62	1344.1
338.12	1462
338.62	1470.6
339.12	1515.2
339.62	1462
340.12	1497
340.63	1488.1
341.13	1488.1
341.63	1524.4
342.13	1436.8
342.63	1488.1
343.13	1515.2
343.63	1470.6
344.13	1462
344.63	1543.2
345.13	1488.1
345.63	1506
346.13	1420.5

Table 1  
Shear Wave Velocity

Depth (ft)	Velocity (ft/sec)
346.63	1488.1
347.13	1515.2
347.63	1470.6
348.13	1562.5
348.63	1351.4
349.13	1582.3
349.63	1366.1
350.13	1420.5
350.63	1592.4
351.13	1373.6
351.63	1329.8
352.13	1533.7
352.63	1572.3
353.13	1524.4
353.63	1428.6
354.13	1412.4
354.63	1388.9
355.13	1453.5
355.63	1428.6
356.14	1428.6
356.64	1381.2
357.14	1412.4
357.64	1488.1
358.14	1445.1
358.64	1462
359.14	1479.3
359.64	1506
360.14	1515.2
360.64	1506
361.14	1373.6
361.64	1381.2
362.14	1562.5
362.64	1582.3
363.14	1666.7
363.64	1344.1
364.14	1592.4
364.64	1445.1

Table 1  
Shear Wave Velocity

Depth (ft)	Velocity (ft/sec)
365.14	1533.7
365.64	1420.5
366.14	1462
366.64	1506
367.14	1533.7
367.64	1396.6
368.14	1404.5
368.64	1396.6
369.14	1315.8
369.64	1506
370.14	1436.8
370.64	1644.7
371.15	1533.7
371.65	1506
372.15	1470.6
372.65	1524.4
373.15	1497
373.65	1592.4
374.15	1488.1
374.65	1445.1
375.15	1445.1
375.65	1420.5
376.15	1412.4
376.65	1428.6
377.15	1412.4
377.65	1479.3
378.15	1420.5
378.65	1515.2
379.15	1396.6
379.65	1428.6
380.15	1479.3
380.65	1524.4
381.15	1470.6
381.65	1515.2
382.15	1552.8
382.65	1524.4
383.15	1533.7

Table 1  
Shear Wave Velocity

Depth (ft)	Velocity (ft/sec)
383.65	1533.7
384.15	1533.7
384.65	1428.6
385.15	1445.1
385.65	1677.9
386.15	1572.3
386.66	1572.3
387.16	1497
387.66	1488.1
388.16	1428.6
388.66	1428.6
389.16	1428.6
389.66	1412.4
390.16	1428.6
390.66	1428.6
391.16	1428.6
391.66	1428.6
392.16	1445.1
392.66	1506
393.16	1445.1
393.66	1428.6
394.16	1524.4
394.66	1506
395.16	1533.7
395.66	1533.7
396.16	1524.4
396.66	1533.7
397.16	1543.2
397.66	1543.2
398.16	1543.2
398.66	1543.2
399.16	1543.2
399.66	1543.2
400.16	1543.2
400.66	1543.2
401.16	1543.2
401.67	1543.2

Table 1  
Shear Wave Velocity

Depth (ft)	Velocity (ft/sec)
402.17	1543.2
402.67	1533.7
403.17	1533.7
403.67	1543.2
404.17	1533.7
404.67	1533.7
405.17	1412.4
405.67	1428.6
406.17	1420.5
406.67	1453.5
407.17	1524.4
407.67	1533.7
408.17	1533.7
408.67	1533.7
409.17	1533.7
409.67	1533.7
410.17	1533.7
410.67	1533.7
411.17	1533.7
411.67	1533.7
412.17	1533.7
412.67	1533.7
413.17	1533.7
413.67	1533.7
414.17	1533.7
414.67	1543.2
415.17	1543.2
415.67	1509.9
416.17	1509.9
416.67	1509.9
417.18	1509.9
417.68	1500.8
418.18	1505.4
418.68	1516.9
419.18	1528.6
419.68	1538
420.18	1519.3

Table 1  
Shear Wave Velocity

Depth (ft)	Velocity (ft/sec)
420.68	1519.3
421.18	1519.3
421.68	1519.3
422.18	1531
422.68	1531
423.18	1531
423.68	1531
424.18	1540.5
424.68	1498.7
425.18	1446.4
425.68	1446.4
426.18	1498.7
426.68	1550
427.18	1540.5
427.68	1483.3
428.18	1481
428.68	1496.4
429.18	1478.7
429.68	1507.7
430.18	1528.6
430.68	1519.3
431.18	1519.3
431.68	1528.6
432.19	1528.6
432.69	1519.3
433.19	1519.3
433.69	1510.1
434.19	1489.8
434.69	1489.8
435.19	1489.8
435.69	1519.3
436.19	1519.3
436.69	1519.3
437.19	1519.3
437.69	1498.7
438.19	1448.6
438.69	1448.6

Table 1  
Shear Wave Velocity

Depth (ft)	Velocity (ft/sec)
439.19	1461.4
439.69	1501.1
440.19	1521.7
440.69	1521.7
441.19	1531
441.69	1521.7
442.19	1564.8
442.69	1579.7
443.19	1579.7
443.69	1602.6
444.19	1636.8
444.69	1626.2
445.19	1751.5
445.69	1689.2
446.19	1642
446.69	1610.2
447.19	1709.3
447.7	1592.4
448.2	1666.7
448.7	1589.7
449.2	1555.1
449.7	1550
450.2	1519.3
450.7	1501.1
451.2	1531
451.7	1540.5
452.2	1540.5
452.7	1531
453.2	1510.1
453.7	1510.1
454.2	1521.7
454.7	1552.6
455.2	1552.6
455.7	1564.8
456.2	1564.8
456.7	1552.6
457.2	1510.1

Table 1  
Shear Wave Velocity

Depth (ft)	Velocity (ft/sec)
457.7	1510.1
458.2	1510.1
458.7	1519.3
459.2	1519.3
459.7	1519.3
460.2	1489.8
460.7	1489.8
461.2	1481
461.7	1489.8
462.2	1489.8
462.71	1481
463.21	1489.8
463.71	1501.1
464.21	1501.1
464.71	1531
465.21	1519.3
465.71	1519.3
466.21	1507.7
466.71	1528.6
467.21	1569.5
467.71	1540.5
468.21	1531
468.71	1540.5
469.21	1550
469.71	1559.7
470.21	1579.4
470.71	1559.7
471.21	1528.6
471.71	1519.3
472.21	1519.3
472.71	1538
473.21	1524.4
473.71	1524.4
474.21	1533.7
474.71	1515.2
475.21	1515.2
475.71	1497

Table 1  
Shear Wave Velocity

Depth (ft)	Velocity (ft/sec)
476.21	1506
476.71	1524.4
477.21	1515.2
477.71	1515.2
478.22	1515.2
478.72	1515.2
479.22	1506
479.72	1506
480.22	1506
480.72	1506
481.22	1506
481.72	1515.2
482.22	1515.2
482.72	1506
483.22	1396.6
483.72	1404.5
484.22	1412.4
484.72	1412.4
485.22	1404.5
485.72	1412.4
486.22	1404.5
486.72	1404.5
487.22	1404.5
487.72	1428.6
488.22	1428.6
488.72	1420.5
489.22	1428.6
489.72	1436.8
490.22	1533.7
490.72	1533.7
491.22	1533.7
491.72	1533.7
492.22	1533.7
492.72	1524.4
493.23	1524.4
493.73	1524.4
494.23	1524.4

Table 1  
Shear Wave Velocity

Depth (ft)	Velocity (ft/sec)
494.73	1420.5
495.23	1524.4
495.73	1533.7
496.23	1533.7
496.73	1533.7
497.23	1533.7
497.73	1533.7
498.23	1533.7
498.73	1533.7
499.23	1533.7
499.73	1524.4
500.23	1420.5
500.73	1420.5
501.23	1428.6
501.73	1428.6
502.23	1428.6
502.73	1436.8
503.23	1388.9
503.73	1428.6
504.23	1428.6
504.73	1445.1
505.23	1420.5
505.73	1412.4
506.23	1462
506.73	1412.4
507.23	1404.5
507.73	1428.6
508.23	1428.6
508.74	1420.5
509.24	1384.1
509.74	1446.4
510.24	1446.4
510.74	1421.8
511.24	1519
511.74	1545
512.24	1535.5
512.74	1505.3

Table 1  
Shear Wave Velocity

Depth (ft)	Velocity (ft/sec)
513.24	1505.3
513.74	1471.9
514.24	1485.1
514.74	1485.1
515.24	1485.1
515.74	1497.2
516.24	1497.2
516.74	1495.9
517.24	1495.9
517.74	1495.9
518.24	1483.8
518.74	1503.6
519.24	1503.6
519.74	1503.6
520.24	1491.4
520.74	1479.4
521.24	1471.5
521.74	1471.5
522.24	1471.5
522.74	1471.5
523.24	1394.7
523.75	1477.1
524.25	1295.4
524.75	1407.4
525.25	1491.4
525.75	1462.1
526.25	1497.8
526.75	1497.8
527.25	1457.3
527.75	1457.3
528.25	1516
528.75	1462.1
529.25	1471.5
529.75	1459.8
530.25	1459.8
530.75	1491.4
531.25	1556.3

Table 1  
Shear Wave Velocity

Depth (ft)	Velocity (ft/sec)
531.75	1556.3
532.25	1445.1
532.75	1445.1
533.25	1445.1
533.75	1453.5
534.25	1445.1
534.75	1445.1
535.25	1462
535.75	1436.8
536.25	1445.1
536.75	1582.3
537.25	1582.3
537.75	1592.4
538.25	1497
538.75	1479.3
539.26	1479.3
539.76	1479.3
540.26	1479.3
540.76	1479.3
541.26	1479.3
541.76	1479.3
542.26	1572.3
542.76	1572.3
543.26	1479.3
543.76	1462
544.26	1462
544.76	1453.5
545.26	1462
545.76	1445.1
546.26	1462
546.76	1479.3
547.26	1479.3
547.76	1562.5
548.26	1612.9
548.76	1488.1
549.26	1479.3
549.76	1488.1

Table 1  
Shear Wave Velocity

Depth (ft)	Velocity (ft/sec)
550.26	1445.1
550.76	1470.6
551.26	1506
551.76	1497
552.26	1470.6
552.76	1436.8
553.26	1453.5
553.76	1388.9
554.27	1515.2
554.77	1488.1
555.27	1592.4
555.77	1634
556.27	1436.8
556.77	1396.6
557.27	1470.6
557.77	1396.6
558.27	1479.3
558.77	1488.1
559.27	1488.1
559.77	1497
560.27	1445.1
560.77	1436.8
561.27	1373.6
561.77	1479.3
562.27	1479.3
562.77	1488.1
563.27	1412.4
563.77	1404.5
564.27	1479.3
564.77	1497
565.27	1515.2
565.77	1524.4
566.27	1533.7
566.77	1515.2
567.27	1515.2
567.77	1515.2
568.27	1462

Table 1  
Shear Wave Velocity

Depth (ft)	Velocity (ft/sec)
568.77	1404.5
569.27	1506
569.78	1506
570.28	1445.1
570.78	1373.6
571.28	1470.6
571.78	1396.6
572.28	1445.1
572.78	1428.6
573.28	1428.6
573.78	1412.4
574.28	1404.5
574.78	1396.6
575.28	1497
575.78	1420.5
576.28	1428.6
576.78	1420.5
577.28	1420.5
577.78	1420.5
578.28	1396.6
578.78	1506
579.28	1412.4
579.78	1412.4
580.28	1428.6
580.78	1404.5
581.28	1404.5
581.78	1396.6
582.28	1420.5
582.78	1445.1
583.28	1428.6
583.78	1445.1
584.28	1396.6
584.79	1506
585.29	1562.5
585.79	1552.8
586.29	1470.6
586.79	1404.5

Table 1  
Shear Wave Velocity

Depth (ft)	Velocity (ft/sec)
587.29	1506
587.79	1479.3
588.29	1543.2
588.79	1592.4
589.29	1358.7
589.79	1381.2
590.29	1428.6
590.79	1453.5
591.29	1453.5
591.79	1436.8
592.29	1428.6
592.79	1428.6
593.29	1436.8
593.79	1428.6
594.29	1428.6
594.79	1428.6
595.29	1428.6
595.79	1436.8
596.29	1445.1
596.79	1428.6
597.29	1420.5
597.79	1428.6
598.29	1412.4
598.79	1404.5
599.29	1488.1
599.79	1420.5
600.3	1428.6
600.8	1404.5
601.3	1428.6
601.8	1479.3
602.3	1470.6
602.8	1412.4
603.3	1445.1
603.8	1428.6
604.3	1428.6
604.8	1428.6
605.3	1428.6

Table 1  
Shear Wave Velocity

Depth (ft)	Velocity (ft/sec)
605.8	1436.8
606.3	1420.5
606.8	1436.8
607.3	1453.5
607.8	1445.1
608.3	1445.1
608.8	1445.1
609.3	1436.8
609.8	1445.1
610.3	1453.5
610.8	1445.1

## Appendix D: Geological Logging Results

---



**SCDNR**  
SOUTH CAROLINA DEPARTMENT OF  
NATURAL RESOURCES

**SCGS**

SOUTH CAROLINA  
GEOLOGICAL SURVEY



Project Name: Deep Soil Test Boring to Determine Shear  
Wave Velocities across South Carolina  
Client: SCDOT  
Location: Conway, SC

Project ID: SPR-731  
Boring No.: B-CON  
Geology Well ID: HOR-1328  
Tested By: Joe Gellici

LITHOLOGY_ID	UNIT_DESCRIPTION	OBS_METHOD	Depth (ft)	
			From	To
No Recovery	no recovery	COREHOLE	0	119
Sand	calcareous clayey sand; silt to medium sand, moderately sorted; weakly cemented with calcium carbonate; friable to hard; clay 15-20%; trace very fine to fine muscovite; trace fine to coarse shell fragments; weak to strong reaction with HCl; very irregular structure; light olive gray (5Y6/1)	COREHOLE	119	121
Sand	calcareous clayey sand; very fine to fine sand in a 10-15% clay matrix; moderately sorted; loose to friable; cemented with calcium carbonate in spots; calcium carbonate concretions; trace very fine to fine muscovite; dark opaque grains may be heavy minerals; very irregular/convoluted structures; burrowed; possible loading structures; olive gray (5Y4/1); strong reaction with HCl, slightly less of a reaction with depth	COREHOLE	121	124
No Recovery	no recovery	COREHOLE	124	125
Sand	calcareous clayey sand; silt to very fine sand in a 15-20% clay matrix; well sorted, friable, weakly cemented with HCl; strong reaction with HCl; trace very fine muscovite; minor dark opaque minerals; very irregular/convoluted structures, appears strongly bioturbated; light olive gray (5Y6/1)	COREHOLE	125	127
Clay	silty clay; well sorted, 30-50% clay/silt; trace very fine sand; minor dark opaque minerals; burrows common; loose; olive gray (5Y4/1); moderate reaction with HCl	COREHOLE	127	128
No Recovery	no recovery	COREHOLE	128	131
Sand	calcareous clayey sand; very fine to fine, silty; well sorted, hard, well cemented with carbonate; 15-20% clay matrix; minor to common dark opaque minerals (5-15%) (possibly glauconite); trace muscovite; strong reaction with HCl; very irregular structures; light olive gray (5Y6/1)	COREHOLE	131	132
Sand	very similar to section above but this section is loose to friable; it lacks the carbonate cement, trace shell fragments; still has strong reaction with HCl; olive gray (5Y4/1)	COREHOLE	132	133
Sand	calcareous clayey sand; very similar to section above; very fine to fine; silty, well sorted; hard; well cemented with carbonate, 10-15% clay matrix; 5-15% dark opaque minerals; irregular structures; possibly loading structures or burrows; strong reaction with HCl; light olive gray (5Y6/1)	COREHOLE	133	136
Sand	calcareous clayey sand; very fine to fine; silty; well sorted; loose to friable; 15-20% clay matrix; minor to common dark opaque minerals (5-15%) (possibly glauconite); trace muscovite; strong reaction with HCl throughout core; massive to lenticular bedding; olive gray (5Y4/1); trace shell fragments throughout core	COREHOLE	136	141
Sand	alternating layers of loose and hard beds caused by carbonate cementation; calcareous clayey sand; very fine to fine; silty; well sorted; 15-20% clay matrix; loose to hard; hard zones are cemented with carbonate; loose zones lack cement; 5-15% dark opaque minerals (possibly glauconite); strong reaction with HCl throughout core; irregular/convoluted structures that are more distinct in hard zones; trace shell fragments; trace muscovite throughout core; hard zones are light olive gray (5Y6/1) and loose zones are olive gray (5Y4/1)	COREHOLE	141	146
Sand	calcareous clayey sand; very fine to fine; silty; well sorted; 15-20% clay matrix; loose to hard caused by carbonate cementation; 5-15% opaque minerals (possibly glauconite); strong reaction with HCl; trace shell fragments, trace muscovite, same irregular/convoluted structures as above; hard zones are light olive gray (5Y6/1); loose zones olive gray (5Y4/1); lower section is silty clay, plastic/sticky, olive black (5Y2/1)	COREHOLE	146	149
No Recovery	no recovery	COREHOLE	149	151
Clay	calcareous silty clay; well sorted; loose to friable; trace very fine muscovite; trace shell fragments; faint clay/silt laminations; faint lenticular bedding; olive black (5Y2/1); strong reaction with HCl	COREHOLE	151	153
Clay	calcareous silty clay; well sorted; 10-15% very fine to fine sand; loose to friable; trace shell fragments; trace very fine muscovite; lenticular bedding structure prevalent; clay is olive black (5Y2/1); silty and sandy zones olive gray (5Y4/1); strong reaction with HCl; this lower zone is slightly sandier than upper zone	COREHOLE	153	156



**SCDNR**  
SOUTH CAROLINA DEPARTMENT OF  
NATURAL RESOURCES

**SCGS**  
SOUTH CAROLINA  
GEOLOGICAL SURVEY



Project Name: Deep Soil Test Boring to Determine Shear  
Wave Velocities across South Carolina  
Client: SCDOT  
Location: Conway, SC

Project ID: SPR-731  
Boring No.: B-CON  
Geology Well ID: HOR-1328  
Tested By: Joe Gellici

LITHOLOGY_ID	UNIT_DESCRIPTION	OBS_METHOD	Depth (ft)	
			From	To
Clay	calcareous silty clay; well sorted; 10-15% very fine to fine sand occurring primarily as thin undulating laminations; loose to friable core; trace very fine muscovite and shell fragments; moderate to strong reaction with HCl; faint lenticular bedding with clay and silt/sand lamination; olive black (5Y21); very fine to fine sand occurs as small (5-10 mm) lenses encased in clay and silt (lenticular bedding); opaque minerals no longer present as above	COREHOLE	156	161
Clay	calcareous silty clay; well sorted; 10-15% very fine to fine sand; loose to friable; trace very fine muscovite and shell fragments; moderate to strong reaction with HCl; faint lenticular bedding; olive black (5Y2/1); very silty core; increasing sand content with depth; very similar to core above but slightly sandier and slightly weaker reaction with HCl	COREHOLE	161	165
No Recovery	no recovery	COREHOLE	165	166
Clay	calcareous sandy clay; 20-30% very fine to medium sand; well sorted; loose to friable; trace muscovite and shell fragments; moderate reaction with HCl; 5-10% opaque minerals; increasing sand toward bottom of core	COREHOLE	166	168
Sand	clayey sand; very fine to medium sand in a 25-30% clay matrix; sandy zones are hard and well cemented with carbonate; clay zones are loose, uncemented, very convoluted, bedding structures; sand is yellowish gray (5Y81) and clay is olive black (5Y2/1)	COREHOLE	168	169
Clay	calcareous sandy clay; 20-30% very fine to medium sand; well sorted; loose to friable; trace muscovite and shell fragments; moderate reaction with HCl; 5-10% opaque minerals; increasing sand toward bottom of core	COREHOLE	169	171
Sand	calcareous clayey sand; fine to medium sand in a 30-40% clay matrix; moderately sorted; loose to friable; trace very fine to fine muscovite; 3-5% dark opaque minerals; massive to faintly laminated (lenticular bedding); moderate reaction with HCl; olive black (5Y2/1)	COREHOLE	171	174
Sand	hard, well carbonate cemented, sandy zone; 15-20% clay flaser bedding structures; sandstone, very convoluted bedding; sand yellowish gray (5Y8/1) and clay olive black; very strong reaction with HCl	COREHOLE	174	175
Sand	calcareous clayey sand; very similar to top of core; slightly finer grained (very fine to fine); moderate reaction with HCl; trace shell fragments	COREHOLE	175	176
Clay	calcareous sandy clay; 30-40% very fine to medium sand; moderately sorted; loose to friable; trace fine-grained muscovite, trace shell fragments; laminated clay and sand; lenticular bedding structure (clay dominates); moderate reaction with HCl; trace dark opaque minerals; olive black (5Y2/1)	COREHOLE	176	181
Clay	calcareous sandy clay; 30-40% very fine to fine sand; well sorted; loose to friable; trace very fine to fine muscovite and shell fragments; lenticular bedding structures; moderate reaction with HCl; olive black (5Y2/1); @ 183'6": hard zone, carbonate-cemented sandstone, strong reaction with HCl	COREHOLE	181	185
No Recovery	no recovery	COREHOLE	185	186
Clay	calcareous silty clay; 5-15% very fine to fine sand occurring as lenses; well sorted; loose to friable; trace very fine muscovite and shell fragments; faintly laminated; lenticular bedding structures; slight to moderate reaction with HCl; olive black (5Y2/1)	COREHOLE	186	191
Clay	calcareous silty clay; 5-15% very fine to fine sand occurring as lenses; well sorted; loose to friable; trace very fine muscovite and shell fragments; faintly laminated; lenticular bedding structures; slight to moderate reaction with HCl; olive black (5Y2/1)	COREHOLE	191	196
Clay	calcareous silty clay; 5-15% very fine to fine sand occurring as lenses; well sorted; loose to friable; trace very fine muscovite and shell fragments; faintly laminated; lenticular bedding structures; slight to moderate reaction with HCl; olive black (5Y2/1); increasing sand content in lower 0.4'	COREHOLE	196	201
Clay	carbonate-cemented sandstone in upper 0.2'; calcareous silty clay; 10-15% very fine to fine sand occurring as stringers and laminations; well sorted; trace very fine to fine muscovite and shell fragments; core is loose to friable; slight reaction with HCl; olive black (5Y2/1); outer surface of core is not smooth but is marked by open holes and elongated tunnel-like structures that are possibly burrows; were probably sand-filled burrows whereby the sand was washed out by the coring operation; there is evidence of sand filled burrows deeper within the core	COREHOLE	201	204



**SCDNR**  
SOUTH CAROLINA DEPARTMENT OF  
NATURAL RESOURCES

**SCGS**  
SOUTH CAROLINA  
GEOLOGICAL SURVEY



Project Name: Deep Soil Test Boring to Determine Shear  
Wave Velocities across South Carolina  
Client: SCDOT  
Location: Conway, SC

Project ID: SPR-731  
Boring No.: B-CON  
Geology Well ID: HOR-1328  
Tested By: Joe Gellici

LITHOLOGY_ID	UNIT_DESCRIPTION	OBS_METHOD	Depth (ft)	
			From	To
No Recovery	no recovery	COREHOLE	204	206
Clay	silty clay to clay; very tight clay beds interbedded with thin (10-30 mm) sand beds, sand beds are more common toward bottom of core; most of the core is silty clay and clay; some clay beds are very dense; core has slight reaction with HCl; sand beds are loose (unconsolidated) and no longer cemented with carbonate; sand is very fine to fine, well sorted, and loose; sand is yellowish gray (5Y8/1) and clay is olive black (5Y2/1)	COREHOLE	206	209
No Recovery	no recovery	COREHOLE	209	211
Sand	sandy clay to clayey sand; very fine to medium sand in a 40-50% clay matrix; moderately sorted; loose; trace muscovite and sparse to common dark opaque minerals; slight reaction with HCl; olive black (5Y2/1)	COREHOLE	211	212
Clay	silty clay; 5-10% very fine sand; well sorted; trace muscovite; trace shell fragments; faint lamination clay/sand, but dominated by clay and silt; slight reaction with HCl; olive black (5Y2/1)	COREHOLE	212	214
No Recovery	no recovery	COREHOLE	214	216
Clay	silty clay; very tight in spots; trace fine-grained muscovite; faintly laminated; slight reaction with HCl; olive black (5Y2/1); thin (<10 mm) bed of very fine-grained unconsolidated sand at 219'; thin sand bed at 219'6"	COREHOLE	216	221
Sand	clayey sand; moderately sorted, fine to medium sand in a 20-30% clay matrix; core is friable; trace muscovite; 3-5% dark opaque minerals; trace shell fragments (white); sandy in the lower 0.4'; weak to moderate reaction with HCl; massive structure; greenish black (5G2/1)	COREHOLE	221	222
No Recovery	no recovery	COREHOLE	222	226
Clay	laminated sand and clay; sand is fine to medium, moderately to well sorted and loose; 1-2% muscovite; green sand grains suggest glauconite (5-15%); most of the recovered core consists of clay laminae 3-5 mm thick that are separated by fine to medium-grained sand laminae 3-5 mm thick; laminations are planar to wavy; the core is poorly consolidated (loose); core has a very weak to no reaction with HCl; clay is greenish black (5G2/1) and sand is greenish gray (5GY6/1)	COREHOLE	226	227
No Recovery	no recovery	COREHOLE	227	231
Sand	core appears to be disturbed; clayey sand; sand is fine to medium, moderately sorted in a 20-25% clay matrix; 1-2% fine-grained muscovite; 3-5% dark opaque grains (glauconite); weak reaction with HCl; sand is greenish gray (5GY6/1); there is a greenish black (5G2/1) clay bed 10 mm thick at the bottom of the interval	COREHOLE	231	232
No Recovery	no recovery	COREHOLE	232	236
Clay	laminated sand and clay; sand is fine to medium, moderately to well sorted and unconsolidated; sand contains 1-2% muscovite and 3-5% dark grains believed to be glauconite; the core is interlaminated with sand and clay in roughly equal parts; laminae are 1-5 mm thick and are planar to wavy and cut across entire width of core; the sand is greenish gray (5GY6/1) and the clay is greenish black (5G2/1)	COREHOLE	236	237
No Recovery	no recovery	COREHOLE	237	241
Clay	laminated sand and clay very similar to the previous run (above), dominated by clay (lenticular bedding); from 241'6" to 242': sandstone; carbonate-cemented sand; very hard; strong reaction with HCl; core has salt and pepper appearance with dark grains possibly being glauconite; overall color is light bluish gray (5D7/1)	COREHOLE	241	242
Clay	sandy clay that grades downward to a dense clay; greenish black (5G2/1)	COREHOLE	242	243
No Recovery	no recovery	COREHOLE	243	246
Sand	clayey sand; fine to medium sand in a 30-40% clay matrix; sand coarsens toward bottom of interval (medium to coarse) and clay content decreases; moderately sorted; core is loose (unconsolidated) to friable where clay content increases; 5-7% dark opaque grains thought to be glauconite; trace shell fragments; very weak reaction with HCl; massive to faintly laminated; greenish black (5G2/1); lignite fragment ~ 20 mm long @ 246'8"	COREHOLE	246	248
No Recovery	no recovery	COREHOLE	248	251
Sand	clayey sand; fine to medium, moderately to well sorted sand in a 10-20% clay matrix; sand is loose and massive; 5-10% dark minerals (possibly glauconite); trace muscovite; greenish gray (5GY6/1) to dark greenish gray (5GY4/1); no reaction with HCl	COREHOLE	251	252
Clay	dense clay; greenish black (5GY2/1); no reaction with HCl; hard	COREHOLE	252	253



**SCDNR**  
SOUTH CAROLINA DEPARTMENT OF  
NATURAL RESOURCES

**SCGS**  
SOUTH CAROLINA  
GEOLOGICAL SURVEY



Project Name: Deep Soil Test Boring to Determine Shear  
Wave Velocities across South Carolina  
Client: SCDOT  
Location: Conway, SC

Project ID: SPR-731  
Boring No.: B-CON  
Geology Well ID: HOR-1328  
Tested By: Joe Gellici

LITHOLOGY_ID	UNIT_DESCRIPTION	OBS_METHOD	Depth (ft)	
			From	To
No Recovery	no recovery	COREHOLE	253	256
Clay	laminated sand and clay (mostly clay); laminae are 1-30 mm thick; planar to wavy to slightly inclined; clay is plastic and sticky; sand is fine to medium-grained; 1-2% fine-grained muscovite; 5-7% dark opaque minerals (glauconite); no reaction with HCl in sand layers and very weak reaction with HCl in clay layers; clay is greenish black (5GY2/1) and sand is light olive gray (5Y6/1)	COREHOLE	256	258
No Recovery	no recovery	COREHOLE	258	261
Clay	clay; very tight, hard and dense; sparsely interlaminated with fine to medium-grained sand; sand appears as small (5-15 mm) lenses similar to what you would see in lenticular bedding; very weak reaction with HCl; clay is greenish black (5GY62/1) and sand is light olive gray (5Y6/1)	COREHOLE	261	267
No Recovery	no recovery	COREHOLE	267	271
Sandstone	possible lag bed; hard to describe; very chaotic structure; conglomerate of shell fragments and other clasts; shelly sandstone; shell fragments up to 30 mm in length; appear to be phosphatic grains tightly cemented with carbonate; very hard; large clasts up to 35 mm; very strong reaction with HCl	COREHOLE	271	272
Clay	clay; tight, hard and dense; sparsely interlaminated with shell fragments and fine-grained sand; slight to moderate reaction with HCl; clay is greenish black (5GY2/1) and sand is light olive gray (5Y6/1)	COREHOLE	272	275
No Recovery	no recovery	COREHOLE	275	276
Clay	clay; tight, hard and dense; contains thin laminations of fine to medium-grained sand in spots; weak reaction with HCl; greenish black (5GY2/1); same as above	COREHOLE	276	278
No Recovery	no recovery	COREHOLE	278	281
Clay	laminated clay and sand (mainly clay); sand is well sorted, very fine to fine, containing 5-10% dark opaque grains; trace very fine muscovite, laminations are 1-5 mm thick; dominated by clay laminae; lenticular bedding; slight reaction with HCl; clay is greenish black (5GY2/1) and sand is light olive gray (5Y6/1); top of core appears to be burrowed; surface of core contains voids and tunnel-like structure that may have been sand-filled burrows	COREHOLE	281	285
No Recovery	no recovery	COREHOLE	285	286
Clay	laminated clay and sand (mainly clay); sand is well sorted, very fine to fine, containing 5-10% dark opaque grains; trace very fine muscovite, laminations are 1-5 mm thick; dominated by clay laminae; lenticular bedding; weak to no reaction with HCl; clay is greenish black (5GY2/1) and sand is light olive gray (5Y6/1); top of core appears to be burrowed; surface of core contains voids and tunnel-like structure that may have been sand-filled burrows	COREHOLE	286	290
No Recovery	no recovery	COREHOLE	290	291
Clay	laminated clay and sand (mainly clay); sand is well sorted, very fine to fine, containing 5-10% dark opaque grains; trace very fine muscovite, laminations are 1-10 mm thick; dominated by clay laminae; lenticular bedding; weak reaction with HCl; clay is sticky and tight; clay is greenish black (5GY2/1) and sand is light olive gray (5Y6/1); top of core appears to be burrowed; surface of core contains voids and tunnel-like structure that may have been sand-filled burrows	COREHOLE	291	295
No Recovery	no recovery	COREHOLE	295	296
Limestone	shelly limestone; shell fragments up to 20 mm in length; tightly cemented with calcium carbonate; core is very hard; vuggy porosity noted along surface of core; dominated by mollusks; very irregular structures; very light gray (N3); pebble zone and lignite @ 296'6", pebbles 10 mm, possibly fine to medium-grained limestone	COREHOLE	296	298
No Recovery	no recovery	COREHOLE	298	306
Sandstone	sandstone; tightly cemented with calcium carbonate; very hard core; finely laminated (1-2 mm) with dark and light grains; 10-15 mm vugs noted along surface of core; very strong reaction with HCl; light gray (N7)	COREHOLE	306	309
No Recovery	no recovery	COREHOLE	309	311
Sandstone	sandstone; tightly cemented with calcium carbonate; very hard core; finely laminated (1-2 mm) with dark and light grains; 10-15 mm vugs noted along surface of core; very strong reaction with HCl; light gray (N7)	COREHOLE	311	312



**SCDNR**  
SOUTH CAROLINA DEPARTMENT OF  
NATURAL RESOURCES

**SCGS**  
SOUTH CAROLINA  
GEOLOGICAL SURVEY



Project Name: Deep Soil Test Boring to Determine Shear  
Wave Velocities across South Carolina  
Client: SCDOT  
Location: Conway, SC

Project ID: SPR-731  
Boring No.: B-CON  
Geology Well ID: HOR-1328  
Tested By: Joe Gellici

LITHOLOGY_ID	UNIT_DESCRIPTION	OBS_METHOD	Depth (ft)	
			From	To
Clay	sandy clay; 20-30% sand; sand is very fine to fine, well sorted and contains 10-15% dark opaque minerals, which appear to be glauconite; core has been disturbed so it is difficult to see structures; core is loose (unconsolidated); slight to moderate reaction with HCl; greenish black (5GY2/1)	COREHOLE	312	313
No Recovery	no recovery	COREHOLE	313	316
Sandstone	sandy clay at very top (0.1') of core; sandstone; tightly cemented with calcium carbonate; very hard core; finely laminated (1-2 mm) with dark and light grains; 10-15 mm vugs noted along surface of core; very strong reaction with HCl; light gray (N7)	COREHOLE	316	317
No Recovery	no recovery	COREHOLE	317	346
Clay	sandy clay; 15-20% very fine to medium sand in a tight clay matrix; sand is moderately sorted and unconsolidated; trace muscovite and 10-15% dark opaque minerals; entire core has lignite running through it; some lignite fragments are 20-40 mm in length; it appears that some lignite occurs wrapped around circular (5-10 mm) sand-filled burrows; HCl reaction only around shell fragments; other lignite fragments are scattered throughout the core; sparse shell fragments; clay is olive black (5Y2/1)	COREHOLE	346	347
No Recovery	no recovery	COREHOLE	347	351
Sand	sand; fine to medium (mostly fine); well sorted, loose sand in 2-5% clay matrix; very clean sand; unconsolidated; trace muscovite; 5-7% dark minerals (glauconite); massive structure; no reaction with HCl; light olive gray (5Y6/1); clay at bottom 0.2' of core	COREHOLE	351	352
No Recovery	no recovery	COREHOLE	352	356
Clay	sandy clay; 15-20% fine to medium sand in a tight sticky clay matrix; sand increases to about 50% toward bottom of core, core is unconsolidated; trace shell fragments; weak reaction with HCl; olive black (5Y2/1)	COREHOLE	356	357
No Recovery	no recovery	COREHOLE	357	366
Clay	sandy clay; 15-25% fine-grained sand in a tight clay matrix; core is unconsolidated to friable; trace muscovite; 5-7% dark minerals; the core is mainly massive but with streaks/lenses of sand; weak reaction with HCl; olive black (5Y2/1); increasing sand with depth	COREHOLE	366	370
No Recovery	no recovery	COREHOLE	370	371
Sand	clayey sand; moderately sorted, fine to medium sand in a 30-40% clay matrix; core is unconsolidated to friable; trace muscovite and thin-walled shell fragments that are scattered throughout core; massive to faintly cross-laminated (very low angle); moderate reaction with HCl; olive black (5Y2/1)	COREHOLE	371	372
No Recovery	no recovery	COREHOLE	372	381
Sand	glauconitic sand; fine to medium, well sorted in a 2-5% clay matrix; dark opaque minerals are likely glauconite (10-15%); trace muscovite; trace shell fragments; trace lignite fragments; core is loose (unconsolidated); no reaction with HCl; sand is massive; sand is greenish gray (5GY6/1); clay at the top and bottom of core, weak reaction with HCl, clay is grayish black (N2)	COREHOLE	381	383
No Recovery	no recovery	COREHOLE	383	386
Clay	clay; hard and tight; very sparse stringers and lenses of fine-grained sand occur throughout the core but the core is primarily clay; no shell fragments; no HCl reaction; grayish black (N2); @ 389': 0.1' sand bed	COREHOLE	386	396
Clay	clay; hard and tight, a few sand stringers (1-2 mm); no reaction with HCl, grayish black (N2); at the top of sample: sandy clay, 20-30% sand in a sticky clay matrix	COREHOLE	396	397
Sand	sand; fine to medium sand in a 5-10% clay matrix; moderately sorted; 10-15% dark minerals that are probably glauconite; core is loose (unconsolidated); no reaction with HCl; shell hash at 2978"; large (40 mm) mollusk shell fragments; dark greenish gray (5G4/1)	COREHOLE	397	398
No Recovery	no recovery	COREHOLE	398	401
Sand	clayey sand; fine to medium, moderately sorted sand in a 15-20% clay matrix; trace shell fragments; 10-20% dark minerals (glauconite); loose core; massive; weak reaction with HCl; dark greenish gray (5GY4/1); core is massive to faintly laminated; carbonate cemented zone at 403'; hard sandstone 0.5'	COREHOLE	401	404
No Recovery	no recovery	COREHOLE	404	411
Clay	clay; very tight, sticky clay; grayish black (N2)	COREHOLE	411	412



**SCDNR**  
SOUTH CAROLINA DEPARTMENT OF  
NATURAL RESOURCES

**SCGS**  
SOUTH CAROLINA  
GEOLOGICAL SURVEY



Project Name: Deep Soil Test Boring to Determine Shear  
Wave Velocities across South Carolina  
Client: SCDOT  
Location: Conway, SC

Project ID: SPR-731  
Boring No.: B-CON  
Geology Well ID: HOR-1328  
Tested By: Joe Gellici

LITHOLOGY_ID	UNIT_DESCRIPTION	OBS_METHOD	Depth (ft)	
			From	To
Clay	sandy clay; 20-30% fine to medium sand in tight clay matrix; lignite; minor shell fragments; shell hash in places; core is friable; grayish black (N2); last 6": sandstone; very hard, well cemented with calcium carbonate; shell fragments up to 50% of core; shark tooth; strong reaction with HCl; light gray (N7)	COREHOLE	412	413
No Recovery	no recovery	COREHOLE	413	421
Clay	silty clay; hard and tight; non-plastic; gritty; laminated with thin (1-3 mm) sand, sand is very fine to fine with 1-2% muscovite and 10-15% dark opaque minerals which appear to be glauconite, laminations are planar to very slightly (5°) inclined; in some cases only thin sand lenses are observed; very weak to no reaction with HCl; clay is olive black (5Y2/1) and sand is dark greenish gray (5G4/1); bulk sand 3-5% of core	COREHOLE	421	425
No Recovery	no recovery	COREHOLE	425	426
Clay	silty clay; hard and tight; non-plastic; gritty; laminated with thin (1-3 mm) sand, sand is very fine to fine with 1-2% muscovite and 10-15% dark opaque minerals which appear to be glauconite, laminations are planar to very slightly (5°) inclined; the sand laminae do not occur throughout the core; the core is 95-97% silt and clay; very weak to no reaction with HCl; clay is olive black (5Y2/1) and sand is dark greenish gray (5G4/1)	COREHOLE	426	431
Clay	silty clay; hard, gritty clay; laminated with very fine to fine sand; trace muscovite and shell fragments; weak to no reaction with HCl; voids occur along the outside surface of the core that may have been sand laminations/lenses whose sand has been washed out; clay is olive black (5Y2/1)	COREHOLE	431	432
No Recovery	no recovery	COREHOLE	432	446
Clay	laminated sand and silty clay (predominantly clay); clay is dense, slightly plastic and gritty; sand is very fine to fine, well sorted, loose and contains trace very fine to fine muscovite and 5-10% opaques (glauconite); very weak reaction with HCl; overall, the core is 85-90% clay and silt, and 10-15% sand; sand laminae are 1-5 mm thick; sand also occurs as isolated lenses typical of lenticular bedding; laminations are planar and slightly wavy; sand is light greenish gray (5GY8/1) clay is olive black (5Y2/1)	COREHOLE	446	447
No Recovery	no recovery	COREHOLE	447	451
Sandstone	shelly sandstone; fine to medium sand, well cemented with carbonate; core is well indurated (hard); sections of the core contain 50% shell fragments; some shell fragments cut across the entire diameter of the core; surface of the core is marked by voids; faintly laminated sand contains 5-10% dark opaque minerals; light blue gray (5B7/1); strong reaction with HCL	COREHOLE	451	455
No Recovery	no recovery	COREHOLE	455	456
Clay	silty clay; hard, dense and gritty; laminated with very fine to fine, well sorted sand; sand contains trace muscovite and 5-10% dark opaque minerals; sand occurs as thin (1-2 mm) laminae and as thin lenses, typical of lenticular bedding; overall, core is 95% clay and 5% sand; weak reaction with HCl	COREHOLE	456	459
No Recovery	no recovery	COREHOLE	459	461
Clay	silty clay; hard, dense and gritty; laminated with very fine to fine, well sorted sand; sand contains trace muscovite and 5-10% dark opaque minerals; sand occurs as thin (1-2 mm) laminae and as thin lenses, typical of lenticular bedding; overall, core is 95% clay and 5% sand; weak reaction with HCl	COREHOLE	461	468
No Recovery	no recovery	COREHOLE	468	471
Limestone	sandy limestone; well indurated (hard); well cemented with carbonate; large (up to 40 mm) micrite-filled molds occur along surface of core; core is mainly a well-cemented shell hash with 20-40% sand; very strong reaction with HCl	COREHOLE	471	472
Clay	limestone grades downward to a cemented sandstone that transitions to clay; clay is olive black (5Y2/1); weak to no reaction with HCl	COREHOLE	472	473
No Recovery	no recovery	COREHOLE	473	476
Clay	silty clay; dense; gritty clay that is finely laminated with well sorted, very fine to fine sand; sand contains trace very fine to fine muscovite and 5-10% dark minerals; and occurs as wisps of sand and as thin (1-3 mm) laminations; overall, core is 95% clay/silt and 5% sand; weak reaction with HCl; clay is olive black (5Y2/1) sand is light olive gray (5Y61)	COREHOLE	476	477
No Recovery	no recovery	COREHOLE	477	481



**SCDNR**  
SOUTH CAROLINA DEPARTMENT OF  
NATURAL RESOURCES

**SCGS**  
SOUTH CAROLINA  
GEOLOGICAL SURVEY



Project Name: Deep Soil Test Boring to Determine Shear  
Wave Velocities across South Carolina  
Client: SCDOT  
Location: Conway, SC

Project ID: SPR-731  
Boring No.: B-CON  
Geology Well ID: HOR-1328  
Tested By: Joe Gellici

LITHOLOGY_ID	UNIT_DESCRIPTION	OBS_METHOD	Depth (ft)	
			From	To
Clay	silty clay; dense; gritty clay that is finely laminated with well sorted, very fine to fine sand; sand contains trace very fine to fine muscovite and 5-10% dark minerals; and occurs as wisps of sand and as thin (1-3 mm) laminations; overall, core is 95% clay/silt and 5% sand; weak reaction with HCl; clay is olive black (5Y2/1) sand is light olive gray (5Y61)	COREHOLE	481	482
No Recovery	no recovery	COREHOLE	482	491
Sand	sand; fine to medium, moderately sorted sand in a 5-10% clay matrix; trace muscovite; trace iron-stained grains; 10-15% dark opaque minerals; core is unconsolidated and massive; sand light olive gray (5Y6/1); clay olive gray (5Y4/1); lower 0.5' is sandy clay bed; no reaction with HCl	COREHOLE	491	493
No Recovery	no recovery	COREHOLE	493	496
Sand	sand; very fine to fine, well sorted sand in a 5-10% clay matrix; trace muscovite; 10-15% opaques; sand is unconsolidated (loose) and massive; olive gray (5Y4/1); no HCl reaction	COREHOLE	496	497
Clay	silty clay; dense; gritty clay that is finely laminated with well sorted, very fine to fine sand; sand contains trace very fine to fine muscovite and 5-10% dark minerals; and occurs as wisps of sand and as thin (1-3 mm) laminations; overall, core is 95% clay/silt and 5% sand; weak reaction with HCl; clay is olive black (5Y2/1) sand is light olive gray (5Y61)	COREHOLE	497	499
No Recovery	no recovery	COREHOLE	499	501



**SCDNR**  
SOUTH CAROLINA DEPARTMENT OF  
NATURAL RESOURCES

**SCGS**  
SOUTH CAROLINA  
GEOLOGICAL SURVEY



Project Name: Deep Soil Test Boring to Determine Shear  
Wave Velocities across South Carolina  
Client: SCDOT  
Location: Andrews, SC

Project ID: SPR-731  
Boring No.: B-FMG  
Geology Well ID: WIL-0358  
Tested By: Joe Gellici

LITHOLOGY_ID	UNIT_DESCRIPTION	OBS_METHOD	Depth (ft)	
			From	To
top soil	top soil- humus; sandy clay; organic-rich, 15-20% fine-medium sand in organic-rich clay; olive black (5Y2/1)	Corehole	0	1
clay	sandy clay; fine-medium sand in a dense , plastic matrix; 15-20% sand; moderately sorted; trace very fine-fine opaque heavy minerals; mottled; clay is light olive gray (5Y6/1), iron-stained light brown (5YR5/6)	Corehole	1	2
top soil	top soil- silty clay; silt and soft, organic-rich clay; trace (1-2%) fine-medium quartz sand; sparse (2-4%) very fine-fine muscovite; olive black (5Y2/1)	Corehole	2	3
clay	sandy clay; fine-medium sand in a dense, sticky, plastic matrix; quartz sand "floating" in a clay matrix; 15-20% quartz sand; moderately sorted; trace very fine-fine muscovite and opaque heavies; clay is light olive gray (5Y6/1); iron-stained light brown (5YR5/6)	Corehole	3	4
clay	sandy clay; fine-coarse sand in a dense, sticky clay matrix; quartz sand "floating" in a dense clay matrix; sand is poorly sorted; contains 20-25% quartz sand; trace weathered sand is angular; 2-5% opaque heavies; trace granule size (2-4mm) quartz grains; clay is light olive gray (5Y6/1); iron-stained moderate brown (5Y4/4)	Corehole	4	6
sand	clayey sand; fine-very coarse granule (2-4mm), very poorly sorted sand in a 20-30% clay matrix; trace fine muscovite; trace very fine opaque heavy minerals; 1-2% weathered feldspar; trace small pebbles up to 6mm; friable; light olive gray, iron-stained light brown	Corehole	6	8
sand	sand; fine-pebbly quartz sand in a 3-5% clay matrix; very poorly sorted; loose, unconsolidated; quartz grains are angular to subrounded; 1-2% weathered feldspar; trace lignite and red quartz, possibly garnet; pebbles up to 5mm; pale yellowish brown (10YR6/2)	Corehole	8	10
no recovery	no recovery	Corehole	10	11
sand	glaucconitic sand; very fine-fine, well sorted quartz sand; 3-5% clay; unconsolidated; sparse bivalve shell fragments up to 6mm; glauconite up to 50%; slight reaction with HCl; partly cemented in places; dark greenish gray (5G2/4)	Corehole	11	13
sand	glaucconitic sand; very fine-fine, well sorted sand; 3-5% clay; unconsolidated; glauconite up to 40%; partly cemented in places with CO3; slight reaction with HCl especially where cemented; olive gray (5Y4/1)	Corehole	13	15
sand	glaucconitic sand; fine-medium (mostly fine); moderately sorted; 5-10% clay matrix; glauconite up to 30%; partly cemented in places with CO3; slight reaction with HCl; unconsolidated except where cemented; trace PO4; olive gray	Corehole	15	17
sand	glaucconitic sand; fine-medium; moderately sorted; 20-30% glauconite; 5-10% clay matrix; unconsolidated except where cemented with CO3; trace bivalve shells up to 10mm; trace coarse-very coarse PO4; slight reaction with HCl; olive gray	Corehole	17	18
sandstone	glaucconitic sandstone; same as above but cemented with CO3	Corehole	18	19
no recovery	no recovery	Corehole	19	21
limestone	shelly limestone (biomicrite); bivalve fragments (up to 20mm, but mostly <5m) in a micritic matrix; some zones are well-indurated and cemented with a fine-grained CO3 cement, other zones are friable where bivalves fragments occur in a soft micritic matrix; no apparent bedding; light olive gray (5Y6/1)	Corehole	21	23
limestone	shelly limestone (biosparite); bivalve fragments, molds, and casts in a CO3 cement; most of the core is tightly cemented, but some zones are friable; it appears that most of the core consists of clay (micrite) or sparry-filled casts and moldic porosity in a CO3 cement; molds up to 30mm long (bivalve molds); outside surface of the core contains numerous molds that may represent casts that were stripped away during the drilling operation; well indurated; very light gray (N8) to yellowish gray (5Y8/1)	Corehole	23	25
no recovery	no recovery	Corehole	25	26



**SCDNR**  
SOUTH CAROLINA DEPARTMENT OF  
NATURAL RESOURCES

**SCGS**  
SOUTH CAROLINA  
GEOLOGICAL SURVEY



Project Name: Deep Soil Test Boring to Determine Shear  
Wave Velocities across South Carolina  
Client: SCDOT  
Location: Andrews, SC

Project ID: SPR-731  
Boring No.: B-FMG  
Geology Well ID: WIL-0358  
Tested By: Joe Gellici

LITHOLOGY_ID	UNIT_DESCRIPTION	OBS_METHOD	Depth (ft)	
			From	To
limestone	shelly limestone (biosparite that grades downward to biomicrite); bivalve casts of sparry calcite and micrite in a sparry/micritic matrix; upper 3 ft is well indurated and tightly cemented with CO <sub>3</sub> ; lower part of core moderately indurated to friable and contains more micrite in the matrix; locally 1-2% black vitreous grains (fine-very coarse) that are very angular; these might be sparry calcite or possibly PO <sub>4</sub> ; these grains look like glass shards; molds up to 28mm long (bivalve molds); very light gray to yellowish gray	Corehole	26	30
no recovery	no recovery	Corehole	30	36
limestone	shelly limestone (biosparite to biomicrite); highly moldic shelly limestone in a well indurated sparry to micritic matrix; most of the shell fragments have been replaced by sparite or micrite; core has the appearance of a shell hash but the shells are missing, having been replaced by micrite and/or sparite; moldic porosity up to 40%; core is well indurated; most of the casts are of bivalve shell fragments with rare gastropod cast; most of the core is broken into biscuit-shaped pieces 30-40mm wide; olive gray to light olive gray; locally yellowish gray	Corehole	36	39
no recovery	no recovery	Corehole	39	41
limestone	shelly limestone (same as above); highly moldic; high moldic porosity; moderate to strong reaction with HCl; light olive gray	Corehole	41	42
no recovery	no recovery	Corehole	42	46
limestone	shelly limestone (same as above); highly moldic; high moldic porosity; moderate to strong reaction with HCl; core has the appearance of a shell hash (coquina) but most of shells have either been replaced with calcite/micrite, or all of the shells have dissolved leaving a calcite-cemented clay matrix in its place; abundant molds/casts; trace glauconite; most molds/casts are bivalves; light olive gray	Corehole	46	47
no recovery	no recovery	Corehole	47	51
sandstone	calcite-cemented sandstone; fine-medium, subrounded, moderately sorted, quartz sand weakly cemented with CO <sub>3</sub> ; loose to friable; 2-3% opaque heavy minerals that appear to be glauconite; 1-2% fine-coarse muscovite; weak to moderate reaction with HCl; massive; light olive gray	Corehole	51	52
no recovery	no recovery	Corehole	52	55
sandstone	calcite-cemented sandstone; fine-medium, subrounded, well sorted, quartz sand in a CO <sub>3</sub> cement; very similar to core above but this core is slightly finer-grained and strongly cemented with CO <sub>3</sub> ; well indurated; 2-3% opaque heavy minerals (may be glauconite); 1-2% fine-coarse muscovite; trace glauconite; strong reaction with HCl; massive; light olive gray to yellowish gray	Corehole	55	56
no recovery	no recovery	Corehole	56	60
sandstone	calcite-cemented sandstone; fine-medium, subrounded, well sorted, quartz sand in a CO <sub>3</sub> cement; very similar to core above but this core is slightly finer-grained and strongly cemented with CO <sub>3</sub> ; well indurated; 2-3% opaque heavy minerals (may be glauconite); 1-2% fine-coarse muscovite; trace glauconite; strong reaction with HCl; massive; light olive gray to yellowish gray; shark tooth noted	Corehole	60	61
no recovery	no recovery	Corehole	61	71
sand	sand and calcite-cemented sandstone; very fine-fine, subrounded, very well sorted, quartz sand; loose to well indurated where locally cemented with CO <sub>3</sub> ; 3-5% very fine-fine opaque heavy minerals; 1-2% fine-medium muscovite; weak to strong reaction with HCl, weak reaction where sediment is loose, strong reaction where sediment is cemented with CO <sub>3</sub> ; finely laminated, appears to be heavy mineral banding 0.5-1.0mm; loose sediment is light olive gray; cemented sediment is very light gray	Corehole	71	72
no recovery	no recovery	Corehole	72	81
sand	silty sand; very fine-fine, subrounded, very well sorted quartz sand in a 10-15% clay matrix; loose; 3-5% very fine-fine opaque heavy minerals; 1-2% fine-medium muscovite; massive; olive gray; weak reaction with HCl	Corehole	81	82



**SCDNR**  
SOUTH CAROLINA DEPARTMENT OF  
NATURAL RESOURCES

**SCGS**  
SOUTH CAROLINA  
GEOLOGICAL SURVEY



Project Name: Deep Soil Test Boring to Determine Shear  
Wave Velocities across South Carolina  
Client: SCDOT  
Location: Andrews, SC

Project ID: SPR-731  
Boring No.: B-FMG  
Geology Well ID: WIL-0358  
Tested By: Joe Gellici

LITHOLOGY_ID	UNIT_DESCRIPTION	OBS_METHOD	Depth (ft)	
			From	To
limestone	sandy, shelly limestone (biosparite); vuggy/moldic limestone; well indurated; 30-40% quartz sand; quartz is fine-medium cemented with CO <sub>3</sub> ; sparry-lined vugs; possible trace PO <sub>4</sub> ; bivalve shell fragments but core dominated by molds/casts; light olive gray; strong reaction with HCl	Corehole	82	83
no recovery	no recovery	Corehole	83	86
sand	silty sand; very fine-fine, subrounded, well sorted quartz sand in a 15-20% clay matrix; loose; 2-3% very fine-fine opaque heavy minerals; trace muscovite; 1-2mm sparse shell fragments; very weak reaction with HCl; massive; olive gray	Corehole	86	87
no recovery	no recovery	Corehole	87	96
sand	silty sand (same as above); very fine-fine, well sorted quartz sand in a 15-20% clay matrix; unconsolidated; very weak reaction with HCl; massive; olive gray	Corehole	96	98
no recovery	no recovery	Corehole	98	101
sand	clayey, silty sand; very fine-fine, rounded, very well sorted quartz sand in a 20-25% clay matrix; unconsolidated; 1-2% very fine-fine opaque heavy minerals; trace fine muscovite; massive; very weak reaction with HCl; olive gray	Corehole	101	102
sandstone	shelly sandstone; very fine-fine, well sorted quartz sand tightly cemented with CO <sub>3</sub> ; well indurated; 5-15% shell fragments; finely laminated, dark/light 0.5-2mm laminae; very light gray to light gray; string reaction with HCl	Corehole	102	103
no recovery	no recovery	Corehole	103	106
clay	interlaminated clay (60%) and sand (40%); silt and very fine-fine, very well sorted, quartz sand interlaminated/interbedded with sticky plastic dark organic-rich clay; unconsolidated; trace muscovite; 2-3% opaque heavy minerals; no reaction with HCl; bedding is convoluted in places; core appears burrowed; convoluted to lenticular bedding; sand lenses up to 15mm thick encased in clay; sand-filled burrows; sand is light olive gray, clay is olive black	Corehole	106	109
no recovery	no recovery	Corehole	109	111
clay	interlaminated clay (50%) and sand (50%); very similar to core above; very fine-fine, well sorted quartz sand interlaminated with dark, organic-rich clay; convoluted bedding structures; bioturbated; some of the sandier zones are cemented with CO <sub>3</sub> , otherwise the core is unconsolidated; sand occurs as laminations/beds that cut across width of core or as isolated lenses; trace muscovite; 2-3% opaque heavy minerals; weak to no reaction with HCl; increasing clay content with depth; picks up shell fragments; wisps of very thin shell fragments increase with depth; sand is light olive gray, clay is olive black	Corehole	111	116
sandstone	shelly sandstone; very fine-fine, well sorted quartz sand strongly cemented with CO <sub>3</sub> ; well indurated (very hard); strong reaction with HCl; casts of bivalves up to 18mm; thin (<1mm) white shell fragments occur locally and in trace amounts; moldic porosity is prominent toward the bottom of the core, molds are 2-10mm diameter; trace very fine-fine muscovite; core appears to be finely laminated (0.5-1mm) with alternating light and dark laminae, but this might be an artifact of the drilling operation; light gray (N7) to very light gray (N8)	Corehole	116	117
no recovery	no recovery	Corehole	117	121
sandstone	snappy sandstone (similar to above core); very fine-fine, well sorted quartz sand tightly cemented with CO <sub>3</sub> ; well indurated (very hard); trace muscovite; common white shell fragments (bivalves); local moldic porosity; outside surface of core appears "porket marked" with molds (voids) that are 1-10mm diameter; fossils appear to be bivalves; strong reaction with HCl; light gray to very light gray	Corehole	121	122
sand	sand; very fine-fine, subrounded, well sorted, quartz sand in a 5-10% clay matrix; trace fine muscovite; 3-5% very fine-fine opaque heavy minerals; no reaction with HCl; massive; heavies may be glauconite; olive black	Corehole	122	123
no recovery	no recovery	Corehole	123	125
sand	sand; very fine-fine, subrounded, well sorted, quartz sand in a 10-15% clay matrix; trace fine muscovite; 3-5% very fine-fine opaque heavy minerals; no reaction with HCl; massive; heavies may be glauconite; olive black	Corehole	125	126
no recovery	no recovery	Corehole	126	141



**SCDNR**  
SOUTH CAROLINA DEPARTMENT OF  
NATURAL RESOURCES

**SCGS**  
SOUTH CAROLINA  
GEOLOGICAL SURVEY



Project Name: Deep Soil Test Boring to Determine Shear  
Wave Velocities across South Carolina  
Client: SCDOT  
Location: Andrews, SC

Project ID: SPR-731  
Boring No.: B-FMG  
Geology Well ID: WIL-0358  
Tested By: Joe Gellici

LITHOLOGY_ID	UNIT_DESCRIPTION	OBS_METHOD	Depth (ft)	
			From	To
sand	clayey, silty sand; laminated; very fine-fine, well sorted quartz sand and silt in a 15-20% clay matrix; unconsolidated; 2-3% opaque heavy (VF) minerals; trace very fine muscovite; no reaction with HCl; faint light/dark laminations that are very irregular/convoluted possibly from bioturbation; olive black	Corehole	141	142
no recovery	no recovery	Corehole	142	146
sand	interlaminated sand and clay; very fine-fine, well sorted quartz sand interlaminated with silt and clay (70% sand, 30% clay); unconsolidated; 2-3% opaque heavies (VF); trace very fine muscovite; very little to no reaction with HCl; laminae are up to 10mm thick but they are very irregular; it is difficult to trace a lamination completely across width of core without being broken/disturbed; core appears to be highly burrowed (sand-filled); zone from 147-148ft is tightly cemented with CO3 (sandstone); strong reaction with HCl; sand is light gray, clay is olive black	Corehole	146	149
no recovery	no recovery	Corehole	149	151
clay	interlaminated sand, silt, and clay (60-70% clay and silt, 30-40% sand); very fine-fine, well sorted sand and silt interlaminated with carbonaceous clay; trace very fine muscovite and opaque heavy minerals; unconsolidated; very weak to no reaction with HCl; laminations are broken by sand-filled burrows; consoluted/distorted bedding possibly load structure; bedding appears to be similar to lenticular bedding where by very fine-fine sand is deposited in clay-dominated ripple troughs; the core is speckled with 1-20mm sand lenses and sand "blebs"; not much continuity to sand; some (or many) of the sand "layers" may be sand-filled burrows	Corehole	151	154
no recovery	no recovery	Corehole	154	156
clay	same as above; interlaminated sand, silt, and clay; very fine-fine, well sorted sand and silt interlaminated with carbonaceous clay; unconsolidated to poorly consolidated; weak reaction with HCl; reaction stronger in sand lenses; trace very fine muscovite and opaque heavy minerals; lenticular bedding, sand-filled burrows; clay is slightly plastic but also waxy in places; sand is light gray and clay is olive black	Corehole	156	159
no recovery	no recovery	Corehole	159	161
clay	calcareous, silty clay; silt and clay that is waxy and very finely laminated with light colored, paper-thin, very fine sand or bioclastic grains (possibly plankton); laminations are very thin and wispy (<0.5mm) and are seen running across the width of the core; cannot determine if these laminae are composed of sand or fossils; core has a weak to moderate reaction with HCl; core is moderately indurated; trace very fine/silt size muscovite; fine grained laminae are very light gray, clay/silt is medium dark gray (N4)	Corehole	161	163
no recovery	no recovery	Corehole	163	166
clay	calcareous, silty clay (marl); waxy, moderately indurated; local very fine to fine quartz or bioclastic lenses; trace very fine muscovite; moderate reaction with HCl in clay and fine-grain lenses; lenses are light gray, clay dark gray	Corehole	166	167
no recovery	no recovery	Corehole	167	168
clay	calcareous, silty clay; 10-15% very fine-fine quartz sand (possibly bioclastic fragments) in a calcareous, silty clay matrix; trace very fine muscovite; moderate reaction with HCl; ("marl"); olive black	Corehole	168	170
no recovery	no recovery	Corehole	170	171
clay	calcareous, silty clay; 10-15% very fine-fine, well sorted quartz sand (possibly also containing bioclastic fragments) in a calcareous clay matrix; moderately indurated; moderate reaction with HCl; trace very fine muscovite; common sand-filled burrows; lenticular bedding; sand-filled burrows and lenses are very gray (N8), clay is dark gray (N3)	Corehole	171	173
no recovery	no recovery	Corehole	173	176



**SCDNR**  
SOUTH CAROLINA DEPARTMENT OF  
NATURAL RESOURCES

**SCGS**  
SOUTH CAROLINA  
GEOLOGICAL SURVEY



Project Name: Deep Soil Test Boring to Determine Shear  
Wave Velocities across South Carolina  
Client: SCDOT  
Location: Andrews, SC

Project ID: SPR-731  
Boring No.: B-FMG  
Geology Well ID: WIL-0358  
Tested By: Joe Gellici

LITHOLOGY_ID	UNIT_DESCRIPTION	OBS_METHOD	Depth (ft)	
			From	To
clay	calcareous, silty clay ("marl"); 20-25% very fine-fine, well sorted quartz sand (may also contain bioclastic fragments) in a calcareous clay matrix; sand occurs as laminae and in sand-filled burrows; lenticular to wavy bedding, convoluted in places; laminae broken by sand-filled burrows; sandy zones locally weakly cemented with CO <sub>3</sub> ; moderately indurated; breaks at "sand" partings; appear to be crystals growing along parting surfaces; trace very fine muscovite; lignite fragments at top of core; dark yellowish orange (10YR6/6)	Corehole	176	179
clay	increasing clay downward; moderate reaction with HCl; sand lenses light gray (N7); clay/silt medium gray (N5) to dark gray (N3)	Corehole	179	181
clay	clay, dense, slightly plastic, carbonaceous clay, waxy texture towards bottom, weak reaction with HCl; massive; moderately indurated; dark gray to black (N1)	Corehole	181	182
clay	calcareous, silty clay ("marl"); 10-15% very fine-fine quartz sand (possibly bioclastic fragments) in a calcareous clay matrix; trace very fine muscovite; lenticular bedding; dark gray; weak reaction with HCl	Corehole	182	183
no recovery	no recovery	Corehole	183	186
clay	calcareous, sandy clay; 20-30%, very fine-fine, moderately sorted quartz sand in a calcareous clay matrix; trace very fine muscovite; 1-2% PO <sub>4</sub> ; 2-3% opaque, fine heavy minerals (might be PO <sub>4</sub> ); trace 2-4mm shell fragments; moderately indurated; lenticular to wavy bedding; sand-filled burrows; weak reaction with HCl; olive black (5Y2/1)	Corehole	186	188
sandstone	sandstone is very fine-fine quartz sand tightly cemented with CO <sub>3</sub> ; very strong reaction with HCl; very hard, well indurated; 3-5% thin shell fragments; light gray (N7)	Corehole	188	190
no recovery	no recovery	Corehole	190	191
sand	sand is very fine-fine, well sorted, quartz in a 20-25% clay matrix; trace very fine muscovite; trace PO <sub>4</sub> ; 2-3% opaque heavy minerals; no reaction with HCl; very loose; massive; greenish black (5G2/1)	Corehole	191	192
no recovery	no recovery	Corehole	192	196
sandstone	shelly sandstone; very fine-fine quartz sand strongly cemented with CO <sub>3</sub> ; trace very fine-fine muscovite; 5-10% shell fragments; salt/pepper specked appearance possibly due to opaque heavy minerals; very well indurated (very hard); faintly laminated; strong reaction with HCl; moldic porosity 3-5%; very light gray (N8) to light gray (N7)	Corehole	196	197
no recovery	no recovery	Corehole	197	200
sandstone	shelly sandstone; very fine-fine quartz sand strongly cemented with CO <sub>3</sub> ; trace very fine-fine muscovite; 5-10% shell fragments; salt/pepper specked appearance possibly due to opaque heavy minerals; very well indurated (very hard); faintly laminated; strong reaction with HCl; moldic porosity 3-5%; very light gray (N8) to light gray (N7)	Corehole	200	201
no recovery	no recovery	Corehole	201	210
sandstone	shelly sandstone; very fine-fine quartz sand strongly cemented with CO <sub>3</sub> ; trace very fine-fine muscovite; 5-10% shell fragments; salt/pepper specked appearance possibly due to opaque heavy minerals; very well indurated (very hard); faintly laminated; strong reaction with HCl; moldic porosity 3-5%; very light gray (N8) to light gray (N7)	Corehole	210	211
no recovery	no recovery	Corehole	211	215
clay	silty clay; carbonaceous, plastic clay; slightly calcareous; weak reaction with HCl; sand-filled burrows; moderately indurated (firm); dark gray (N3) to grayish black (N2)	Corehole	215	217
sandstone	shelly sandstone; very fine-fine quartz sand strongly cemented with CO <sub>3</sub> ; trace very fine-fine muscovite; 5-10% shell fragments (most appear to be bivalves); shell fragments range from 1-25mm but most are 5-15mm and most are thin, wispy fragments (bowl shaped); core is very well indurated (very hard); faintly and thinly laminated (<3mm); strong reaction with HCl; locally moldic; very light gray	Corehole	217	218
no recovery	no recovery	Corehole	218	221



**SCDNR**  
SOUTH CAROLINA DEPARTMENT OF  
NATURAL RESOURCES

**SCGS**  
SOUTH CAROLINA  
GEOLOGICAL SURVEY



Project Name: Deep Soil Test Boring to Determine Shear  
Wave Velocities across South Carolina  
Client: SCDOT  
Location: Andrews, SC

Project ID: SPR-731  
Boring No.: B-FMG  
Geology Well ID: WIL-0358  
Tested By: Joe Gellici

LITHOLOGY_ID	UNIT_DESCRIPTION	OBS_METHOD	Depth (ft)	
			From	To
sandstone	shaly sandstone; very fine-fine quartz sand strongly cemented with CO <sub>3</sub> ; trace very fine-fine muscovite; 5-10% shell fragments (most appear to be bivalves); shell fragments range from 1-25mm but most are 5-15mm and most are thin, wispy fragments (bowl shaped); core is very well indurated (very hard); faintly and thinly laminated (<3mm); strong reaction with HCl; locally moldic; very light gray	Corehole	221	222
sand	calcareous clayey sand; very fine-fine, well sorted silty quartz sand in a 25-30% calcareous clay matrix; unconsolidated (soft); trace very fine-fine muscovite, 10-15% fine-very coarse phosphate; massive; weak to moderate reaction HCl; olive black; phosphate component is very poorly sorted, ranging from fine to very coarse with one clast ~3mm in diameter, polished (glossy) clasts	Corehole	222	223
no recovery	no recovery	Corehole	223	226
sand	calcareous, clayey sand; very fine-fine, well sorted silty quartz sand in a 25-30% calcareous clay matrix; unconsolidated (soft); 1-2% very fine-fine muscovite, 10-15% fine-very coarse phosphate, phosphate coated bone fragments, shark tooth, trace shell fragments up to 7mm; weak to moderate reaction with HCl; massive; olive black; calcite-cemented sand clasts (5mm), common toward bottom of core	Corehole	226	229
no recovery	no recovery	Corehole	229	231
clay	clay to sandy clay; very fine-fine, very well sorted, silty quartz sand (10-20%) in an 80-90%, medium dense (firm) clay matrix; 1-2% very fine-fine muscovite; 2-3% very fine-fine opaque heavy minerals; massive to faintly laminated; olive gray (5Y3/2); no reaction with HCl; rare sand-filled burrow; clay increase with depth	Corehole	231	236
clay	clay to sandy clay; very fine-fine, very well sorted, silty quartz sand (10-20%) in an 80-90%, medium dense (firm) clay matrix; 1-2% very fine-fine muscovite; 2-3% very fine-fine opaque heavy minerals; massive to faintly laminated; olive gray (5Y3/2); rare sand-filled burrow; clay increase with depth; very weak reaction with HCl	Corehole	236	238
no recovery	no recovery	Corehole	238	241
clay	sandy clay; very fine-fine, well sorted, silty quartz sand (10-20%) in an 80-90% medium dense (firm) clay matrix; 1-2% very fine-fine muscovite; 2-3% very fine-fine opaque heavy minerals; massive to faintly laminated with minor sand-filled burrows; very weak reaction with HCl; olive gray (5Y3/2)	Corehole	241	243
no recovery	no recovery	Corehole	243	246
clay	calcareous, sandy clay; very fine-fine, well sorted, silty quartz sand (10-20%) in a dense (firm) clay matrix; 1-2% very fine-fine muscovite; 2-3% very fine-fine opaque heavy minerals; massive to faintly laminated with sand-filled burrows; very weak reaction with HCl; olive gray; large sand-filled burrow cuts across entire width of core at 246.1 ft with burrow 8mm wide by 55mm long	Corehole	246	249
no recovery	no recovery	Corehole	249	251
clay	calcareous, sandy clay; very fine-fine, well sorted, silty quartz sand (10-20%) in a dense (firm) clay matrix; 1-2% very fine-fine muscovite; 2-3% very fine-fine opaque heavy minerals; massive to faintly laminated with sand-filled burrows; very weak reaction with HCl; olive gray; large sand-filled burrow cuts across entire width of core at 246.1 ft with burrow 8mm wide by 55mm long	Corehole	251	253
no recovery	no recovery	Corehole	253	256
clay	calcareous, silty clay; soft sticky, plastic silty clay; massive; olive gray	Corehole	256	257
claystone	claystone-sandstone; very fine-fine, well sorted, silty quartz sand that is well-cemented with CO <sub>3</sub> ; well indurated (very hard); massive to faintly laminated; strong reaction with HCl; light olive gray (5Y5/2)	Corehole	257	258
no recovery	no recovery	Corehole	258	261



**SCDNR**  
SOUTH CAROLINA DEPARTMENT OF  
NATURAL RESOURCES

**SCGS**  
SOUTH CAROLINA  
GEOLOGICAL SURVEY



Project Name: Deep Soil Test Boring to Determine Shear  
Wave Velocities across South Carolina  
Client: SCDOT  
Location: Andrews, SC

Project ID: SPR-731  
Boring No.: B-FMG  
Geology Well ID: WIL-0358  
Tested By: Joe Gellici

LITHOLOGY_ID	UNIT_DESCRIPTION	OBS_METHOD	Depth (ft)	
			From	To
sand	clayey sand to sandy clay; calcareous, very fine-fine, well sorted, silty quartz sand (40-60%) in a clay matrix (40-60%); friable (can be broken by hand) but firm; 1-2% very fine-fine muscovite; 1-2% very fine-fine opaque heavy minerals; trace small (1-2mm) shell fragments; faintly laminated (appears to be lenticular bedding); moderate reaction with HCl; olive gray	Corehole	261	262
no recovery	no recovery	Corehole	262	266
sandstone	calcareous sandstone; very fine-fine, well sorted, silty quartz sand tightly cemented with CO <sub>3</sub> ; 1-2% very fine-fine muscovite; alternating light and dark laminae may be heavy minerals; well indurated (hard); some areas of core show very convoluted bedding structures possibly burrowed or loading structures; other areas show planar laminations (1-3mm); strong reaction with HCl; light gray (N7) to light olive gray (5Y5/2)	Corehole	266	267
clay	sandy clay; very fine-fine, well sorted quartz sand (30-40%) in a dense clay matrix; 1-2% very fine-fine muscovite; trace 1-2mm shell fragments; weak to moderate reaction with HCl; lenticular bedding; core is friable but firm; olive gray (5Y3/2)	Corehole	267	269
sandstone	calcareous sandstone; very fine-fine, well sorted, silty quartz sand tightly cemented with CO <sub>3</sub> ; 1-2% very fine-fine muscovite; alternating light and dark laminae may be heavy minerals; well indurated (hard); some areas of core show very convoluted bedding structures possibly burrowed or loading structures; other areas show planar laminations (1-3mm); strong reaction with HCl; light gray (N7) to light olive gray (5Y5/2)	Corehole	269	270
no recovery	no recovery	Corehole	270	271
clay	calcareous, sandy clay; very fine-fine, well sorted quartz sand (20-30%) in a dense clay matrix; friable (can be broken with hand) but firm; 1-2% very fine-fine muscovite; lenticular bedding; olive gray (5Y3/2); weak to moderate reaction with HCl	Corehole	271	274
no recovery	no recovery	Corehole	274	276
clay	calcareous, sandy clay (mostly clay); very fine-fine, well sorted silty quartz sand (10-20%) in a dense clay matrix; friable but firm; 1-2% very fine-fine muscovite; trace shell fragments up to 4mm; weak to moderate reaction with HCl; massive to faintly laminated; olive gray; lower part of core is similar to above but weakly cemented with CO <sub>3</sub> , core is slightly harder	Corehole	276	279
no recovery	no recovery	Corehole	279	281
clay	calcareous, sandy clay (mostly clay); very fine-fine, well sorted silty quartz sand (10-20%) in a dense clay matrix; friable but firm; 1-2% very fine-fine muscovite; weak to moderate reaction with HCl; massive to faintly laminated; olive gray	Corehole	281	284
no recovery	no recovery	Corehole	284	286
clay	calcareous, sandy clay (mostly clay); very fine-fine, well sorted, silty quartz sand (10-20%) in a dense clay matrix; friable but firm; 1-2% very fine-fine muscovite; weak to moderate reaction with HCl; sand-filled burrows; massive to faintly laminated; olive gray	Corehole	286	289
no recovery	no recovery	Corehole	289	291
clay	core is weakly to moderately cemented with CO <sub>3</sub> ; calcareous, sandy clay (mostly clay); very fine-fine, well sorted, silty quartz sand (10-20%) in a dense, weakly to moderately well cemented matrix; 1-2% very fine-fine muscovite; trace 1-2mm shell fragments; moderate to strong reaction with HCl; core is well indurated (hard) except toward the bottom 0.5 ft; massive to faintly laminated; olive gray; (claystone to sandstone)	Corehole	291	294
no recovery	no recovery	Corehole	294	296
clay	calcareous, sandy clay (mostly clay); very fine-fine, well sorted, silty quartz sand (10-20%) in a dense clay matrix; friable (can break with hand) but firm; 1-2% very fine-fine muscovite; 1-2% shell fragments (1-4mm); massive to faintly laminated; olive gray	Corehole	296	299
no recovery	no recovery	Corehole	299	301



**SCDNR**  
SOUTH CAROLINA DEPARTMENT OF  
NATURAL RESOURCES

**SCGS**  
SOUTH CAROLINA  
GEOLOGICAL SURVEY



Project Name: Deep Soil Test Boring to Determine Shear  
Wave Velocities across South Carolina  
Client: SCDOT  
Location: Andrews, SC

Project ID: SPR-731  
Boring No.: B-FMG  
Geology Well ID: WIL-0358  
Tested By: Joe Gellici

LITHOLOGY_ID	UNIT_DESCRIPTION	OBS_METHOD	Depth (ft)	
			From	To
clay	calcareous, sandy clay; very fine-fine, well sorted, silty quartz sand (10-20%) in a dense clay matrix; friable but moderately hard (can break with hand); 1-2% very fine-fine muscovite; trace shell fragments; massive to faintly laminated; olive gray; sand fraction appears to be concentrated in thin laminae and lenses, as opposed to being disseminated throughout core	Corehole	301	304
no recovery	no recovery	Corehole	304	306
clay	calcareous, sandy clay; very fine-fine, well sorted, silty quartz sand (20-30%) in a dense clay matrix; friable to moderately well indurated; core is weakly cemented with CO <sub>3</sub> and is hard in places; 1-2% very fine muscovite; moderate reaction with HCl; burrowed; olive gray	Corehole	306	309
no recovery	no recovery	Corehole	309	311
clay	calcareous, silty clay; dense, slightly plastic, hard clay containing 5-10% silt and very fine sand; trace 1-2mm shell fragments; trace very fine muscovite; weak reaction with HCl; massive; olive gray to grayish black (N2); less sand than section above	Corehole	311	313
no recovery	no recovery	Corehole	313	316
clay	calcareous, silty clay; dense, slightly plastic, hard clay containing 5-10% silt and very fine sand; trace 1-2mm shell fragments; trace very fine muscovite; weak reaction with HCl; massive; olive gray to grayish black (N2); less sand than section above	Corehole	316	319
no recovery	no recovery	Corehole	319	321
clay	calcareous, silty clay, dense clay containing 5-10% silt and very fine quartzs and moderate reaction with HCl; massive; olive gray; becomes increasingly sandier with depth (20-30%) and weakly cemented with CO <sub>3</sub>	Corehole	321	325
no recovery	no recovery	Corehole	325	326
clay	calcareous, sandy clay; very fine-fine, well sorted, silty quartz sand (10-20%) in a dense clay matrix; friable to moderately well indurated; trace very fine muscovite; moderate reaction with HCl; massive; olive gray; the cretaceous section can be classified as a "marl" consisting of a mixture of clay and lime mud, all cretaceous has reaction with HCl	Corehole	326	329
no recovery	no recovery	Corehole	329	331
clay	calcareous, silty clay; slightly sticky and slightly plastic, dense clay containing 5-10% silt; massive; olive gray; moderate reaction with HCl	Corehole	331	334
no recovery	no recovery	Corehole	334	336
clay	calcareous, silty clay; slightly waxy (shaves like a candle), dense clay containing 5-10% silt; massive; olive gray; moderate reaction with HCl	Corehole	336	339
no recovery	no recovery	Corehole	339	341
clay	calcareous, silty clay; waxy, dense clay with 5-10% silt; massive; olive gray; weak to moderate reaction with HCl	Corehole	341	344
no recovery	no recovery	Corehole	344	346
clay	calcareous, sandy clay; very fine-fine, well sorted, silty quartz sand (10-20%) in a dense, calcareous clay matrix; moderate to strong reaction with HCl; friable to moderately well indurated; hard zones are weakly cemented with CO <sub>3</sub> ; burrowed in places; olive gray	Corehole	346	349
no recovery	no recovery	Corehole	349	351
clay	calcareous, silty clay; waxy, dense clay containing 5-10% silt; friable but very firm; massive to very faintly laminated; weak reaction with HCl; olive gray	Corehole	351	354
no recovery	no recovery	Corehole	354	356
clay	calcareous, silty clay; waxy dense clay containing 5-10% silt; friable (can break by hand) but firm (hard); massive to very faintly laminated; weak reaction with HCl; olive gray	Corehole	356	359
no recovery	no recovery	Corehole	359	361
clay	calcareous, sandy clay; very fine-fine, well sorted quartz sand (30-40%) in a dense, calcareous clay matrix; upper 0.5 ft is well cemented with CO <sub>3</sub> ; core is friable but firm; trace very fine muscovite; trace 1-2mm shell fragments; massive to faintly laminated; sand-filled burrows; light olive gray (5Y5/2) to olive gray (5Y3/2); moderate to strong reaction with HCl; sandier with depth	Corehole	361	363
no recovery	no recovery	Corehole	363	366



**SCDNR**  
SOUTH CAROLINA DEPARTMENT OF  
NATURAL RESOURCES

**SCGS**  
SOUTH CAROLINA  
GEOLOGICAL SURVEY



Project Name: Deep Soil Test Boring to Determine Shear  
Wave Velocities across South Carolina  
Client: SCDOT  
Location: Andrews, SC

Project ID: SPR-731  
Boring No.: B-FMG  
Geology Well ID: WIL-0358  
Tested By: Joe Gellici

LITHOLOGY_ID	UNIT_DESCRIPTION	OBS_METHOD	Depth (ft)	
			From	To
clay	calcareous, sandy clay; very fine-medium, moderately-well sorted quartz sand (40-50%) in a dense calcareous clay matrix, weakly cemented with CO <sub>3</sub> ; moderately well indurated (hard); trace very fine muscovite; trace green mineral (glauconite?); possibly trace PO <sub>4</sub> ; trace 1-3mm shell fragments; massive; olive gray; lower part of core- calcareous, clayey sand, fine-coarse, moderately sorted quartz sand in a 20-30% clay matrix; unconsolidated; strong reaction with HCl, 3-5% PO <sub>4</sub> , trace muscovite, shell fragments up to 20mm, massive, chaotic structure, light olive gray	Corehole	366	369
no recovery	no recovery	Corehole	369	371
sand	calcareous, clayey sand; fine-coarse, moderately sorted quartz sand in a 20-30% calcareous clay matrix; unconsolidated; 2-3% PO <sub>4</sub> ; trace muscovite; trace shell fragments; strong reaction with HCl; massive; light olive gray; may be a lag bed	Corehole	371	374
no recovery	no recovery	Corehole	374	376
sand	calcareous, clayey sand; fine-coarse, moderately sorted quartz sand in a 20-30% calcareous clay matrix; unconsolidated; 2-3% PO <sub>4</sub> ; trace muscovite; trace shell fragments; strong reaction with HCl; massive; light olive gray; may be a lag bed; hard from CO <sub>3</sub> cement	Corehole	376	378
no recovery	no recovery	Corehole	378	381
sand	calcareous, clayey sand to sandy clay; very fine-medium, moderately sorted quartz sand in a dense calcareous matrix; friable but firm; 50% sand and 50% clay; 1-2% dark minerals that appear to be PO <sub>4</sub> ; moderate reaction with HCl; massive; light olive gray to olive gray	Corehole	381	384
no recovery	no recovery	Corehole	384	386
clay	laminated calcareous, silty clay; dense clay interlaminated with silt; silt laminae are 0.5-1mm; core break along the silt laminae (silt partings) and has "poker-chip" appearance; 1-2% very fine muscovite in the silt laminae; moderate reaction with HCl in clay and strong reaction in silt; clay is grayish black (N2) and silt is light gray (N7)	Corehole	386	390
no recovery	no recovery	Corehole	390	391
clay	laminated calcareous, silty clay; dense clay interlaminated with silt; silt laminae are 0.5-1mm; core break along the silt laminae (silt partings) and has "poker-chip" appearance; 1-2% very fine muscovite in the silt laminae; moderate reaction with HCl in clay and strong reaction in silt; clay is grayish black (N2) and silt is light gray (N7); predominantly clay ~90%	Corehole	391	394
no recovery	no recovery	Corehole	394	396
clay	laminated, calcareous silt and clay; predominantly clay (90%); silt laminae 0.5-1mm; 1-2% very fine muscovite (or possibly other mica) in silt layers; moderate reaction with HCl in clay and strong reaction in silt; clay is grayish black and silt is light gray	Corehole	396	399
no recovery	no recovery	Corehole	399	401
clay	laminated calcareous silt and clay (clay~80%); 1-2% very fine muscovite (or other mica) occurs in silt laminae; moderate reaction with HCl in clay layers, strong reaction with HCl in silt layers; friable (can break with hand) but firm; silt laminae are very irregular; they have a 'blotchy' appearance; some may be silt-filled burrows; silt laminae appear to be disrupted and are not always continuous across width of core; clay grayish black (N2), silt light gray (N7)	Corehole	401	403
no recovery	no recovery	Corehole	403	406
clay	laminated calcareous silt and clay (clay~80%); 1-2% very fine muscovite (or other mica) occurs in silt laminae; moderate reaction with HCl in clay layers, strong reaction with HCl in silt layers; friable (can break with hand) but firm; silt laminae are very irregular; they have a 'blotchy' appearance; some may be silt-filled burrows; silt laminae appear to be disrupted and are not always continuous across width of core; clay grayish black (N2), silt light gray (N7)	Corehole	406	409
no recovery	no recovery	Corehole	409	411



**SCDNR**  
SOUTH CAROLINA DEPARTMENT OF  
NATURAL RESOURCES

**SCGS**  
SOUTH CAROLINA  
GEOLOGICAL SURVEY



Project Name: Deep Soil Test Boring to Determine Shear  
Wave Velocities across South Carolina  
Client: SCDOT  
Location: Andrews, SC

Project ID: SPR-731  
Boring No.: B-FMG  
Geology Well ID: WIL-0358  
Tested By: Joe Gellici

LITHOLOGY_ID	UNIT_DESCRIPTION	OBS_METHOD	Depth (ft)	
			From	To
clay	calcareous, sandy clay; very fine, well sorted, quartz sand and silt (30-40%) in a dense clay matrix; 1-2% very fine muscovite, 1-2% opaque heavy minerals; core is friable to loose in spots; silt and sand occurs as laminae and lenses; sand-filled burrows; clay is olive gray (5Y3/2) and silt/sand is light olive gray (5Y5/2); moderate reaction with HCl	Corehole	411	414
no recovery	no recovery	Corehole	414	416
clay	calcareous, sandy clay; very fine, well sorted, quartz sand and silt (20-30%) in a dense clay matrix; 2-3% very fine muscovite; friable but firm; silt and sand occur as irregular laminae and lenses; silt and sand-filled burrows; moderate reaction with HCl	Corehole	416	419
no recovery	no recovery	Corehole	419	421
clay	calcareous, sandy clay; very fine, well sorted, quartz sand and silt (20-30%) in a dense clay matrix; 2-3% very fine muscovite; friable but firm; silt and sand occur as irregular laminae and lenses; silt and sand-filled burrows; moderate reaction with HCl	Corehole	421	424
no recovery	no recovery	Corehole	424	426
clay	calcareous, sandy clay; very fine-fine, well sorted, silty quartz sand (20-30%) in a dense clay matrix; 1-2% very fine-fine muscovite; moderate reaction with HCl; friable but firm; silt and sand occur as irregular lenses and laminae and sand-filled burrows; clay olive gray and silt/sand light olive gray	Corehole	426	429
no recovery	no recovery	Corehole	429	431
clay	calcareous, sandy clay; very fine-fine, well sorted, silty quartz sand (20-30%) in a dense clay matrix; 1-2% very fine-fine muscovite; moderate reaction with HCl; friable but firm; silt and sand occur as irregular lenses and laminae and sand-filled burrows; clay olive gray and silt/sand light olive gray	Corehole	431	433
no recovery	no recovery	Corehole	433	436
clay	calcareous, sandy clay; very fine-fine, well sorted, silty quartz sand (20-30%) in a dense clay matrix; 1-2% very fine-fine muscovite; moderate reaction with HCl; friable but firm; silt and sand occur as irregular lenses and laminae and sand-filled burrows; clay olive gray and silt/sand light olive gray; increasing clay content with depth	Corehole	436	439
no recovery	no recovery	Corehole	439	441
clay	calcareous, sandy clay; very fine-fine, well sorted, silty, quartz sand (10-20%) in a dense clay matrix; 1-2% very fine muscovite; moderate to strong reaction with HCl; friable but firm; bottom 0.5 ft weakly cemented with CO3; increasing sand toward bottom of core; most of the sand and silt occurs as irregular laminae lenses, and sand-filled burrows; olive gray (5Y3/2)	Corehole	441	444
no recovery	no recovery	Corehole	444	446
clay	calcareous, sandy clay (more sand than core above); very fine-fine, well sorted, silty, quartz sand (30-40%) in a dense clay matrix; friable to loose in spots; 1-2% very fine muscovite; strong reaction with HCl; massive to faintly laminated, sand-filled burrows; olive gray to light olive gray	Corehole	446	449
no recovery	no recovery	Corehole	449	451
clay	calcareous, sandy clay; very fine-fine, well sorted, silty, quartz sand (10-20%) in a dense clay matrix; 1-2% very fine muscovite; moderate to strong reaction with HCl; friable but firm; sand and silt occur as irregular laminae, lenses and sand-filled burrows; olive gray	Corehole	451	454
no recovery	no recovery	Corehole	454	456
clay	calcareous, sandy clay; very fine-fine, well sorted, silty, quartz sand (10-20%) in a dense clay matrix; 1-2% very fine muscovite; moderate to strong reaction with HCl; friable but firm; sand and silt occur as irregular laminae, lenses and sand-filled burrows; olive gray	Corehole	456	459
no recovery	no recovery	Corehole	459	461



**SCDNR**  
SOUTH CAROLINA DEPARTMENT OF  
NATURAL RESOURCES

**SCGS**  
SOUTH CAROLINA  
GEOLOGICAL SURVEY



Project Name: Deep Soil Test Boring to Determine Shear  
Wave Velocities across South Carolina  
Client: SCDOT  
Location: Andrews, SC

Project ID: SPR-731  
Boring No.: B-FMG  
Geology Well ID: WIL-0358  
Tested By: Joe Gellici

LITHOLOGY_ID	UNIT_DESCRIPTION	OBS_METHOD	Depth (ft)	
			From	To
clay	calcareous, sandy clay; very fine-fine, well sorted, silty, quartz sand (10-20%) in a dense clay matrix; 1-2% very fine muscovite; moderate to strong reaction with HCl; friable but firm; sand and silt occur as irregular laminae, lenses and sand-filled burrows; olive gray	Corehole	461	463
no recovery	no recovery	Corehole	463	466
clay	calcareous, sandy clay; very fine-fine, well sorted, silty, quartz sand (20-40%) in a dense clay matrix; friable to firm; 1-2% very fine muscovite; sections of the core display very convoluted bedding structures; has a 'blotchy' look to it possibly from burrows; sandier zone are weakly cemented with CO <sub>3</sub> , have a strong reaction with HCl, and are moderately to well indurated; sandy zones very light gray (N8), clay olive gray	Corehole	466	469
no recovery	no recovery	Corehole	469	471
clay	calcareous, sandy clay; very fine-fine, well sorted, silty, quartz sand (20-40%) in a dense clay matrix; friable to firm; 1-2% very fine muscovite; sections of the core display very convoluted bedding structures; has a 'blotchy' look to it possibly from burrows; sandier zone are weakly cemented with CO <sub>3</sub> , have a strong reaction with HCl, and are moderately to well indurated; sandy zones very light gray (N8), clay olive gray	Corehole	471	472
clay	shelly, silty clay; hard, dense, waxy silty clay; up to 10% shell fragments in places, trace very fine muscovite, trace PO <sub>4</sub> ; weak to strong reaction with HCl; strong where shell fragments are concentrated; core is moderately indurated and breaks along bedding planes where shell fragments are concentrated; most shell fragments are small (1-4mm) but can be up to 12mm; clay is dark gray (N3)	Corehole	472	474
no recovery	no recovery	Corehole	474	476
clay	shelly, silty clay; hard, dense, waxy, silty clay containing 0-40% shell fragments; fragments up to 13mm but most are 1-4mm; trace very fine muscovite; weak to strong reaction with HCl; sand/silt-filled burrows and convoluted laminae; some of these sandy/silty zones are weakly cemented with CO <sub>3</sub> ; clay dark gray, shell fragments white (N9) to very light gray (N8)	Corehole	476	479
no recovery	no recovery	Corehole	479	481
clay	shelly, silty clay; hard, dense, waxy, silty clay containing 0-40% shell fragments; fragments up to 13mm but most are 1-4mm; trace very fine muscovite; weak to strong reaction with HCl; sand/silt-filled burrows and convoluted laminae; some of these sandy/silty zones are weakly cemented with CO <sub>3</sub> ; clay dark gray, shell fragments white (N9) to very light gray (N8)	Corehole	481	484
no recovery	no recovery	Corehole	484	486
clay	shelly, silty clay; hard, dense, waxy, silty clay containing 0-40% shell fragments; fragments up to 13mm but most are 1-4mm; trace very fine muscovite; weak to strong reaction with HCl; sand/silt-filled burrows and convoluted laminae; some of these sandy/silty zones are weakly cemented with CO <sub>3</sub> ; clay dark gray, shell fragments white (N9) to very light gray (N8)	Corehole	486	489
no recovery	no recovery	Corehole	489	491
clay	silty clay; silty, waxy clay; trace very fine muscovite, trace shell fragments; core is friable but firm; very silty core possibly up to 50% silt in places; appears to be finely (0.5-1mm) interlaminated with silt and clay; less shell fragments than section above and core is not as dense; large bivalve shell (20mm) at 491.8 ft; olive gray to light olive gray; core has weak reaction with HCl	Corehole	491	494
no recovery	no recovery	Corehole	494	496
clay	silty clay; silty, waxy clay; trace very fine muscovite, trace shell fragments; core is friable but firm; very silty core possibly up to 50% silt in places; appears to be finely (0.5-1mm) interlaminated with silt and clay; less shell fragments than section above and core is not as dense; large bivalve shell (20mm) at 491.8 ft; olive gray to light olive gray; core has weak reaction with HCl	Corehole	496	499
no recovery	no recovery	Corehole	499	501



**SCDNR**  
SOUTH CAROLINA DEPARTMENT OF  
NATURAL RESOURCES

**SCGS**  
SOUTH CAROLINA  
GEOLOGICAL SURVEY



Project Name: Deep Soil Test Boring to Determine Shear  
Wave Velocities across South Carolina  
Client: SCDOT  
Location: Andrews, SC

Project ID: SPR-731  
Boring No.: B-FMG  
Geology Well ID: WIL-0358  
Tested By: Joe Gellici

LITHOLOGY_ID	UNIT_DESCRIPTION	OBS_METHOD	Depth (ft)	
			From	To
clay	clay; tight, slightly plastic clay; friable but firm; trace very fine muscovite disseminated throughout core; locally silty; grayish black (N7); weak reaction with HCl	Corehole	501	504
no recovery	no recovery	Corehole	504	506
clay	clay; tight, slightly plastic clay; friable but firm; trace very fine muscovite disseminated throughout core; locally silty; grayish black (N7); weak reaction with HCl	Corehole	506	508
clay	calcareous, sandy clay; very fine, well sorted, silty quartz sand (10-20%) in a dense clay matrix; friable but hard; clay has a waxy texture; trace very fine muscovite, trace shell fragments; massive to faintly laminated; weak reaction with HCl; dark gray (N3)	Corehole	508	509
no recovery	no recovery	Corehole	509	511
clay	calcareous, sandy clay- same as above; sandier zones occur as irregular laminae, lenses, and sand-filled burrows; these zones react strongly with HCl; clay layers react weakly with HCl	Corehole	511	514
no recovery	no recovery	Corehole	514	516
clay	calcareous, sandy clay; very fine-medium, well sorted, quartz sand (10-40%) in a dense clay matrix; trace very fine muscovite, trace shell fragments; friable but firm; massive to faintly laminated; sand-filled burrows; moderate reaction with HCl; olive gray	Corehole	516	519
no recovery	no recovery	Corehole	519	521
sandstone	sandstone; very fine-medium, quartz sand well-cemented with CO <sub>3</sub> ; locally abundant shell fragments; well-indurated (very hard); thinly laminated (planar) to very convoluted bedding at base of interval; strong reaction with HCl; very light gray (N8) to medium light gray (N6)	Corehole	521	522
sand	calcareous, clayey sand; fine-medium, moderately sorted quartz sand in a 20-30% calcareous clay matrix; 3-5% dark opaque minerals, some of which appear to be PO <sub>4</sub> (one grain was 3mm long); trace shell fragments; trace muscovite; greenish hue may be due to presence of glauconite; core is unconsolidated and massive; strong reaction with HCl; olive gray	Corehole	522	524
no recovery	no recovery	Corehole	524	526
sand	calcareous, clayey sand; fine-medium, moderately sorted quartz sand in a 20-30% calcareous clay matrix; 3-5% dark opaque minerals, some of which appear to be PO <sub>4</sub> (one grain was 3mm long); trace shell fragments; trace muscovite; greenish hue may be due to presence of glauconite; core is unconsolidated and massive; strong reaction with HCl; olive gray; increasing clay content with depth	Corehole	526	529
no recovery	no recovery	Corehole	529	531
clay	sandy clay; very fine-fine, well sorted, silty, quartz sand (30-40%) in a dense clay matrix; weak reaction with HCl; 2-3% very fine opaque heavy minerals; locally abundant shell fragments; friable but firm; massive to faintly laminated; sand-filled burrows; olive gray	Corehole	531	534
no recovery	no recovery	Corehole	534	536
clay	sandy clay; very fine-fine, well sorted, silty, quartz sand (30-40%) in a dense clay matrix; weak reaction with HCl; 2-3% very fine opaque heavy minerals; locally abundant shell fragments; friable but firm; massive to faintly laminated; sand-filled burrows; olive gray	Corehole	536	539
no recovery	no recovery	Corehole	539	541
clay	sandy clay; very fine-fine, well sorted, silty, quartz sand (30-40%) in a dense clay matrix; weak reaction with HCl; 2-3% very fine opaque heavy minerals; locally abundant shell fragments; friable but firm; massive to faintly laminated; sand-filled burrows; olive gray; increasing sand content with depth	Corehole	541	544
no recovery	no recovery	Corehole	544	546



**SCDNR**  
SOUTH CAROLINA DEPARTMENT OF  
NATURAL RESOURCES

**SCGS**  
SOUTH CAROLINA  
GEOLOGICAL SURVEY



Project Name: Deep Soil Test Boring to Determine Shear  
Wave Velocities across South Carolina  
Client: SCDOT  
Location: Andrews, SC

Project ID: SPR-731  
Boring No.: B-FMG  
Geology Well ID: WIL-0358  
Tested By: Joe Gellici

LITHOLOGY_ID	UNIT_DESCRIPTION	OBS_METHOD	Depth (ft)	
			From	To
sand	calcareous, clayey sand; very fine-fine (mostly fine), well sorted quartz sand in a 20-30% clay matrix; 5-7% very fine-fine dark opaque minerals difficult to determine if these are PO4, glauconite, or heavy minerals; however, there are some larger grains (up to 2mm) that are definitely PO4; trace muscovite; weak reaction with HCl; friable to loose; convoluted laminations; olive gray to light olive gray	Corehole	546	548
no recovery	no recovery	Corehole	548	551
sandstone	sandstone; very fine-fine quartz sand tightly cemented with CO3; moderate to strong reaction with HCl; well indurated (very hard); appears to be thinly laminated (<3mm); has a 'salt and pepper' look; medium dark gray (N4) and very light gray (N8)	Corehole	551	552
no recovery	no recovery	Corehole	552	556
sandstone	sandstone; very fine-fine quartz sand tightly cemented with CO3; moderate to strong reaction with HCl; well indurated (very hard); appears to be thinly laminated (<3mm); has a 'salt and pepper' look; medium dark gray (N4) and very light gray (N8); trace local shell fragments	Corehole	556	557
no recovery	no recovery	Corehole	557	566
sandstone	sandstone; very fine-fine quartz sand tightly cemented with CO3; moderate to strong reaction with HCl; well indurated (very hard); appears to be thinly laminated (<3mm); has a 'salt and pepper' look; medium dark gray (N4) and very light gray (N8)	Corehole	566	567
no recovery	no recovery	Corehole	567	571
sand	clayey sand; very fine-medium, well sorted quartz sand in a 20-30% clay matrix; friable to loose; 3-5% dark opaque minerals (could be glauconite), trace muscovite; little to no reaction with HCl; massive; olive gray	Corehole	571	573
no recovery	no recovery	Corehole	573	576
sand	clayey sand; very fine-fine, well sorted quartz sand in a 30-40% clay matrix; friable to loose; 3-5% very fine-fine dark opaque minerals (could be glauconite), trace muscovite; little to no reaction with HCl; massive; olive gray	Corehole	576	578
no recovery	no recovery	Corehole	578	581
sand	clayey sand; very fine-fine, well sorted quartz sand in a 30-40% clay matrix; friable to loose; 3-5% very fine-fine dark opaque minerals (could be glauconite), trace muscovite; little to no reaction with HCl; massive; olive gray	Corehole	581	582
sandstone	sandstone; very fine-fine, well sorted quartz sand tightly cemented with CO3; well indurated (very hard); locally shelly, trace very fine-fine muscovite; convoluted bedding structures, appear to be clay drapes/laminae that are not well cemented, interlaminated with sand that is well cemented; 'salt and pepper' look; very light gray to medium dark gray; strong reaction with HCl	Corehole	582	583
no recovery	no recovery	Corehole	583	586
sandstone	sandstone; very fine-fine, well sorted quartz sand tightly cemented with CO3; well indurated (very hard); locally shelly, trace very fine-fine muscovite; convoluted bedding structures, appear to be clay drapes/laminae that are not well cemented, interlaminated with sand that is well cemented; 'salt and pepper' look; very light gray to medium dark gray; strong reaction with HCl	Corehole	586	587
clay	calcareous, sandy clay; very fine-fine, well sorted quartz sand (10-20%) in a dense, plastic clay matrix; trace muscovite; friable but firm; sand-filled burrows; grayish black (N2); weak reaction with HCl	Corehole	587	588
no recovery	no recovery	Corehole	588	591
clay	interlaminated sand and clay (mostly clay); very fine, well sorted quartz sand interlaminated with silty clay; friable, breaks at sand partings; core is about 70-80% clay and 20-30% sand; 1-2% very fine muscovite in sand layers; little to no reaction with HCl; clay is dark gray (N3) and sand is slight gray (N7)	Corehole	591	592
no recovery	no recovery	Corehole	592	595
clay	interlaminated sand and clay (mostly clay); very fine, well sorted quartz sand interlaminated with silty clay; friable, breaks at sand partings; core is about 70-80% clay and 20-30% sand; 1-2% very fine muscovite in sand layers; little to no reaction with HCl; clay is dark gray (N3) and sand is slight gray (N7)	Corehole	595	596



**SCDNR**  
SOUTH CAROLINA DEPARTMENT OF  
NATURAL RESOURCES

**SCGS**  
SOUTH CAROLINA  
GEOLOGICAL SURVEY



Project Name: Deep Soil Test Boring to Determine Shear  
Wave Velocities across South Carolina  
Client: SCDOT  
Location: Andrews, SC

Project ID: SPR-731  
Boring No.: B-FMG  
Geology Well ID: WIL-0358  
Tested By: Joe Gellici

LITHOLOGY_ID	UNIT_DESCRIPTION	OBS_METHOD	Depth (ft)	
			From	To
sand	sand bed; consists of medium-coarse, moderately to well sorted; loose; glauconitic sand; glauconite 20-30%, trace muscovite; no reaction with HCl; dark greenish gray (SGY4/1)	Corehole	596	597
clay	interlaminated sand and clay (mostly clay); very fine, well sorted quartz sand interlaminated with silty clay; friable, breaks at sand partings; core is about 70-80% clay and 20-30% sand; 1-2% very fine muscovite in sand layers; little to no reaction with HCl; clay is dark gray (N3) and sand is slight gray (N7)	Corehole	597	599
no recovery	no recovery	Corehole	599	601
sand	interlaminated/interbedded sand and clay; very fine-fine, well sorted quartz sand interlaminated/interbedded with clay; unconsolidated (loose); trace muscovite; 10-15% opaque minerals which appear to be glauconite (sands have an overall green coloration); local bivalve shell fragments up to 10mm; very little to no reaction with HCl except where shell fragments occur; core is ~ 60 % sand and 40% clay; beds are up to 20mm thick; massive in spots; dark greenish gray	Corehole	601	602
no recovery	no recovery	Corehole	602	606
sand	interlaminated/interbedded sand and clay; very fine-fine, well sorted quartz sand interlaminated/interbedded with clay; unconsolidated (loose); trace muscovite; 10-15% opaque minerals which appear to be glauconite (sands have an overall green coloration); local bivalve shell fragments up to 10mm; very little to no reaction with HCl except where shell fragments occur; core is ~ 60 % sand and 40% clay; beds are up to 20mm thick; massive in spots; dark greenish gray	Corehole	606	607
no recovery	no recovery	Corehole	607	611
sand	interlaminated/interbedded sand and clay; very fine-fine, well sorted quartz sand interlaminated/interbedded with clay; unconsolidated (loose); trace muscovite; 10-15% opaque minerals which appear to be glauconite (sands have an overall green coloration); local bivalve shell fragments up to 10mm; very little to no reaction with HCl except where shell fragments occur; core is ~ 60 % sand and 40% clay; beds are up to 20mm thick; massive in spots; dark greenish gray	Corehole	611	612
no recovery	no recovery	Corehole	612	616

## Appendix E: Index Testing Results

---



**University of South Carolina**  
 Department of Civil and Environmental Engineering  
 Project Name: Deep Soil Test Boring to Determine Shear  
 Wave Velocities across South Carolina

Client: SCDOT  
 Project ID: SPR-731  
 Boring No.: B-CON  
 Location: Conway, SC

Sample #	Depth (ft)		$\omega_{lab}$ (%)	Fine Content (%)	LL (%)	PL (%)	PI (%) <i>np - nonplastic</i>	USCS / Rock Type	ASSHTO	
	From	To								
C-SS-1	1	0.0	2.0	9.8	10.8	-	-	np	SC-SM	A-1-a
C-SS-2	2	2.0	4.0	13.2	8.0	-	-	np	SC-SM	A-3
C-SS-3	3	4.0	6.0	17.0	44.0					A-4
C-SS-4	4	6.0	8.0	16.8	39.0	27	12	15	SC	A-6 (2)
C-SS-5	5	8.0	10.0	31.3	90.0	37	17	20	CL	A-6 (18)
C-UD-1	1	10.0	12.5	43.4	95.1	51	23	28	CH	A-7-6 (30)
C-SS-6	6	12.5	14.5	50.5	90.0	38	26	12	ML	A-6 (12)
C-UD-2	2	14.5	17.0		8.0	-	-	-	SC-SM	
C-SS-7	7	17.0	19.0	40.2	37.6	25	20	5	SC-SM	A-4
C-SS-8	8	19.0	21.0	24.3	31.6	-	-	np	SM	A-2-4
C-SS-9	9	21.0	23.0	21.9	18.0	-	-	np	SM	A-1-b
C-SS-10	10	23.0	25.0	29.3	22.0	-	-	np	SM	A-1-b
C-SS-11	11	25.0	27.0	37.6	29.0	-	-	np	SM	A-2-4
C-SS-12	12	27.0	29.0	34.7	26.0	-	-	np	SM	A-2-4
C-SS-13	13	29.0	31.0	57.4	49.0	-	-	np	SM	A-4
C-SS-14	14	31.0	33.0	52.8	41.0	-	-	np	SM	A-4
C-SS-15	15	33.0	35.0	37.2	30.8	-	-	np	SM	A-2-4
C-SS-16	16	35.0	37.0	24.9	14.0	-	-	np	SM	A-1-a
C-SS-17	17	37.0	39.0	26.8	8.4	-	-	-	SC-SM	
C-SS-18	18	39.0	41.0	20.6	19.0	32	27	5	SM	A-1-b
C-SS-19	19	41.0	43.0	32.9	7.6	-	-	-	SC-SM	
C-SS-20	20	43.0	45.0	21.8	9.2	-	-	-	SC-SM	
C-SS-21	21	45.0	47.0	22.0	18.0	-	-	np	SM	A-1-b
C-SS-22	22	47.0	49.0	17.5	33.0	-	-	np	SM	A-2-4
C-SS-23	23	49.0	51.0	24.8	35.0	20	17	3	SM	A-2-4
C-SS-24	24	51.0	53.0	28.4	31.0	-	-	np	SM	A-2-4
C-SS-25	25	53.0	55.0	37.3	94.2	58	32	26	MH	A-7-5 (30)
C-UD-3	3	55.0	57.5	35.3	91.6	68	24	44	CH	A-7-6 (45)
C-UD-4	4	57.5	60.0							
C-SS-26	26	60.0	62.0	34.5	97.0	66	35	31	MH	A-7-5 (38)
C-SS-27	27	62.0	64.0	34.9	96.0	59	28	31	CH	A-7-6 (35)
C-SS-28	28	64.0	66.0	35.6	93.8	58	35	23	MH	A-7-5 (27)
C-SS-29	29	66.0	68.0	34.3	82.6	50	44	6	MH	A-5 (9)
C-SS-30	30	68.0	70.0	38.2	98.2	62	36	26	MH	A-7-5 (33)
C-SS-31	31	70.0	72.0	38.7	96.0	63	35	28	MH	A-7-5 (34)
C-UD-5	5	72.0	74.5							
C-UD-6	6	74.5	77.0							
C-SS-32	32	77.0	79.0	30.1	85.0	43	31	12	ML	A-7-5 (12)
C-SS-33	33	79.0	81.0	30.3	88.8	47	27	20	ML	A-7-6 (20)
C-SS-34	34	81.0	83.0	32.9	92.0	46	23	23	CL	A-7-6 (23)
C-UD-7	7	83.0	85.5	40.7	87.0	68	25	43	CH	A-7-6 (41)
C-UD-8	8	85.5	88.0	42.6	93.8	74	27	47	CH	A-7-6 (51)
C-SS-35	35	88.0	90.0	30.2	91.6	55	33	22	MH	A-7-5 (25)
C-UD-9	9	90.0	94.0							
C-SS-36	36	94.0	96.0	32.1	96.0	57	35	22	MH	A-7-5 (27)



**University of South Carolina**  
 Department of Civil and Environmental Engineering  
 Project Name: Deep Soil Test Boring to Determine Shear  
 Wave Velocities across South Carolina

Client: SCDOT  
 Project ID: SPR-731  
 Boring No.: B-CON  
 Location: Conway, SC

Sample #	Depth (ft)		$\omega_{lab}$ (%)	Fine Content (%)	LL (%)	PL (%)	PI (%) <i>np - nonplastic</i>	USCS / Rock Type	ASSHTO
	From	To							
C-SS-37	96.0	98.0	33.9	93.0	53	33	20	MH	A-7-5 (23)
C-SS-38	98.0	100.0	34.6	88.0	51	28	23	CH	A-7-6 (23)
C-SS-39	100.0	102.0	27.0	86.0	51	30	21	MH	A-7-6 (21)
C-SS-40	102.0	104.0	32.0	92.6	47	29	18	ML	A-7-6 (20)
N/A	104	106.5	-	-	-	-	-	No Sample	
C-SS-41	106.5	108.5	29.2	92.0	43	25	18	CL	A-7-6 (18)
C-SS-42	108.5	110.5	31.1	88.0	46	23	23	CL	A-7-6 (22)
C-SS-43	110.5	112.5	13.4	81.0	33	25	8	ML	A-4
C-SS-44	112.5	114.5	19.3	58.2	34	18	16	CL	A-6 (7)
N/A	114.5	119.2	-	-	-	-	-	No Sample	
C-SC-1	119.2	120.7	3.9	28.0	21	17	4	SC-SM	A-2-4
C-SC-2	120.7	125.7	16.4	24.0	23	18	5	SC-SM	A-1-b
C-SC-3	125.7	130.7	27.8	28.6	29	22	7	SC	A-2-4
C-SC-4	130.7	135.7	14.2	29.0	-	-	np	SM	A-2-4
C-SC-4R	130.7	135.7	-	-	-	-	-	Sandstone	
C-SC-5	135.7	140.7	16.4	33.4	46	29	17	SM	A-2-7 (1)
C-SC-6	140.7	145.7	16.5	40.8	33	23	10	SC	A-4
C-SC-7	145.7	150.7	18.5	39.4	33	17	16	SC	A-6 (2)
C-SC-8	150.7	155.7	26.1	83.0	63	40	23	MH	A-7-5 (24)
C-SC-9	155.7	160.7	19.4	30.6	34	20	14	SC	A-2-6 (1)
C-SC-10	160.7	165.7	16.8	29.0	24	22	2	SM	A-2-4
C-SC-11	165.7	170.7	22.8	27.0	32	27	5	SM	A-2-4
C-SC-12	170.7	175.7	21.3	23.0	31	24	7	SM	A-2-4
C-SC-13	175.7	180.7	21.6	31.0	35	18	17	SC	A-2-6 (1)
C-SC-14	180.7	185.7	22.1	45.0	40	20	20	SC	A-6 (5)
C-SC-15	185.7	190.7	44.0	70.2	50	31	19	MH	A-7-5 (14)
C-SC-16	190.7	195.7	28.9	69.0	54	25	29	CH	A-7-6 (19)
C-SC-17	195.7	200.7	29.0	42.0	43	17	26	SC	A-7-6 (6)
C-SC-18	200.7	205.7	27.4	50.0	49	21	28	SC	A-7-6 (10)
C-SC-19	205.7	210.7	46.5	17.0	49	23	26	SC	A-2-7 (0)
C-SC-20	210.7	215.7	23.9	39.0	32	21	11	SC	A-6 (1)
C-SC-21	215.7	220.7	27.5	54.0	53	30	23	MH	A-7-6 (10)
C-SC-22	220.7	225.7	18.8	33.0	36	14	22	SC	A-2-6 (2)
C-SC-23	225.7	230.7	-	-	-	-	-	No Sample	
C-SC-24	230.7	235.7	-	-	-	-	-	No Sample	
C-SC-25	235.7	240.7	46.9	43.0	38	16	22	SC	A-6 (5)
C-SC-26	240.7	245.7	30.8	41.0	-	-	np	SM	A-4
C-SC-27	245.7	250.7	31.5	32.8	36	21	15	SC	A-2-6 (1)
C-SC-28	250.7	255.7	20.3	25.0	32	28	4	SM	A-1-b
C-SC-29	255.7	260.7	28.1	84.4	39	30	9	ML	A-4
C-SC-30	260.7	265.7	40.0	89.6	40	8	32	CL	A-6 (27)
C-SC-31	265.7	270.7	19.8	94.6	82	38	44	MH	A-7-5 (52)
C-SC-32	270.7	275.7	19.0	33.0	38	15	23	SC	A-2-6 (2)
C-SC-33	275.7	280.7	36.2	41.2	39	12	27	SC	A-6 (6)
C-SC-34	280.7	285.7	30.4	43.6	39	24	15	SC	A-6 (3)



**University of South Carolina**  
 Department of Civil and Environmental Engineering  
 Project Name: Deep Soil Test Boring to Determine Shear  
 Wave Velocities across South Carolina

Client: SCDOT  
 Project ID: SPR-731  
 Boring No.: B-CON  
 Location: Conway, SC

Sample #	Depth (ft)		$\omega_{lab}$ (%)	Fine Content (%)	LL (%)	PL (%)	PI (%) <i>np - nonplastic</i>	USCS / Rock Type	ASSHTO
	From	To							
C-SC-35	285.7	290.7	31.9	57.0	43	29	14	ML	A-7-6 (6)
C-SC-36	290.7	295.7	23.6	30.0	44	37	7	SM	A-2-5
C-SC-37	295.7	300.7	25.3	30.0	36	23	13	SC	A-2-6 (0)
C-SC-38	300.7	305.7	-	-	-	-	-	Sandstone	
C-SC-39	305.7	310.7	-	-	-	-	-	Sandstone	
C-SC-39R	305.7	310.7	-	-	-	-	-	Sandstone	
C-SC-40	310.7	315.7	24.5	36.0	36	16	20	SC	A-6 (2)
C-SC-40R	310.7	315.7	-	-	-	-	-	Sandstone	
C-SC-41	315.7	320.7	-	-	-	-	-	Sandstone	
C-SC-41R	315.7	320.7	-	-	-	-	-	Sandstone	
C-SC-42	320.7	325.7	-	-	-	-	-	Sandstone	
C-SC-43	325.7	330.7	-	-	-	-	-	Sandstone	
C-SC-44	330.7	335.7	-	-	-	-	-	Sandstone	
C-SC-45	335.7	340.7	-	-	-	-	-	Sandstone	
C-SC-46	340.7	345.7	-	-	-	-	-	Sandstone	
C-SC-47	345.7	350.7	40.8	45.0	43	19	24	SC	A-7-6 (6)
C-SC-48	350.7	355.7	17.5	21.0	30	24	6	SM	A-1-b
C-SC-49	355.7	360.7	25.2						
C-SC-50	360.7	365.7	-	-	-	-	-	No Sample	
C-SC-51	365.7	370.7	29.9	38.0	34	25	9	SM	A-4
C-SC-52	370.7	375.7	30.1	28.0	33	18	15	SC	A-2-6 (1)
C-SC-53	375.7	380.7	-	-	-	-	-	No Sample	
C-SC-54	380.7	385.7	43.9	17.0	23	21	2	SM	A-1-b
C-SC-55	385.7	390.7	14.5	79.0	80	38	42	MH	A-7-5 (38)
C-SC-56	390.7	395.7	24.0	95.7	60	26	34	CH	A-7-6 (38)
C-SC-57	395.7	400.7	40.4	85.0	110	49	61	MH	A-7-5 (63)
C-SC-58	400.7	405.7	30.3	16.0	28	24	4	SM	A-1-b
C-SC-59	405.7	410.7	33.3	37.0	51	21	30	SC	A-7-6 (5)
C-SC-60	410.7	415.7	41.3	53.0	46	21	25	CL	A-7-6 (10)
C-SC-61	415.7	420.7	35.8	-	-	-	-	No Sample	
C-SC-62	420.7	425.7	35.2	77.0	70	43	27	MH	A-7-5 (25)
C-SC-63	425.7	430.7	45.7	80.0	64	25	39	CH	A-7-6 (33)
C-SC-64	430.7	435.7	44.6	67.6	99	30	69	CH	A-7-6 (47)
C-SC-65	435.7	440.7	-	-	-	-	-	No Sample	
C-SC-66	440.7	445.7	-	-	-	-	-	No Sample	
C-SC-67	445.7	450.7	34.9	67.6	48	36	12	ML	A-7-5 (9)
C-SC-68	450.7	455.7	-	-	-	-	-	Sandstone	
C-SC-68R	450.7	455.7	-	-	-	-	-	Sandstone	
C-SC-69	455.7	460.7	31.9	96.2	94	61	33	MH	A-7-5 (47)
C-SC-70	460.7	465.7	19.6	37.6	99	59	40	SM	A-7-5 (8)
C-SC-71	465.7	470.7	32.9	95.6	97	36	61	CH	A-7-5 (70)
C-SC-72	470.7	475.7	23.8	41.6	45	32	13	SM	A-7-5 (2)
C-SC-73	475.7	480.7	42.7	46.0	100	24	76	SC	A-7-6 (26)
C-SC-74	480.7	485.7	35.2	38.0	34	29	5	SM	A-4
C-SC-75	485.7	490.7	-	-	-	-	-	No Sample	



**University of South Carolina**  
Department of Civil and Environmental Engineering  
Project Name: Deep Soil Test Boring to Determine Shear  
Wave Velocities across South Carolina

Client: SCDOT  
Project ID: SPR-731  
Boring No.: B-CON  
Location: Conway, SC

Sample #	Depth (ft)		$w_{lab}$ (%)	Fine Content (%)	LL (%)	PL (%)	PI (%) <i>np - nonplastic</i>	USCS / Rock Type	ASSHTO
	From	To							
C-SC-76	490.7	495.7	26.7	3.0	-	-	-	SP	A-3
C-SC-77	495.7	500.7	44.9	78.0	110	62	48	MH	A-7-5 (48)
C-SC-78	500.7	505.7	27.9	53.0	61	25	36	CH	A-7-6 (15)



**University of South Carolina**  
 Department of Civil and Environmental Engineering  
 Project Name: Deep Soil Test Boring to Determine Shear  
 Wave Velocities across South Carolina

Client: SCDOT  
 Project ID: SPR-731  
 Boring No.: B-FMG  
 Location: Andrews, SC

Sample #	Depth (ft)		$\omega_{lab}$ (%)	Fine Content (%)	LL (%)	PL (%)	PI (%) <i>np - nonplastic</i>	USCS / Rock Type	ASSHTO
	From	To							
A-SS-1A	0	1.2	17.6	44.4	25	19	6	SC-SM	A-4
A-SS-1B	1.2	2	17.6	60.8	41	24	17	CL	A-7-6 (8)
A-SS-2A	2	3.1	30.2	51.0	29	25	4	ML	A-4 (0)
A-SS-2B	3.1	4	22.9	62.0	47	25	22	CL	A-7-6 (12)
A-SS-3	4	6	29.2	66.8	50	21	29	CH	A-7-6 (18)
A-UD-1	4	6	22.6	30.5	51	24	27	SC	A-2-7 (1)
A-SS-4A	6	6.2	22.1	-	-	-	-	No Sample	
A-SS-4B	6.2	8	17.0	41.4	34	14	20	SC	A-6 (4)
A-UD-2	6	8	14.3	23.2	16	15	1	SM	A-1-b
A-SS-5	8	10	18.4	32.4	26	19	7	SC-SM	A-2-4
A-UD-3	8	10		14.3	-	-	-	SM	
N/A	10	11.4	-	-	-	-	-	No Sample	
A-SS-6	11.4	12.7	34.8	27.4	-	-	np	SM	A-2-4
A-SS-7	12.7	14.7	27.0	34.2	-	-	np	SM	A-2-4
A-SS-8	14.7	16.7	28.4	34.8	22	20	2	SM	A-2-4
A-SS-9	16.7	18.5	29.0	33.2	27	22	5	SC-SM	A-2-4
A-SS-10	18.5	20.5	16.5	-	-	-	-	Sandstone	
A-SS-11	20.5	20.7	-	-	-	-	-	Limestone	
A-SC-1	20.7	25.7	-	-	-	-	-	Limestone	
A-SC-2	25.7	30.7	-	-	-	-	-	Limestone	
A-SC-3	30.7	35.7	-	-	-	-	-	Limestone	
A-SC-4	35.7	40.7	-	-	-	-	-	Limestone	
A-SC-5	40.7	45.7	-	-	-	-	-	Limestone	
A-SC-6	45.7	50.7	-	-	-	-	-	Limestone	
A-SC-7	50.7	55.7	-	-	-	-	-	Sandstone	
A-SC-8	55.7	60.7	-	-	-	-	-	Sandstone	
A-SC-9	60.7	65.7	-	-	-	-	-	Rock	
A-SC-10	65.7	70.7	-	-	-	-	-	Rock	
A-SC-11	70.7	75.7	23.6	-	-	-	-	Rock	
A-SC-12	75.7	80.7	-	-	-	-	-	Rock	
A-SC-13	80.7	85.7	28.0	40.4	-	-	-	SM	
A-SC-14	85.7	90.7	32.6	35.4	32	25	7	SM	A-4
A-SC-15	90.7	95.7	-	-	-	-	-	No Sample	
A-SC-16	95.7	100.7	34.2	37.2	-	-	np	SM	A-4
A-SC-17	100.7	105.7	36.9	44.4	29	22	7	SC	A-4
A-SC-18	105.7	110.7	28.5	33.6	29	23	6	SM	A-2-4
A-SC-19	110.7	115.7	38.6	35.8	30	28	2	SM	A-4
A-SC-20	115.7	120.7	-	-	-	-	-	Rock	
A-SC-21	120.7	125.7	34.4	22.2	26	24	2	SM	A-1-b
A-SC-22	125.7	130.7	-	-	-	-	-	Rock	
A-SC-23	130.7	135.7	-	-	-	-	-	Rock	
A-SC-24	135.7	140.7	-	-	-	-	-	Rock	
A-SC-25	140.7	145.7	35.1	45.0	-	-	np	SM	A-4
A-SC-26	145.7	150.7	34.8	46.2	-	-	np	SM	A-4
A-UD-4	145	148							



**University of South Carolina**  
 Department of Civil and Environmental Engineering  
 Project Name: Deep Soil Test Boring to Determine Shear  
 Wave Velocities across South Carolina

Client: SCDOT  
 Project ID: SPR-731  
 Boring No.: B-FMG  
 Location: Andrews, SC

Sample #	Depth (ft)		$\omega_{lab}$ (%)	Fine Content (%)	LL (%)	PL (%)	PI (%) <i>np - nonplastic</i>	USCS / Rock Type	ASSHTO	
	From	To								
A-UD-	5	148	151	0.0	-	-	-	SP	A-3	
A-SC-	27	150.7	155.7	35.2	64.2	38	25	13	CL	A-6 (7)
A-UD-	6	151	154	26.0	57.5	38	27	11	ML	A-6 (5)
A-SC-	28	155.7	160.7	32.6	84.2	51	26	25	CH	A-7-6 (23)
A-SC-	29	160.7	165.7	39.5	93.8	68	45	23	MH	A-7-5 (30)
A-SC-	30	165.7	167.7	43.4	81.8	64	35	29	MH	A-7-5 (28)
A-SC-	31	167.7	170.7	29.2	50.2	-	-	np	ML	A-4
A-SC-	32	170.7	175.7	40.1	81.8	46	38	8	ML	A-5 (9)
A-SC-	33	175.7	180.7	56.2	83.4	54	40	14	MH	A-7-5 (16)
A-SC-	34	180.7	185.7	52.9	71.2	54	47	7	MH	A-5 (8)
A-SC-	35	185.7	190.7	34.7	60.0	35	26	9	ML	A-4
A-SC-	36	190.7	195.7	34.4	12.6	-	-	np	SM	A-1-a
A-SC-	37	195.7	200.7	-	-	-	-	-	Rock	
A-SC-	38	200.7	205.7	-	-	-	-	-	Rock	
A-SC-	39	205.7	210.7	-	-	-	-	-	Rock	
A-SC-	40	210.7	215	-	-	-	-	-	Rock	
A-SC-	41	215	215.7	30.8	69.8	43	26	17	CL	A-7-6 (11)
A-SC-	42	215.7	220.7	49.3	41.4	32	26	6	SM	A-4
A-SC-	42R	215.7	220.7	-	-	-	-	-	Sandstone	
A-SC-	43	220.7	225.7	27.9	54.4	27	22	5	ML	A-4
A-SC-	44T	225.7	230.7	41.9	40.6	45	19	26	SC	A-7-6 (5)
A-SC-	44B				51.6	32	26	6	ML	A-4
A-SC-	45	230.7	235.7	36.8	46.8	42	26	16	SC	A-7-6 (4)
A-SC-	46	235.7	240.7	33.6	63.8	44	26	18	CL	A-7-6 (10)
A-SC-	47	240.7	245.7	32.7	64.8	45	26	19	CL	A-7-6 (11)
A-SC-	48	245.7	250.7	32.4	68.0	40	30	10	ML	A-4
A-SC-	49	250.7	255.7	32.6	68.0	54	21	33	CH	A-7-6 (21)
A-SC-	50	255.7	260.7	48.5	68.0	43	27	16	ML	A-7-6 (10)
A-SC-	51	260.7	265.7	31.7	58.6	47	27	20	CL	A-7-6 (10)
A-SC-	52	265.7	270.7	28.4	55.6	34	23	11	CL	A-6 (4)
A-SC-	52R	265.7	270.7	-	-	-	-	-	Claystone	
A-SC-	53	270.7	275.7	25.3	72.2	44	24	20	CL	A-7-6 (14)
A-SC-	54	275.7	280.7	24.4	61.0	41	24	17	CL	A-7-6 (9)
A-SC-	55	280.7	285.7	23.8	65.2	41	24	17	CL	A-7-6 (10)
A-SC-	56	285.7	290.7	25.2	74.0	43	25	18	CL	A-7-6 (13)
A-SC-	57	290.7	295.7	25.8	72.2	38	24	14	CL	A-6 (9)
A-SC-	58	295.7	300.7	26.0	82.2	47	25	22	CL	A-7-6 (19)
A-SC-	59	300.7	305.7	26.6	81.2	45	23	22	CL	A-7-6 (18)
A-SC-	59R	300.7	305.7	-	-	-	-	-	Sandstone	
A-SC-	60	305.7	310.7	18.3	77.4	42	25	17	CL	A-7-6 (13)
A-SC-	60R	305.7	310.7	-	-	-	-	-	Sandstone	
A-SC-	61	310.7	315.7	28.5	85.2	48	34	14	ML	A-7-5 (15)
A-SC-	62	315.7	320.7	17.1	82.4	45	27	18	ML	A-7-6 (16)
A-SC-	63	320.7	325.7	17.5	81.0	38	25	13	ML	A-6 (11)
A-SC-	64	325.7	330.7	27.2	90.0	46	37	9	ML	A-5 (12)



**University of South Carolina**  
 Department of Civil and Environmental Engineering  
 Project Name: Deep Soil Test Boring to Determine Shear  
 Wave Velocities across South Carolina

Client: SCDOT  
 Project ID: SPR-731  
 Boring No.: B-FMG  
 Location: Andrews, SC

Sample #	Depth (ft)		$\omega_{lab}$ (%)	Fine Content (%)	LL (%)	PL (%)	PI (%) <i>np - nonplastic</i>	USCS / Rock Type	ASSHTO
	From	To							
A-SC-65	330.7	335.7	21.2	93.0	45	28	17	ML	A-7-6 (19)
A-SC-66	335.7	340.7	32.1	88.6	49	23	26	CL	A-7-6 (25)
A-SC-67	340.7	345.7	30.7	94.0	34	21	13	CL	A-6 (12)
A-SC-68	345.7	350.7	20.5	86.2	37	26	11	ML	A-6 (10)
A-SC-69	350.7	355.7	24.6	94.2	49	35	14	ML	A-7-5 (18)
A-SC-70	355.7	360.7	19.9	92.2	41	30	11	ML	A-7-6 (12)
A-SC-71	360.7	365.7	26.8	82.6	41	22	19	CL	A-7-6 (16)
A-SC-72	365.7	370.7	12.6	63.4	36	23	13	CL	A-6 (7)
A-SC-73	370.7	375.7	19.5	34.4	24	20	4	SC-SM	A-2-4
A-SC-74	375.7	380.7	12.2	38.4	24	19	5	SC-SM	A-4
A-SC-75	380.7	385.7	25.4	37.8	29	23	6	SM	A-4
A-SC-76	385.7	390.7	44.7	47.4	60	30	30	SC	A-7-6 (10)
A-SC-77	390.7	395.7	33.2	62.0	57	33	24	MH	A-7-5 (14)
A-SC-78	395.7	400.7	34.4	67.2	48	32	16	ML	A-7-5 (11)
A-SC-79	400.7	405.7	26.7	45.8	35	31	4	SM	A-4
A-SC-80	405.7	410.7	26.9	46.6	36	28	8	SM	A-4
A-SC-81	410.7	415.7	24.2	61.2	37	23	14	CL	A-6 (7)
A-SC-82	415.7	420.7	28.8	78.2	50	34	16	MH	A-7-5 (15)
A-SC-83	420.7	425.7	25.4	41.2					
A-SC-84	425.7	430.7	29.5	47.4	39	25	14	SM	A-6 (4)
A-SC-85	430.7	435.7	25.9	56.4	48	25	23	CL	A-7-6 (11)
A-SC-86	435.7	440.7	28.4	73.0	54	25	29	CH	A-7-6 (21)
A-SC-87	440.7	445.7	27.7	59.0	46	25	21	CL	A-7-6 (10)
A-SC-88	445.7	450.7	19.8	48.8	35	23	12	SC	A-6 (3)
A-SC-89	450.7	455.7	27.9	75.2	45	27	18	ML	A-7-6 (14)
A-SC-90	455.7	460.7	28.2	80.6	50	23	27	CH	A-7-6 (23)
A-SC-91	460.7	465.7	29.1	82.2	51	24	27	CH	A-7-6 (23)
A-SC-92	465.7	470.7	28.0	52.6	39	23	16	CL	A-6 (6)
A-SC-93	470.7	475.7	29.4	66.2	70	22	48	CH	A-7-6 (30)
A-SC-94	475.7	480.7	36.0	76.2	81	26	55	CH	A-7-6 (44)
A-SC-95	480.7	485.7	29.6	67.0	81	24	57	CH	A-7-6 (37)
A-SC-96	485.7	490.7	29.8	75.0	64	31	33	CH	A-7-5 (27)
A-SC-97	490.7	495.7	40.3	91.8	80	35	45	CH	A-7-5 (50)
A-SC-98	495.7	500.7	59.1	94.8	80	45	35	MH	A-7-5 (44)
A-SC-99	500.7	505.7	37.5	81.0	60	29	31	CH	A-7-6 (28)
A-SC-100	505.7	510.7	36.9	71.6	67	24	43	CH	A-7-6 (31)
A-SC-101	510.7	515.7	26.3	41.8	40	25	15	SC	A-6 (3)
A-SC-102	515.7	520.7	39.2	43.8	37	24	13	SC	A-6 (2)
A-SC-103	520.7	525.7	21.9	31.0	26	21	5	SC-SM	A-2-4
A-SC-104	525.7	530.7	21.1	34.2	31	22	9	SC	A-2-4
A-SC-105	530.7	535.7	25.7	43.0	42	22	20	SC	A-7-6 (4)
A-SC-106	535.7	540.7	28.6	31.2	41	23	18	SC	A-2-7 (1)
A-SC-107	540.7	545.7	31.0	43.0	43	26	17	SC	A-7-6 (4)
A-SC-108	545.7	550.7	26.7	34.0	40	21	19	SC	A-2-6 (2)
A-SC-109	550.7	555.7	-	-	-	-	-	Rock	



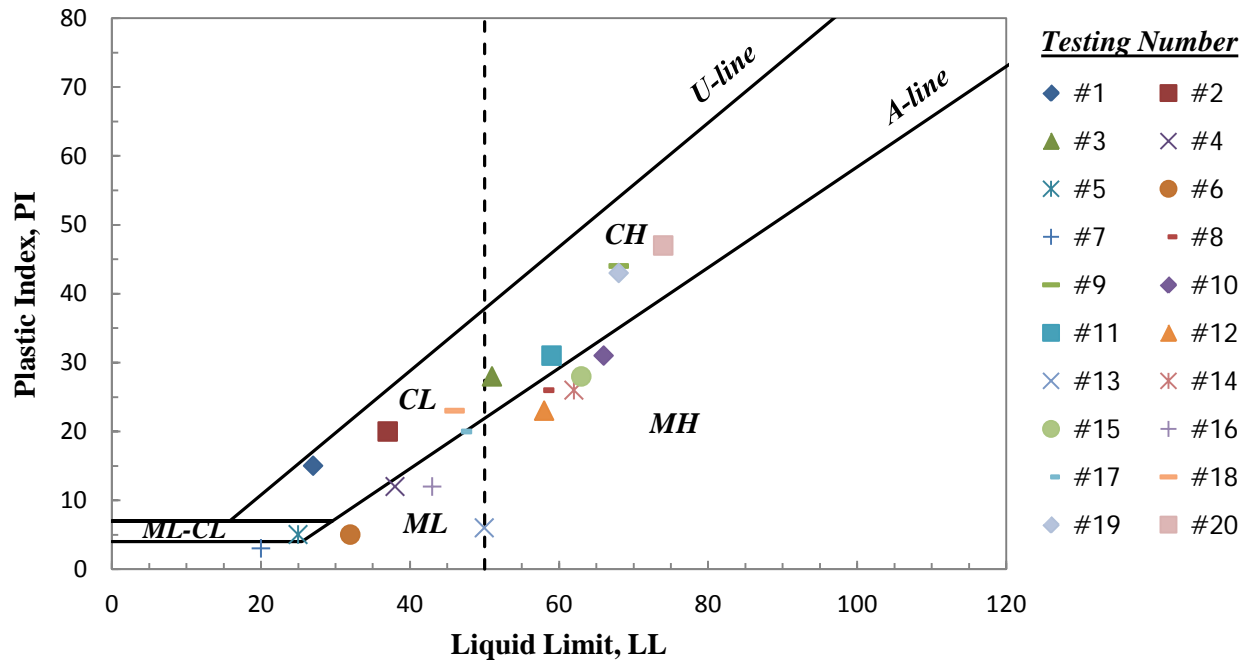
**University of South Carolina**  
 Department of Civil and Environmental Engineering  
 Project Name: Deep Soil Test Boring to Determine Shear  
 Wave Velocities across South Carolina

Client: SCDOT  
 Project ID: SPR-731  
 Boring No.: B-FMG  
 Location: Andrews, SC

Sample #	Depth (ft)		$\omega_{lab}$ (%)	Fine Content (%)	LL (%)	PL (%)	PI (%) <small>np - nonplastic</small>	USCS / Rock Type	ASSHTO
	From	To							
A-SC-109R	550.7	555.7	-	-	-	-	-	Sandstone	
A-SC-110	555.7	560.7	-	-	-	-	-	Rock	
A-SC-110R	555.7	560.7	-	-	-	-	-	Sandstone	
A-SC-111	560.7	565.7	-	-	-	-	-	Rock	
A-SC-112	565.7	570.7	-	-	-	-	-	Rock	
A-SC-112R	565.7	570.7	-	-	-	-	-	Sandstone	
A-SC-113	570.7	575.7	25.9	25.0	30	22	8	SC	A-2-4
A-SC-114	575.7	580.7	29.0	26.8					
A-SC-115	580.7	585.7	28.6	25.6	31	20	11	SC	A-2-6 (0)
A-SC-115R	580.7	585.7	-	-	-	-	-	Sandstone	
A-SC-116	585.7	590.7	33.0	81.8	82	43	39	MH	A-7-5 (39)
A-SC-116R	585.7	590.7	-	-	-	-	-	Sandstone	
A-SC-117	590.7	595.7	31.1	90.6	87	50	37	MH	A-7-5 (45)
A-SC-118	595.7	600.7	22.8	29.0	30	21	9	SC	A-2-4
A-SC-119	600.7	605.7	37.9	36.4	37	22	15	SC	A-6 (1)
A-SC-120	605.7	610.7	27.6	16.8	24	21	3	SM	A-1-b
A-SC-121	610.7	615.7	39.6	16.2	38	19	19	SC	A-2-6 (0)



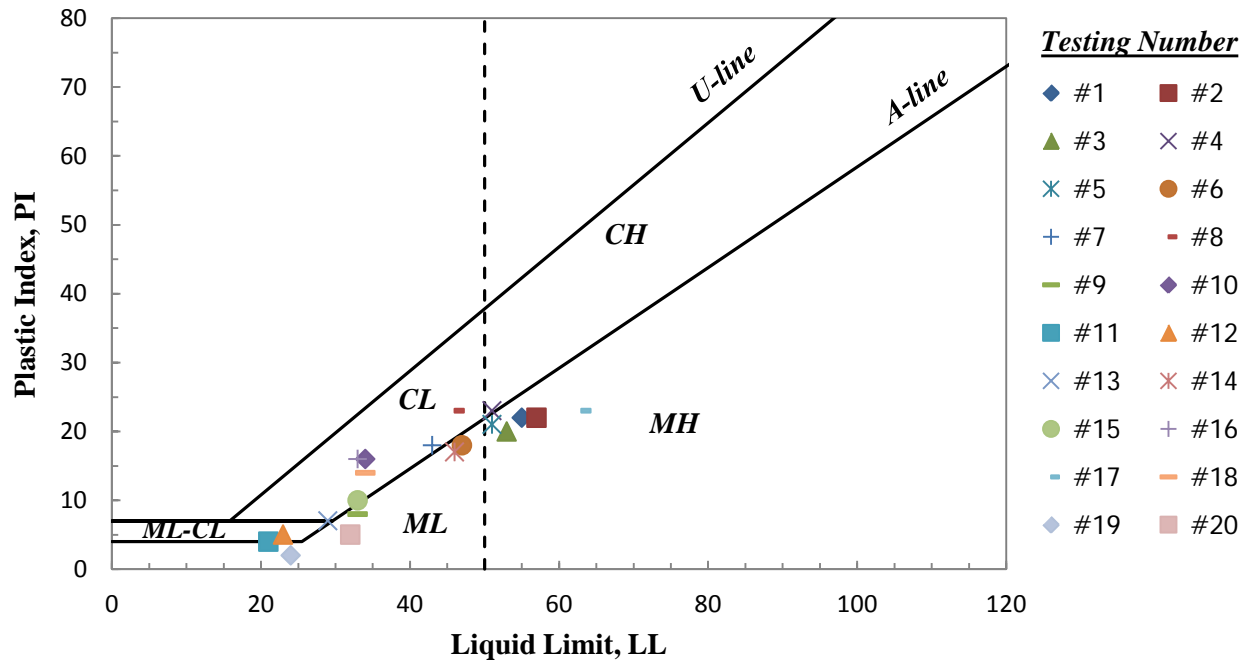
### Plasticity Chart



#	Sample #	Depth (ft)		$\omega_{lab}$ (%)	Fine Content (%)	LL (%)	PL (%)	PI (%)	USCS
		From	To						
1	SS4	6.0	8.0	16.8	39.0	27	12	15	SC
2	SS5	8.0	10.0	31.3	90.0	37	17	20	CL
3	UD1	10.0	12.5	43.4	95.1	51	23	28	CH
4	SS6	12.5	14.5	50.5	90.0	38	26	12	ML
5	SS7	17.0	19.0	40.2	37.6	25	20	5	SC-SM
6	SS18	39.0	41.0	20.6	19.0	32	27	5	SM
7	SS23	49.0	51.0	24.8	35.0	20	17	3	SM
8	SS25	53.0	55.0	37.3	94.2	58	32	26	MH
9	UD3	55.0	57.5	35.3	91.6	68	24	44	CH
10	SS26	60.0	62.0	34.5	97.0	66	35	31	MH
11	SS27	62.0	64.0	34.9	96.0	59	28	31	CH
12	SS28	64.0	66.0	35.6	93.8	58	35	23	MH
13	SS29	66.0	68.0	34.3	82.6	50	44	6	MH
14	SS30	68.0	70.0	38.2	98.2	62	36	26	MH
15	SS31	70.0	72.0	38.7	96.0	63	35	28	MH
16	SS32	77.0	79.0	30.1	85.0	43	31	12	ML
17	SS33	79.0	81.0	30.3	88.8	47	27	20	ML
18	SS34	81.0	83.0	32.9	92.0	46	23	23	CL
19	UD7	83.0	85.5	40.7	87.0	68	25	43	CH
20	UD8	85.5	88.0	42.6	93.8	74	27	47	CH



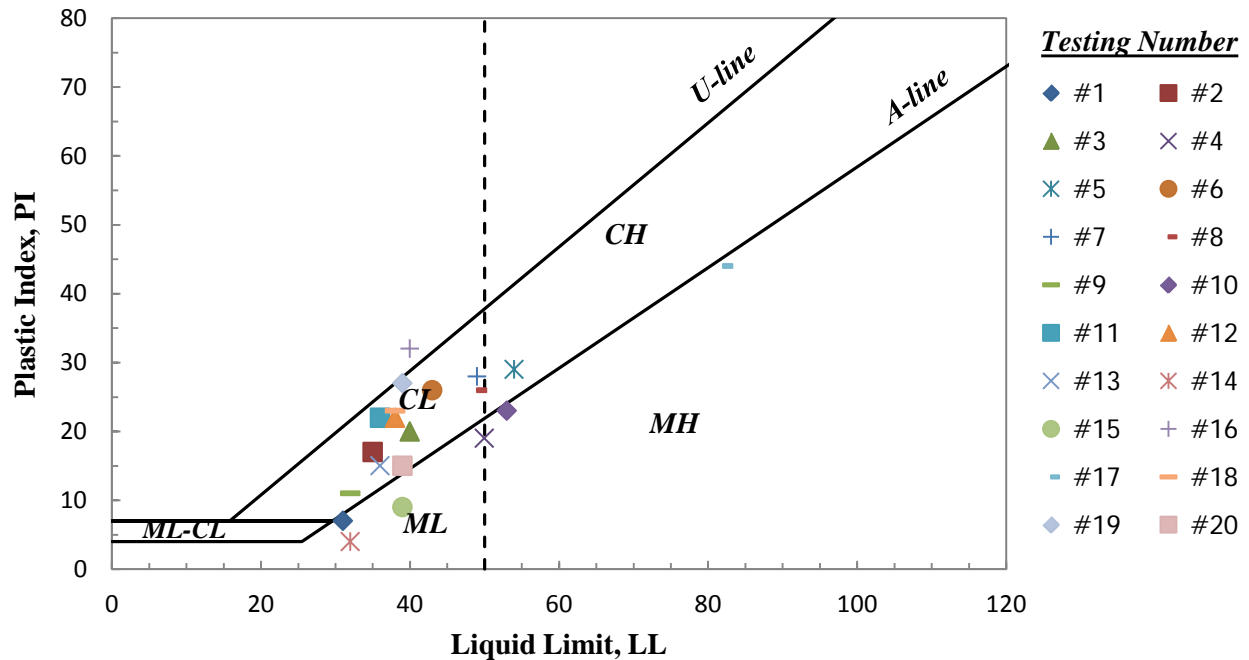
### Plasticity Chart



#	Sample #	Depth (ft)		$\omega_{lab}$ (%)	Fine Content (%)	LL (%)	PL (%)	PI (%)	USCS
		From	To						
1	SS35	88.0	90.0	30.2	91.6	55	33	22	MH
2	SS36	94.0	96.0	32.1	96.0	57	35	22	MH
3	SS37	96.0	98.0	33.9	93.0	53	33	20	MH
4	SS38	98.0	100.0	34.6	88.0	51	28	23	CH
5	SS39	100.0	102.0	27	86.0	51	30	21	MH
6	SS40	102.0	104.0	32	92.6	47	29	18	ML
7	SS41	106.5	108.5	29.2	92.0	43	25	18	CL
8	SS42	108.5	110.5	31.1	88.0	46	23	23	CL
9	SS43	110.5	112.5	13.4	81.0	33	25	8	ML
10	SS44	112.5	114.5	19.3	58.2	34	18	16	CL
11	SC1	119.2	120.7	3.9	28.0	21	17	4	SC-SM
12	SC2	120.7	125.7	16.4	24.0	23	18	5	SC-SM
13	SC3	125.7	130.7	27.8	28.6	29	22	7	SC
14	SC5	135.7	140.7	16.4	33.4	46	29	17	SM
15	SC6	140.7	145.7	16.5	40.8	33	23	10	SC
16	SC7	145.7	150.7	18.5	39.4	33	17	16	SC
17	SC8	150.7	155.7	26.1	83.0	63	40	23	MH
18	SC9	155.7	160.7	19.4	30.6	34	20	14	SC
19	SC10	160.7	165.7	16.8	29.0	24	22	2	SM
20	SC11	165.7	170.7	22.8	27.0	32	27	5	SM



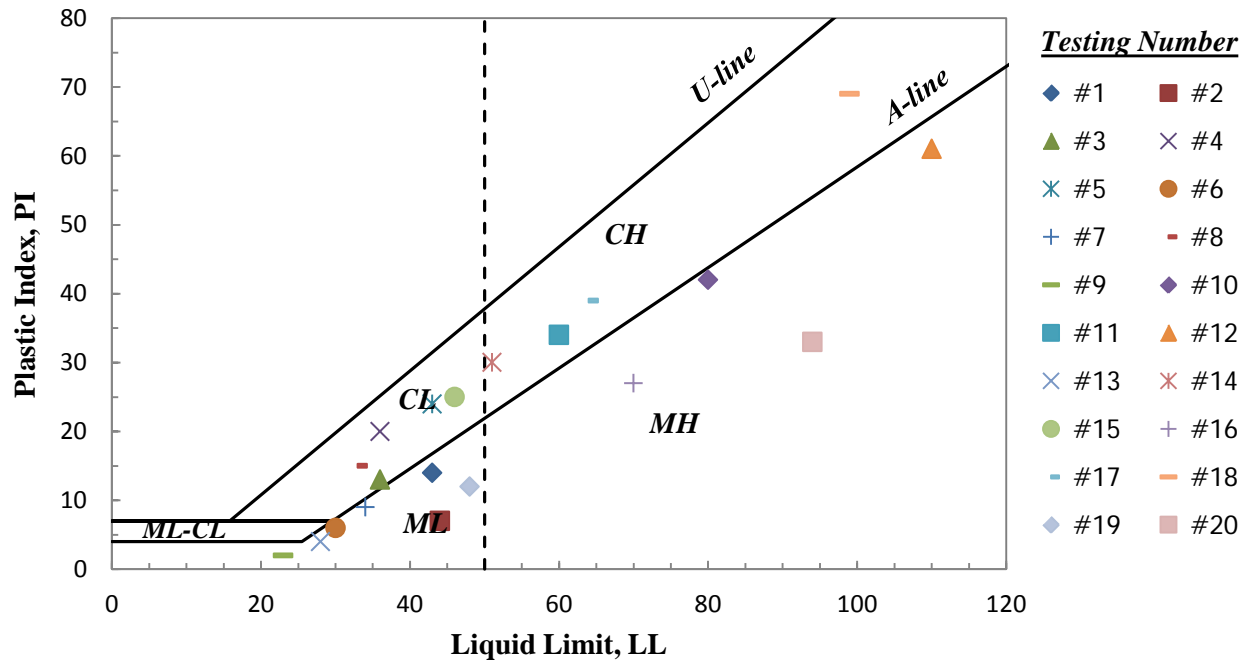
### Plasticity Chart



#	Sample #	Depth (ft)		$\omega_{lab}$ (%)	Fine Content (%)	LL (%)	PL (%)	PI (%)	USCS
		From	To						
1	SC12	170.7	175.7	21.3	23.0	31	24	7	SM
2	SC13	175.7	180.7	21.6	31.0	35	18	17	SC
3	SC14	180.7	185.7	22.1	45.0	40	20	20	SC
4	SC15	185.7	190.7	44.0	70.2	50	31	19	MH
5	SC16	190.7	195.7	28.9	69.0	54	25	29	CH
6	SC17	195.7	200.7	29.0	42.0	43	17	26	SC
7	SC18	200.7	205.7	27.4	50.0	49	21	28	SC
8	SC19	205.7	210.7	46.5	17.0	49	23	26	SC
9	SC20	210.7	215.7	23.9	39.0	32	21	11	SC
10	SC21	215.7	220.7	27.5	54.0	53	30	23	MH
11	SC22	220.7	225.7	18.8	33.0	36	14	22	SC
12	SC25	235.7	240.7	46.9	43.0	38	16	22	SC
13	SC27	245.7	250.7	31.5	32.8	36	21	15	SC
14	SC28	250.7	255.7	20.3	25.0	32	28	4	SM
15	SC29	255.7	260.7	28.1	84.4	39	30	9	ML
16	SC30	260.7	265.7	40.0	89.6	40	8	32	CL
17	SC31	265.7	270.7	19.8	94.6	82	38	44	MH
18	SC32	270.7	275.7	19.0	33.0	38	15	23	SC
19	SC33	275.7	280.7	36.2	41.2	39	12	27	SC
20	SC34	280.7	285.7	30.4	43.6	39	24	15	SC



### Plasticity Chart

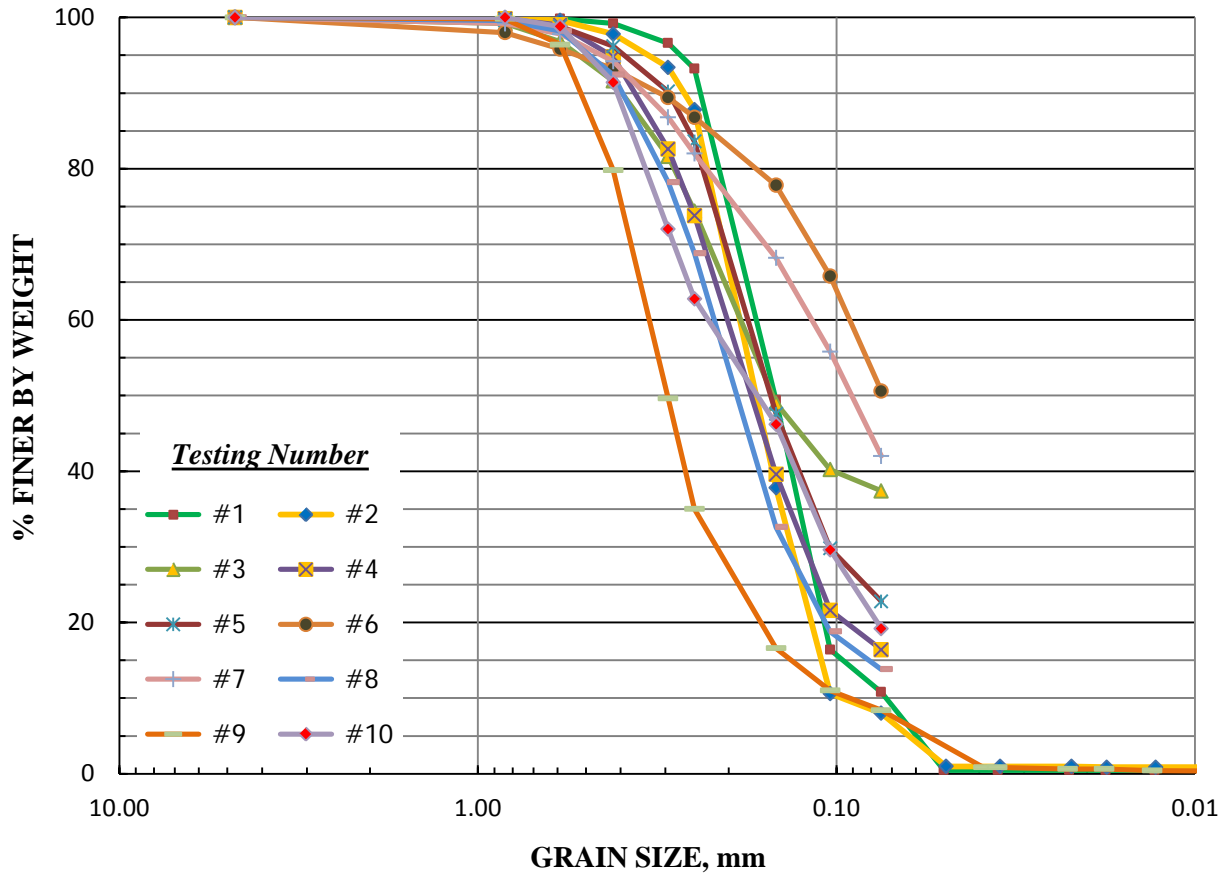


#	Sample #	Depth (ft)		$\omega_{lab}$ (%)	Fine Content (%)	LL (%)	PL (%)	PI (%)	USCS
		From	To						
1	SC35	285.7	290.7	31.9	57.0	43	29	14	ML
2	SC36	290.7	295.7	23.6	30.0	44	37	7	SM
3	SC37	295.7	300.7	25.3	30.0	36	23	13	SC
4	SC40	310.7	315.7	24.5	36.0	36	16	20	SC
5	SC47	345.7	350.7	40.8	45.0	43	19	24	SC
6	SC48	350.7	355.7	17.5	21.0	30	24	6	SM
7	SC51	365.7	370.7	29.9	38.0	34	25	9	SM
8	SC52	370.7	375.7	30.1	28.0	33	18	15	SC
9	SC54	380.7	385.7	43.9	17.0	23	21	2	SM
10	SC55	385.7	390.7	14.5	79.0	80	38	42	MH
11	SC56	390.7	395.7	24	95.7	60	26	34	CH
12	SC57	395.7	400.7	40.4	85.0	110	49	61	MH
13	SC58	400.7	405.7	30.3	16.0	28	24	4	SM
14	SC59	405.7	410.7	33.3	37.0	51	21	30	SC
15	SC60	410.7	415.7	41.3	53.0	46	21	25	CL
16	SC62	420.7	425.7	35.2	77.0	70	43	27	MH
17	SC63	425.7	430.7	45.7	80.0	64	25	39	CH
18	SC64	430.7	435.7	44.6	67.6	99	30	69	CH
19	SC67	445.7	450.7	34.9	67.6	48	36	12	ML
20	SC69	455.7	460.7	31.9	96.2	94	61	33	MH





### GRAIN SIZE DISTRIBUTION

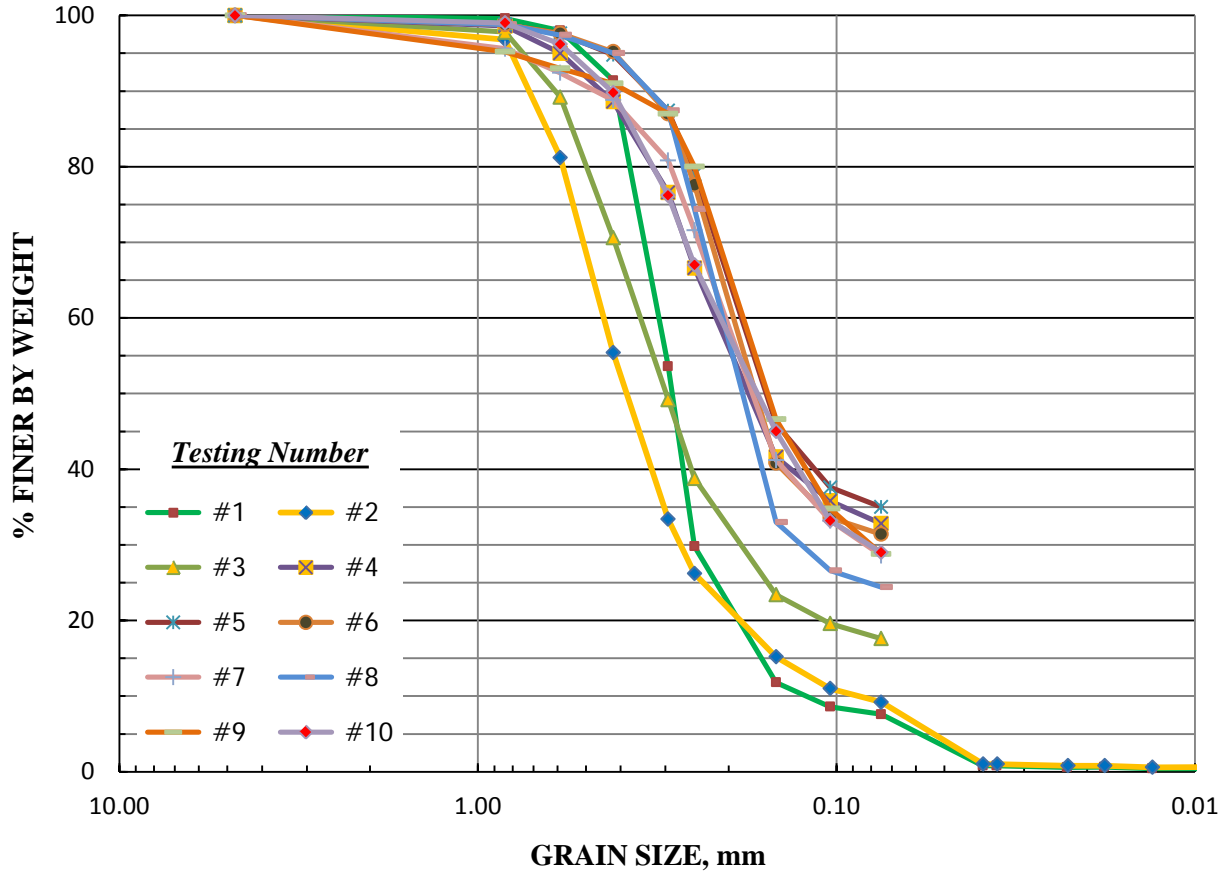


GRAVEL	SAND			SILT or CLAY
	coarse	medium	fine	

#	Sample #	Depth (ft)		%Gravel	%Sand	%Silt %Clay	D <sub>60</sub>	D <sub>30</sub>	D <sub>10</sub>	Cc	Cu
		From	To								
1	SS-1	0.0	2.0	100.0	89.2	10.8	0.17	0.12	0.07	1.21	2.43
2	SS-2	2.0	4.0	100.0	92.0	8.0	0.19	0.13	0.10	0.89	1.90
3	SS-3	4.0	6.0	100.0	62.6	37.4	0.18	-	-	-	-
4	SS-8	19.0	21.0	100.0	83.6	16.4	0.20	0.13	-	-	-
5	SS-10	23.0	25.0	100.0	77.2	22.8	0.18	0.11	-	-	-
6	SS-13	29.0	31.0	100.0	49.4	50.6	0.09	-	-	-	-
7	SS-14	31.0	33.0	100.0	58.0	42.0	0.12	-	-	-	-
8	SS-16	35.0	37.0	100.0	86.2	13.8	0.22	0.13	-	-	-
9	SS-17	37.0	39.0	100.0	91.6	8.4	0.33	0.22	0.09	1.63	3.67
10	SS-18	39.0	41.0	100.0	80.8	19.2	0.23	0.11	-	-	-



### GRAIN SIZE DISTRIBUTION

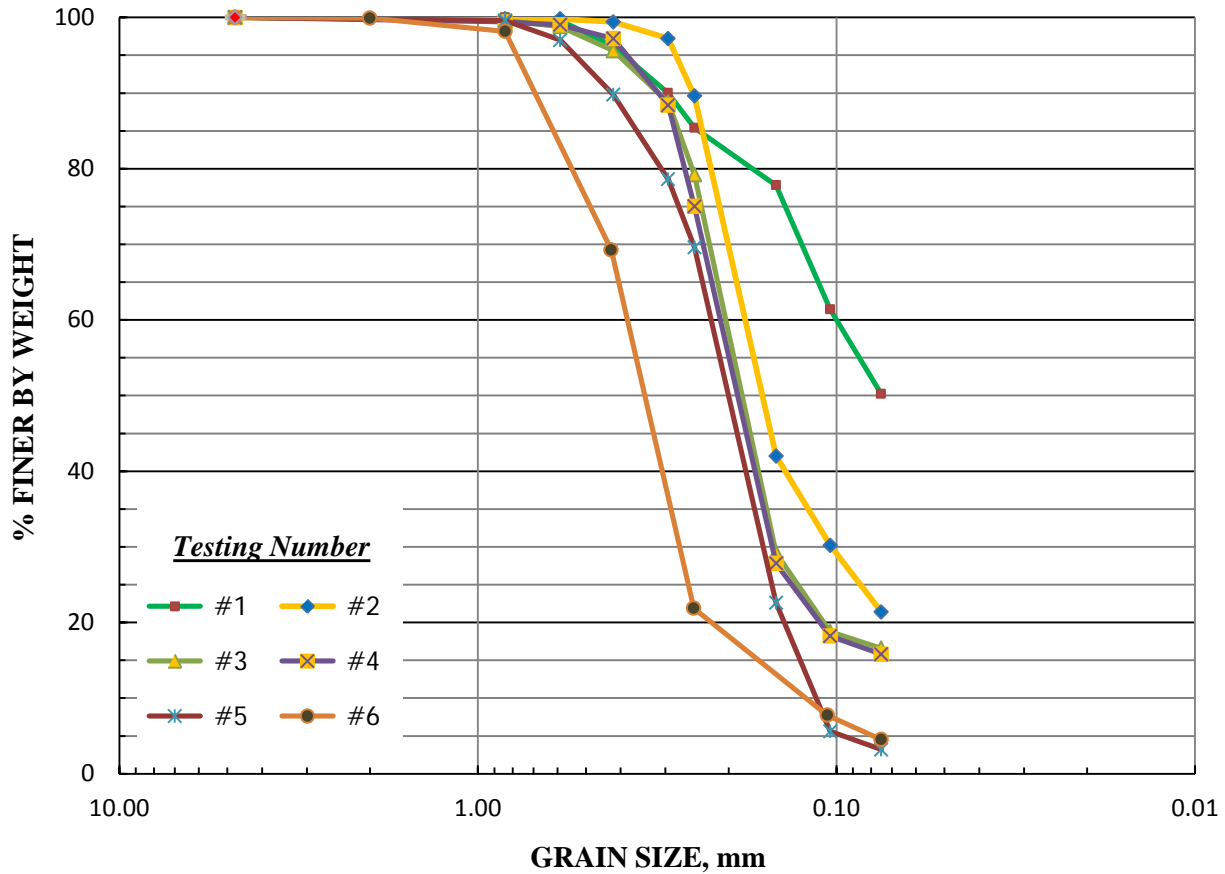


GRAVEL	SAND			SILT or CLAY
	coarse	medium	fine	

#	Sample #	Depth (ft)		%Gravel	%Sand	%Silt %Clay	D <sub>60</sub>	D <sub>30</sub>	D <sub>10</sub>	Cc	Cu
		From	To								
1	SS-19	41	43	100.0	92.4	7.6	0.31	0.25	0.13	1.55	2.38
2	SS-20	43	45	100.0	90.8	9.2	0.43	0.28	0.09	2.03	4.78
3	SS-21	45	47	100.0	82.4	17.6	0.33	0.18	-	-	-
4	SS-22	47	49	100.0	67.2	32.8	0.22	-	-	-	-
5	SS-23	49	51	100.0	65.0	35.0	0.18	-	-	-	-
6	SS-24	51	53	100.0	68.6	31.4	0.19	-	-	-	-
7	SC-01	119.2	120.7	100.0	71.4	28.6	0.20	0.08	-	-	-
8	SC-02	120.7	125.7	100.0	75.6	24.4	0.21	0.13	-	-	-
9	SC-04	130.7	135.7	100.0	71.2	28.8	0.18	0.08	-	-	-
10	SC-10	160.7	165.7	100.0	71.0	29.0	0.22	0.08	-	-	-



### GRAIN SIZE DISTRIBUTION

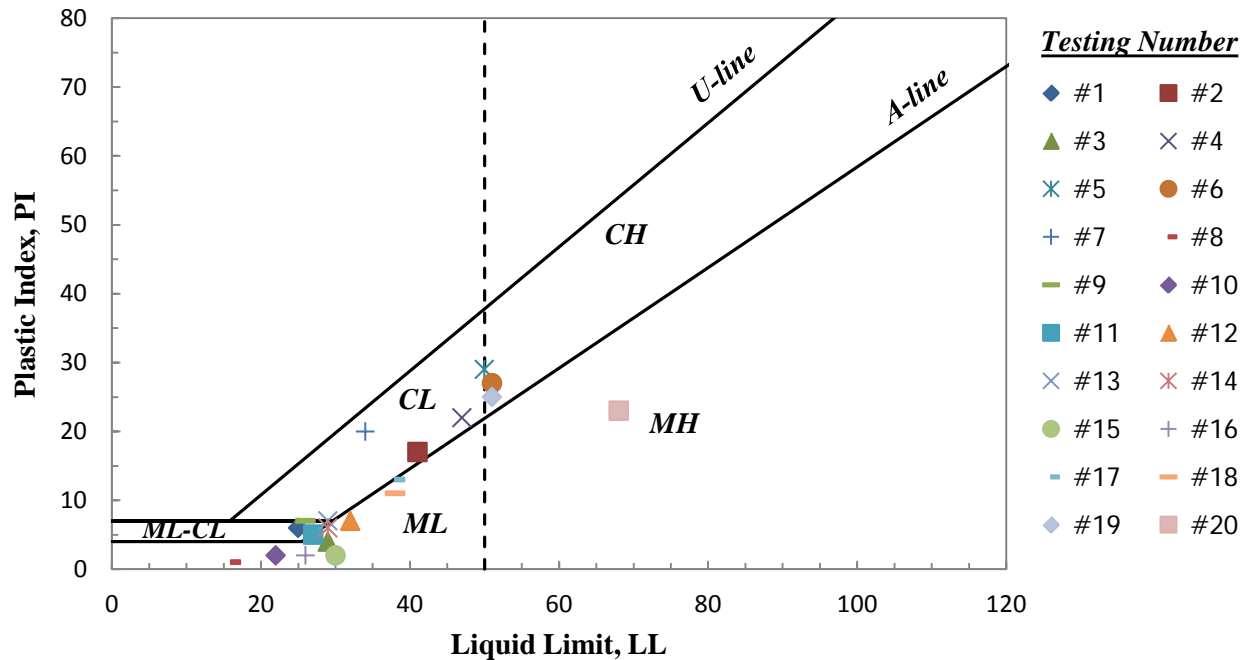


GRAVEL	SAND			SILT or CLAY
	coarse	medium	fine	

#	Sample #	Depth (ft)		%Gravel	%Sand	%Silt %Clay	D <sub>60</sub>	D <sub>30</sub>	D <sub>10</sub>	Cc	Cu
		From	To								
1	SC-18	200.7	205.7	100.0	49.8	50.2	0.10	-	-	-	-
2	SC-48	350.7	355.7	100.0	78.6	21.4	0.17	0.10	-	-	-
3	SC-54	380.7	385.7	100.0	83.4	16.6	0.20	0.14	-	-	-
4	SC-58	400.7	405.7	100.0	84.2	15.8	0.22	0.15	-	-	-
5	SC-76	490.7	495.7	100.0	96.8	3.2	0.23	0.16	0.12	0.93	1.92
6	UD-2	14.5	17.0	100.0	95.5	4.5	0.39	0.27	0.12	1.56	3.25



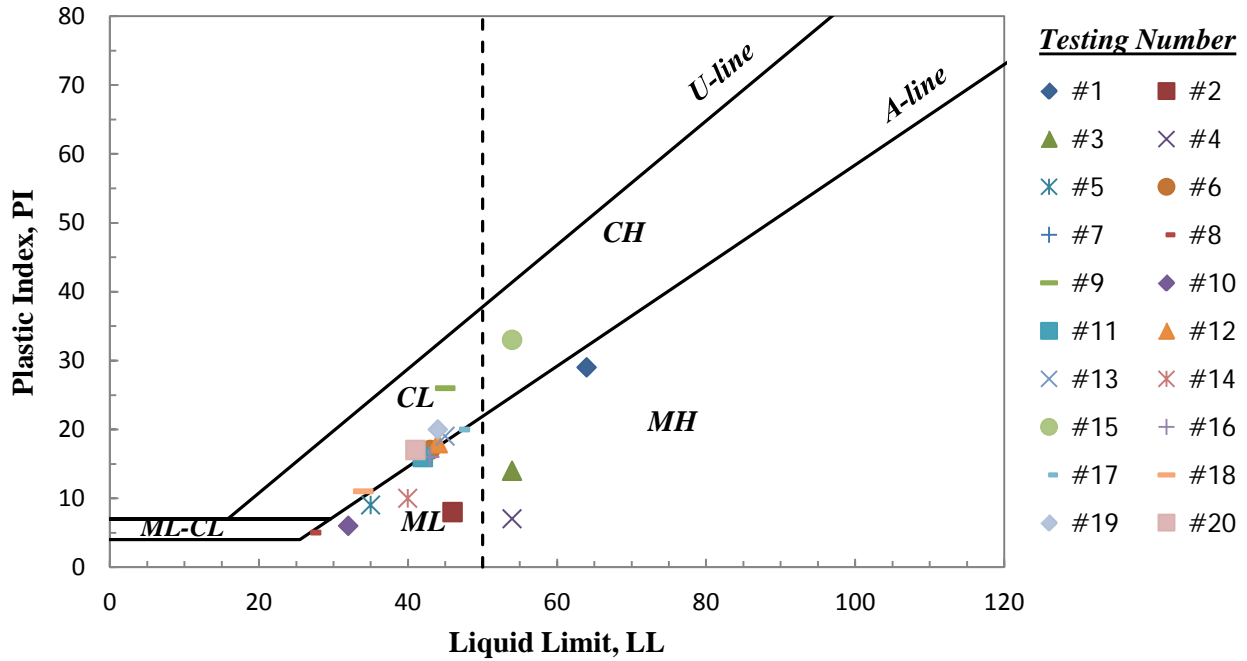
### Plasticity Chart



#	Sample #	Depth (ft)		$\omega_{lab}$ (%)	Fine Content (%)	LL (%)	PL (%)	PI (%)	USCS
		From	To						
1	SS1A	0.0	1.2	17.6	44.4	25	19	6	SC-SM
2	SS1B	1.2	2.0	17.6	60.8	41	24	17	CL
3	SS2A	2.0	3.1	30.2	51.0	29	25	4	ML
4	SS2B	3.1	4.0	22.9	62.0	47	25	22	CL
5	SS3	4.0	6.0	29.2	66.8	50	21	29	CH
6	UD1	4.0	6.0	22.6	30.5	51	24	27	SC
7	SS4B	6.2	8.0	17	41.4	34	14	20	SC
8	UD2	6.0	8.0	14.3	23.2	16	15	1	SM
9	SS5	8.0	10.0	18.4	32.4	26	19	7	SC-SM
10	SS8	14.7	16.7	28.4	34.8	22	20	2	SM
11	SS9	16.7	18.5	29	33.2	27	22	5	SC-SM
12	SC14	85.7	90.7	32.6	35.4	32	25	7	SM
13	SC17	100.7	105.7	36.9	44.4	29	22	7	SC
14	SC18	105.7	110.7	28.5	33.6	29	23	6	SM
15	SC19	110.7	115.7	38.6	35.8	30	28	2	SM
16	SC21	120.7	125.7	34.4	22.2	26	24	2	SM
17	SC27	150.7	155.7	35.2	64.2	38	25	13	CL
18	UD6	151.0	154.0	26	57.5	38	27	11	ML
19	SC28	155.7	160.7	32.6	84.2	51	26	25	CH
20	SC29	160.7	165.7	39.5	93.8	68	45	23	MH



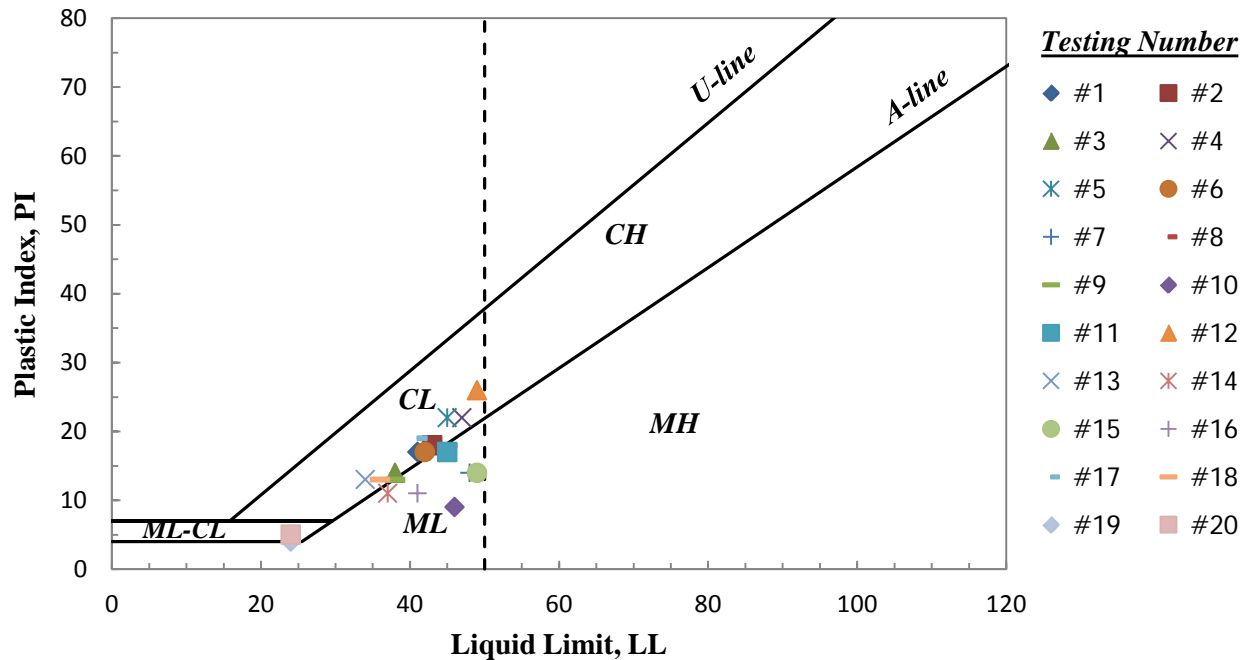
### Plasticity Chart



#	Sample #	Depth (ft)		$\omega_{lab}$ (%)	Fine Content (%)	LL (%)	PL (%)	PI (%)	USCS
		From	To						
1	SC30	165.7	167.7	43.4	81.8	64	35	29	MH
2	SC32	170.7	175.7	40.1	81.8	46	38	8	ML
3	SC33	175.7	180.7	56.2	83.4	54	40	14	MH
4	SC34	180.7	185.7	52.9	71.2	54	47	7	MH
5	SC35	185.7	190.7	34.7	60.0	35	26	9	ML
6	SC41	215.0	215.7	30.8	69.8	43	26	17	CL
7	SC42	215.7	220.7	49.3	41.4	32	26	6	SM
8	SC43	220.7	225.7	27.9	54.4	27	22	5	ML
9	SC44T	225.7	230.7	41.9	40.6	45	19	26	SC
10	SC44B	225.7	230.7	41.9	51.6	32	26	6	ML
11	SC45	230.7	235.7	36.8	46.8	42	26	16	SC
12	SC46	235.7	240.7	33.6	63.8	44	26	18	CL
13	SC47	240.7	245.7	32.7	64.8	45	26	19	CL
14	SC48	245.7	250.7	32.4	68.0	40	30	10	ML
15	SC49	250.7	255.7	32.6	68.0	54	21	33	CH
16	SC50	255.7	260.7	48.5	68.0	43	27	16	ML
17	SC51	260.7	265.7	31.7	58.6	47	27	20	CL
18	SC52	265.7	270.7	28.4	55.6	34	23	11	CL
19	SC53	270.7	275.7	25.3	72.2	44	24	20	CL
20	SC54	275.7	280.7	24.4	61.0	41	24	17	CL



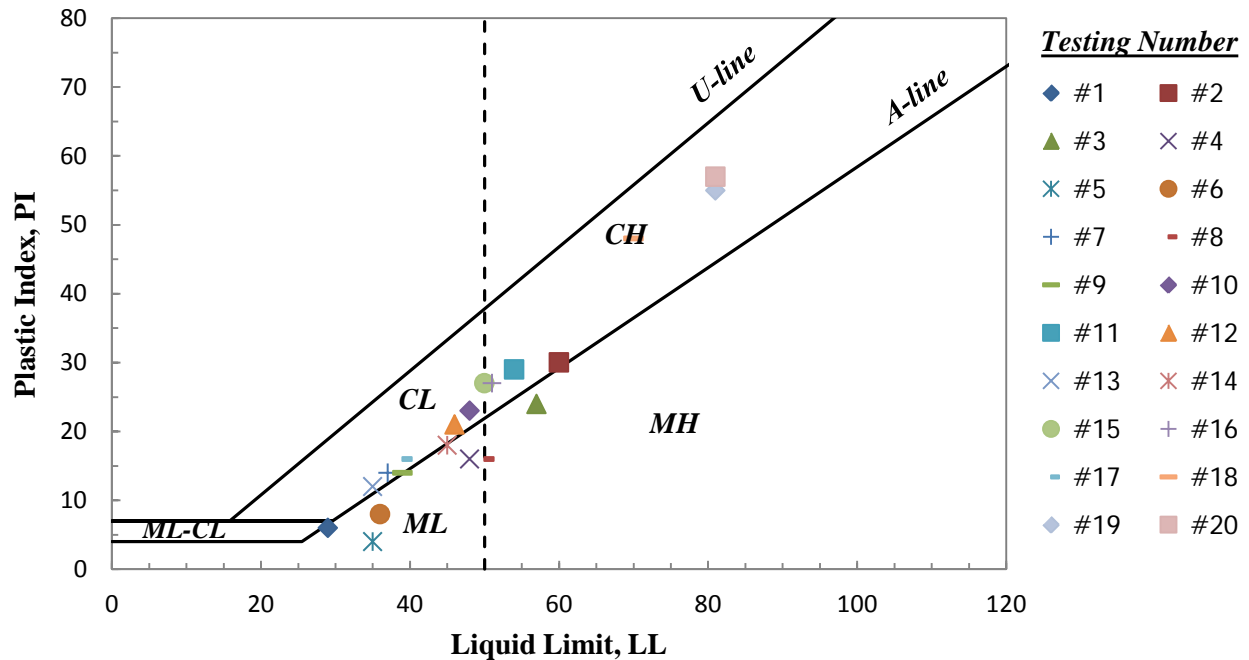
### Plasticity Chart



#	Sample #	Depth (ft)		$\omega_{lab}$ (%)	Fine Content (%)	LL (%)	PL (%)	PI (%)	USCS
		From	To						
1	SC55	280.7	285.7	23.8	65.2	41	24	17	CL
2	SC56	285.7	290.7	25.2	74.0	43	25	18	CL
3	SC57	290.7	295.7	25.8	72.2	38	24	14	CL
4	SC58	295.7	300.7	26	82.2	47	25	22	CL
5	SC59	300.7	305.7	26.6	81.2	45	23	22	CL
6	SC60	305.7	310.7	18.3	77.4	42	25	17	CL
7	SC61	310.7	315.7	28.5	85.2	48	34	14	ML
8	SC62	315.7	320.7	17.1	82.4	45	27	18	ML
9	SC63	320.7	325.7	17.5	81.0	38	25	13	ML
10	SC64	325.7	330.7	27.2	90.0	46	37	9	ML
11	SC65	330.7	335.7	21.2	93.0	45	28	17	ML
12	SC66	335.7	340.7	32.1	88.6	49	23	26	CL
13	SC67	340.7	345.7	30.7	94.0	34	21	13	CL
14	SC68	345.7	350.7	20.5	86.2	37	26	11	ML
15	SC69	350.7	355.7	24.6	94.2	49	35	14	ML
16	SC70	355.7	360.7	19.9	92.2	41	30	11	ML
17	SC71	360.7	365.7	26.8	82.6	41	22	19	CL
18	SC72	365.7	370.7	12.6	63.4	36	23	13	CL
19	SC73	370.7	375.7	19.5	34.4	24	20	4	SC-SM
20	SC74	375.7	380.7	12.2	38.4	24	19	5	SC-SM



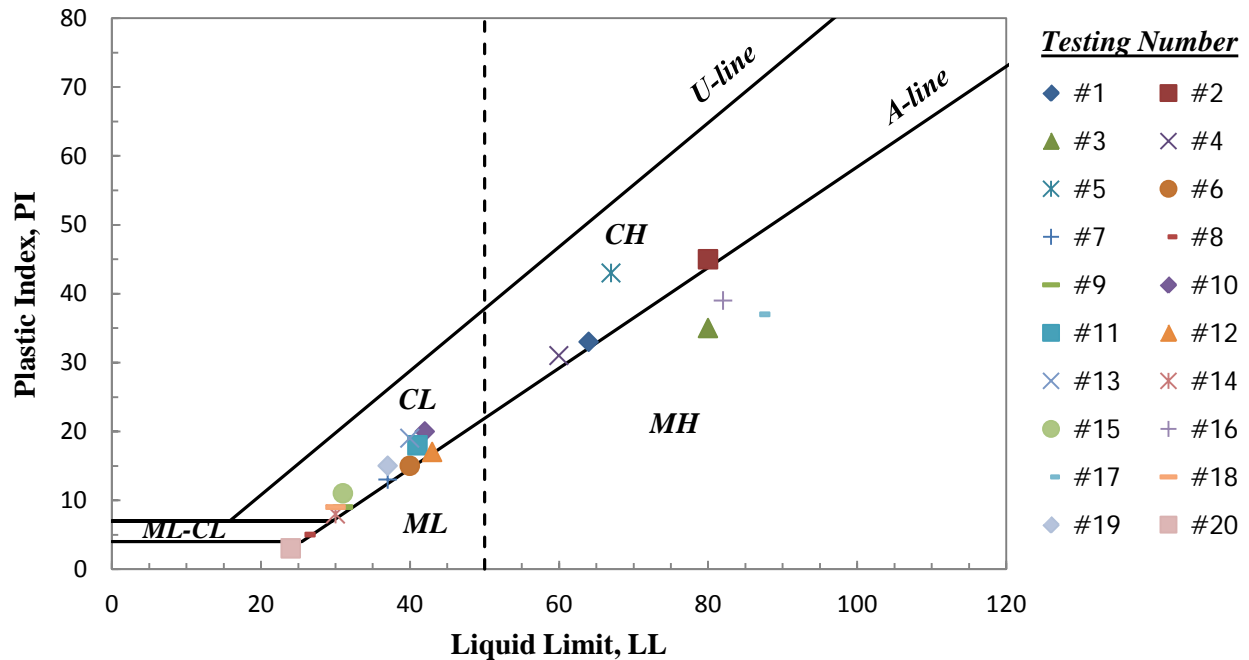
### Plasticity Chart



#	Sample #	Depth (ft)		$\omega_{lab}$ (%)	Fine Content (%)	LL (%)	PL (%)	PI (%)	USCS
		From	To						
1	SC75	380.7	385.7	25.4	37.8	29	23	6	SM
2	SC76	385.7	390.7	44.7	47.4	60	30	30	SC
3	SC77	390.7	395.7	33.2	62.0	57	33	24	MH
4	SC78	395.7	400.7	34.4	67.2	48	32	16	ML
5	SC79	400.7	405.7	26.7	45.8	35	31	4	SM
6	SC80	405.7	410.7	26.9	46.6	36	28	8	SM
7	SC81	410.7	415.7	24.2	61.2	37	23	14	CL
8	SC82	415.7	420.7	28.8	78.2	50	34	16	MH
9	SC84	425.7	430.7	29.5	47.4	39	25	14	SM
10	SC85	430.7	435.7	25.9	56.4	48	25	23	CL
11	SC86	435.7	440.7	28.4	73.0	54	25	29	CH
12	SC87	440.7	445.7	27.7	59.0	46	25	21	CL
13	SC88	445.7	450.7	19.8	48.8	35	23	12	SC
14	SC89	450.7	455.7	27.9	75.2	45	27	18	ML
15	SC90	455.7	460.7	28.2	80.6	50	23	27	CH
16	SC91	460.7	465.7	29.1	82.2	51	24	27	CH
17	SC92	465.7	470.7	28	52.6	39	23	16	CL
18	SC93	470.7	475.7	29.4	66.2	70	22	48	CH
19	SC94	475.7	480.7	36	76.2	81	26	55	CH
20	SC95	480.7	485.7	29.6	67.0	81	24	57	CH



### Plasticity Chart

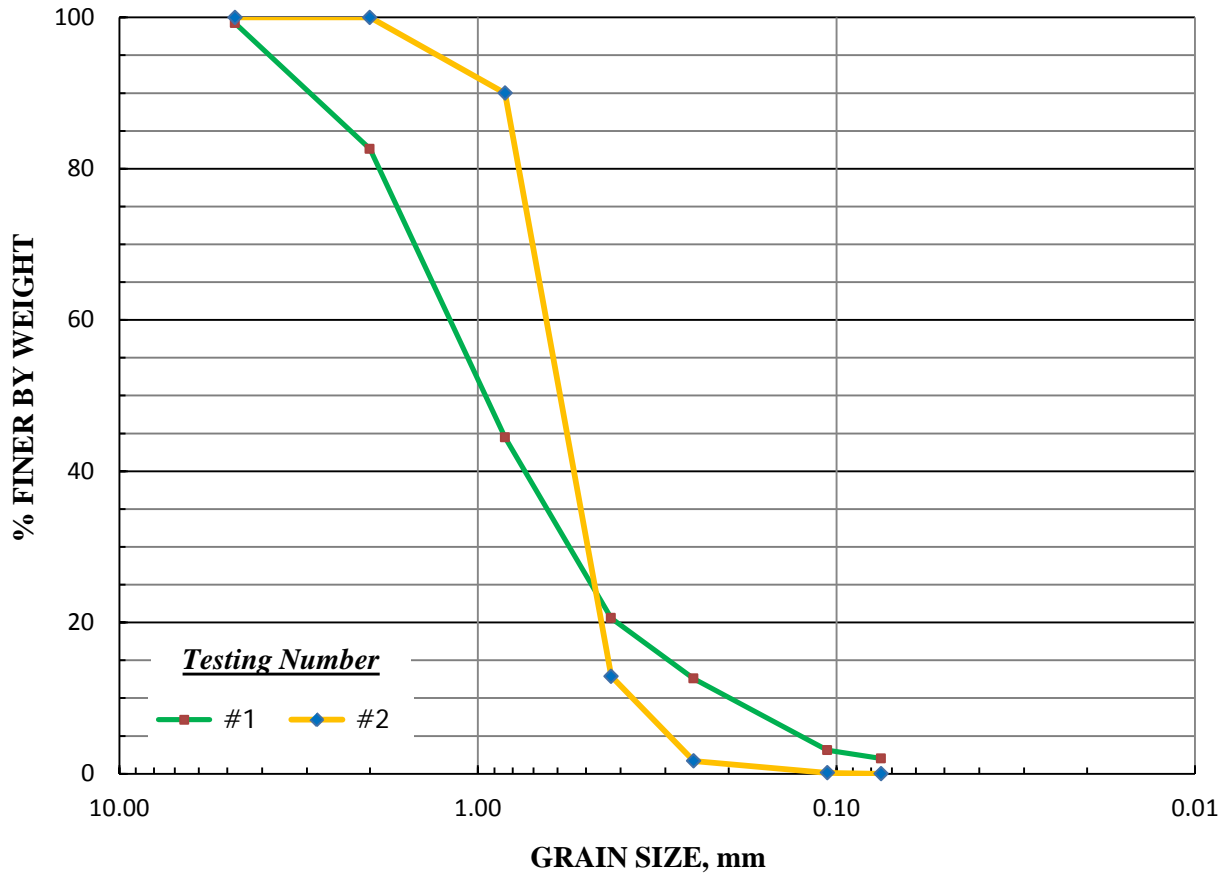


#	Sample #	Depth (ft)		$\omega_{lab}$ (%)	Fine Content (%)	LL (%)	PL (%)	PI (%)	USCS
		From	To						
1	SC96	485.7	490.7	29.8	75.0	64	31	33	CH
2	SC97	490.7	495.7	40.3	91.8	80	35	45	CH
3	SC98	495.7	500.7	59.1	94.8	80	45	35	MH
4	SC99	500.7	505.7	37.5	81.0	60	29	31	CH
5	SC100	505.7	510.7	36.9	71.6	67	24	43	CH
6	SC101	510.7	515.7	26.3	41.8	40	25	15	SC
7	SC102	515.7	520.7	39.2	43.8	37	24	13	SC
8	SC103	520.7	525.7	21.9	31.0	26	21	5	SC-SM
9	SC104	525.7	530.7	21.1	34.2	31	22	9	SC
10	SC105	530.7	535.7	25.7	43.0	42	22	20	SC
11	SC106	535.7	540.7	28.6	31.2	41	23	18	SC
12	SC107	540.7	545.7	31	43.0	43	26	17	SC
13	SC108	545.7	550.7	26.7	34.0	40	21	19	SC
14	SC113	570.7	575.7	25.9	25.0	30	22	8	SC
15	SC115	580.7	585.7	28.6	25.6	31	20	11	SC
16	SC116	585.7	590.7	33	81.8	82	43	39	MH
17	SC117	590.7	595.7	31.1	90.6	87	50	37	MH
18	SC118	595.7	600.7	22.8	29.0	30	21	9	SC
19	SC119	600.7	605.7	37.9	36.4	37	22	15	SC
20	SC120	605.7	610.7	27.6	16.8	24	21	3	SM





### GRAIN SIZE DISTRIBUTION



GRAVEL	SAND			SILT or CLAY
	coarse	medium	fine	

#	Sample #	Depth (ft)		%Gravel	%Sand	%Silt %Clay	D <sub>60</sub>	D <sub>30</sub>	D <sub>10</sub>	Cc	Cu
		From	To								
1	UD-03	8.0	10.0	100.0	98.0	2.0	1.30	0.54	0.20	1.12	6.50
2	UD-05	148.0	151.0	100.0	100.0	0.0	0.63	0.50	0.37	1.07	1.70

## **Appendix F: Resonant Column and Torsional Shear Testing Procedures and Results**

---

## General Testing Procedures for Resonant column (RC) and Torsional Shear (TS) Tests

### 1. Sample Preparation

- 1.1. For Shelby tube samples, the tube is cut to an appropriate length and then cut lengthwise to be able to split into two sections (Fig. 1-a). The soil sample is carefully removed and placed on the trimming device (see in Fig. 1-b). The sample is then trimmed to 1.4 inches in diameter and 2:1 (length to diameter) dimensional ratio. (Fig. 1-c to 2-a).



**Fig. 1** Soil Sample Preparation: (a) Cutting, (b) Removing Tube and (c) Trimming

- 1.2. For core samples (soil and rock), the sample is very stiff due to cementation so it can not be trimmed radially without disturbing the sample. As a result, the sample is tested “as-is” at approximately 2.5 inches in diameter and 2:1 (length to diameter) dimensional ratio (Fig. 2-b). Top and bottom surfaces of the sample are leveled before installing in the RCTS equipment to avoid tilting during testing (Fig. 2-c). The top and bottom surface of rock samples are scratched to create friction between top and bottom platen (see in Figs. 2-b to c).

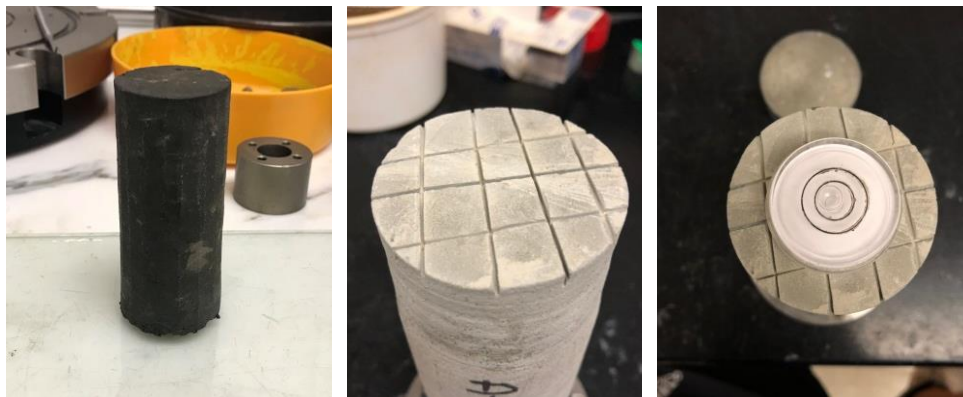


**Fig. 2** Core Sample Preparation for RC and TS Tests: (a) Soil Core Sample, (b) Rock Core Sample and (c) Leveling Rock Sample

- 1.3. Filter paper discs are then installed at the top and bottom of the sample and six filter strips are installed along the length of the sample to accelerate consolidation process (Fig. 3-a). For the rock sample, the top and bottom platens are glued to the sample using epoxy resin. The resin is allowed to cure for at least 24 hours (see in Fig.3-d).
- 1.4. A rubber membrane is installed around the sample (Fig. 3-b) and secured with o-rings (Fig. 3-b). Vacuum grease is used in this process to improve contact force between the metal and rubber membrane. A water bath is installed around soil samples (Fig. 3-c). The rubber membrane and water bath are not used for the rock samples.



**Fig. 3** Sample Setup in RCTS Device: (a) Disc Filter Paper and Filter Drainages, (b) Radius Drainages Installation with Soil Sample, (c) Rock Sample Installation on Bottom Plate and (d) Top Cap Installation above Rock Sample

- 1.5. The RCTS drive plate system is then installed (Fig. 4-a) and the accelerometer, two proximeters and a LVDT at the drive plate system are setup (Fig. 4-b)
- 1.6. The RCTS chamber is then installed and the sample is ready for consolidation.

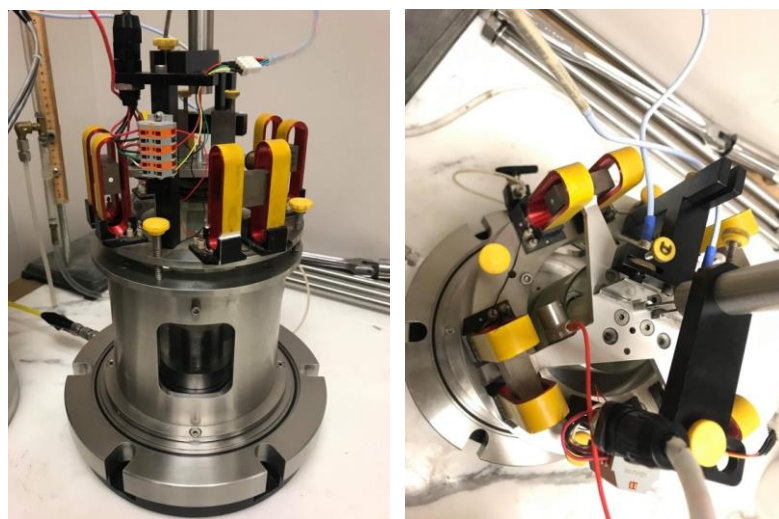


**Fig. 4** Drive Plate System Installation: (a) Drive Plate, and (b) Accelerometer, LVDT and Proximeter Sensors

## **2. Consolidation**

- 2.1. A drainage valve is opened and a target confining pressure is applied to the desired confining stress.
- 2.2. Sample settlement is monitored and recorded using an LVDT. Low-strain shear modulus is also observed during consolidation process. The end of primary consolidation is determined based on the settlement and observing when the ratio between the change of low-strain shear modulus and the shear modulus at 1000 minutes after applying the confining pressure ( $\Delta G/G_{1000}$  or  $N_G$ ) is less than 15%.
- 2.3. Once the RC and TS tests are completed as described in 3.1 and 3.2, the confining pressure is increased to the next level.

## **3. Testing procedure**

- 3.1. Upon a completion of the consolidation process, the RC and TS tests are performed at the lowest shear strain level possible. For the RC test, the first mode resonant frequency of the sample is determined from the response curves. The TS test is performed at a frequency of 1 Hz and 10 cycles.
- 3.2. The RC and TS tests are then repeated at higher strain amplitude. For the first and second confining pressure, the tests stop at  $G/G_{\max}$  of approximately 0.8 to avoid sample disturbance. For the highest confining pressure, the tests stop at  $G/G_{\max}$  approximately 0.55 as it reaches the maximum capacity of the RCTS equipment.



## RESONANT COLUMN (RC) AND TORSIONAL SHEAR (TS) TESTING SUMMARY

Project Name: Deep Soil Test Boring to Determine Shear  
Wave Velocities across South Carolina

Boring No.: B-CON and B-BMF  
Location: Conway and Andrews, SC

Client: SCDOT  
Project ID: SPR-731

**Summary Table for Site A: B-CON (Conway, SC)**

#	Sample #	Depth (ft)	$\sigma'_{mo}$ (psi)	Soil / Rock Type	% Finer	PI	LL	$\omega_1$ (%)	$\omega_2$ (%)	Total Unit Weight (lb/ft <sup>3</sup> )	Sample Height (inch)	D <sub>min,RC</sub> (%)	D <sub>min,TS</sub> (%)	G <sub>max,RC</sub> (ksf)	G <sub>max,TS</sub> (ksf)	Geology Formation	Age.
1	C-UD-01	11	5	CH	95.1	28	51	43.4	37.1	110	2.77	1.54	1.59	769	813	QUATERNARY (Penholoway allo Fm.)	2.6 - 0.01 MYA
2	C-UD-02*	16	6	SC-SM	8.0	np	-	0	0	92	6.00	0.62	0.77	1156	1117		
3	C-UD-03	56	17	CH	91.6	44	68	35.34	37.1	113	3.61	3.20	1.48	2728	2499	CRETACEOUS (Middle Peedee Fm.)	69.5 - 66.0 MYA
4	C-UD-07	84	25	CH	87.0	43	68	40.7	35.8	109	3.83	2.93	1.98	1306	1330		
5	C-UD-08	87	26	MH	93.8	47	74	42.6	37.7	110	2.84	3.34	2.01	1341	1406		
6	C-SC-09	158	48	SC	30.6	14	34	20.3	26.4	112	2.80	4.57	1.72	3323	3163	CRETACEOUS (Lower Peedee Fm.)	72.1 - 69.5 MYA
7	C-SC-15	188	57	MH	70.2	19	50	31.2	28.3	113	3.17	3.65	1.86	2980	2811		
8	C-SC-04R	133	45	Sandstone	-	-	-	-	-	157	5.53	0.38	-	85619	-	CRETACEOUS (Black Creek Group)	83.6 - 72.1 MYA
9	C-SC-34	283	83	SC	43.6	15	39	30.1	27	106	3.52	3.61	1.56	2508	2405		
10	C-SC-56	393	113	CH	95.7	34	60	36.5	36.1	105	2.79	4.4	2.07	2153	1852		
11	C-SC-63	428	121	CH	80.0	39	64	43.5	40.5	106	3.44	5.31	1.98	1844	1609		
12	C-SC-39R	308	93	Sandstone	-	-	-	-	-	167	5.32	1.19	-	97066	-		
13	C-SC-40R	313	110	Sandstone	-	-	-	-	-	166	5.62	0.69	-	101401	-		
14	C-SC-41R	318	103	Sandstone	-	-	-	-	-	165	5.28	0.94	-	101853	-		
15	C-SC-68R	454	160	Sandstone	-	-	-	-	-	165	4.93	1.97	-	77964	-		

UD = shelly tube sample; SC = core sample;  $\sigma'_{mo}$  = effective insitu mean stress; np = nonplastic; \* reconstituted sample

**Summary Table for Site B: B-FMG (Andrews, SC)**

#	Sample #	Depth (ft)	$\sigma'_{mo}$ (psi)	Soil / Rock Type	% Finer	PI	LL	$\omega_1$ (%)	$\omega_2$ (%)	Total Unit Weight (lb/ft <sup>3</sup> )	Sample Height (inch)	D <sub>min,RC</sub> (%)	D <sub>min,TS</sub> (%)	G <sub>max,RC</sub> (ksf)	G <sub>max,TS</sub> (ksf)	Geology Formation	Age.
1	A-UD-01	5.0	2.2	SC	30.5	27	51	22.6	17.6	123	3.32	-	3.33	-	958	QUATERNARY (Ten Mile Hill Fm.)	(N.A.)
2	A-UD-02	7.0	2.7	SM	23.2	1	16	14.3	13.9	106	3.41	2.54	1.38	747	786		
3	A-UD-03*	9.0	3.3	SM	14.3	np	-	0	0	107	6.10	1.60	1.47	307	309	TERTIARY (Williams Burg Fm. and Lower Bridge Member)	58.0 - 56.0 MYA
4	A-UD-05*	149.5	41.4	SP	0.0	np	-	0	0	90	5.35	0.28	0.48	3823	3754		
5	A-UD-06	152.5	43.1	ML	57.5	11	38	26	23.5	118	3.54	1.88	0.97	2436	2422	TERTIARY (Rhems Fm.)	65.0 - 61.0 MYA
6	A-SC-27	153.2	43.2	CL	64.2	13	38	33.3	30.2	117	3.65	1.52	1.00	2190	2382		
7	A-SC-42R	218	68	Sandstone	-	-	-	-	-	161	5.84	1.01	-	48667	-	CRETACEOUS (Peedee Fm.)	72.1 - 66.0 MYA
8	A-SC-49	253.2	68.2	CH	68.0	33	54	30.2	24.8	115	3.53	5.01	1.83	2598	2230		
9	A-SC-77	393	110	MH	62.0	24	57	35.4	33.5	105	2.94	5.46	2.05	2077	1985		
10	A-SC-86	438.2	122.1	CH	72.6	29	54	25.7	24.3	118	3.42	4.03	1.17	6408	5767		
11	A-SC-52R	268	89	Sandstone	-	-	-	-	-	160	5.66	0.95	-	75353	-		
12	A-SC-59R	303	100	Claystone	-	-	-	-	-	152	4.78	1.09	-	53424	-		
13	A-SC-60R	308	98	Claystone	-	-	-	-	-	148	5.57	0.47	-	79100	-		
14	A-SC-96	488.2	136.0	CH	74.9	33	64	31.3	30.9	115	3.08	4.77	1.62	5336	4757	CRETACEOUS (Black Creek Group)	83.6 - 72.1 MYA
15	A-SC-105	533.2	147.8	SC	42.9	20	42	25.6	22.1	118	3.83	5.04	2.21	6861	5683		
16	A-SC-109R	553	184	Sandstone	-	-	-	-	-	167	5.80	0.28	-	110089	-		
17	A-SC-110R	558	174	Sandstone	-	-	-	-	-	168	5.70	1.54	-	118799	-		
18	A-SC-112R	568	177	Sandstone	-	-	-	-	-	167	5.30	1.86	-	92715	-		
19	A-SC-115R	583	197	Sandstone	-	-	-	-	-	163	5.34	1.92	-	72416	-		
20	A-SC-116R	588	190	Sandstone	-	-	-	-	-	167	5.93	1.42	-	114815	-		

UD = shelly tube sample; SC = core sample;  $\sigma'_{mo}$  = effective insitu mean stress; np = nonplastic; \* reconstituted sample



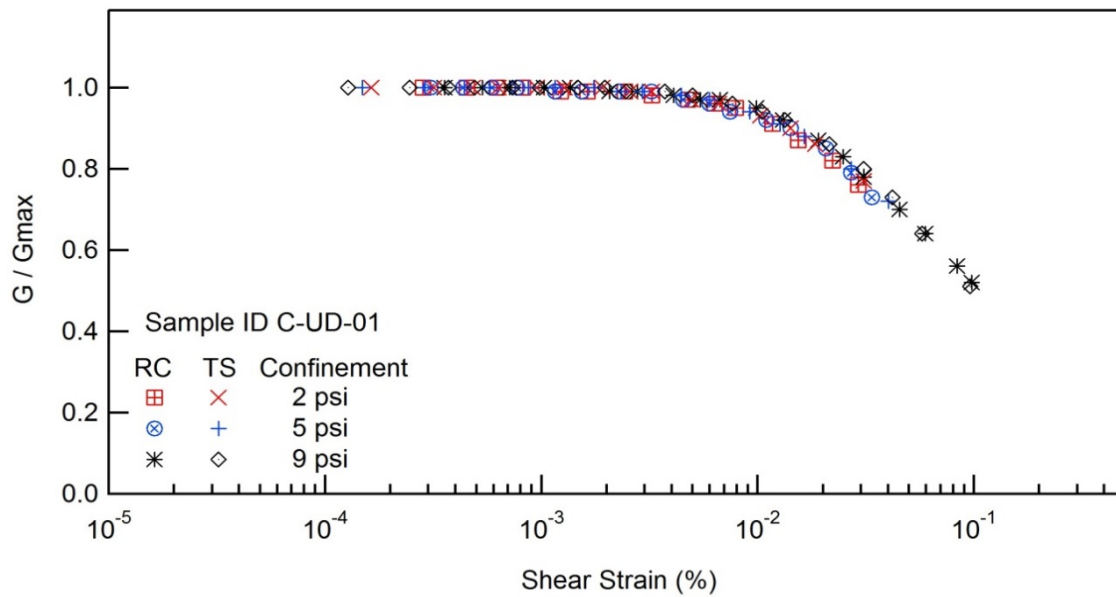
## RESONANT COLUMN (RC) AND TORSIONAL SHEAR (TS) TEST

Project Name: Deep Soil Test Boring to Determine Shear  
Wave Velocities across South Carolina

Client: SCDOT  
Location: Conway, SC

Project ID: SPR-731  
Boring No.: B-CON

Sample ID : C-UD-01





## RESONANT COLUMN (RC) AND TORSIONAL SHEAR (TS) TEST

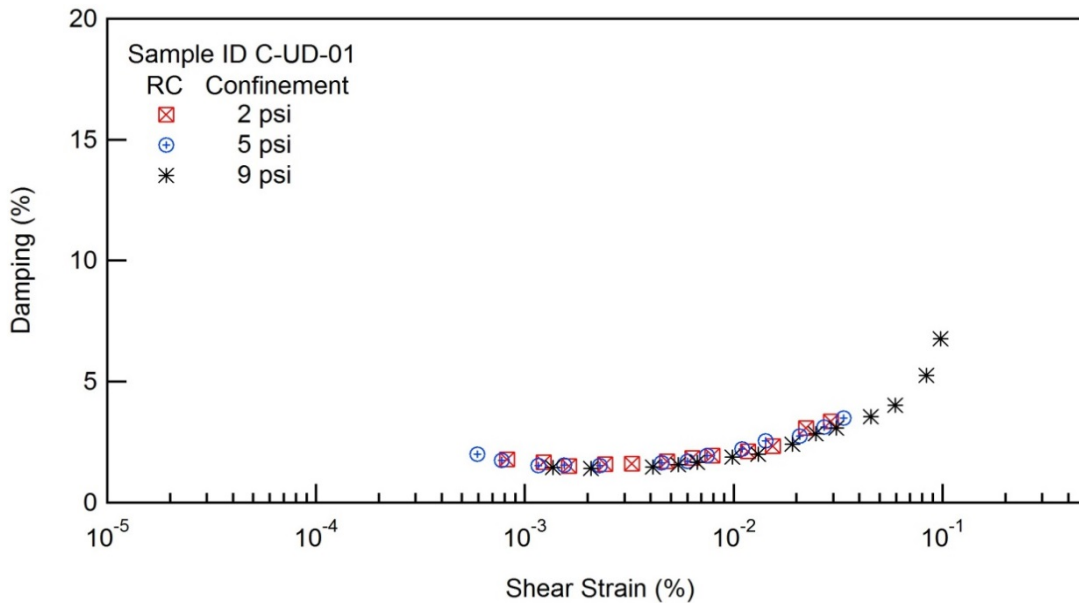
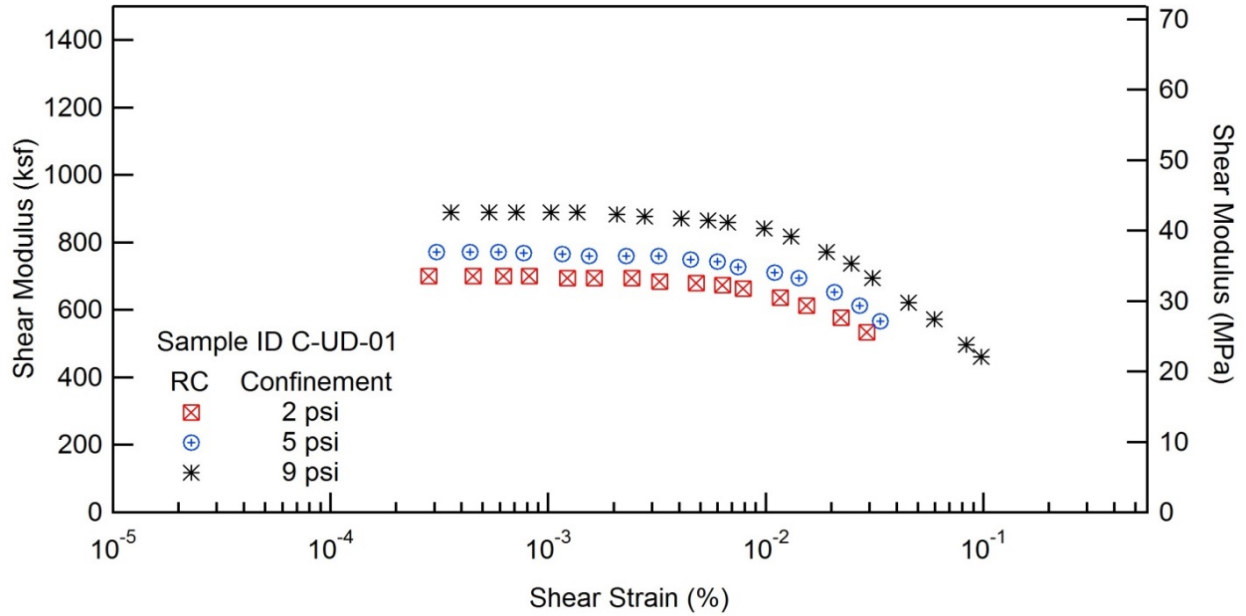
Project Name: Deep Soil Test Boring to Determine Shear  
Wave Velocities across South Carolina

Client: SCDOT

Project ID: SPR-731

Location: Conway, SC

Boring No.: B-CON



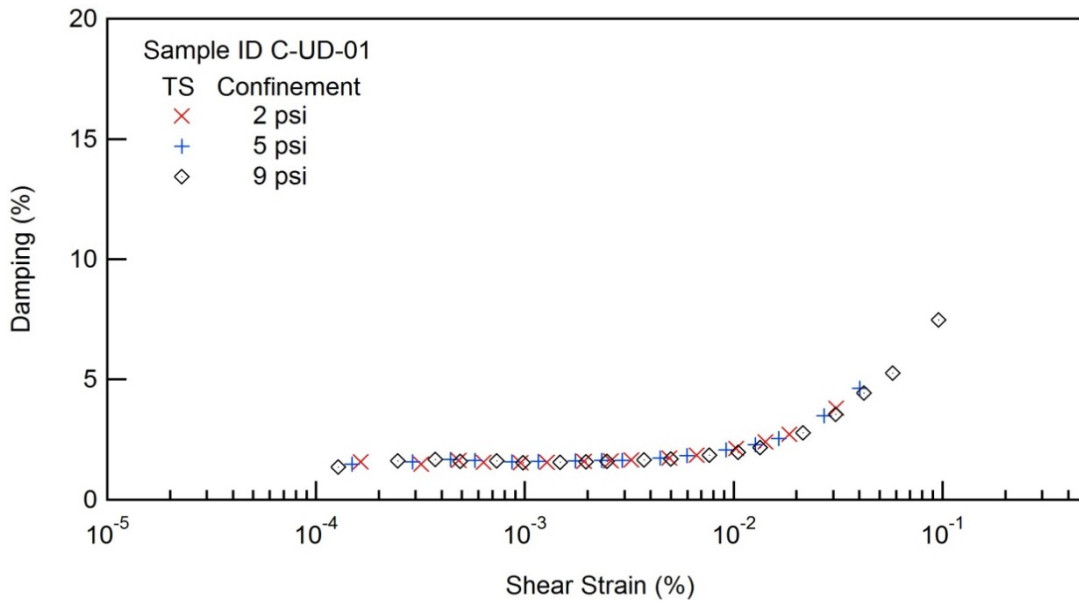
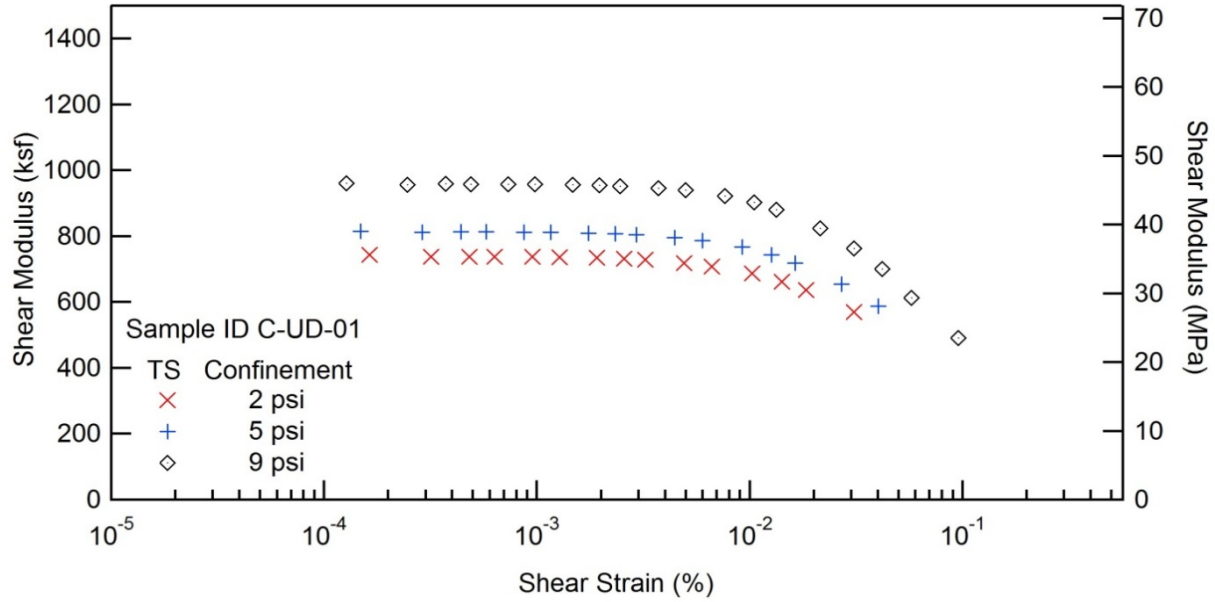


### RESONANT COLUMN (RC) AND TORSIONAL SHEAR (TS) TEST

Project Name: Deep Soil Test Boring to Determine Shear  
Wave Velocities across South Carolina

Client: SCDOT  
Location: Conway, SC

Project ID: SPR-731  
Boring No.: B-CON









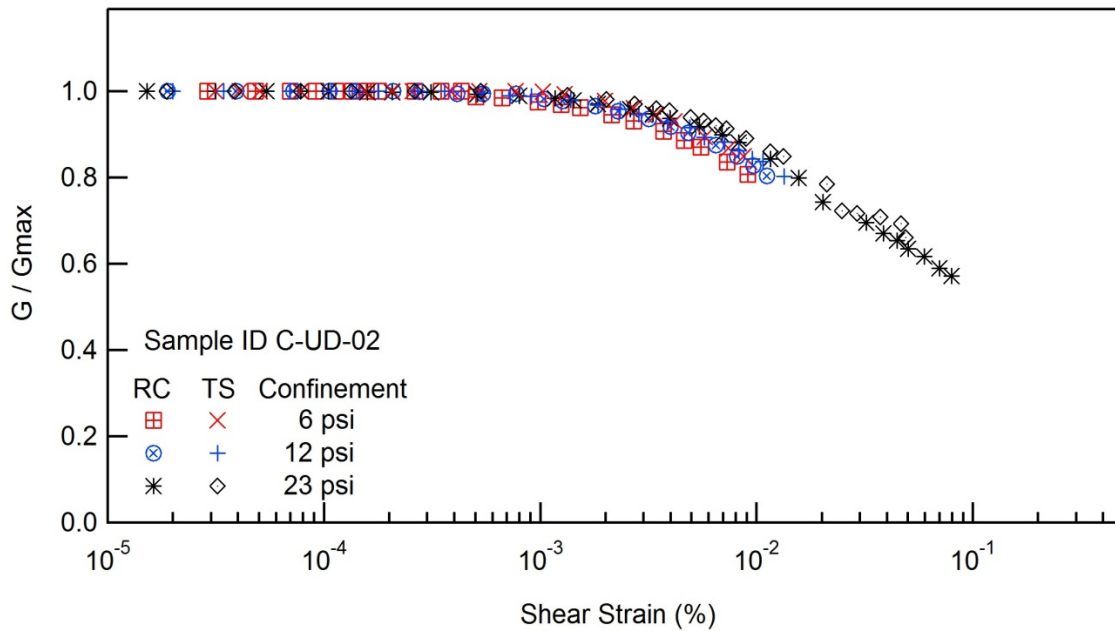
## RESONANT COLUMN (RC) AND TORSIONAL SHEAR (TS) TEST

Project Name: Deep Soil Test Boring to Determine Shear  
Wave Velocities across South Carolina

Client: SCDOT  
Location: Conway, SC

Project ID: SPR-731  
Boring No.: B-CON

Sample ID : C-UD-02



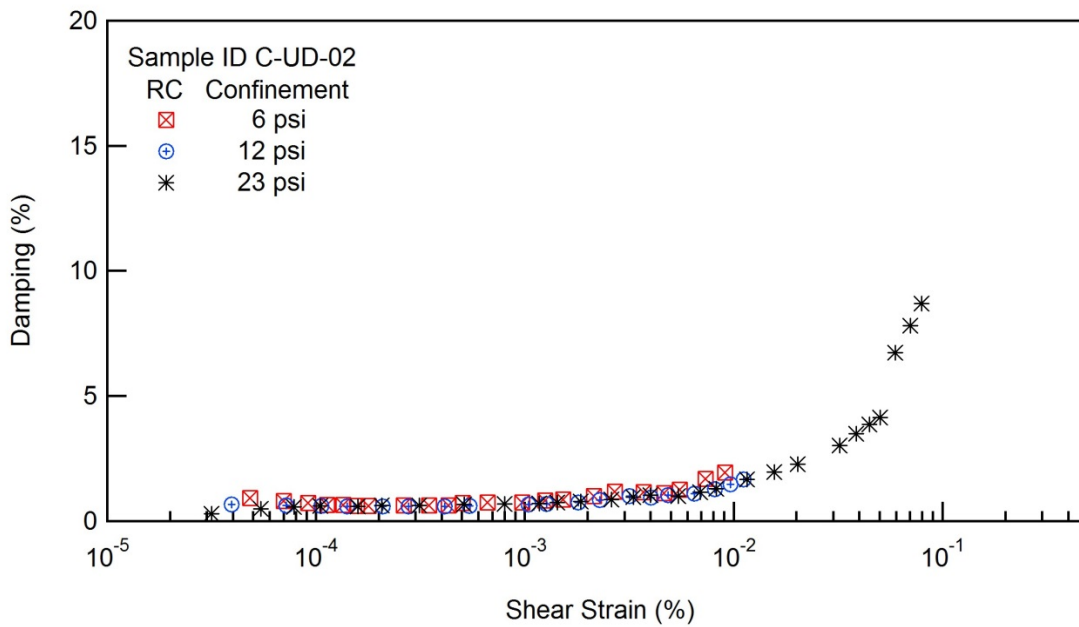
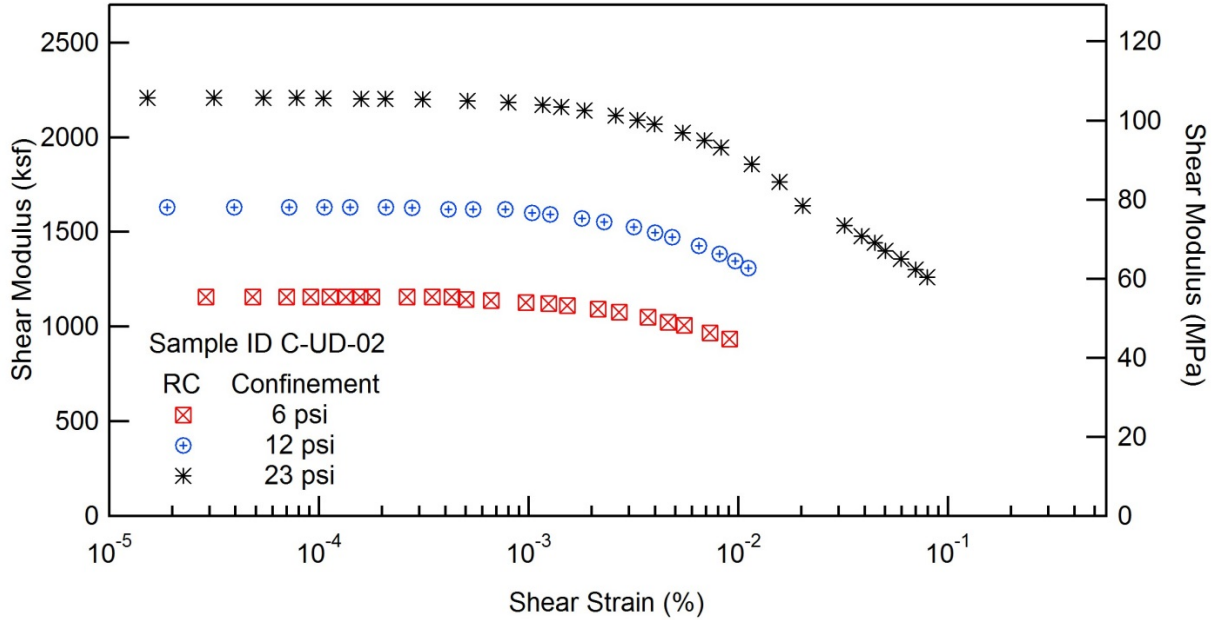


### RESONANT COLUMN (RC) AND TORSIONAL SHEAR (TS) TEST

Project Name: Deep Soil Test Boring to Determine Shear  
Wave Velocities across South Carolina

Client: SCDOT  
Location: Conway, SC

Project ID: SPR-731  
Boring No.: B-CON



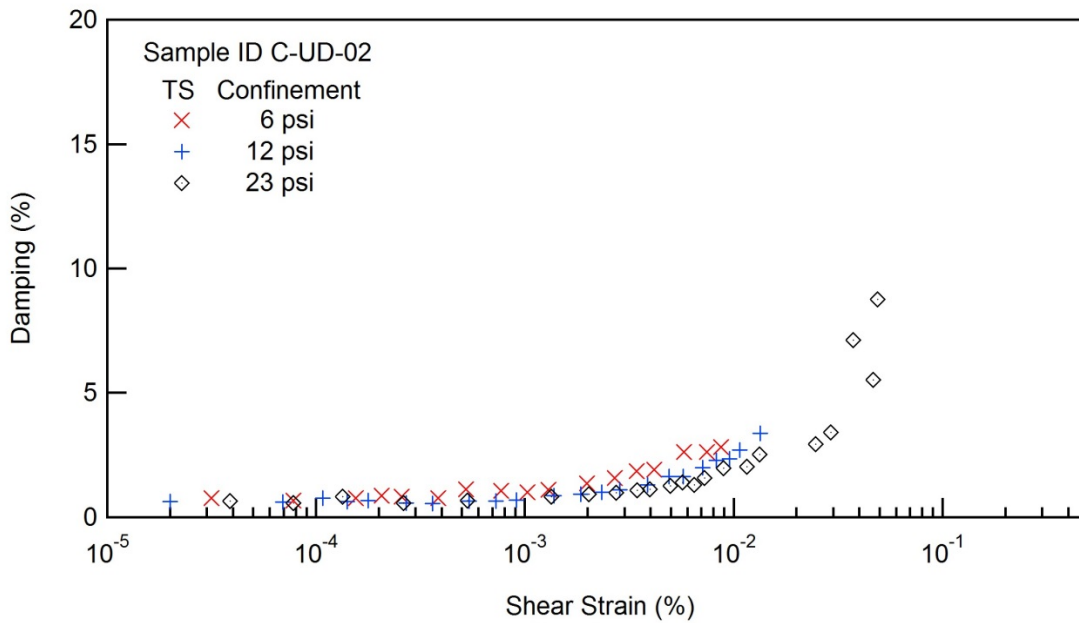
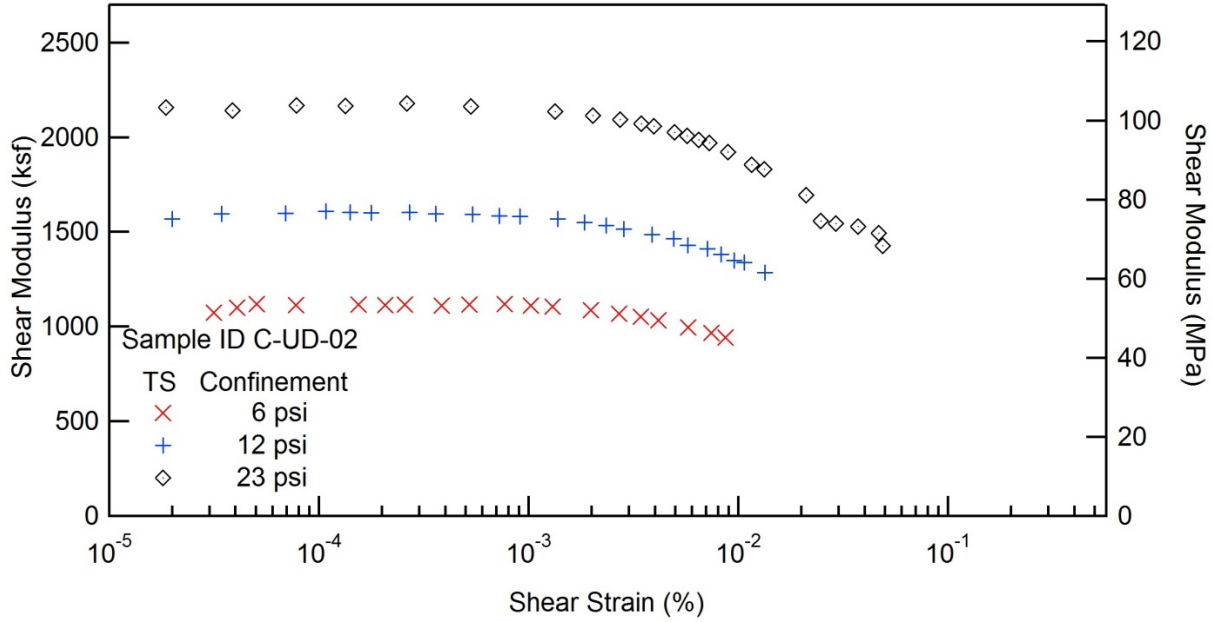


# RESONANT COLUMN (RC) AND TORSIONAL SHEAR (TS) TEST

Project Name: Deep Soil Test Boring to Determine Shear  
Wave Velocities across South Carolina

Client: SCDOT  
Location: Conway, SC

Project ID: SPR-731  
Boring No.: B-CON









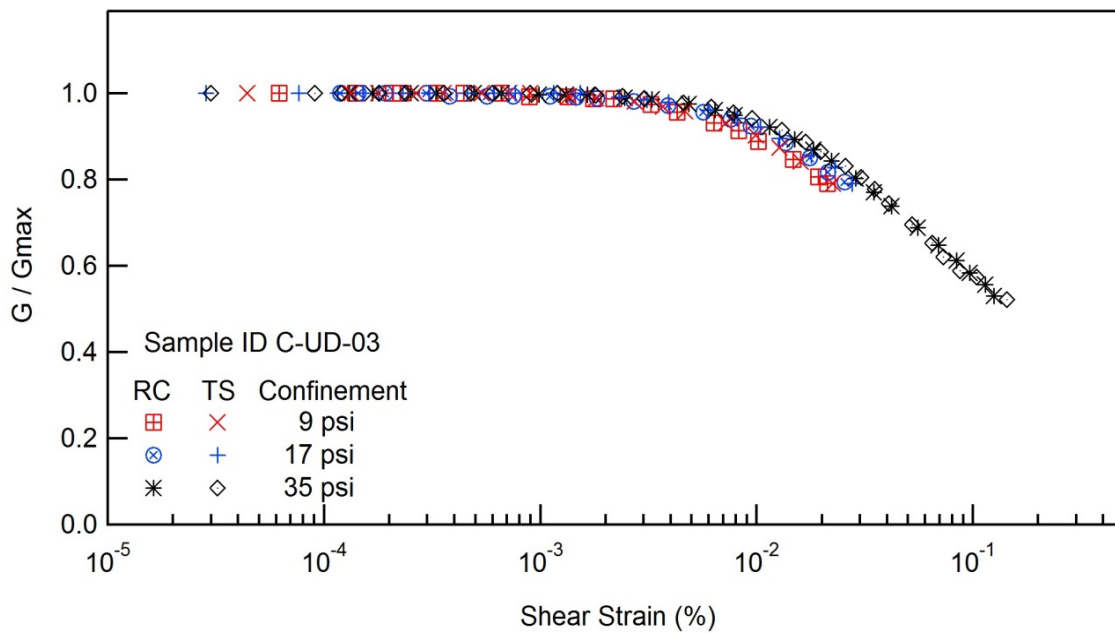
## RESONANT COLUMN (RC) AND TORSIONAL SHEAR (TS) TEST

Project Name: Deep Soil Test Boring to Determine Shear  
Wave Velocities across South Carolina

Client: SCDOT  
Location: Conway, SC

Project ID: SPR-731  
Boring No.: B-CON

Sample ID : C-UD-03





## RESONANT COLUMN (RC) AND TORSIONAL SHEAR (TS) TEST

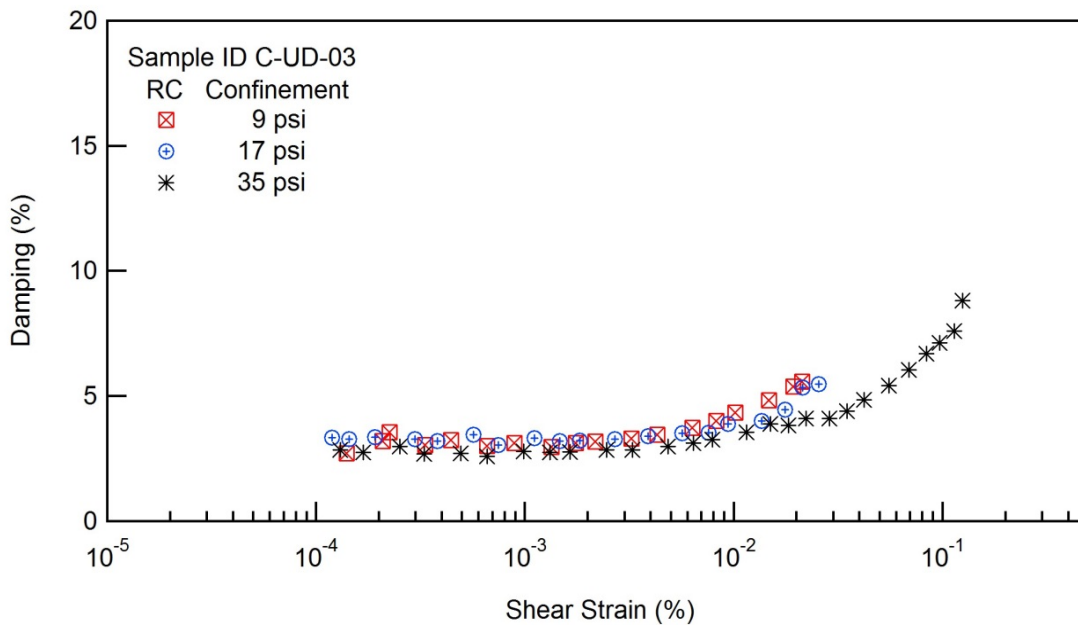
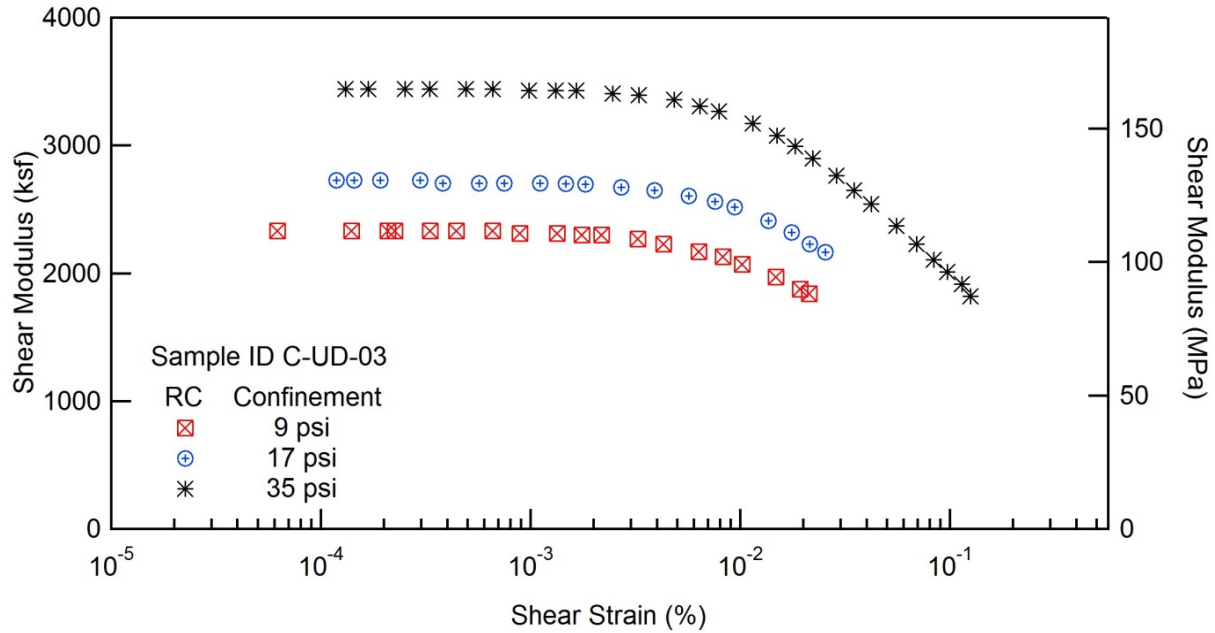
Project Name: Deep Soil Test Boring to Determine Shear  
Wave Velocities across South Carolina

Client: SCDOT

Project ID: SPR-731

Location: Conway, SC

Boring No.: B-CON



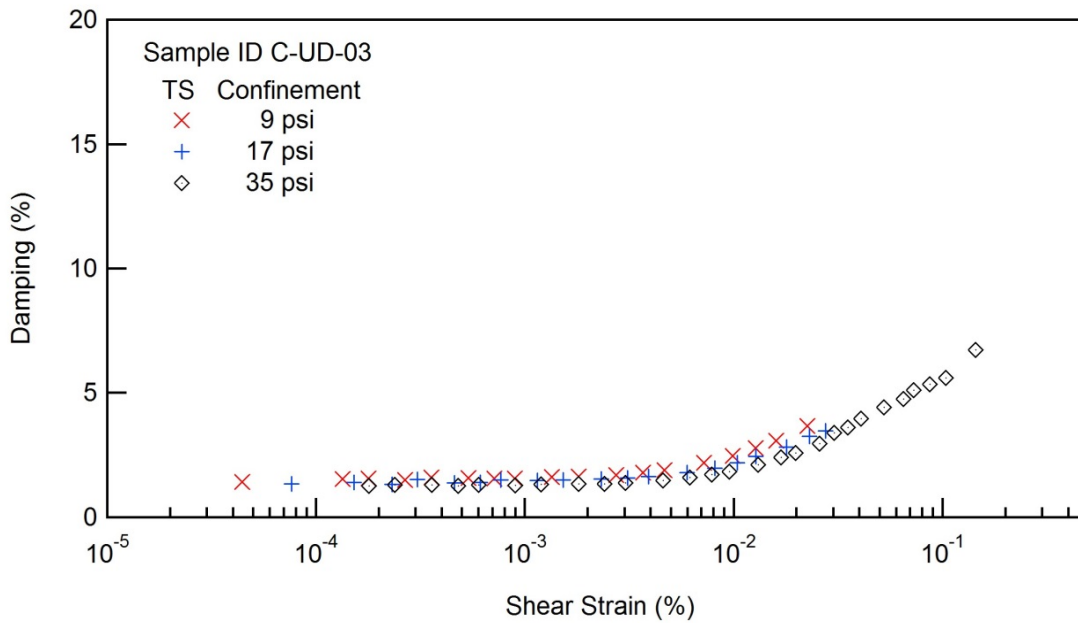
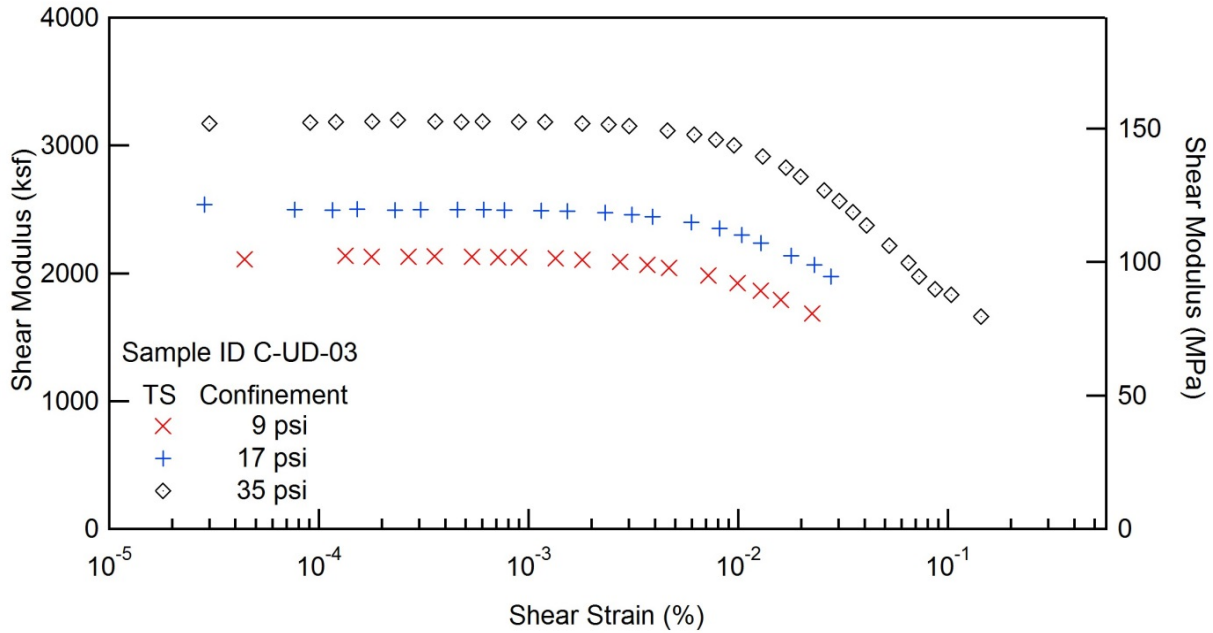


## RESONANT COLUMN (RC) AND TORSIONAL SHEAR (TS) TEST

Project Name: Deep Soil Test Boring to Determine Shear  
Wave Velocities across South Carolina

Client: SCDOT  
Location: Conway, SC

Project ID: SPR-731  
Boring No.: B-CON









## RESONANT COLUMN (RC) AND TORSIONAL SHEAR (TS) TEST

Project Name: Deep Soil Test Boring to Determine Shear  
Wave Velocities across South Carolina

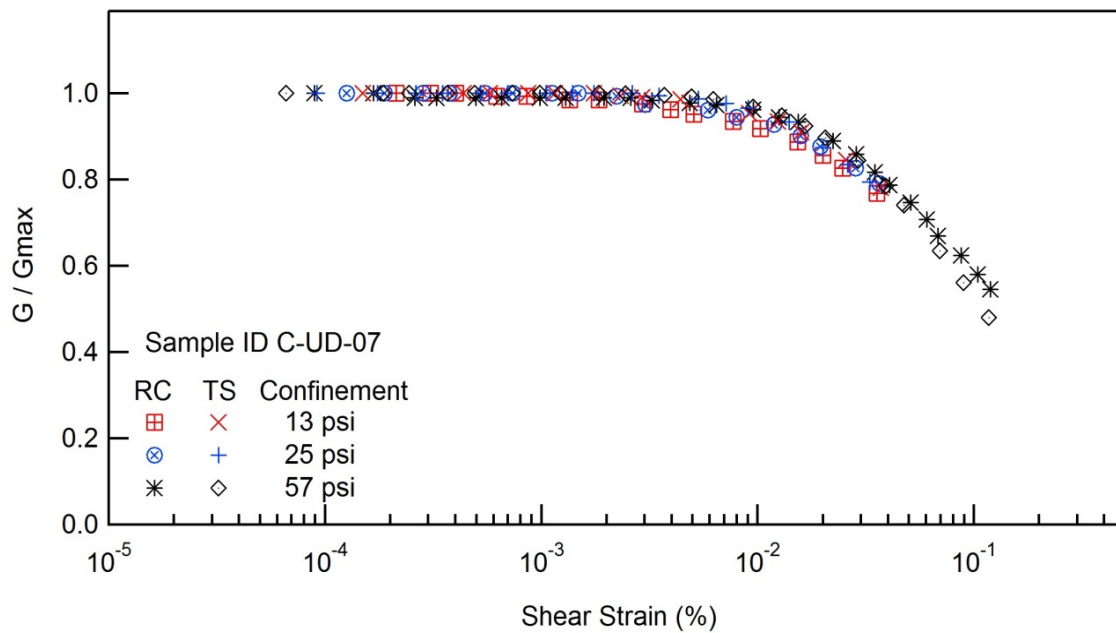
Client: SCDOT

Project ID: SPR-731

Location: Conway, SC

Boring No.: B-CON

Sample ID : C-UD-07



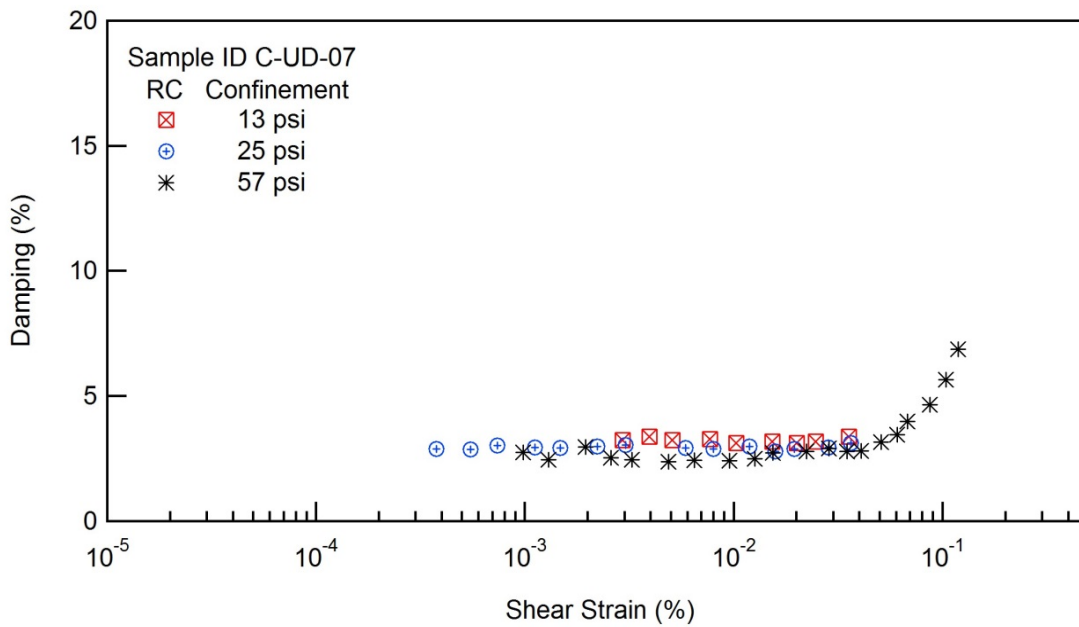
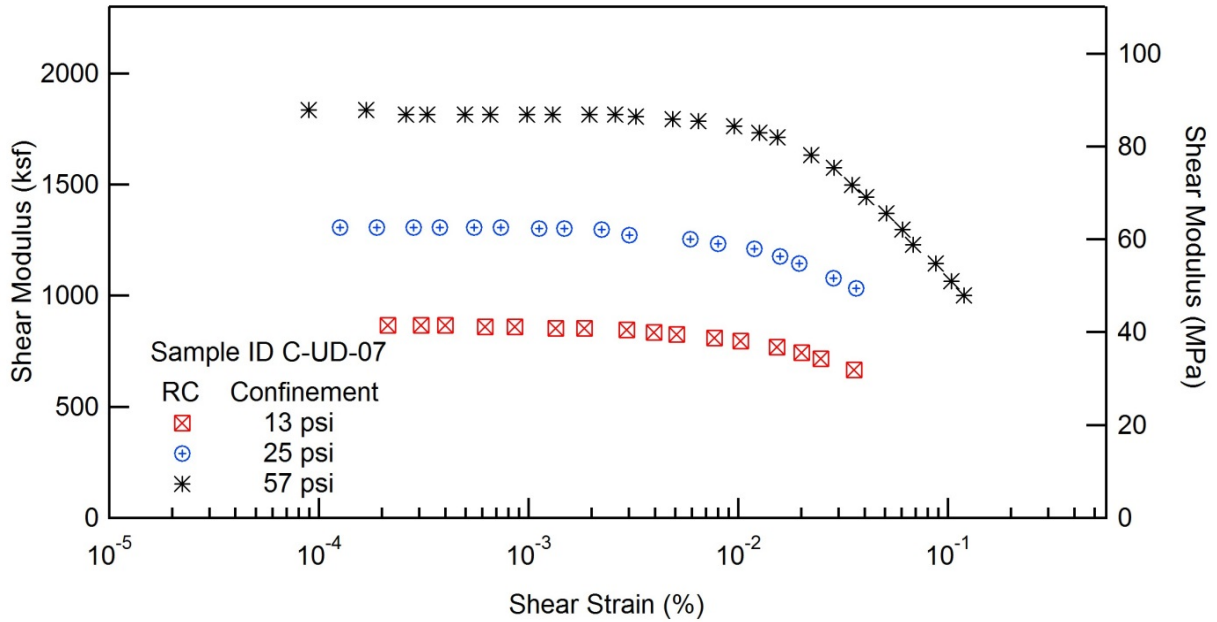


### RESONANT COLUMN (RC) AND TORSIONAL SHEAR (TS) TEST

Project Name: Deep Soil Test Boring to Determine Shear  
Wave Velocities across South Carolina

Client: SCDOT  
Location: Conway, SC

Project ID: SPR-731  
Boring No.: B-CON



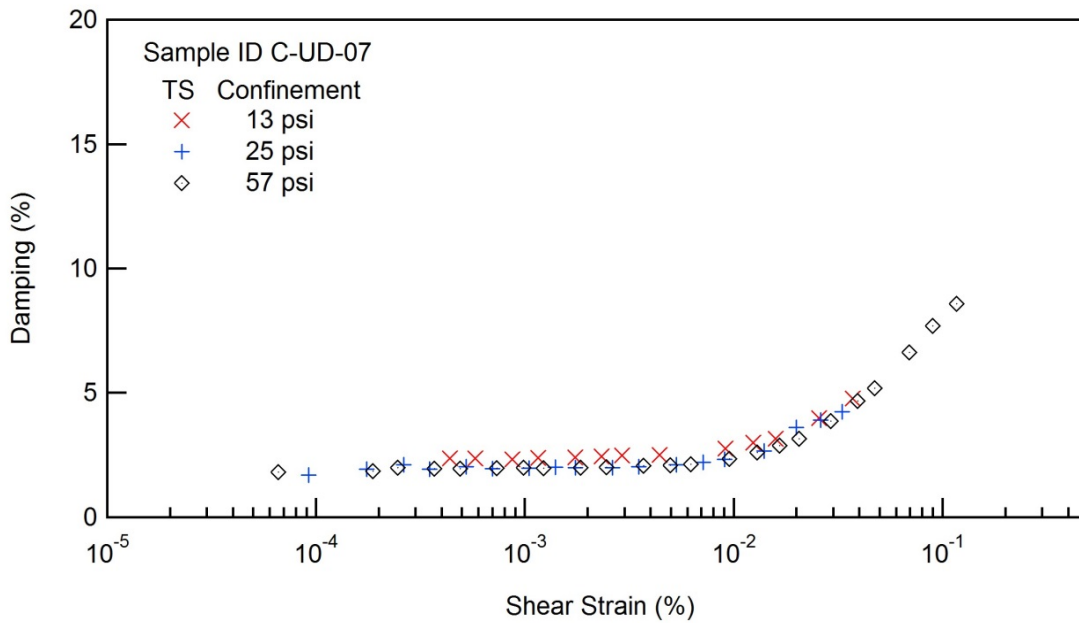
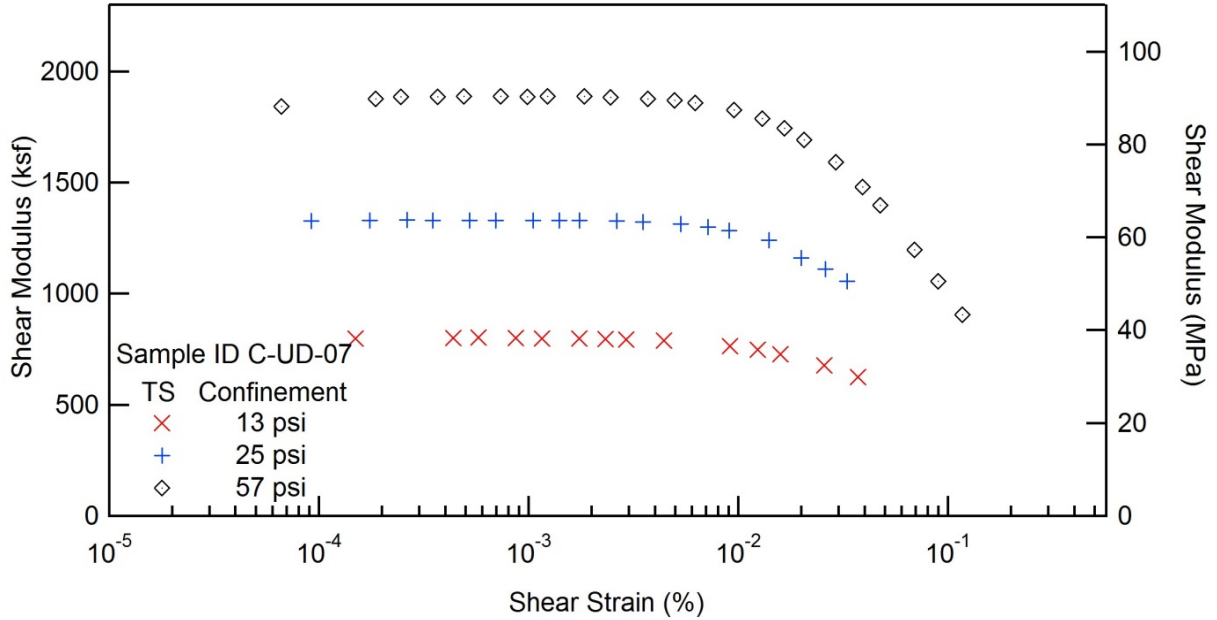


### RESONANT COLUMN (RC) AND TORSIONAL SHEAR (TS) TEST

Project Name: Deep Soil Test Boring to Determine Shear  
Wave Velocities across South Carolina

Client: SCDOT  
Location: Conway, SC

Project ID: SPR-731  
Boring No.: B-CON









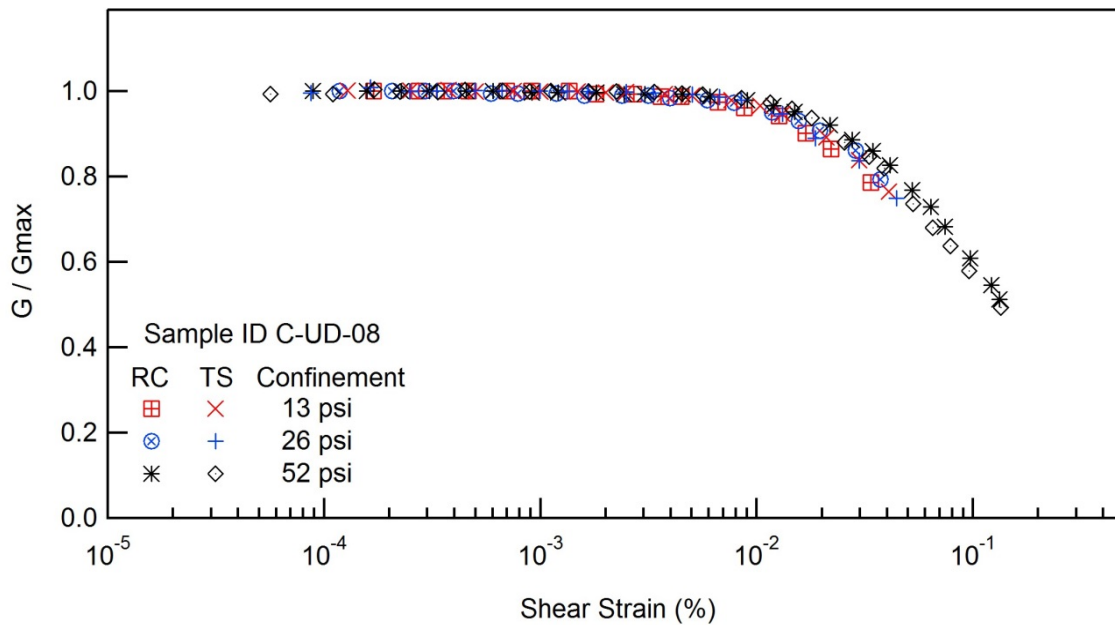
## RESONANT COLUMN (RC) AND TORSIONAL SHEAR (TS) TEST

Project Name: Deep Soil Test Boring to Determine Shear  
Wave Velocities across South Carolina

Client: SCDOT  
Location: Conway, SC

Project ID: SPR-731  
Boring No.: B-CON

Sample ID : C-UD-08



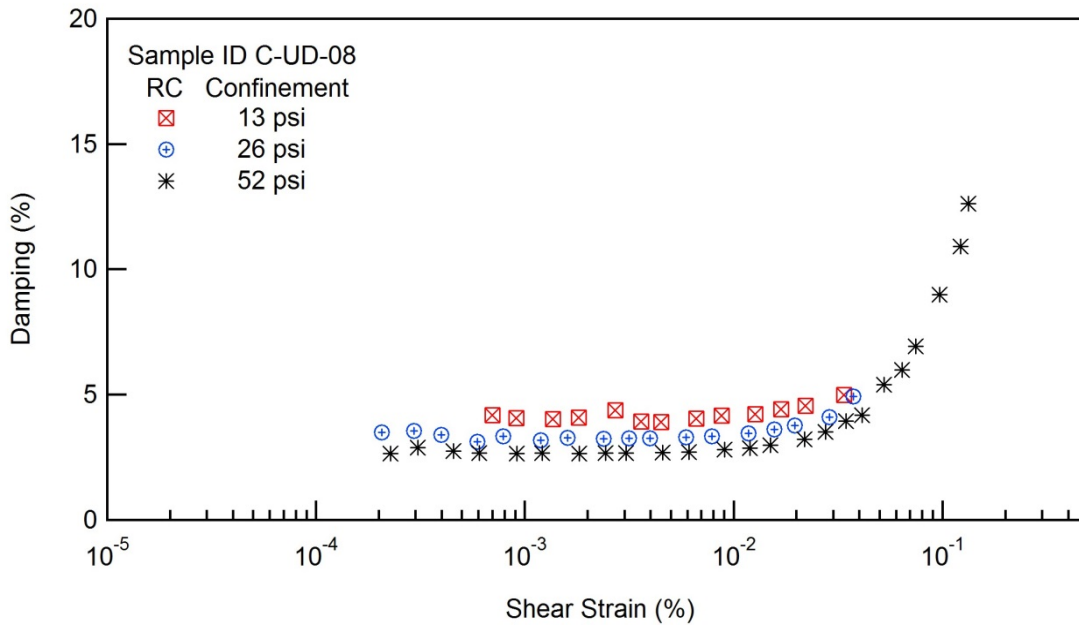
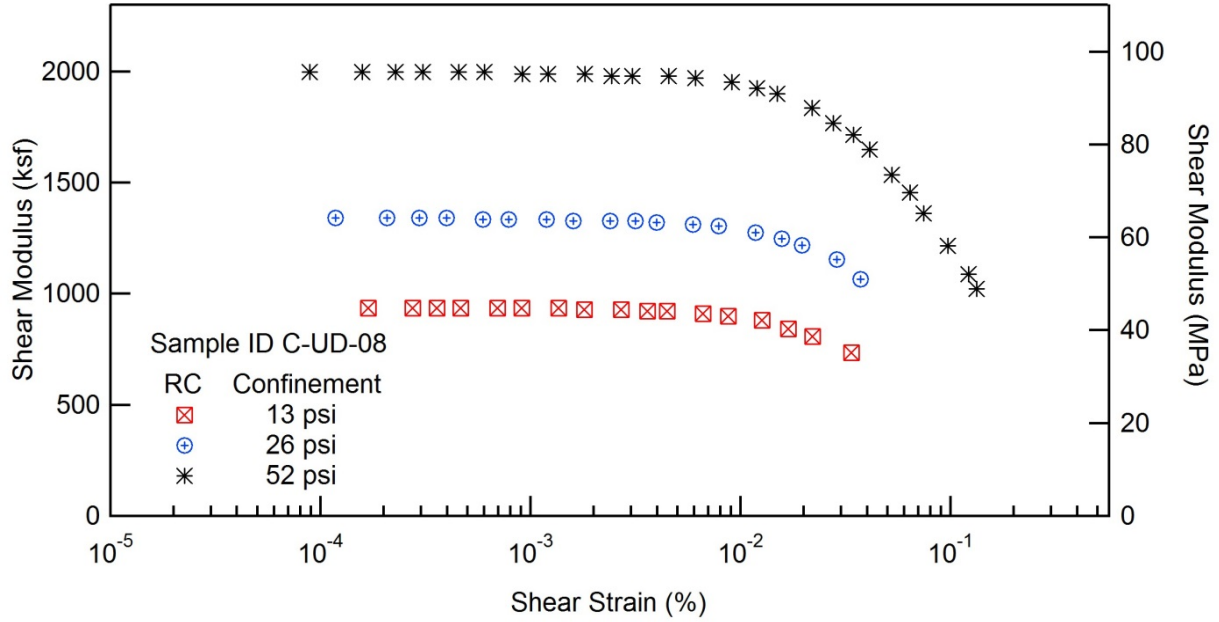


### RESONANT COLUMN (RC) AND TORSIONAL SHEAR (TS) TEST

Project Name: Deep Soil Test Boring to Determine Shear  
Wave Velocities across South Carolina

Client: SCDOT  
Location: Conway, SC

Project ID: SPR-731  
Boring No.: B-CON



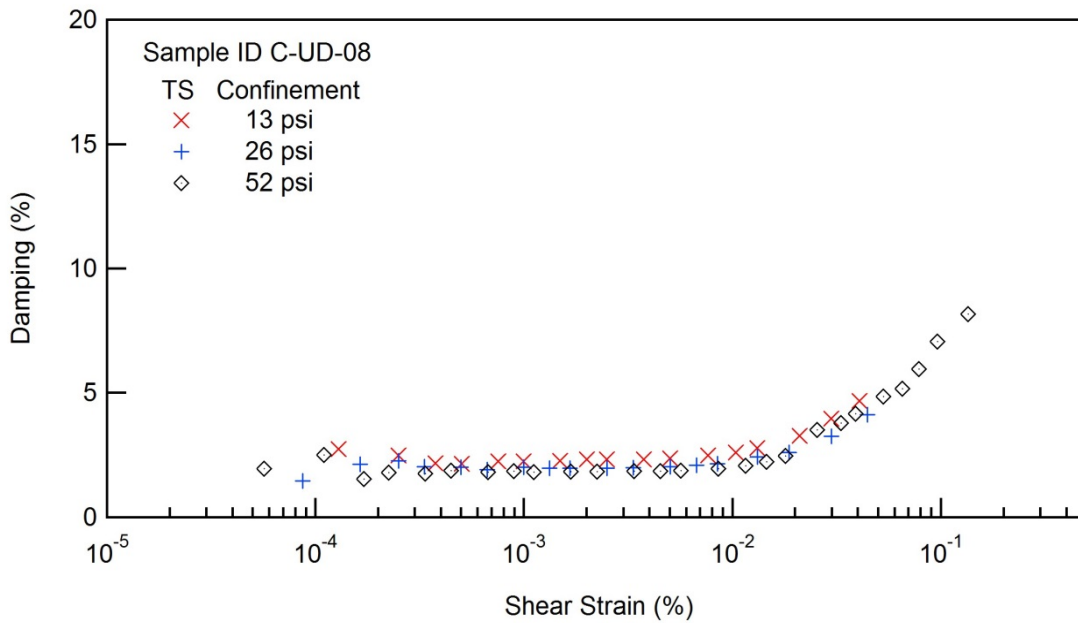
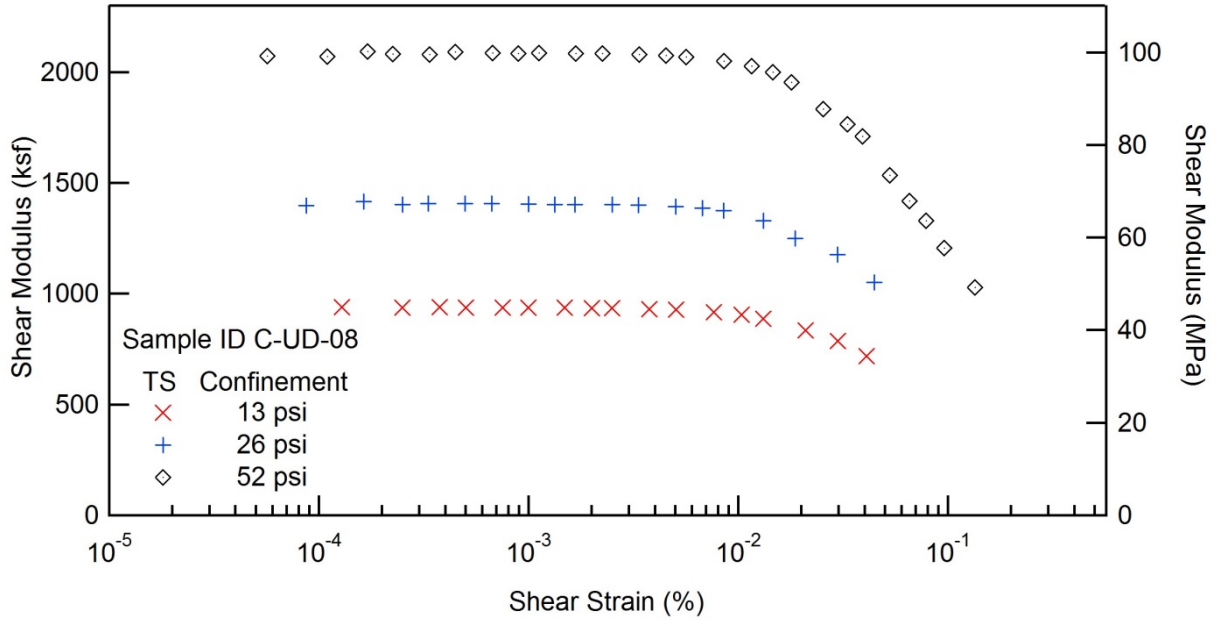


### RESONANT COLUMN (RC) AND TORSIONAL SHEAR (TS) TEST

Project Name: Deep Soil Test Boring to Determine Shear  
Wave Velocities across South Carolina

Client: SCDOT  
Location: Conway, SC

Project ID: SPR-731  
Boring No.: B-CON









## RESONANT COLUMN (RC) AND TORSIONAL SHEAR (TS) TEST

Project Name: Deep Soil Test Boring to Determine Shear  
Wave Velocities across South Carolina

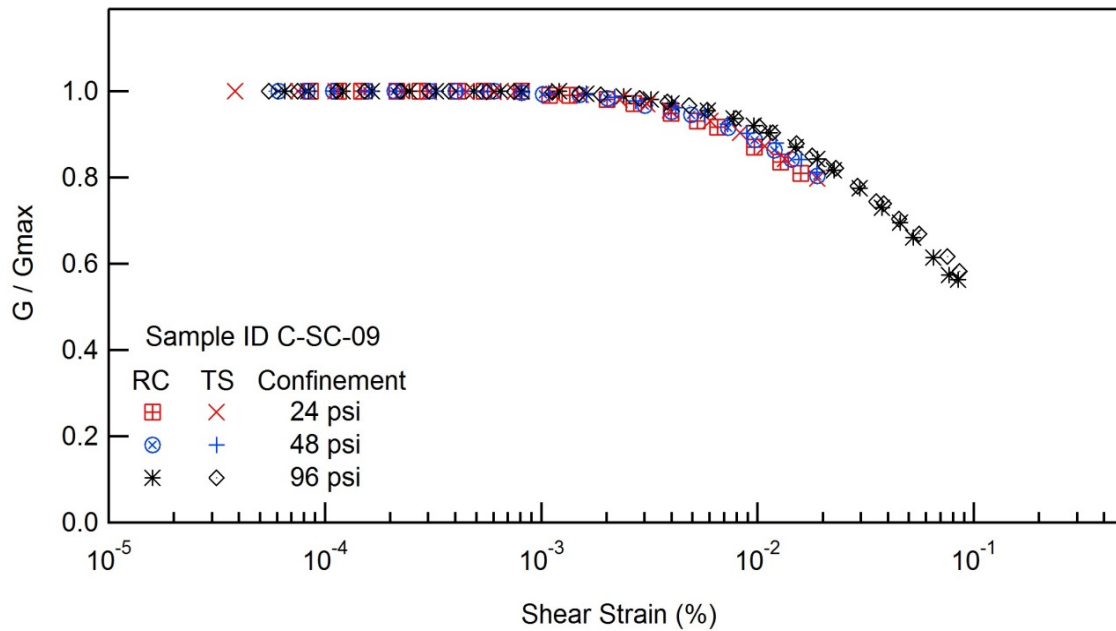
Client: SCDOT

Project ID: SPR-731

Location: Conway, SC

Boring No.: B-CON

Sample ID : C-SC-09



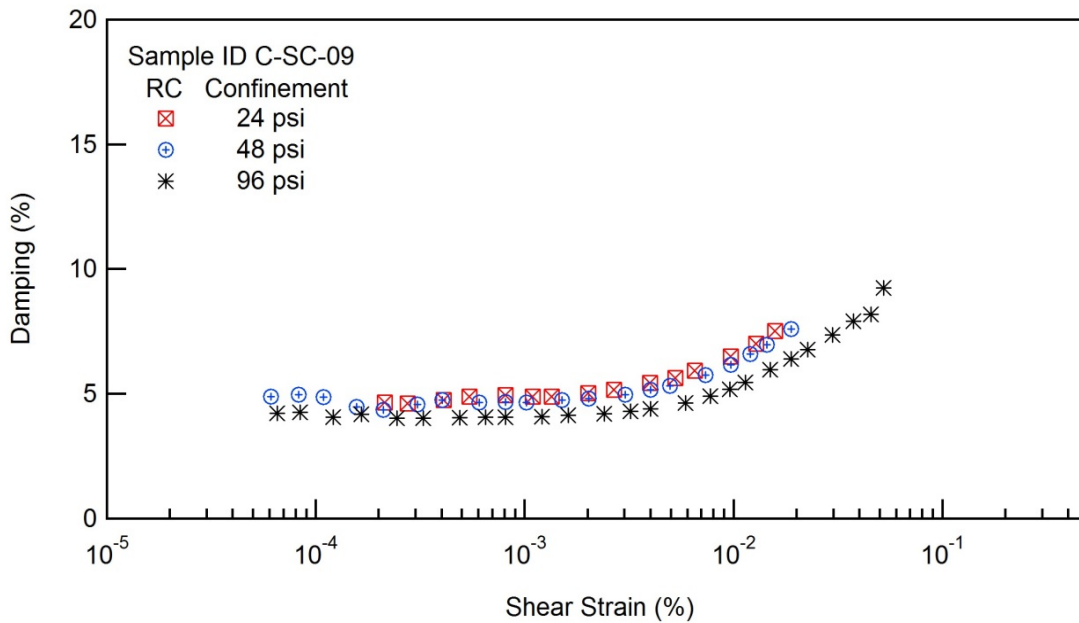
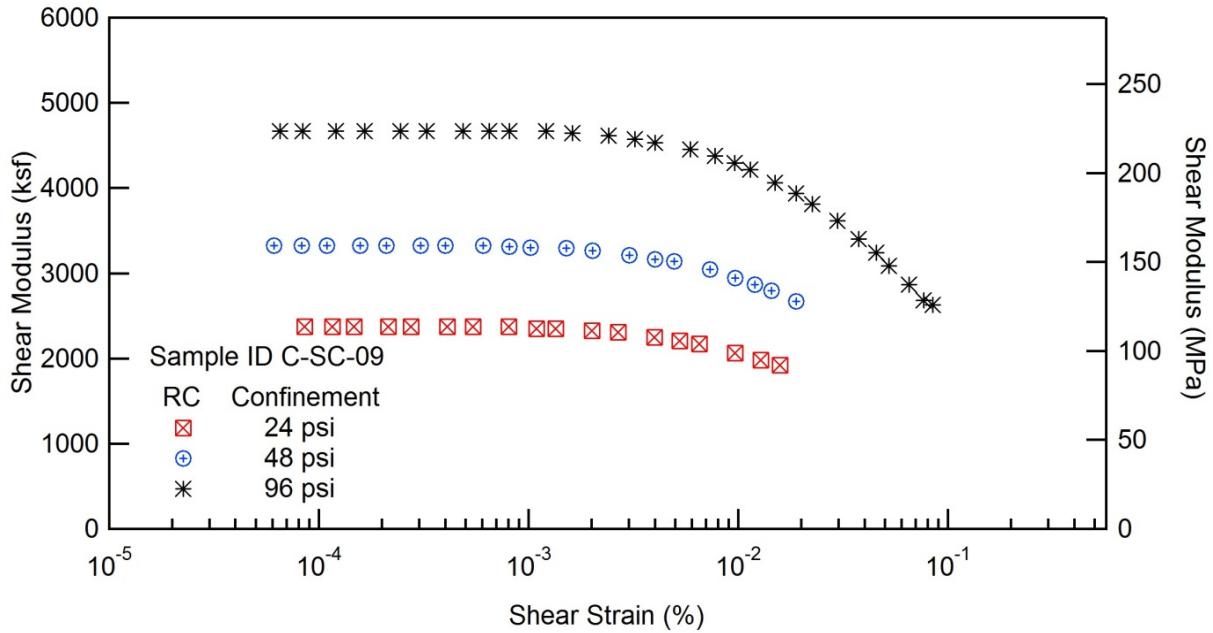


# RESONANT COLUMN (RC) AND TORSIONAL SHEAR (TS) TEST

Project Name: Deep Soil Test Boring to Determine Shear  
Wave Velocities across South Carolina

Client: SCDOT  
Location: Conway, SC

Project ID: SPR-731  
Boring No.: B-CON



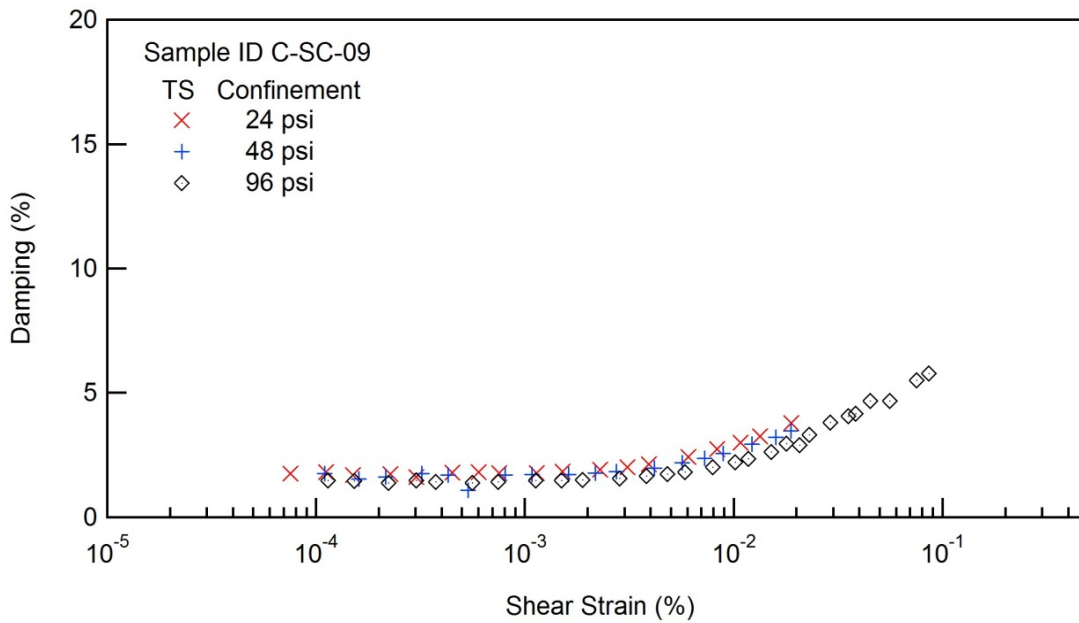
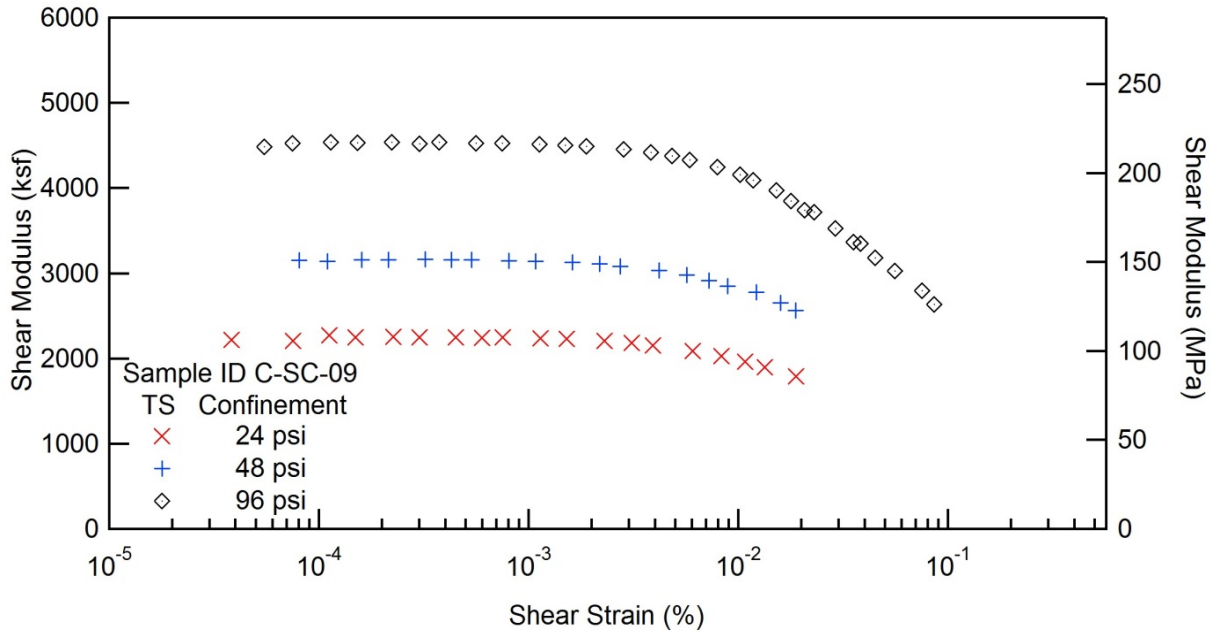


# RESONANT COLUMN (RC) AND TORSIONAL SHEAR (TS) TEST

Project Name: Deep Soil Test Boring to Determine Shear  
Wave Velocities across South Carolina

Client: SCDOT  
Location: Conway, SC

Project ID: SPR-731  
Boring No.: B-CON









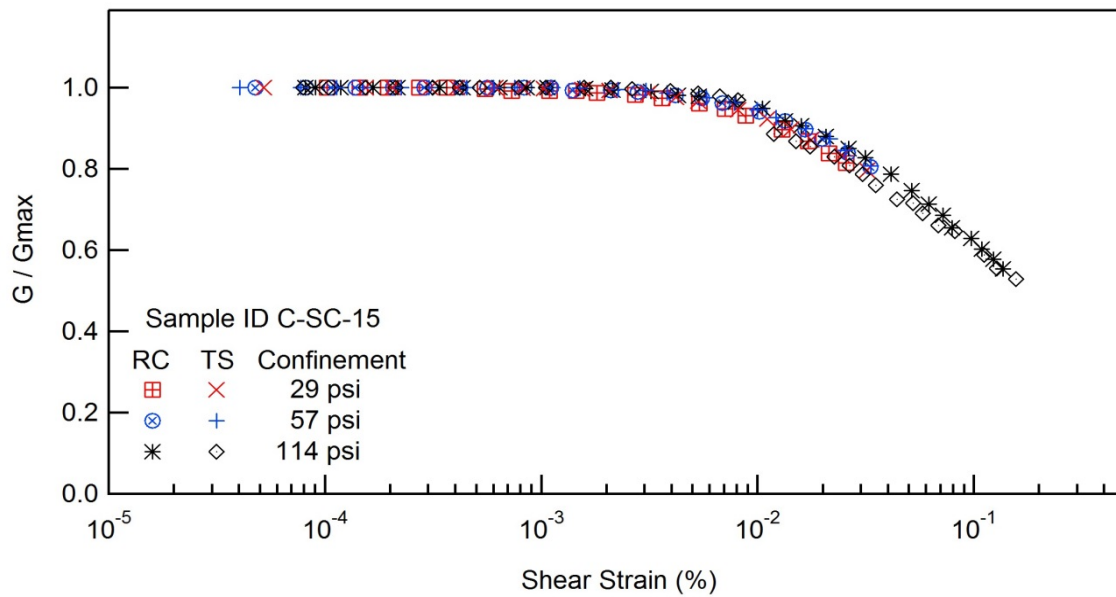
## RESONANT COLUMN (RC) AND TORSIONAL SHEAR (TS) TEST

Project Name: Deep Soil Test Boring to Determine Shear  
Wave Velocities across South Carolina

Client: SCDOT  
Location: Conway, SC

Project ID: SPR-731  
Boring No.: B-CON

Sample ID : C-SC-15





## RESONANT COLUMN (RC) AND TORSIONAL SHEAR (TS) TEST

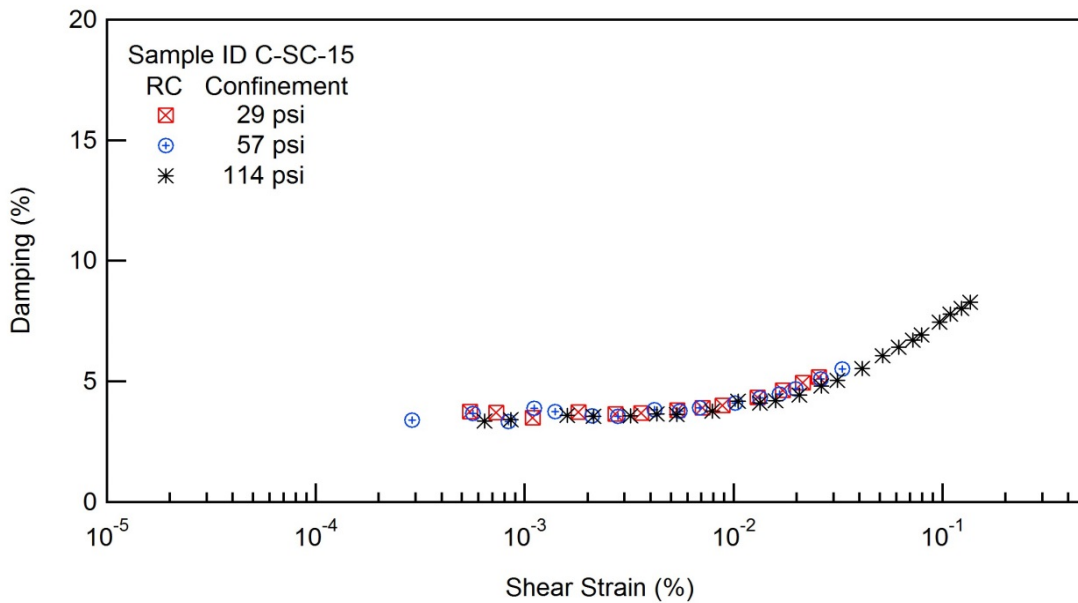
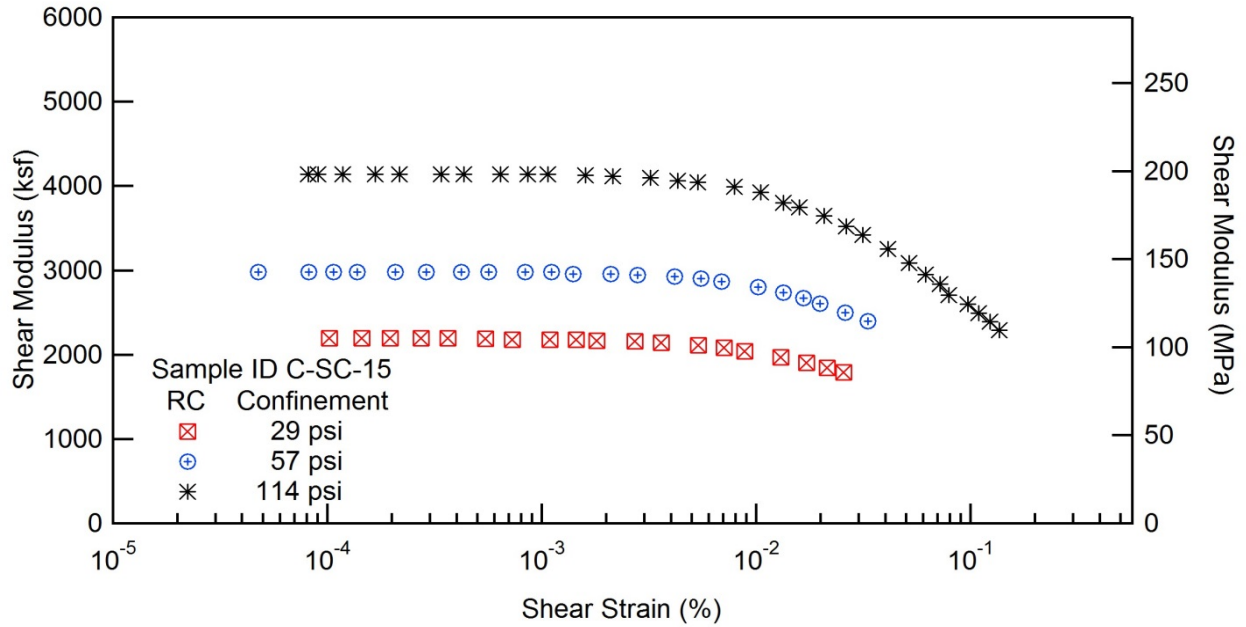
Project Name: Deep Soil Test Boring to Determine Shear  
Wave Velocities across South Carolina

Client: SCDOT

Project ID: SPR-731

Location: Conway, SC

Boring No.: B-CON



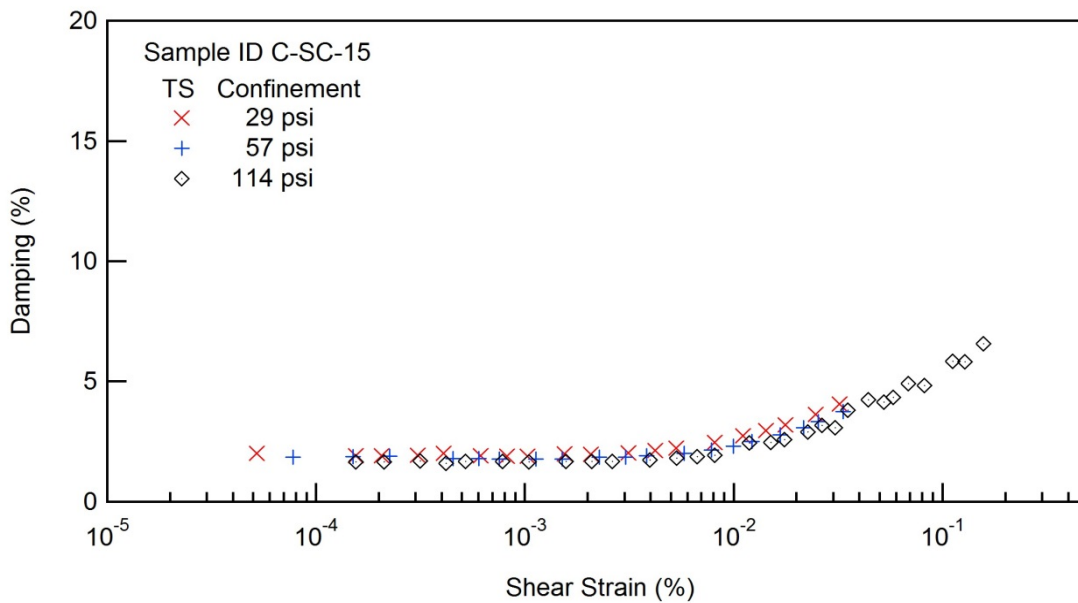
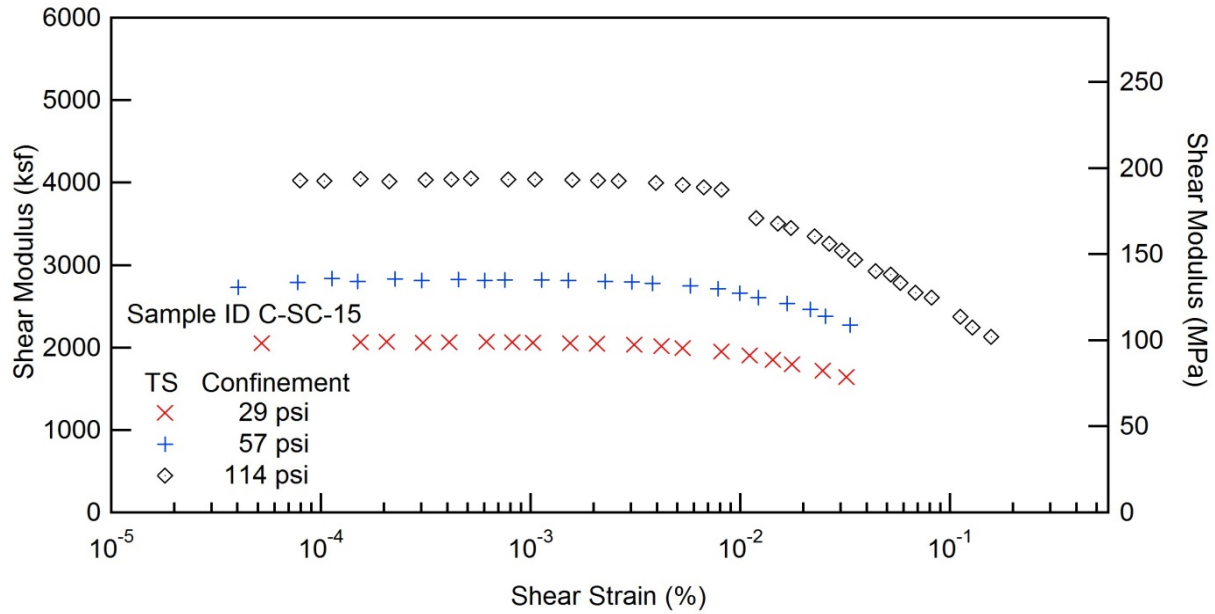


## RESONANT COLUMN (RC) AND TORSIONAL SHEAR (TS) TEST

Project Name: Deep Soil Test Boring to Determine Shear  
Wave Velocities across South Carolina

Client: SCDOT  
Location: Conway, SC

Project ID: SPR-731  
Boring No.: B-CON





**UNIVERSITY OF SOUTH CAROLINA**  
 Department of Civil and Environmental Engineering  
 300 Main street, Columbia, SC, 29208

**RESONANT COLUMN (RC) TEST REPORT**

Project Name: Deep Soil Test Boring to Determine Shear  
 Wave Velocities across South Carolina  
 Client: SCDOT Project ID: SPR-731  
 Location: Conway, SC Boring No.: B-CON

Table 1 Results for Sample ID C-SC-15 for RC Test

Confining Pressure 29 PSI				Confining Pressure 57 PSI				Confining Pressure 114 PSI			
$\gamma$ (%)	G (ksf)	G/G <sub>max</sub>	D (%)	$\gamma$ (%)	G (ksf)	G/G <sub>max</sub>	D (%)	$\gamma$ (%)	G (ksf)	G/G <sub>max</sub>	D (%)
1.02E-04	2196	1.000		4.77E-05	2980	1.000		8.14E-05	4139	1.000	
1.45E-04	2196	1.000		8.17E-05	2980	1.000		9.04E-05	4139	1.000	
1.96E-04	2196	1.000		1.07E-04	2980	1.000		1.18E-04	4139	1.000	
2.73E-04	2196	1.000		1.38E-04	2980	1.000		1.67E-04	4139	1.000	
3.66E-04	2196	1.000		2.07E-04	2980	1.000		2.17E-04	4139	1.000	
5.48E-04	2187	0.996	3.747	2.89E-04	2980	1.000	3.404	3.39E-04	4139	1.000	
7.31E-04	2177	0.991	3.711	4.21E-04	2980	1.000		4.33E-04	4139	1.000	
1.09E-03	2177	0.991	3.495	5.65E-04	2980	1.000	3.668	6.42E-04	4139	1.000	3.356
1.45E-03	2177	0.991		8.35E-04	2980	1.000	3.341	8.59E-04	4139	1.000	3.421
1.81E-03	2167	0.987	3.729	1.11E-03	2980	1.000	3.887	1.07E-03	4139	1.000	
2.72E-03	2158	0.982	3.664	1.40E-03	2957	0.992	3.741	1.60E-03	4125	0.997	3.589
3.61E-03	2138	0.974	3.689	2.10E-03	2957	0.992	3.565	2.14E-03	4112	0.994	3.547
5.37E-03	2110	0.960	3.812	2.80E-03	2946	0.989	3.545	3.21E-03	4099	0.990	3.585
7.09E-03	2081	0.947	3.905	4.17E-03	2923	0.981	3.827	4.30E-03	4059	0.981	3.651
8.83E-03	2042	0.930	4.013	5.52E-03	2901	0.974	3.764	5.34E-03	4046	0.978	3.625
1.30E-02	1968	0.896	4.326	6.89E-03	2867	0.962	3.898	7.93E-03	3992	0.964	3.761
1.72E-02	1904	0.867	4.628	1.02E-02	2800	0.940	4.115	1.05E-02	3926	0.949	4.183
2.14E-02	1841	0.838	4.952	1.34E-02	2734	0.918	4.305	1.34E-02	3797	0.917	4.106
2.56E-02	1787	0.814	5.180	1.66E-02	2669	0.896	4.468	1.59E-02	3746	0.905	4.197
				1.98E-02	2605	0.874	4.699	2.07E-02	3644	0.880	4.437
				2.61E-02	2499	0.839	5.097	2.63E-02	3519	0.850	4.813
				3.32E-02	2396	0.804	5.516	3.14E-02	3421	0.827	5.046
								4.13E-02	3252	0.786	5.537
								5.17E-02	3087	0.746	6.071
								6.18E-02	2950	0.713	6.413
								7.20E-02	2838	0.686	6.717
								7.93E-02	2706	0.654	6.930
								9.71E-02	2599	0.628	7.462
								1.09E-01	2493	0.602	7.795
								1.23E-01	2390	0.578	8.033
								1.36E-01	2289	0.553	8.295



**UNIVERSITY OF SOUTH CAROLINA**  
 Department of Civil and Environmental Engineering  
 300 Main street, Columbia, SC, 29208

**TORSIONAL SHEAR (TS) TEST REPORT**

Project Name: Deep Soil Test Boring to Determine Shear  
 Wave Velocities across South Carolina  
 Client: SCDOT Project ID: SPR-731  
 Location: Conway, SC Boring No.: B-CON

Table 2 Results for Sample ID C-SC-15 for TS Test

Confining Pressure 29 PSI				Confining Pressure 57 PSI				Confining Pressure 114 PSI			
$\gamma$ (%)	G (ksf)	G/G <sub>max</sub>	D (%)	$\gamma$ (%)	G (ksf)	G/G <sub>max</sub>	D (%)	$\gamma$ (%)	G (ksf)	G/G <sub>max</sub>	D (%)
5.22E-05	2049	1.000	2.006	4.03E-05	2729	1.000		7.96E-05	4024	1.000	
1.55E-04	2062	1.000	1.912	7.75E-05	2788	1.000	1.856	1.04E-04	4021	1.000	
2.06E-04	2069	1.000	1.909	1.13E-04	2834	1.000		1.55E-04	4046	1.000	1.656
3.08E-04	2058	1.000	1.940	1.50E-04	2803	1.000	1.880	2.12E-04	4014	1.000	1.656
4.09E-04	2066	1.000	2.017	2.25E-04	2831	1.000	1.885	3.16E-04	4029	1.000	1.703
6.16E-04	2067	1.000	1.914	3.02E-04	2811	1.000		4.20E-04	4036	1.000	1.596
8.21E-04	2063	0.999	1.890	4.52E-04	2824	1.000	1.786	5.21E-04	4049	1.000	1.681
1.03E-03	2059	0.997	1.900	6.03E-04	2814	1.000	1.799	7.85E-04	4039	1.000	1.684
1.55E-03	2054	0.995	1.986	7.53E-04	2817	1.000	1.785	1.05E-03	4035	1.000	1.654
2.07E-03	2048	0.992	1.981	1.13E-03	2816	1.000	1.780	1.58E-03	4032	1.000	1.670
3.13E-03	2033	0.985	2.043	1.51E-03	2814	0.999	1.770	2.10E-03	4025	0.998	1.677
4.21E-03	2016	0.976	2.127	2.27E-03	2803	0.995	1.856	2.63E-03	4018	0.996	1.667
5.31E-03	1994	0.966	2.215	3.04E-03	2793	0.992	1.856	3.97E-03	3996	0.991	1.741
8.15E-03	1950	0.945	2.465	3.82E-03	2777	0.986	1.915	5.33E-03	3972	0.985	1.817
1.11E-02	1903	0.922	2.740	5.79E-03	2745	0.975	2.012	6.71E-03	3945	0.978	1.870
1.43E-02	1851	0.897	2.954	7.83E-03	2709	0.962	2.149	8.12E-03	3910	0.969	1.944
1.77E-02	1797	0.871	3.189	9.96E-03	2661	0.945	2.312	1.19E-02	3568	0.885	2.441
2.47E-02	1718	0.832	3.629	1.22E-02	2607	0.926	2.509	1.51E-02	3500	0.868	2.474
3.22E-02	1644	0.796	4.060	1.67E-02	2532	0.899	2.785	1.75E-02	3450	0.855	2.588
				2.16E-02	2459	0.873	3.067	2.27E-02	3349	0.830	2.898
				2.54E-02	2379	0.845	3.344	2.66E-02	3259	0.808	3.170
				3.34E-02	2274	0.807	3.737	3.06E-02	3176	0.787	3.066
								3.53E-02	3062	0.759	3.796
								4.42E-02	2924	0.725	4.247
								5.24E-02	2884	0.715	4.147
								5.81E-02	2783	0.690	4.335
								6.86E-02	2662	0.660	4.920
								8.19E-02	2605	0.646	4.828
								1.12E-01	2372	0.588	5.828
								1.28E-01	2240	0.555	5.815
								1.57E-01	2129	0.528	6.562



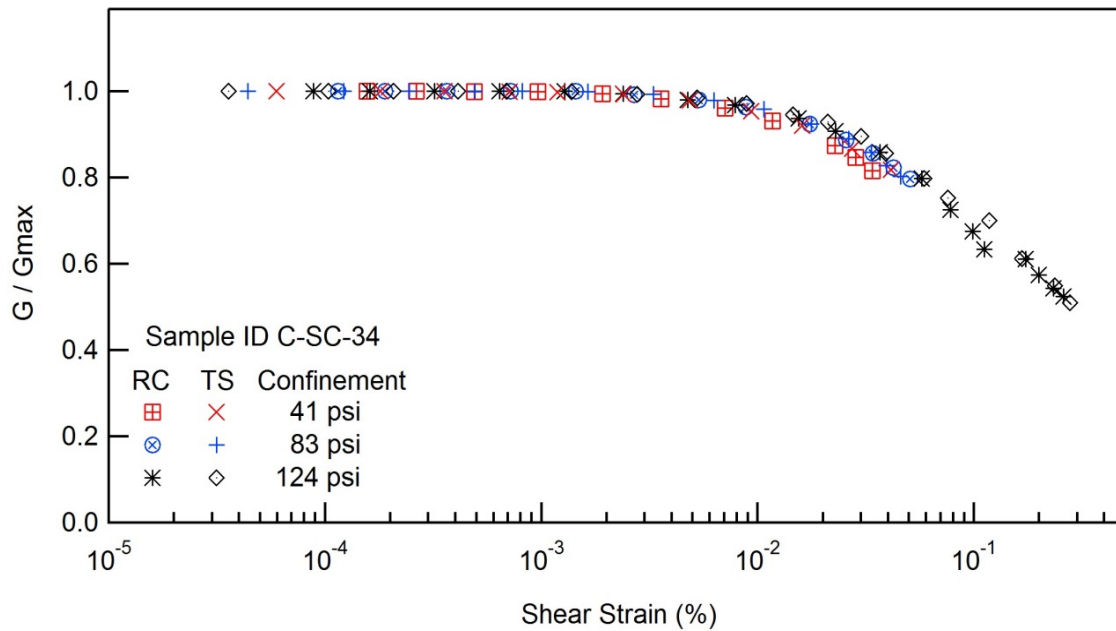
## RESONANT COLUMN (RC) AND TORSIONAL SHEAR (TS) TEST

Project Name: Deep Soil Test Boring to Determine Shear  
Wave Velocities across South Carolina

Client: SCDOT  
Location: Conway, SC

Project ID: SPR-731  
Boring No.: B-CON

Sample ID : C-SC-34



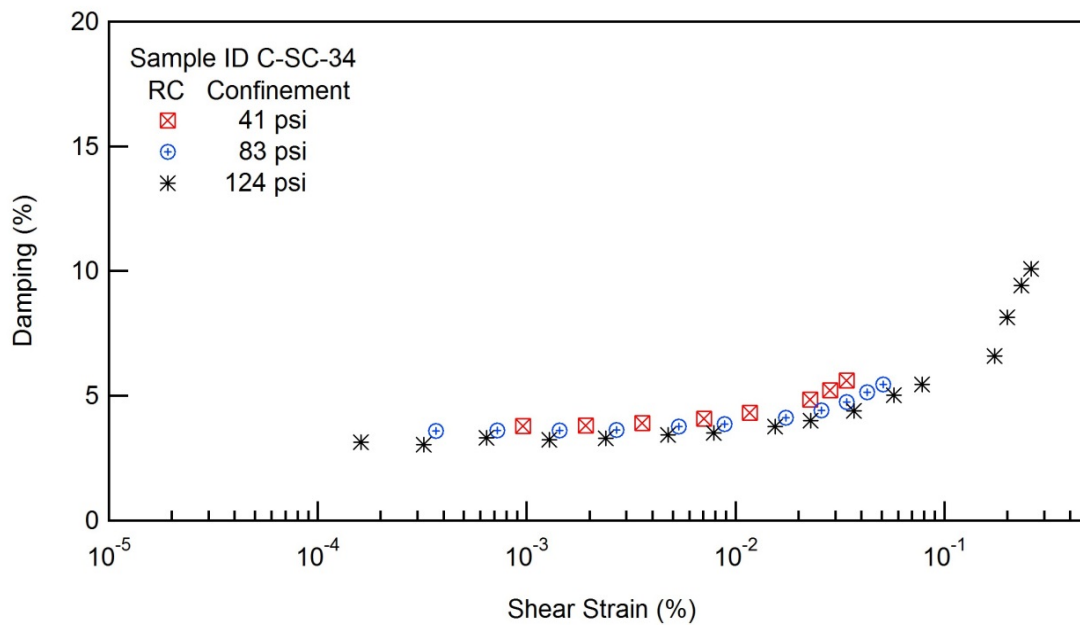
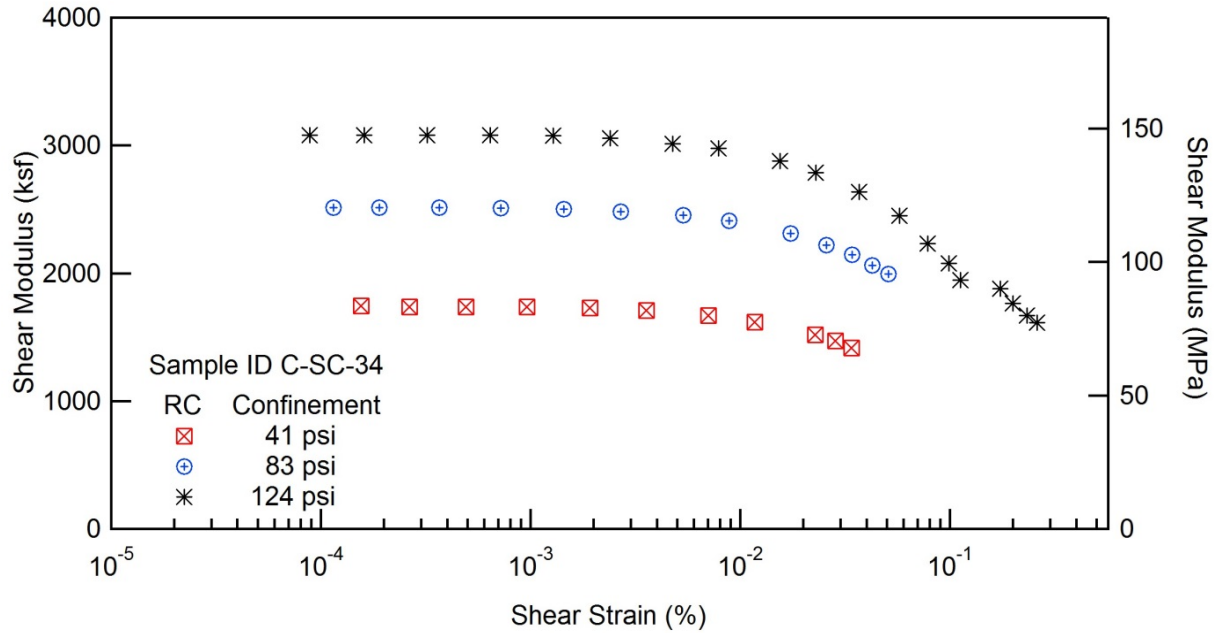


## RESONANT COLUMN (RC) AND TORSIONAL SHEAR (TS) TEST

Project Name: Deep Soil Test Boring to Determine Shear  
Wave Velocities across South Carolina

Client: SCDOT  
Location: Conway, SC

Project ID: SPR-731  
Boring No.: B-CON



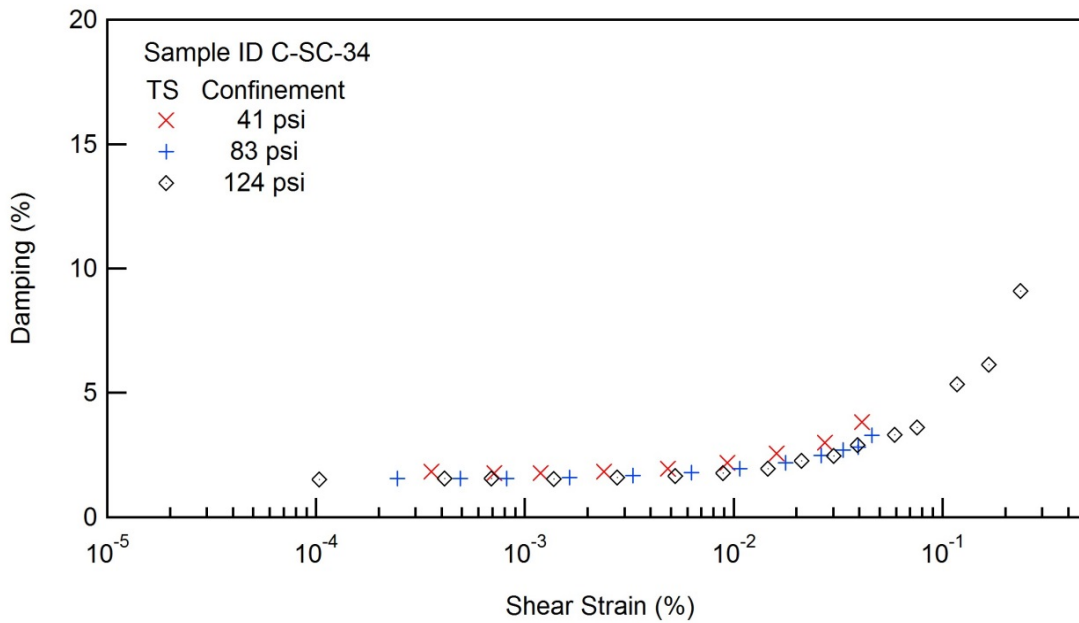
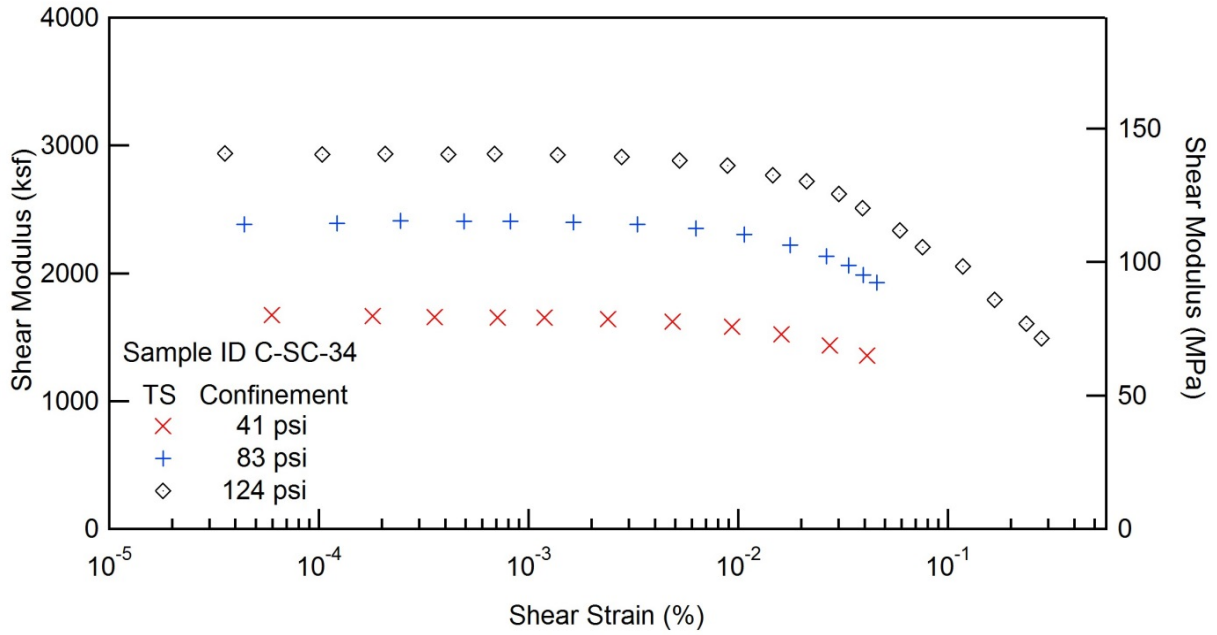


### RESONANT COLUMN (RC) AND TORSIONAL SHEAR (TS) TEST

Project Name: Deep Soil Test Boring to Determine Shear  
Wave Velocities across South Carolina

Client: SCDOT  
Location: Conway, SC

Project ID: SPR-731  
Boring No.: B-CON









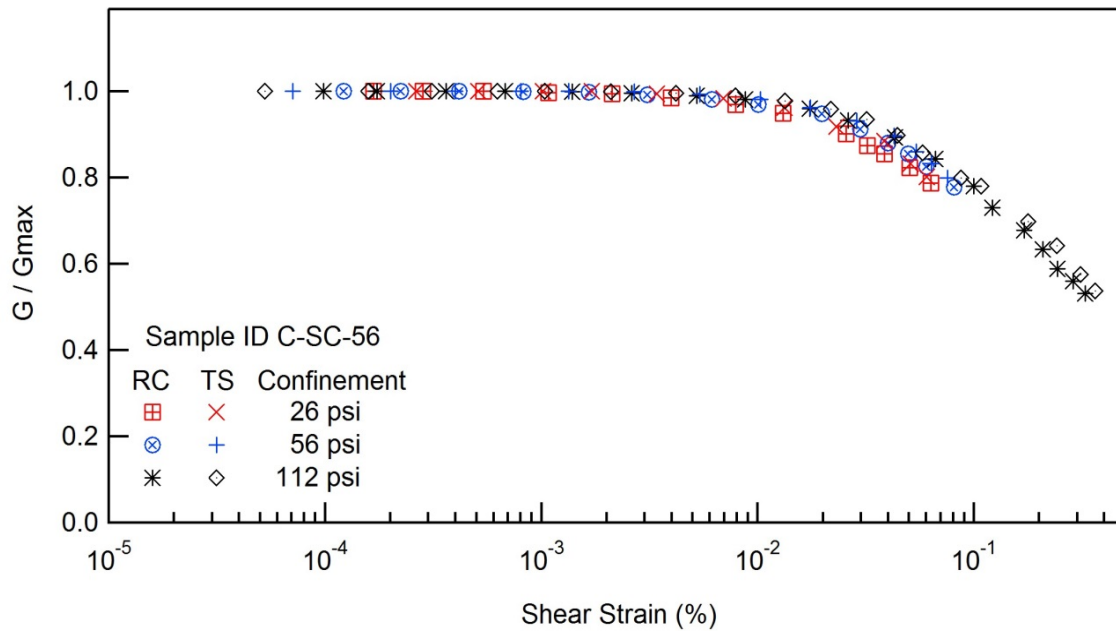
## RESONANT COLUMN (RC) AND TORSIONAL SHEAR (TS) TEST

Project Name: Deep Soil Test Boring to Determine Shear  
Wave Velocities across South Carolina

Client: SCDOT  
Location: Conway, SC

Project ID: SPR-731  
Boring No.: B-CON

Sample ID : C-SC-56



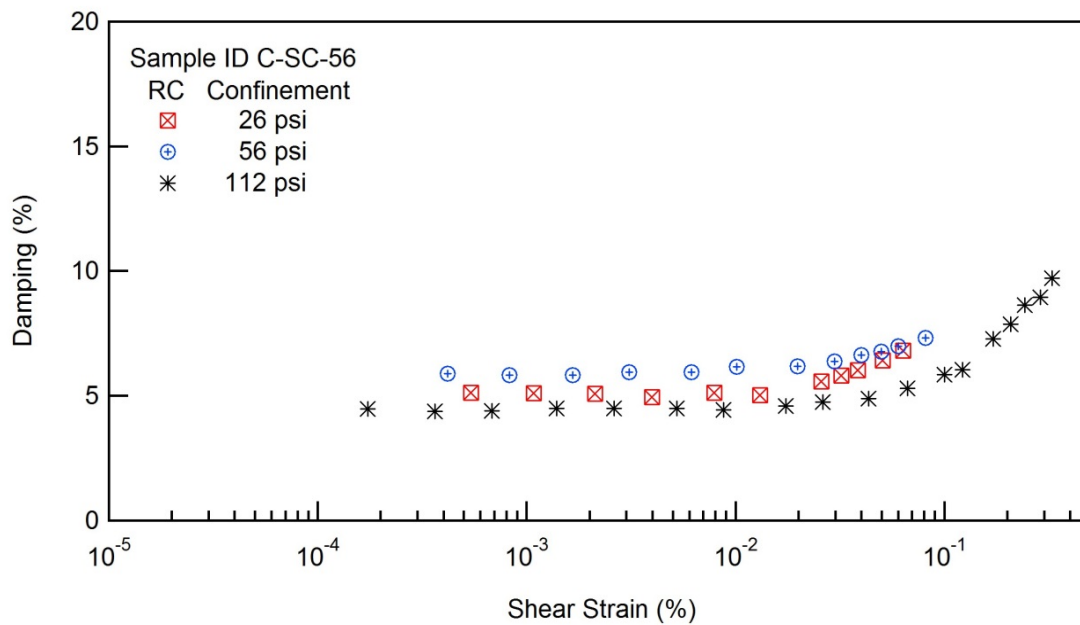
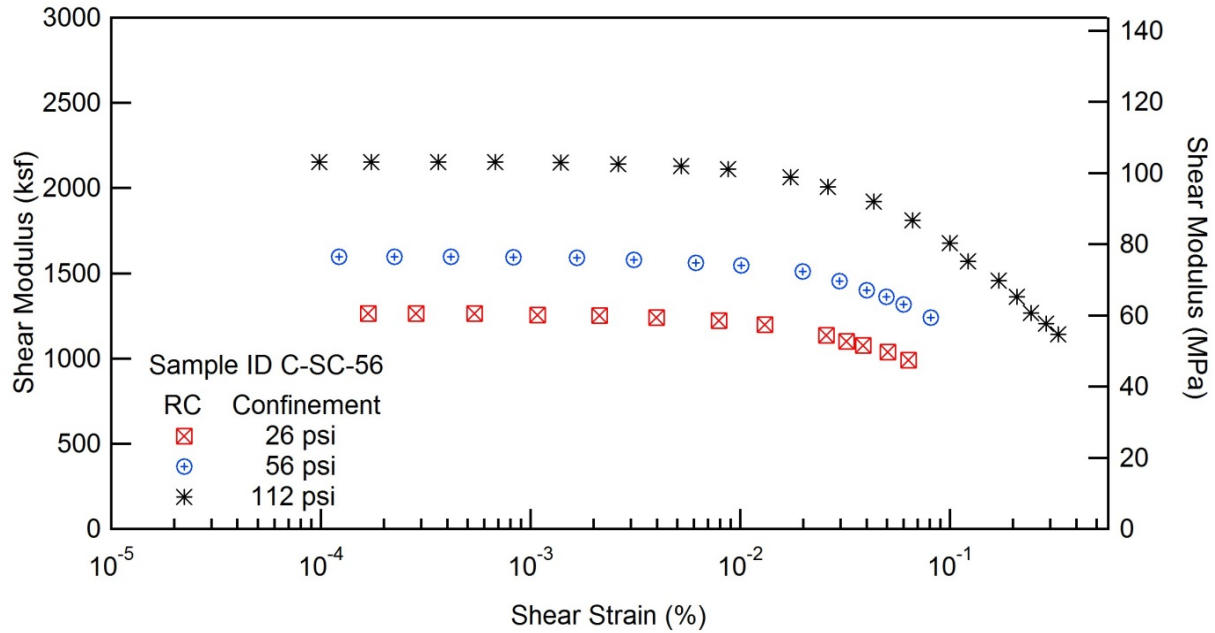


## RESONANT COLUMN (RC) AND TORSIONAL SHEAR (TS) TEST

Project Name: Deep Soil Test Boring to Determine Shear  
Wave Velocities across South Carolina

Client: SCDOT  
Location: Conway, SC

Project ID: SPR-731  
Boring No.: B-CON



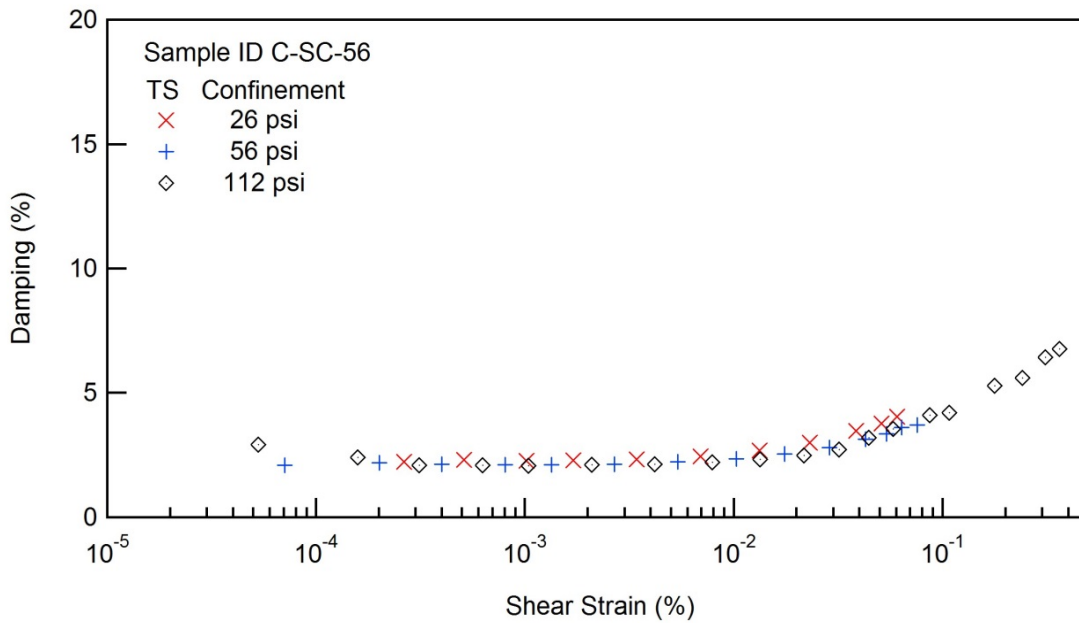
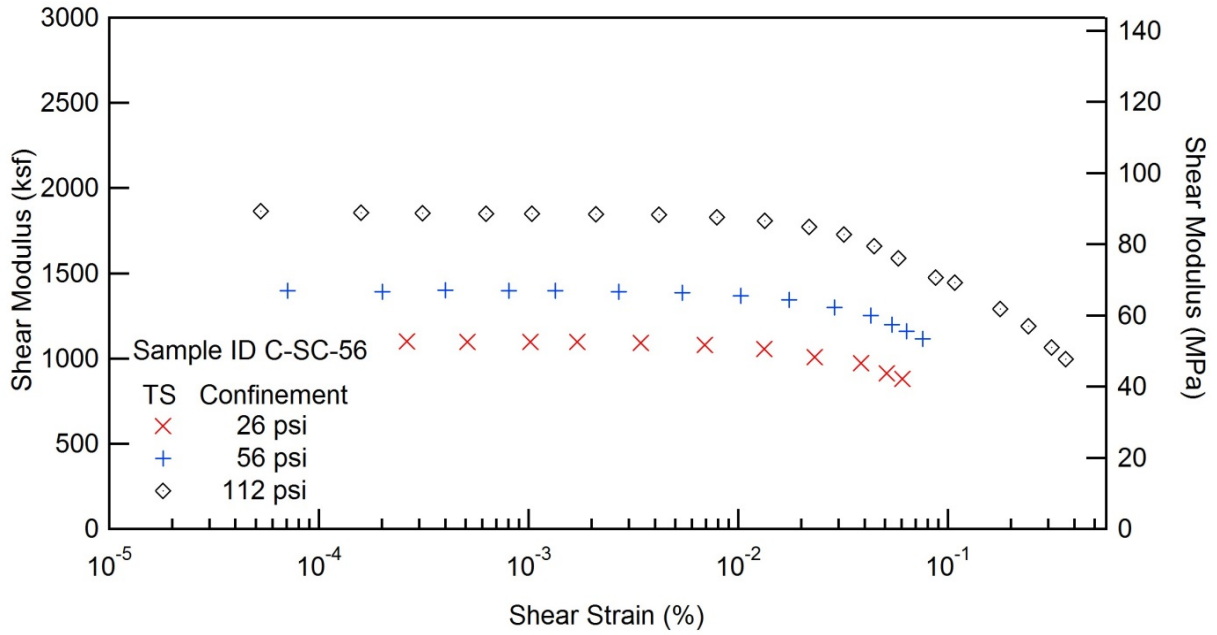


### RESONANT COLUMN (RC) AND TORSIONAL SHEAR (TS) TEST

Project Name: Deep Soil Test Boring to Determine Shear  
Wave Velocities across South Carolina

Client: SCDOT  
Location: Conway, SC

Project ID: SPR-731  
Boring No.: B-CON









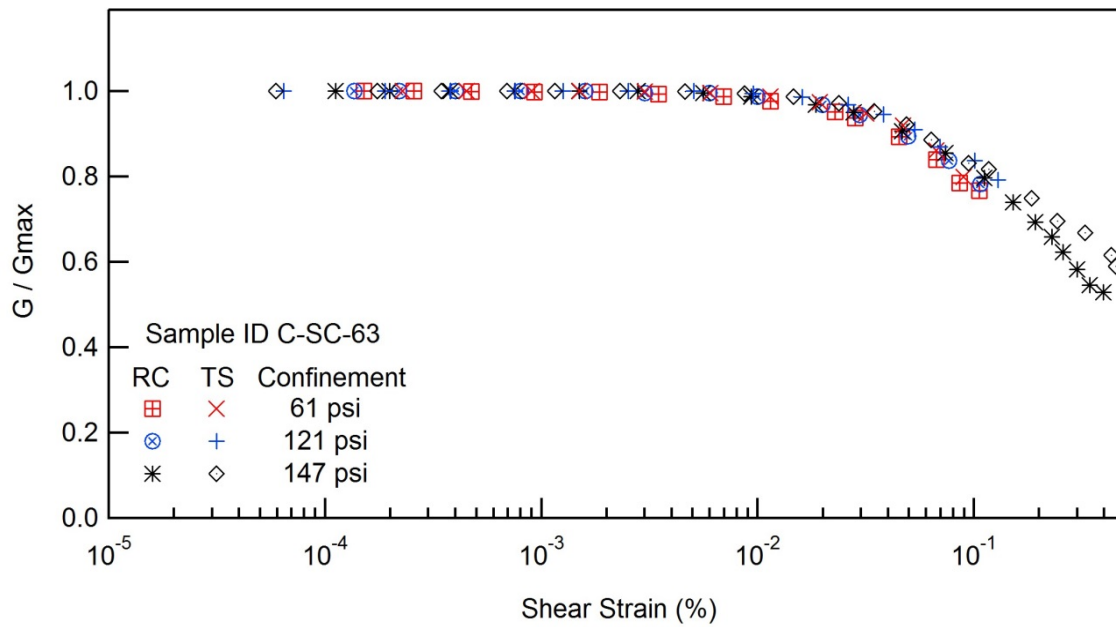
## RESONANT COLUMN (RC) AND TORSIONAL SHEAR (TS) TEST

Project Name: Deep Soil Test Boring to Determine Shear  
Wave Velocities across South Carolina

Client: SCDOT  
Location: Conway, SC

Project ID: SPR-731  
Boring No.: B-CON

Sample ID : C-SC-63



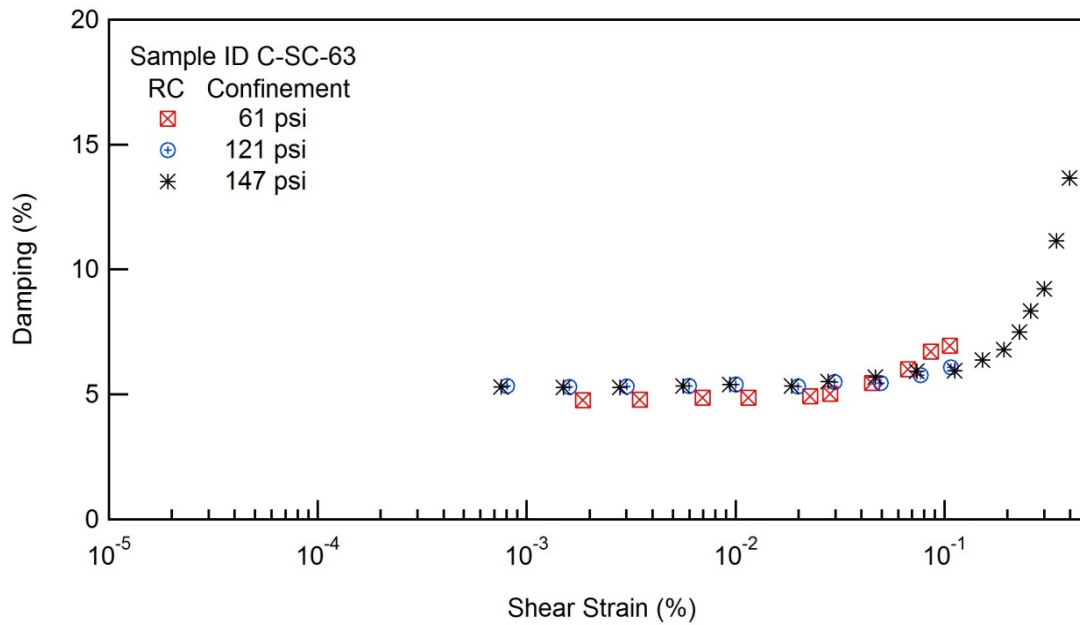
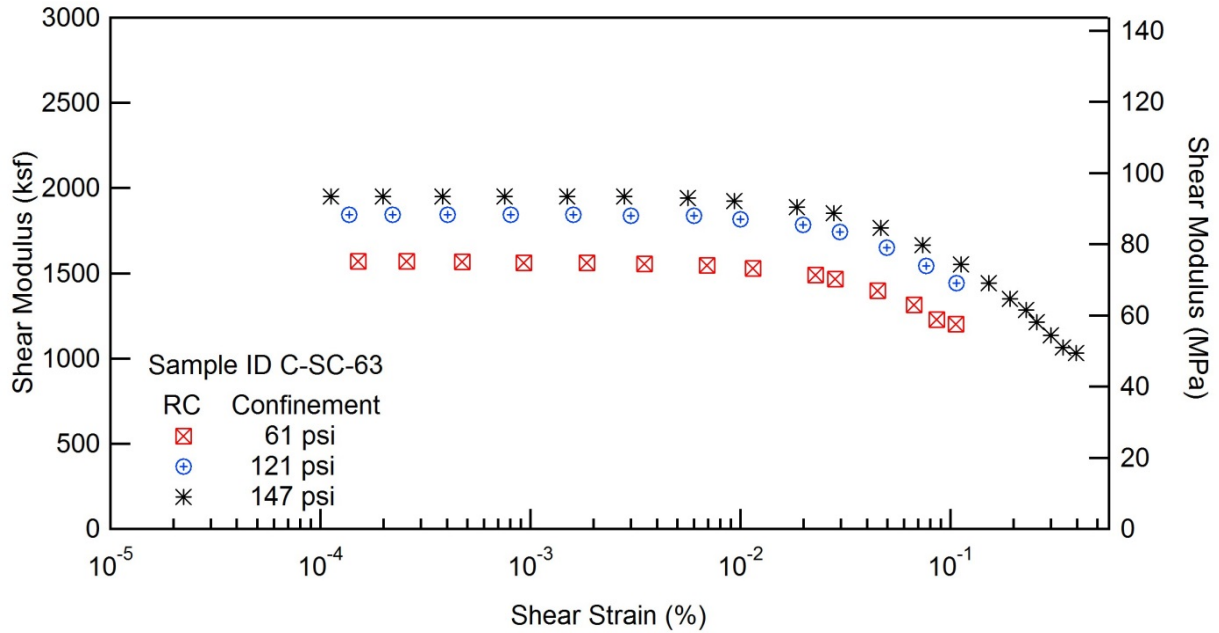


## RESONANT COLUMN (RC) AND TORSIONAL SHEAR (TS) TEST

Project Name: Deep Soil Test Boring to Determine Shear  
Wave Velocities across South Carolina

Client: SCDOT  
Location: Conway, SC

Project ID: SPR-731  
Boring No.: B-CON



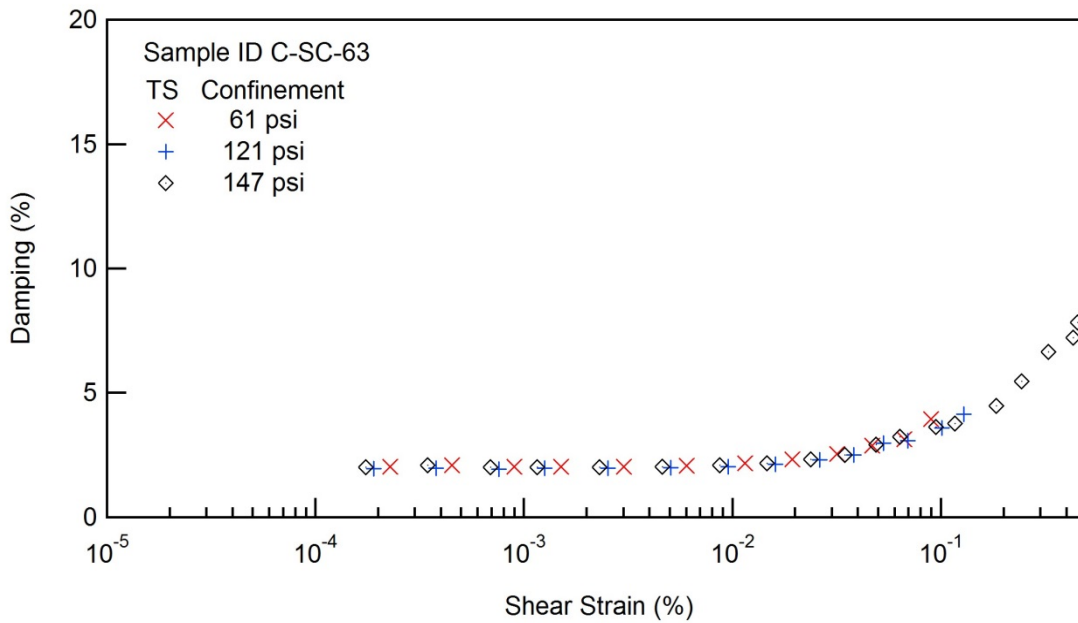
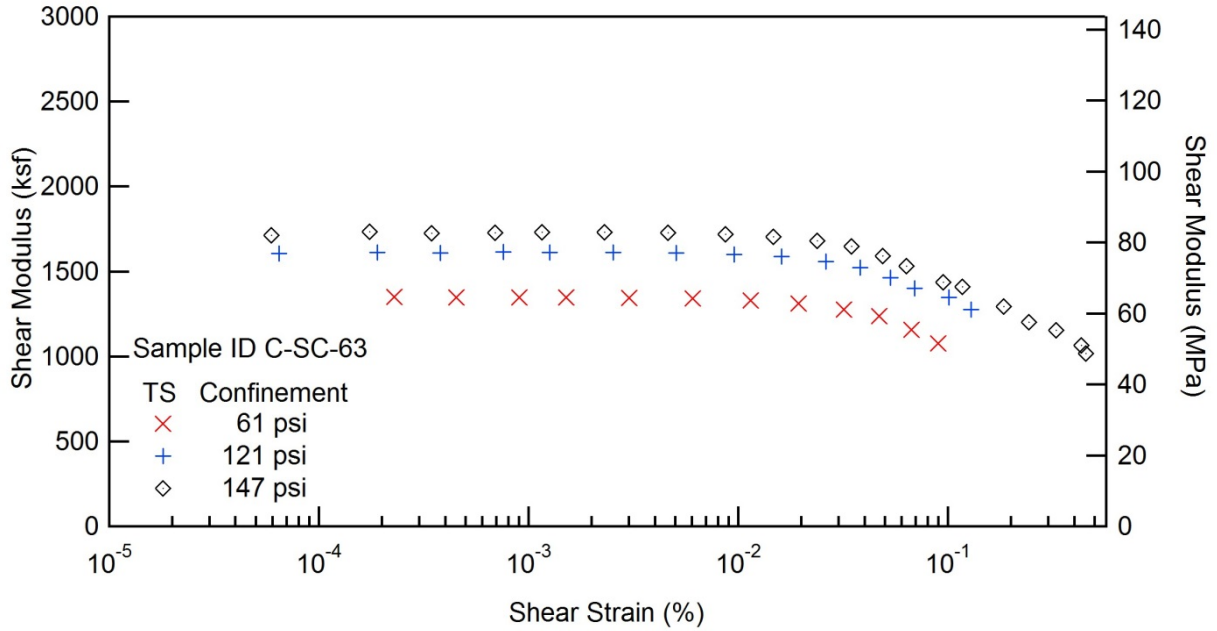


### RESONANT COLUMN (RC) AND TORSIONAL SHEAR (TS) TEST

Project Name: Deep Soil Test Boring to Determine Shear  
Wave Velocities across South Carolina

Client: SCDOT  
Location: Conway, SC

Project ID: SPR-731  
Boring No.: B-CON









## RESONANT COLUMN (RC) AND TORSIONAL SHEAR (TS) TEST

Project Name: Deep Soil Test Boring to Determine Shear  
Wave Velocities across South Carolina

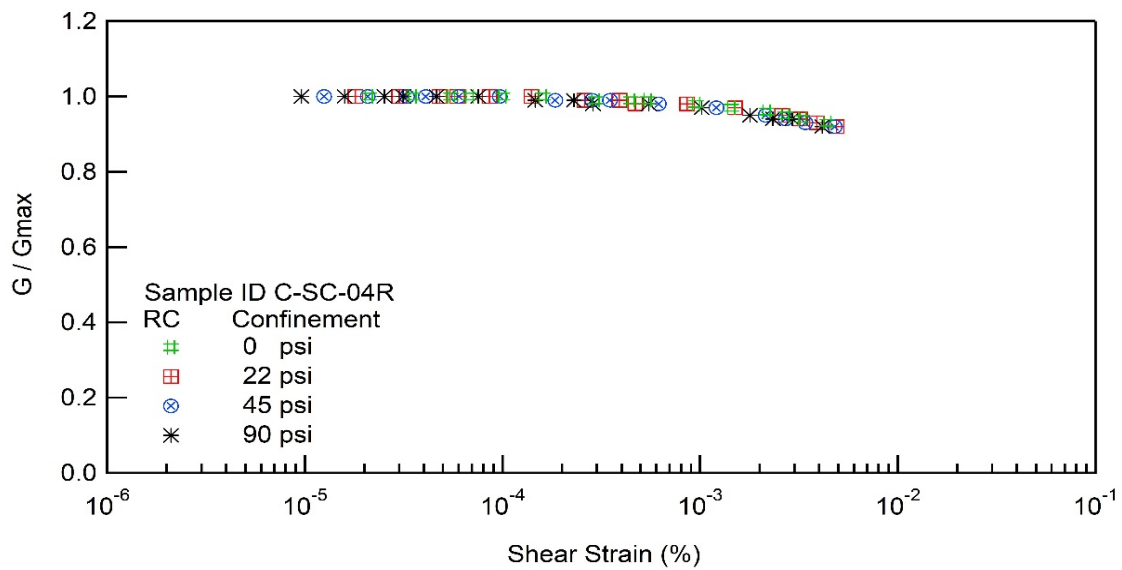
Client: SCDOT

Project ID: SPR-731

Location: Conway, SC

Boring No.: B-CON

Sample ID : C-SC-04R





## RESONANT COLUMN (RC) AND TORSIONAL SHEAR (TS) TEST

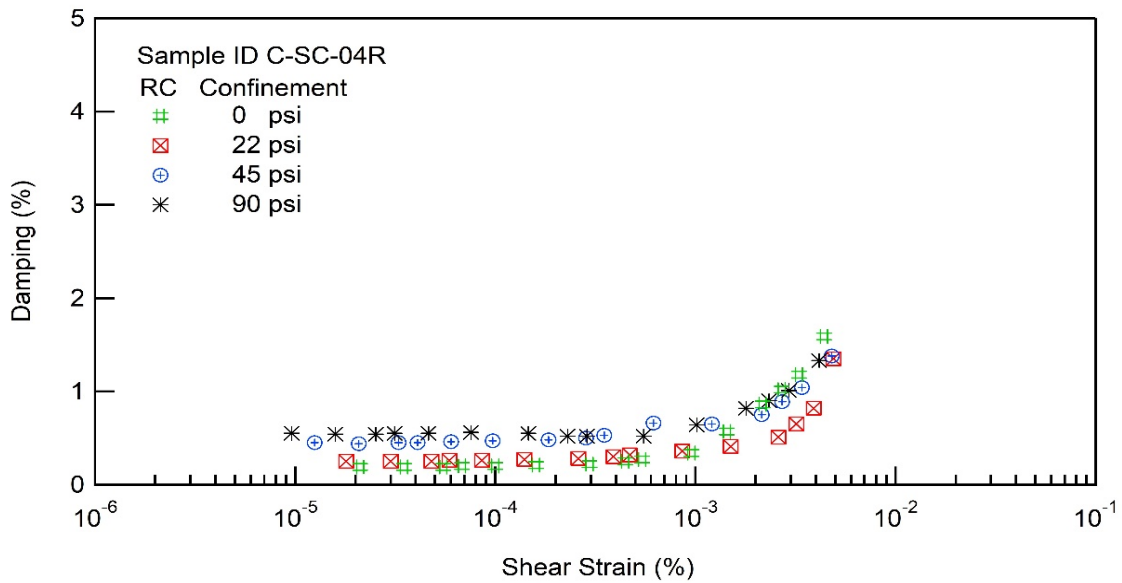
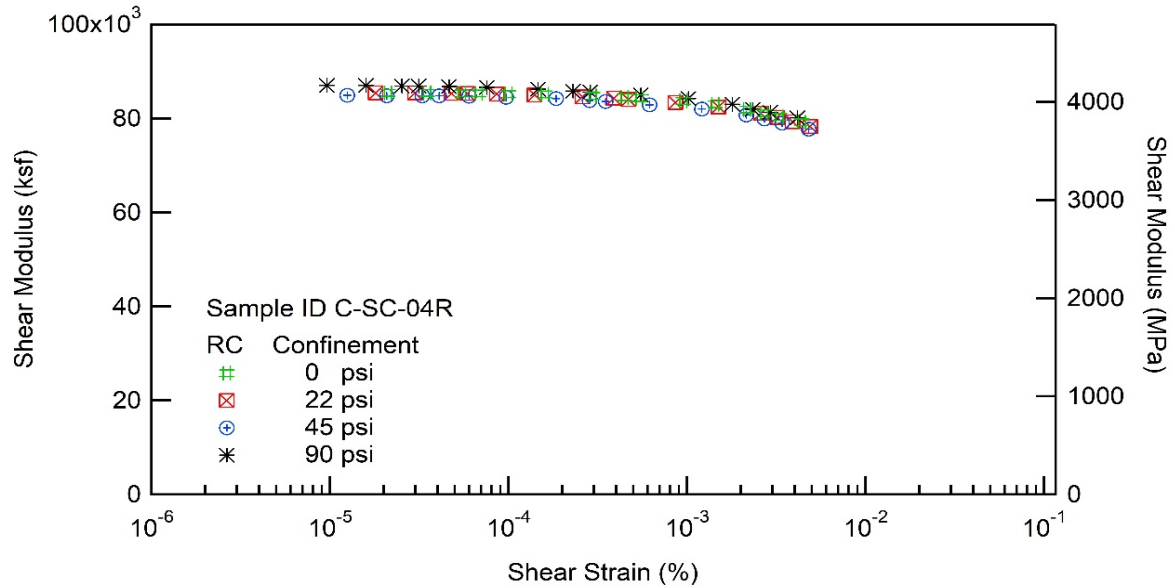
Project Name: Deep Soil Test Boring to Determine Shear  
Wave Velocities across South Carolina

Client: SCDOT

Project ID: SPR-731

Location: Conway, SC

Boring No.: B-CON





**UNIVERSITY OF SOUTH CAROLINA**  
 Department of Civil and Environmental Engineering  
 300 Main street, Columbia, SC, 29208

**RESONANT COLUMN (RC) TEST REPORT**

Project Name: Deep Soil Test Boring to Determine Shear  
 Wave Velocities across South Carolina  
 Client: SCDOT Project ID: SPR-731  
 Location: Conway, SC Boring No.: B-CON

Table 1 Results for Sample ID C-SC-04R for RC Test

No Confining Pressure				Confining Pressure 22 PSI				Confining Pressure 45 PSI			
$\gamma$ (%)	G (ksf)	G/G <sub>max</sub>	D (%)	$\gamma$ (%)	G (ksf)	G/G <sub>max</sub>	D (%)	$\gamma$ (%)	G (ksf)	G/G <sub>max</sub>	D (%)
2.11E-05	85351	1.001	0.188	1.83E-05	85375	1.001	0.247	1.25E-05	84871	1.001	0.446
3.50E-05	85375	1.001	0.188	3.02E-05	85375	1.001	0.249	2.08E-05	84772	1.000	0.444
5.50E-05	85275	1.000	0.192	4.76E-05	85275	1.000	0.252	3.29E-05	84772	1.000	0.446
6.81E-05	85275	1.000	0.195	5.88E-05	85275	1.000	0.257	4.09E-05	84772	1.000	0.452
9.99E-05	85173	0.999	0.198	8.55E-05	85173	0.999	0.262	6.01E-05	84670	0.999	0.460
1.60E-04	85073	0.998	0.206	1.37E-04	84974	0.996	0.267	9.70E-05	84471	0.997	0.470
2.96E-04	84772	0.994	0.225	2.55E-04	84570	0.992	0.276	1.85E-04	84171	0.993	0.483
4.46E-04	84471	0.991	0.248	3.86E-04	84270	0.988	0.298	2.84E-04	83769	0.988	0.503
5.42E-04	84270	0.988	0.267	4.72E-04	83970	0.985	0.325	3.50E-04	83569	0.986	0.533
9.54E-04	83671	0.981	0.338	8.61E-04	83369	0.978	0.355	6.17E-04	82871	0.978	0.664
1.44E-03	82972	0.973	0.570	1.54E-03	82378	0.966	0.409	1.21E-03	81980	0.967	0.652
2.17E-03	81883	0.960	0.863	2.59E-03	81092	0.951	0.511	2.15E-03	80701	0.952	0.752
2.70E-03	81092	0.951	1.018	3.21E-03	80211	0.941	0.649	2.71E-03	79918	0.943	0.889
3.29E-03	80308	0.942	1.184	3.89E-03	79332	0.930	0.822	3.41E-03	79041	0.933	1.037
4.40E-03	79236	0.929	1.591	4.93E-03	78267	0.918	1.349	4.80E-03	77689	0.917	1.375

Table 2 Results for Sample ID C-SC-04R for RC Test (Cont.)

Confining Pressure 90 PSI			
$\gamma$ (%)	G (ksf)	G/G <sub>max</sub>	D (%)
9.60E-06	86996	1.00	0.55
1.59E-05	86996	1.00	0.54
2.53E-05	86895	1.00	0.54
3.14E-05	86895	1.00	0.55
4.64E-05	86795	1.00	0.55
7.55E-05	86591	1.00	0.56
1.46E-04	86184	0.99	0.55
2.30E-04	85780	0.99	0.52
2.87E-04	85578	0.98	0.52
5.51E-04	84974	0.98	0.52
1.02E-03	84171	0.97	0.64
1.79E-03	82972	0.95	0.82
2.33E-03	81883	0.94	0.90
2.93E-03	81289	0.94	1.01
4.15E-03	80114	0.92	1.33



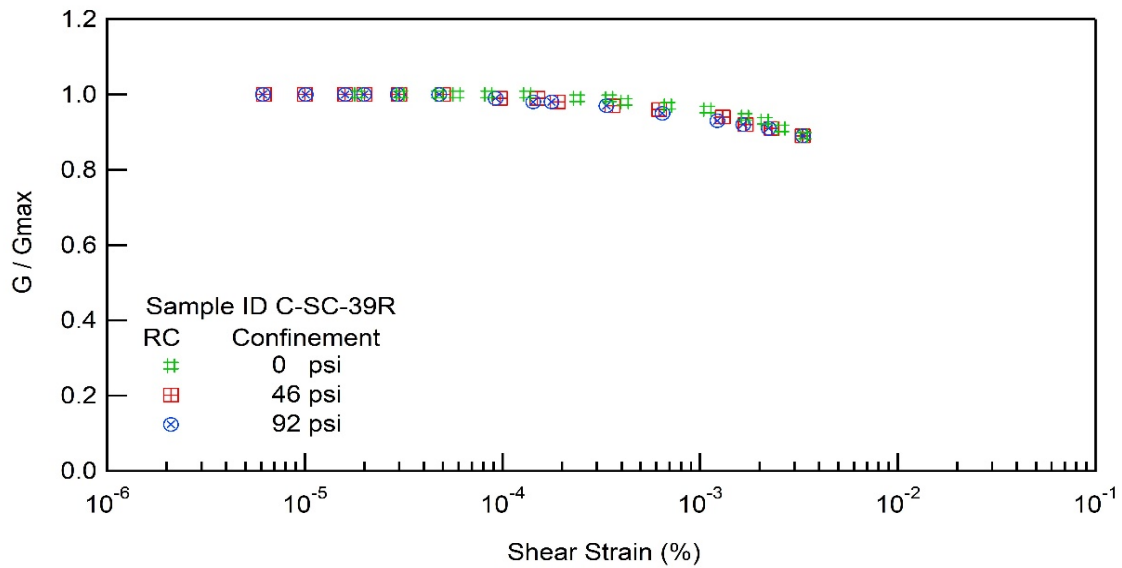
## RESONANT COLUMN (RC) AND TORSIONAL SHEAR (TS) TEST

Project Name: Deep Soil Test Boring to Determine Shear  
Wave Velocities across South Carolina

Client: SCDOT  
Location: Conway, SC

Project ID: SPR-731  
Boring No.: B-CON

Sample ID : C-SC-39R





## RESONANT COLUMN (RC) AND TORSIONAL SHEAR (TS) TEST

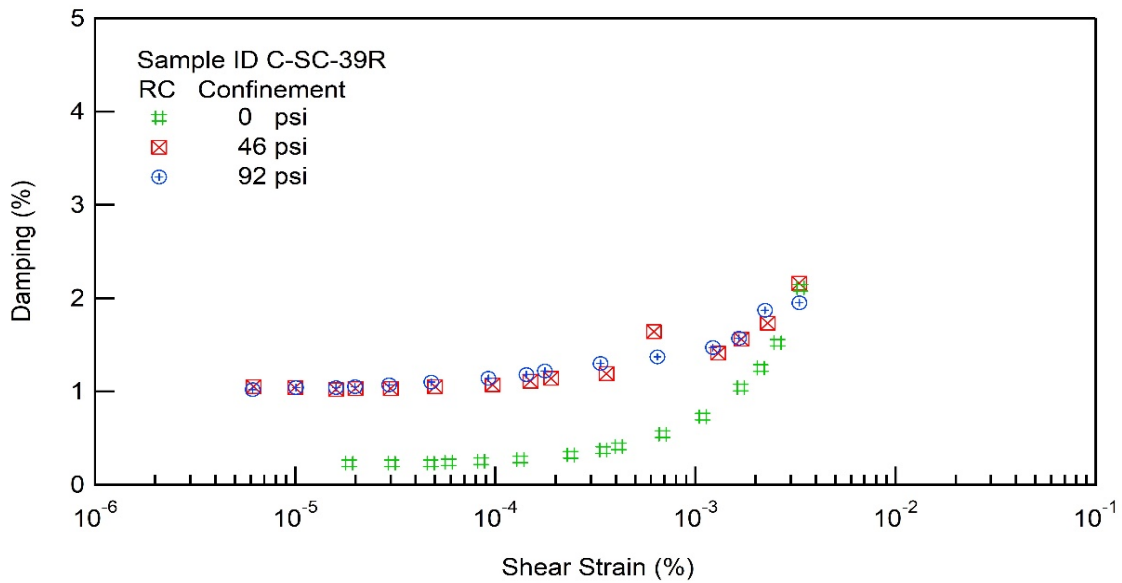
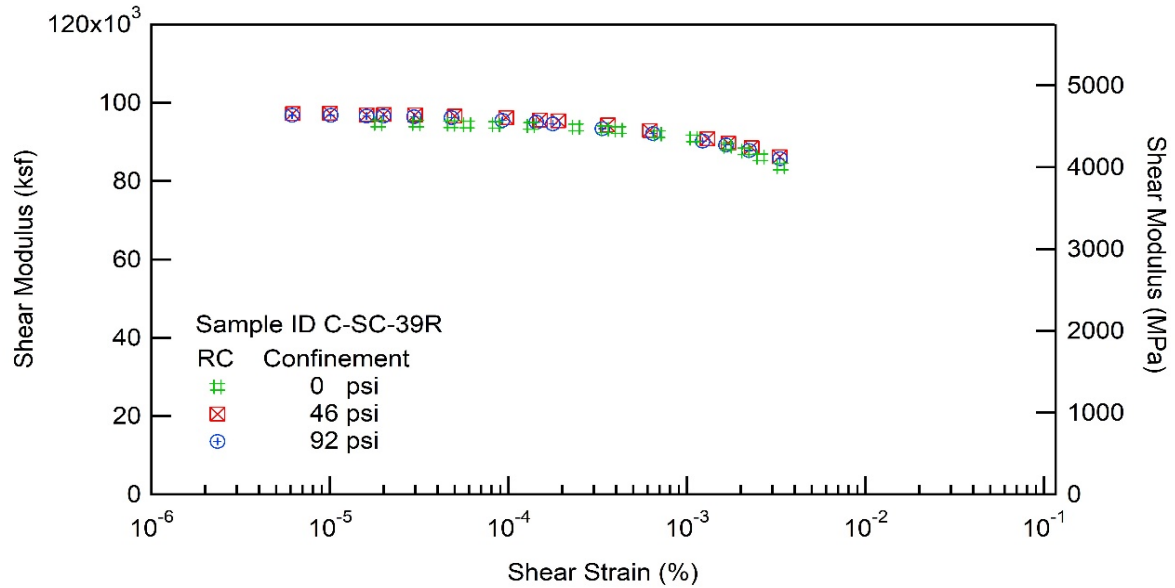
Project Name: Deep Soil Test Boring to Determine Shear  
Wave Velocities across South Carolina

Client: SCDOT

Project ID: SPR-731

Location: Conway, SC

Boring No.: B-CON







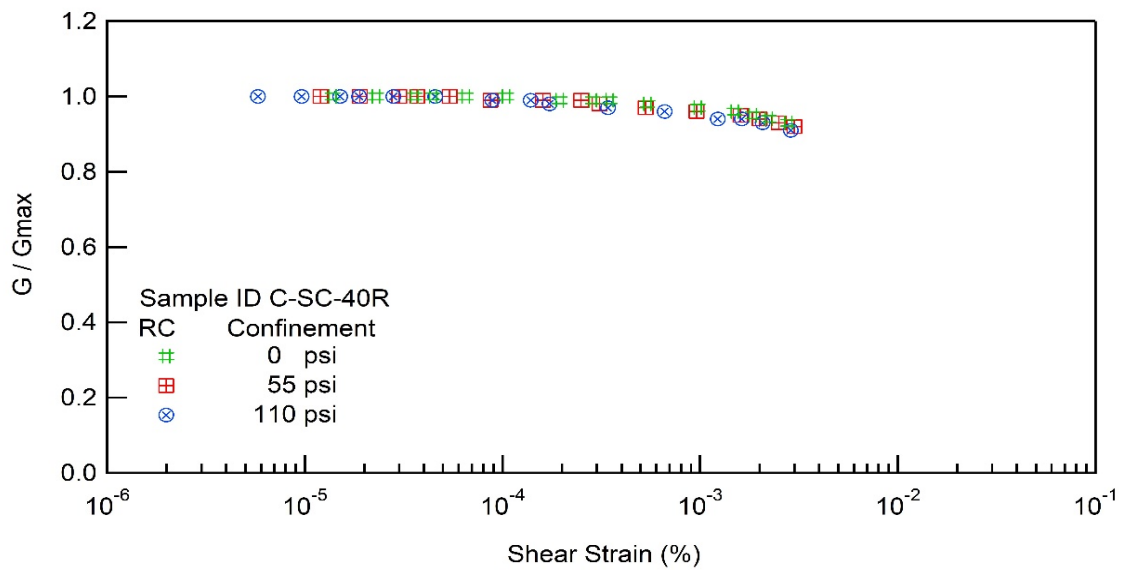
## RESONANT COLUMN (RC) AND TORSIONAL SHEAR (TS) TEST

Project Name: Deep Soil Test Boring to Determine Shear  
Wave Velocities across South Carolina

Client: SCDOT  
Location: Conway, SC

Project ID: SPR-731  
Boring No.: B-CON

Sample ID : C-SC-40R





## RESONANT COLUMN (RC) AND TORSIONAL SHEAR (TS) TEST

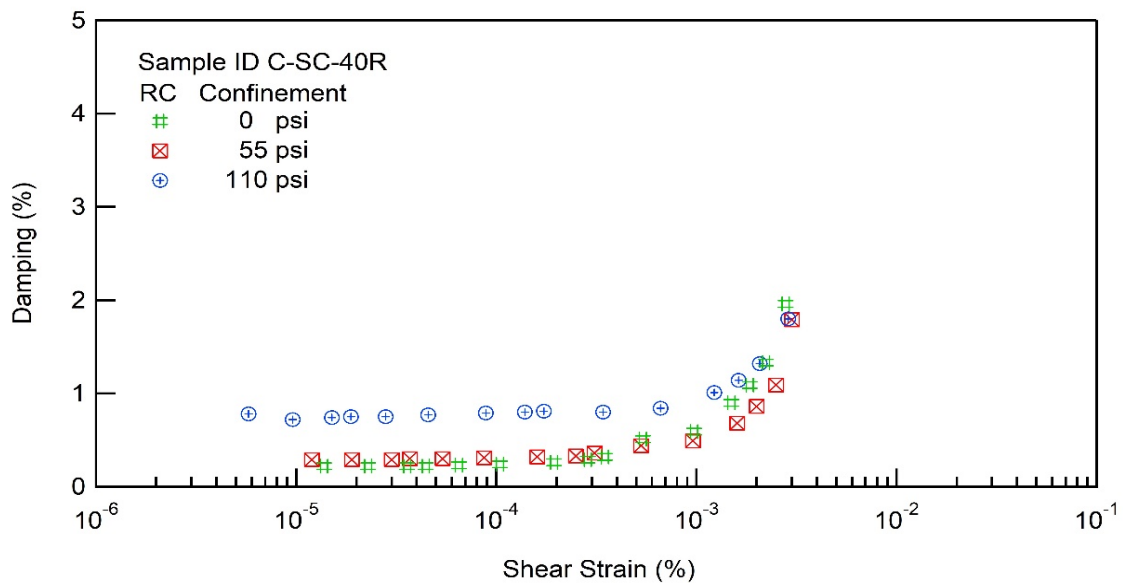
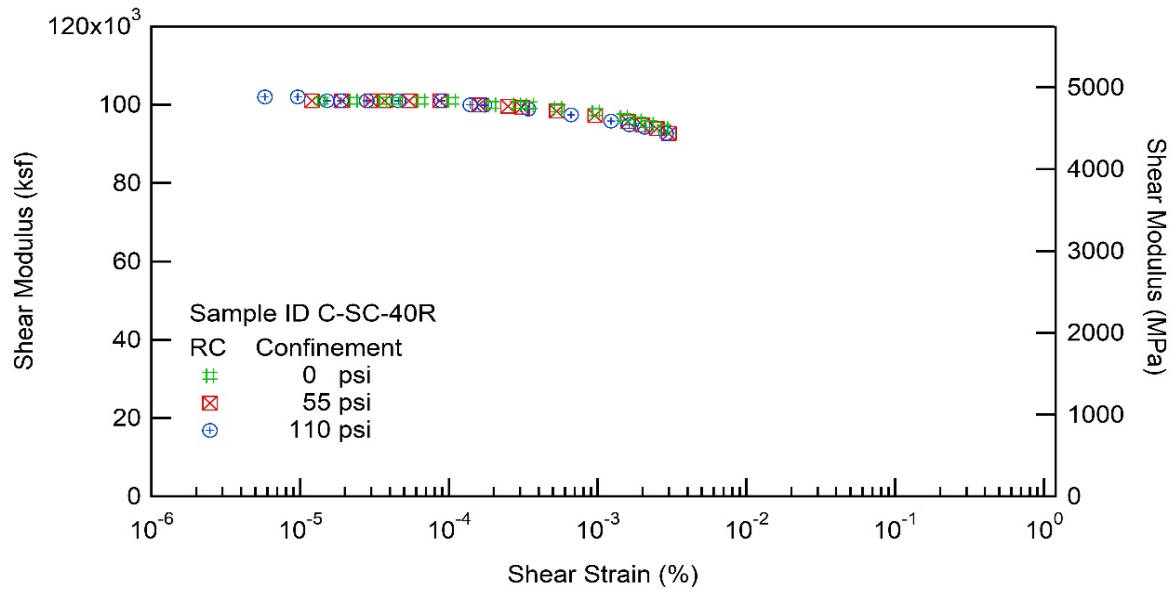
Project Name: Deep Soil Test Boring to Determine Shear  
Wave Velocities across South Carolina

Client: SCDOT

Project ID: SPR-731

Location: Conway, SC

Boring No.: B-CON







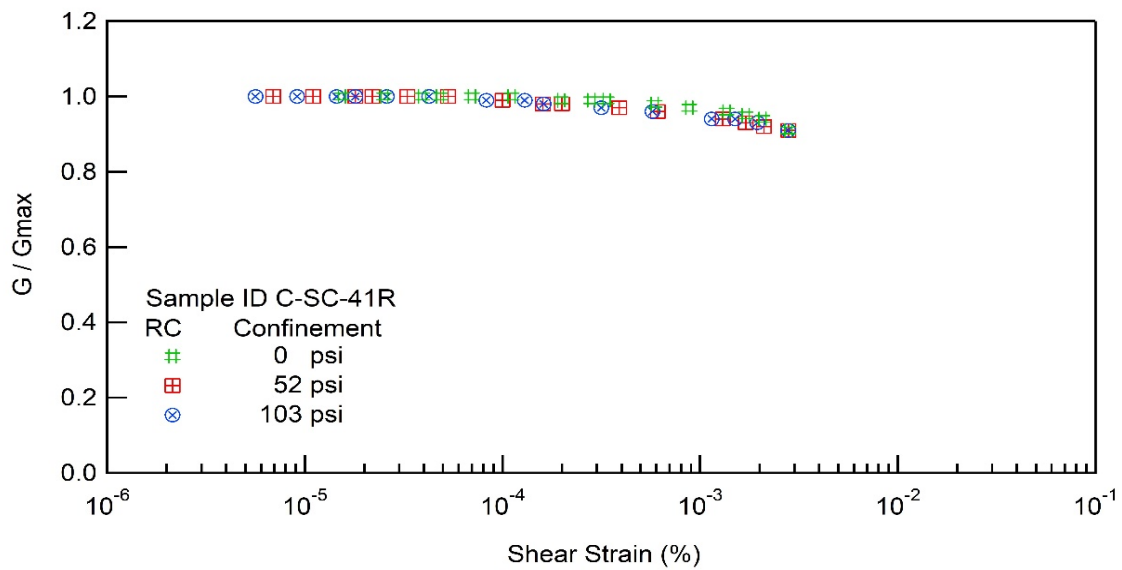
## RESONANT COLUMN (RC) AND TORSIONAL SHEAR (TS) TEST

Project Name: Deep Soil Test Boring to Determine Shear  
Wave Velocities across South Carolina

Client: SCDOT  
Location: Conway, SC

Project ID: SPR-731  
Boring No.: B-CON

Sample ID : C-SC-41R



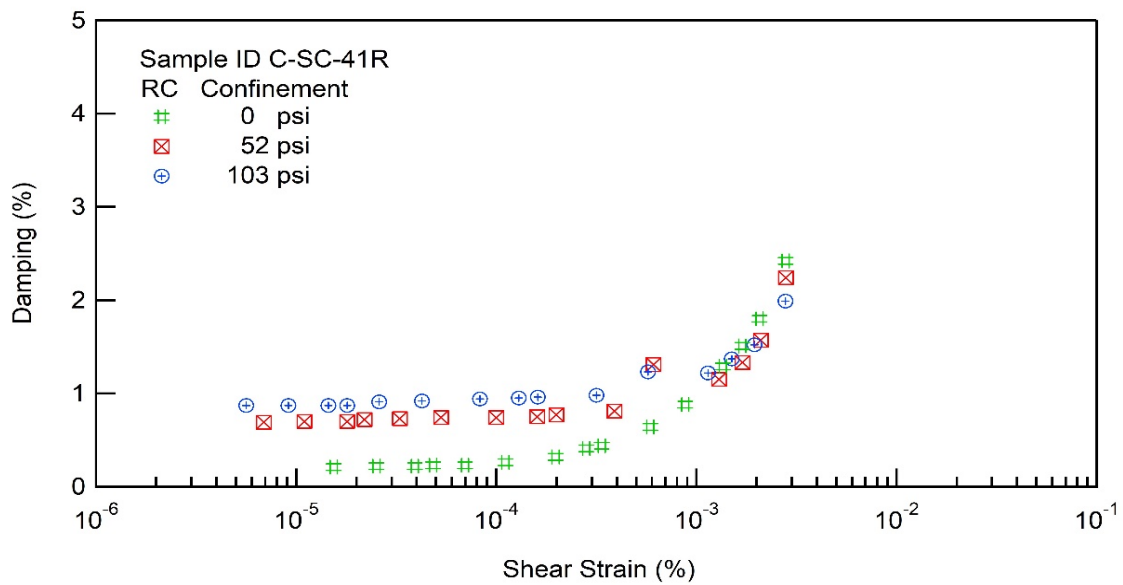
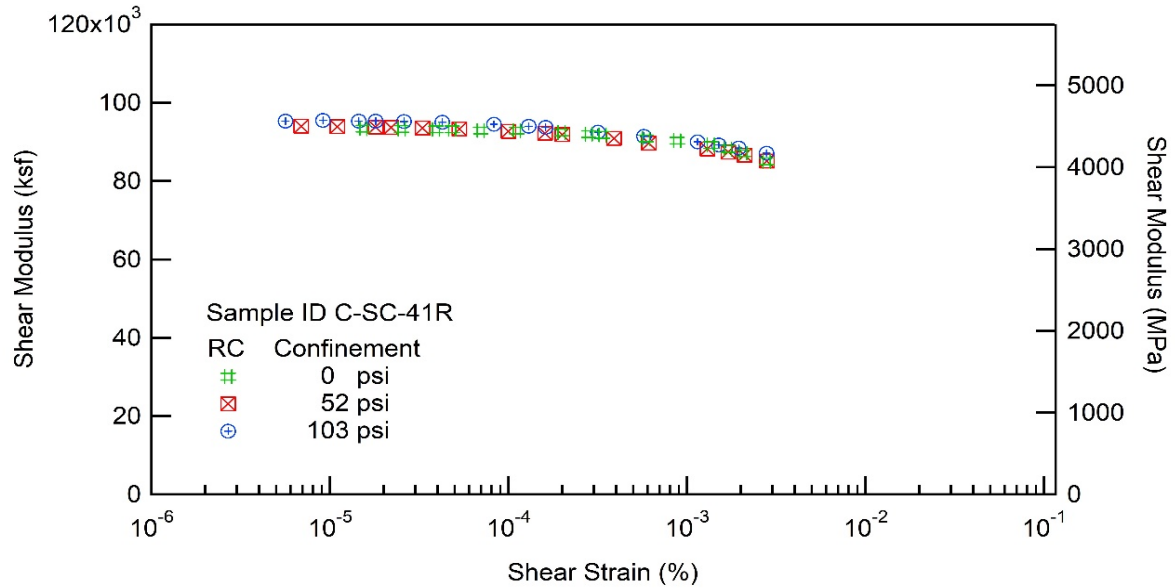


## RESONANT COLUMN (RC) AND TORSIONAL SHEAR (TS) TEST

Project Name: Deep Soil Test Boring to Determine Shear  
Wave Velocities across South Carolina

Client: SCDOT  
Location: Conway, SC

Project ID: SPR-731  
Boring No.: B-CON







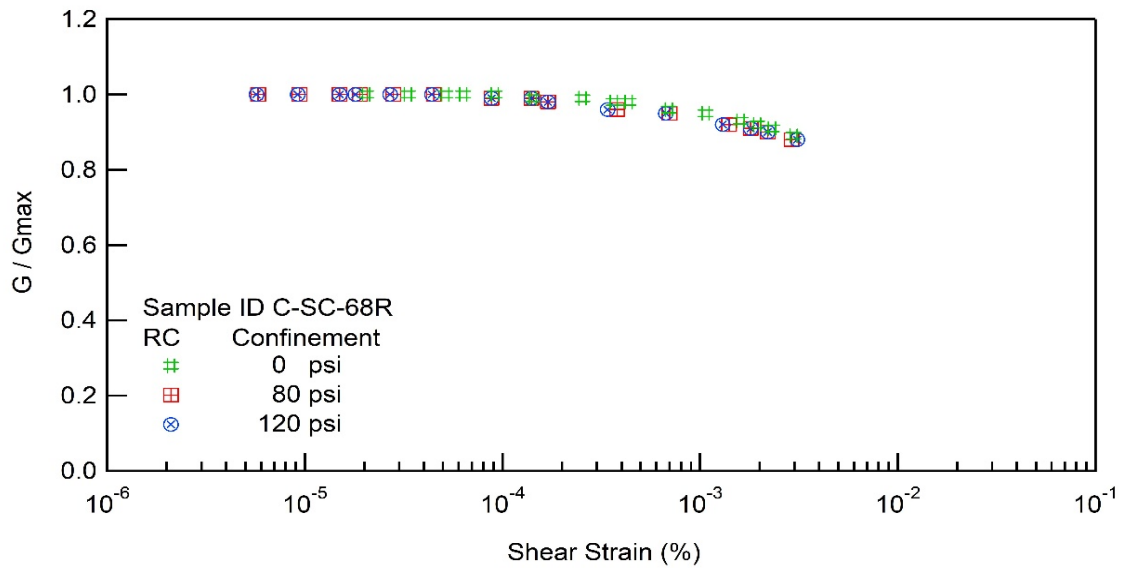
## RESONANT COLUMN (RC) AND TORSIONAL SHEAR (TS) TEST

Project Name: Deep Soil Test Boring to Determine Shear  
Wave Velocities across South Carolina

Client: SCDOT  
Location: Conway, SC

Project ID: SPR-731  
Boring No.: B-CON

Sample ID : C-SC-68R





## RESONANT COLUMN (RC) AND TORSIONAL SHEAR (TS) TEST

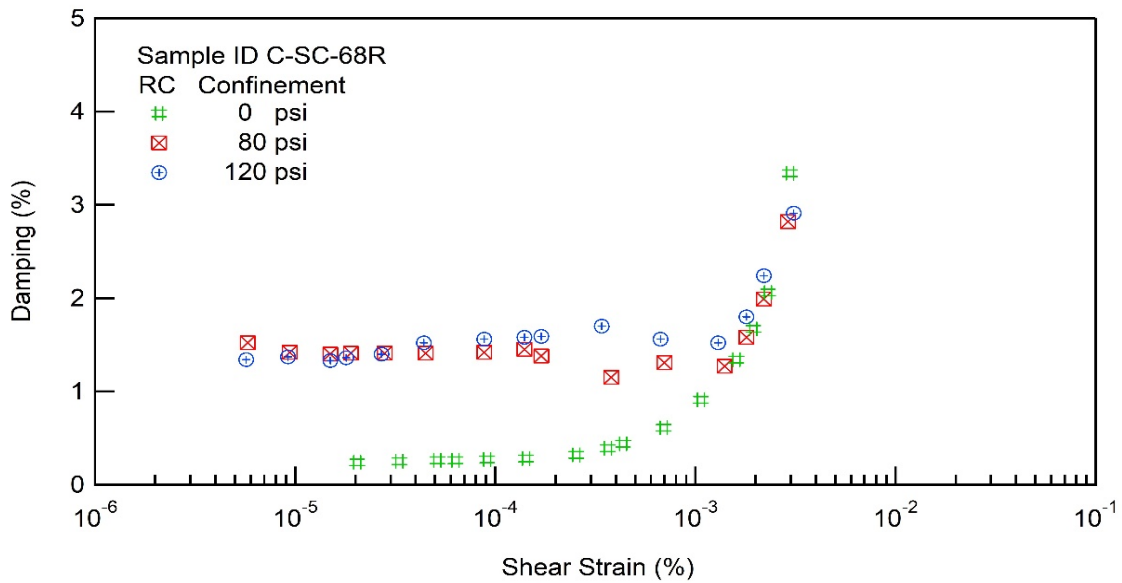
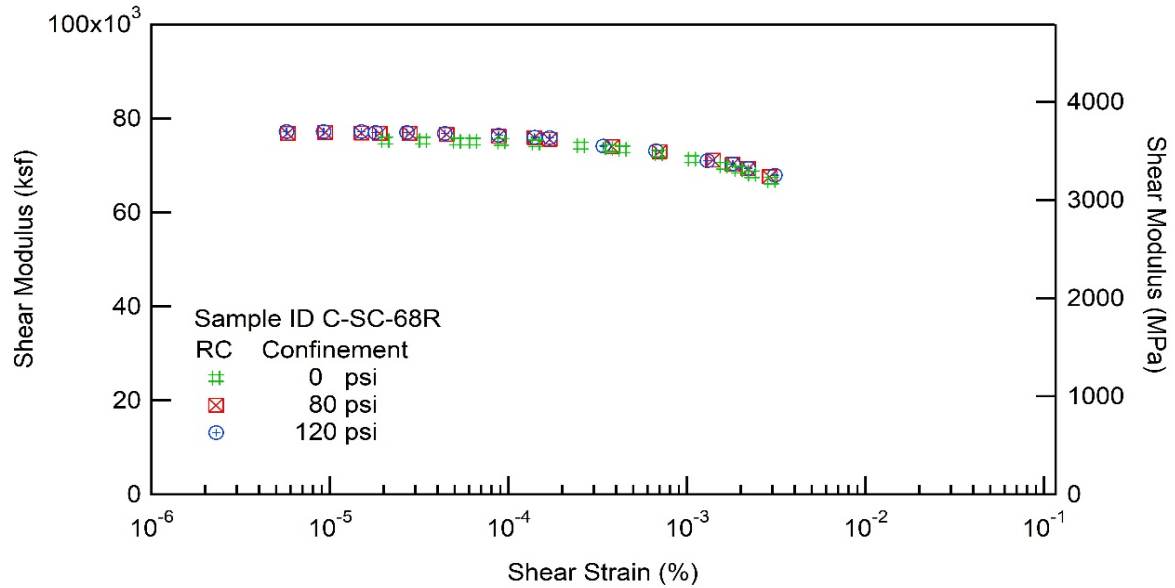
Project Name: Deep Soil Test Boring to Determine Shear  
Wave Velocities across South Carolina

Client: SCDOT

Project ID: SPR-731

Location: Conway, SC

Boring No.: B-CON







## RESONANT COLUMN (RC) AND TORSIONAL SHEAR (TS) TEST

Project Name: Deep Soil Test Boring to Determine Shear  
Wave Velocities across South Carolina

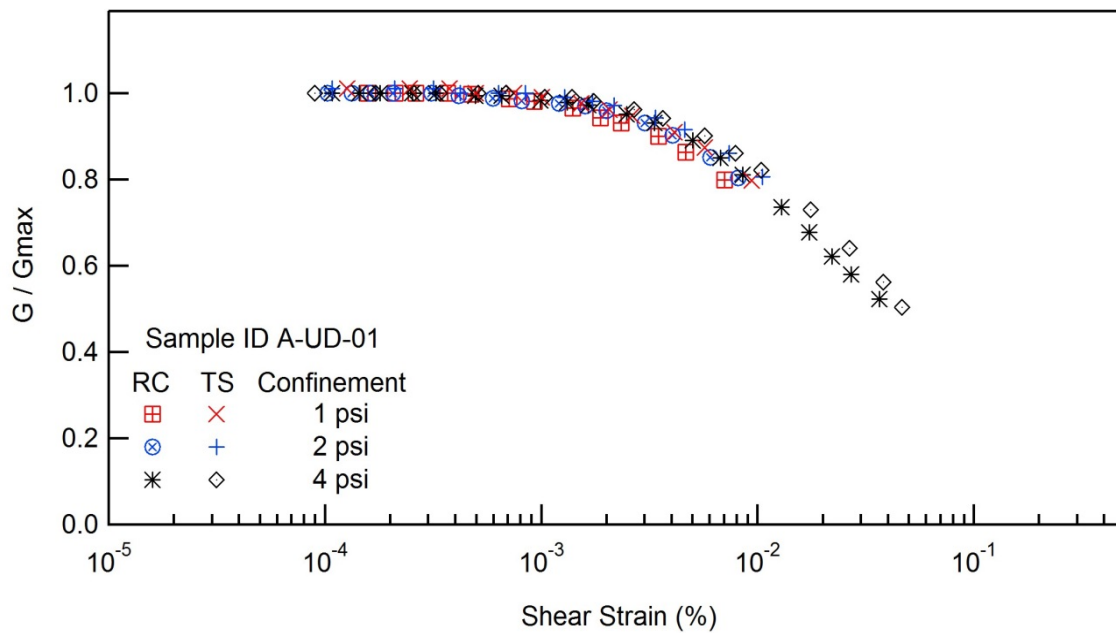
Client: SCDOT

Project ID: SPR-731

Location: Andrews, SC

Boring No.: B-FMG

Sample ID : A-UD-01





### RESONANT COLUMN (RC) AND TORSIONAL SHEAR (TS) TEST

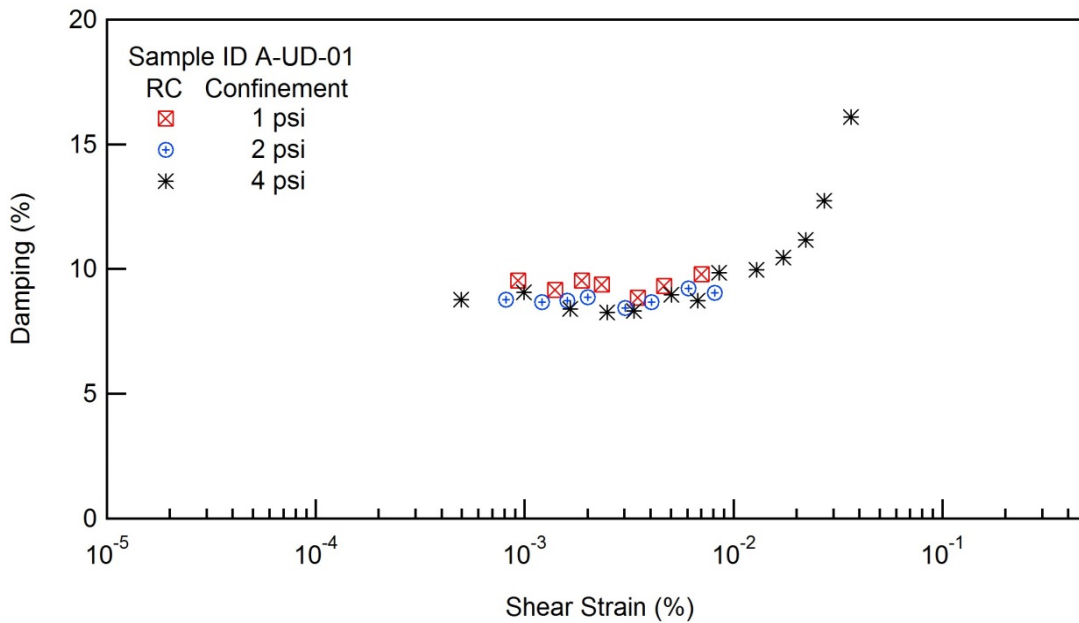
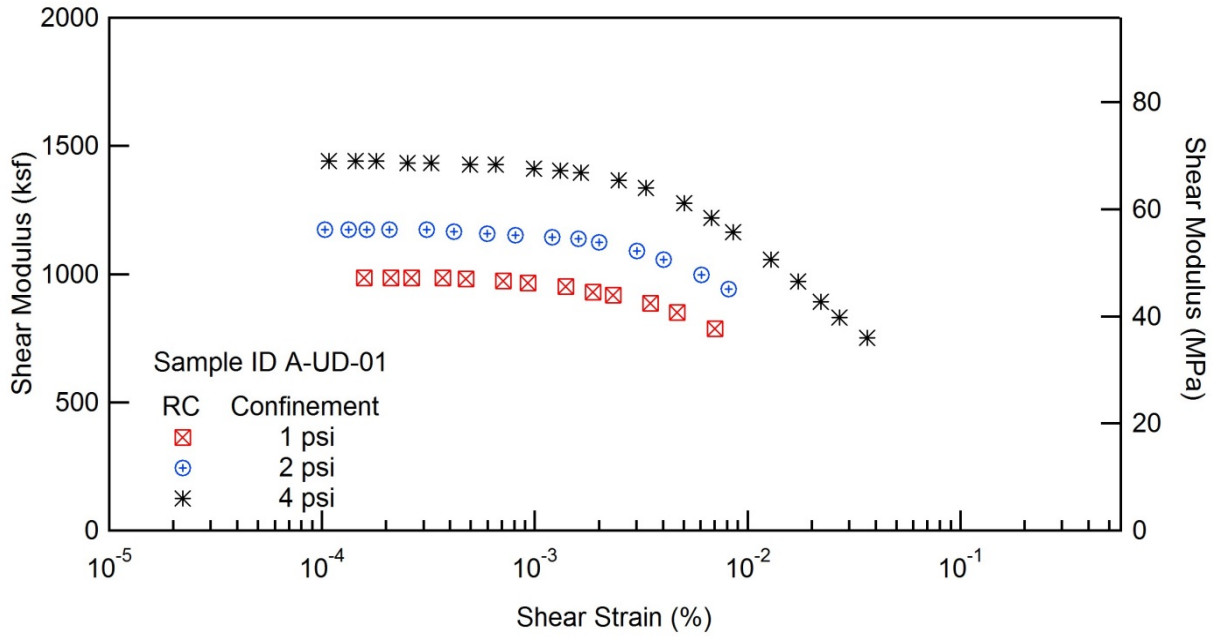
Project Name: Deep Soil Test Boring to Determine Shear  
Wave Velocities across South Carolina

Client: SCDOT

Project ID: SPR-731

Location: Andrews, SC

Boring No.: B-FMG





## RESONANT COLUMN (RC) AND TORSIONAL SHEAR (TS) TEST

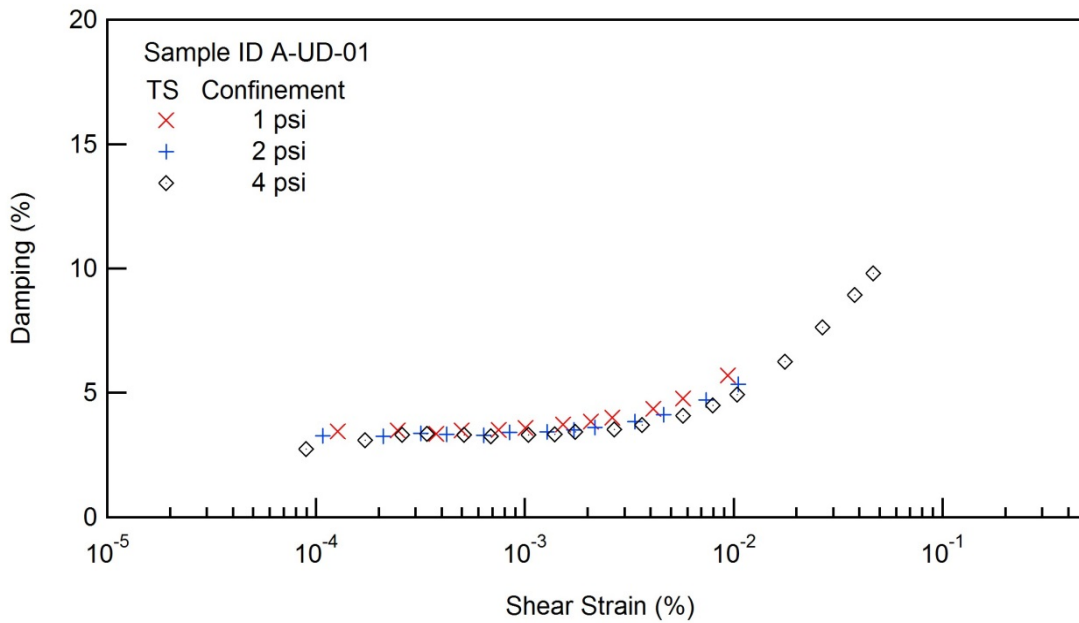
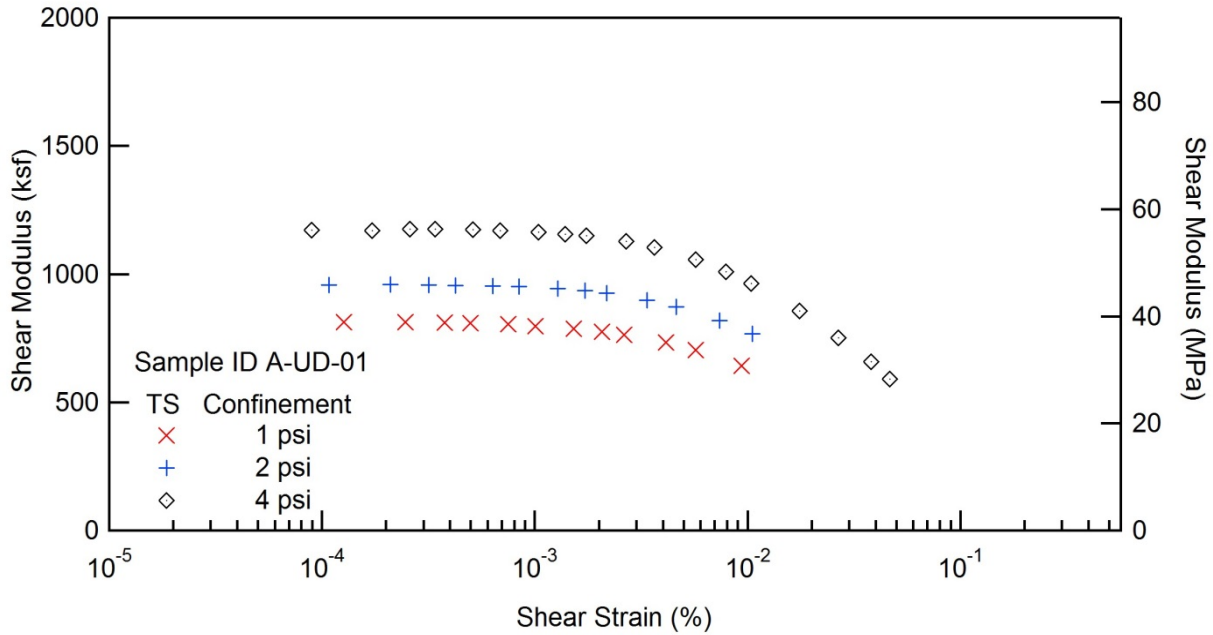
Project Name: Deep Soil Test Boring to Determine Shear  
Wave Velocities across South Carolina

Client: SCDOT

Project ID: SPR-731

Location: Andrews, SC

Boring No.: B-FMG









## RESONANT COLUMN (RC) AND TORSIONAL SHEAR (TS) TEST

Project Name: Deep Soil Test Boring to Determine Shear  
Wave Velocities across South Carolina

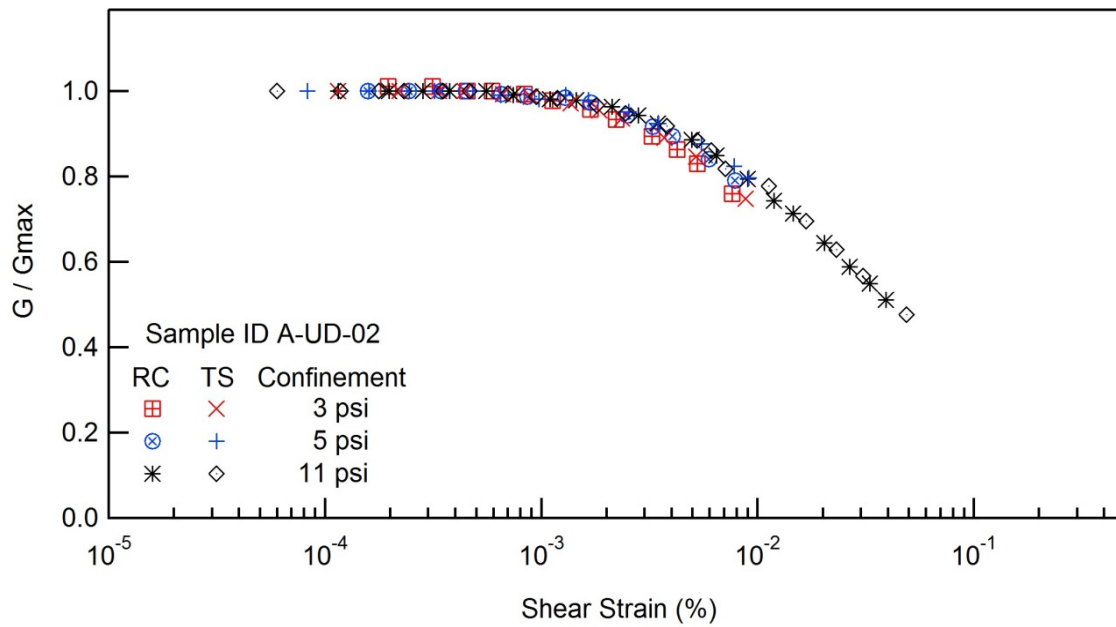
Client: SCDOT

Project ID: SPR-731

Location: Andrews, SC

Boring No.: B-FMG

Sample ID : A-UD-02





## RESONANT COLUMN (RC) AND TORSIONAL SHEAR (TS) TEST

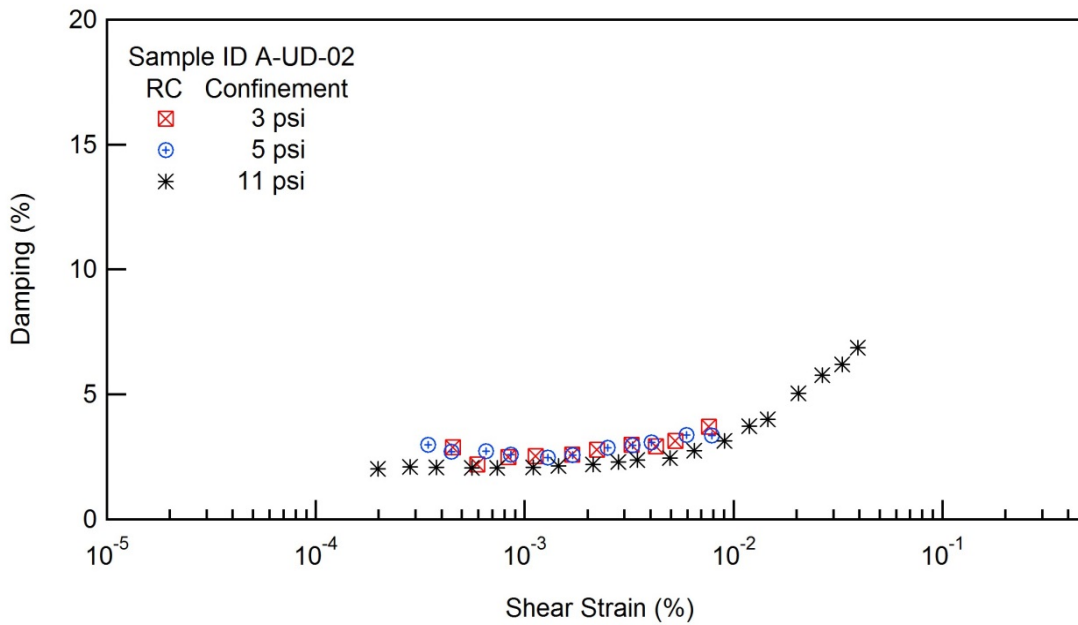
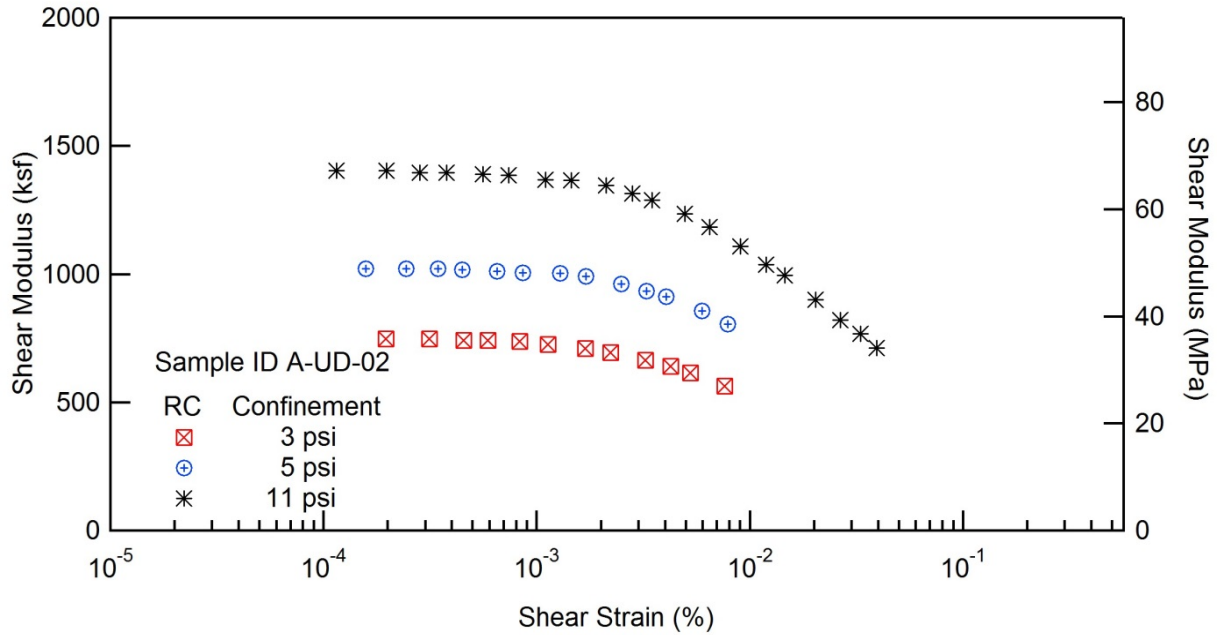
Project Name: Deep Soil Test Boring to Determine Shear  
Wave Velocities across South Carolina

Client: SCDOT

Project ID: SPR-731

Location: Andrews, SC

Boring No.: B-FMG





### RESONANT COLUMN (RC) AND TORSIONAL SHEAR (TS) TEST

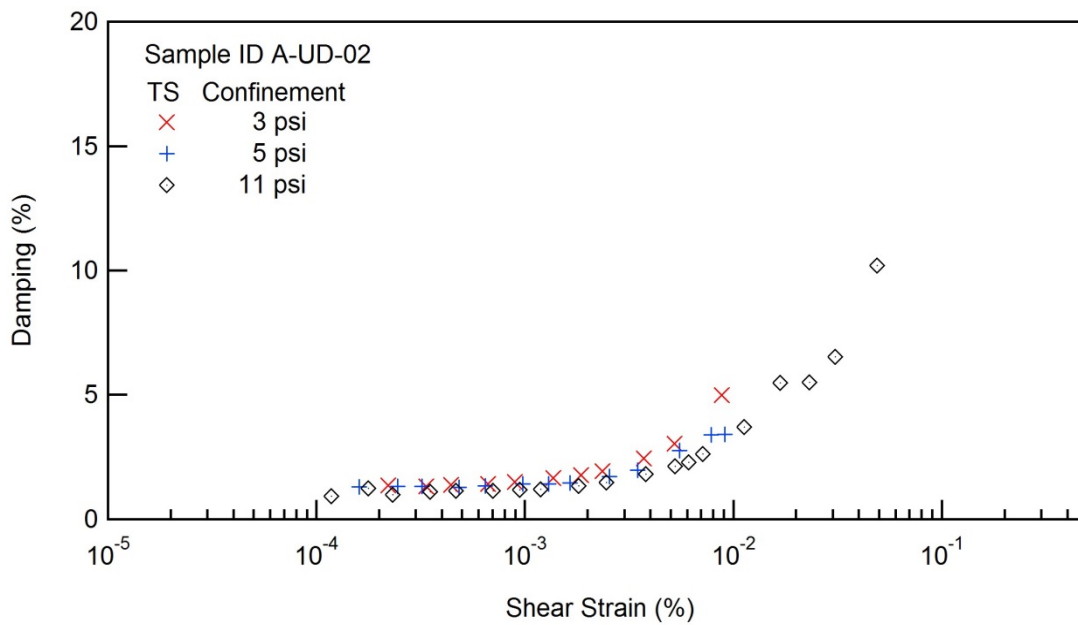
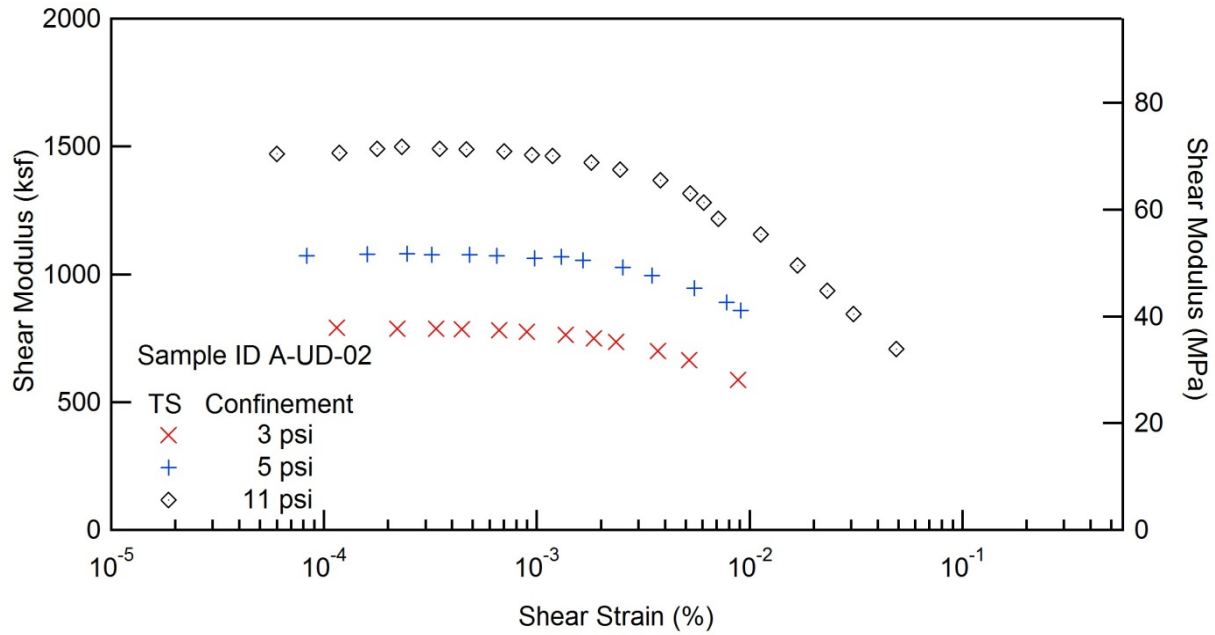
Project Name: Deep Soil Test Boring to Determine Shear  
Wave Velocities across South Carolina

Client: SCDOT

Project ID: SPR-731

Location: Andrews, SC

Boring No.: B-FMG









## RESONANT COLUMN (RC) AND TORSIONAL SHEAR (TS) TEST

Project Name: Deep Soil Test Boring to Determine Shear  
Wave Velocities across South Carolina

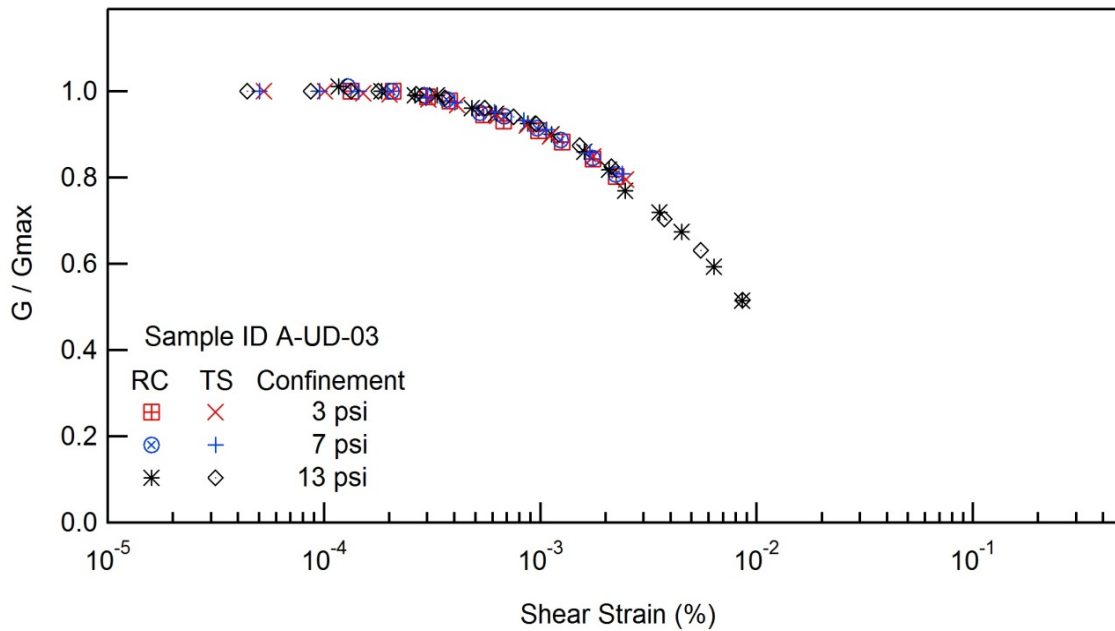
Client: SCDOT

Project ID: SPR-731

Location: Andrews, SC

Boring No.: B-FMG

Sample ID : A-UD-03





## RESONANT COLUMN (RC) AND TORSIONAL SHEAR (TS) TEST

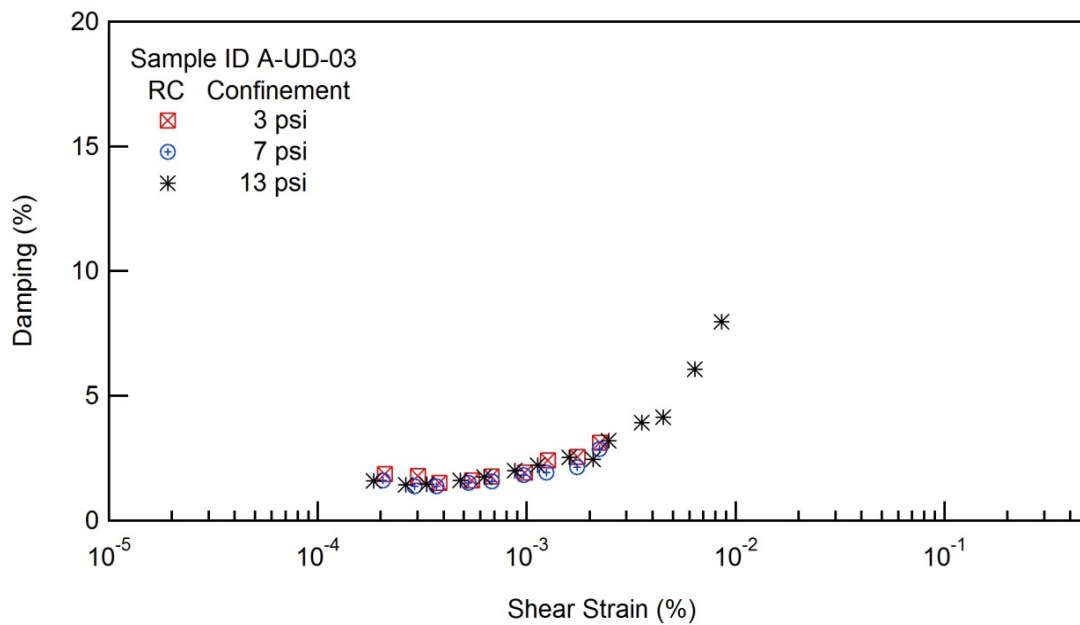
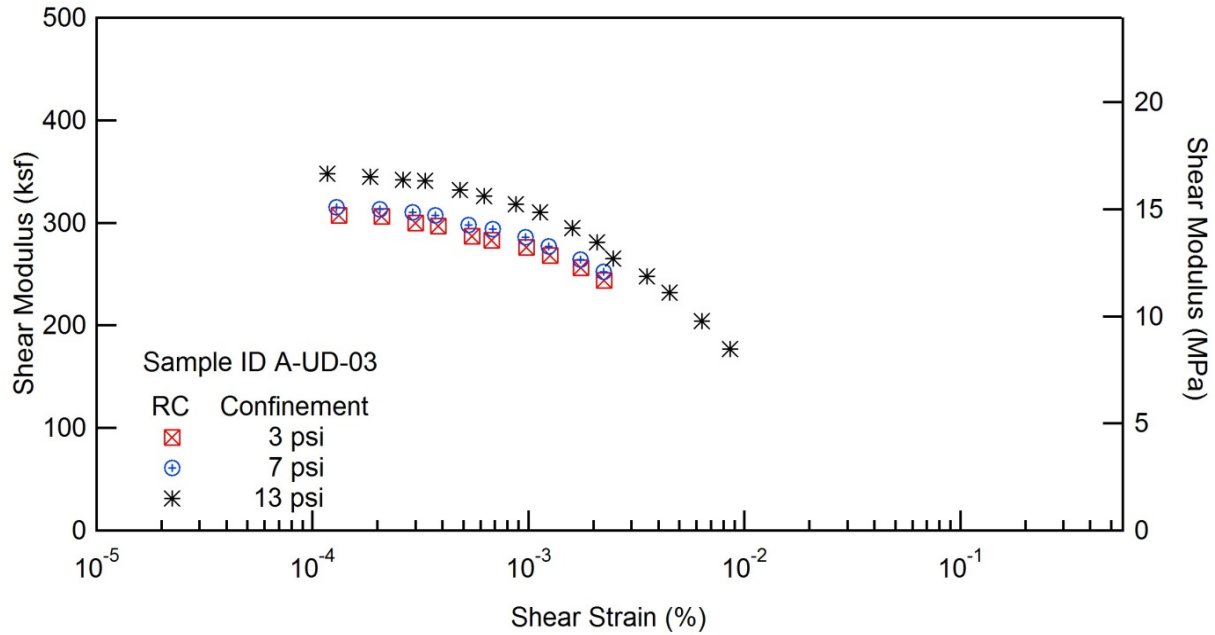
Project Name: Deep Soil Test Boring to Determine Shear  
Wave Velocities across South Carolina

Client: SCDOT

Project ID: SPR-731

Location: Andrews, SC

Boring No.: B-FMG





## RESONANT COLUMN (RC) AND TORSIONAL SHEAR (TS) TEST

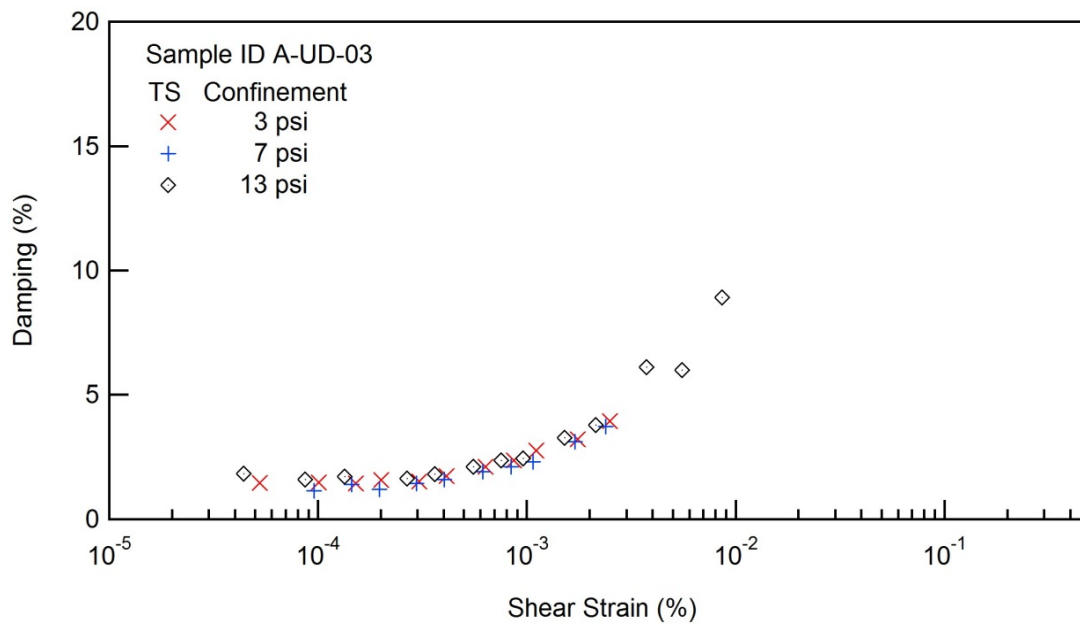
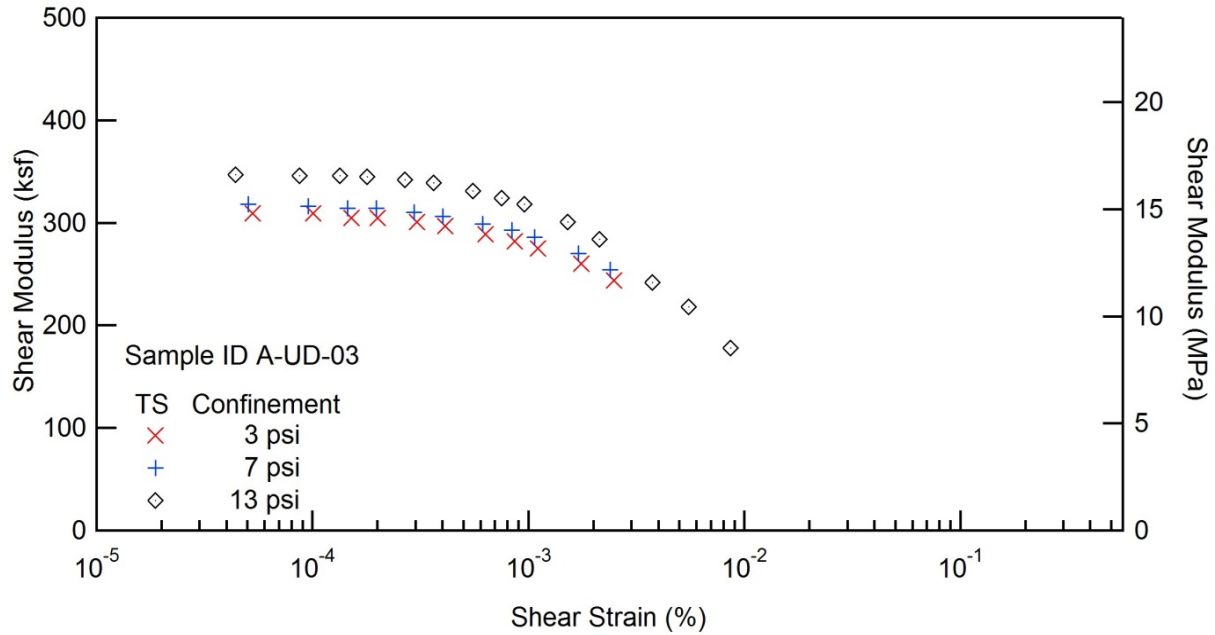
Project Name: Deep Soil Test Boring to Determine Shear  
Wave Velocities across South Carolina

Client: SCDOT

Project ID: SPR-731

Location: Andrews, SC

Boring No.: B-FMG









## RESONANT COLUMN (RC) AND TORSIONAL SHEAR (TS) TEST

Project Name: Deep Soil Test Boring to Determine Shear  
Wave Velocities across South Carolina

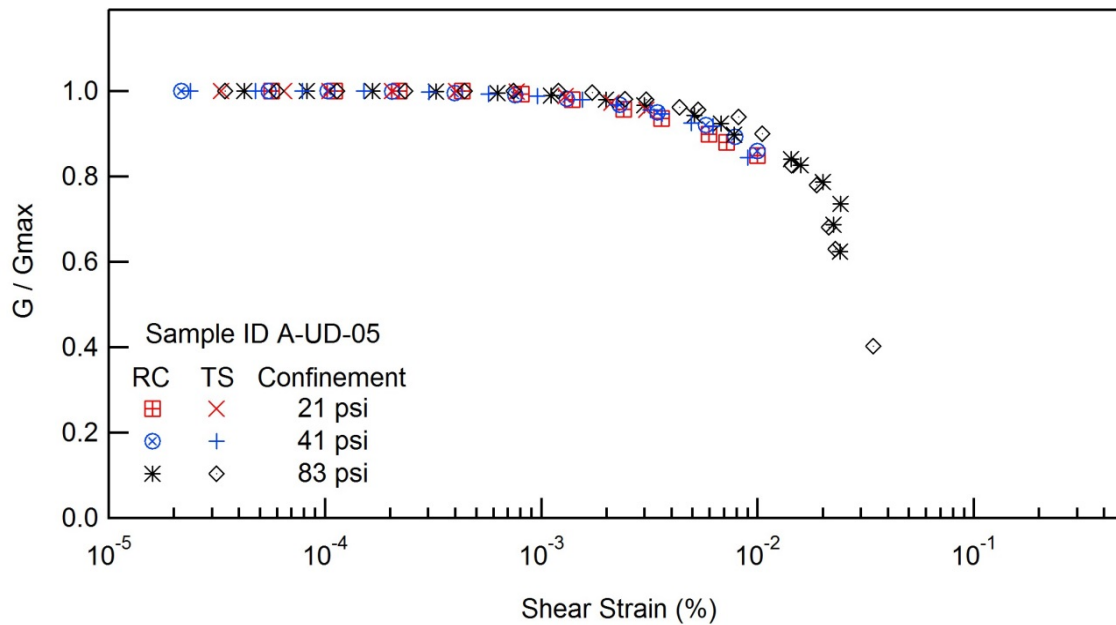
Client: SCDOT

Project ID: SPR-731

Location: Andrews, SC

Boring No.: B-FMG

Sample ID : A-UD-05





## RESONANT COLUMN (RC) AND TORSIONAL SHEAR (TS) TEST

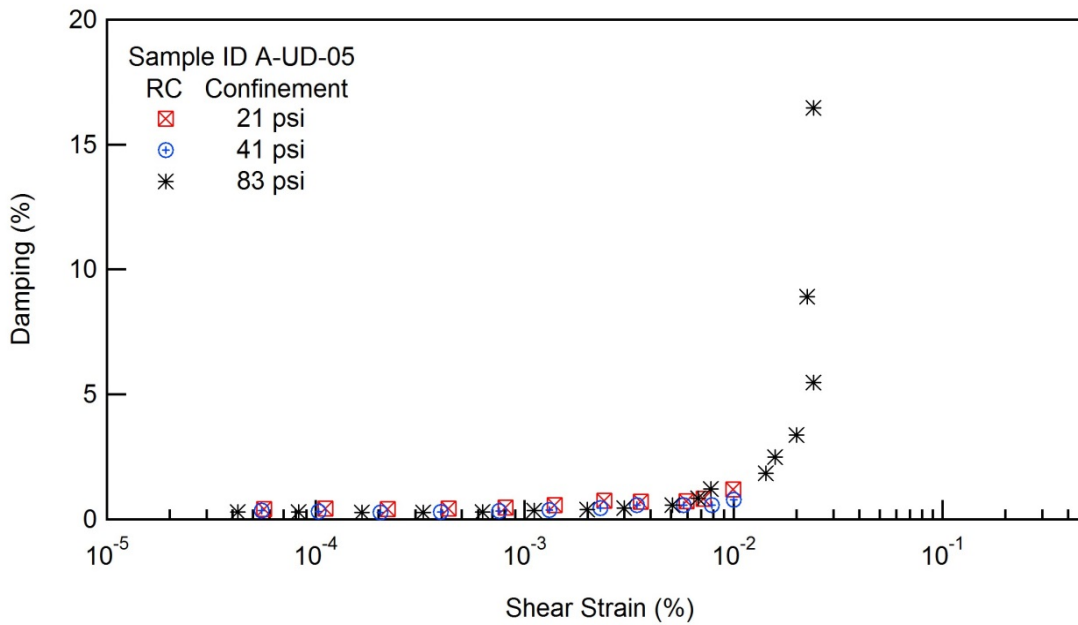
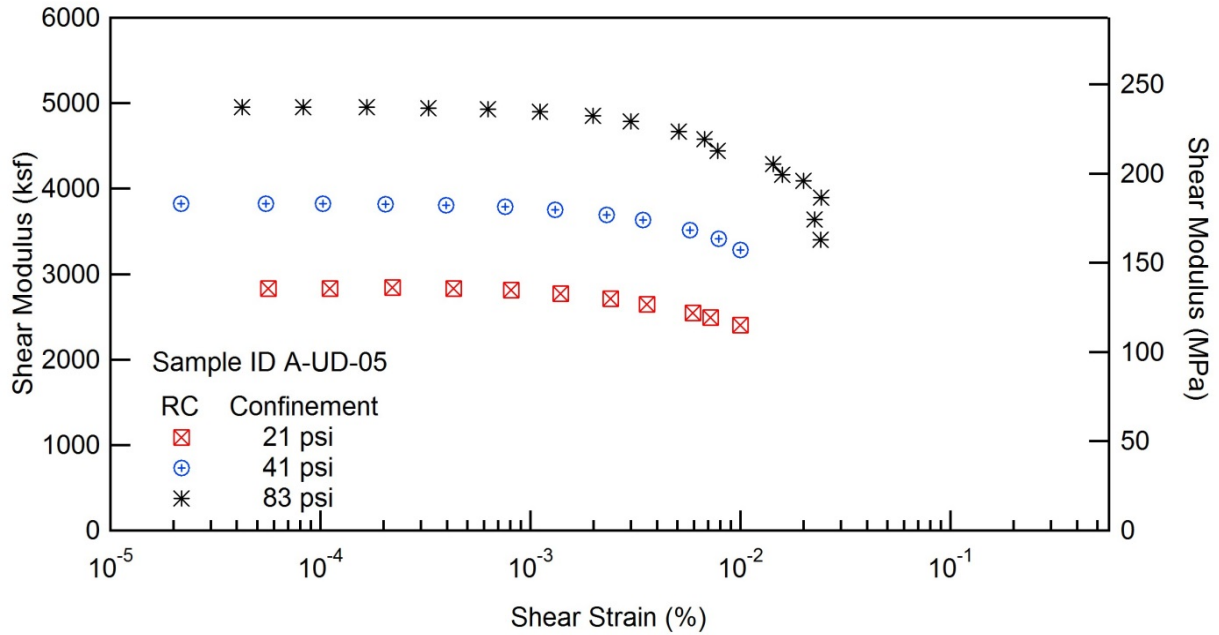
Project Name: Deep Soil Test Boring to Determine Shear  
Wave Velocities across South Carolina

Client: SCDOT

Project ID: SPR-731

Location: Andrews, SC

Boring No.: B-FMG





### RESONANT COLUMN (RC) AND TORSIONAL SHEAR (TS) TEST

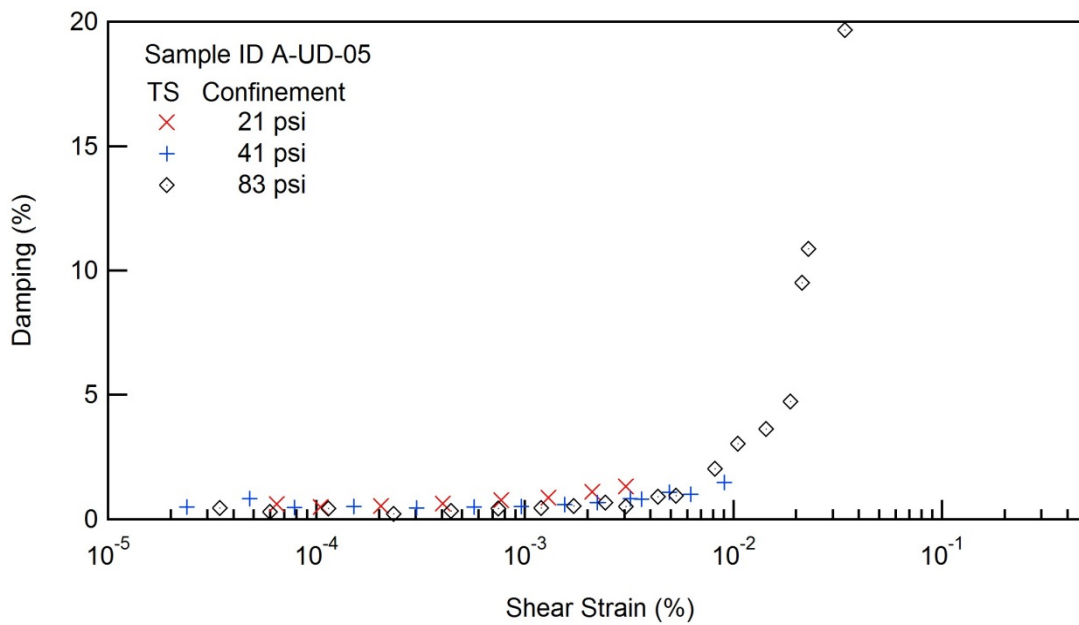
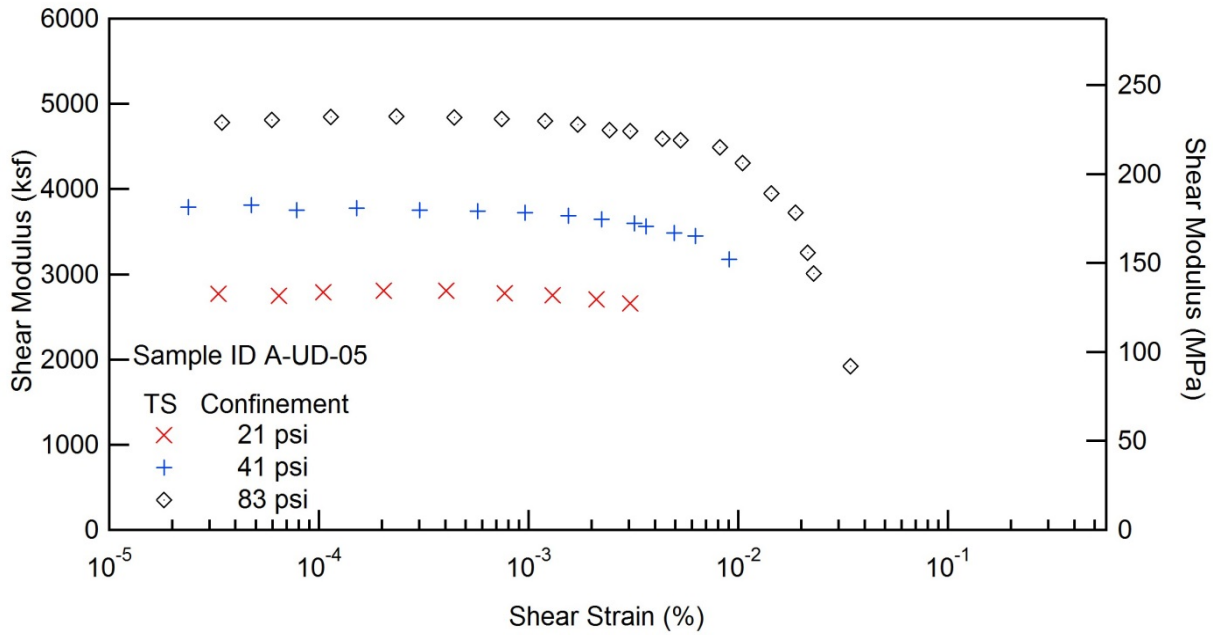
Project Name: Deep Soil Test Boring to Determine Shear  
Wave Velocities across South Carolina

Client: SCDOT

Project ID: SPR-731

Location: Andrews, SC

Boring No.: B-FMG









## RESONANT COLUMN (RC) AND TORSIONAL SHEAR (TS) TEST

Project Name: Deep Soil Test Boring to Determine Shear  
Wave Velocities across South Carolina

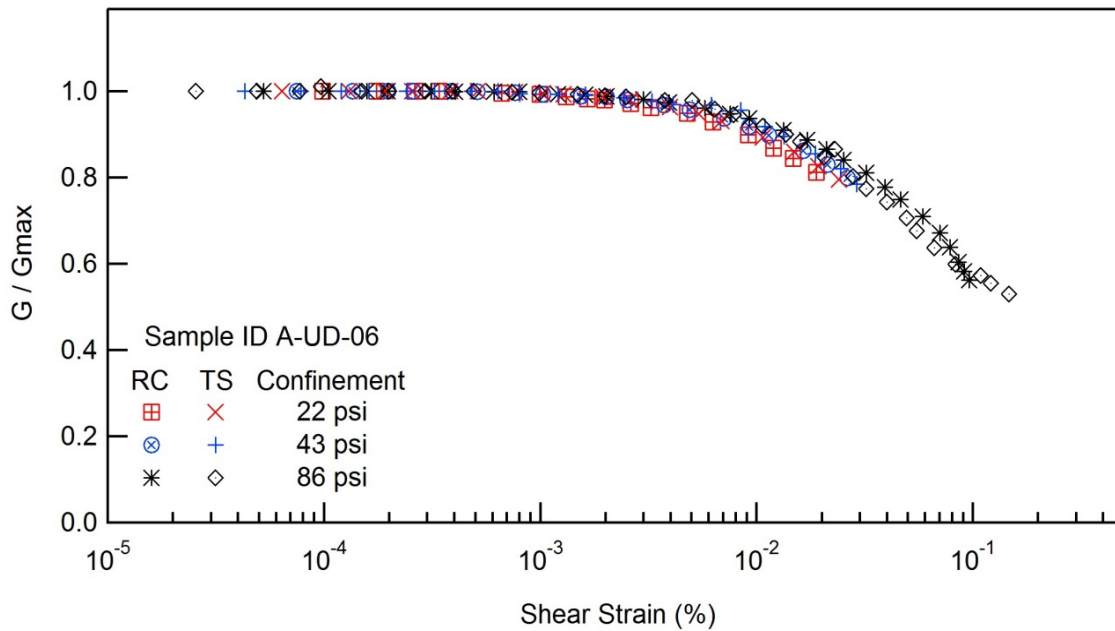
Client: SCDOT

Project ID: SPR-731

Location: Andrews, SC

Boring No.: B-FMG

Sample ID : A-UD-06



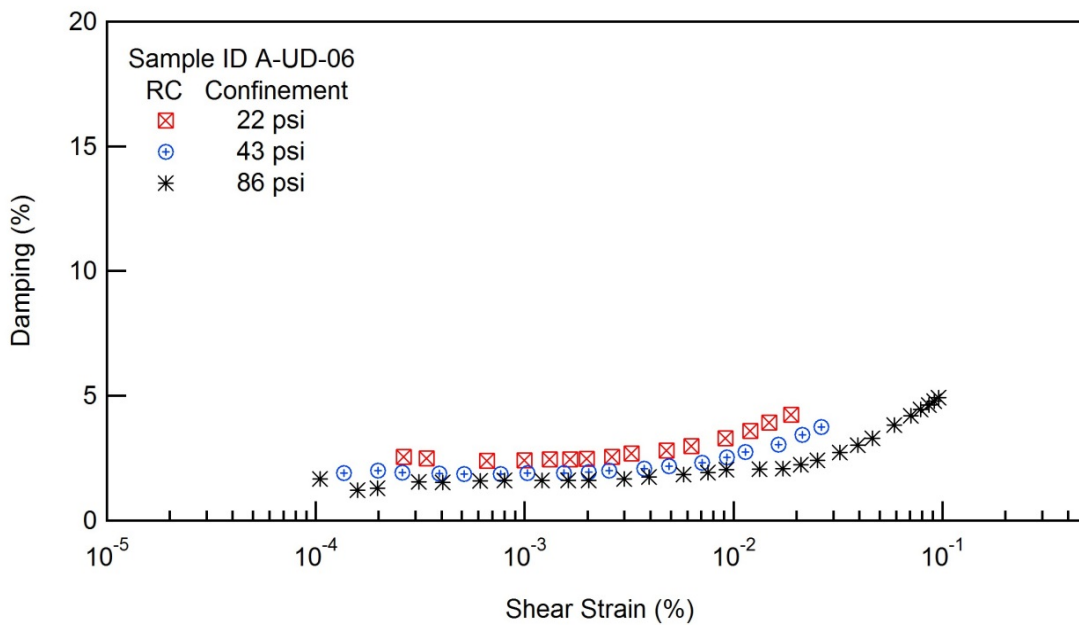
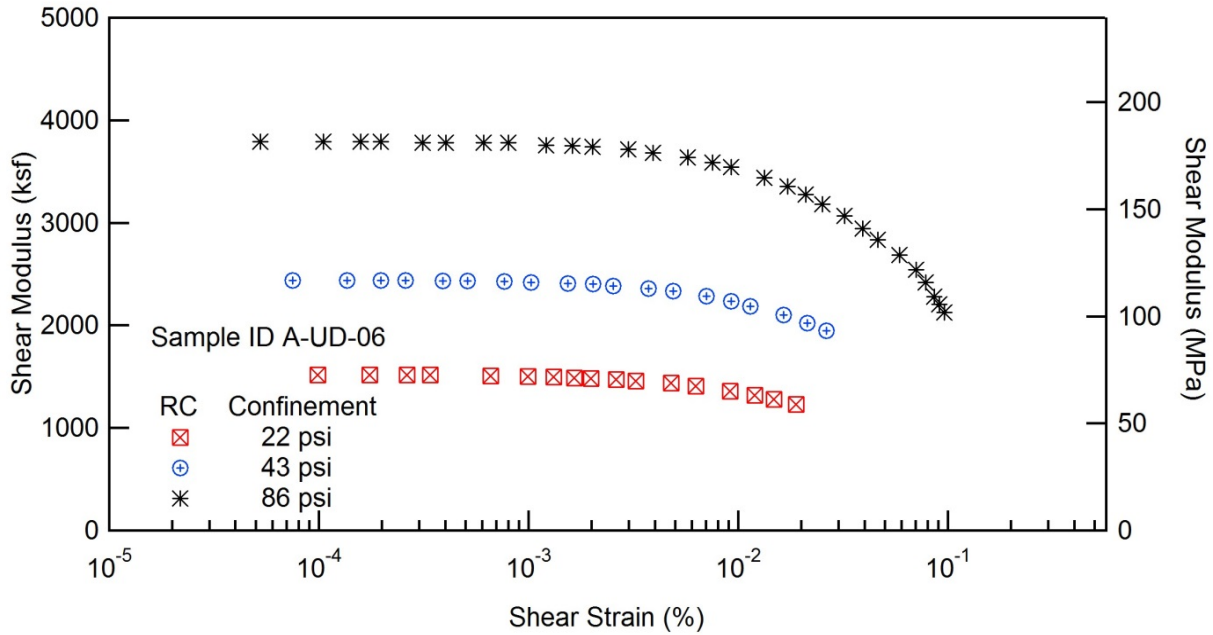


# RESONANT COLUMN (RC) AND TORSIONAL SHEAR (TS) TEST

Project Name: Deep Soil Test Boring to Determine Shear  
Wave Velocities across South Carolina

Client: SCDOT  
Location: Andrews, SC

Project ID: SPR-731  
Boring No.: B-FMG



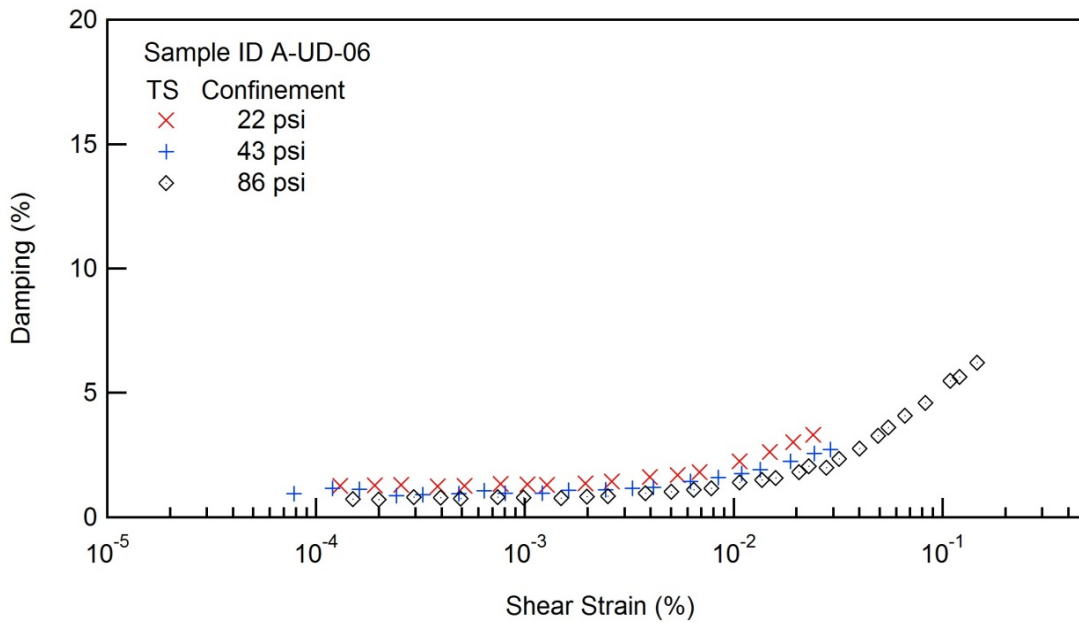
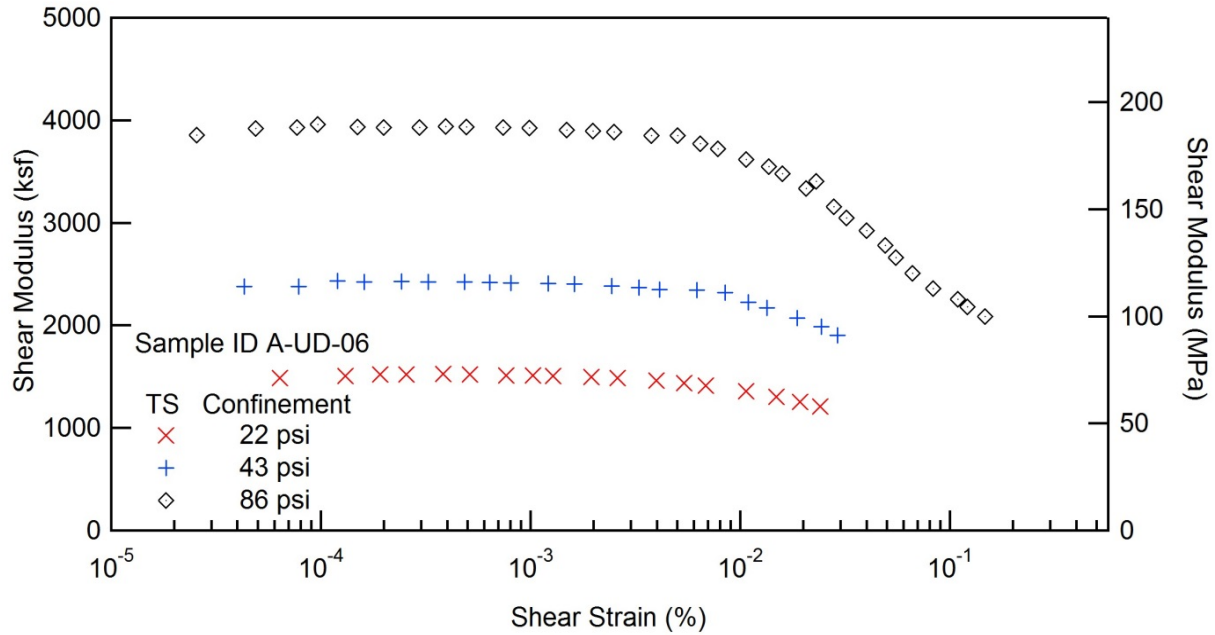


## RESONANT COLUMN (RC) AND TORSIONAL SHEAR (TS) TEST

Project Name: Deep Soil Test Boring to Determine Shear  
Wave Velocities across South Carolina

Client: SCDOT  
Location: Andrews, SC

Project ID: SPR-731  
Boring No.: B-FMG







**UNIVERSITY OF SOUTH CAROLINA**  
 Department of Civil and Environmental Engineering  
 300 Main street, Columbia, SC, 29208

**TORSIONAL SHEAR (TS) TEST REPORT**

Project Name: Deep Soil Test Boring to Determine Shear  
 Wave Velocities across South Carolina  
 Client: SCDOT Project ID: SPR-731  
 Location: Andrews, SC Boring No.: B-FMG

Table 2 Results for Sample ID A-UD-06 for TS Test

Confining Pressure 22 PSI				Confining Pressure 43 PSI				Confining Pressure 86 PSI			
$\gamma$ (%)	G (ksf)	G/G <sub>max</sub>	D (%)	$\gamma$ (%)	G (ksf)	G/G <sub>max</sub>	D (%)	$\gamma$ (%)	G (ksf)	G/G <sub>max</sub>	D (%)
6.40E-05	1486	1.000		4.30E-05	2379	1.000		4.90E-05	3920	1.000	
1.31E-04	1504	1.000	1.271	7.83E-05	2378	1.000	0.951	7.72E-05	3928	1.000	
1.92E-04	1523	1.000	1.276	1.20E-04	2433	1.000	1.175	9.68E-05	3960	1.000	
2.56E-04	1523	1.000	1.297	1.61E-04	2422	1.000	1.134	1.50E-04	3936	1.000	0.739
3.83E-04	1524	1.000	1.238	2.42E-04	2428	1.000	0.868	2.00E-04	3929	1.000	0.719
5.15E-04	1520	1.000	1.270	3.25E-04	2421	0.999	0.909	2.95E-04	3932	1.000	0.804
7.68E-04	1513	0.997	1.344	4.83E-04	2421	0.998	0.942	3.95E-04	3941	1.000	0.792
1.03E-03	1512	0.995	1.318	6.38E-04	2417	0.997	1.059	4.94E-04	3935	0.999	0.759
1.28E-03	1506	0.992	1.296	8.05E-04	2411	0.994	0.969	7.42E-04	3928	0.997	0.810
1.95E-03	1497	0.986	1.367	1.21E-03	2406	0.992	0.975	9.89E-04	3923	0.996	0.796
2.61E-03	1487	0.979	1.433	1.62E-03	2401	0.990	1.076	1.49E-03	3906	0.992	0.778
3.98E-03	1462	0.963	1.618	2.44E-03	2385	0.984	1.108	1.99E-03	3897	0.989	0.832
5.40E-03	1438	0.947	1.697	3.28E-03	2368	0.976	1.171	2.50E-03	3883	0.986	0.848
6.87E-03	1412	0.930	1.815	4.12E-03	2350	0.969	1.204	3.78E-03	3852	0.978	0.966
1.07E-02	1356	0.893	2.242	6.20E-03	2346	0.967	1.430	5.04E-03	3852	0.978	1.032
1.49E-02	1305	0.859	2.625	8.46E-03	2318	0.956	1.592	6.44E-03	3771	0.958	1.106
1.93E-02	1255	0.826	3.012	1.09E-02	2225	0.918	1.759	7.82E-03	3720	0.945	1.165
2.41E-02	1208	0.795	3.323	1.34E-02	2170	0.895	1.908	1.07E-02	3618	0.919	1.410
				1.87E-02	2073	0.855	2.236	1.37E-02	3546	0.900	1.503
				2.44E-02	1987	0.820	2.566	1.59E-02	3477	0.883	1.584
				2.91E-02	1902	0.784	2.729	2.06E-02	3337	0.847	1.814
								2.30E-02	3406	0.865	2.046
								2.79E-02	3158	0.802	1.986
								3.21E-02	3048	0.774	2.345
								4.01E-02	2925	0.743	2.772
								4.93E-02	2779	0.706	3.269
								5.51E-02	2662	0.676	3.604
								6.63E-02	2508	0.637	4.080
								8.30E-02	2357	0.598	4.604
								1.09E-01	2253	0.572	5.490
								1.21E-01	2180	0.554	5.637
								1.47E-01	2087	0.530	6.22



### RESONANT COLUMN (RC) AND TORSIONAL SHEAR (TS) TEST

Project Name: Deep Soil Test Boring to Determine Shear  
Wave Velocities across South Carolina

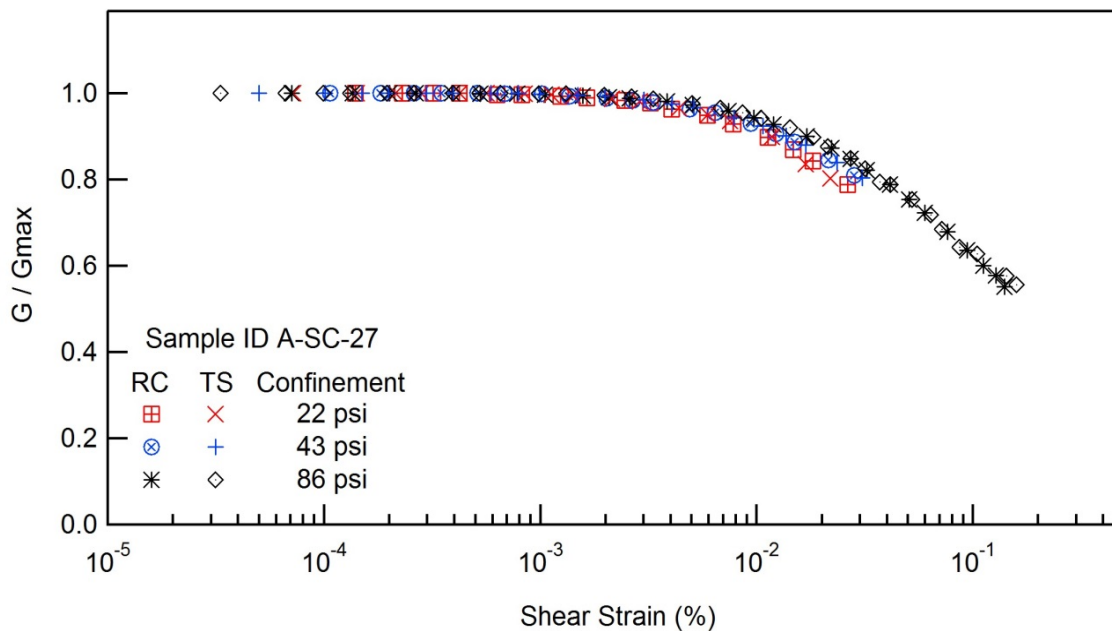
Client: SCDOT

Project ID: SPR-731

Location: Andrews, SC

Boring No.: B-FMG

Sample ID : A-SC-27





### RESONANT COLUMN (RC) AND TORSIONAL SHEAR (TS) TEST

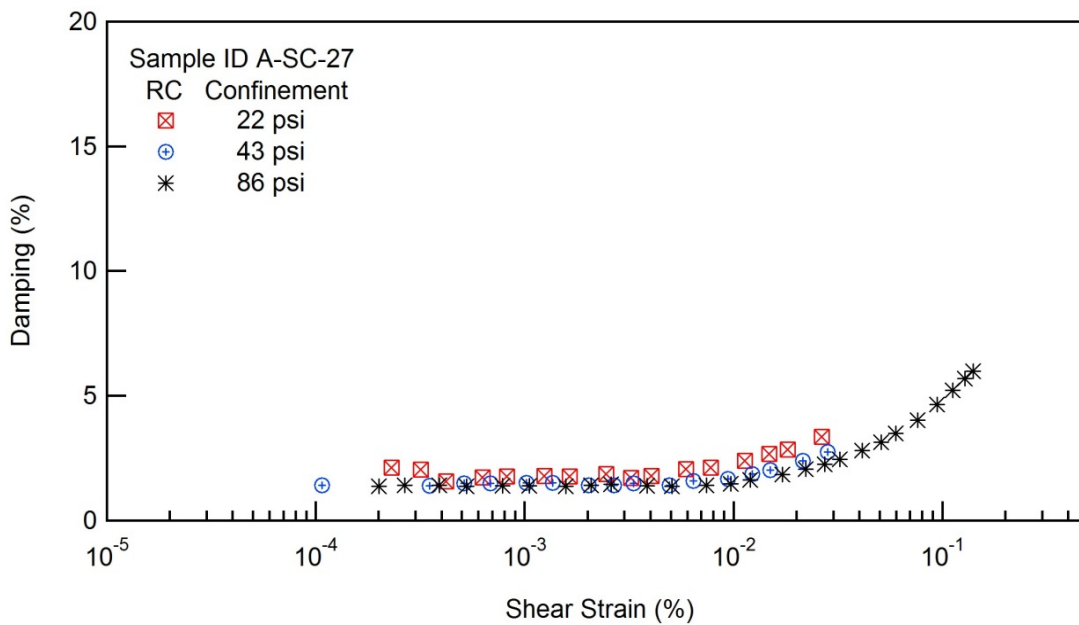
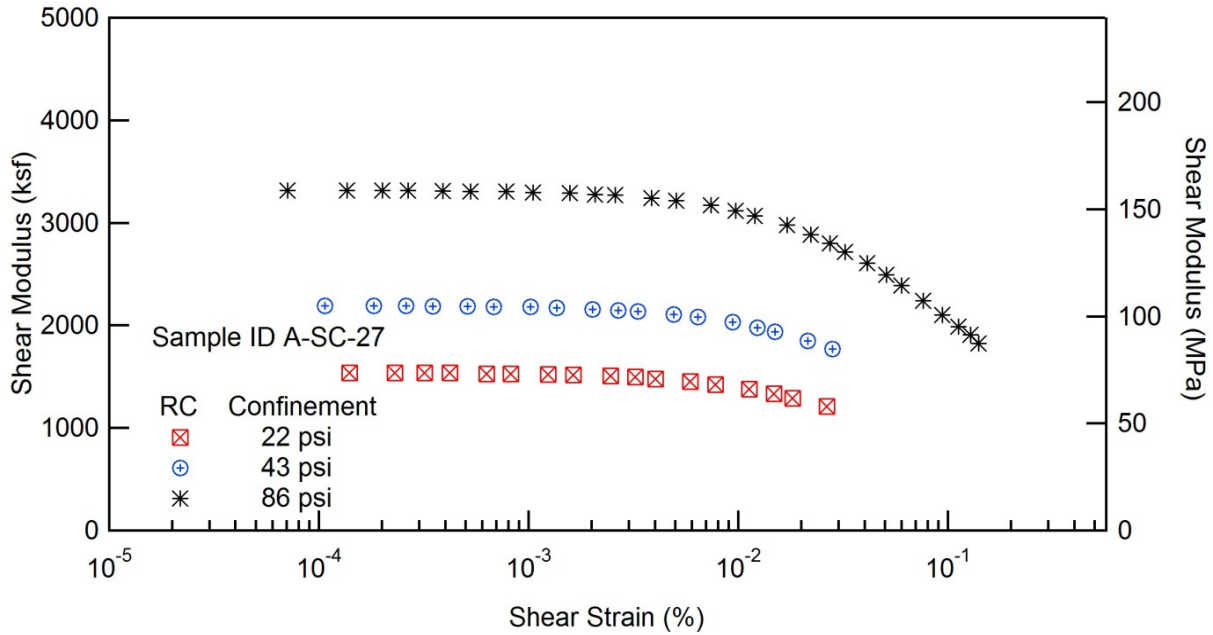
Project Name: Deep Soil Test Boring to Determine Shear  
Wave Velocities across South Carolina

Client: SCDOT

Project ID: SPR-731

Location: Andrews, SC

Boring No.: B-FMG



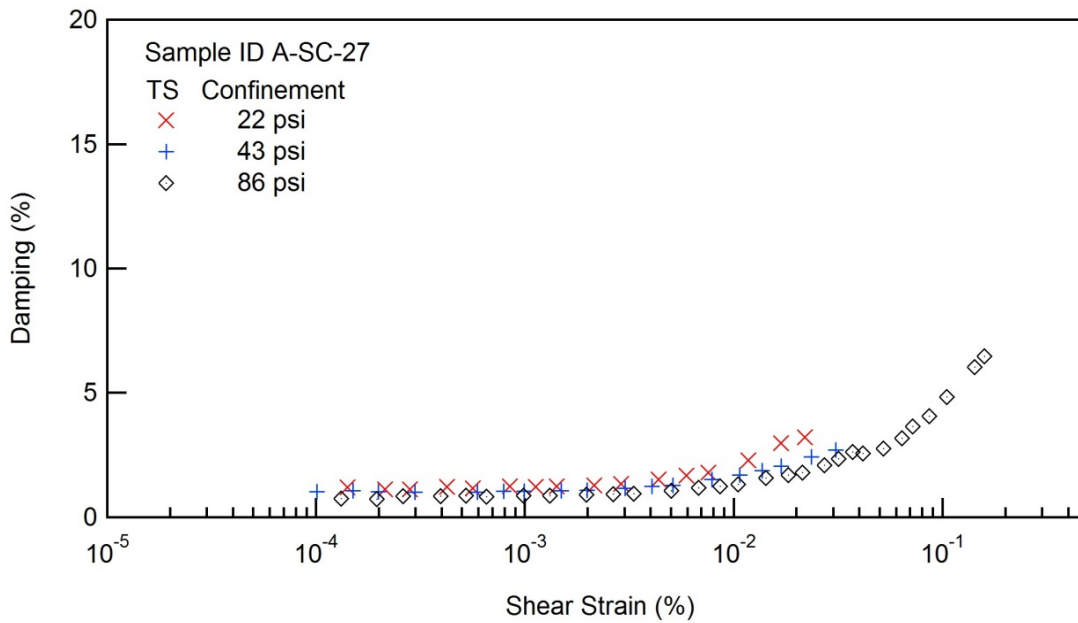
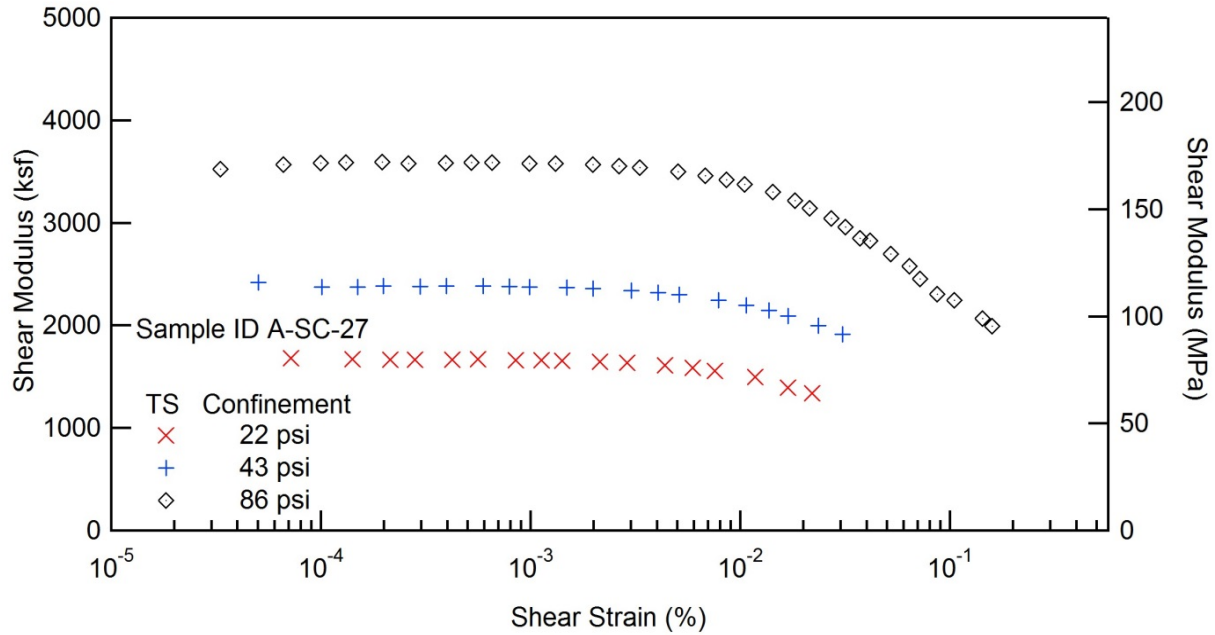


## RESONANT COLUMN (RC) AND TORSIONAL SHEAR (TS) TEST

Project Name: Deep Soil Test Boring to Determine Shear  
Wave Velocities across South Carolina

Client: SCDOT  
Location: Andrews, SC

Project ID: SPR-731  
Boring No.: B-FMG







**UNIVERSITY OF SOUTH CAROLINA**  
 Department of Civil and Environmental Engineering  
 300 Main street, Columbia, SC, 29208

**TORSIONAL SHEAR (TS) TEST REPORT**

Project Name: Deep Soil Test Boring to Determine Shear  
 Wave Velocities across South Carolina  
 Client: SCDOT Project ID: SPR-731  
 Location: Andrews, SC Boring No.: B-FMG

Table 2 Results for Sample ID A-SC-27 for TS Test

Confining Pressure 22 PSI				Confining Pressure 43 PSI				Confining Pressure 86 PSI			
$\gamma$ (%)	G (ksf)	G/G <sub>max</sub>	D (%)	$\gamma$ (%)	G (ksf)	G/G <sub>max</sub>	D (%)	$\gamma$ (%)	G (ksf)	G/G <sub>max</sub>	D (%)
7.21E-05	1678	1.000		5.02E-05	2417	1.000		3.33E-05	3525	1.000	
1.42E-04	1670	1.000	1.198	1.01E-04	2372	1.000	1.029	6.65E-05	3569	1.000	
2.14E-04	1665	1.000	1.135	1.50E-04	2375	1.000	1.071	9.98E-05	3582	1.000	
2.82E-04	1663	1.000	1.134	1.99E-04	2382	1.000	1.017	1.32E-04	3586	1.000	0.754
4.24E-04	1667	1.000	1.228	2.97E-04	2379	1.000	1.015	1.96E-04	3593	1.000	0.731
5.63E-04	1668	1.000	1.175	3.96E-04	2383	1.000		2.62E-04	3579	1.000	0.855
8.50E-04	1662	0.998	1.242	5.93E-04	2382	1.000	1.003	3.95E-04	3583	1.000	0.855
1.13E-03	1660	0.996	1.224	7.91E-04	2379	1.000	1.046	5.24E-04	3586	1.000	0.871
1.42E-03	1656	0.994	1.240	9.91E-04	2374	0.997	1.047	6.56E-04	3587	1.000	0.823
2.15E-03	1645	0.987	1.289	1.49E-03	2368	0.995	1.055	9.87E-04	3579	0.998	0.870
2.89E-03	1634	0.980	1.355	1.99E-03	2361	0.992	1.083	1.32E-03	3578	0.998	0.861
4.39E-03	1609	0.965	1.515	3.02E-03	2341	0.984	1.158	1.98E-03	3566	0.995	0.900
5.95E-03	1584	0.950	1.678	4.06E-03	2321	0.975	1.237	2.65E-03	3552	0.991	0.924
7.56E-03	1558	0.935	1.794	5.12E-03	2300	0.966	1.286	3.33E-03	3538	0.987	0.956
1.18E-02	1496	0.898	2.294	7.87E-03	2244	0.943	1.522	5.05E-03	3499	0.976	1.074
1.69E-02	1392	0.835	2.976	1.07E-02	2197	0.923	1.700	6.81E-03	3459	0.965	1.176
2.20E-02	1336	0.802	3.225	1.37E-02	2145	0.901	1.871	8.61E-03	3418	0.954	1.248
				1.69E-02	2093	0.879	2.051	1.05E-02	3374	0.941	1.322
				2.36E-02	1996	0.839	2.425	1.43E-02	3299	0.920	1.574
				3.08E-02	1912	0.803	2.709	1.83E-02	3214	0.897	1.706
								2.14E-02	3142	0.876	1.800
								2.72E-02	3041	0.848	2.092
								3.18E-02	2956	0.825	2.352
								3.72E-02	2847	0.794	2.633
								4.16E-02	2825	0.788	2.563
								5.23E-02	2698	0.753	2.763
								6.40E-02	2575	0.718	3.174
								7.20E-02	2451	0.684	3.647
								8.68E-02	2305	0.643	4.071
								1.05E-01	2247	0.627	4.842
								1.43E-01	2064	0.576	6.038
								1.59E-01	1992	0.556	6.461



## RESONANT COLUMN (RC) AND TORSIONAL SHEAR (TS) TEST

Project Name: Deep Soil Test Boring to Determine Shear  
Wave Velocities across South Carolina

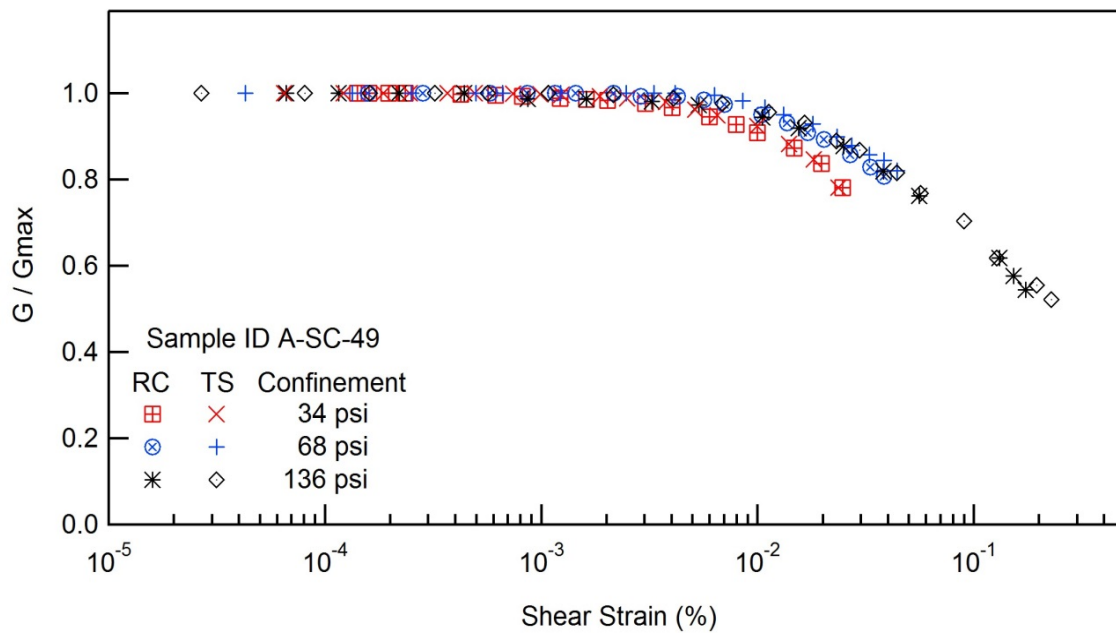
Client: SCDOT

Project ID: SPR-731

Location: Andrews, SC

Boring No.: B-FMG

Sample ID : A-SC-49





## RESONANT COLUMN (RC) AND TORSIONAL SHEAR (TS) TEST

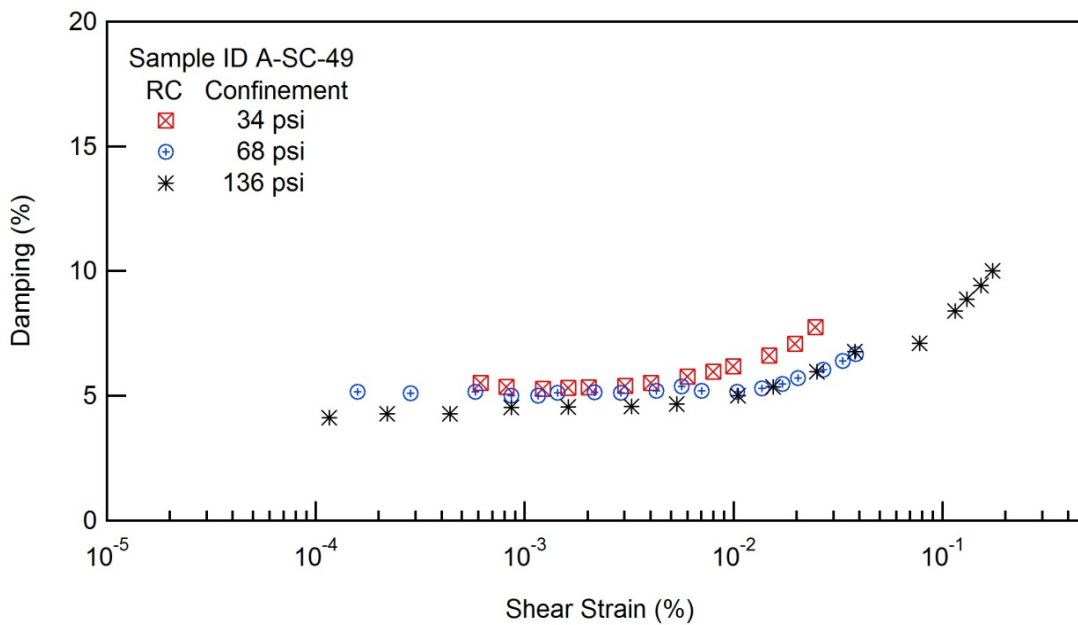
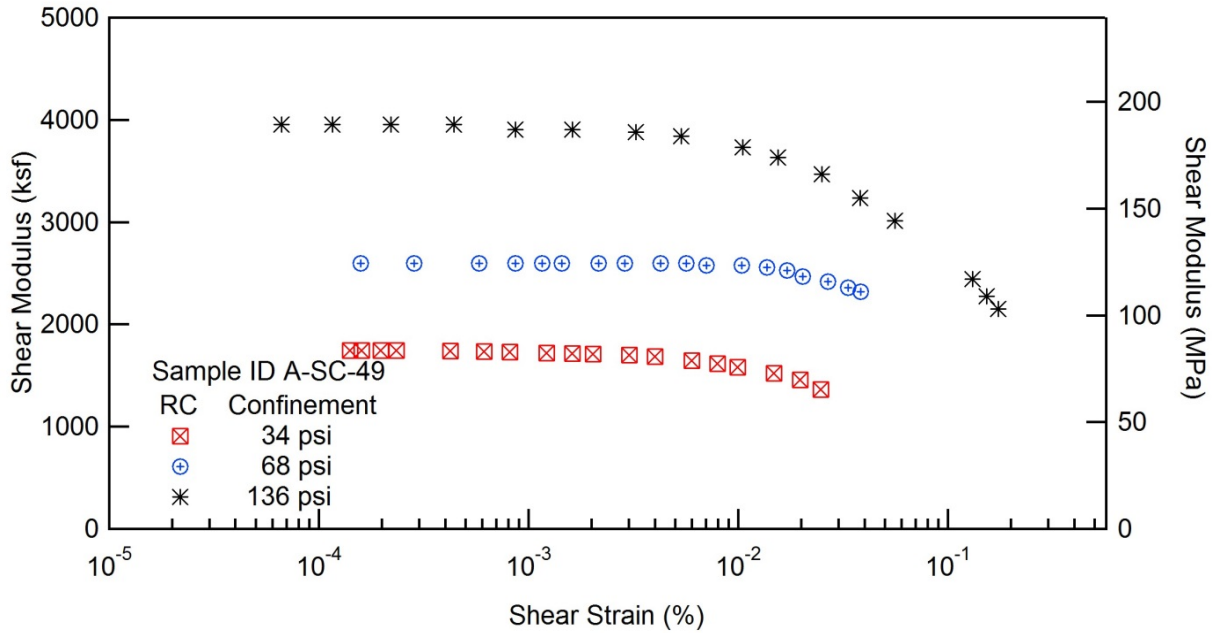
Project Name: Deep Soil Test Boring to Determine Shear  
Wave Velocities across South Carolina

Client: SCDOT

Project ID: SPR-731

Location: Andrews, SC

Boring No.: B-FMG





## RESONANT COLUMN (RC) AND TORSIONAL SHEAR (TS) TEST

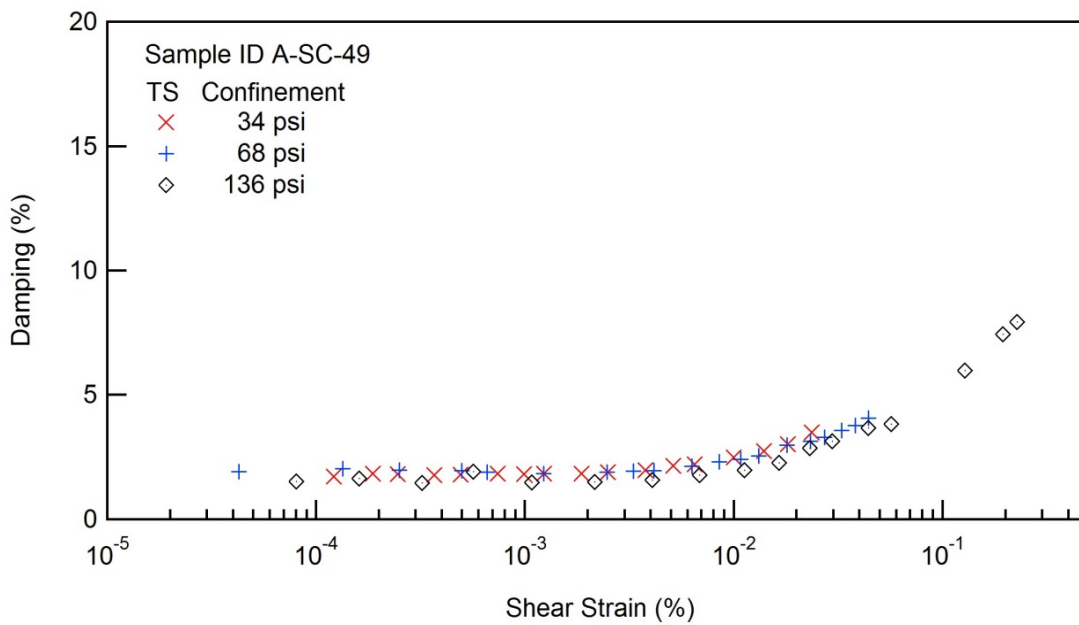
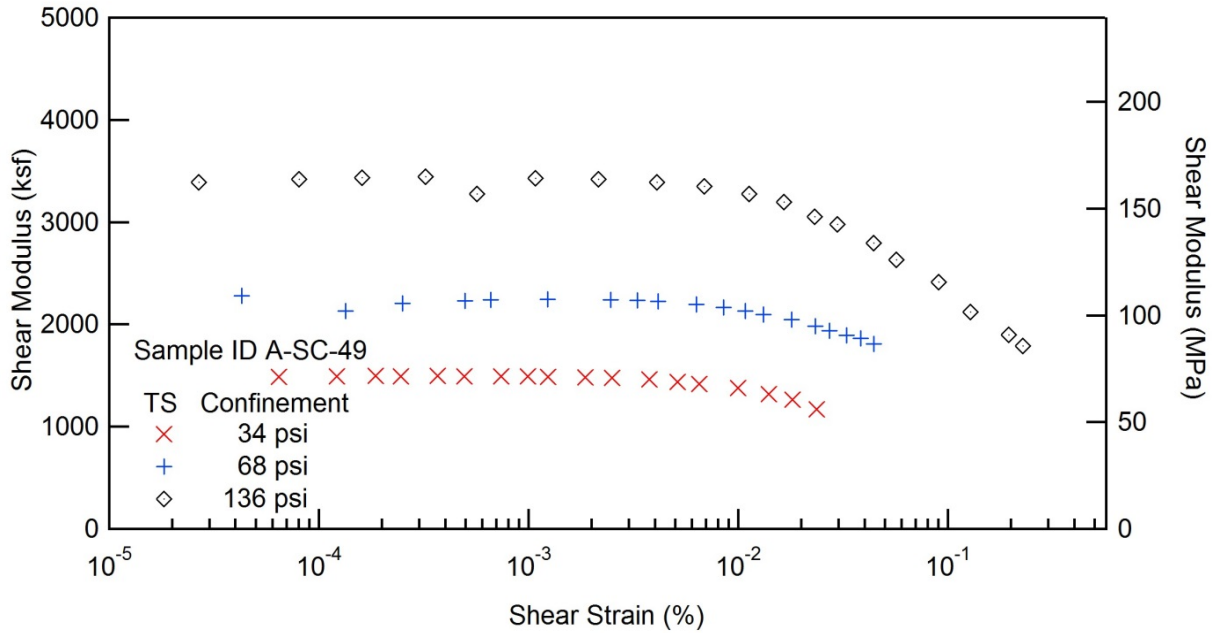
Project Name: Deep Soil Test Boring to Determine Shear  
Wave Velocities across South Carolina

Client: SCDOT

Project ID: SPR-731

Location: Andrews, SC

Boring No.: B-FMG









## RESONANT COLUMN (RC) AND TORSIONAL SHEAR (TS) TEST

Project Name: Deep Soil Test Boring to Determine Shear  
Wave Velocities across South Carolina

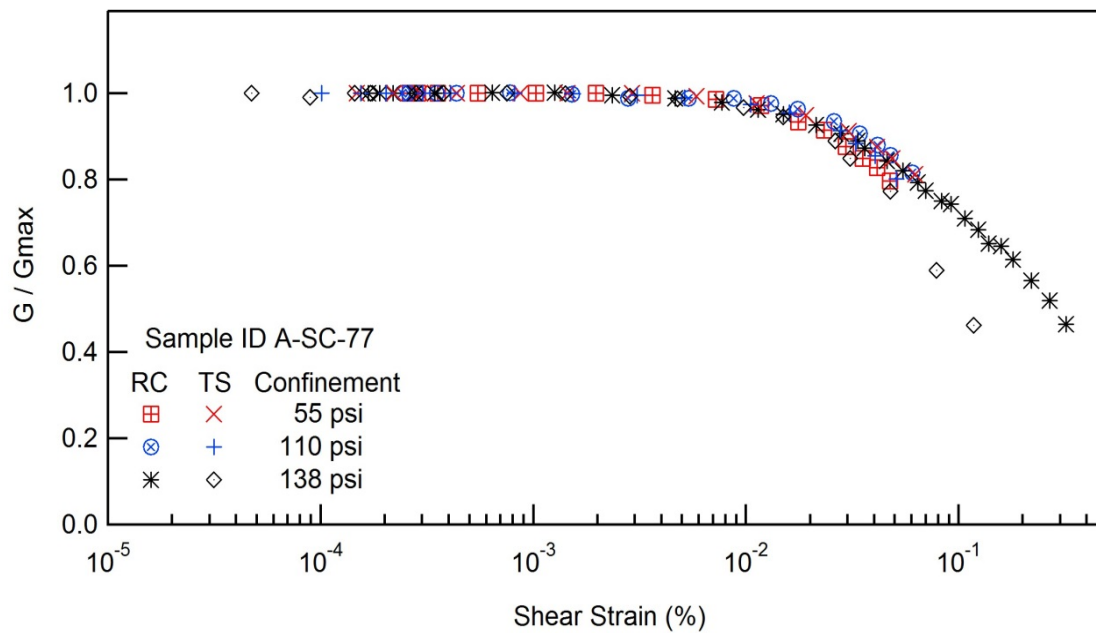
Client: SCDOT

Project ID: SPR-731

Location: Andrews, SC

Boring No.: B-FMG

Sample ID : A-SC-77



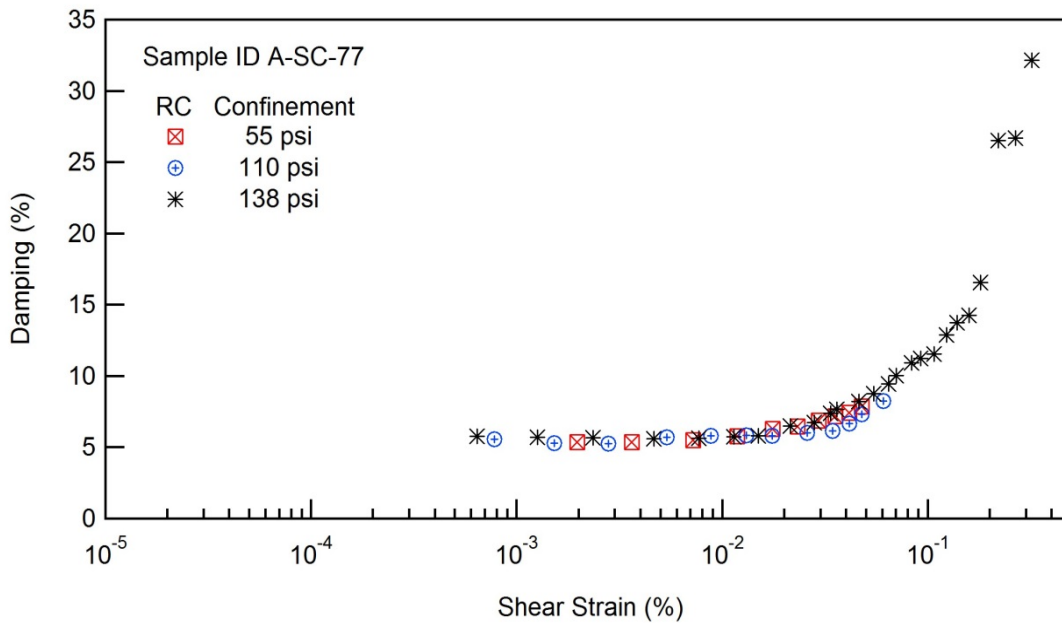
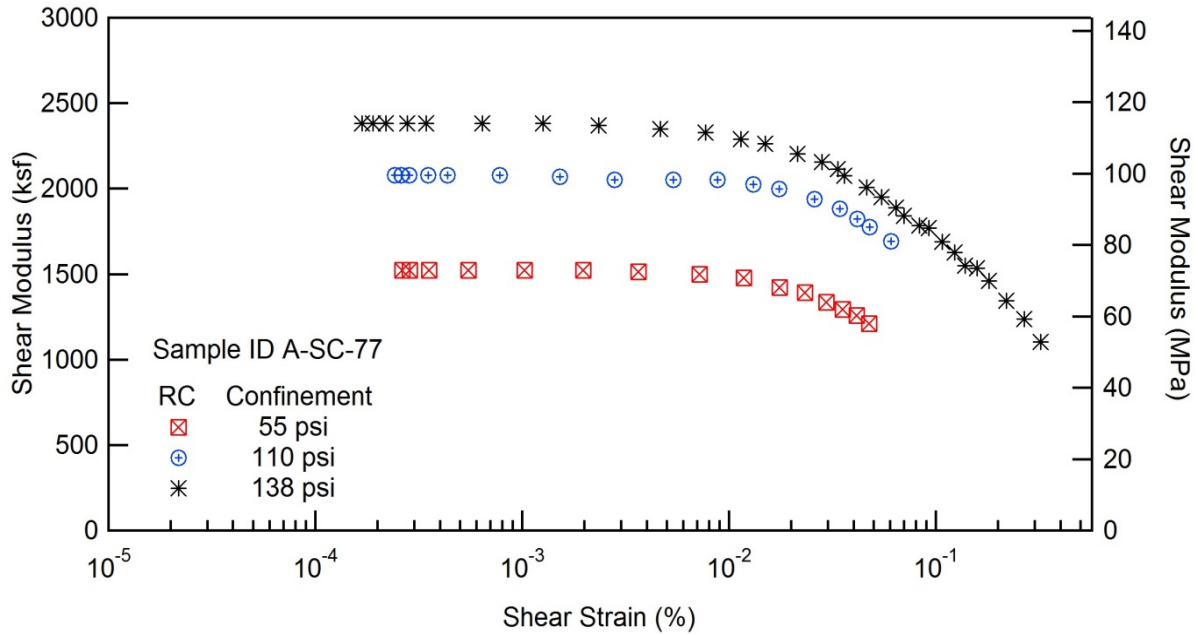


# RESONANT COLUMN (RC) AND TORSIONAL SHEAR (TS) TEST

Project Name: Deep Soil Test Boring to Determine Shear  
Wave Velocities across South Carolina

Client: SCDOT  
Location: Andrews, SC

Project ID: SPR-731  
Boring No.: B-FMG



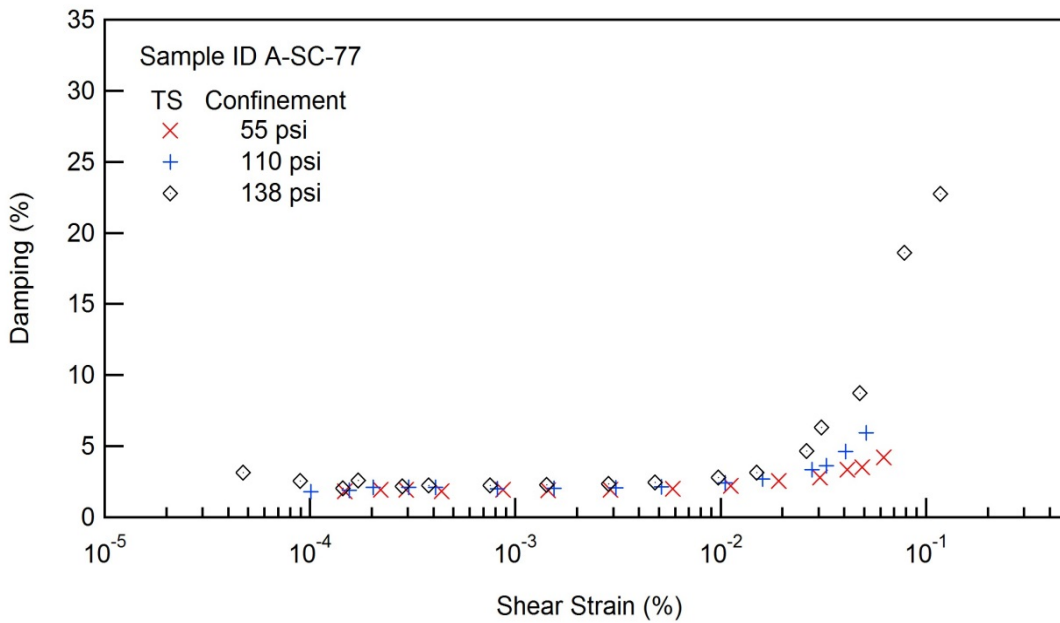
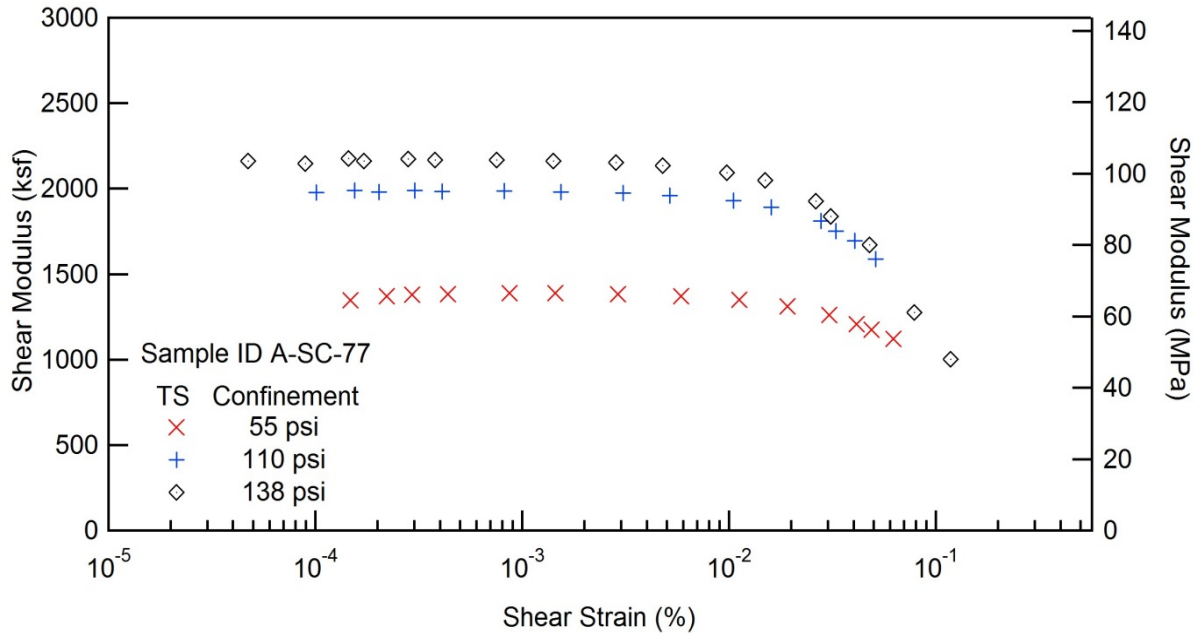


# RESONANT COLUMN (RC) AND TORSIONAL SHEAR (TS) TEST

Project Name: Deep Soil Test Boring to Determine Shear  
Wave Velocities across South Carolina

Client: SCDOT  
Location: Andrews, SC

Project ID: SPR-731  
Boring No.: B-FMG









## RESONANT COLUMN (RC) AND TORSIONAL SHEAR (TS) TEST

Project Name: Deep Soil Test Boring to Determine Shear  
Wave Velocities across South Carolina

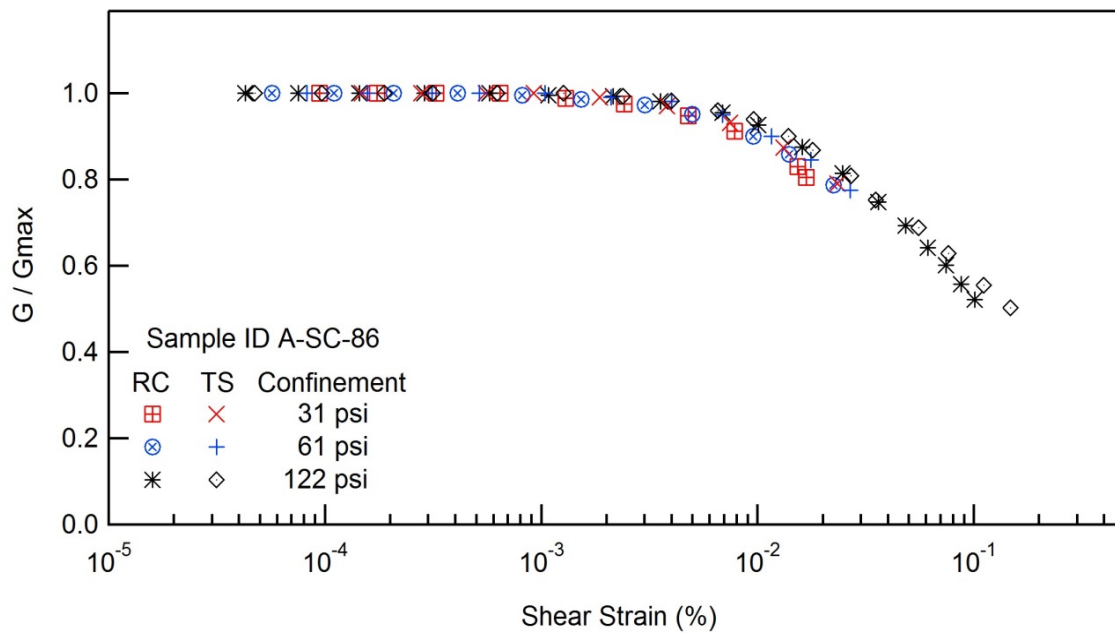
Client: SCDOT

Project ID: SPR-731

Location: Andrews, SC

Boring No.: B-FMG

Sample ID : A-SC-86



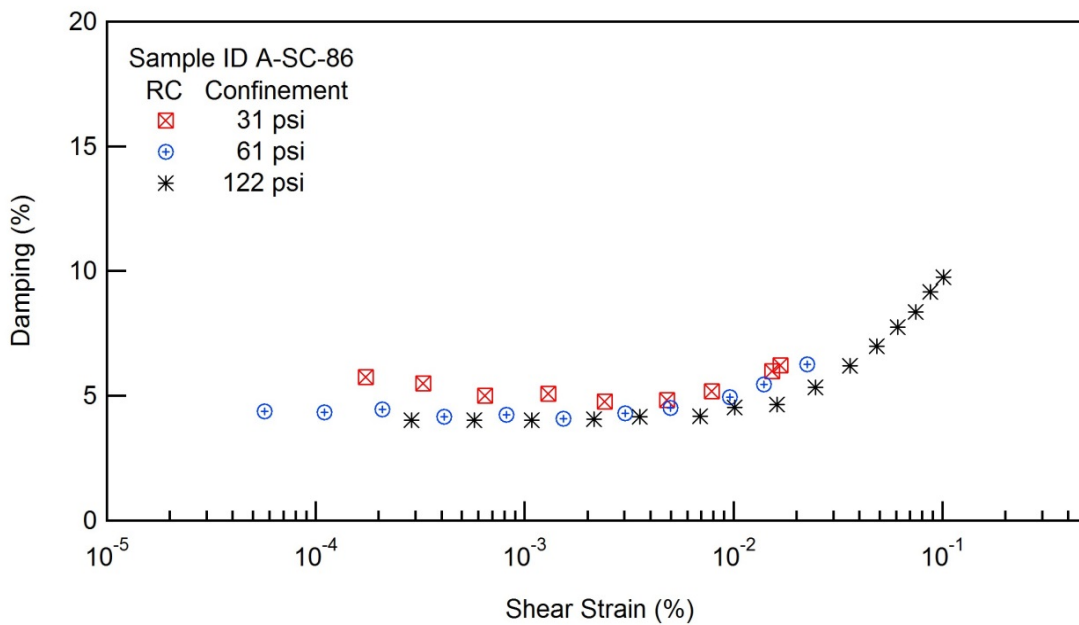
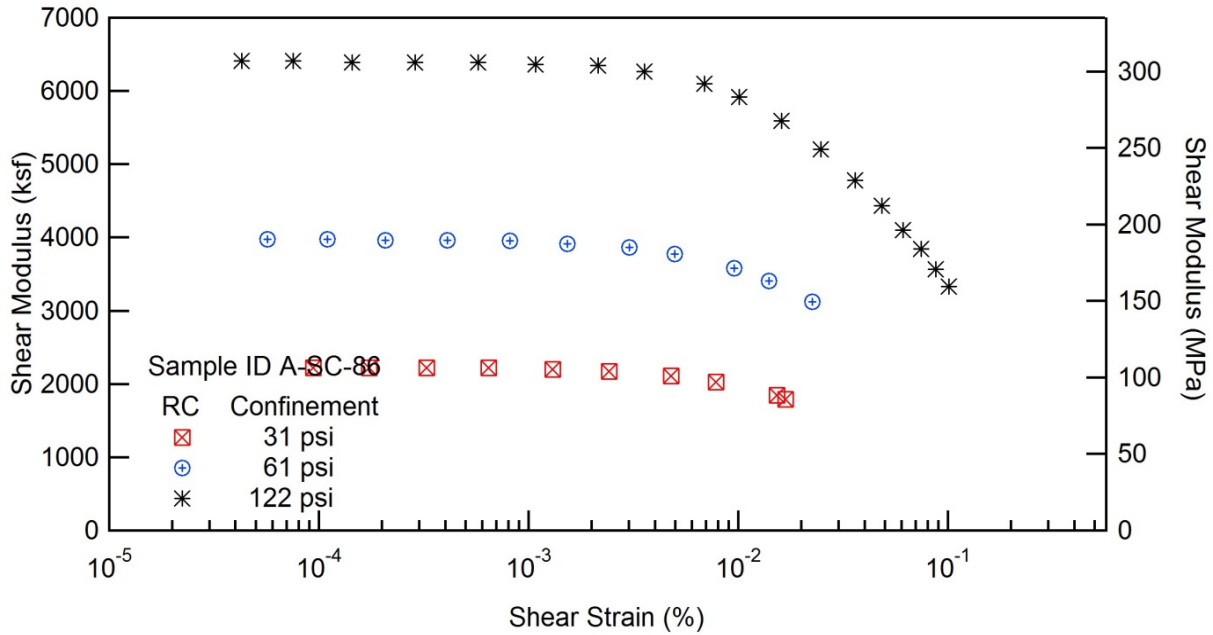


## RESONANT COLUMN (RC) AND TORSIONAL SHEAR (TS) TEST

Project Name: Deep Soil Test Boring to Determine Shear  
Wave Velocities across South Carolina

Client: SCDOT  
Location: Andrews, SC

Project ID: SPR-731  
Boring No.: B-FMG



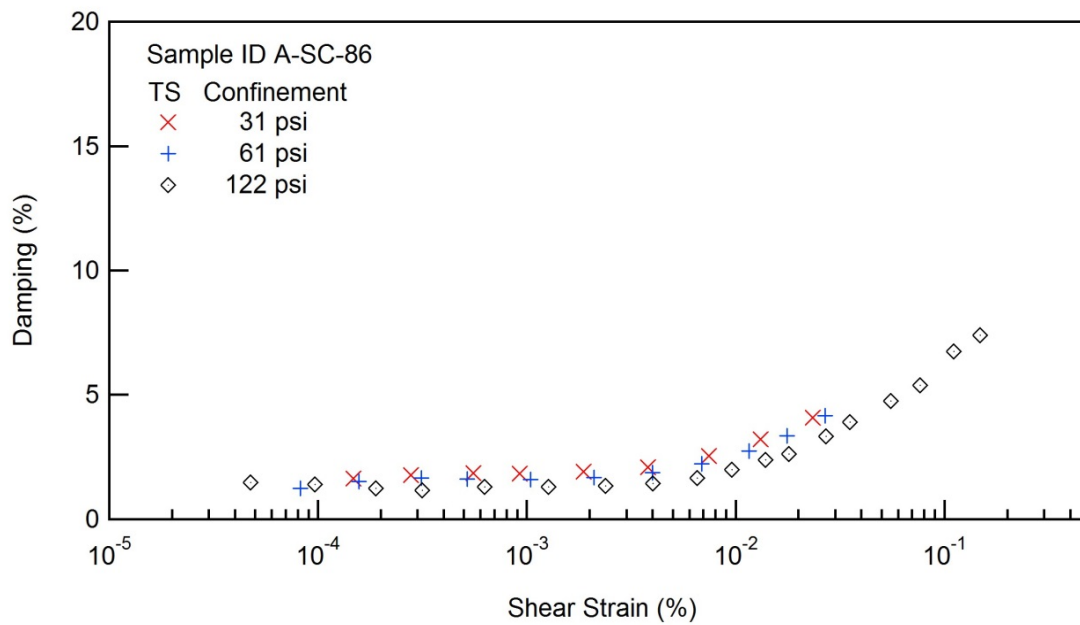
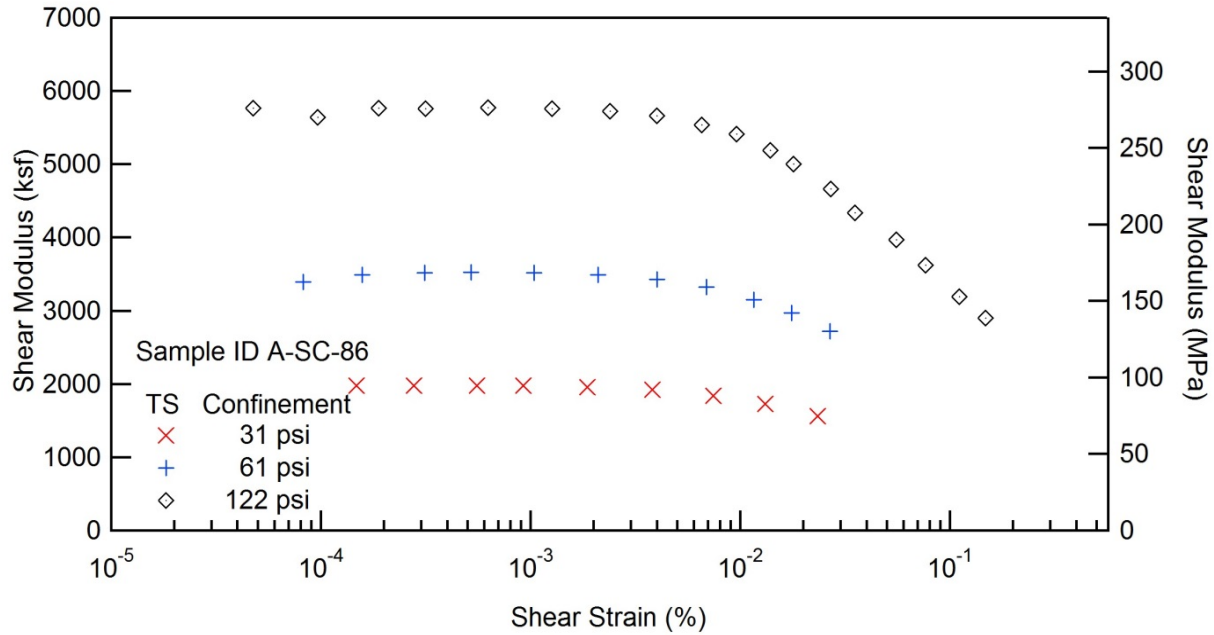


## RESONANT COLUMN (RC) AND TORSIONAL SHEAR (TS) TEST

Project Name: Deep Soil Test Boring to Determine Shear  
Wave Velocities across South Carolina

Client: SCDOT  
Location: Andrews, SC

Project ID: SPR-731  
Boring No.: B-FMG









## RESONANT COLUMN (RC) AND TORSIONAL SHEAR (TS) TEST

Project Name: Deep Soil Test Boring to Determine Shear  
Wave Velocities across South Carolina

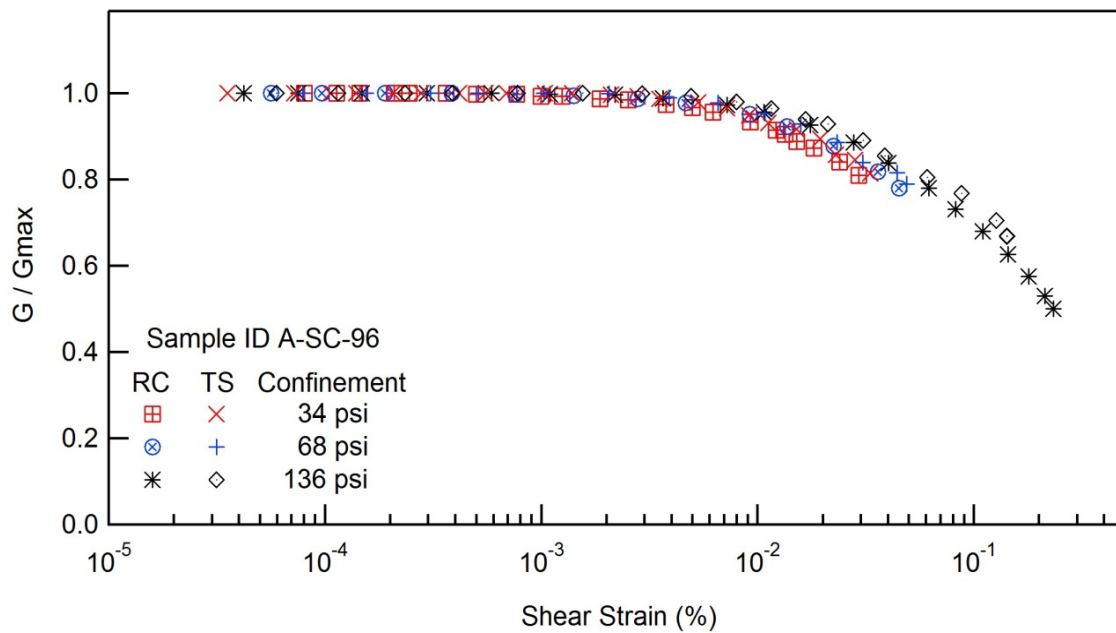
Client: SCDOT

Project ID: SPR-731

Location: Andrews, SC

Boring No.: B-FMG

Sample ID : A-SC-96





## RESONANT COLUMN (RC) AND TORSIONAL SHEAR (TS) TEST

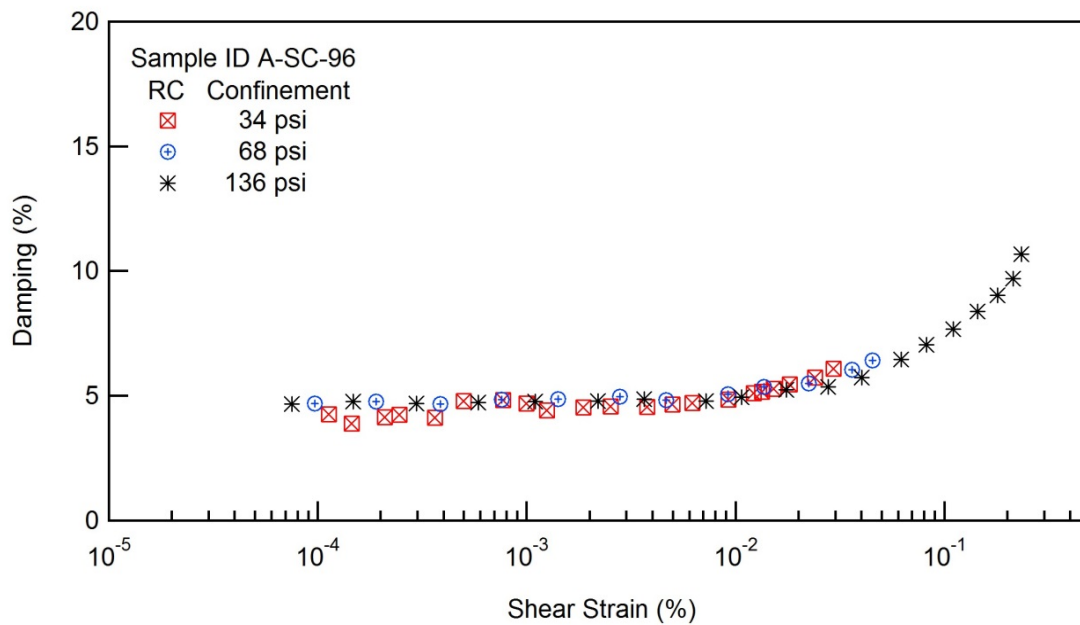
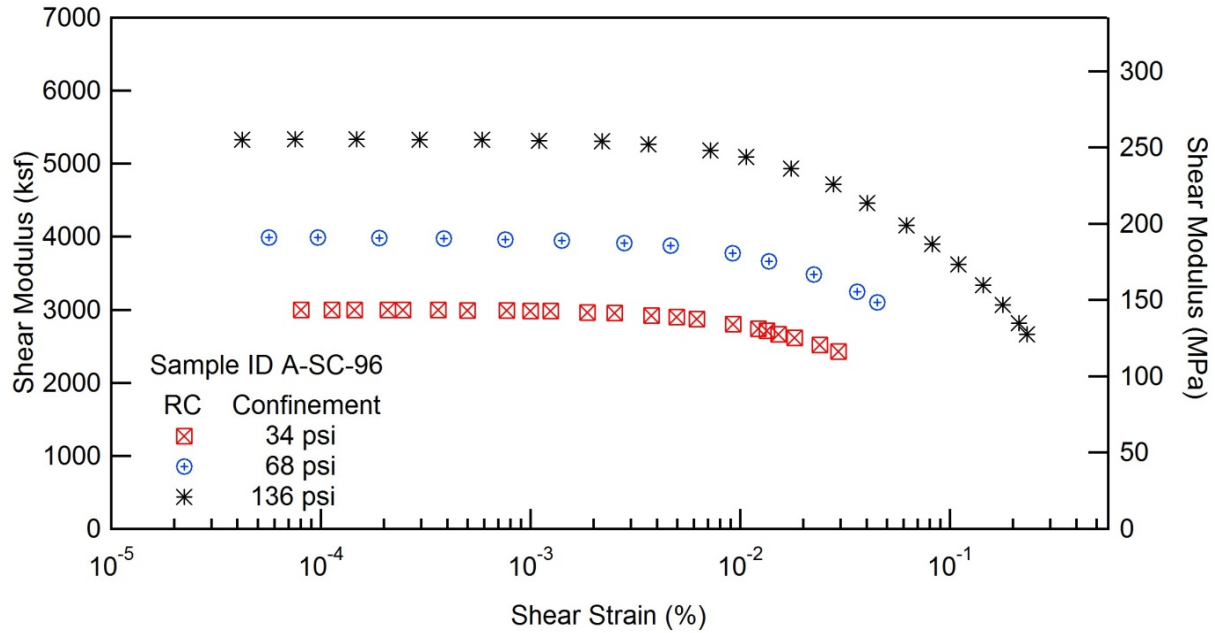
Project Name: Deep Soil Test Boring to Determine Shear  
Wave Velocities across South Carolina

Client: SCDOT

Project ID: SPR-731

Location: Andrews, SC

Boring No.: B-FMG



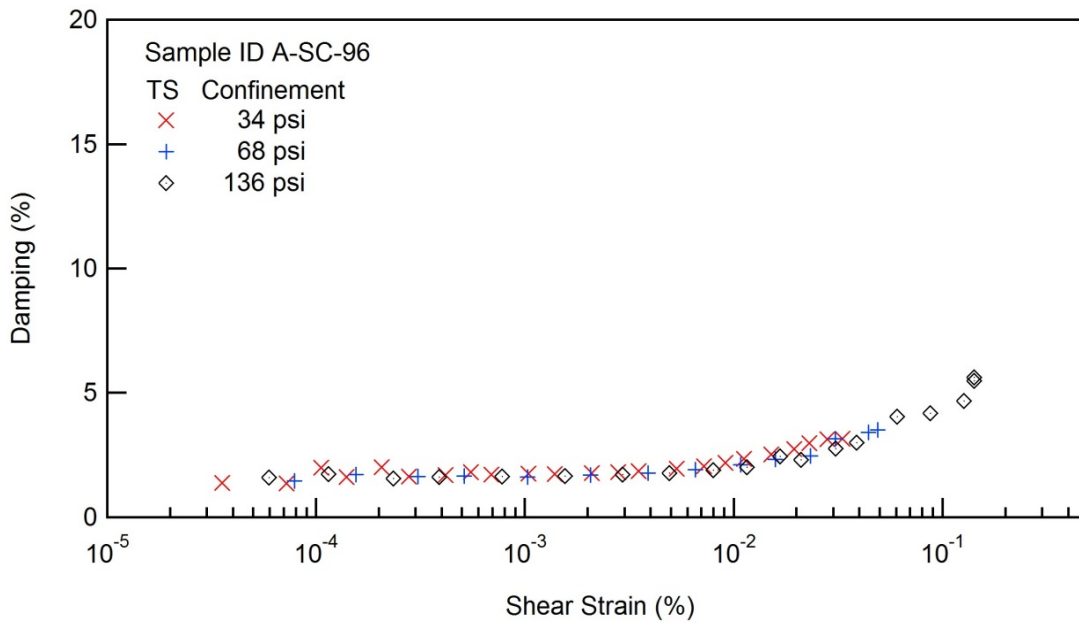
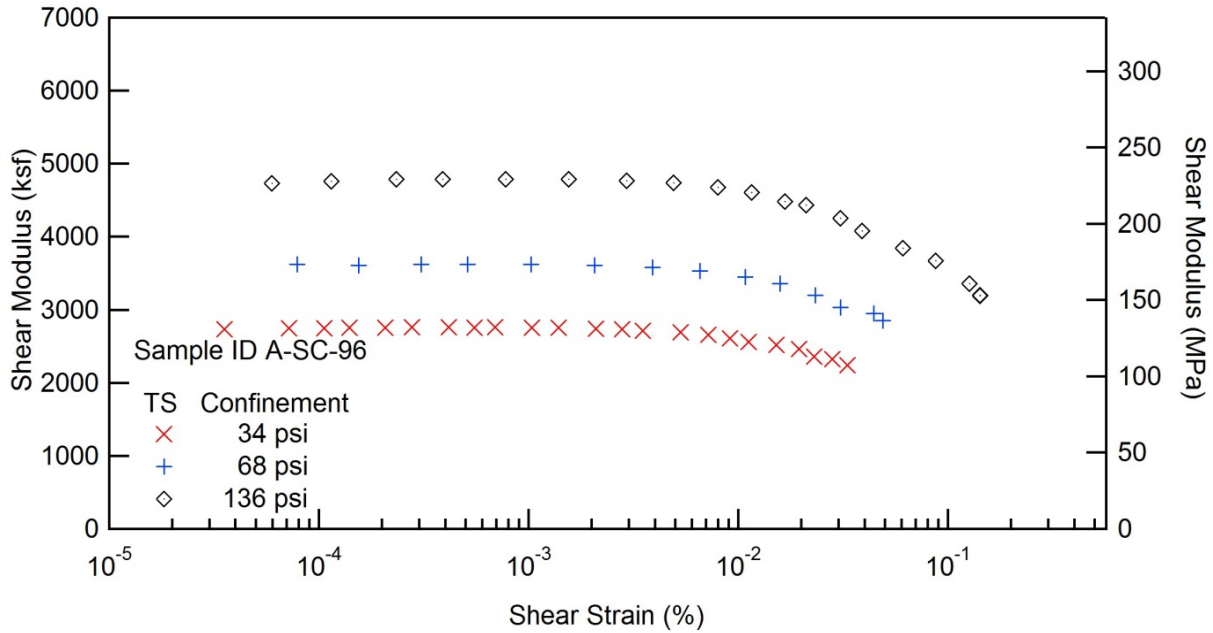


### RESONANT COLUMN (RC) AND TORSIONAL SHEAR (TS) TEST

Project Name: Deep Soil Test Boring to Determine Shear  
Wave Velocities across South Carolina

Client: SCDOT  
Location: Andrews, SC

Project ID: SPR-731  
Boring No.: B-FMG









## RESONANT COLUMN (RC) AND TORSIONAL SHEAR (TS) TEST

Project Name: Deep Soil Test Boring to Determine Shear  
Wave Velocities across South Carolina

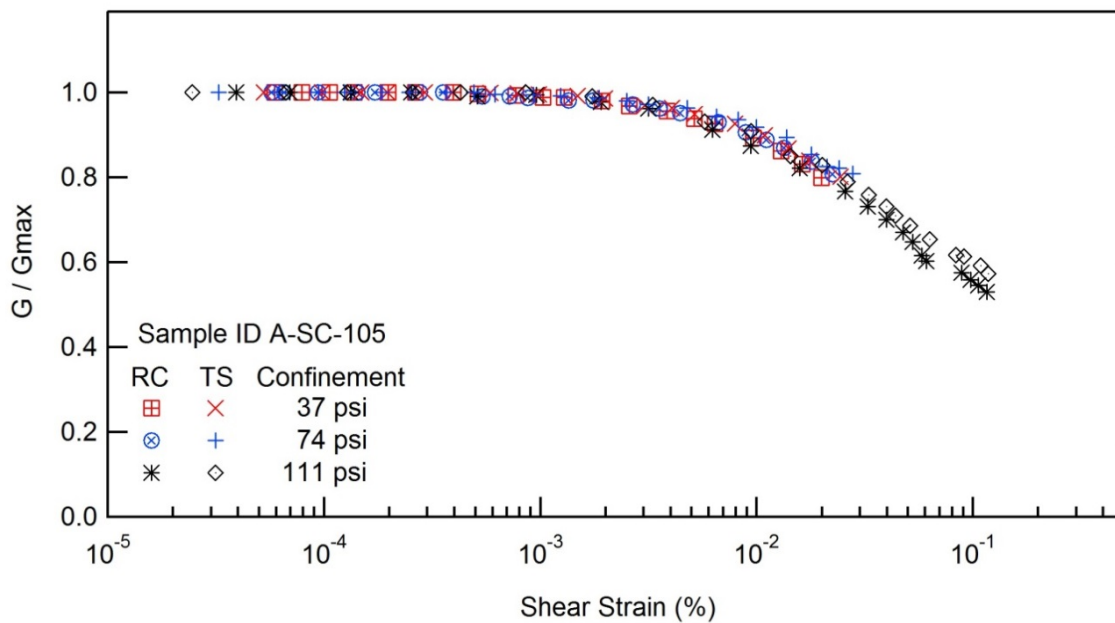
Client: SCDOT

Project ID: SPR-731

Location: Andrews, SC

Boring No.: B-FMG

Sample ID : A-SC-105





## RESONANT COLUMN (RC) AND TORSIONAL SHEAR (TS) TEST

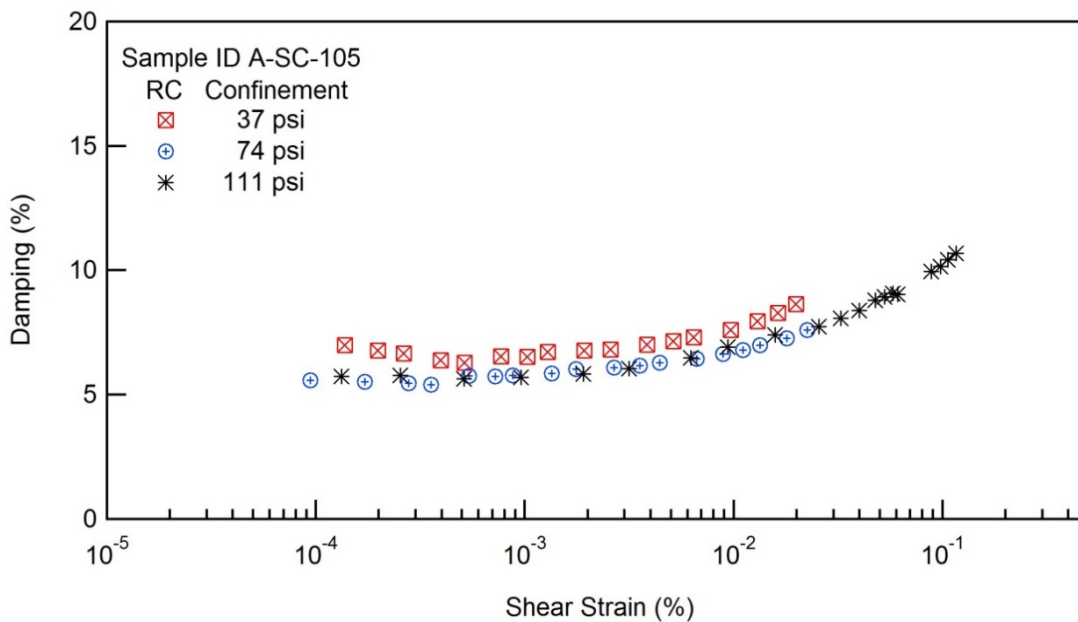
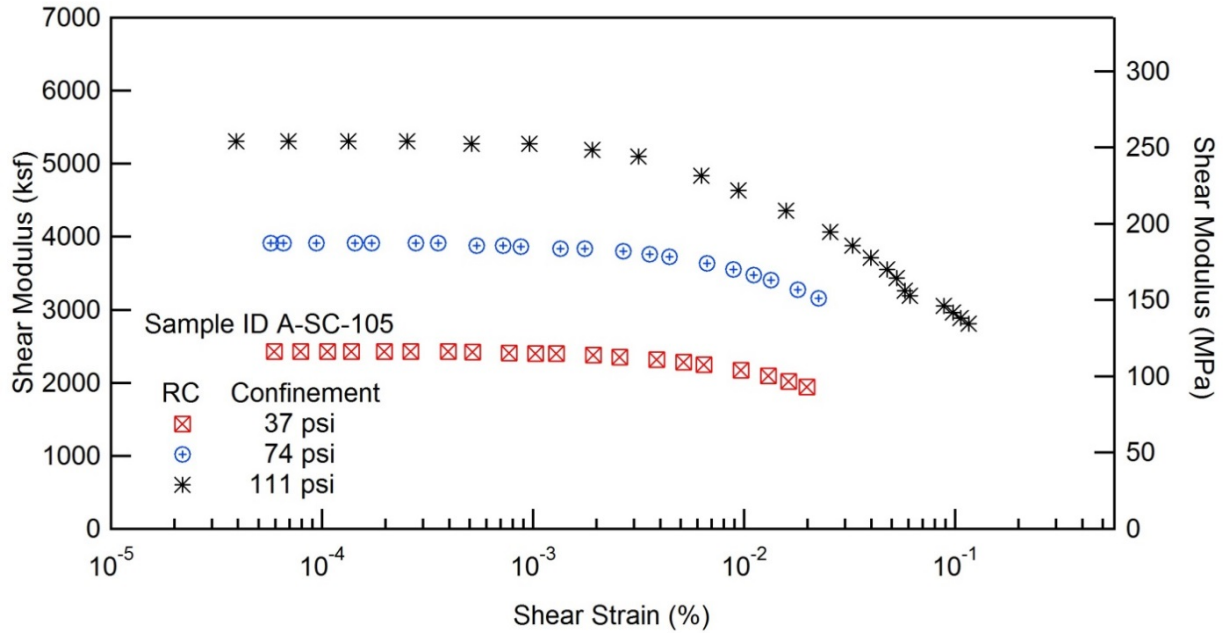
Project Name: Deep Soil Test Boring to Determine Shear  
Wave Velocities across South Carolina

Client: SCDOT

Project ID: SPR-731

Location: Andrews, SC

Boring No.: B-FMG



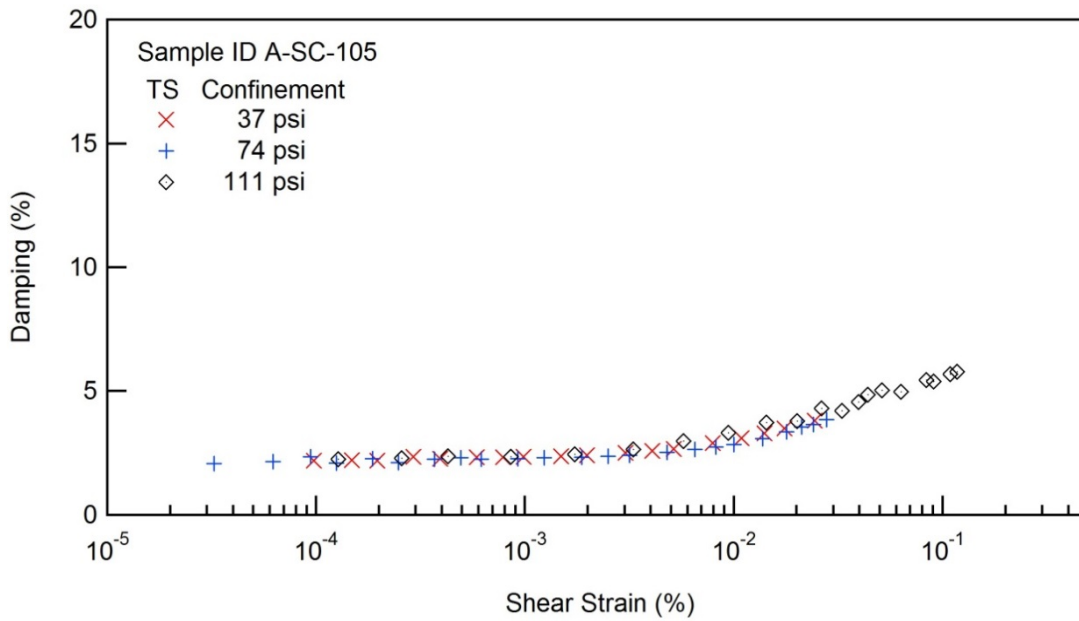
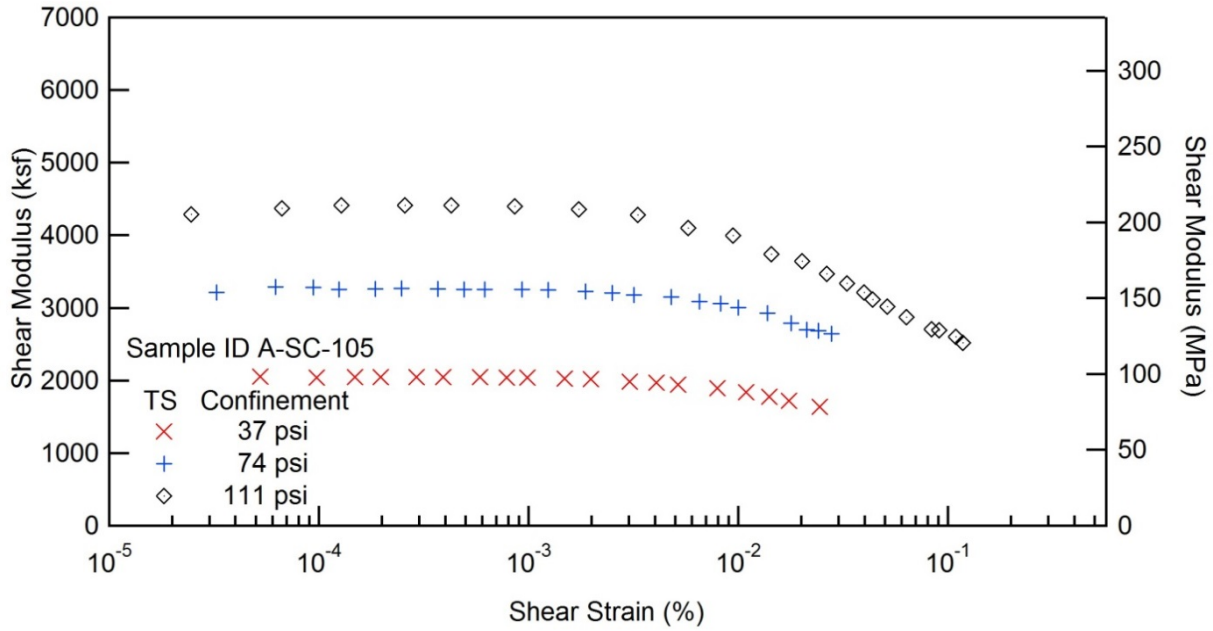


### RESONANT COLUMN (RC) AND TORSIONAL SHEAR (TS) TEST

Project Name: Deep Soil Test Boring to Determine Shear  
Wave Velocities across South Carolina

Client: SCDOT  
Location: Andrews, SC

Project ID: SPR-731  
Boring No.: B-FMG









## RESONANT COLUMN (RC) AND TORSIONAL SHEAR (TS) TEST

Project Name: Deep Soil Test Boring to Determine Shear  
Wave Velocities across South Carolina

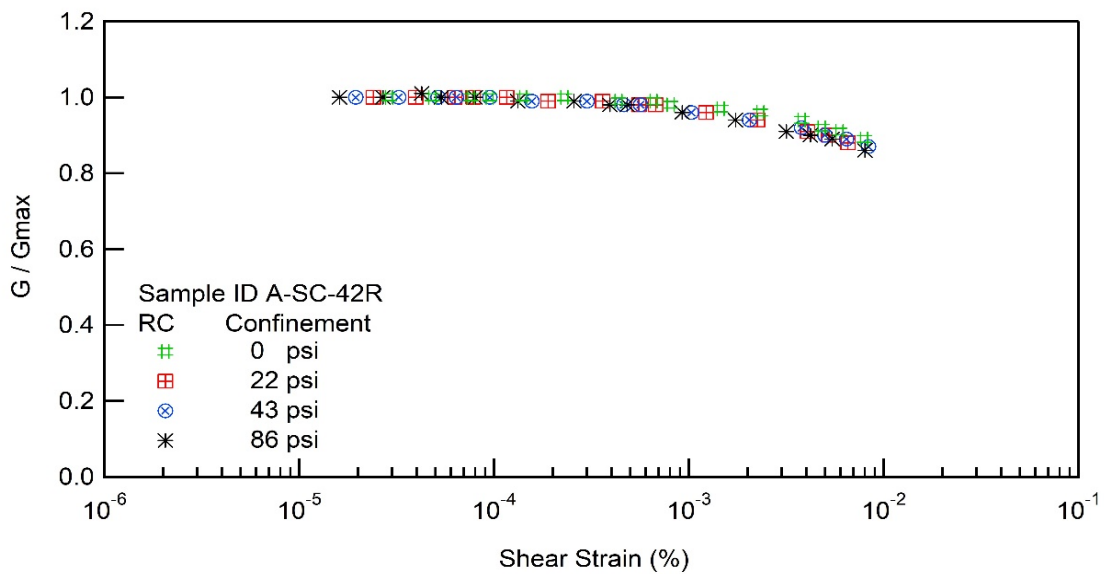
Client: SCDOT

Project ID: SPR-731

Location: Andrews, SC

Boring No.: B-FMG

Sample ID : A-SC-42R





## RESONANT COLUMN (RC) AND TORSIONAL SHEAR (TS) TEST

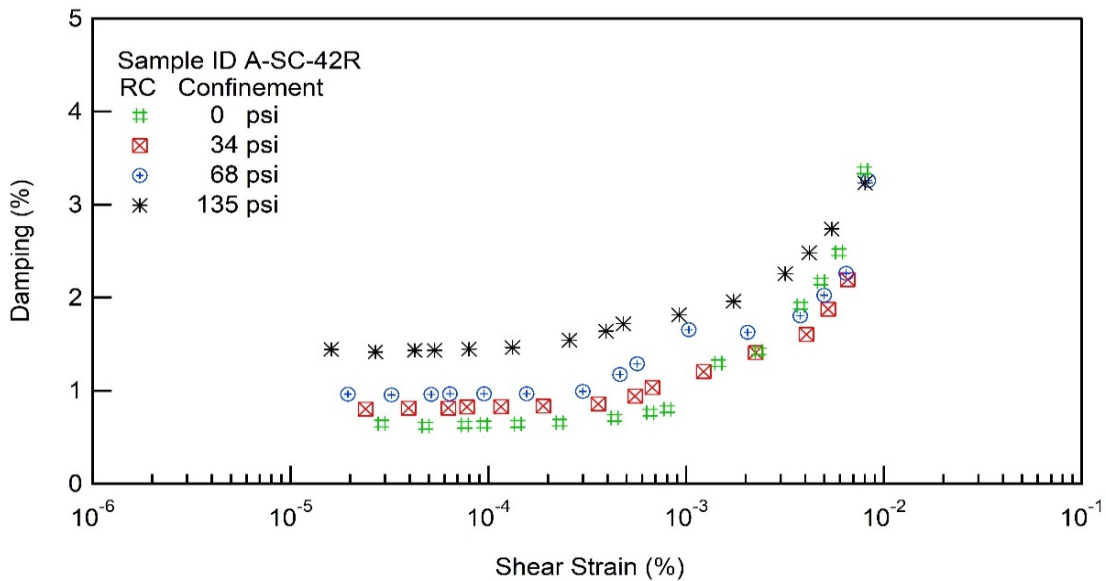
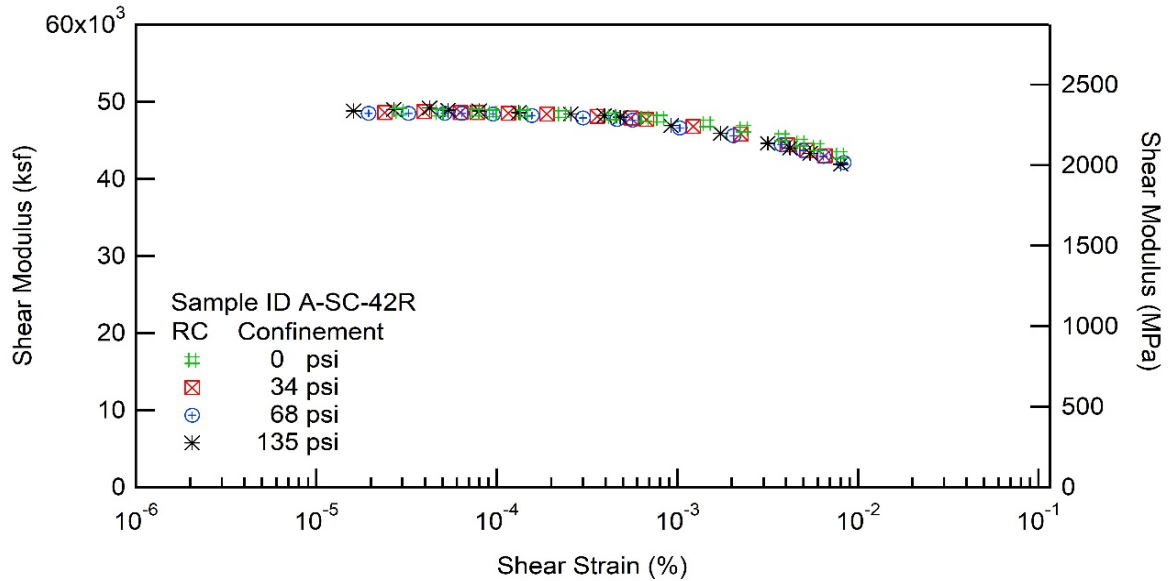
Project Name: Deep Soil Test Boring to Determine Shear  
Wave Velocities across South Carolina

Client: SCDOT

Project ID: SPR-731

Location: Andrews, SC

Boring No.: B-FMG





**UNIVERSITY OF SOUTH CAROLINA**  
 Department of Civil and Environmental Engineering  
 300 Main street, Columbia, SC, 29208

**RESONANT COLUMN (RC) TEST REPORT**

Project Name: Deep Soil Test Boring to Determine Shear  
 Wave Velocities across South Carolina  
 Client: SCDOT Project ID: SPR-731  
 Location: Andrews, SC Boring No.: B-FMG

Table 1 Results for Sample ID A-SC-42R for RC Test

No Confining Pressure				Confining Pressure 34 PSI				Confining Pressure 68 PSI			
$\gamma$ (%)	G (ksf)	G/G <sub>max</sub>	D (%)	$\gamma$ (%)	G (ksf)	G/G <sub>max</sub>	D (%)	$\gamma$ (%)	G (ksf)	G/G <sub>max</sub>	D (%)
2.89E-05	48693	1.003	0.646	2.40E-05	48622	1.000	0.801	1.95E-05	48535	1.001	0.963
4.82E-05	48609	1.001	0.622	3.96E-05	48706	1.002	0.812	3.24E-05	48535	1.001	0.954
7.61E-05	48622	1.001	0.633	6.29E-05	48622	1.000	0.812	5.15E-05	48535	1.001	0.961
9.49E-05	48535	1.000	0.636	7.81E-05	48622	1.000	0.823	6.40E-05	48451	1.000	0.967
1.41E-04	48451	0.998	0.644	1.16E-04	48535	0.998	0.827	9.52E-05	48368	0.998	0.967
2.29E-04	48368	0.996	0.656	1.89E-04	48368	0.995	0.834	1.56E-04	48198	0.994	0.967
4.35E-04	48112	0.991	0.706	3.60E-04	48112	0.990	0.858	3.00E-04	47945	0.989	0.992
6.58E-04	47945	0.987	0.764	5.53E-04	47859	0.984	0.940	4.63E-04	47690	0.984	1.175
8.04E-04	47776	0.984	0.801	6.75E-04	47690	0.981	1.033	5.65E-04	47607	0.982	1.289
1.45E-03	47187	0.972	1.296	1.23E-03	46769	0.962	1.205	1.03E-03	46602	0.961	1.656
2.33E-03	46520	0.958	1.422	2.25E-03	45774	0.941	1.407	2.04E-03	45611	0.941	1.627
3.79E-03	45446	0.936	1.913	4.06E-03	44385	0.913	1.604	3.78E-03	44385	0.916	1.804
4.81E-03	44709	0.921	2.174	5.23E-03	43738	0.900	1.875	4.99E-03	43656	0.901	2.025
5.93E-03	44059	0.907	2.487	6.55E-03	43014	0.885	2.194	6.44E-03	42935	0.886	2.261
7.94E-03	43096	0.888	3.367					8.34E-03	42141	0.869	3.259

Table 2 Results for Sample ID A-SC-42R for RC Test (Cont.)

Confining Pressure 135 PSI			
$\gamma$ (%)	G (ksf)	G/G <sub>max</sub>	D (%)
1.61E-05	48790	0.997	1.444
2.69E-05	48961	1.000	1.415
4.25E-05	49217	1.005	1.433
5.36E-05	48877	0.998	1.434
7.99E-05	48790	0.997	1.446
1.33E-04	48622	0.993	1.464
2.57E-04	48368	0.988	1.543
3.94E-04	48198	0.984	1.639
4.83E-04	48028	0.981	1.718
9.23E-04	46854	0.957	1.814
1.74E-03	45940	0.938	1.960
3.17E-03	44628	0.912	2.258
4.20E-03	43980	0.898	2.482
5.44E-03	43336	0.885	2.739
8.02E-03	41904	0.856	3.231



## RESONANT COLUMN (RC) AND TORSIONAL SHEAR (TS) TEST

Project Name: Deep Soil Test Boring to Determine Shear  
Wave Velocities across South Carolina

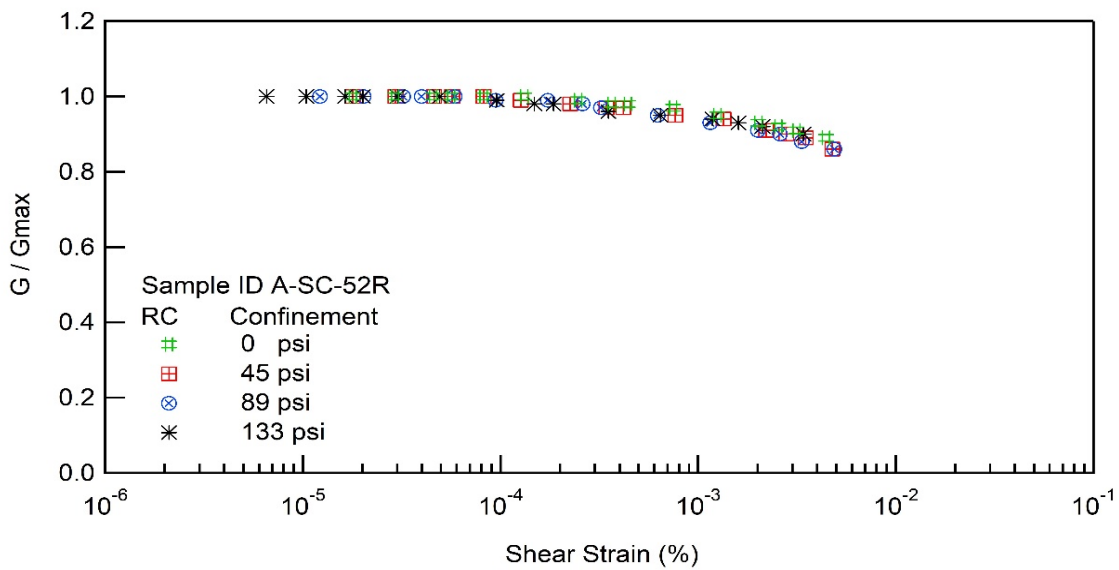
Client: SCDOT

Project ID: SPR-731

Location: Andrews, SC

Boring No.: B-FMG

Sample ID : A-SC-52R





## RESONANT COLUMN (RC) AND TORSIONAL SHEAR (TS) TEST

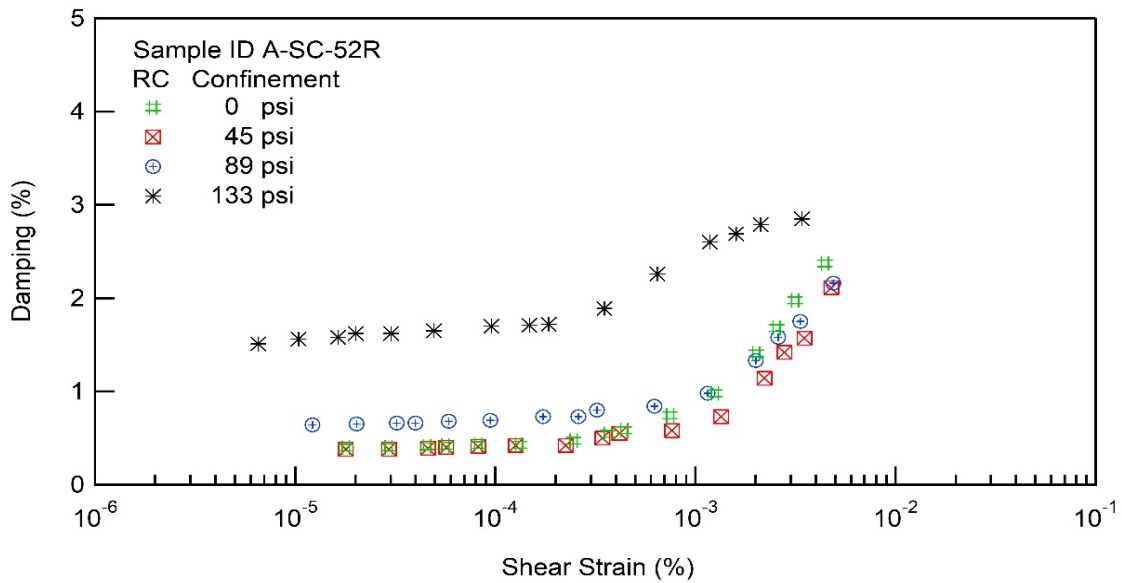
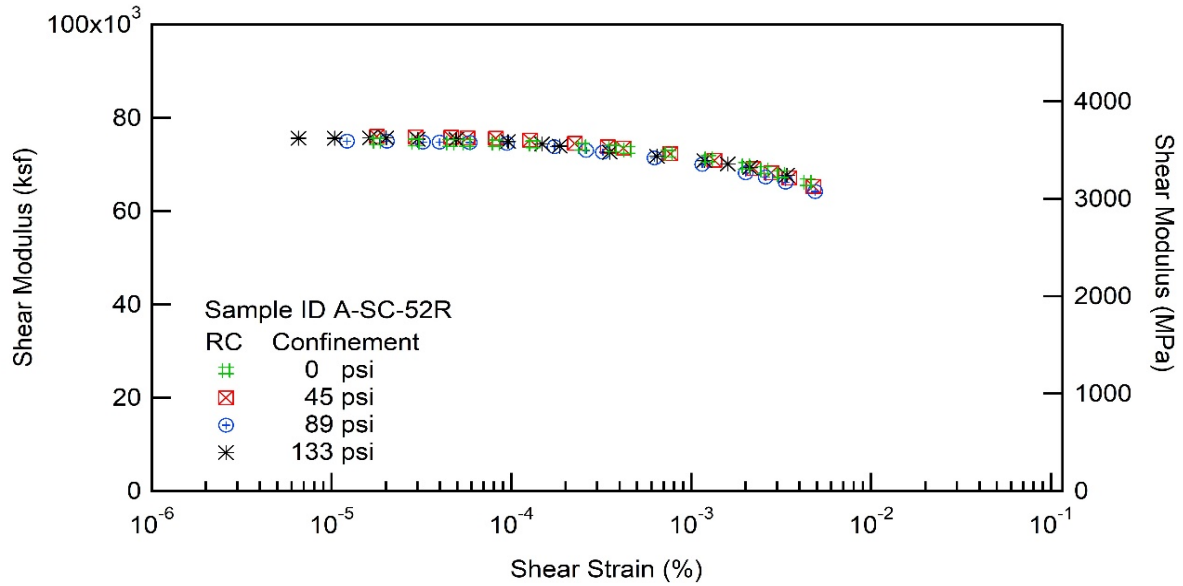
Project Name: Deep Soil Test Boring to Determine Shear  
Wave Velocities across South Carolina

Client: SCDOT

Project ID: SPR-731

Location: Andrews, SC

Boring No.: B-FMG





**UNIVERSITY OF SOUTH CAROLINA**  
 Department of Civil and Environmental Engineering  
 300 Main street, Columbia, SC, 29208

**RESONANT COLUMN (RC) TEST REPORT**

Project Name: Deep Soil Test Boring to Determine Shear  
 Wave Velocities across South Carolina  
 Client: SCDOT Project ID: SPR-731  
 Location: Andrews, SC Boring No.: B-FMG

Table 1 Results for Sample ID A-SC-52R for RC Test

No Confining Pressure				Confining Pressure 45 PSI				Confining Pressure 89 PSI			
$\gamma$ (%)	G (ksf)	G/G <sub>max</sub>	D (%)	$\gamma$ (%)	G (ksf)	G/G <sub>max</sub>	D (%)	$\gamma$ (%)	G (ksf)	G/G <sub>max</sub>	D (%)
1.79E-05	74938	1.004	0.396	1.79E-05	76015	1.003	0.377	1.22E-05	75037	1.002	0.642
2.93E-05	74746	1.002	0.399	2.94E-05	75918	1.002	0.379	2.03E-05	75037	1.002	0.648
4.56E-05	74647	1.000	0.412	4.62E-05	75819	1.001	0.386	3.22E-05	74842	1.000	0.655
5.63E-05	74647	1.000	0.418	5.69E-05	75722	0.999	0.397	3.99E-05	74842	1.000	0.661
8.21E-05	74455	0.998	0.425	8.21E-05	75622	0.998	0.408	5.86E-05	74746	0.998	0.675
1.32E-04	74260	0.995	0.428	1.27E-04	75233	0.993	0.424	9.45E-05	74455	0.994	0.692
2.47E-04	73776	0.989	0.472	2.25E-04	74455	0.983	0.420	1.73E-04	73776	0.985	0.731
3.65E-04	73388	0.983	0.545	3.43E-04	73776	0.974	0.504	2.60E-04	73005	0.975	0.732
4.41E-04	73100	0.980	0.584	4.19E-04	73487	0.970	0.553	3.22E-04	72620	0.970	0.800
7.48E-04	72304	0.969	0.742	7.66E-04	72333	0.955	0.575	6.25E-04	71379	0.953	0.836
1.25E-03	71189	0.954	0.980	1.34E-03	70905	0.936	0.733	1.15E-03	69960	0.934	0.980
2.01E-03	69679	0.934	1.408	2.21E-03	69117	0.912	1.139	2.01E-03	68185	0.911	1.332
2.54E-03	68837	0.922	1.679	2.79E-03	68185	0.900	1.416	2.59E-03	67259	0.898	1.579
3.15E-03	67907	0.910	1.975	3.50E-03	67074	0.885	1.575	3.35E-03	66248	0.885	1.752
4.43E-03	66155	0.887	2.373	4.78E-03	65336	0.862	2.112	4.88E-03	64248	0.858	2.164

Table 2 Results for Sample ID A-SC-52R for RC Test (Cont.)

Confining Pressure 133 PSI			
$\gamma$ (%)	G (ksf)	G/G <sub>max</sub>	D (%)
6.55E-06	75596	1.000	1.506
1.04E-05	75622	1.000	1.560
1.64E-05	75722	1.001	1.581
2.01E-05	75722	1.001	1.616
3.02E-05	75429	0.997	1.619
4.93E-05	75429	0.997	1.651
9.58E-05	74941	0.991	1.697
1.48E-04	74356	0.983	1.714
1.85E-04	73871	0.977	1.724
3.52E-04	72594	0.960	1.891
6.46E-04	71784	0.949	2.257
1.18E-03	70834	0.937	2.597
1.60E-03	70056	0.926	2.692
2.12E-03	69305	0.916	2.786
3.40E-03	67721	0.896	2.852



## RESONANT COLUMN (RC) AND TORSIONAL SHEAR (TS) TEST

Project Name: Deep Soil Test Boring to Determine Shear  
Wave Velocities across South Carolina

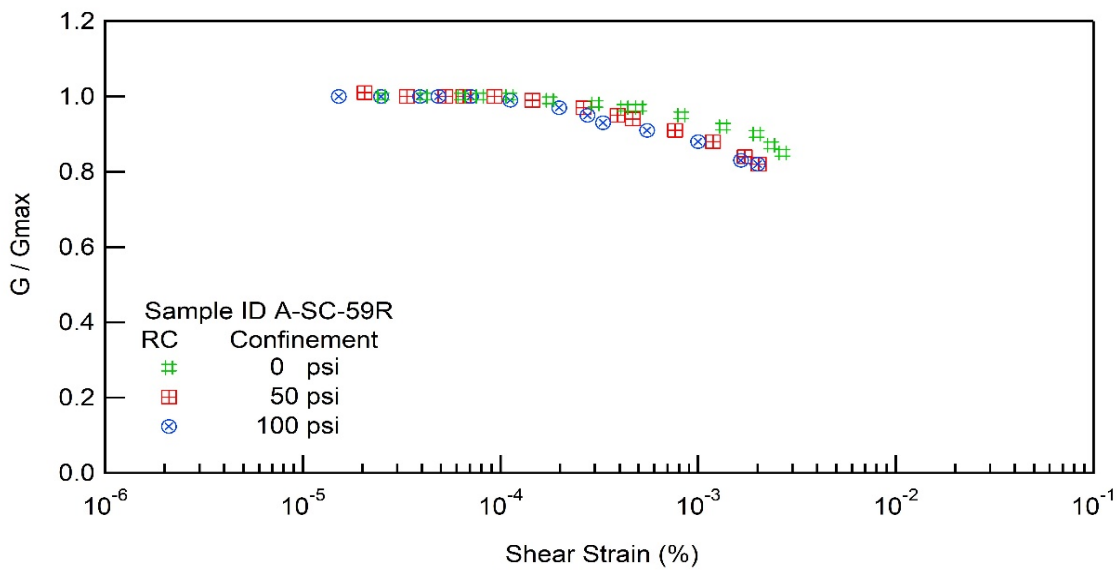
Client: SCDOT

Project ID: SPR-731

Location: Andrews, SC

Boring No.: B-FMG

Sample ID : A-SC-59R





## RESONANT COLUMN (RC) AND TORSIONAL SHEAR (TS) TEST

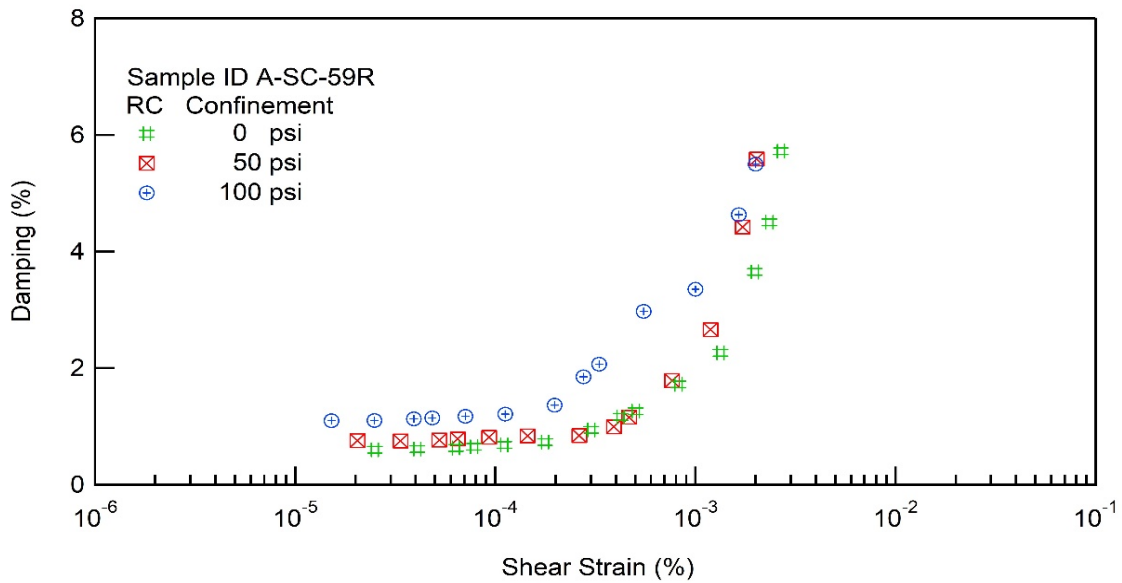
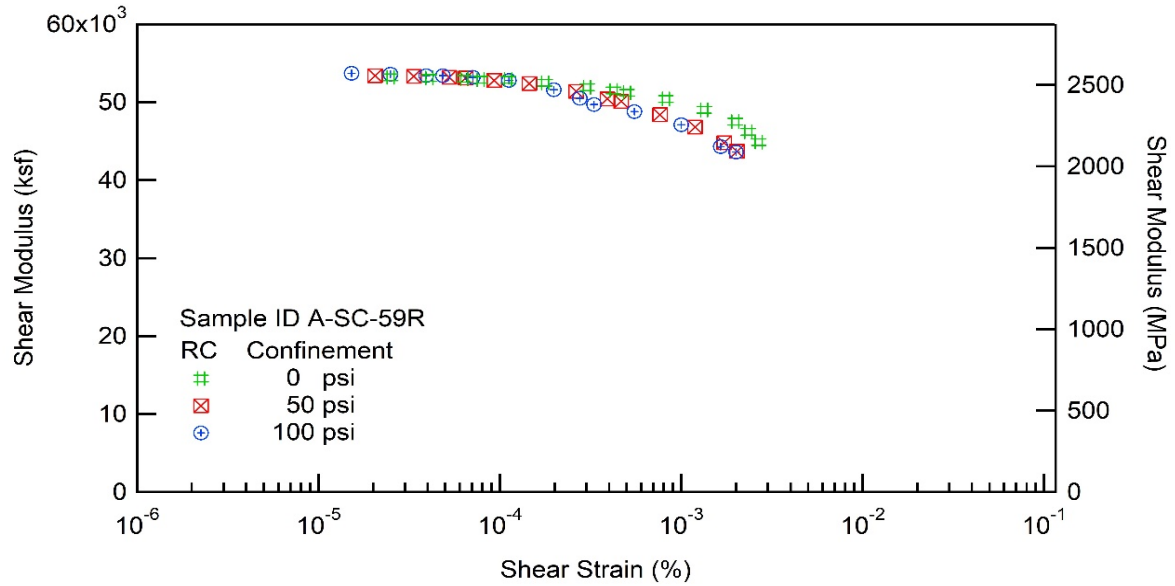
Project Name: Deep Soil Test Boring to Determine Shear  
Wave Velocities across South Carolina

Client: SCDOT

Project ID: SPR-731

Location: Andrews, SC

Boring No.: B-FMG







## RESONANT COLUMN (RC) AND TORSIONAL SHEAR (TS) TEST

Project Name: Deep Soil Test Boring to Determine Shear  
Wave Velocities across South Carolina

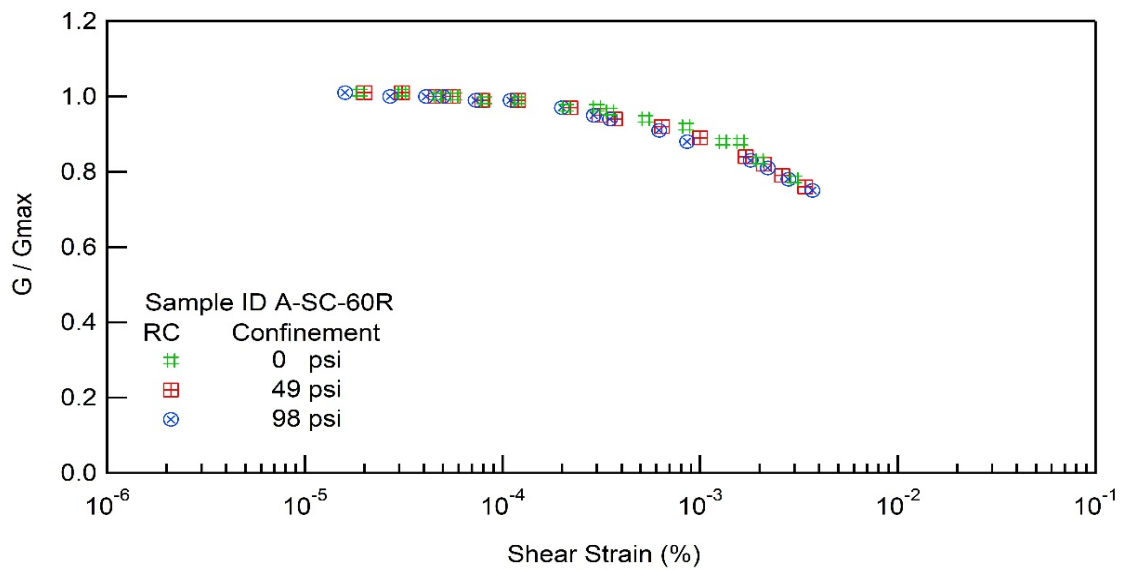
Client: SCDOT

Project ID: SPR-731

Location: Andrews, SC

Boring No.: B-FMG

Sample ID : A-SC-60R





## RESONANT COLUMN (RC) AND TORSIONAL SHEAR (TS) TEST

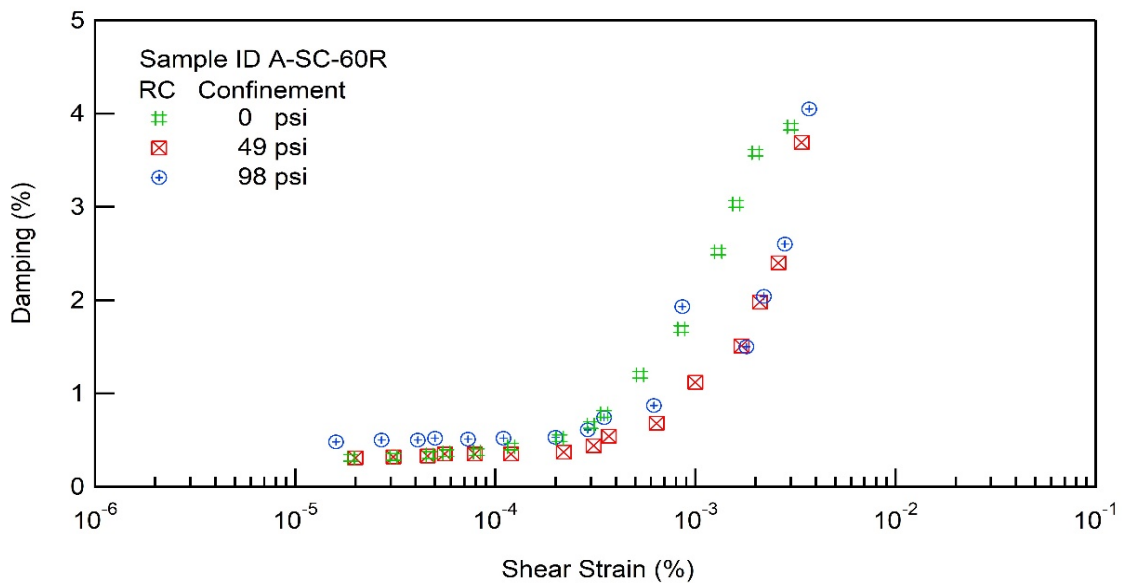
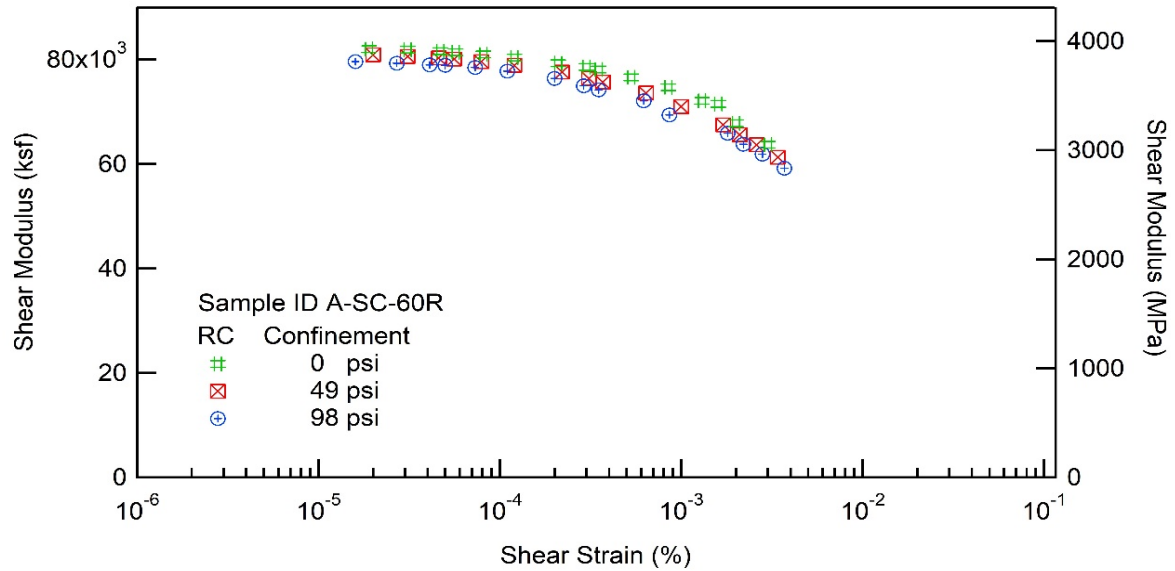
Project Name: Deep Soil Test Boring to Determine Shear  
Wave Velocities across South Carolina

Client: SCDOT

Project ID: SPR-731

Location: Andrews, SC

Boring No.: B-FMG







## RESONANT COLUMN (RC) AND TORSIONAL SHEAR (TS) TEST

Project Name: Deep Soil Test Boring to Determine Shear  
Wave Velocities across South Carolina

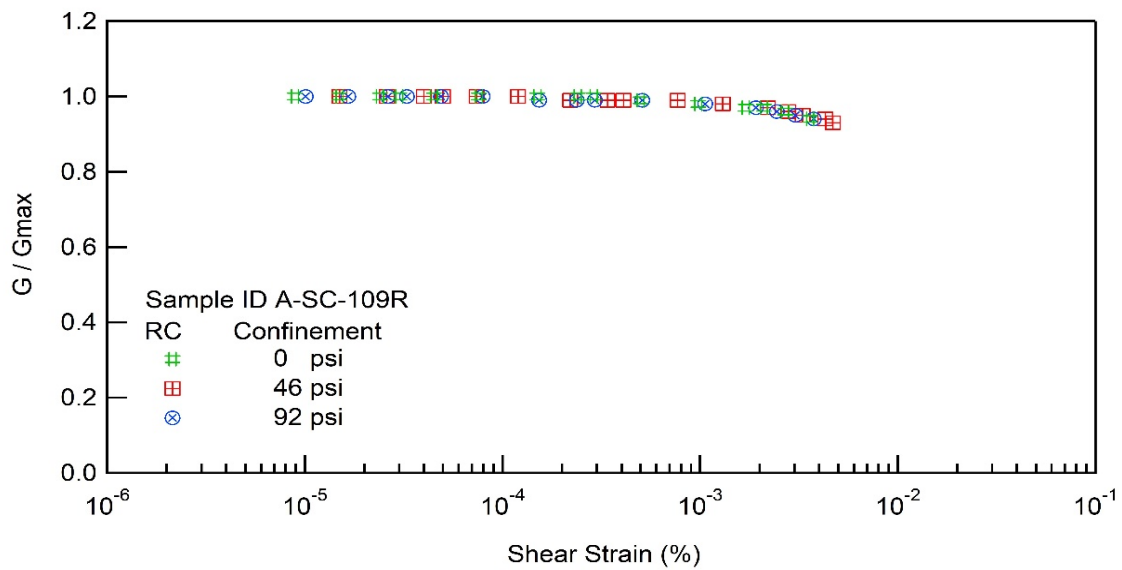
Client: SCDOT

Project ID: SPR-731

Location: Andrews, SC

Boring No.: B-FMG

Sample ID : A-SC-109R





## RESONANT COLUMN (RC) AND TORSIONAL SHEAR (TS) TEST

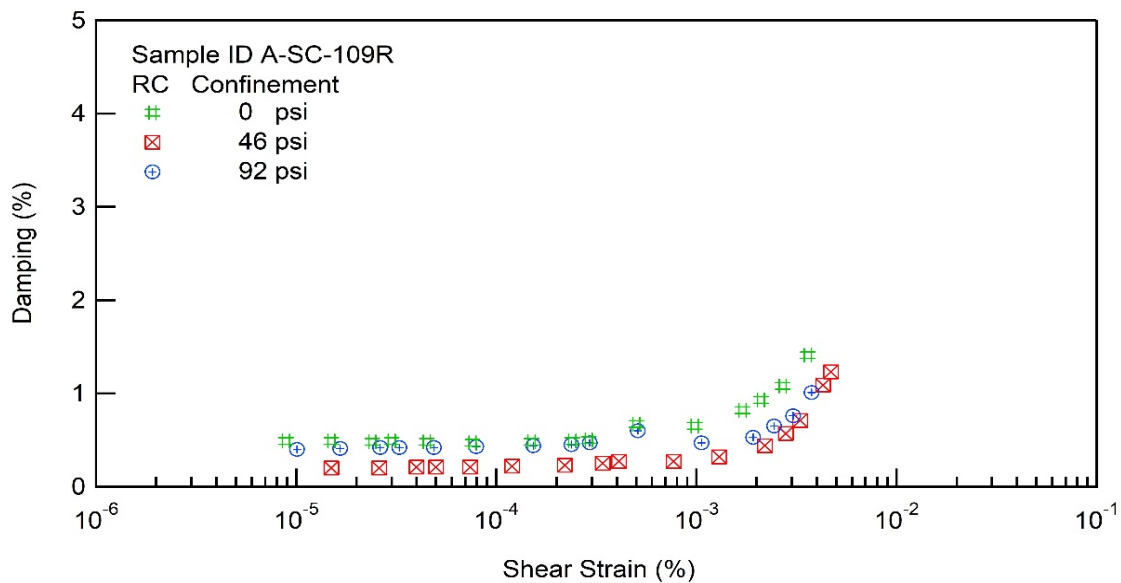
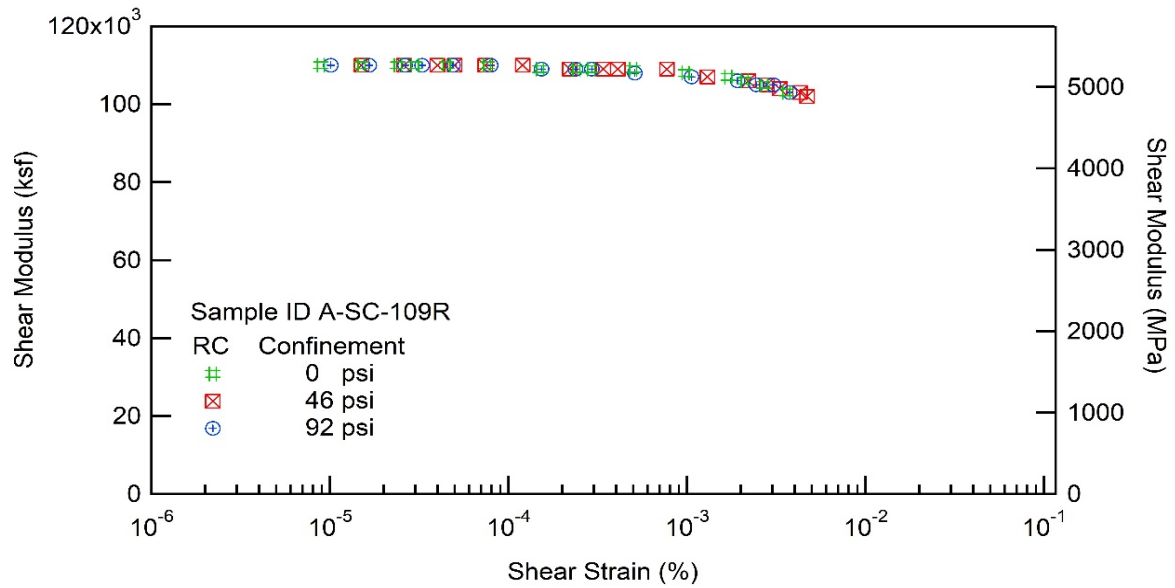
Project Name: Deep Soil Test Boring to Determine Shear  
Wave Velocities across South Carolina

Client: SCDOT

Project ID: SPR-731

Location: Andrews, SC

Boring No.: B-FMG







## RESONANT COLUMN (RC) AND TORSIONAL SHEAR (TS) TEST

Project Name: Deep Soil Test Boring to Determine Shear  
Wave Velocities across South Carolina

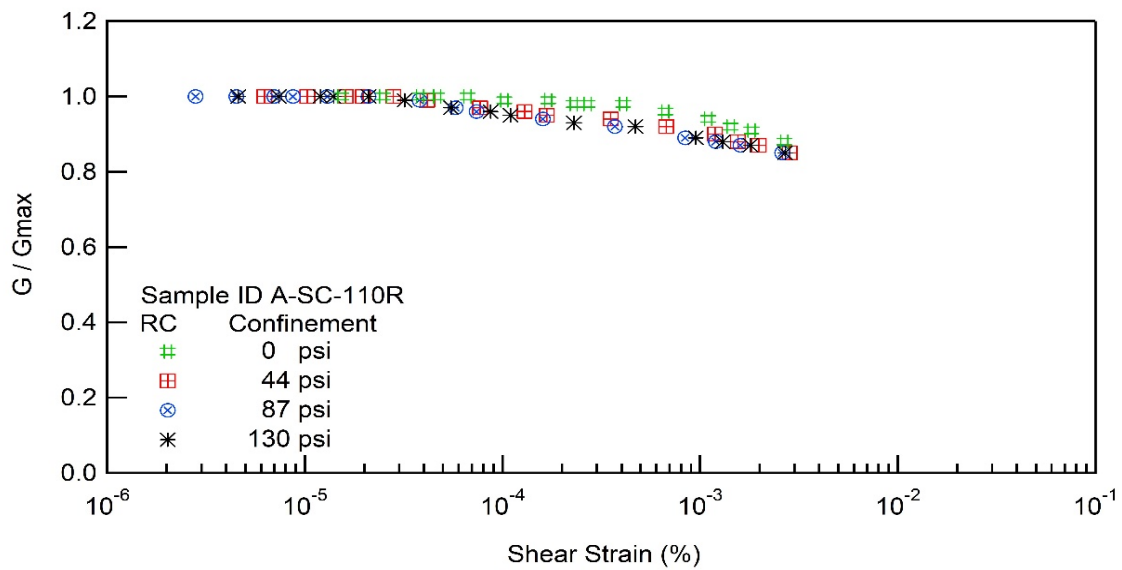
Client: SCDOT

Project ID: SPR-731

Location: Andrews, SC

Boring No.: B-FMG

Sample ID : A-SC-110R





## RESONANT COLUMN (RC) AND TORSIONAL SHEAR (TS) TEST

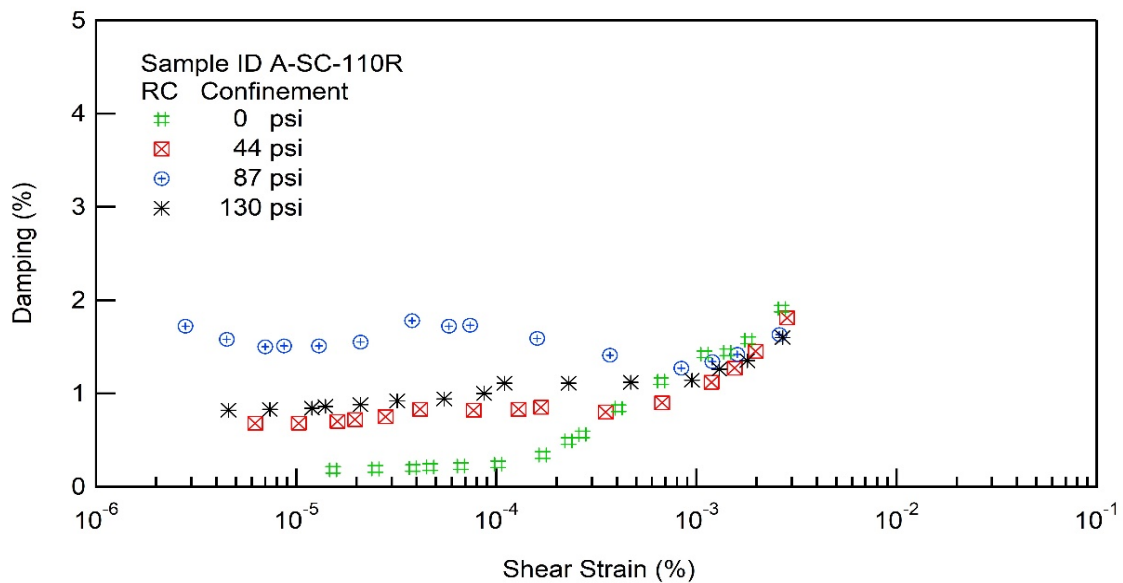
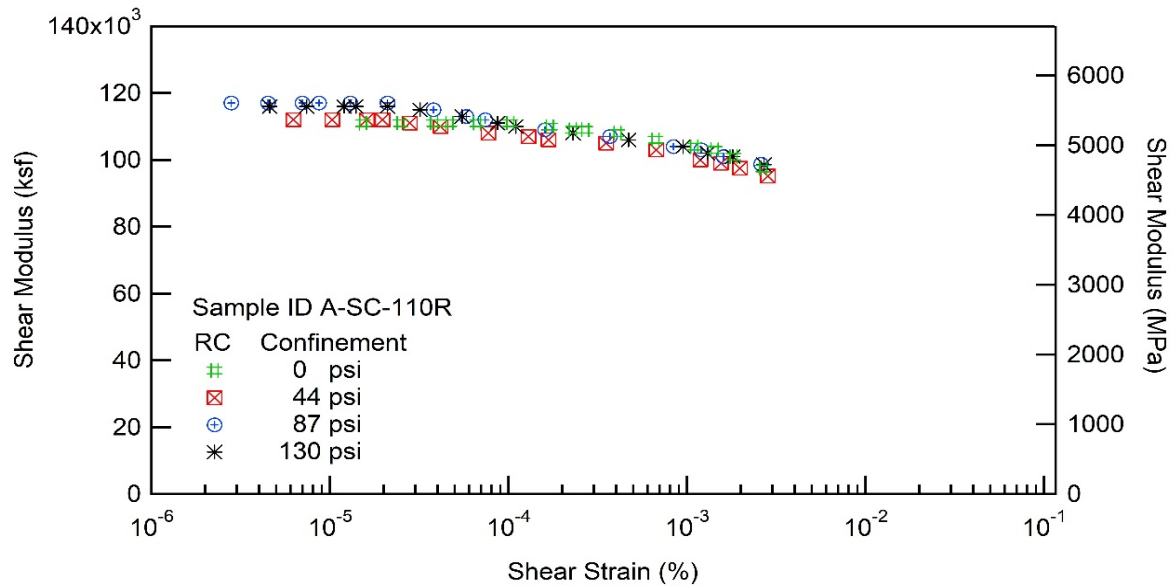
Project Name: Deep Soil Test Boring to Determine Shear  
Wave Velocities across South Carolina

Client: SCDOT

Project ID: SPR-731

Location: Andrews, SC

Boring No.: B-FMG





**UNIVERSITY OF SOUTH CAROLINA**  
 Department of Civil and Environmental Engineering  
 300 Main street, Columbia, SC, 29208

**RESONANT COLUMN (RC) TEST REPORT**

Project Name: Deep Soil Test Boring to Determine Shear  
 Wave Velocities across South Carolina  
 Client: SCDOT Project ID: SPR-731  
 Location: Andrews, SC Boring No.: B-FMG

Table 1 Results for Sample ID A-SC-110R for RC Test

No Confining Pressure				Confining Pressure 44 PSI				Confining Pressure 87 PSI			
$\gamma$ (%)	G (ksf)	G/G <sub>max</sub>	D (%)	$\gamma$ (%)	G (ksf)	G/G <sub>max</sub>	D (%)	$\gamma$ (%)	G (ksf)	G/G <sub>max</sub>	D (%)
1.53E-05	111421	1.002	0.184	6.24E-06	112311	1.004	0.675	2.76E-06	116530	0.998	1.716
2.49E-05	111330	1.001	0.187	1.03E-05	112189	1.003	0.679	4.47E-06	116658	0.999	1.580
3.83E-05	111205	1.000	0.199	1.61E-05	111943	1.001	0.695	7.05E-06	116906	1.001	1.496
4.67E-05	111205	1.000	0.208	1.97E-05	111818	1.000	0.716	8.71E-06	116906	1.001	1.510
6.66E-05	110963	0.998	0.220	2.80E-05	111330	0.996	0.755	1.30E-05	116530	0.998	1.512
1.02E-04	110597	0.995	0.244	4.16E-05	110229	0.986	0.834	2.09E-05	116654	0.999	1.546
1.70E-04	109864	0.988	0.345	7.71E-05	108046	0.966	0.817	3.83E-05	115034	0.985	1.781
2.29E-04	109137	0.982	0.494	1.29E-04	106843	0.955	0.832	5.84E-05	112805	0.966	1.719
2.69E-04	109013	0.981	0.560	1.68E-04	106248	0.950	0.854	7.41E-05	111943	0.959	1.734
4.08E-04	108412	0.975	0.839	3.53E-04	104578	0.935	0.802	1.64E-04	109500	0.938	1.587
6.67E-04	106484	0.958	1.127	6.74E-04	102569	0.917	0.904	3.73E-04	107444	0.920	1.405
1.10E-03	104106	0.936	1.423	1.19E-03	100234	0.896	1.119	8.40E-04	104460	0.895	1.274
1.43E-03	102569	0.923	1.440	1.55E-03	98958	0.885	1.273	1.18E-03	103041	0.883	1.344
1.82E-03	100698	0.906	1.573	1.98E-03	97463	0.872	1.455	1.62E-03	101400	0.869	1.423
2.67E-03	97377	0.876	1.908	2.84E-03	95188	0.851	1.812	2.60E-03	98730	0.846	1.631

Table 2 Results for Sample ID A-SC-110R for RC Test (Cont.)

Confining Pressure 130 PSI			
$\gamma$ (%)	G (ksf)	G/G <sub>max</sub>	D (%)
4.56E-06	116279	1.002	0.824
7.41E-06	116279	1.002	0.826
1.16E-05	116155	1.001	0.835
1.43E-05	115905	0.999	0.862
2.06E-05	115654	0.997	0.879
3.19E-05	115034	0.992	0.915
5.49E-05	112927	0.974	0.937
8.72E-05	110839	0.956	0.997
1.09E-04	110108	0.949	1.105
2.27E-04	108289	0.934	1.109
4.68E-04	106366	0.917	1.122
9.55E-04	103748	0.894	1.144
1.31E-03	102337	0.882	1.264
1.77E-03	100816	0.869	1.352
2.73E-03	98612	0.850	1.595



## RESONANT COLUMN (RC) AND TORSIONAL SHEAR (TS) TEST

Project Name: Deep Soil Test Boring to Determine Shear  
Wave Velocities across South Carolina

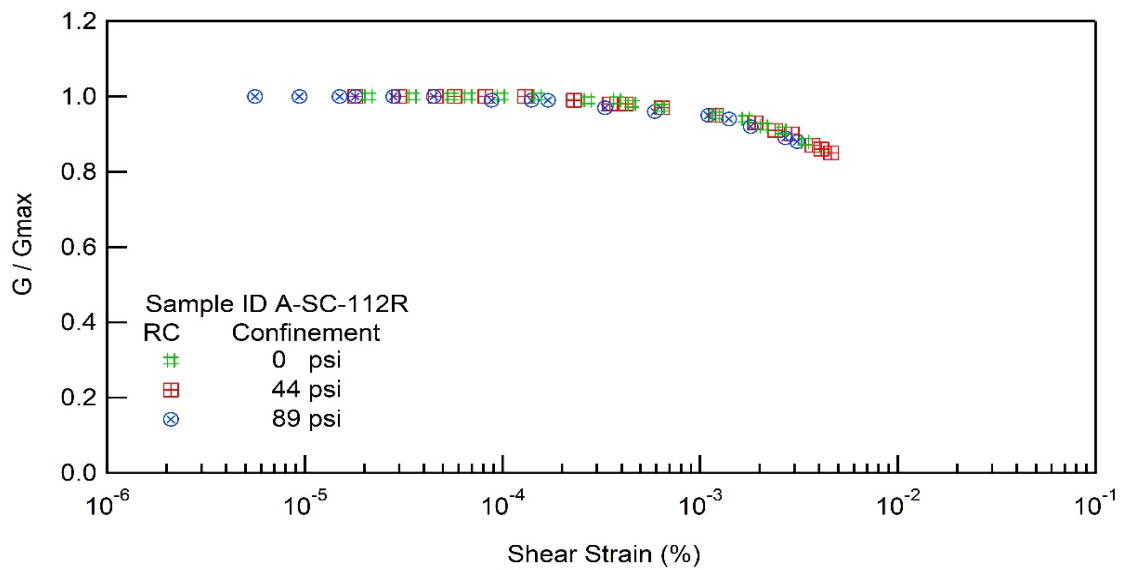
Client: SCDOT

Project ID: SPR-731

Location: Andrews, SC

Boring No.: B-FMG

Sample ID : A-SC-112R





## RESONANT COLUMN (RC) AND TORSIONAL SHEAR (TS) TEST

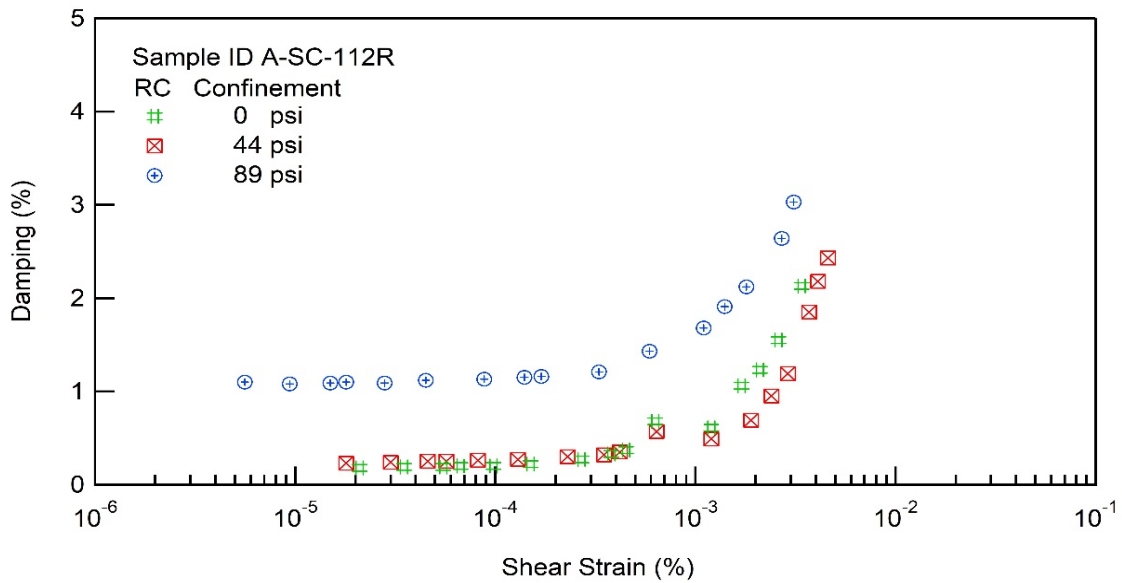
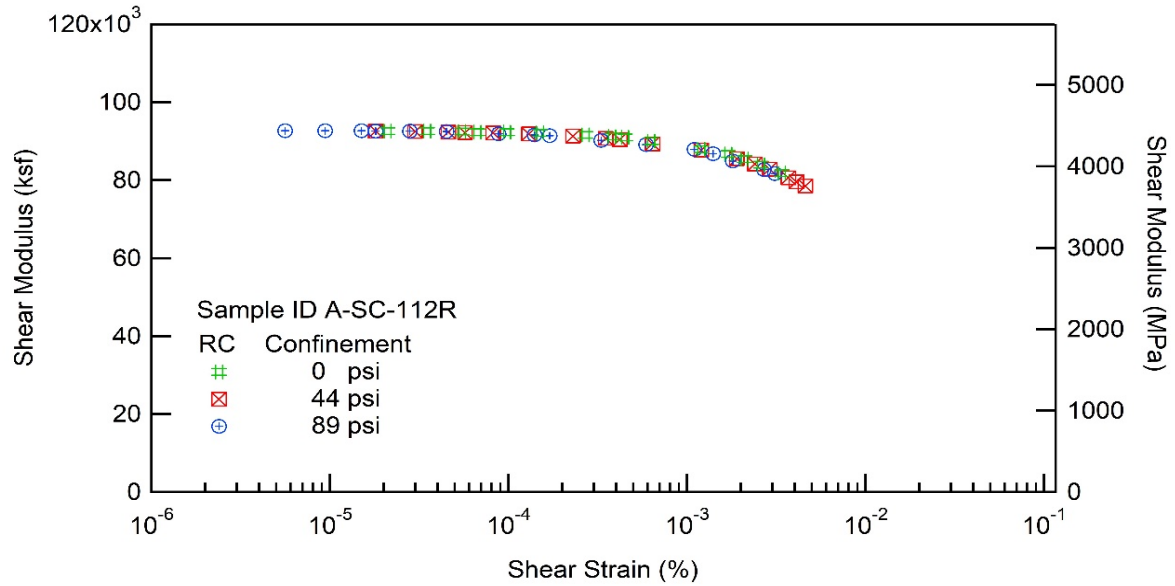
Project Name: Deep Soil Test Boring to Determine Shear  
Wave Velocities across South Carolina

Client: SCDOT

Project ID: SPR-731

Location: Andrews, SC

Boring No.: B-FMG







## RESONANT COLUMN (RC) AND TORSIONAL SHEAR (TS) TEST

Project Name: Deep Soil Test Boring to Determine Shear  
Wave Velocities across South Carolina

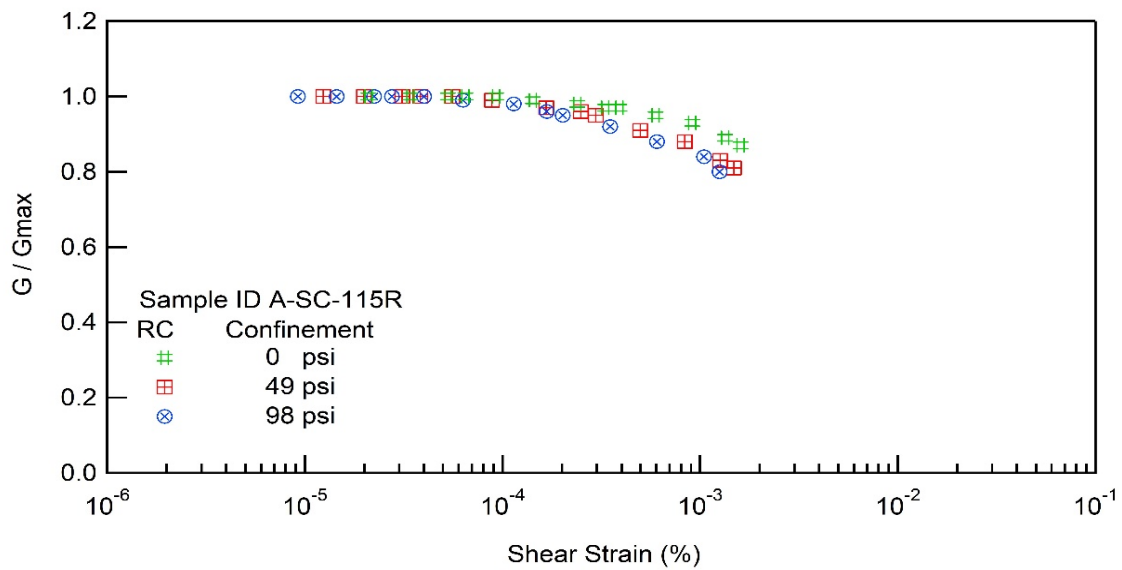
Client: SCDOT

Project ID: SPR-731

Location: Andrews, SC

Boring No.: B-FMG

Sample ID : A-SC-115R





## RESONANT COLUMN (RC) AND TORSIONAL SHEAR (TS) TEST

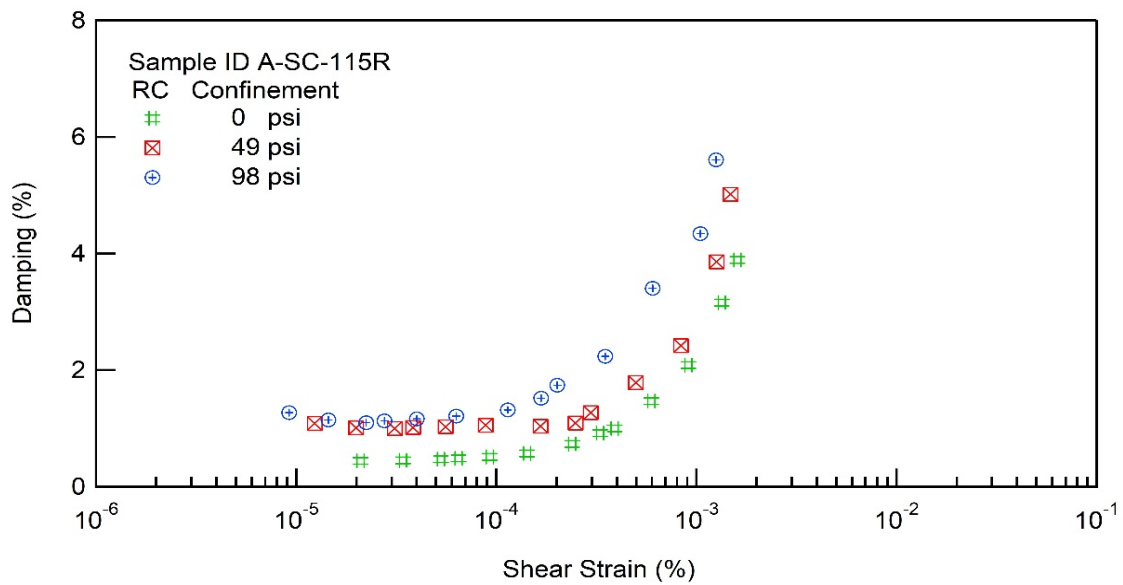
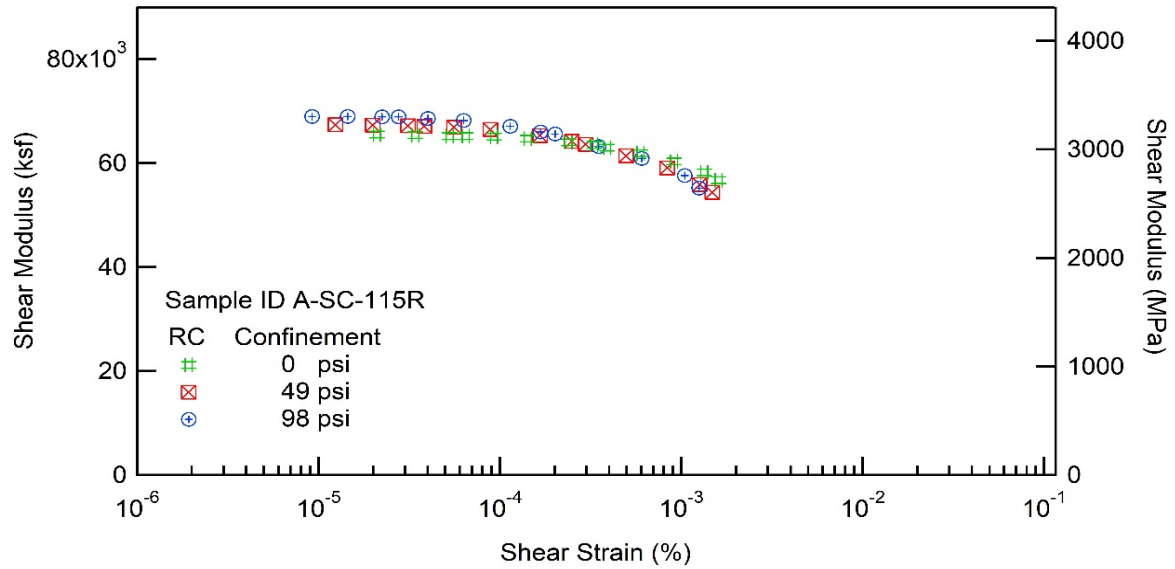
Project Name: Deep Soil Test Boring to Determine Shear  
Wave Velocities across South Carolina

Client: SCDOT

Project ID: SPR-731

Location: Andrews, SC

Boring No.: B-FMG







## RESONANT COLUMN (RC) AND TORSIONAL SHEAR (TS) TEST

Project Name: Deep Soil Test Boring to Determine Shear  
Wave Velocities across South Carolina

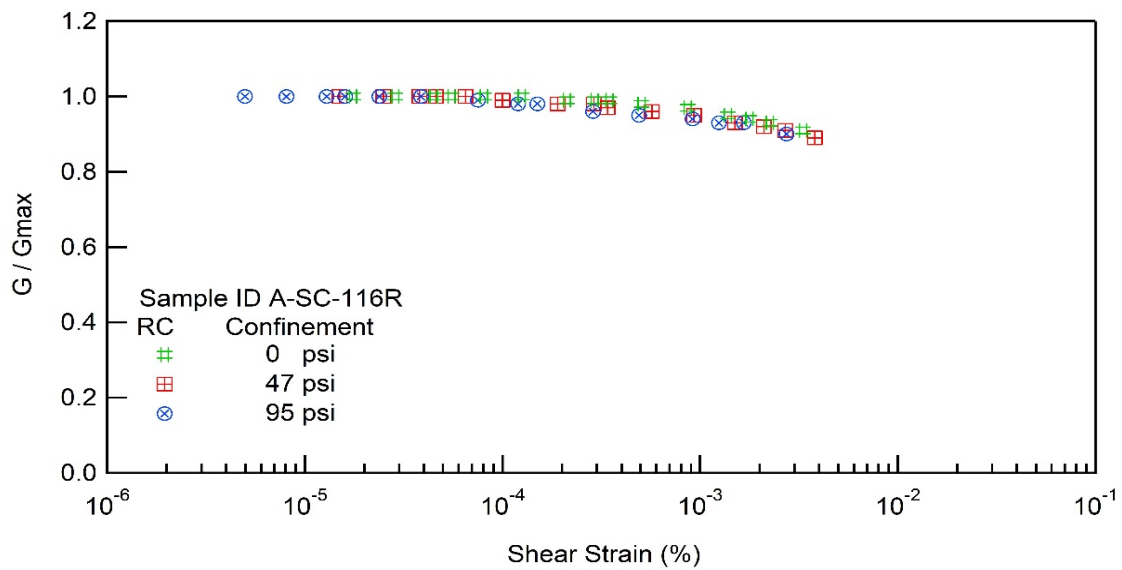
Client: SCDOT

Project ID: SPR-731

Location: Andrews, SC

Boring No.: B-FMG

Sample ID : A-SC-116R





## RESONANT COLUMN (RC) AND TORSIONAL SHEAR (TS) TEST

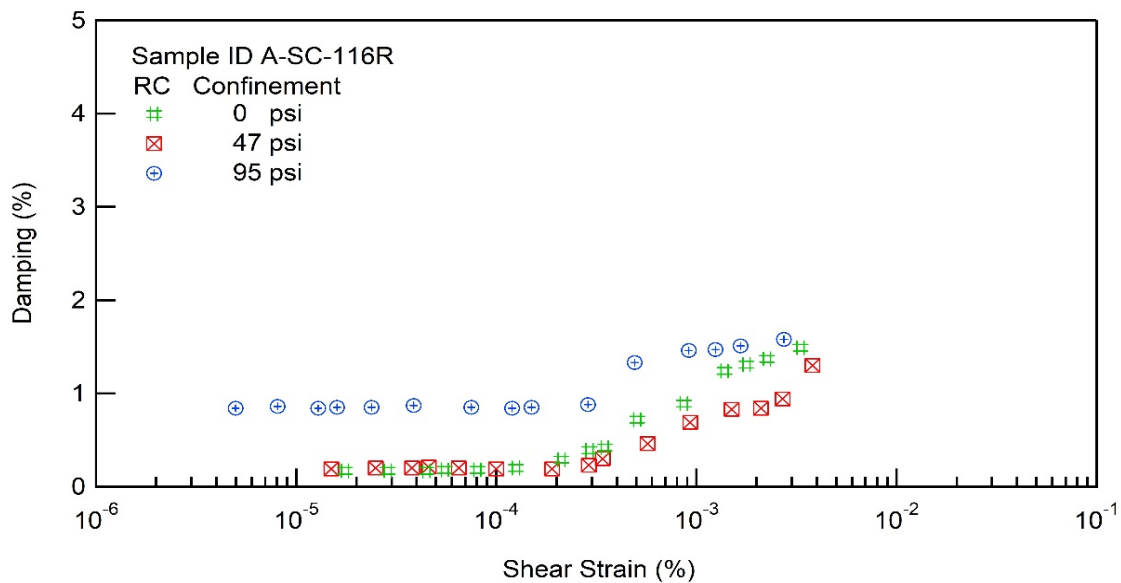
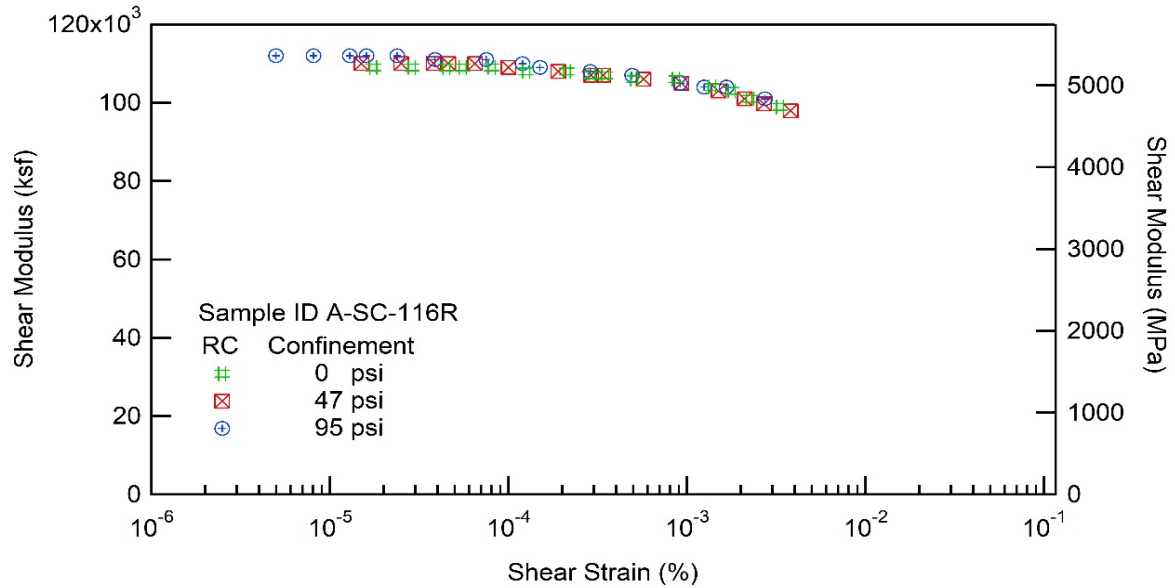
Project Name: Deep Soil Test Boring to Determine Shear  
Wave Velocities across South Carolina

Client: SCDOT

Project ID: SPR-731

Location: Andrews, SC

Boring No.: B-FMG





## Appendix G: Statistical Analysis of $G/G_{\max}$ and Damping Curves

---

## Quaternary Deposits

Sample	C-UD-02	A-UD-03	A-UD-02	A-UD-01	C-UD-01
Geologic Unit	QUATERNARY (Ten Mile Hill Fm. And Penholoway allo Fm. )				
Age (MYA)	2.6 - 0.01 MYA				
USCS	SC-SM	SM	SM	SC	CH
PI	-	-	1	27	28
$\alpha$	0.990	1.151	1.213	1.215	1.258

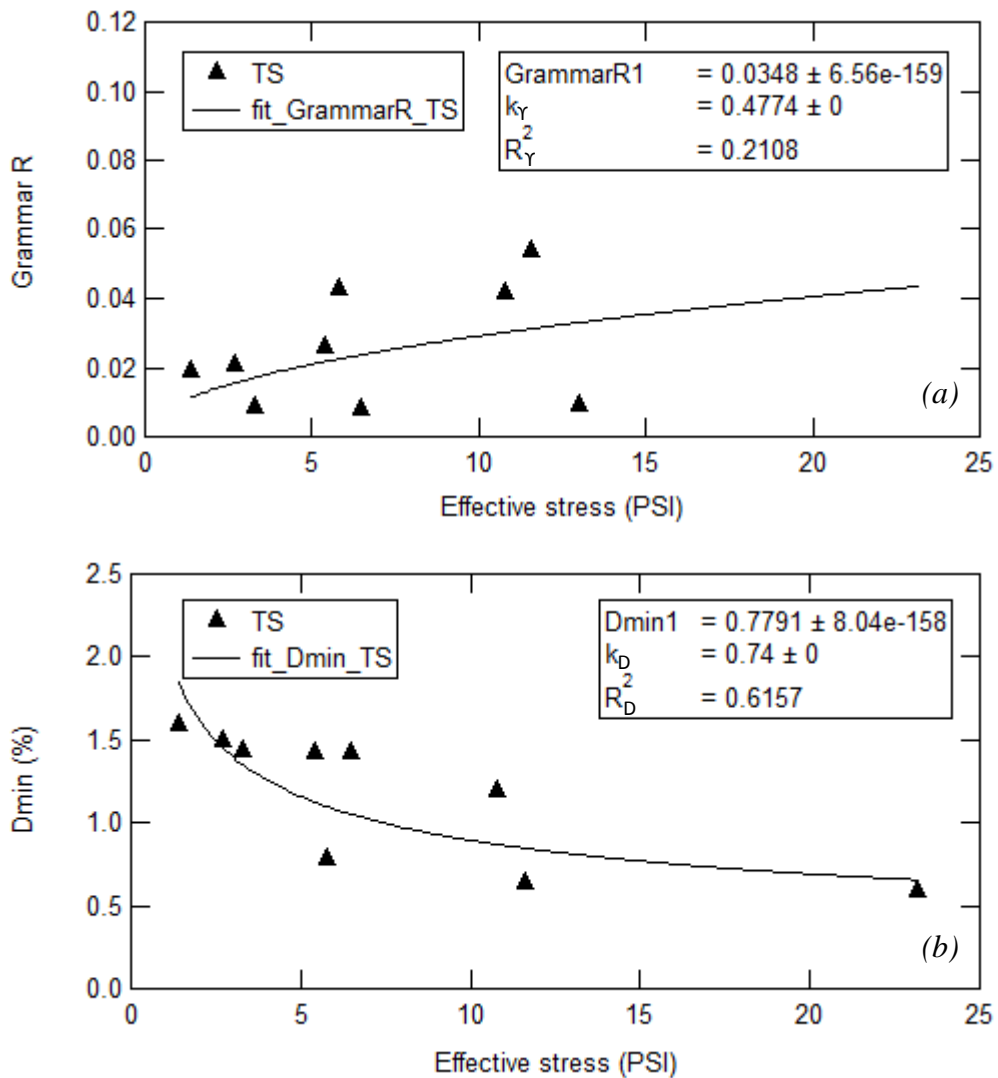


**Figure G1** Statistic Analysis for Model Parameters for non-PI of Quaternary Deposits:  
(a)  $Y_{r1}$  and  $k_Y$ , and (b)  $D_{min1}$  and  $k_D$

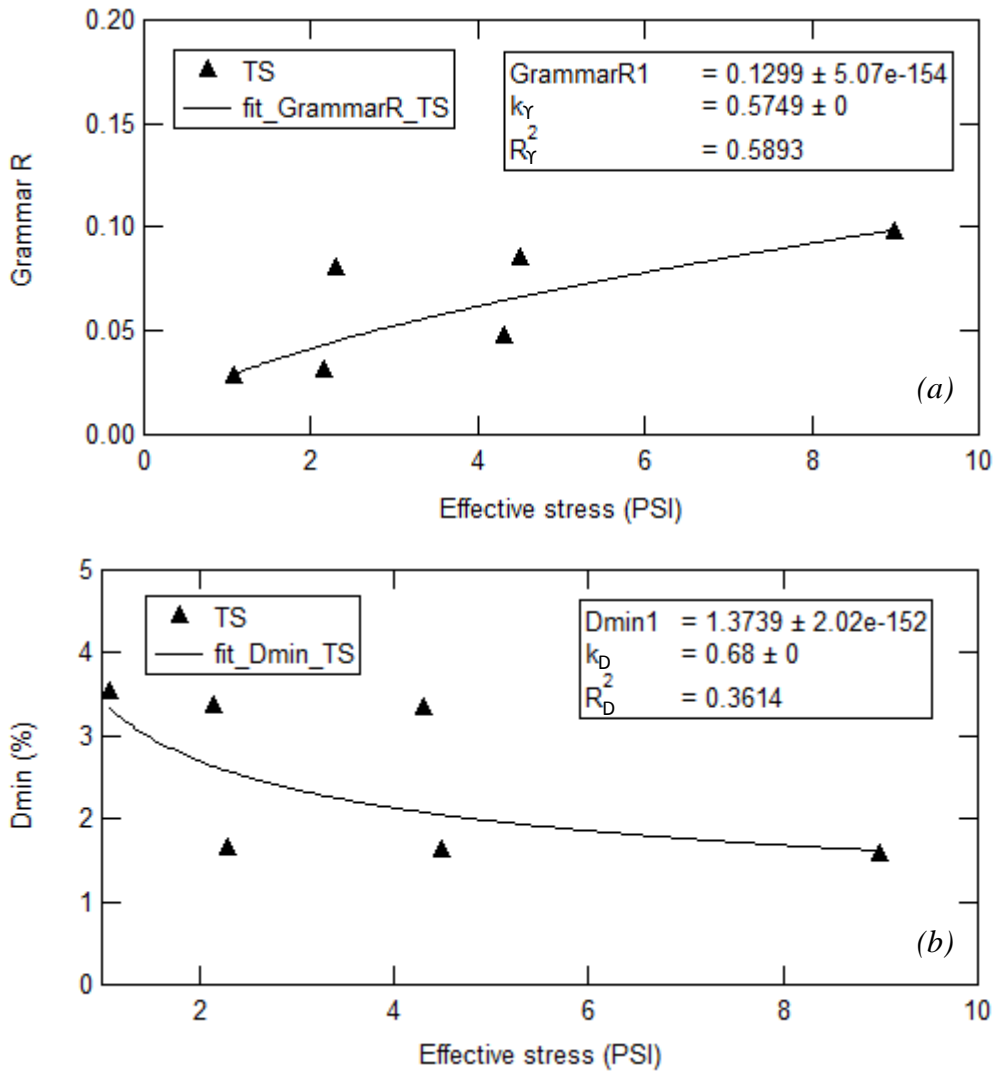


**Figure G2** Statistic Analysis for Model Parameters for PI between 21 and 30 of Quaternary Deposits: (a)  $\gamma_{r1}$  and  $k_Y$ , and (b)  $D_{min1}$  and  $k_D$

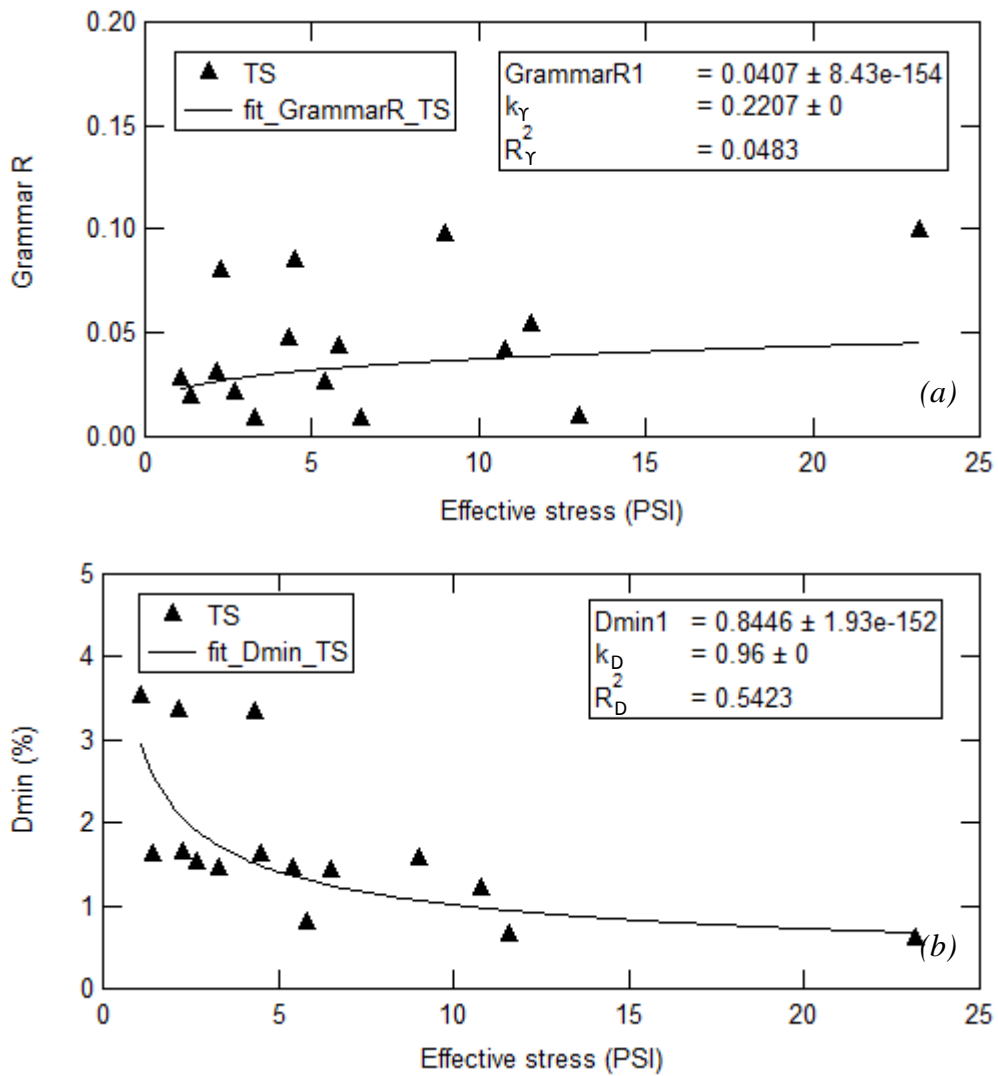


**Figure G3** Statistic Analysis for Model Parameters for PI between non-PI and 30 (all of soils) of Quaternary Deposits: (a)  $\Upsilon_{r1}$  and  $k_Y$ , and (b)  $D_{min1}$  and  $k_D$

## Tertiary Deposits

<i>Sample</i>	<i>A-UD-05</i>	<i>A-UD-06</i>	<i>A-SC-27</i>
<i>Geologic Unit</i>	<i>TERTIARY</i> <i>(Williams Burg Fm. and Lower Bridge Member)</i>		
<i>Age (MYA)</i>	<i>58.0 - 56.0 MYA</i>		
<i>USCS</i>	<i>SP</i>	<i>ML</i>	<i>CL</i>
<i>PI</i>	-	<i>11</i>	<i>13</i>
<i>α</i>	1.535	1.052	1.077

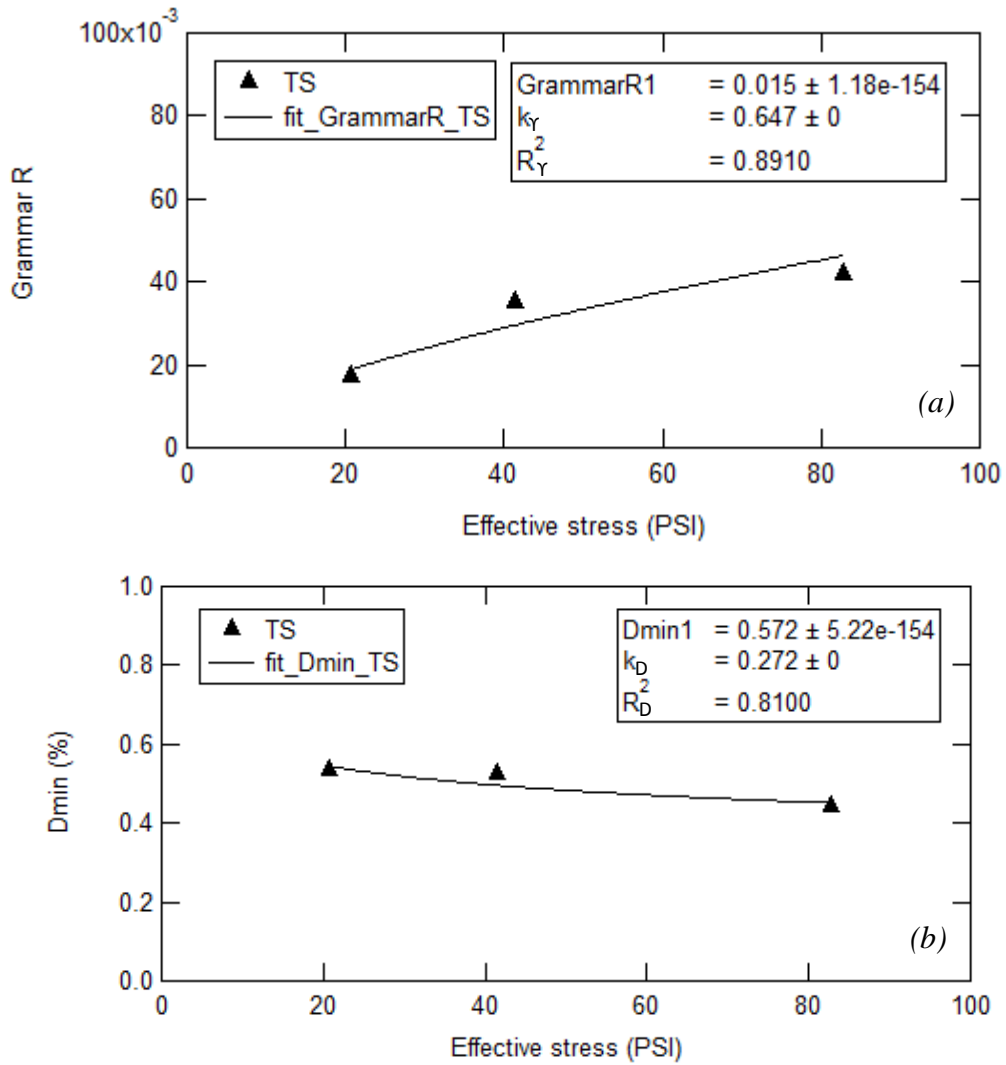


**Figure G4** Statistic Analysis for Model Parameters for non-PI of Tertiary Deposits:

(a)  $\Upsilon_{r1}$  and  $k_Y$ , and (b)  $D_{min1}$  and  $k_D$

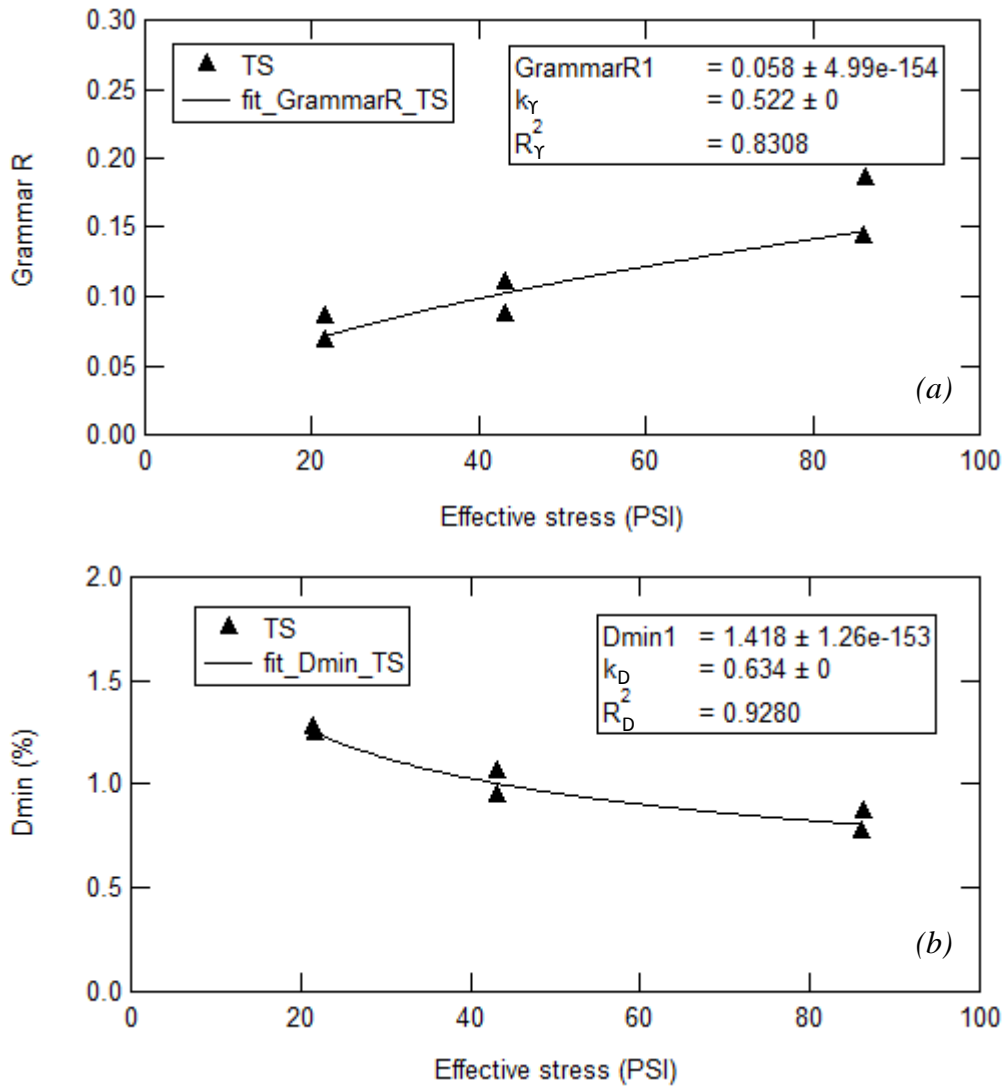


**Figure G5** Statistic Analysis for Model Parameters for PI between 11 and 20 of Tertiary Deposits: (a)  $\gamma_{r1}$  and  $k_Y$ , and (b)  $D_{min1}$  and  $k_D$

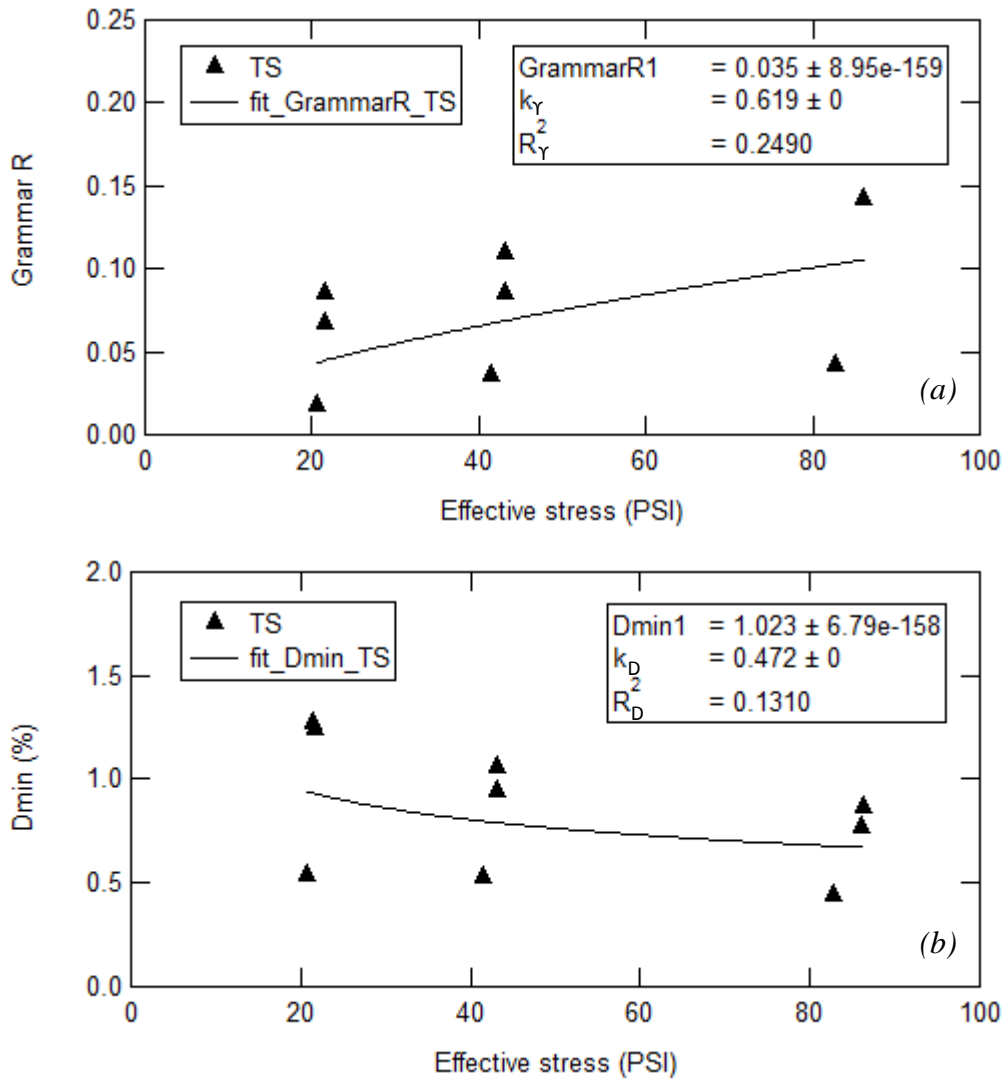


**Figure G6** Statistic Analysis for Model Parameters for PI between non-PI and 20 (all of soils) of Tertiary Deposits: (a)  $\gamma_{r1}$  and  $k_\gamma$ , and (b)  $D_{min1}$  and  $k_D$

## Cretaceous Deposits and Rocks

<i>Sample</i>	<i>C-SC-09</i>	<i>C-SC-34</i>	<i>A-SC-105</i>	<i>C-SC-15</i>	<i>A-SC-77</i>	<i>A-SC-86</i>
<i>Geologic Unit</i>	<i>CRETACEOUS (Peedee Fm. and Black Creek Group)</i>					
<i>Age (MYA)</i>	<i>83.6 - 66.0 MYA</i>					
<i>USCS</i>	<i>SC</i>	<i>SC</i>	<i>SC</i>	<i>MH</i>	<i>MH</i>	<i>CH</i>
<i>PI</i>	<i>14</i>	<i>15</i>	<i>20</i>	<i>19</i>	<i>24</i>	<i>29</i>
<i>α</i>	<i>1.085</i>	<i>1.059</i>	<i>0.963</i>	<i>1.059</i>	<i>1.396</i>	<i>1.107</i>

<i>Sample</i>	<i>A-SC-49</i>	<i>A-SC-96</i>	<i>C-SC-56</i>	<i>C-SC-63</i>	<i>C-UD-07</i>	<i>C-UD-03</i>	<i>C-UD-08</i>
<i>Geologic Unit</i>	<i>CRETACEOUS (Peedee Fm. and Black Creek Group)</i>						
<i>Age (MYA)</i>	<i>83.6 - 66.0 MYA</i>						
<i>USCS</i>	<i>CH</i>	<i>CH</i>	<i>CH</i>	<i>CH</i>	<i>CH</i>	<i>CH</i>	<i>CH</i>
<i>PI</i>	<i>33</i>	<i>33</i>	<i>34</i>	<i>39</i>	<i>43</i>	<i>44</i>	<i>47</i>
<i>α</i>	<i>1.186</i>	<i>1.070</i>	<i>1.148</i>	<i>1.196</i>	<i>1.356</i>	<i>1.104</i>	<i>1.411</i>

<i>Sample</i>	<i>C-SC-04R</i>	<i>C-SC-39R</i>	<i>C-SC-40R</i>	<i>C-SC-41R</i>	<i>C-SC-68R</i>	<i>A-SC-52R</i>	<i>A-SC-59R</i>
<i>Geologic Unit</i>	<i>CRETACEOUS (Peedee Fm. And Black Creek Group)</i>						
<i>Age (MYA)</i>	<i>83.6 - 66.0 MYA</i>						
<i>Rock types</i>	<i>Sandstone</i>	<i>Sandstone</i>	<i>Sandstone</i>	<i>Sandstone</i>	<i>Sandstone</i>	<i>Sandstone</i>	<i>Claystone</i>
<i>PI</i>	<i>-</i>	<i>-</i>	<i>-</i>	<i>-</i>	<i>-</i>	<i>-</i>	<i>-</i>
<i>α</i>	<i>0.795</i>	<i>0.772</i>	<i>0.750</i>	<i>0.781</i>	<i>0.757</i>	<i>0.503</i>	<i>0.928</i>

<i>Sample</i>	<i>A-SC-60R</i>	<i>A-SC-109R</i>	<i>A-SC-110R</i>	<i>A-SC-112R</i>	<i>A-SC-115R</i>	<i>A-SC-116R</i>
<i>Geologic Unit</i>	<i>CRETACEOUS (Peedee Fm. And Black Creek Group)</i>					
<i>Age (MYA)</i>	<i>83.6 - 66.0 MYA</i>					
<i>Rock types</i>	<i>Claystone</i>	<i>Sandstone</i>	<i>Sandstone</i>	<i>Sandstone</i>	<i>Sandstone</i>	<i>Sandstone</i>
<i>PI</i>	<i>-</i>	<i>-</i>	<i>-</i>	<i>-</i>	<i>-</i>	<i>-</i>
<i>α</i>	<i>0.840</i>	<i>0.959</i>	<i>0.606</i>	<i>0.918</i>	<i>0.994</i>	<i>0.713</i>

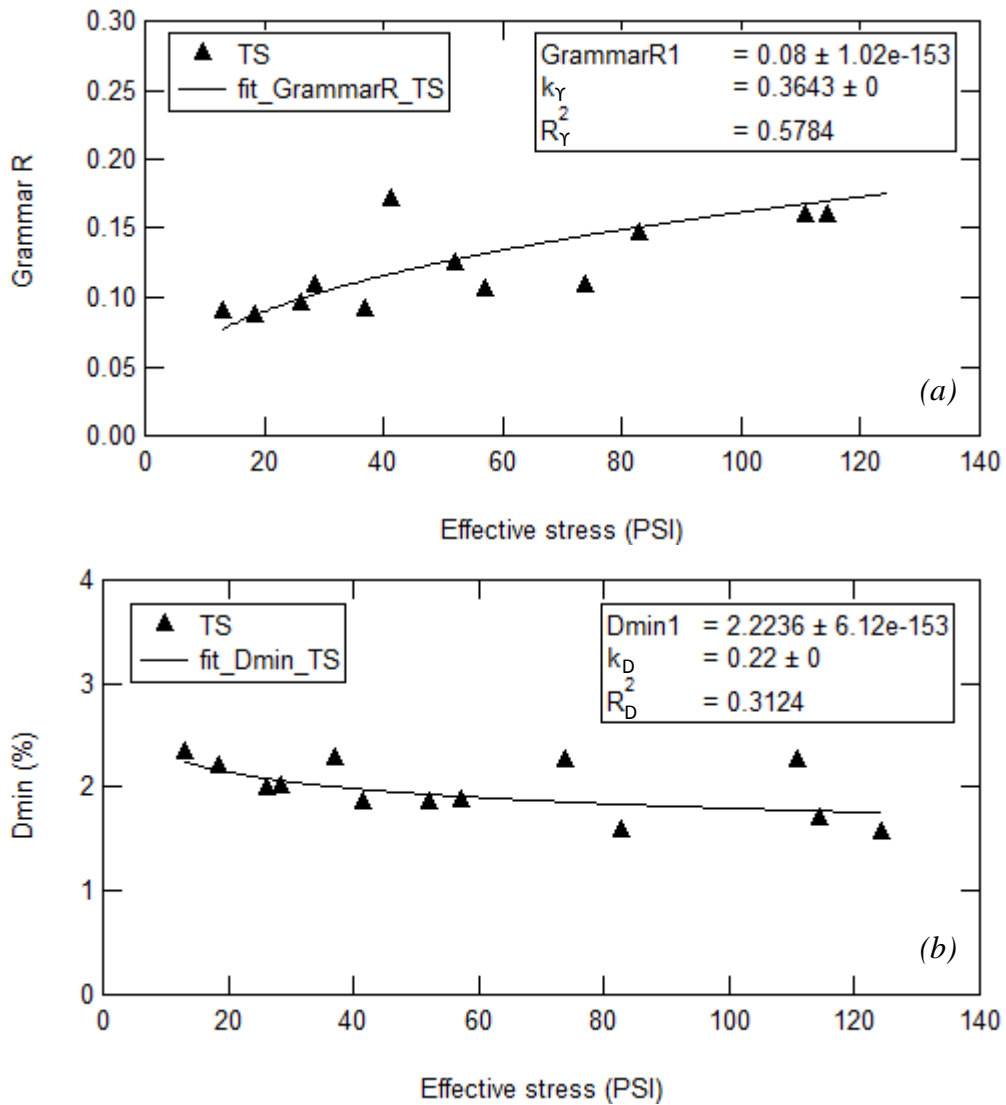


**Figure G7** Statistic Analysis for Model Parameters for PI between 11 and 20 of Cretaceous Deposits: (a)  $\gamma_{r1}$  and  $k_Y$ , and (b)  $D_{min1}$  and  $k_D$

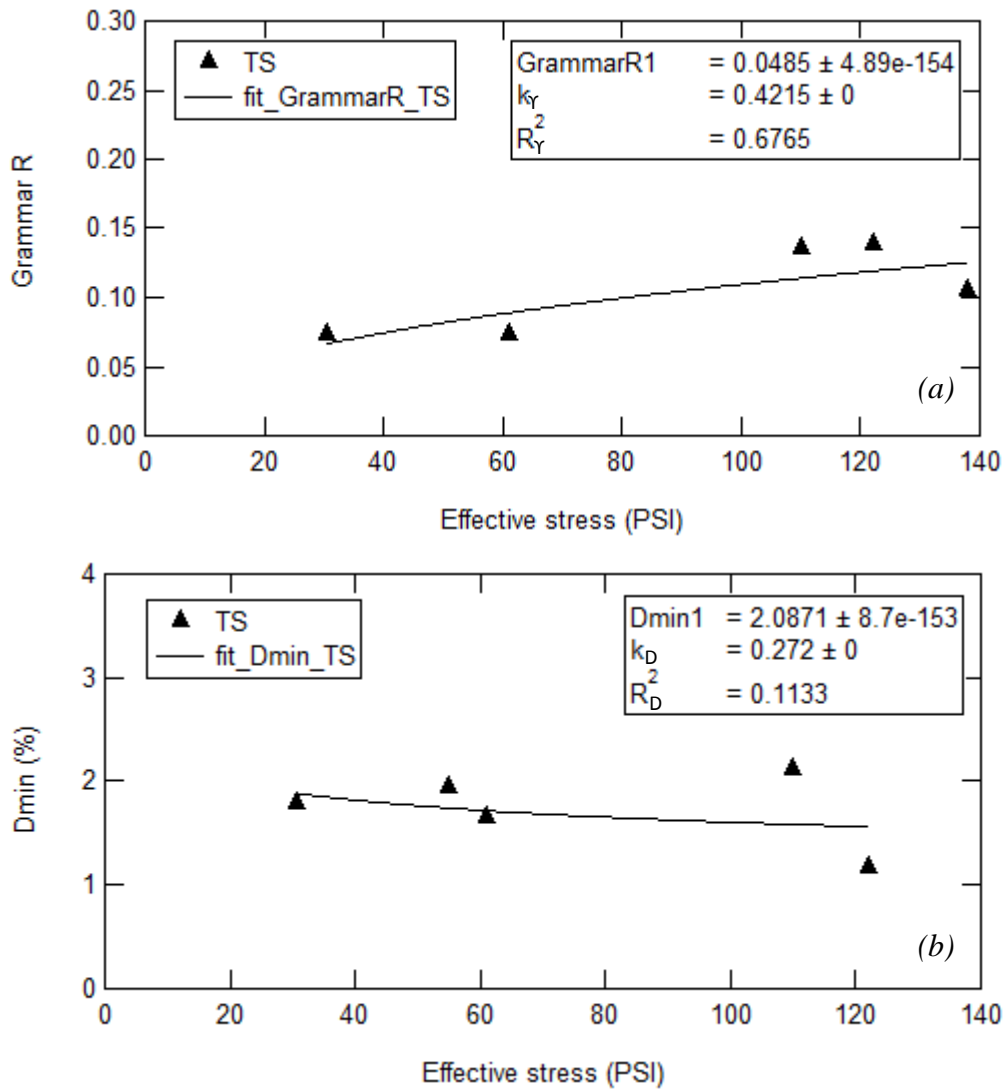


**Figure G8** Statistic Analysis for Model Parameters for PI between 21 and 30 of Cretaceous Deposits: (a)  $\gamma_{r1}$  and  $k_Y$ , and (b)  $D_{min1}$  and  $k_D$

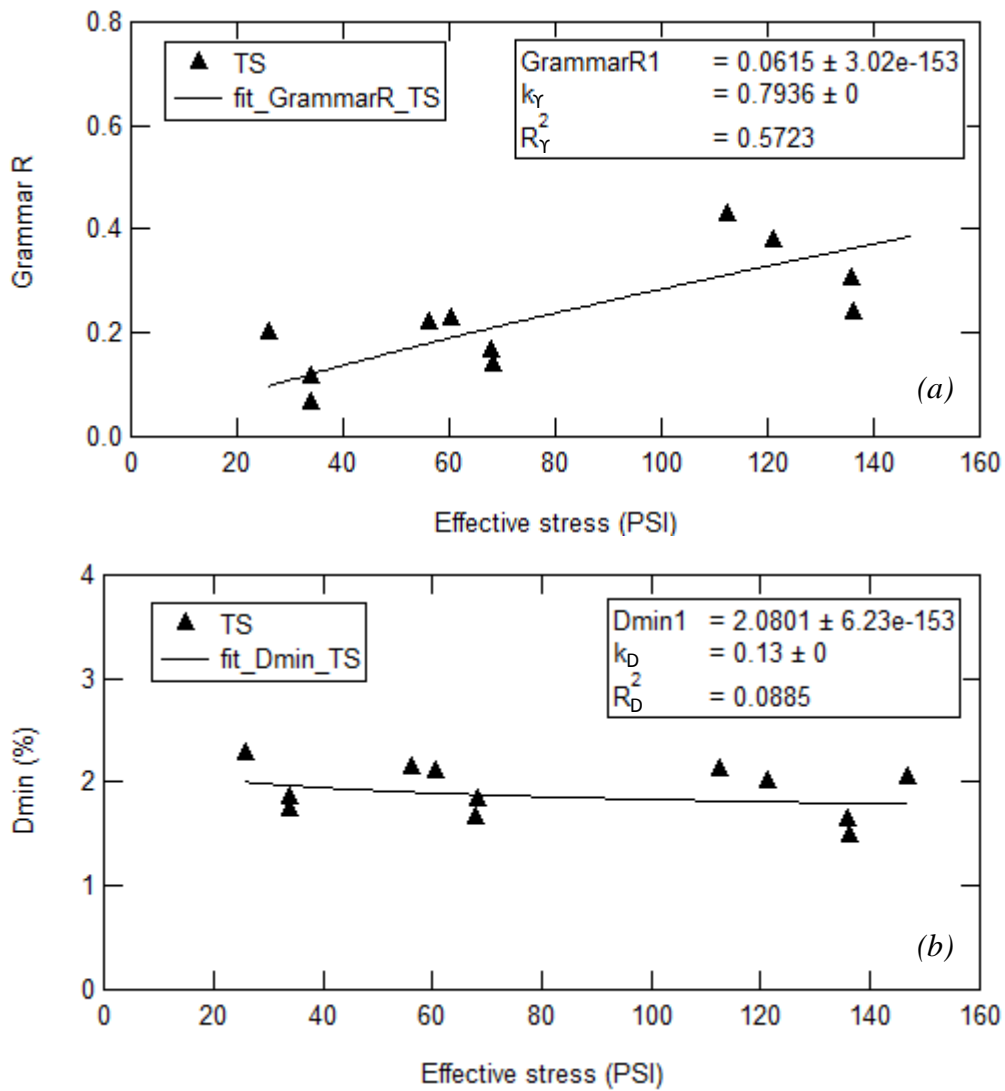


**Figure G9** Statistic Analysis for Model Parameters for PI between 31 and 40 of Cretaceous Deposits: (a)  $\gamma_{r1}$  and  $k_Y$ , and (b)  $D_{min1}$  and  $k_D$

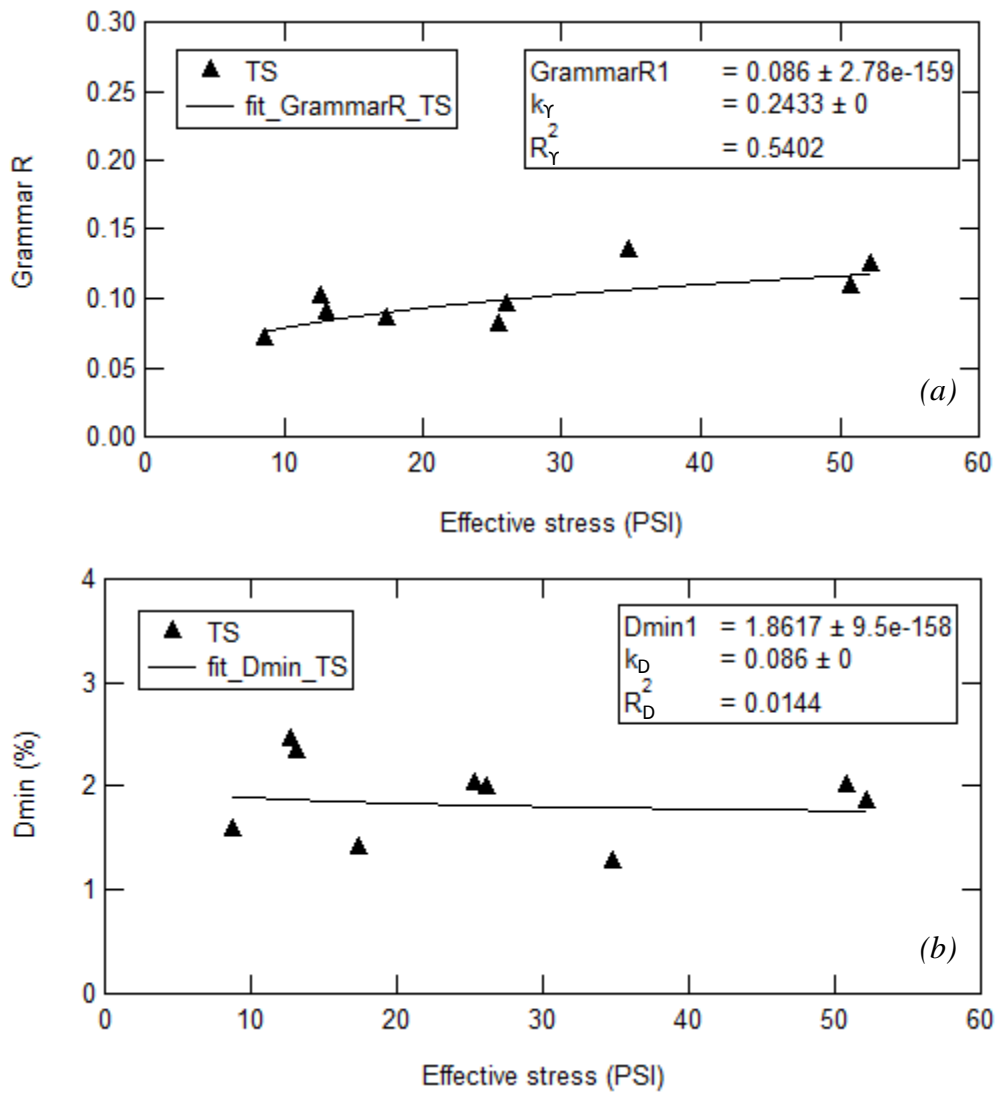


**Figure G10** Statistic Analysis for Model Parameters for PI between 41 and 50 of Cretaceous Deposits: (a)  $Y_{r1}$  and  $k_Y$ , and (b)  $D_{min1}$  and  $k_D$

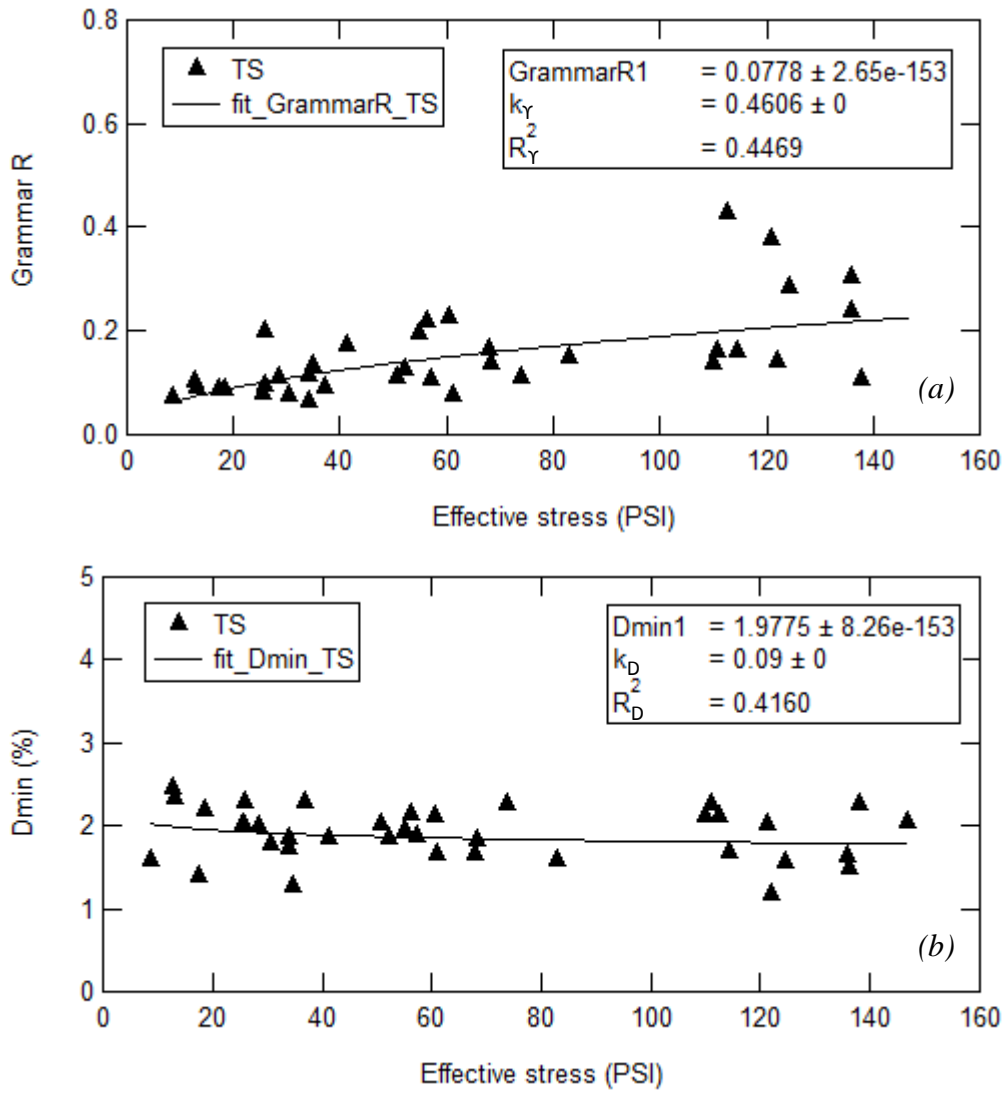


**Figure G11** Statistic Analysis for Model Parameters for PI between 11 and 50 (all of soils) of Cretaceous Deposits: (a)  $\gamma_{r1}$  and  $k_Y$ , and (b)  $D_{min1}$  and  $k_D$

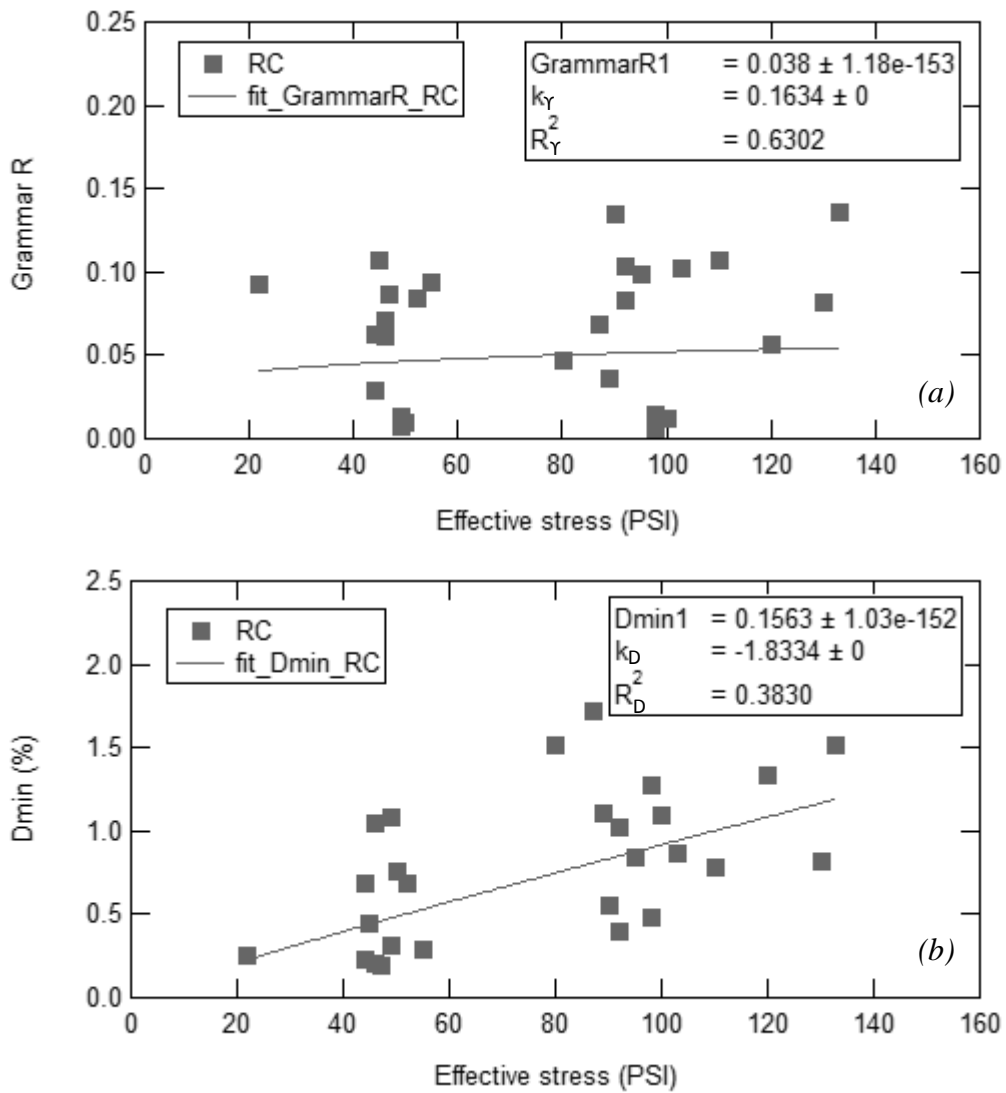


**Figure G12** Statistic Analysis for Model Parameters for Cretaceous Rocks:  
 (a)  $\gamma_{r1}$  and  $k_Y$ , and (b)  $D_{min1}$  and  $k_D$